

Files are in or Adobe format.
Download the newest version from Adobe.

24th International Symposium on BALLISTICS

New Orleans, LA

September 22-26, 2008

Conference Agenda

TUESDAY, SEPTEMBER 23, 2008

GENERAL SESSION

- *"IBC Presentation 2008",* Bo Janzon, IBC Chairman, SECRAB, Sweden
- *"GS009 A Brief History of Shaped Charges"*, William Walters, USA
- *"GS104 Numerical Simulation of Muzzle Exit and Separation Process for Sabot-Guided Projectiles at M > 1"*, Jorn van Keuk, Germany; Arno Klomfass, Germany

TERMINAL BALLISTICS

- "*TB068 Performance and Production of Jacketed Penetrators having Different Jacket Thickness*", B.J. van der Meer, The Netherlands; Mark Dijkstra, The Netherlands; Erik Carton, The Netherlands
- *"TB227 Loading Mechanisms on a Target from Detonation of a Buried Charge",* Leslie Taylor, USA; William Fourney, USA; Ulrich Leiste, USA; Bryan Cheesman, USA
- *"TB167 Predicting the Onset of Lateral Instability of Long Rod Penetrators in a Particulate Target",* Melissa Hankins, USA; S. E. Jones, USA; Karen L. Torres, USA
- *"TB135 A Comparative Study of Penetration Codes for Brittle Materials",* Sikhanda Satapathy, USA; Anthony Dawson, USA; Gregory Rodin, USA
- "*TB200 Radial Jet Dispersion Due to Current Interaction in an Electric Armour Application"*, Patrik Lundberg, Sweden; Patrik Appelgren, Sweden; Melker Skoglund, Sweden; Lars Westerling, Sweden; Tomas Hurtig, Sweden; Anders Larsson, Sweden

WARHEAD MECHANISMS

- *"WM056 Munitions Effects: A Schematic Overview of Munitions and Warheads, Trends for the Future"*, Andre Diederen, The Netherlands
- *"WM097 Initiation Controlled Multimode Warheads",* Thomas Falter, Germany
- *"WM203 Combined Effects Aluminized Explosives",* Ernest Baker, USA; Leonard Stiel, USA; Christos Capellos, USA; Wendy Balas, USA; Jack Pincay, USA
- *"WM134 Multiple Effects Warheads for Defeat of Urban Structures and Armour"*, Anthony Whelan, UK
- *"WM161 Development of the NLOS-LS PAM Warhead"*, Melissa Hobbs, USA; Christopher English, USA; David Hunter, USA; Jim Strom, USA; William Zarr, USA

EXTERIOR BALLISTICS & LAUNCH DYNAMICS

- "EB113 Range Extension of Gun-Launched Smart Munitions", Frank Fresconi, USA
- "EB166 Numerical Prediction of Magnus of Spin-Stabilized Projectiles", James DeSpirito, USA; Sidra Silton, USA
- "EB206 Mine Countermeasure Dart Dispense Modeling & Simulation", Gary Prybyla, USA; Michael Dean Neaves, USA; Kevin Losser, USA; James Baltar, USA; William Dietz, USA
- " EB178 Trajectory Deflection of Fin- and Spin-Stabilized Projectiles using Paired Lateral Impulses", Pierre Wey, France; Daniel Corriveau, Canada
- "LD011 Numerical Analysis of Bi-Metallic Explosive Shock-Loading and Release Experiments", Geremy Kleiser, USA; Brian Plunkett, USA; Lalit Chhabildas, USA

WEDNESDAY SEPTEMBER 24, 2008

ARMOUR & PERSONAL PROTECTION

- *"APP032 Assessment and Measurement of Potential Blunt Trauma Under Ballistic Helmets",* Celia Watson, UK; Annette Webb, Australia; Ian Horsfall, UK
- *"APP171 Ballistic Performance Assessment of Lightweight Body Armour Material Systems Against IED Threat",* Gilles Pageau, Canada; Kevin Williams, Canada; Daniel Bourget, Canada; Ming Cheng, Canada; Clint Hedge, Canada; Benoit Anctil, Canada
- *"APP001 Experimental Validation of the Origin of the Bodywork Effect (K-Effect) in the Up-Armouring of Civil and Military Vehicles"*, Frederik Coghe, Belgium; Bernard Kestelyn, Belgium; Marc Pirlot, Belgium
- *"APP075 Half Scale Experiments with Rig for Measuring Structural Deformation and Impulse Transfer from Land Mines",* Björn Zakrisson, Sweden; Bo Johansson, Sweden; Bengt Wikman, Sweden
- *"APP062 A Computational Study of the Energy Dissipation through an Acrylic Target Impacted by Various Size FSP",* Costas Fountzoulas, USA; Peter Dehmer, USA; Jian Yu, USA; James Sands, USA

TERMINAL BALLISTICS

- "*TB035 High Speed Penetration into Low Strength Concrete Target*", Vincent Luk, USA; James Dykes, USA; Joseph Bishop, USA; John Ludwigsen, USA; Douglas Dederman, USA; P. A. Taylor, USA
- "*TB168 Fragment Penetration Modeling of Anthropometric Ballistic Mannequins"*, William Bruchey, USA; Amy Tank, USA
- *"TB230 Effects of Small Caliber Ammunition Through Intermediate Barriers",* Jeremy Lucid, USA; Chris Gandy, USA

THURSDAY SEPTEMBER 25, 2008

GENERAL SESSION

- *"EB139 Numerical Computations of Dynamic Pitch-Damping Derivatives using Time-Accurate CFD Techniques",* Jubaraj Sahu, USA
- *"GS137 Consideration of the Ignition Delay of Gun Propellants",* Clive Woodley, UK; Michael Taylor, UK; Steve Fuller, UK; Steve Gilbert, UK; Joseph Gransden, UK
- "*GS232 U.S. Army Tactical Wheeled Vehicle Vulnerability Test & Evaluation Methodology",* Stephanie Koch, USA
- "*The Effect of Velocity on Jacketed Rod Efficiency",* Brad Pederson, Stephan Bless, Robert Fromm

WARHEAD MECHANISMS

- *"WM085 The Appendix",* Eitan Hirsch, Israel; Meir Mayseless, Israel
- "WM256 Behind Armour Effects at Shaped Charge Attacks", Manfred Held, Germany
- *"WM016 Warhead Filling and Casing Interactions Affect the Blast Field Performance"*, Paul Locking, UK; Dennis Flynn, UK; J. Dunnett, UK
- *"WM234 Reaction of Metal Fragments from Cased Explosive Charges",* Laura Donahue, Canada; Robert Ripley, Canada; Jeff Leadbetter, Canada; Yasuyuki Horie, USA; Fan Zhang, Canada

INTERIOR BALLISTICS & LAUNCH DYNAMICS

- "*IB098 Numerical Simulation of Projectile Acceleration Process Using Solid/Gas Two-Phase Reacting Flow Model*", Hiroaki Miura, Japan; Akiko Matsuo, Japan; Yuichi Nakamura, Japan
- *"IB015 Two-Dimensional Modelling of Modular Charge Gun Firings",* Clive Woodley, UK; Steve Fuller, UK
- "*LD027 Launch Dynamics Environment of a Water Piercing Missile Launcher"*, Jon Yagla, USA; John Busic, USA; Samuel Koski, USA; Chris Weiland, USA
- *"LD065 Experiments with Gun Launched Penetrators into Gelatin Target Materials",* John Stubberfield, UK; Nicholas Lynch, UK; Clive Woodley, UK; Alan Hepper, UK

WOUND BALLISTICS & VULNERABILITY

- *"WB053 The Validation of a Thoracic and Abdominal Test Rig for BABT Soft Body Armour Testing"*, Kate Hewins, UK; Ian Horsfall, UK; Celia Watson, UK
- *"WB242 Survivability Measures for Evaluation of Personnel in Military Systems",* Natalie Eberius, USA; Patricia Frounfelker, USA; Kelly Benjamin, USA
- *"WB144 Diagnostic Techniques for Multiphase Blast Fields"*, Richard Ames, USA; Michael Murphy, USA

FRIDAY SEPTEMBER 26, 2008

GENERAL SESSION

- *"GS023 Predicting Hazard Response Scenarios in Weapon Systems",* Ian Cullis, UK; I.H. Brown, UK; P.D. Church, UK; P. Gould, UK; V.E. Ingamells, UK
- *"GS130 Experimental Validation of a Kevlar Fabric Model for Ballistic Impact"*, Chian Yen, USA; Tusit Weerasooriya, USA; Paul Moy, USA; Brian Scott, USA; Bryan Cheeseman, USA
- *"GS205 Shaped Charge Penetration of Gas Saturated Sandstone",* Brenden Grove, USA; Jeremy Harvey, USA

TERMINAL BALLISTICS

- *"TB025 Penetration Resistance of Glass and a Glass Ceramic"*, Stephan Bless, USA; Don Berry, USA
- *"TB111 Long-Rod Penetration into Intact and Pre-Damaged SiC Ceramic"*, Charles Anderson, USA; Thilo Behner, Germany; Dennis Orphal, USA; Arthur Nicholls, USA; Timothy Holmquist, USA; Matthias Wickert, Germany
- *"TB058 The Shock Response Of a Cemented Tungsten Carbide",* Koen Herlaar, The Netherlands; Andre Diederen, The Netherlands; Gareth Appleby-Thomas, UK; Paul J Hazell, UK
- *"TB038 GRC's Impact Behavior"*, Alejandro Enfedaque Diaz, Spain; David Cendón Franco, Spain; Francisco Gálvez Díaz-Rubio, Spain; Vicente Sánchez Gálvez, Spain
- *"TB248 The Mechanics of Projectile Arrest for Compliant Cross Plied Unidirectional Laminates",* Brian Scott, USA; Bryan Cheeseman, USA

NATIONAL DEFENSE INDUSTRIAL ASSOCIATION
NDIA
STRENGTH THROUGH INDUSTRY & TECHNOLOGY

PROMOTING NATIONAL SECURITY SINCE 1919

24th International Symposium on BALLISTICS

New Orleans, Louisiana, USA

Sponsored by the Ballistics Division of NDIA in association with the International Ballistics Committee

IBC International Ballistics Committee

SEPTEMBER 22-26, 2008
WWW.NDIA.ORG/MEETINGS/8210

CONFERENCE AGENDA
SHERATON NEW ORLEANS ▸ NEW ORLEANS, LA

24TH INTERNATIONAL SYMPOSIUM ON BALLISTICS:

SEPTEMBER 22-26, 2008 ▶ SHERATON NEW ORLEANS NEW ORLEANS, LA

The 24th International Symposium on Ballistics is jointly organized and supported by the National Defense Industrial Association, USA in conjunction with the International Ballistics Committee

Symposium Co-Chairmen:
Dr. Stephan Bless
Dr. James Walker

PREVIOUS INTERNATIONAL SYMPOSIA ON BALLISTICS

Orlando, Florida, USA	1974
Daytona, Florida, USA	1976
Karlsruhe, Germany	1977
Monterey, California, USA	1978
Toulouse, France	1980
Orlando, Florida, USA	1981
The Hague, The Netherlands	1983
Orlando, Florida, USA	1984
Shrivenham, UK	1986
San Diego, California, USA	1987
Brussels, Belgium	1989
San Antonio, Texas, USA	1990
Stockholm, Sweden	1992
Quebec City, Canada	1993
Jerusalem, Israel	1995
San Francisco, California, USA	1996
Midrand, South Africa	1998
San Antonio, Texas, USA	1999
Interlaken, Switzerland	2001
Orlando, Florida, USA	2002
Adelaide, South Australia	2004
Vancouver, BC, Canada	2005
Tarragona, Spain	2007

SYMPOSIUM ATTIRE

Appropriate dress for this symposium is business for civilians (coat and tie) and class A uniform or uniform of the day for military.

PAPER SELECTION COMMITTEE

Dr. Charles E. Anderson, Jr., USA
Mr. Joseph Backofen, USA
Dr. Dennis Baum, USA
Dr. Stephan Bless, USA
Mme. Manon Bolduc, Canada
Dr. Donald Carlucci, USA
Dr. James Cazamias, USA
Mr. Pierre Chanteret, France
Dr. Sidney Chocron, USA
Dr. Ian Cullis, UK
Mr. Philip Cunniff, USA
Dr. Andre Diederen, Netherlands
Dr. Eric Fahrenthold, USA
Dr. William Flis, USA
Dr. Richard Fong, USA
Dr. Francisco Galvez, Spain
Dr. Marc Giraud, France
Dr. Manfred Held, Germany
Dr. Bo Janzon, Sweden
Dr. Valeriy Kartuzov, Ukraine
Dr. Michael Murphy, USA
Dr. Dennis Nandlall, Canada
Mr. Dennis Orphal, USA
Dr. Ake Persson, Sweden
Dr. Xiangyang Quan, USA
Mr. Jack P. Riegel, III, USA
Mr. Erick Sagebiel, USA
Dr. Sikhanda Satapathy, USA
Dr. Douglas Templeton, USA
Dr. James Walker, USA
Dr. Paul Weinacht, USA
Mr. Carl Weiss, USA
Dr. Joe Wells, USA

INTERNATIONAL BALLISTICS COMMITTEE

Executive Committee
Dr. Bo Janzon, Sweden
Chairman
Mr. Jack Riegel, USA
Vice-Chairman
Dr. Ian Cullis, UK
Secretary
Prof. Ron Brown, USA
Bursar #1
Dr. Richard Fong, USA
Bursar #2
Dr. Pieter Nel, South Africa
Immediate Past Chairman
Dr. Roxan Cayzac, France
POC Europe
Dr. Meir Mayseless, Israel
POC Other Nations
Dr. Joe Carleone, USA
POC North America

Members
Dr. Charles Anderson, Jr., USA
Mr. Joe Backofen, USA
Dr. Dennis Baum, USA
Dr. Ronald Brown, USA
Dr. Norbert Burman, Australia
Dr. Joseph Carleone, USA
Dr. Roxan Cayzac, France
Mr. Pierre Chanteret, France
Dr. Sidney Chocron, USA
Dr. Ian Cullis, UK
Dr. Andre Diederen, The Netherlands
Dr. William Flis, USA
Mr. Richard Fong, USA
Dr. Francisco Galvez, Spain
Dr. Marc Giraud, France
Prof. Dr. Manfred Held, Germany
Dr. Dieter Hensel, France
Dr. Eitan Hirsch, Israel
Dr. Bo Janzon, Sweden
Dr. Hanspeter Kaufmann, Switzerland
Dr. Eva Liden, Sweden
Dr. Meir Mayseless, Israel
Dr. Frederick Mostert, South Africa
Dr. Michael Murphy, USA
Dr. Dennis Nandall, Canada
Dr. Pieter Nel, South Africa
Dr. Ake Persson, Sweden
Dr. Moshe Ravid, Israel
Dr. William Reinecke, USA
Mr. Jack Riegel, USA
Dr. Brian Scott, USA
Prof. Dr. Klaus Thoma, Germany
Prof. Zhongyuan Wang, China
Dr. Paul Weinacht, USA

Emeritus Members
Dr. Brucs Burns
Prof. Eduard Celens, Belgium
Dr. Pei Chi Chou, USA
Dr. Rudi Heiser, Germany
Dr. Albert Horst, USA
Dr. Gunther Krauth, Germany
Dr. Ir. Hans Pasman, The Netherlands
Dr. E. Schmidt, USA
Dr. Gustav-Adolf Schroeder, Germany
Mr. David Scott, UK
Dr. Alois Stilp, Germany
Dr. Louis Zernow, USA

Guest Members
Mr. P. U. Deshpande, India
Professor Tan Hua, China
Dr. Carlos Navarro, Spain
Acad. Victor S. Soloviev, Russia

MONDAY, SEPTEMBER 22, 2008

7:00 am - 7:00 pm **Registration Open**

9:00 am - 4:30 pm **Independent Tutorials**
Additional Registration Fee Applies
Presented by Professor Dr. Manfred Held

AM SESSION

9:00 am	Warhead Mechanism
	1.1 Blast Charges
	1.2 Shaped Charges
	1.3 Flat Cone Charges
10:45 am	Coffee Break
11:00 am	Warhead Mechanism Continued
	1.4 EFP Charges
	1.5 Fragment Charges (Anti-AC/Anti-TBM)

PM SESSION

1:30 pm	Overview on Armour for MBT´s and APC´s
	2.1 RHA
	2.2 Ceramics
	2.3 Glass
3:00 pm	Coffee Break
3:15 pm	Overview on Armour for MBT´s and APC´s Cont.
	2.4 Composites
	2.5 ERA
	2.6 NERA or Bulging
	2.7 Active Defence Concepts

10:00 am - 4:00 pm **Exhibitor Move In**

5:00 pm **Exhibit Hall Open**

5:00 pm - 7:00 pm **Opening Reception - Exhibit Hall**
Featuring the New Orleans Spice Jazz Band

These tutorials will provide attendees with a better understanding of the many very specialized papers in the 24th International Symposium on Ballistics. Every course attendee will receive a handout of the slides used in the lectures.

Prof. Dr. Held is one of the foremost experts in the world in ballistics. The material in this course is drawn from his lectures at the Military University in Munich.

TUESDAY, SEPTEMBER 23, 2008

7:00 am **Continental Breakfast & Registration**

8:00 am **Welcome & Administrative Remarks**

8:10 am - 9:50 am **General Session**
Chaired by Pieter Nel & Marc Giraud

8:10 am *GS009 A Brief History of Shaped Charges*
William Walters, USA

8:50 am *GS109 Interface Defeat for Unconfined SiC Ceramics*
Thilo Behner, Germany; Charles Anderson, USA; Timothy Holmquist, USA; Matthias Wickert, Germany; Doug Templeton, USA

9:10 am *GS104 Numerical Simulation of Muzzle Exit and Separation Process for Sabot-Guided Projectiles at M > 1*
Jorn van Keuk, Germany; Arno Klomfass, Germany

9:30 am *GS117 Origin and Magnitude of the Pressure and Temperature Increase Behind Defeated Armor*
Andreas Heine, Germany; Matthias Wickert, Germany

9:30 am - 5:30 pm **Exhibit Hall Open**

9:50 am - 10:10 am **Coffee Break in Exhibit Hall**

10:10 am - 10:30 am **Presentation on Proposed International Ballistics Society**

10:30 am - 12:10 pm **Terminal Ballistics**
Chaired by Dennis Nandlall & Sikhanda Satapathy

10:30 am *TB068 Performance and Production of Jacketed Penetrators having Different Jacket Thickness*
B.J. van der Meer, The Netherlands; Mark Dijkstra, The Netherlands; Erik Carton, The Netherlands

10:50 am *TB227 Loading Mechanisms on a Target from Detonation of a Buried Charge*
Leslie Taylor, USA; William Fourney, USA; Ulrich Leiste, USA; Bryan Cheesman, USA

11:10 am *TB167 Predicting the Onset of Lateral Instability of Long Rod Penetrators in a Particulate Target*
Melissa Hankins, USA; S. E. Jones, USA; Karen L. Torres, USA

11:30 am *TB135 A Comparative Study of Penetration Codes for Brittle Materials*
Sikhanda Satapathy, USA; Anthony Dawson, USA; Gregory Rodin, USA

11:50 am *TB200 Radial Jet Dispersion Due to Current Interaction in an Electric Armour Application*
Patrik Lundberg, Sweden; Patrik Appelgren, Sweden; Melker Skoglund, Sweden; Lars Westerling, Sweden; Tomas Hurtig, Sweden; Anders Larsson, Sweden

12:10 pm - 12:30 pm **Introduction to Poster Sessions**

12:30 pm - 2:00 pm **Lunch - Armstrong Ballroom; 8th Floor**

2:00 pm - 3:40 pm **Warhead Mechanisms**
Chaired by Pierre Chanteret & Richard Fong

2:00 pm *WM056 Munitions Effects: A Schematic Overview of Munitions and Warheads, Trends for the Future*
Andre Diederen, The Netherlands

2:20 pm *WM097 Initiation Controlled Multimode Warheads*
Thomas Falter, Germany

2:40 pm *WM203 Combined Effects Aluminized Explosives*
Ernest Baker, USA; Leonard Stiel, USA; Christos Capellos, USA; Wendy Balas, USA; Jack Pincay, USA

3:00 pm *WM134 Multiple Effects Warheads for Defeat of Urban Structures and Armour*
Anthony Whelan, UK

3:20 pm *WM161 Development of the NLOS-LS PAM Warhead*
Melissa Hobbs, USA; Christopher English, USA; David Hunter, USA; Jim Strom, USA; William Zarr, USA

3:40 pm - 5:30 pm **Terminal Ballistics Poster Session**

3:40 pm **Coffee Break in Exhibit Hall**

4:00 pm - 5:40 pm **Exterior Ballistics & Launch Dynamics**
Chaired by Paul Weinacht & Roxan Cayzac

4:00 pm *EB113 Range Extension of Gun-Launched Smart Munitions*
Frank Fresconi, USA

4:20 pm *EB166 Numerical Prediction of Magnus of Spin-Stabilized Projectiles*
James DeSpirito, USA; Sidra Silton, USA

4:40 pm *EB206 Mine Countermeasure Dart Dispense Modeling & Simulation*
Gary Prybyla, USA; Michael Dean Neaves, USA; Kevin Losser, USA; James Baltar, USA; William Dietz, USA

5:00 pm *EB178 Trajectory Deflection of Fin- and Spin-Stabilized Projectiles using Paired Lateral Impulses*
Pierre Wey, France; Daniel Corriveau, Canada

5:20 pm *LD011 Numerical Analysis of Bi-Metallic Explosive Shock-Loading and Release Experiments*
Geremy Kleiser, USA; Brian Plunkett, USA; Lalit Chhabildas, USA

TERMINAL BALLISTICS POSTER SESSION

3:40 pm - 5:30 pm

CHAIRMEN: JACK RIEGEL, CARL WEISS & KOEN HERLAAR

TB002 Ballistic Performance of Protective Liners

Moshe Ravid, Israel; Shlomo Birger, Israel; Nimi Shapira, Israel; Avi Ya'akobovith, Israel; Yoav Hirschberg, Israel

TB008 Non-Invasive Ballistic Impact Damage Diagnostics Capabilities with XCT: Now and in the Future

Joe Wells, USA

TB018 Protection Capability of Steel Armor with Liquid Filled Cavities Against Shaped Charge Jets

Andreas Holzwarth, Germany

TB020 Deformation and Breakup of Tungsten Alloy Cubes, Cylinders and Spheres on Aluminum Plates

Karl Weber, Germany

TB030 Penetration of Tube-Like Projectiles into Metal Targets

Vladislav Veldanov, Russia; Sergey Fedorov, Russia; Victor Kozlov, Russia; Mikhail Maximov, Russia

TB031 Penetration Model Taking in Mind Viscosity Properties of the Impacted Body Materials. Comparison with Test.

Vladislav Veldanov, Russia; Victor Kozlov, Russia

TB045 The Effect of a Copper Buffer on Interface Defeat

Timothy Holmquist, USA; Charles Anderson, USA; Thilo Behner, Germany

TB050 On Penetration/Perforation of Concretes Struck by Rigid Projectiles

Xiaowei Chen, China

TB052 Study on the Effect of Reinforcement of Concrete Targets upon the Penetration Performance of a Projectile

Hak Jun Kim, Korea; Leeju Park, Korea; Hyungwon Kim, Korea

TB057 Ballistic Impact Experiments of Tungsten Carbide Projectiles onto Tungsten Carbide Targets

Koen Herlaar, The Netherlands; Andre Diederen, The Netherlands; Gareth Appleby-Thomas, UK; Paul Hazell, UK

TB058 The Shock Response Of a Cemented Tungsten Carbide

Koen Herlaar, The Netherlands; Andre Diederen, The Netherlands; Gareth Appleby-Thomas, UK; Paul J Hazell, UK

TB060 Modeling of Defects in Transparent Ceramics for Improving Military Armor

Costas Fountzoulas, USA; James Sands, USA; Gary Glide, USA; Parimal Patel, USA

TB064 Modeling the Influence of Damage in Compression on the Spall Strength of Alumina

Zvi Cooper, Israel; Miles Rubin, Israel

TB067 New Analytical Model of Expansion of Spherical Cavity in Porous Plastic Material and Penetration into Such Materials

Boris Galanov, Ukraine; Valeriy Kartuzov, Ukraine; Sergei Ivanov, Ukraine

TB080 An Experimental Study of Penetration Behavior of Shaped Charge Jet in Water Filled Targets

Dev Raj Saroha, India; Gurmit Singh, India; Virendra Kumar Mahala, India

TB083 Ricochet of AP Projectiles from Hard Concrete Targets

Meir Mayseless, Israel; Yehiel Reifen, Israel; David Touati, Israel; Dan Yaziv, Israel; G. Tibon, Israel

TB089 Numerical Study or the Relations between Material Properties of Tungsten-Alloy Rod and its Ballistic Performance

Lou Jianfeng, China; He Changjiang, China; Hong Tao, China; Wang Zheng, China; Hang Yihong, China

TB106 Numerical and Experimental Study of the Defeating the RPG-7

Stanislav Rolc, Czech Republic; Jaroslav Buchar, Czech Republic; Zbynek Akstein, Czech Republic; Giovanni Cozzani, Italy; C. De Giorgi, Italy

TB128 New Lightweight Metals for Armors

Frans van Wegen, The Netherlands; Erik Carton, The Netherlands

TB132 An Analytical Investigation of the Energy-Volume Relationship Observed in Concrete Targets Penetrated by Shaped Charge Jets

Milton Frick Maritz, South Africa; Frikkie Mostert, South Africa; Cornelis Tereblanche, South Africa

TB138 The Effect of Velocity on Jacketed Rod Efficiency

Brad Pedersen, USA; Stephan Bless, USA; Robert Fromm, USA

TB141 Preliminary Results From Firings of Glass Shaped Charge Jets into Steel Targets

Michael Edwards, UK; Rhydian Harries, UK; Euan Henderson, UK

TB146 An Accuracy and Efficiency Assessment of Beanbags

Alexandre Papy, Belgium; Fatiha Id-Boufker, Belgium

TB148 A Comparison of the Ballistic Performance between Rolled Plate in AZ31B-H24 Magnesium & 5083-H131 Aluminum

Tyrone Jones, USA; Matthew Burkins, USA; Rick DeLorme, USA

TB149 In Situ Penetration Testing of Darts with 15-Inch Mobile Gas Gun

Douglas Dederman, USA; James Dykes, USA; John Foster, USA; Damon Burnett, USA

TB190 How to Model Fracture Behaviour in Long Rod Projectile

Ewa Lidén, Sweden

TB192 Concept Analysis and Impact Performance of Kinetic Energy Penetrators against Composite Hard Targets

A. K. Sharma, India

TB197 Multiple Hit Performance of 7.62 mm Hardened Steel and 30 mm APFSDS Projectiles in Brick and Reinforced Concrete Walls

Stephan Lampert, Switzerland; Hanspeter Kaufmann, Switzerland; Dieter Hoffmann, Germany

TB201 Supersonic Penetration by Wedges and Cones into Dry Sand

William Flis, USA; David Jann, USA; Lucia Shan, USA

TB207 Constitutive Properties of Transparent Nylon during High Velocity Impact

Nicholas Tsantinis, USA; John Song, USA; Jason Parker, USA; Phillip Cunniff, USA

TB217 Penetration Performance of Geopenetrators in the High Velocity Regime

Norbert Heider, Germany; Arno Klomfass, Germany; Makfred Salk, Germany

TB229 Simple Explicit Analysis for the Effect of Ceramic Thickness on the Dwell/ Penetration Transition

Jerry LaSalvia, USA

WEDNESDAY, SEPTEMBER 24, 2008

7:00 am **Continental Breakfast & Registration**

8:00 am **Administrative Remarks**

8:00 am - 1:30 pm **Exhibit Hall Open**

8:10 am - 10:10 am **Armour & Personal Protection**
Chaired by Doug Templeton & Eric Fahrenthold

8:10 am *APP032 Assessment and Measurement of Potential Blunt Trauma Under Ballistic Helmets*
Celia Watson, UK; Annette Webb, Australia; Ian Horsfall, UK

8:30 am *APP171 Ballistic Performance Assessment of Lightweight Body Armour Material Systems Against IED Threat*
Gilles Pageau, Canada; Kevin Williams, Canada; Daniel Bourget, Canada; Ming Cheng, Canada; Clint Hedge, Canada; Benoit Anctil, Canada

8:50 am *APP001 Experimental Validation of the Origin of the Bodywork Effect (K-Effect) in the Up-Armouring of Civil and Military Vehicles*
Frederik Coghe, Belgium; Bernard Kestelyn, Belgium; Marc Pirlot, Belgium

9:10 am *APP075 Half Scale Experiments with Rig for Measuring Structural Deformation and Impulse Transfer from Land Mines*
Björn Zakrisson, Sweden; Bo Johansson, Sweden; Bengt Wikman, Sweden

9:30 am *APP062 A Computational Study of the Energy Dissipation through an Acrylic Target Impacted by Various Size FSP*
Costas Fountzoulas, USA; Peter Dehmer, USA; Jian Yu, USA; James Sands, USA

9:50 am *APP163 Simulation of Damage to a Vehicle by Explosion of an Improvised Explosive Device*
Chris Quan, USA; John Pavon, USA

8:10 am - 10:30 am **Warhead Mechanisms Poster Session**

10:10 am - 10:30 am **Coffee Break in Exhibit Hall**

10:30 am - 12:00 pm **Terminal Ballistics**
Chaired by Klaus Thoma & Ake Persson

10:30 am *TB035 High Speed Penetration into Low Strength Concrete Target*
Vincent Luk, USA; James Dykes, USA; Joseph Bishop, USA; John Ludwigsen, USA; Douglas Dederman, USA; P. A. Taylor, USA

10:50 am *TB168 Fragment Penetration Modeling of Anthropometric Ballistic Mannequins*
William Bruchey, USA; Amy Tank, USA

11:10 am *TB230 Effects of Small Caliber Ammunition Through Intermediate Barriers*
Jeremy Lucid, USA; Chris Gandy, USA

11:30 am *TB222 Protecting the New Horizons Spacecraft's Radioisotope Thermoelectric Generator from Potential Fragment Impacts during Launch Self Destruct*
James Walker, USA; Walt Gray, USA

12:00 am - 1:30 pm **Lunch - Armstrong Ballroom; 8th Floor**

1:30 pm - 5:30 pm **Tour of the French Quarter (included in attendee registration)**

Conference attendees will be split into 4 groups, determined by bead theme and color given at registration. Groups will convene in the lobby of the Sheraton before taking off for Bourbon Street! Stay with your group to enjoy New Orleans' famous bars and restaurants!

WARHEAD MECHANISMS POSTER SESSION

8:10 am - 10:30 am

CHAIRMEN: EITAN HIRSCH, FRIKKIE MOSTERT, DAVE LAMBERT

WM003 Experimental, Numerical and Analytical Studies on Two Linear Demolition Shape Charges for Two Initiation Modes

Shakeel Abbas Rofi, China; Huang Fenglei, China

WM004 Experimental and Numerical Investigations on the Formation and Penetration of Jet Projectile Charges against Concrete Targets

Shakeel Abbas Rofi, China; Huang Fenglei, China; Zhang Leilei, China

WM010 Softening of Shaped Charge Jet Particles While Penetrating Air

Joe Backofen, USA

WM019 Lethality Enhancer Against TBMs with Demanding Submunition Payloads

Werner Arnold, Germany; Ernst Rottenkolber, Germany

WM022 Optimisation of Fragmentation Warheads

Lawrence Davey, UK; John Curtis, UK; Andrew Bowden, UK

WM029 Near Field Impulse Loading Measurement Techniques for Evaluating Explosive Blast Performance

Thuvan Piehler, USA; Avi Birk, USA; Richard Benjamin, USA; Vincent Boyle, USA; Eugene Summers, USA; Stephen Aubert, USA

WM040 Study on Virtual Prototyping Design Method for Conventional Warhead

Yang Yunbin, China; Qian Lixin, China; Sun Chuanjie, China; Zhou Yan, China

WM094 Influence of Peripheral Frame Parameters on Fragments Dispersion

Alex Zlatkis, Israel; Natanel Korin, Israel; Ilan Azulay, Israel; David Touati, Israel; Evgeny Gofman, Israel

WM101 Multi-Purpose Projectile Concept to Balance the Conflicting Requirements for Peace Support Operations

Gawie De la Bat, South Africa; Jean Louis Du Plessis, South Africa; Donovan Wilson, South Africa; Dieter Peters, South Africa; Johan Mare, South Africa

WM155 Development of the M982 Excalibur Unitary Warhead

Richard Szczepanski, USA; Terry Young, USA

WM156 Development of Fielding of the Guided Multi-Launch Rocket System (GMRLS) Unitary Warhead

Renita Friese, USA; Richard Tuznik, USA; Tracey Westmoreland, USA

WM164 Small EFP Charge for Armor Development

David Davison, USA; Dan Pratt, USA; James Bustamante, USA

WM185 The Effect of Corner Turning on Wave Shaper Performance

Andreas Helte, Sweden; Jonas Lundgren, Sweden; Håkan Örnhed, Sweden

WM189 SDSC – A Structure Destroying Shaped Charge

Lippe Sadwin, Israel; Eitan Hirsch, Israel

WM193 The Jetting Cavity Test – A Multi Parameter Material Properties Measurement Tool

Sergi Chanukaev, Israel; Eitan Hirsch, Israel

WM202 Warhead Venting Design Technology Development

Timothy Madsen, USA; Ernest Baker, USA; Stanley DeFisher, USA; Nausheen Al-Shehab, USA; Daniel Suarez, USA; Brian Fuchs, USA

WM204 PIMS: Particle Impact Mitigation Sleeves

James Pham, USA; Arthur Daniels, USA; Ernest Baker, USA; Koon-Wing Ng, USA; David Pfau, USA

WM212 Effects of Computational Zoning on Resolving Partitioning and Jet Formation from Small Caliber Nitromethane Shaped Charges

Ronald Brown, USA; Hung Cao, USA; Richard Zamberlan, USA; Dave Gerace, USA; Pedro Freitas, USA; Jose O. Sinibaldi, USA; Andreas Holzwarth, Germany

WM214 Frangible Munitions for Reduced Collateral Damage

Michael Minnicino, USA; Ryan Emerson, USA

THURSDAY, SEPTEMBER 25, 2008

7:00 am **Continental Breakfast & Registration**

8:00 am **Administrative Remarks**

8:10 am - 9:50 am **General Session**
Chaired by Zhongyuan Wang & Ed Schmidt

8:10 am *EB139 Numerical Computations of Dynamic Pitch-Damping Derivatives using Time-Accurate CFD Techniques*
Jubaraj Sahu, USA

8:30 am *GS195 Impact Effects of Light Shaped Charge Rockets with Ignition Failure on Thin Metal Armour Plates*
Hanspeter Kaufmann, Switzerland; Stephan Lampert, Switzerland

8:50 am *GS137 Consideration of the Ignition Delay of Gun Propellants*
Clive Woodley, UK; Michael Taylor, UK; Steve Fuller, UK; Steve Gilbert, UK; Joseph Gransden, UK

9:10 am *GS046 Electromagnetic Artillery*
Jerome Tzeng, USA; Ed Schmidt, USA

9:30 am *GS232 U.S. Army Tactical Wheeled Vehicle Vulnerability Test & Evaluation Methodology*
Stephanie Koch, USA

9:30 am - 3:30 pm **Exhibit Hall Open**

9:50 am - 10:10 am **Coffee Break in Exhibit Hall**

9:50 am - 11:50 am **Exterior Ballistics; Interior Ballistics; Launch Dynamics Poster Sessions**

10:10 am - 12:00 pm **Warhead Mechanisms**
Chaired by Chris Quan & Michael Murphy

10:10 am *WM085 The Appendix*
Eitan Hirsch, Israel; Meir Mayseless, Israel

10:30 am *WM256 Behind Armour Effects at Shaped Charge Attacks*
Manfred Held, Germany

10:50 am *WM211 Effect of Detonation Front Inversion on Directed Energy Output*
Ronald Brown, USA; Dimitrios Fanaras, USA; David Amondson, USA; Ronald Williams, USA; James Stork, USA; John Gamble, USA; Jose O. Sinibaldi, USA

11:10 am *WM016 Warhead Filling and Casing Interactions Affect the Blast Field Performance*
Paul Locking, UK; Dennis Flynn, UK; J. Dunnett, UK

11:30 am *WM234 Reaction of Metal Fragments from Cased Explosive Charges*
Laura Donahue, Canada; Robert Ripley, Canada; Jeff Leadbetter, Canada; Yasuyuki Horie, USA; Fan Zhang, Canada

12:00 pm - 1:30 pm **Lunch - Armstrong Ballroom; 8th Floor**

1:30 pm - 3:30 pm **Armour & Personal Protection; Wound Ballistics & Vulnerability Poster Sessions**

1:30 pm - 3:10 pm **Interior Ballistics & Launch Dynamics**
Chaired by Don Carlucci & Ken Kuo

1:30 pm *IB098 Numerical Simulation of Projectile Acceleration Process Using Solid/Gas Two-Phase Reacting Flow Model*
Hiroaki Miura, Japan; Akiko Matsuo, Japan; Yuichi Nakamura, Japan

1:50 pm *IB015 Two-Dimensional Modelling of Modular Charge Gun Firings*
Clive Woodley, UK; Steve Fuller, UK

2:10 pm *IB110 Numerical Simulation of Interior Ballistics Processes of a High Speed Counter-Mass Propelling Gun*
Xiaobing Zhang, China; Weiping Zhou, China; Haiqing Li, China

2:30 pm *LD027 Launch Dynamics Environment of a Water Piercing Missile Launcher*
Jon Yagla, USA; John Busic, USA; Samuel Koski, USA; Chris Weiland, USA

2:50 pm *LD065 Experiments with Gun Launched Penetrators into Gelatin Target Materials*
John Stubberfield, UK; Nicholas Lynch, UK; Clive Woodley, UK; Alan Hepper, UK

3:10 pm - 3:30 pm **Coffee Break in Exhibit Hall**

3:30 pm - 8:30 pm **Exhibitor Move Out (Exhibit Hall CLOSED)**

3:30 pm - 5:10 pm **Wound Ballistics & Vulnerability**
Chaired by Phil Cunniff & Joe Backofen

3:30 pm *WB053 The Validation of a Thoracic and Abdominal Test Rig for BABT Soft Body Armour Testing*
Kate Hewins, UK; Ian Horsfall, UK; Celia Watson, UK

3:50 pm *WB005 Using LS-Dyna to Estimate After-barrier-effectiveness of Small Arms Projectiles*
Mark Minisi, USA

4:10 pm *WB240 An Overview of the Operational Requirement-based Casualty Assessment (ORCA) Model and its Military Applications*
William Mermagen, USA; Patrick Gillich, USA

4:30 pm *WB242 Survivability Measures for Evaluation of Personnel in Military Systems*
Natalie Eberius, USA; Patricia Frounfelker, USA; Kelly Benjamin, USA

4:50 pm *WB144 Diagnostic Techniques for Multiphase Blast Fields*
Richard Ames, USA; Michael Murphy, USA

7:00 pm - 9:00 pm **Symposium Banquet - Armstrong Ballroom; 8th Floor (included in attendee registration)**

Join us for an evening of New Orleans-inspired food, traditional jazz music, and dancing!

INTERIOR BALLISTICS POSTER SESSION

LAUNCH DYNAMICS POSTER SESSION

EXTERIOR BALLISTICS POSTER SESSION

9:50 am - 11:50 am
CHAIRMAN: CHRIS VAN DRIEL

IB049 Effects of Condensed Phases in Primer Output on Charge Ignition in Small Ammunition

Lang-Mann Chang, USA; Anthony Williams, USA

IB051 A Study on the Erosion Characteristics of K9 Thunder 155mm 52Cal. SPH (Self Propelled Howitzer)

Jae Kab Kim, Korea; Byung Doo Choi, Korea; Seong Ho Park, Korea; No Seok Park, Korea; Yeon-Sik Cho, Korea

IB054 The Effect of a Balanced Breech 120 mm Tank Gun System on Gun Dynamics and Firing Accuracy

Eugene Adamovski, Israel; Ilan Azulay, Israel; Yoav Gur, Israel; Davis Touati, Israel; Boris Manilov, Israel

IB074 Ignition Behaviour of LOVA Propellant

Chris Van Driel, The Netherlands

IB078 Linking Ignition and Transient Loading on a Medium Caliber Projectile

Richard Beyer, USA; Albert Horst, USA

IB090 Medium Caliber Lead Free Electric Primer

Robert Brewer, USA; Sarah Ford, USA; Kelvin Higa, USA

IB098 Numerical Simulation of Projectile Acceleration Process Using Solid/Gas Two-Phase Reacting Flow Model

Hiroaki Miura, Japan; Akiko Matsuo, Japan; Yuichi Nakamura, Japan

IB131 Interior Ballistics Characterization of a 40-mm Cartridge

Andrew Brant, USA; Joseph Colburn, USA; Anthony Williams, USA

IB147 Combustion Model for TAGzT and TAGzT Mixtures

Clint Conner, USA; William Anderson, USA

IB151 Revised Model for RDX Combustion

William Anderson, USA; Gabriel da Silva, USA; Clint Conner, USA; Rubik Asatryan, USA; Joseph Bozzelli, USA

IB169 The Effects of Igniter Design on the Interior Ballistic Performance of Deterrent Coated Propellants

Thelma Manning, USA; Kelly Moran, USA; Steven Ritchie, USA; Joseph Colburn, USA; Barrie Homan, USA; Carlton Adam, USA; Michael Ellis, USA; D. Park, USA; E. Rozumov, USA; S. M. Gilbert, USA; C.R. McMurray, USA

IB196 Experimental and Numerical Study of Reduction of Pressure Wave in Large Caliber Gun Chamber

Yuichi Nakamura, Japan; Hiroaki Miura, Japan; Akiko Matsuo, Japan

IB219 Matching Internal Ballistics Code Fidelity to Gun System and Analysis Complexity

Martin Pocock, UK; T. Melvin, UK; I. Robertson, UK; C. Woodley, UK; Chris Guyott, UK

IB223 Collection and Modelling of 155mm Artillery Projectile In-Bore Ballistic Data

George Yorke, USA; Don Carlucci, USA

IB249 Study for the Bore Resistance Factors Due to Friction and Engraving in NATO STANAG 4367, Edition 3

James Matts, USA; Ari Tuomainen, Finland

LD013 A Case Study on Flight Failure of a Supersonic Spinning Rocket and Successful Problem Solving through Modal Analysis & Testing

K M Rajan, India; Anil Datar, India; Surendra Kumar, India

LD024 Balloting in a Frenet Frame

Satoru Shoji, Japan

LD081 3D Unsteady Intermediate Ballistics Modelling: Muzzle Brake and Sabot Separation

Roxan Cayzac, France; T. Alziary de Roquefort, France; E. Carette, France

LD165 Occasion-to-Occasion Tank Gun Error Sources

Mark Bundy, USA; Jim Garner, USA; Dave Webb, USA; Paul Durkin, USA

EB039 Miss to Hit

Petrus Karsten, South Africa; Chris Botha, South Africa

EB059 Mathematical Modeling of Lift Sabot Separation Process

Ravindra Shriram Acharya, India; Smita D. Naik, India

EB076 Dual Mode Mortar Munition System

Yanina Rubenchik, Israel; Haim Yahia, Israel; Boris Manilov, Israel; Aron Pila, Israel; David Touati, Israel; Albert Mamane, Israel; Yuval Levy, Israel

EB082 Computational Fluid Dynamics Modeling of a Course Corrected Artillery Projectile at Transonic Speeds

Jubaraj Sahu, USA; Karen Heavey, USA; Richard Buretta, USA

EB086 NATO Shareable Software Developing into True Suite Supporting National Operational, Fire Control Systems

André Sowa, USA

EB087 NATO Testing in Turkey Shows Benefit of Meteorological Forecast Data to Indirect Fire Support

André Sowa, USA; Birger Hansen, Denmark; Sevsay Aytar Ortaç, Turkey

EB088 Liquid Payloads Impact on the Trajectory of Spinning Projectiles

Gene Cooper, USA; Mark Costello, USA

EB096 Aerodynamic and Ballistic Analysis of Rifled Mortar Munition

Hyunsung Jung, Korea; Ui Chang Hwang, Korea; Joo-Sung Kim, Korea

EB118 Research of Aerodynamic Structure and Correctional Ability for One-Dimensional Trajectory Correction Projectile

Zhongyuan Wang, China; Xiaobing Zhang, China; Jinguang Shi, China; Wenjun Yi, China; Zhiming Qiu, China

EB120 Algorithm Scheme for Tightly Integrated GPS/INS Navigation System in Large Dynamic Occasions

Lee Being, China

EB194 Fast Safety Checks for Numerical Trajectory Calculations

Alexander Kuhrt, Germany; Hendrik Rothe, Germany

EB255 On The Stagnation Point Reynolds Number of Supersonic Projectiles

William Reinecke, USA

ARMOR & PERSONAL PROTECTION POSTER SESSION

1:30 pm - 3:30 pm

CHAIRMEN: EWA LIDEN, ERICK SAGEBIEL & VELERIY KARTUZOV

APP007 On the XCT Diagnostics of Ballistic Impact Damage in a B_4C Ceramic Body Armor Plate

Joe Wells, USA; Nevin Rupert, USA

APP012 Numerical Simulation of Mine Detonation Beneath a Generalized Add-On Armor Structure

Sharon Peles, Israel; David Touati, Israel; Avi Neuberger, Israel; Ilan Azulay, Israel

APP034 Nondestructive Damage Assessment of Alumina Structural Ceramics

Raymond Brennan, USA; William Green, USA; James Sands, USA; Jian H. Yu, USA

APP044 Advances in Ballistic Performance of Commercially Available Saint-Gobain Sapphire Transparent Armor Composites

Christopher Jones, USA; Jeff Rioux, USA; John Locher, USA

APP055 Armour Materials: A Preview into a Resource-Poor Future, Implications for the Development of Armour Materials

Andre Diederen, The Netherlands

APP062 A Computational Study of the Energy Dissipation through an Acrylic Target Impacted by Various Size FSP

Costas Fountzoulas, USA; Peter Dehmer, USA; Jian Yu, USA; James Sands, USA

APP066 Analysis of Terminal Metallic Armor Plate Free-Surface Bulging

Edward Rapacki, USA

APP099 Collateral Damage Caused by Reactive Armour Protection Against PG-7-Like Threats

Martin van de Voorde, The Netherlands; Koen Bakker, The Netherlands; Frans van Wegen, The Netherlands

APP105 Response of the Plate to the Buried Blast Mine Explosion

Stanislav Rolc, Czech Republic; Jaroslav Buchar, Czech Republic; Josef Kratky, Czech Republic; Rolf Graeber, Czech Republic; Jaroslav Pechacek, Czech Republic; M.Havlicek, Czech Republic

APP121 Effect of Ceramics, Fibre Reinforced Plastics and Aluminium Used as Confinement Plates for Explosive Reactive Armours

Stefano Bianchi, Switzerland; Hanspeter Kaufmann, Switzerland; André Koch, Switzerland

APP122 Ballistic Protection of Fragment Vests Against IED Threat

Hans Broos, The Netherlands; M.J. van der Jagt–Deutekom, The Netherlands; M.J. van de Voorde, The Netherlands

APP126 Experimental Tests and Numerical Calculations using ALE and SPH Approaches on Mine Blast Effects on Structure

Geneviève Toussaint, Canada; Amal Bouamoul, Canada

APP140 Investigation of a Methodology for Producing Variable Damage in Structural Armor Ceramics

William Green, USA; Jian Yu, USA; Raymond Brennan, USA; James Sands, USA

APP153 High-Speed Photographic Study of Wave Propagation and Impact Damage in Novel Glass Laminates

James McCauley, USA; Elmar Strassburger, Germany; Parimal Patel, USA; Doug Templeton, USA; Arun Varshneya, USA

APP160 Structure, Properties and Dynamic Response of Polypropylene Fibers and Textiles

Michael Sennett, USA; Elizabeth Welsh, USA; Peter Stenhouse, USA; Philip Cunniff, USA; Thomas Godfrey, USA; Deana Archambault, USA

APP163 Simulation of Damage to a Vehicle by Explosion of an Improvised Explosive Device

Chris Quan, USA; John Pavon, USA

APP170 Hybrid Particle-Element Simulation of Body Armor Impact Physics

Kwon Joong Son, USA; Eric Fahrenthold, USA

APP172 A Possible Approach in Support of the Chacterization of Body Armors

Nevin Rupert, USA

APP183 Ballistic Impact Performance of Clothing Items Under Impact by Munition Fragments

Phillip Cunniff, USA

APP184 Variability in Ballistic Impact Performance due to Projectile Physical Properties and Dimensions

Phillip Cunniff, USA

APP186 The Importance of Off-Normal Obliquity Impact Performance to the Casualty Reduction Potential of Ballistic Protective Helmets

Phillip Cunniff, USA

APP187 Assessment of the Ballistic Impact Performance of Variable Response Armor Systems

Phillip Cunniff, USA

APP188 The Effect of Preform Shape on Ballistic Impact Performance, Coverage and Seam Density in Combat Helmets

Jason Parker, USA; Phillip Cunniff, USA

APP198 Developing Simulation Capabilities to Link Textile Manufacturing to Ballistic Performance

Bryan Cheeseman, USA; Chian Yen, USA; Brian Scott, USA; Bruce LaMattina, USA; Yuyang Miao, USA; Youqi Wang, USA

APP199 Ballistic Testing of SSAB Ultra-High Hardness Steel for Armor Applications

Matthew Burkins, USA; William Gooch, USA; Dwight Showalter, USA; Rosmari Stockman Koch, Sweden

APP209 Ballistic Properties of Hybrid Systems for Transparent Armor Applications

John Song, USA; Nicholas Tsantinis, USA; Roy Paulson, USA

APP220 Characterizing Collateral Damage to Dismounted Troops and Other Personnel located near Active Counter Measures

Patricia Frounfelker, USA; Kathleen Doonan, USA

APP236 Ballistic Evaluation of Aluminum 2139-T8

Bryan Cheeseman, USA; Matthew Burkins, USA; William Gooch, USA

APP244 Impact of Soldier Helmet Configuration on Survivability

Natalie Eberius, USA; Patrick Gillich, USA

WOUND BALLISTICS & VULNERABILITY POSTER SESSION

1:30 pm - 3:30 pm

CHAIRMEN: BO JANZON & JOE WELLS

V041 V/L TARVAC BBN Based Understanding of Combat Damage and Operational Readiness Consequences to Assess Proportional Fire Power (Lethality)

Theo Verhagen, The Netherlands; M.F.G. van der Wurff, The Netherlands; Th.P.J. Van Rijn, The Netherlands; L.J. van Peteghem, The Netherlands

V042 (In)Sensitive Ammunition Impact on V/L TARVAC Modelling

Theo Verhagen, The Netherlands; R.H.B. Bouma, The Netherlands; R. Boeschoten, The Netherlands

V043 Munition – MOUT Effects Modelling: Embedding Experimental Research in V/L TARVAC Assessment

Theo Verhagen, The Netherlands; M.J. van de Voorde, The Netherlands; E. van Meerten, The Netherlands; Th.P.J. van Rijn, The Netherlands

V123 Comparison of Methods to Measure the Blast Impulse Loading of an Explosive Charge

Pieter Smith, South Africa; Frikkie Mostert, South Africa; Izak Snyman, South Africa

V124 Terminal Ballistics of HE Ammunition for Counter-RAM Systems

Markus Graswald, Germany; Hendrik Rothe, Germany

V142 Perspectives on the Requirements, Development, and Outputs of an X-Ray Computed Tomography Image Processing Application for Ballistic Impact Analysis in Armor Samples

Jeffrey Wheeler, USA; Nevin Rupert, USA; Joe Wells, USA

V173 Damage Assessment Method of Complex Shape Surface Target Based on Image Manipulation

Lu Yonggang, China

V245 Lethality of Bursting Munitions and Their Effect on Survivability

Natalie Eberius, USA; Kathleen Doonan, USA

V254 The Measurements of Overpressure of Thermobaric Grenade and Analysis of its Power

Chen Hao, China; Tao Gang, China

WB005 Using LS-Dyna to Estimate After-barrier-effectiveness of Small Arms Projectiles

Mark Minisi, USA

WB006 Simulating Ordinace Gelatin Impacts Using LSDyna; Correlations and Challenges

Mark Minisi, USA

WB069 Computational and Experimental Study of Paintball Impact Ocular Trauma

Walt Gray, USA; James Walker, USA; William Sponsel, USA; Carl Weiss, USA

WB071 Theoretical Study of the Motion of a Rigid Gyro-Stabilized Projectile into Homogeneous Dense Medium

Nestor Nsiampa, UK; Gunther Dyckmans, UK

WB114 Ensemble Effect for the Penetration by Non-Metallic Particles

Matthias Wickert, Germany

WB116 How to Quantify the Effects of Non-lethal Kinetic Weapons

Philippe Drapela, Switzerland; Stephan Lampert, Switzerland; R. Lorenzo, Switzerland

WB218 U.S. Army Research Laboratory Support to the Small Arms Capabilities Based Assessment

Gregory Dietrich, USA; James Newill, USA; William McLaughlin, USA

WB241 A New Small Caliber Evaluation Methodology Using Operational Requirement-based Casualty Assessment (ORCA)

Patrick Gillich, USA; Timothy Myers, USA

FRIDAY, SEPTEMBER 26, 2008

7:00 am **Continental Breakfast & Registration**

8:00 am **Administrative Remarks**

8:10 am - 9:30 am **General Session**
Chaired by Francisco Galvez & Dennis Baum

8:10 am *TB020 Deformation and Breakup of Tungsten Alloy Cubes, Cylinders and Spheres on Aluminum Plates*
Karl Weber, Germany

8:30 am *GS023 Predicting Hazard Response Scenarios in Weapon Systems*
Ian Cullis, UK; I.H. Brown, UK; P.D. Church, UK; P. Gould, UK; V.E. Ingamells, UK

8:50 am *GS130 Experimental Validation of a Kevlar Fabric Model for Ballistic Impact*
Chian Yen, USA; Tusit Weerasooriya, USA; Paul Moy, USA; Brian Scott, USA; Bryan Cheeseman, USA

9:10 am *GS205 Shaped Charge Penetration of Gas Saturated Sandstone*
Brenden Grove, USA; Jeremy Harvey, USA

9:30 am - 9:50 am **Coffee Break**

9:50 am - 12:00pm **Terminal Ballistics**
Chaired by James Cazamias & Patrik Lundberg

9:50 am *TB025 Penetration Resistance of Glass and a Glass Ceramic*
Stephan Bless, USA; Don Berry, USA

10:10 am *TB111 Long-Rod Penetration into Intact and Pre-Damaged SiC Ceramic*
Charles Anderson, USA; Thilo Behner, Germany; Dennis Orphal, USA; Arthur Nicholls, USA; Timothy Holmquist, USA; Matthias Wickert, Germany

10:30 am *TB058 The Shock Response Of a Cemented Tungsten Carbide*
Koen Herlaar, The Netherlands; Andre Diederen, The Netherlands; Gareth Appleby-Thomas, UK; Paul J Hazell, UK

10:50 am *TB038 GRC's Impact Behavior*
Alejandro Enfedaque Diaz, Spain; David Cendón Franco, Spain; Francisco Gálvez Díaz-Rubio, Spain; Vicente Sánchez Gálvez, Spain

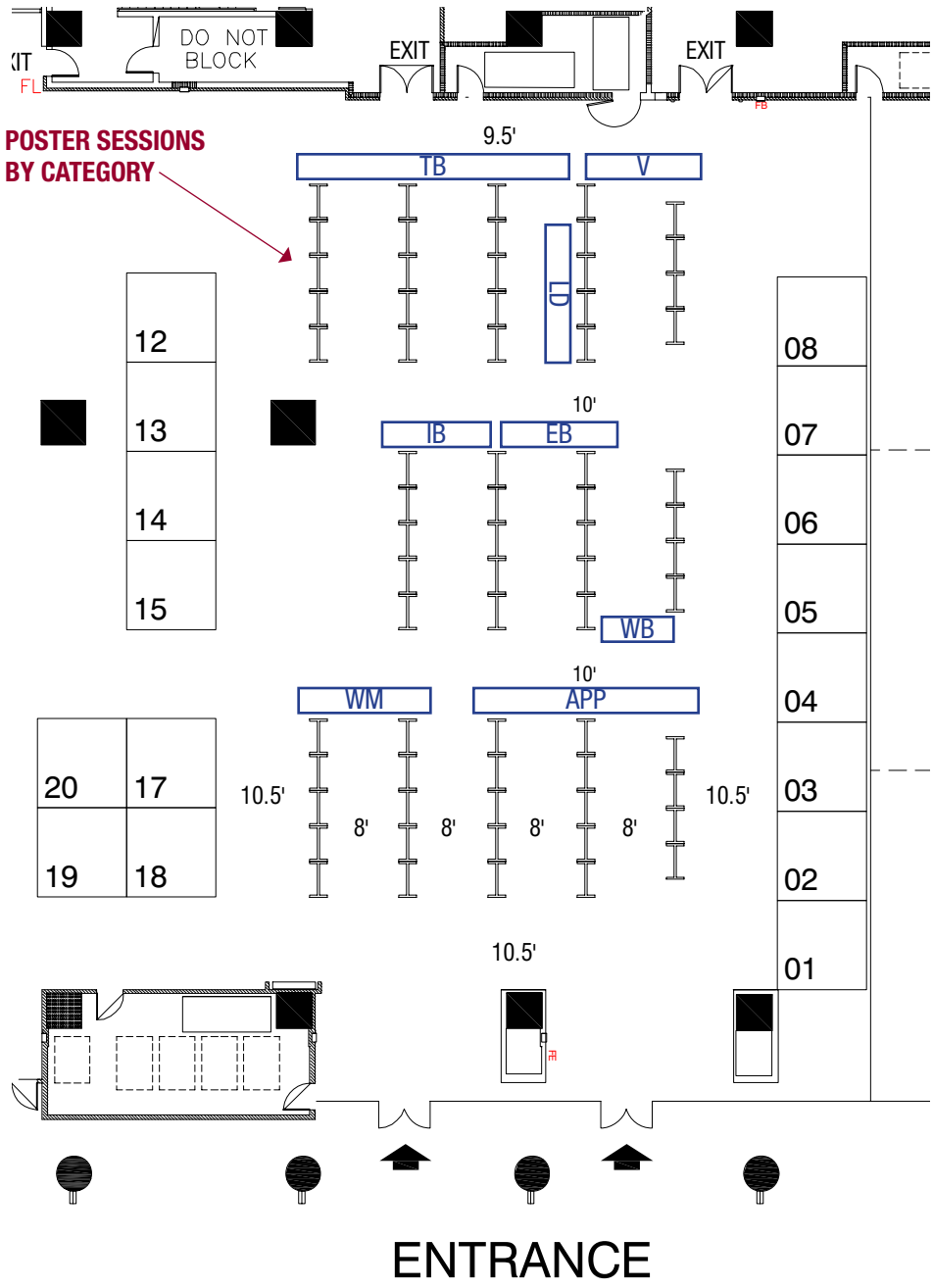
11:10 am *TB237 Experimental Determination of Strain in Fabrics under Ballistic Impact*
Sidney Chocron, USA; K. Samant, USA; Arthur Nicholls, USA; Carl Weiss, USA; James Walker, USA; Charles Anderson, USA

11:30 am *TB248 The Mechanics of Projectile Arrest for Compliant Cross Plied Unidirectional Laminates*
Brian Scott, USA; Bryan Cheeseman, USA

12:00 pm - 12:30 pm **Presentation of Awards**

12:30 pm - 12:45 pm **Future Symposia Announcements**
- **25th International Symposium on Ballistics - China**
- **26th International Symposium on Ballistics - USA**

12:45 pm **Symposium Adjourns**



ANSYS, INC.....4
ARROW TECH ASSOCIATES.....14
DRS DATA & IMAGING SYSTEMS.....6
FRAZER-NASH CONSULTANCY.....5
KISTLER INSTRUMENTS.....3
MS INSTRUMENTS PLC.....7
25TH IBC - BEIJING.....8
NATIONAL TECHNICAL SYSTEMS CORP.....15
NEW LENOX MACHINE CO. INC.....13
PHOTO-SONICS, INC.....1
SAINT-GOBAIN CERAMICS & PLASTICS, INC 12
UTRON, INC.....2
WEIBEL.....17

PROMOTIONAL PARTNERS

Arrow Tech

Formed in 1987 Arrow Tech Associates Inc. has been providing world-class support in ammunition design and analysis including structural analysis, dynamic analysis, weapons system simulation.

Throughout history there has been a need for rapid, accurate analysis of ammunition performance. With strong skills in both engineering analysis and software development, we have been able to answer this need for our customers. Arrow Tech has been a crucial and integral team member on many weapon system design teams in both civilian and government industry ranging from Olympic Archery to Artillery Systems and everything in between.

In 1992 Arrow Tech decided to make available our internal engineering software tools that we used to accomplish our design and analysis tasks and thus the first commercially available comprehensive ammunition design package came into being. PRODAS, (Projectile Rocket Ordnance Design and Analysis Software) is now one of the most widely used and advanced ammunition design toolkits available, with over 500 users worldwide and continual development and improvements.

Analysis modules help the user estimate mass properties, predict aerodynamics and stability, fly trajectories including guided projectiles and simulate interior ballistics, in bore balloting, or rocket motors. The latest release of PRODAS captures over 45 years of experience within the industry.

Arrow Tech is proud to be a co-sponsor of this year's International Ballistics Symposium with the NDIA in New Orleans. Please feel free to stop by our booth (#14) as we look forward to talking to our current and future customers.

Foster-Miller, Inc.

LAST® Armor, the largest approved supplier of armor for fixed-wing aircraft in the United States, supports C-130s, C-17s and C-5s with add-on armor. LAST® Armor also makes a unique add-on armor appliqué system for armored vehicles and rotary-wing aircraft that installs without any cutting, welding or drilling on the base vehicle. LAST® tactical vehicle armor kits can be sent forward to deployed vehicles and the simple installation can be performed by the vehicle crew itself. It is most often affixed using a patented, high-strength Velcro® hook-and-loop fastening system.

LAST® Armor is a division of QinetiQ North America's Technology Solutions Group (TSG). Headquartered in Waltham, MA, TSG includes the businesses of Foster-Miller, Inc., and its subsidiaries Planning Systems Incorporated, Automatika, Applied Perception, Spectro, Inc., and the research and development activities of Apogen Technologies, Inc. It is a technology and product development group with an international reputation for delivering innovative products and systems that perform under the most demanding conditions.

Weibel

Weibel Scientific A/S is a designer and manufacturer of scientific measurement equipment for testing and experimental applications. Its customers include armies, navies, and air forces; test ranges; research and development establishments; ordnance industries; and security forces. Weibel's products include Doppler radar-based equipment ranging from small compact Doppler radar systems to high-performance, on-line, 3-D Doppler radar tracking systems for long-range (>1,000 km) flight analysis. Weibel Doppler radar systems are based on the most up-to-date radar, computer, and software technologies, and incorporate such unique features as self-calibration and multi-object tracking. Weibel Scientific manufactures all mechanical parts, electronics and software in house in it's company owned facility just outside of Copenhagen, Denmark.

THANK YOU TO OUR PROMOTIONAL PARTNERS

ARROW TECH

LAST® ARMOR
QinetiQ North America

WEIBEL
DOPPLER RADARS

PDF Complete
Your complimentary use period has ended. Thank you for using PDF Complete.
Click Here to upgrade to Unlimited Pages and Expanded Features



Diagnostic Techniques for Multiphase Blast Fields

Richard Ames
Raytheon Missile Systems

Michael Murphy
Lawrence Livermore National Laboratory

With Contributions from

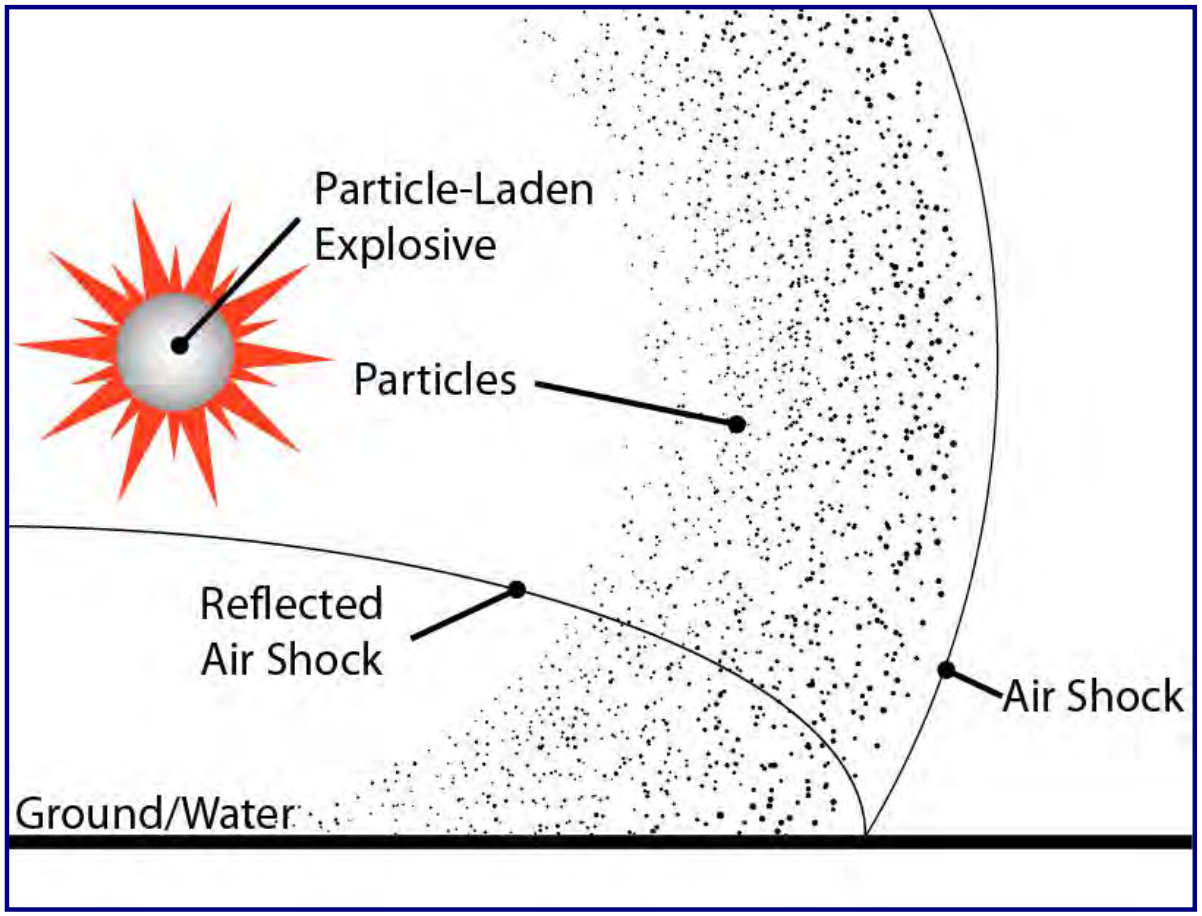
Scott Groves, Mitch Moffett
LLNL
Don Cunard, Alan Orht
AFRL Eglin
Jason Drotar
NSWC Dahlgren

APPROVED FOR UNLIMITED DISTRIBUTION

PDF Complete
Your complimentary use period has ended. Thank you for using PDF Complete.
Click Here to upgrade to Unlimited Pages and Expanded Features

ulti-Phase Blast Flows

- Multi-Phase Blast Flows are produced by particle-laden explosives
- Can also be produced when a standard explosive entrains dust and debris
- A key unknown is how much energy/momentum is transported in each phase within the blast field

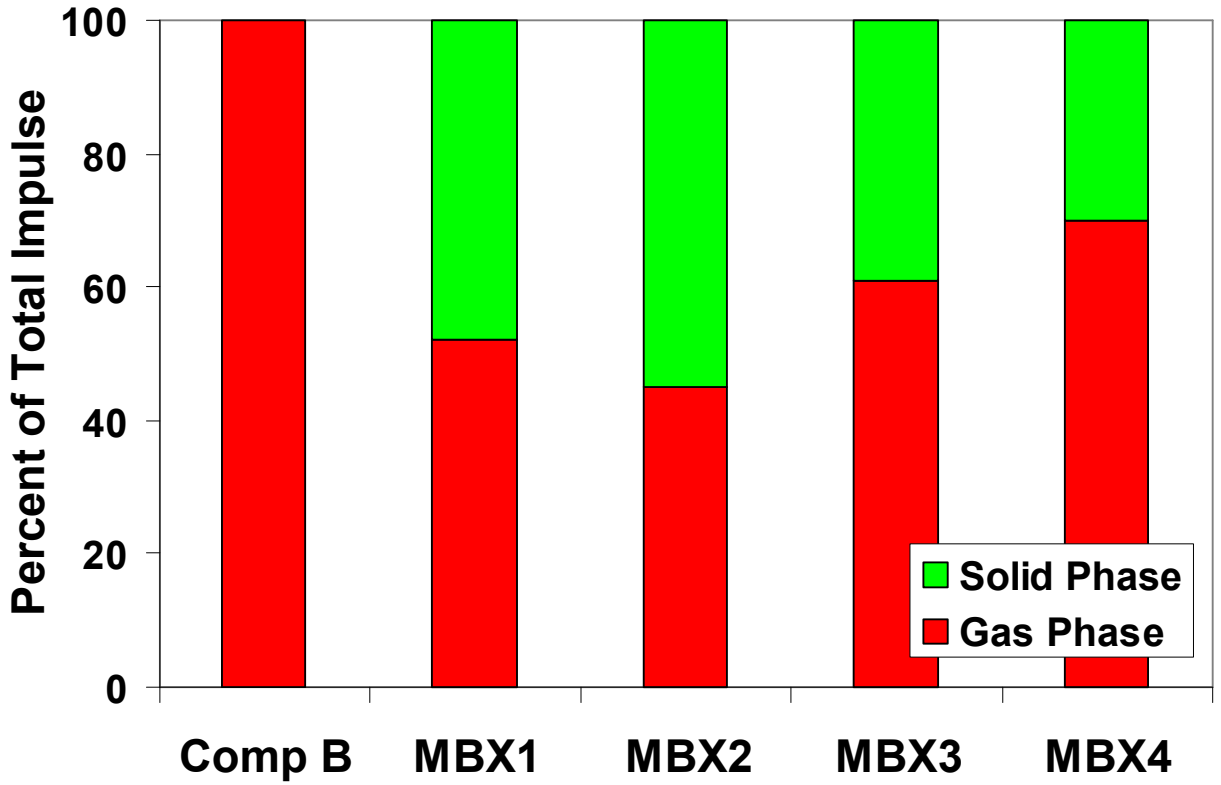


Typical MBX Blast Field

PDF Complete
Your complimentary use period has ended. Thank you for using PDF Complete.
Click Here to upgrade to Unlimited Pages and Expanded Features

ve Amounts of Momentum ux in MBX Blast Flows

Measurements of Momentum Transfer Against a Flat-Plate Target for Four Types of Multiphase Blast Explosives (MBX)



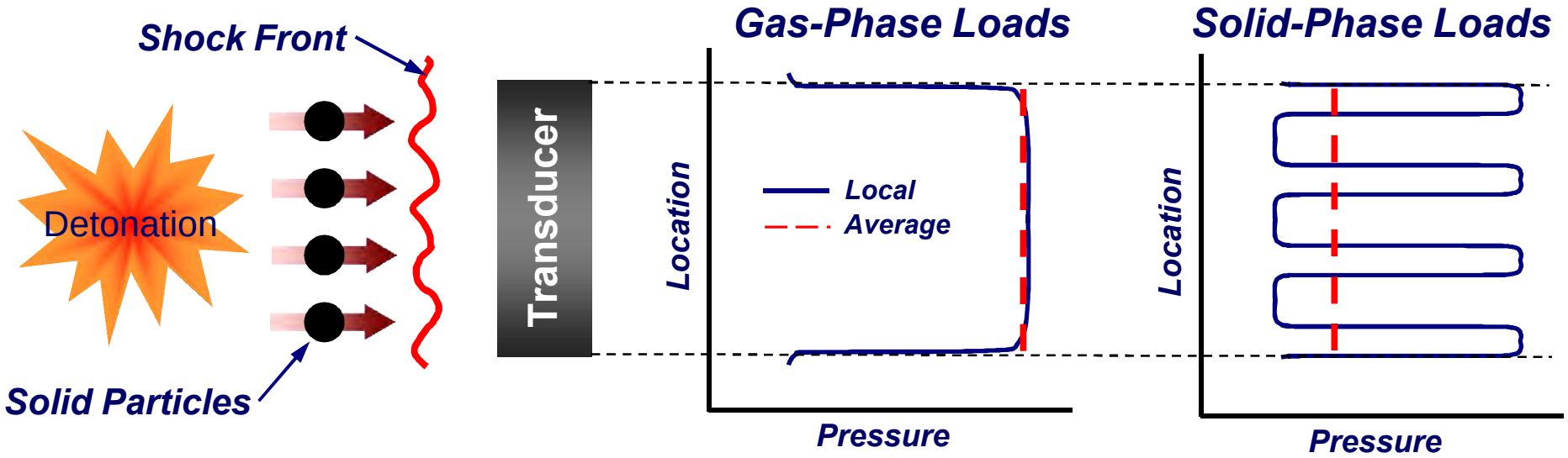
- The solid-phase component of MBX blast fields carries a substantial amount of momentum and energy
  - Can be as much as 50% for some blast flows
- As a consequence, characterization of this class of multiphase flows must accurately account for the solid phase

PDF Complete
Your complimentary use period has ended. Thank you for using PDF Complete.
Click Here to upgrade to Unlimited Pages and Expanded Features

Diagnostic Techniques

PDF Complete
Your complimentary use period has ended. Thank you for using PDF Complete.
Click Here to upgrade to Unlimited Pages and Expanded Features

asurement Problem for Multi-Phase Blast Flows



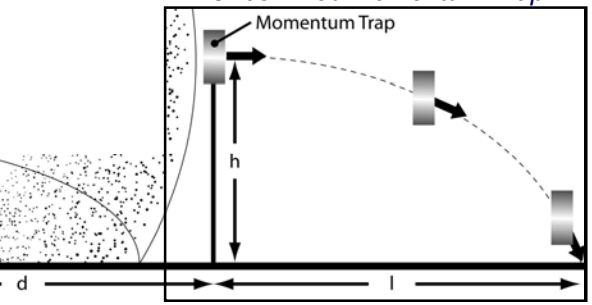
- Most pressure transducers are designed under the assumption of rough equivalence between small-scale, local loads and global, average loads
  - Good assumption for gas-phase loads because the impulse associated with individual molecular impacts is extremely small
- Not valid for distributed solid-phase loads
  - Local loads much larger than global average

PDF Complete
Your complimentary use period has ended. Thank you for using PDF Complete.
Click Here to upgrade to Unlimited Pages and Expanded Features

ily of Diagnostic Techniques

Impulse Traps

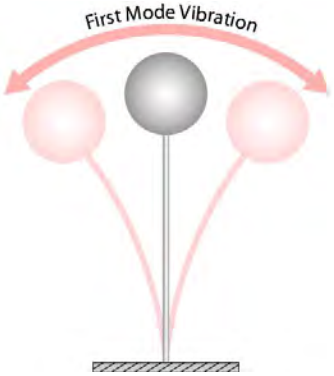
Unconfined Momentum Trap



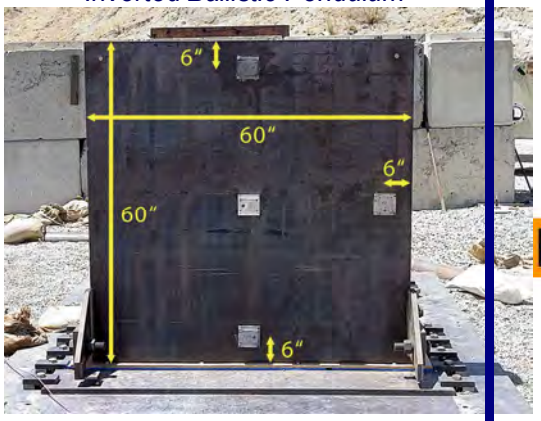
Confined Momentum Trap



Cantilevered Ball Gauge



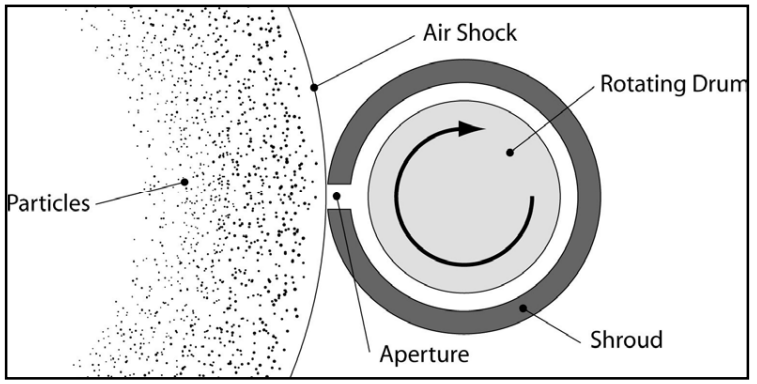
Inverted Ballistic Pendulum



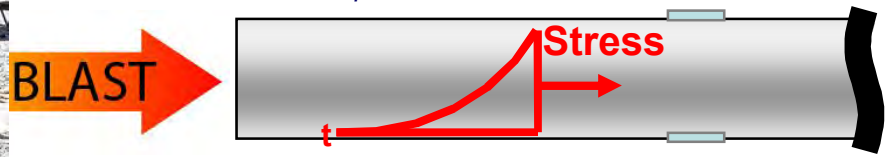
- No time history information available
- Easy to deploy
- Simple physics

Time-Varying Diagnostics

Particle Streak Recorder



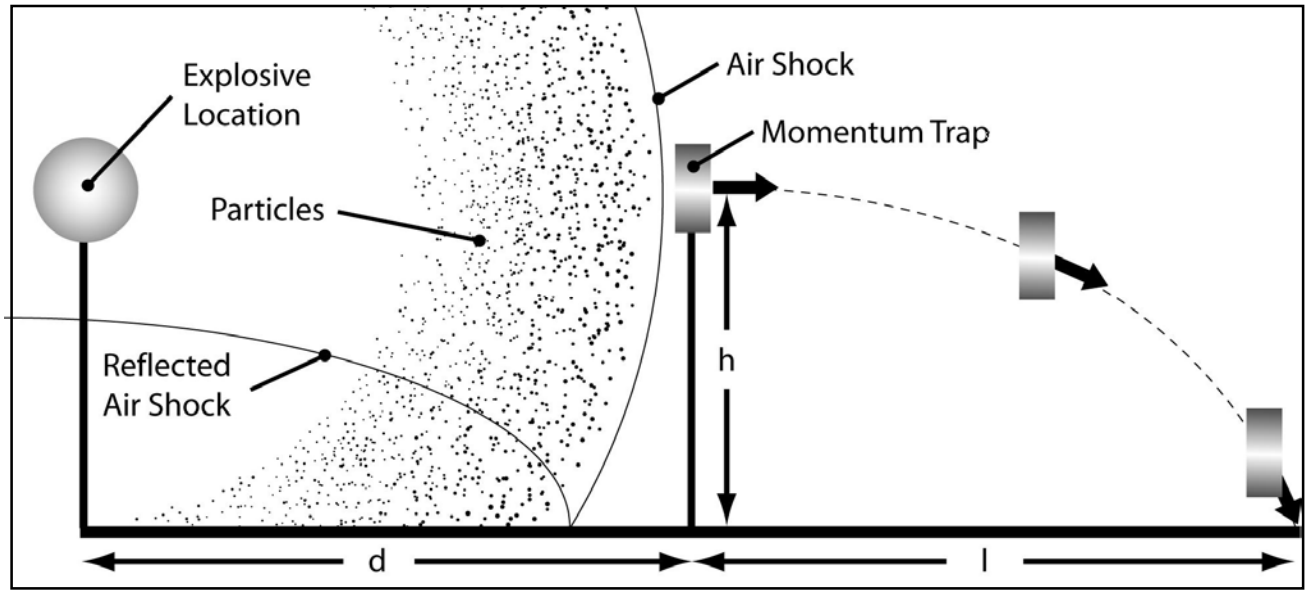
Hopkinson Pressure Bar



- Provide time history information
- Somewhat difficult to deploy
- Requires assumption-laden post-processing

PDF Complete
Your complimentary use period has ended. Thank you for using PDF Complete.
Click Here to upgrade to Unlimited Pages and Expanded Features

Unconfined Momentum Trap (UMT)

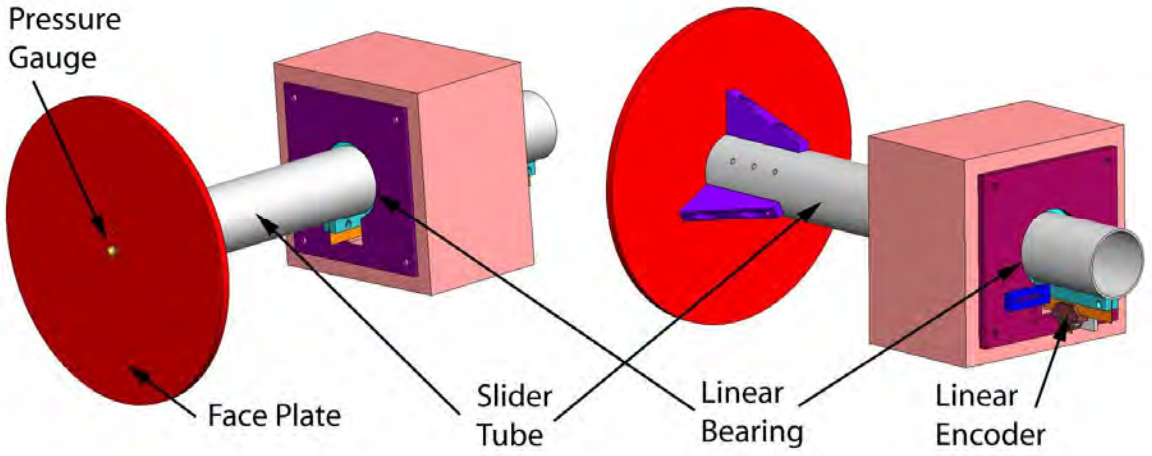


$$I = \frac{m_b l}{\sqrt{2h/g}}$$

- The Unconfined Momentum Trap (UMT) is a disk placed normal to the charge at some height
- The distance the trap is thrown is proportional to the impulse delivered to the face
  - Assumes time scales associated with loads are much less than time scales associated with loading
  - Neglects drag
- Different shapes can be used to provide information regarding target geometry effects

PDF Complete
Your complimentary use period has ended. Thank you for using PDF Complete.
Click Here to upgrade to Unlimited Pages and Expanded Features

Confined Momentum Trap



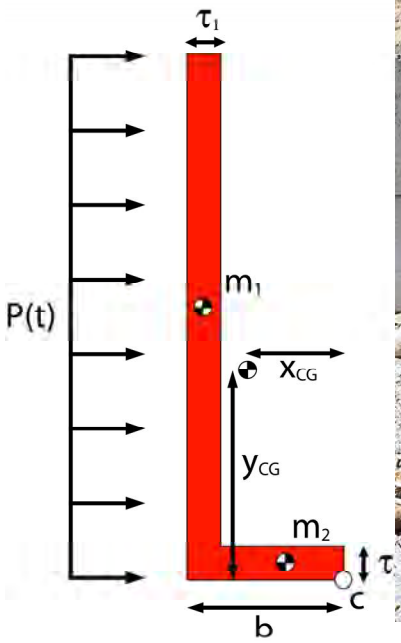


- Uses a disc on a slider tube with optical position encoder
- The time-history of the motion provides a measure of the impulse delivered to the Face Plate
- Face plate also includes a pressure gauge so that gas-phase loads may be measured

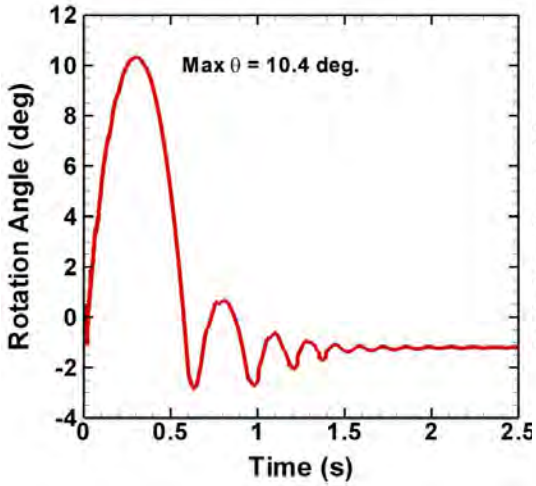
PDF Complete
Your complimentary use period has ended. Thank you for using PDF Complete.
Click Here to upgrade to Unlimited Pages and Expanded Features

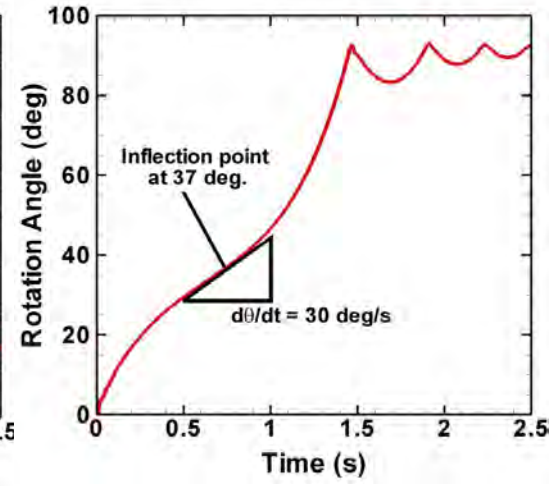
erted Ballistic Pendulum (IBP)

- The IBP is a large flat plate on a pivoting base
- Tip angle is proportional to impulse
- If the wall tips over the impulse is measured by the angular speed as the CG passes vertically over the pivot









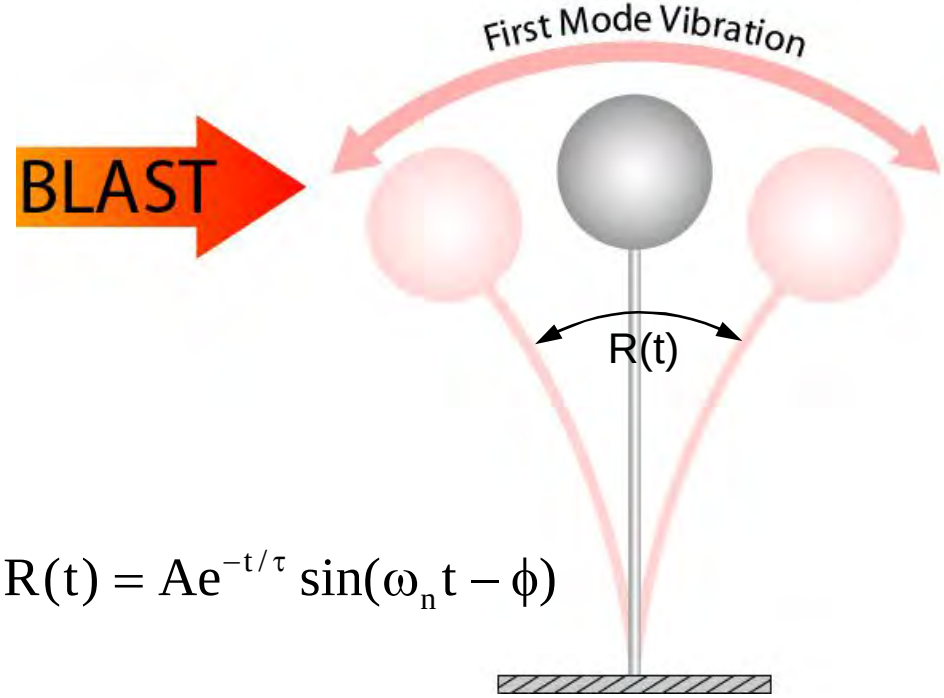
$\theta < \theta_{tip}$ $$I = \left[\frac{8(m_1+m_2)gJ_c\left(\sqrt{x_{cg}^2+y_{cg}^2}\sin(\theta+\theta_0)-y_{cg}\right)}{h^4w^2}\right]^{\frac{1}{2}}$$

$\theta > \theta_{tip}$ $$I = \left[\frac{8J_c}{h^4w^2}\left[(m_1+m_2)g\left(\sqrt{x_{cg}^2+y_{cg}^2}-y_{cg}\right)+\frac{1}{2}J_C\dot{\theta}_{IP}^2\right]\right]^{\frac{1}{2}}$$

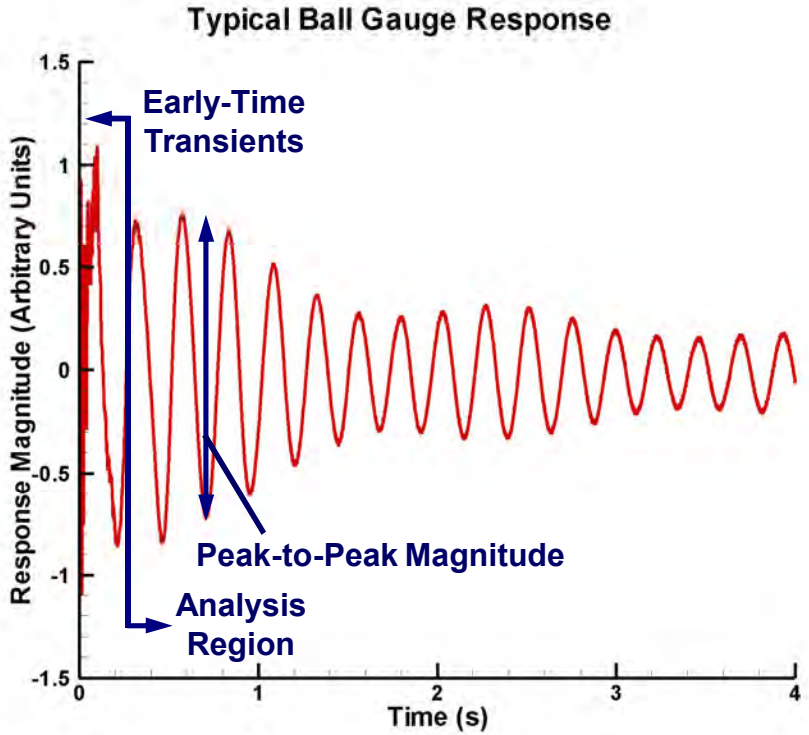
$\theta = \theta_{tip}$ $$I_{min} = \left[\frac{8(m_1+m_2)gJ_c\left(\sqrt{x_{cg}^2+y_{cg}^2}-y_{cg}\right)}{h^4w^2}\right]^{\frac{1}{2}}$$

PDF Complete
Your complimentary use period has ended. Thank you for using PDF Complete.
Click Here to upgrade to Unlimited Pages and Expanded Features

e Cantilevered Ball Gauge



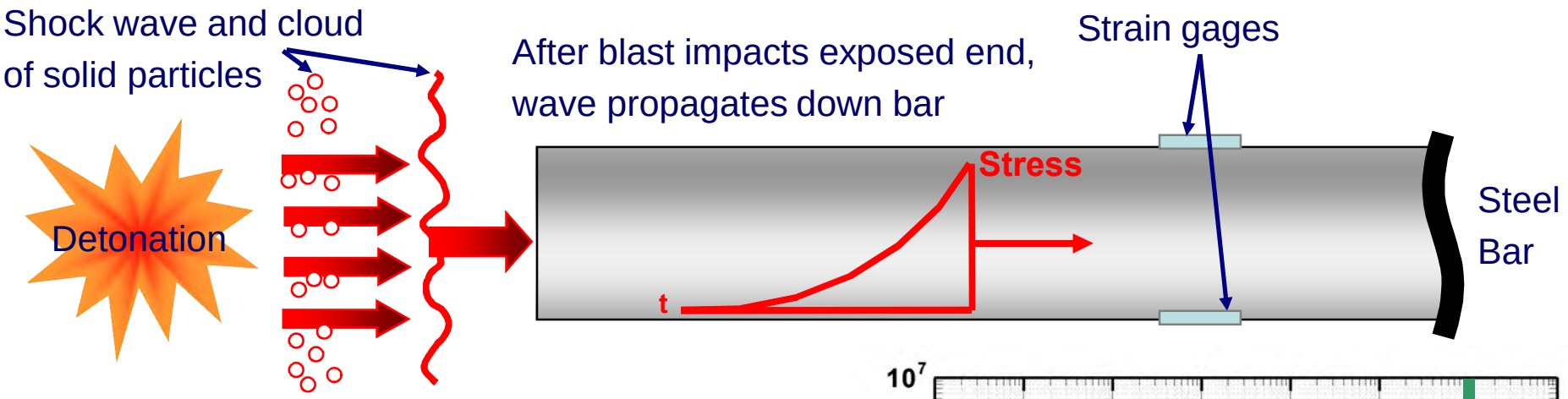
$$R(t) = Ae^{-t/\tau}\sin(\omega_n t - \phi)$$



- Measures the total impulse delivered to a sphere on a slender rod via strain measurements that capture the vibratory motion
- Measurements taken in orthogonal directions in order to compute total loading in a plane normal to the sting mount
- Under the assumption that the loading time scales << structural response time scales, total impulse is proportional to the magnitude of the structural response in the first bending mode

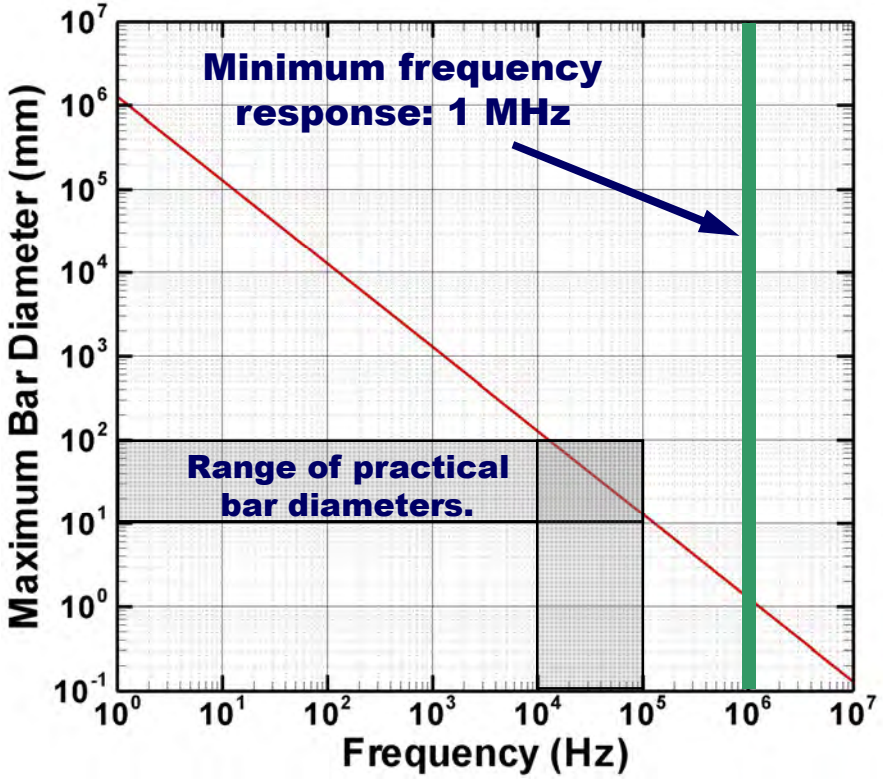
PDF Complete
Your complimentary use period has ended. Thank you for using PDF Complete.
Click Here to upgrade to Unlimited Pages and Expanded Features

The Hopkinson Bar



$$r < \frac{0.465 c_0}{2\pi \upsilon f}$$

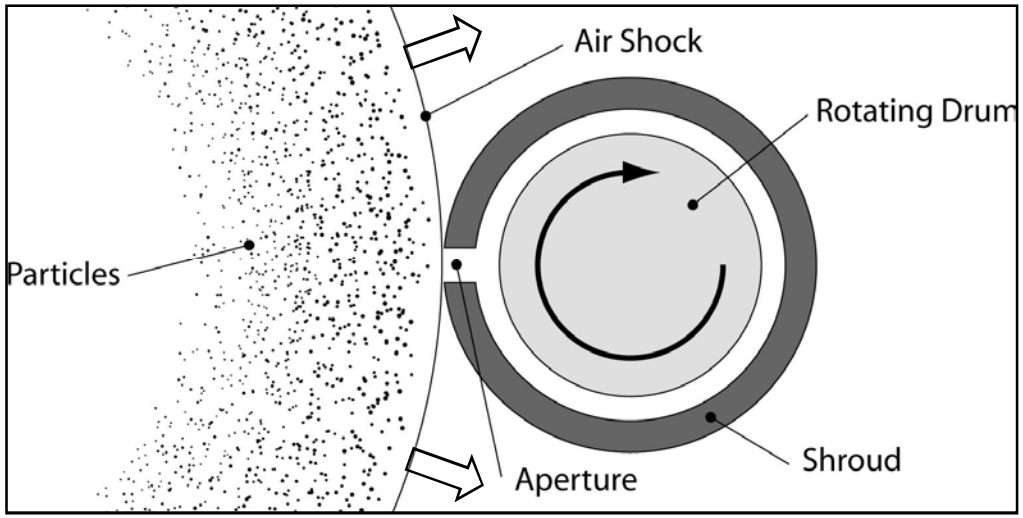
For less than 5% dispersion.



- High Frequency components of the load move more slowly through the bar, altering the signal

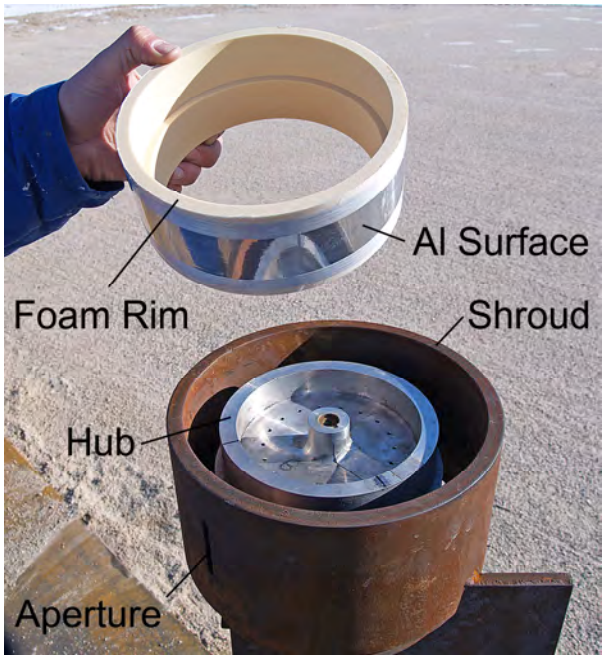
PDF Complete
Your complimentary use period has ended. Thank you for using PDF Complete.
Click Here to upgrade to Unlimited Pages and Expanded Features

rticle Streak Recorder (PSR)



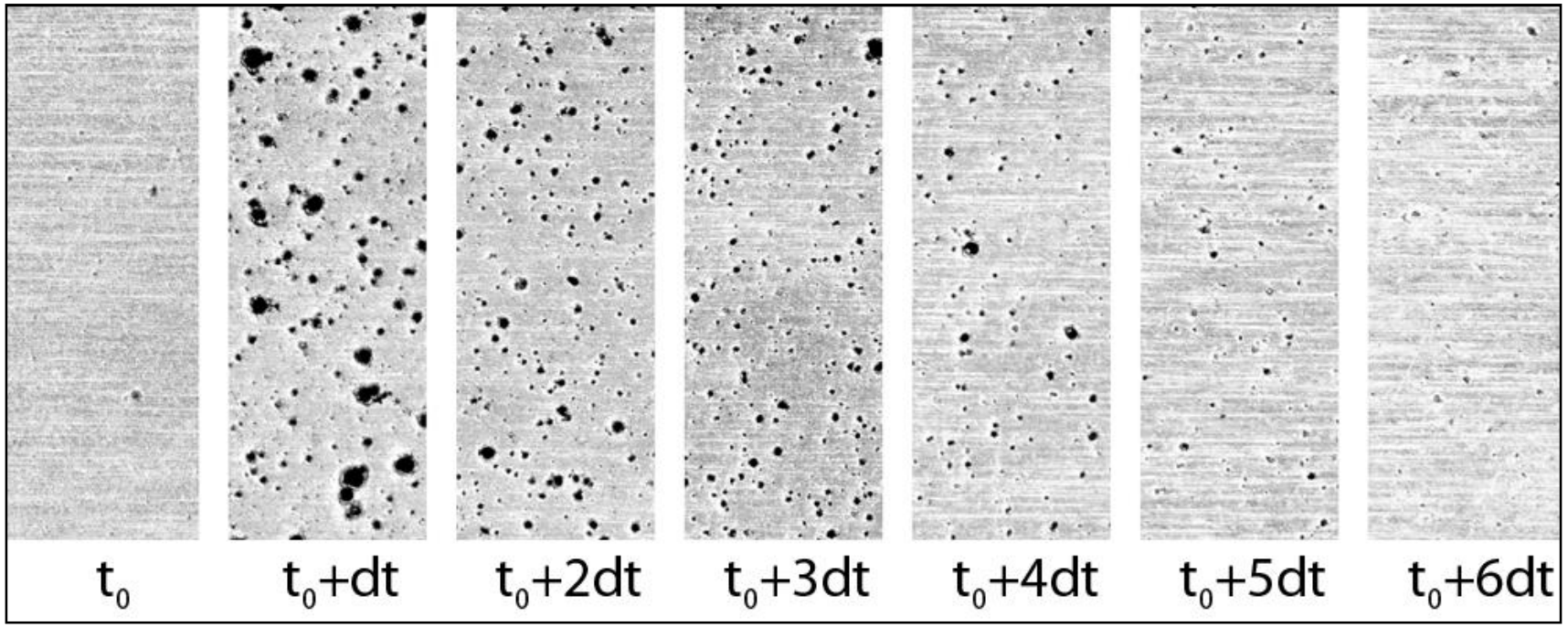


- Uses a rotating disc behind a thin aperture
  - Thin aluminum on a high-density foam core attached to an aluminum hub
  - Different RPMs used at different standoffs to account for differences in blast duration
- Provides a measure of the time history of the number density of particles
  - Can be used to estimate momentum flux given assumptions about the time dependence



PDF Complete
Your complimentary use period has ended. Thank you for using PDF Complete.
Click Here to upgrade to Unlimited Pages and Expanded Features

al Data from Particle Streak Recorders



- The PSR data records give a measure of the time history of particle number density passing through the aperture
  - Normally expressed as number of particles per unit area
  - Errors arise when multiple particles produce a single hole
- Also provides statistics on hole sizes
  - Relationship to actual particle sizes is difficult to define

PDF Complete
Your complimentary use period has ended. Thank you for using PDF Complete.
Click Here to upgrade to Unlimited Pages and Expanded Features

R Impact Surface Analysis Technique

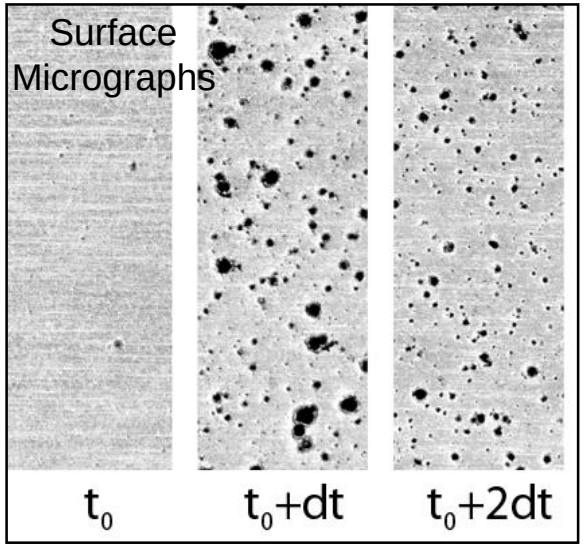
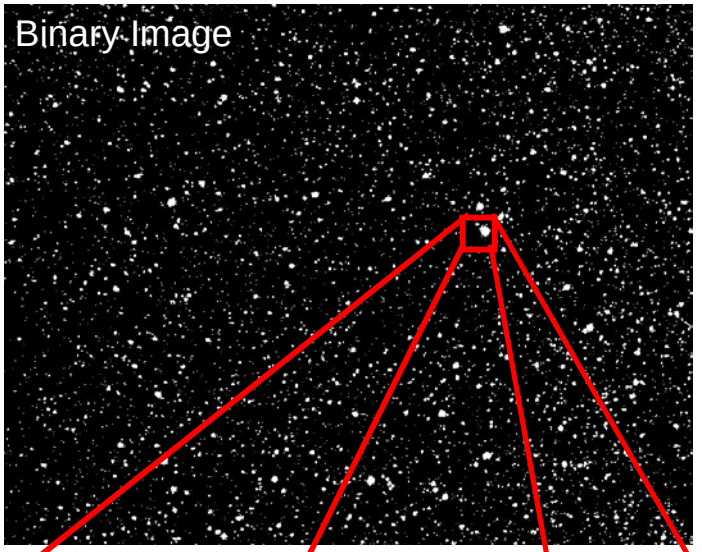
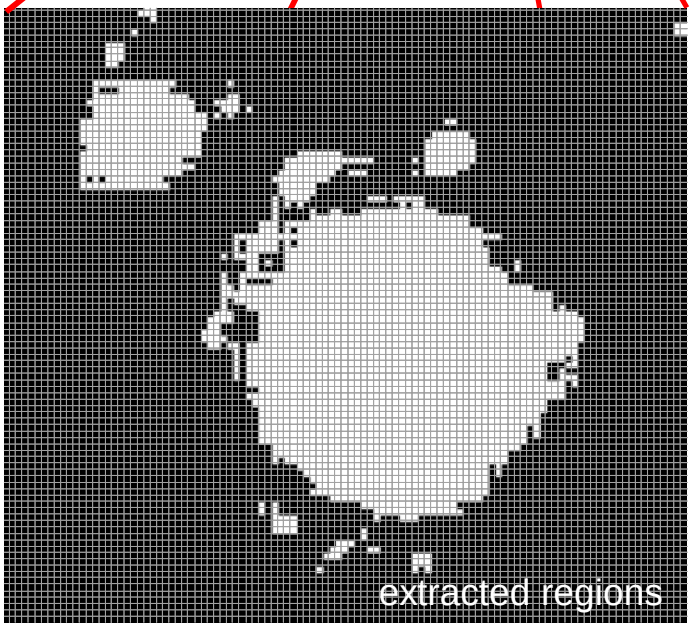
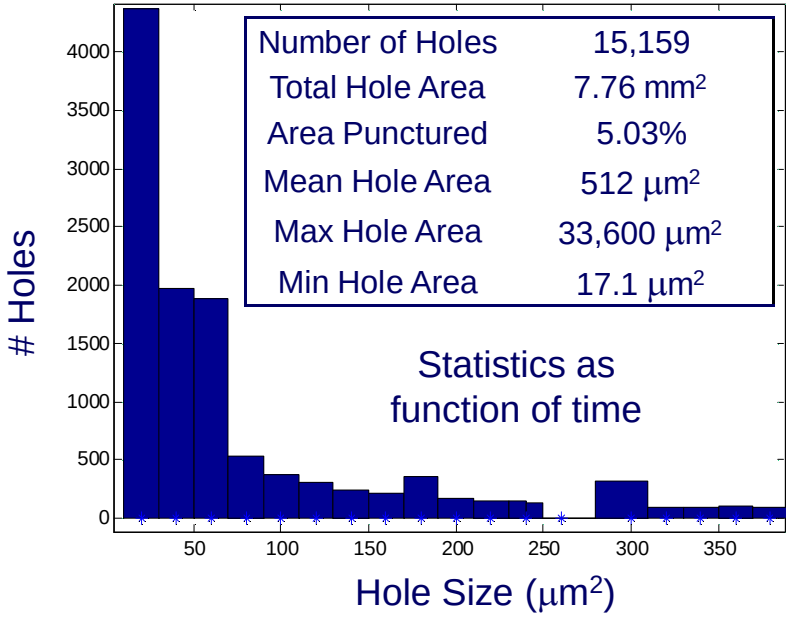


Image processing algorithm implemented in Matlab





Connectivity algorithm implemented in Matlab



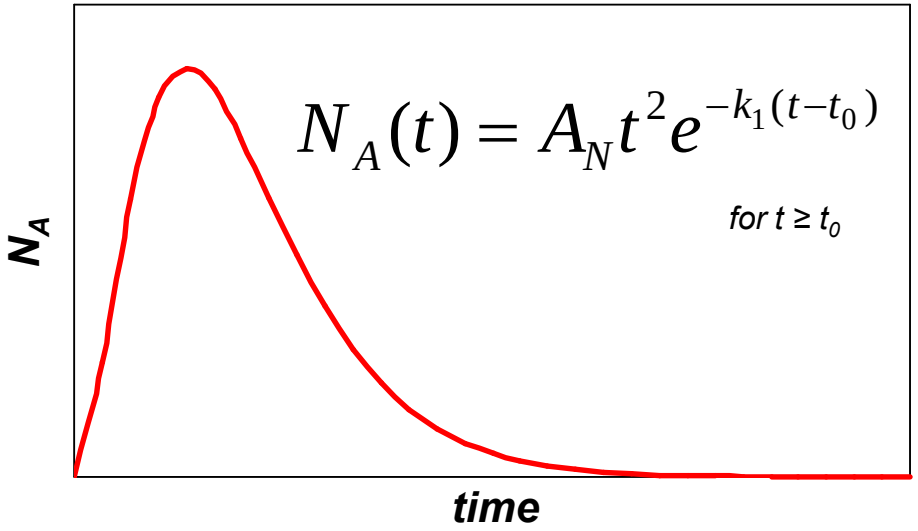
PDF Complete
Your complimentary use period has ended. Thank you for using PDF Complete.
Click Here to upgrade to Unlimited Pages and Expanded Features

Data Analysis Procedure

- Momentum flux rate is simply the mass per particle times the average particle speed times number density flux rate

$$\frac{dp_A}{dt} = m_p V_p \frac{dN_A}{dt}$$

- Data from a number of tests show that the number density flux has a modified decaying exponential behavior
  - t^2 term accounts for behavior at the front of the particle wave



- Particle speed is calculated based on arrival time and allowed to decay exponentially

$$V_p = \frac{d}{t} e^{-k_2(t-t_0)} \quad \text{for } t \geq t_0$$

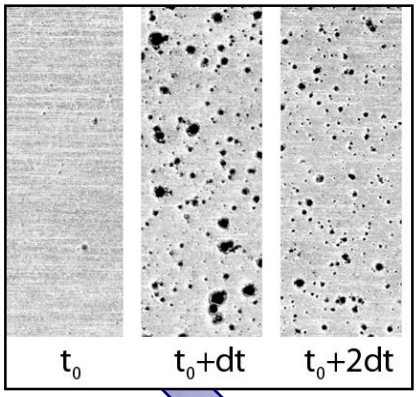
PDF Complete
Your complimentary use period has ended. Thank you for using PDF Complete.
Click Here to upgrade to Unlimited Pages and Expanded Features

Data Analysis Procedure

The data analysis procedure then reduces to finding four parameters:

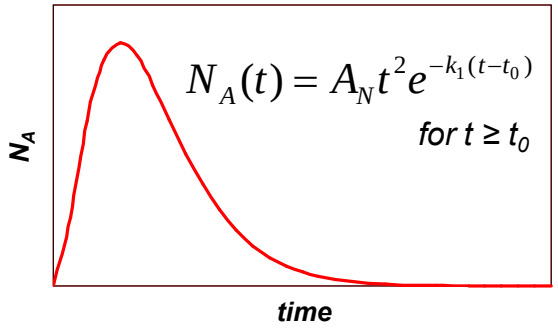
A_N, k_1, k_2, and t_0

A_N

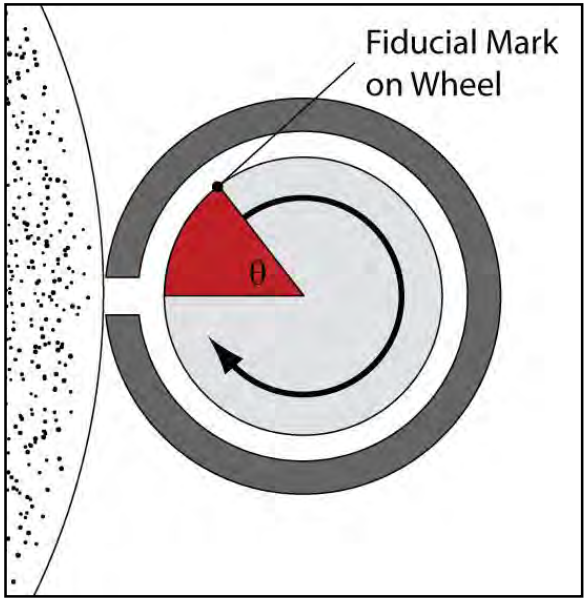


k_1

The values of A_N and k_1 are determined by fitting the PSR data to the modified exponential model



t_0



A fiducial provides a relationship between angular position around the wheel surface and time

PDF Complete
Your complimentary use period has ended. Thank you for using PDF Complete.
Click Here to upgrade to Unlimited Pages and Expanded Features

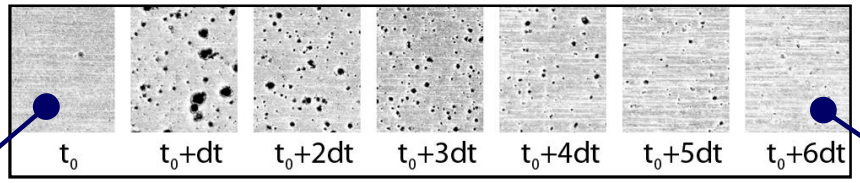
Data Analysis Procedure

The data analysis procedure then reduces to finding four parameters:

A_N, k_1, k_2, and t_0

k_2

For a given particle material and PSR surface material, the minimum marking speed V_{min} can be estimated.



First appearance of particles: t_0

Last evidence of particles: t_1

The estimate for V_{min} along with measurements of t_0 and t_1 will give the particle velocity decay constant k_2.

$$V_p = \frac{d}{t} e^{-k_2(t-t_0)} \Rightarrow V_{min} = \frac{d}{t_1} e^{-k_2(t_1-t_0)} \Rightarrow k_2 = \frac{1}{t_0 - t_1} ln\left(\frac{V_{min} t_1}{d}\right)$$

PDF Complete
Your complimentary use period has ended. Thank you for using PDF Complete.
Click Here to upgrade to Unlimited Pages and Expanded Features

ing the Impulse from the PSR Data

- Once the constants A_N, k_1, k_2, and t_0 are determined, the solid-phase impulse can be computed
- The impulse (per unit area) is the time integral of the momentum flux rate
  - Assumes particle impacts are perfectly plastic
- Given the total impulse measurement from the Unconfined Momentum Trap, the difference between the two is the gas-phase impulse
  - Note that these values are usually normalized to surface area

$$I_{A,SP} = \int_{t_0}^{\infty} \frac{dp_A}{dt} dt$$

$$I_{A,SP} = \frac{m_p d A_N \left[1 + (k_1 + k_2) t_0\right]}{(k_1 + k_2)^2}$$

$$I_{A,tot} = I_{A,GP} + I_{A,SP}$$

From momentum trap ***From PSR***

PDF Complete
Your complimentary use period has ended. Thank you for using PDF Complete.
Click Here to upgrade to Unlimited Pages and Expanded Features

Wrap-Up and Summary

PDF Complete
Your complimentary use period has ended. Thank you for using PDF Complete.
Click Here to upgrade to Unlimited Pages and Expanded Features

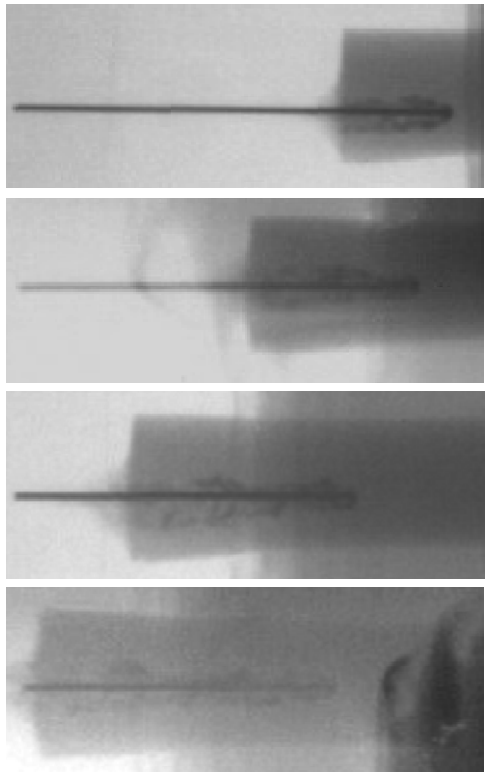
erview of Techniques

Diagnostic Technique	Time varying?	Separates loads by phase?	Measurement Fidelity
Unconfined Momentum Trap	No	No ï total only	High
Confined Momentum Trap	No	Yes	Moderate
Inverted Ballistic Pendulum	No	Yes	Moderate
Cantilevered Ball Gauge	No	No ï total only	Low
Hopkinson Pressure Bar	Yes	No ï total only	Moderate
Particle Streak Recorder	Yes	No ï solid phase only	Low

- This presentation has given an introduction to the state-of-the art in multiphase blast diagnostic techniques
- These techniques are generally time-integrated
  - Time-varying measurement techniques for solid-phase loads are relatively immature
- Improvements in hole detection will allow increases in the fidelity of the Particle Streak Recorder Technique
  - Currently investigating alternate impact surface configurations to enable higher signal-to-noise ratio

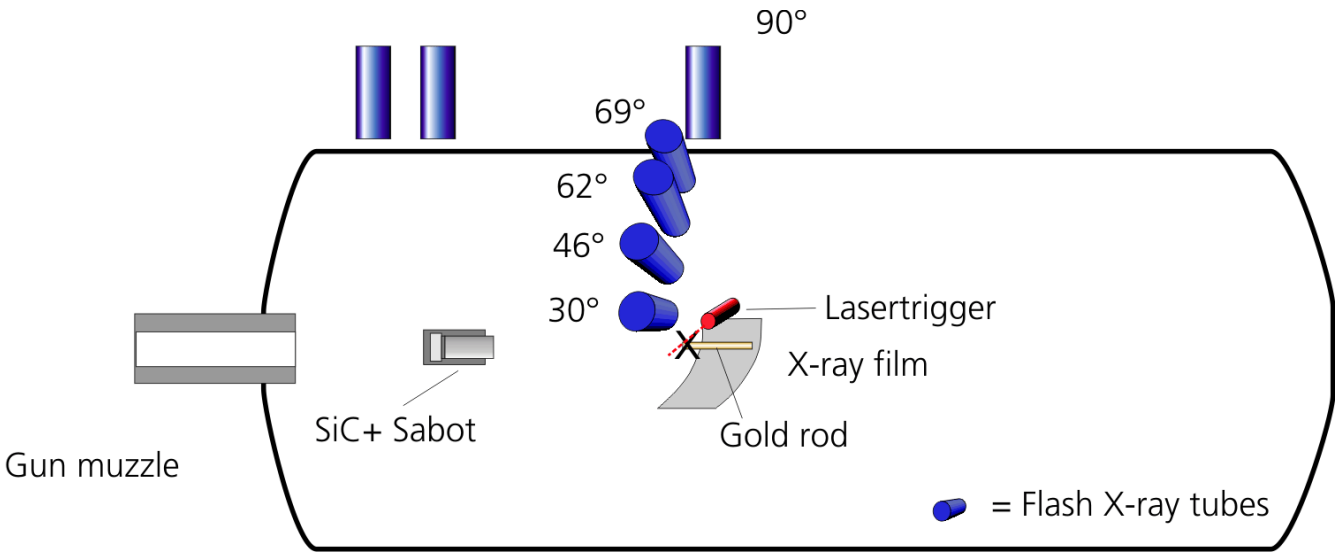
Long-Rod Penetration into Intact and Pre-Damaged SiC Ceramic

Charles E. Anderson, Jr.
Thilo Behner
Dennis L. Orphal
Arthur E. Nicholls
Timothy J. Holmquist
Matthias Wickert



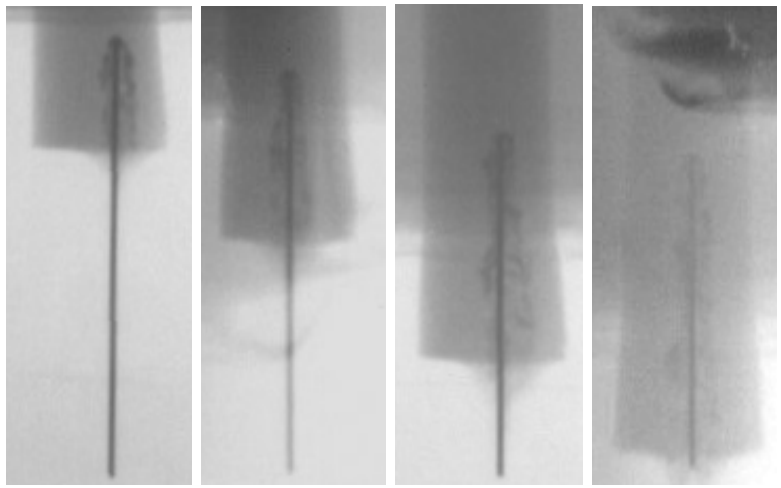
September 2008

Experimental Set-up

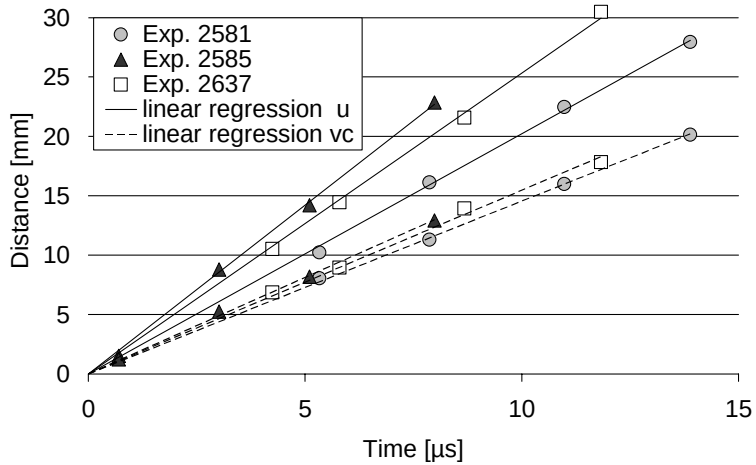


- *Reverse ballistics experiments*
- *Flash radiography used to measure position of nose and tail of rod versus time*

Penetration Experiments

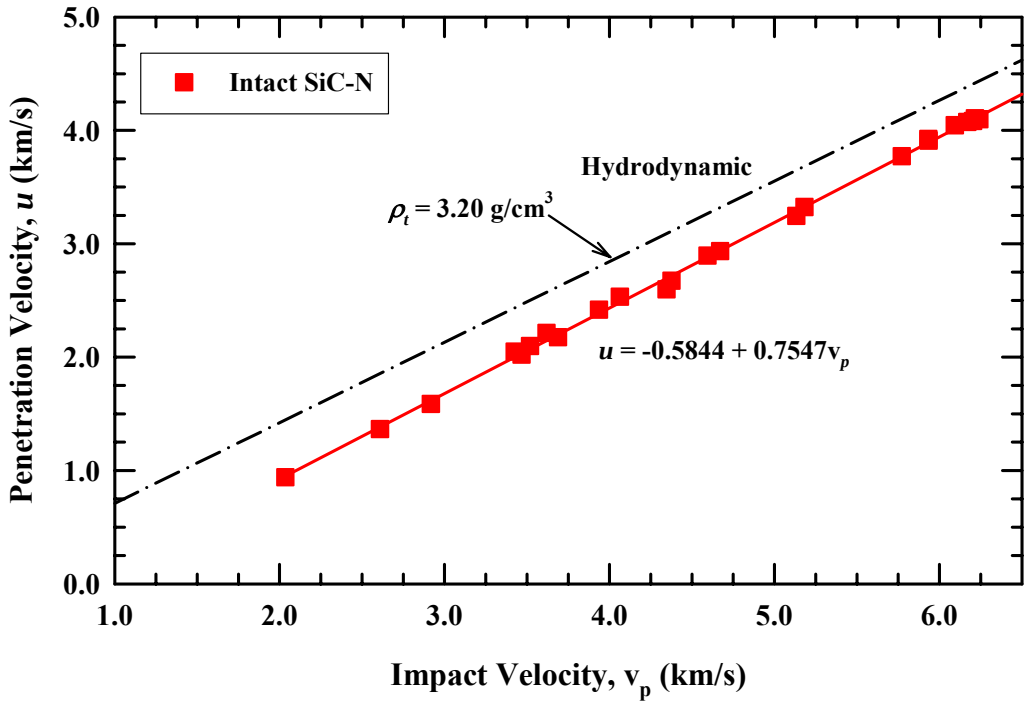


Expt 2581



- *Regression fits*
  - *Penetration vs. time*
  - *Rod length vs. time*
- *Slopes of regression fits*
  - *Penetration velocity*
  - *Consumption velocity*

Penetration Velocity vs. Impact Velocity



Experiments & Analysis: 2002 - 2005

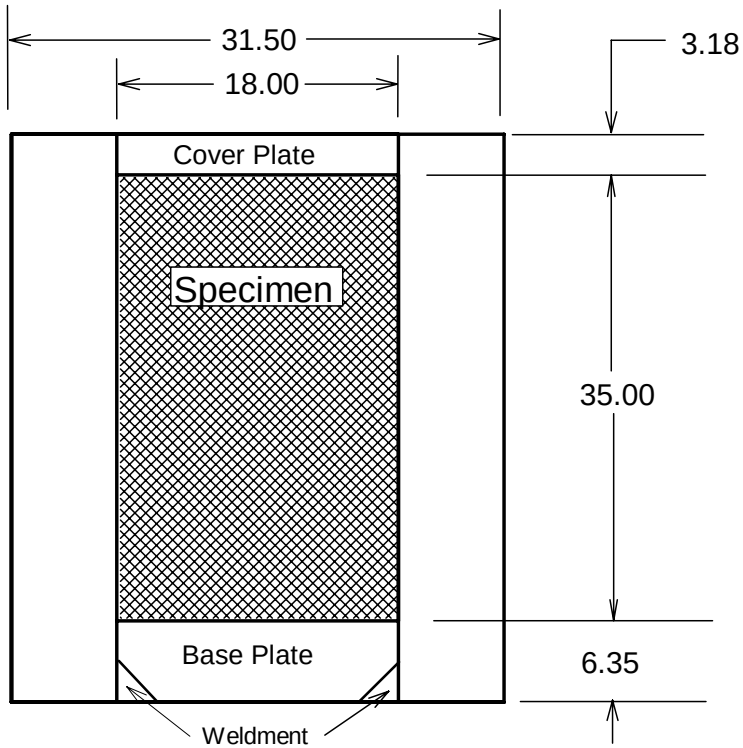
Experiments to Explore Penetration of Damaged Ceramic

- *Conflicting interpretations for strength of damaged ceramic*
- *Designed experiments to investigate penetration response of various "damaged" SiC*
  - *Pre-damaged (thermal cycles that induced cracks)*
  - *In-situ comminuted (thermal cycle plus load/reload cycles in a MTS machine)*
  - *Compacted powder*

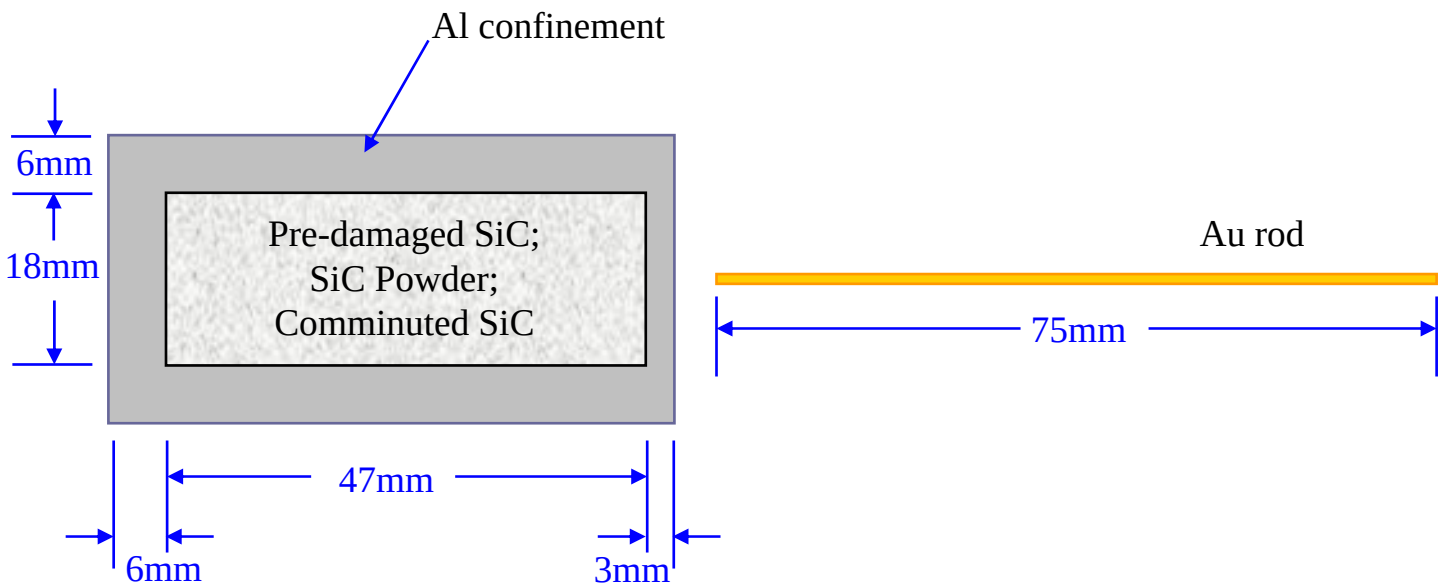
Experiments & Analysis: 2006 - 2007

Target Design

- *7075-T6 aluminum sleeve*
- *Base plate welded*
- *Cover plate press-fit w/superglue*

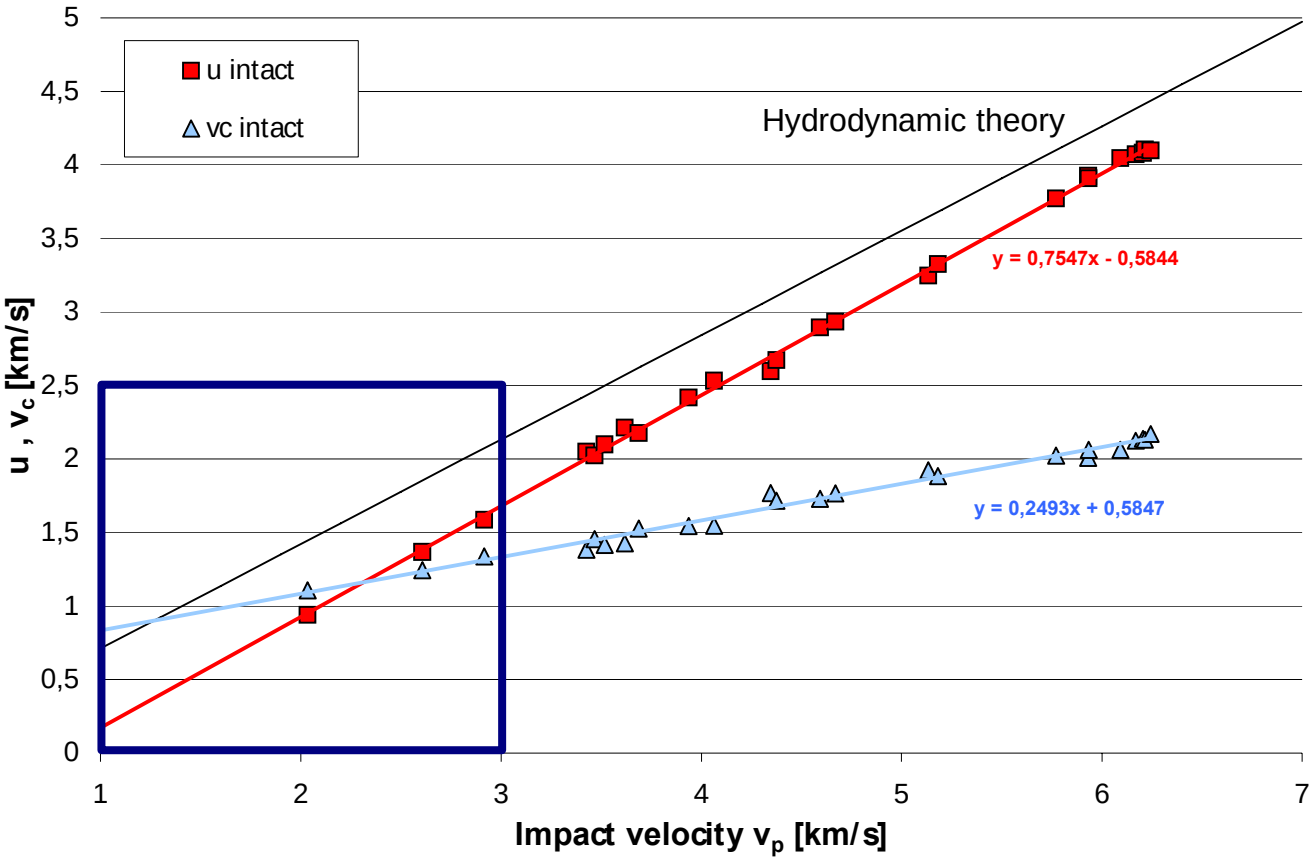


Schematic of EMI Experiments

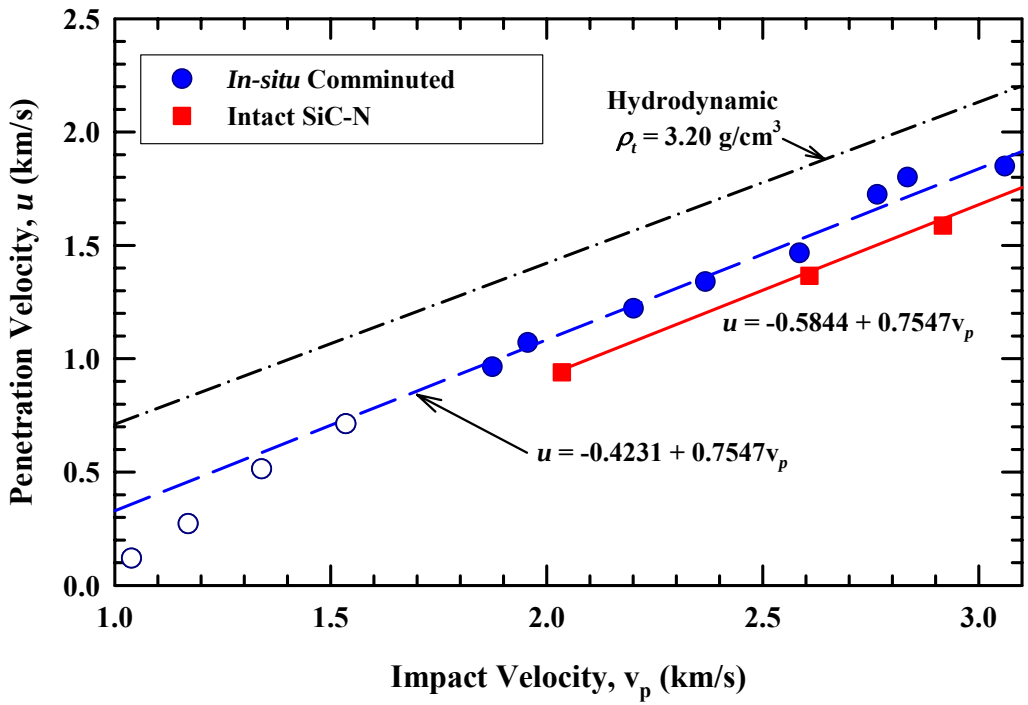


- *Differences in experiments relative to previous experiments*
  - *Aluminum confinement w/cover plate*
  - *1.00-mm diameter Au rod instead of 0.75-mm diameter rod*

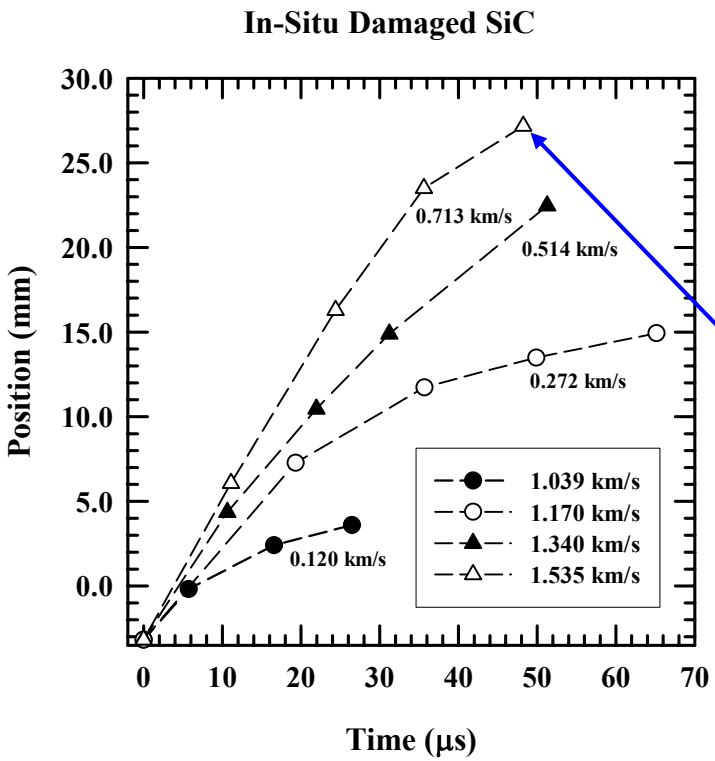
Velocity Range

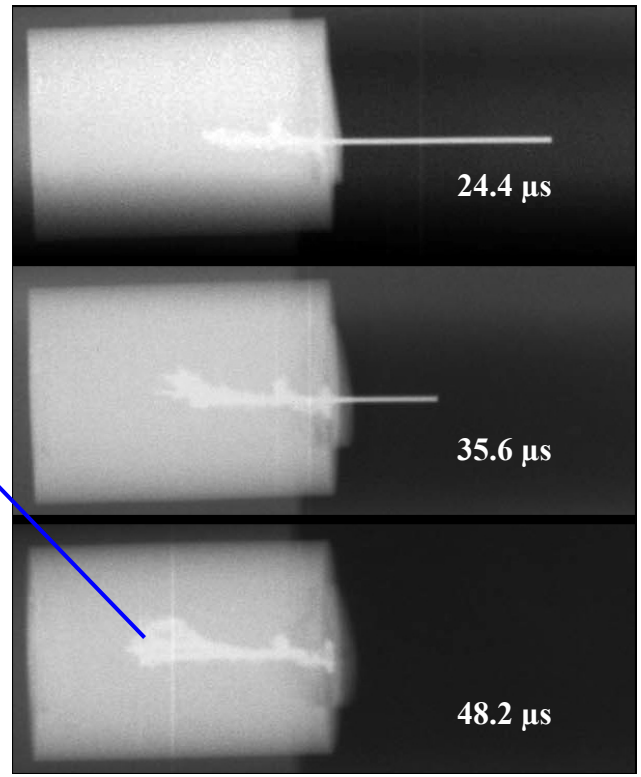


In-Situ Comminuted SiC



Lowest Impact Velocities

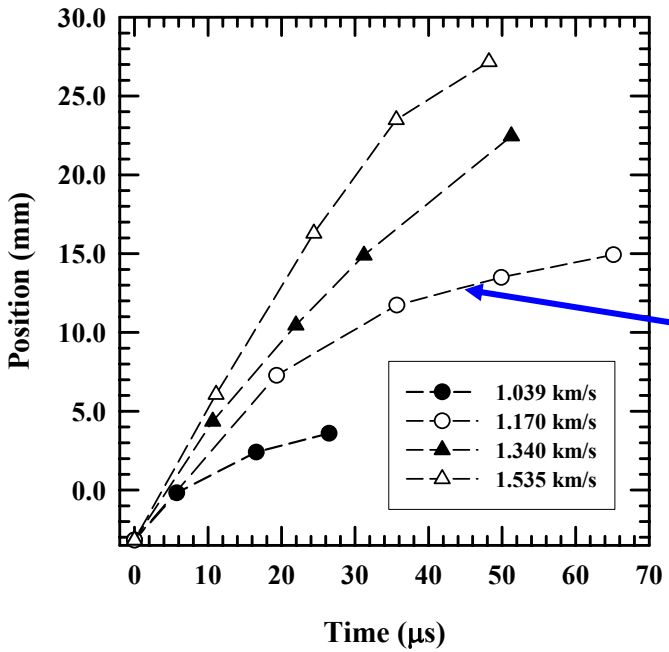


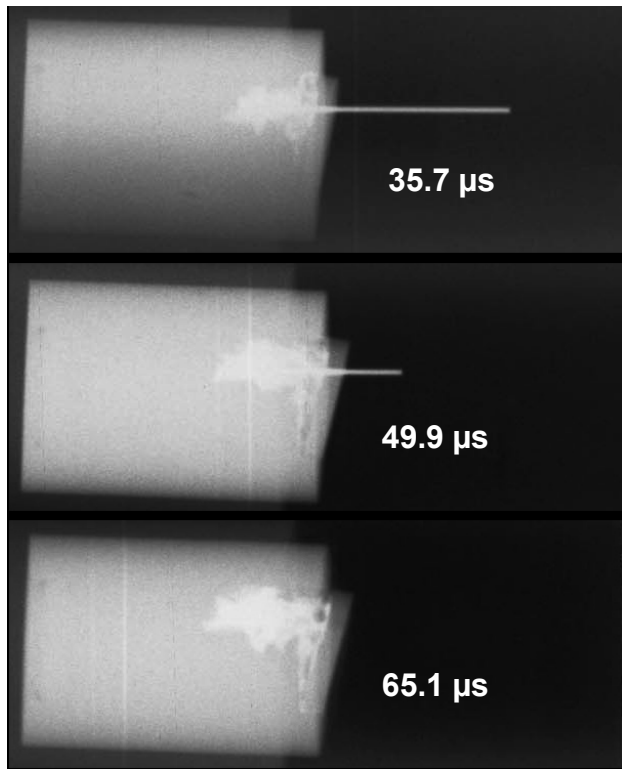


v_p = 1.535 km/s

- *When $u \leq v_c$, nonlinear penetration response*

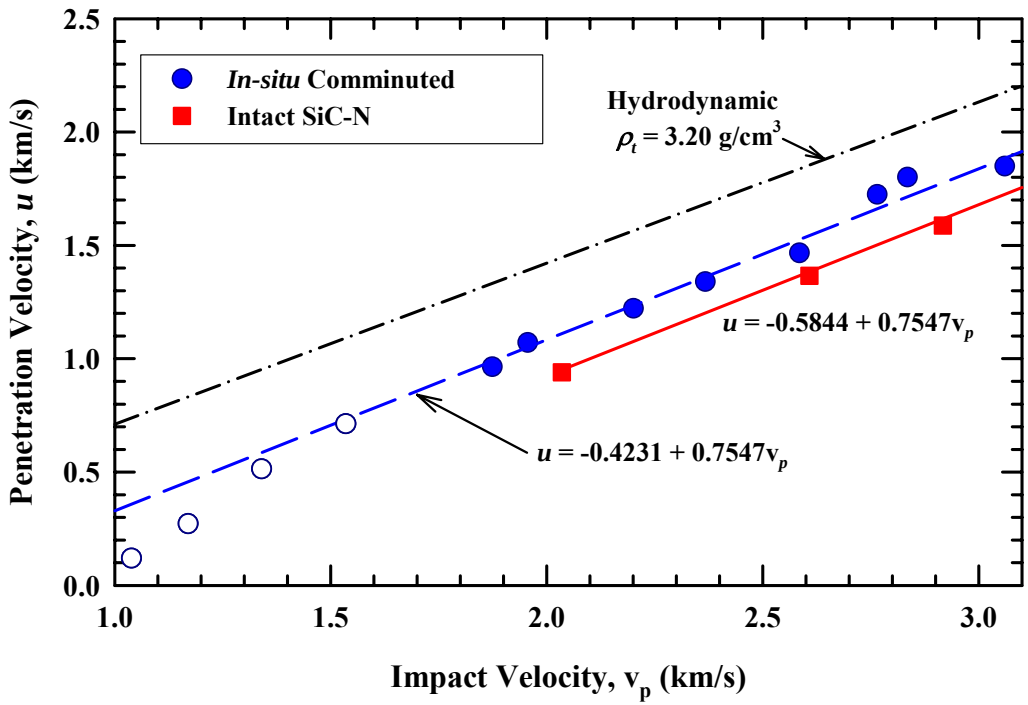
Dwell-Like Behavior



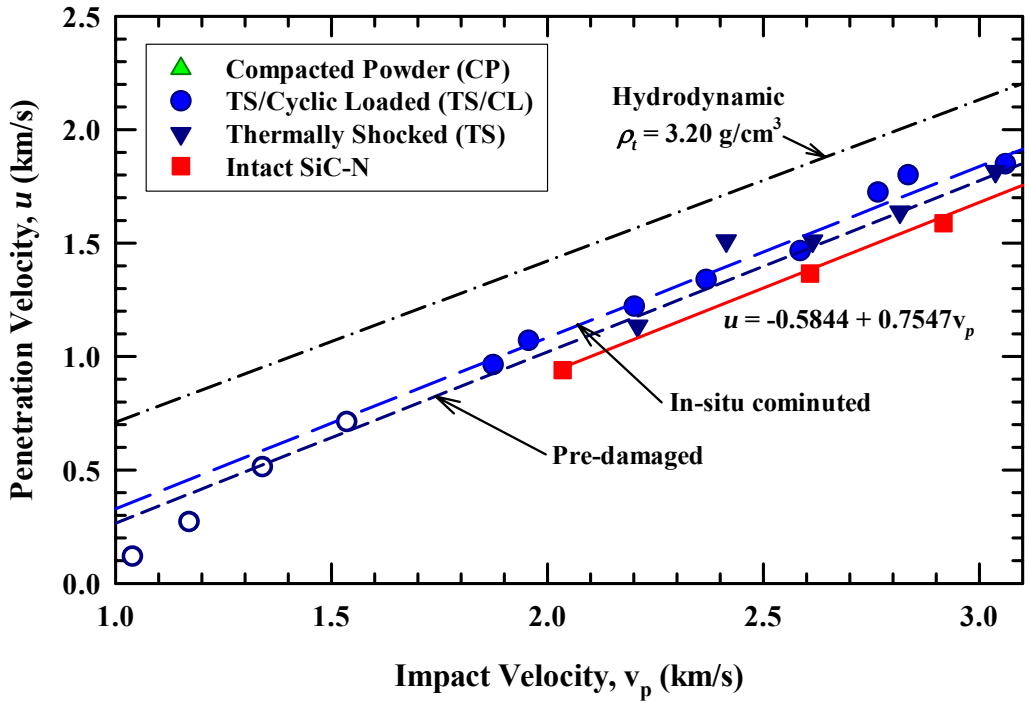


v_p = 1.170 km/s

In-Situ Comminuted SiC

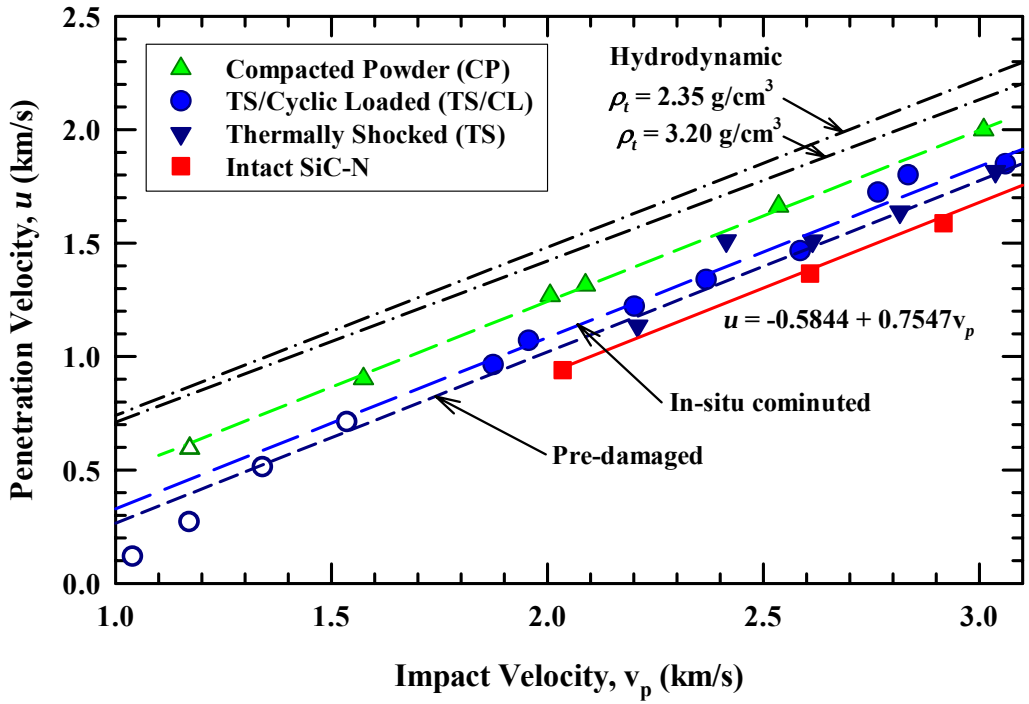


Thermally Shocked SiC



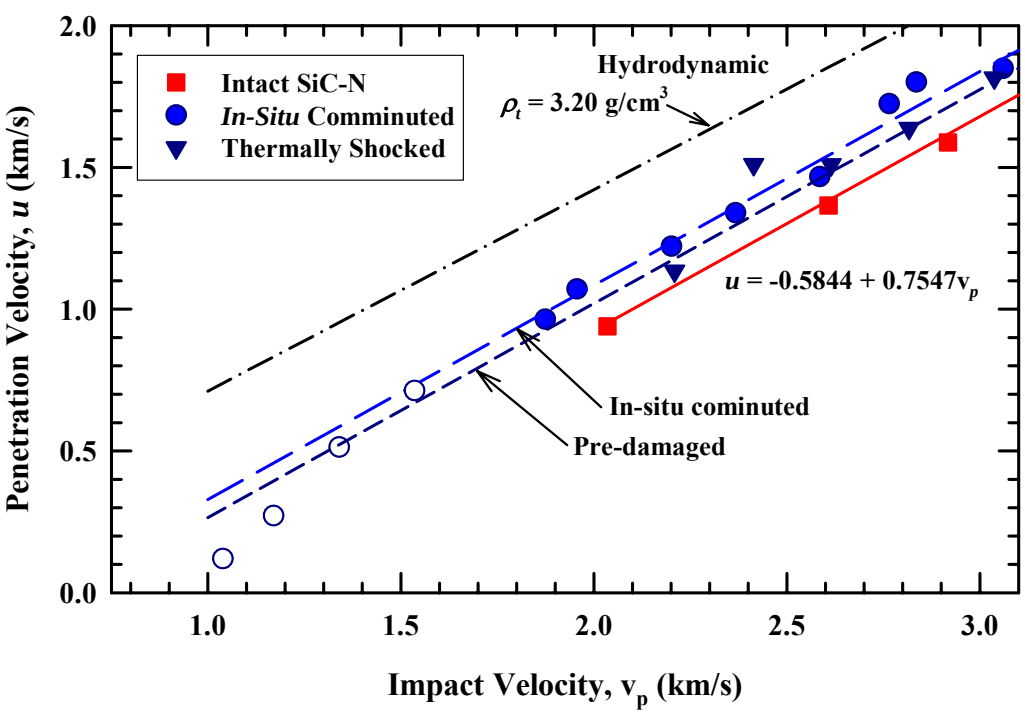
- *Regression fit through pre-damaged results ignored the datum point at 2.4 km/s*

Compacted SiC Powder



- $u_{intact} < u_{predamaged} < u_{comminuted} < u_{powder} < u_{hydro}$

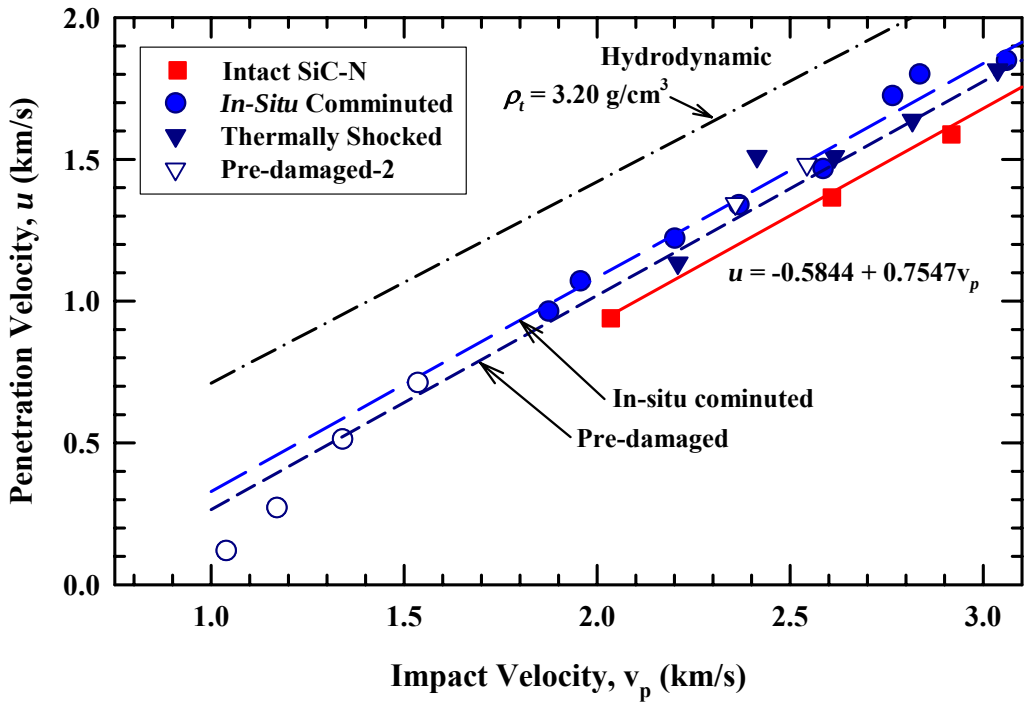
New Experiments



- *Extend pre-damaged sleeved data to lower impact velocities*
- *Check to see if data point at 2.4 km/s is an outlier*
- *Demonstrate that bare and sleeved intact ceramic have the same penetration response*
- *Extend intact data to lower impact velocities*

Pre-Damaged SiC Results

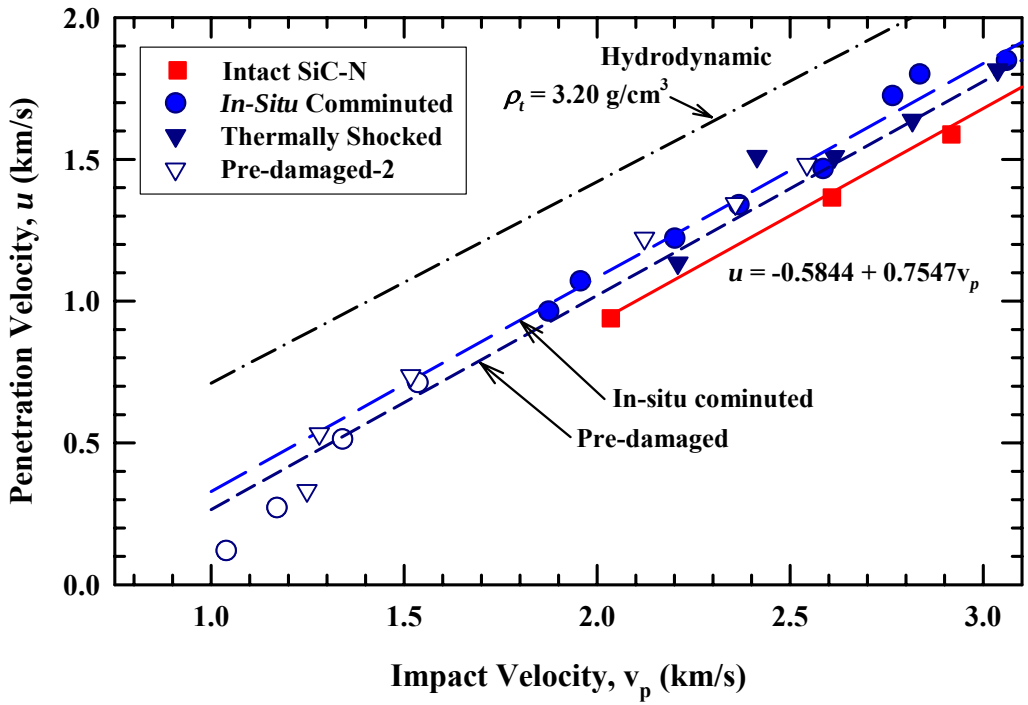
- *Was datum at 2.4 km/s anomalously high?*



- *Yes, it appears to be!*

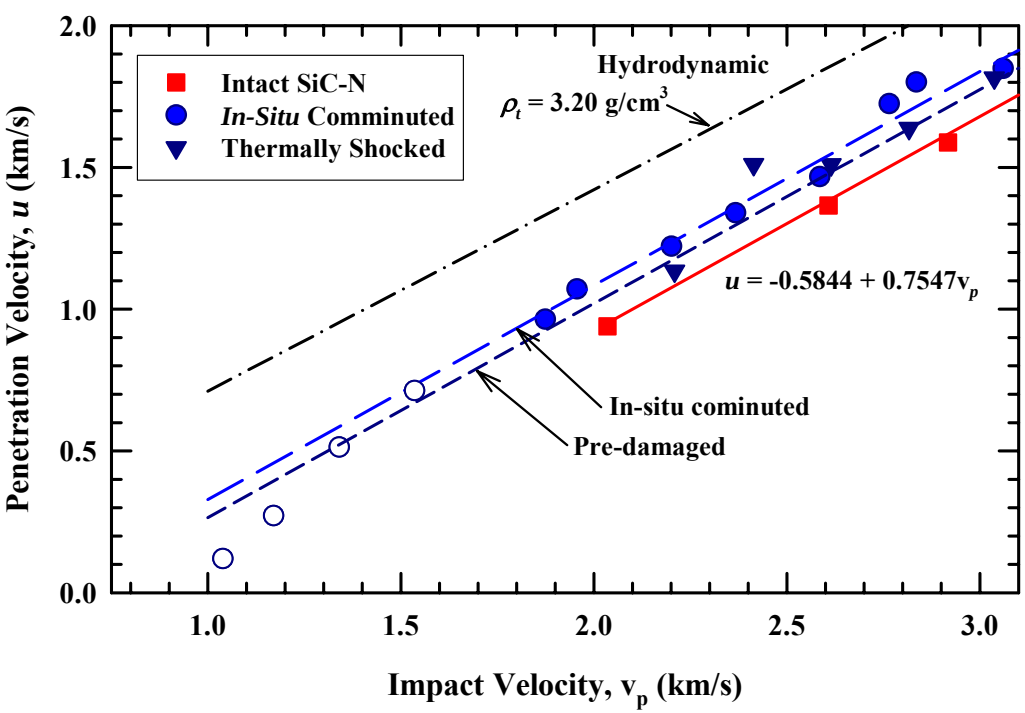
Pre-Damaged Results

- *Extend results to lower impact velocities*



- *Cannot differentiate between pre-damaged and in-situ comminuted experiments (within data scatter)*

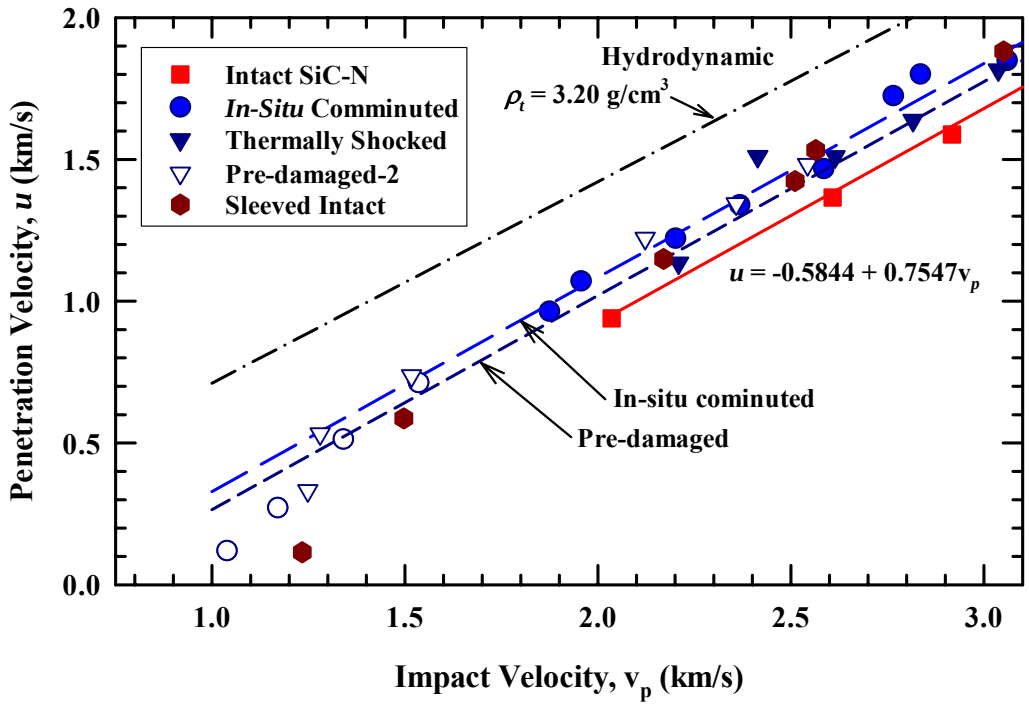
New Experiments



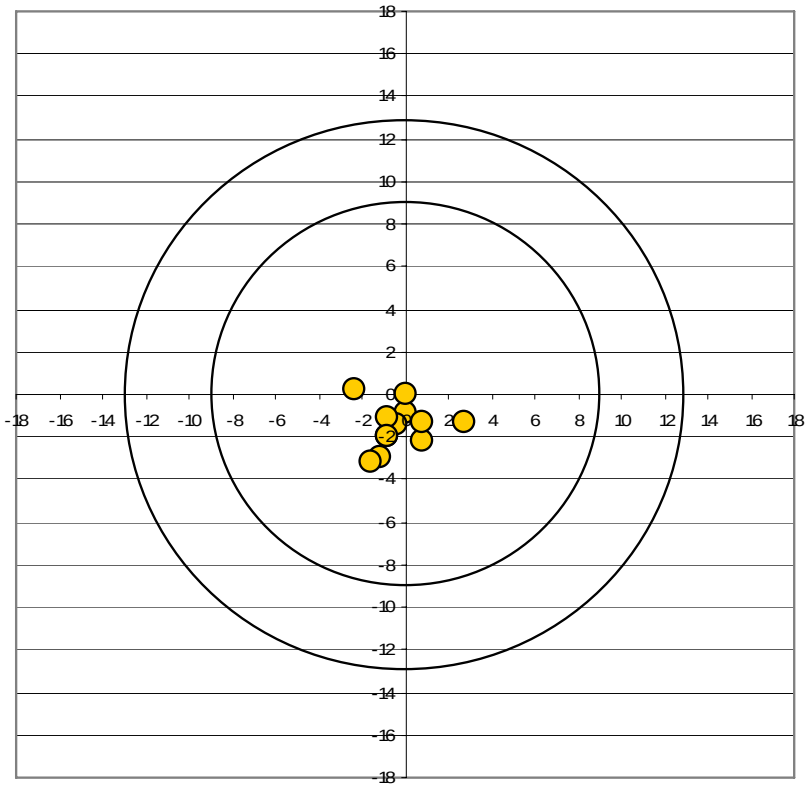
- *Extend pre-damaged sleeved data to lower impact velocities*
- *Check to see if data point at 2.4 km/s is an outlier*
- *Demonstrate that bare and sleeved intact ceramic have the same penetration response*
- *Extend intact data to lower impact velocities*

Sleeved Intact SiC

- *Begin experiments at high impact velocity (results should be independent of confinement)*

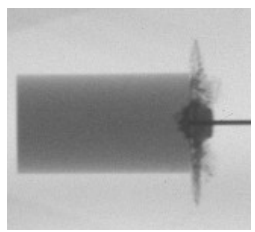


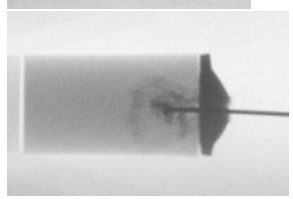
Good Impacts

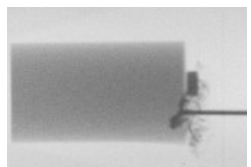


Results

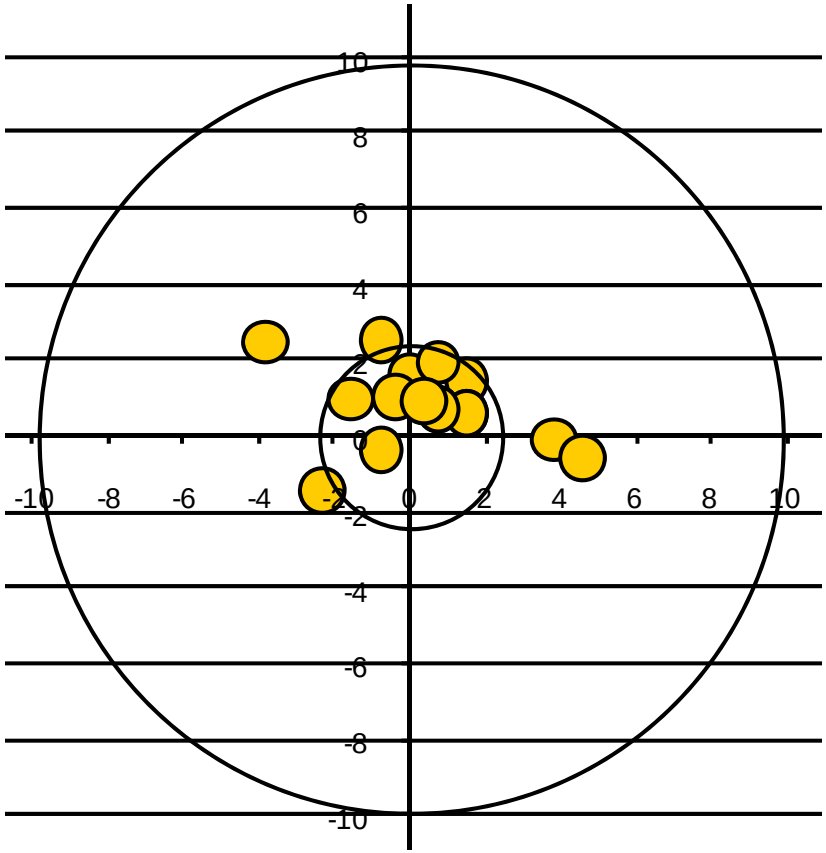
- *Cannot differentiate intact data from pre-damaged and in-situ comminuted data*
- *The new experiments were encased in the aluminum sleeve*
- *Had additional experiments to investigate interface defeat*
  - *Unconfined ceramic*
  - *With and w/o Cu buffer*
    - *Cu nub*
    - *Cu plate*



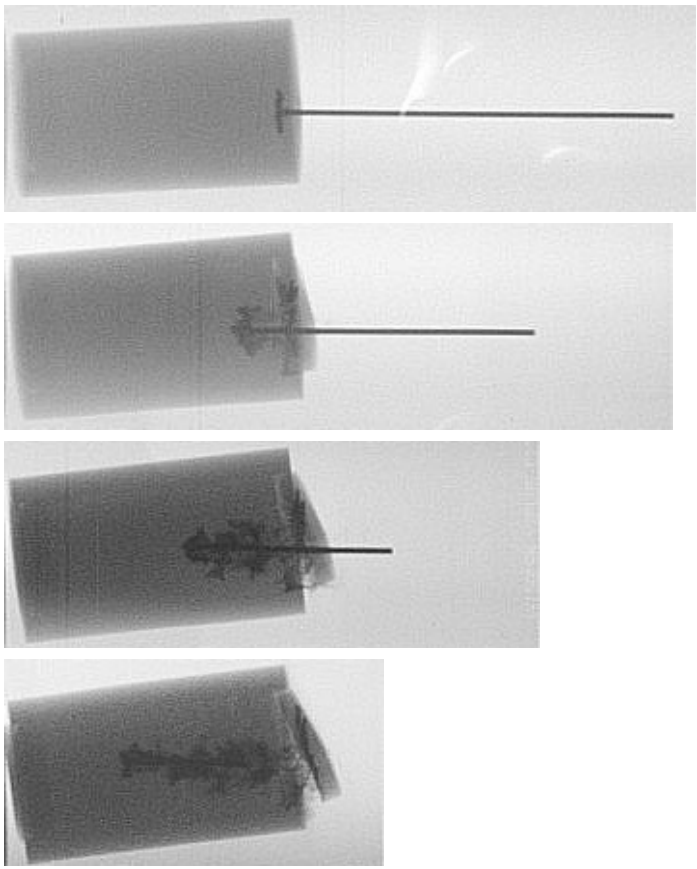




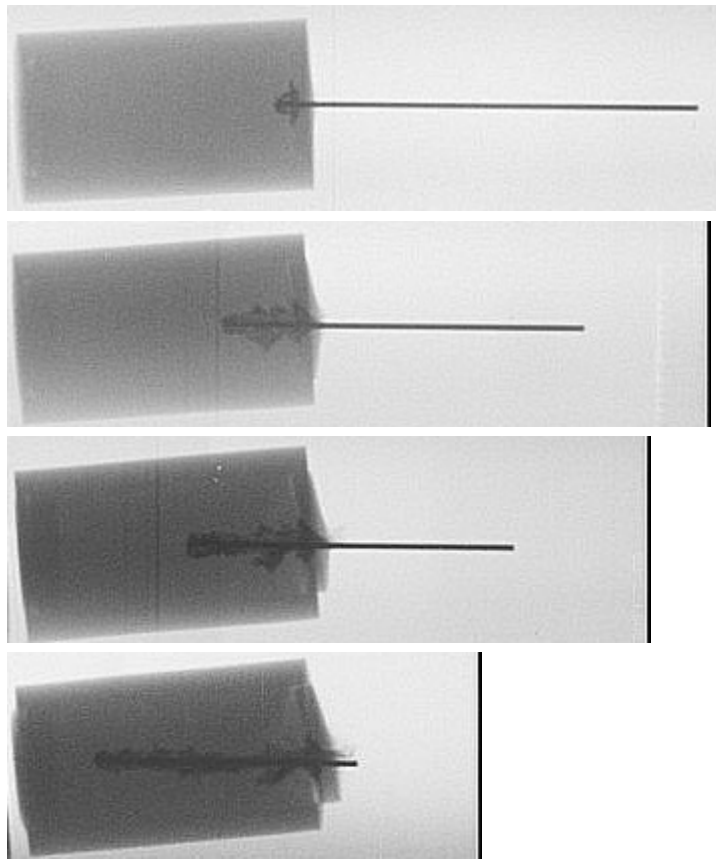
Impact Locations



Incipient Dwell w/Cover

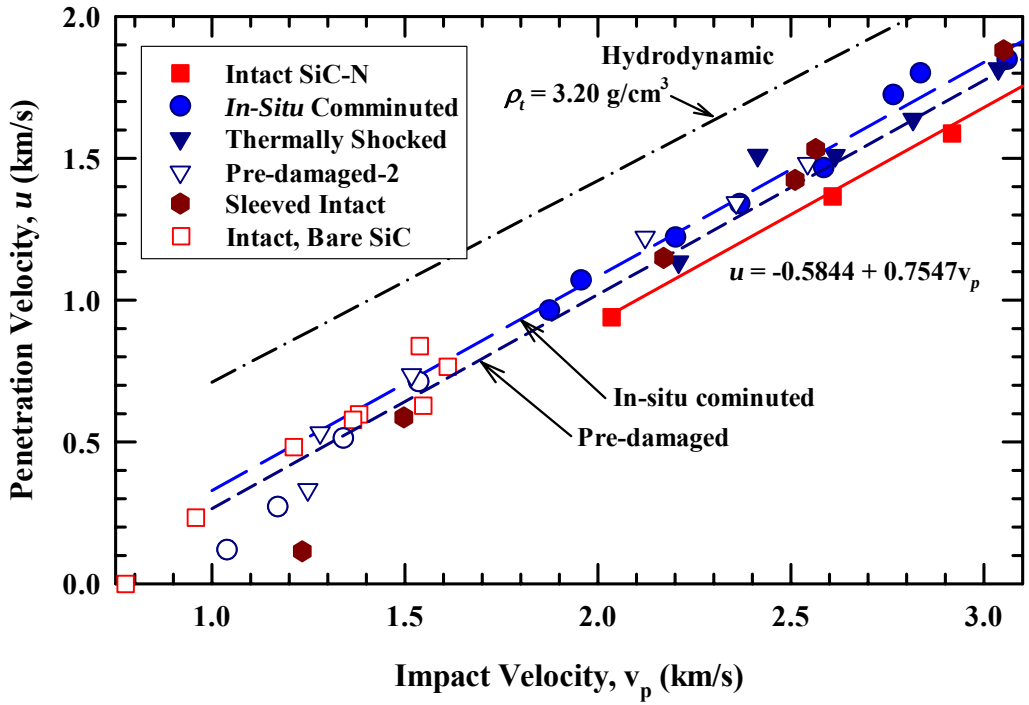


Test 11340
v_p = 1.497 km/s

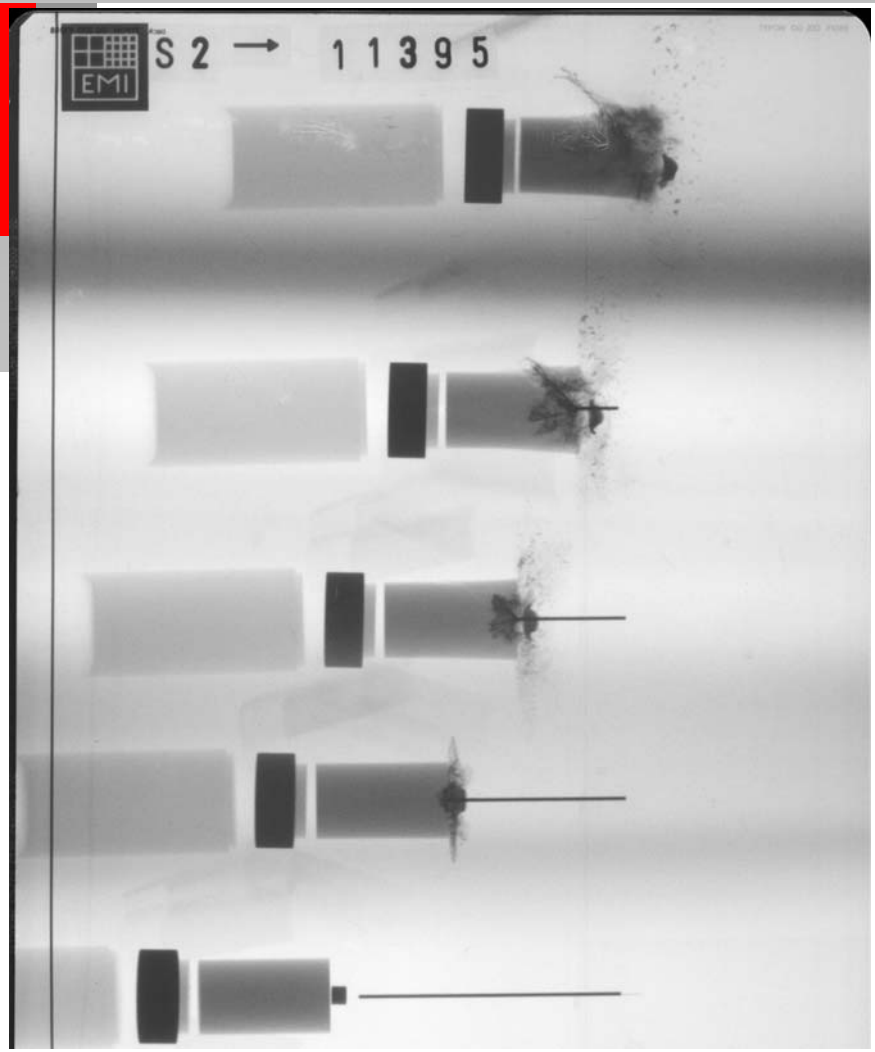


Test 11342
v_p = 2.170 km/s

Interface Defeat Expts.

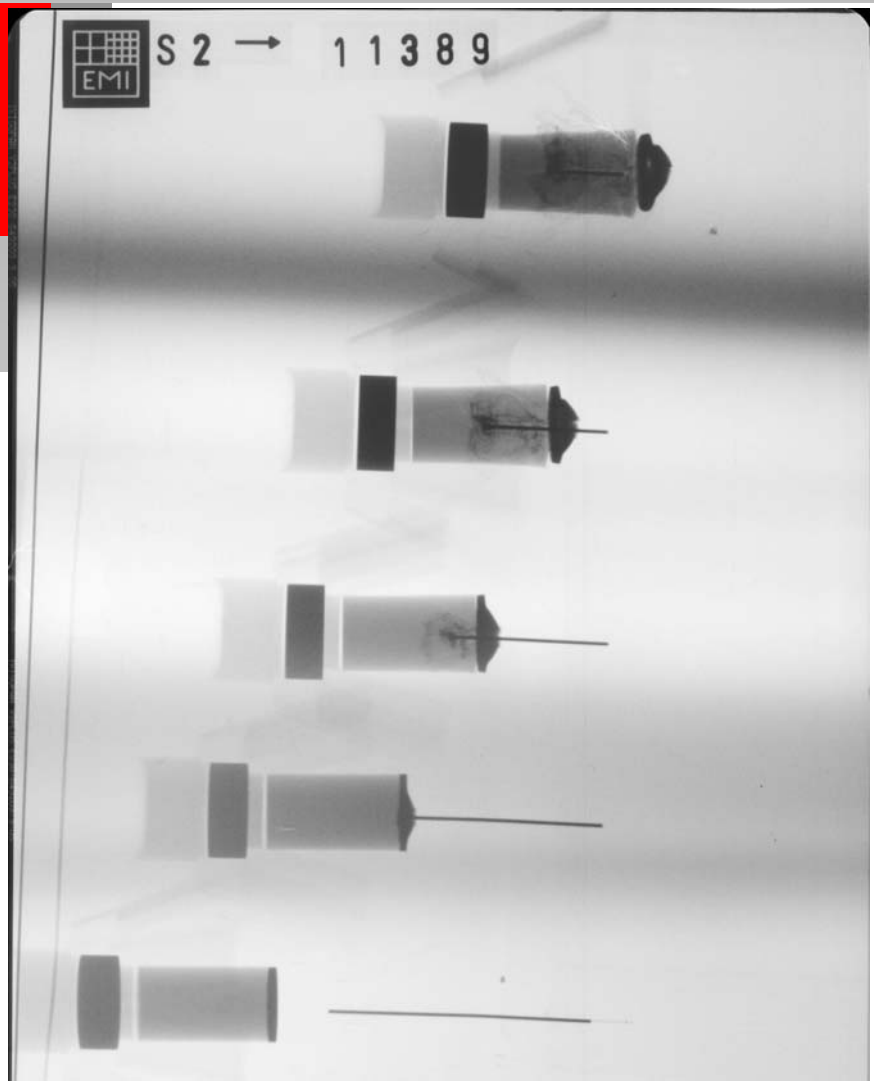


Dwell Experiment



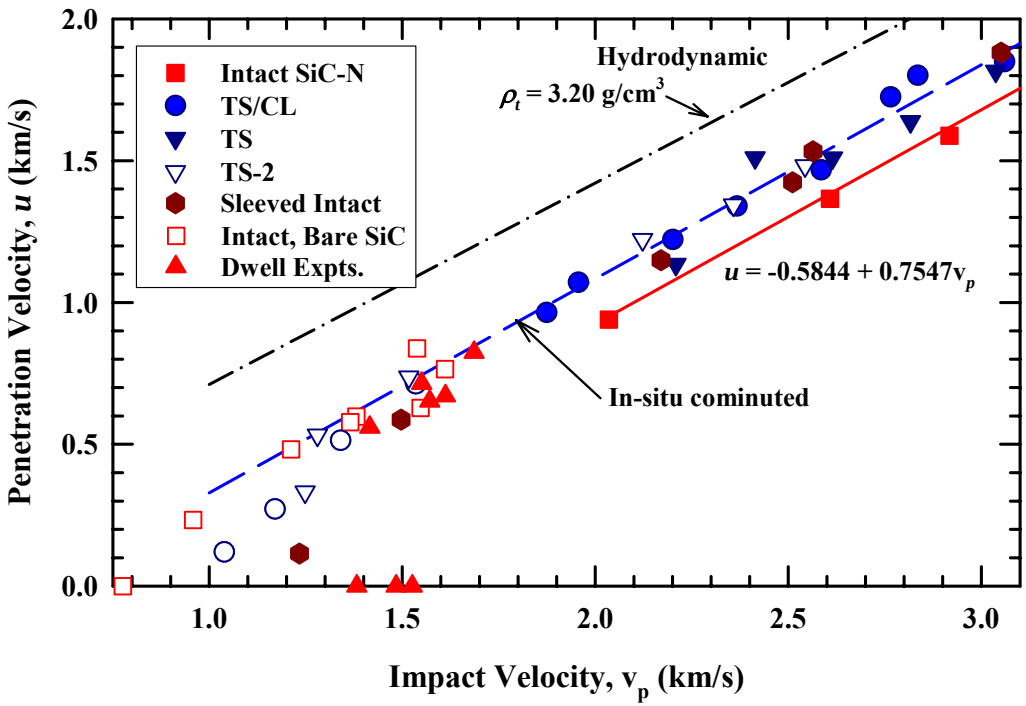
- *Test 11395*
- *Cu buffer*
- *Impact velocity: 1.526 km/s*
- *Dwelled for ~10.4 μs*

Dwell Experiment



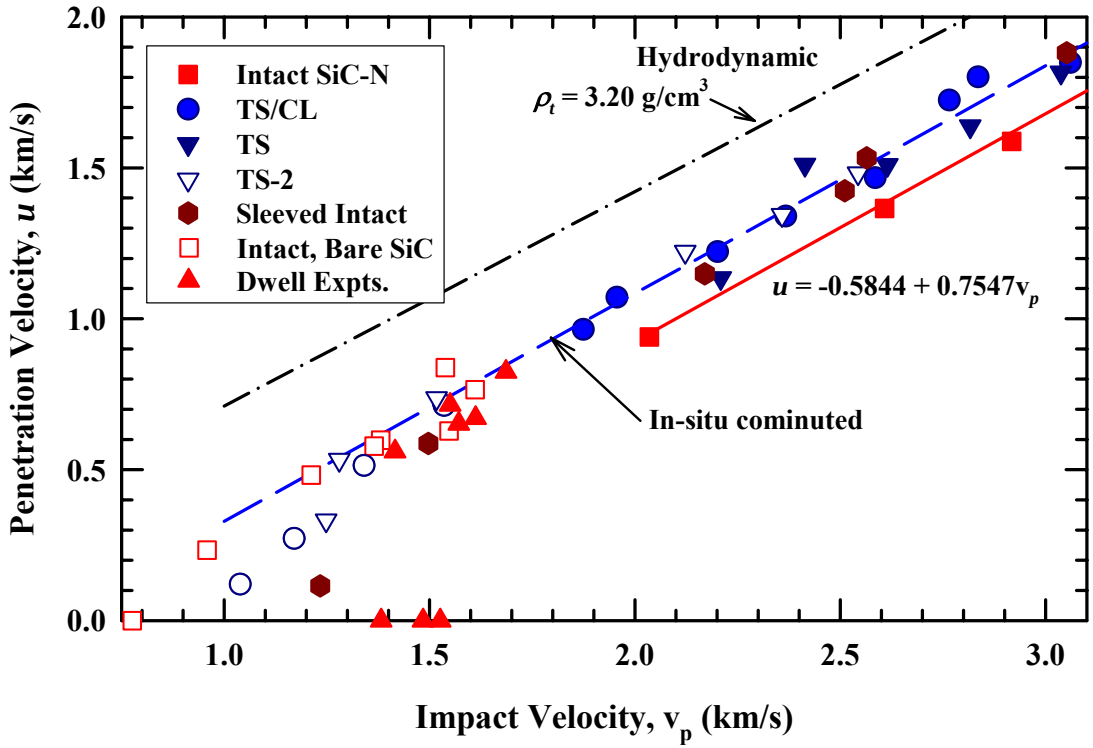
- *Test 11389*
- *Cu plate*
- *Impact velocity: 1.571 km/s*
- *Dwelled for ~11 μs*

Transition from Dwell to Penetration



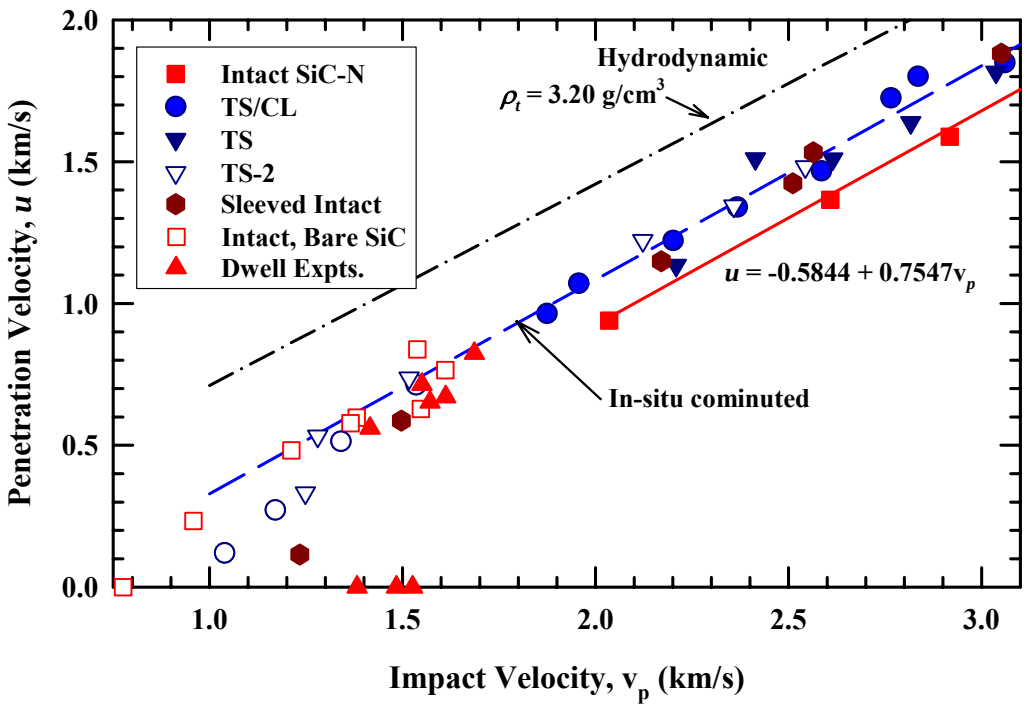
- *Within data scatter, $u_{1.00}$ for intact, pre-damaged, and in-situ comminuted are the same (sleeved or bare)*
- *$u_{1.00} > u_{0.75}$*
- *Once begin penetrating, experimental data and high-speed photography imply penetrating failed material*

Summary of Data



- ~~$u_{intact} < u_{predamaged} < u_{comminuted} < u_{powder} < u_{hydro}$~~
- $u_{intact} = u_{predamaged} = u_{comminuted} < u_{powder} < u_{hydro}$

Further Experiments



- *20-mm diameter, bare, SiC-N cylinders*
- *Impact velocity: ~2.2 – 3.0 km/s*
- *Conduct ~5 experiments with 0.75-mm diameter Au rods*
- *Conduct ~5 experiments with 1.00-mm diameter Au rods*

In physics, you don't have to go around making trouble for yourself—

Nature does it for you

- Frank Wilczek

Radial jet dispersion due to current interaction in an electric armour application

Authors

- Patrik Appelgren
- Lars Westerling
- Melker Skoglund
- Patrik Lundberg*
- Tomas Hurtig
- Anders Larsson

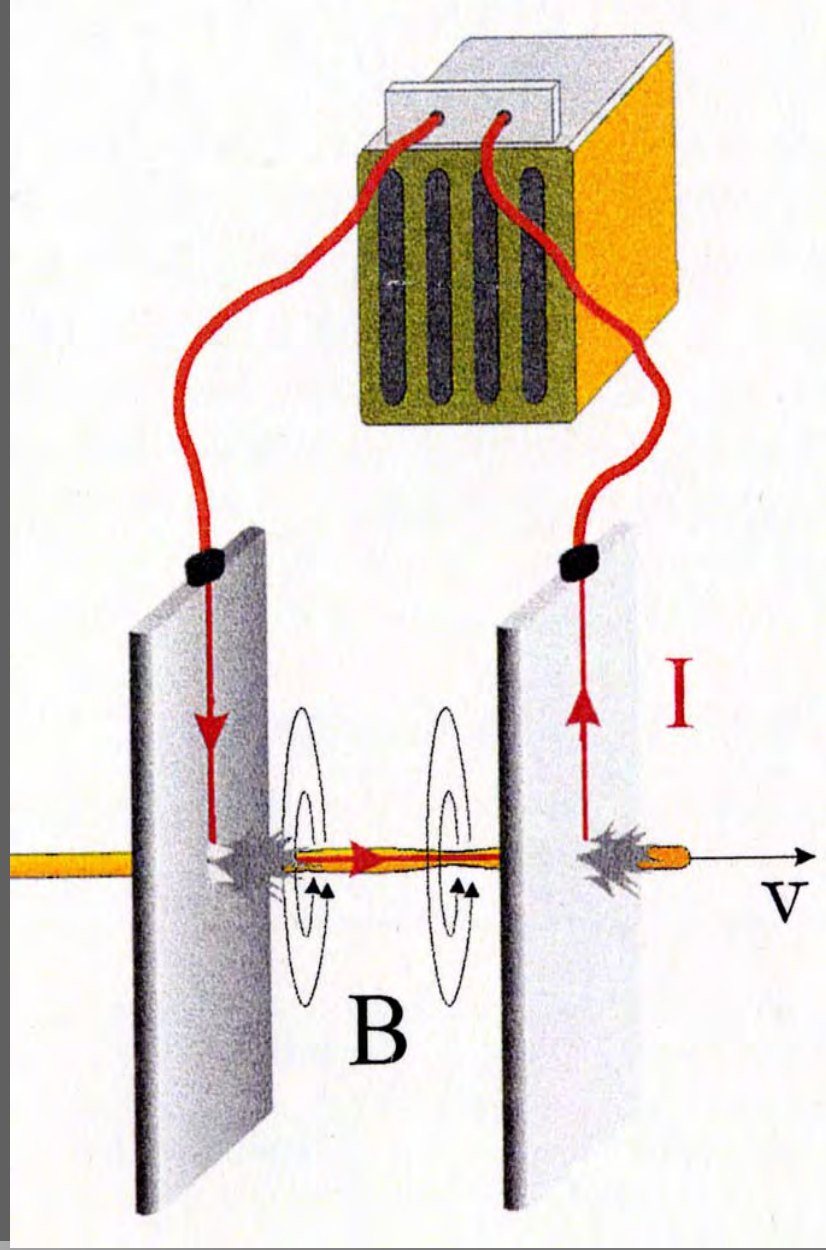
Contents

- Introduction – electric armour (electromagnetic armour)
- Shaped charge experiments
  - Observations - results
- Modelling of jet - current interaction
  - results
- Conclusions

Electric armour

Effects on jet by:

- Joule heating
  - Heating, melting
  - Local vaporisation
- Lorentz forces
  - Local instability growth
  - Fragmentation, disintegration



Electric armour – protective mechanism

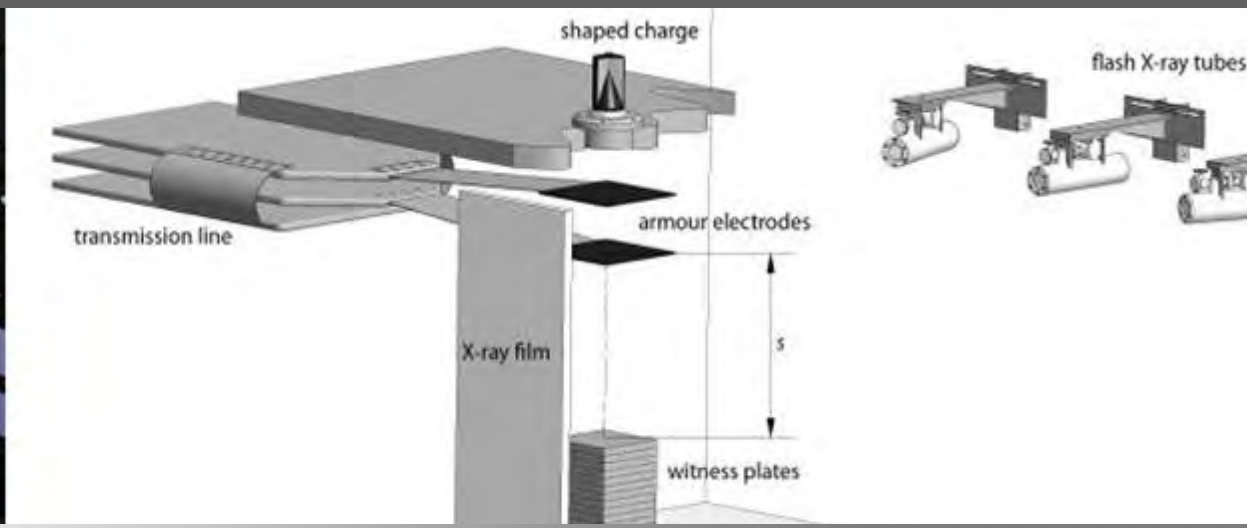
- Magnetic forces transforms the jet from a cylindrical shape (axial coherence) to ring- or disc shaped structures



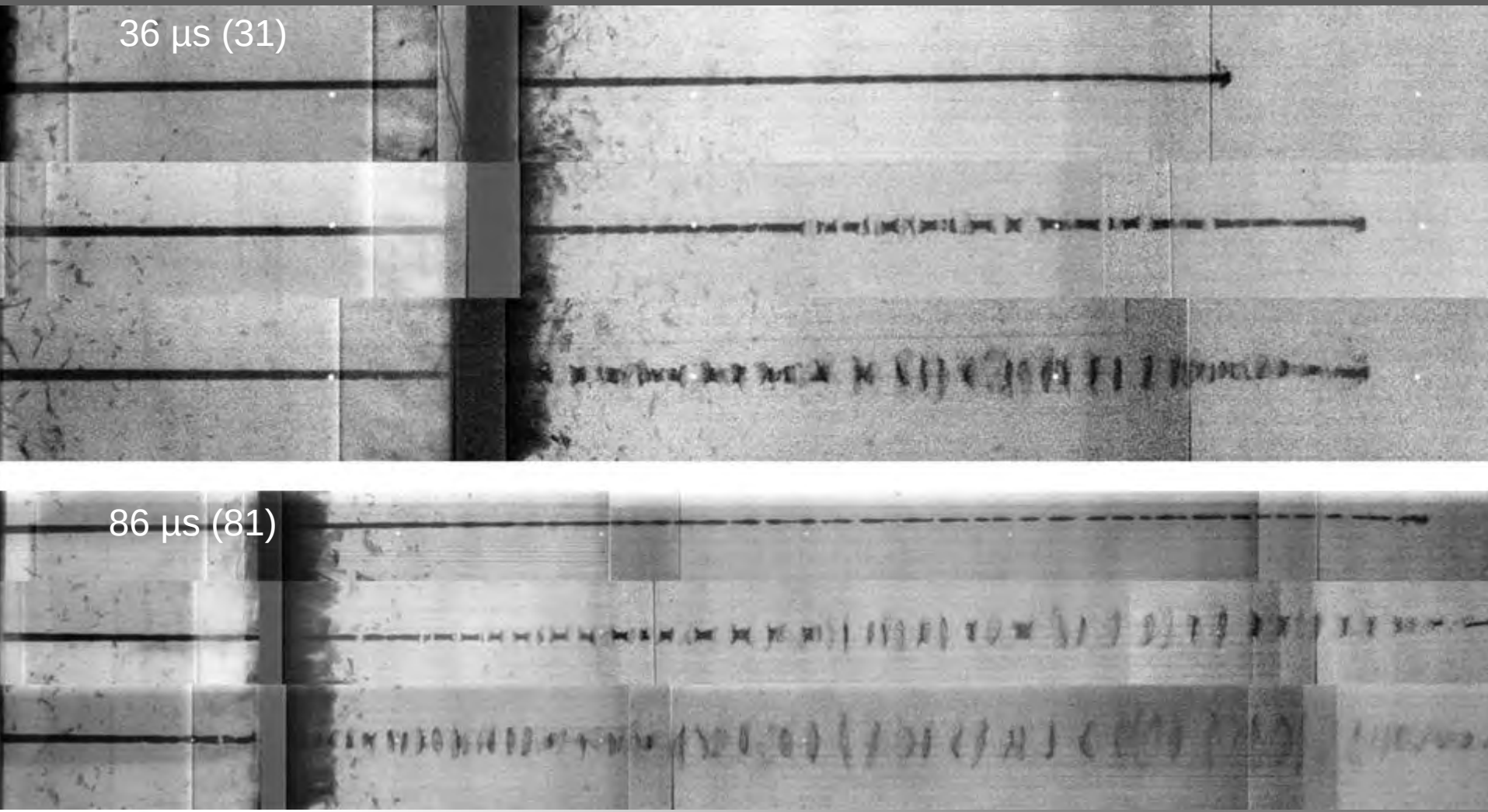
Experimental test setup

- A 1.7 mF, 400 kJ pulsed power supply
  - Two-plate electrode arrangement
  - Current and voltage diagnostics
  - Three X-rays to depict the jet



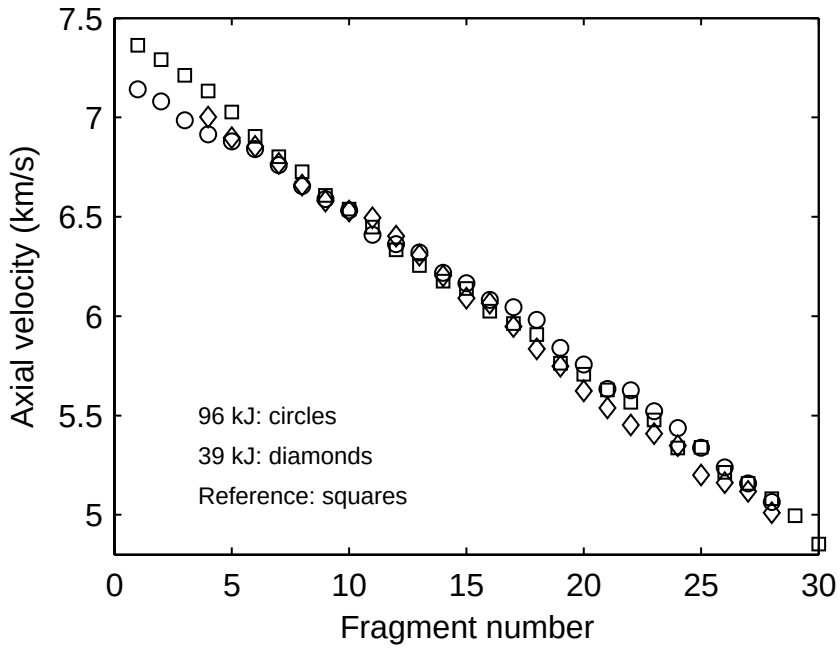


Experimental results (0, 39 kJ, 96 kJ)



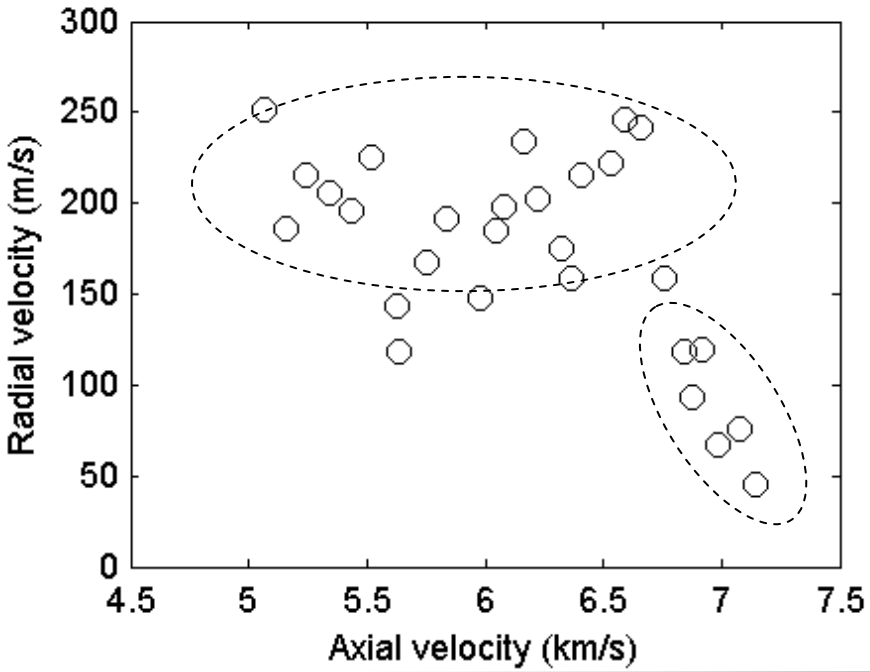
Experimental results 39 and 96 kJ

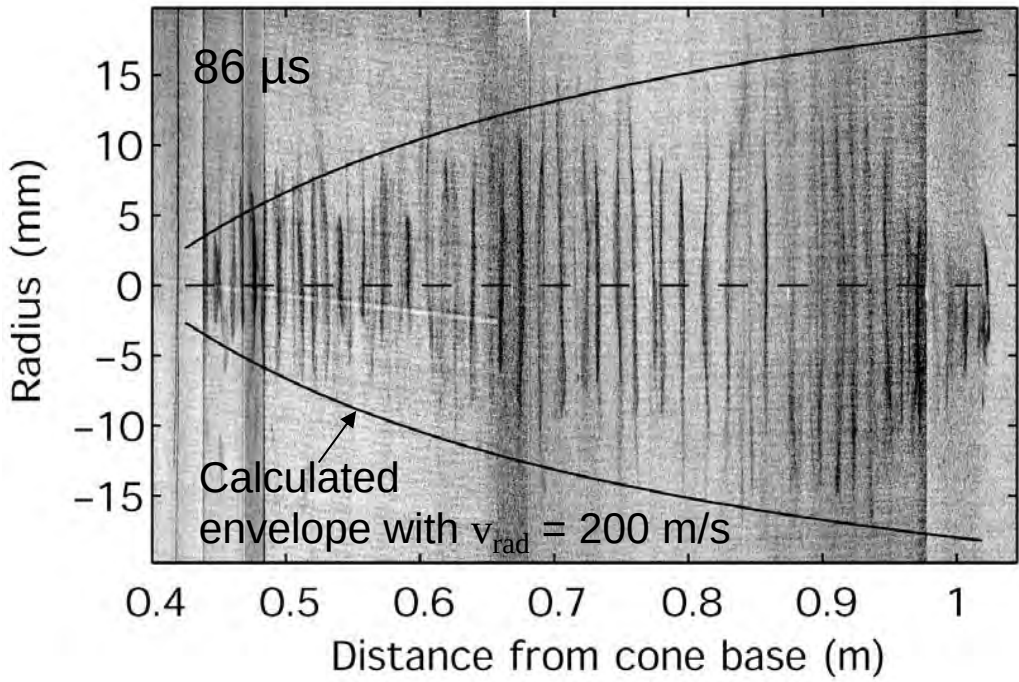
- Number of fragments independent of electric energy
  - Same fragmentation behaviour but more rapid



Experimental results 96 kJ

- Radial expansion velocity of jet elements:
  - Around 200 m/s ($3 < v_{axial} < 6.6$ km/s)



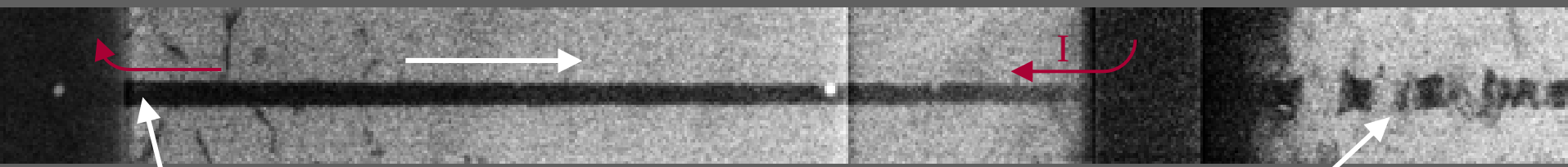


Experimental results 96 kJ

- No clear mechanical effect in-between the electrodes
- Rapid transformation at exit of electrode region
  - Fragmentation
  - Disk- and ring formation

Electrode 1

Electrode 2

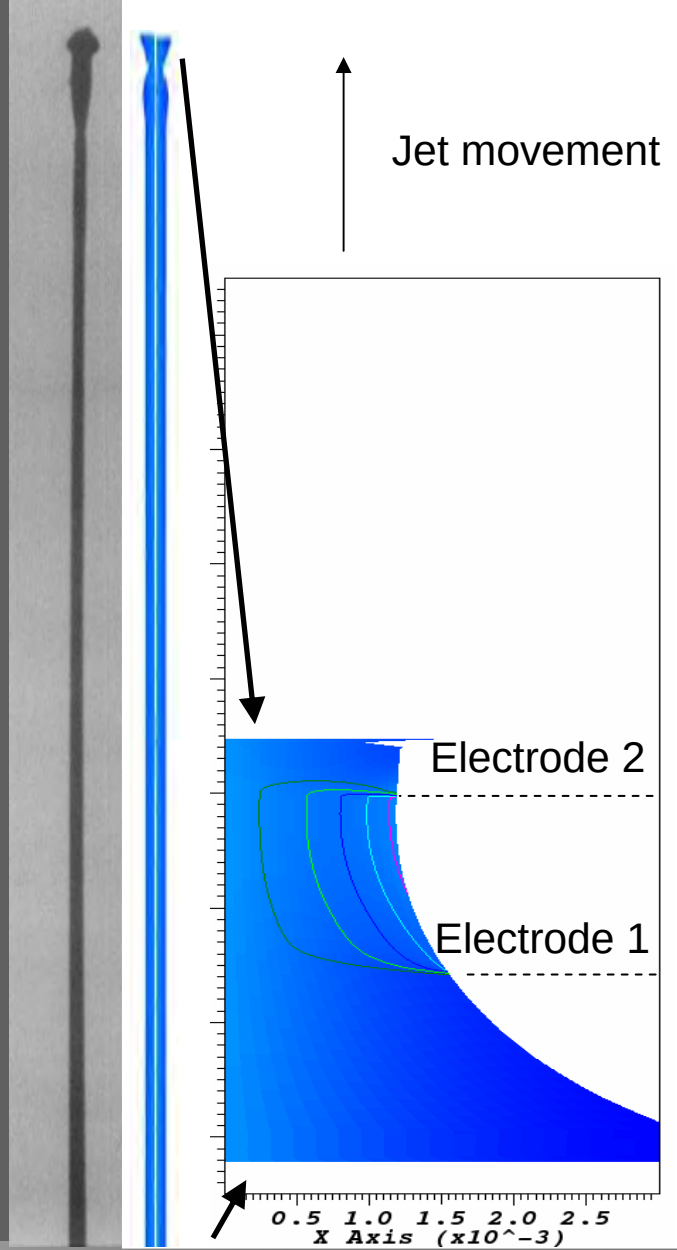


The jet enters electrode region

The jet transforms to discs or rings

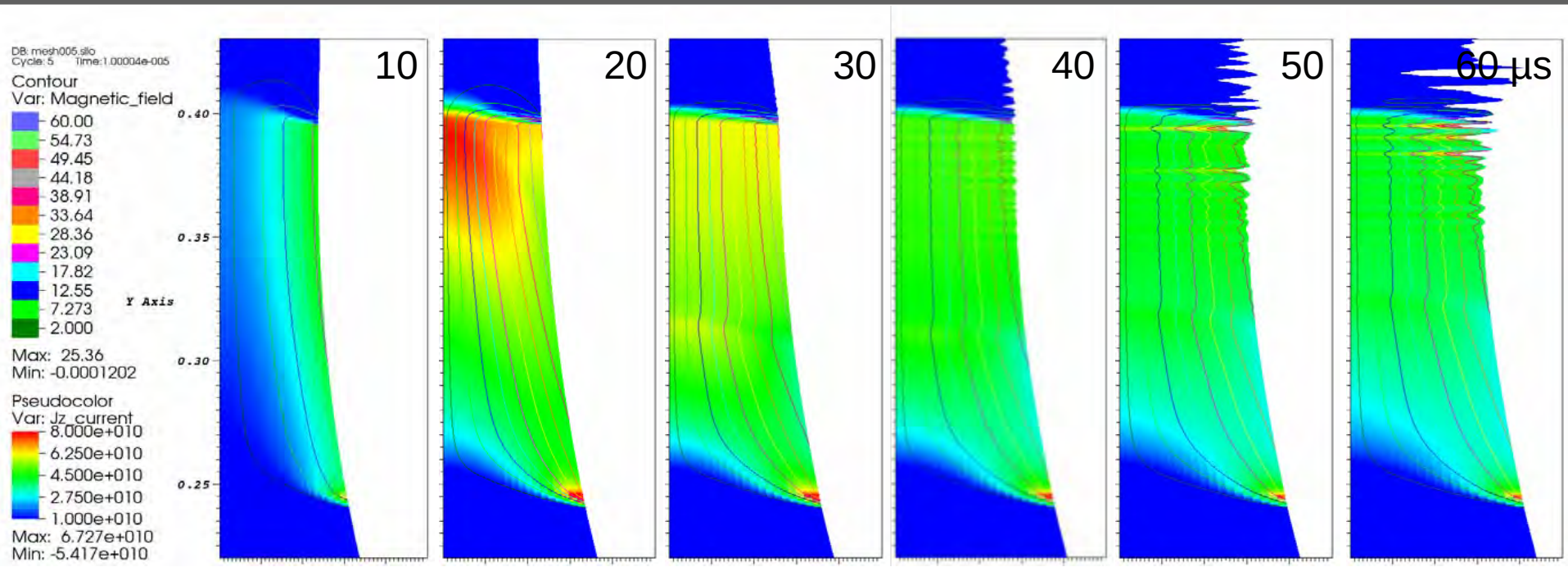
Modelling of jet – current interaction

- GRALE
  - Hydrodynamic 2D ALE code
    - Axial symmetry and plane problems
  - Magnetohydrodynamic (MDH) capability included
    - Only Lagrange-coordinates for the MHD-module
    - Pulsed power supply included as current source
  - Material model includes:
    - Thermal softening
    - Temperature dependent resistivity
    - Melt (vaporisation) energies



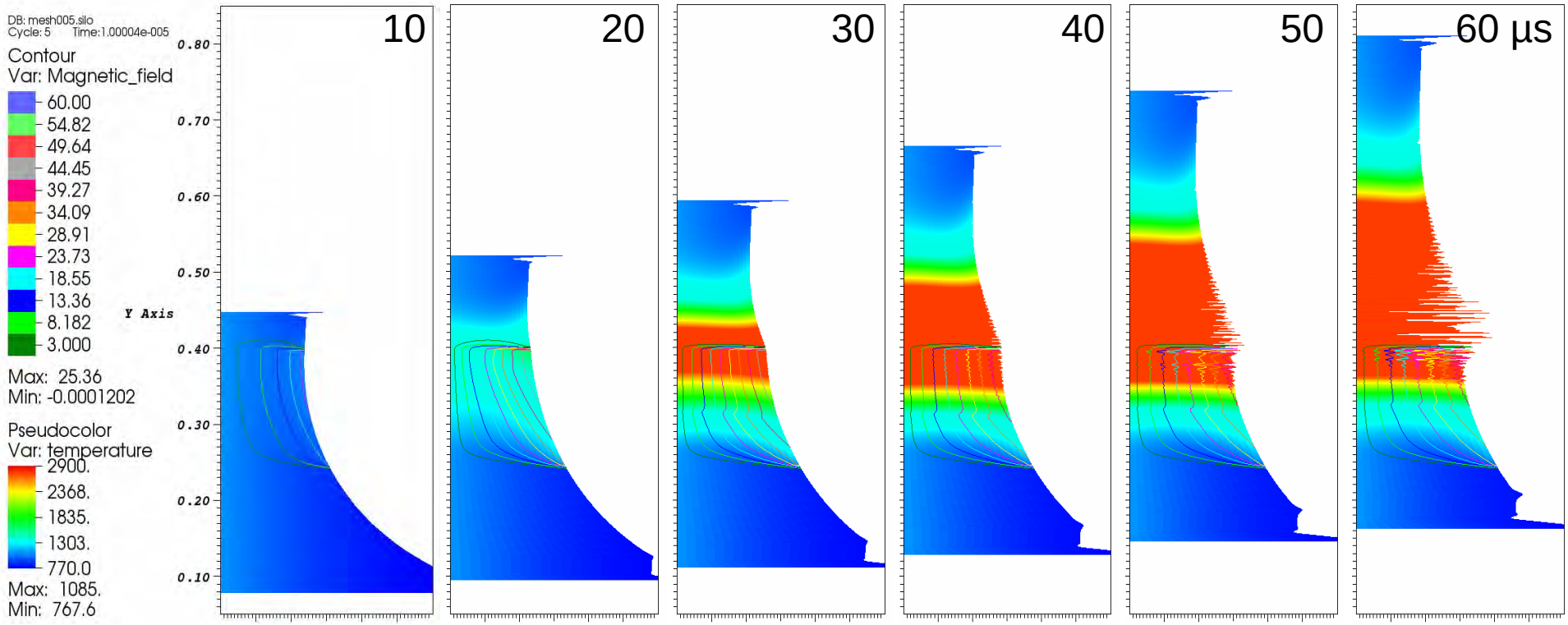
Current density and magnetic field (96 kJ)

- Diffusion of magnetic field and current into the jet (skin effect)
  - Homogeneous current distribution at times >30 µs



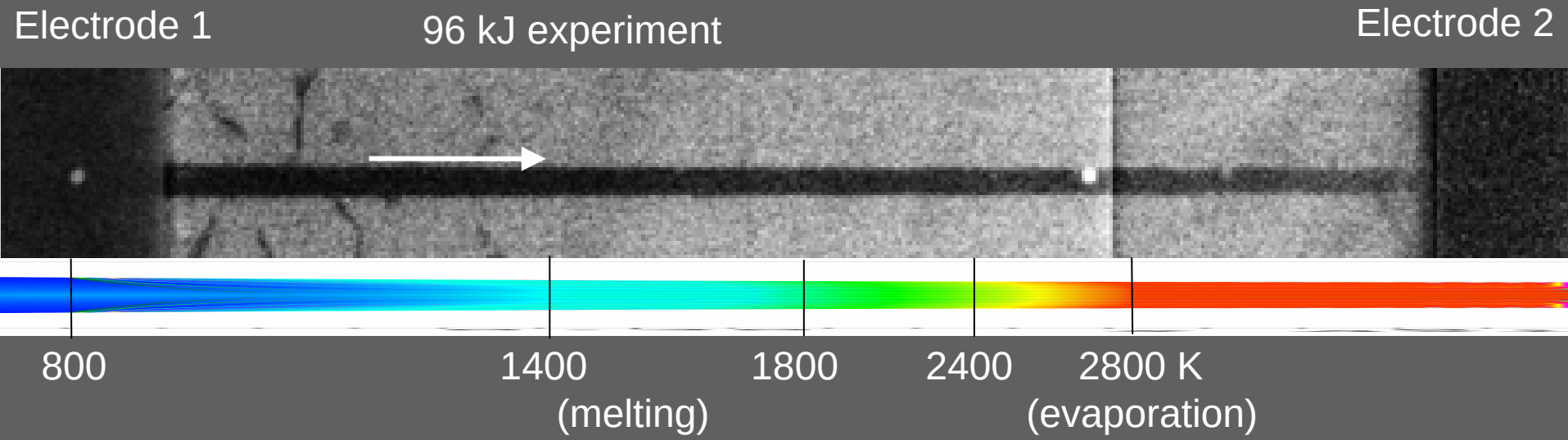
Temperature and magnetic field (96 kJ)

- Temperature distribution homogenous radially
  - Reaches melting- and evaporation temperatures rapidly



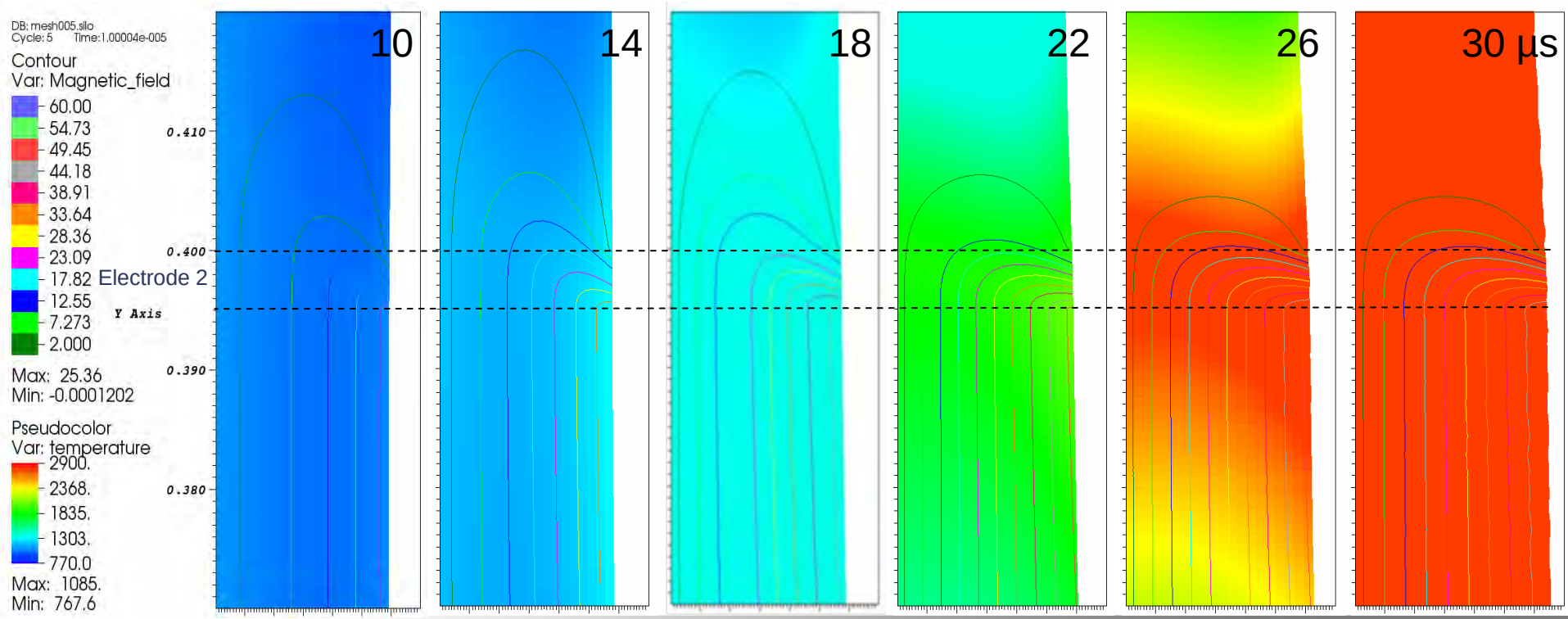
Temperature distribution (96 kJ)

- Temperature distribution homogenous radially
  - Reaches melting- and evaporation temperatures rapidly



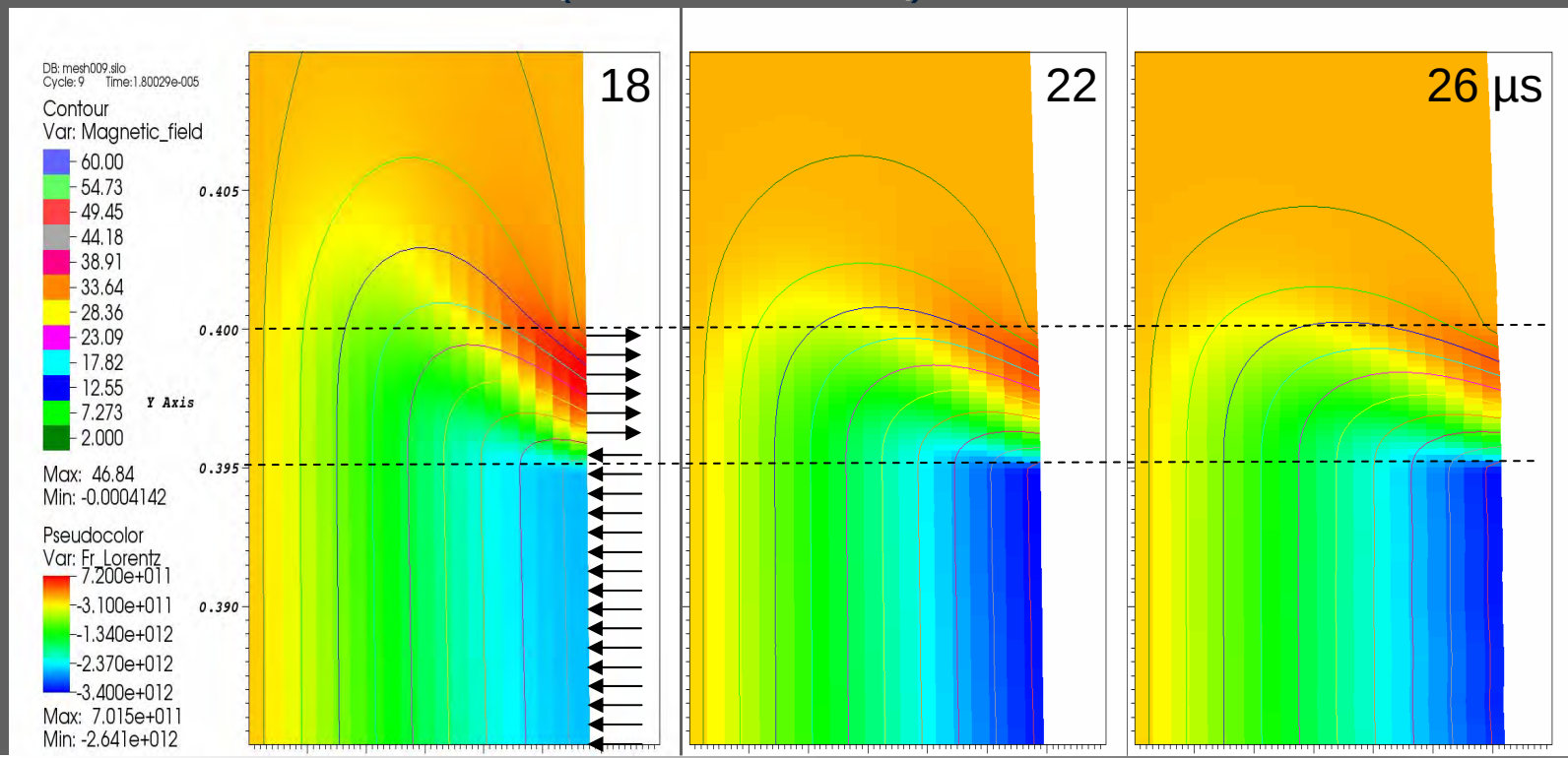
Magnetic field

- Magnetic field frozen in when conductivity is high (low temperature)
  - Diffusion velocity increases with temperature (low conductivity)



Lorentz force

- Radial component of the Lorentz' force is:
  - Compressible in-between electrodes (≈ 3 KN/mm^3)
  - Tensile at electrode 2 (≈ 0.7 KN/mm^3)

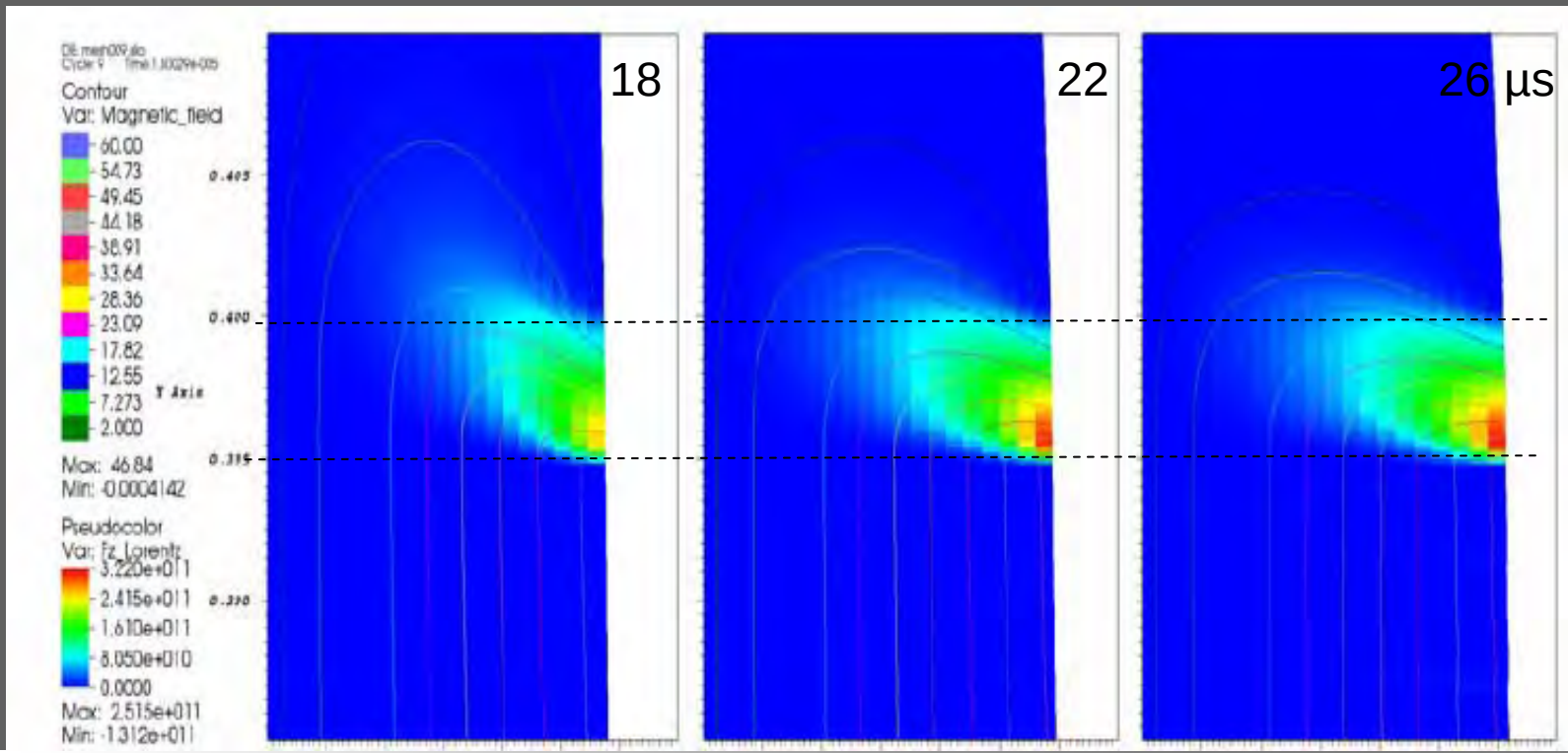


Electrode 2

Lorentz force

- Axial component of the Lorentz' force is:
  - Zero in-between electrodes
  - Tensile at electrode 2 (≈ 0.3 KN/mm^3)

Electrode 2



Conclusions

- The experiments shows:
  - Jet fragmentation (particulation) accelerates with increasing electric energy
    - Similar number of fragments (disks- or rings).
  - Close to exit of the electrode region, the jet is rapidly transformed into discs or rings
    - Radial velocity of around 200 m/s for the 96 kJ experiment

Conclusions

- Modelling shows:
  - The jet is homogenously heated radially
    - Temperature reaches vaporisation temperatures
  - Magnetic field is compressive in-between the electrodes
    - May enhance the natural necking of the stretching jet
  - Magnetic field is pulled out of the electrode region causing a rapid change in direction of magnetic forces
    - From compressive to tensile in radial direction
    - From zero to tensile in axial direction
- These tensile forces may contribute to the rapid disc- or ring formation after current interaction ends

RDECOM

TECHNOLOGY DRIVEN. WARFIGHTER FOCUSED.

Combined Effects Aluminized Explosives

Dr. Ernest L. Baker

L.I. Stiel, W. Balas, C. Capellos and J. Pincay

23 SEP 2008

Outline

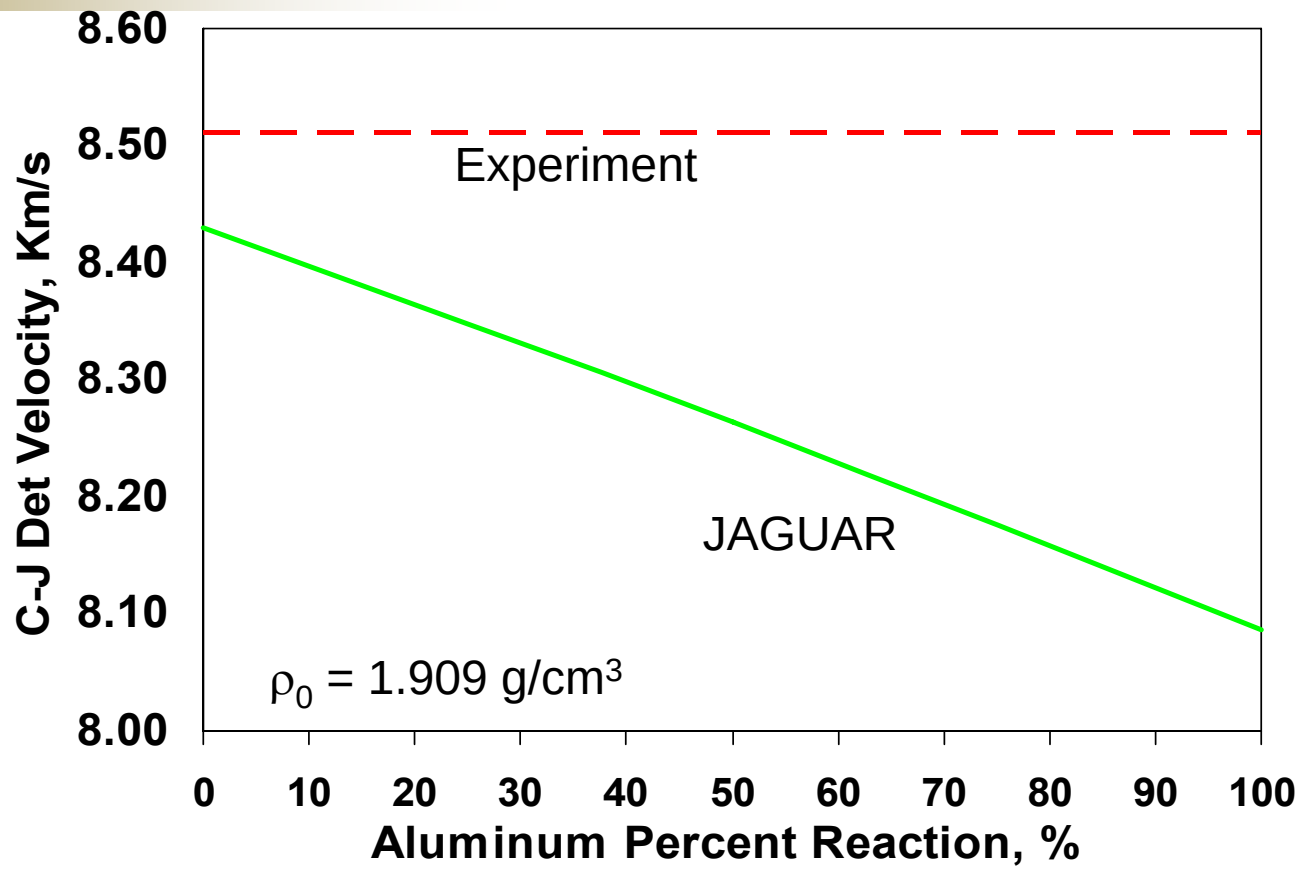
- Combined Effects Explosives
- Eigenvalue Detonation
- Detonation Velocities
- Cylinder Velocities
- Equations of State
- Conclusions

Combined Effects Explosive

- High Energy Explosive
  - High nitramine content
  - High early work output (before 7V/V0)
- High Blast Explosive
  - Typically aluminum and additional oxidizer
  - Later work output (after 7V/V0)
- Combined Effects Explosive
  - Nitramine with fine aluminum: micron & submicron
  - Aluminum reaction occurs very early and contributes to early work

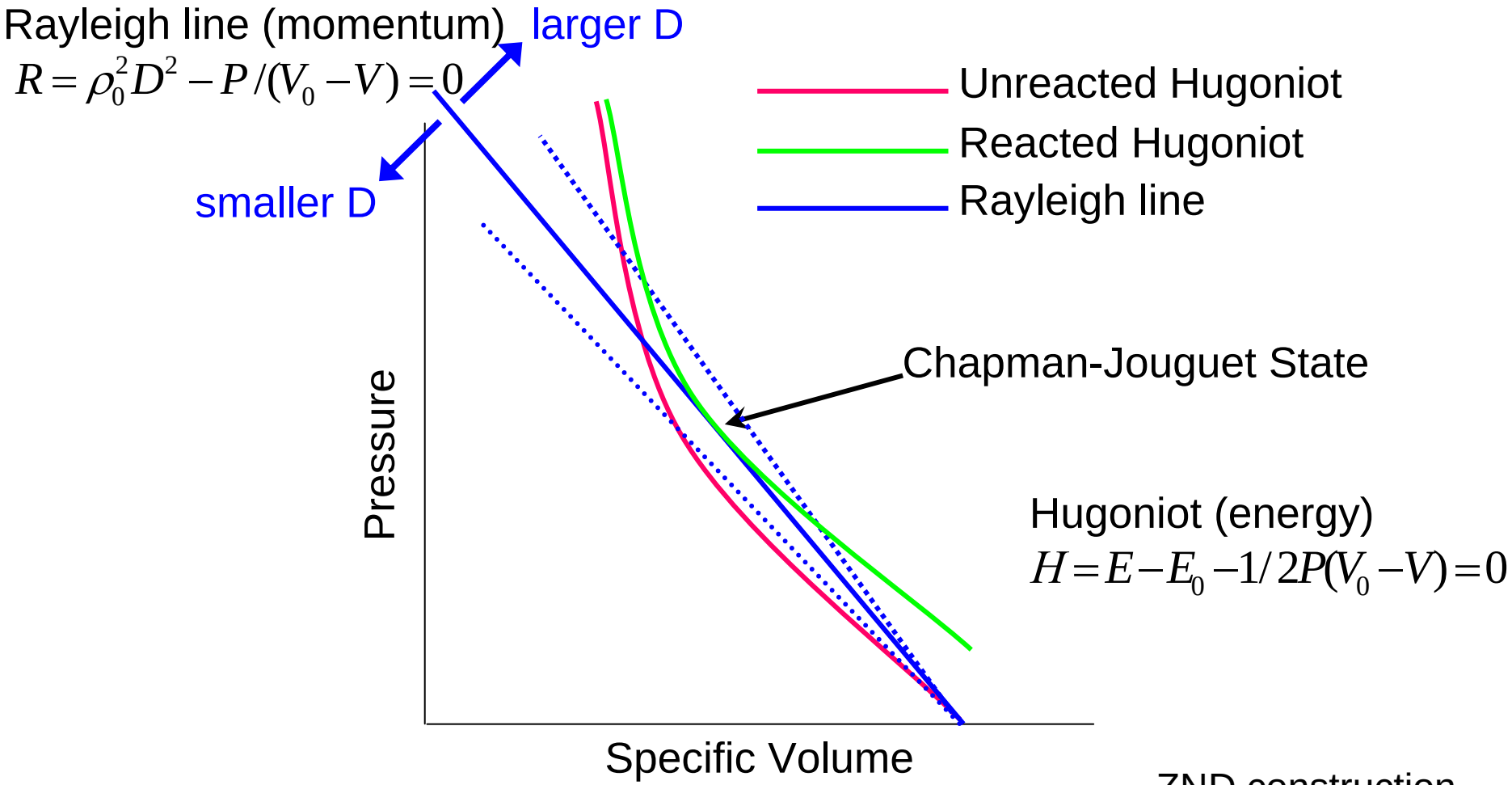
PAX-29: 77/15 Cl-20/Al
PAX-30: 77/15 HMX/Al
PAX-42 77/15 RDX/Al

Combined Effects Explosives PAX-30 (HMX, 15%Al)



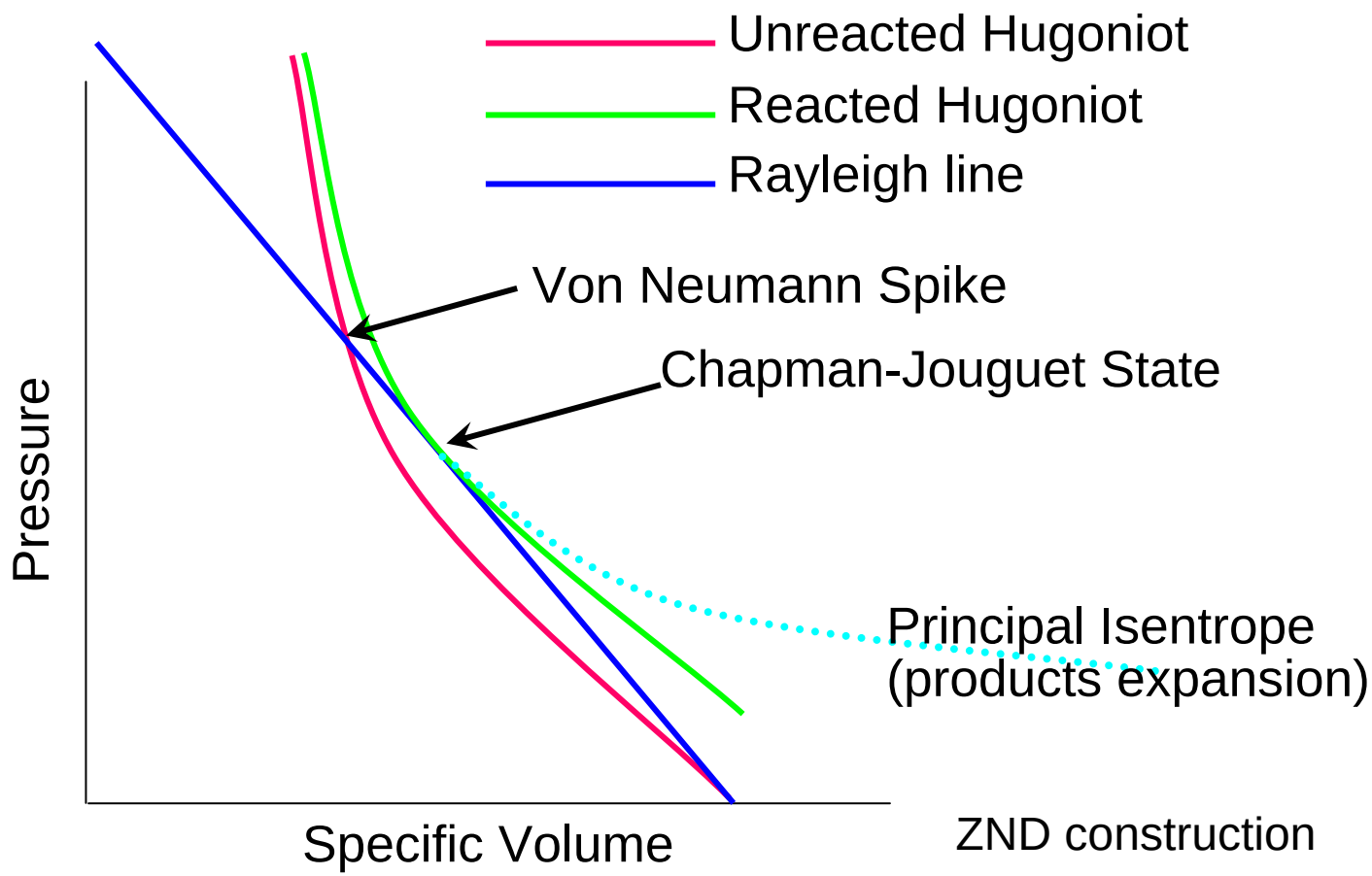
- ***C-J Detonation velocity decreases with extent of Al reaction***
- ***Experiments:***
  - ***–Detonation velocity agrees with 0% Al reaction***
  - ***–Cylinder velocity agrees with 100% Al reaction @ 7V/V0***
    0%: 1.69Km/s, 100%: 1.90Km/s, Experiment: 1.88Km/s

ZND Model

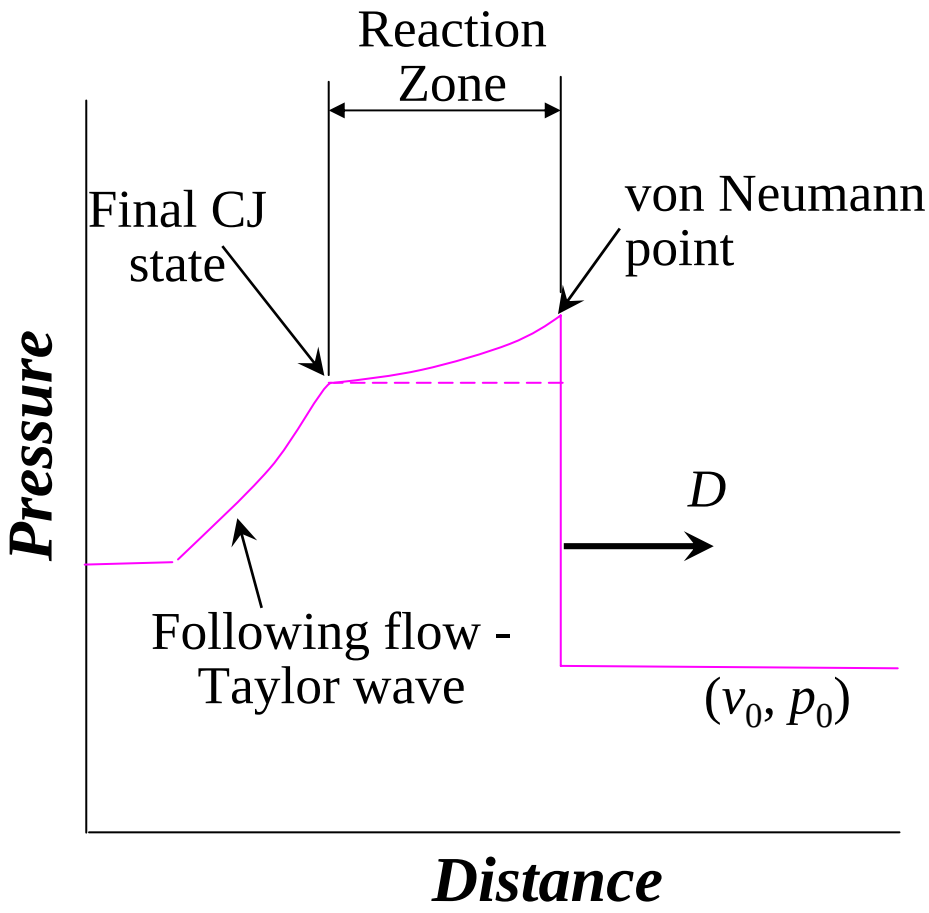


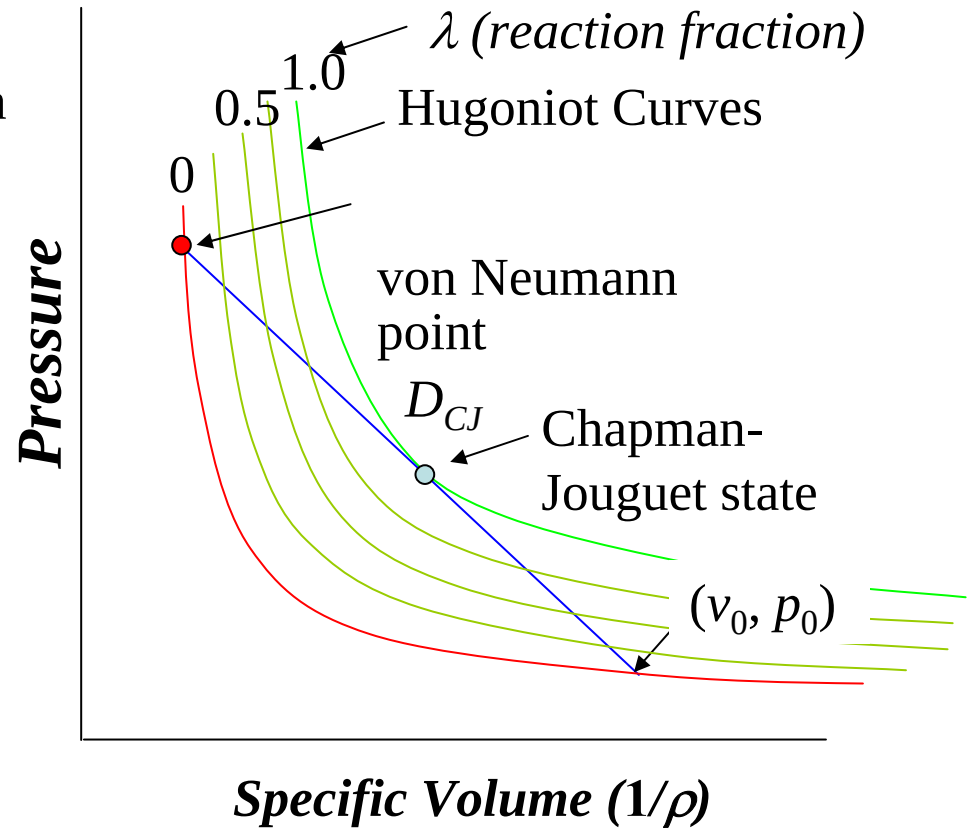
ZND construction

ZND Model

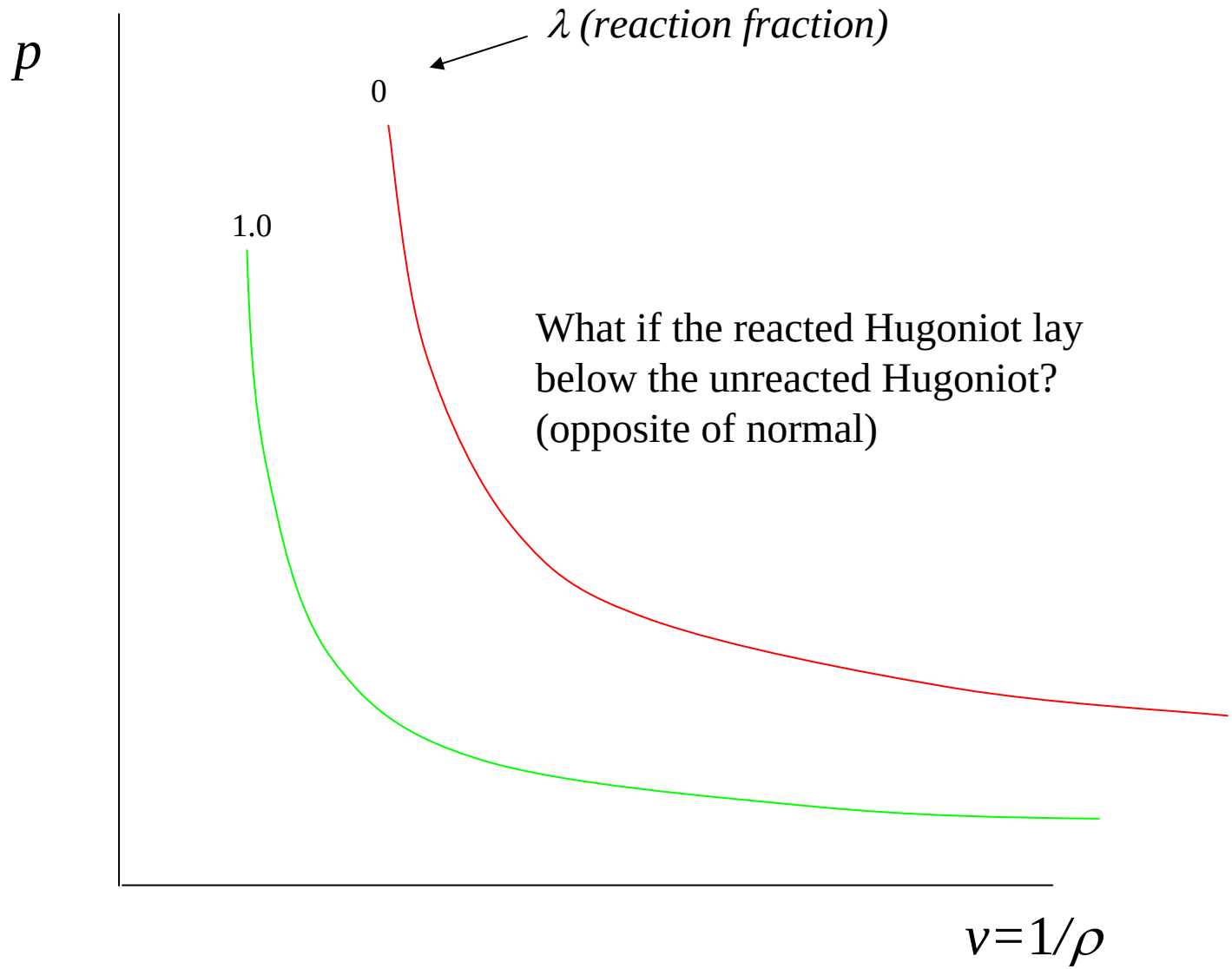

Unreacted Hugoniot
Reacted Hugoniot
Rayleigh line
Von Neumann Spike
Chapman-Jouguet State
Principal Isentrope
(products expansion)
Pressure
Specific Volume
ZND construction

ZND Model

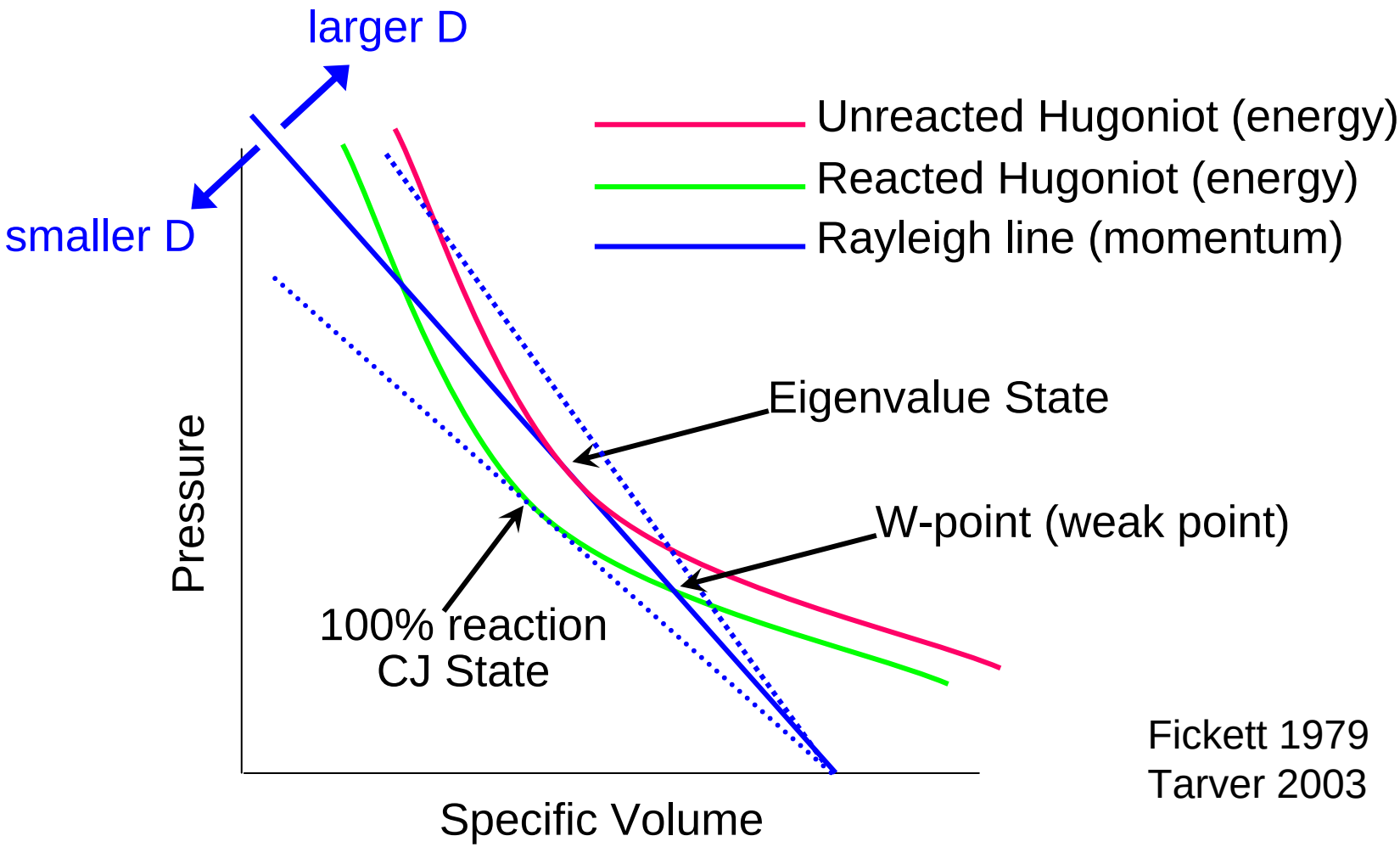

Reaction Zone
Final CJ state
von Neumann point
D
Following flow - Taylor wave
(v_0, p_0)
Pressure
Distance


λ (reaction fraction)
1.0
0.5
0
Hugoniot Curves
von Neumann point
D_{CJ}
Chapman-Jouguet state
(v_0, p_0)
Pressure
Specific Volume (1/ρ)

Eigenvalue Detonation

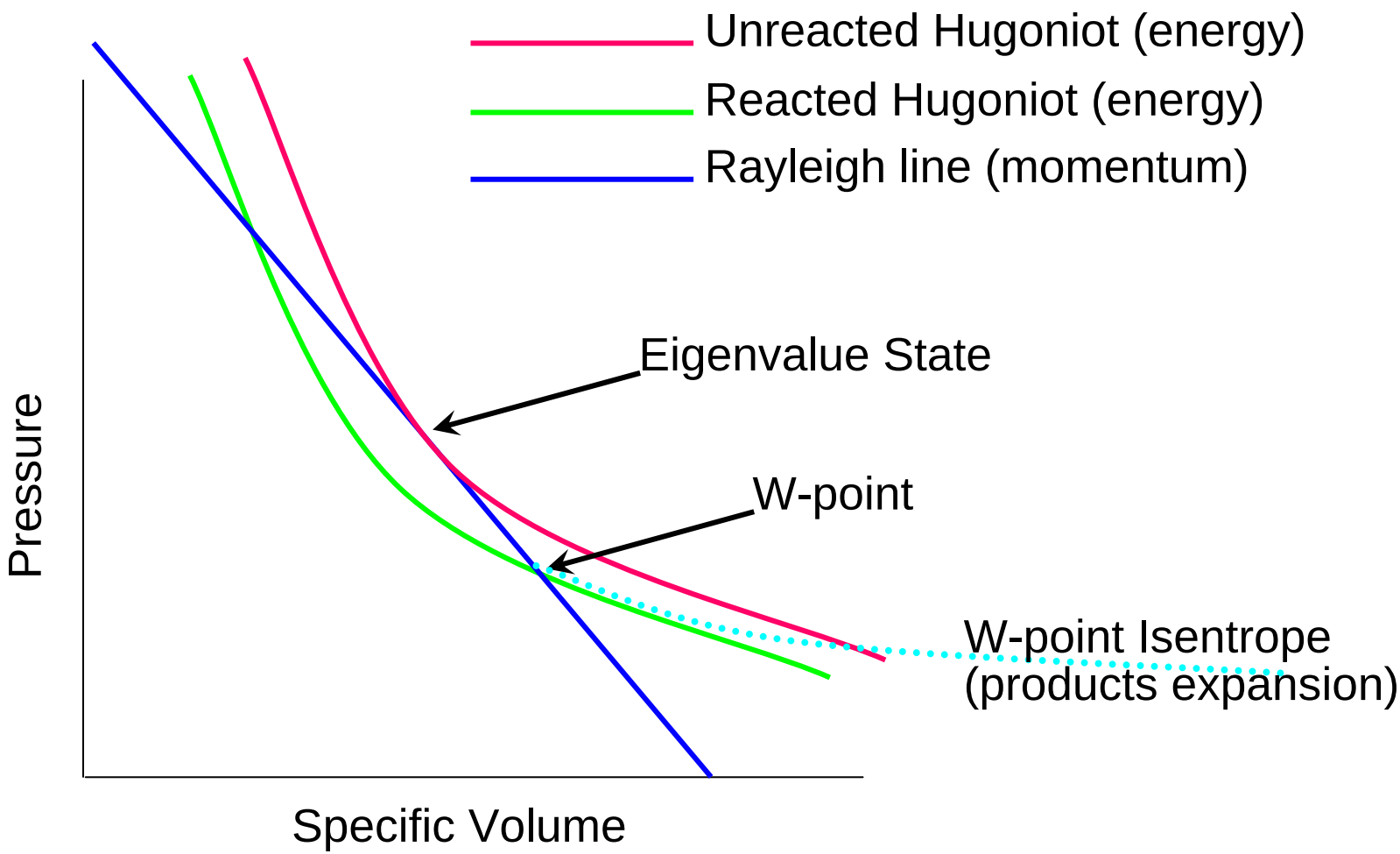


Eigenvalue Detonation

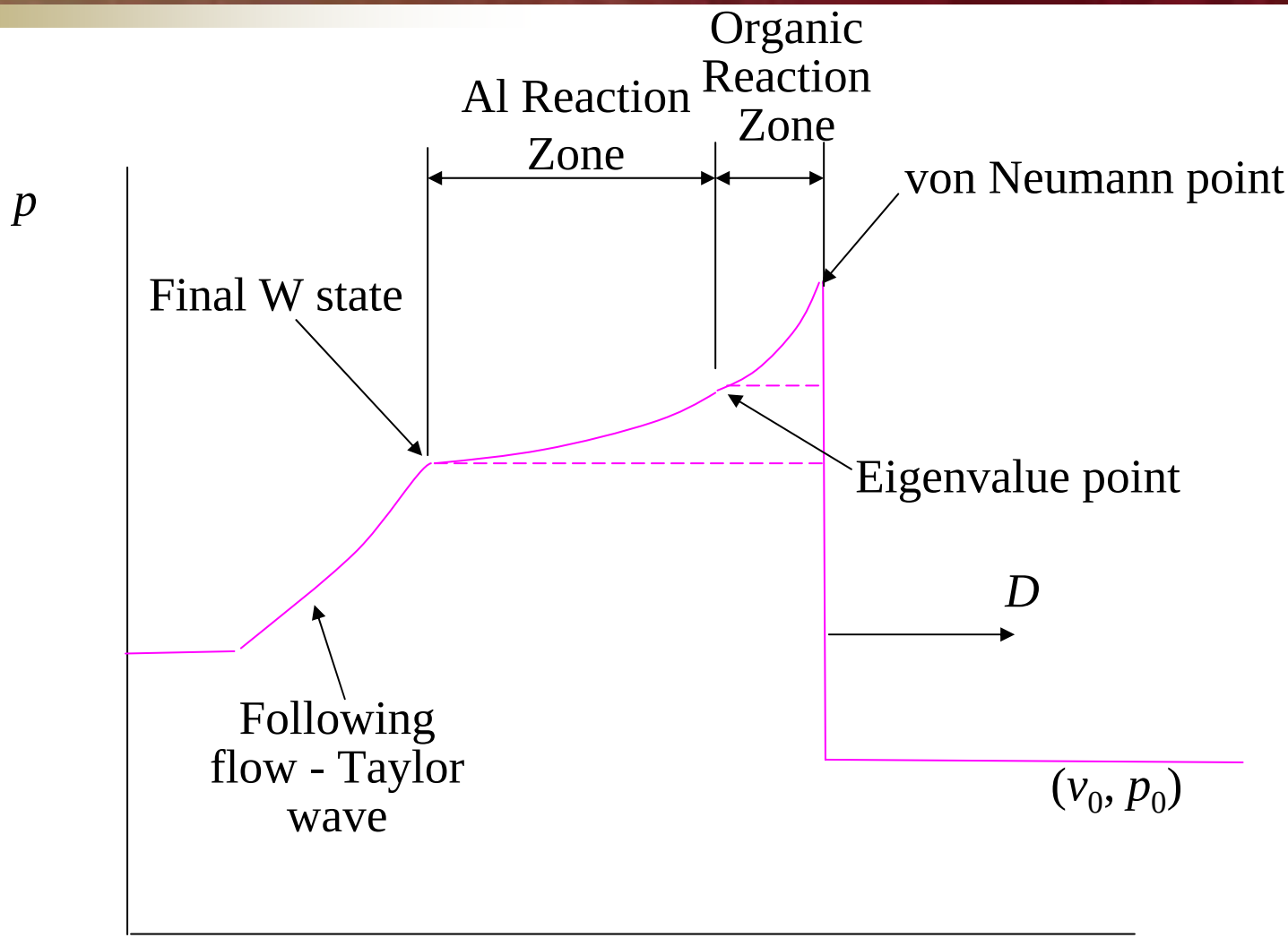


Fickett 1979
Tarver 2003

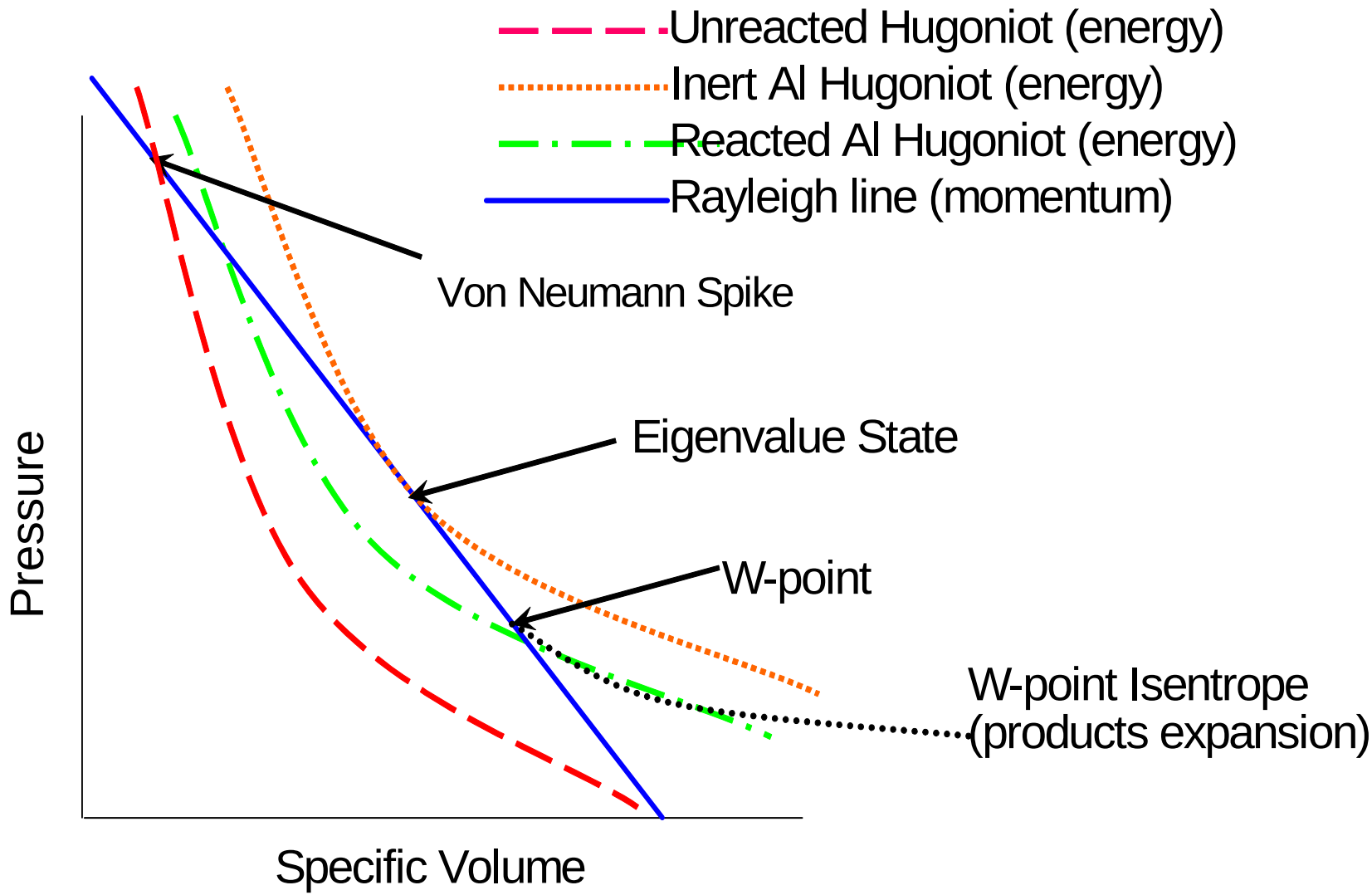
Eigenvalue Detonation



Eigenvalue Detonation Aluminized Explosive



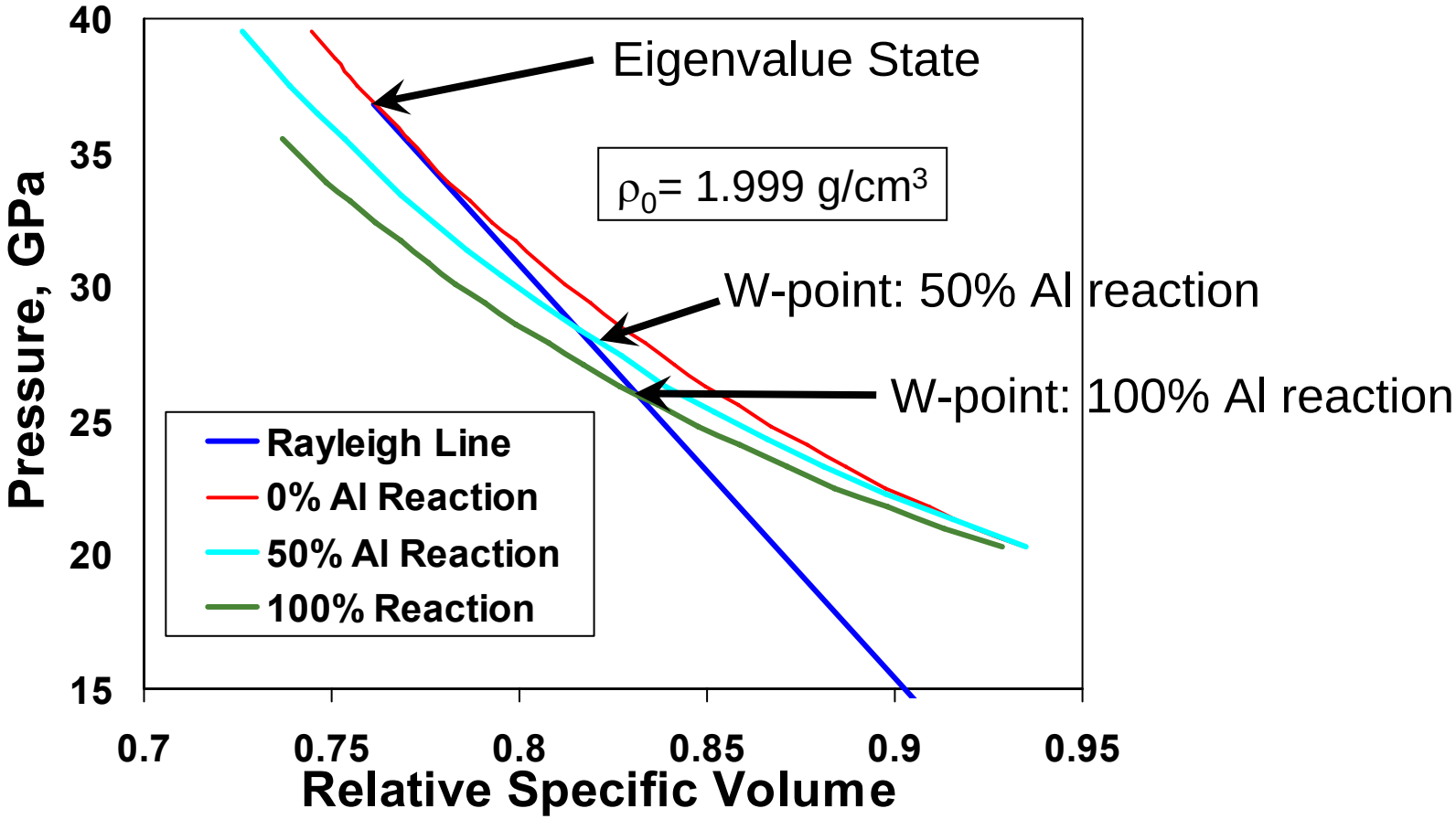
Eigenvalue Detonation Aluminized Explosive



Eigenvalue Detonation Combined Effects Explosive

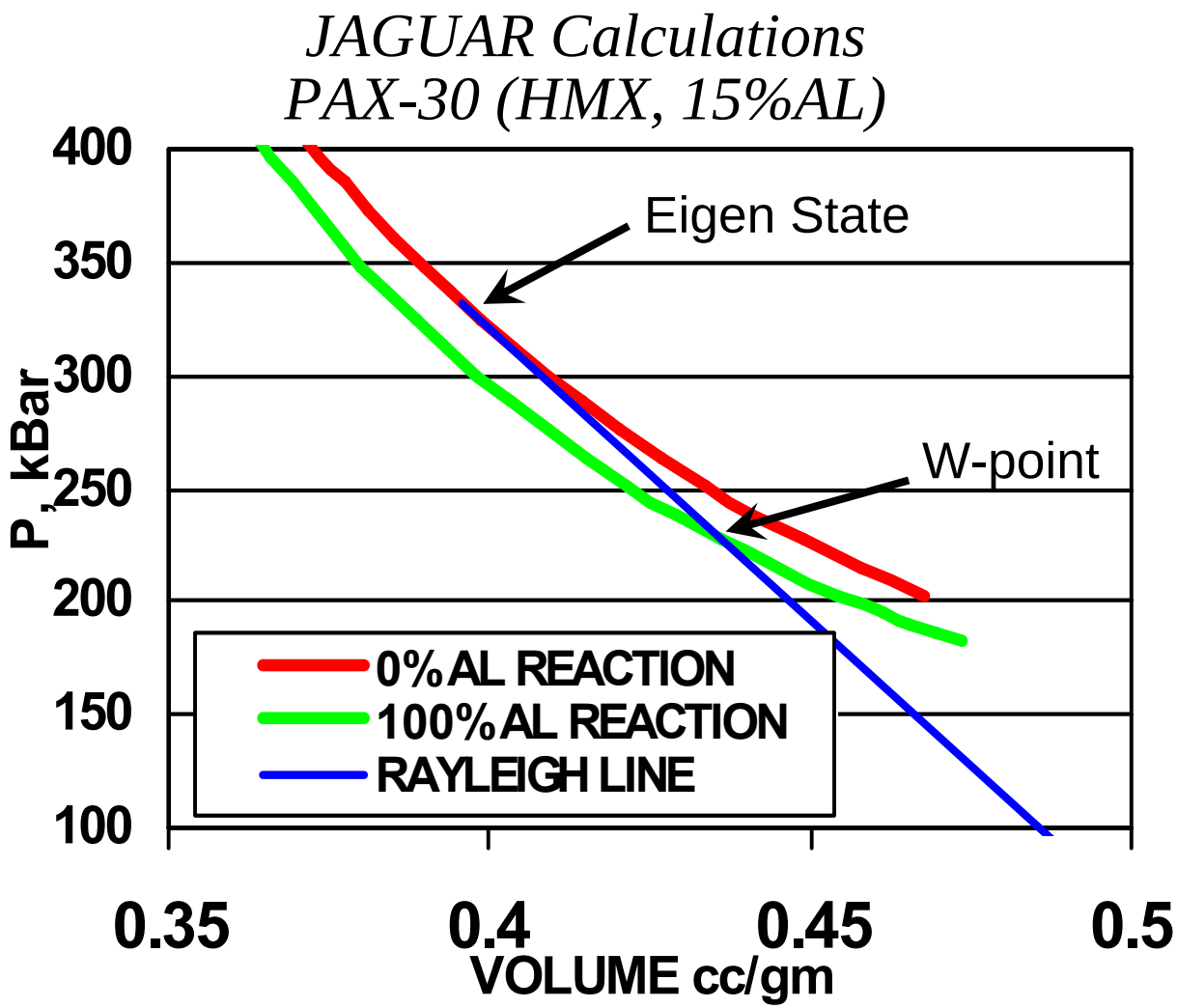
JAGUAR Calculations

PAX-29 (CL-20, 15%Al)



Aluminum reaction produces lower Hugoniots

Eigenvalue Detonation Combined Effects Explosive



Detonation velocity controlled by 0% AL reaction Hugoniot!

Detonation Velocity Aluminized Explosives Data

EXPLOSIVE	Al%	ρ_0(gm/cc)	Experiment D (Km/s)	JAGUAR Calculations Inert Al D (Km/s)	JAGUAR Calculations Reacting Al D (Km/s)
HMX	5	1.84	8.71	8.66	8.53
HMX	15	1.87	8.45	8.42	7.95
HMX	25	1.95	8.55	8.35	7.32
BTNEN	15	1.96	8.29	8.38	7.45
BTNEN	15	1.91	8.06	8.16	7.24
NG	15	1.74	7.94	8.07	7.93
TNT	20	1.64	6.41	6.38	5.77
TNT	30	1.84	6.74	6.63	4.92
TNT	10	1.67	6.51	6.68	6.52
PAX-3	18	1.87	7.96	8.05	7.65
PAX-29	15	2.0	8.95	8.79	8.16
PAX-30	15	1.91	8.51	8.43	8.09
PAX-42	15	1.83	8.25	8.14	7.75
			AVERAGE ERROR %	**1.22**	**7.52**

Detonation velocities agree with little or no aluminum reaction

Cylinder Velocity
Analytic Cylinder Model

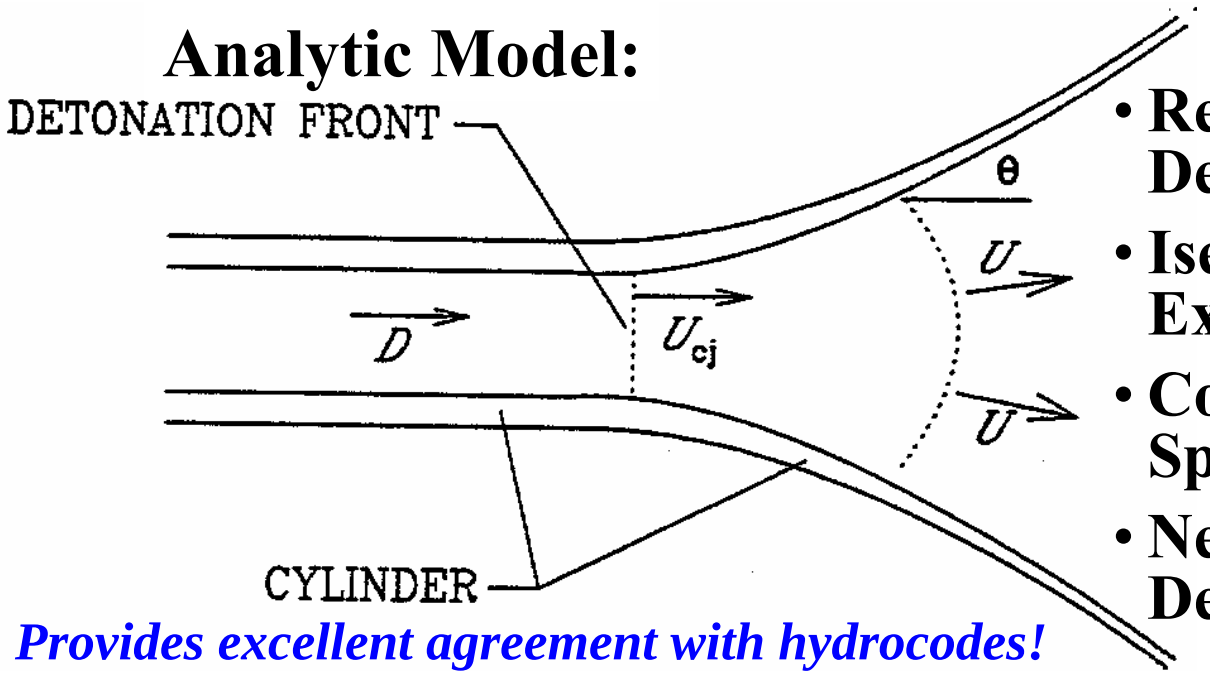
JWLB Equation of State:

$$P = \sum_i \mathrm{A}i\left(1 - \frac{\lambda}{\mathrm{R}iV^*}\right)e^{-\mathrm{R}iV^*} + \frac{\lambda E}{V^*} + \mathrm{C}\left(1 - \frac{\lambda}{\omega}\right)V^{*-(\omega+1)}$$

Gruneisen Parameter:

$$\lambda \equiv \sum\left(\mathrm{A}\lambda\mathrm{i}V^* + \mathrm{B}\lambda\mathrm{i}\right)e^{-\mathrm{R}\lambda iV^*} + \omega$$

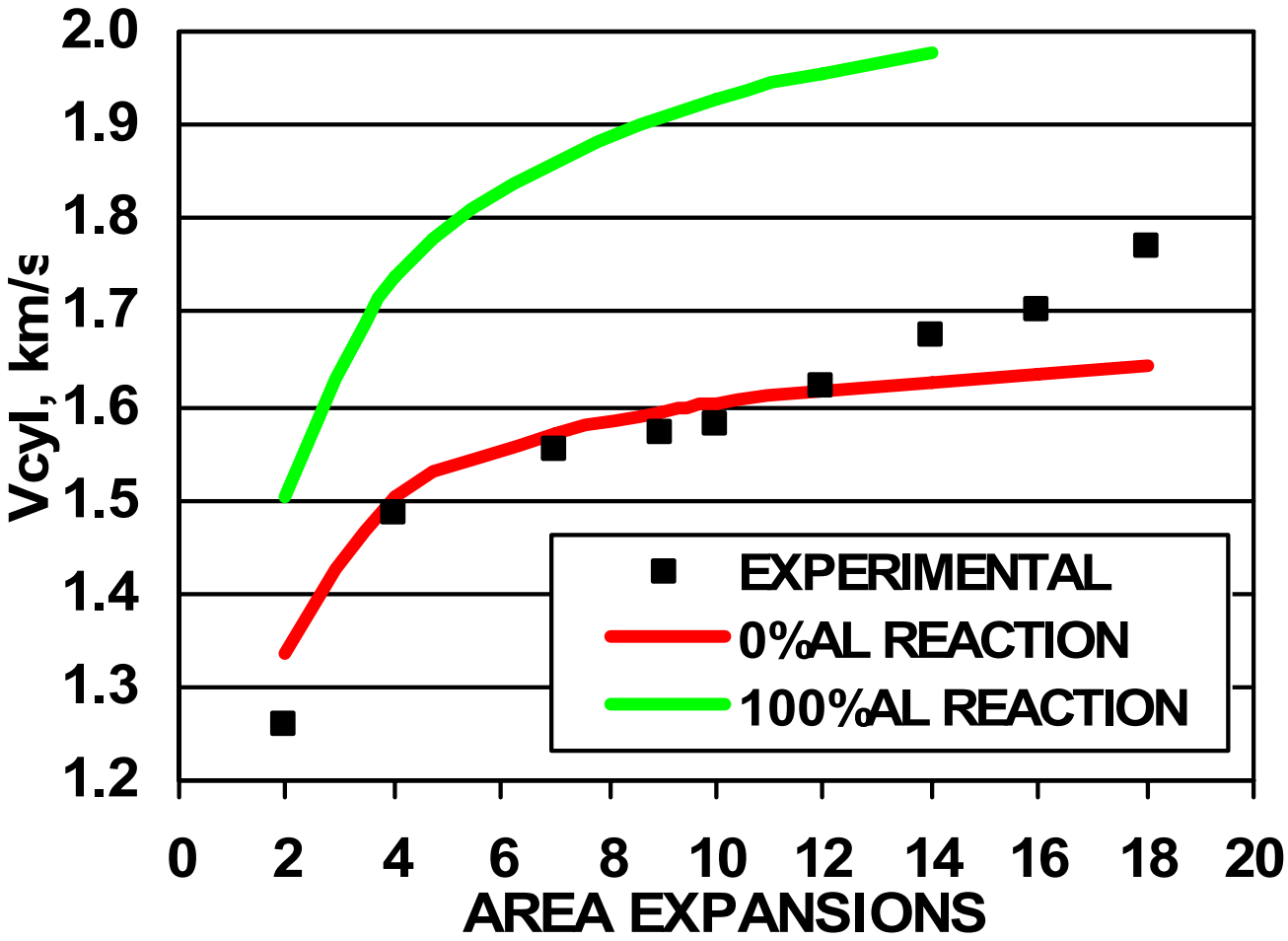
Analytic Model:



- **Reference Frame at Detonation Velocity**
- **Isentropic Products Expansion**
- **Constant Properties Along Spherical Surfaces**
- **New: Modified for Eigen Detonation W-point**

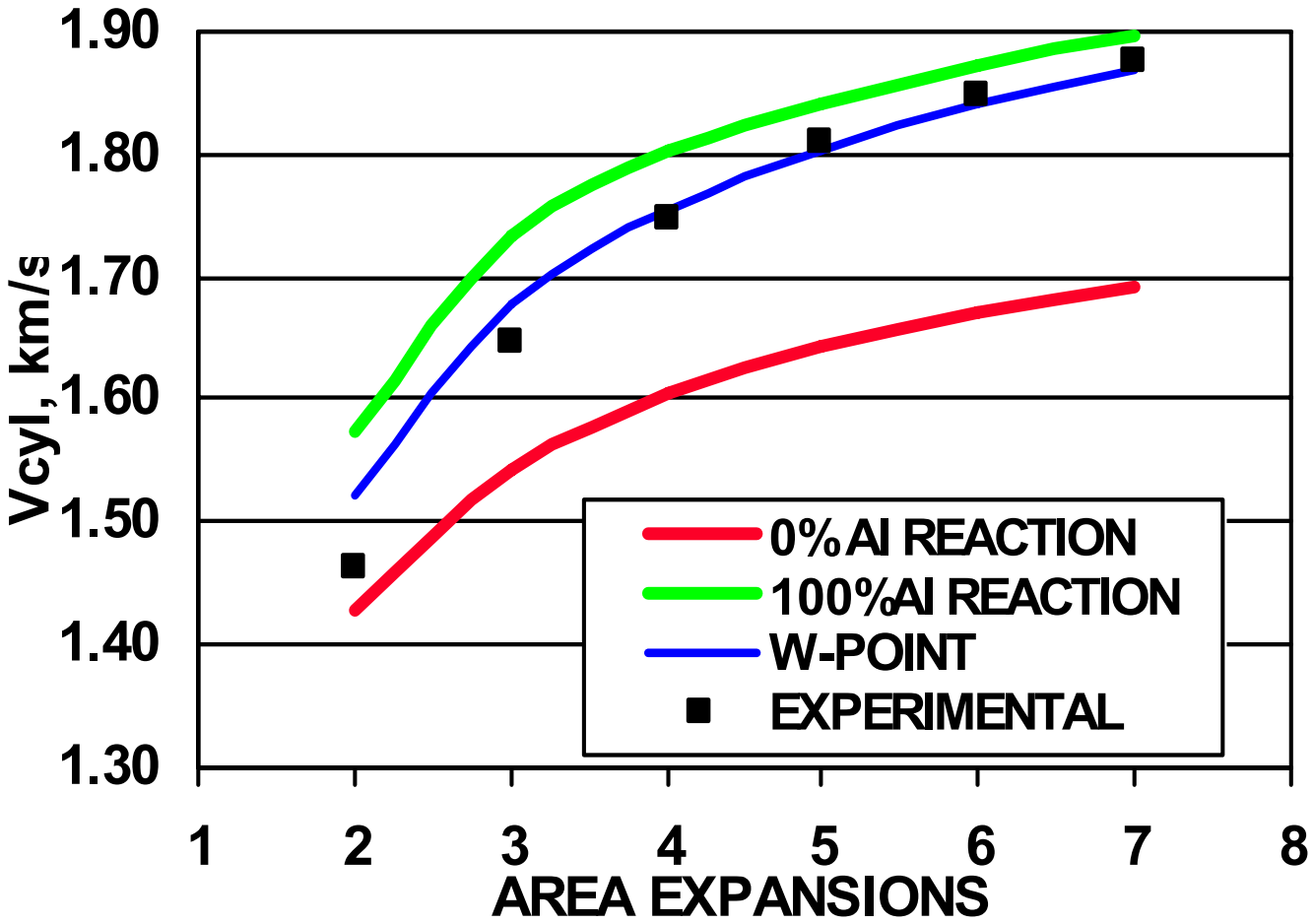
Provides excellent agreement with hydrocodes!

Cylinder Test Results
PAX-3 (HMX, 18%AL - large)



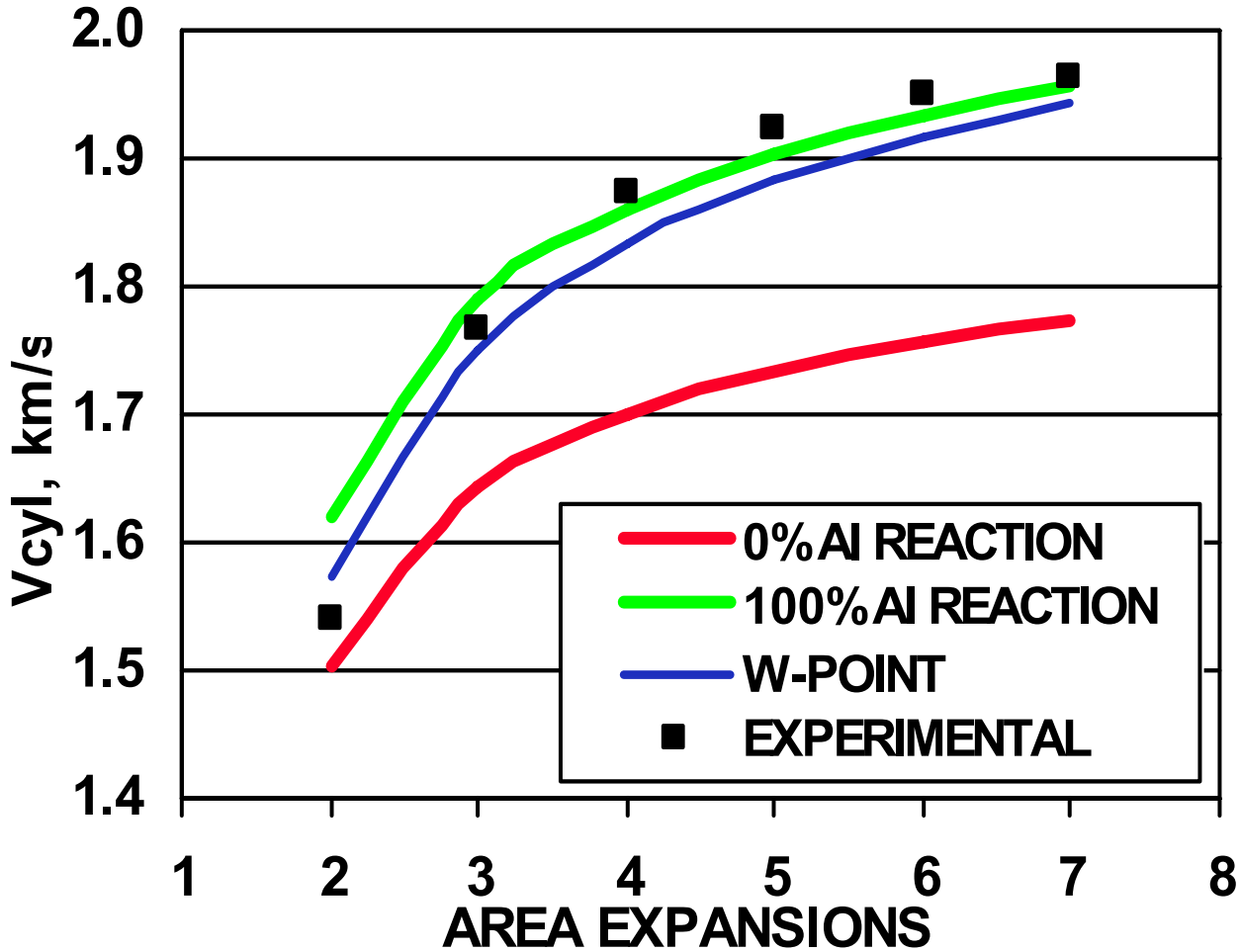
HMX with large particle size Aluminum: AL reacts late!

Cylinder Test Results
PAX-30 (HMX, 15%AL - small)



HMX with small particle size aluminum: AL reacts early!

Cylinder Test Results
PAX-29 (CL-20, 15%AL - small)



CL-20 with small particle size Aluminum: AL reacts early!

JWLB Equations of State

	PAX-3 (Al INERT)	PAX-29	PAX-30	PAX-42
ρ0 (g/cc)	1.866	1.999	1.885	1.827
E0 (Mbar)	0.08223	0.14611	0.13568	0.13109
D (cm/μs)	0.8023	0.8784	0.8342	0.8137
P (Mbar)	0.2937	0.2599	0.2419	0.2339
A1 (Mbar)	601.643	400.407	406.224	400.717
A2 (Mbar)	3.9482	82.630	135.309	16.5445
A3 (Mbar)	0.9403	1.5507	1.311	1.45169
A4 (Mbar)	0.049688	0.006126	0.006772	0.006103
R1	13.6055	20.9887	26.9788	13.6945
R2	3.69901	9.6288	10.6592	8.67402
R3	24.9093	24.2441	2.52342	2.5320
R4	1.04285	0.328128	0.335585	0.33570
C (Mbar)	0.007691	0.014626	0.013561	0.014057
ω	0.27780	0.24286	.234742	0.242371

D and P are from W-Point (not C-J values)

JWL Equations of State

	LX14	PAX-2A	PAX-29	PAX-30	PAX-42
ρ0 (g/cc)	1.819	1.770	1.999	1.885	1.827
E0 (Mbar)	0.10213	0.09953	**0.14714**	**0.135755**	**0.12994**
D (cm/μs)	0.8630	0.8391	0.8784	0.8342	0.8137
P (Mbar)	0.3349	0.3124	0.2599	0.2419	0.2339
A1 (Mbar)	26.1406	27.0134	8.58373	7.19151	13.8484
A2 (Mbar)	.763619	.762675	0.168261	0.097112	0.145102
R1	6.93245	7.22237	4.7726	4.59098	5.74864
R2	1.94159	1.95979	1.03613	0.84089	0.99404
C (Mbar)	0.010994	0.010919	0.014556	0.013492	0.015193
ω	0.384193	0.375812	0.242252	0.233665	0.253095

Combined effects explosives: note large blast energies!

Conclusions

- New combined effects explosives produce both high metal pushing (early) and high blast (late) work output.
- Detonation velocities agree with little or no Al reaction even with sub-micron particles
- However, with small particles, complete Al reaction is indicated during early products expansion
- Eigen detonation theory used for EOS development

Interface Defeat for Unconfined SiC Ceramics

Th. Behner[1], Ch. E. Anderson Jr.[2], T. J. Holmquist[3]
M. Wickert[1], and D. W. Templeton[4]

[1] Fraunhofer Institut für Kurzzeitdynamik (EMI), Eckerstr. 4, 79104 Freiburg, Germany

[2] Southwest Research Institute, P.O. Drawer 28510, San Antonio, TX 78228, USA

[3] Southwest Research Institute, 5353 Wayzata Blvd., Minneapolis, MN 55416, USA

[4] U.S. Army TARDEC-RDECOM, AMSRD-TAR-R, Warren, MI 48397, USA



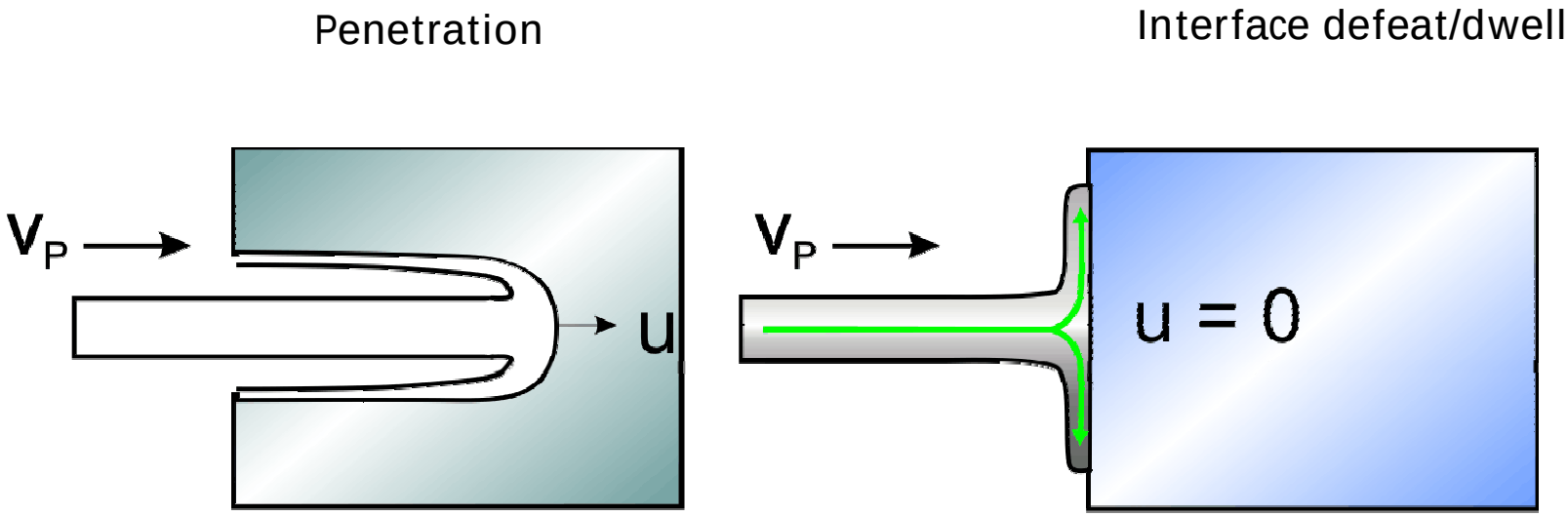




Motivation - Objectives

- Interface defeat/dwell on ceramics

  ➡ ideal mechanism for an passive armor system



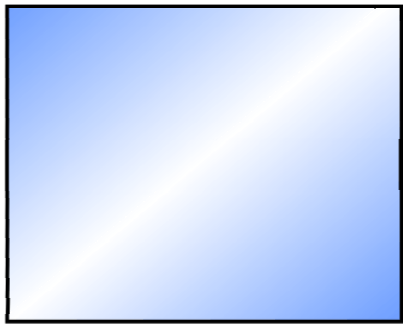
Behner 09/2008

© 2008 Fraunhofer EMI

Fraunhofer EMI Institut Kurzzeitdynamik Ernst-Mach-Institut

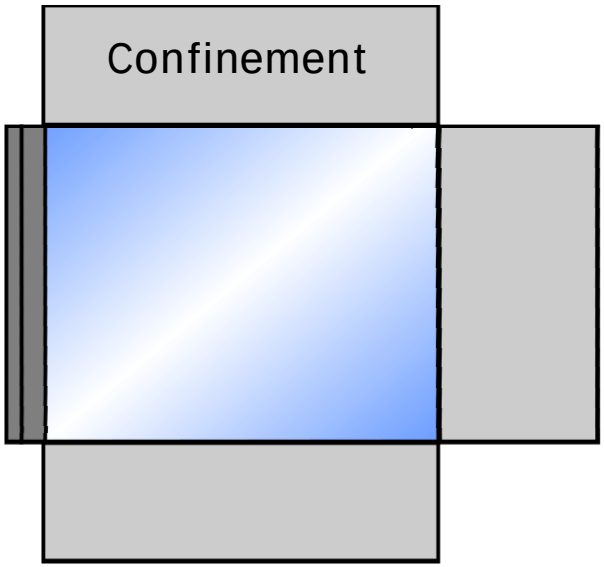
Motivation - Objectives

- Experimental study with an unconfined target design
  - ➡ focuses on dwell potential of the material and not on target arrangement
  - ➡ input for numerical model



Unconfined

Coverplate system



Behner 09/2008

© 2008 Fraunhofer EMI

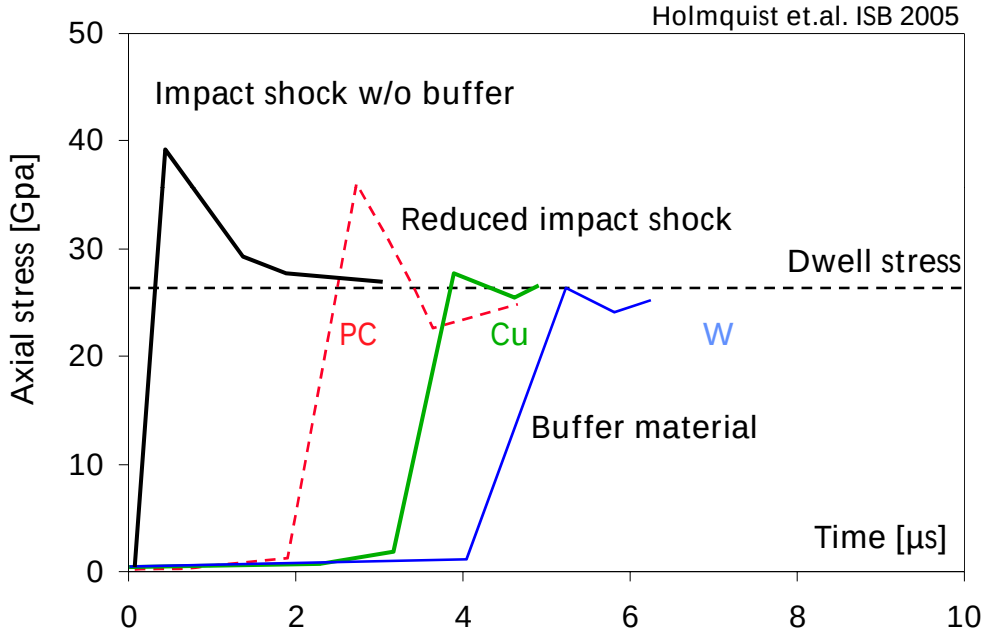
Fraunhofer EMI Institut Kurzzeitdynamik Ernst-Mach-Institut

TARDEC

Motivation - Objectives

- Buffering the impact shock

  ➡ increase transition velocity for interface defeat substantially



Behner 09/2008

© 2008 Fraunhofer EMI

Fraunhofer EMI Institut Kurzzeitdynamik Ernst-Mach-Institut

Experimental Set-Up

- Target: SiC-N cylinders, 35 mm long , Ø 20 mm
  - 3 types: ➡ bare
    - ➡ small Cu-buffer (Ø 5 mm, 4 mm height)
    - ➡ 20 mm Ø Cu-plate with 2 mm height

- Penetrator: pure gold rods (70 mm with Ø 1 mm)
  - ➡ low strength but high density
  - ➡ @ 1.6 km/s pressure/stress at target interface same as for WSA

- Reverse ballistic method
  - ➡ target launched at stationary rod

- Impact velocity v_P from 750 to 1700 m/s



Behner 09/2008

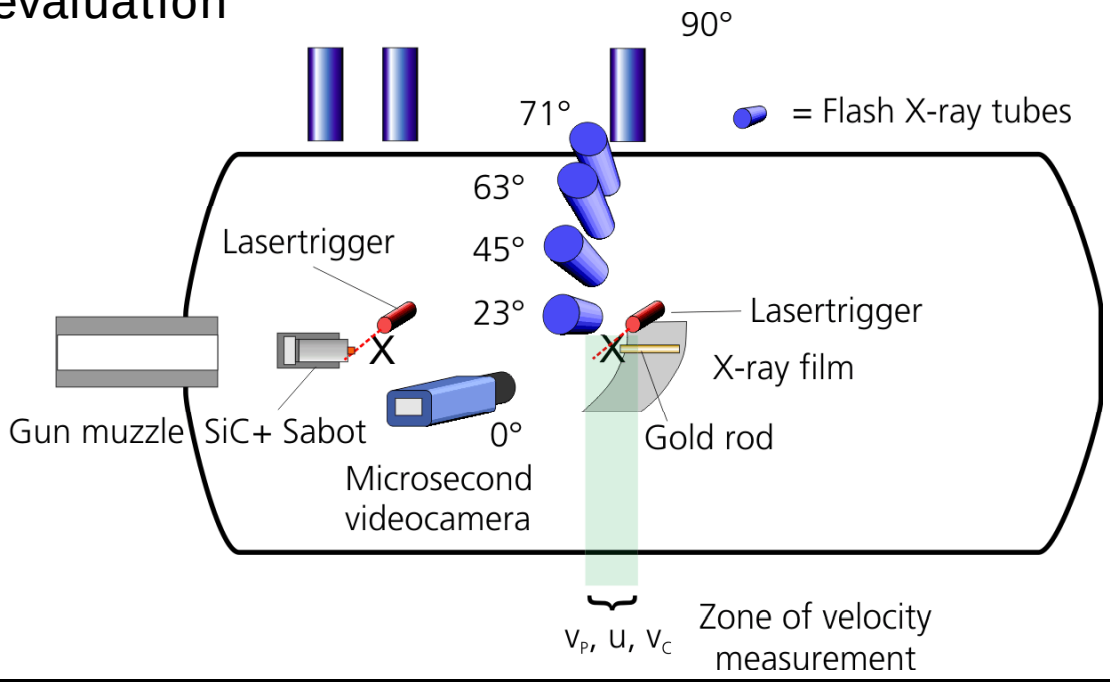
© 2008 Fraunhofer EMI

Fraunhofer EMI Institut Kurzzeitdynamik Ernst-Mach-Institut

TARDEC

Experimental Set-Up

- 5 X-ray tubes in a single plane to monitor impact
- Optional a Microsecond video camera (up to 1 MFps) for optical evaluation
- All velocities measured in zone of impact
  - ➡ high accuracy necessary



Behner 09/2008

© 2008 Fraunhofer EMI

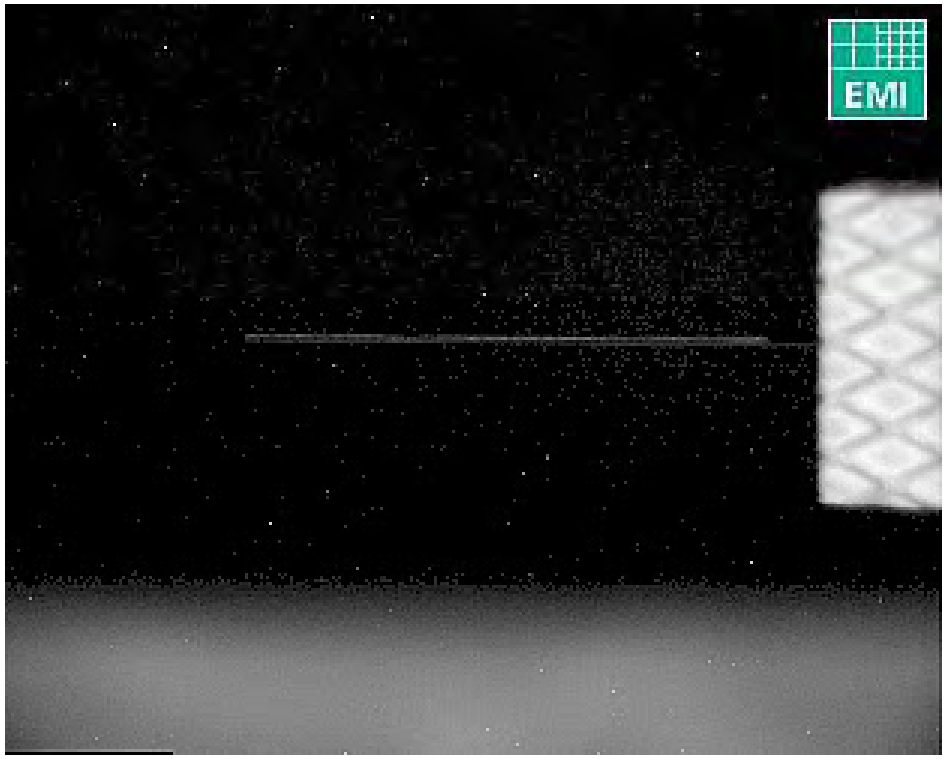
Fraunhofer EMI Institut Kurzzeitdynamik Ernst-Mach-Institut

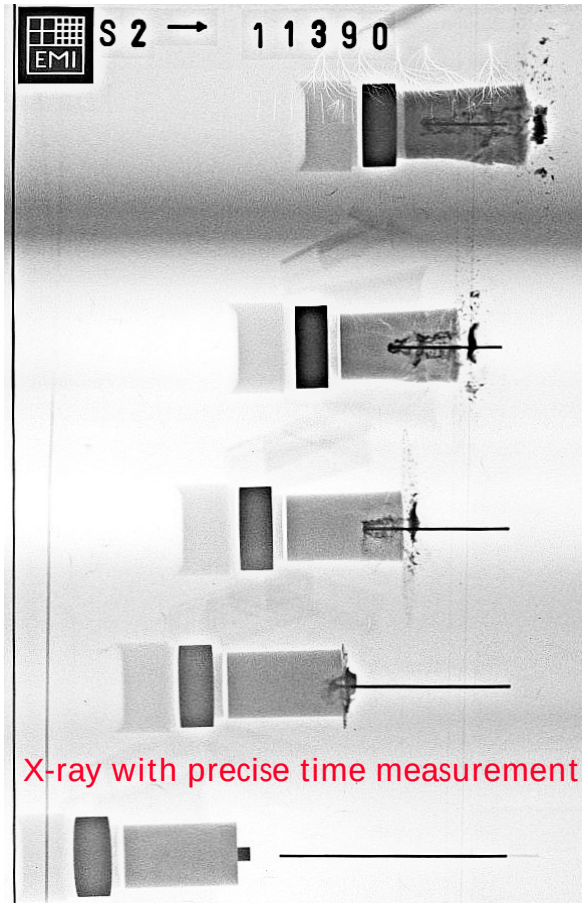
TARDEC

Observation of Dwell/Penetration

Exp. 11390, v_P = 1550 m/s

Video: 2 µs interframe time / 500 ns exposure





X-ray with precise time measurement

Behner 09/2008

© 2008 Fraunhofer EMI

Fraunhofer Institut Kurzzeitdynamik Ernst-Mach-Institut

TARDEC

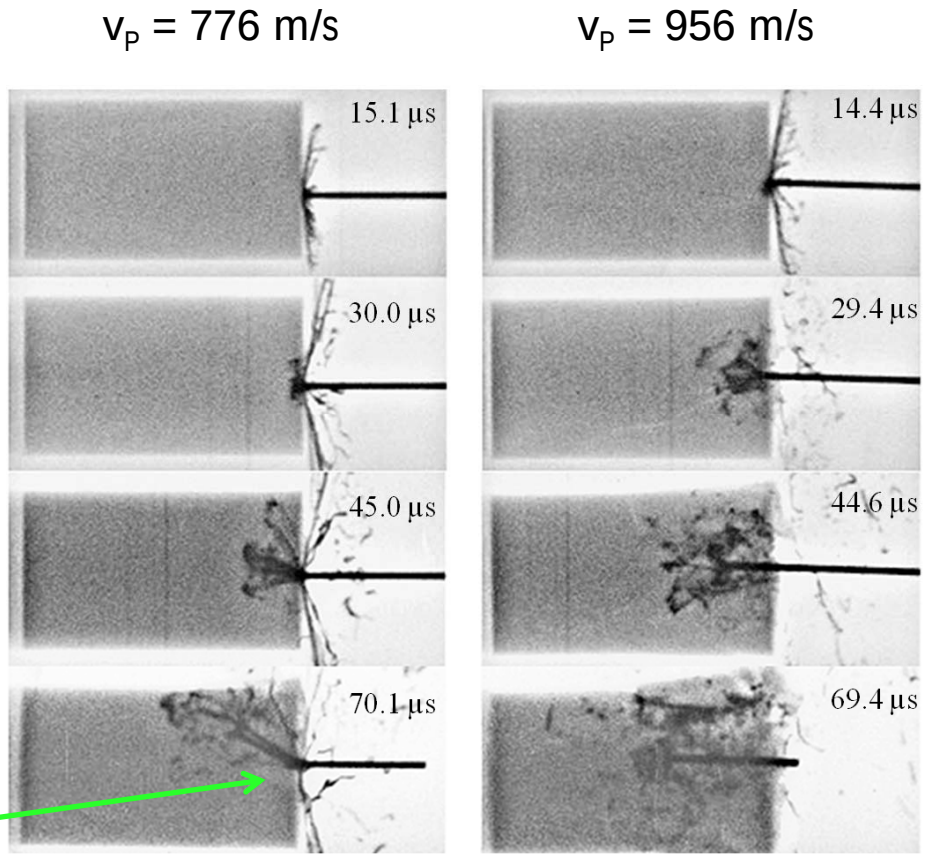
Results – Bare SiC Experiments

Time after impact

Left: sustained dwell

Right: short dwell phase with penetration

➡ Dwell possible up to 800 m/s impact velocity



Diversion of rod at front surface

Behner 09/2008

© 2008 Fraunhofer EMI

Fraunhofer EMI Institut Kurzzeitdynamik Ernst-Mach-Institut

TARDEC

Results – Buffered SiC Experiments

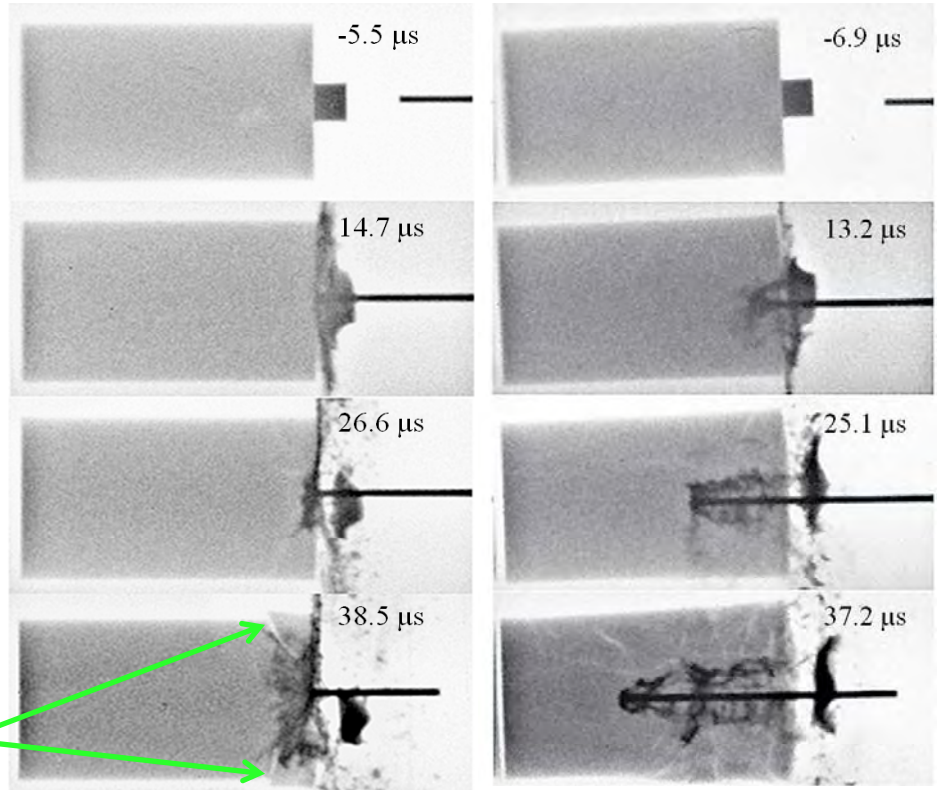
Cu-buffer (Ø 5 mm, 4 mm height)

Left: sustained dwell

Right: short dwell phase with penetration

➡ Dwell velocity substantially higher with buffer (≈ 1530 m/s)

Conical shaped crack



Behner 09/2008

© 2008 Fraunhofer EMI

Fraunhofer Institut Kurzzeitdynamik Ernst-Mach-Institut

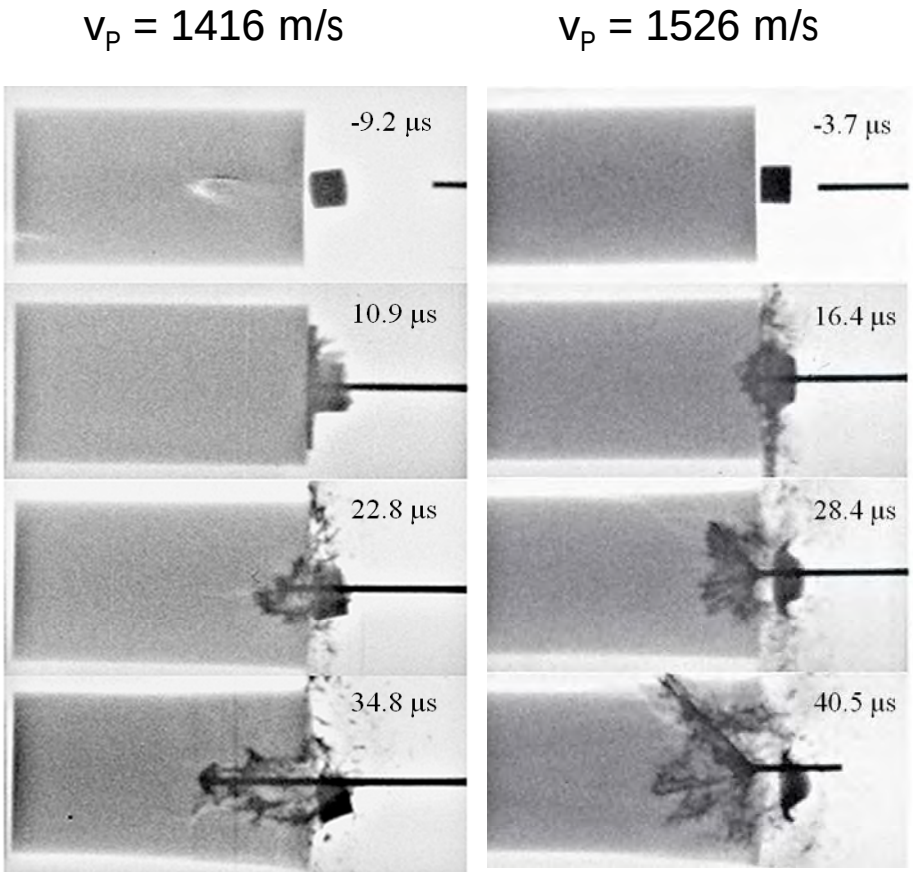
Results – Buffered SiC Experiments

Separation of buffer before impact (accidental)

Left: large gap – short dwell

Right: short gap – sust. dwell

➡ Buffer separation influences dwell behavior (Holmquist et. al. TB045 Poster session)



Behner 09/2008

© 2008 Fraunhofer EMI

Fraunhofer EMI Institut Kurzzeitdynamik Ernst-Mach-Institut

TARDEC

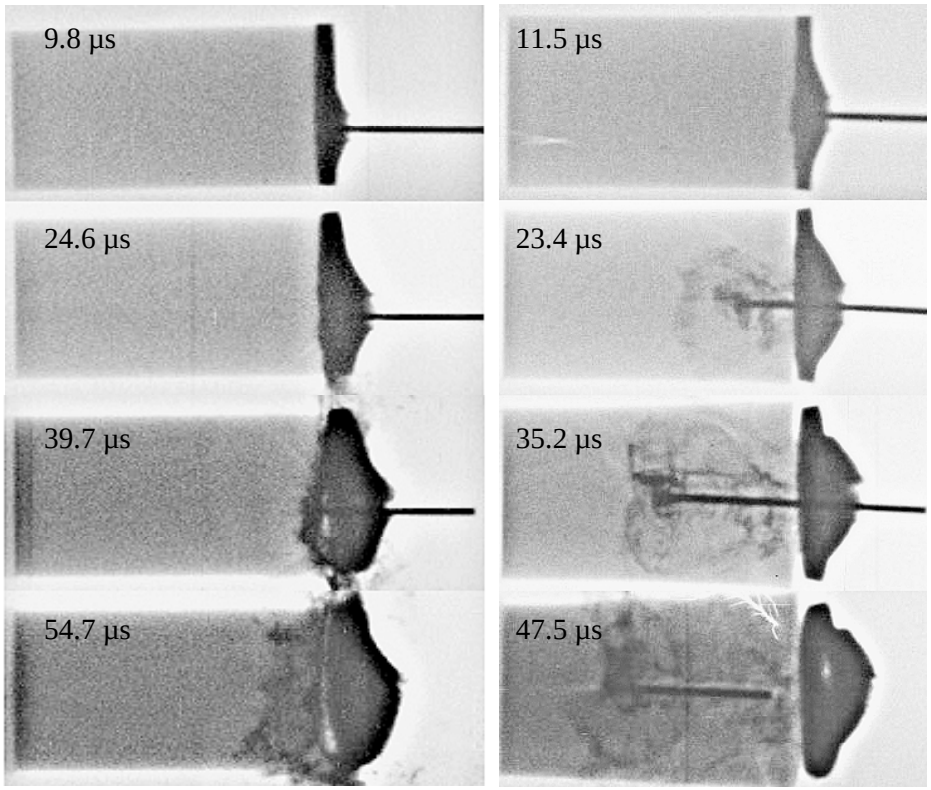
Results – Coverplate SiC Experiments

Cu-plate (Ø 20 mm, 2 mm height)

Left: sustained dwell

Right: short dwell phase with penetration

➡ Similar behavior as small buffer



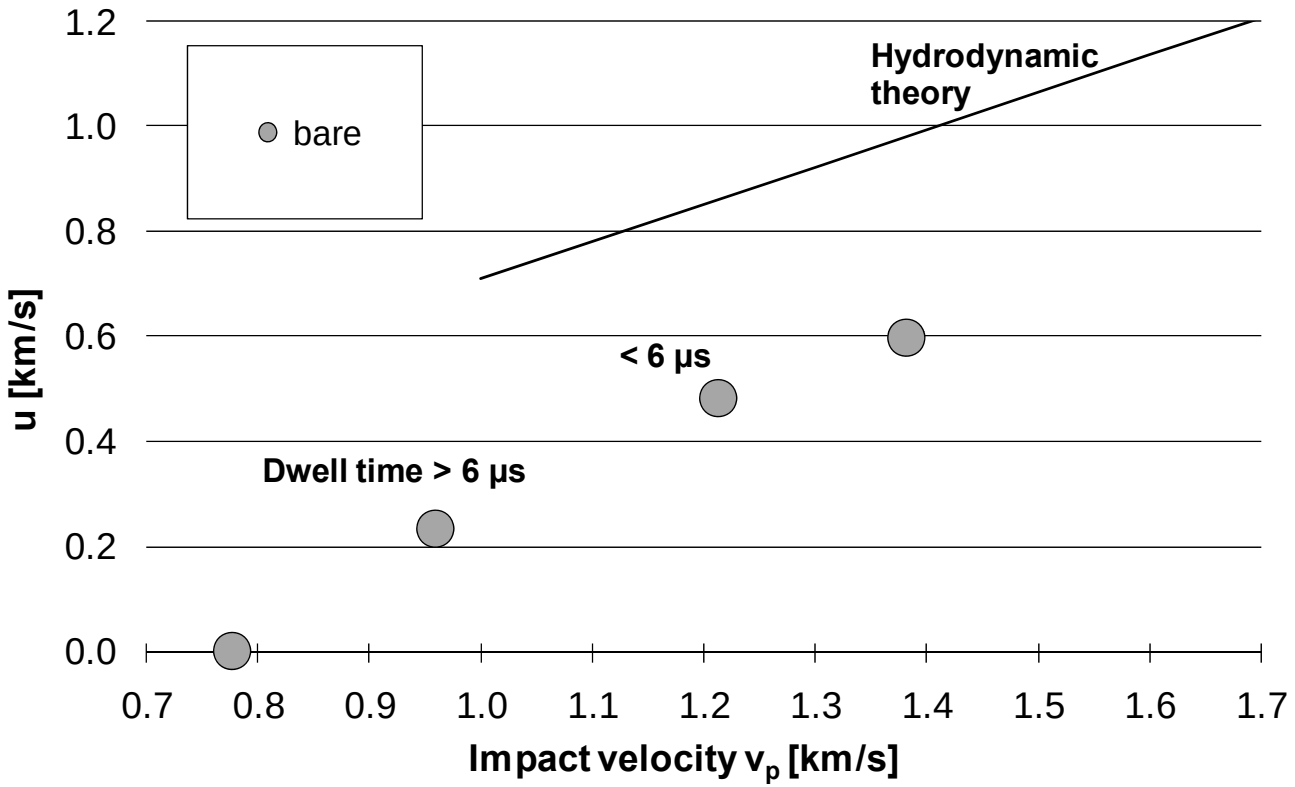
Behner 09/2008

© 2008 Fraunhofer EMI

Fraunhofer Institut Kurzzeitdynamik Ernst-Mach-Institut

Transition from Dwell to Penetration

Pentration velocity vs. Impact velocity



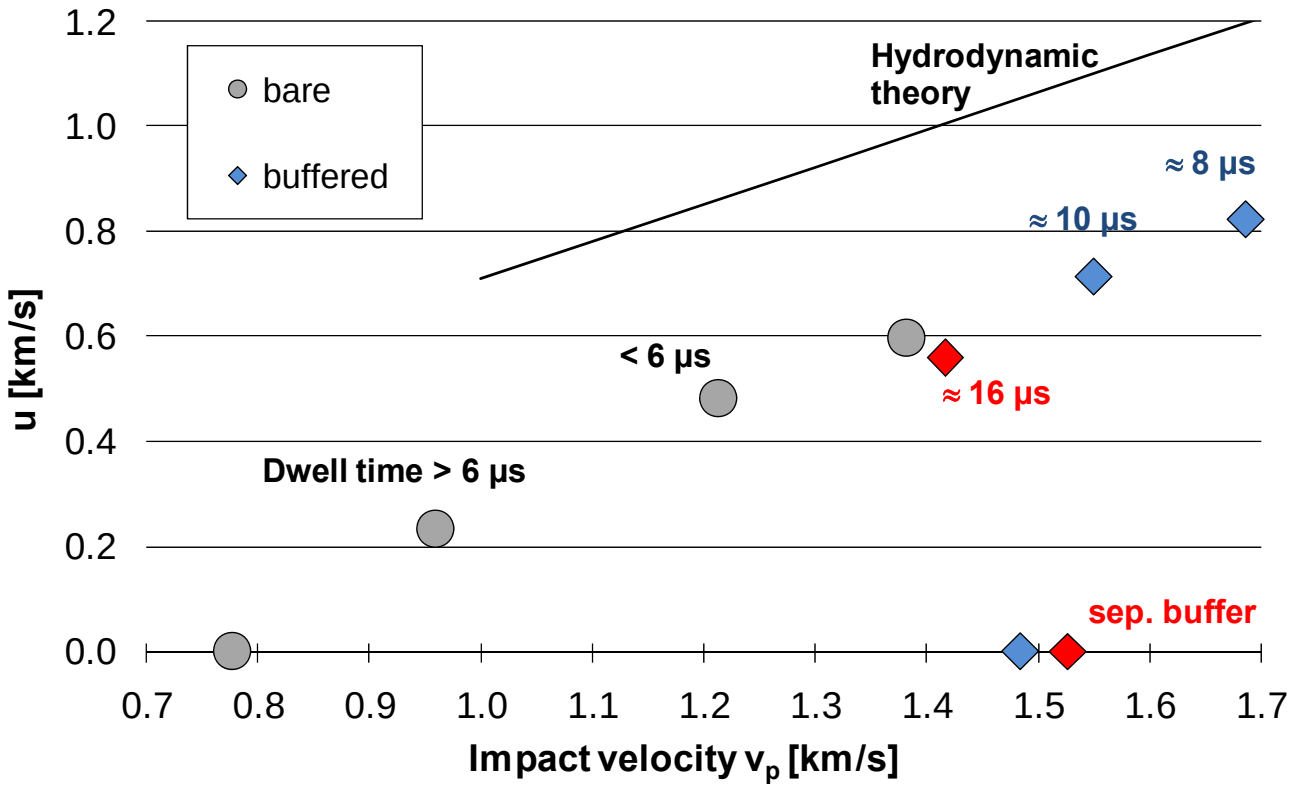
Behner 09/2008

© 2008 Fraunhofer EMI

Fraunhofer Institut Kurzzeitdynamik Ernst-Mach-Institut

Transition from Dwell to Penetration

Pentration velocity vs. Impact velocity



Behner 09/2008

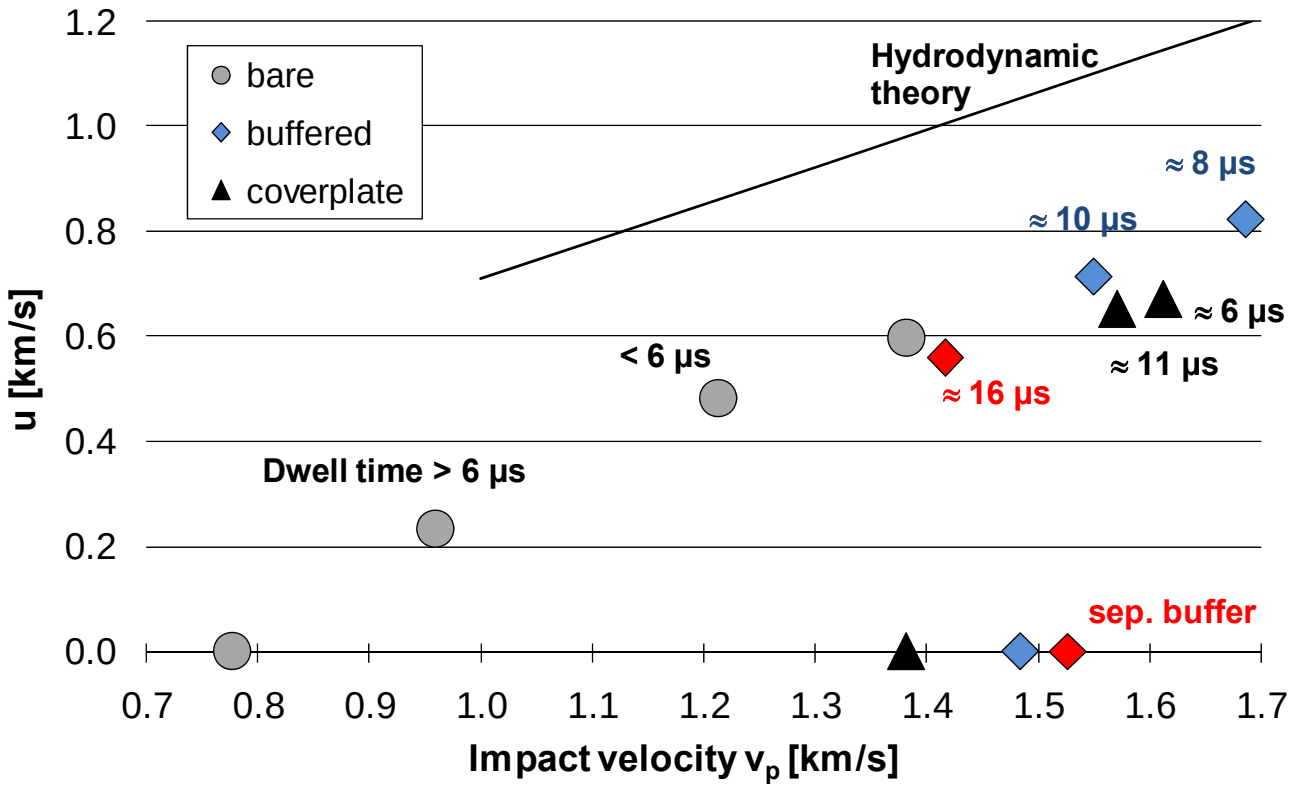
© 2008 Fraunhofer EMI

Fraunhofer EMI Institut Kurzzeitdynamik Ernst-Mach-Institut

TARDEC

Transition from Dwell to Penetration

Pentration velocity vs. Impact velocity



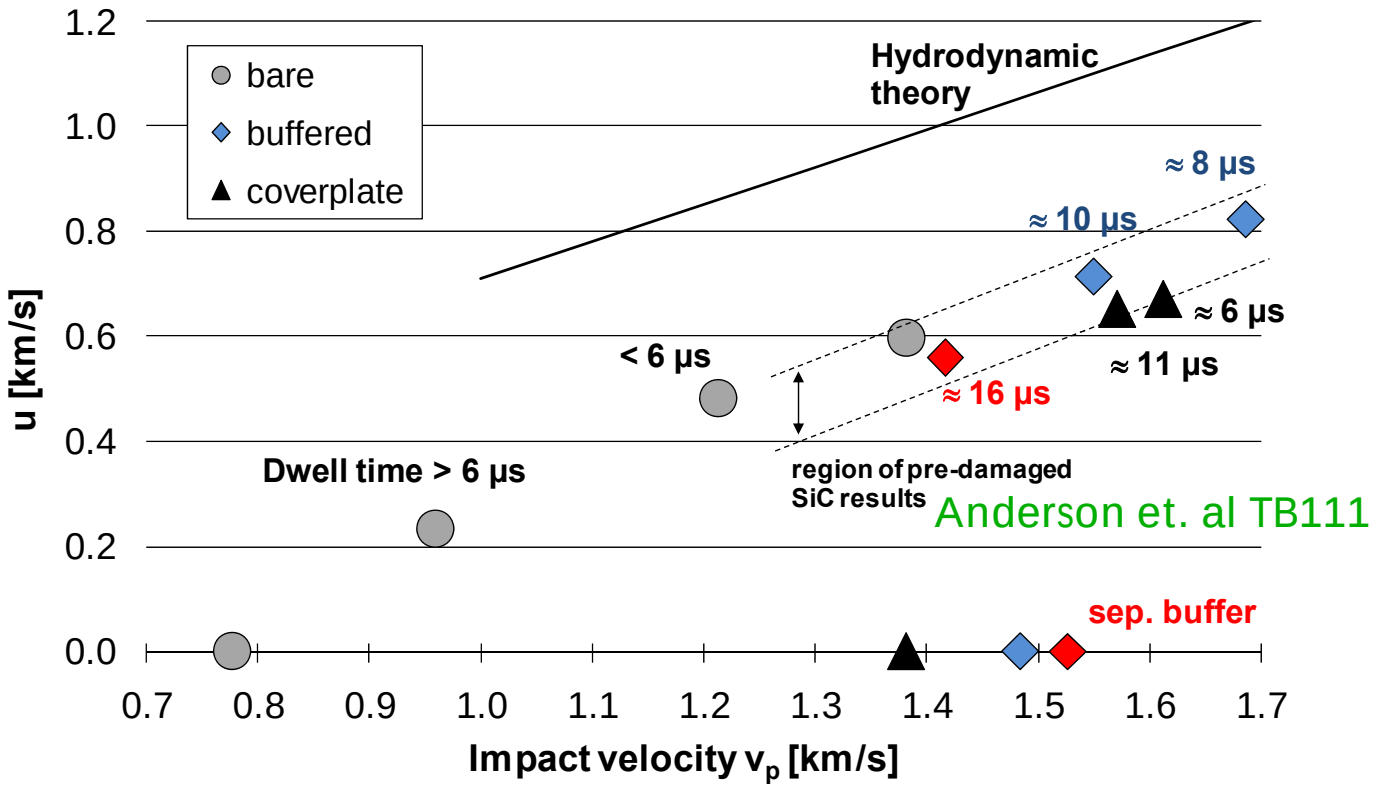
Behner 09/2008

© 2008 Fraunhofer EMI

Fraunhofer Institut Kurzzeitdynamik Ernst-Mach-Institut

Transition from Dwell to Penetration

Pentration velocity vs. Impact velocity



Behner 09/2008

© 2008 Fraunhofer EMI

Fraunhofer Institut Kurzzeitdynamik Ernst-Mach-Institut

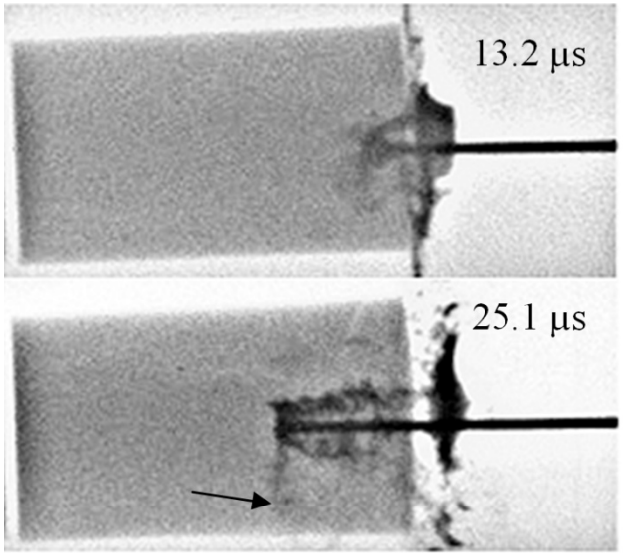
TARDEC

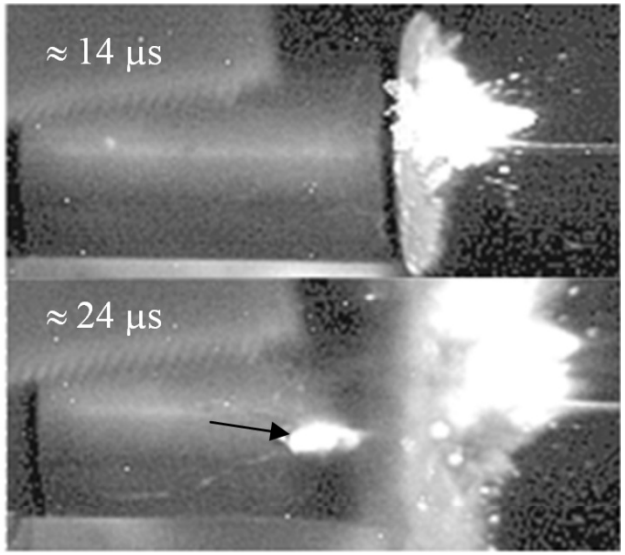
Comparing X-ray with Video still image

At nearly same time after impact

Upper section: diverted rod is forming into disc shape

Lower section: during penetration material emerges from cracks





v_P = 1550 m/s

Behner 09/2008

© 2008 Fraunhofer EMI

Fraunhofer Institut Kurzzeitdynamik Ernst-Mach-Institut

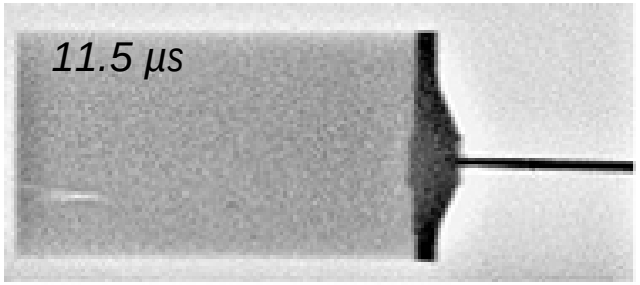
TARDEC

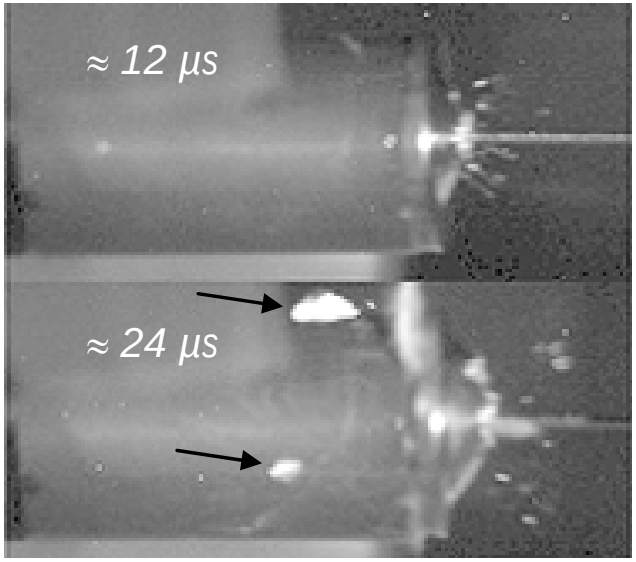
Comparing X-ray with Video still image

At nearly same time after impact

Upper section: Cover plate starts to bulge

Lower section: during penetration material emerges from cracks





v_P = 1571 m/s

Behner 09/2008

© 2008 Fraunhofer EMI

Fraunhofer Institut Kurzzeitdynamik Ernst-Mach-Institut

TARDEC

Summary and Conclusions

- Bare SiC samples dwell up to 800 m/s impact velocity
- A small Cu-buffer attached to front increase transition velocity to ≈1530 m/s
- A coverplate performs similar to a (smaller) buffer
- Microsecond video camera can reveal additional information during impact
- Further Experiments are planned to “pin down” on transition velocity

Behner 09/2008

© 2008 Fraunhofer EMI

Fraunhofer Institut Kurzzeitdynamik Ernst-Mach-Institut

PDF Complete
Your complimentary use period has ended. Thank you for using PDF Complete.
Click Here to upgrade to Unlimited Pages and Expanded Features

RDECOM

Survivability Measures for Evaluation of Personnel in Military Systems

24th International Symposium on Ballistics
22 - 26 September 2008

TECHNOLOGY DRIVEN. WARFIGHTER FOCUSED.

Kelly Benjamin
Natalie Eberius
Patricia Frounfelker

U.S. Army Research Laboratory
Survivability/Lethality Analysis Directorate

PDF Complete
Your complimentary use period has ended. Thank you for using PDF Complete.
Click Here to upgrade to Unlimited Pages and Expanded Features

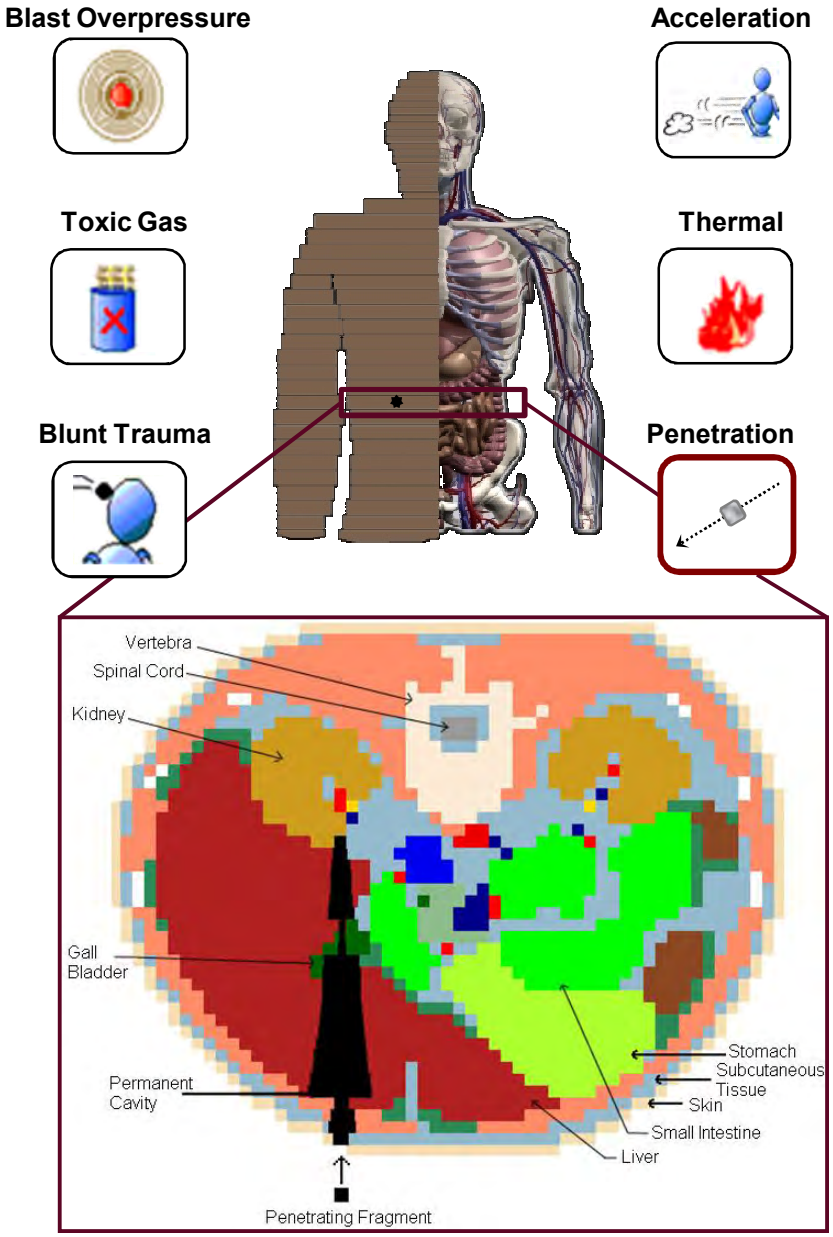
Outline

- ORCA overview
- Survivability and lethality discussion and metrics
- Crew casualty assessment
- Predictive personnel analysis of vehicle crew
- Sample analysis

PDF Complete
Your complimentary use period has ended. Thank you for using PDF Complete.
Click Here to upgrade to Unlimited Pages and Expanded Features

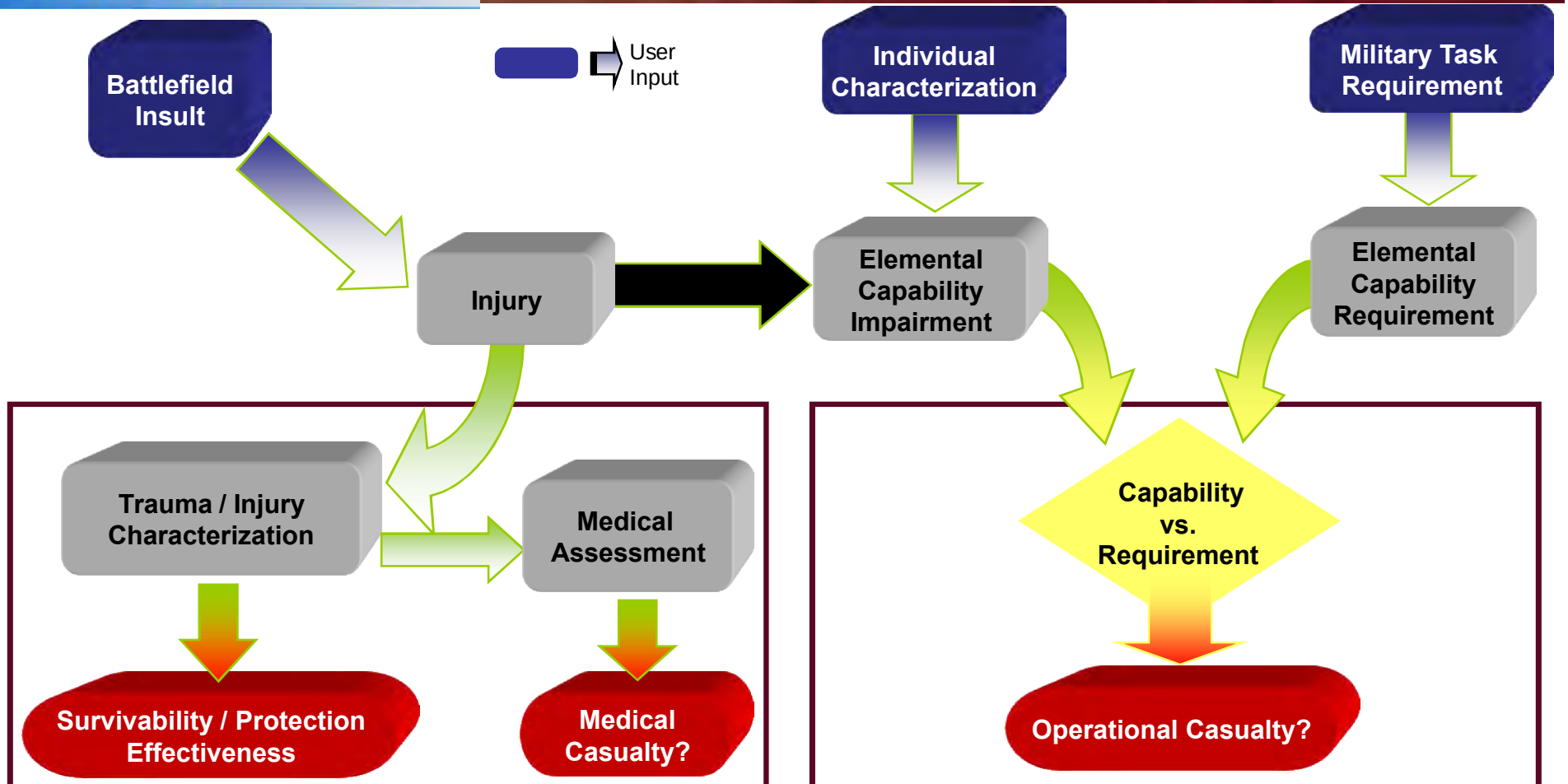
erational Requirement-based asualty Assessment (ORCA)

- ORCA is a high-resolution computerized human vulnerability model that is used to assess the impact of various casualty-causing insults on personnel.
- ORCA calculates several injury severity trauma metrics that may be used to characterize both an individual injury as well as multiple injuries to a single person.
- ORCA is used to assess the impact of various casualty-causing mechanisms on the ability of military personnel to perform battlefield tasks.
  - It considers the operational tasks that personnel must perform, and determines the extent to which penetration and other battlefield insults degrade the ability to perform these tasks.
  - The model can be applied to personnel occupying any crew position and posture on any combat platform.
  - Based on a given insult or set of insults, ORCA assesses whether personnel becomes impaired to the extent that the personnel is incapacitated based on his specific job/military occupational specialty (MOS).



PDF Complete
Your complimentary use period has ended. Thank you for using PDF Complete.
Click Here to upgrade to Unlimited Pages and Expanded Features

ORCA Methodology



Survivability Metric (Injury)

- Typically Red on Blue analyses
- Focus is the survivability of Blue forces
- ORCA output metric: MAIS
- Example analysis: Vehicle Up-armor programs

Lethality Metric (Incapacitation)

- Typically Blue on Red analyses
- Focus is the lethality of a Blue system
- ORCA output metrics: WTAI, JI and Casualty
- Example analysis: Munition lethality evaluation

PDF Complete
Your complimentary use period has ended. Thank you for using PDF Complete.
Click Here to upgrade to Unlimited Pages and Expanded Features

ORCA Metrics

SURVIVABILITY (Injury Metric): ORCA utilizes the Abbreviated Injury Scale (AIS). AIS is an anatomically-based, consensus-derived, international severity scoring system that classifies each injury by body region according to its relative importance on a 6-point ordinal scale. AIS values provide information on the type, location, and severity of anatomical injuries. AIS scores each single injury.

- **MAIS** – Maximum Abbreviated Injury Score (MAIS) is an anatomical measure of injury severity. This score classifies injury severity on the basis of the single injury having the greatest AIS severity value. The MAIS is between 0 and 6.

MAIS	Injury Level	Head Injury Example	Type of Injury
1	Minor	Minor laceration of scalp	Superficial
2	Moderate	Major laceration of scalp, blood loss < 20%	Reversible injuries; medical attention required
3	Serious	Fracture of skull, penetration < 2 cm	Reversible injuries; hospitalization required
4	Severe	Depressed skull fracture, penetration > 2 cm	Non-reversible injuries; not fully recoverable without care
5	Critical	Depressed skull fracture, laceration of spinal artery	Non-reversible injuries; not fully recoverable even with care
6	Maximal	Massive brain stem crush	Nearly Unsurvivable

LETHALITY (Incapacitation Metric): ORCA provides operational metrics derived from evaluating the impact of injuries from one or more insults on the capabilities that humans use to accomplish tasks for a particular set of operational requirements.

- **WTAI** – Weighted Task Average Impairment metric provides an average characterization of an individual's post-injury capability. ORCA examines the reduction in capability to perform individual tasks for a given job with respect to a minimum performance level. WTAI makes use of all task capability information by computing the average level of impairment over all of the task elements that constitute the job under consideration.

PDF Complete
Your complimentary use period has ended. Thank you for using PDF Complete.
Click Here to upgrade to Unlimited Pages and Expanded Features

Crew Casualty Assessment

Survivability Assessment

- Injury/Medical metrics:
  - Severity of Injuries
  - Are the injuries treatable?
  - Are there medical casualties?
  - Trauma scoring metrics
- Operational Metrics (secondary questions):
  - Are there operational casualties?
  - Is our mission intact?

Example:

Effectiveness of Added Vehicle Protection



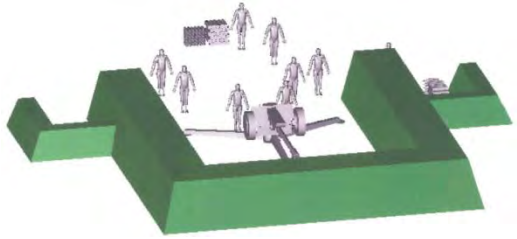
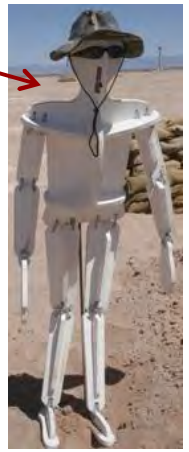



Lethality Assessment

- Operational Metrics:
  - Quantitative measure of weapon performance
  - Can soldier perform certain military tasks?
    - » Dependent on soldierôs tactical role and time after wounding
  - Has the threat been neutralized?
  - Is the enemyôs mission intact?

Example:

Effectiveness of an Air-bursting Munition

PDF Complete
Your complimentary use period has ended. Thank you for using PDF Complete.
Click Here to upgrade to Unlimited Pages and Expanded Features

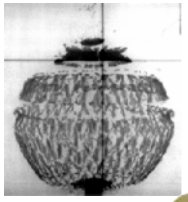
MUVES-S2 and ORCA

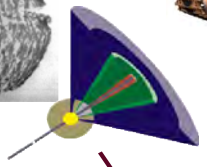
A Survivability/Lethality/Vulnerability (SLV) computer model capable of analyzing the effects of one or more munitions against aircraft or ground-mobile targets.

ORCA Methodology
allows for:

- discrete shot lines through anatomy based on orientation of threat trajectory to personnel
- projectile penetration mechanics through various anatomic structures
- velocity retardation of threat through wound track
- injury description by type, severity, and frequency
- in-depth description of operational effectiveness

Threat Characterization

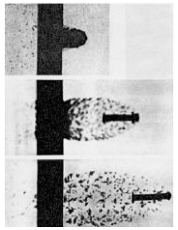






Target Geometry

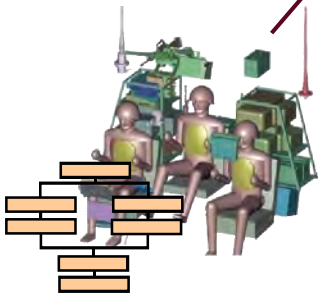
Behind-Armor Debris





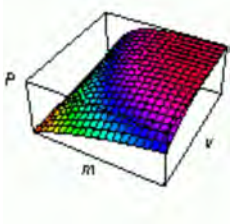
Crew Casualty

Vehicular SLV Analysis



Criticality Analysis of Components and Subsystems

Component Defeat Criteria





Engagement Conditions

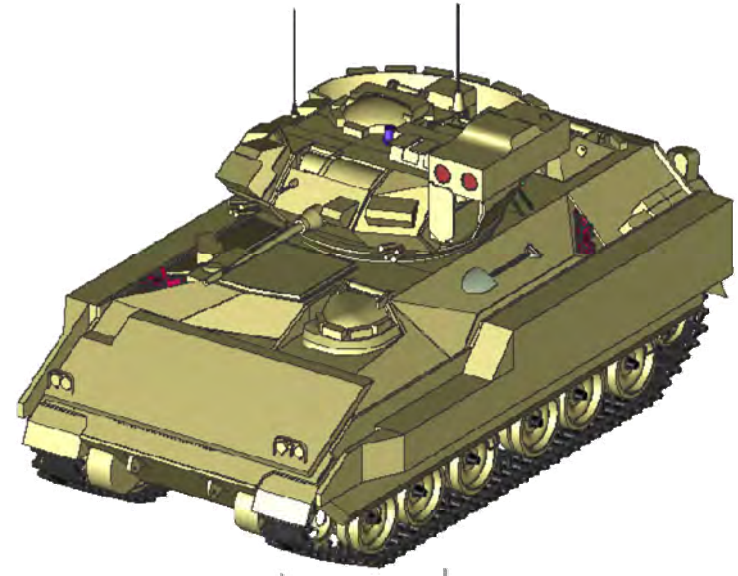
Analysis Outputs

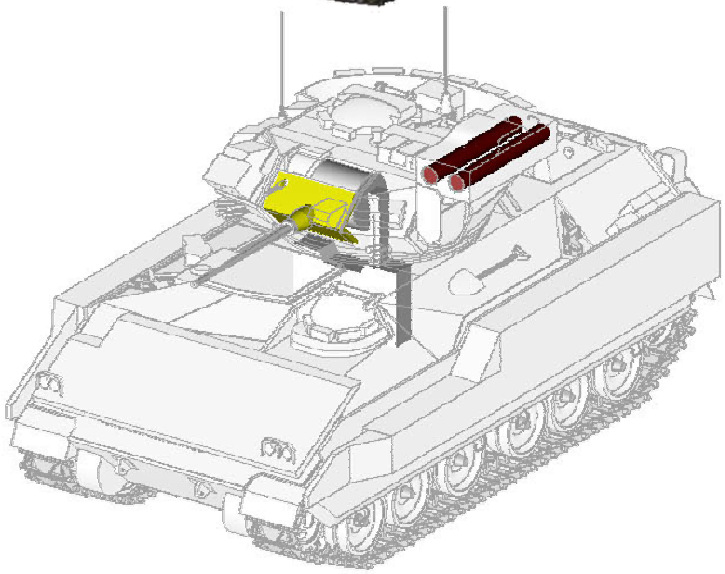
- personnel injury and incapacitation
- system-level kills / loss of function
- residual penetration & velocity
- component damage
- subsystem capabilities
- remaining system utility
- user-defined criteria
- tabular & graphical products

PDF Complete
Your complimentary use period has ended. Thank you for using PDF Complete.
Click Here to upgrade to Unlimited Pages and Expanded Features

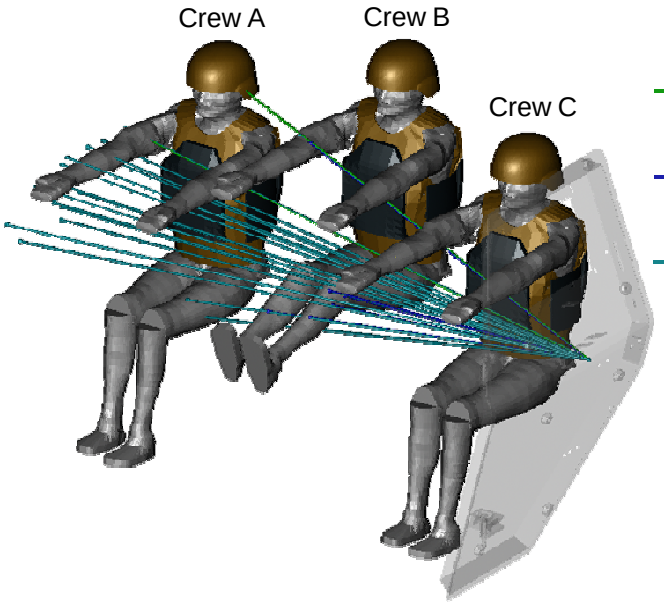
get and Threat Characterizations

Target Description





Threat Interaction





Copper Fragment Threat
vs.
Modeled Vehicle

Engine Component
Material: Mild Steel

Front Seat Frame
Material: Aluminum

Driver Arm
Material: Personnel Soft Tissue

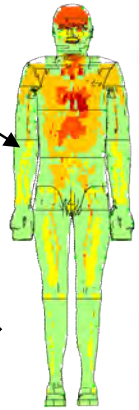
ORCA Module

HVAC
Material: Bonded Nylon

Window Frame
Material: Aluminum

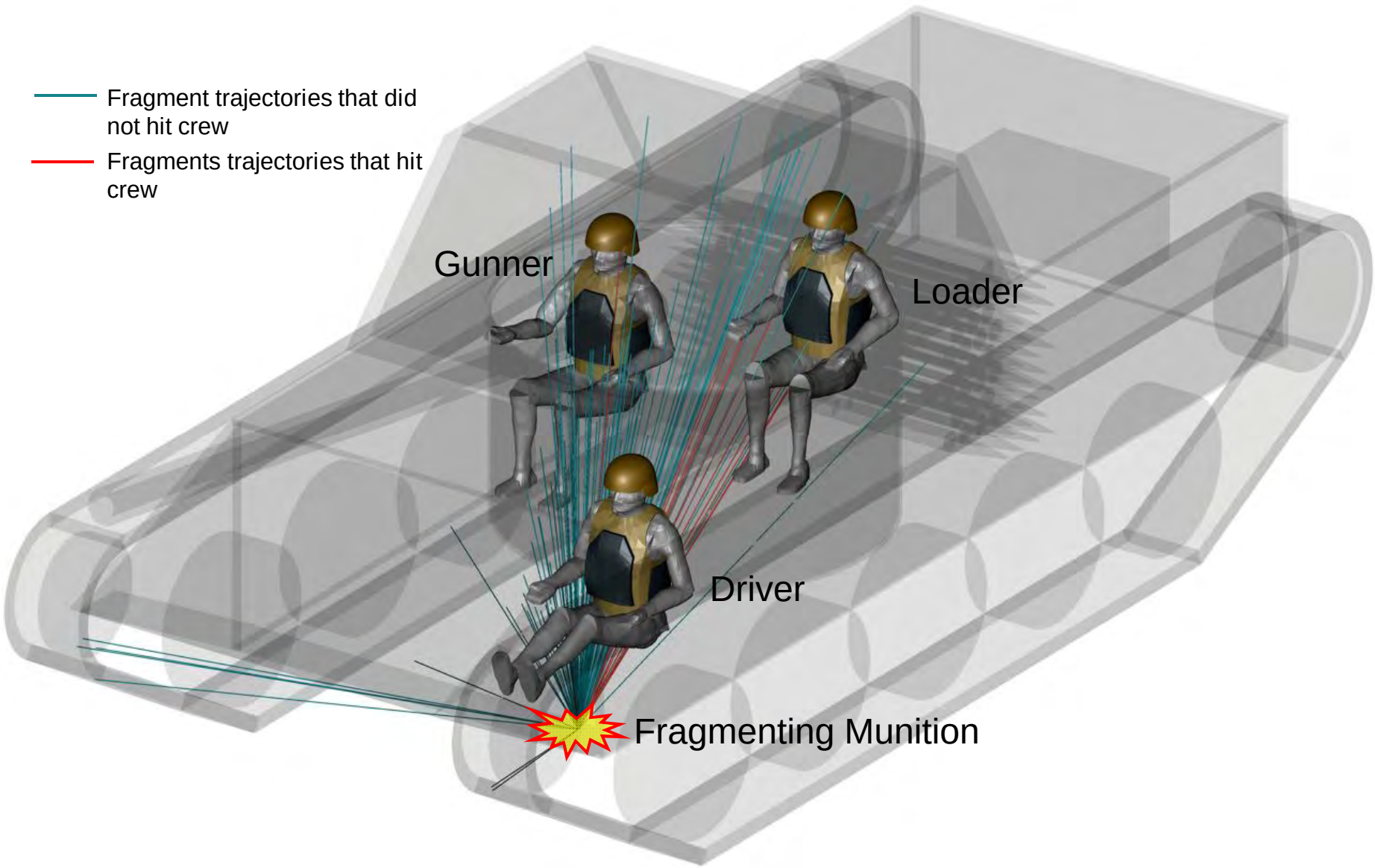
Exit Vehicle

Arm Hit
MAIS: 2



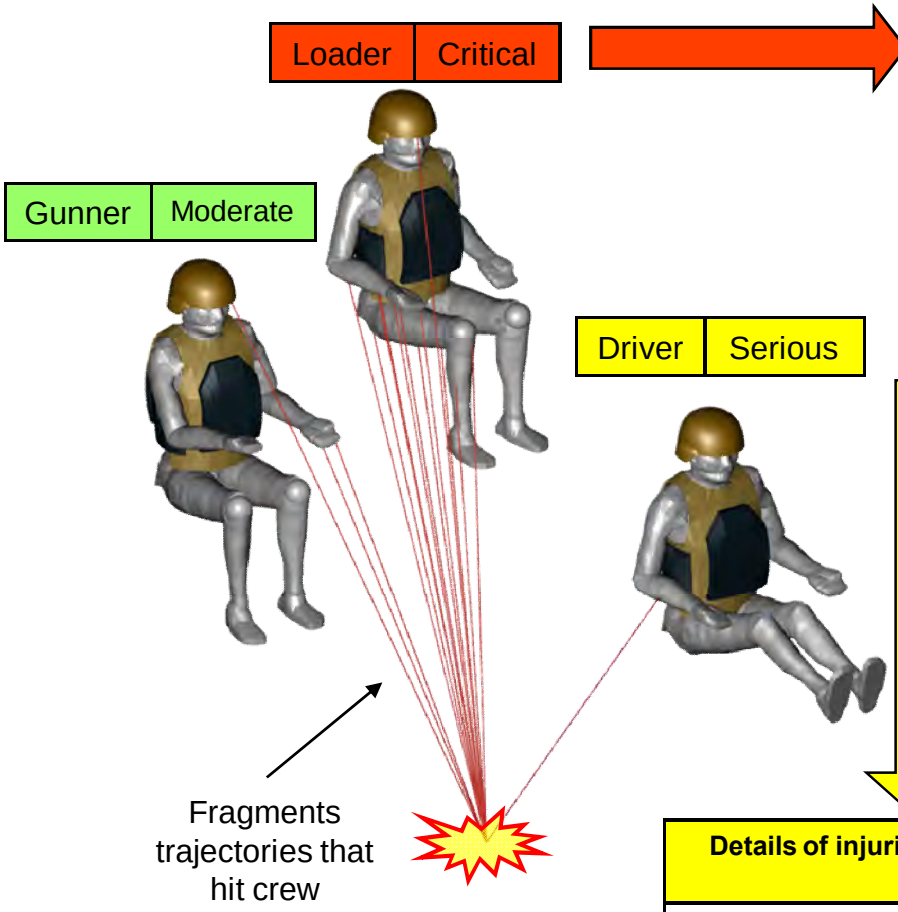
PDF Complete
Your complimentary use period has ended. Thank you for using PDF Complete.
Click Here to upgrade to Unlimited Pages and Expanded Features

enting Munition vs. Tank Crew (1 of 4)



PDF Complete
Your complimentary use period has ended. Thank you for using PDF Complete.
Click Here to upgrade to Unlimited Pages and Expanded Features

Injury Details (2 of 4)



Details of 6 injurious fragments hitting Loader

frag #	mass (g)	vel (m/s)	Body Region	MAIS
1	63.8	753.6	forearm	Serious (3)
2	36.2	512.8	forearm	Moderate (2)
6	5.9	9.6	hand	Minor (1)
7	83.8	524.0	upper leg	Serious (3)
8	83.8	306.5	abdomen	Critical (5)
13	17.9	261.1	head	Critical (5)

Details of injuries caused by fragment 7 (MAIS 3)

Tissue Name	Severity
Skin	17.69cm^2 damaged
Muscle (quadriceps femoris)	> 80% damage
Muscle (sartorius)	20% < damage < 50%
Bone (femur)	Comminuted fracture

Details of injuries caused by fragment 8 (MAIS 5)

Tissue Name	Severity
Skin	10.29 cm^2 damaged
Small and large intestines	> 50% damage
Liver and kidney (R)	> 50% damage, fracture
Muscle (diaphragm)	< 20% damage
Lung (inferior lobe, R)	1.3 cc damaged

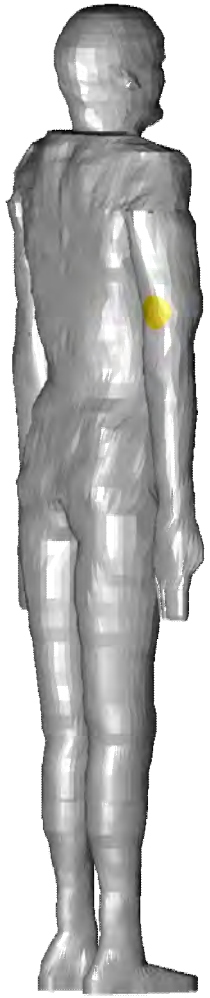
PDF Complete
Your complimentary use period has ended. Thank you for using PDF Complete.
Click Here to upgrade to Unlimited Pages and Expanded Features

Surface Injury Mapping (3 of 4)

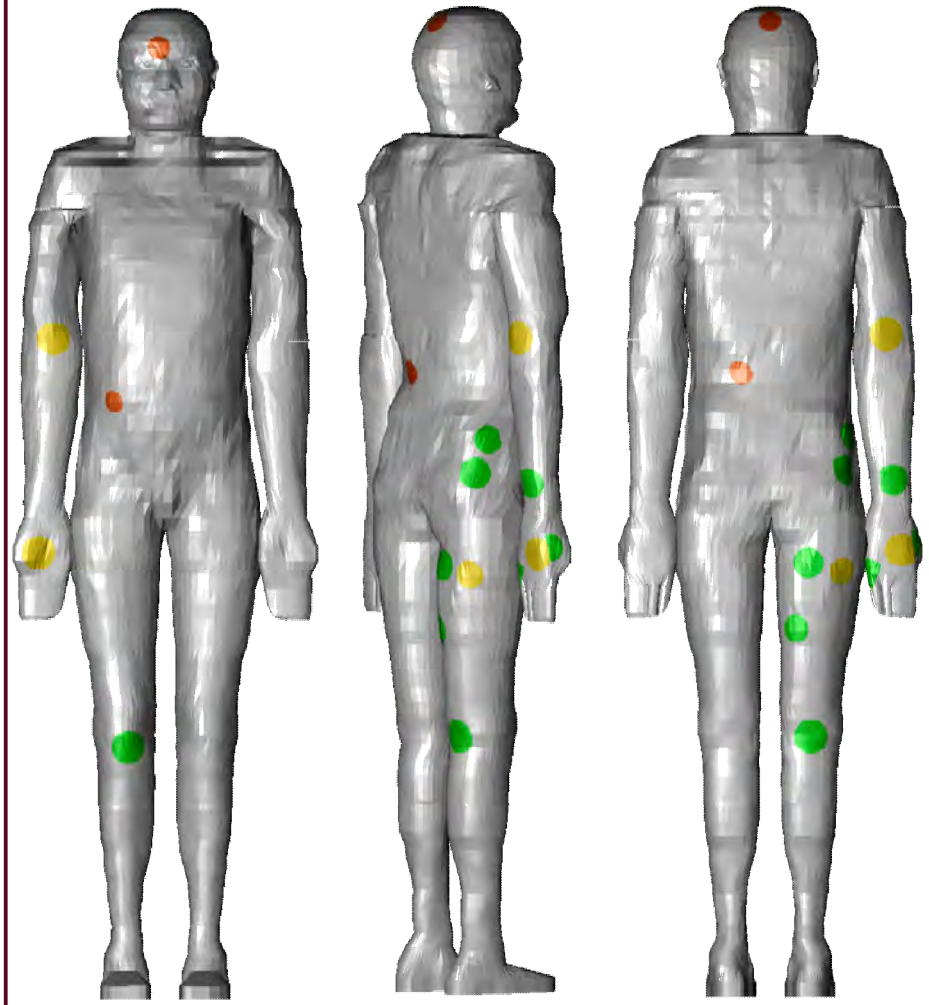
MAIS	Injury Level
1	Minor
2	Moderate
3	Serious
4	Severe
5	Critical
6	Maximal

Size of the surface damage reflects the size of damaged skin tissue and the color indicates the severity of the wound track.

Driver
1 fragment hit
MAIS 3
Serious



Loader
15 fragment hits
MAIS 5
Critical



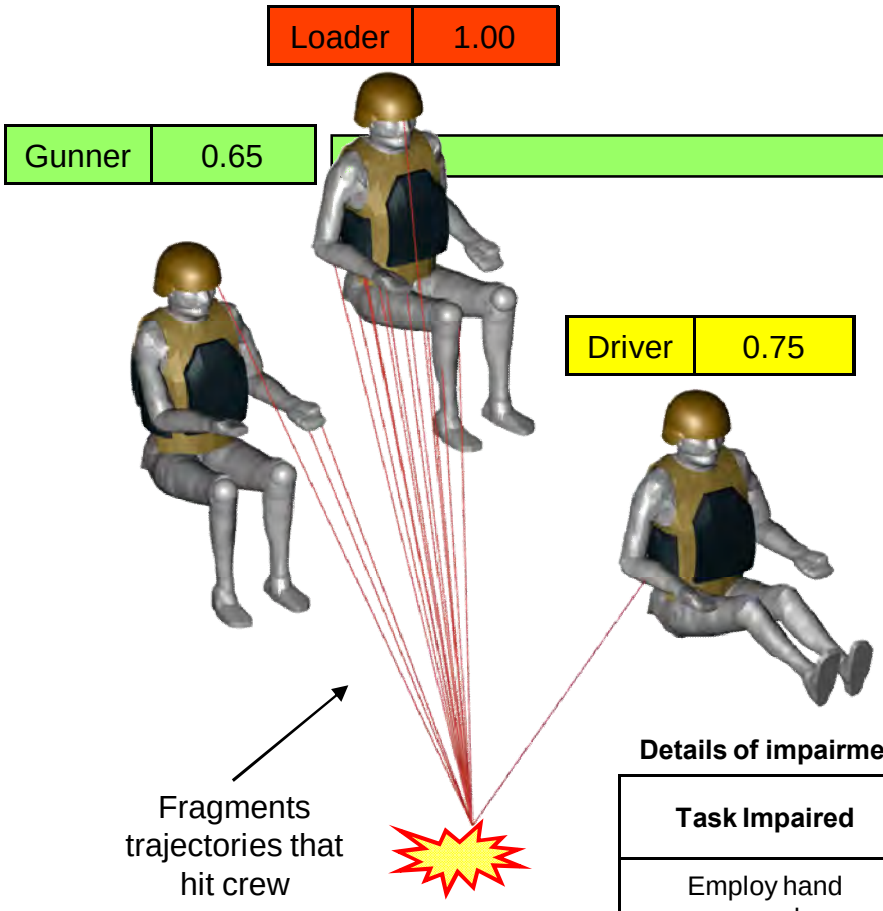
Gunner
3 fragment hits
MAIS 2
Moderate



PDF Complete
Your complimentary use period has ended. Thank you for using PDF Complete.
Click Here to upgrade to Unlimited Pages and Expanded Features

Impairment Details (4 of 4)

capacitation For a Given Tactical Role and Time Period



Details of 3 impairing fragments hitting Gunner				
frag #	**mass (gm)**	**vel (m/s)**	**Body Region**	**WTAI @ 5 min**
1	2.1	91.5	hand	0.15
2	27.3	9.6	hand	0.26
3	3.4	180.4	head (ear)	0.36

Details of impairment caused by fragment 2

Task Impaired	Elemental Capability Degraded
Employ hand grenade	Arm / wrist strength (L)
Load and engage targets with carbine	Arm / wrist dexterity (L)
Evacuate a casualty	Psychomotor mental processing
Operate night vision goggles	

Details of impairment caused by fragment 3

Task Impaired	Elemental Capability Degraded
Move under direct fire	Speech intelligibility clarity
Move as a member of a fire team	Vocal clarity
Navigate check point to check point	Auditory mental processing
React to indirect fire	Balance

PDF Complete
Your complimentary use period has ended. Thank you for using PDF Complete.
Click Here to upgrade to Unlimited Pages and Expanded Features

Conclusion

- MUVES-S2 with ORCA improves personnel casualty assessment for SLV analysis of combat systems.
- ORCA provides improvements for all phases of the casualty assessment process from operational casualty assessment needed to address lethality questions to survivability-based metrics.
- These new survivability metrics provide injury type and severity leading to higher resolution outputs to better serve survivability assessments.
- This new and unique capability in MUVES-S2 allows careful analysis and design of vehicle and body armor systems and configurations.

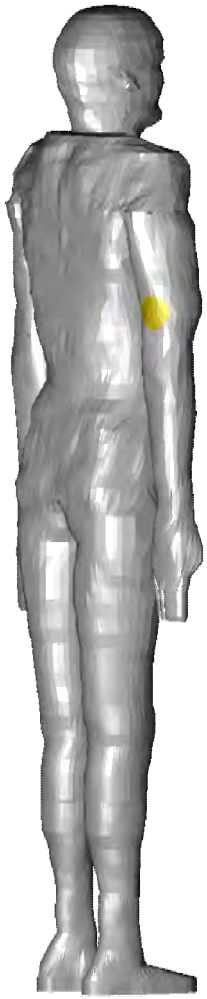
PDF Complete
Your complimentary use period has ended. Thank you for using PDF Complete.
Click Here to upgrade to Unlimited Pages and Expanded Features

Surface Injury Mapping (3 of 4)

MAIS	Injury Level
1	Minor
2	Moderate
3	Serious
4	Severe
5	Critical
6	Maximal

Size of the surface damage reflects the size of damaged skin tissue and the color indicates the severity of the wound track.

Driver
1 fragment hit
MAIS 3
Serious



Crew 1
15 fragment hits
MAIS 5
Critical



Crew 2
3 fragment hits
MAIS 2
Moderate



Resistance to FSP Penetration of Some Transparent Materials

24th International Ballistics Symposium

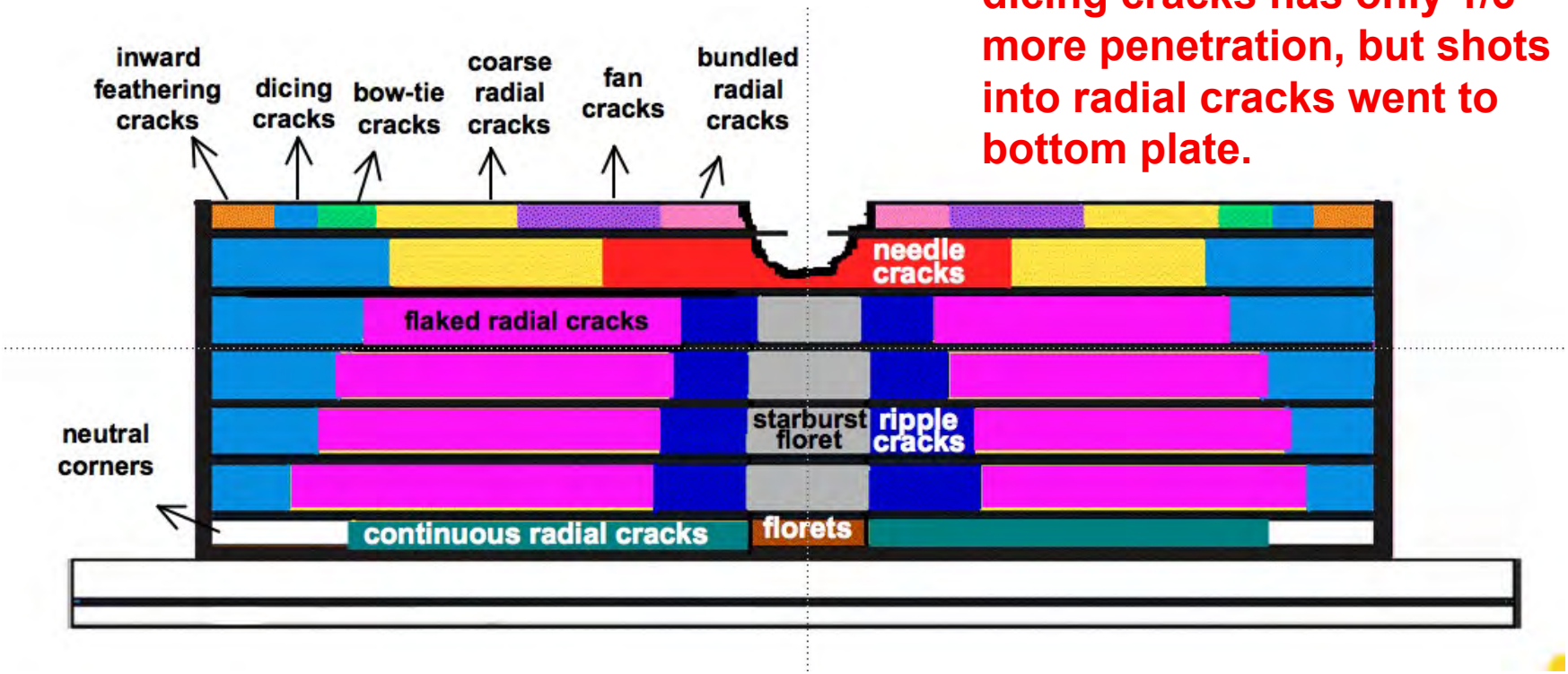
22-26 September 2008

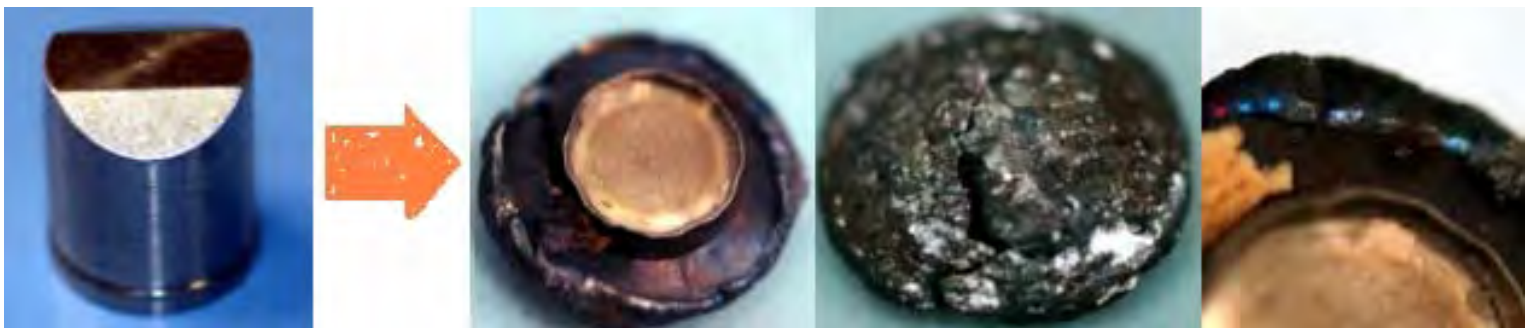
S.Bless, D.Berry

sbless@iat.utexas.edu

Last ISB: Experiments with .50 FSP into 7-layer glass targets.

Subsequent shots into dicing cracks has only 1/3 more penetration, but shots into radial cracks went to bottom plate.





Experiments with 4-layer targets turned out to give very similar results.

Four-layer targets was tested. First 4 layers same as 7 layer target.

Damage patterns were the same as 7-layer target.

1st shot: P = 24mm. No bulge.

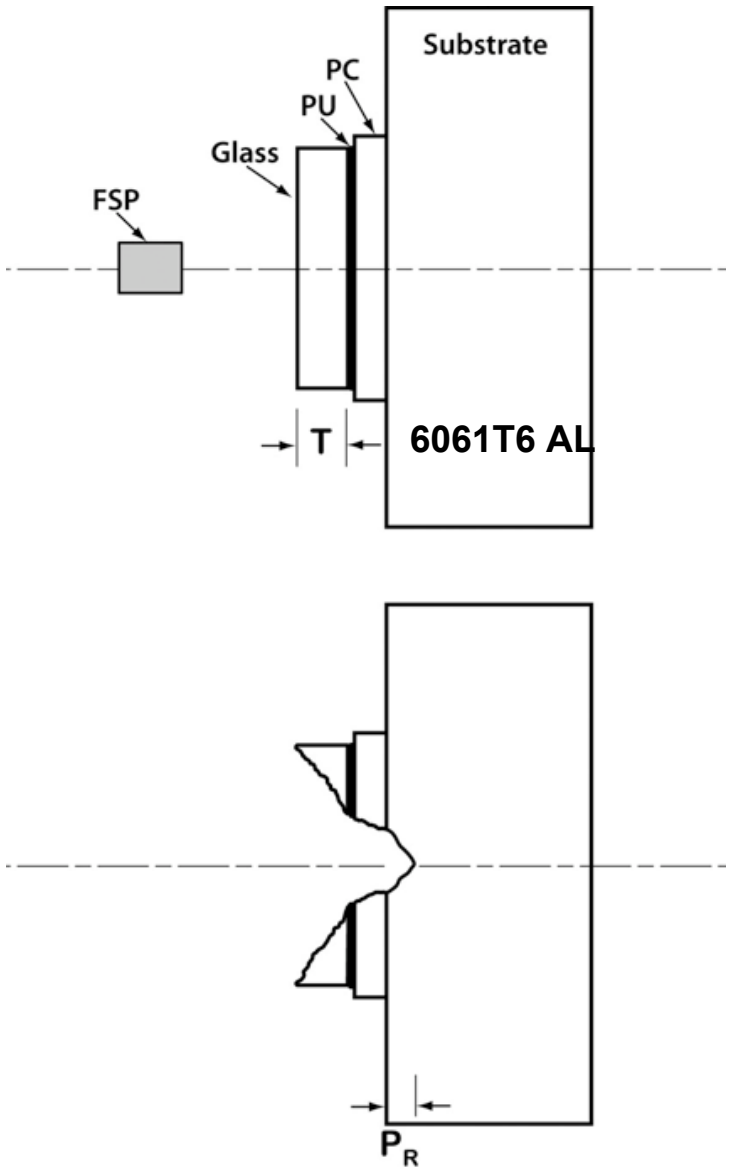
2nd shot into dicing cracks: No change in damage distribution except at impact point. P = 42mm. Slight bulge.

3rd shot into bundled radial cracks (surrounding first impact site): Result was complete penetration.

4th shot into dicing cracks: P=45mm, slight bulge.



DOP testing also gave same result



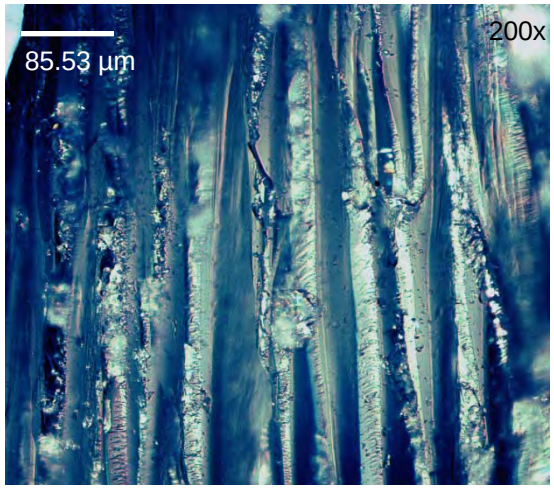


20-shot series.

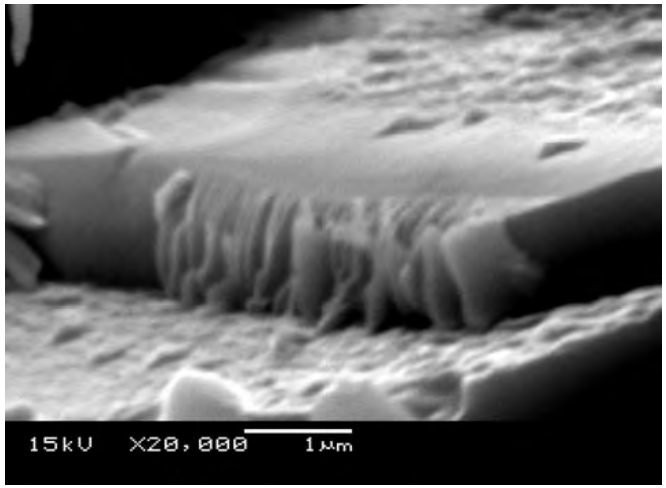
Mass efficiency (rel. to aluminum) was 1.2-1.4. Did not depend on thickness. Edge proximity had little effect.
Performance for 1st and 2nd hits very similar to what was seen in multilayer target.

Recovered particles show fast communition

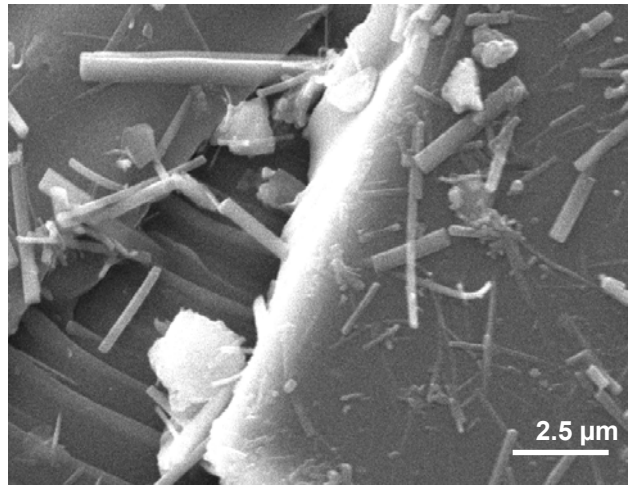
This material exhibited many features indicating very fast fracture, but very few grains showed the FW structure: e.g. conventional elastic-brittle cavity expansion.



Long parallel hackles

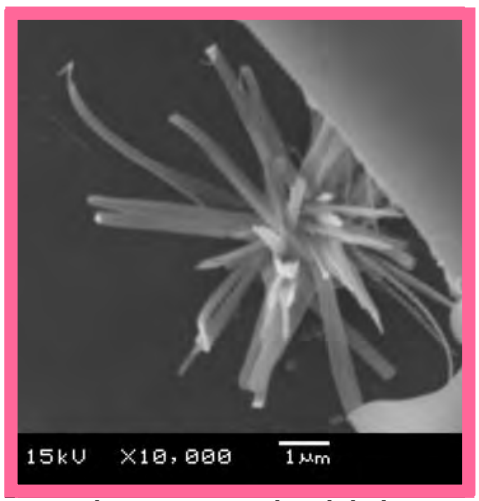


Nano “stairsteps” with hackle on steps.

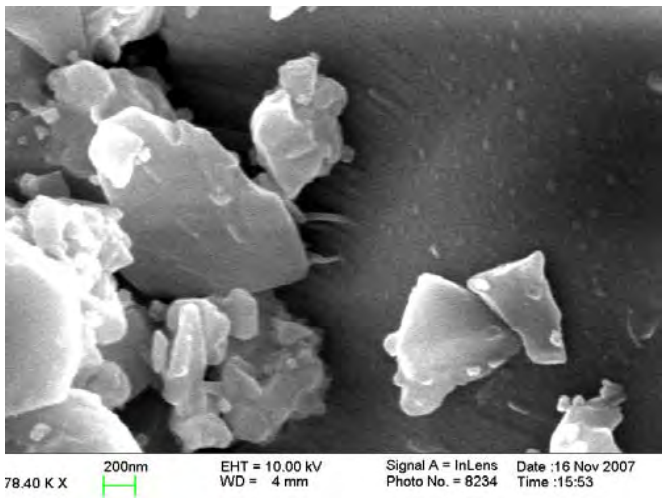


Fields of nano whiskers

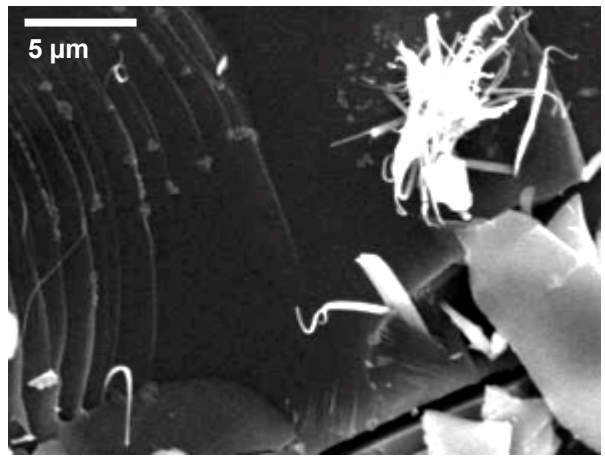
*Note that whiskers may be associated with adjacent hackles



Agglomerated whiskers

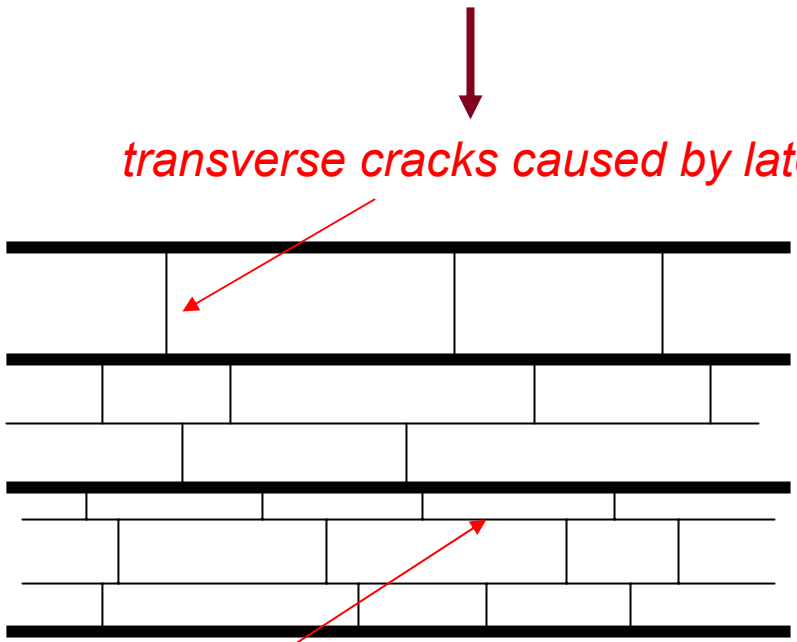


Rounded nano particles



Curvature of whiskers

Hypothesis for radial crack structure within the targets



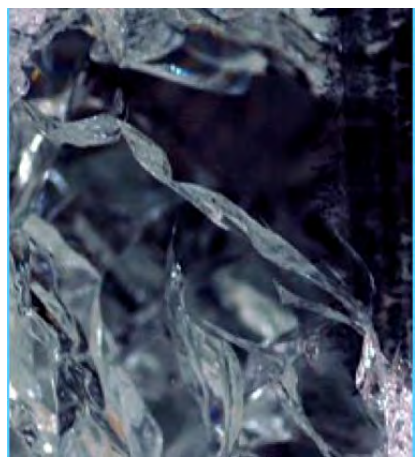
Summary of results concerning how damage degrades multi-layer glass targets

Close in cavity expansion transitions to far-reaching radial crack pattern.

First shot sets up damage pattern. Two basic kinds of crack damage: dicing cracks and radial cracks, which are flaked in inner layers and pie-sections in outer layers. This pattern does not change significantly in subsequent shots.

The radial cracks very seriously degrade ballistic performance. The dicing cracks do not.

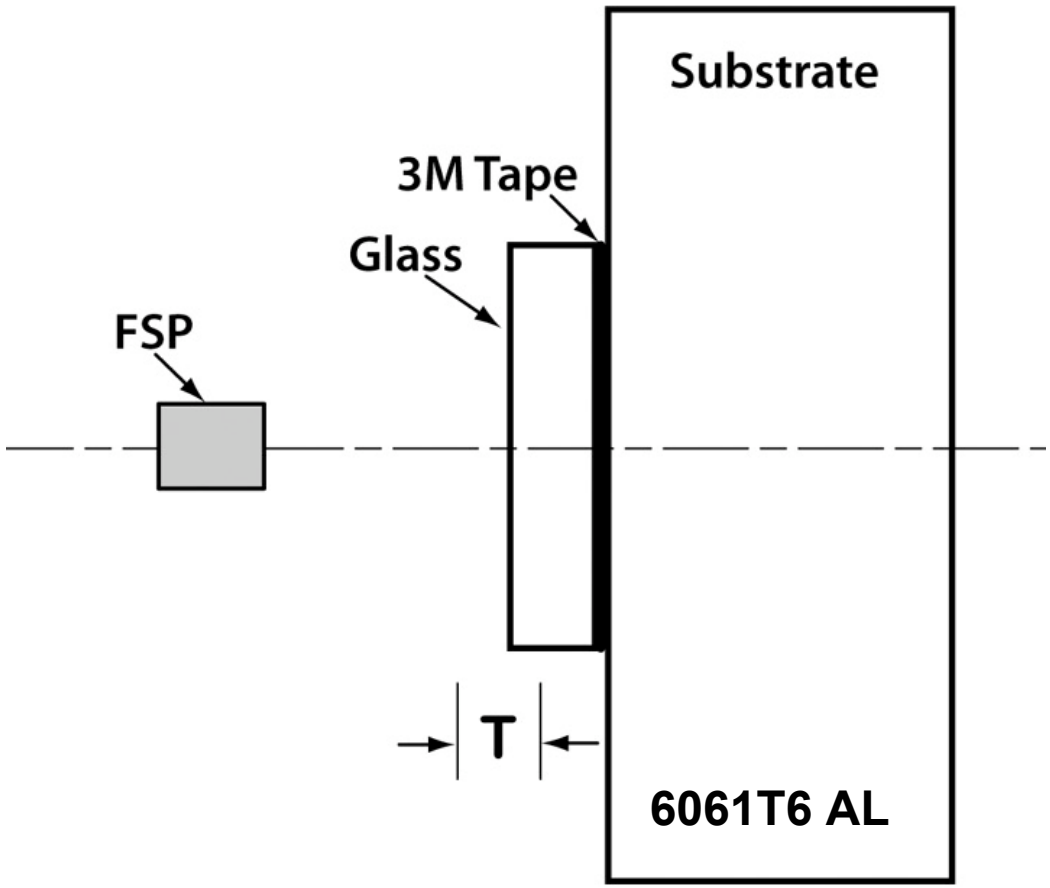




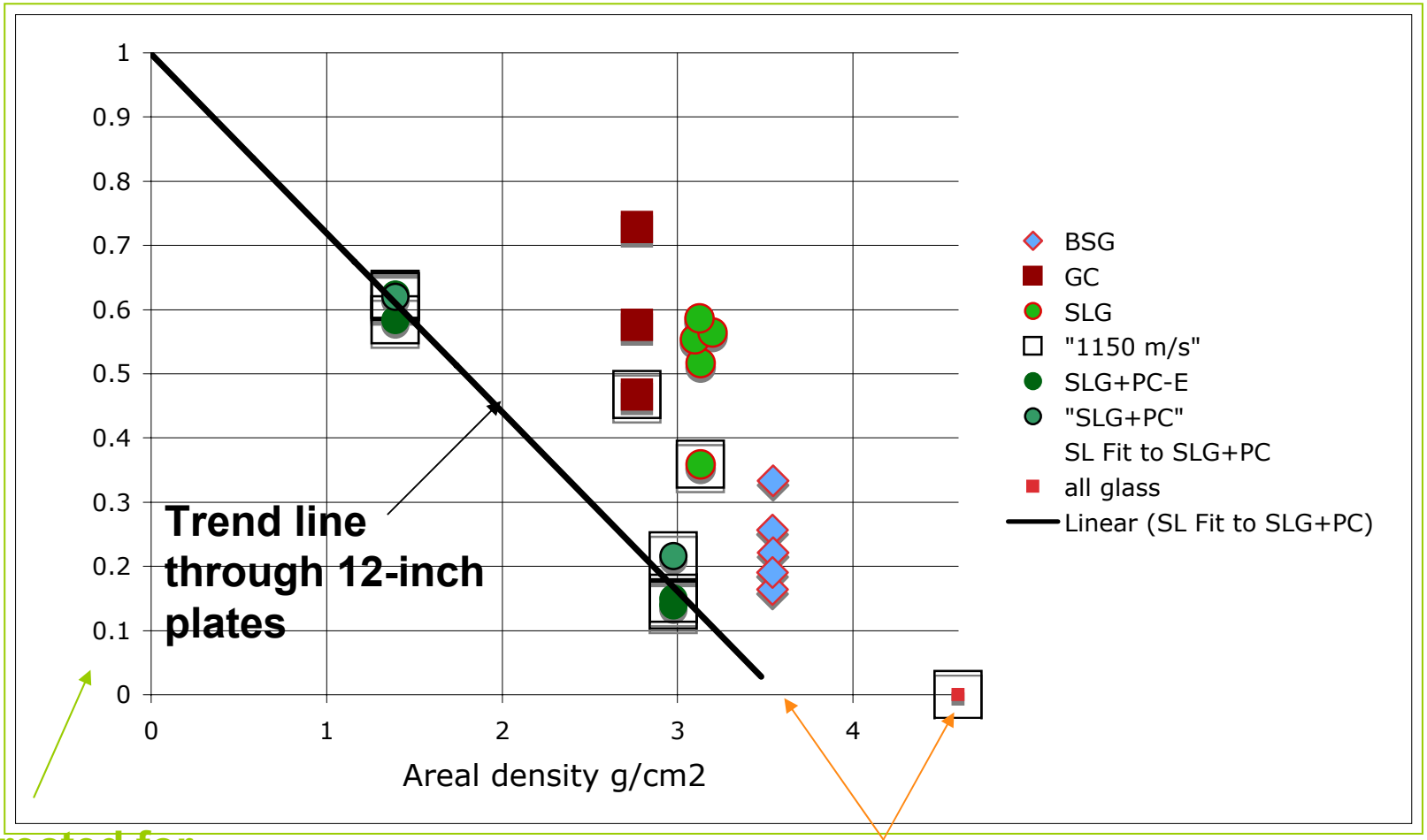
3 Materials compared to investigate effect of properties

Parameter	Soda lime glass	Boro-silicate glass	Glass ceramic (Corning)
Density (g/cm3)	2.5	2.2	2.78
E (GPa)	72	61	72

Modified DOP test geometry for 4-inch test coupons



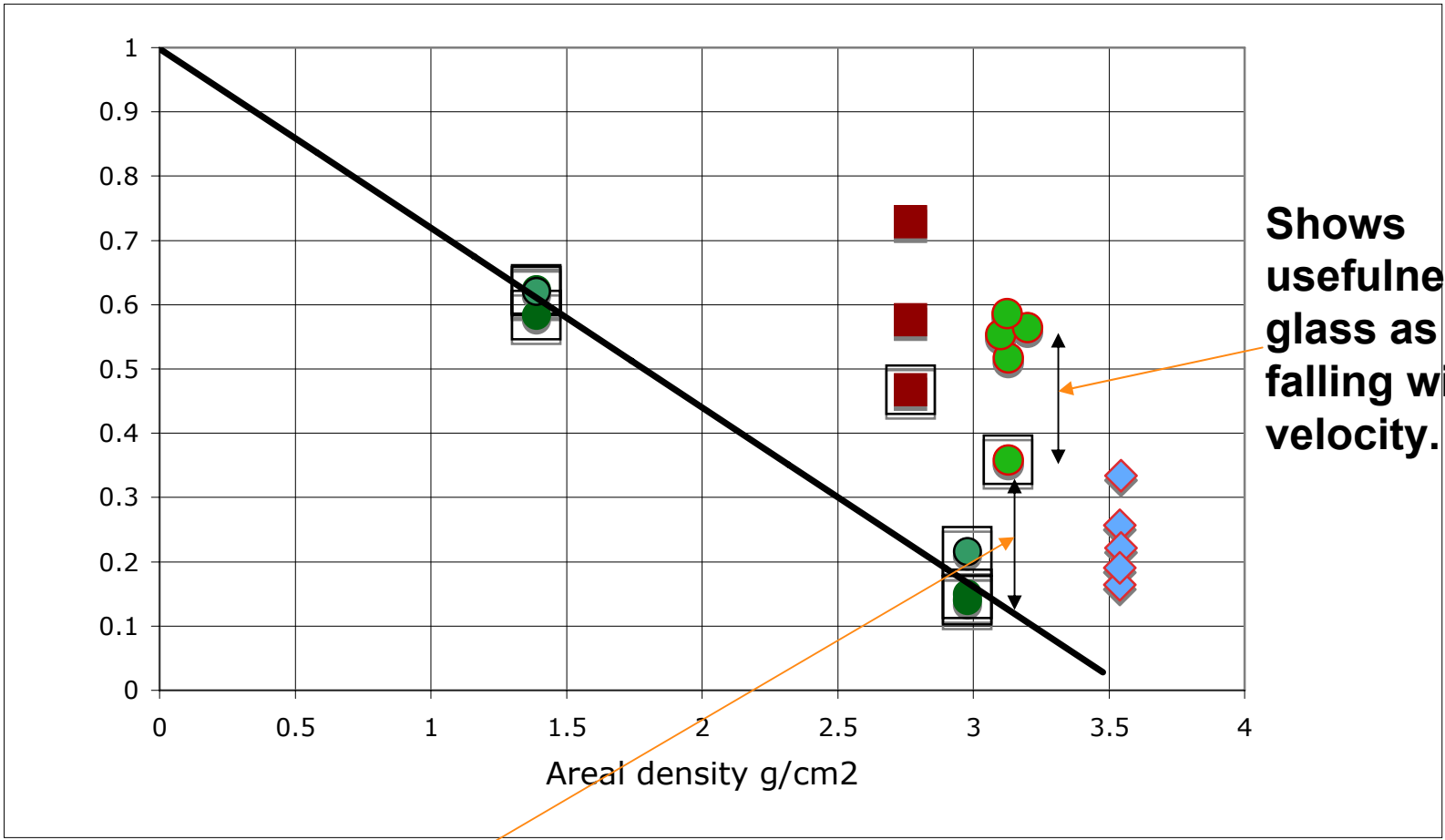
Connection of DOP tests and laminate target tests



Corrected for effect of PC.

Penetration is more in an all glass target than would be predicted from DOP trend. This is probably due to loss of strength which allows projectile to "coast" to s stop in glass.

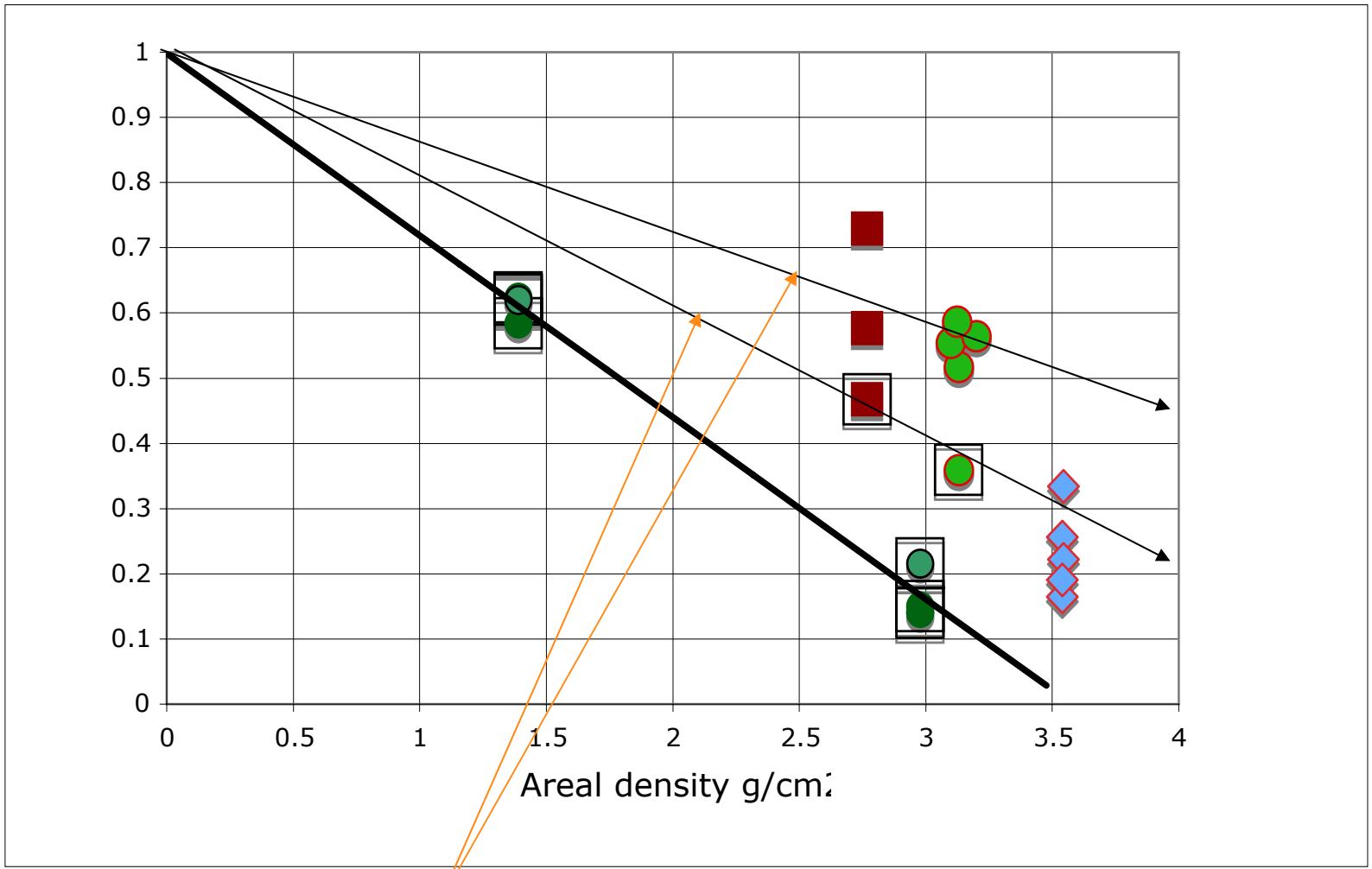
Effects of Mounting and Velocity



Shows usefulness of glass as armor falling with velocity.

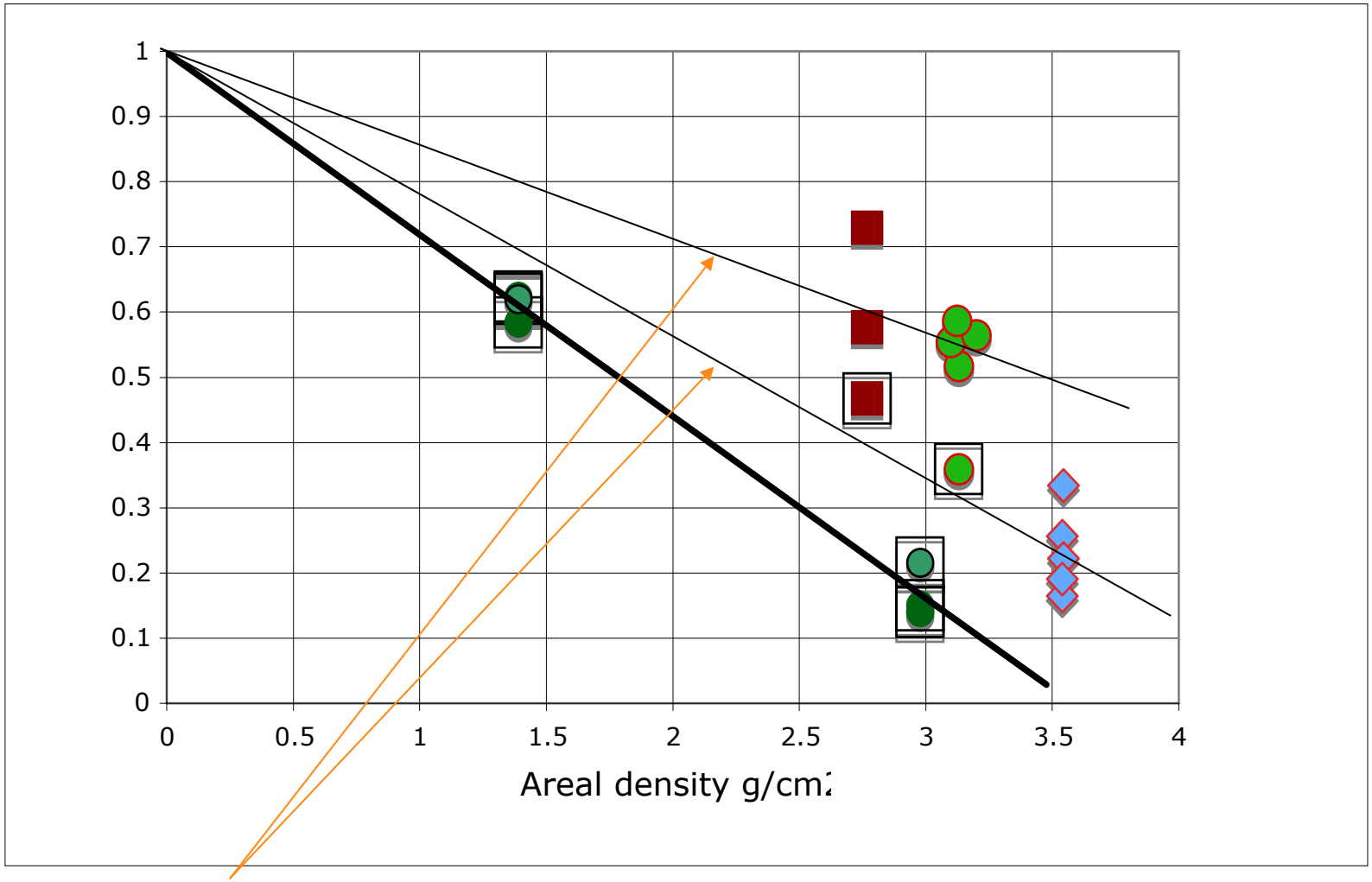
Shows SLG with 3M tape was about 34% less effective than with PU/PC mounting.

Comparison SLG and GC



Shows the efficiencies of SLG and GC are very similar.

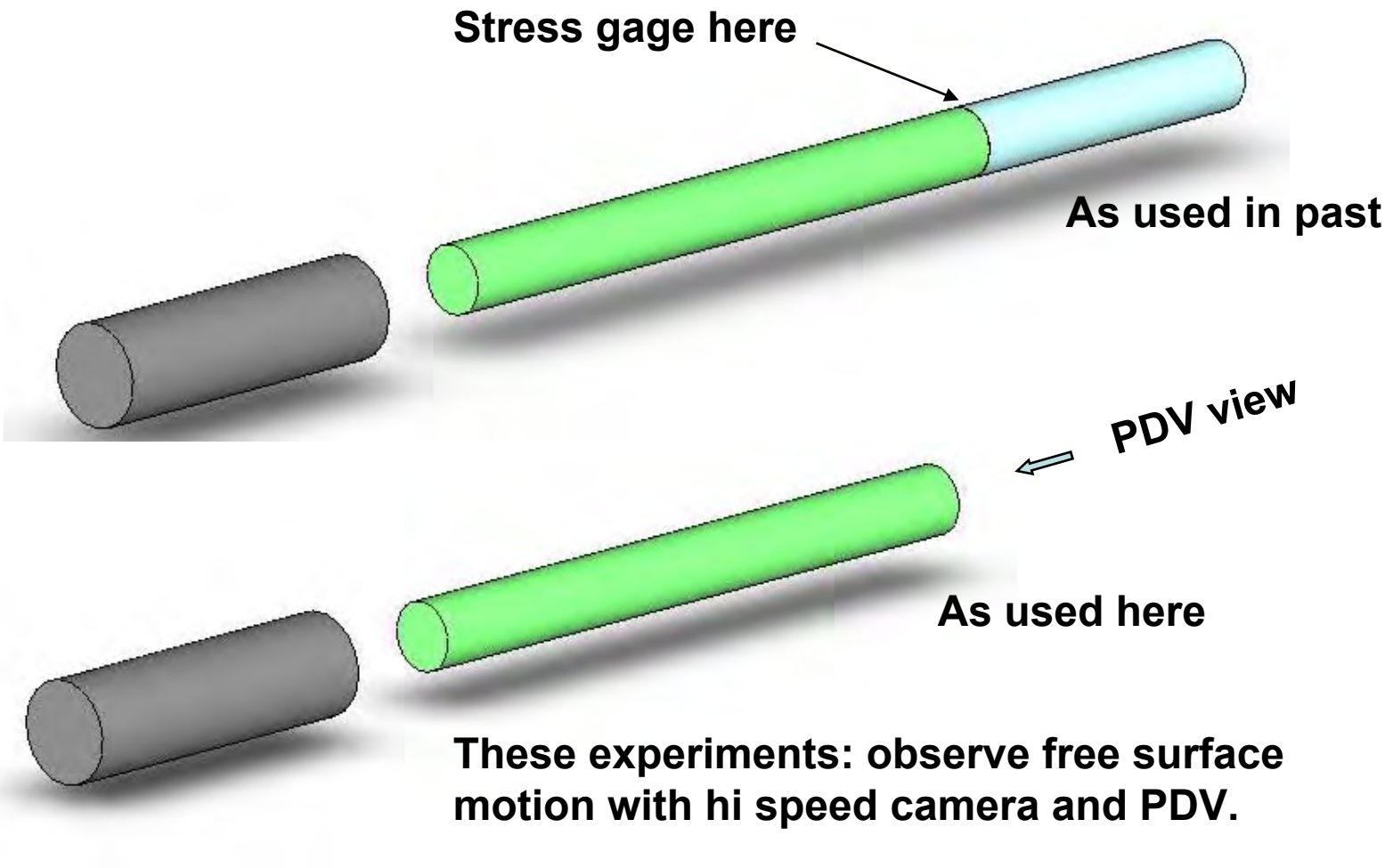
Comparison BSG and SLG



Shows that BSG is much better than SLG. Probably due to the importance of density.

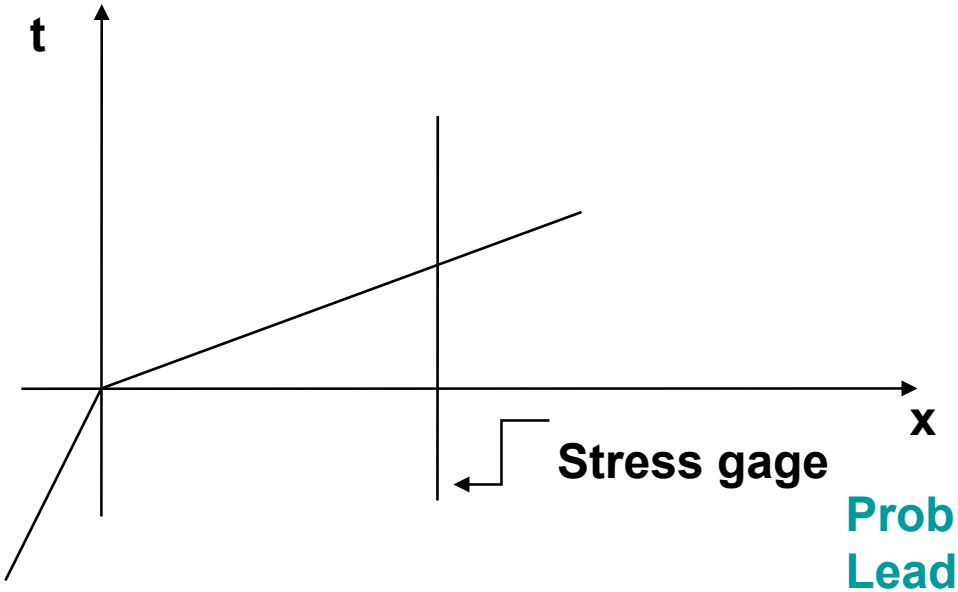
Strength Measurements on Glass

Goal: Develop technique to measure strength of glasses

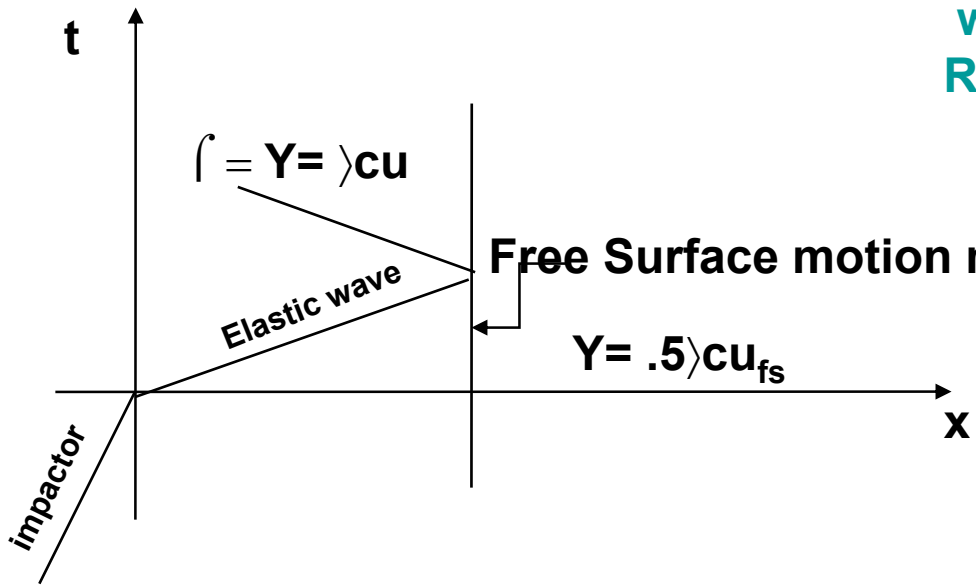


These experiments: observe free surface motion with hi speed camera and PDV.

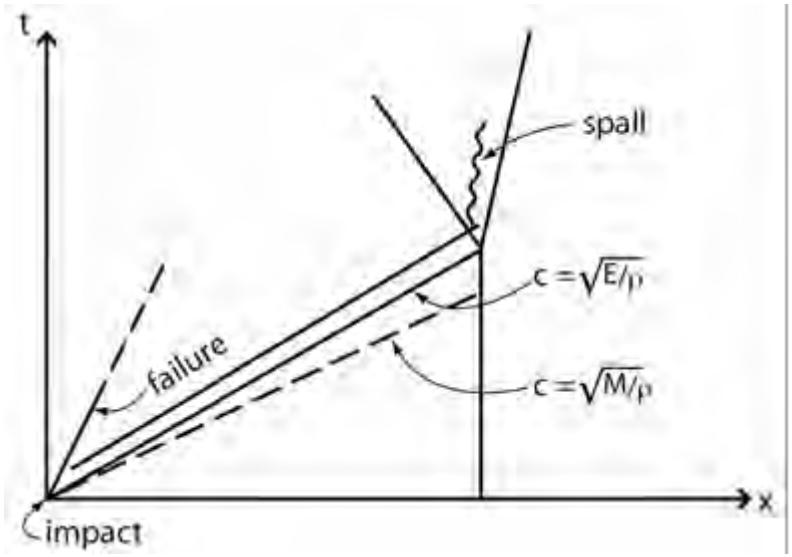
Theory (for ductile materials)



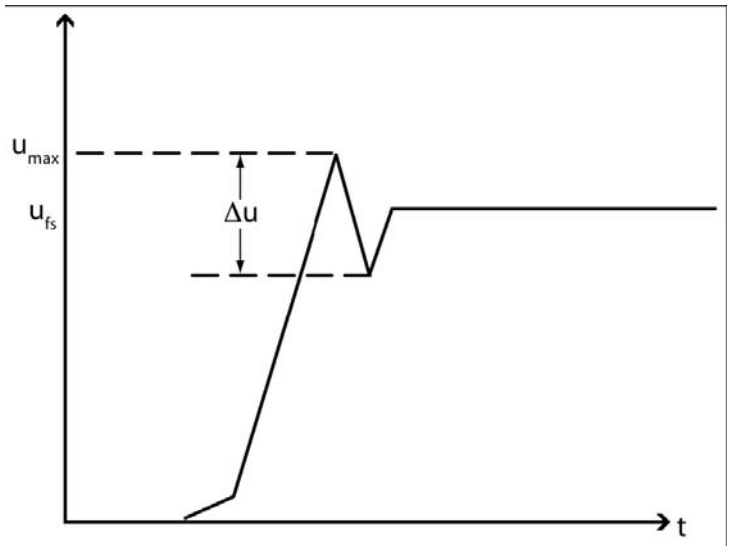
Problems with gauge –
Leads break
Very short lifetime
when used with brittle materials
Risetime limited



Theory for brittle materials



Spall equaiton

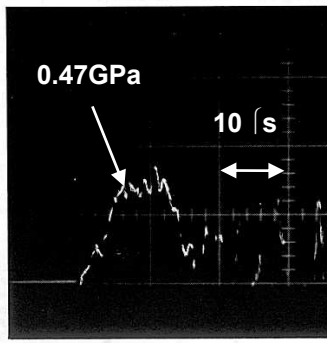


Failure causes release near impact, resulting in triangular instead of square pulse. For many brittle materials, spall strength is less than compressive strength, resulting in a "spall signal" at free surface.

(M=K+4G/3. K,G,E are elastic moduli)

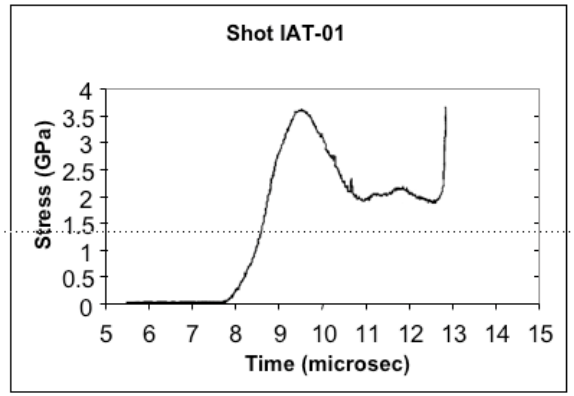
Examples of Previous work

Strength of a Mild Steel



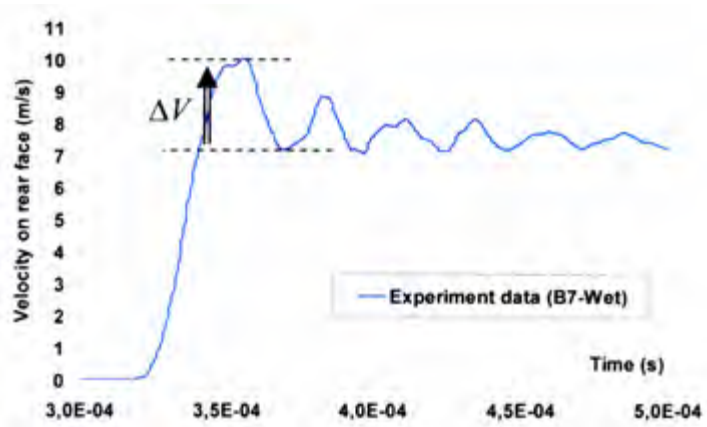
Rosenberg & Bless, 1986

Strength of Alumina



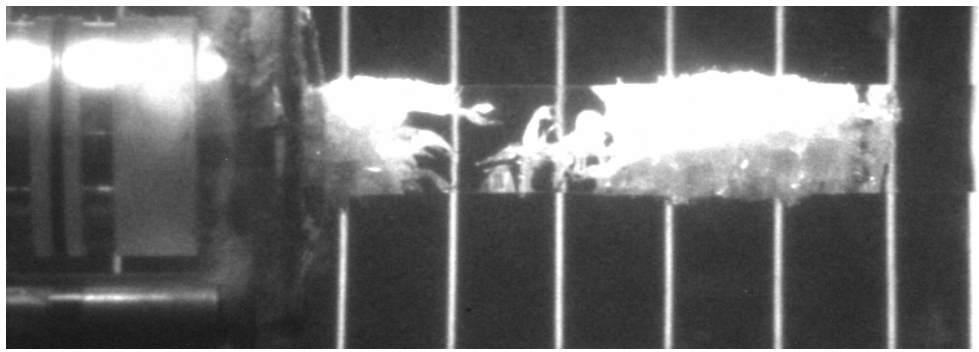
T. Beno at al, 2006, strength of alumina = 3.6 GPa

Spall in Concrete



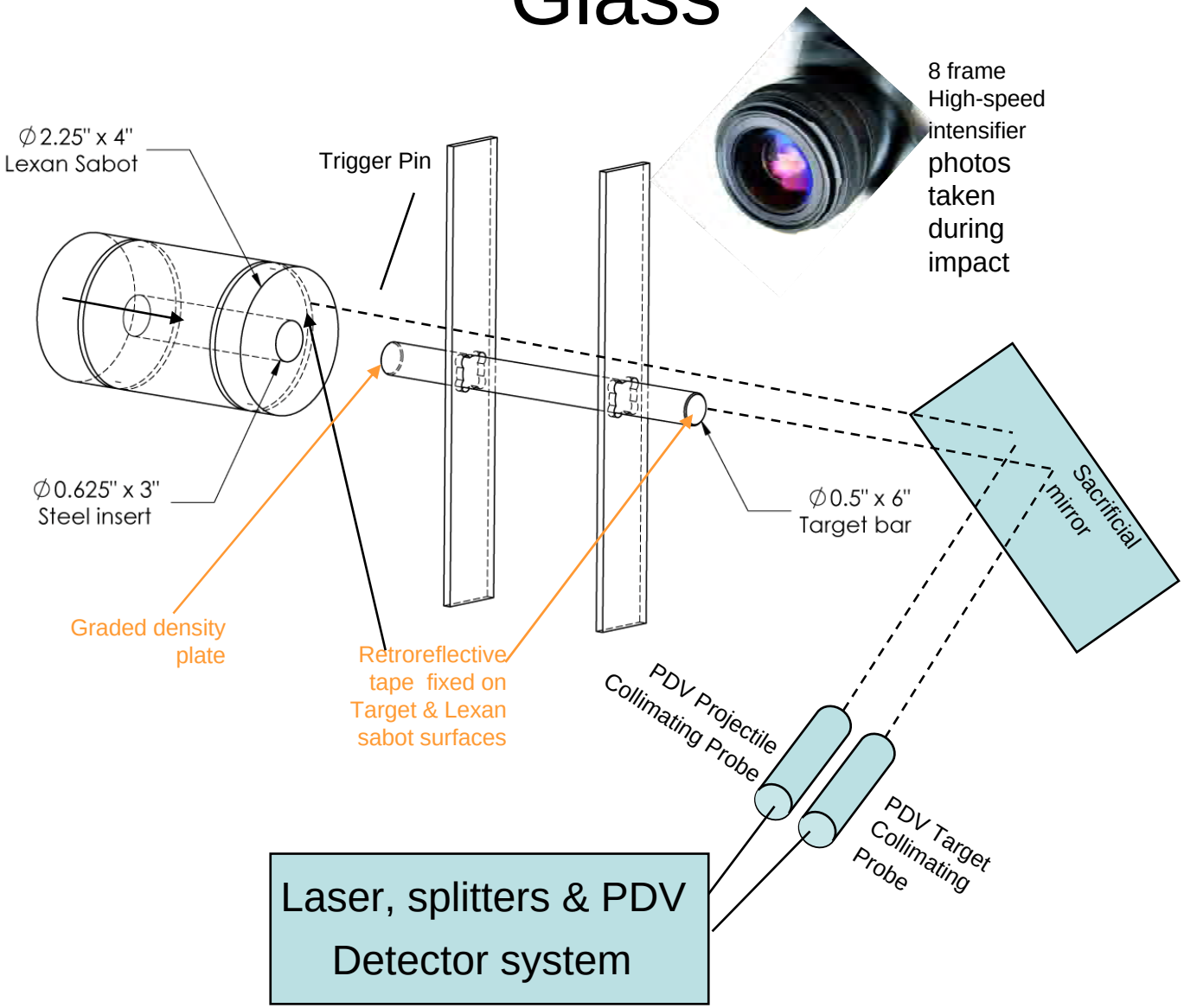
P. Forquin, & Erzan, 2008

Failure in homalite bar



Bless, 2003

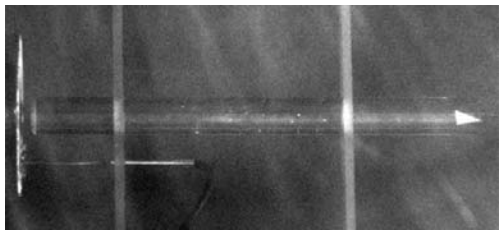
Experimental Setup for Glass



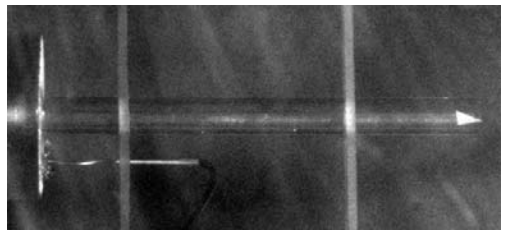
Failure process in BSG

shot A1008
borosilicate glass

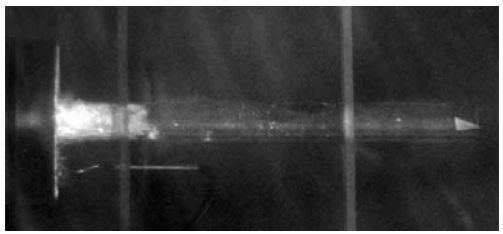
Direction of travel



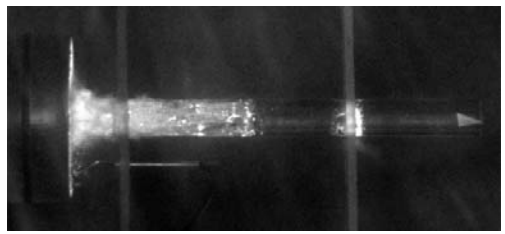
150 ✪s



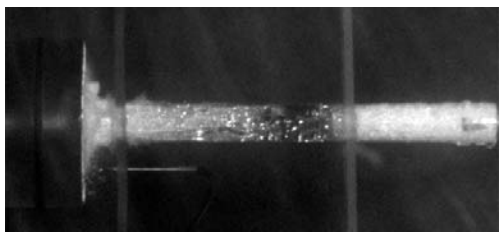
160 ✪s



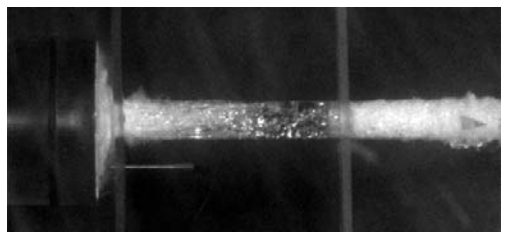
170 ✪s



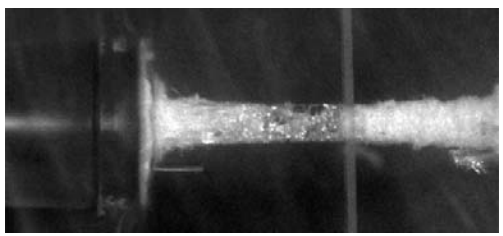
175 ✪s



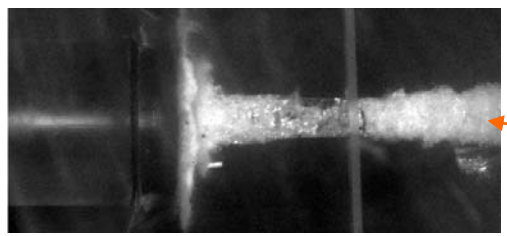
180 ✪s



200 ✪s



250 ✪s



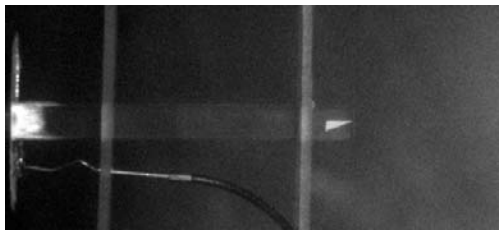
300 ✪s

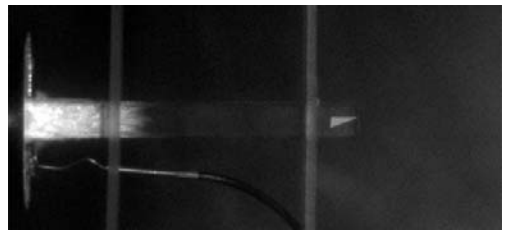
explosive tensile failure

Failure of GC rod generally very similar to glass rod

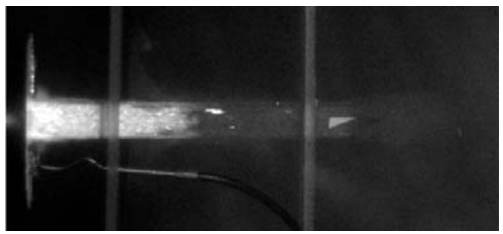
Direction of travel

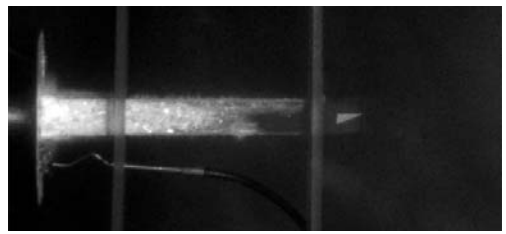
shot A1011
glass ceramic

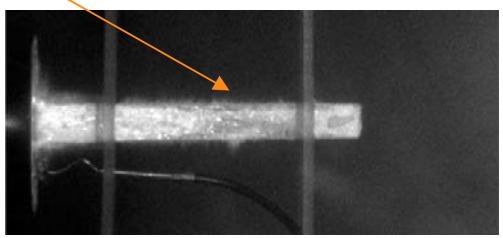

145 ✪s

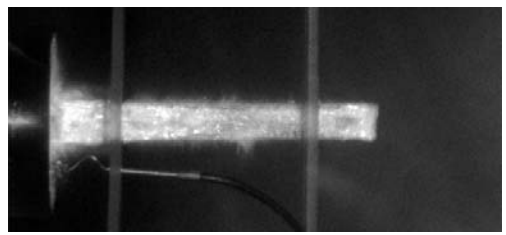

150 ✪s

No damage-free zone in middle

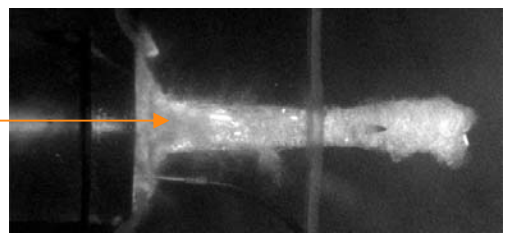

153 ✪s

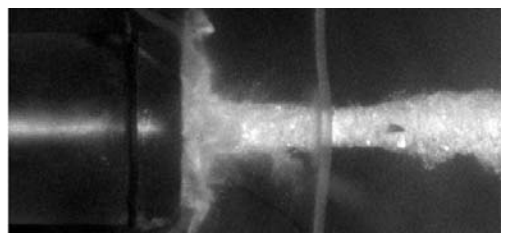

175 ✪s


180 ✪s

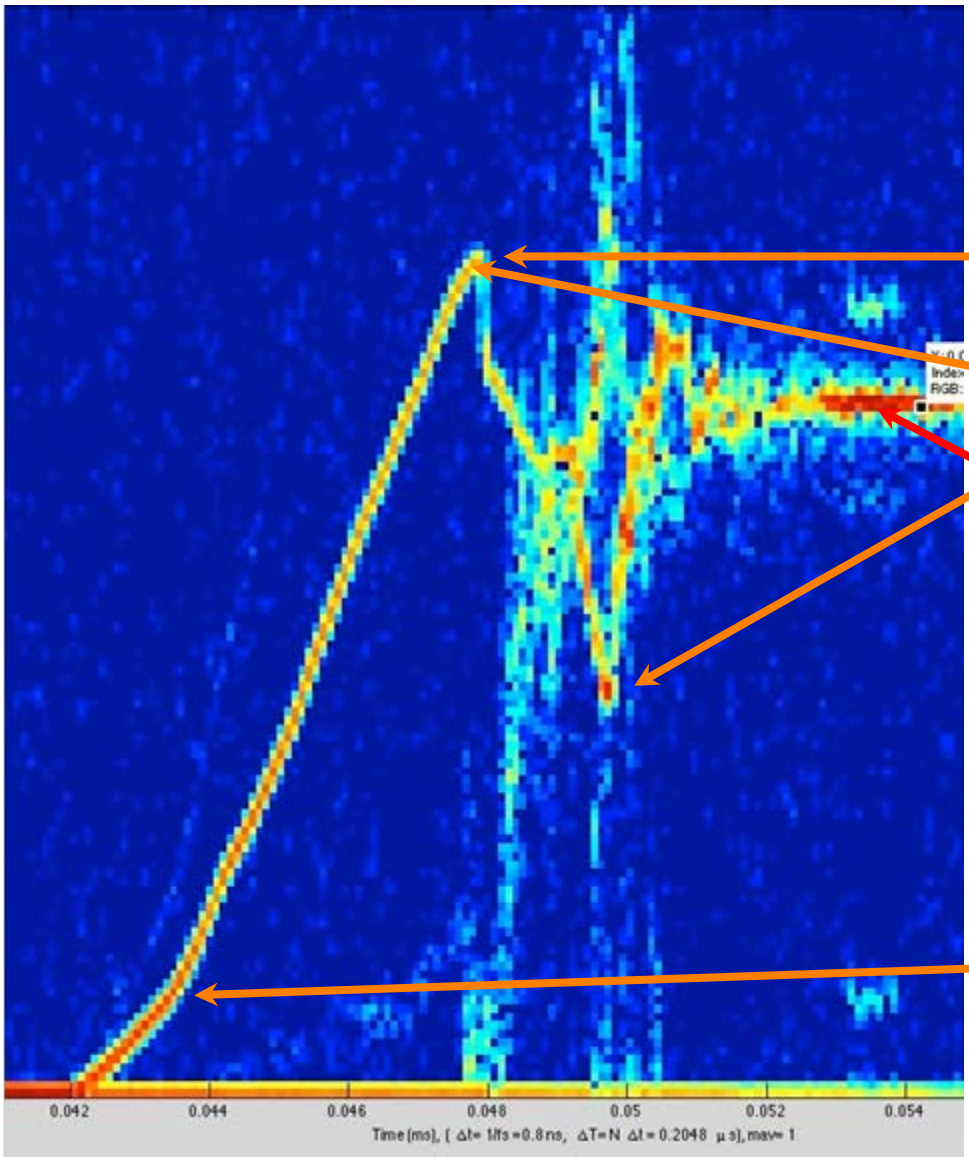

200 ✪s

More expansion in compressive zone


250 ✪s


300 ✪s

Free surface velocity data



Borosilicate glass

Peak stress = 2.2 GPa

spall pull back? = 187 m/s
spall stress = 1.1 GPa

final velocity = 307 m/s

.

Break between 1-D strain and 1-D stress waves.

10 Tests conducted

All impact velocities between 250 and 310 m/s

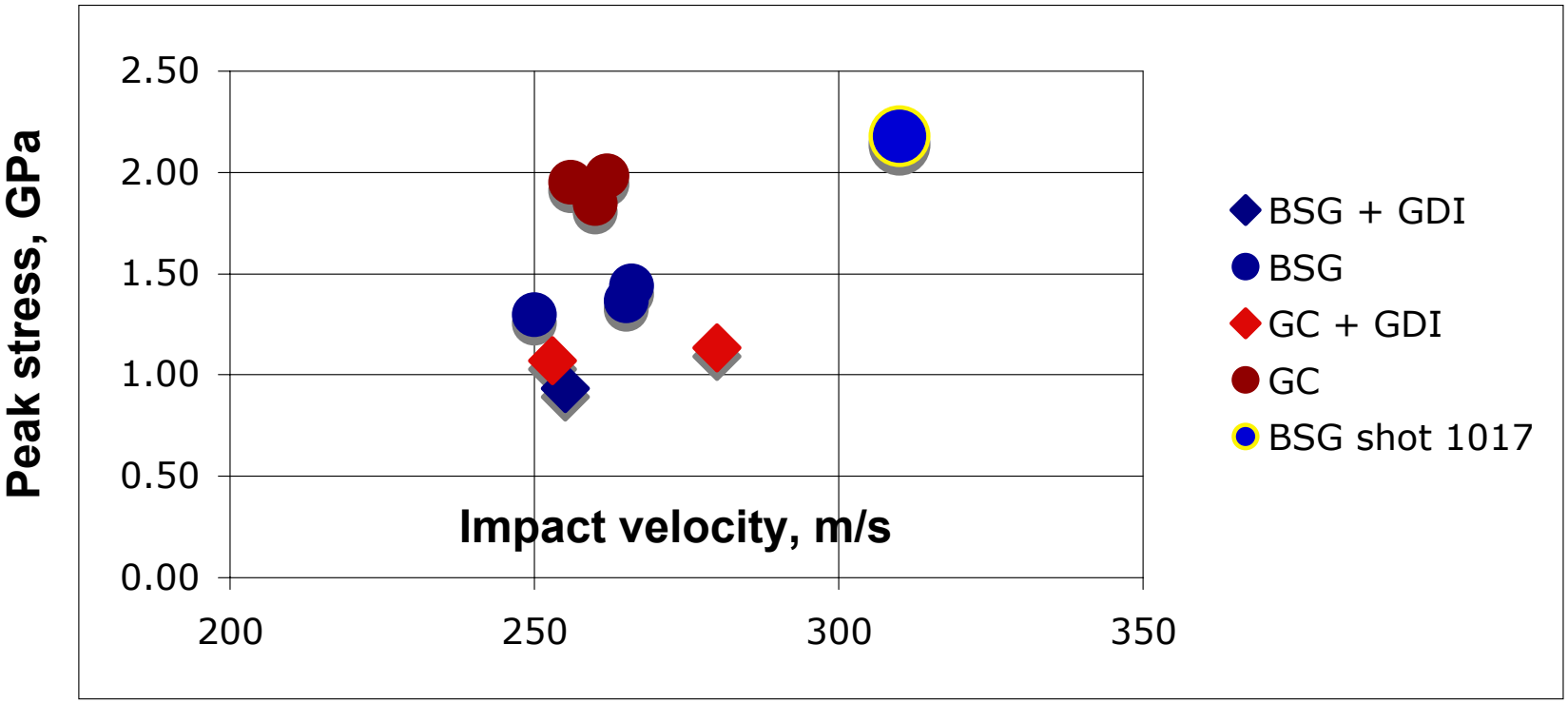
Values of stress plateau (after spall), from photos or PDV.

Test	Material	Impact Velocity (m/s)	Free Surface Velocity (m/s)	Stres (Gpa)
a1004	GC	260	287	1.84
a1007	GC	256	275	1.95
a1011	GC	262	280	1.99
a1013	GC+GDI	280	160	1.13
a1014	GC+GDI	253	151	0.84
a1015	BSG+GDI	255	160	0.93
a1003	BSG	266	247	1.44
a1008	BSG	250	223	1.30
a1012	BSG	265	235	1.37
a1017	BSG w/o Retro	310	374	2.18

GC = Glass Ceramic, BSG = Borosilicate glass

GDI=graded density impactor

Peak stress data (from PDV records)



For both materials, adding the GDI reduces measured stress.

GC is 30% stronger than BSG.

There appears to be a strong rate effect of measured peak stress.

Summary of what we learned

FSPs produce characteristic damage patterns in glass single sheets or laminates: generally radial cracks (many species) and dicing cracks.

Dicing cracks are relatively benign; not so radial cracks.

Density is much more important than strength in defeating FSP projectiles.

.

Experimental validation of the origin of the bodywork effect (K-effect) in the up-armouring of civil and military vehicles

F. Coghe[1], B. Kestelyn[2] and M. Pirlot[1]

[1] *Dept. Weapon Systems & Ballistics, Royal Military Academy*

[2] *DG Material Resources, Belgian Defence*

Overview

- Introduction
- Experimental setup, results and discussion
- Conclusion

Introduction



VIP vehicles





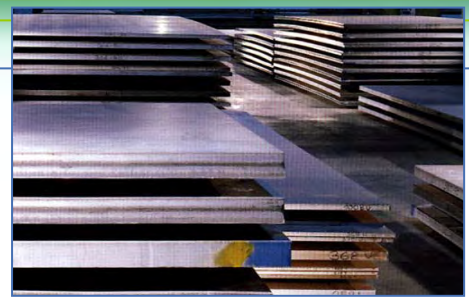
Light armoured vehicles

- Small calibre ammunition
- Fragments
- IED
-...



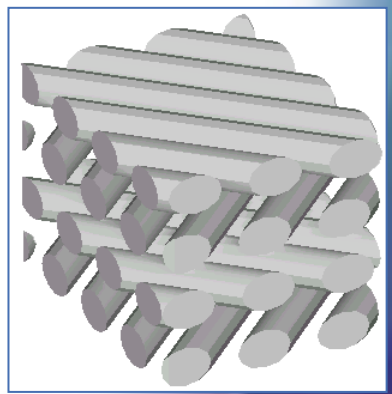
Logistic vehicles

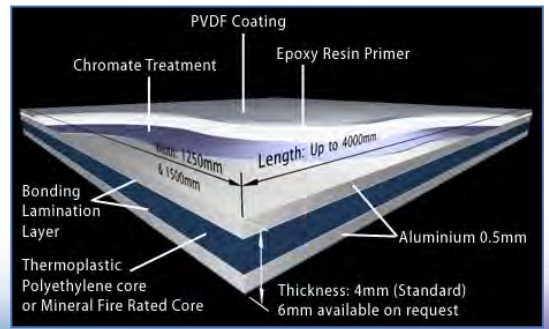
Introduction







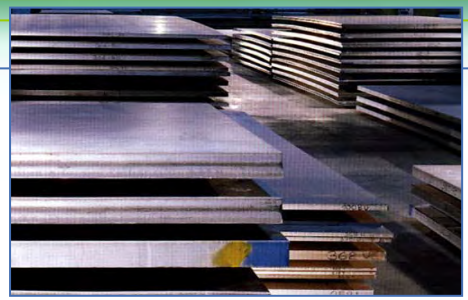




Armour materials:

- -Metals
- -Ceramics
- -Fibre
- -Composites
- -...

Introduction



STANAG 4569 Level 1



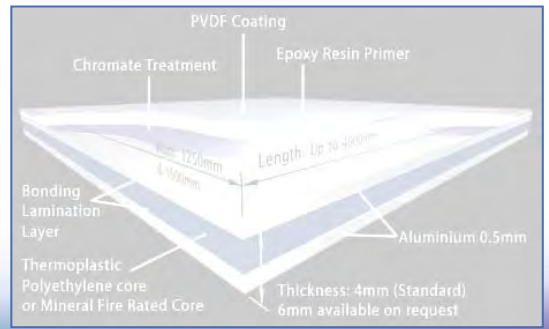
High hardness steel plates:

- -Moderate cost
- -Known processing path
- -Not weight-inefficient



Armour materials:

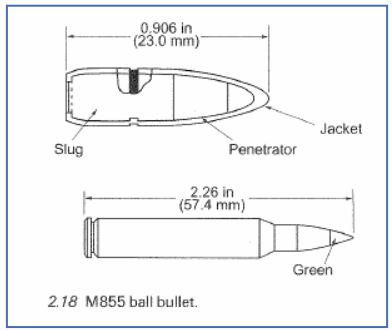
- -Metals
- -Ceramics
- -Fibre
- -Composites
- -...



Introduction

Threat

5.56 x 45 NATO Ball (M855, SS109,...)



2.18 M855 ball bullet.



Protection

Thyssen-Krupp Secure 500

(high hardness ballistic armour plate, 480-530 HB)

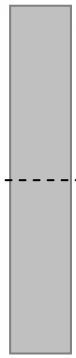
Classification	Weapon		Bullet		Test Conditions		SECURE 500 (480-530 HB)
EN 1063 / EN 1522	Type	Calibre	Type	Mass [g]	Test range [m]	Bullet velocity [1] [m·s^{-1}]	Minimum thickness for bullet resistance [mm]
BR / FB 3	hand-gun	.357 Magnum	FJ/CB/SC	10.2	5	430 ± 10	3.0 [2]
BR / FB 4		.44 Magnum	FJ/FN/SC	15.6	5	440 ± 10	3.0
BR / FB 5	rifle	5.56 mm x 45 (SS 109) *twist length: 178 ± 10 mm*	FJ/PB/SCP1	4.0	10	950 ± 10	6.5
BR / FB 6		7.62 mm x 51	FJ/PB/SC	9.5	10	830 ± 10	6.5
BR / FB 7		7.62 mm x 51 (AP) *twist length: 254 ± 10 mm*	FJ/PB/HC1	9.8	10	820 ± 10	15.5

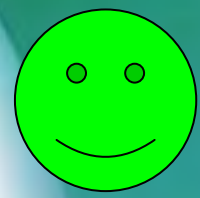
no classification	hand-gun	.44 Magnum	FJ/FN/SC	15.6	3	435 - 455	3.0
	rifle	7.62 mm x 39 (Kalashnikov)	FJ/PB/SC	7.9	25	710 ± 15	4.0
			API	7.7	25	730 ± 15	12.0
		7.62 mm x 51	FJ/PB/SC	9.5	10	785 - 795	5.5
		7.62 mm x 51 (AP)	FJ/PB/HC1	9.8	25	800 - 810	14.5
		5.56 mm x 45 (SS 92)	FJ/PB/SC	3.6	25	965 - 975	9.0

Introduction

Single armour plate





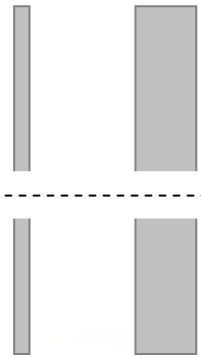


V_{50} OK

More material, less protection!!!

Armour plate behind car door panel







V_{50} not OK!!!

Experimental setup, results & discussion

Explanation

Bodywork effect

Explanation 1:

Steel penetrator loses jacket after penetration of first plate.

Steel penetrator penetrates second (armour) plate due to increased energy density.

Experimental setup, results & discussion

Validation

Analytically*:

Case 1: complete projectile

$$ED = \frac{mass_{projectile}.(speed_{projectile})^2}{2.\left(\frac{diameter_{projectile}}{2}\right)^2.\pi} = \frac{0{,}004kg.(1000m/s)^2}{2.\left(\frac{0{,}889.10^{-3}m}{2}\right)^2.\pi} = 3222kJ/m^2$$

Case 2: steel penetrator and lead slug

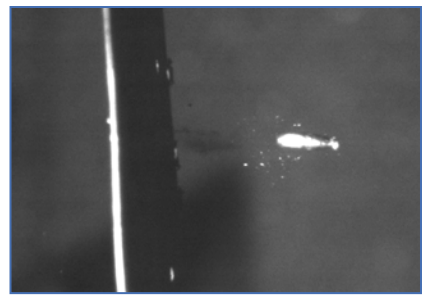
$$ED = \frac{mass_{projectile}.(speed_{projectile})^2}{2.\left(\frac{diameter_{projectile}}{2}\right)^2.\pi} = \frac{0{,}00324kg.(1000m/s)^2}{2.\left(\frac{2{,}68210^{-3}m}{2}\right)^2.\pi} = 457kJ/m^2$$

+ Nsiampa et al. (23rd ISB)

* Based on the technical drawings FN SS109

Experimentally:

High speed photography (1mm mild steel plate)



Soft recovery

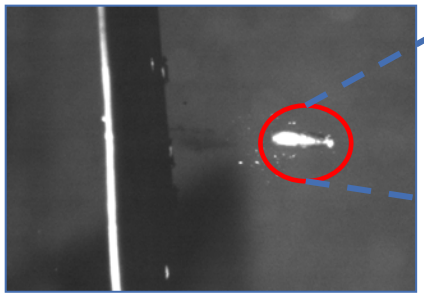


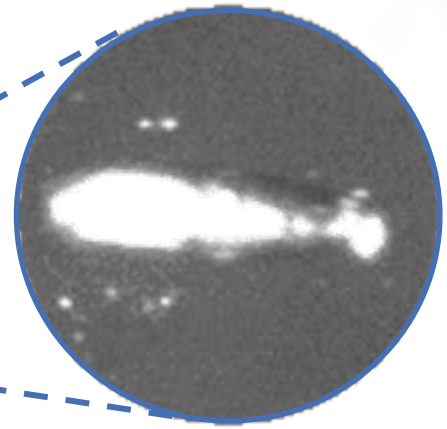
Experimental setup, results & discussion

Validation

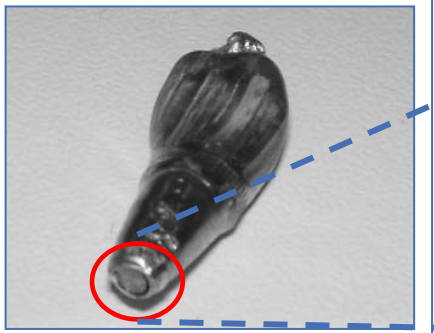
Experimentally:

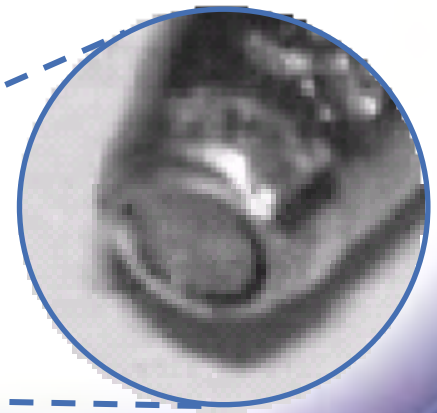
High speed photography (1mm mild steel plate)





Soft recovery





Experimental setup, results & discussion

Explanation

Bodywork effect



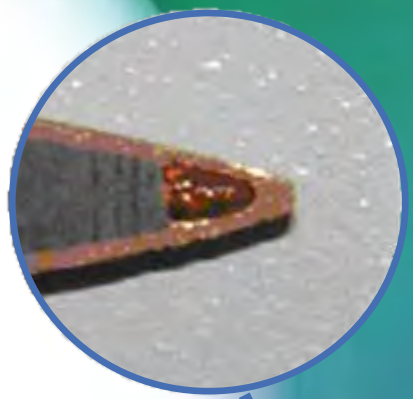
Steel [illegible]tor loses jac[illegible] after
[illegible]etra[illegible] of first pla[illegible]

Steel [illegible]netrator p[illegible]trates [illegible]cond
(armou[illegible]late due to [illegible]eas[illegible]energy
density.

Experimental setup, results & discussion

Explanation

Bodywork effect



Explanation 2:

Penetration through first plate changes geometry of projectile nose (flattening).

Changed geometry changes penetration mechanism during impact on the second (armour) plate.



Experimental setup, results & discussion

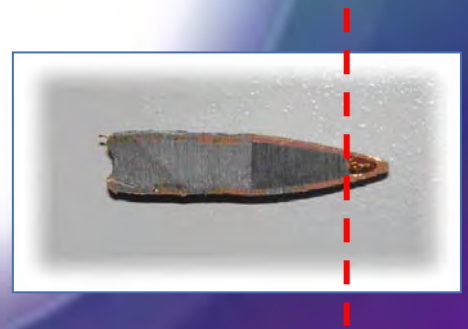
Validation

- Adapted projectile geometry:





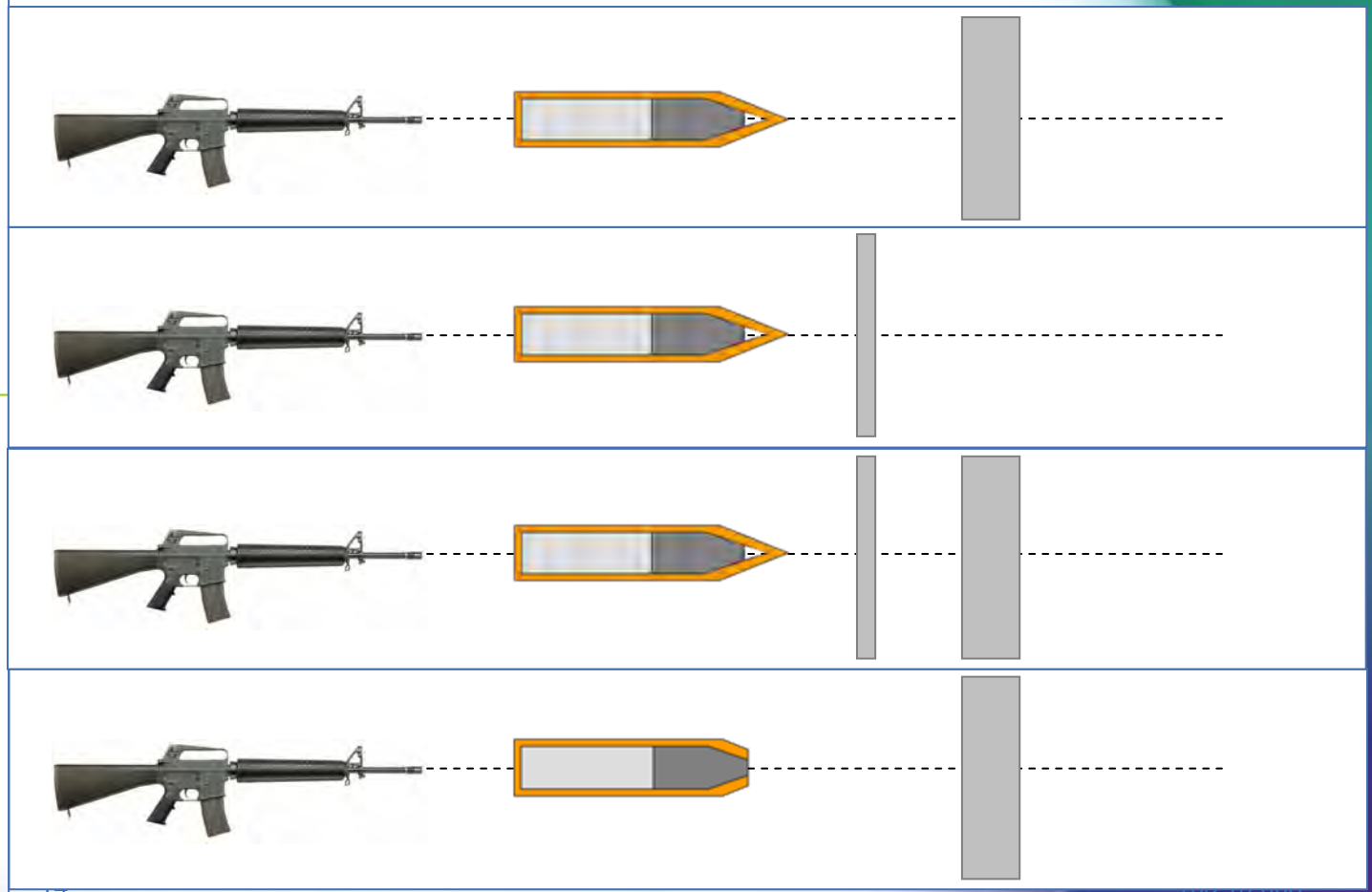
Truncated nose



Experimental setup, results & discussion

Validation

4 different projectile – target combinations:



Experimental setup, results & discussion

Validation

Test	Projectile	Thickness bodywork plate (mm)	Thickness armour plate (mm)	V_{50} (m/s)
1		/	6.5	**1002.5**
2		1	/	**40.2****
3*		1	6.5	**963.9**
4		/	6.5	**910.2**

* 10 mm air gap
** Residual velocity measurement

Experimental setup, results & discussion

Validation

Test	Projectile	Thickness bodywork plate (mm)	Thickness armour plate (mm)	V_{50} (m/s)
1		/	6.5	**1002.5**
2		1	/	**40.2****
3*		1	6.5	**963.9**
4		/	6.5	**910.2**

±40m/s

* 10 mm air gap
** Residual velocity measurement

Experimental setup, results & discussion

Validation

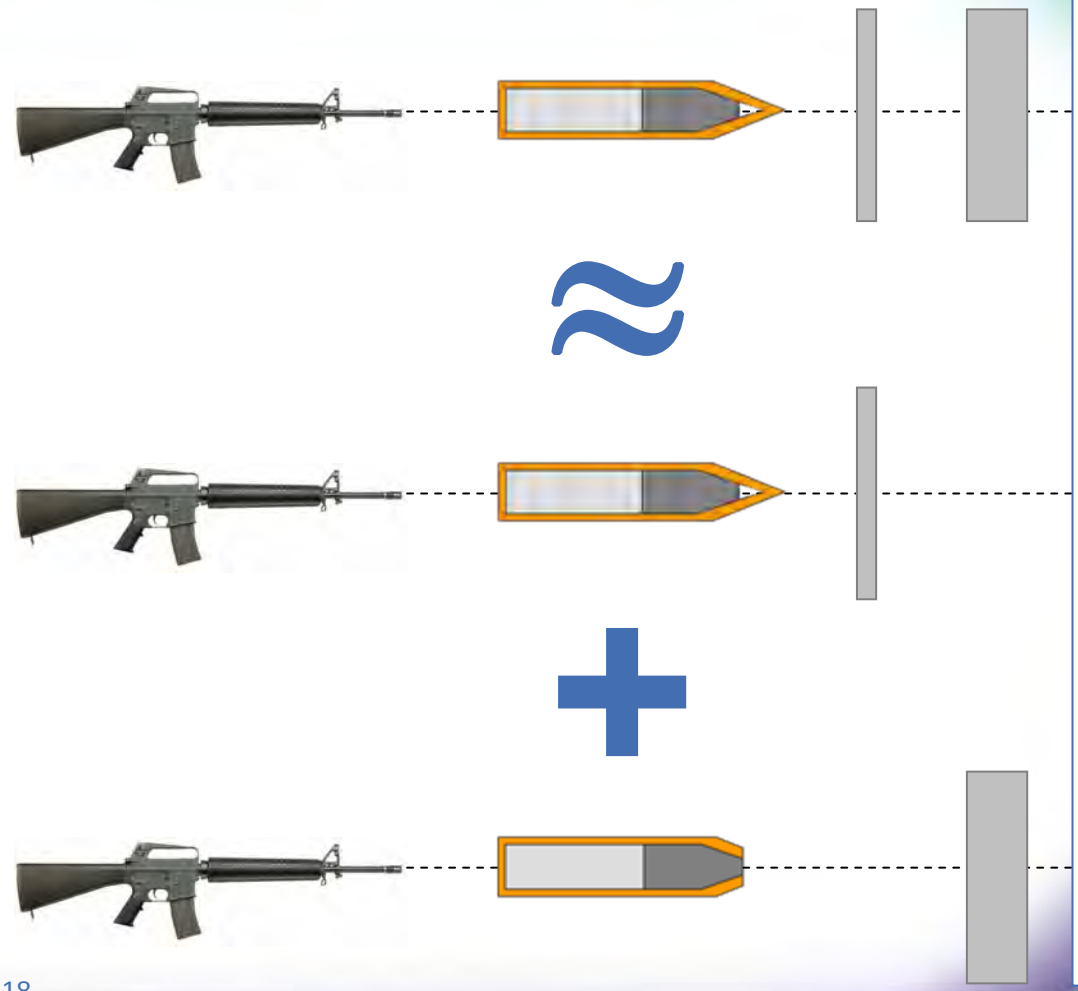
Test	Projectile	Thickness bodywork plate (mm)	Thickness armour plate (mm)	V_{50} (m/s)
1		/	6.5	**1002.5**
2		1	/	**40.2****
3*		1	6.5	**963.9**
4		/	6.5	**910.2**

±90m/s

* 10 mm air gap
** Residual velocity measurement

Experimental setup, results & discussion

Validation



V_{50}:

963 m/s

≈

40 m/s

+

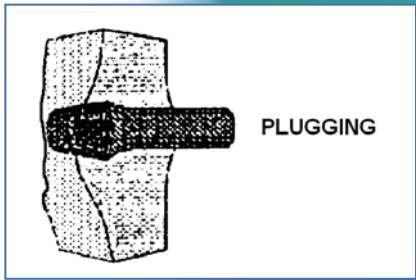
910 m/s

Experimental setup, results & discussion

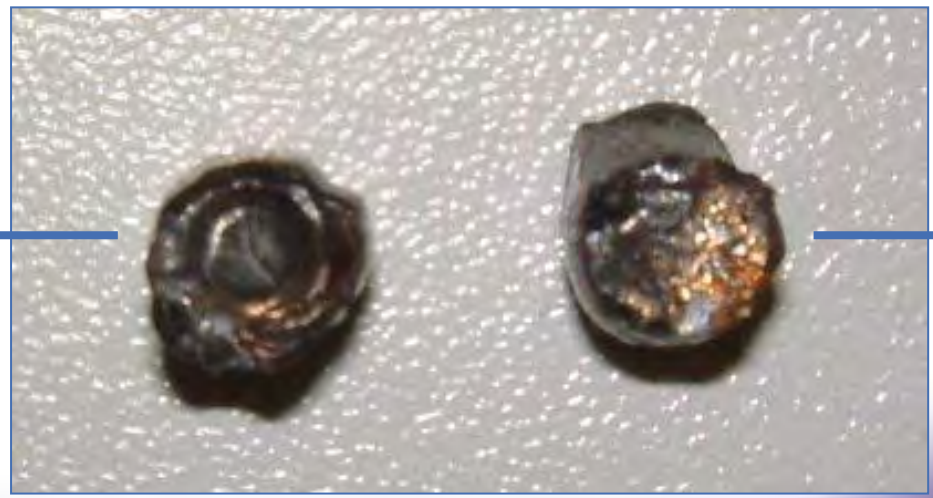
Failure mechanism

Limited ductility even further reduced due to shear localization

Plugging



Adapted projectile



Standard projectile

Conclusion

Summary

- Bodywork effect caused by changed projectile shape, which leads to enhanced plugging failure.
- Importance of in-situ testing!!!
- Be careful with norms and standards!!! Check real value.

Conclusion

Further work

- Numerical simulation
  - Dynamic material characterization
- Other projectiles
  - 7.62 x 39 M1943 Soviet
  - AP (hard core)




Questions???

Predicting Hazard Response Scenarios in Weapon Systems

Ian Cullis, I Brown, P Church, P Gould, V Ingamells

A presentation to: 24th International Symposium on Ballistics



Date: 22nd - 25th September 2008

© Copyright QinetiQ limited 2008

Contents

01 Background

02 Material Models: EOS

03 Material Models: Constitutive Response

04 CHARM

05 Munition System Application

06 Conclusions

07 Acknowledgements



© Copyright QinetiQ limited 2008

01 Background

The changes in the way the UK armed forces are being asked to deploy as part of Rapid Reaction peacekeeping forces and their long-term evolution into the Balanced Force concept demands the transport and store in forward ammunition dumps of different mixes of weapon systems and ammunition. An understanding of the associated hazard would allow this to be achieved with a minimum and well-defined risk factor.

It is an essential element of the MoD's Duty of Care to the Armed Forces.

© Copyright QinetiQ limited 2008

01 Background

Camp Falcon: US Army Ammunition Holding Area Iraq.

- 10th October 2006 Insurgent attack with 82mm mortars.
- Struck storage area for flares & illumination munitions. Started fire which spread to other stores.
- 7 EOD teams fully committed dawn to dusk
- Needed to secure area 1000ft radius.
- FIRE is an important hazard!





© Copyright QinetiQ limited 2008

01 Background

Hazard Responses.

- Type 1: Detonation, characterised by a supersonic decomposition reaction.
- Type II: Partial detonation.
- Type III: Fast combustion of confined material (explosion) with a local pressure build up.
- Type IV: Combustion/deflagration characterised by a non-violent pressure release.
- Type V: Combustion.

Research Context.

- Need a fundamental understanding of the controlling physics and chemistry within energetic materials.
- This applies to ALL systems that contain an energetic material component.
- It provides a key component in establishing Through Life Cost of any munition procurement.

© Copyright QinetiQ limited 2008

01 Background

Building Blocks

- Constitutive Response: deformation heating
- Chemical Response: ignition & growth
- Burning Response: deflagration, detonation

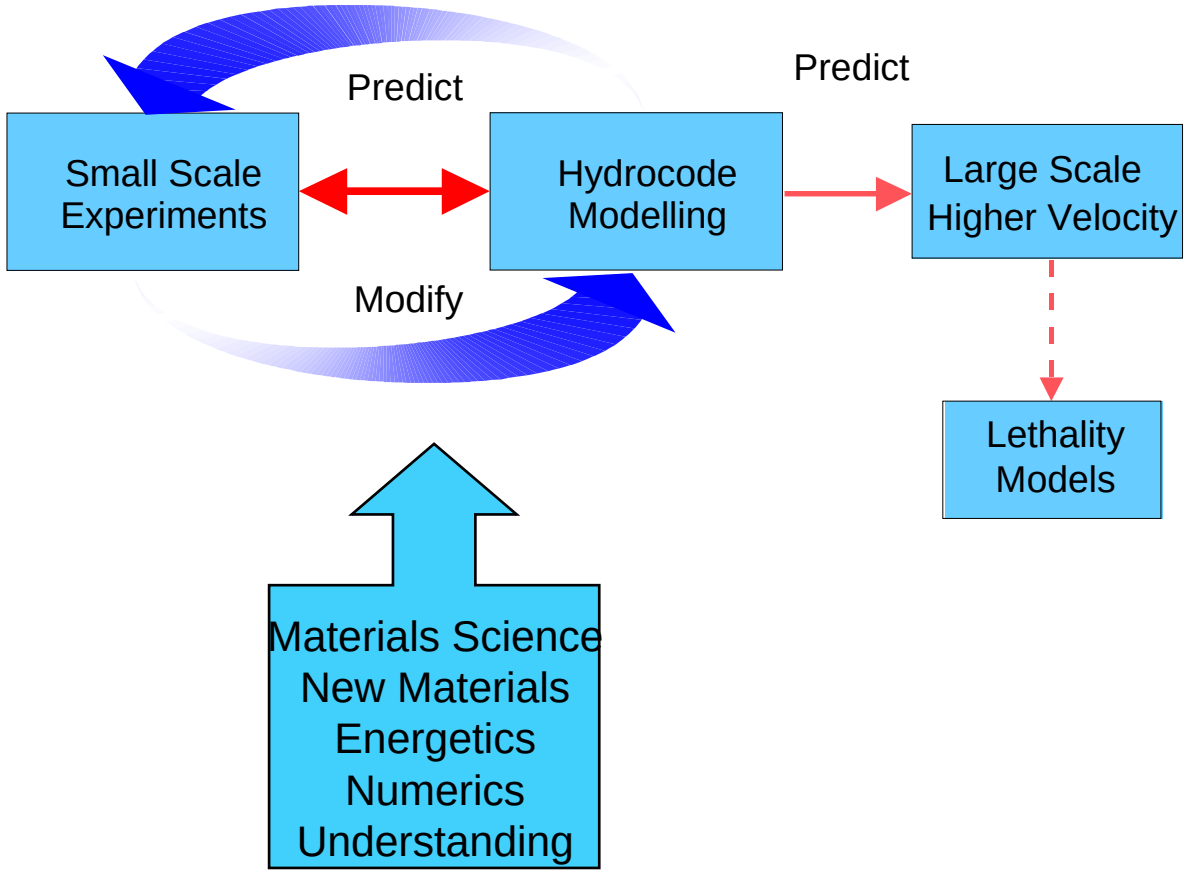
Needs

- Material models: EoS, constitutive, damage, fracture
- Ignition mechanisms and their description
- Link between constitutive response (damage) and ignition source term
- Burning models
- Experiments: characterisation, validation

© Copyright QinetiQ limited 2008

01 Background

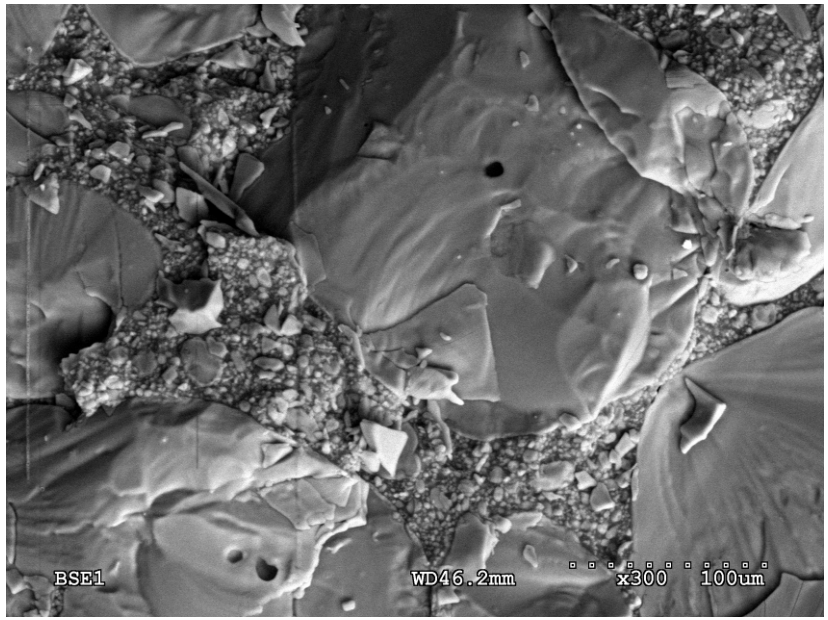
Integrated Modelling



© Copyright QinetiQ limited 2008

02

Material Model: Equation of State



© Copyright QinetiQ limited 2008

02 Materials Models

Objective

To develop predictive Equations of State based on materials science with as few fitting parameters as possible – ideally none. Porter-Gould methodology, based on Group Interaction Modelling.

To develop predictive continuum based deformation and failure algorithms. These attempt to link the meso-macro scale and deal with anisotropic plastic deformation, failure and fracture.

Active strategy for the past 25 years – pioneered by Barry Goldthorpe, Philip Church.

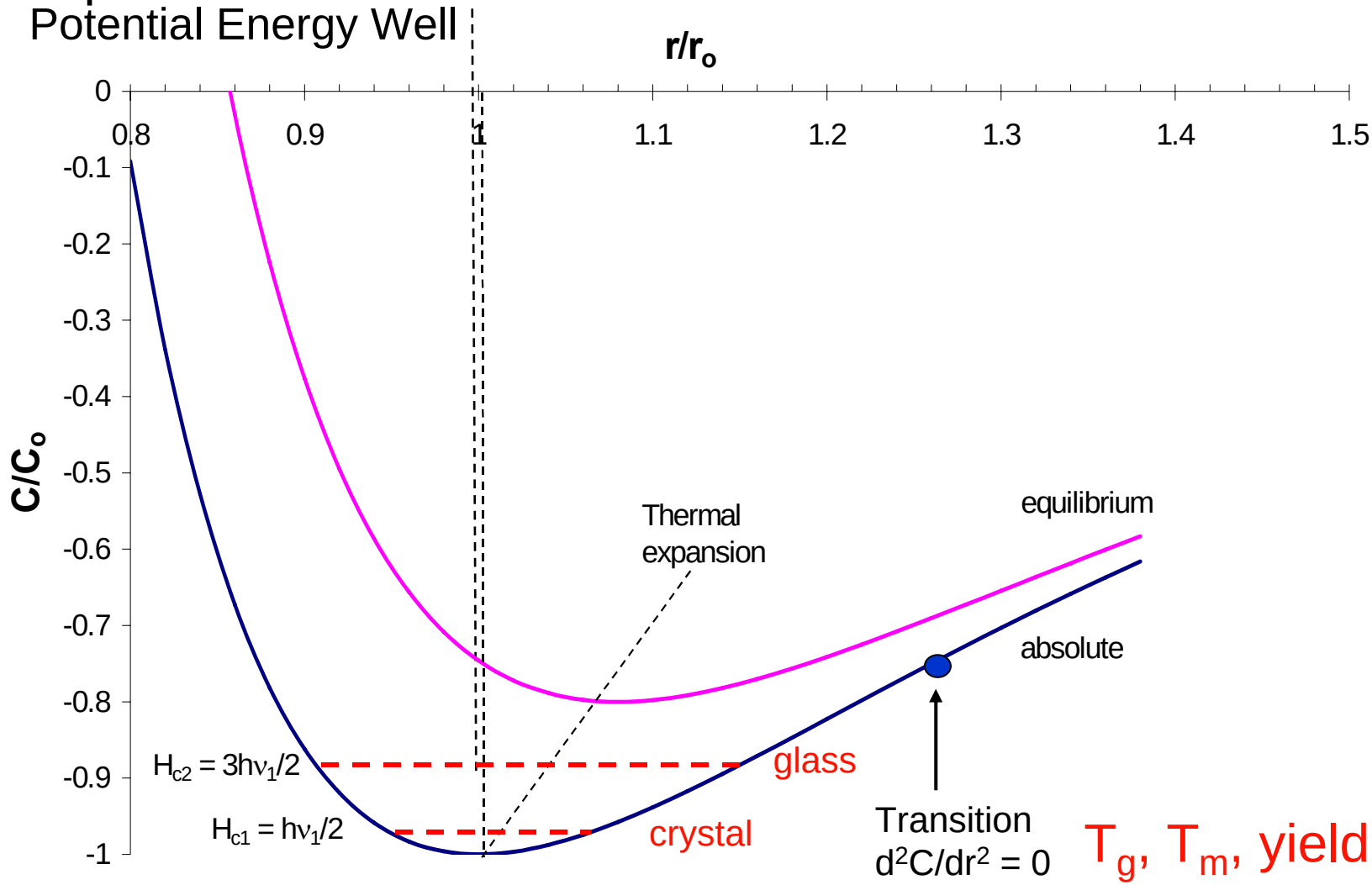
Different approach to materials tests and models.

Predictive - within 5% of experiment or within experimental error.

© Copyright QinetiQ limited 2008

02 Equations of State

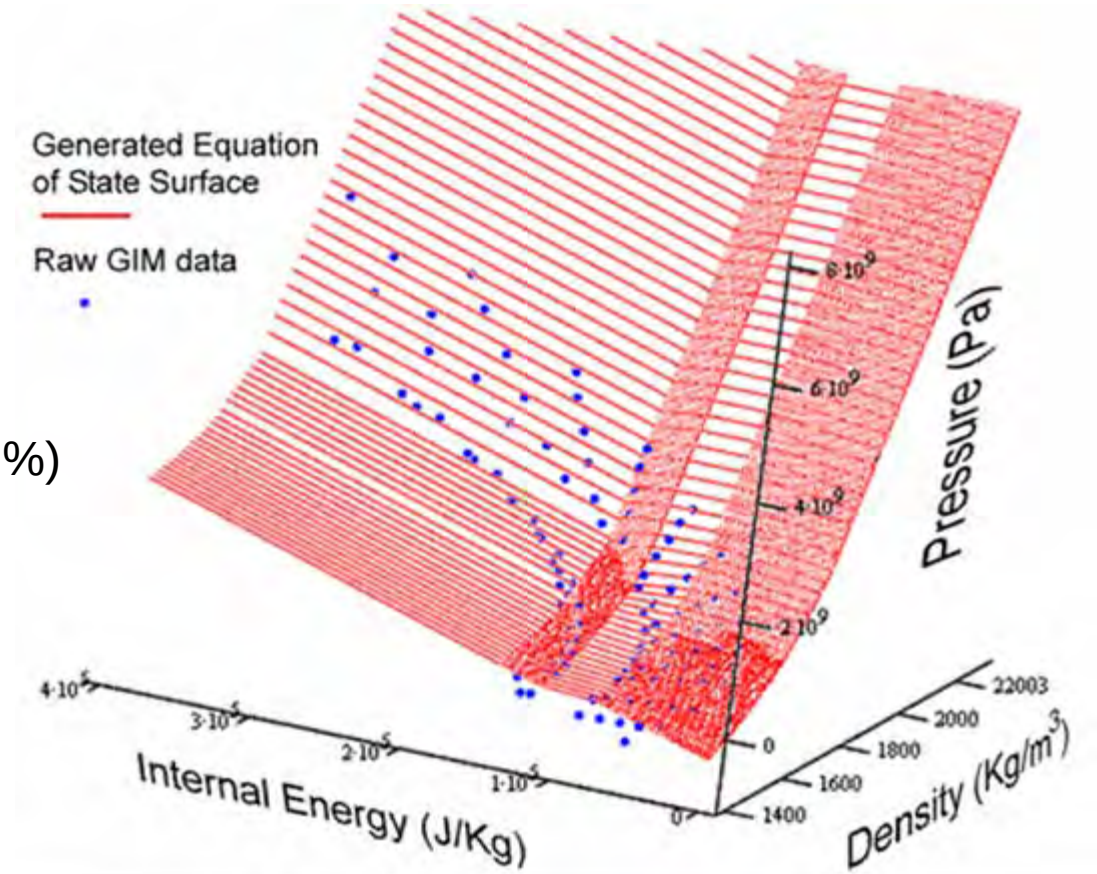
Potential Energy Well



© Copyright QinetiQ limited 2008

02 Equations of State

RX1100
(RDX:HTPB :: 88%:12%)



© Copyright QinetiQ limited 2008

02 Equations of State

Specific Heat

Activation Model

Prediction of reaction properties: HTPB

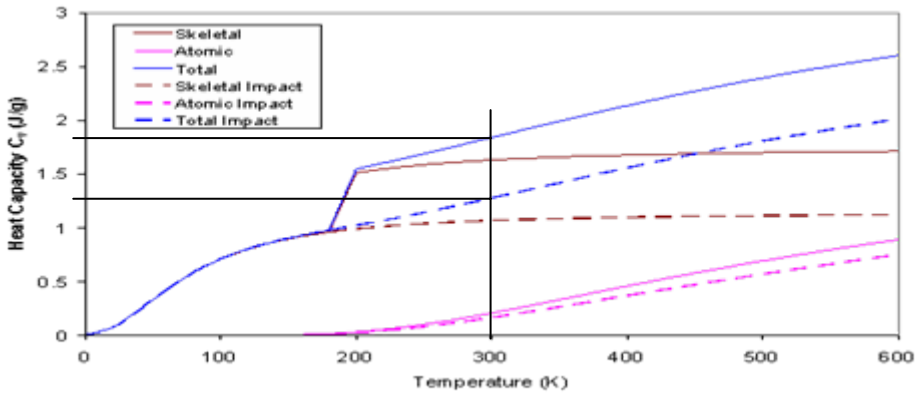
Experimental: C_p = 1.95 Jg^{-1} at 300K

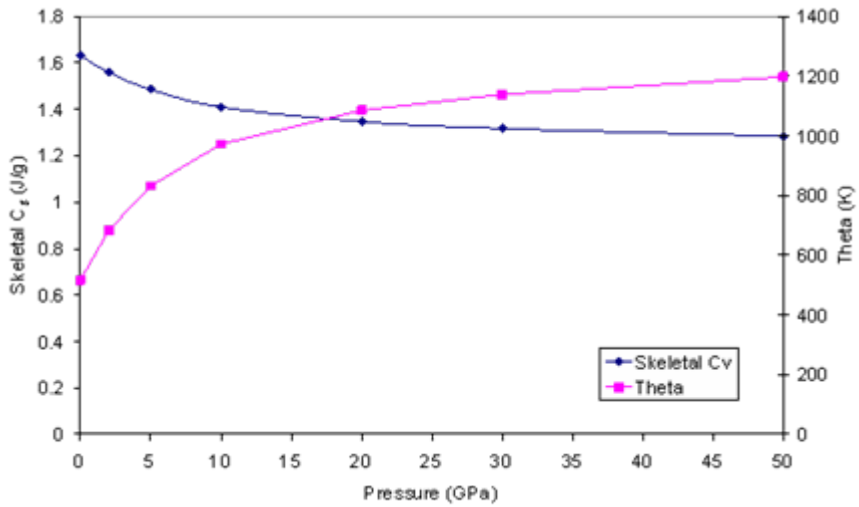
Model: C_v = 1.86 Jg^{-1} at 300K

Menikoff: C_p and C_v differ by only 5% for these materials

RDX: Cv = 0.96 Jg^{-1} compared with experimental Cp = 1.0 Jg^{-1}

Can also predict the dependency with pressure, a significant effect and crucial for hazard studies





© Copyright QinetiQ limited 2008

03

Material Model: Constitutive Response



© Copyright QinetiQ limited 2008

03 Constitutive Response

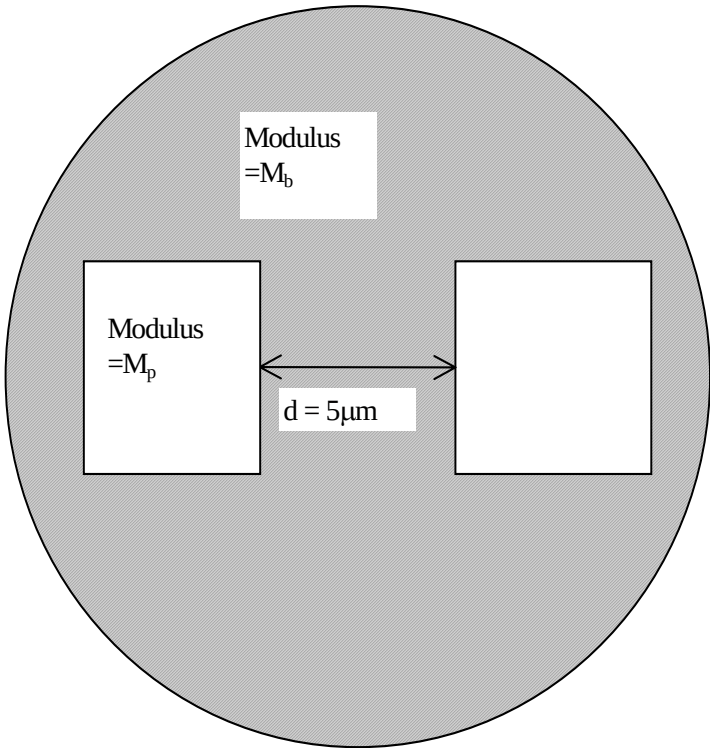
Binder properties

- Predicted from chemistry via Group Interaction Modelling
- Particle size distribution magnifies the binder effects
- Hierarchical model built up through multiple length scales
- Elastic material with an elastic limit
- Unique approach

© Copyright QinetiQ limited 2008

03 Constitutive Response

Hierarchical model



Local composite modulus

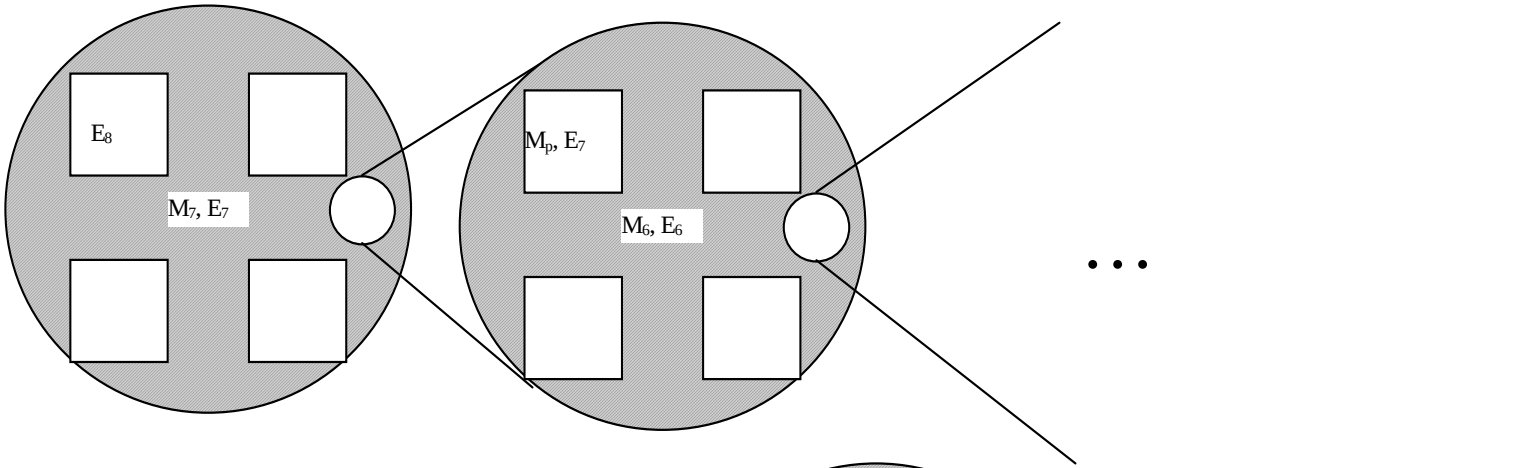
$$\frac{1}{M_{local}} = \frac{f_{V,particle}}{M_{particle}} + \frac{f_{V,binder}}{M_{binder}}$$

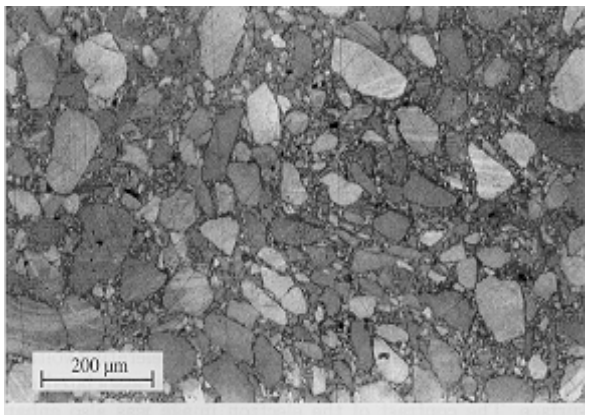
Schematic of smallest length scale within composite

QINETIQ/08/02238

© Copyright QinetiQ limited 2008

03 Constitutive Response





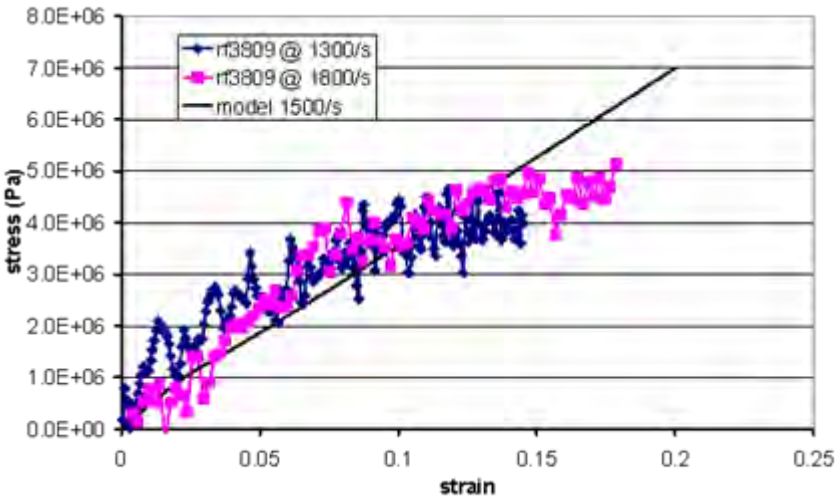
Micrograph from: PJ Rae, HT Goldrein, SJP Palmer, JE Field, AL Lewis, Proc. Roy. Soc. Lond. A**458** (2002) pp743-762

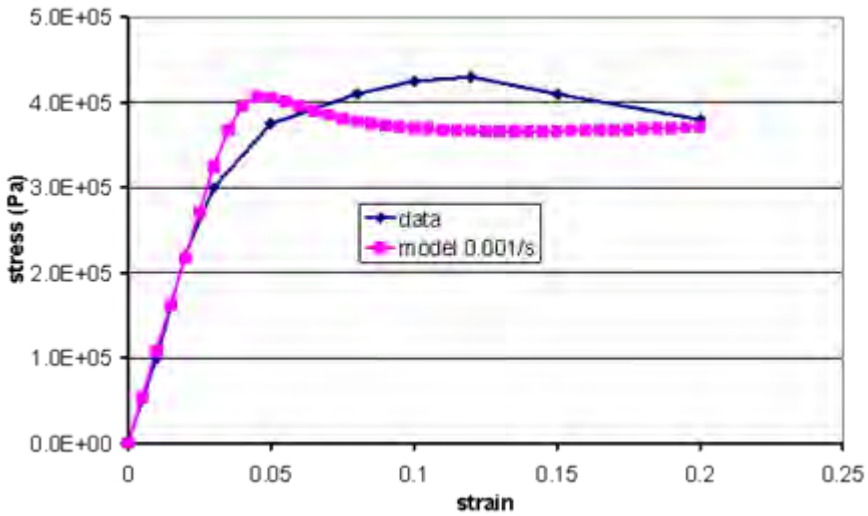
© Copyright QinetiQ limited 2008

03 Constitutive Response

Basic Model

- Can predict stress – strain behaviour over a range of strain rates.





© Copyright QinetiQ limited 2008

03 Constitutive Response

Two types of failure:

- damage
- fracture

Damage is local failure and may lead to hazard response

Fracture is complete failure - material can no longer support load

Need to quantify the effect upon deformation and upon hazard response

addressing specific microstructural events

© Copyright QinetiQ limited 2008

03 Constitutive Response

Energy segregation gives most deformation energy in binder.

Work to fracture the binder is significantly lower than for interface or for filler particles.

Most likely damage is local brittle failure of binder leading to voids and removal of constraint.

Fracture of filler particles will lead to increased hazard.

© Copyright QinetiQ limited 2008

03 Constitutive Response

Polymer properties calculated by considering the separation distance of polymer chains. (GIM)

Chain separation beyond a certain distance breaks the weak bond between chains on one side.

This relaxes any constraint on the polymer chain but still allows it to support load via bonds with chains on other sides.

On a continuum level we can introduce the concept of a “failed” state – a polymer chain that has been separated from some of its neighbours by a cavitation event. As crazing is a general nucleation of cavitation sites then in any particular volume, there will be a fraction of “failed” states that do not contribute to constraint – although they will contribute to modulus.

Crazes link to form planes.

QINETIQ/08/02238

© Copyright QinetiQ limited 2008

03 Constitutive Response

Evolution of binder modulus can be determined as a function of damage.

$$M_b = 2.5 - 1.9 * f_f$$

$$f_f = \frac{2 * \exp\left(-E_0 / E\right)}{1 + \exp\left(-E_0 / E\right)}$$

We can predict:

- spacing of craze planes and thus surface area
- craze size and number of voids in each craze
- void size

- Craze planes close up on unloading
- Can predict conditions under which particles will crack

© Copyright QinetiQ limited 2008

03 Constitutive Response

Material Damage

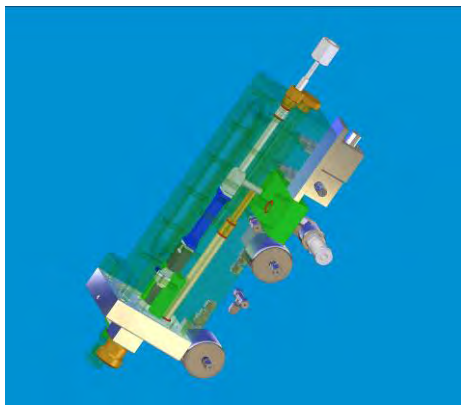
- Extensive research in polymers on this subject.
- Damage in composite due to debonding.
- Tomography provided validation. Can estimate created surface area caused by debonding.
- Implemented in GRIM and tested on different insults to ROWANEX1100.
- Basis for a variable hotspot density model in ignition and growth models.
- Ideas successfully being developed to describe cement composites.

© Copyright QinetiQ limited 2008

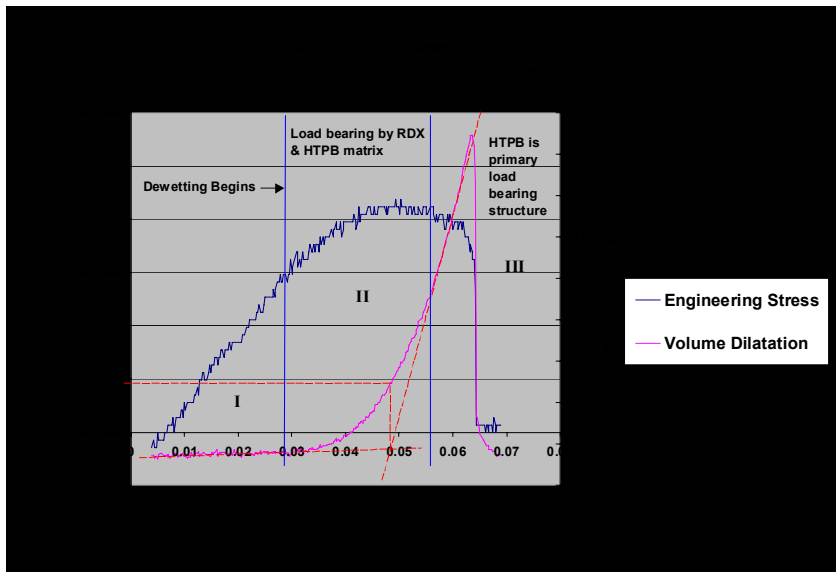
03 Constitutive Response

Gas Dilatometer

- Direct measurement of porosity and Poisson's ratio.
- Direct measurement of damage as a function of tensile strain.



Dilatometer

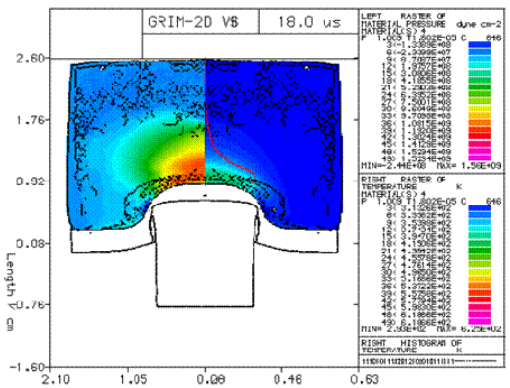


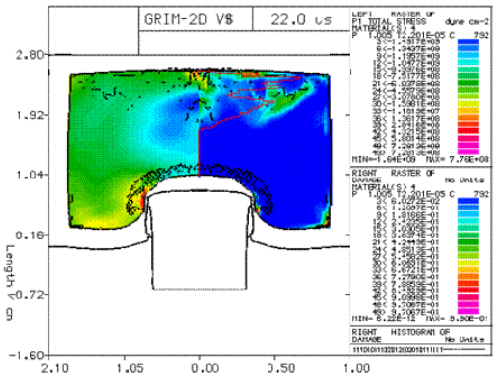
Damage and stress histories

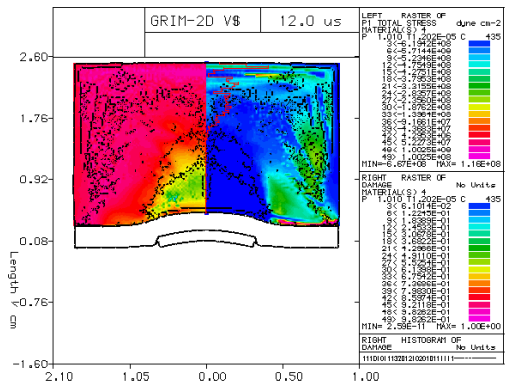
© Copyright QinetiQ limited 2008

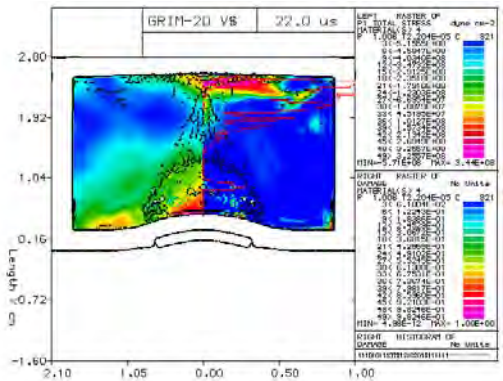
03 Constitutive Response

Material Damage







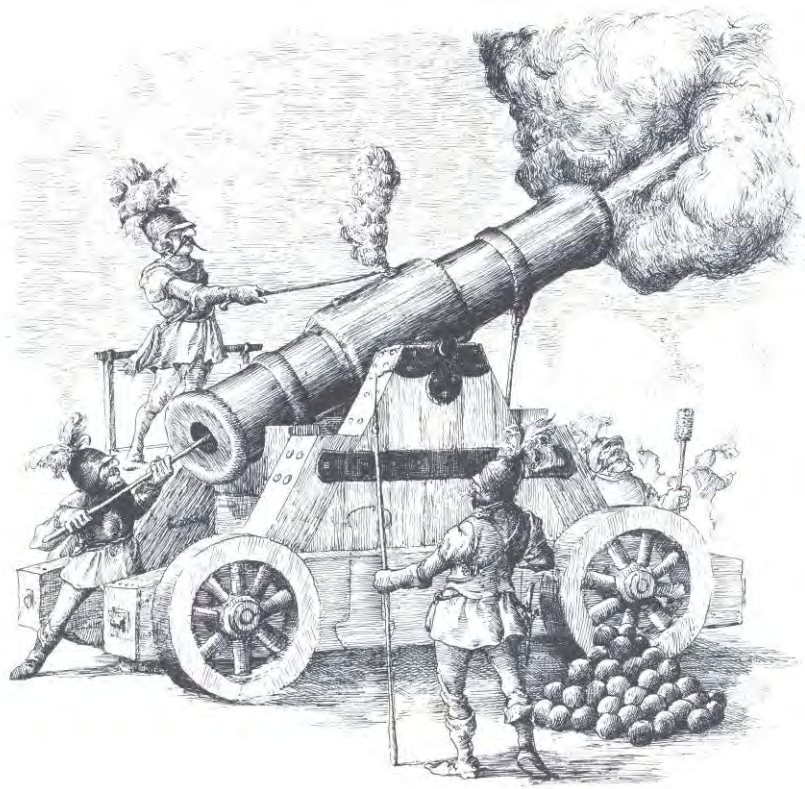


Fragment attack v=450m/s

© Copyright QinetiQ limited 2008

04

CHARM



QINETIQ/08/02238

© Copyright QinetiQ limited 2008

04 CHARM

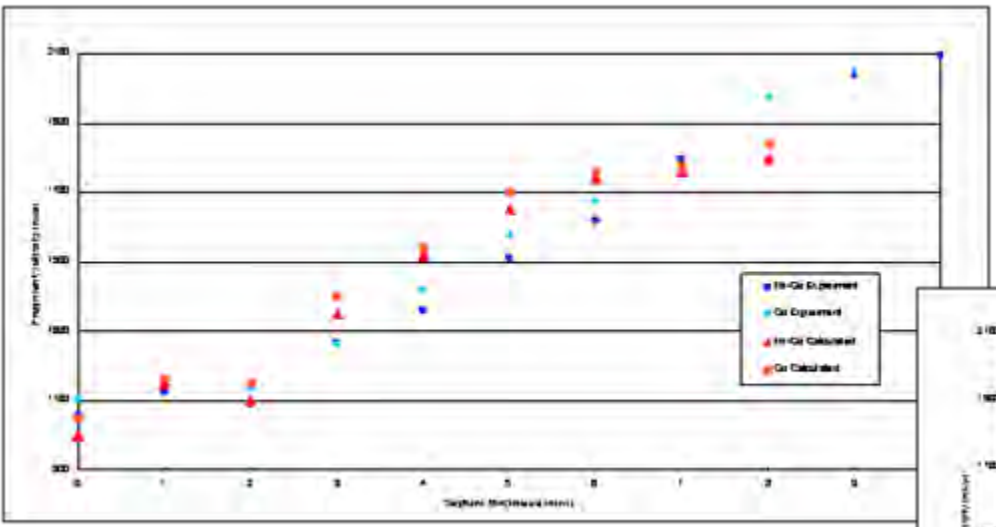
CHARM Modelling

- Temperature driven 3-step Arrhenius chemistry to describe chemical reaction in solid to produce gaseous products and release of energy.
- Ideally fit the chemistry to ODTX.
- Predict fragment impact experiments (13.15mm diameter projectiles etc.)
- Adjust model to obtain best fit.
- Predict other diameter fragments
- Predict response of weapon.
- BUT, needs material data, needs ‘chemistry’ of explosive, often has to use literature data of ‘similar’ explosives.

© Copyright QinetiQ limited 2008

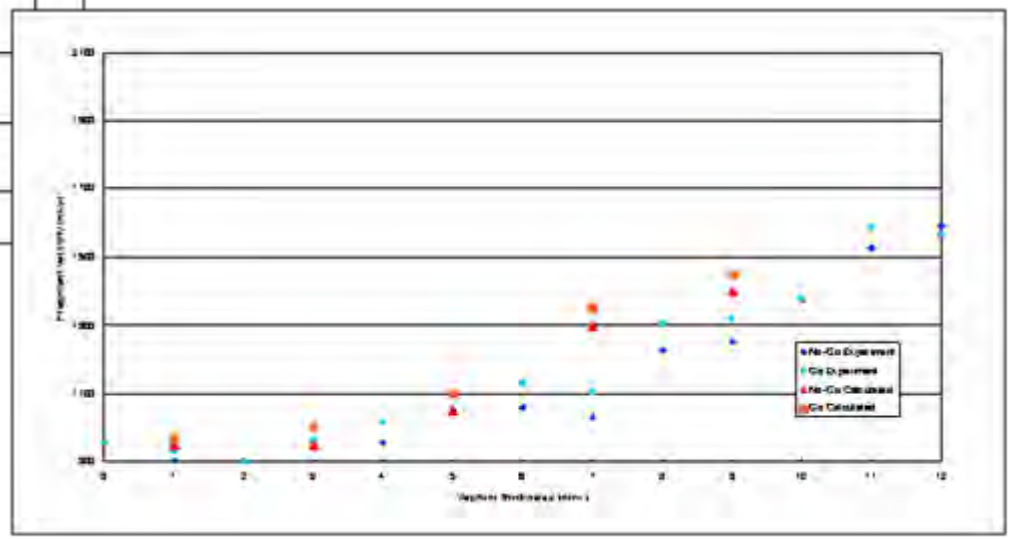
04 CHARM

CHARM: Rowanex 1001 fragment impact SDT Threshold data



13.15mm diameter projectile

20mm diameter projectile

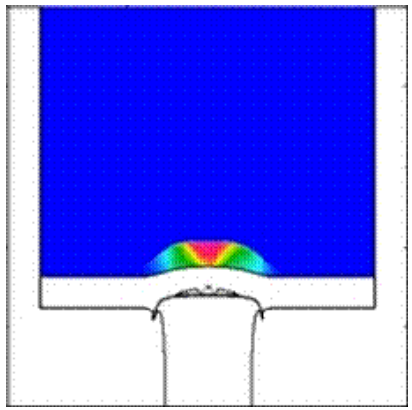


Experimental point: blue
Calculated: red

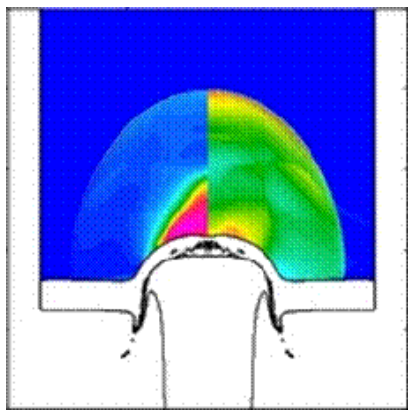
© Copyright QinetiQ limited 2008

CHARM: Rowanex 1001 fragment impact SDT Threshold data

Pressure - Energy

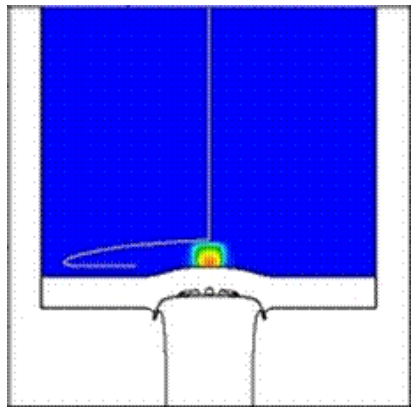


1.5µs

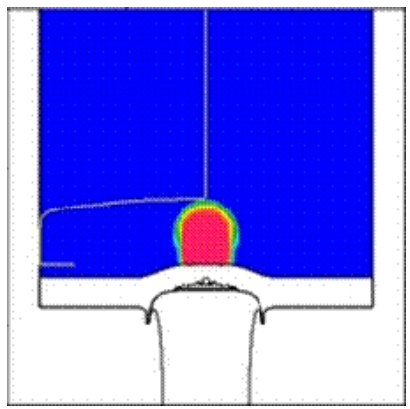


6.0µs

Gas Evolution



1.5µs



2.25µs

© Copyright QinetiQ limited 2008

04 CHARM

Rowanex 1100 fragment impact SDT Threshold data

PG EOS

PG Constitutive Model

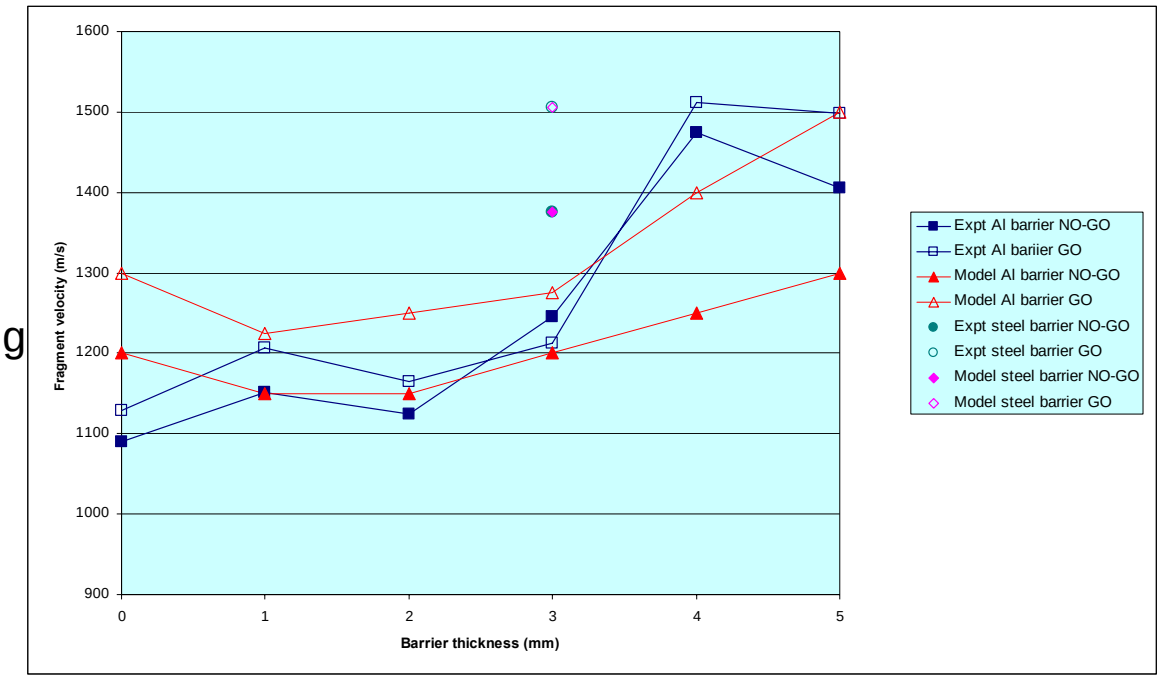
Pore number (size 5μm)

- $5.10^{10}m^{-3}$ in crystals
- $5.10^{10}m^{-3}$ due to debonding
- Porosity $6.5.10^{-6}$

Chemistry

- -1st step adjusted

Experimental point: blue
Calculated: red



13.15mm diameter projectile

© Copyright QinetiQ limited 2008

05

Munition System



© Copyright QinetiQ limited 2008

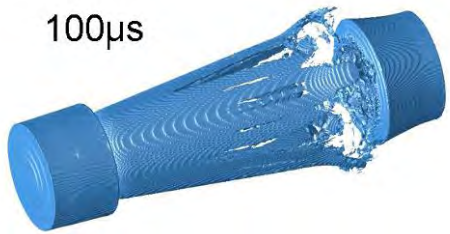
05 Munition System

Tube Test Explosiveness Levels



I – Pressure Burst





II - Deflagration

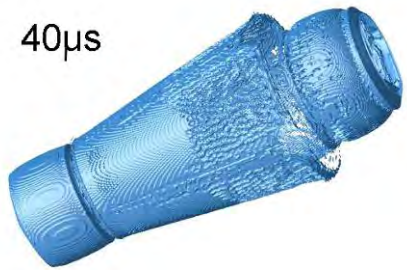


III - Explosion





IV - Detonation



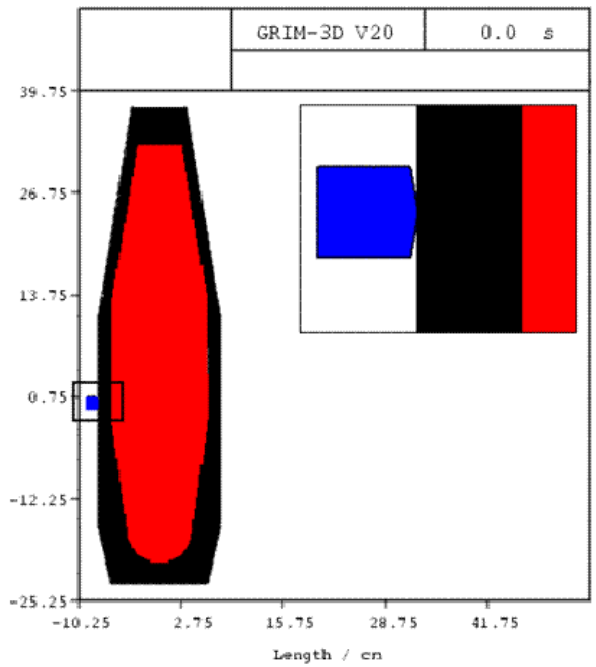
© Copyright QinetiQ limited 2008

05 Munition System

Artillery Shell Fragment Attack Hazard

- CHARM, employing the advanced Equations of State (EOS), the Porter-Gould constitutive model and a physically based hotspot density distribution to predict the fragment attack experiments of an artillery shell.

STANAG Fragment v=2536m.s^{-1}



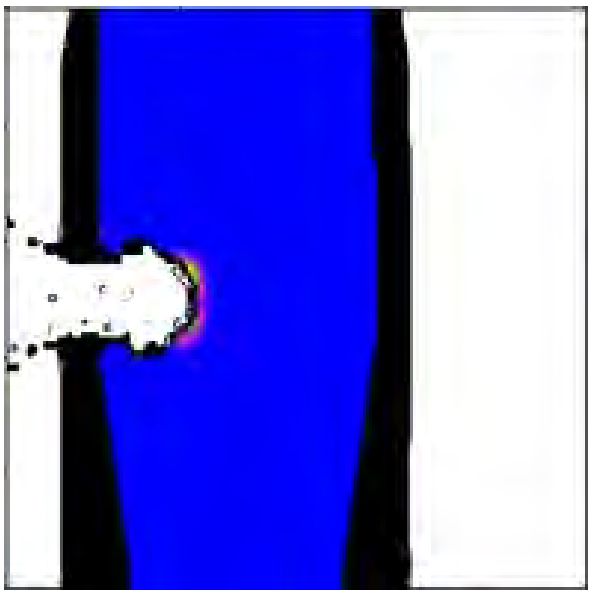
© Copyright QinetiQ limited 2008

05 Munition System

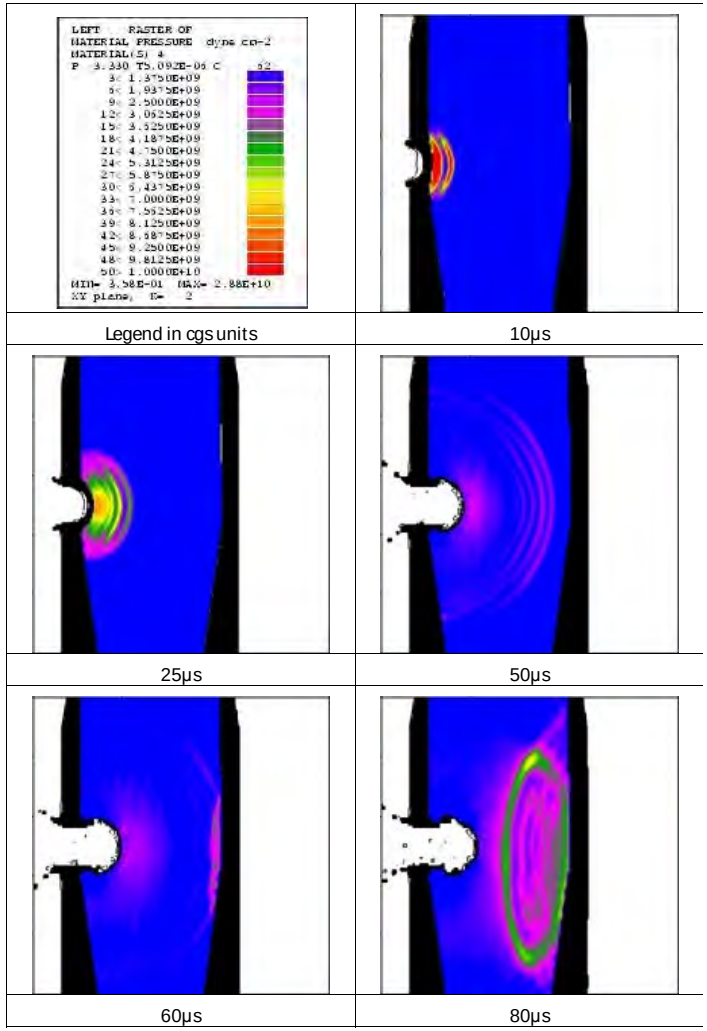
Artillery Shell Fragment Attack Hazard

Pressure field shows SDT not a mechanism

Gas evolution suggests low level BVR



Gas evolution 80µs

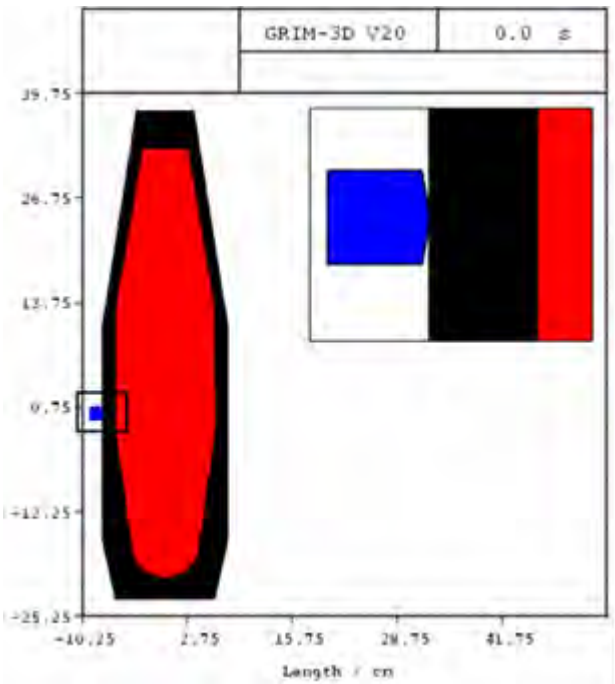


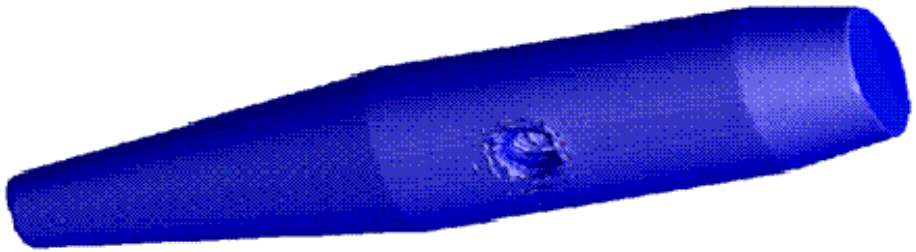
© Copyright QinetiQ limited 2008

05 Munition System

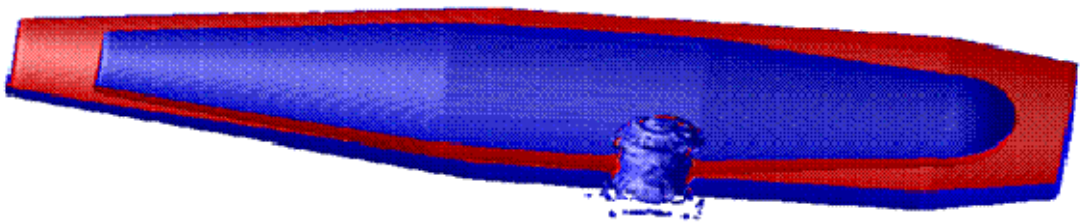
Artillery Shell Fragment Attack Hazar

Comparison with experiment









STANNAG Fragment v=2536m.s^{-1}

© Copyright QinetiQ limited 2008

05 Munition System

Comparison with experiment.

- Modelling, in good agreement with the experiments, predicted that fragment attack of the artillery shell would not lead to an SDT event and that any subsequent reaction would be a BVR event.
- The size of the hole in the shell case and the destruction of the fragment were in excellent agreement with the experiment
- The model was able to show the generation of a small amount of gaseous reaction products around the cavity produced by the fragment in the shell filling.
- However, it was unable to predict how any subsequent reactions would grow.

© Copyright QinetiQ limited 2008

06
Conclusions



© Copyright QinetiQ limited 2008

06 Conclusions

The ability to predict the hazard response of a munition is an important requirement for the IM certification process of a munition.

Materials science can predict the basic behaviour of the mechanical response of a PBX:-

- Equation of State
- Constitutive response
- Damage and failure

Integration with an ignition and growth model can predict the SDT hazard response of munitions subjected to fragment attack.

A BVR model is required to predict non-SDT events and their resulting violence.

The long term UK objective is ‘Certification by Simulation’

© Copyright QinetiQ limited 2008

07 Acknowledgments

- Hazard UK II Consortium:
  - QinetiQ
  - BAESYSTEMS
  - Fluid Gravity Engineering
  - Cranfield University
- Defence Technology Innovation Centre, MOD for providing financial support.

© Copyright QinetiQ limited 2008



Independent expertise where it matters most.

www.QinetiQ.com/iX

© Copyright QinetiQ limited 2007

Numerical Predictions of Magnus of Spin-Stabilized Projectiles

James DeSpirito and Sidra I. Silton
U.S. Army Research Laboratory
Aberdeen Proving Ground, Maryland

TECHNOLOGY DRIVEN. WARFIGHTER FOCUSED.

24th International Symposium on Ballistics
New Orleans, Louisiana
22–26 September 2008

Introduction

- Nonlinear Magnus moments
  - Observed for nearly all spin-stabilized projectiles in subsonic and transonic flight.
  - Accurate prediction important to predict dynamic stability and trim angles.
- Prediction capabilities
  - Steady-state RANS provides accurate results in supersonic and high transonic flight regimes, as demonstrated in 1980s.
  - Recent work found issues in subsonic and transonic flight regimes for some projectile configurations.
    - Predictions too high at these flight speeds.
    - Time-accurate hybrid RANS/LES simulations can lead to more accurate results.



Steady-State RANS

M910 Projectile
Mach 0.6



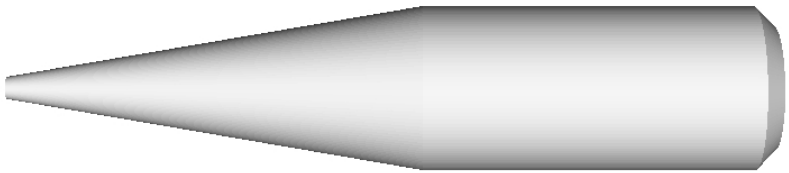
Unsteady RANS/LES

Numerical Approach

- Full 3-D Navier-Stokes calculations
- CFD++, Metacomp Technologies, Inc.
  - Implicit, dual time-stepping
  - Unstructured, finite-volume discretization
- Second order space/time accuracy
- Steady-state RANS simulations
  - Goldberg's three-equation k-ε-R turbulence model
  - Two-equation realizable k-ε turbulence model
  - Two-equation cubic k-ε turbulence model
- Unsteady hybrid RANS/LES
  - Batten-Goldberg turbulence model
    - Cubic k-ε in RANS region (handles anisotropy)
    - Anisotropic form of the Smagorinsky model in LES regions
- y^+ values <0.5

Configurations Investigated

M910 Target Practice Round



D=16.2 mm
L=4.7 cal.

*DeSpirito and Heavey, 2004
*DeSpirito, 2007

0.50-caliber round

D=12.7 mm
L=4.55 cal.

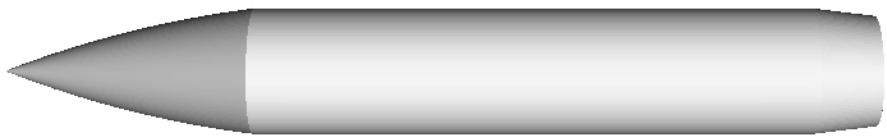


*Silton, 2005

U.S. Army-Navy Spinner Rocket (ANSR)



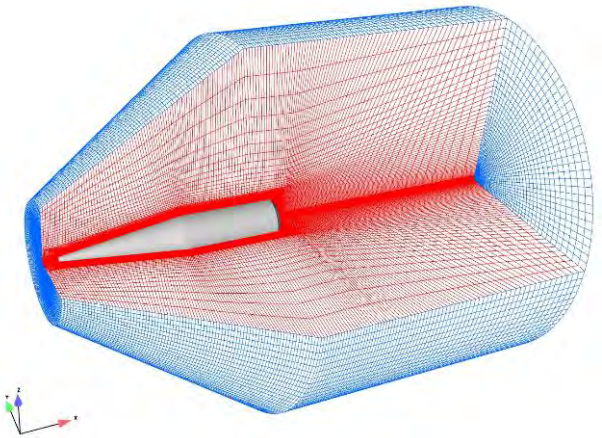
D=20.0 mm
L=7 cal.



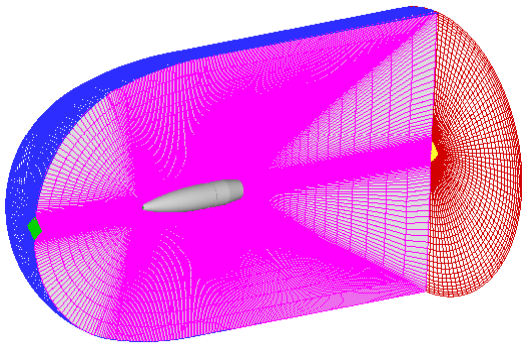
*DeSpirito, 2008

Computational Meshes

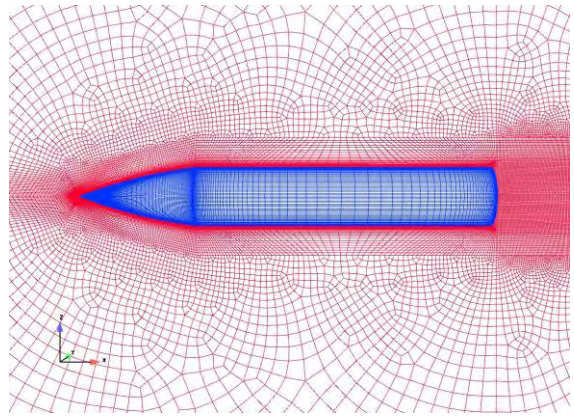
M910

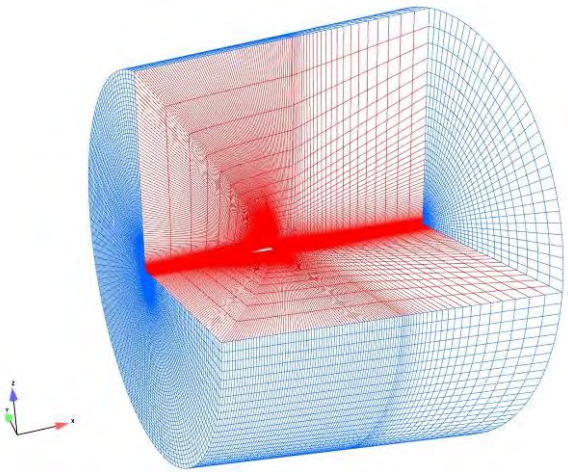


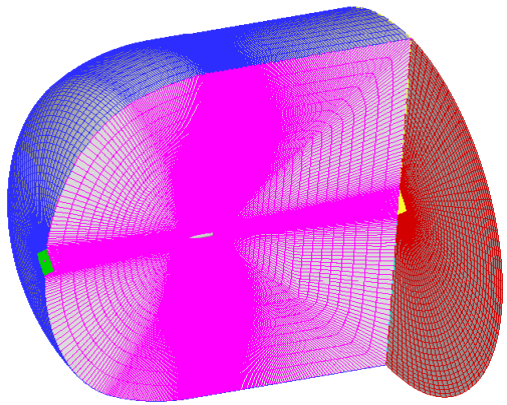
0.05-cal

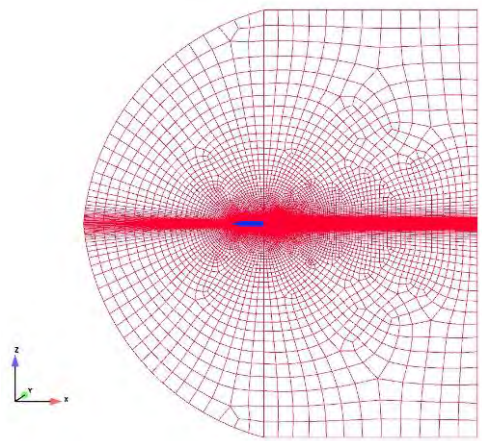


ANSR

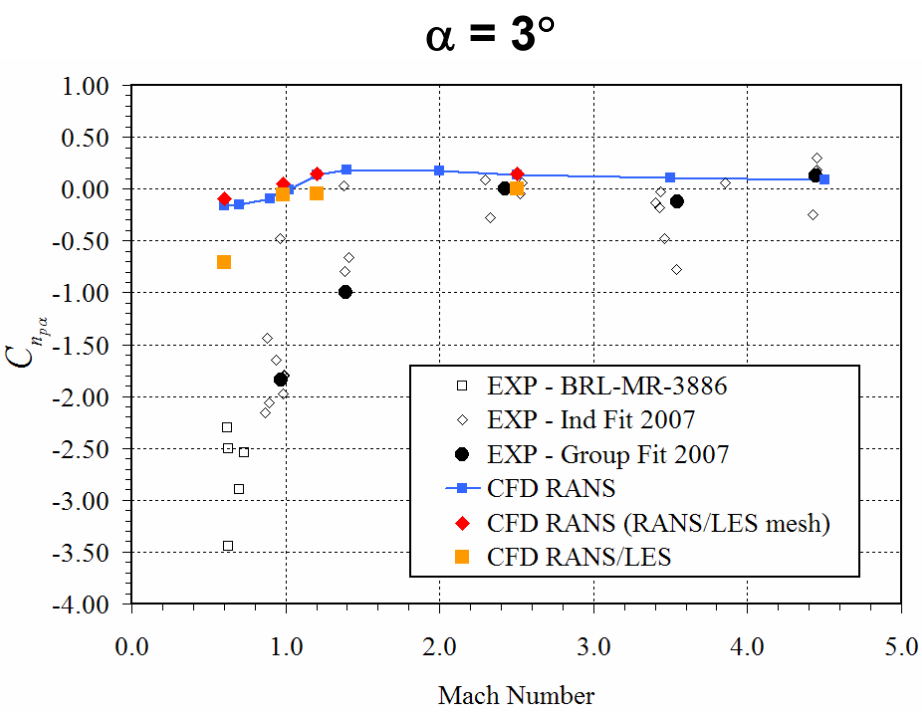


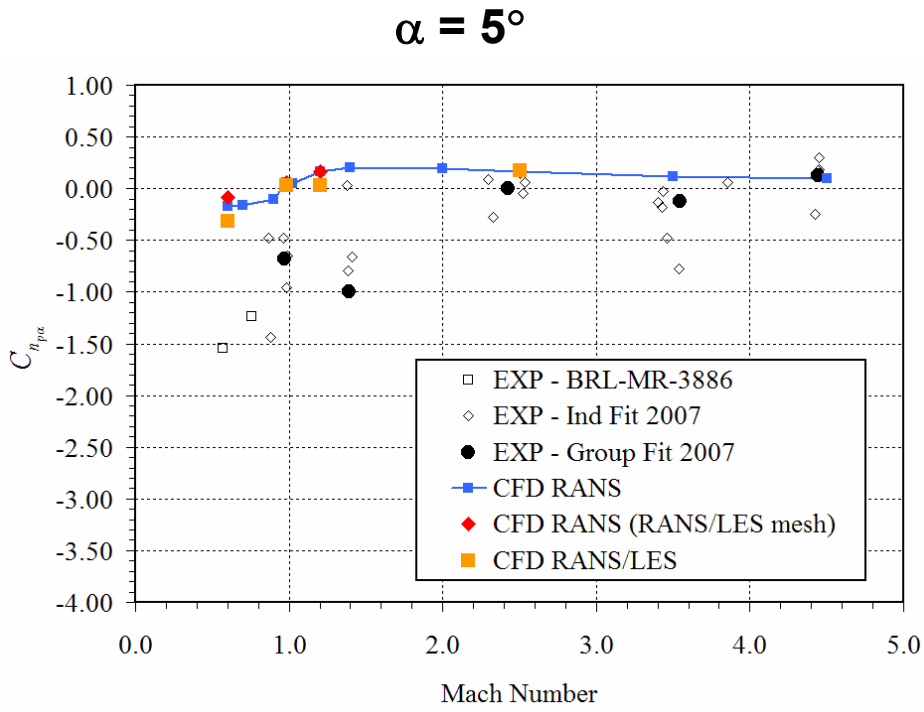






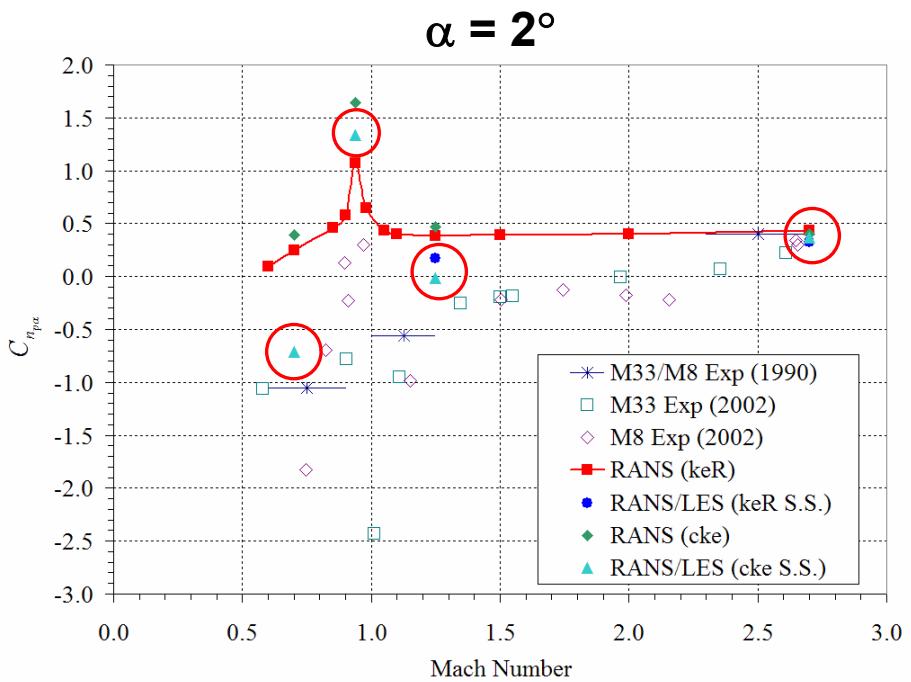
M910 Results

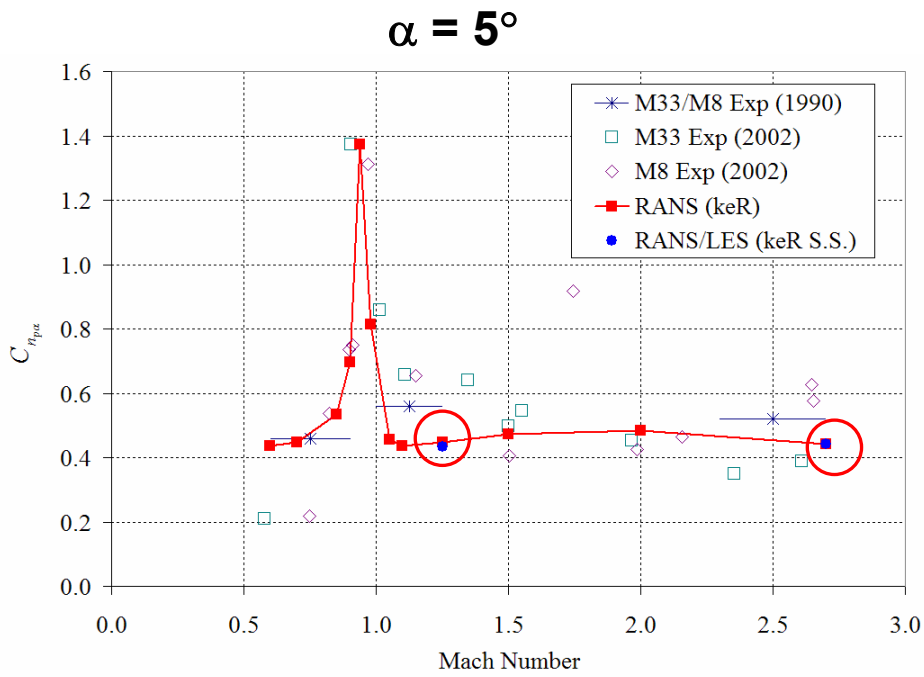




- Steady-state RANS accurate in supersonic regime.
- Time-accurate RANS/LES
  - More accurately predict negative trend at lower Mach numbers (though not as sharp a decrease).
  - Predicts nonlinearity with α, not observed in steady-state RANS simulations.

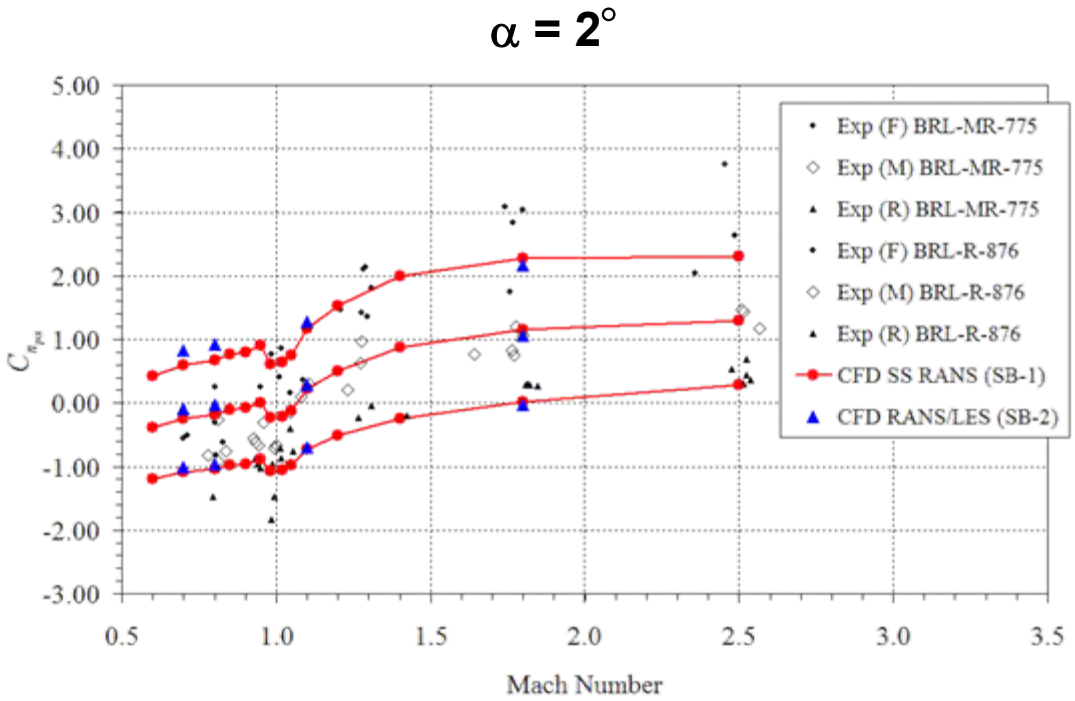
0.50-cal. Results





- Critical behavior in transonic region predicted by both solution methods.
- At α=5° RANS predictions compare well with experimental data.
  - Magnus moment under predicted as Mach 1 approached from above.
  - Over predicted in subsonic range.
- At α=2° time-accurate RANS/LES (circled) more accurate.
- RANS turbulence model has small effect on Magnus moment but did not improve prediction in subsonic range.

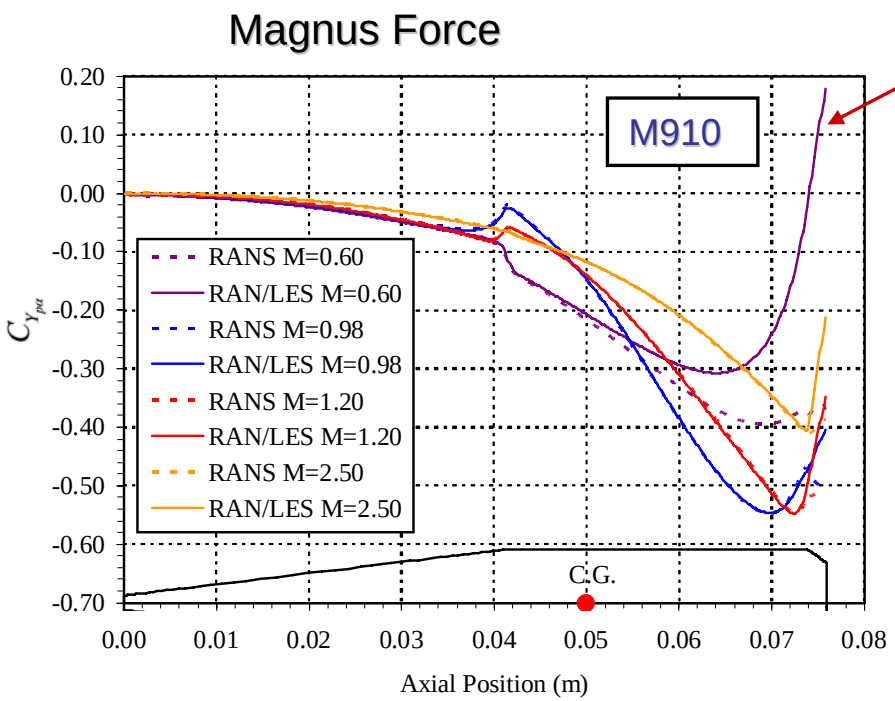
ANSR Results
Square-base, no boattail

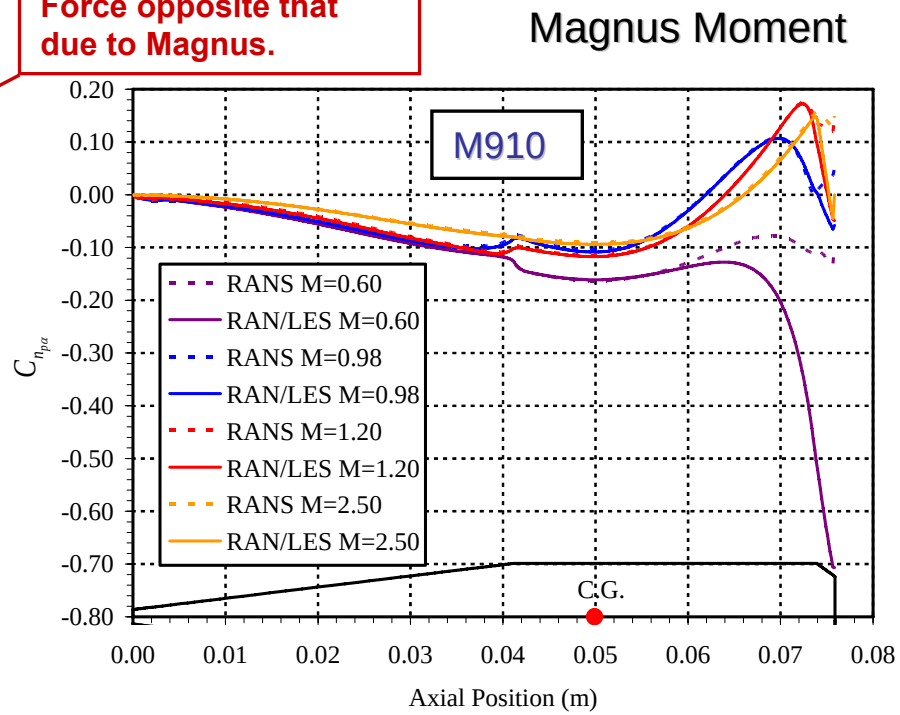


- Sharp edge on base, unlike rounded 0.50-cal. and chamfered M910.
- 3 c.g. locations.
- Little difference between RANS and RANS/LES (regardless of Mach number or c.g. location).
  - Excellent agreement for $M \geq 0.98$.
  - Slightly over predicted in subsonic range but not a great as 0.50-cal or M910.
- Similar result for 0.5-cal, 7° boattail ANSR configuration.
- Results indicates that a sharp edge (corner) on base of projectile may inhibit impact of unsteady flow phenomena on accuracy of steady-state RANS solution.
  - Weinacht (2007) previously found sharp edge reduces nonlinear Magnus effect.

Magnus Distribution on Projectile
M910

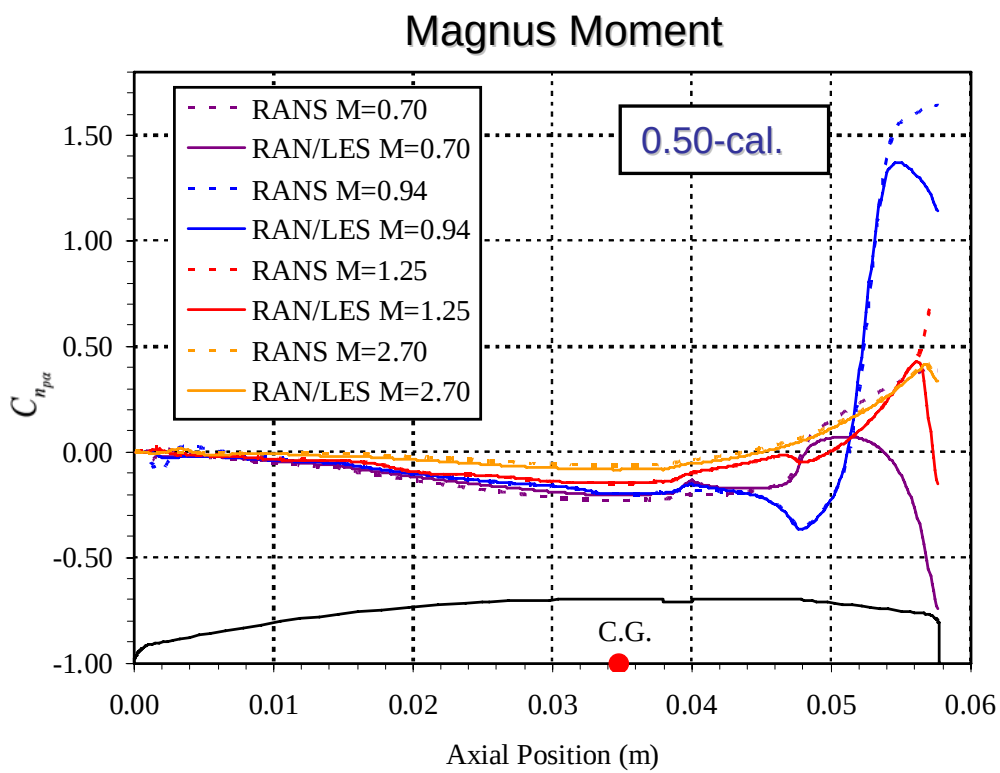
Force opposite that due to Magnus.





- Effects of Magnus confined to rear end of projectile.
- RANS vs. RANS/LES differences
  - Small for transonic and supersonic Mach numbers and confined to chamfer region.
  - Large difference at Mach 0.6 and begins farther forward on projectile.
- Subsonic (Mach 0.6) Magnus
  - Positive force indicates flow interactions have overtaken Magnus effects.
    - Magnus force usually negative (normal pointing to port side for right hand spin).
  - Magnus force center of pressure has moved rear of c.g.

Magnus Distribution on Projectile
0.50-cal.



- Virtually no difference between RANS and RANS/LES at Mach 2.7.
- As Mach number decreases
  - Difference between simulation methods increases.
  - Difference between the two distributions diverge farther forward.

(ANSR results showed only minor differences in Magnus distributions for the two simulations methods.)

M910 Flow Field
RANS vs. RANS/LES

Mach 0.6

Instantaneous RANS/LES



Time-averaged RANS/LES



Steady-state RANS



Mach 0.98

Instantaneous RANS/LES



Time-averaged RANS/LES



Steady-state RANS



Numerical Schlieren Visualizations, $\|\nabla\rho\|$

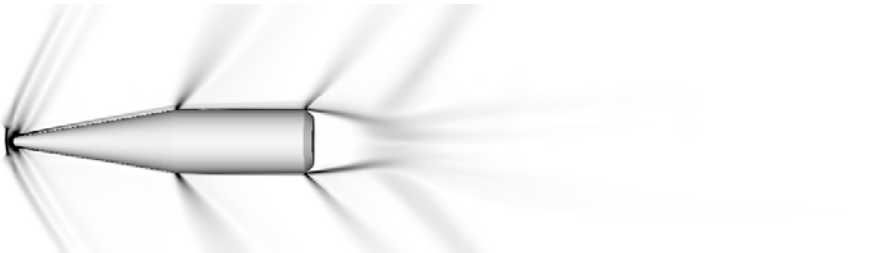
M910 Flow Field
RANS vs. RANS/LES

Mach 1.2

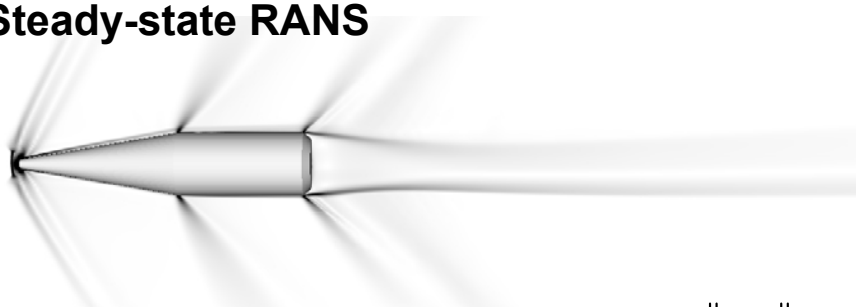
Instantaneous RANS/LES



Time-averaged RANS/LES

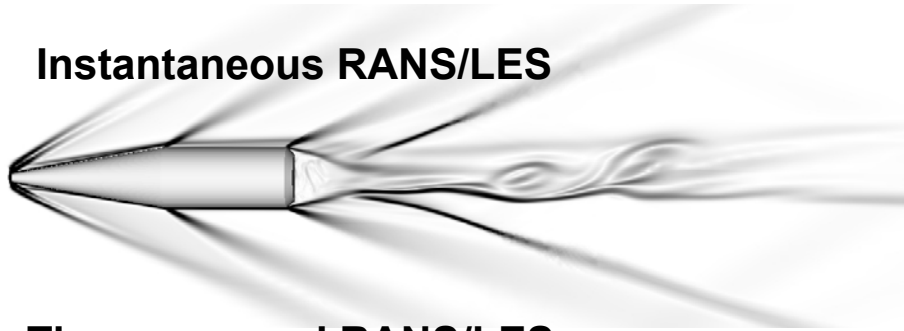


Steady-state RANS

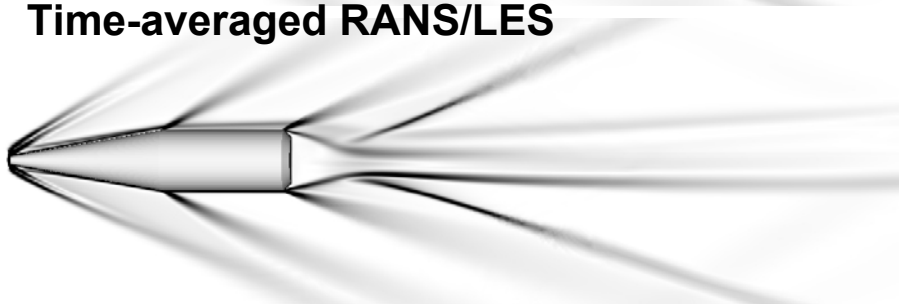


Mach 2.5

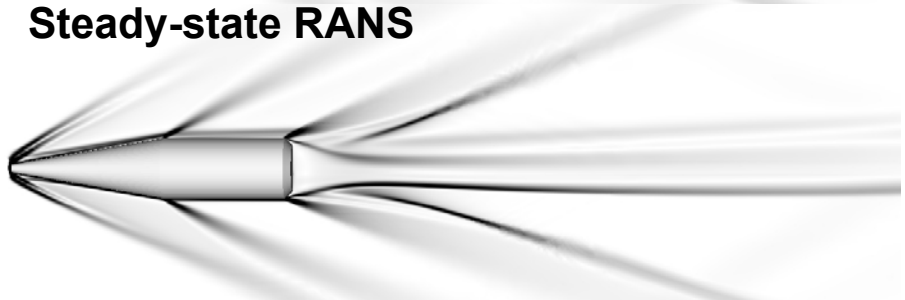
Instantaneous RANS/LES



Time-averaged RANS/LES



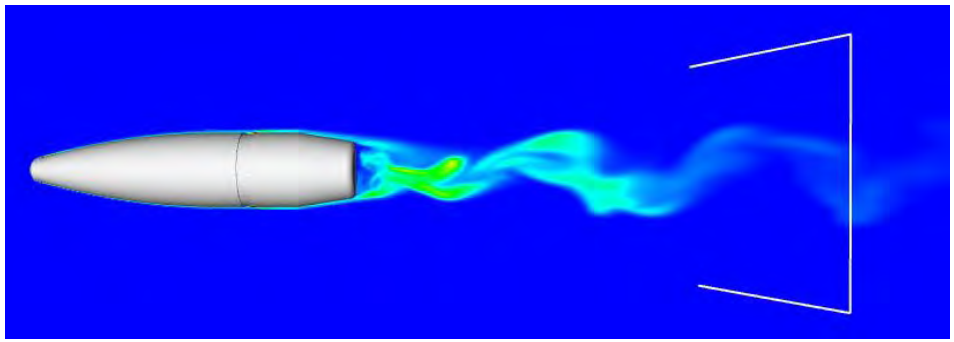
Steady-state RANS



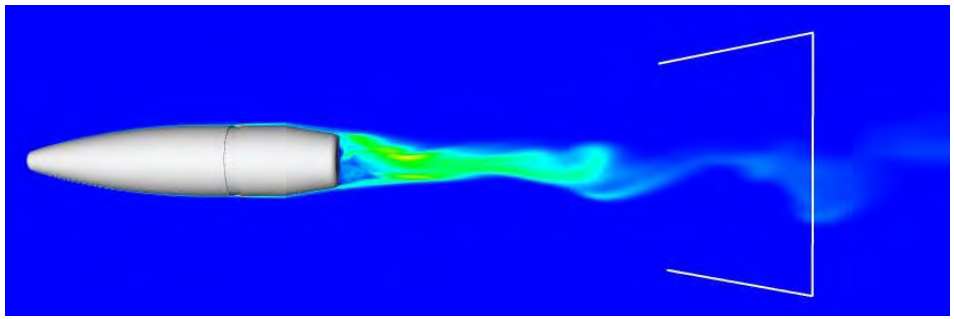
Numerical Schlieren Visualizations, $\|\nabla\rho\|$

0.50-cal. Flow Field
Turbulent Kinetic Energy

Mach 0.7



Mach 1.25



- Similar flow field results for 0.50-cal. and ANSR (not shown).

Conclusions & Future Work

- Projectile base shape is an important parameter.
  - Rounded or chamfered bases
    - Time-accurate RANS/LES simulations improve the Magnus moment prediction.
    - Higher nonlinear Magnus effects (Weinacht, 2007).
  - Sharp cornered base leads to less nonlinear Magnus and improved steady-state RANS predictions.
- Turbulent eddies resolved in RANS/LES simulations impact the pressure distribution on projectile at lower Mach numbers.
- Future work
  - More detailed analysis of unsteady flow field.
    - Separation
    - Pressure distribution
  - Higher angle of attack simulations ($5° \leq \alpha \leq 15°$).

This work was supported in part by a grant of high-performance computing time from the U.S. Department of Defense High Performance Computing Modernization program at the ARL Major Shared Resource Center, Aberdeen Proving Ground, Maryland.

Contact Information

Dr. James DeSpirito
U.S. Army Research Laboratory
Aberdeen Proving Ground, MD 21005-5069
410-306-0778
james.despirito@us.army.mil

Munitions effects: a schematic overview of munitions and warheads, trends for the future

24th International Symposium on Ballistics
New Orleans, LA, September 22−26, 2008

TNO | Knowledge for business



Dr. A.M. Diederen
andre.diederen@tno.nl

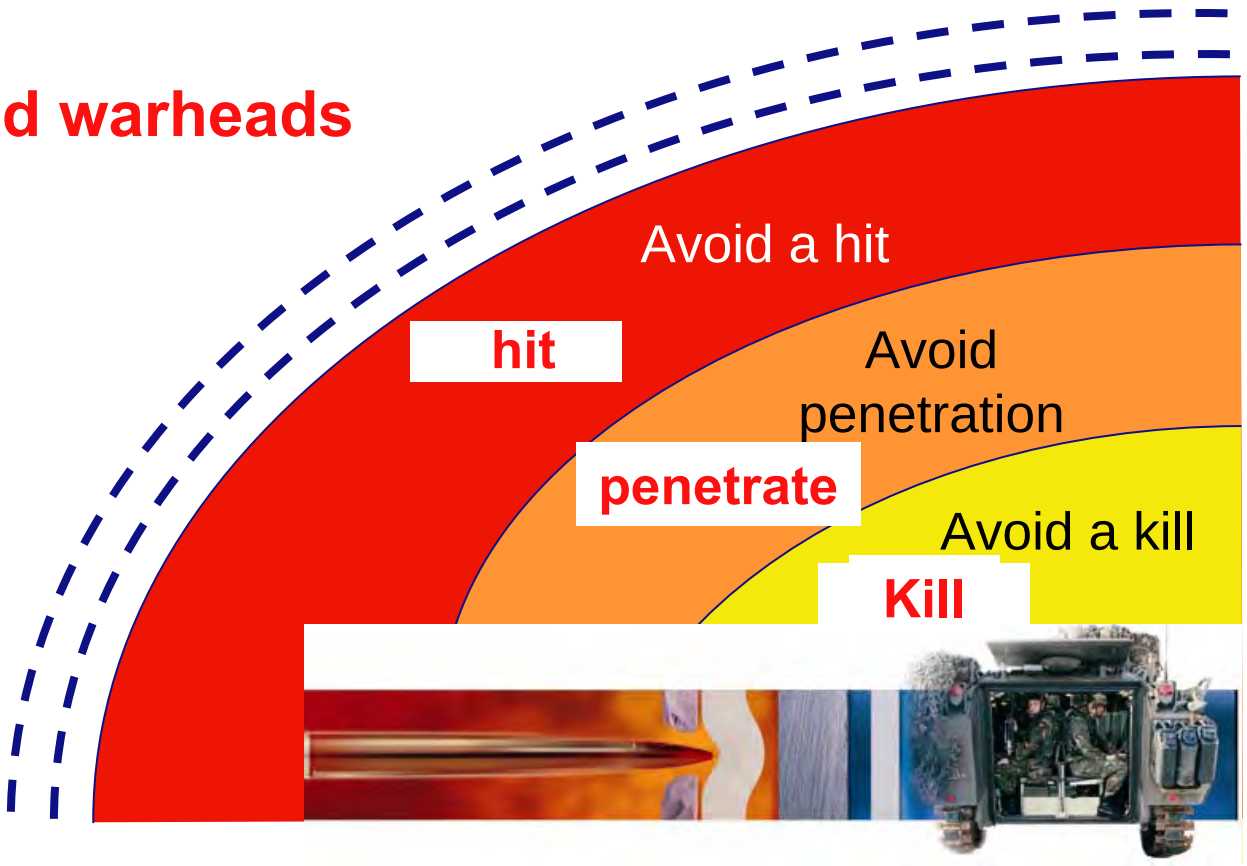
Outline

- Types of energy transfer media
  atoms, electrons and photons
- Classification scheme of munitions and weapons effects
  examples for kinetic energy, blast and heat, electric current and electromagnetic radiation
- Trends
  - adaptive effects and enhanced lethality

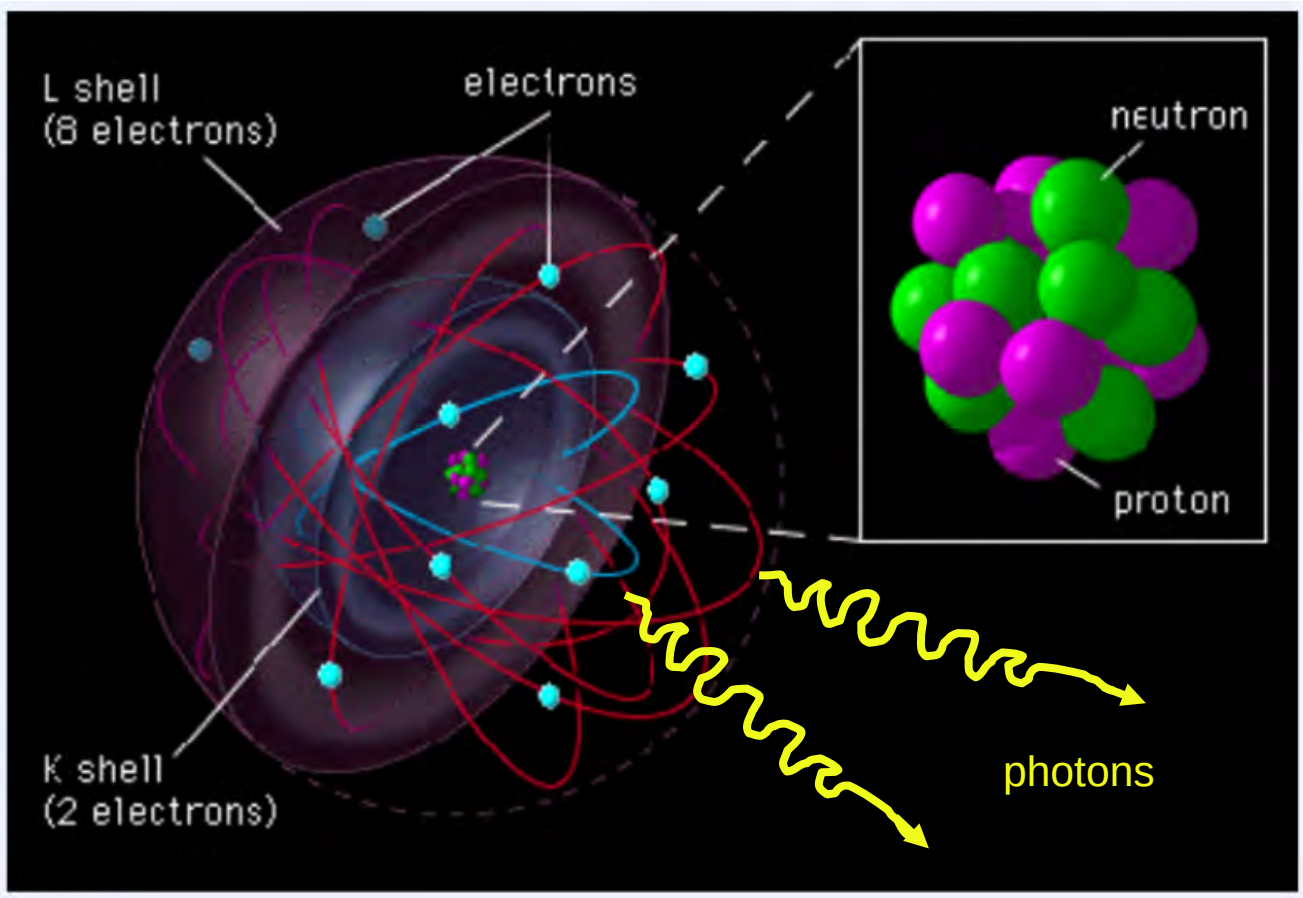
Layers of { protection / attack

Passive, reactive and hard-kill active armour

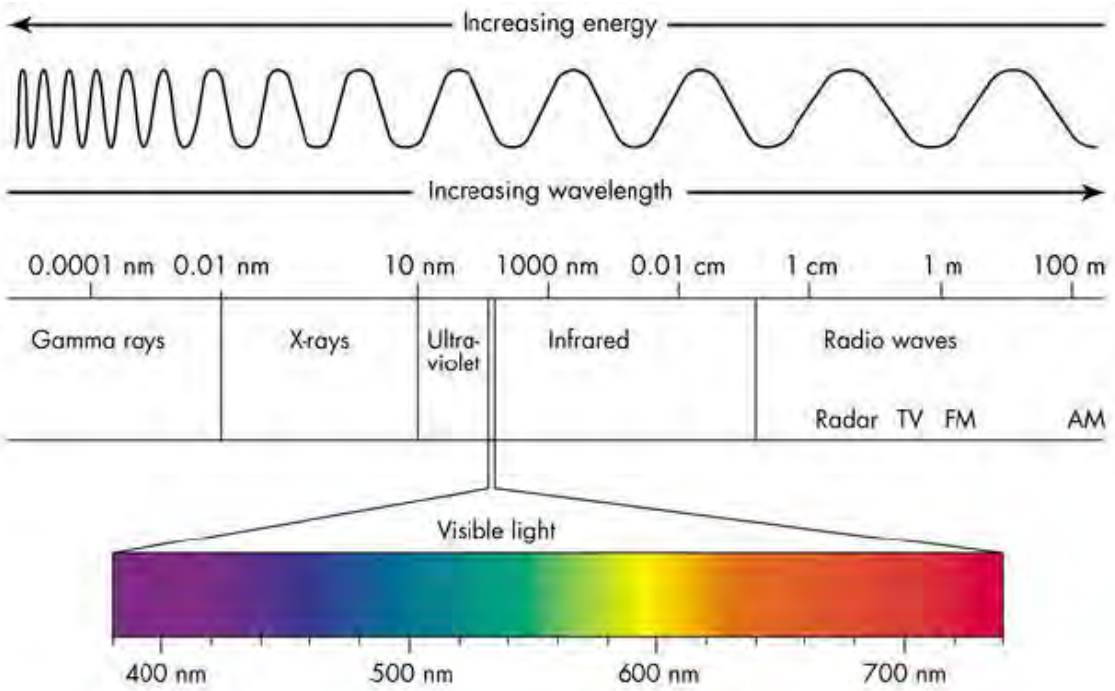
Projectiles and warheads



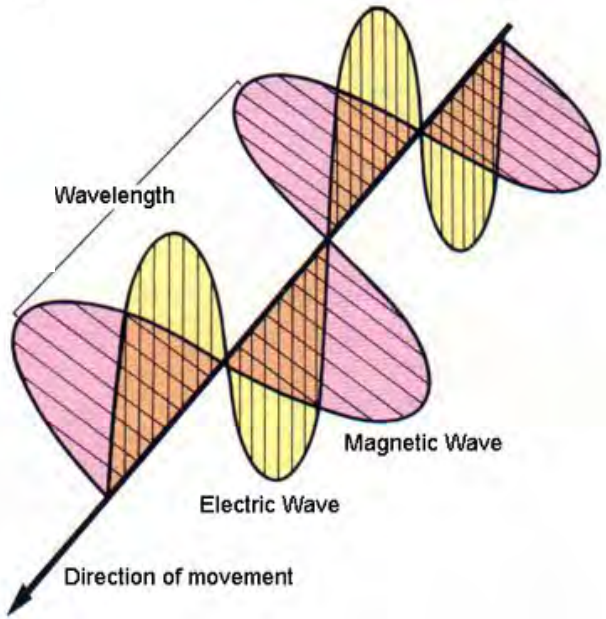
Munitions effects: atoms, electrons and photons as energy transfer medium



Photons as energy transfer medium: wave behaviour

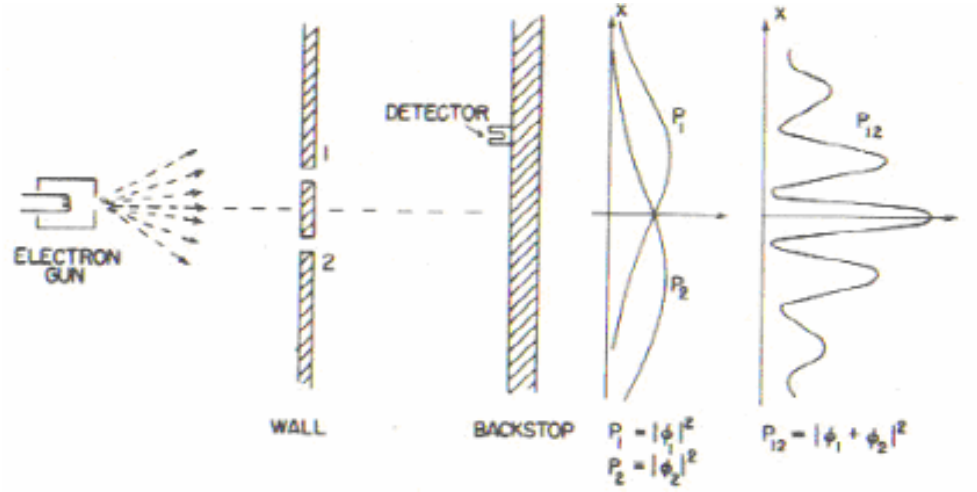


oscillating electromagnetic field



energy per photon:
Planck constant x frequency

Wave aspects:
besides photons, also electrons and atoms exhibit diffraction and interference





particles of matter: pressure waves and shock waves could be interpreted as “waves of excess density”

Atoms, electrons and photons: strength in numbers

Example: energy transfer of 100 KJ

- Burning a hole in a metal target:
  10^{24} photons (at typical wavelength)
- Shortcutting a shaped charge jet (electric armour):
  10^{19} electrons (at typical high voltage)
- 200 g steel penetrator at 1000 m/s:
  10^{24} atoms

Classification scheme of munitions and weapons effects

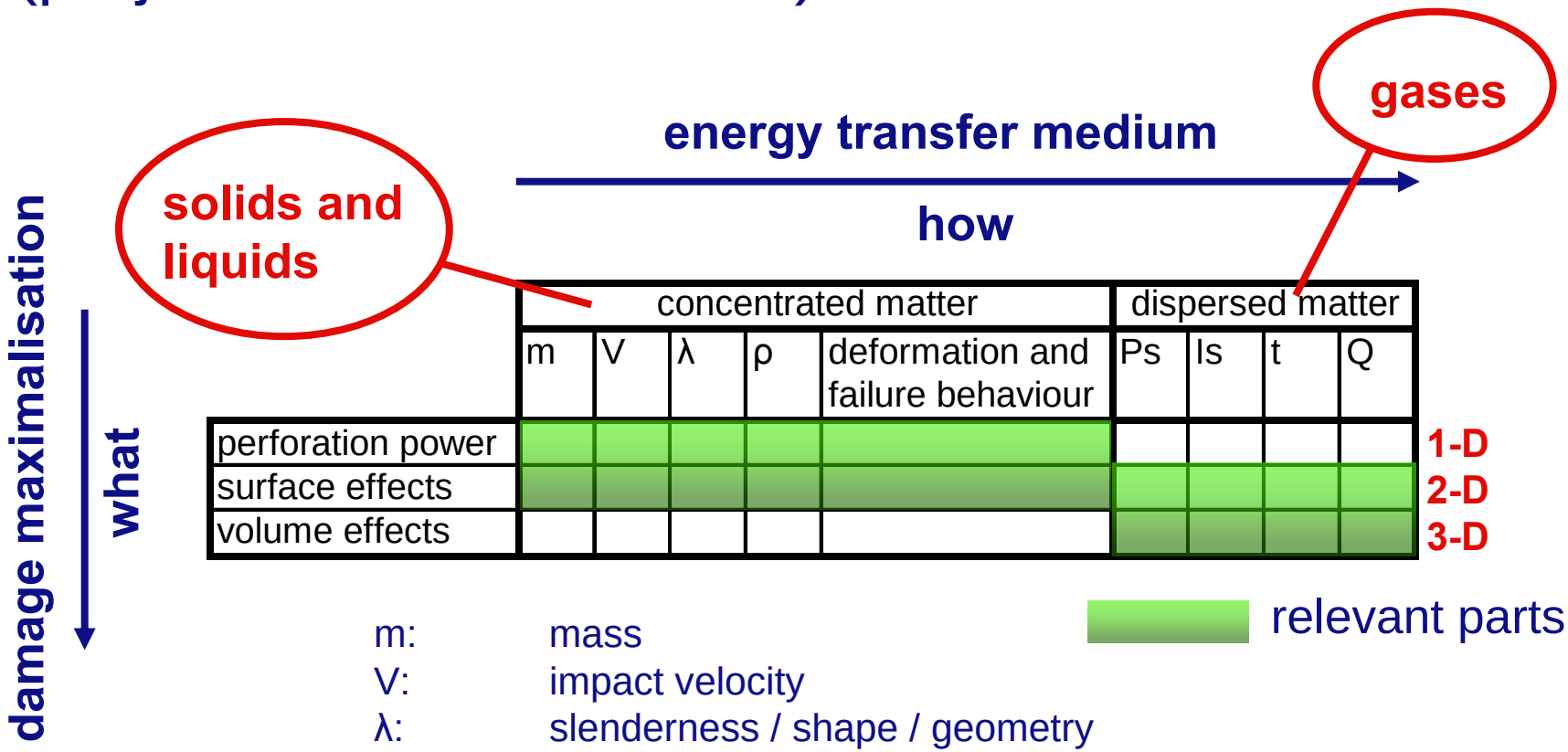
energy transfer medium

damage maximalisation

	matter									electrons				photons			
	solid/liquid-like					gaseous											
	m	V	λ	ρ	deformation and failure behaviour	Ps	Is	t	Q	I	V	t	spotsize	n	h.v	t	spotsize
perforation power	■	■	■	■	■									■	■	■	■
lateral effects	■	■	■	■	■	■	■	■	■					■	■	■	■
volume effects						■	■	■	■	■	■	■	■				

■ relevant parts

Classification scheme: particles of matter (projectiles and warheads)



m: mass
V: impact velocity
λ: slenderness / shape / geometry
ρ: density
Ps: maximum static overpressure
Is: impulse of the positive phase of the blast wave
t: duration / time
Q: heat flux

Desired effects determine parameter choices

Example:
highly lethal versus non-lethal

	concentrated matter					dispersed matter			
	m	V	λ	ρ	deformation and failure behaviour	Ps	ls	t	Q
perforation power									
surface effects									
volume effects									

M1028



tungsten spheres

rubber projectiles

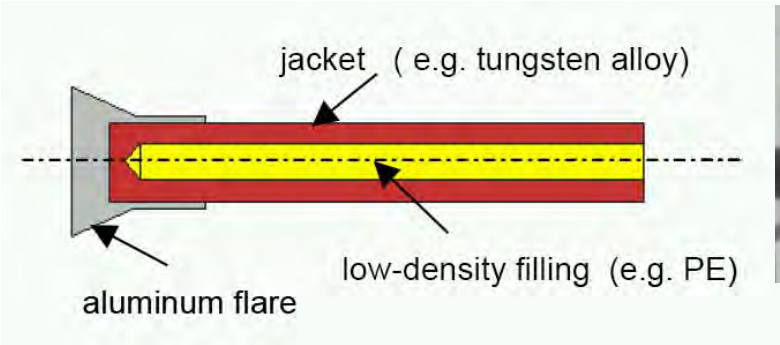


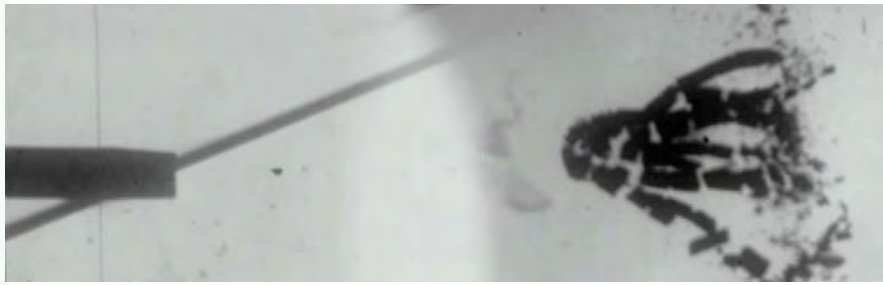
A schematic overview of munitions and warheads

Example: penetrators with enhanced / advanced lateral efficiency (PELE®, ALP®)

	concentrated matter					dispersed matter			
	m	V	λ	ρ	deformation and failure behaviour	Ps	Is	t	Q
perforation power									
surface effects									
volume effects									

longitudinal section of a typical PELE projectile:





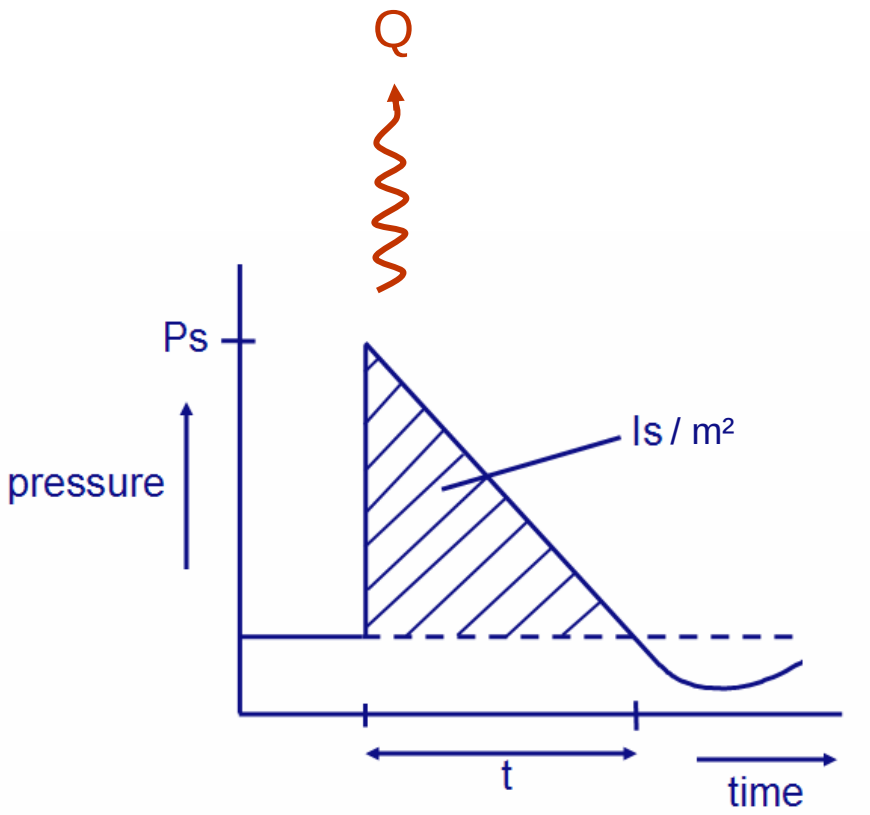
wall breach after 3 hits of large calibre PELE



(source: ISL/ Diehl/ Rheinmetall)

Blast (and heat)

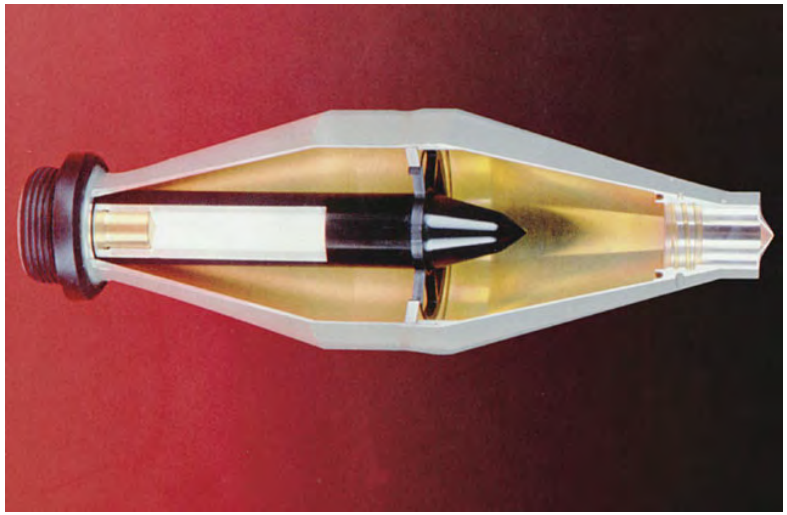
	concentrated matter					dispersed matter			
	m	V	λ	ρ	deformation and failure behaviour	Ps	Is	t	Q
perforation power									
surface effects									
volume effects									





Combination of penetration/ perforation and blast

Example: Modular Explosive Penetrator (RUAG)



	concentrated matter					dispersed matter			
	m	V	λ	ρ	deformation and failure behaviour	Ps	Is	t	Q
perforation power									
surface effects									
volume effects									

Classification scheme: electrons and photons

energy transfer medium

how

damage maximalisation

what

	electrons				photons			
	I	V	t	spotsize	n	h.v	t	spotsize
perforation power					■	■	■	■
lateral effects					■	■	■	■
volume effects	■	■	■	■				

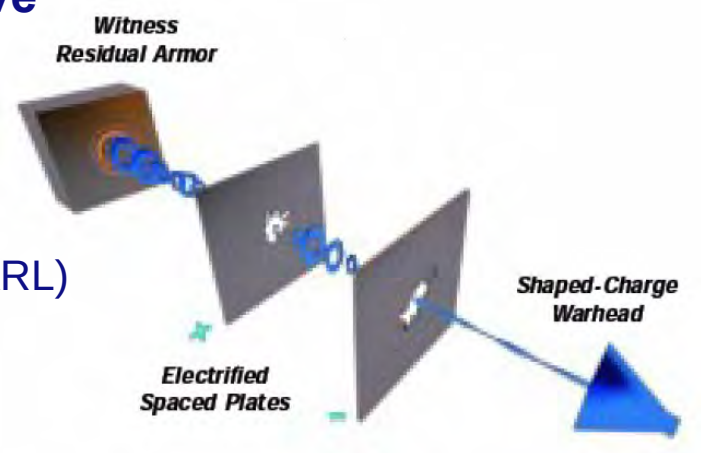
■ relevant parts

I: strength of current
V: voltage
t: duration / time
spotsize: representative conducting cross-section / impact area
n: number of photons
h: Planck constant
v: frequency

Electrons as transfer medium

	electrons				photons			
	I	V	t	spotsize	n	h.v	t	spotsize
perforation power								
lateral effects								
volume effects								

- **Electric reactive armour**



(figure: ARL)

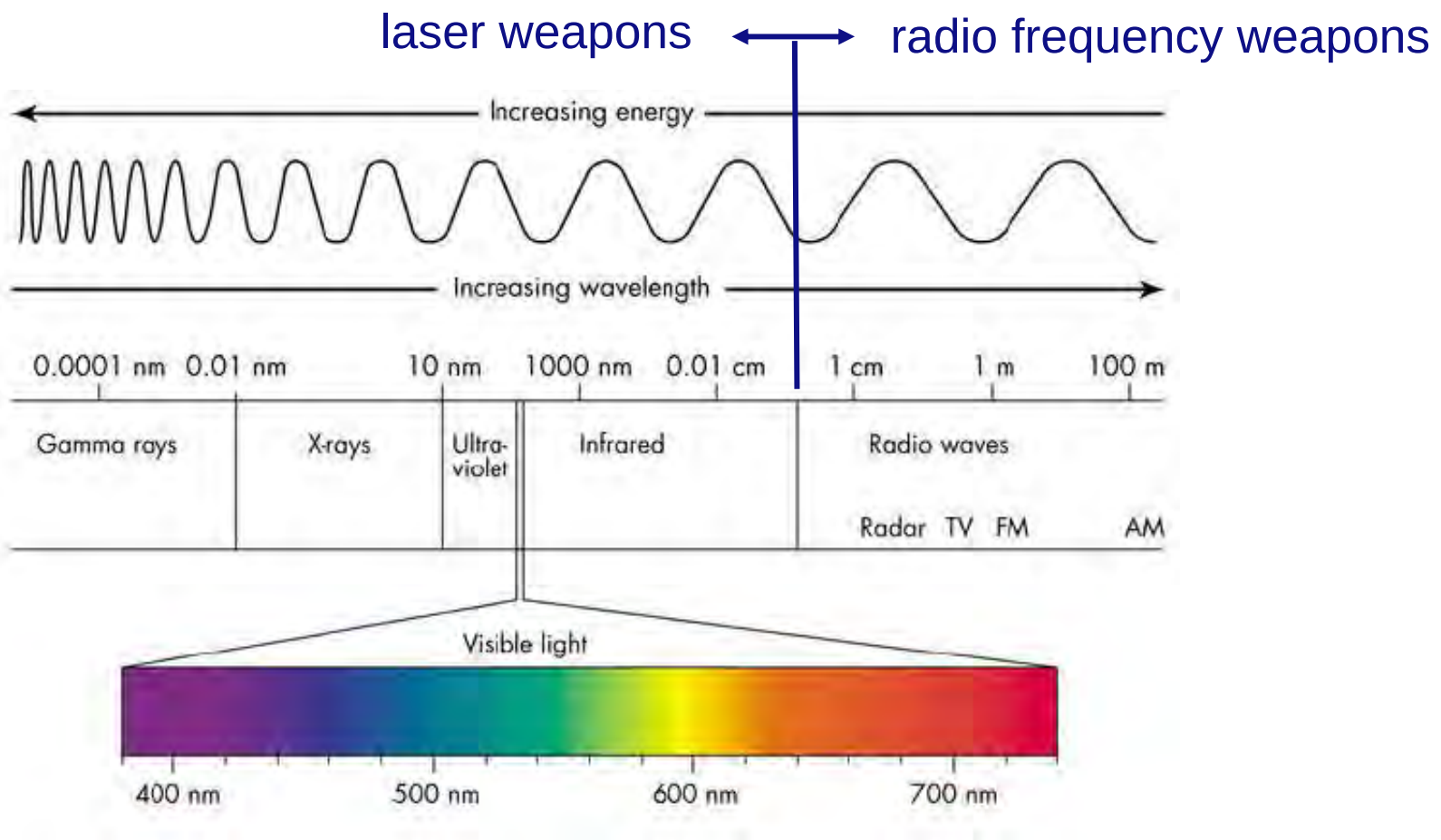
disturbance of the shaped charge jet due to magnetohydrodynamic instabilities

- **Taser**



less lethal: incapacitation by electric current through body

Photons as energy transfer medium: EM spectrum



Photons as transfer medium

	electrons				photons			
	I	V	t	spotsize	n	h.v	t	spotsize
perforation power								
lateral effects								
volume effects								

- **Radio frequency weapons**





95 GHz

Effective beam volume:
1m x 1m x 250m

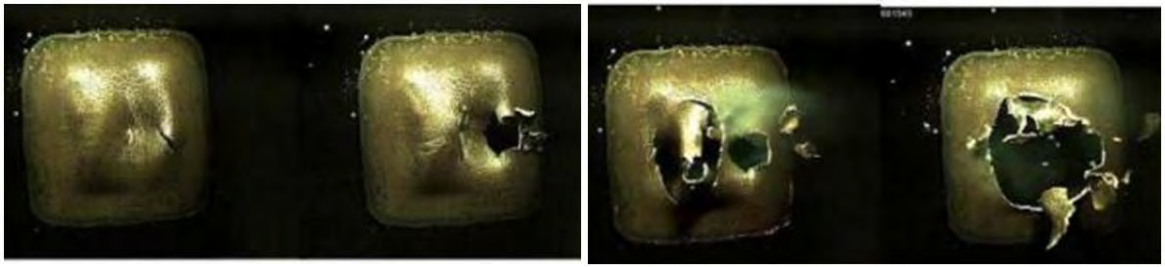
Silent Guardian (30 KW, left),
formerly known as Area Denial System (100 KW, right)

(source: Raytheon)

Photons as transfer medium

	electrons				photons			
	I	V	t	spotsize	n	h.v	t	spotsize
perforation power								
lateral effects								
volume effects								

- **Laser weapons**



(photo: Lawrence Livermore National Laboratory)



melting, ‘erosive’ heating or
‘explosive’ heating
of (armour) material

Laser Area Defence System (50 KW),
to be mounted alongside the Phalanx guns
(source: Raytheon/ Air Force Research Lab.)

Combining photons and electrons as transfer medium: “directed lightning”

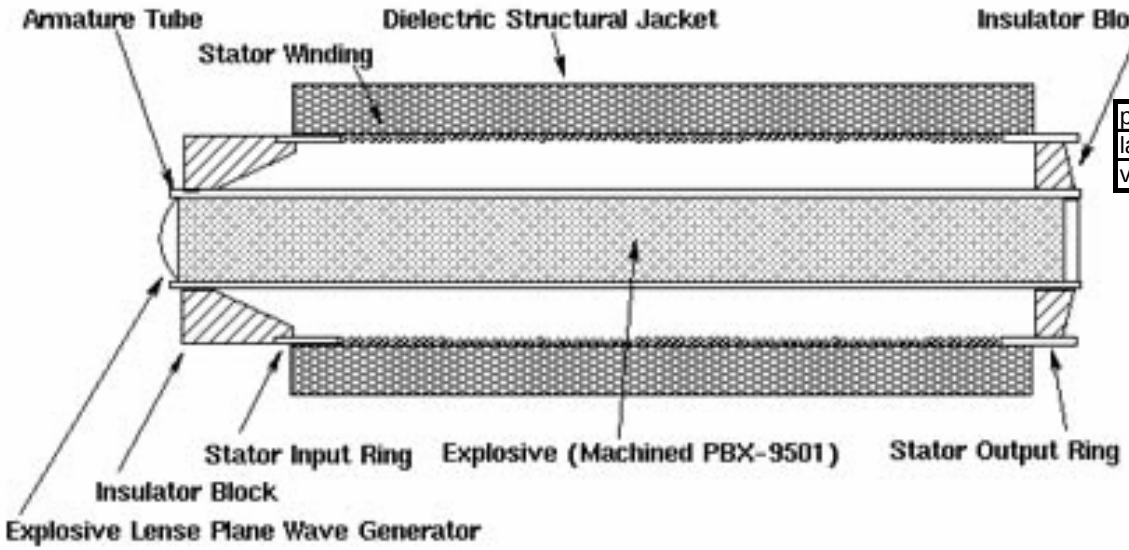


	electrons				photons			
	I	V	t	spotsize	n	h.v	t	spotsize
perforation power								
lateral effects								
volume effects								

facilitating

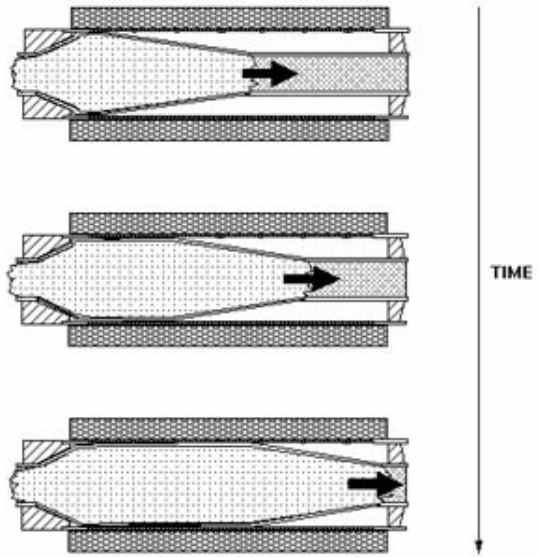
use lasers (or other EM radiation) to ionize the air in the path of the subsequent electric current

Using the high energy density of energetic materials: “E-bomb”, electromagnetic pulse



	electrons				photons			
	I	V	t	spotsize	n	h.v	t	spotsize
perforation power								
lateral effects								
volume effects								

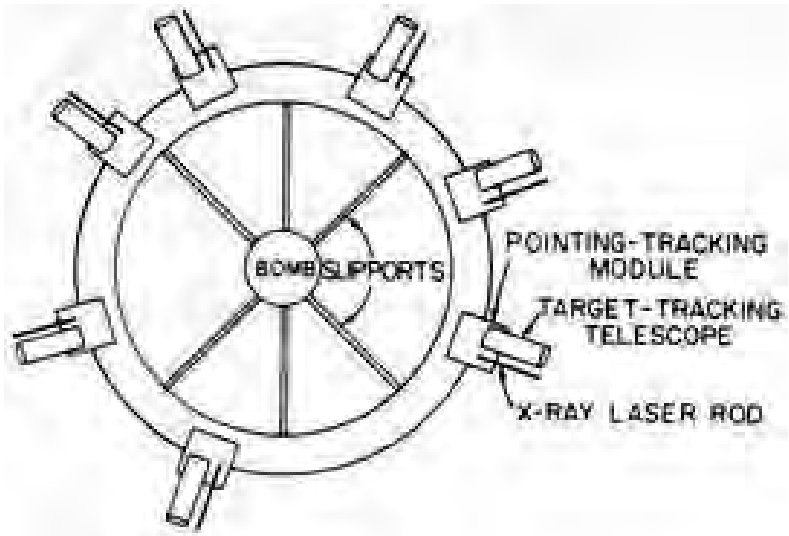
future



explosively pumped coaxial flux compression generator

Using the high energy density of energetic materials: detonation-pumped laser?

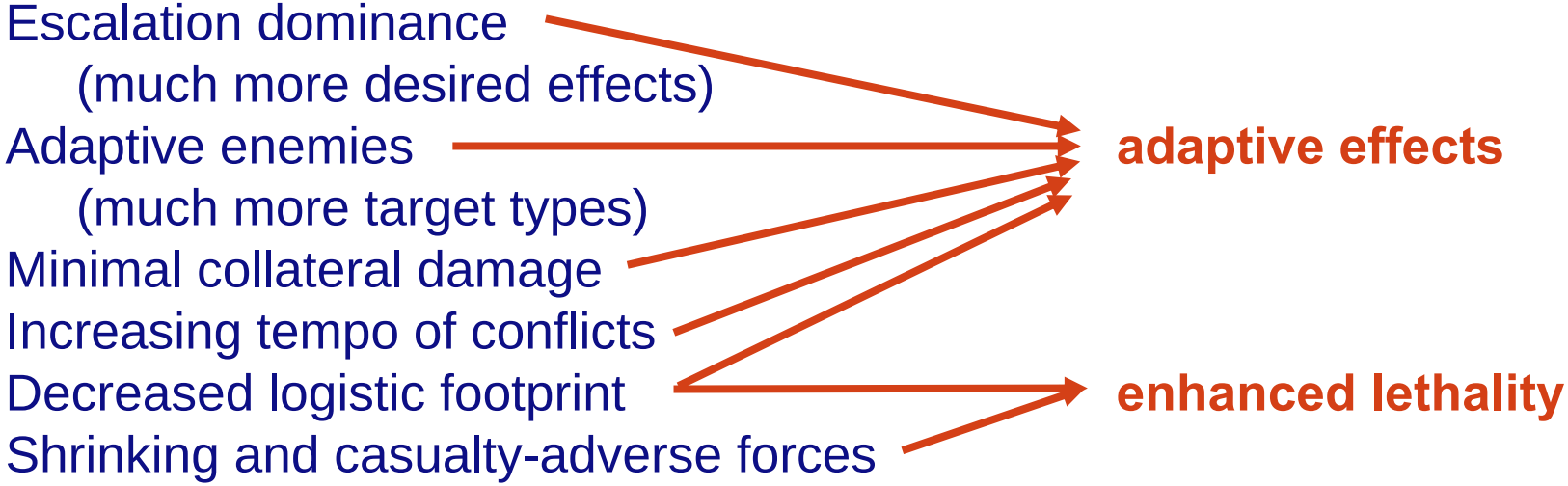




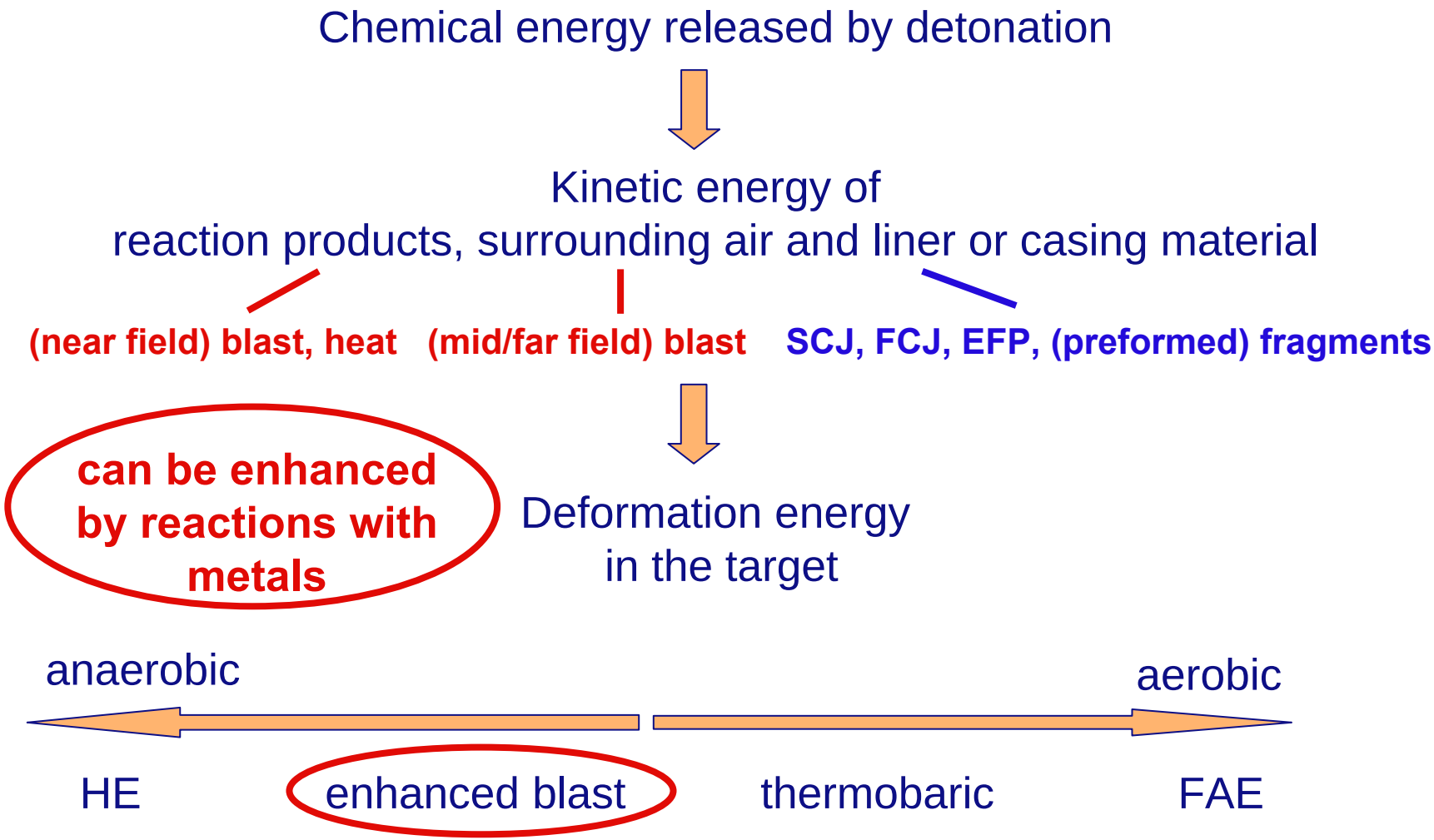
SDI: nuclear explosion pumped X-ray laser (5MJ per laser)

Current and future munitions drivers

Starting conditions: pinpoint accuracy, insensitive energetic materials



Adaptive and enhanced lethal effects: enhanced blast



Examples of enhancement by reactions with metals



	concentrated matter					dispersed matter			
	m	V	λ	ρ	deformation and failure behaviour	Ps	Is	t	Q
perforation power	■	■		■					
surface effects	■	■		■		■	■	■	
volume effects						■	■	■	

(Source: US Air Force Research Laboratory)



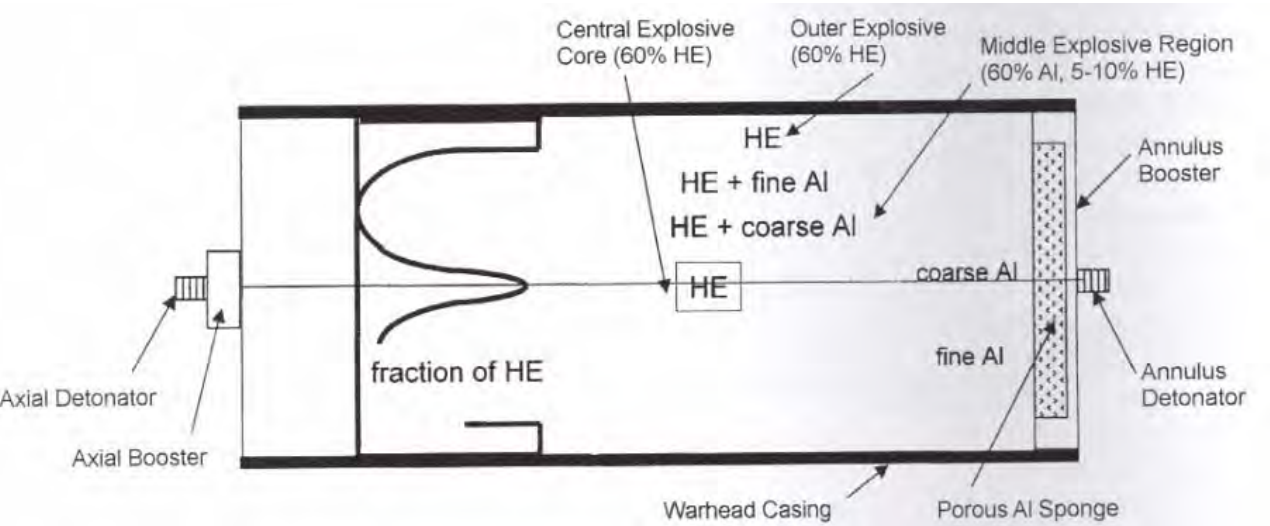
	concentrated matter					dispersed matter			
	m	V	λ	ρ	deformation and failure behaviour	Ps	Is	t	Q
perforation power	■	■		■					
surface effects	■	■		■		■	■	■	■
volume effects						■	■	■	■

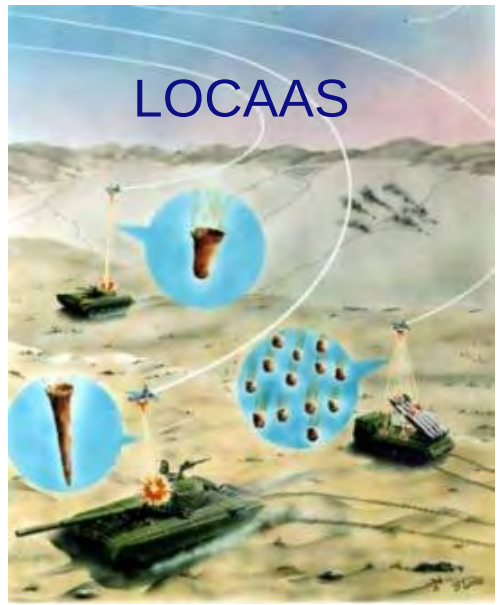
(Source: US Office of Naval Research)

Multimode or adaptive effects

	concentrated matter					dispersed matter			
	m	V	λ	ρ	deformation and failure behaviour	Ps	Is	t	Q
perforation power									
surface effects									
volume effects									

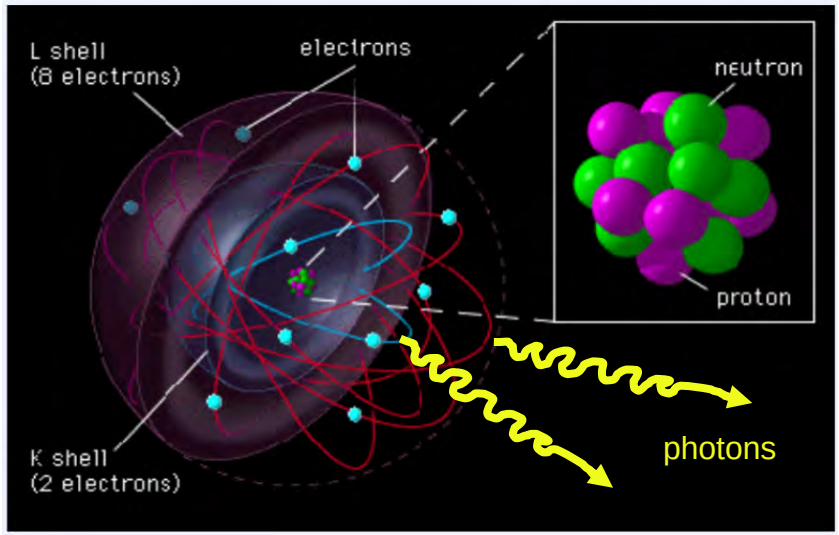
graded explosives (US Navy)





Ultimate multimode or adaptive effects

	matter									electrons				photons			
	solid/liquid-like					gaseous											
	m	V	λ	ρ	deformation and failure behaviour	Ps	Is	t	Q	I	V	t	spotsize	n	h.v	t	spotsize
perforation power																	
lateral effects																	
volume effects																	



Questions?



Contact information

Dr. A.M. Diederen
andre.diederen@tno.nl

TNO Defence, Security and Safety
Business Unit Protection, Munitions and Weapons
Research Group Explosions, Ballistics and Protection
PO Box 45, 2280 AA Rijswijk, The Netherlands

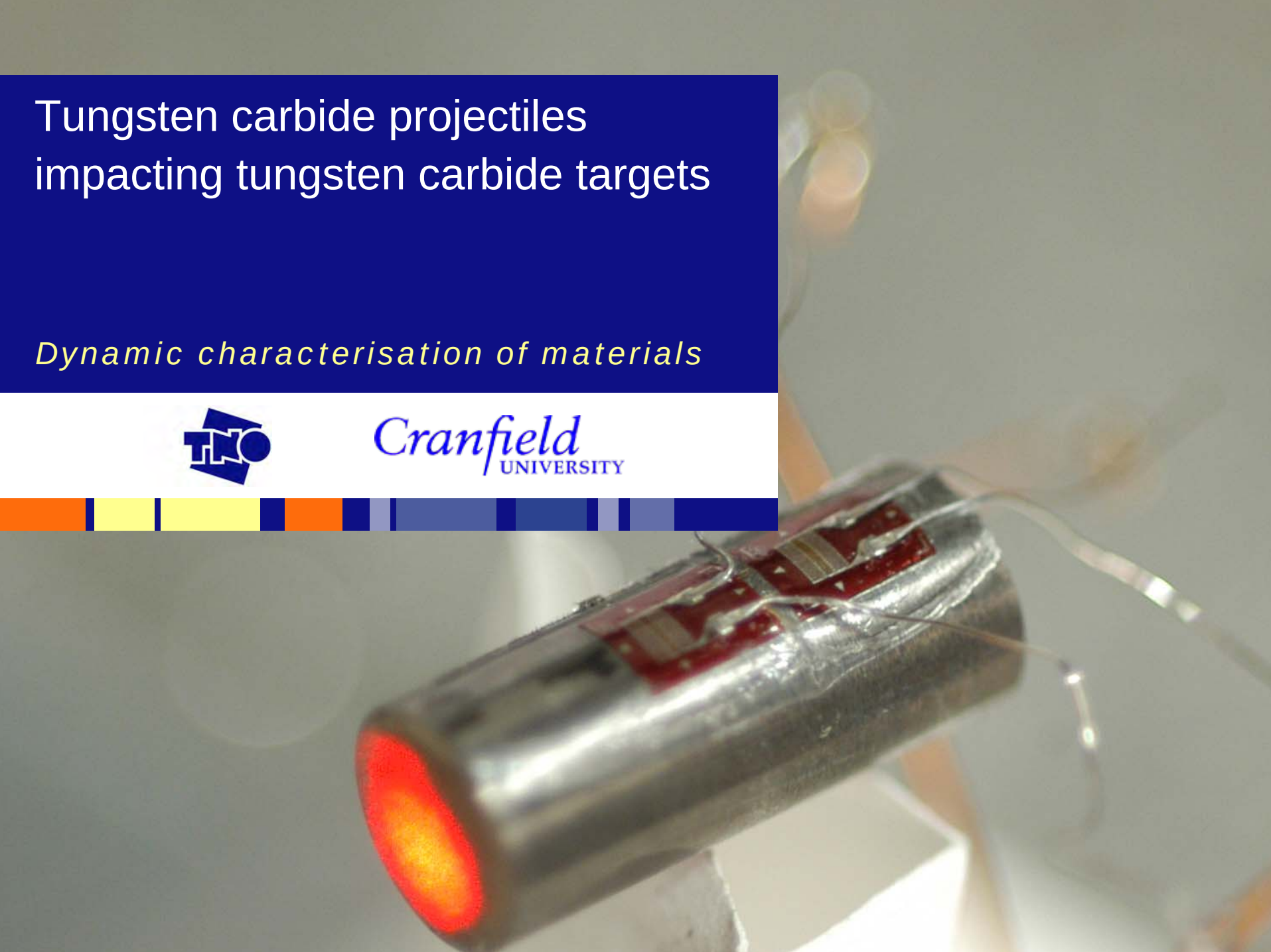
Phone +31 15 284 3509
Mobile +31 6 5184 5221
Fax: +31 15 284 3939

Tungsten carbide projectiles impacting tungsten carbide targets

Dynamic characterisation of materials

TNO

Cranfield UNIVERSITY



Acknowledgements



- Co-author:
  - Dr. André Diederen
- Laboratory for Ballistic Research (Ypenburg, NL)

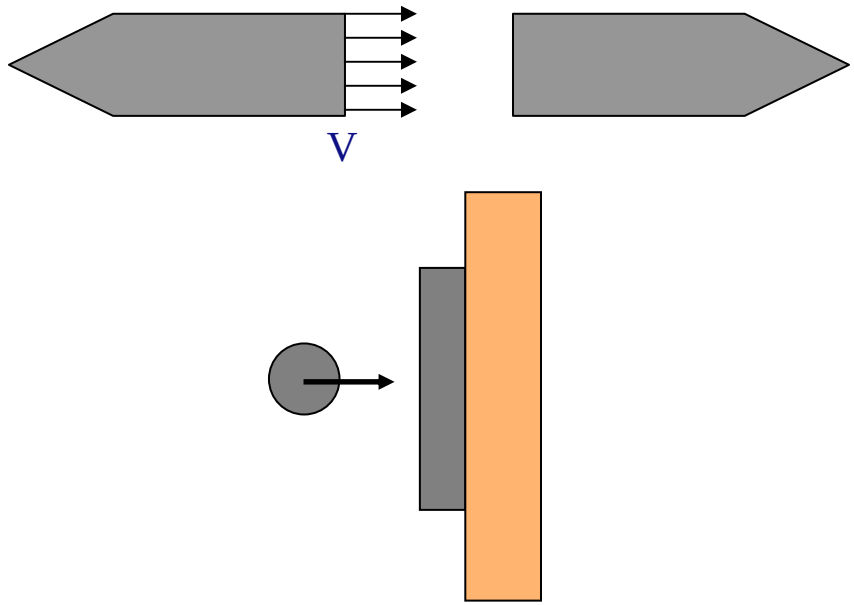
Cranfield UNIVERSITY

- Co-author:
  - Dr. Paul Hazell
  - Mr. Gareth Appleby-Thomas
- Material Characterisation Lab (Shrivenham, UK)

- Funded by the Dutch Ministry of Defense, partly through the research program “Munition and weapons effects”

Contents

- Introduction:
  - Overview of total research project
- Two specialized experiments:
  - Core to Core impact
  - Sphere to Disc impact
- Core to Core impact
  - Set-up
  - Results
- Summarizing
- Further research



Introduction

- In ballistic impacts events → strong interaction between dynamic behaviour of projectile and armour
- Lots of work is done in characterising and modelling armour materials

- However, characterising the dynamic behaviour of Armour Piercing (AP) projectiles is equally important

- Problems:
  - **dynamic** material testing is difficult
  - only small samples of material are available (projectile cores)
  - validation experiments for FE modelling with AP projectiles often involve ‘complex’ armour systems (incl. ceramics)

Overview of total research program

EOS, hardening

- Analysing the composition of AP core material (SEM)
- ‘Standard’ dynamic material tests with material, closely resembling real AP core material: Flyer plate impact testing (*poster TB058*)

1

Failure behaviour

- Special designed dynamic experiments with real AP cores
- Special designed dynamic experiments with simulant material
- Goal: well defined, ‘simple’, experiments (*this presentation*)

2

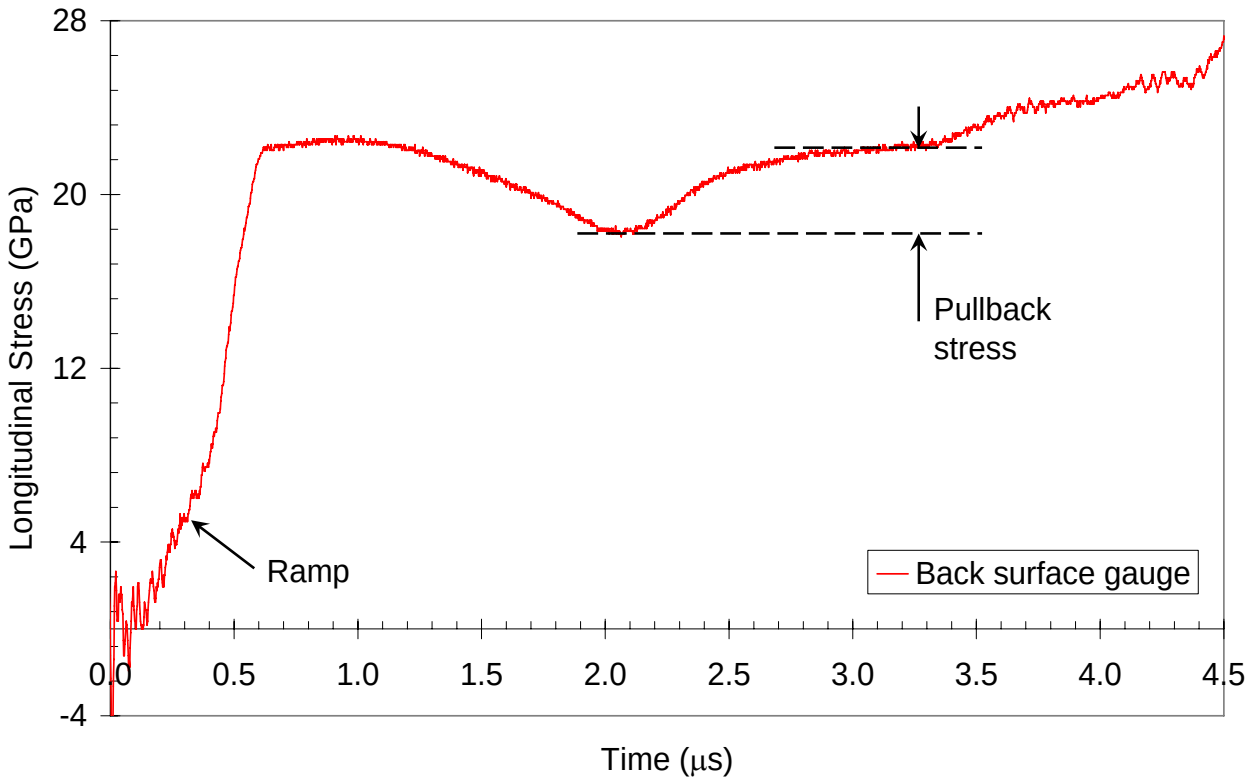
Total material model

- Use the results of step 1 (direct engineering) together with the results of step 2 in order to reverse engineer the dynamic material model for the AP core material (*ongoing research*)

3

TNO Cranfield UNIVERSITY

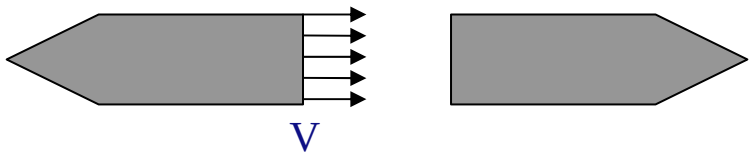
Step 1: flyer plate testing



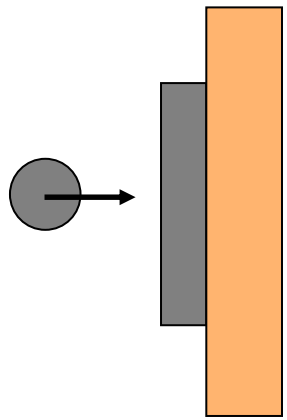
- "Shock response of a cemented Tungsten Carbide" (poster TB058)
- Measured: EOS (shock), Hugoniot Elastic Limit, Dynamic Spall Strength

Step 2: Specialized experiments

- Core to core experiments
- Acceleration of a AP core (in reverse orientation) onto an identical stationary core



- Sphere to disc experiments
- Sphere of ‘simulant’ AP core (WC) material impacting ‘simulant’ (WC) target
- Target: 6 mm WC with 12 mm polycarbonate backing



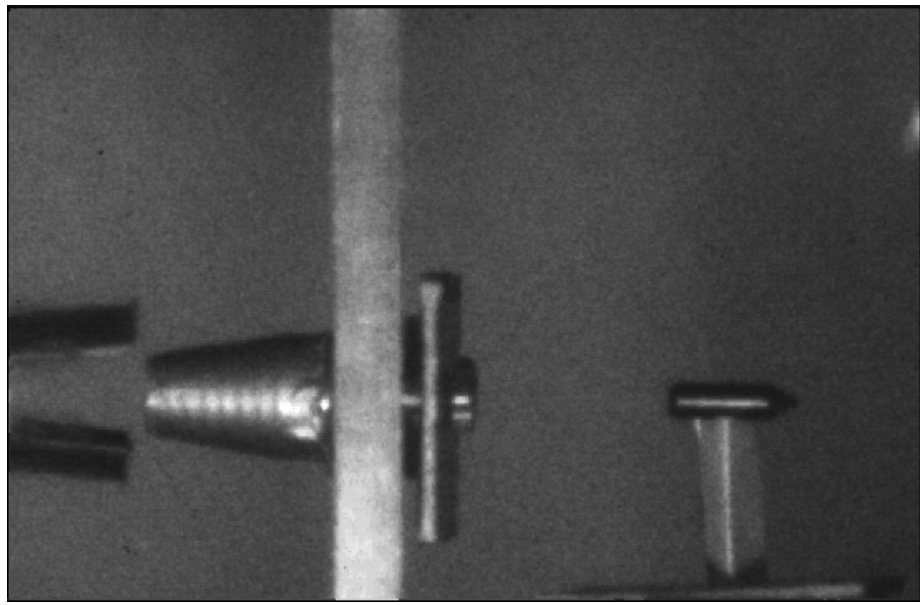
Goal: break-up of WC material with a ‘simple’ experimental set-up

Use the results of the experiments to reverse engineer the failure model

Step 2: Specialized experiments: Core to Core

- Acceleration of a AP core (in reverse orientation) onto an identical stationary core
- Acceleration in a sabot
- Velocity regime: 250 - 500 m/s
- Fragments are captured and collected afterwards for SEM analysis
- Occasionally strain measurements are performed on the stationary core

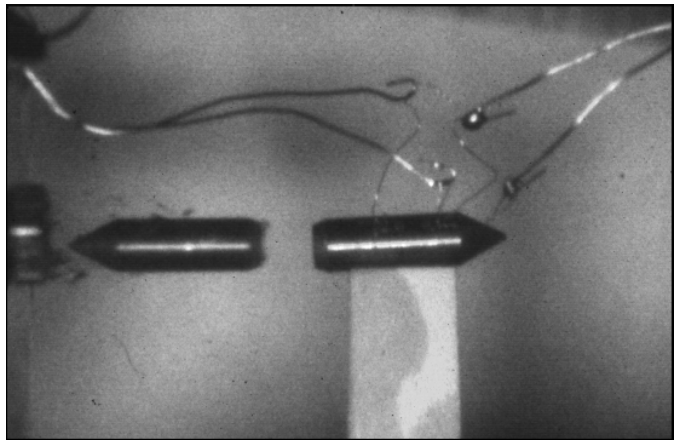


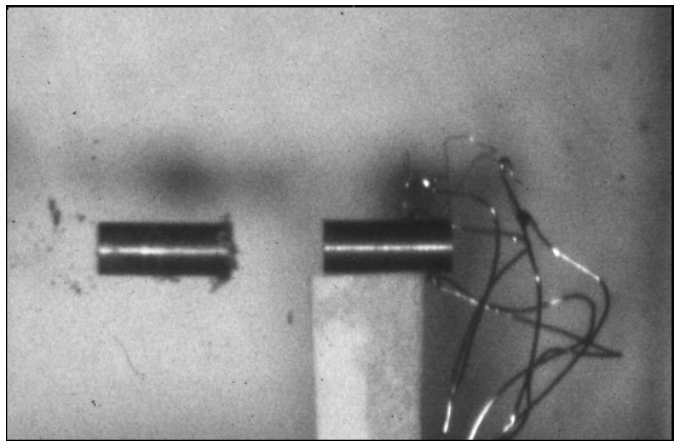



11-09-2007 -000010 0.000 94500 fps

Specialized experiments: Core to Core

- Benefits:
  - Experiments with real core material
  - Only one material is used → only one material needs to be modelled
  - Highly dynamic event (impact velocity up to 500 m/s)
  - Simple small geometry → FE models small and quick





(straight cilinders from AP cores with the use of spark erosion)

Specialized experiments: Core to Core

- Results:
  - Projectiles rapidly erode at impact surface followed by fragmentation along length



v = 250 m/s



v = 370 m/s

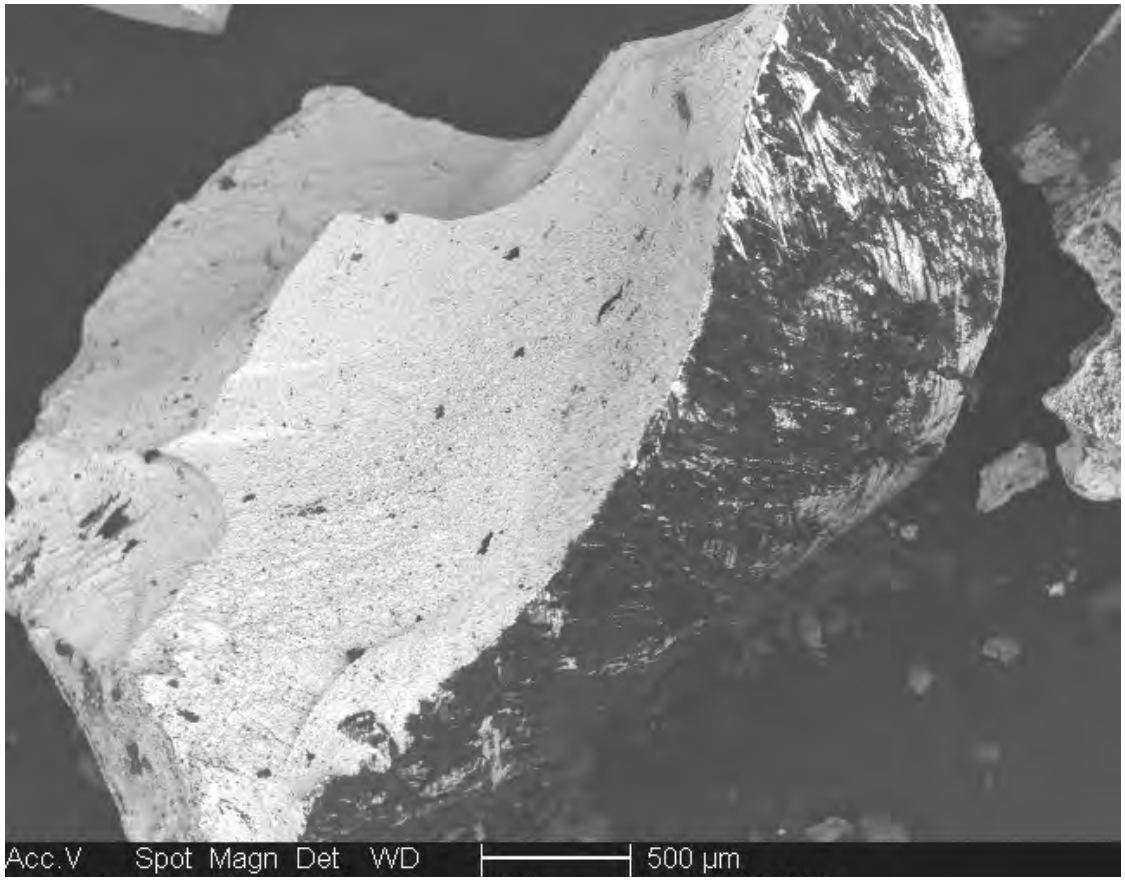


v = 500 m/s

  - Comminution of material increases with impact velocity
  - Complete fragmentation of cores with v = 500 m/s

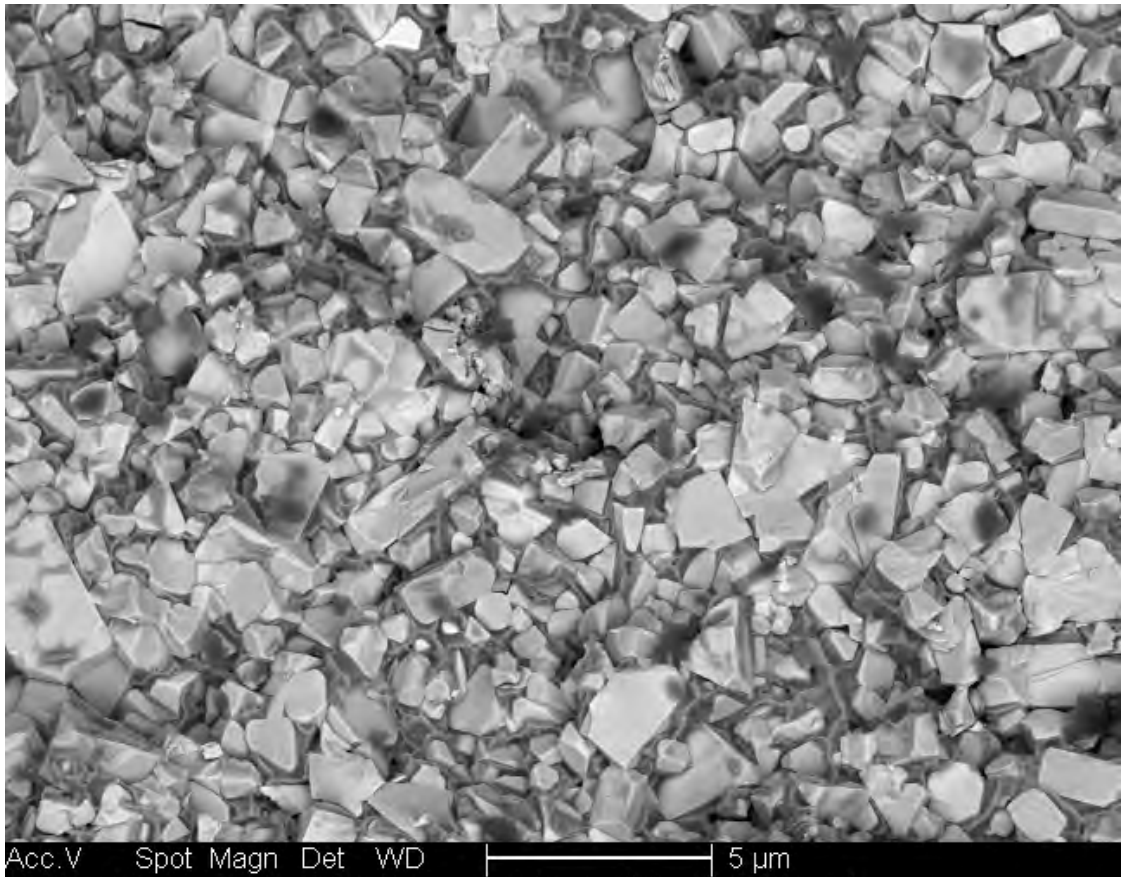
Koen Herlaar, ISB 2008, New Orleans (koen.herlaar@tno.nl)

SEM pictures recovered fragments after impact



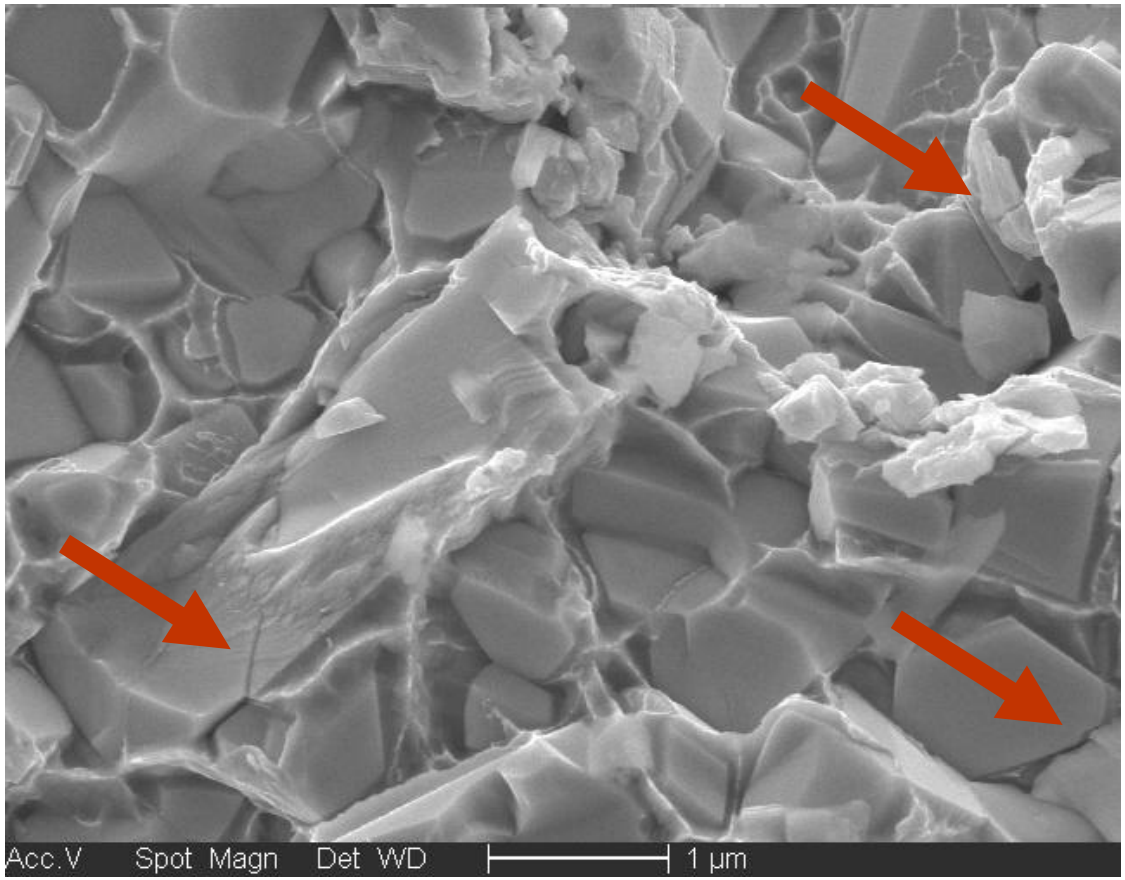
33 x magnification

SEM pictures recovered fragments after impact



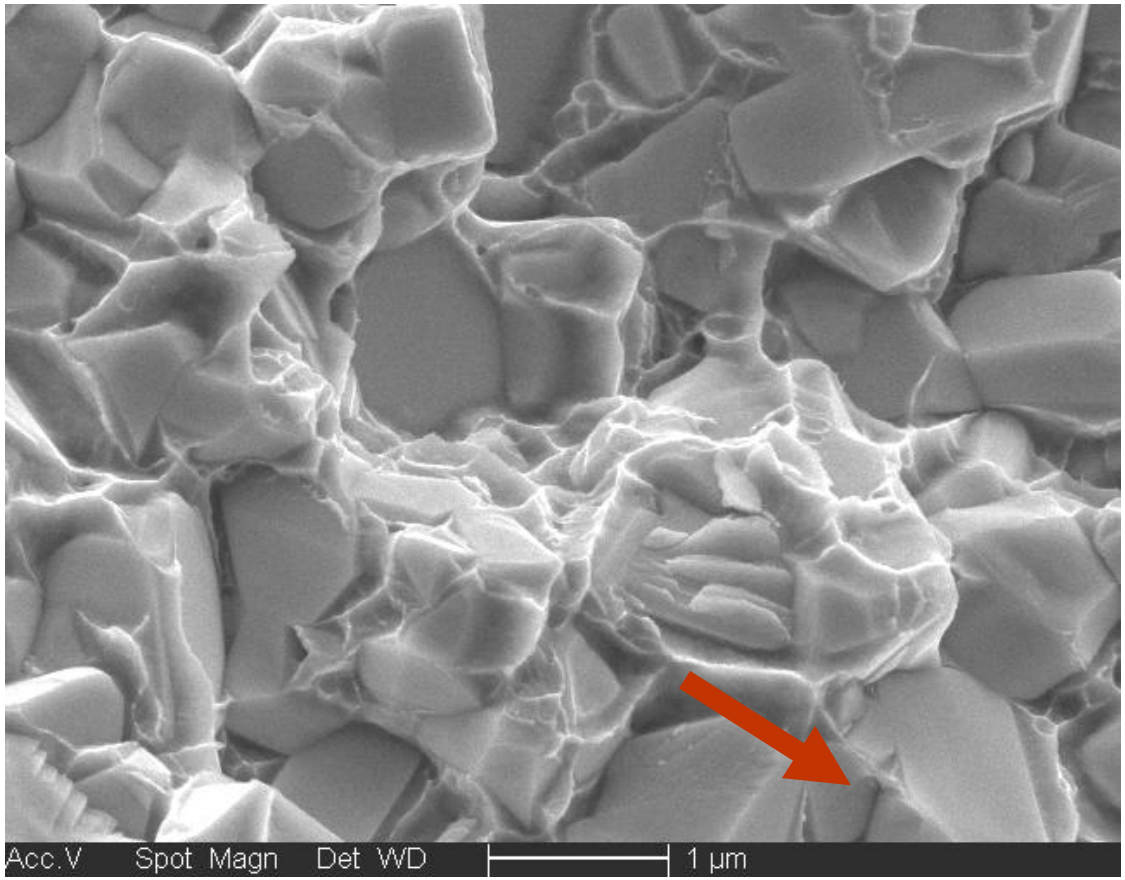
5.000 x magnification

SEM pictures recovered fragments after impact



20.000 x magnification, v = 500 m/s

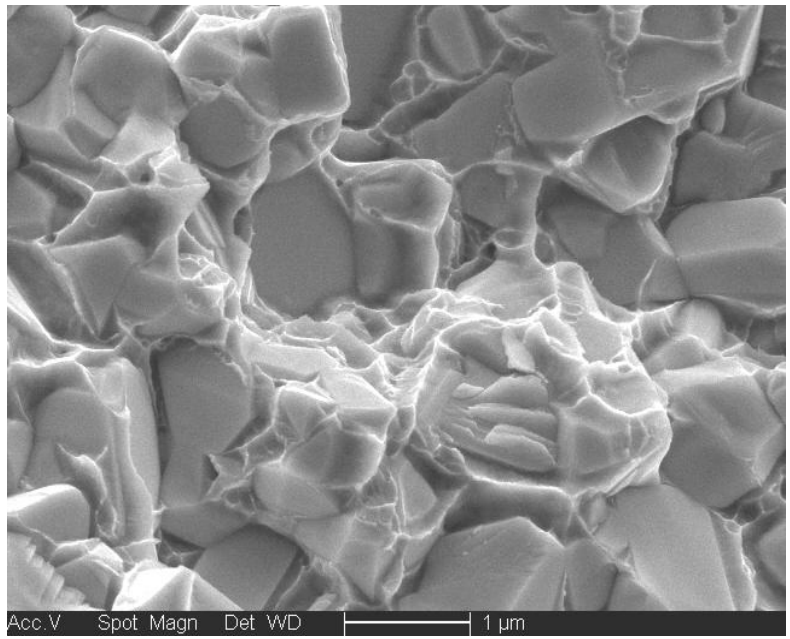
SEM pictures recovered fragments after impact



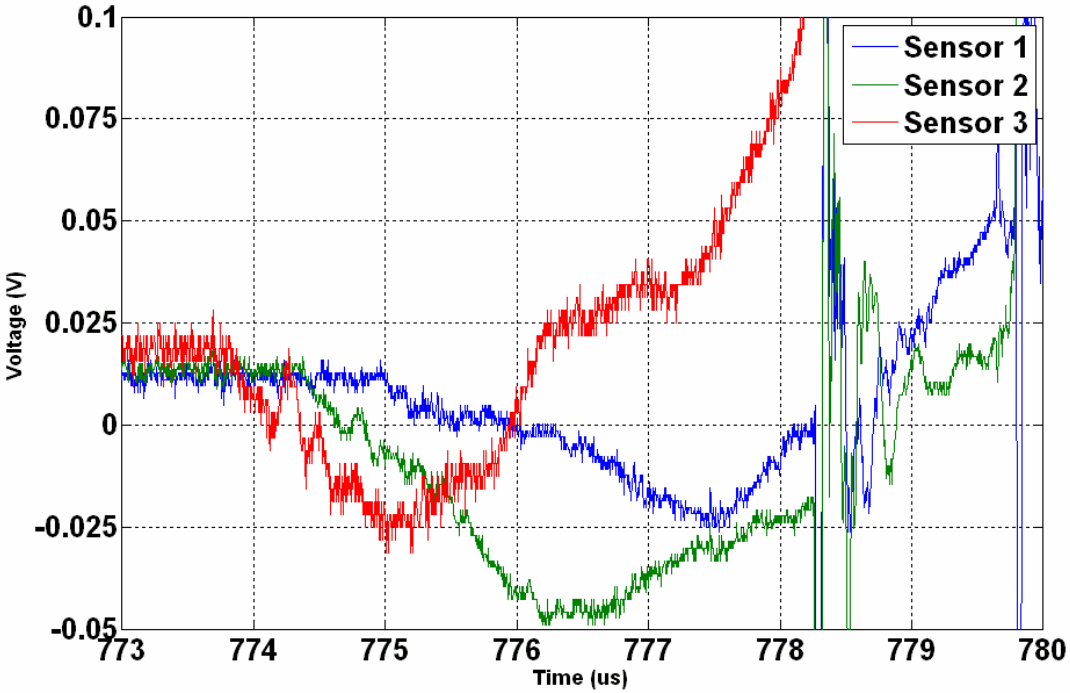
20.000 x magnification, v = 250 m/s

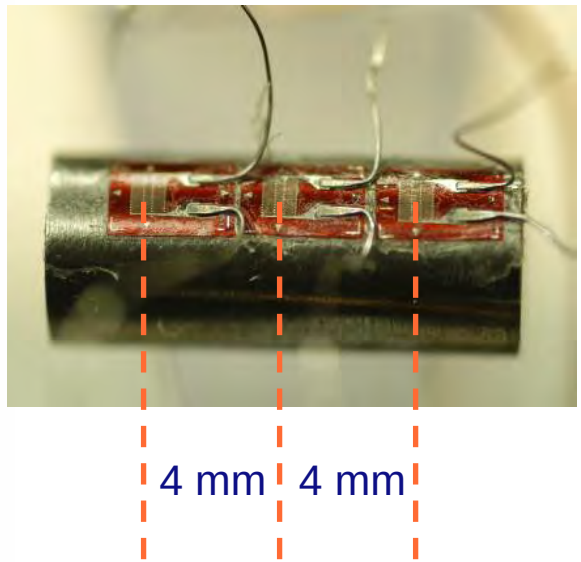
SEM pictures recovered fragments after impact

- Failure dominated by trans-granular failure in Co-matrix
- Trans-granular failure seems to be more brittle at higher impact velocities
- Inter-granular failure is rare



Results strain gauges





- Successful measurements of strain for approximately 4 µs
- Measured wave velocity corresponds well with measured EOS

Summarizing

EOS, hardening

- Analysing the composition of AP core material (SEM)
- ‘Standard’ dynamic material tests with material, closely resembling real AP core material: Flyer plate impact testing (*poster TB058*)

1

Failure behaviour

- Special designed dynamic experiments with real AP cores
- Special designed dynamic experiments with simulant material
- Goal: well defined, ‘simple’, experiments (*this presentation*)

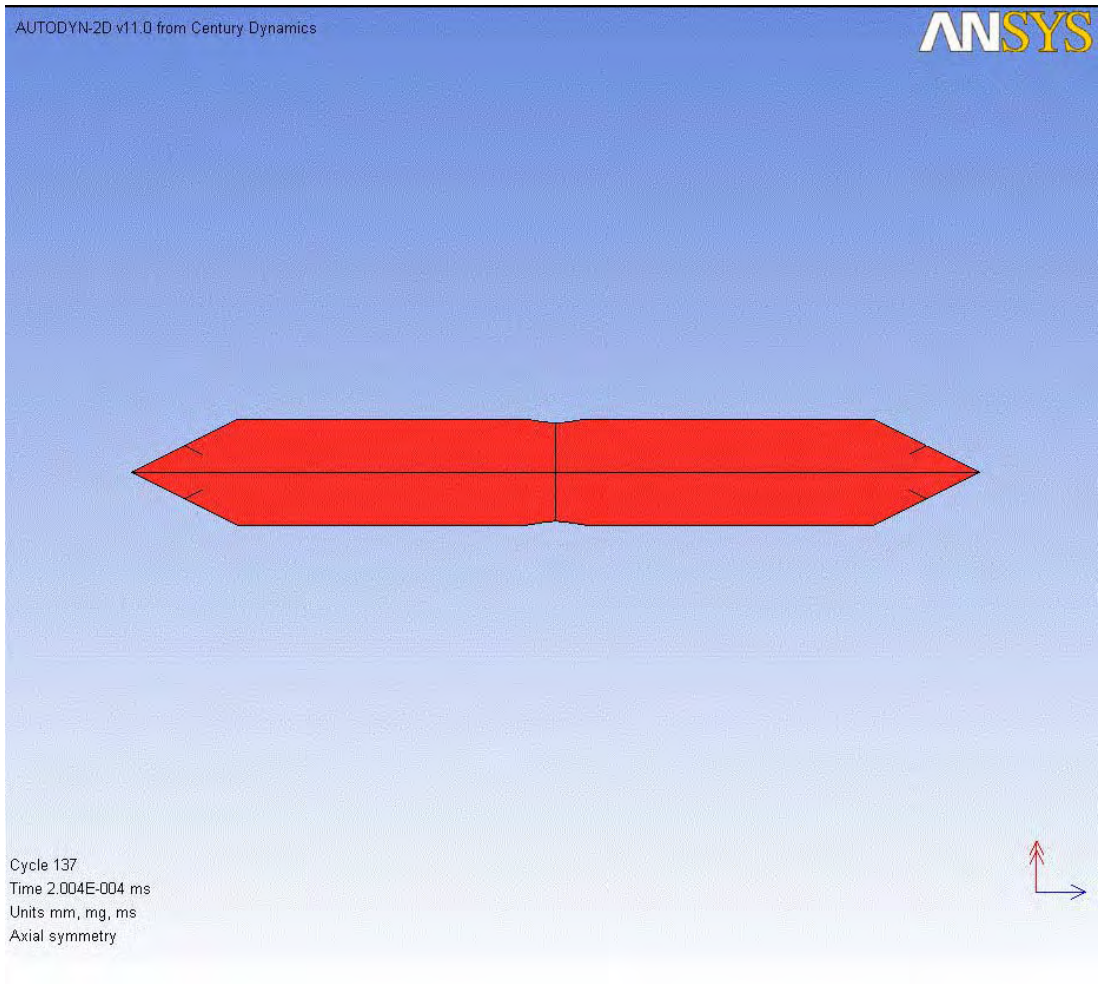
2

Total material model

- Use the results of step 1 (direct engineering) together with the results of step 2 in order to reverse engineer the dynamic material model for the AP core material (*ongoing research*)

3

Step 3, *in progress*

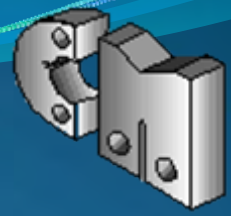


Thank you for your attention

Questions … ??

Dynamic characterisation of materials

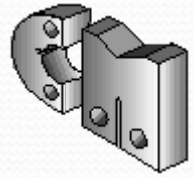




GRC's impact behavior

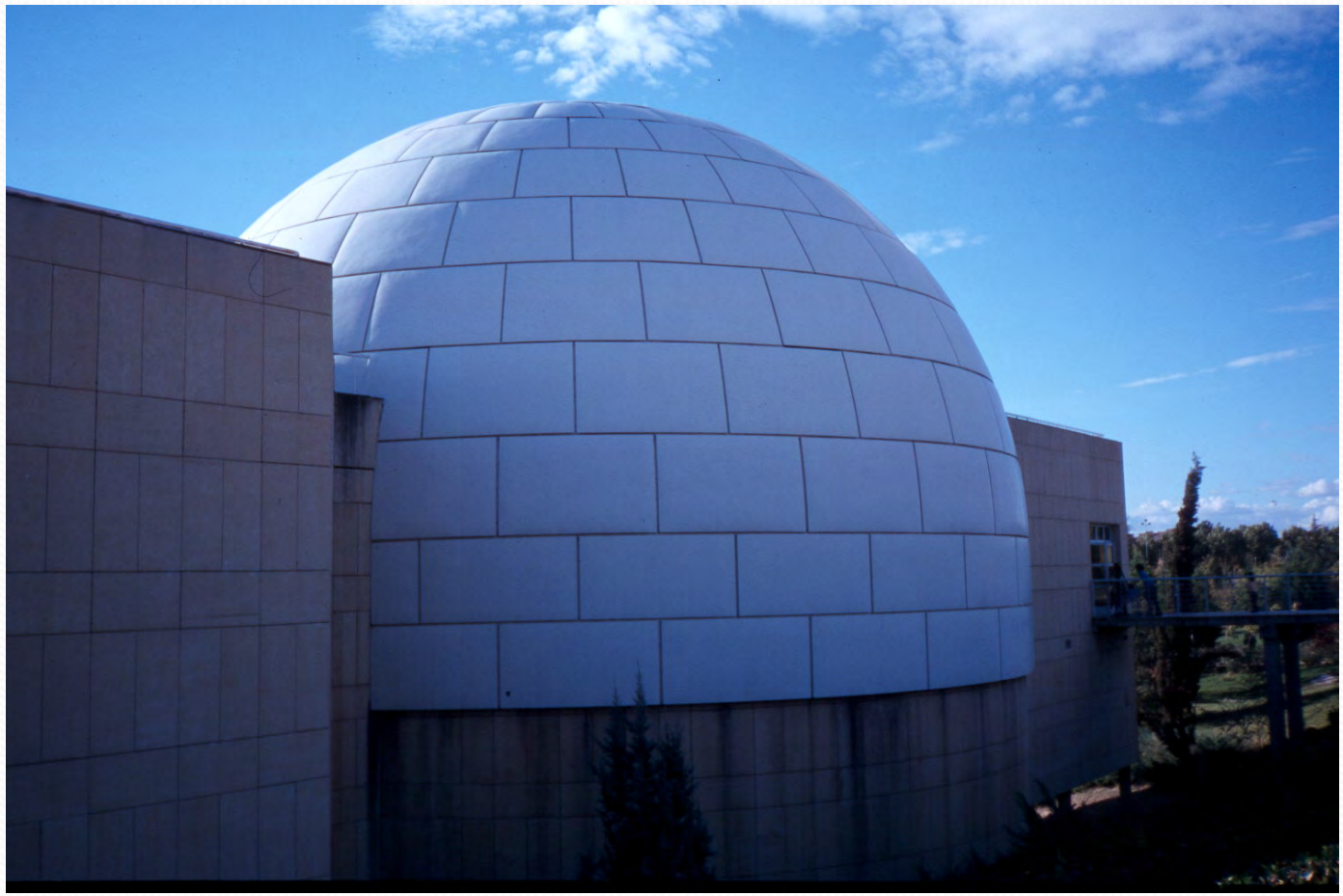
A. Enfedaque, F. Gálvez, D. Cendón, V. Sánchez Gálvez
Material Science Department
Polytechnic University of Madrid

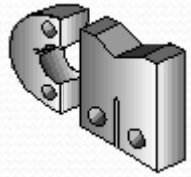
Contents



1. Introduction
   - What is GRC?
   - GRC's mechanical properties
2. GRC production and tests
   - GRC formulation
   - Testing facilities and projectiles
   - Velocity measuring systems
3. Numerical simulations
4. Conclusions

Introduction





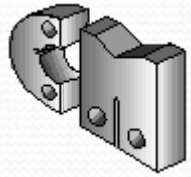
What is GRC?

¿What does GRC stand for?

GRC stands for Glass Fiber Reinforced Cement. This material is produced by spraying chopped glass fibers simultaneously with cement mortar.







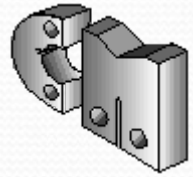
What is GRC?

Why are glass fibers added to cement mortar?

Glass fibers increase cement mortar's ductility and prevent cracking caused by shrinkening.







GRC's mechanical properties

GRC static mechanical properties

Density	1.900 – 2.250 Kg/m^3
Compressive strength	48 – 83 MPa.
Young modulus	10 – 20 GPa.
Flexural strength -First cracking -Rupture	 6 – 10 MPa. 17 – 25 MPa.
Tensile strength -First cracking -Rupture	 4,8 – 7 MPa. 7 – 11 MPa
Failure strain	0,6 – 1,2 %

GRC's mechanical properties

What about GRC's behavior under high strain rates?

Strain rates over 10^1 s^{-1} have not been studied.



GRC production and tests



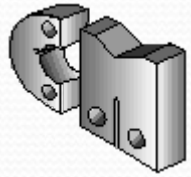
Material production

GRC was produced using a 10% metakolin addition.

Cement	Sand	Water	Plasticizer	Metakaolin
50 Kg.	50 Kg.	22 l.	0.5 liters	5 Kg.



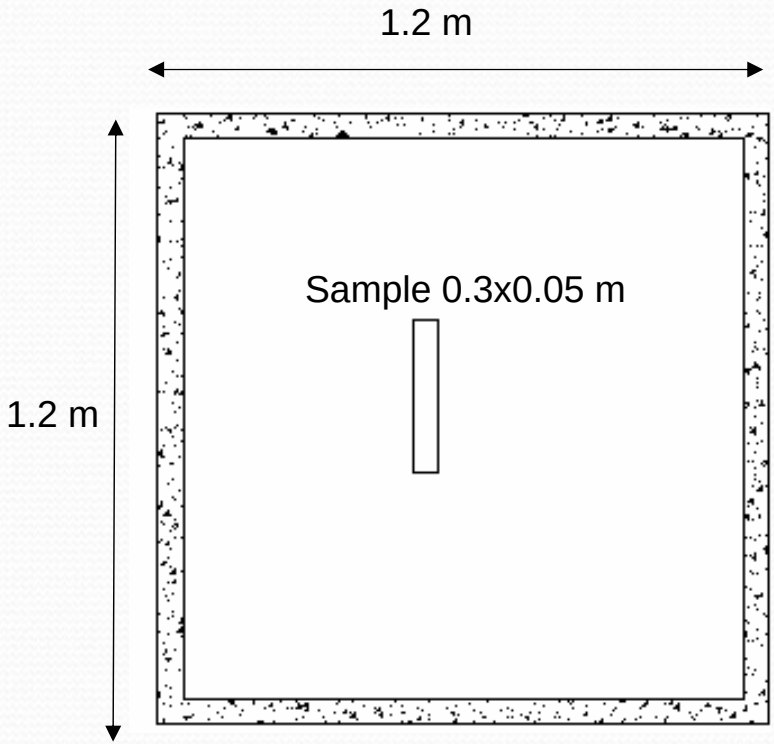


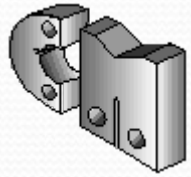


Material production

GRC tensile tested samples were cut from 1.2x1.2m test boards

Samples dimensions were 0.3x0.05 m.



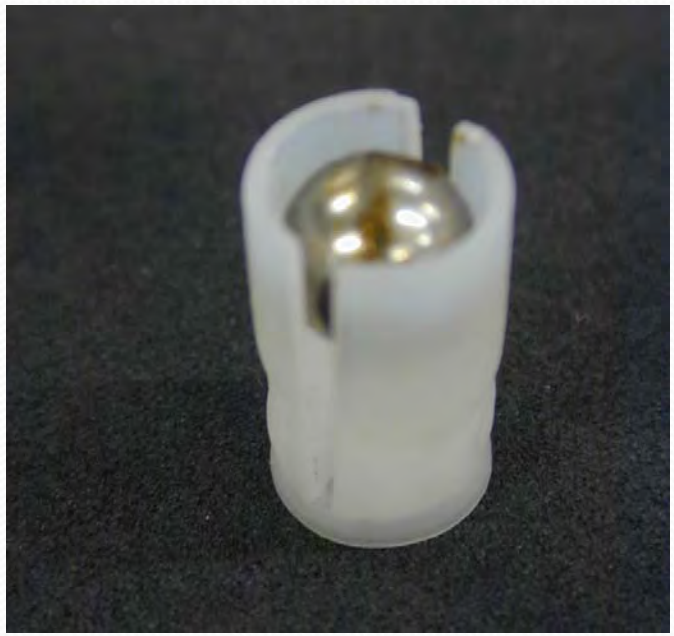


Test set up

Gas gun

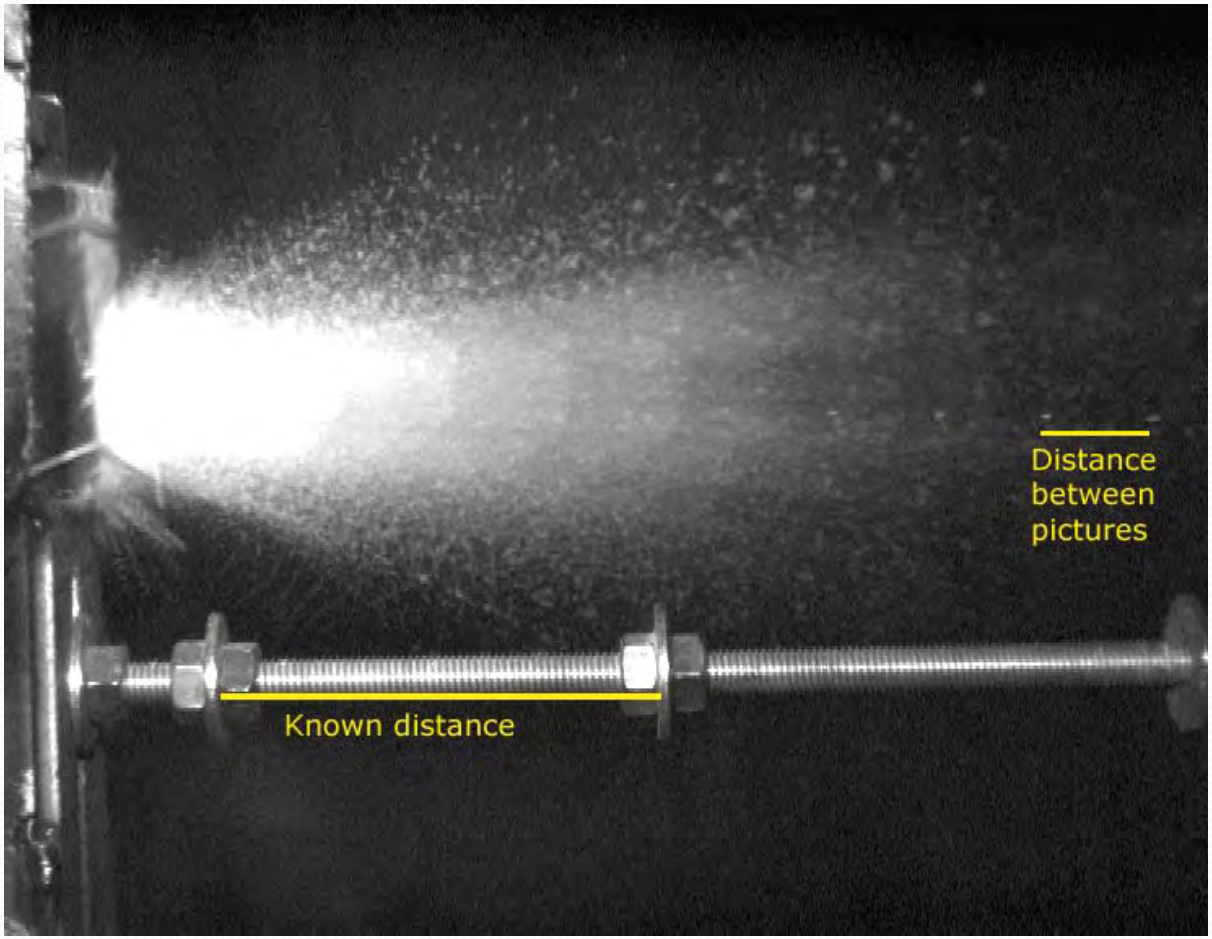


5.5 mm diameter steel spheres and sabot



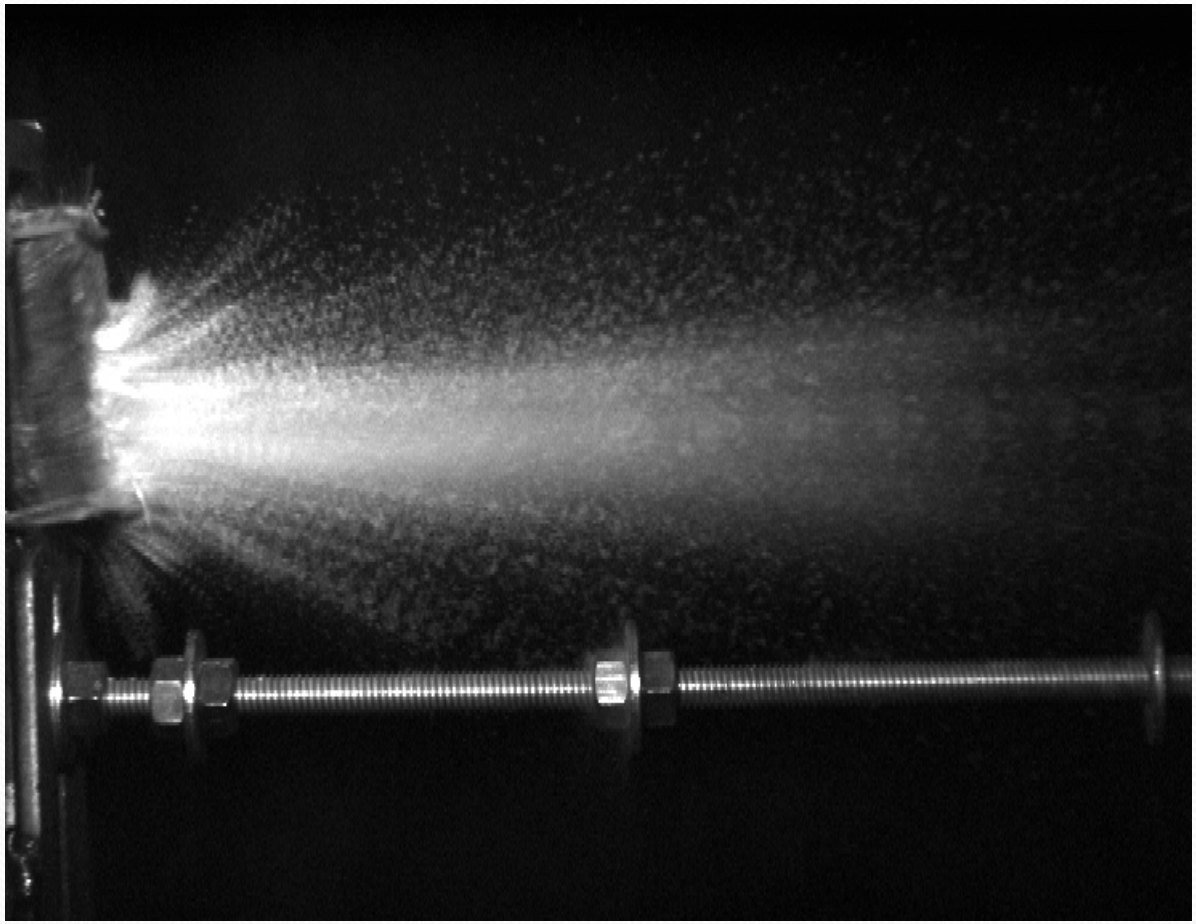
Velocity measuring systems

High speed rate pictures for high speeds (>400 m/s)

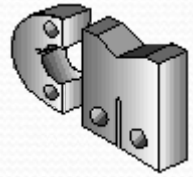


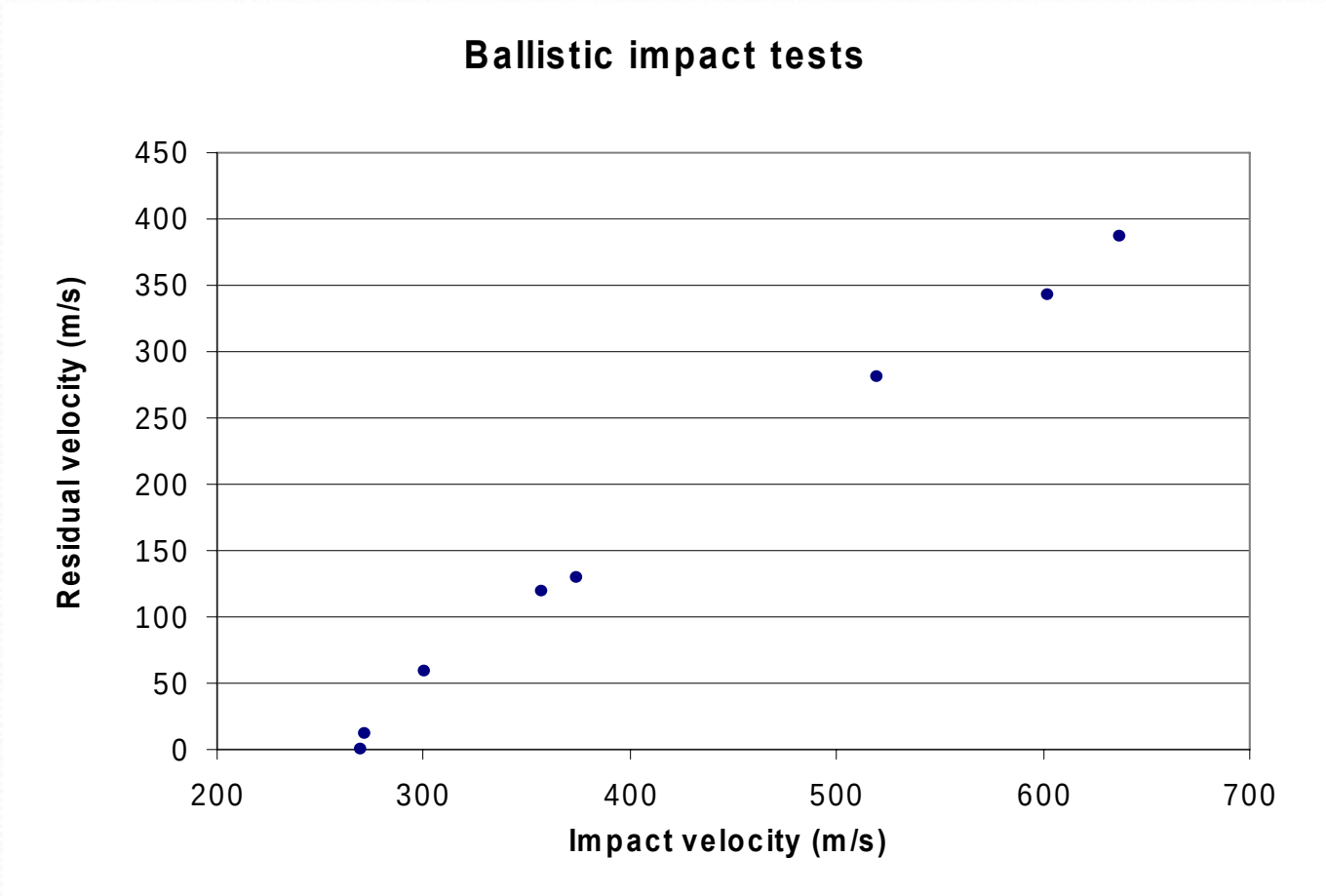
Velocity measuring systems

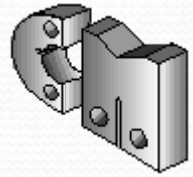
For low speeds a calibrated molding clay was used (< 400 m/s)



Test results







Numerical simulations

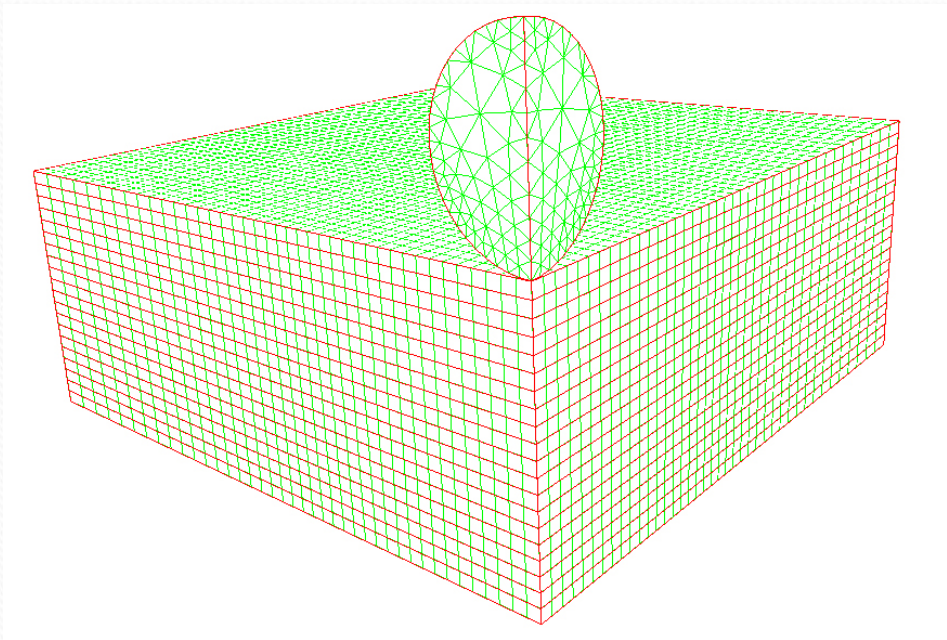
Autodyn v6 was used for calculations

GRC samples idealized as 10 mm thick plates

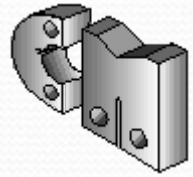
Cement simulated as Concrete-L Autodyn library material

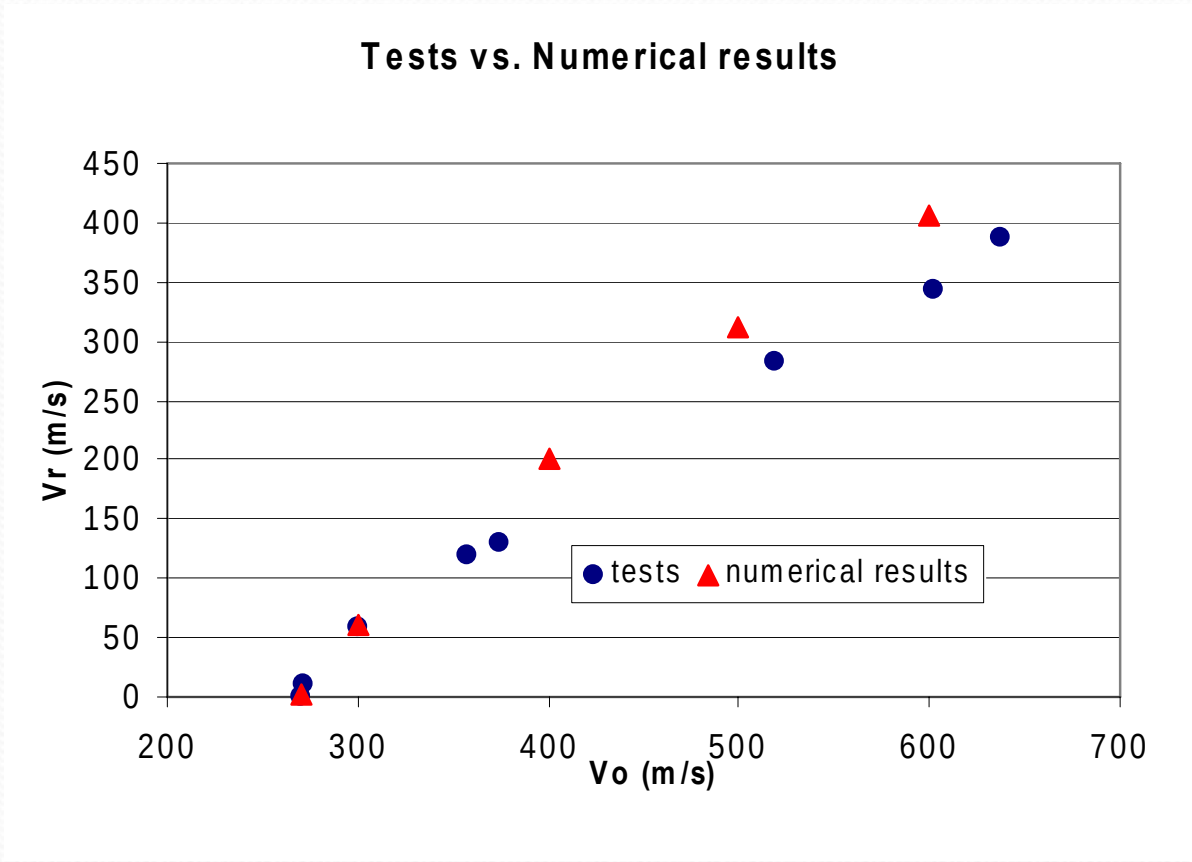
Glass fibers introduced in the model as membrane layers between cement ones

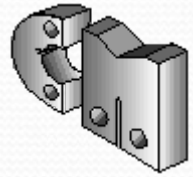
Spheres simulated as a rigid body



Testing vs. Numerical simulations





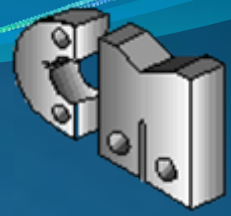


Conclusions

1. A complete residual velocity vs. impact velocity curve for GRC panels has been achieved.

2. Velocity measurement through high velocity photographs and indirect measurement using molding clay have been proved to be consistent.

3. Numerical simulations using Autodyn 3-D v6. are able to predict GRC's impact behavior accurately.



GRC's impact behavior

A. Enfedaque, F. Gálvez, D. Cendón, V. Sánchez Gálvez
Material Science Department
Polytechnic University of Madrid

DIEHL
BGT Defence

Initiation Controlled Multimode Warheads



Dr. Thomas Falter
DBD E-MK
09/23/2008

DIEHL
BGT Defence

Outline

- Introduction & Motivation
  - Multimode warhead
- Theory
  - Computational tool: ANSYS AUTODYN®
  - Underlying physics
- Simulation of an Initiation Controlled Multimode Warhead
  - EFP Mode
  - Jetting Mode
  - Fragmentation Mode
- Summary

Copyright Diehl BGT Defence GmbH & Co. KG

DIEHL
BGT Defence

Motivation

- Conventional HE warhead types (examples)

Warhead	Penetration performance	Standoff	Focus
SC	High (≥10 CD)	Low (~6 CD)	Directed
EFP	Medium (≥1 CD)	High (≥150m)	Directed
Fragmentation	Low	Medium	Omnidirectional

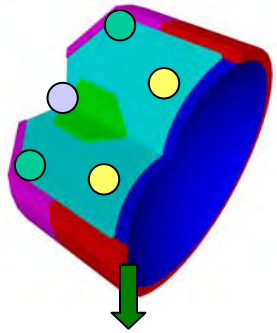
Objective → 1 single multimode warhead that can switch between the three different modes

Copyright Diehl BGT Defence GmbH & Co. KG

DIEHL
BGT Defence

Motivation

single charge
(e.g. EFP)



multiple points of
initiation

EFP Mode





hard targets
large standoff



e.g. (main battle) tank

Jetting (SC) Mode



hard targets
small standoff



e.g. main battle tank

Fragmentation Mode





semi hard /
soft targets
medium
standoff



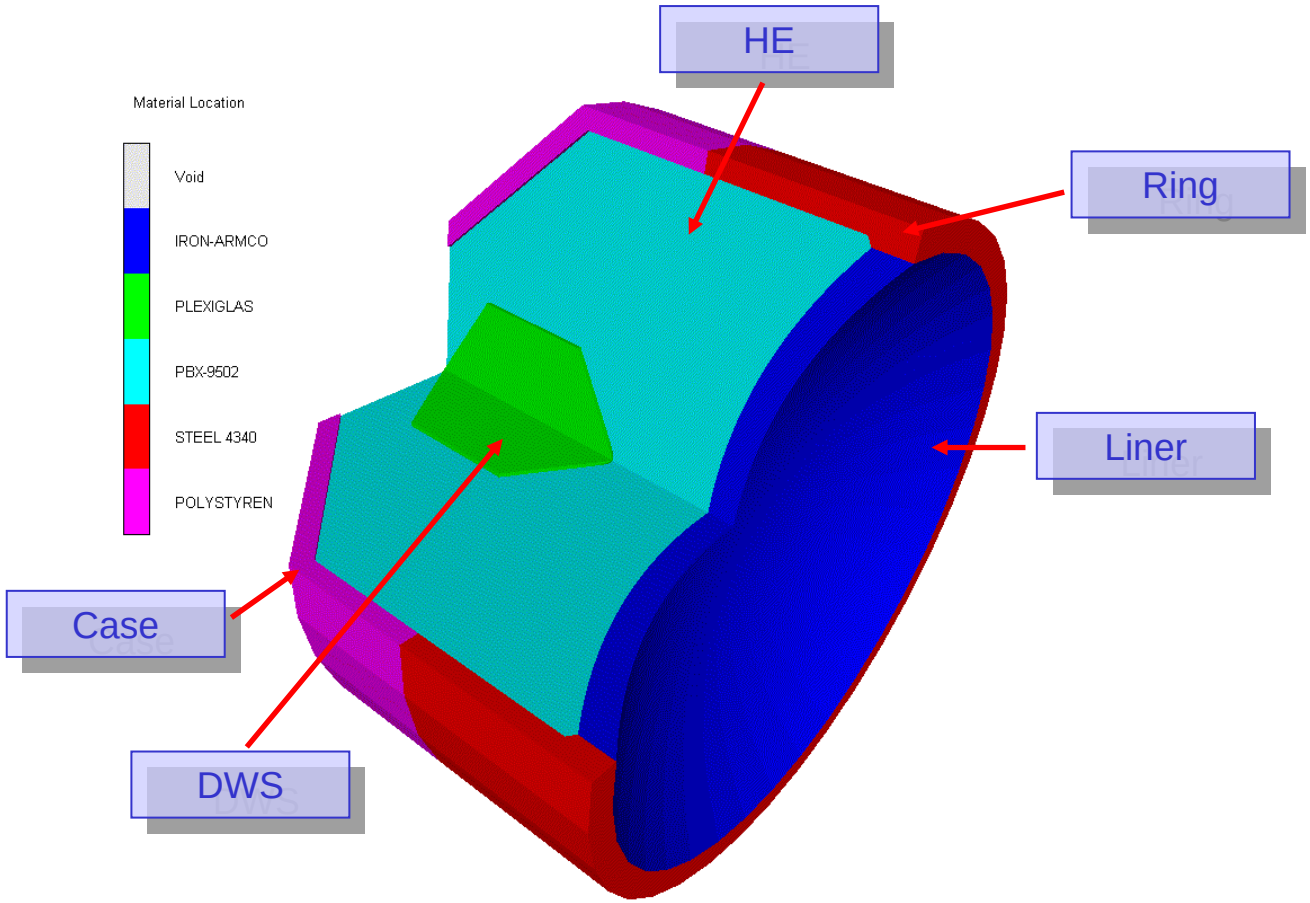
e.g. truck, radar, etc.

Copyright Diehl BGT Defence GmbH & Co. KG

DIEHL
BGT Defence

Multimode Warhead

- Basis: EFP warhead

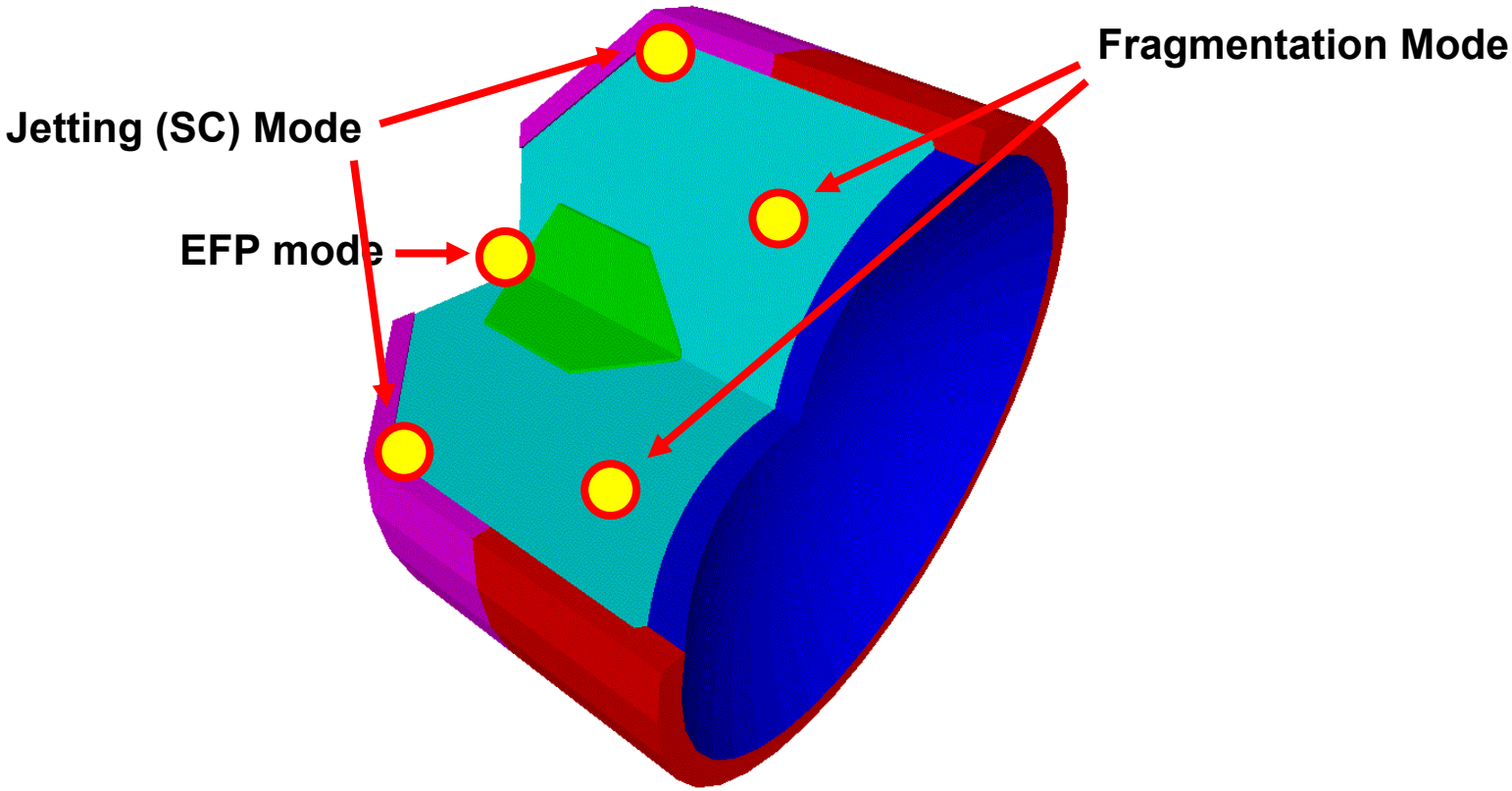


Copyright Diehl BGT Defence GmbH & Co. KG

DIEHL
BGT Defence

Multimode Warhead

- Choose warhead mode by means of initiation with EFI



Copyright Diehl BGT Defence GmbH & Co. KG

DIEHL
BGT Defence

AUTODYN®

- Hydrocode simulation with ANSYS AUTODYN®
  - Explicit analysis tool for simulating non-linear short time dynamics of
    - solids, fluids, gases
    - fluid-structure interactions
  - Combined method of
    - finite differences
    - finite elements
    - finite volumes
    - (mesh free SPH)

Copyright Diehl BGT Defence GmbH & Co. KG

DIEHL
BGT Defence

Underlying Physics

- Conservation laws
  - Mass

$$\frac{D\rho}{dt} + \rho \sum_{i=1}^{3} \frac{\partial v_i}{\partial x_i} = 0$$

  - Momentum

$$\rho \frac{Dv_i}{Dt} = \sum_{j=1}^{3} \frac{\partial \sigma_{ji}}{\partial x_j} + f_i \qquad (i = 1,2,3)$$

  - Angular Momentum

$$\sigma_{ij} = \sigma_{ji} \qquad (i, j = 1,2,3)$$

  - Energy

$$\rho \frac{Dw_{\text{int}}}{Dt} = \sum_{i,j=1}^{3} \frac{\partial v_i}{\partial x_j} \sigma_{ij} - \sum_{i=1}^{3} \frac{\partial q_i}{\partial x_i} + \rho s$$

- Material laws
  - Equation of State
  - Material strength
  - Material Failure

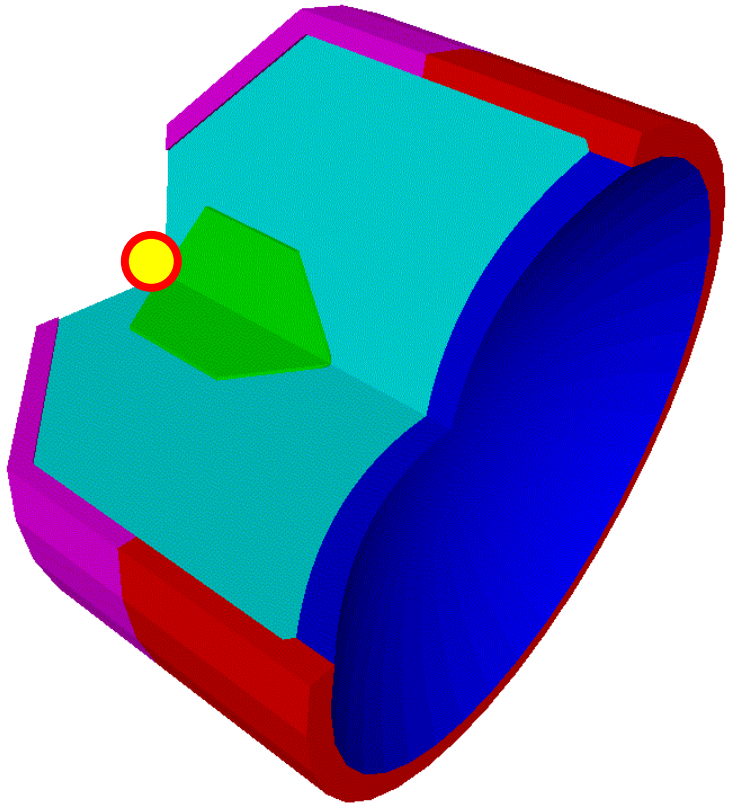
t :	time
x_i :	position
v_i :	velocity
ρ :	local density
σ_{ij} :	stress tensor
f_i :	external force density
w_{int} :	specific internal energy
s :	heat sources
q_i :	heat flux

Copyright Diehl BGT Defence GmbH & Co. KG

DIEHL
BGT Defence

EFP Mode

- Initiation point in front of DWS

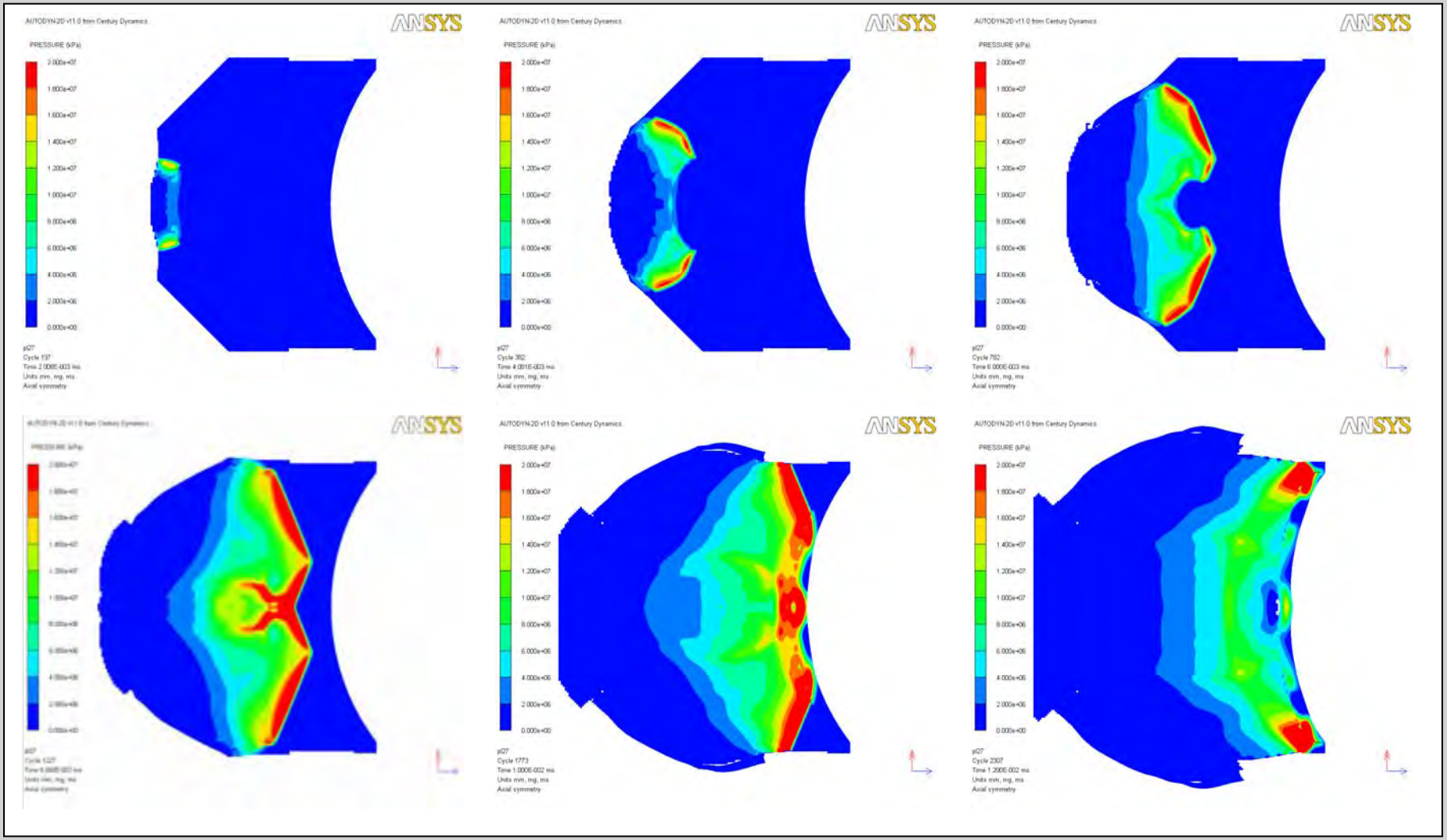


Copyright Diehl BGT Defence GmbH & Co. KG

Initiation Controlled Multimode Warheads

DIEHL
BGT Defence

EFP Mode

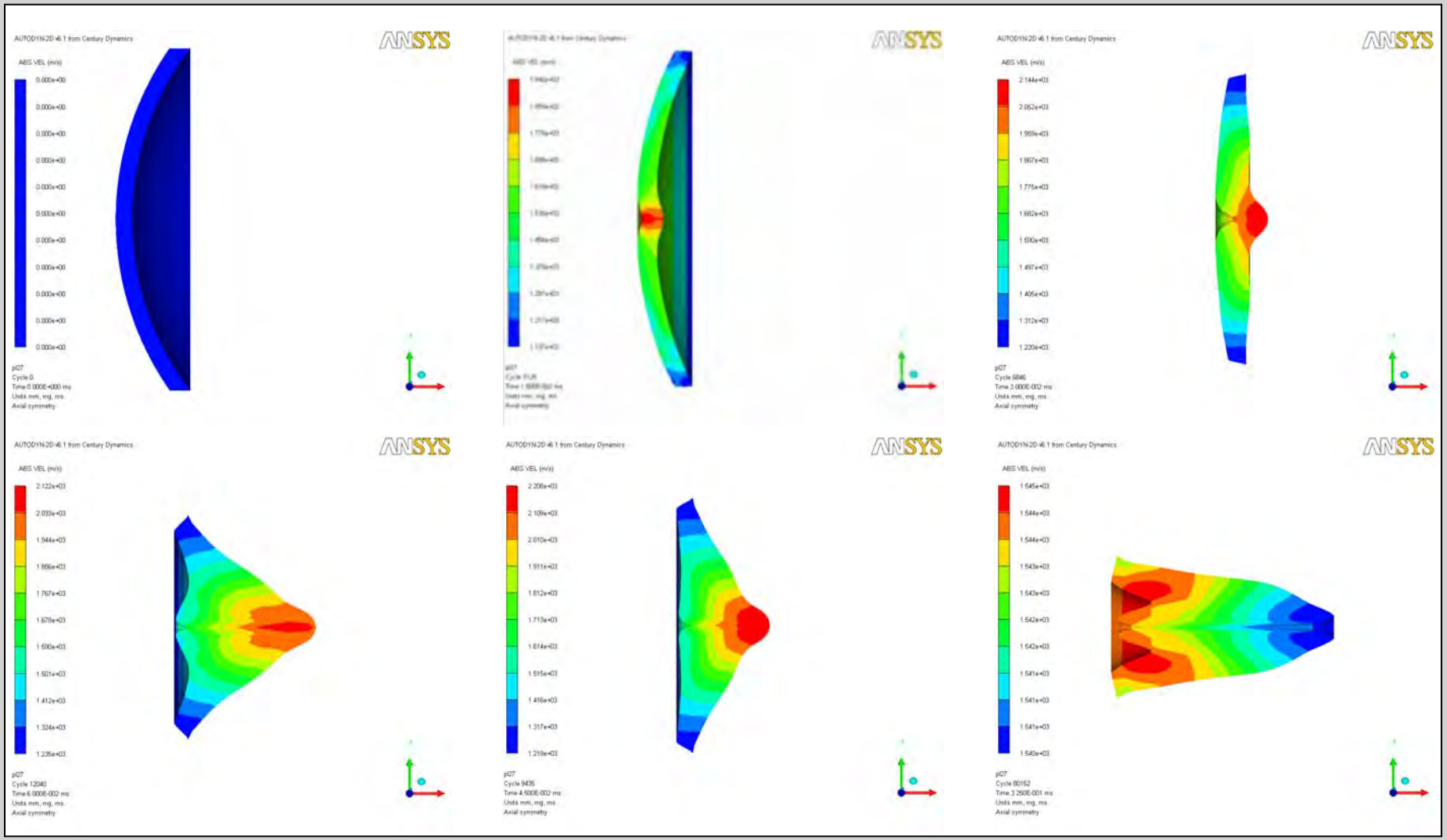


Copyright Diehl BGT Defence GmbH & Co. KG

Initiation Controlled Multimode Warheads

DIEHL
BGT Defence

EFP Mode

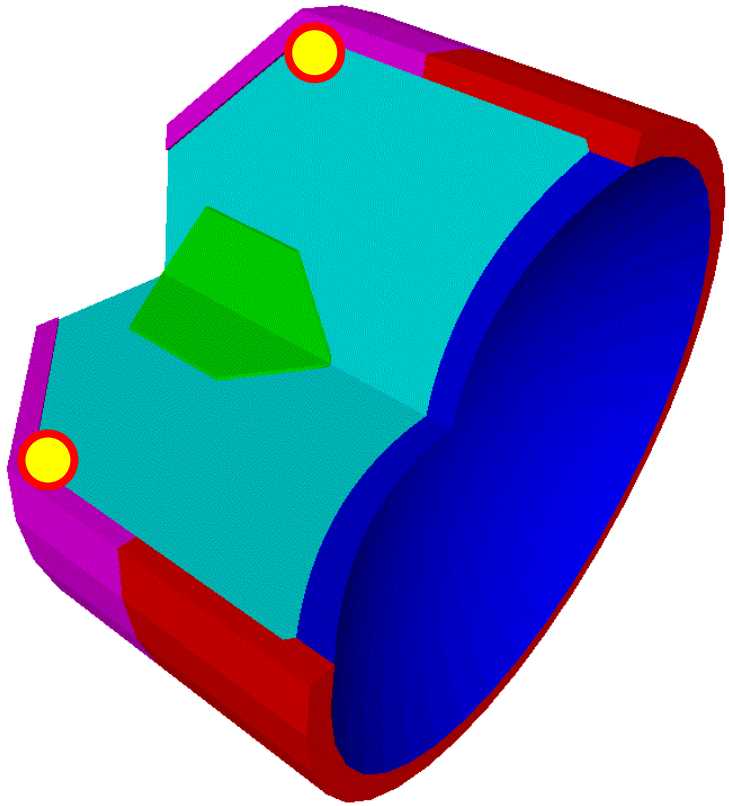


Copyright Diehl BGT Defence GmbH & Co. KG

DIEHL
BGT Defence

Jetting (SC) Mode

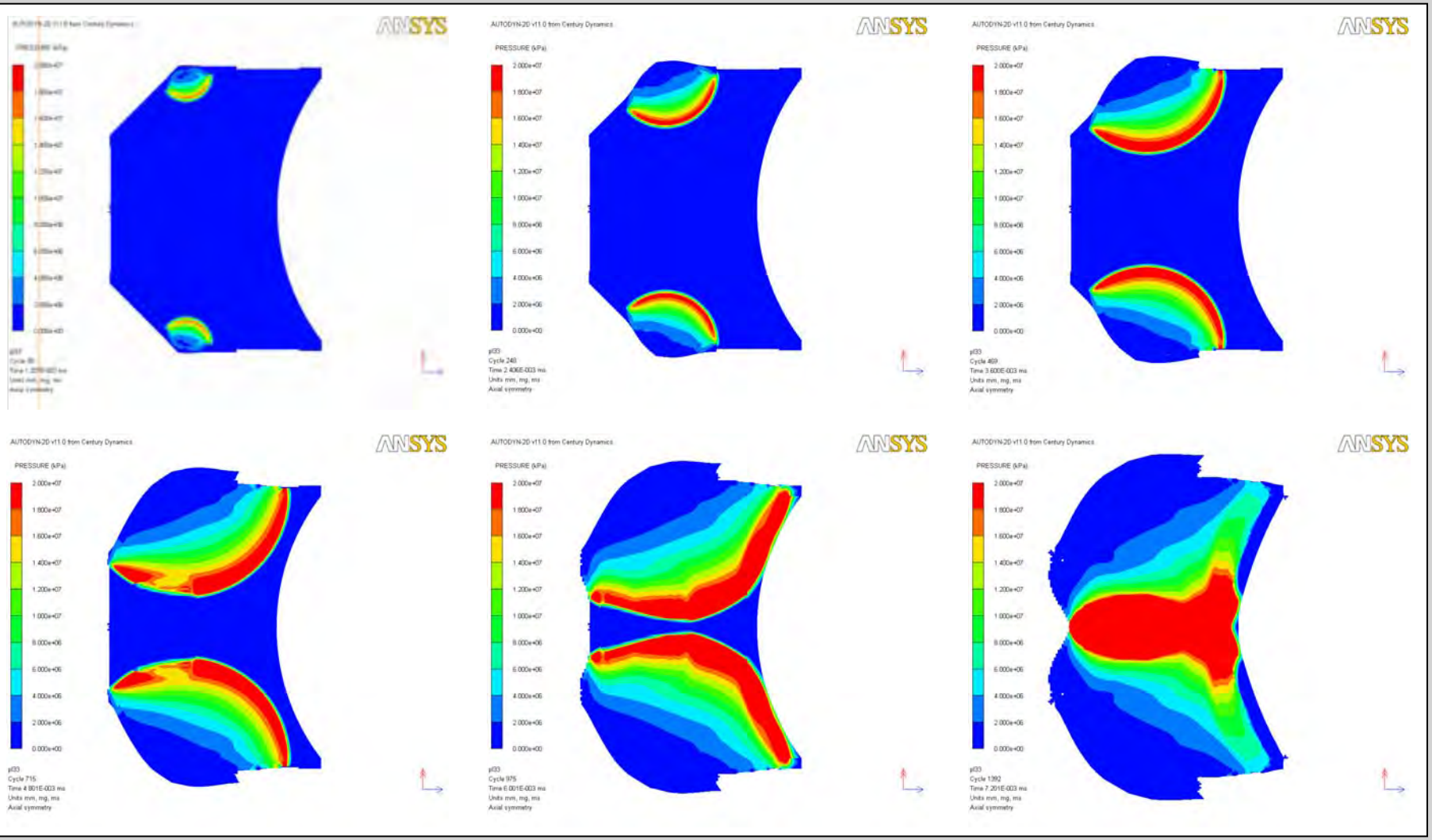
- Multiple initiation points around circumference of warhead case



Copyright Diehl BGT Defence GmbH & Co. KG

DIEHL
BGT Defence

Jetting (SC) Mode

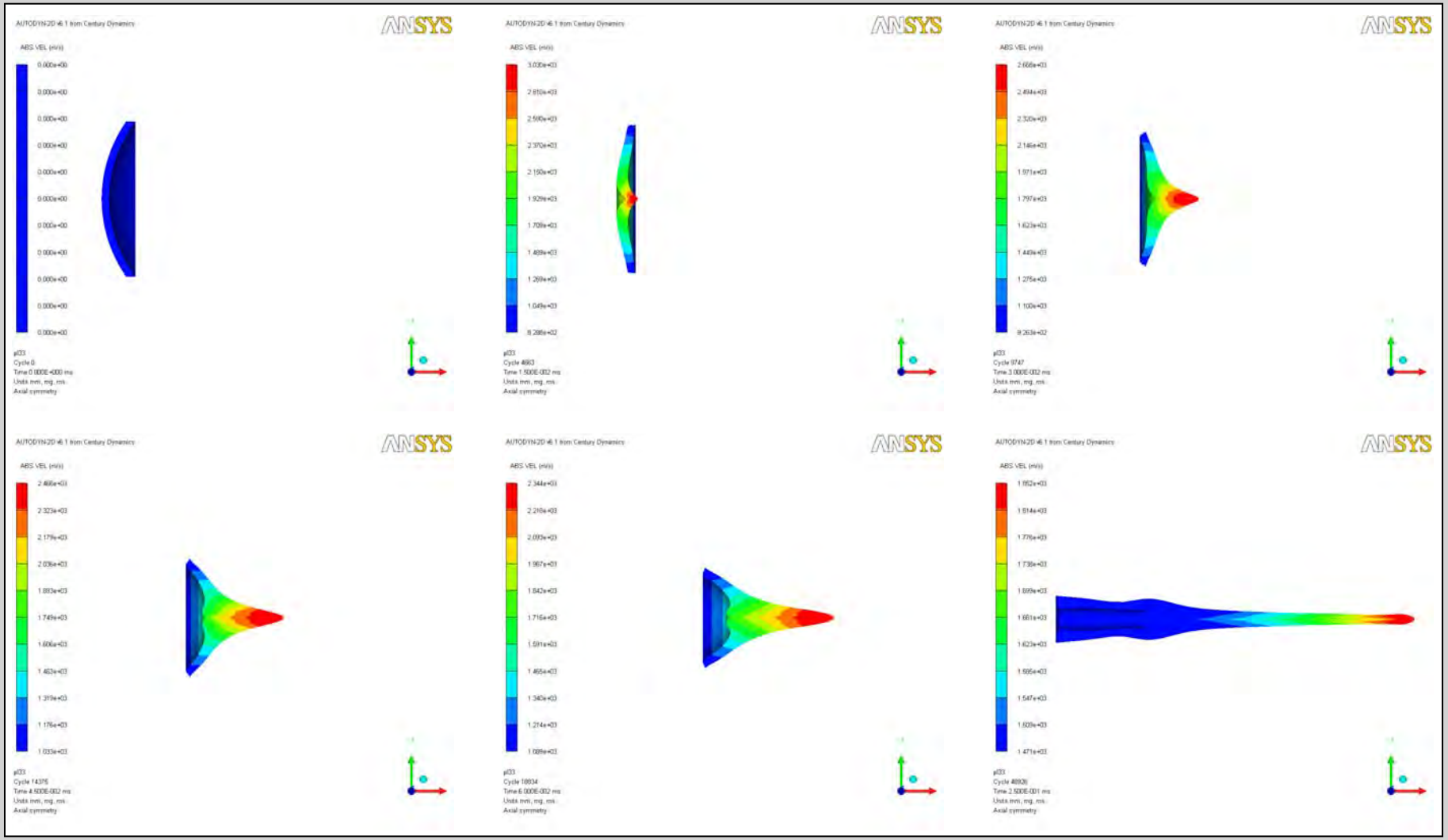


Copyright Diehl BGT Defence GmbH & Co. KG

Initiation Controlled Multimode Warheads

DIEHL
BGT Defence

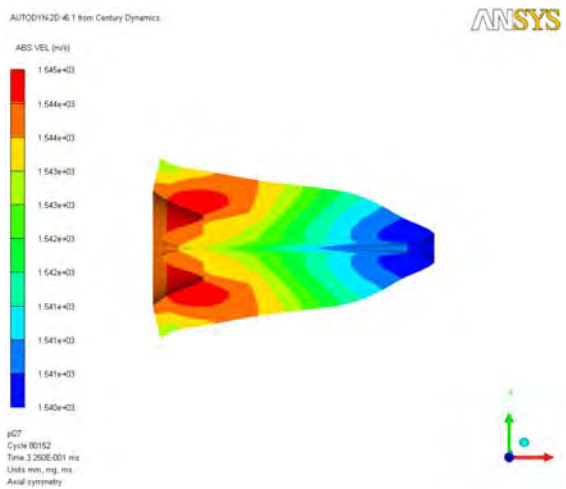
Jetting (SC) Mode



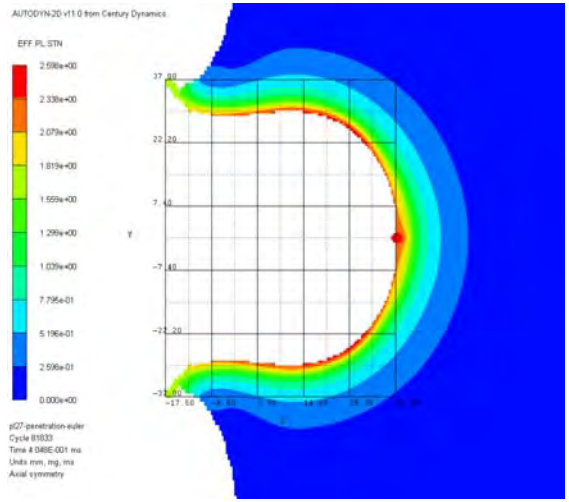
Copyright Diehl BGT Defence GmbH & Co. KG

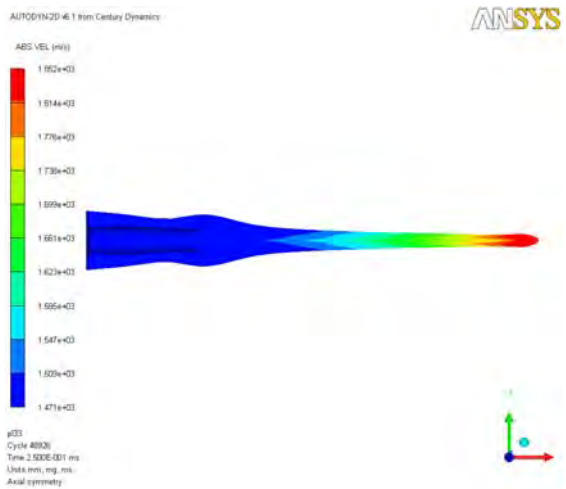
DIEHL
BGT Defence

Comparison of EFP and SC Modes

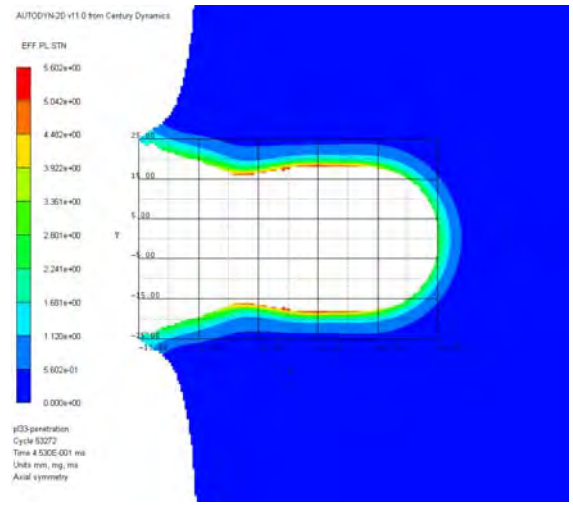


v = 1540 m/s
L/D = 1.6
P_{Steel} = 0.4 CD





v = 1850-1470 m/s
L/D = 7.6 (t=250µs)
P_{Steel} = 0.7 CD

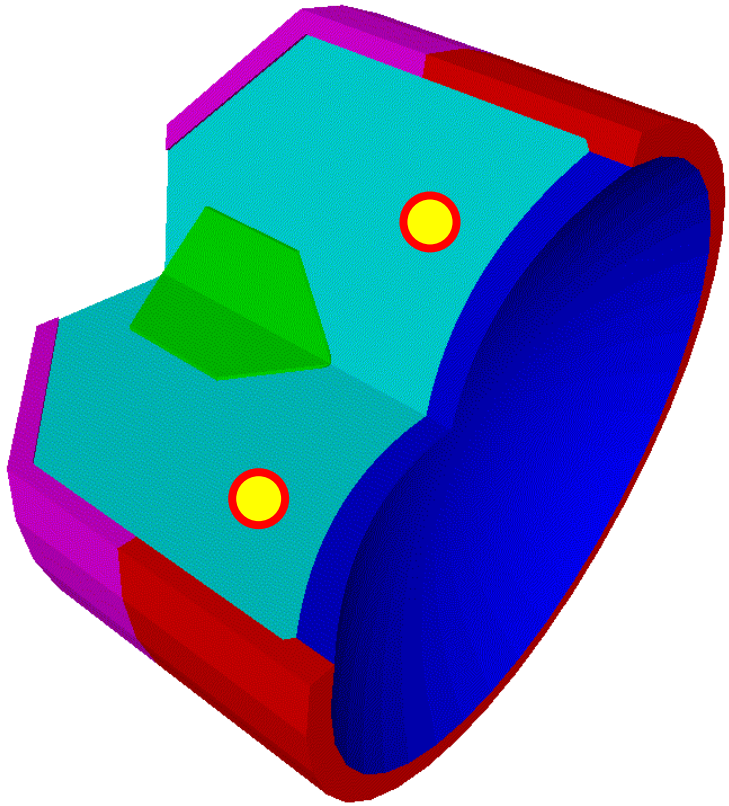


Copyright Diehl BGT Defence GmbH & Co. KG

DIEHL
BGT Defence

Fragmentation Mode

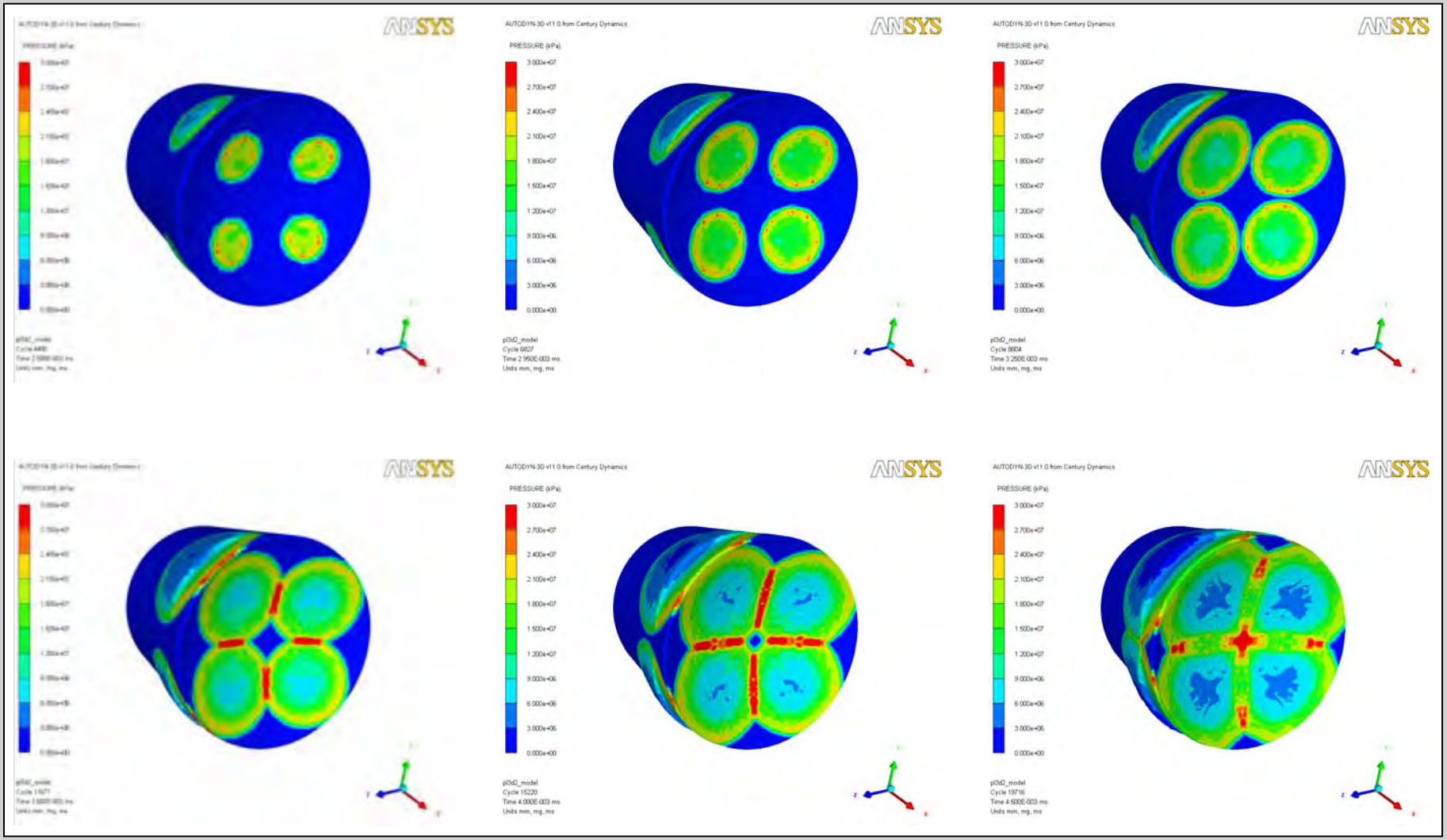
- Few initiation points in front of liner



Copyright Diehl BGT Defence GmbH & Co. KG

DIEHL
BGT Defence

Fragmentation Mode with 4 Initiation Points

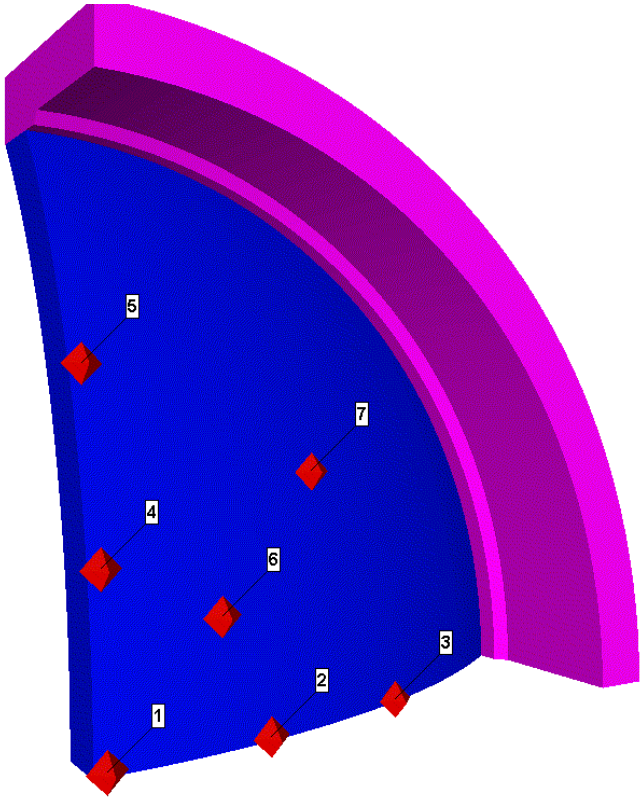


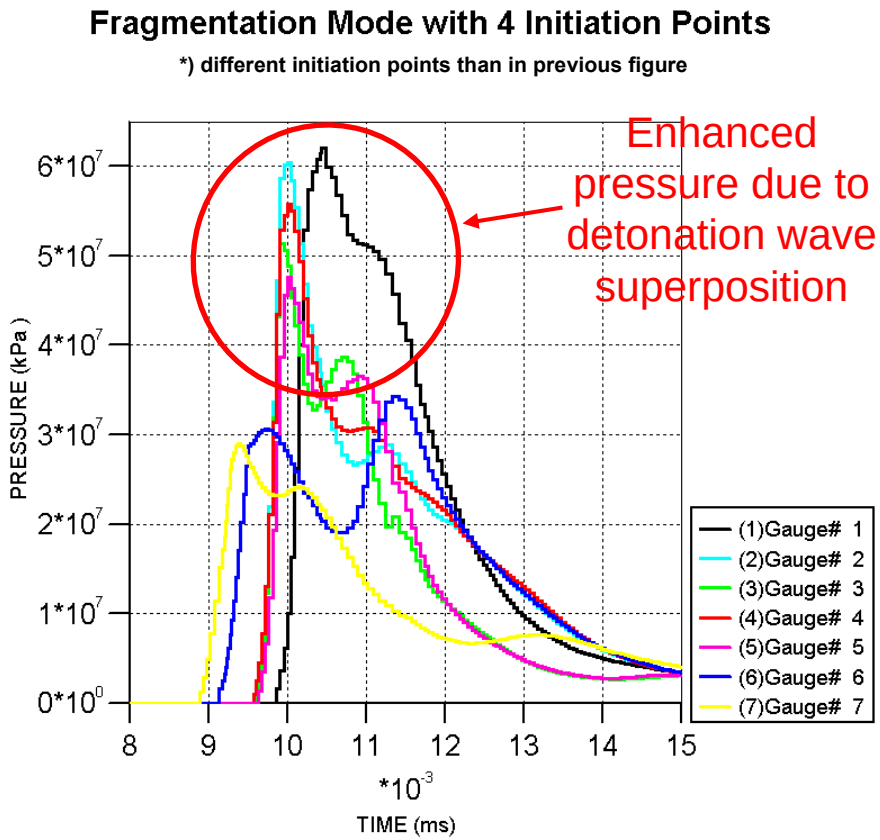
Copyright Diehl BGT Defence GmbH & Co. KG

DIEHL
BGT Defence

Fragmentation Mode

- Fragmentation of liner due to detonation wave superposition
  - Superposition of detonation waves lead to high local impulse densities
    → local failure of liner material



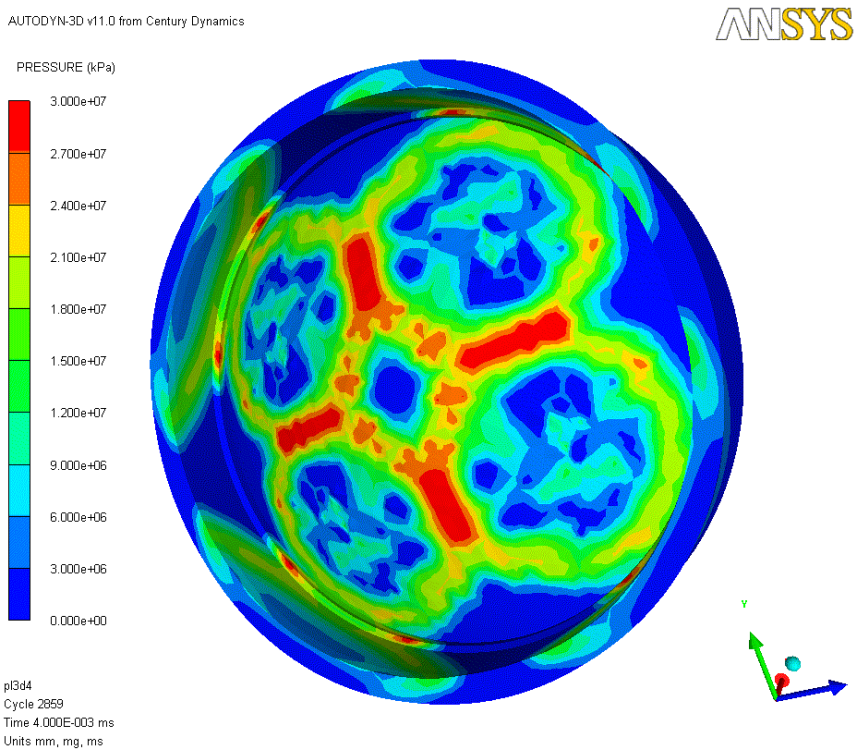


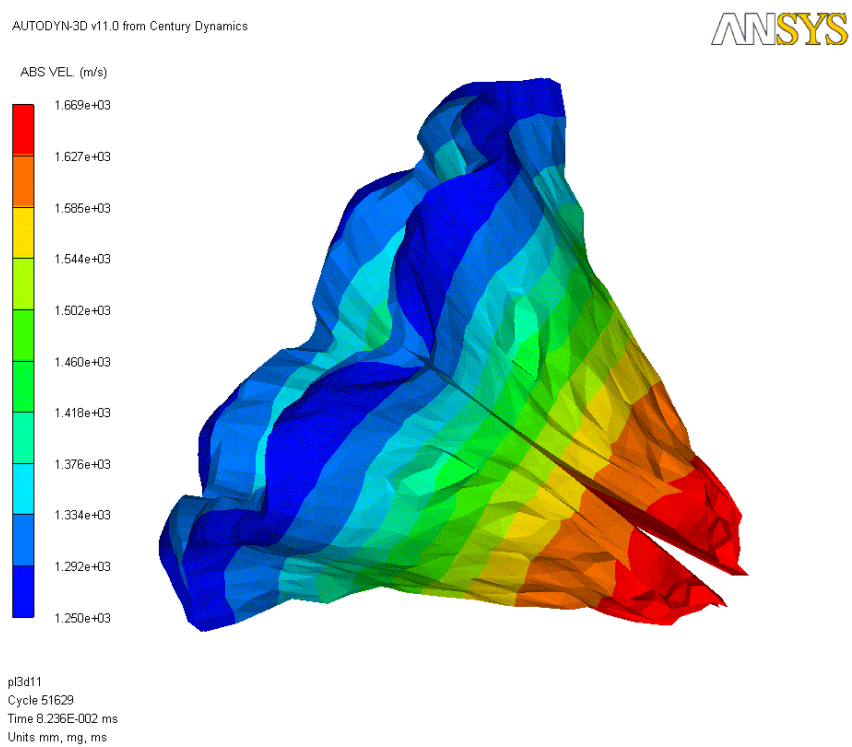
Copyright Diehl BGT Defence GmbH & Co. KG

DIEHL
BGT Defence

Fragmentation Mode

- Formation of liner fragments





Copyright Diehl BGT Defence GmbH & Co. KG

DIEHL
BGT Defence

Limits of Initiation Controlled Multimode Warheads

- Optimum performance only for original warhead mode, i.e.
  - EFP mode for EFP based multimode warhead
  - SC mode for SC based multimode warhead
- EFP basis
  - Thick liner → low collapse velocity → no high velocity SC jet
- SC basis
  - Low liner mass, small opening angle → no EFP
  - Low liner mass → only low mass fragments

Copyright Diehl BGT Defence GmbH & Co. KG

DIEHL
BGT Defence

Summary

- Operating modes of initiation controlled multimode warhead demonstrated by simulation
- EFP charge with multiple initiation points
  - EFP mode: Single initiation point in front of DWL
    - Aerodynamically stable projectile → hard target defeat at long standoffs
  - Jetting (SC) mode: multipoint initiation along warhead circumference
    - Stretched projectile → enhanced penetration performance at small standoffs
  - Fragmentation mode: few initiation points in front of liner
    - Fragments → defeat of semi-hard and soft targets at medium standoffs
- Functionality of EFP and Jetting (SC) mode verified by experimental tests
- Fragmentation mode under current experimental investigation

Copyright Diehl BGT Defence GmbH & Co. KG

DIEHL
BGT Defence

Contact

Dr. Thomas Falter

Diehl BGT Defence GmbH & Co. KG

Phone: +49-(0)911-957-2522

Email: Thomas.Falter@diehl-bgt-defence.de

Copyright Diehl BGT Defence GmbH & Co. KG

PDF Complete
Your complimentary use period has ended. Thank you for using PDF Complete.
Click Here to upgrade to Unlimited Pages and Expanded Features

A Computational Study of the Energy Dissipation Through an Acrylic Target Impacted by Various Size FSP

C. G. Fountzoulas, P. G. Dehmer, J. M. Sands, and J. H. Yu
U.S. Army Research Laboratory
Aberdeen Proving Ground, MD 21005-5069
cfount@arl.army.mil, pdehmer@arl.army.mil, jsands@arl.army.mil, jian.h.yu@arl.army.mil

PDF Complete
Your complimentary use period has ended. Thank you for using PDF Complete.
Click Here to upgrade to Unlimited Pages and Expanded Features

OUTLINE

- *Objective*
- *Background*
- *Experimental Details*
- *Numerical Simulations*
- *Regression Analysis*
- *Summary*
- *Future Plans*

Knowledge of the energy absorption by an impacted material is a necessary requirement for the successful design of an armor

PDF Complete
Your complimentary use period has ended. Thank you for using PDF Complete.
Click Here to upgrade to Unlimited Pages and Expanded Features

Objective

- To study the energy dissipation through acrylic targets of varying thickness and architecture impacted by various size Fragmented Simulated Projectiles (FSPs)
- To produce analytical expressions of the velocity profiles by using regression analysis tools in an effort
  - to produce a general equation of energy absorption of a projectile through a PMMA target

PDF Complete
Your complimentary use period has ended. Thank you for using PDF Complete.
Click Here to upgrade to Unlimited Pages and Expanded Features

et Penetration Factors

- According to M . L. Wilkins et al* ñThe important projectile parameters for target penetration are geometry, material strength, density, and velocity.
  - Geometry refers to the sharp point used in the design of armor piercing projectiles.
  - Material strength is the parameter that permits the projectile to maintain the designed armor-piercing shape during the penetration process.
  - The projectile material strength is important until a target that is stronger than the projectile is encountered.
    - Then, the penetration process is governed by the projectile mass and velocity.
      - For example, ball and armor piercing, and projectiles with the same mass have about the same ballistic limit for ceramic targets strong enough to destroy the tip of the armor piercing projectile.ò

*M: L. Wilkins, R. L. Lamdingham, C. **A.** Honodel, Fifth Progress Report of Light Armor Program, UCRL-50980, University of California, Liveromore.

PDF Complete
Your complimentary use period has ended. Thank you for using PDF Complete.
Click Here to upgrade to Unlimited Pages and Expanded Features

Background

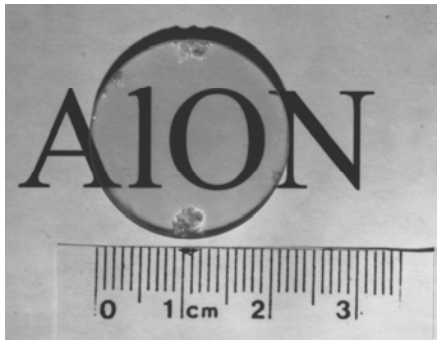
- Commercially available transparent armor systems are used in a variety of military and civilian applications including
  - face shields, goggles, vehicle vision blocks, windshields and windows, blast shields, and aircraft canopies
- High performance transparent armor systems typically consist of several different materials, such as
  - PMMA, float or soda lime glass, sapphire, ALON, spinel, and polycarbonate bonded together with a rubbery interlayer such as polyurethane (PU) or polyvinylbutyral (PVB),
- The lamination sequence, material thicknesses and bonding between layers has been shown to drastically affect system performance and it has been observed that each material serves an important function.

PDF Complete
Your complimentary use period has ended. Thank you for using PDF Complete.
Click Here to upgrade to Unlimited Pages and Expanded Features

sparent Armor Design



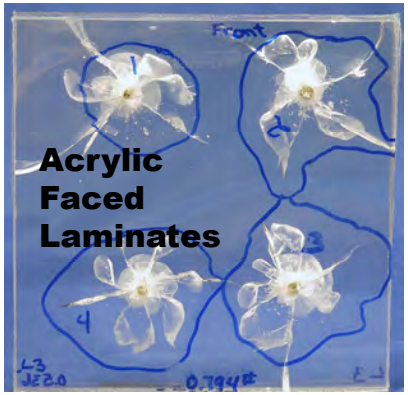
0.12”(3 mm) thick
85.2 % transmittance



4” (10.2 cm) diam. x 0.44" (1.1 cm) thick spinel

Ceramic or glass

Interlayer between polycarbonate



Polymer backing

THREAT

Interlayer





PDF Complete
Your complimentary use period has ended. Thank you for using PDF Complete.
Click Here to upgrade to Unlimited Pages and Expanded Features

Modeling Efforts

- Numerical simulations coupled with experiments provide a more cost-effective way of studying the ballistic performance of monolithic and laminated transparent armor systems
- Accurately simulating polymeric transparent armor material over a range of strain rates has proven challenging
  - Nandlall and Livingstone established that by adjusting the element erosion strain, the constitutive model was capable of accurately simulating the experimental ballistic limits
- Recent development of constitutive equations combining nonlinear viscoelasticity and viscoplasticity capture most of the time-dependent, nonlinear response observed for glassy polymers

PDF Complete
Your complimentary use period has ended. Thank you for using PDF Complete.
Click Here to upgrade to Unlimited Pages and Expanded Features

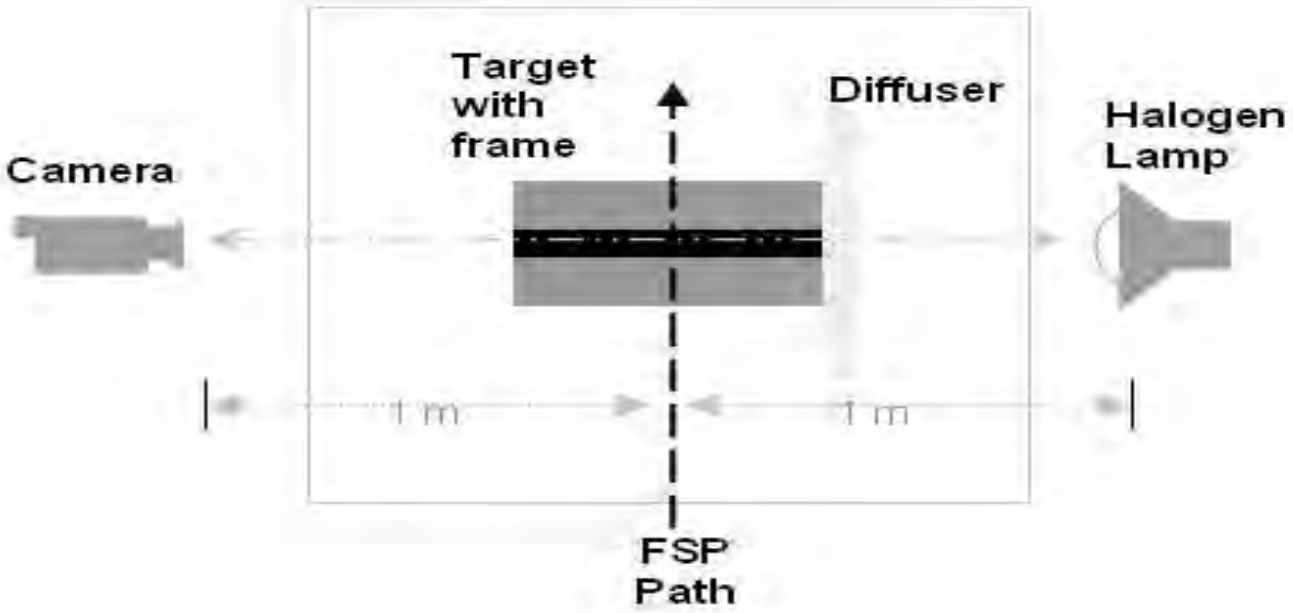
xperimental Details

- Ballistic measurements were carried out at the Experimental Facility of Aberdeen Proving Ground, MD, using a 17-gr (1.1-g weight) .22-cal FSP, and a 5.85-gr (0.37 g weight) .15-cal FSP
- The cross-section area of all the acrylic targets was 152.4-mm x 152.4-mm. The target architecture was
  - Monolithic targets of thickness 11.82-mm and 5.92-mm
    - They were impacted by .22-cal and .15-cal FSP respectively
  - A third target, which was consisted of two 5.92-mm thick plates of acrylic without any adhesive between them-total thickness of the set 11.84-mm-
    - It was impacted by a .22-cal FSP.
- All targets were sandwiched in a transparent frame
- All shots were conducted with the target normal to the projectile line of flight, i.e., 0° obliquity.

PDF Complete
Your complimentary use period has ended. Thank you for using PDF Complete.
Click Here to upgrade to Unlimited Pages and Expanded Features

rimental Details-cont.

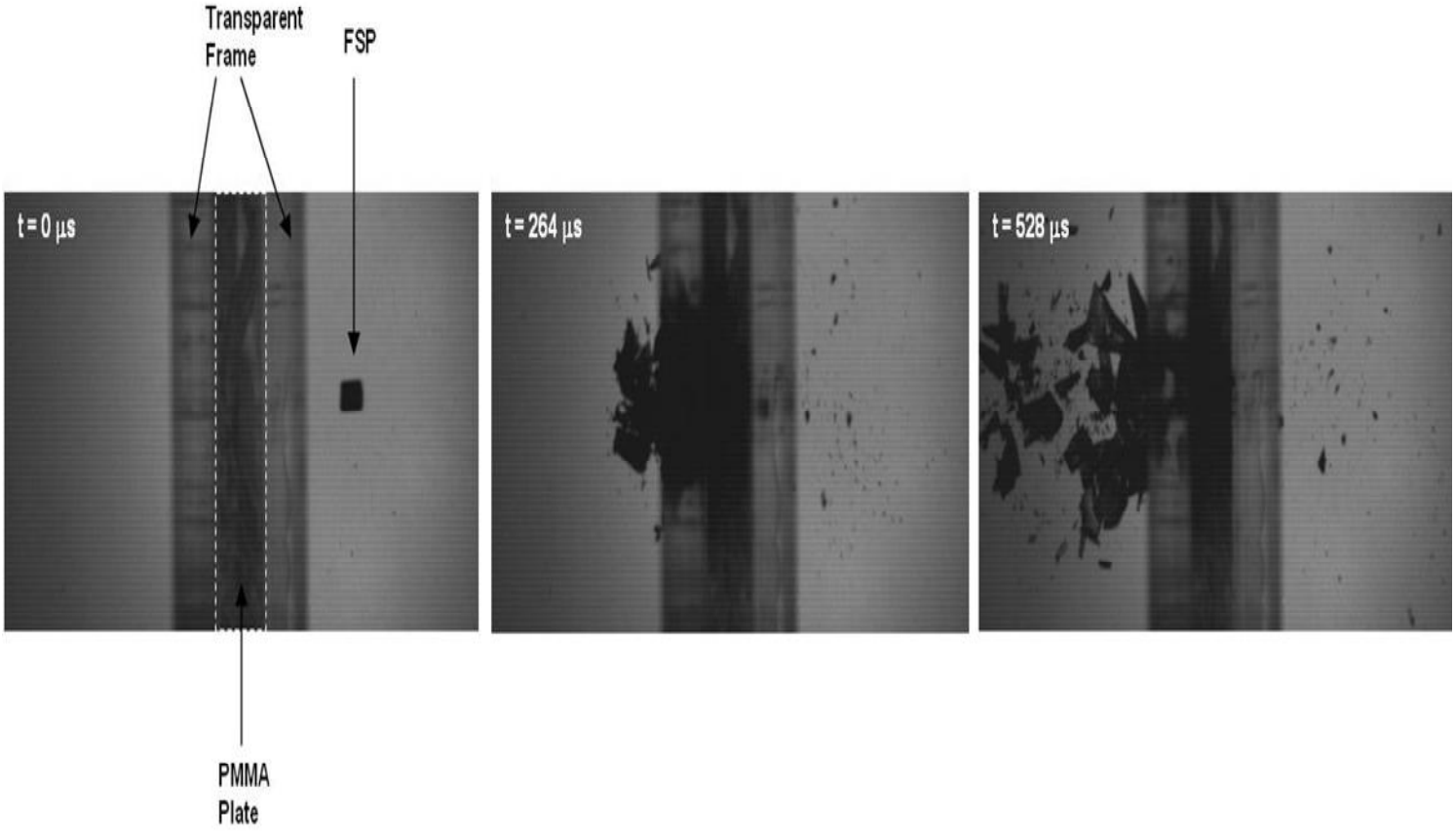
- The impact on the PMMA target was recorded by a Phantom v7, Vision Research, high-speed camera aiming at 90º to the path of the FSP.
- The targeting area was illuminated by backlighting using a high intensity halogen lamp and a diffuser was used to spread out the light intensity.



High-speed camera setup

PDF Complete
Your complimentary use period has ended. Thank you for using PDF Complete.
Click Here to upgrade to Unlimited Pages and Expanded Features

Impact Penetration through a PMMA Plate



PDF Complete
Your complimentary use period has ended. Thank you for using PDF Complete.
Click Here to upgrade to Unlimited Pages and Expanded Features

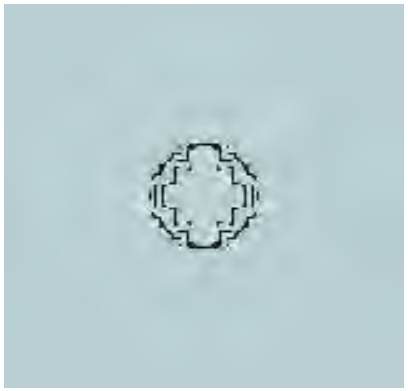
merical Simulations

- The numerical modeling was carried out by using the nonlinear analysis commercial software ANSYS/AUTODYN using
  - 3D axisymmetric models and smooth particle hydrodynamics (SPH) solver
  - The particle size used for SPH solver was 0.5-mm
- The dimensions of the model were equal to the dimensions of the actual size target
- Results were obtained by simulating projectiles impacting the targets at the experimental V50 velocities of
  - 350 m/s for the 11.84-mm thick targets and
  - 210 m/s for the 5.92-mm thick target, respectively.

PDF Complete
Your complimentary use period has ended. Thank you for using PDF Complete.
Click Here to upgrade to Unlimited Pages and Expanded Features

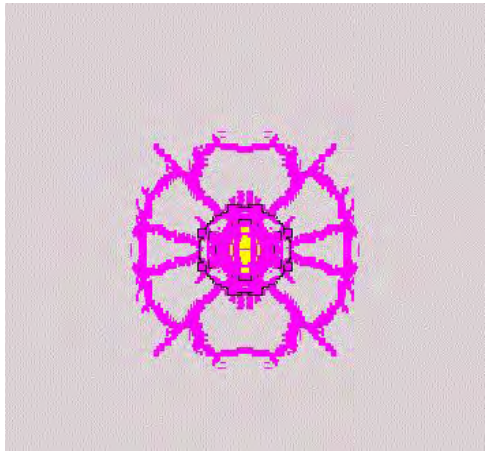
rial Models and Simulation Validation

- **Steel** was modeled using
  - ï shock EOS
  - ï JC strength model.
- **PMMA** was modeled using
  - ï shock EOS
  - ï von Mises strength model
  - ï principle stress failure criterion with crack softening criterion
    - PMMA Material Model in the Autodyn Library has No Strength and No Failure Criterion.



Simulated Impact before material models modification, .22-cal FSP @350m/s





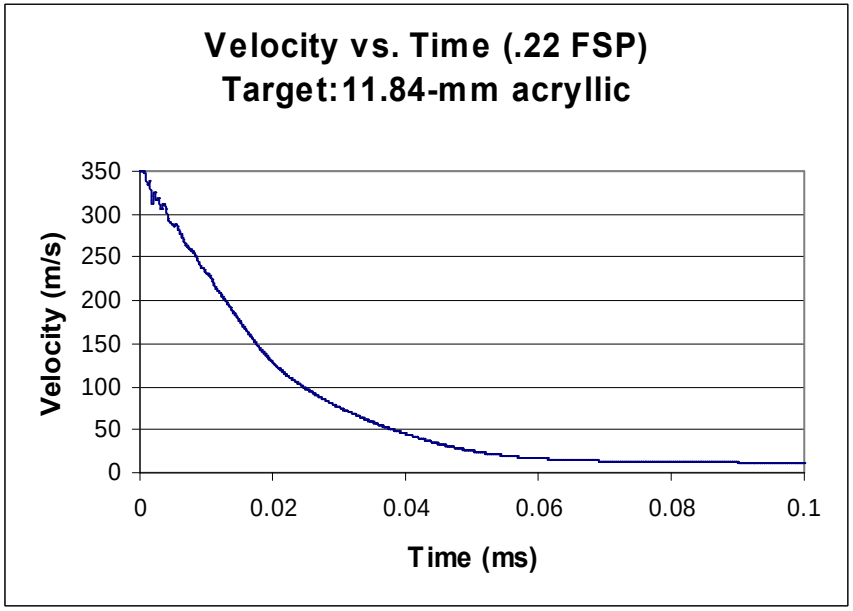
Actual impact **Simulated impact**

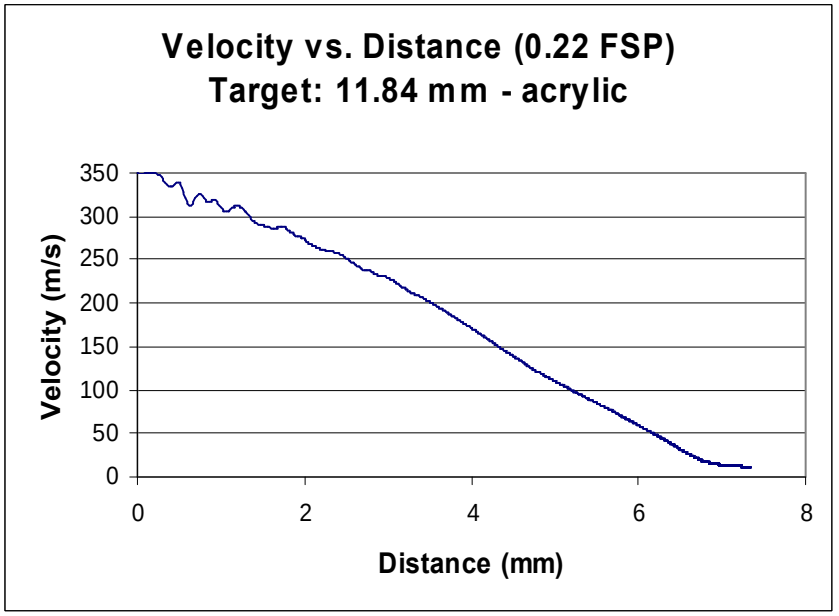
Actual and simulated target were impacted by .22-cal FSP @ 350 m/s

PDF Complete
Your complimentary use period has ended. Thank you for using PDF Complete.
Click Here to upgrade to Unlimited Pages and Expanded Features

Simulation Results

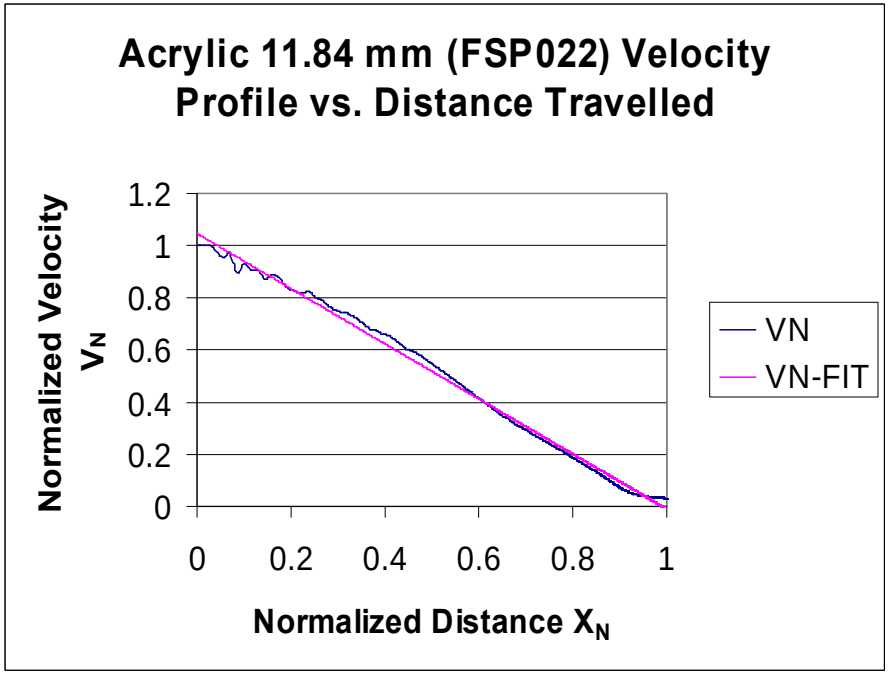
- All simulated exit velocities were within a few meters from the experimental exit velocities
- The analytical expression of the velocity profiles of all impacts was determined by using the LINEST statistical function of the Microsoft Excel

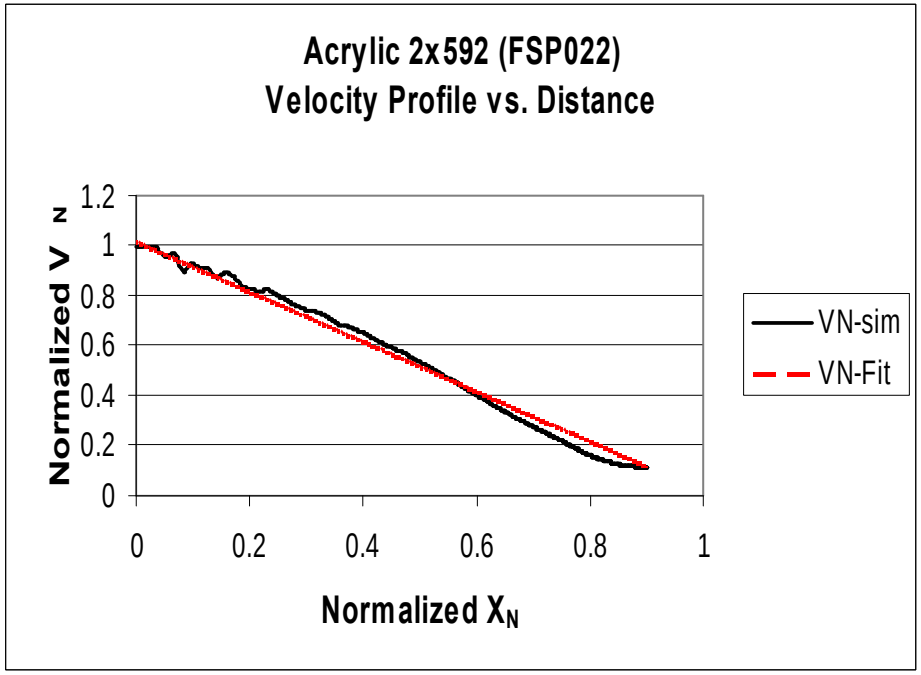




PDF Complete
Your complimentary use period has ended. Thank you for using PDF Complete.
Click Here to upgrade to Unlimited Pages and Expanded Features

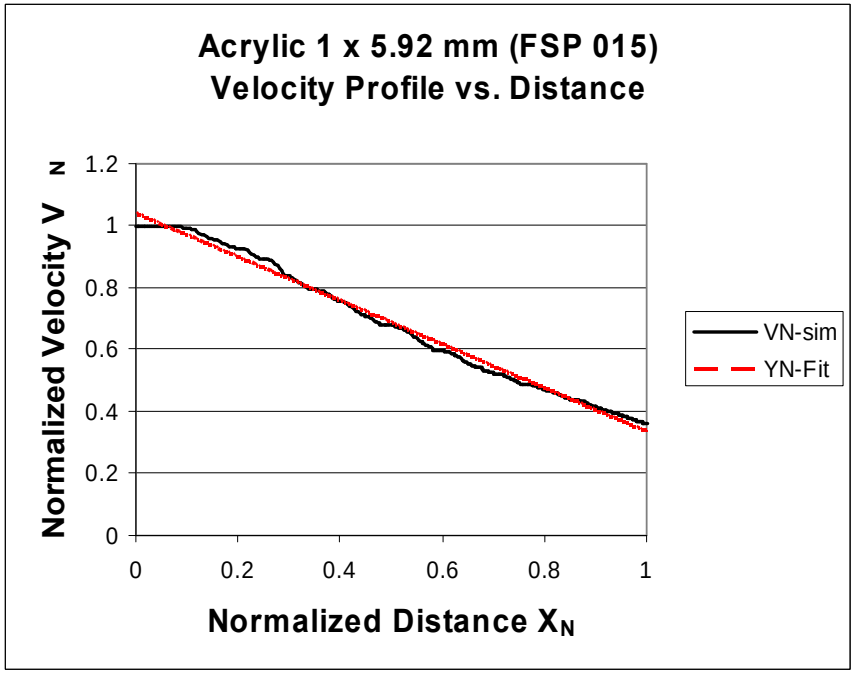
egression Analysis

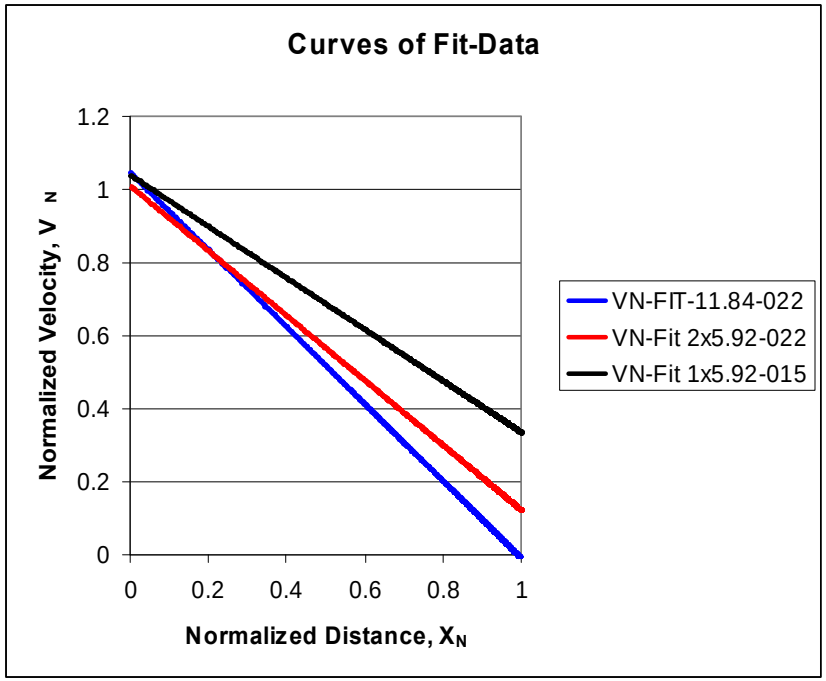




PDF Complete
Your complimentary use period has ended. Thank you for using PDF Complete.
Click Here to upgrade to Unlimited Pages and Expanded Features

egression Analysis





PDF Complete
Your complimentary use period has ended. Thank you for using PDF Complete.
Click Here to upgrade to Unlimited Pages and Expanded Features

TIONS OF THE BEST-FIT CURVE F ALL SIMULATED IMPACTS

Target	Projectile	Velocity	Equation
1x11.84-mm	.22-cal FSP	350 m/s	$V/V_{MAX} = 1.046 - 1.056X_N$
2x5.92-mm (Laminated)	.22-cal FSP	350 m/s	$V/V_{MAX} = 1.010 - 0.888X_N$
1x5.92-mm	.15-cal FSP	210 m/s	$V/V_{MAX} = 1.039 - 0.7045X_N$

V = Instantaneous Projectile Velocity

V_{MAX} = Initial Impact Velocity

PDF Complete
Your complimentary use period has ended. Thank you for using PDF Complete.
Click Here to upgrade to Unlimited Pages and Expanded Features

CONCLUSIONS

- The current paper has demonstrated the powerful use of computational modeling to produce analytical expressions for the prediction of the energy absorption by an acrylic target, which is impacted by various size FSPs.
- The results of the current study verified, the already known experimentally, that the resistance of an acrylic target to impact by FSP projectiles is affected by the
  - Size of the FSP
  - Impact velocity
  - Target architecture.
- The experimental cracking pattern and the exit velocity of 0.22-cal and 0.15-cal FSPs through monolithic and laminated without intermediate adhesive layer PMMA targets were successfully substantiated by our modified existing strength and failure models of PMMA
  - The PMMA material model was modified by introducing a von-Mises strength model
  - a principal tensile strength criterion using published parameters

PDF Complete
Your complimentary use period has ended. Thank you for using PDF Complete.
Click Here to upgrade to Unlimited Pages and Expanded Features

Conclusions

- The equations of the velocity profiles of the various cal FSPs traveling through the PMMA target were produced by regression analysis of the simulated velocity profile using the existing Microsoft Excel software

- An effort was made to produce an energy loss equation which is not only a mathematical expression, i.e. polynomial equation, but to be related to the physical parameters of the impact, such as impact velocity

- The **ideal equation** of the energy absorption profile is expected to be

$$(V/V_{MAX})^2 = [1 - (slope)*(X/X_{MAX})]^2$$

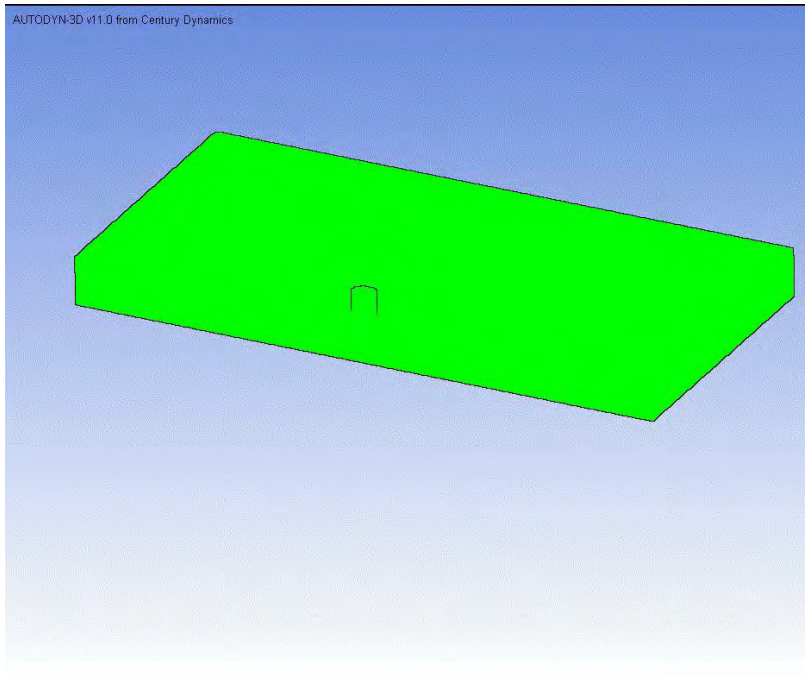
Where: V is the projectile instantaneous velocity and X distance travelled by the projectile within the PMMA target

- Future studies will attempt to
  - Connect the slope of the equation to the FSP mass and target architecture
  - Improve the prediction of the failure of the PMMA by simulation for various loading rates of PMMA and laminate geometries
  - Produce analytical energy absorption expression for a laminate target with more PMMA layers with and without adhesive layer between them.

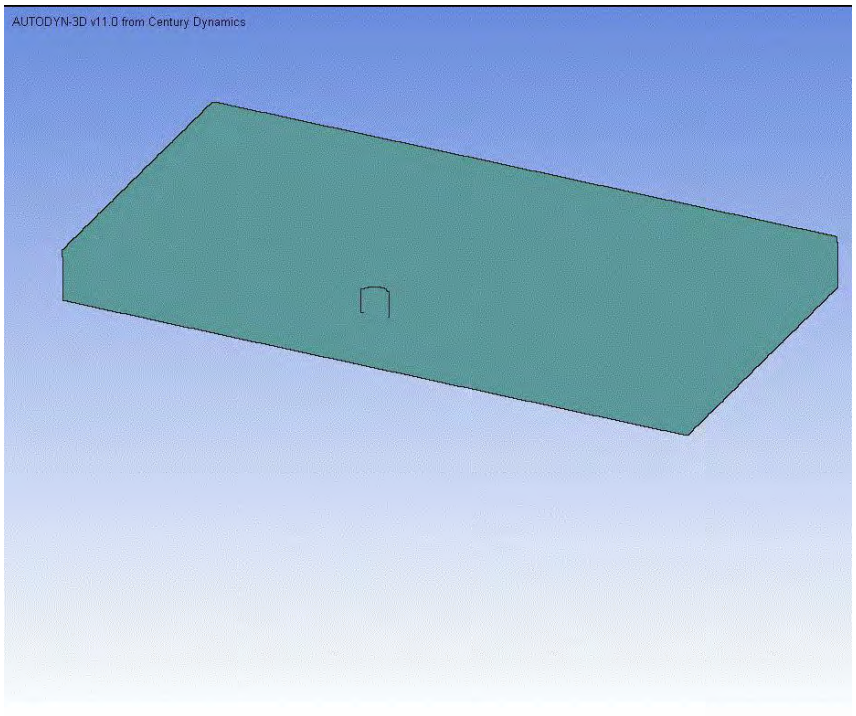
PDF Complete
Your complimentary use period has ended. Thank you for using PDF Complete.
Click Here to upgrade to Unlimited Pages and Expanded Features

MOVIES

1 X 11.84-mm PMMA



2 X 5.92-mm PMMA



Range Extension of Gun-Launched Smart Munitions

TECHNOLOGY DRIVEN. WARFIGHTER FOCUSED.

Dr. Frank Fresconi

Army Research Laboratory

23 September 2008

Introduction

Motivation

- Extending the range of gun-launched smart munitions enables larger area of influence, more timely fires, enhanced effectiveness, and improved urban operations.

Goal

- Identify the critical technical drivers for extended range of precision munitions

Approach

- 105-mm fin-stabilized projectile with rocket motor and general control mechanism studied in six degree-of-freedom simulation
- Guidance, navigation, and control (GNC) techniques
- Optimization of quadrant elevation, ignition time of rocket motor, start time of glide actuation
- Trade-offs in aerodynamic/control mechanism strategies

Configuration of Candidate Projectile

- 105-mm fin-stabilized projectile

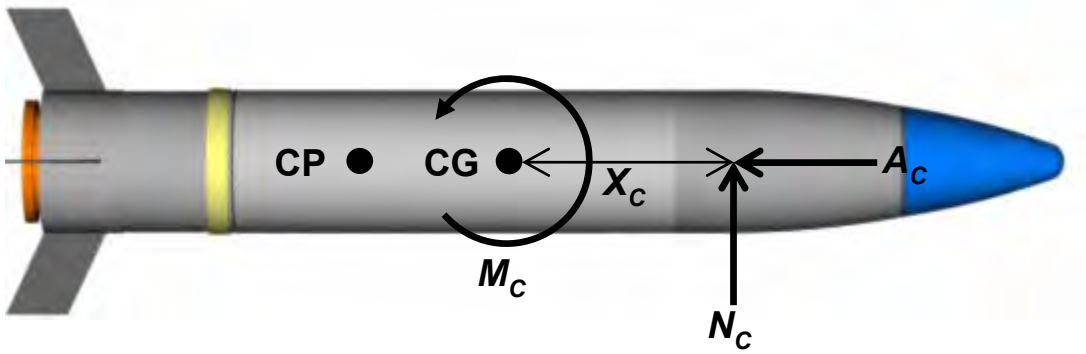
Mass (kg)	Axial Inertia ($kg\text{-}m^2$)	Transverse Inertia ($kg\text{-}m^2$)	Center of Gravity From Nose (mm)	Diameter (mm)	Overall Length (mm)
18.40	0.03199	0.5607	422.7	104.7	762.0

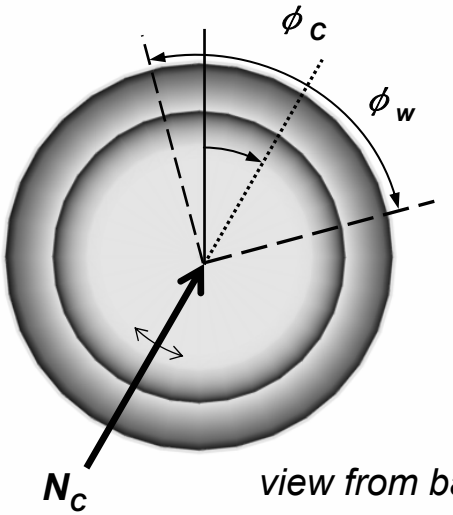
- Generalized control mechanism
- Solid grain rocket motor
  - 3.6 sec burn time
  - 491.8 N thrust
  - Variable ignition time



Modeling of Control Mechanism

- Control mechanism (canards, thrusters, etc.) modeled as axial control force (A_C), normal control force (N_C) with control moment arm (X_C), producing control moment (M_C).
- Maneuver direction of given control mechanism prescribed by commanded roll orientation (ϕ_C) and duration of roll cycle (ϕ_W).





Parameters and Metrics

- Fire control (max charge)
  - quadrant elevation (QE)
  - rocket ignition time (T_R)
  - glide start time (T_G)
- Projectile configuration
  - control normal force
  - control normal-to-axial force ratio
  - control axial location
  - static margin
  - roll window
- Metrics
  - extended range
  - total angle of attack (α_T)

GNC for Maximum Range

- Common sense: control normal force direction (ϕ_c) should be opposite gravity to maximize range.
- Problem: Projectile drift (interaction of gravity, spin, and pitching moment) can significantly bend the trajectory in the crossrange direction and reduce range.
- Solution: develop flight control system to maximize range while minimizing drift.

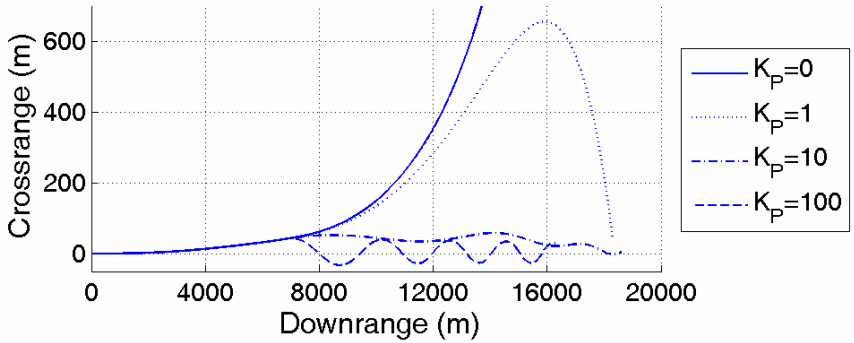
Flight Control Law for Maximum Range

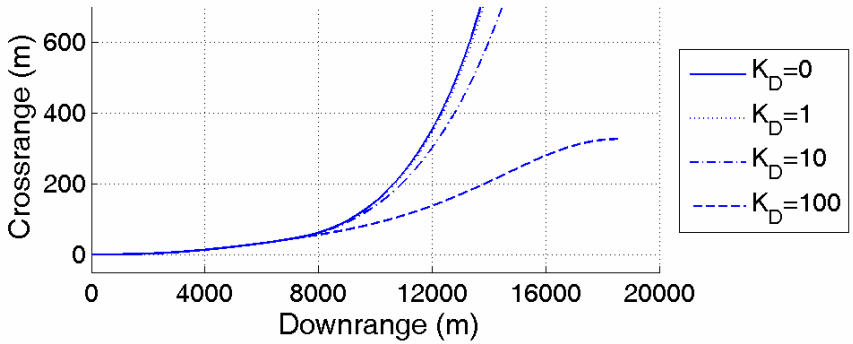
$$\varphi_C = \arctan\left(\frac{K_P e_y + K_D \dot{e}_y}{e_z}\right)$$

$$e_y = y_p - y_t \qquad \dot{e}_y = \dot{y}_p - \dot{y}_t \qquad e_z = z_p - z_t$$

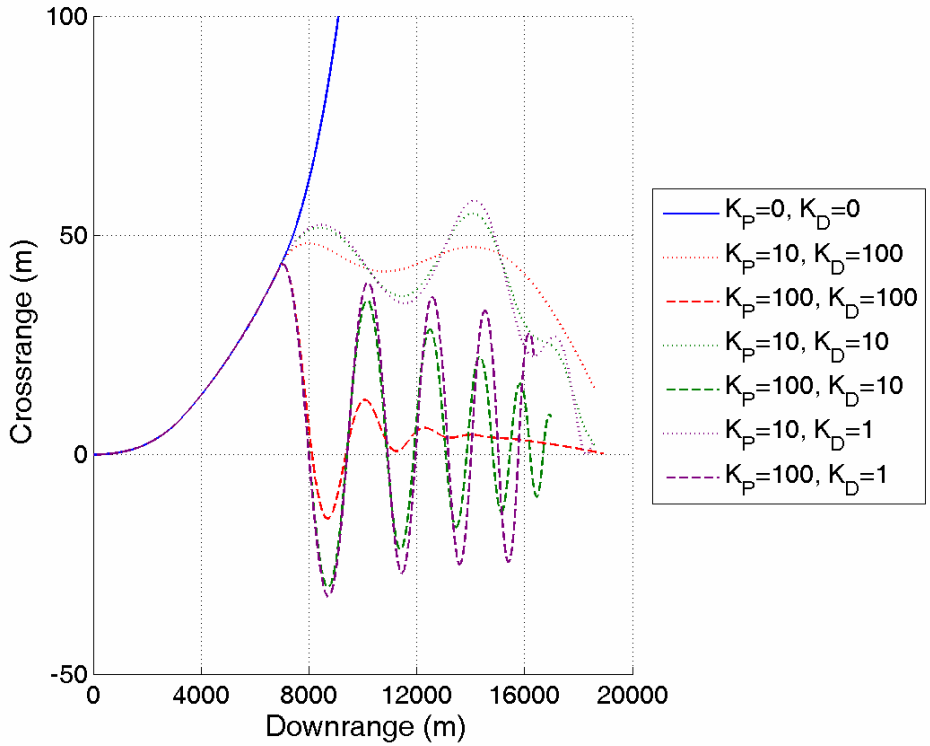
- Projectile inertial position (y_p, z_p) and velocity ($\dot{y}_p$) input from GPS, IMU, etc.
- Target inertial position (y_t, z_t) and velocity ($\dot{y}_t$) provided from fire control
- Proportional (K_P) and derivative (K_D) gains
- Flight controller seeks to maximize pitch angle of attack, minimize yaw angle of attack

Flight Control System Performance



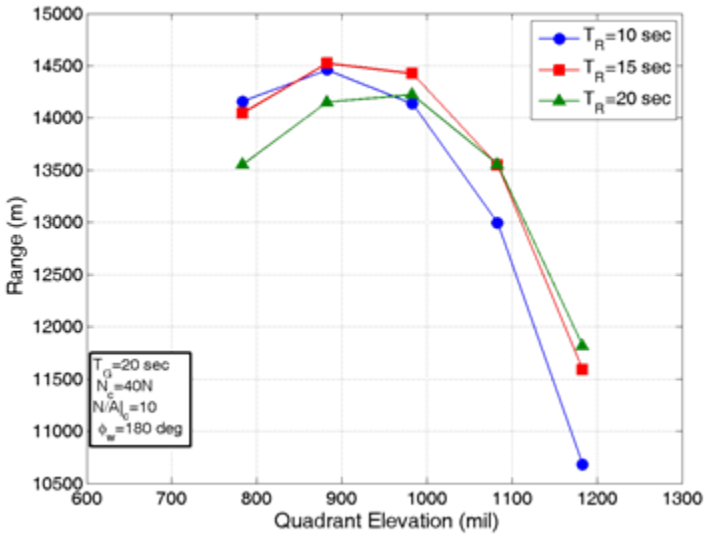


QE = 883 mils
T_R = 13 sec
T_G = 29 sec
N_c = 40 N
N_c / A_c = 10
X_c = 0.4 cal from CG
ϕ_w = 180 deg
static margin = 0.96

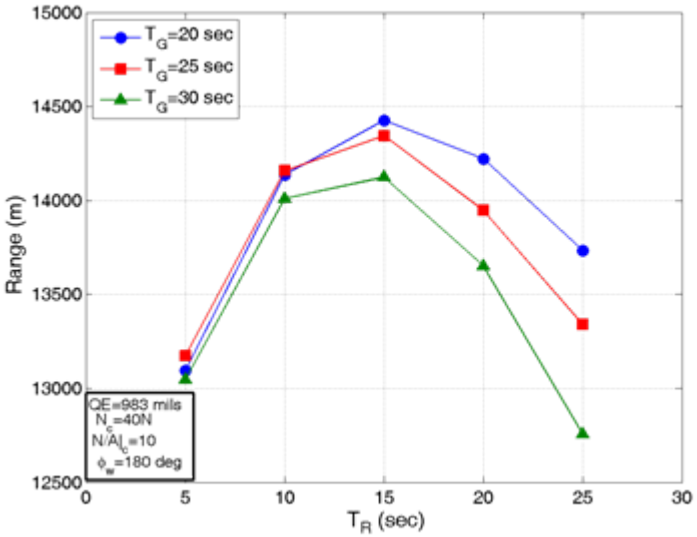


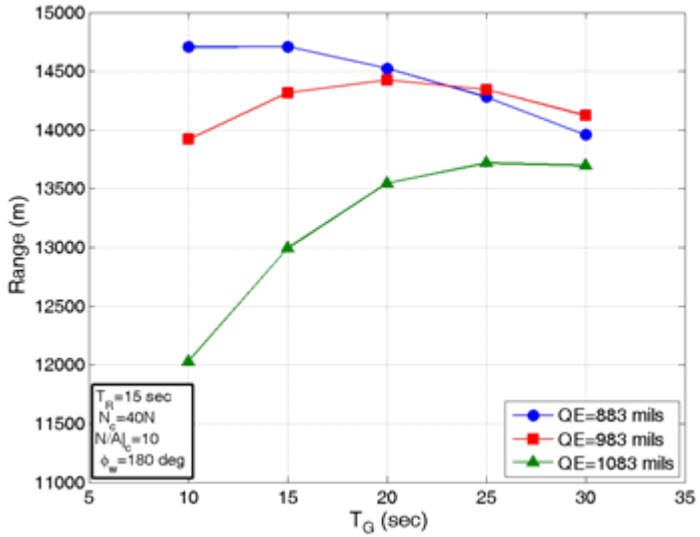
- 3000 m drift without GNC
- best combination of gains gets crossrange to zero without overcorrection and velocity heading along downrange axis (K_P=50, K_D=50).

Fire Control Parameters

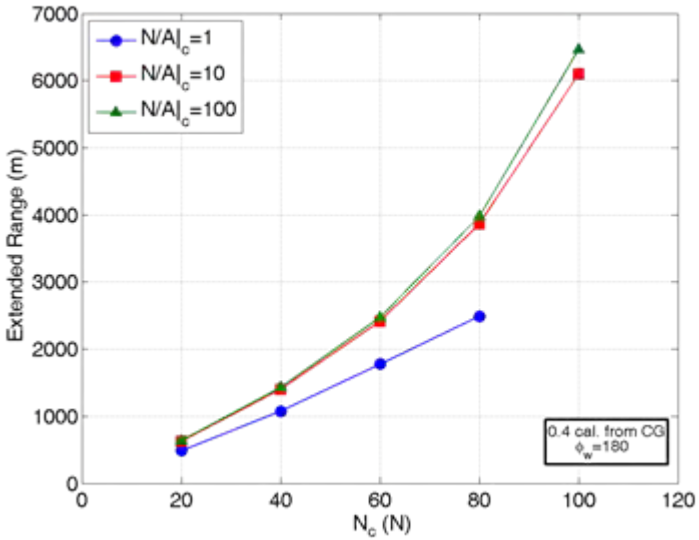


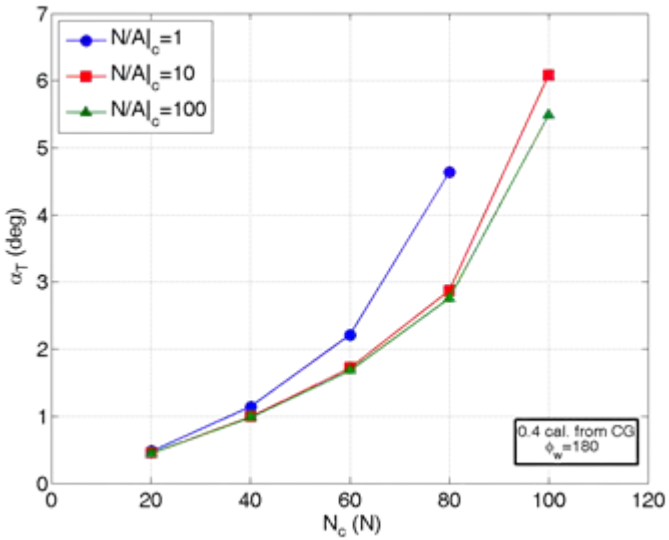
- optimize in parallel
- thrust/drag variation with atmospheric density for rocket ignition time
- lift/drag ratio of control mechanism for glide start time



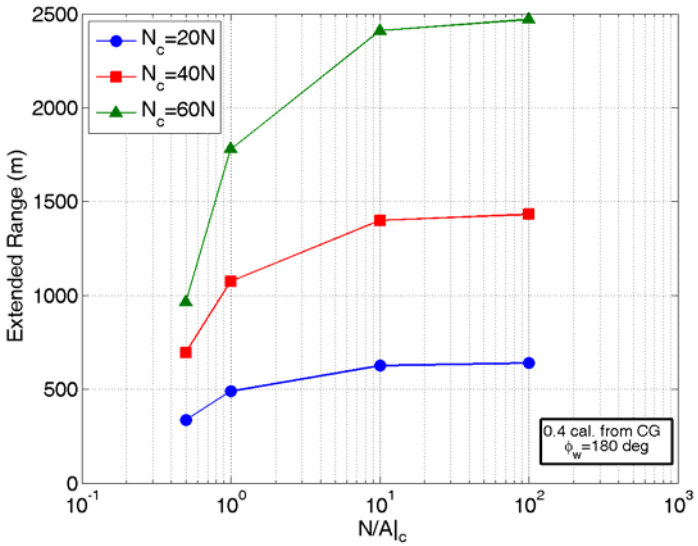


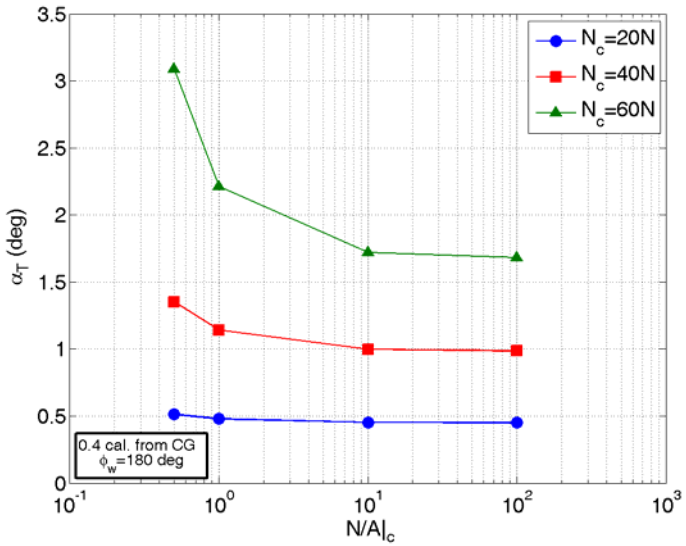
Projectile Parameters



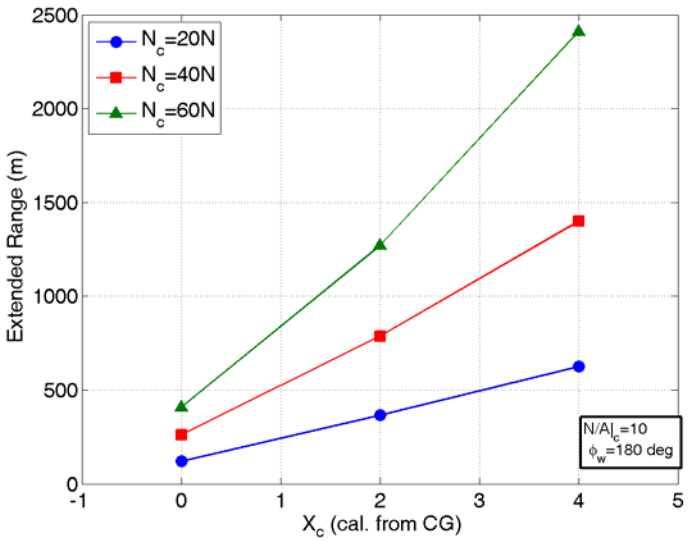


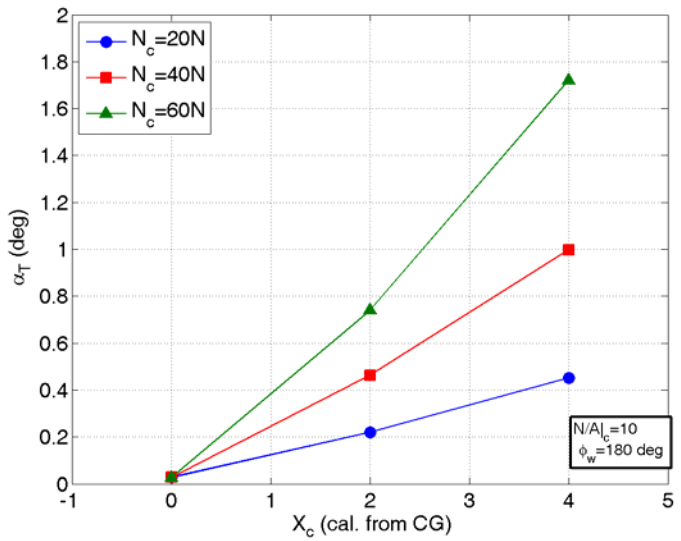
- asymptotic behavior for range increase
- more drag results in lower dynamic pressure which induces higher angle of attack to balance control moment





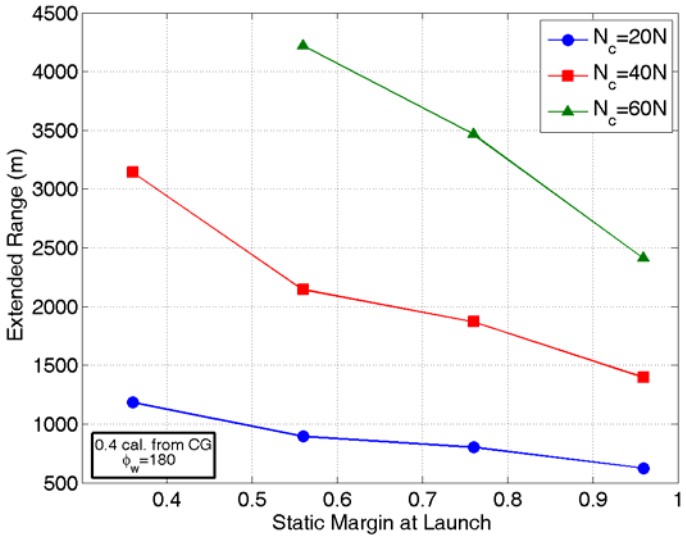
Projectile Parameters

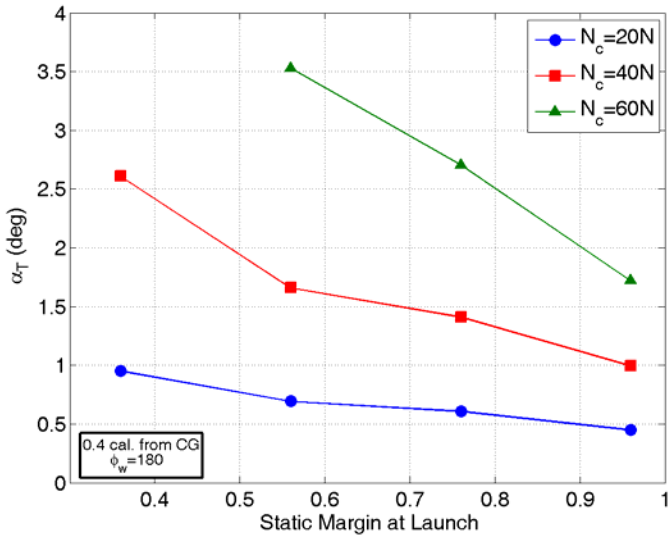




- range increases linearly with control moment arm

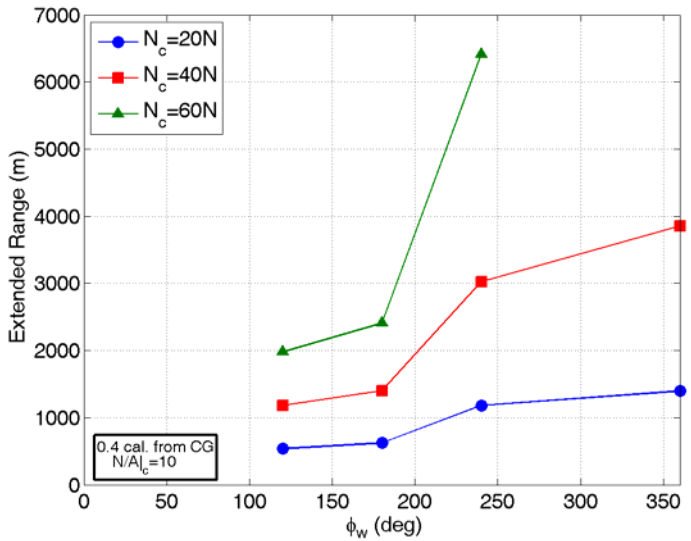
Projectile Parameters

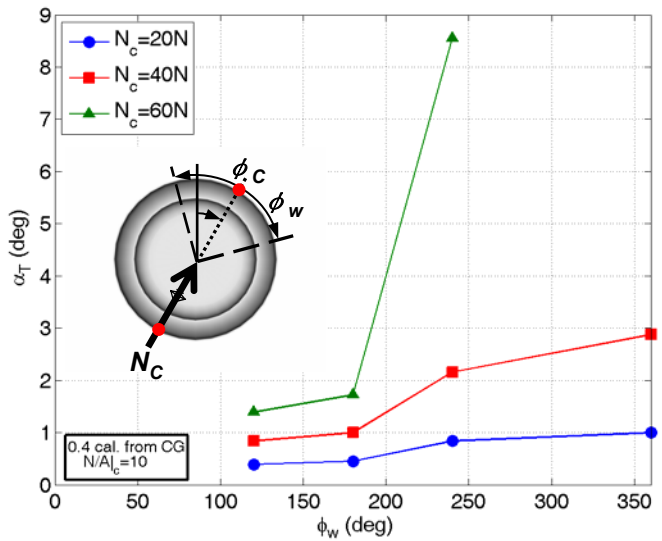




• lower static margin equals shorter moment arm for pitching moment to balance control moment

• adding more than one control element can significantly increase range





Summary

- Examined technical drivers to extending range of gun-launched precision munitions
  - fin-stabilized projectile with rocket motor and general control mechanism studied in six degree-of-freedom environment
  - Flight dynamics (projectile drift) required GNC algorithm development
    - maximize pitch angle and minimize yaw angle
  - Fire control parameters (QE, rocket ignition time, glide start time) must be optimized in parallel
  - Projectile configuration for maximum range: low static margin, large control normal force, control normal-to-axial force ratio of at least 10, control axial location at the nose, and large roll window

Contact Info

- Frank Fresconi, PhD
- U.S. Army Research Laboratory
- AMSRD-ARL-WM-BC, APG, MD 21005
- 410-306-0794

RDECOM

Malcolm Baldrige National Quality Award 2007 Award Recipient

ARMAMENT RESEARCH, DEVELOPMENT AND ENGINEERING CENTER
PICATINNY ARSENAL, NJ

TECHNOLOGY DRIVEN. WARFIGHTER FOCUSED.

Effects of Small Caliber Munitions Through Intermediate Barriers

September 2008

Chris Gandy & Jeremy Lucid – US Army - ARDEC

Introduction

- Can fielded ammunition meet the needs of the war fighter?
- How well do 5.56mm projectiles penetrate automobiles?
- What are the penetration capabilities of small caliber ammunition against intermediate barriers?

Typical Intermediate Barriers

Concrete Wall

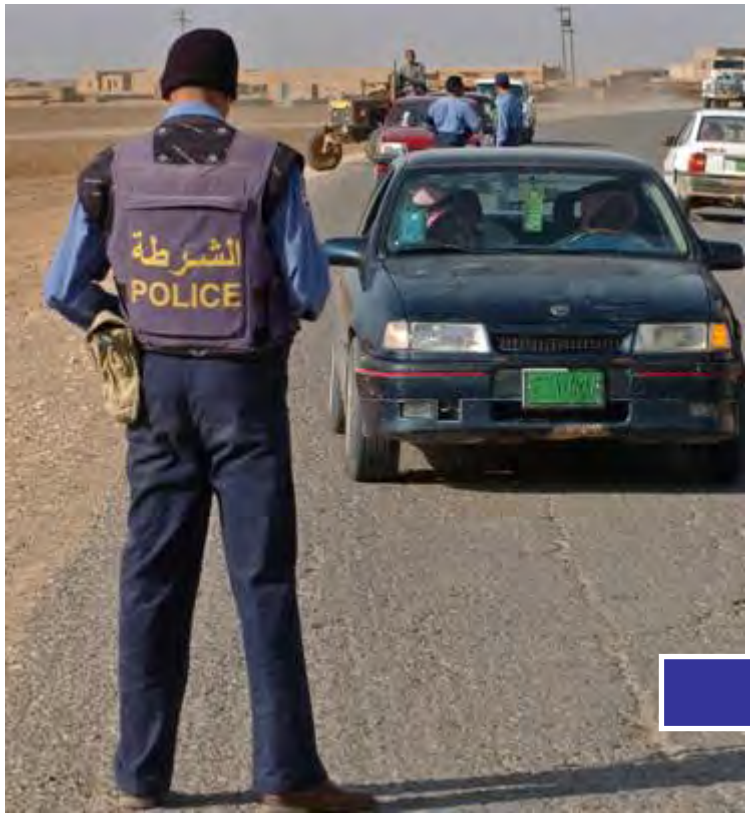


Insurgent Vehicle



This vehicle ran a checkpoint.
Could this have been prevented?

Vehicle Checkpoint



Lab Setup

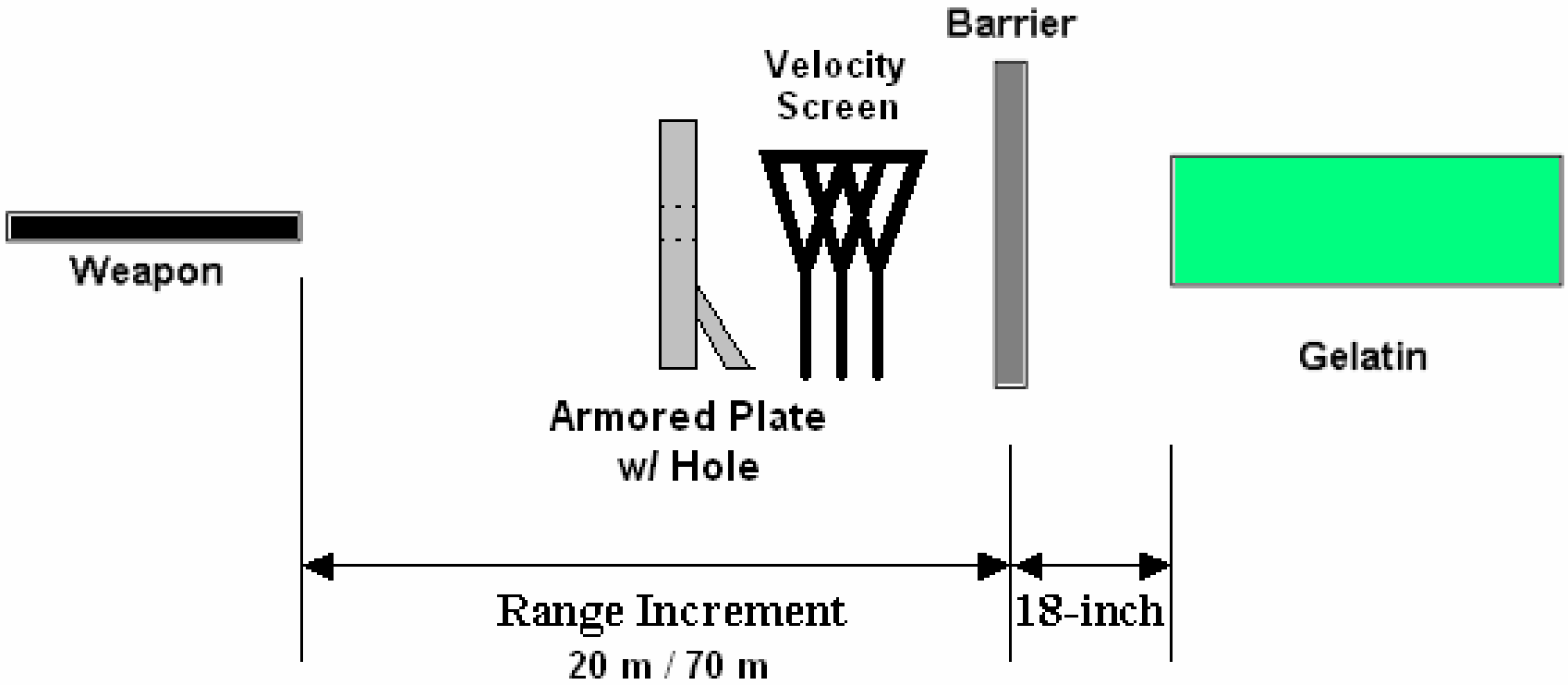


Malcolm Baldrige National Quality Award 2007 Award Recipient

Phase I – Shot Matrix

Weapons → Ammunition	M16 (5.56mm)	M4 (5.56mm)	M240 (7.62mm)
M193 (5.56mm)	Intermediate Barriers • No Barrier (Baseline) • Windshields • Simulated Car Doors		
M855 (5.56mm)			
MK262 (5.56mm)			
M80 (7.62mm)			

Phase I – Range Setup



Malcolm Baldrige National Quality Award 2007 Award Recipient

Phase I – Barrier Setup

90˚ Steel Plates



45˚ Steel Plates



Phase I – Barrier Setup

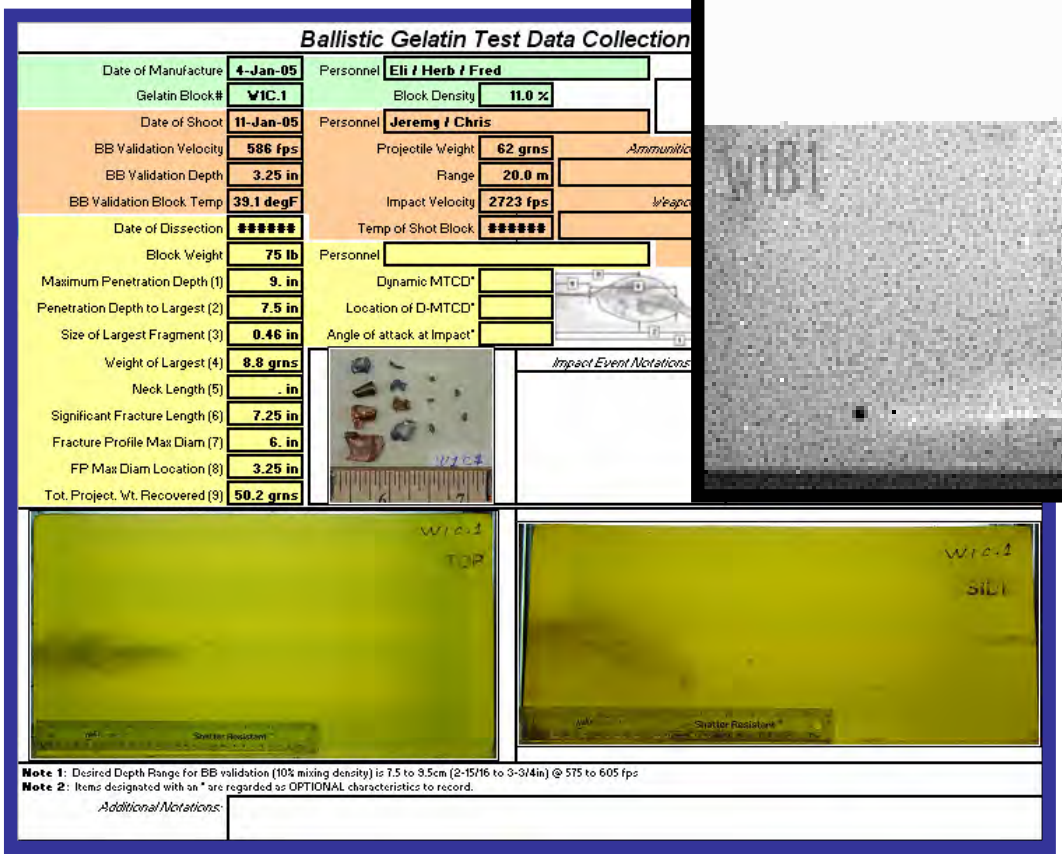
90˚ Windshield



45˚ Windshield



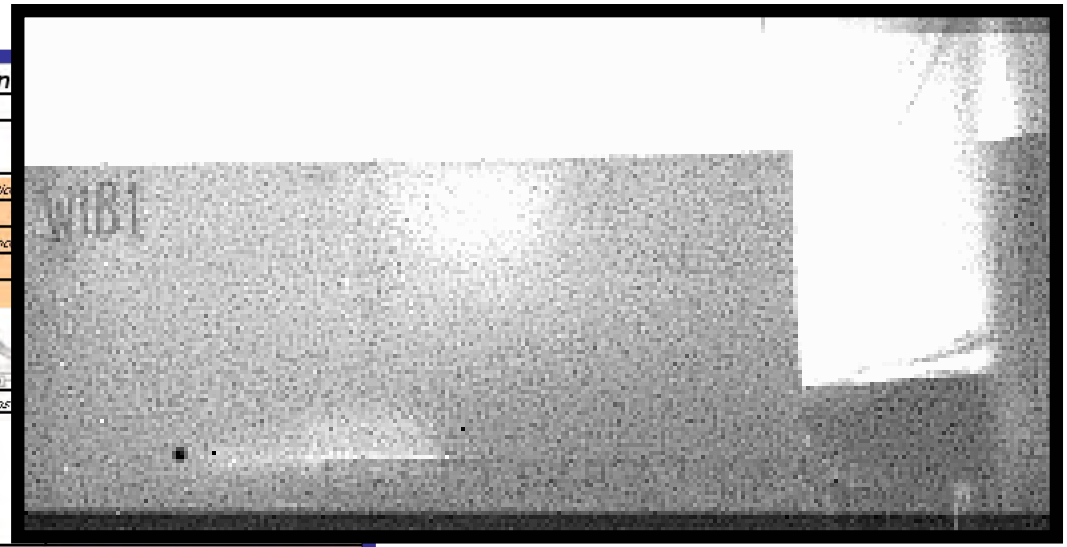
Phase I – Data Extraction



Ballistic Gelatin Test Data Collection

Date of Manufacture	4-Jan-05	Personnel	Eli / Herb / Fred		
Gelatin Block#	W1C.1	Block Density	11.0 %		
Date of Shoot	11-Jan-05	Personnel	Jeremy / Chris		
BB Validation Velocity	586 fps	Projectile Weight	62 grns	Ammunitio	
BB Validation Depth	3.25 in	Range	20.0 m		
BB Validation Block Temp	39.1 degF	Impact Velocity	2723 fps	Weapo	
Date of Dissection	######	Temp of Shot Block	######		
Block Weight	75 lb	Personnel			
Maximum Penetration Depth (1)	9. in	Dynamic MTCD*			
Penetration Depth to Largest (2)	7.5 in	Location of D-MTCD*			
Size of Largest Fragment (3)	0.46 in	Angle of attack at Impact*			
Weight of Largest (4)	8.8 grns				
Neck Length (5)	. in				
Significant Fracture Length (6)	7.25 in				
Fracture Profile Max Diam (7)	6. in				
FP Max Diam Location (8)	3.25 in				
Tot. Project. Wt. Recovered (9)	50.2 grns				

Impact Event Notations:



Note 1: Desired Depth Range for BB validation (10% mixing density) is 7.5 to 9.5cm (2-15/16 to 3-3/4in) @ 575 to 605 fps
Note 2: Items designated with an * are regarded as OPTIONAL characteristics to record.

Additional Notations:

- **Recovered Projectile Parameters**
- **High Speed Video**
- **Gelatin Damage Parameters**

Malcolm Baldrige National Quality Award 2007 Award Recipient

Phase I – EDR Analysis

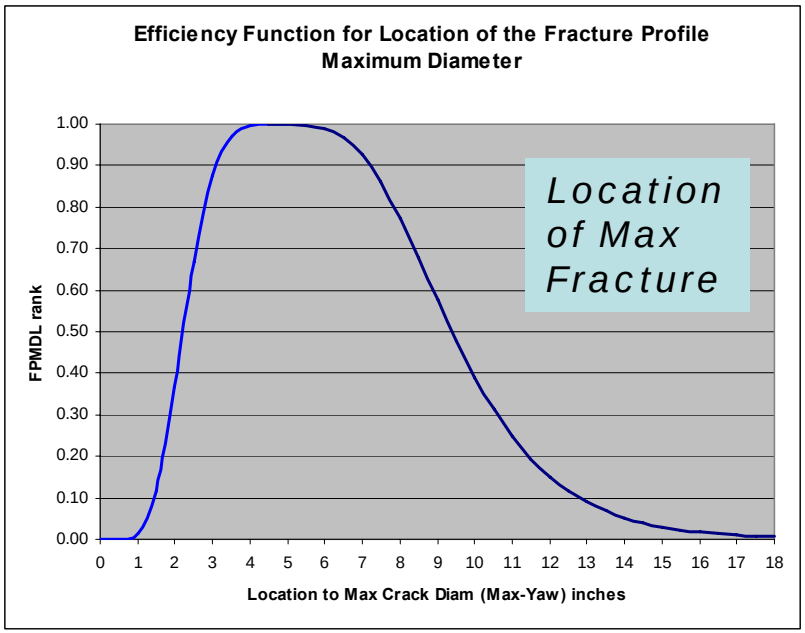
- Effective Damage Rating (EDR) is an abbreviated ranking system designed to quickly estimate the terminal performance of small caliber ammunition against human threats.
- Methodology is defined in Technical Report ARAET-TR-06013

Phase I – EDR Analysis

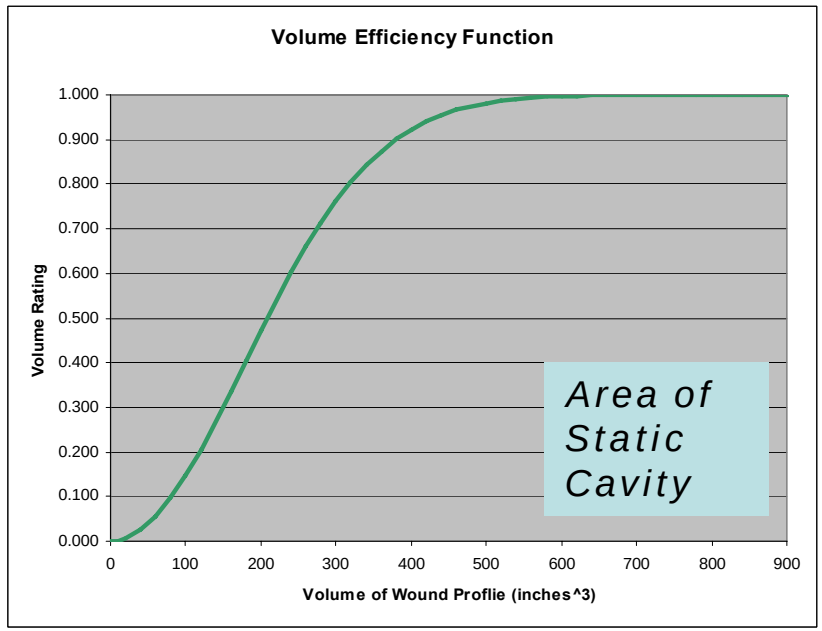
- EDR values range from zero to one
  - (1) One is Good
  - (0) Zero is Bad
- There are four different EDR rankings
  - EDR-1 *Rapid Effects/ Location of Damage*
  - EDR-2 *Quantity of Potential Damage*
  - *EDR-3 Adequate Penetration*
  - *EDR-4 Potential Engagements of Vital Organs*
- Average of all four EDR values was used

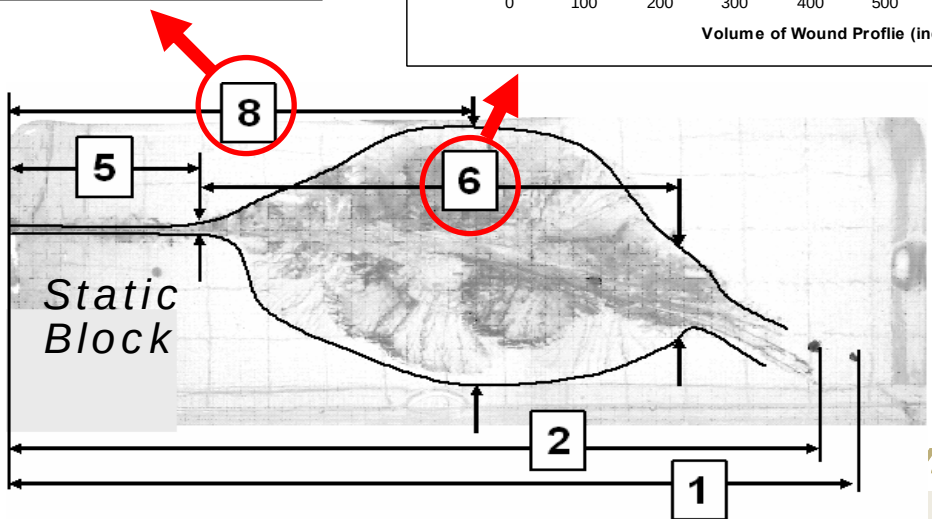
Phase I – EDR Analysis

EDR-1 Rapid Effects/ Location of Damage **25%**



EDR-2 Quantity of Potential Damage **25%**

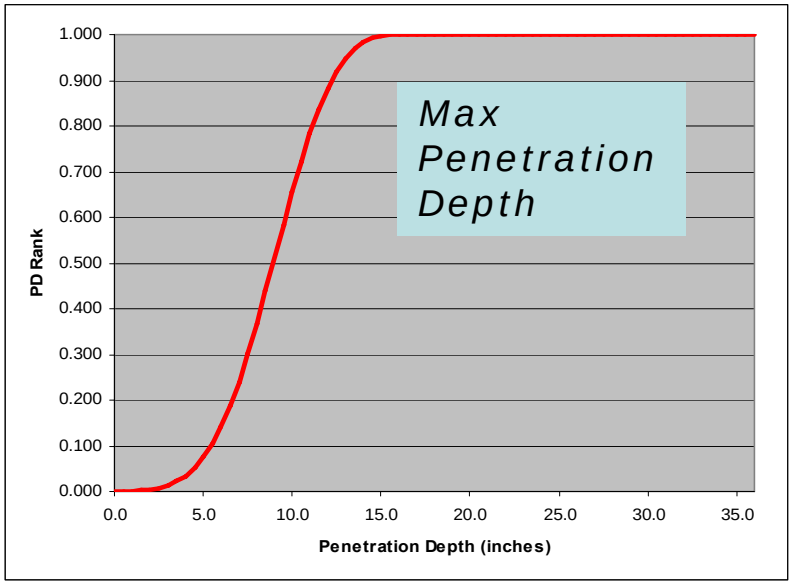




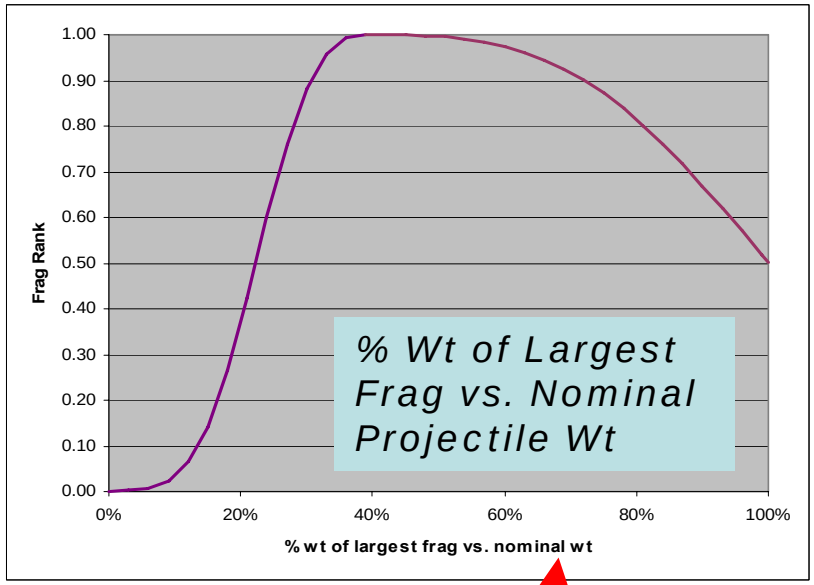
Malcolm Baldrige National Quality Award 2007 Award Recipient

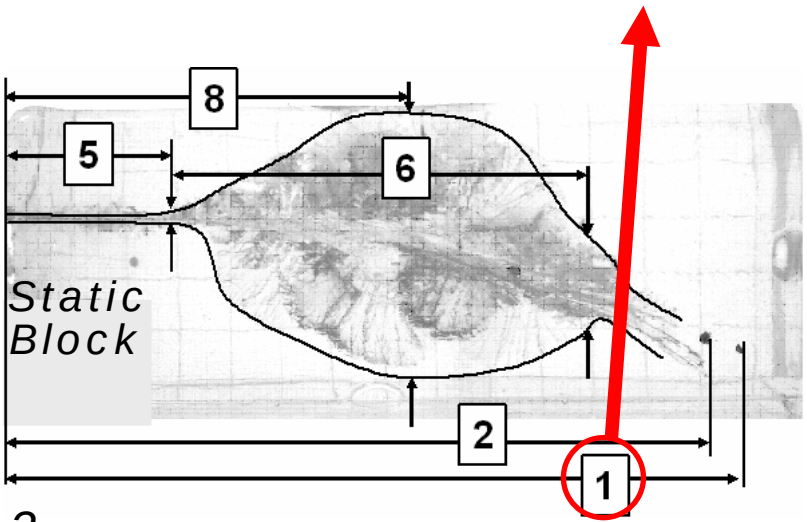
Phase I – EDR Analysis

EDR-3 Adequate Penetration **25%**



EDR-4 Potential Engagements of Vital Organs **25%**

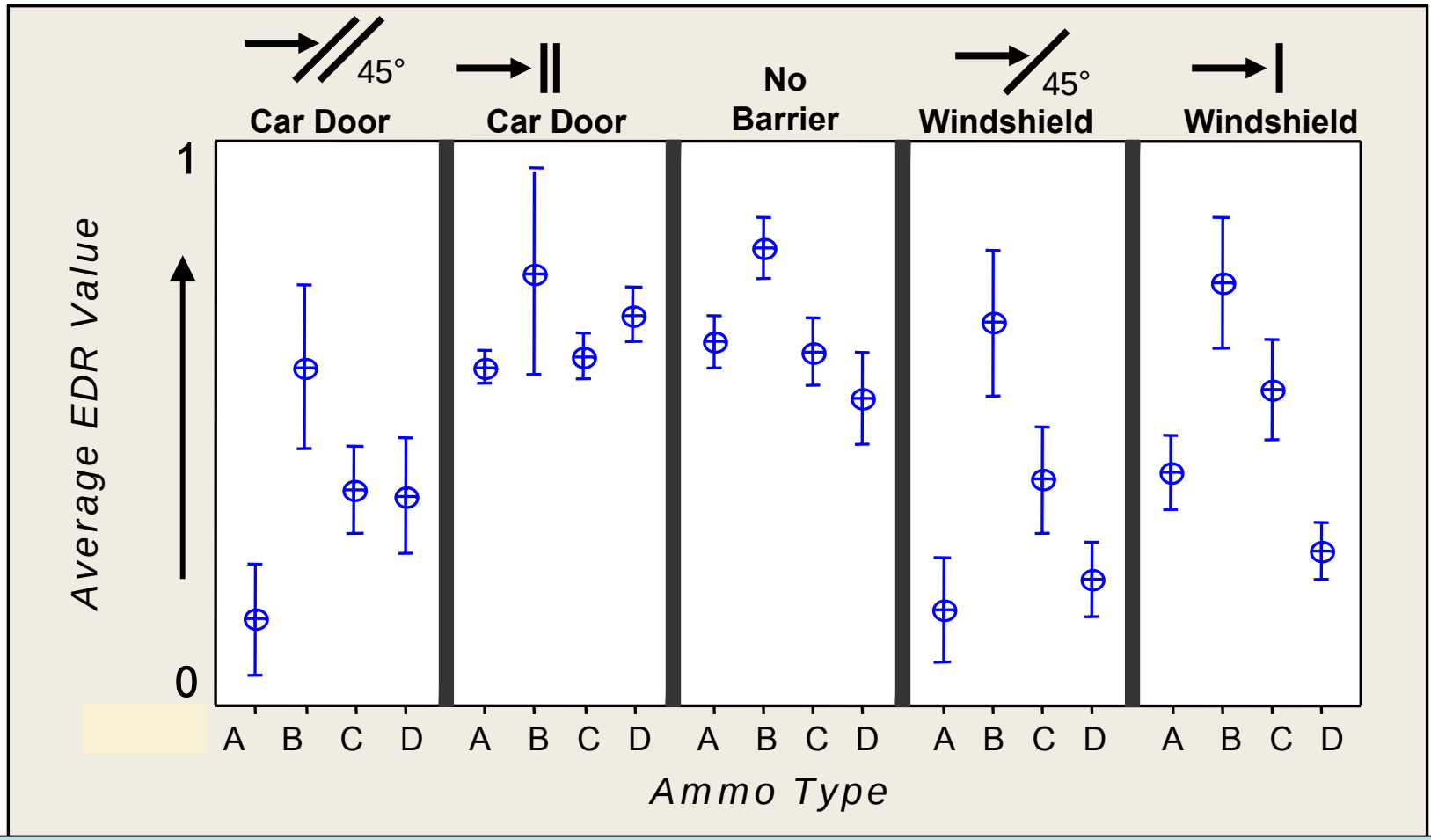






Bullet Fragments

Phase I – Results



Higher Average EDR Value = Better Post-Barrier Effectiveness

Phase II - Overview

- Evaluate terminal effects of 1,600 rounds of 5.56mm & 7.62mm ammunition through:
  - Automobile windshields at steeper angles
  - Simulated truck doors w/ increased shell thickness
  - Concrete blocks
- Establish quick go/no gages for intermediate barriers to assist in assessing the threat

Phase II - Test Setup



USAMU – Ft Benning

Weapons:

- M4
- M16
- M249
- M24
- M240

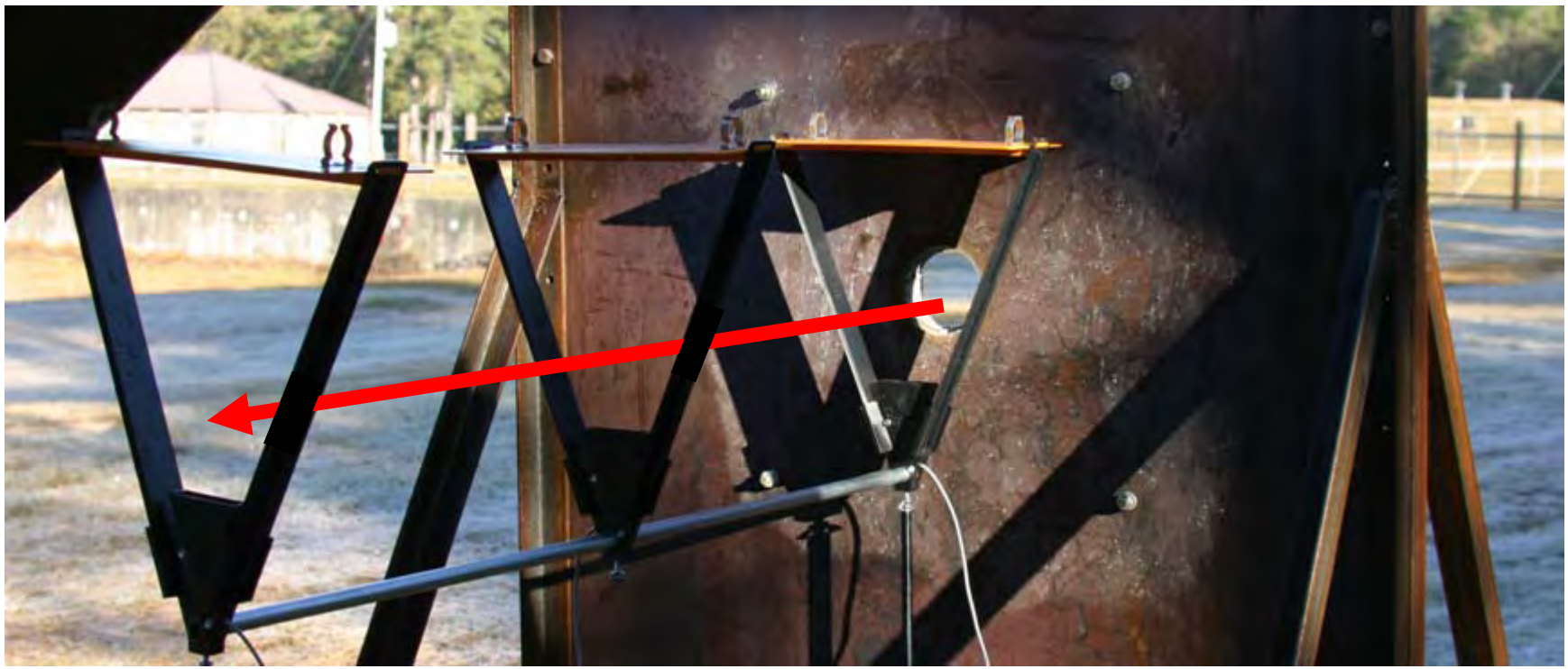
Ranges:

- 75m
- 200m

Malcolm Baldrige National Quality Award
2007 Award Recipient

Phase II - Test Setup

5.56mm Ammo	7.62mm Ammo
M193 M855 MK262 M995	M118LR M80

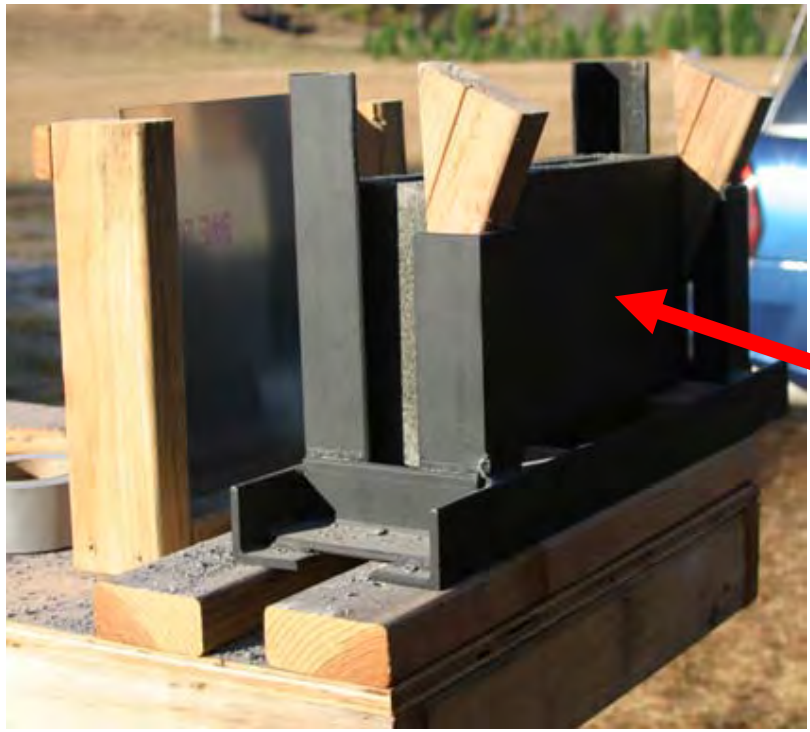


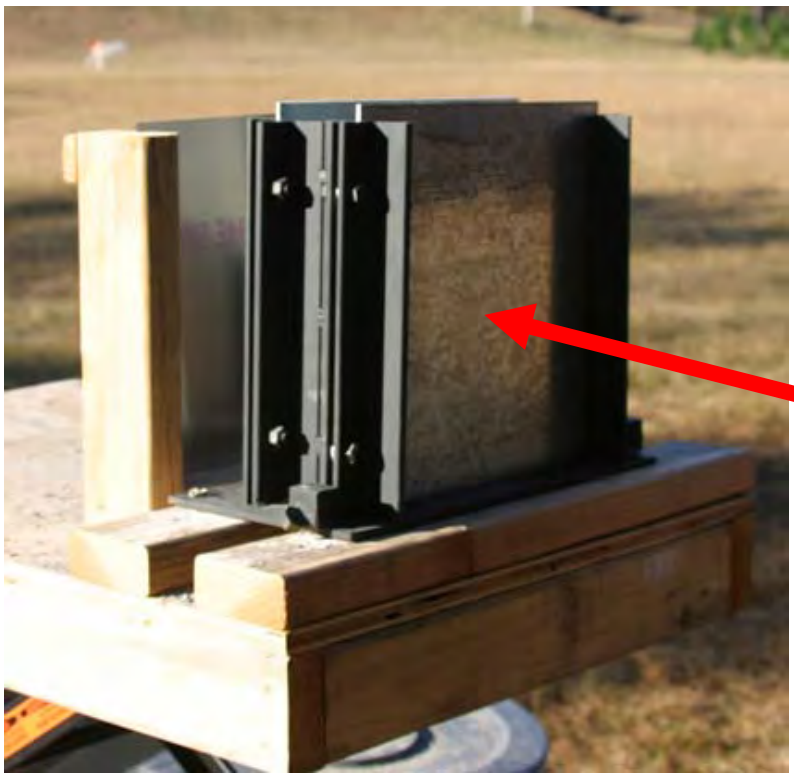
Automobile Windshields



Concrete & Steel

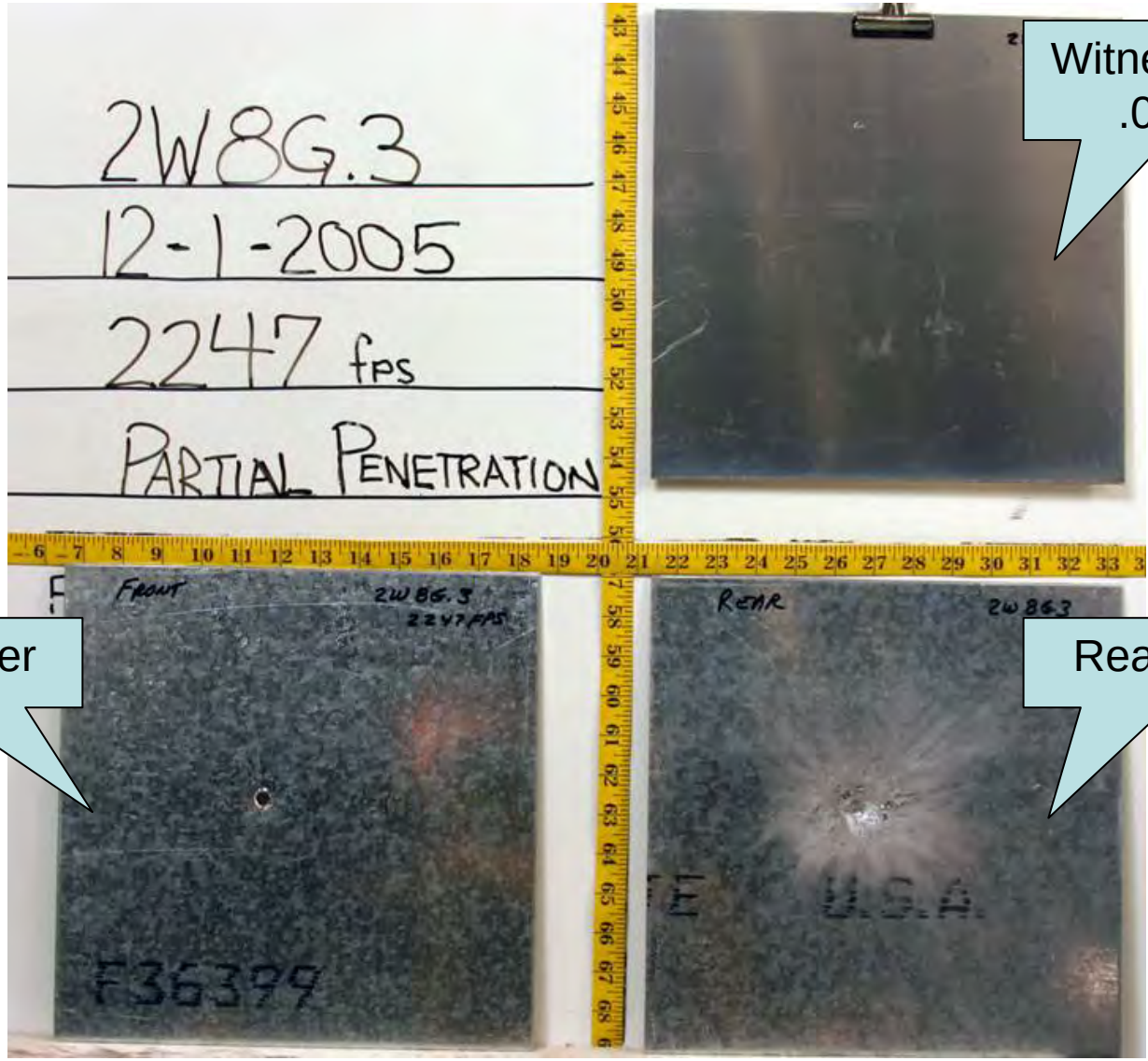
Concrete ➔





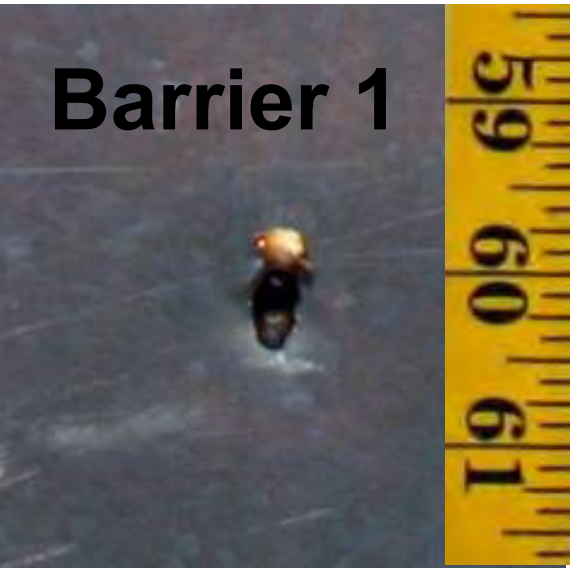
➔ Steel

Data Collection



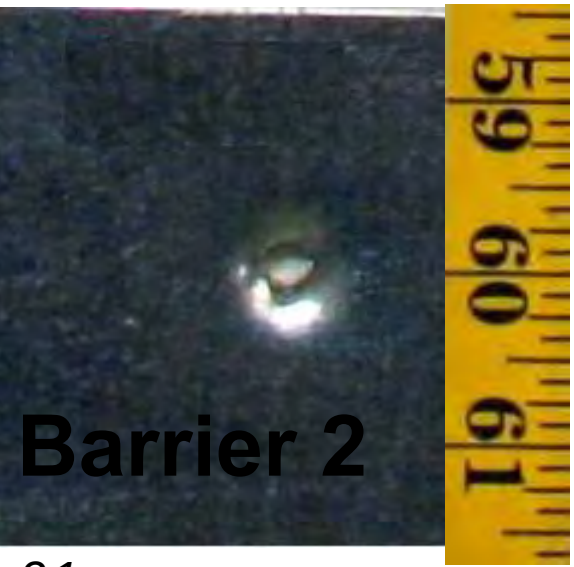
Malcolm Baldrige National Quality Award
2007 Award Recipient

Penetration Assessment



Partial Penetration





Full Penetration



Penetration Assessment of Munitions (PAM) Charts

RND XYZ - XX grain

	Windshield	Heavy Truck Door		Concrete Façade	
Weapon/ Range	Worst Case	Head On	Angle	4" Hollow	4" Filled
Gun 1 - Range 1	1	1	2	1	2
Gun 1 - Range 2	1	2	2	2	3
Gun 2 - Range 1	1	2	2	1	2
Gun 2 - Range 2	1	2	2	1	3

1	Full Penetration - Minimum # of Shots Required to Penetrate Barrier (80% of the rounds fired were able to penetrate the barrier on the first shot)
2	Partial Penetration - Multiple Shots Required To Penetrate Barrier
3	No Penetration - Maximum # of Shots Required To Penetrate Barrier (80% of the rounds fired were unable to penetrate the barrier on the first shot)

Quick assessment of penetration capability across multiple barriers and ranges.

Malcolm Baldrige National Quality Award 2007 Award Recipient

Conclusion

- Provided a quick assessment of currently fielded ammunition
- Determined effectiveness through light intermediate barriers found in field
- Compiled all data for future testing and modeling efforts
- Technical Report ARAET-TR-07030

Requests for this document:

U.S. Army ARDEC
ATTN: AMSRD-AAR-EMK
Picatinny Arsenal, NJ 07806-5000

Contact Information

Questions?

Chris Gandy – chris.gandy@us.army.mil
Jeremy Lucid – jeremy.lucid@us.army.mil



Fragment Penetration Modeling of Anthropometric Ballistic Mannequins



24th International Symposium on Ballistics
22 - 26 September 2008
Presented by: Patrick Gillich

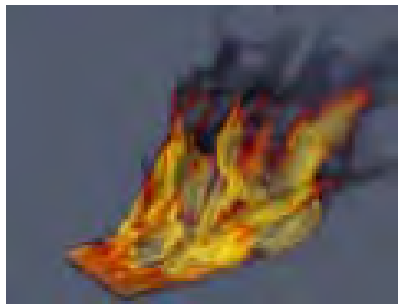
TECHNOLOGY DRIVEN. WARFIGHTER FOCUSED.

William Bruchey
Survice Engineering Company, Belcamp, MD

Amy Tank
U.S. Army Research Laboratory, APG, MD

Introduction

ORCA Model
An Integrated Methodology for Survivability Assessment



BURNSIM - THERMAL
(U.S. Air Force Research Laboratory)

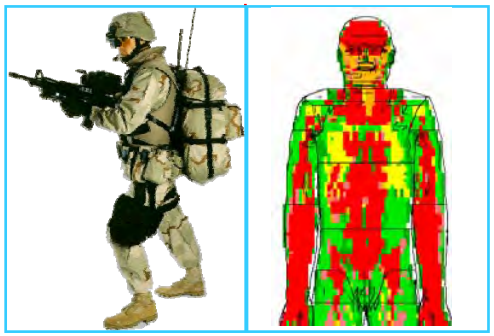


INJURY - BLAST OVERPRESSURE
(U.S. Army Medical Research and Materiel Command)



AMANDA - ACCELERATION
(U.S. Army Aeromedical Research Laboratory)

Operational Requirement-based Casualty Assessment



COMPUTERMAN
(U.S. Army Research Laboratory)



CHEMICAL MAN
(U.S. Army Research Laboratory)

- **Standard Injury Description**
- **Standard Military Task Inputs**
- **Common Integrated Crew Casualty Assessment Methodology**

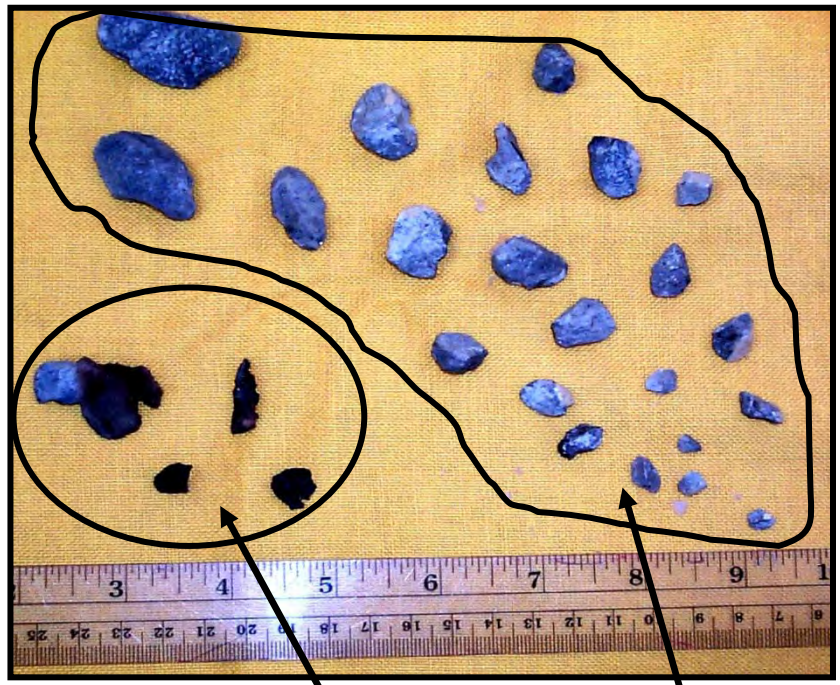
Secondary Debris from Concrete Wall Front Surface

Debris cloud from warhead impact





Recovered steel warhead fragments and aggregate debris

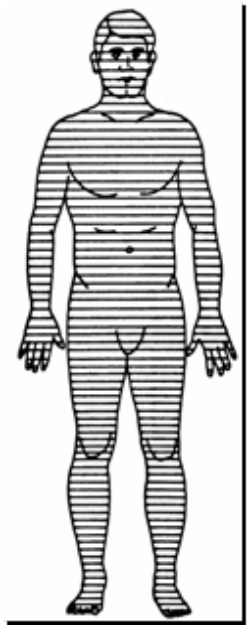


Steel fragments
Mass: 0.13g - 8g

Aggregate (stone)
Mass: 0.05g - 9g

ORCA / Computerman

3-D Anatomical Man





Plywood Mannequin

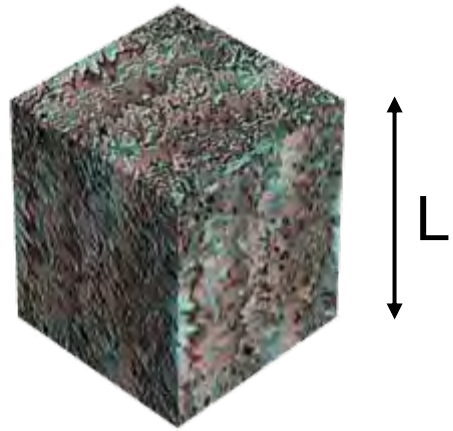


Wound Ballistics Modeling:

- Input : Mass, Velocity, Shape Factor , Entry & Exit Points
- Data Source: Plywood Penetration & Ballistic Gel Retardation
- Output : Expected Incapacitation (EI) of a Soldier

Projectile Characteristics

- Shape: Cube, Natural Aggregate
- Mass: 0.1g – 41g
- Size (Length): 0.22cm – 1.75cm
- Materials**
  - Steel
  - Aluminum
  - Aggregate
  - Granite
- Velocity: 150m/s – 1000m/s



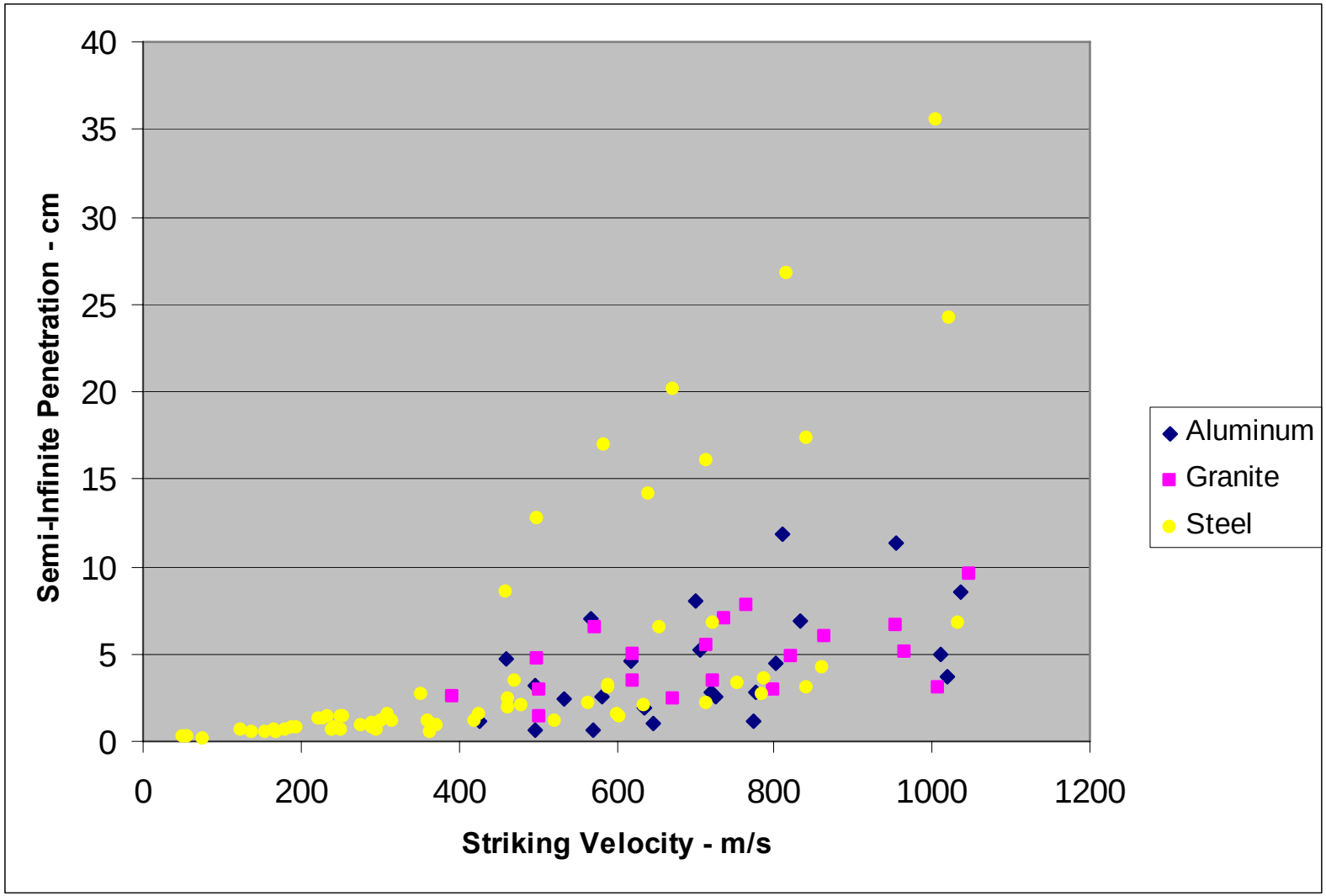
**Note: All projectiles penetrated as rigid bodies

Target Characteristics

- Material: ¾ in Marine Grade Plywood
- Density: 0.35 g/cc
- Configuration
  - Semi-infinite stack, i.e. semi-infinite target
  - Single layer, i.e. finite target
- Obliquity
  - Semi-infinite, 0^o obliquity
  - Finite, 0^o and 60^o obliquity

Semi-Infinite Penetration (All Cubes)

Raw Data – Aluminum, Granite, and Steel



Penetration Model

After Tate and Alekseevskii:

$\dot{L} = V-U$ (erosion kinematics)

$L\dot{U} = -Y/r_r$ (rod deceleration)

$\frac{1}{2} r_r(U-V)^2 + Y = \frac{1}{2} r_t + R$ (interface stress balance)

"Approaches to Penetration Problems", T. Wright, K. Frank, U.S. Army Ballistic Research Laboratory, TR-2957, December 1988

For Fragment Penetration of Plywood:

- $V-U = 0$
- $R > Y$

Semi-Infinite Plywood Penetration Analysis

Differential Form of Penetration Equation:

$$-mv(dv/dx) = \tfrac{1}{2}\, \rho b A v^2 + sA$$

where: $\rho = 0.35$ g/cc

s = strength of plywood, dynes/cm^2

A = Average Presented Area of Fragment, (cubes), cm^2

v = striking velocity, cm/sec

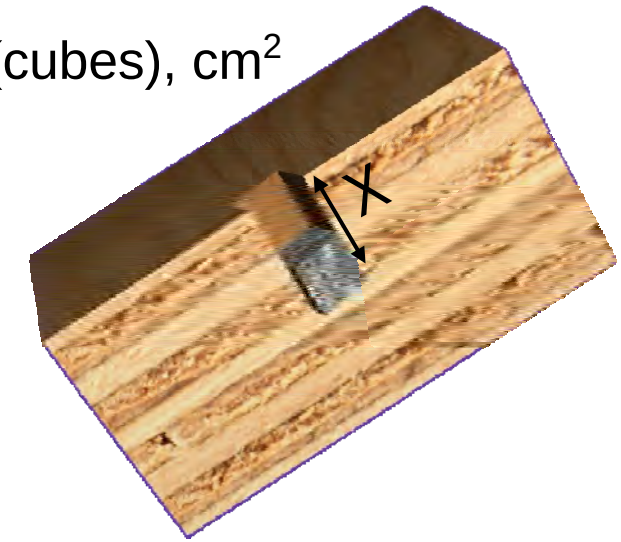
m = fragment mass, g

X = plywood penetration depth, cm

$a = A/m$

$g = \tfrac{1}{2}\, \rho$

b = Shape Factor



Integrating the above equation for v and x:

$$X = \frac{-1}{2} \cdot \frac{\ln(\sigma) - \ln\left(v_0^{\,2} \cdot \gamma \cdot \beta + \sigma\right)}{\alpha \cdot \gamma \cdot \beta}$$

Solution requires determination of two unknowns: b, s (optimized over all fragment masses, areas, and densities => NLLS solution for b,s)

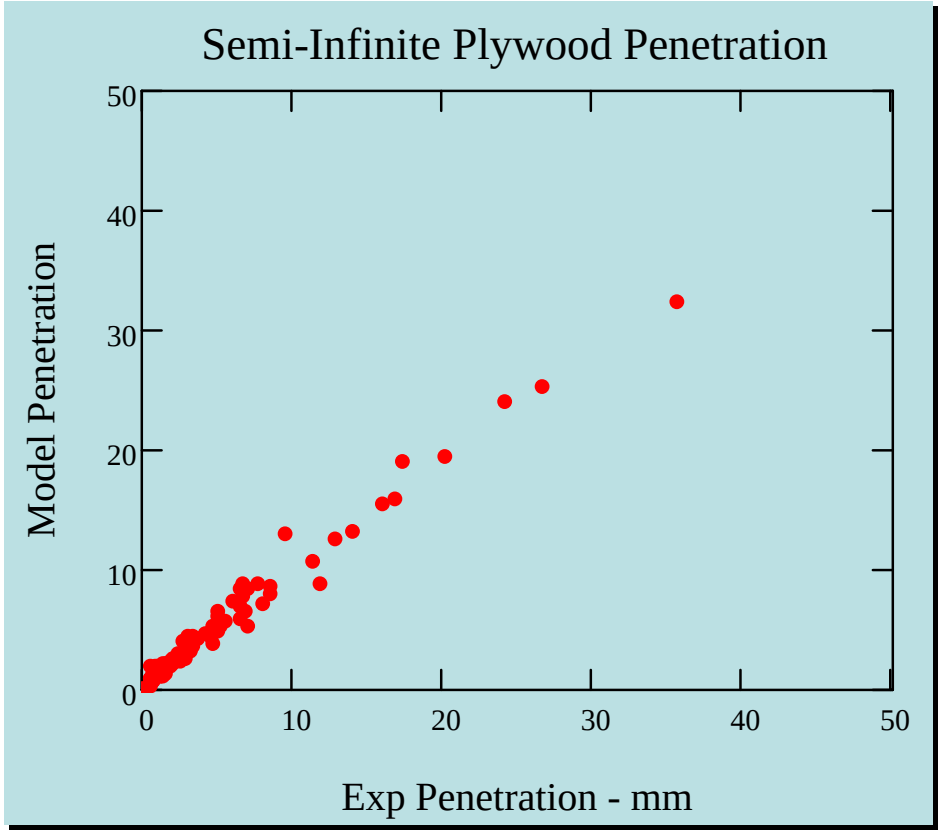
Results of Analysis (Penetration Prediction)

Number of Data Points: 105
Average Miss Distance (average of all (x_{pred} - x_{obs})): -0.253 mm

b = 1.014
s = 7.007 x 10^8 dynes/cm^2

$$X = \frac{-1}{2} \cdot \frac{\ln(\sigma) - \ln\left(v_0^{\,2} \cdot \gamma \cdot \beta + \sigma\right)}{\alpha \cdot \gamma \cdot \beta}$$

Indicates how well penetration is predicted for any fragment at a given striking velocity.

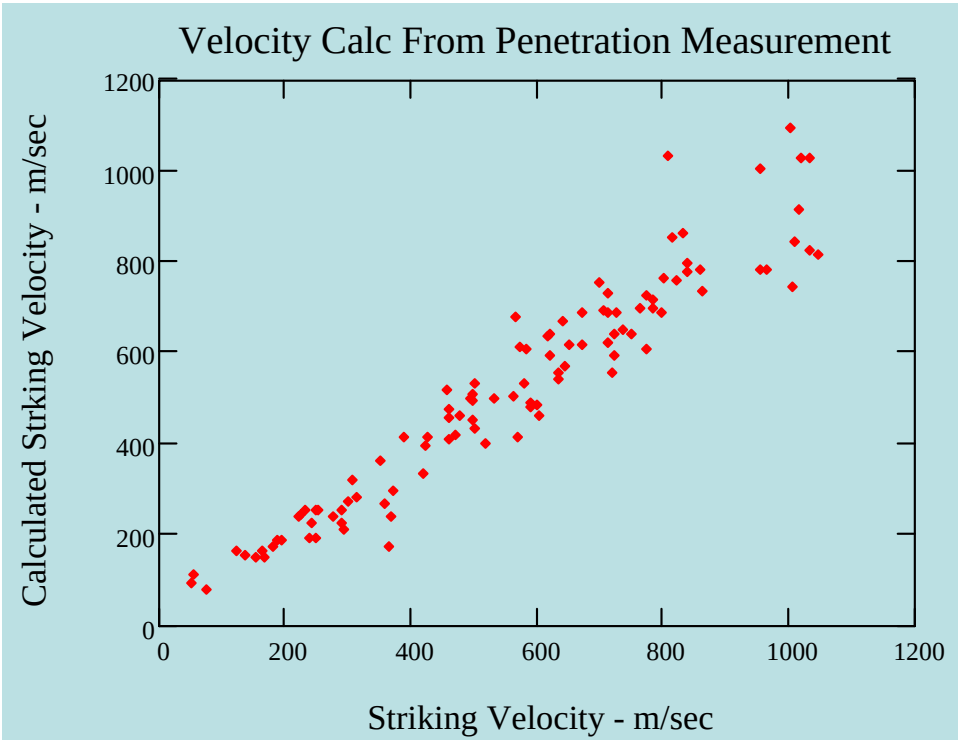


Results of Analysis (Velocity Prediction)

$$V_s = \frac{1}{e^{(-2)\cdot x\cdot\alpha\cdot\gamma\cdot\beta}\cdot\gamma\cdot\beta}\cdot\left[\left[-e^{(-2)\cdot x\cdot\alpha\cdot\gamma\cdot\beta}\right]\cdot\gamma\cdot\beta\cdot\sigma\cdot\left[e^{(-2)\cdot x\cdot\alpha\cdot\gamma\cdot\beta}-1\right]\right]^{\frac{1}{2}}$$

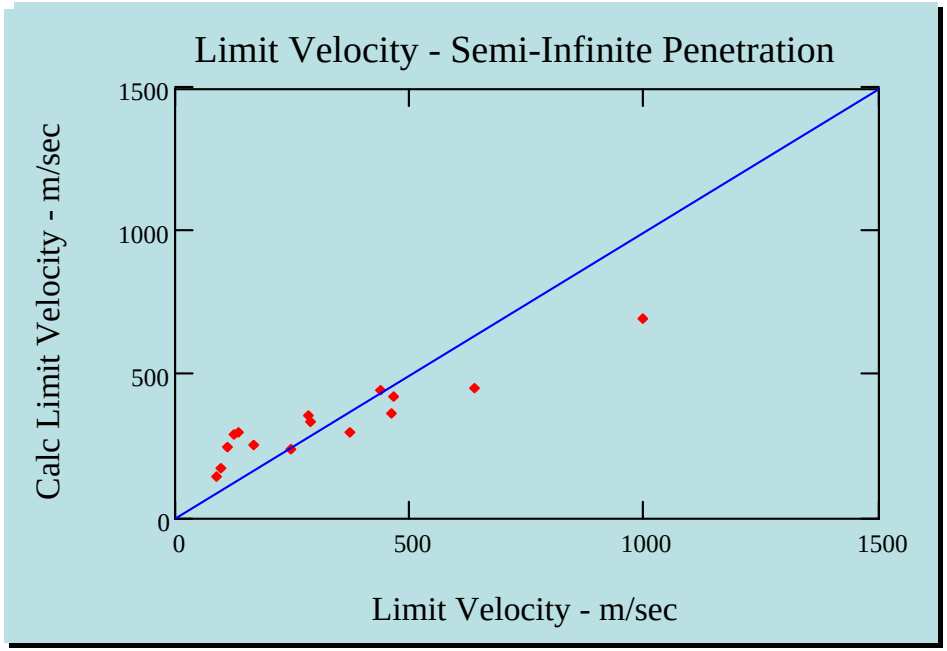
b = 1.014

s = 7.007 x 10^8 dynes/cm^2



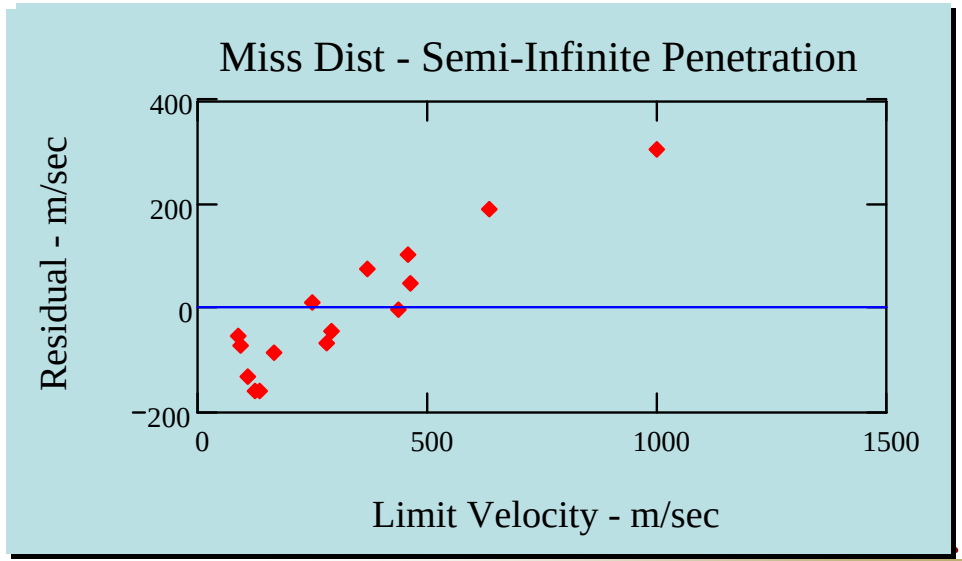
Limit Velocity Prediction ¾” Plywood

- Assume no finite target effect, i.e. limit velocity equals velocity needed to penetrate ¾-in into semi-infinite plywood



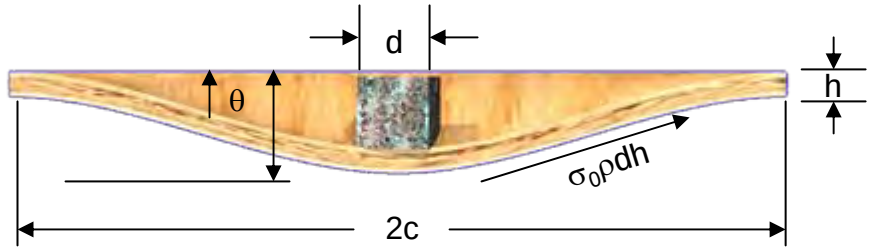
- Analysis of residuals show linear trend → finite thickness effect

*Residual = ($X_{observed} - X_{predicted}$)



Finite Plywood Correction





$$mv \cdot \frac{dv}{dx} = \sigma_0 \cdot \pi \cdot d \cdot h \cdot \frac{x}{c}$$

$$\int_{v_f}^{0} v\,dv = \int_{0}^{x} -\sigma_0 \cdot \pi \cdot d \cdot h \cdot \frac{x}{c \cdot m}\,dx$$

$$v_f^2 = x^2 \cdot \sigma_0 \cdot \pi \cdot d \cdot \frac{h}{c \cdot m} \rightarrow v_f \sim (A_p/m)^{1/2}$$

"The Limit Velocity of Fragments Impacting Lightweight Armor Materials: An Ad Hoc Model", W. Bruchey, BRL MR-2677, Sep 1976

Finite Thickness Correction

Assume:

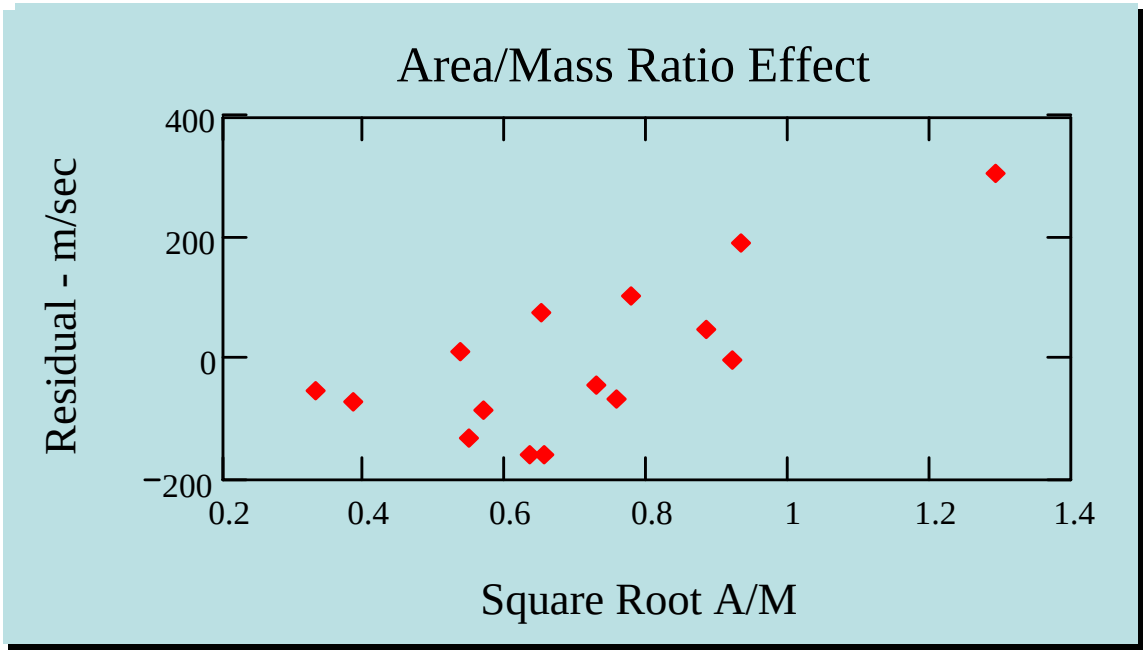
- Initial penetration is given by semi-infinite penetration analysis
- At some thickness < ¾-in, the plywood fails and acts as if it is a membrane
- Membrane analysis shows that the failure velocity is proportional to $(A_p/m)^{1/2}$

Linear relationship ⇒

Residual = $a + b(A_p/m)^{1/2}$

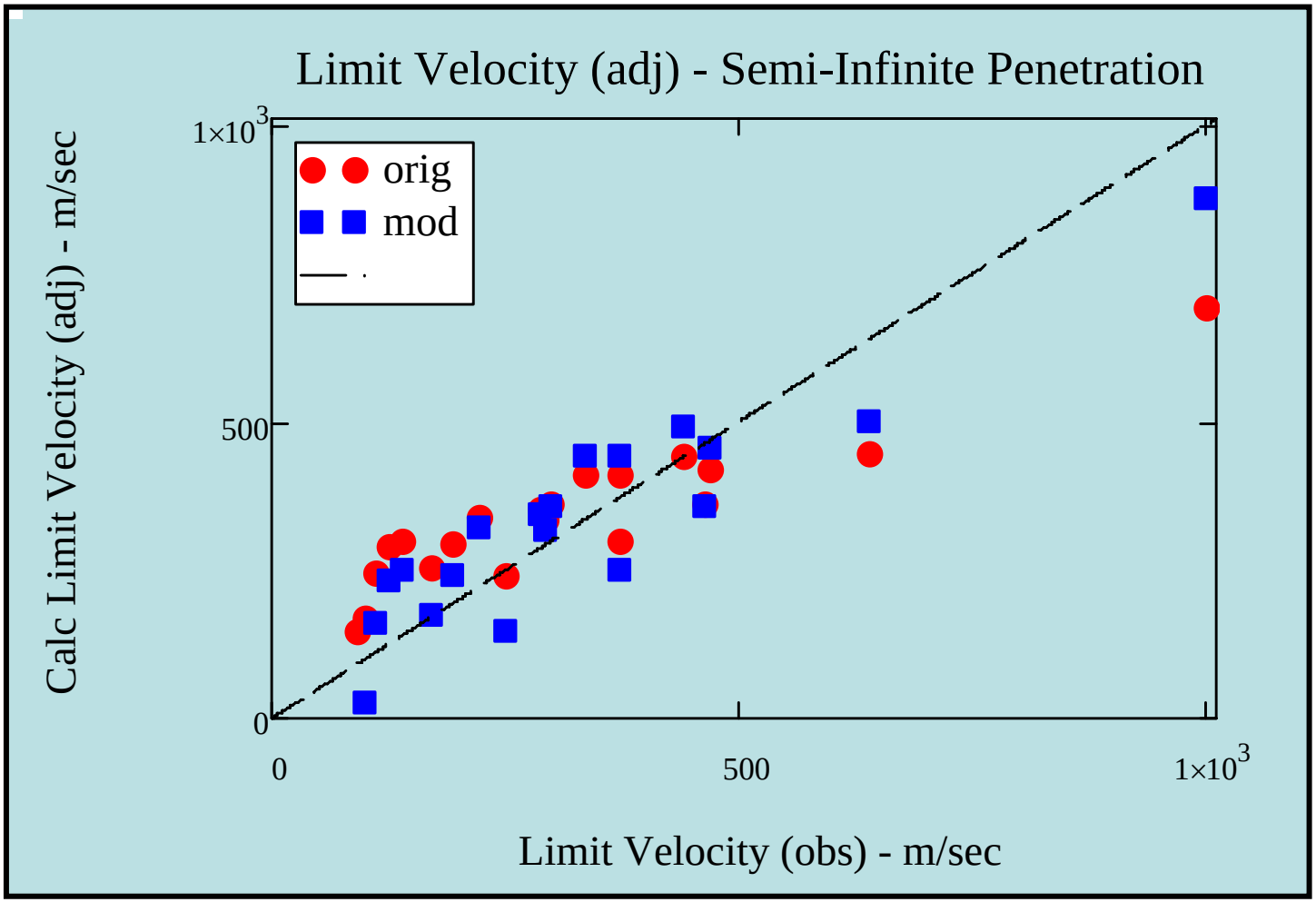
$a = -2.846 * 10^4$

$b = 3.601 * 10^4$



Limit Velocity Calculated from Semi-Infinite Penetration

Calculated Limit Velocity with Adjustment for finite thickness versus the Observed Limit Velocity



Conclusion

This model provides an estimate of fragment penetration into semi-infinite stacks of marine-grade plywood. Limit velocities can be estimated from semi-infinite penetration utilizing a correction factor for finite target breakout effects.

Resulting Equations:

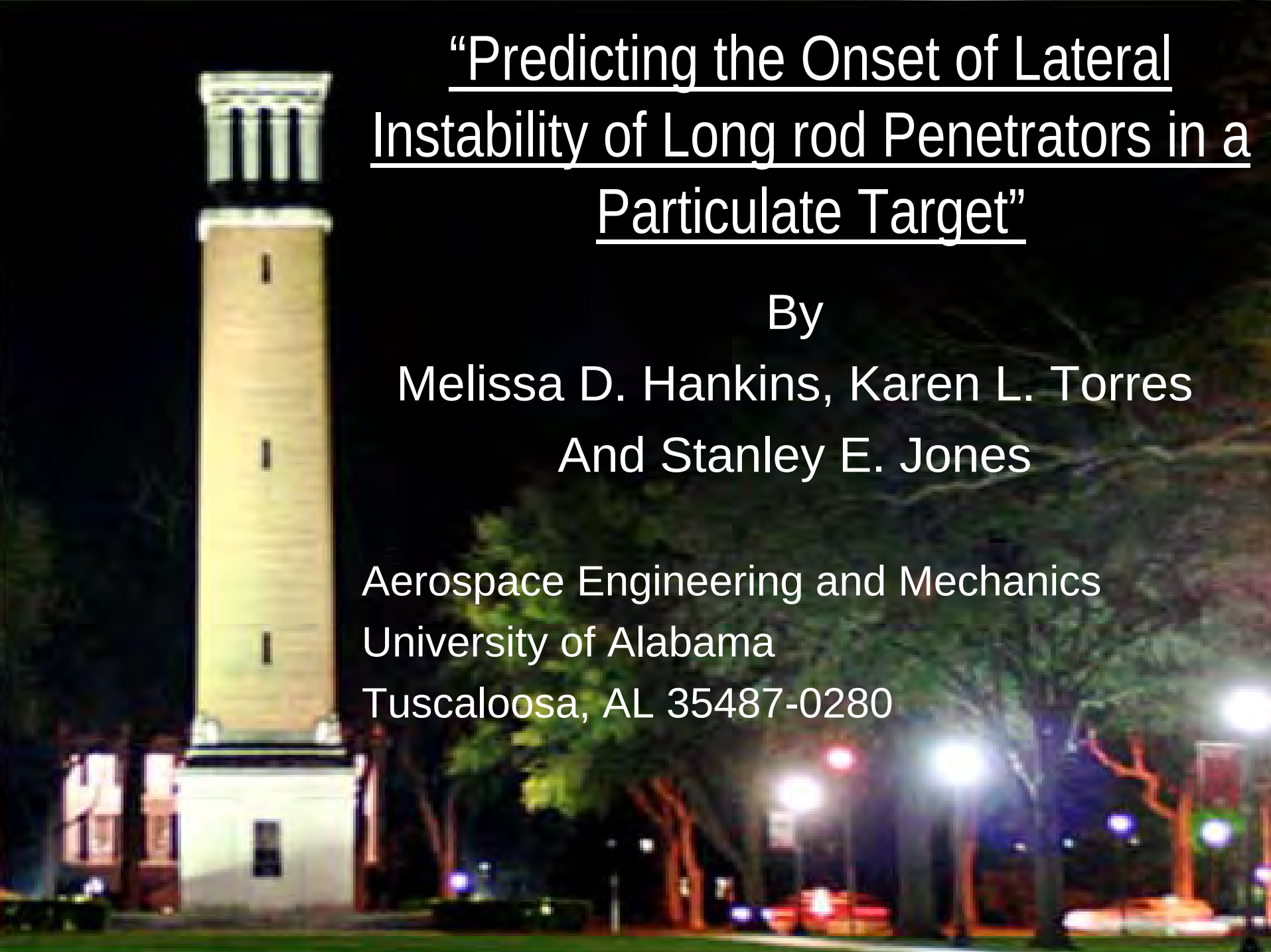
- Semi- Infinite

$$V_s = \frac{1}{e^{(-2)\cdot x\cdot\alpha\cdot\gamma\cdot\beta}\cdot\gamma\cdot\beta}\cdot\left[\left[-e^{(-2)\cdot x\cdot\alpha\cdot\gamma\cdot\beta}\right]\cdot\gamma\cdot\beta\cdot\sigma\cdot\left[e^{(-2)\cdot x\cdot\alpha\cdot\gamma\cdot\beta}-1\right]\right]^{\frac{1}{2}}$$

- Finite (¾-in Marine Plywood)

  Semi- Infinite solution plus breakout correction

  $a + b(A_p/m)^{1/2}$



"Predicting the Onset of Lateral Instability of Long rod Penetrators in a Particulate Target"

By

Melissa D. Hankins, Karen L. Torres

And Stanley E. Jones

Aerospace Engineering and Mechanics

University of Alabama

Tuscaloosa, AL 35487-0280



Topics

- The Instability Problem
- Laboratory Scale Testing
- Normal Penetration of Particulate Targets
- Formulation and Solution of the Problem
- Results
- Conclusions and Future Work

The Instability Problem

Penetrator Material: High Strength Steel
Penetrator Material: 12.7 mm
Target: Remolded Eglin Sand
Impact Velocity: 1525 m/sec

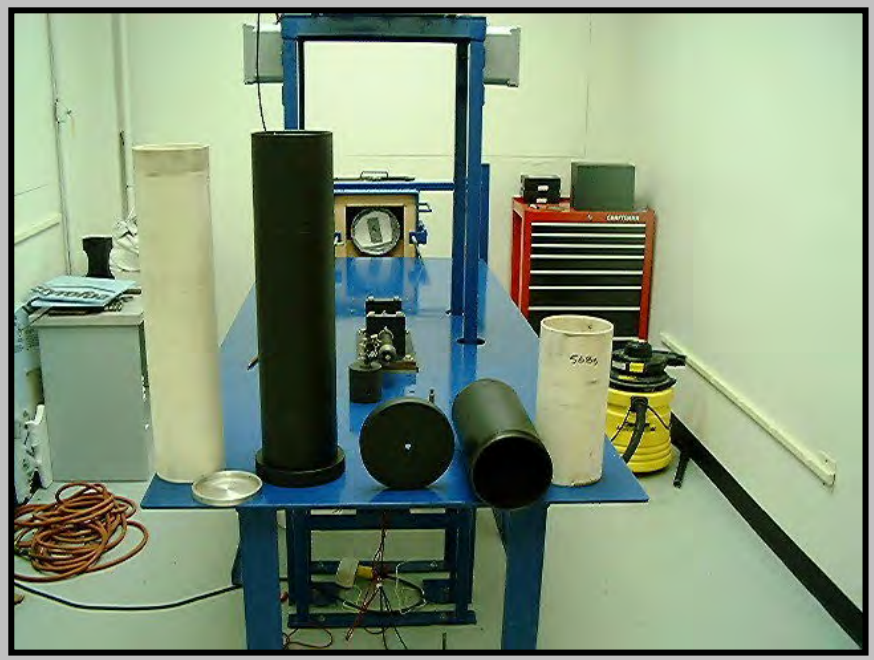


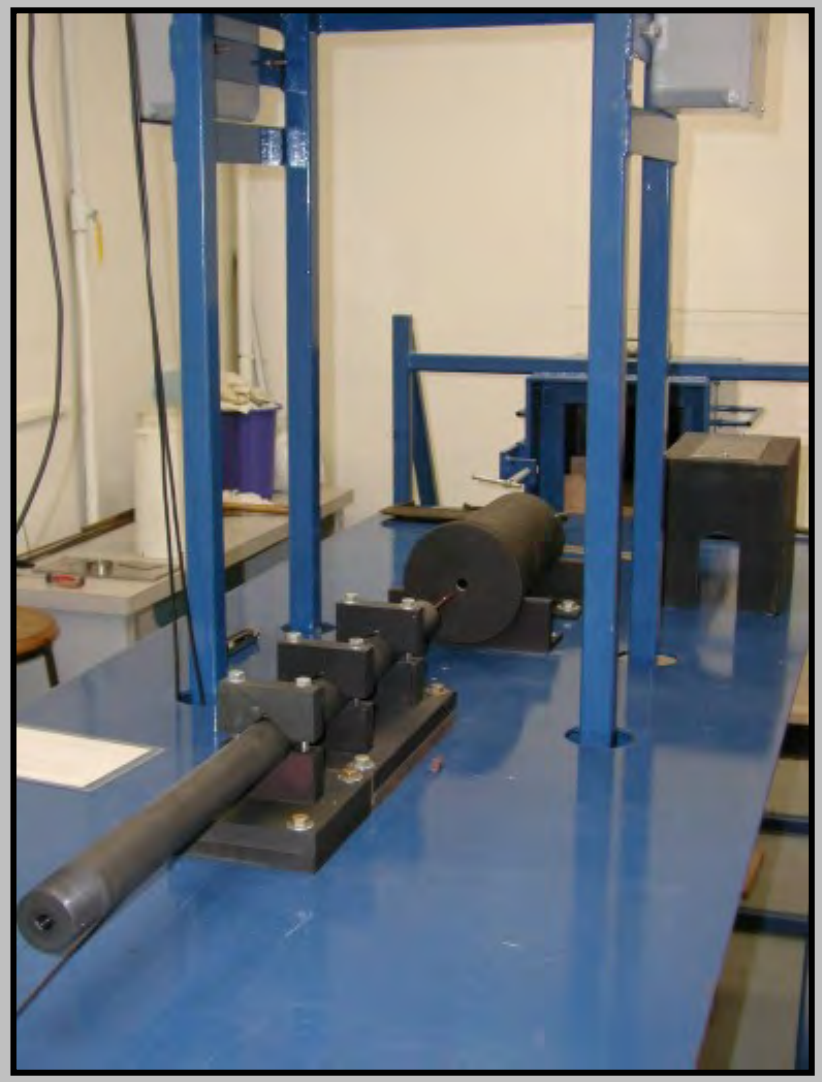
Penetrator Material: 6061-T6 Aluminum
Penetrator Material: 4.17 mm
Target: Alumina Powder
Impact Velocity: 696 m/sec

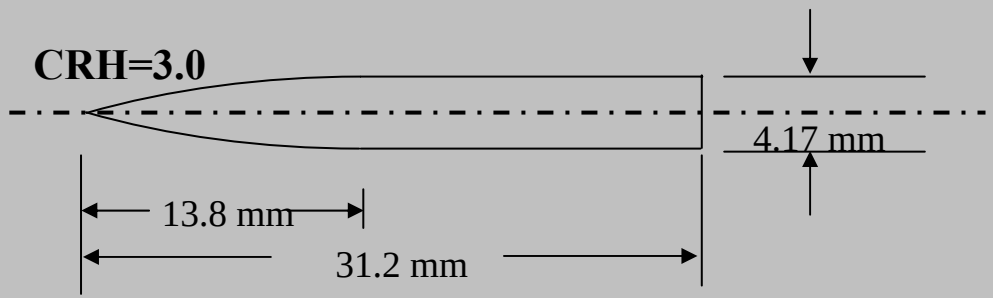


Experimental Data:

University of Alabama Ballistics Facility

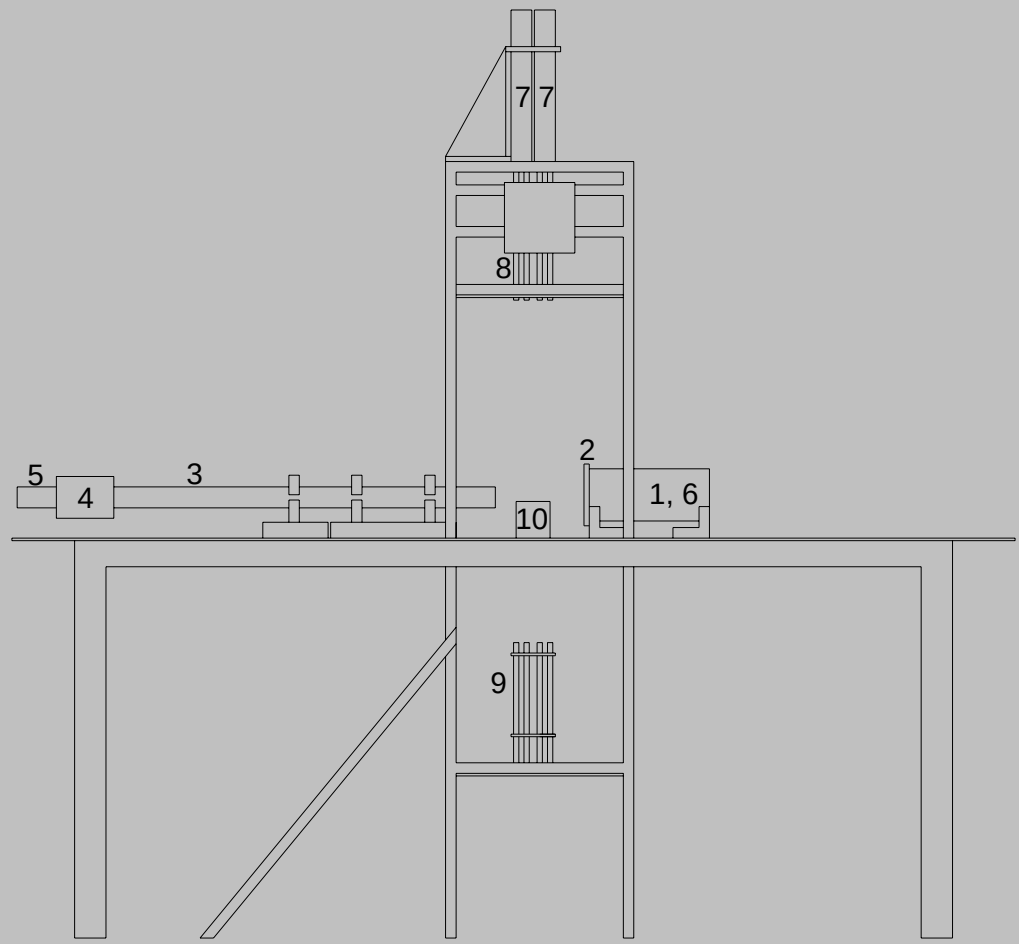






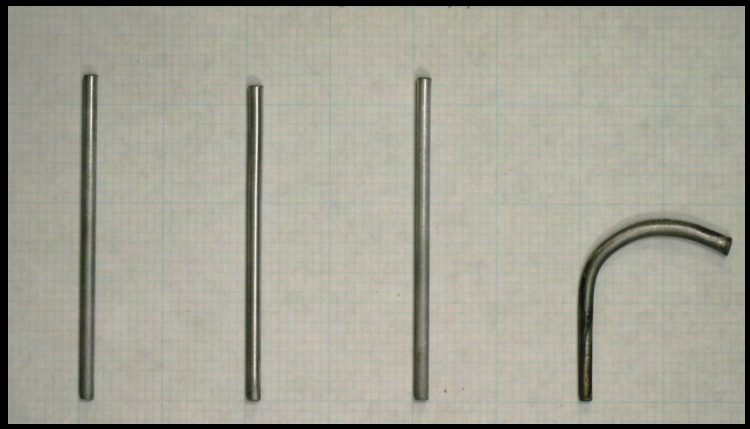
Schematic of Laboratory Penetration Test

1. **Steel target canister**
2. **Steel target face**
3. **Smooth-bore gun tube (167 caliber, 0.167 inch inside diameter bore)**
4. **Breech**
5. **Solenoid driver**
6. **Target sleeve in canister**
7. **Class 3A laser heads**
8. **Lenses which focus the laser beams on the projectile flight path**
9. **Receiving unit for laser beams with photomultiplier tubes**
10. **Small riser to prevent target material from spilling onto the photomultiplier tubes**



Laboratory Scale Penetration Testing

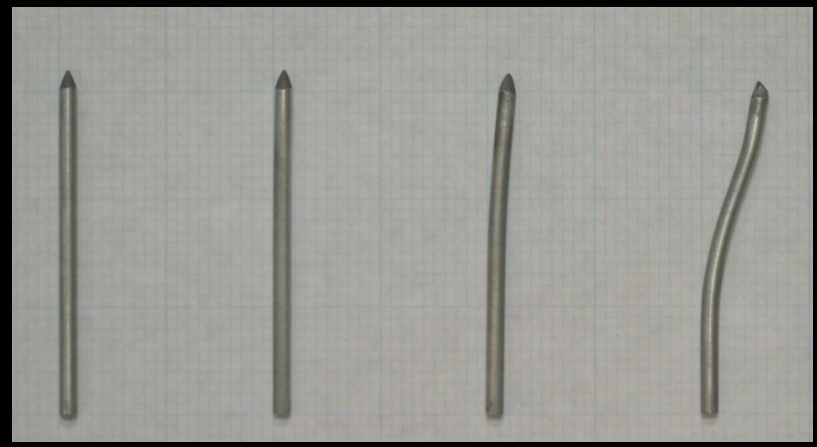
7075-T6 20:1Cylindrical Projectiles in Coarse Foundry Sand



508 m/s 543 m/s 564 m/s 664 m/s

These figures demonstrate the progression of failure occurring after the critical velocity.

6061-T6 CRH 3.0 20:1 Projectiles in Coarse Foundry Sand



475 m/s 513 m/s 574 m/s 639 m/s

Normal Penetration Into Sand

$$P = \gamma \rho_t v_n^2 + R$$ (Pressure)

$$f = \mu P$$ (Friction)

Neglecting friction on the penetrator nose, the total penetration depth >L is

Normal Penetration Into Sand

$$z_f = L + \frac{1}{k}\ell n\left[\frac{e^{-kL_0}\left(v_0^2 + \frac{2\pi a^2 R}{mk} - \frac{4\pi\mu R a}{mk^2}\right) + \frac{4\pi\mu R a}{mk^2}}{\frac{2\pi a^2 R}{mk} + \frac{4\pi\mu R a L_0}{mk}}\right]$$

L = overall penetrator length

L_0 = shank length

$$k = \frac{2\pi a^2 \gamma \rho_t N}{m}$$

$$N = \frac{2}{a^2}\int_0^b \frac{rr'^3}{1+r'^2}dx$$

a= shank radius

b= nose length

μ= friction coefficient

R= target strength factor

m= penetrator mass

p_1= target density

Y= dimensionless drag coefficient

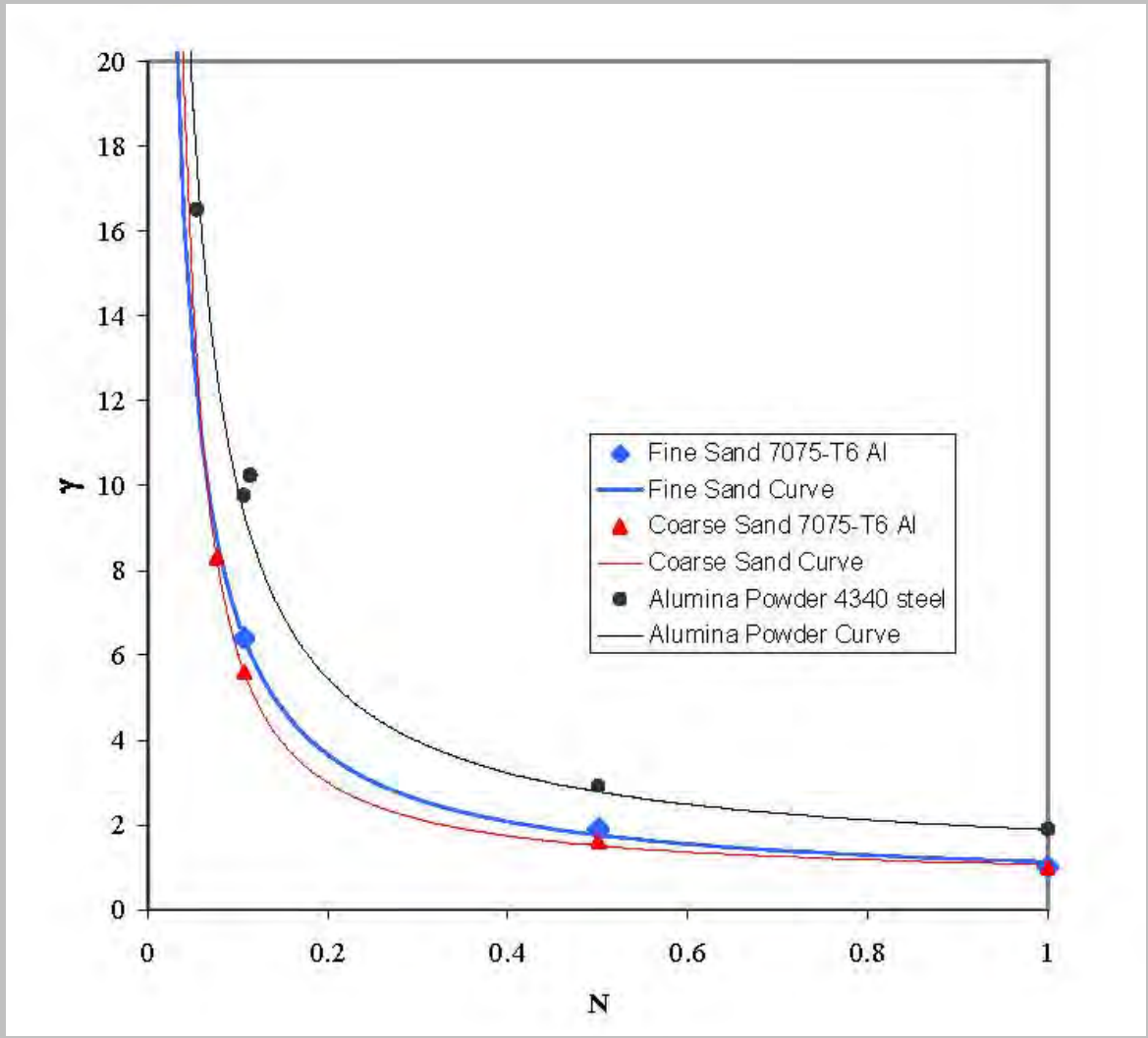
EVALUATION of γ

$$\gamma = \gamma_0 + \gamma_1\left(\frac{1}{N}\right) + \gamma_2\left(\frac{1}{N^2}\right) + \ldots$$

$\gamma = \gamma_0 + \gamma_1\left(\frac{1}{N}\right) + \gamma_2\left(\frac{1}{N^2}\right) + \gamma_3\left(\frac{1}{N^3}\right)$				
	γ_0	γ_1	γ_2	γ_3
Coarse Foundry Sand	0.660	0.397	0.140	0
Fine Foundry Sand	0.500	0.630	0	0
Alumina Powder	1.000	0.891	0	0

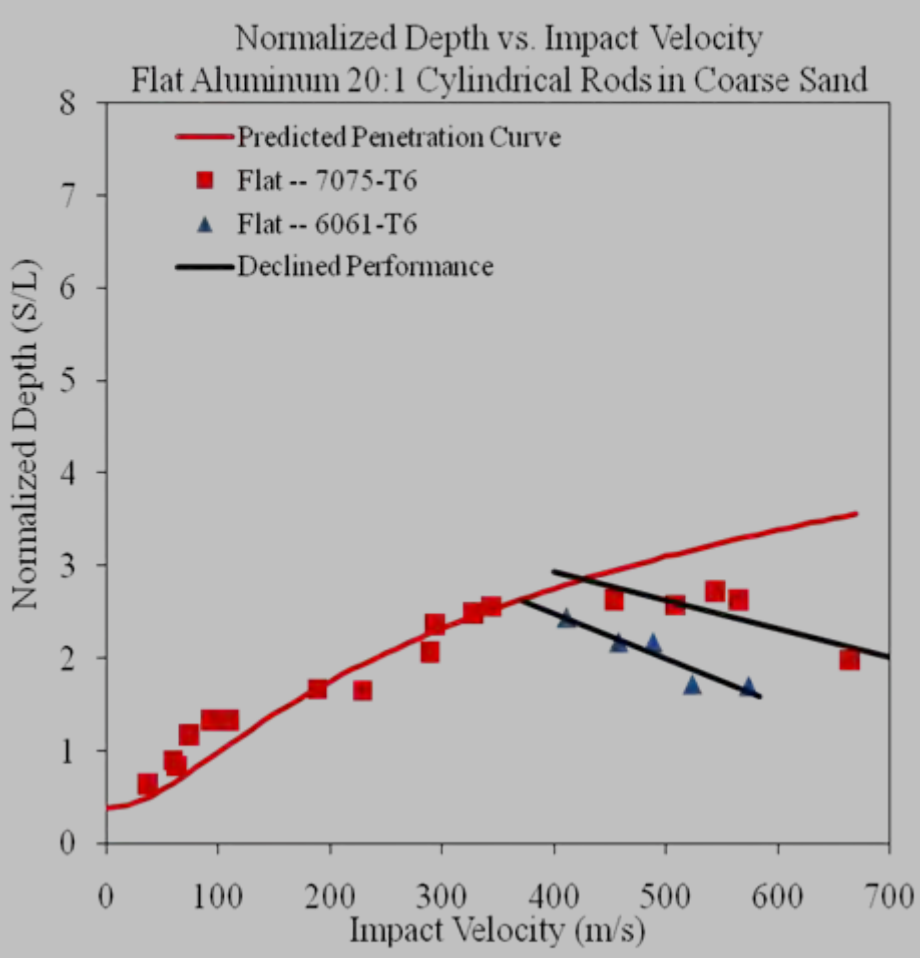
Summary of γ coefficients for three target media

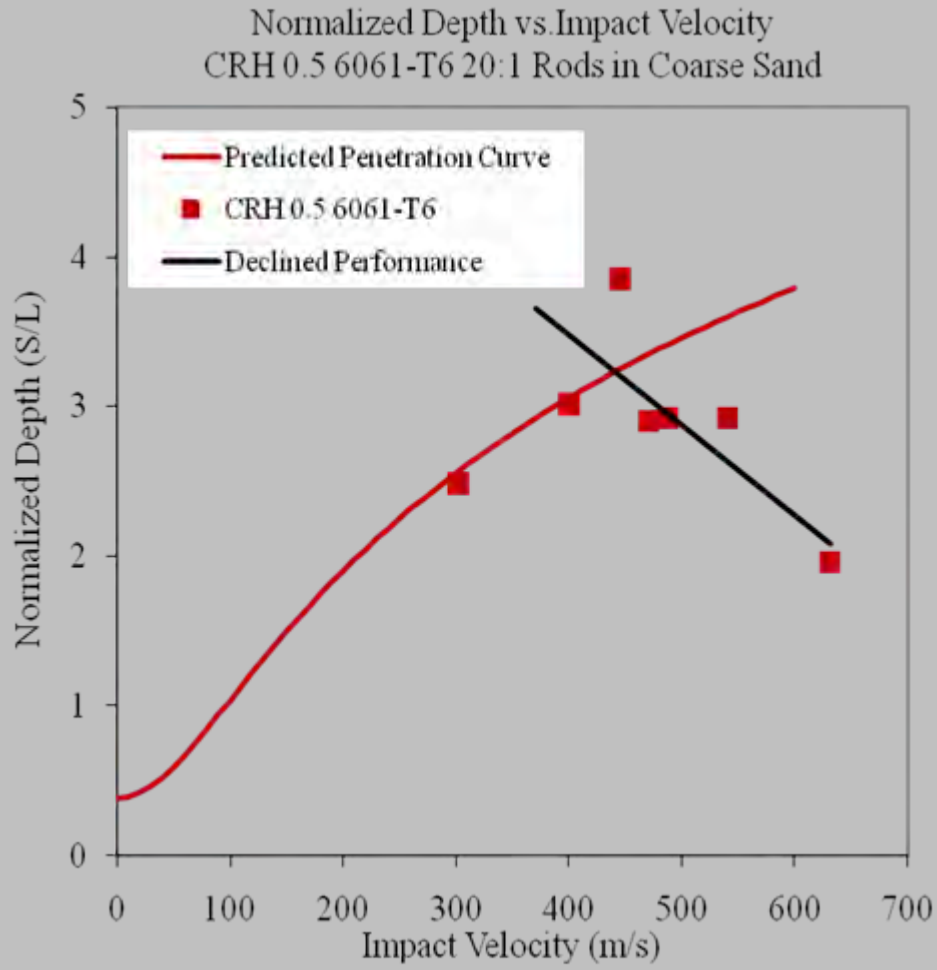
EVALUATION of γ



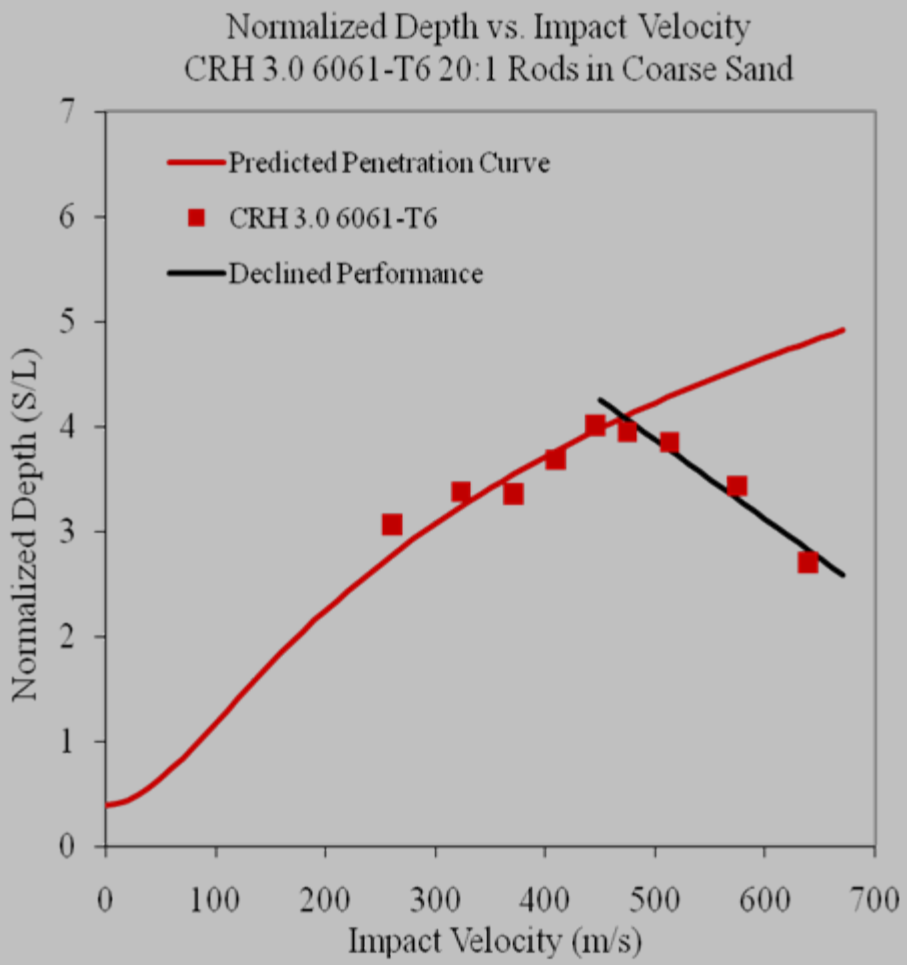
Graph of γ vs. N for each target medium

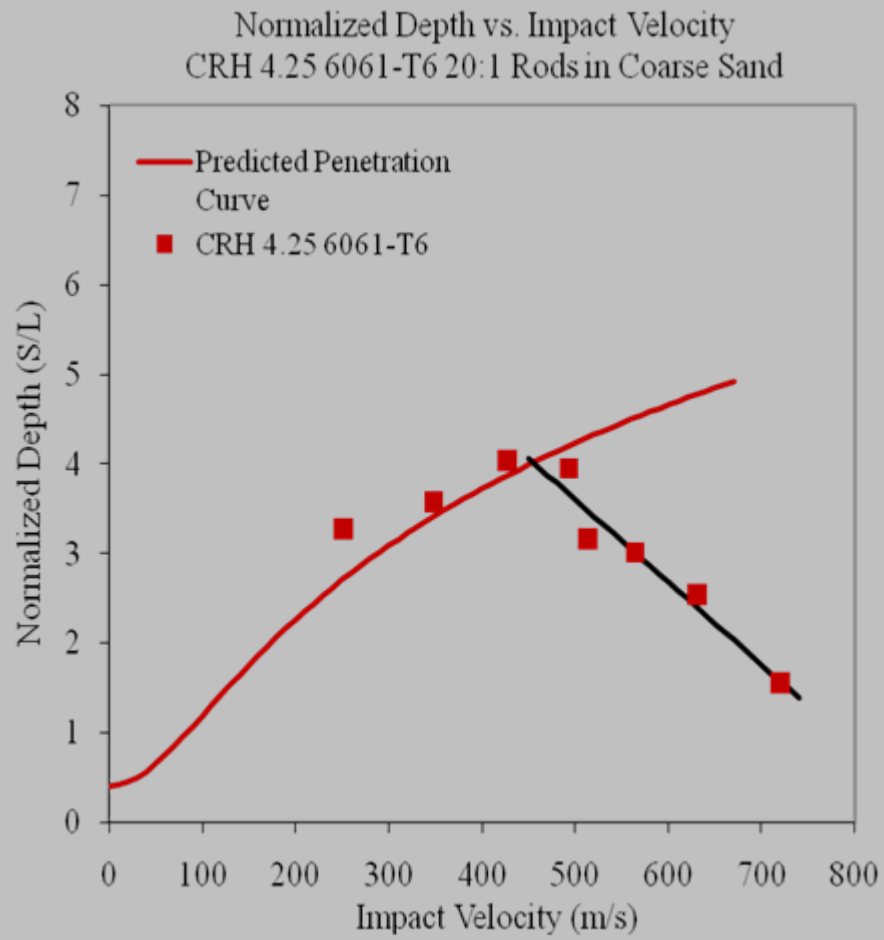
EVALUATION of γ



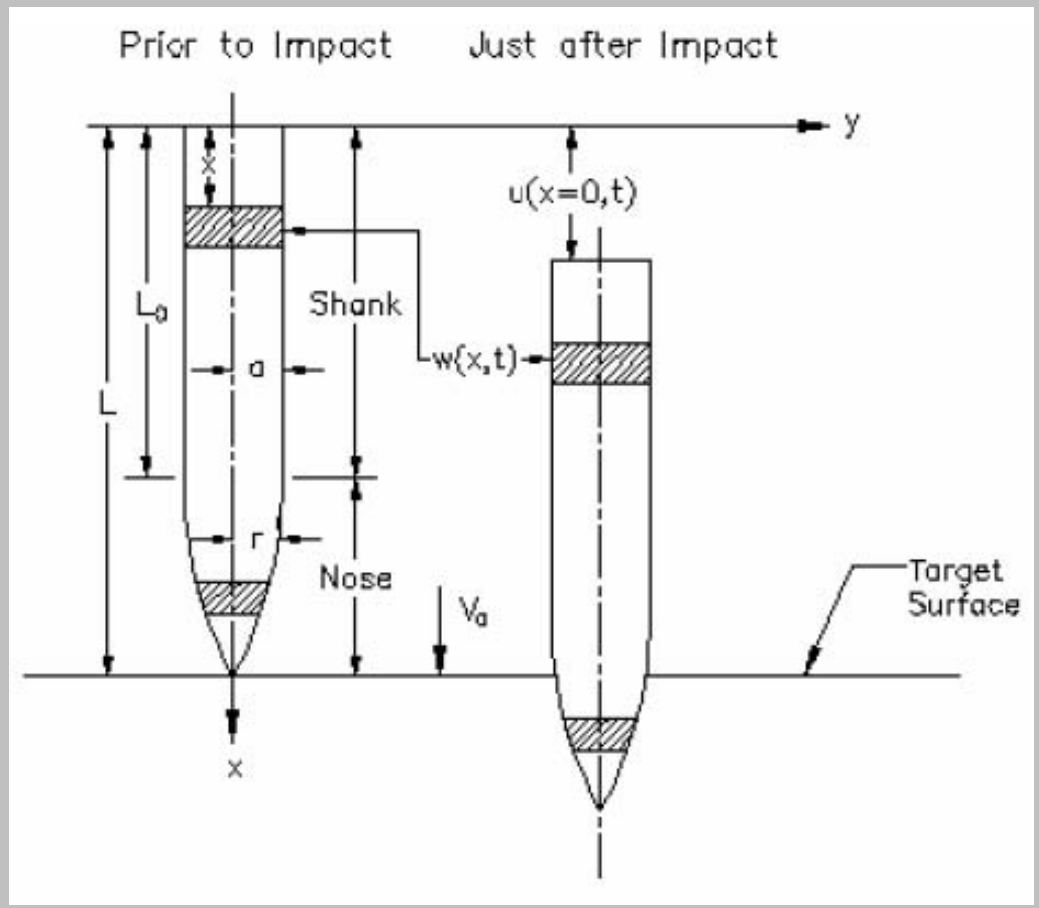


EVALUATION of γ





Formulation and Solution of the Problem



The Lagrangian coordinate system

Formulation and Solution of the Problem

$$\rho \pi r^2 \frac{\partial^2 u}{\partial t^2} = \frac{\partial P}{\partial x}$$

$$\rho \pi r^2 \frac{\partial^2 w}{\partial t^2} = \frac{\partial Q}{\partial x}$$

$$\rho \pi r^2 \frac{\partial^2 w}{\partial t^2} + \frac{\partial^2}{\partial x^2}\left(EI \frac{\partial^2 w}{\partial x^2} \right) - \frac{\partial}{\partial x}\left(P \frac{\partial w}{\partial x} \right) = 0$$

Longitudinal Force

$$m\dot{v}_G = -F(v_G(t))$$

$$\frac{\partial^2 u}{\partial t^2} = \dot{v}_G$$

$$\frac{\partial P}{\partial x} = \rho \pi r^2 \dot{v}_G \qquad 0 < x < L$$

Longitudinal Force

$$P(x,t) = \rho\pi a^2 \dot{v}_G x$$

$$0 < x < L_0$$

$$P(L_0,t) = \rho\pi a^2 \dot{v}_G L_0$$

$$P(x,t) = \rho\pi a^2 \dot{v}_G L_0 + \rho\pi \dot{v}_G \int_{L_0}^{x} r^2(x)dx$$

$$L_0 < x < L$$

Lateral Motion

$$\rho\pi a^2 \frac{\partial^2 w}{\partial t^2} + \frac{\partial^2}{\partial x^2}\left(EI \frac{\partial^2 w}{\partial x^2} \right) - \frac{\partial}{\partial x}\left(\rho\pi a^2 \dot{v}_G x \frac{\partial w}{\partial x} \right) = 0$$

$$0 < x < L_0$$

$$\rho\pi r^2 \frac{\partial^2 w}{\partial t^2} + \frac{\partial^2}{\partial x^2}\left(EI \frac{\partial^2 w}{\partial x^2} \right) - \frac{\partial}{\partial x}\left(\rho\pi \dot{v}_G (a^2 L_0 + \int_{L_0}^{x} r^2(x)dx) \frac{\partial w}{\partial x} \right) = 0$$

$$L_0 < x < L$$

Homogeneous Boundary Conditions

$$\frac{\partial^2 w}{\partial x^2}(0,t) = \frac{\partial^3 w}{\partial x^3}(0,t) = 0$$

$$w(L,t) = 0$$

$$\frac{\partial^2 w}{\partial x^2}(L,t) = 0$$

Dimensionless Variables

$$\xi = \frac{x}{L} \qquad \beta = \frac{r(x)}{a} \qquad z = \frac{w}{a} \qquad \tau = \frac{v_0 t}{L}$$

$$\frac{EI}{\rho \pi a^2 v_0^2 L^2} \frac{\partial^4 z}{\partial \xi^2} + \frac{\partial^2 z}{\partial \tau^2} - \frac{L \dot{v}_G}{v_0^2} \frac{\partial}{\partial \xi} \left(\xi \frac{\partial z}{\partial \xi} \right) = 0$$

$$0 < \xi < \xi_0$$

$$\frac{Ea^2}{\rho \pi v_0^2 L^2 \beta^2} \frac{\partial^2}{\partial \xi^2} \left(\frac{I}{a^4} \frac{\partial^2 z}{\partial \xi^2} \right) + \frac{\partial^2 z}{\partial \tau^2} - \frac{L \dot{v}_G}{\beta^2 v_0^2} \frac{\partial}{\partial \xi} \left(\left(\xi_0 + \int_{\xi_0}^{\xi} \beta^2 d\xi \right) \frac{\partial z}{\partial \xi} \right) = 0$$

$$\xi_0 < \xi < 1$$

Deceleration Approximation

$$\dot{v}_G = -\frac{F}{m} \cong -\frac{\pi a^2 \gamma \rho_t N v_0^2}{m}$$

Separation of Variables

$$z = \Phi(\xi)T(\tau) \qquad \ddot{T} + \omega T = 0$$

$$\frac{EI}{\rho\pi a^2 v_0^2 L^2}\frac{d^4\Phi}{d\xi^4} - \omega\Phi + \frac{L\pi a^2\gamma\rho_t N}{m}\frac{d}{d\xi}\left(\xi\frac{d\Phi}{d\xi}\right) = 0$$

$$0 < \xi < \xi_0$$

$$\frac{Ea^2}{\rho\pi v_0^2 L^2\beta^2}\frac{d^2}{d\xi^2}\left(\frac{I}{a^4}\frac{d^2\Phi}{d\xi^2}\right) - \omega\Phi + \frac{L\pi a^2\gamma\rho_t N}{m\beta^2}\frac{d}{d\xi}\left(\left(\xi_0 + \int_{\xi_0}^{\xi}\beta^2 d\xi\right)\frac{d\Phi}{d\xi}\right) = 0$$

$$\xi_0 < \xi < 1$$

Boundary Conditions

$$\frac{d^2\Phi}{d\xi^2}(0) = \frac{d^3\Phi}{d\xi^3}(0) = 0$$

$$\Phi(1) = \frac{d^2\Phi}{d\xi^2}(1) = 0$$

Separation of Variables

$$\lambda \frac{d^4\Phi}{d\xi^4} - \omega\Phi + \eta \frac{d}{d\xi}\left(\xi \frac{d\Phi}{d\xi} \right) = 0$$

$$0 < \xi < \xi_0$$

$$\lambda \frac{d^2}{d\xi^2}\left(\beta^4 \frac{d^2\Phi}{d\xi^2} \right) - \omega\beta^2\Phi + \eta \frac{d}{d\xi}\left(\left(\xi_0 + \int_{\xi_0}^{\xi} \beta^2 d\xi \right) \frac{d\Phi}{d\xi} \right) = 0$$

$$\xi_0 < \xi < 1$$

$$\lambda = \frac{EI_S}{\rho\pi a^2 v_0^2 L^2}$$

$$\eta = \frac{\pi L a^2 \gamma \rho_t N}{m}$$

Orthogonality of the Eigenfunctions

Consider, for simplicity, the case for a flat-ended cylinder.

$$\lambda \frac{d^4 \Phi_n}{d\xi^4} + \eta \frac{d}{d\xi}\left(\xi \frac{d\Phi_n}{d\xi} \right) - \omega_n \Phi_n = 0$$

It is not difficult to show that

$$\int_0^1 \Phi_m \Phi_n d\xi = 0 \qquad m \neq n$$

$$\omega_n = \frac{\lambda \int_0^1 \left(\frac{d^2 \Phi_n}{d\xi^2} \right)^2 d\xi - \eta \int_0^1 \xi \left(\frac{d\Phi_n}{d\xi} \right)^2 d\xi}{\int_0^1 \Phi_n^2 d\xi}$$

Orthogonality of the Eigenfunctions

Consider

$$\omega = \frac{\lambda \int_0^1 \left(\frac{d^2\Phi}{d\xi^2} \right)^2 d\xi - \eta \int_0^1 \xi \left(\frac{d\Phi}{d\xi} \right)^2 d\xi}{\int_0^1 \Phi^2 d\xi}$$

$$\Phi = k_1\Phi_1 + k_2\Phi_2 + \ldots$$

Orthogonality of the Eigenfunctions

$$\omega = \frac{\omega_1 k_1^2 \int_0^1 \Phi_1^2 d\xi + \omega_2 k_2^2 \int_0^1 \Phi_2^2 d\xi + \ldots + \omega_n k_n^2 \int_0^1 \Phi_n^2 d\xi + \ldots}{k_1^2 \int_0^1 \Phi_1^2 d\xi + k_2^2 \int_0^1 \Phi_2^2 d\xi + \ldots + k_n^2 \int_0^1 \Phi_n^2 d\xi + \ldots}$$

The Stationary Values achieved by this quotient are the Eigenvalues $\omega_1, \omega_2, \ldots$

Ogive Noses

$$\omega_n = \frac{\lambda\left[\int_0^{\xi_0}\left(\frac{d^2\Phi_n}{d\xi^2}\right)^2 d\xi + \int_0^1 \beta^4\left(\frac{d^2\Phi_n}{d\xi^2}\right)^2 d\xi\right] - \eta\left[\int_0^{\xi_0}\xi\left(\frac{d\Phi_n}{d\xi}\right)^2 d\xi + \int_{\xi_0}^1\left(\xi_0 + \int_{\psi_0}^{\xi}\beta^2 d\xi\right)\left(\frac{d\Phi_n}{d\xi}\right)^2 d\xi\right]}{\int_0^{\xi_0}\Phi_n^2 d\xi + \int_{\xi_0}^1 \beta^2\Phi_n^2 d\xi}$$

$$\beta'(\xi_0) = 0$$

Stability Criterion

$$\omega_1 = \frac{\lambda\left[\int_0^{\xi_0}\left(\frac{d^2\Phi_1}{d\xi^2}\right)^2 d\xi + \int_{\xi_0}^{1}\beta^4\left(\frac{d^2\Phi_1}{d\xi^2}\right)^2 d\xi\right] - \eta\left[\int_0^{\xi_0}\xi\left(\frac{d\Phi_1}{d\xi}\right)^2 d\xi + \int_{\xi_0}^{1}\left(\xi_0 + \int_{\xi_0}^{\xi}\beta^2 d\xi\right)\left(\frac{d\Phi_1}{d\xi}\right)^2 d\xi\right]}{\int_0^{\xi_0}\Phi_1^2 d\xi + \int_{\xi_0}^{1}\beta^2\Phi_1^2 d\xi} > 0$$

where ω_1 is the lowest eigenvalue and Φ_1 is the corresponding eigenfunction

Trial Functions

$$\Phi = 1 - \frac{5}{2}\xi^4 + \frac{3}{2}\xi^5 + \left(\xi - \frac{5}{2}\xi^4 + \frac{3}{2}\xi^5\right)C_1 + \left(1 - \frac{20}{3}\xi^4 + 9\xi^5 - \frac{10}{3}\xi^6\right)C_2$$

Choose C_1 and C_2 so that a minimum in the quotient is achieved.

Results

Critical Velocity of 20:1 6061 T-6 Aluminum into Course Foundry Sand				
	Flat	CRH 0.5	CRH 3.0	CRH 4.25
Two Constant Estimate	384.03 (m/s)	405 (m/s)	452 (m/s)	450.2 (m/s)
Experimental	375 (m/s)	435 (m/s)	475 (m/s)	445 (m/s)

Critical Velocity Comparisons

Critical Velocity of 20:1 6061 T-6 Aluminum into Course Foundry Sand				
	Flat	CRH 0.5	CRH 3.0	CRH 4.25
One Constant Estimate	495.25 (m/s)	522.32 (m/s)	589.265 (m/s)	613.934 (m/s)
Two Constant Estimate	384.03 (m/s)	405 (m/s)	452 (m/s)	450.2 (m/s)
Torres Estimate	406 (m/s)	421 (m/s)	472 (m/s)	468 (m/s)

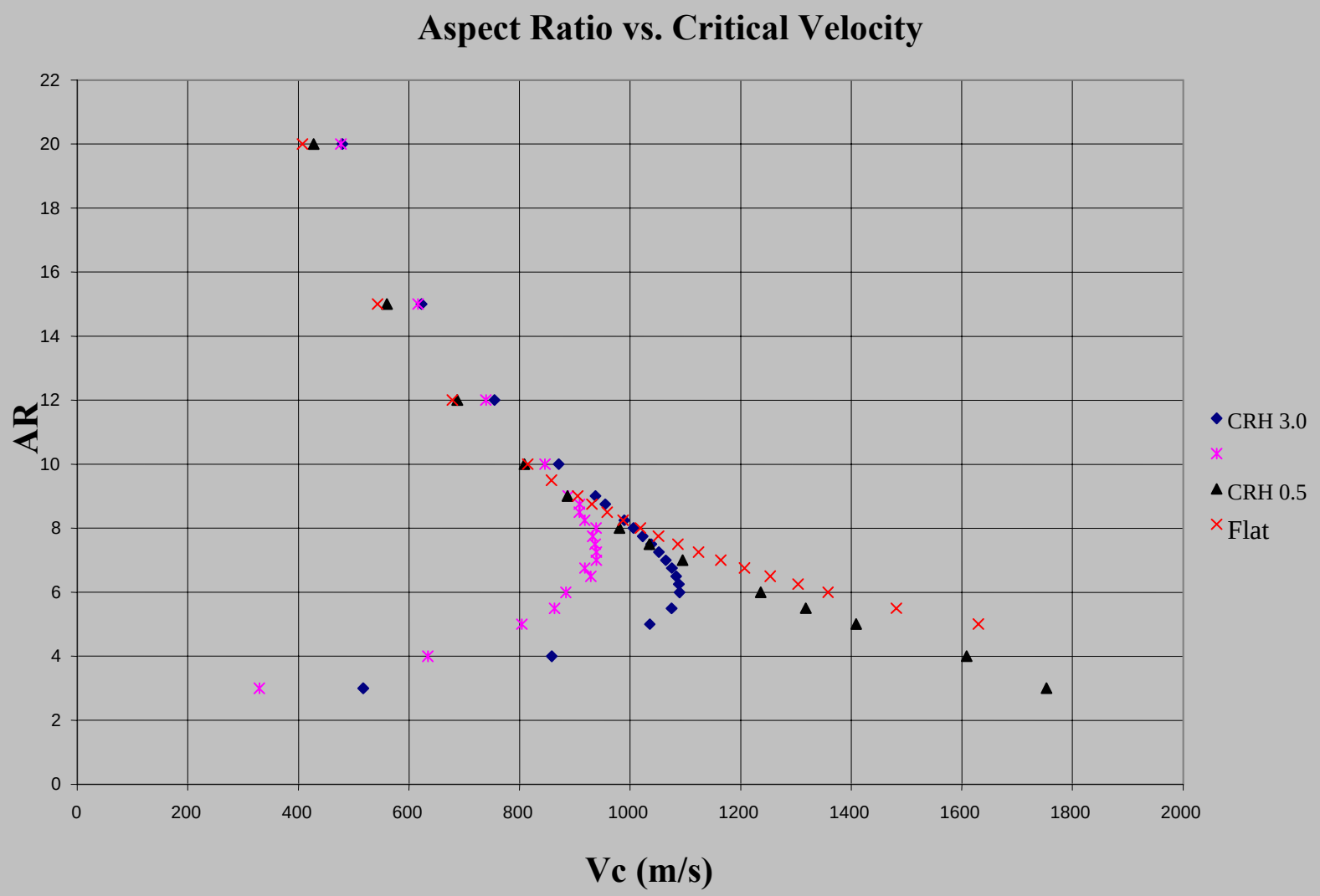
Theory Comparisons

Results

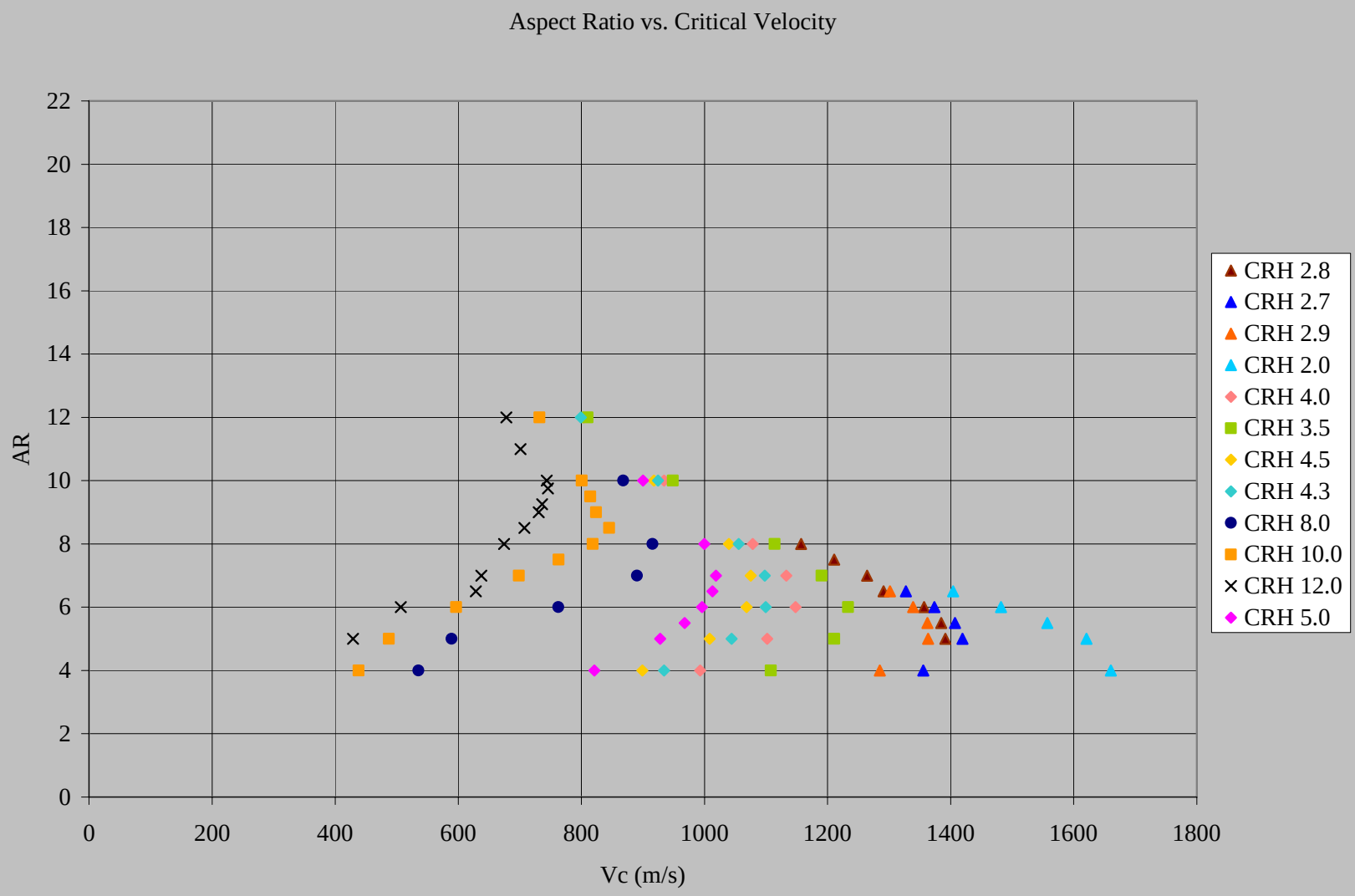
7075- T6 Aluminum CRH 12 into Course Foundry Sand		
	8:1	12:1
One Constant Estimate	819.13 (m/s)	822.76 (m/s)
Two Constant Estimate	679.17 (m/s)	683.14 (m/s)
Torres Estimate	680 (m/s)	680 (m/s)
Experimental Result	700 (m/s)	690 (m/s)

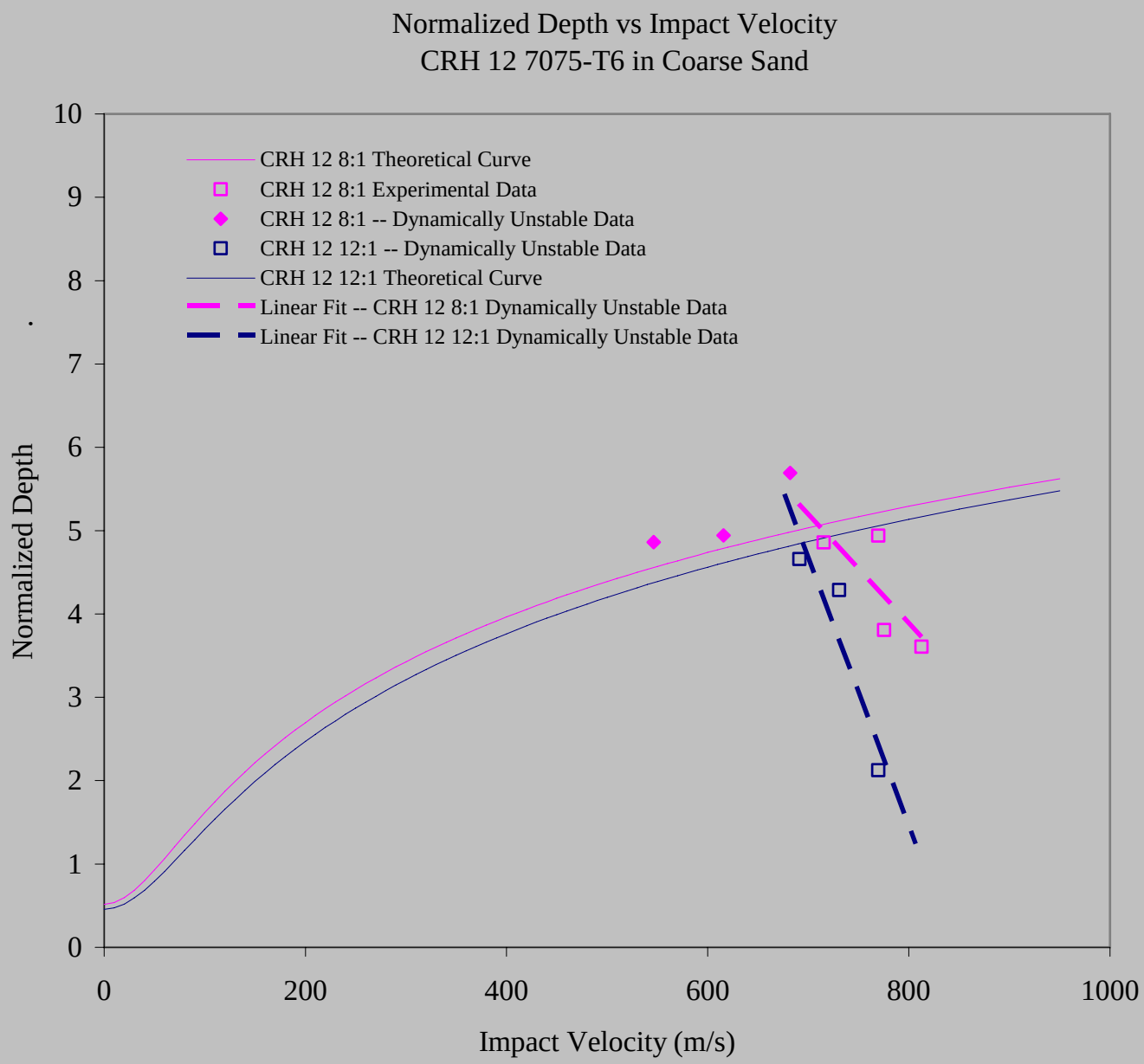
More Theory Comparisons

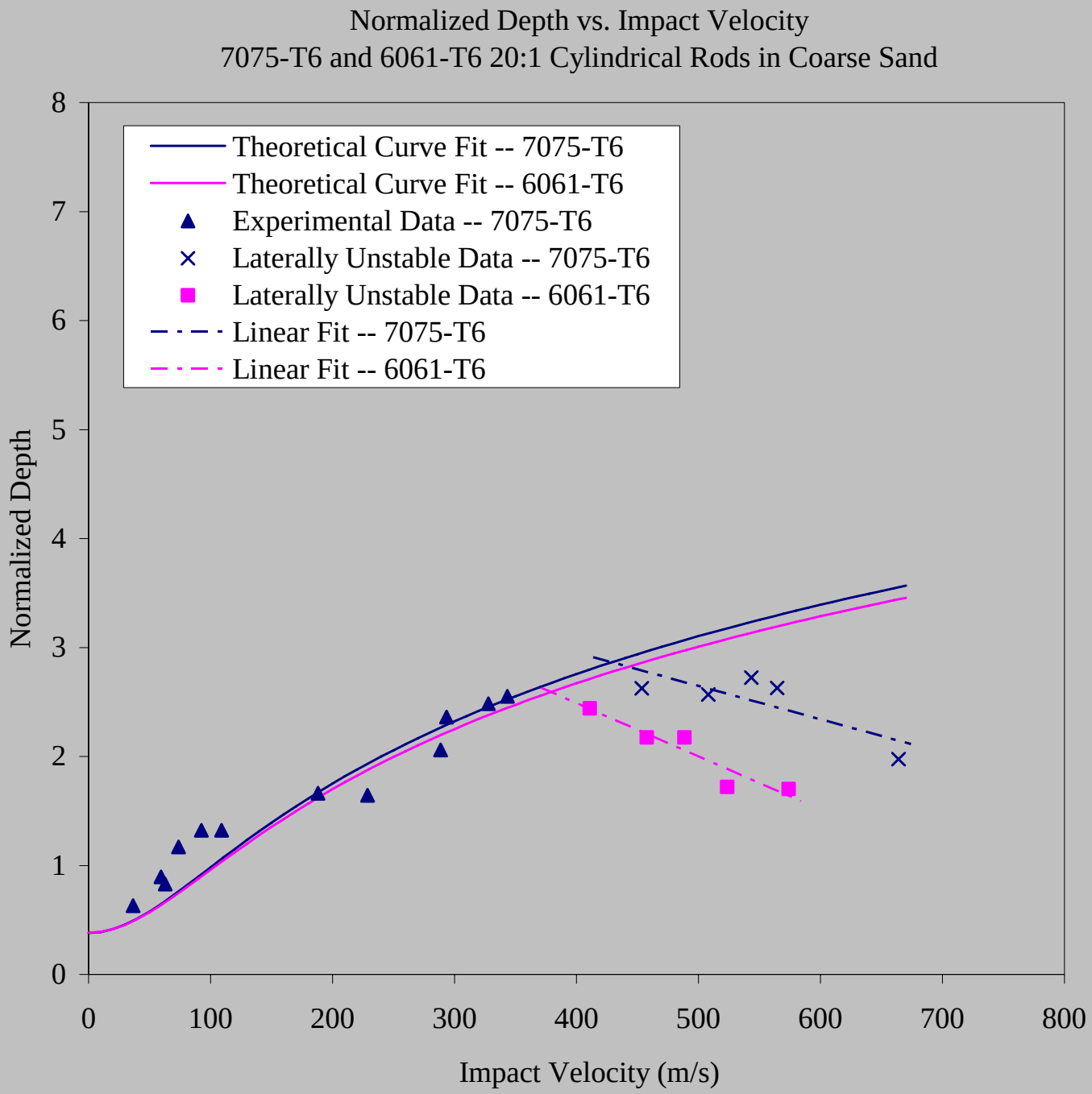
Results

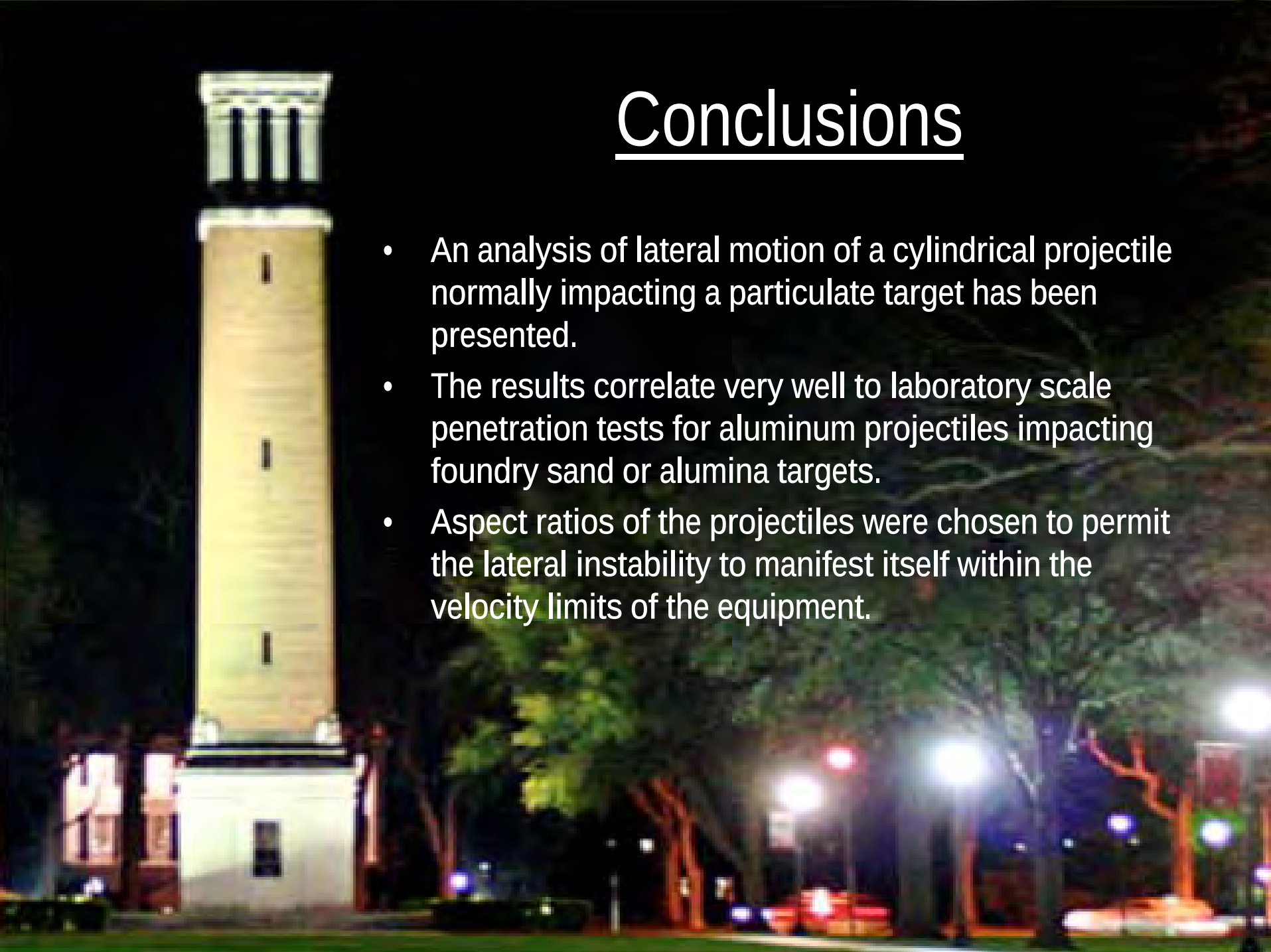

Aspect Ratio vs. Critical Velocity
AR
Vc (m/s)
0
2
4
6
8
10
12
14
16
18
20
22
0
200
400
600
800
1000
1200
1400
1600
1800
2000
CRH 3.0
CRH 0.5
Flat

Results


Aspect Ratio vs. Critical Velocity
AR
Vc (m/s)
0
2
4
6
8
10
12
14
16
18
20
22
0
200
400
600
800
1000
1200
1400
1600
1800
CRH 2.8
CRH 2.7
CRH 2.9
CRH 2.0
CRH 4.0
CRH 3.5
CRH 4.5
CRH 4.3
CRH 8.0
CRH 10.0
CRH 12.0
CRH 5.0

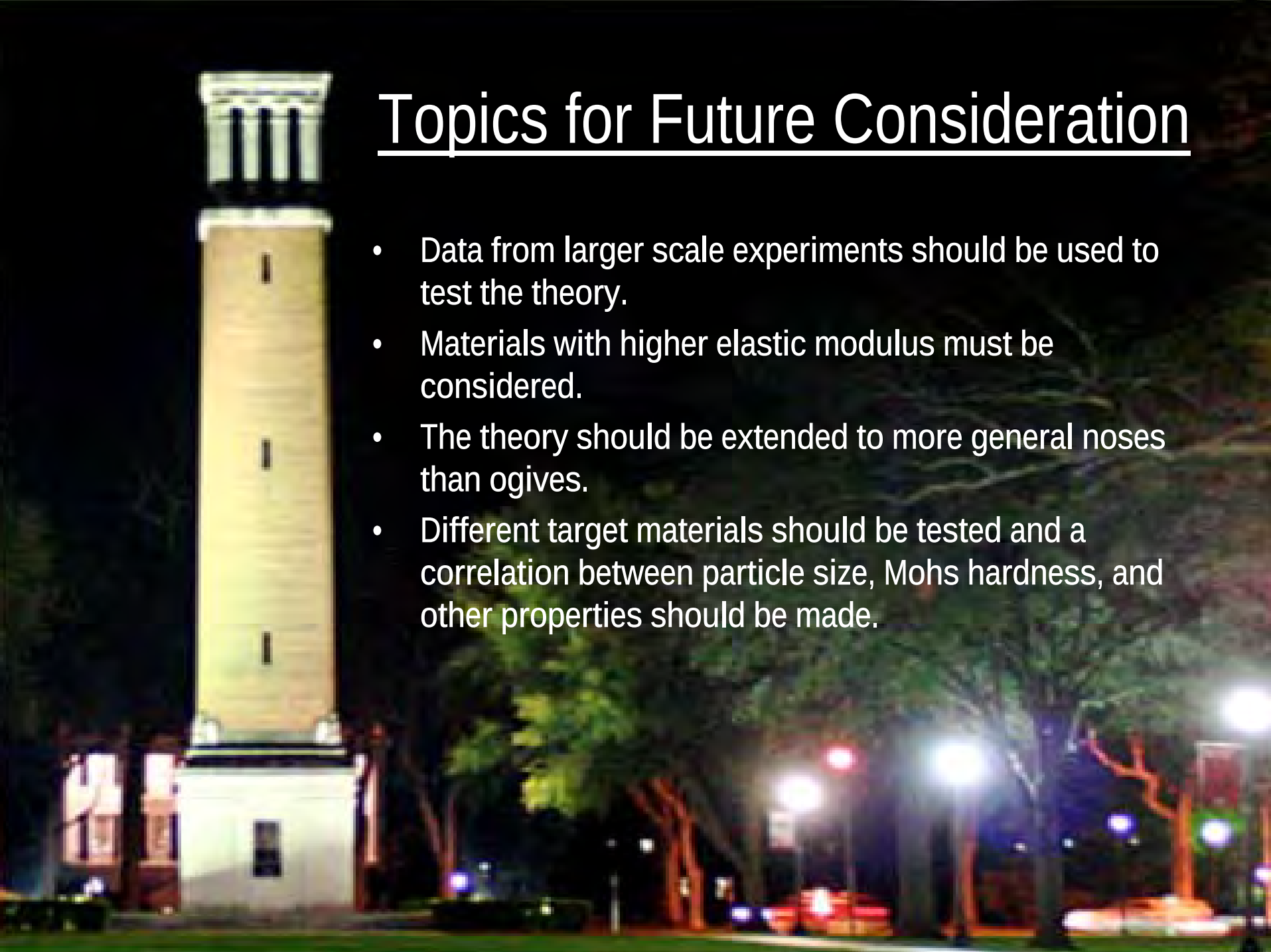

Normalized Depth vs Impact Velocity
CRH 12 7075-T6 in Coarse Sand
CRH 12 8:1 Theoretical Curve
CRH 12 8:1 Experimental Data
CRH 12 8:1 -- Dynamically Unstable Data
CRH 12 12:1 -- Dynamically Unstable Data
CRH 12 12:1 Theoretical Curve
Linear Fit -- CRH 12 8:1 Dynamically Unstable Data
Linear Fit -- CRH 12 12:1 Dynamically Unstable Data
Normalized Depth
Impact Velocity (m/s)
0
1
2
3
4
5
6
7
8
9
10
0
200
400
600
800
1000


Normalized Depth vs. Impact Velocity
7075-T6 and 6061-T6 20:1 Cylindrical Rods in Coarse Sand
Theoretical Curve Fit -- 7075-T6
Theoretical Curve Fit -- 6061-T6
Experimental Data -- 7075-T6
Laterally Unstable Data -- 7075-T6
Laterally Unstable Data -- 6061-T6
Linear Fit -- 7075-T6
Linear Fit -- 6061-T6
Normalized Depth
0
1
2
3
4
5
6
7
8
0
100
200
300
400
500
600
700
800
Impact Velocity (m/s)



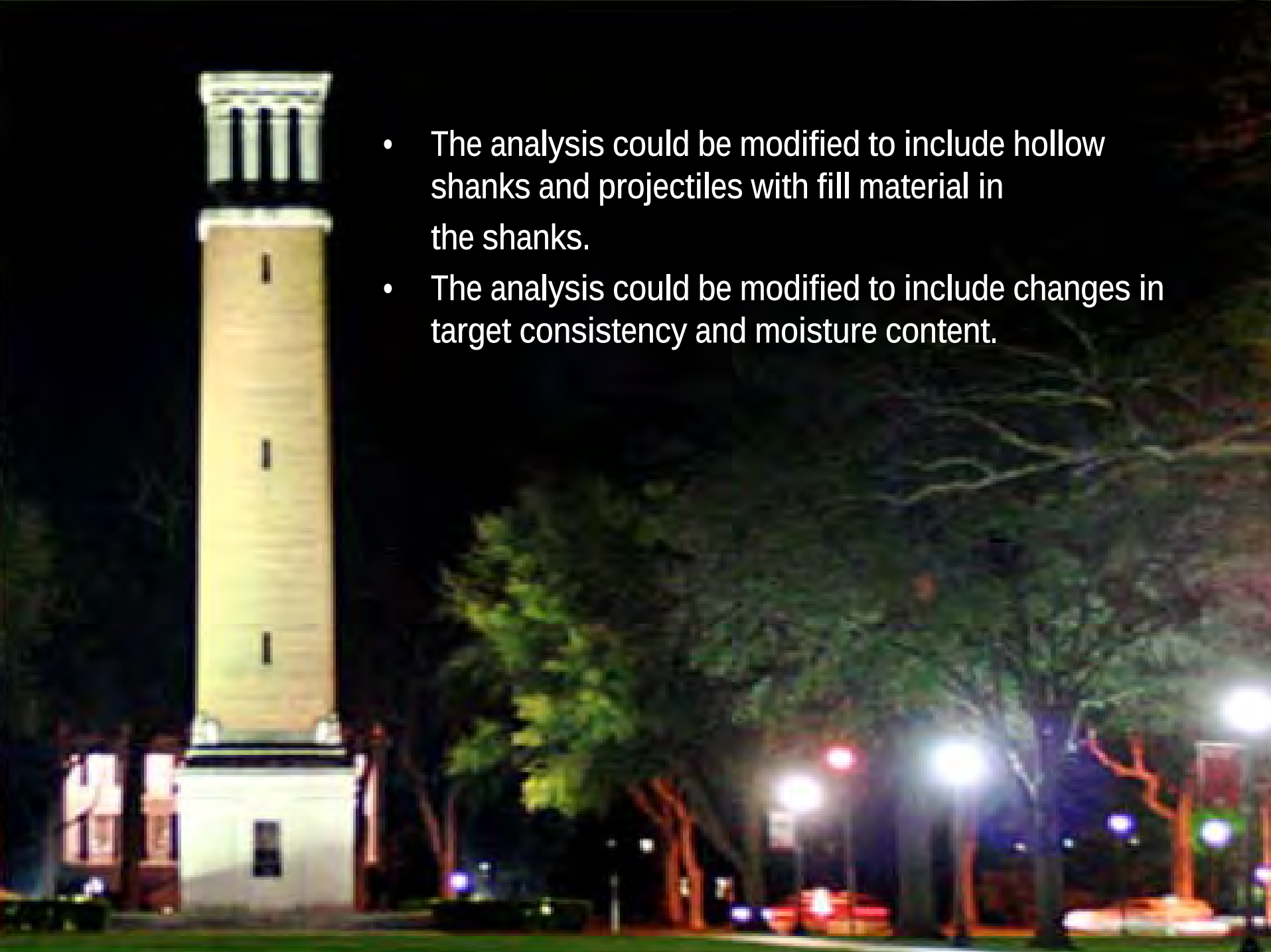
Conclusions

- An analysis of lateral motion of a cylindrical projectile normally impacting a particulate target has been presented.
- The results correlate very well to laboratory scale penetration tests for aluminum projectiles impacting foundry sand or alumina targets.
- Aspect ratios of the projectiles were chosen to permit the lateral instability to manifest itself within the velocity limits of the equipment.



Topics for Future Consideration

- Data from larger scale experiments should be used to test the theory.
- Materials with higher elastic modulus must be considered.
- The theory should be extended to more general noses than ogives.
- Different target materials should be tested and a correlation between particle size, Mohs hardness, and other properties should be made.



- The analysis could be modified to include hollow shanks and projectiles with fill material in the shanks.
- The analysis could be modified to include changes in target consistency and moisture content.

SHAPED CHARGE PENETRATION INTO GAS SATURATED SANDSTONE

Jeremy Harvey, Brenden Grove

24th International Symposium on Ballistics

New Orleans, LA

September 26, 2008

Schlumberger

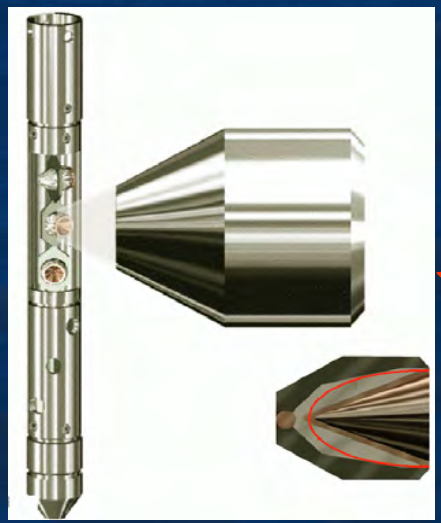
Overview

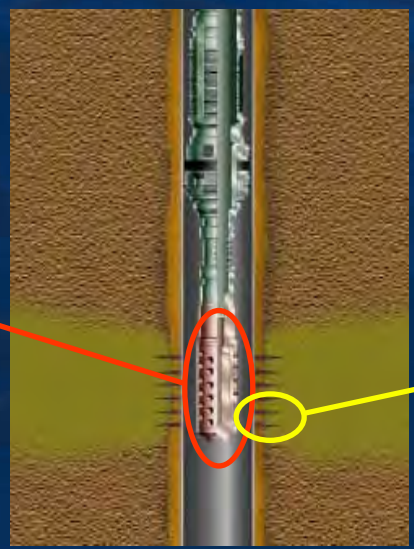
- Introduction / Background
- Recent Experiments
- Conclusions & Future Work

Schlumberger

Introduction

- Oilwell perforators
  - small caliber shaped charges
  - create the pathway for oil or gas to flow from the reservoir rock into the wellbore
- Deep, clean perforations required for well productivity







Schlumberger

Introduction

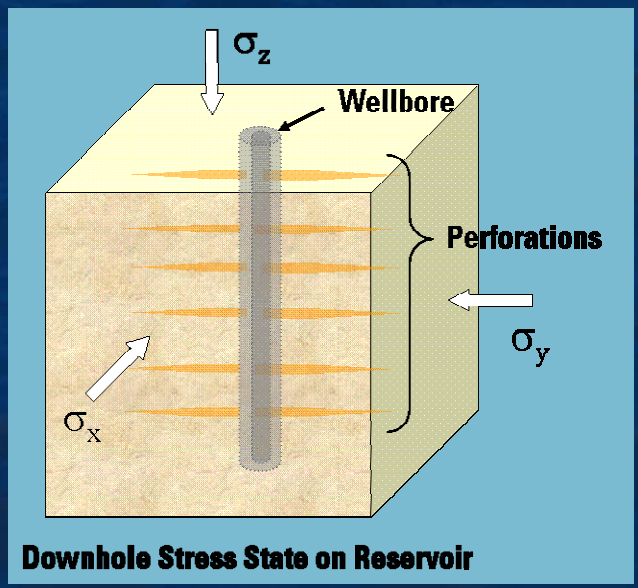
- Reservoir properties influencing perforation depth:
  - Rock strength
  - In-situ stresses (overburden, tectonic)
  - Pore fluid pressure
  - Pore fluid type (liquid vs. gas)

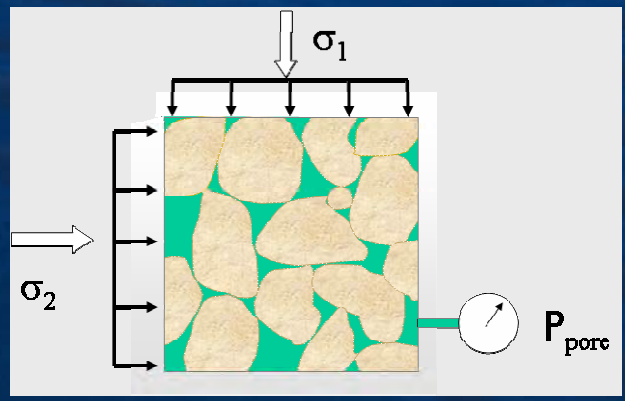
Background

- Geomechanics considerations:
  - In-situ stresses ("total" stress)
  - Pore fluid pressure

Effective stress

$$\sigma_{eff} = (\sigma_{mean} - a * P_p)$$

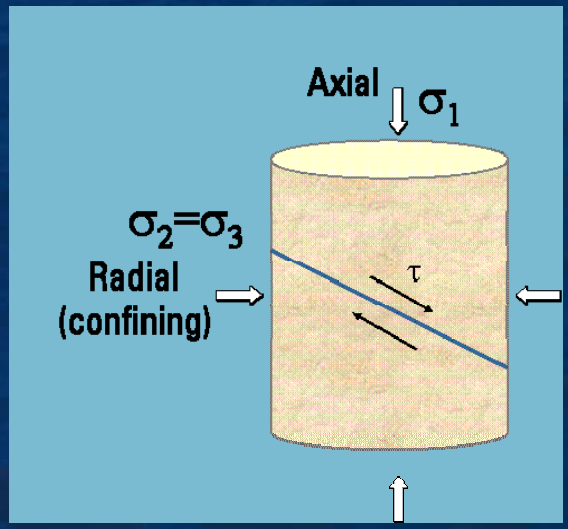


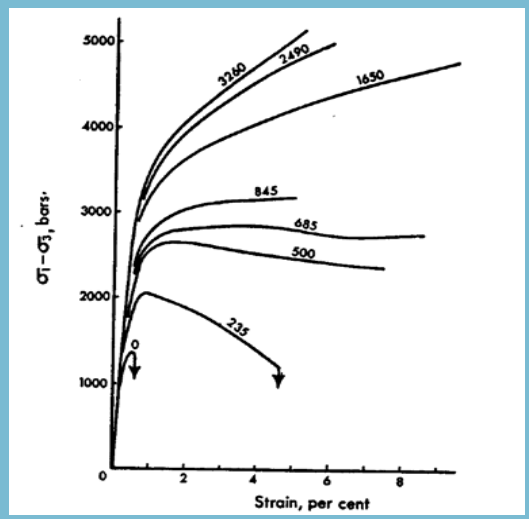


Schlumberger

Background

- Why is in-situ stress important to SC penetration?
  - Rocks are stronger under increasing applied stress





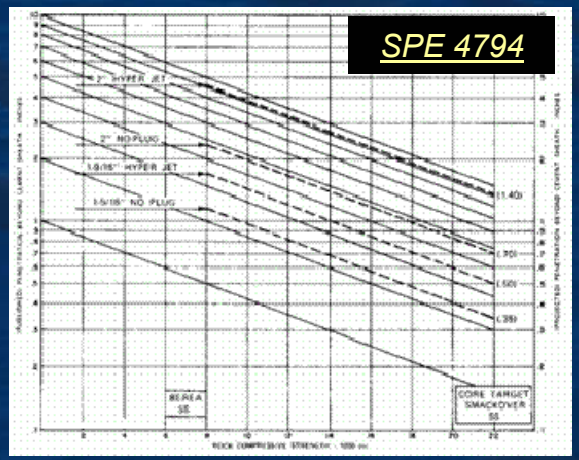
$$\tau = f(\sigma_{mean})$$

Schlumberger

Background

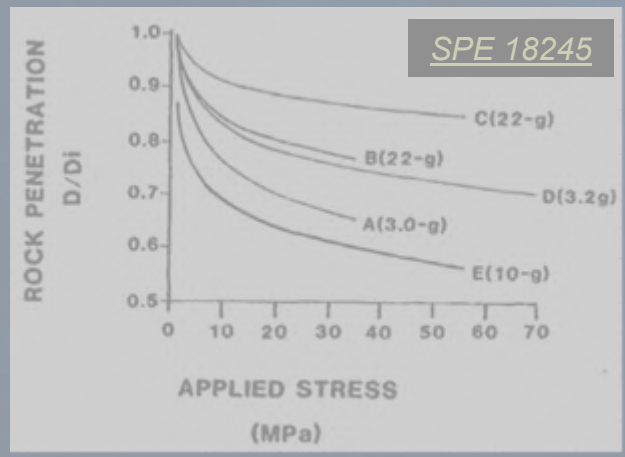
a = "ballistic pore pressure coefficient"

Perforation depth depends on:



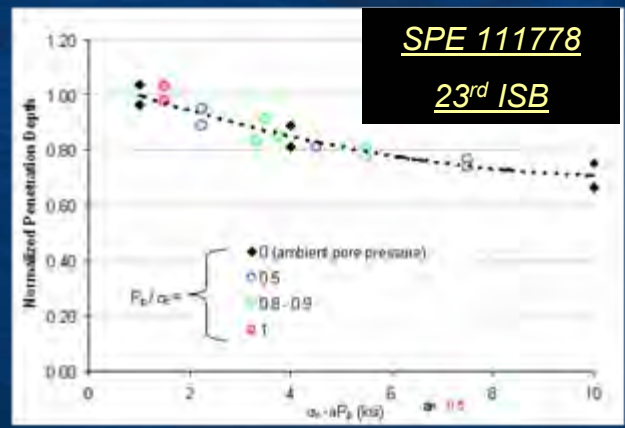
Formation Strength (UCS)

$$\sigma_{eff} = (\sigma_{mean} - P_p)$$



$$\sigma_{eff} = (\sigma_{mean} - a * P_p)$$

$$a \sim 0.5$$



Formation Effective Stress

Schlumberger

Background

- Historical and recent laboratory work consistently demonstrated that perforation depth decreases with…
  - increasing rock strength
  - increasing effective stress
- Recent laboratory work demonstrated
  - pore pressure's influence is less significant than previously thought (i.e. a<1)
  - a new definition of effective stress*

** for purposes of SC penetration depth*

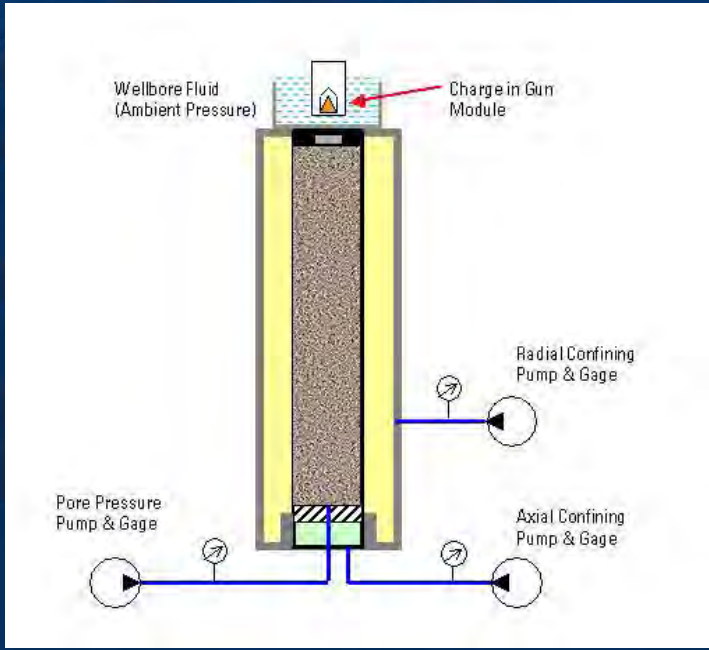
Schlumberger

Background

- Motivation for current work
  - All previous laboratory work (especially into stressed targets) addressed liquid-filled rock
  - Reasonably valid for oil reservoirs, but not necessarily for gas reservoirs
- Focus on perforation depth; tunnel diameter is another variable not addressed here

Current Work

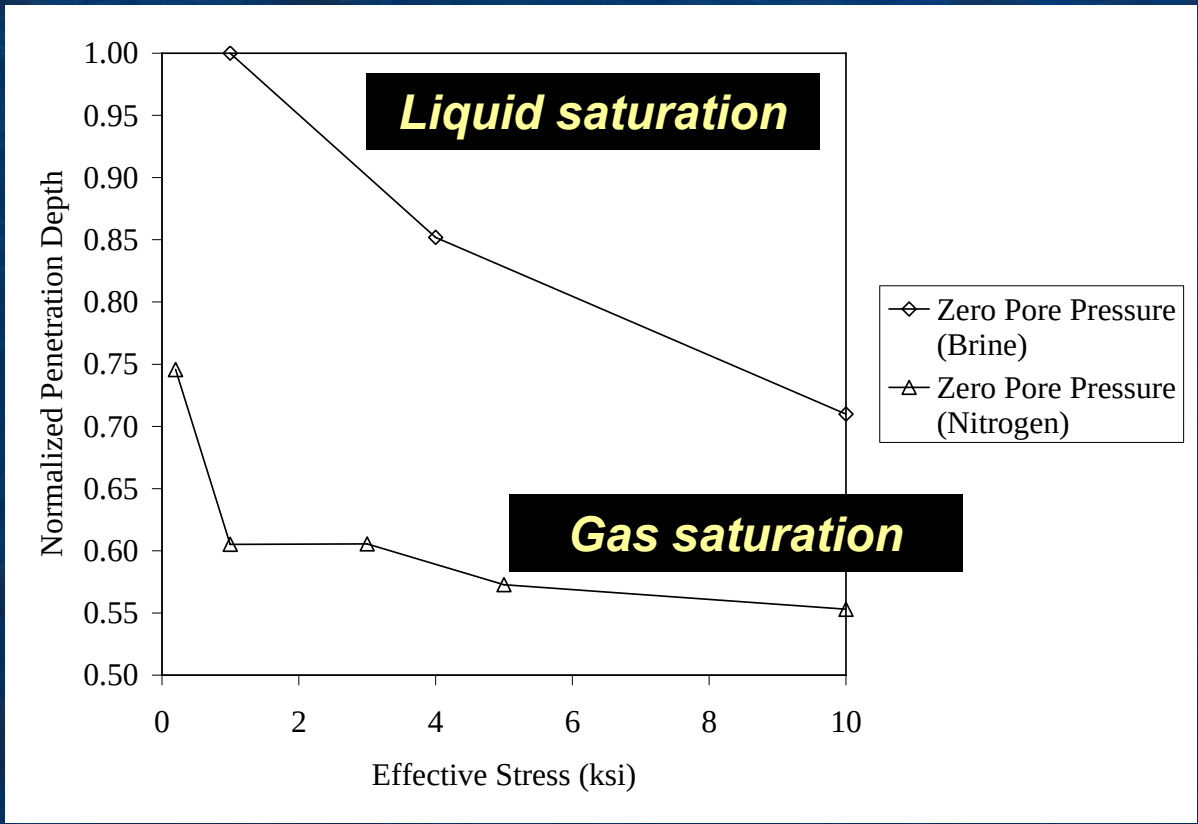
- Penetration experiments into stressed rock targets
  - independent confining and pore pressures, up to 10,000 psi
  - simulates stress levels representative of depths up to 10,000'
  - does not mimic downhole temperature or wellbore fluid pressure
- Berea sandstone
- Pore fluid is dry N_2



Schlumberger

Results: Ambient Pore Pressure

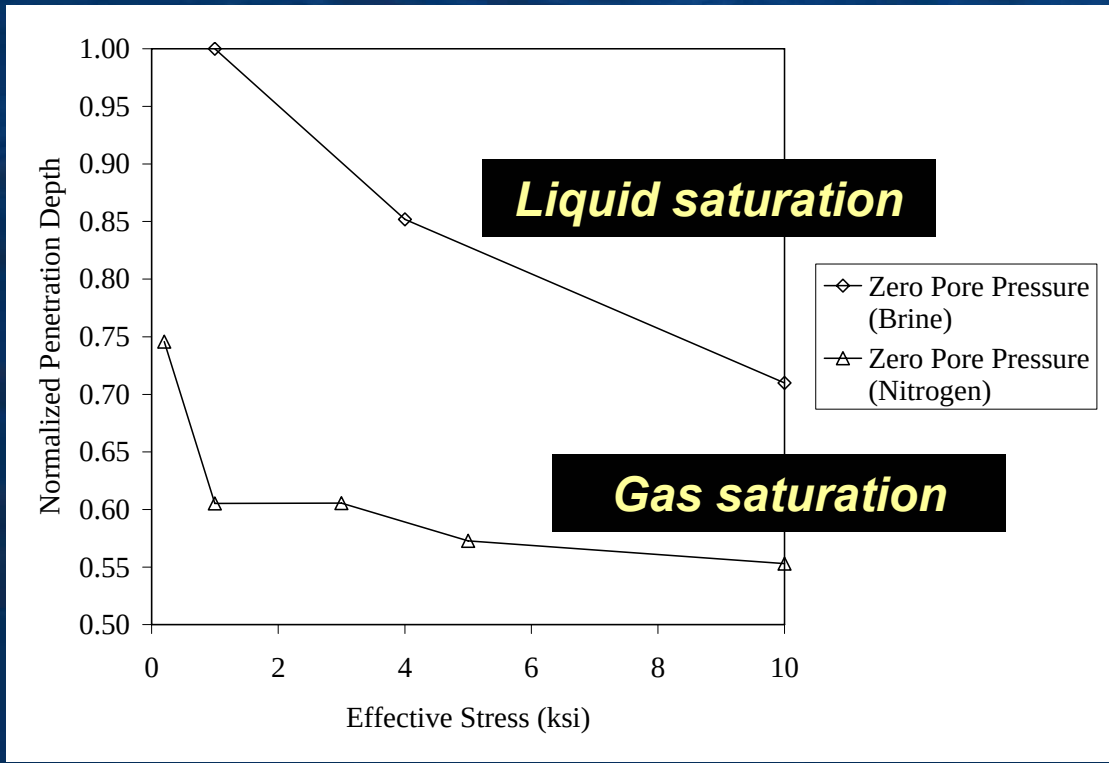
- Perforation depth vs. confining stress
  - for both liquid- and gas-saturated sandstone



Schlumberger

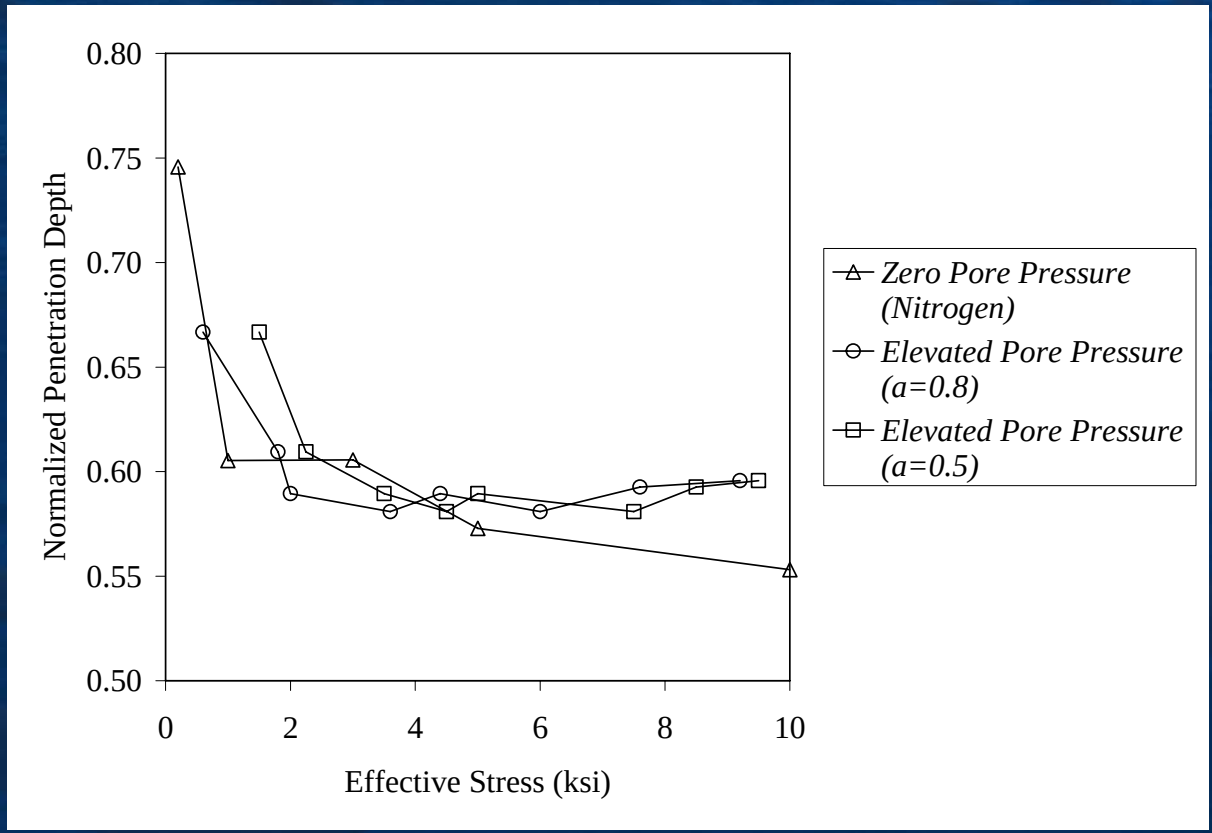
Results: Ambient Pore Pressure

- Two primary observations
  - PD significantly reduced in gas saturated target
  - Stress influence on PD
    - high for liquid
    - minimal for gas
      (above ~1 ksi)



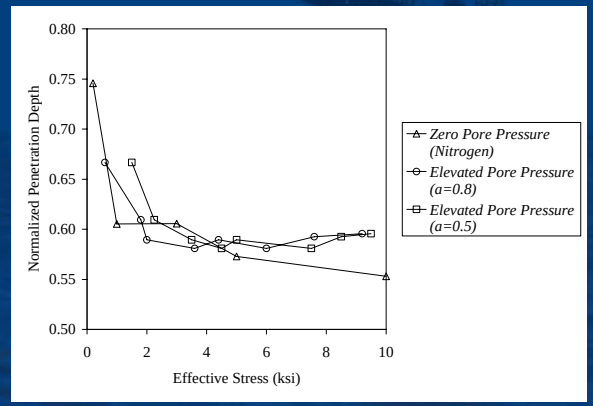
Results: Elevated Pore Pressure

- Perforation depth vs. effective stress $\sigma_{eff} = (\sigma_{mean} - a * P_p)$
  - gas saturation only; both elevated and ambient pore pressure



Schlumberger

Results: Elevated Pore Pressure



- Primary observations
  - Pore pressure influence
    - For stress>2ksi, a=0.5 gives reasonable fit
    - For stress<2ksi, fit is improved with a=0.8
  - Strictly speaking, BPC is not a constant rock property, but *f(stress, pore fluid)*
  - For elevated pore pressure, penetration into gas saturated rock is even less stress dependant

Practically speaking, both stress and pore pressure may be irrelevant to perforation depth for dry gas saturated rock (above some threshold stress value)

Schlumberger

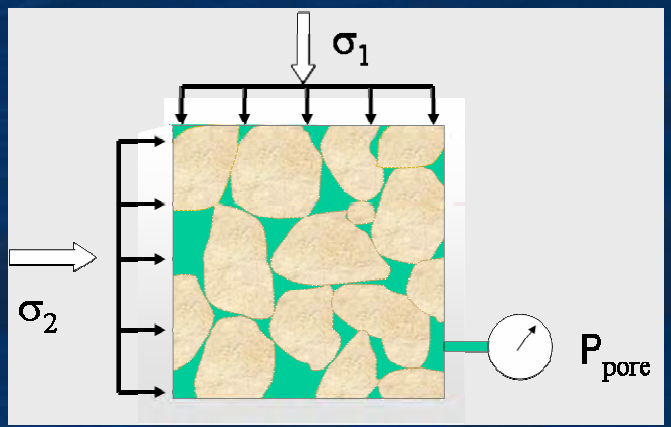
Summary

- Laboratory experiments were conducted
  - shaped charge penetration
  - dry nitrogen-saturated sandstone targets
  - stressed to simulate downhole conditions
- Results:
  - penetration depth into dry gas saturated sandstone is…
    - considerably shallower than into liquid-saturated sandstone
    - essentially independent of effective stress (above 2 ksi)
  - confining stress (and also pore pressure): only important at very low stress levels

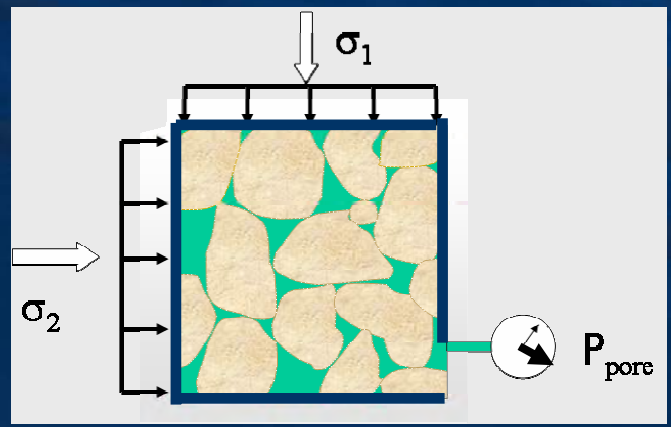
Schlumberger

Possible Mechanisms

- reduced penetration depth
  - dry sandstone is stronger than brine-saturated (surface tension and cementation weakening)
  - energy absorption of pore collapse in target
  - “active target” effect (Aseltine, 1985)
- stress independence
  - shallow penetration = high jet cutoff velocity ~ hydrodynamic penetration
  - for liquid saturation, rapid “undrained” loading may limit the increase in the target’s “dynamic effective stress” (and, therefore, strength)



drained



Undrained, or rapid loading

Schlumberger

Future Work

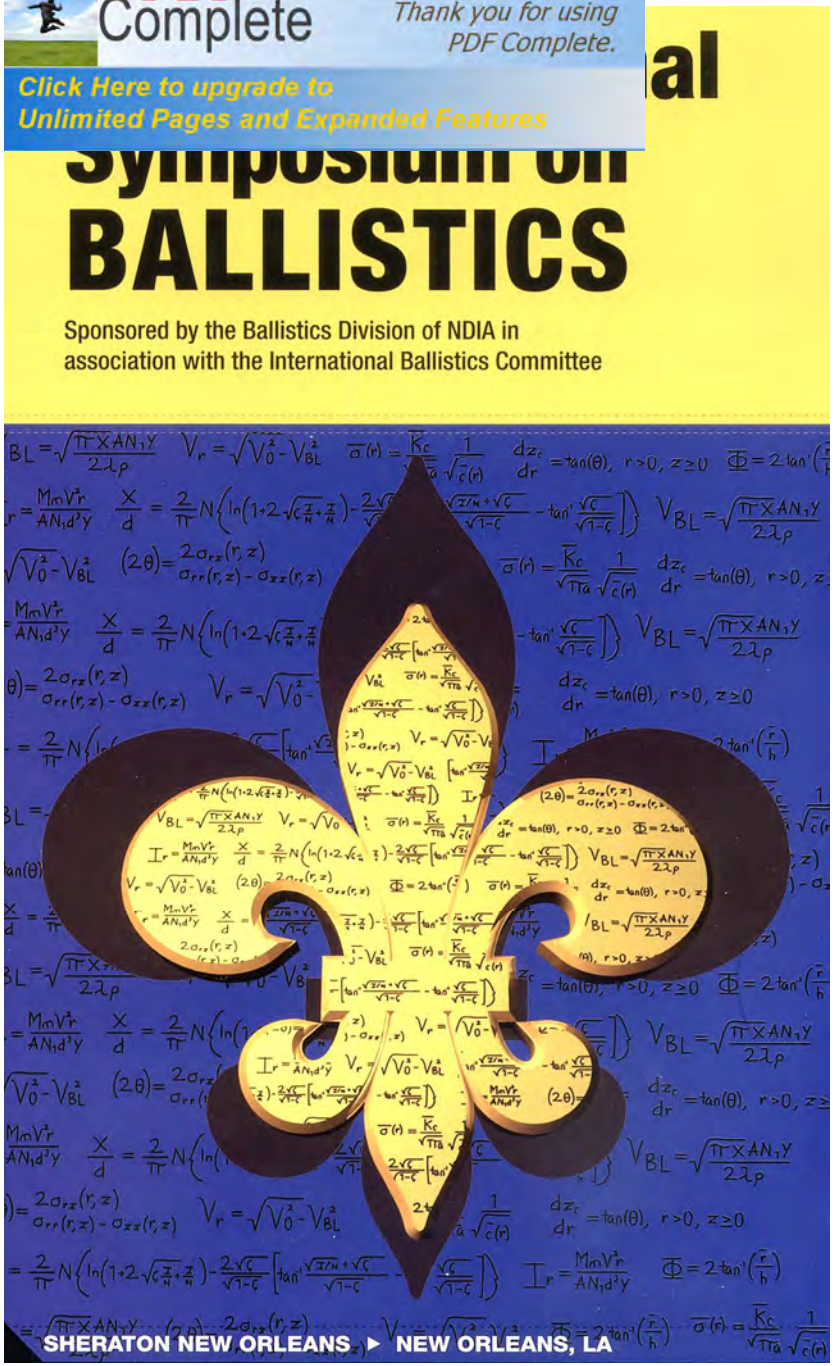
- Future Work
  - Understand the mechanisms responsible for these fundamental differences in ballistic response of liquid and gas saturated sandstones
  - Design of shaped charges optimized for gas saturated reservoirs

Thank You



Schlumberger

PDF Complete
Your complimentary use period has ended. Thank you for using PDF Complete.
Click Here to upgrade to Unlimited Pages and Expanded Features



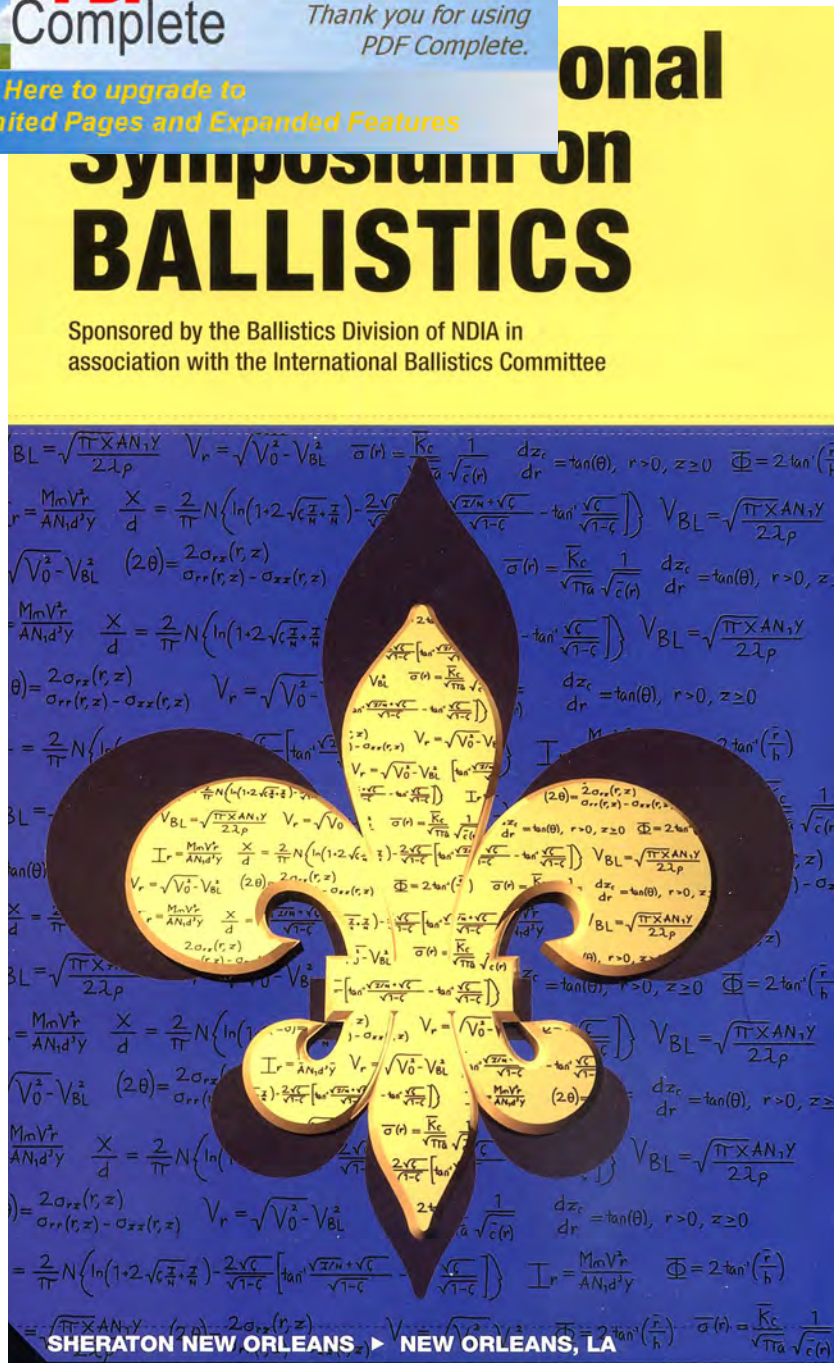
Behind Armour Effects at Shaped Charge Attacks

Prof. Dr. M. Held

EADS DEFENCE & SECURITY

Schrobenhausen, Germany

PDF Complete
Your complimentary use period has ended. Thank you for using PDF Complete.
Click Here to upgrade to Unlimited Pages and Expanded Features



Content

Introduction

Diagnostic vessel

Light effects

Gaseous products

Temperature

Spall fragments

Blast effects &

HE equivalence

Incendiary effects

Ignition & Initiation

Summary

PDF Complete
Your complimentary use period has ended. Thank you for using PDF Complete.
Click Here to upgrade to Unlimited Pages and Expanded Features

EADS DEFENCE & SECURITY

Introduction

PDF Complete
Your complimentary use period has ended. Thank you for using PDF Complete.
Click Here to upgrade to Unlimited Pages and Expanded Features

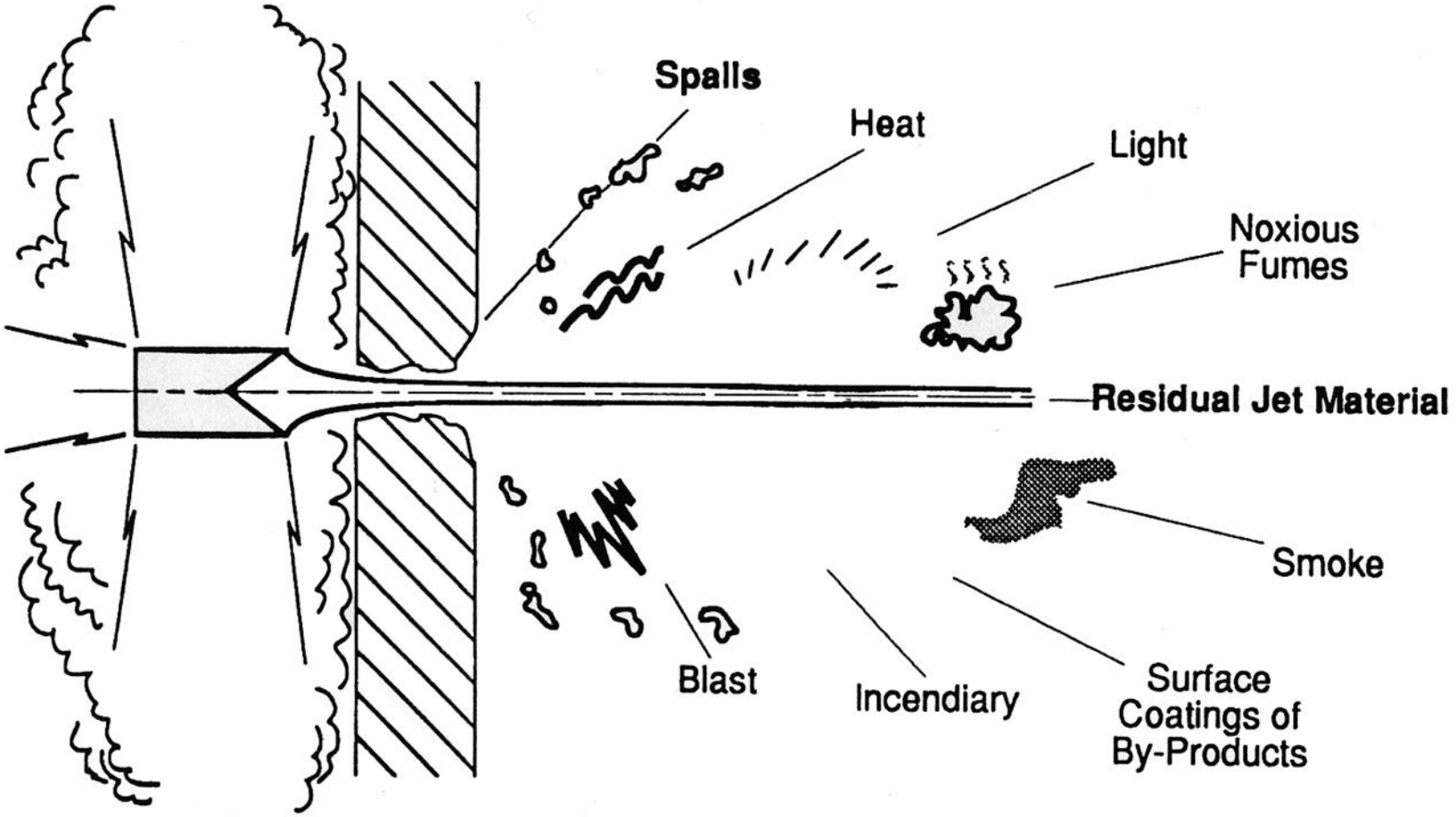
ed Charge Effects

EADS DEFENCE & SECURITY

Location	Phenomena	Efficiency Currier	Percentage
Internal	Mechanical	• Residual Jet • Fragments	
	Blast	Pressure history	
	Thermic	Heat	
	Optical	Dazzle Dust	
	Chemical	Gaseous (HE-Products)	
External	Mechanical	• Fragments • Blast	

PDF Complete
Your complimentary use period has ended. Thank you for using PDF Complete.
Click Here to upgrade to Unlimited Pages and Expanded Features

rmour Effects after Shaped Charge Jets Perforations



Don Kennedy

PDF Complete
Your complimentary use period has ended. Thank you for using PDF Complete.
Click Here to upgrade to Unlimited Pages and Expanded Features

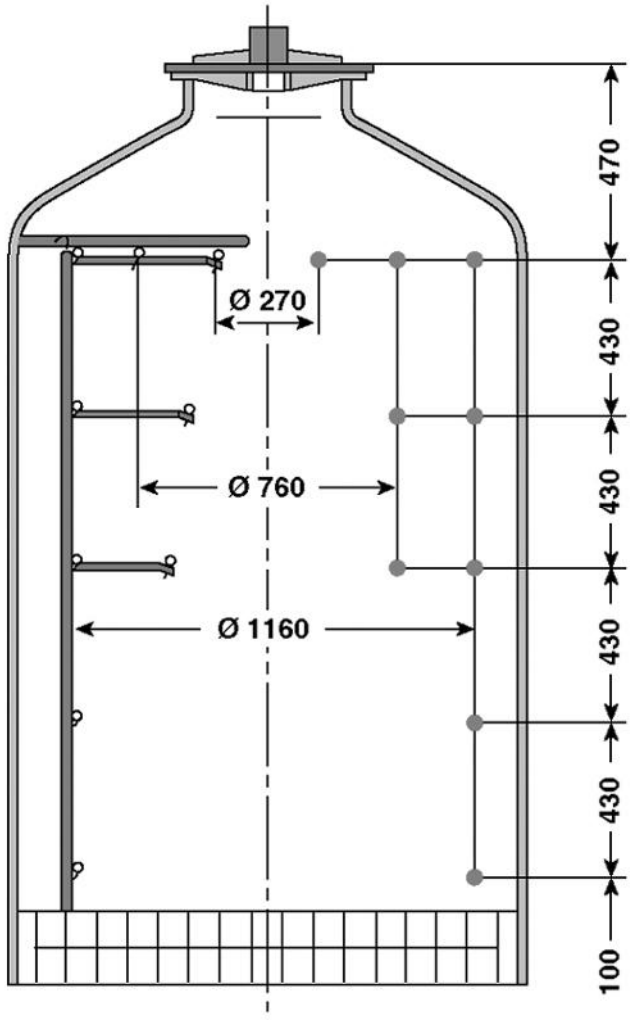
EADS DEFENCE & SECURITY

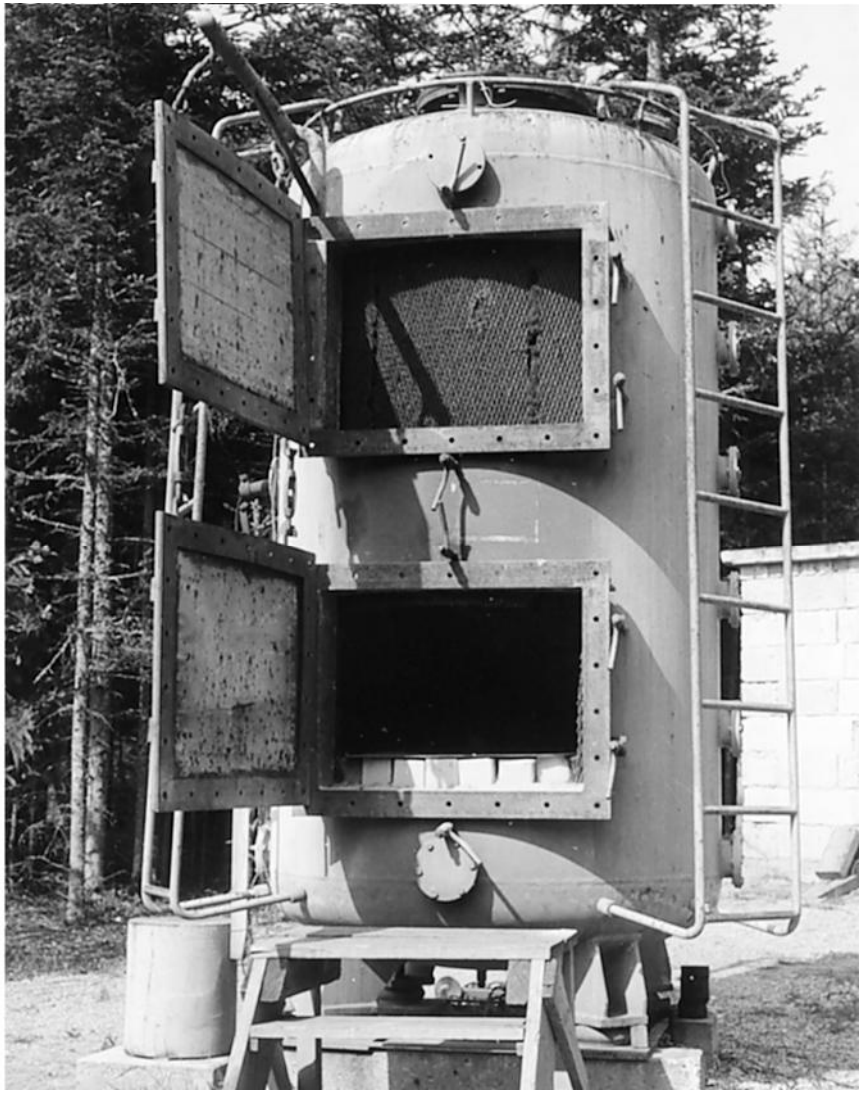
Diagnostic Vessel

PDF Complete
Your complimentary use period has ended. Thank you for using PDF Complete.
Click Here to upgrade to Unlimited Pages and Expanded Features

with 2.4 m³ Volume

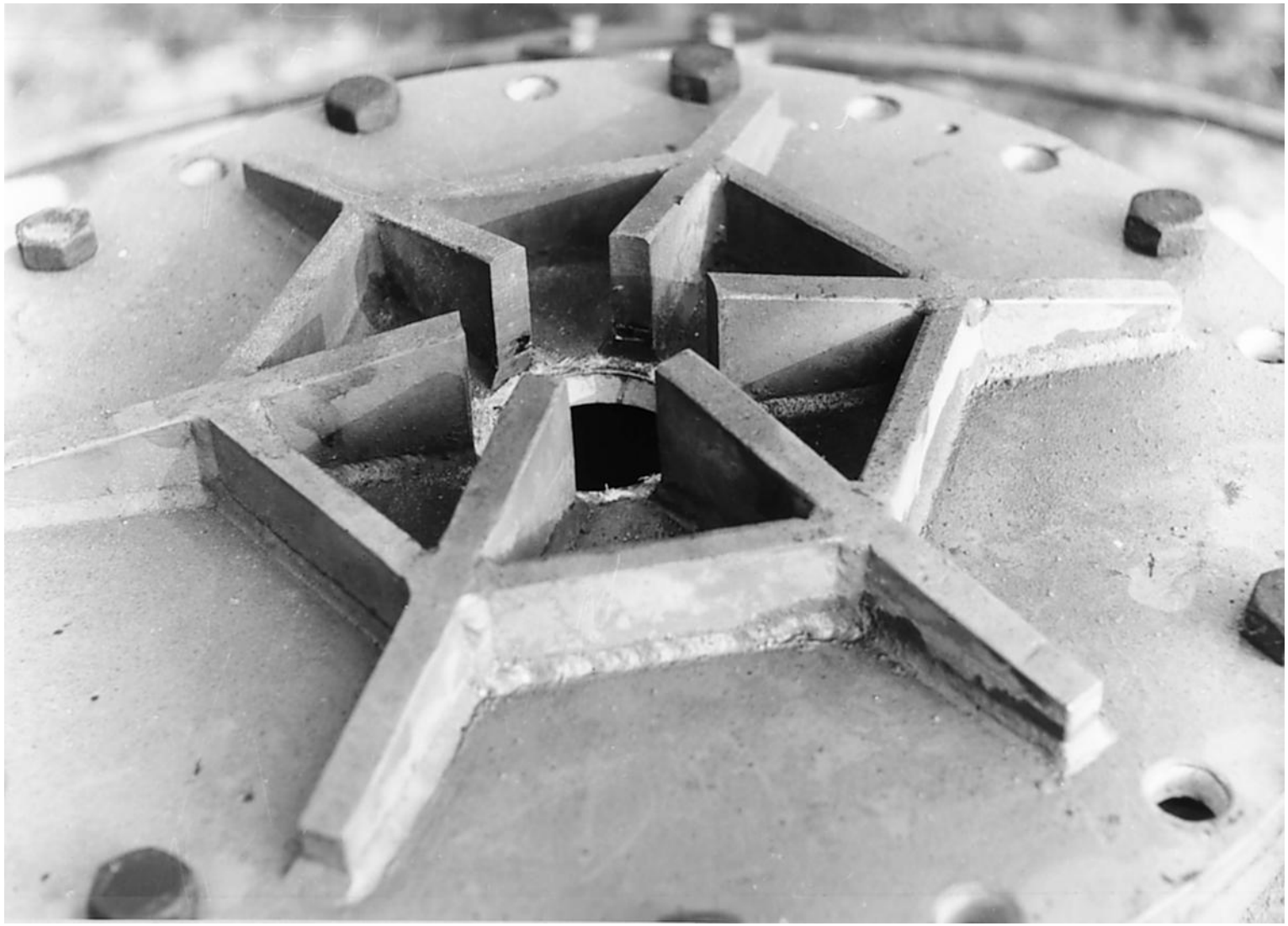
EADS DEFENCE & SECURITY





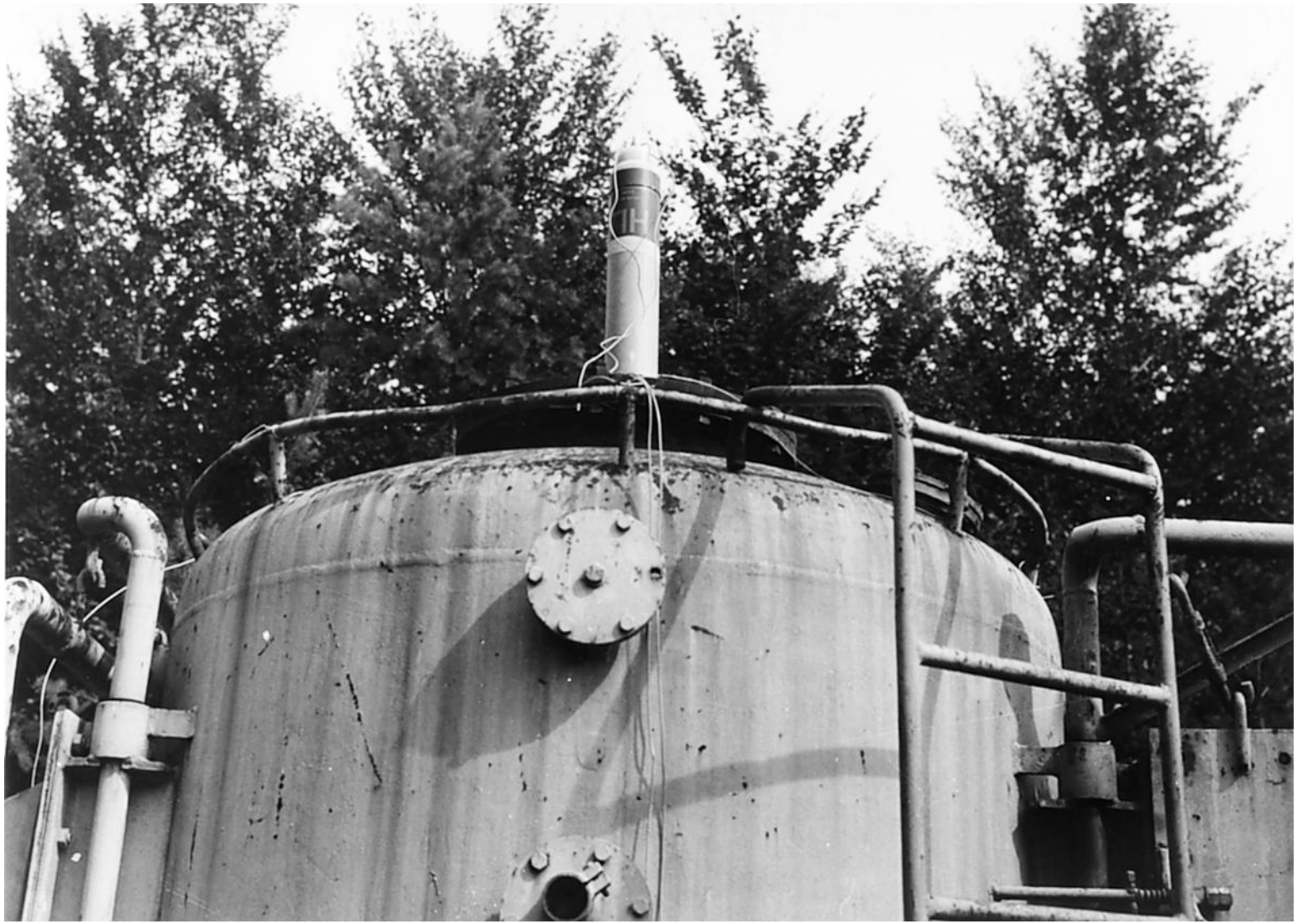
PDF Complete
Your complimentary use period has ended. Thank you for using PDF Complete.
Click Here to upgrade to Unlimited Pages and Expanded Features

EADS DEFENCE & SECURITY



PDF Complete
Your complimentary use period has ended. Thank you for using PDF Complete.
Click Here to upgrade to Unlimited Pages and Expanded Features

rge on Top



EADS DEFENCE & SECURITY

PDF Complete
Your complimentary use period has ended. Thank you for using PDF Complete.
Click Here to upgrade to Unlimited Pages and Expanded Features

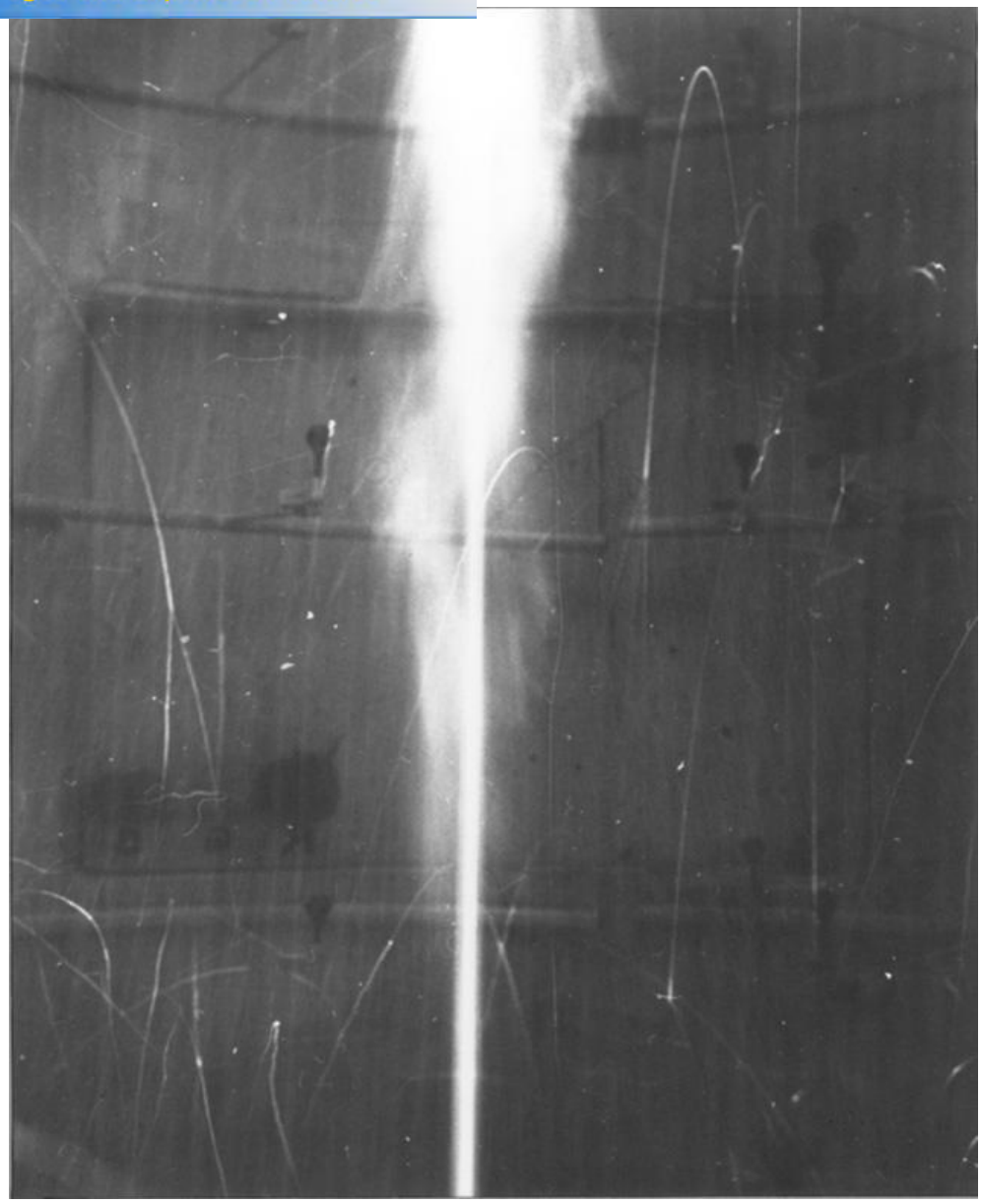
EADS DEFENCE & SECURITY



PDF Complete
Your complimentary use period has ended. Thank you for using PDF Complete.
Click Here to upgrade to Unlimited Pages and Expanded Features

Pictures

EADS DEFENCE & SECURITY



Cobra with Cu liner in the diagnostic vessel

PDF Complete
Your complimentary use period has ended. Thank you for using PDF Complete.
Click Here to upgrade to Unlimited Pages and Expanded Features

EADS DEFENCE & SECURITY

ctures



PDF Complete
Your complimentary use period has ended. Thank you for using PDF Complete.
Click Here to upgrade to Unlimited Pages and Expanded Features

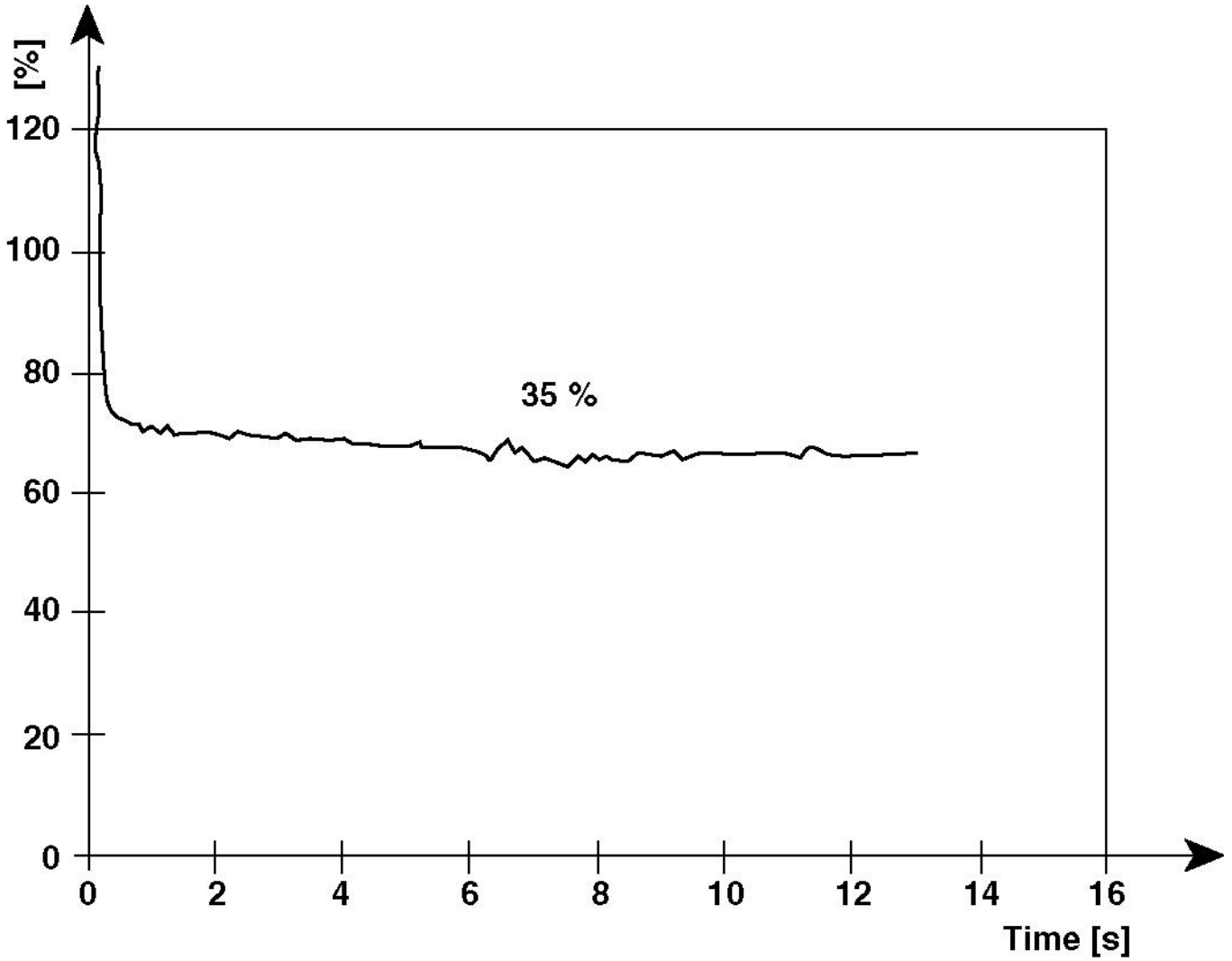
ctures



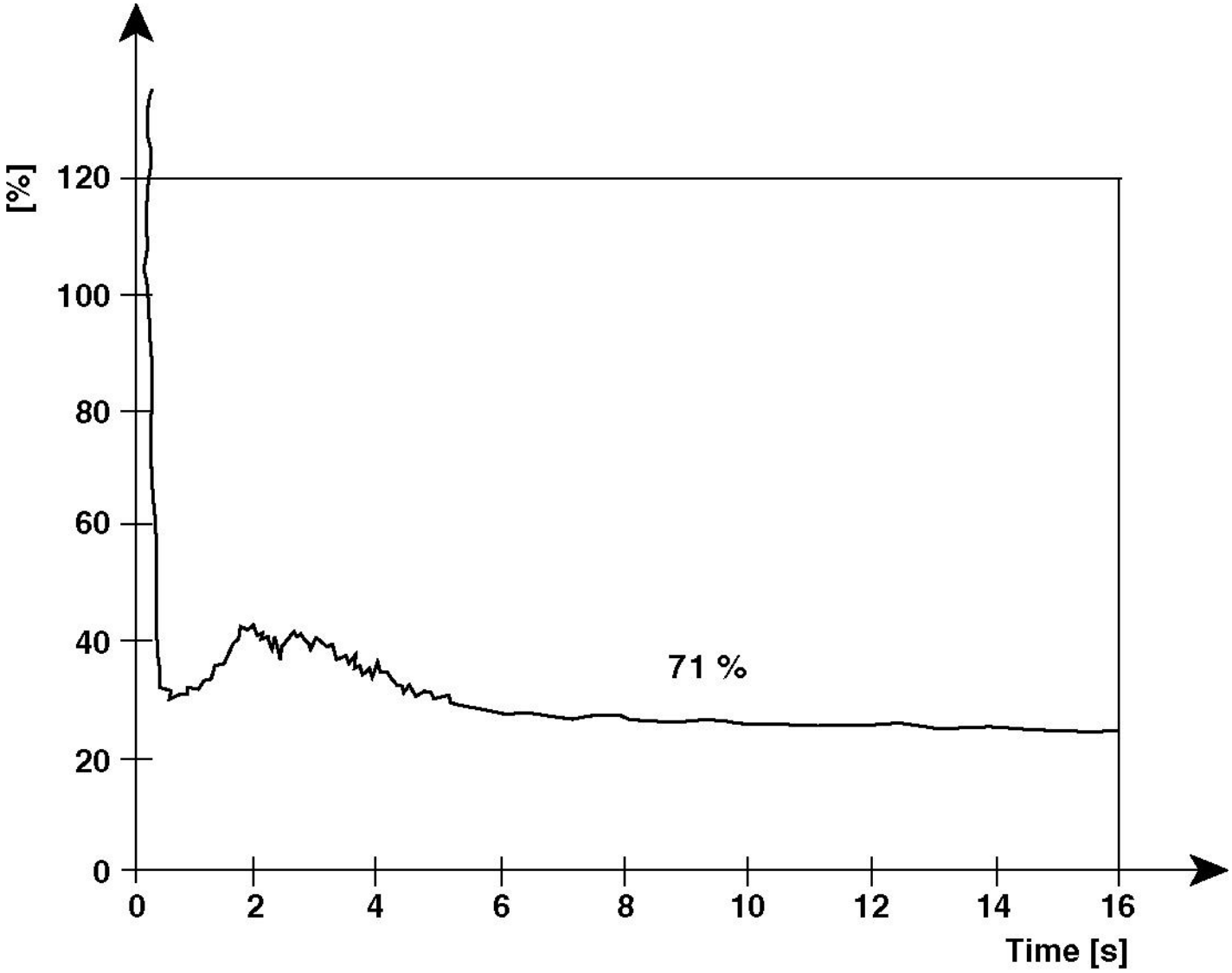
EADS DEFENCE & SECURITY

PDF Complete
Your complimentary use period has ended. Thank you for using PDF Complete.
Click Here to upgrade to Unlimited Pages and Expanded Features

EADS DEFENCE & SECURITY



PDF Complete
Your complimentary use period has ended. Thank you for using PDF Complete.
Click Here to upgrade to Unlimited Pages and Expanded Features



PDF Complete
Your complimentary use period has ended. Thank you for using PDF Complete.
Click Here to upgrade to Unlimited Pages and Expanded Features

EADS DEFENCE & SECURITY

with Gaseous Analysis and Piezoelectric Pressure Gauges



PDF Complete
Your complimentary use period has ended. Thank you for using PDF Complete.
Click Here to upgrade to Unlimited Pages and Expanded Features

EADS DEFENCE & SECURITY

Measuring Tank No.

Shaped Charge	:	Orig. Cobra
HE - Weight	:	1480 g
Cu liner - Weight	:	250 g
Standoff	:	300 mm
Barrier	:	300 mm

Gaseous Analysis

(Oxygen Absorption in Pyrogallol)

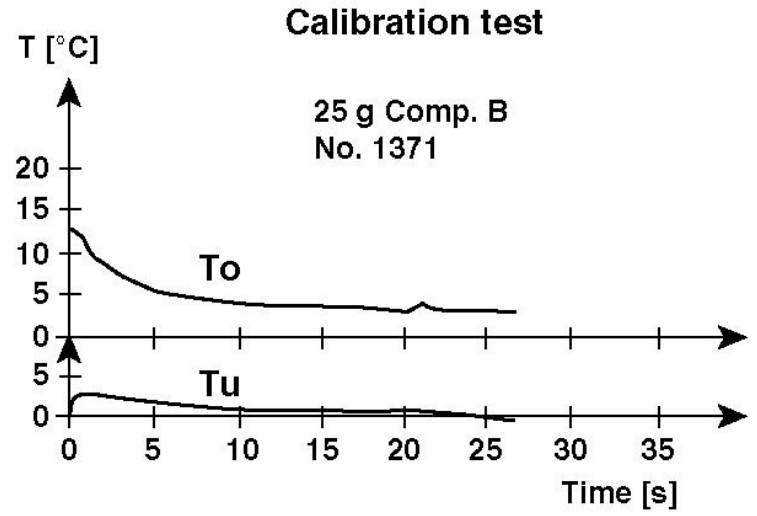
Oxygen before Firing	:	20.9 %
Oxygen after Firing	:	20.6 %

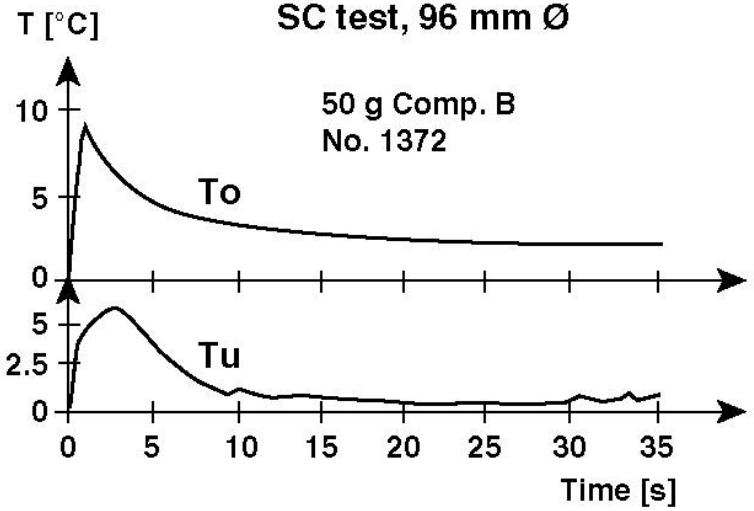
Found in Water after 50 Liter Gas:

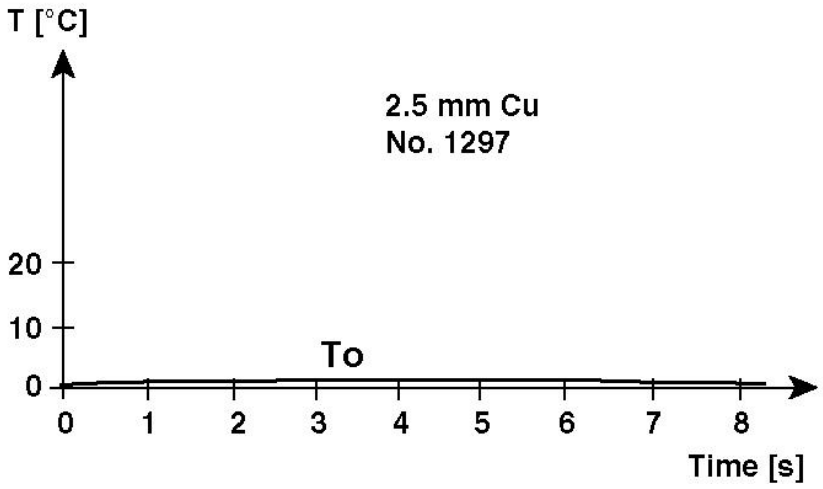
Iron	Fe	0.70 mg
Copper	Cu	1.40 mg
Nitropenoxia	NO	Shows

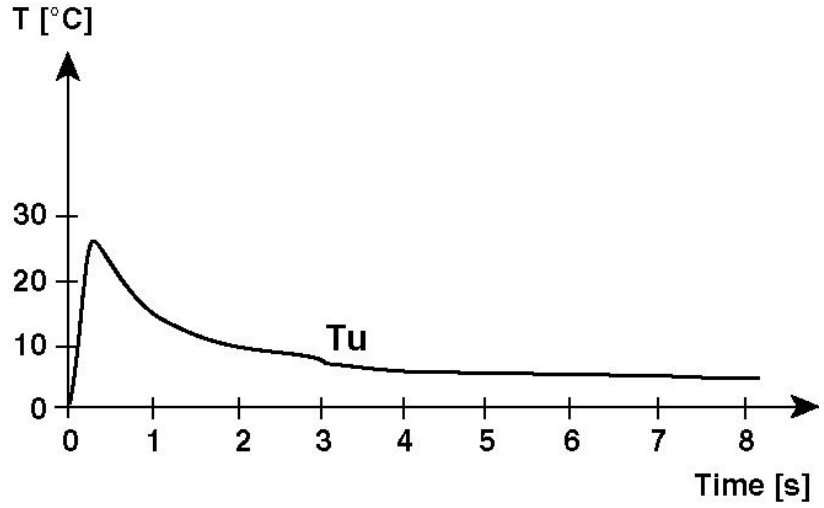
PDF Complete
Your complimentary use period has ended. Thank you for using PDF Complete.
Click Here to upgrade to Unlimited Pages and Expanded Features

EADS DEFENCE & SECURITY





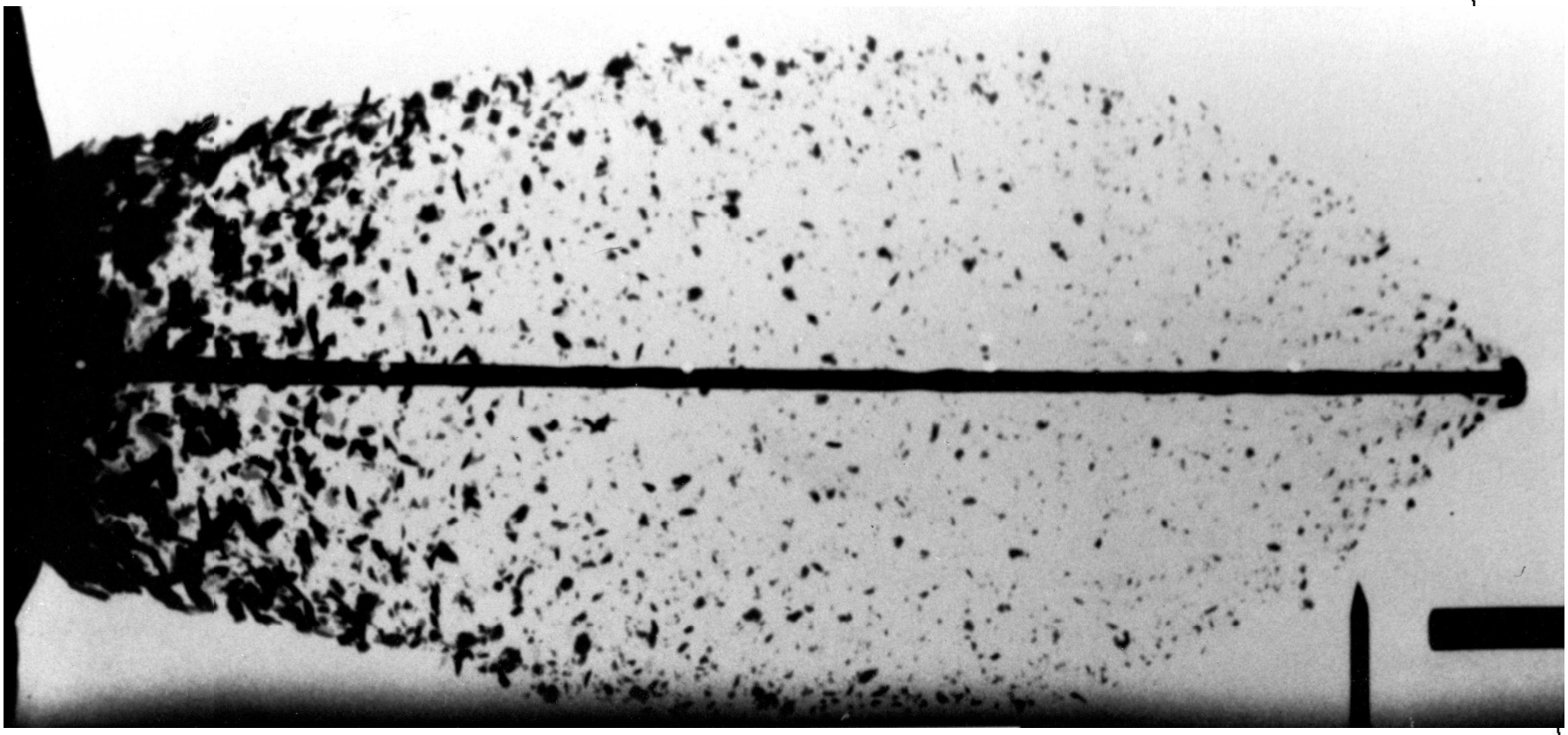




PDF Complete
Your complimentary use period has ended. Thank you for using PDF Complete.
Click Here to upgrade to Unlimited Pages and Expanded Features

Spall Fragments

EADS DEFENCE & SECURITY



PDF Complete
Your complimentary use period has ended. Thank you for using PDF Complete.
Click Here to upgrade to Unlimited Pages and Expanded Features

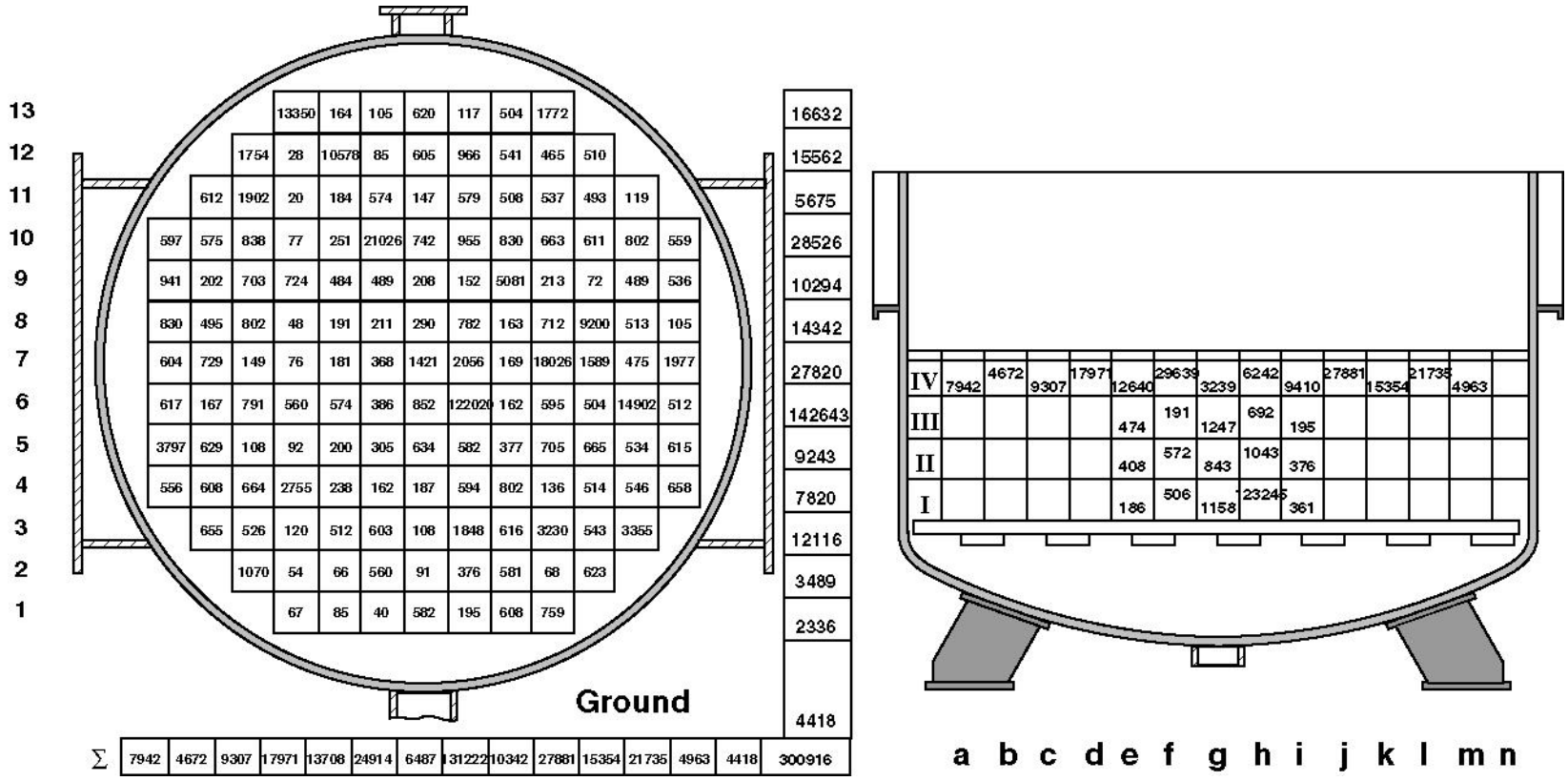
Bottom



PDF Complete
Your complimentary use period has ended. Thank you for using PDF Complete.
Click Here to upgrade to Unlimited Pages and Expanded Features

ses in mg

EADS DEFENCE & SECURITY



4 x 145 = 580 Boxes
of 100 mm³

PDF Complete
Your complimentary use period has ended. Thank you for using PDF Complete.
Click Here to upgrade to Unlimited Pages and Expanded Features

EADS DEFENCE & SECURITY

Blast Load Measurements

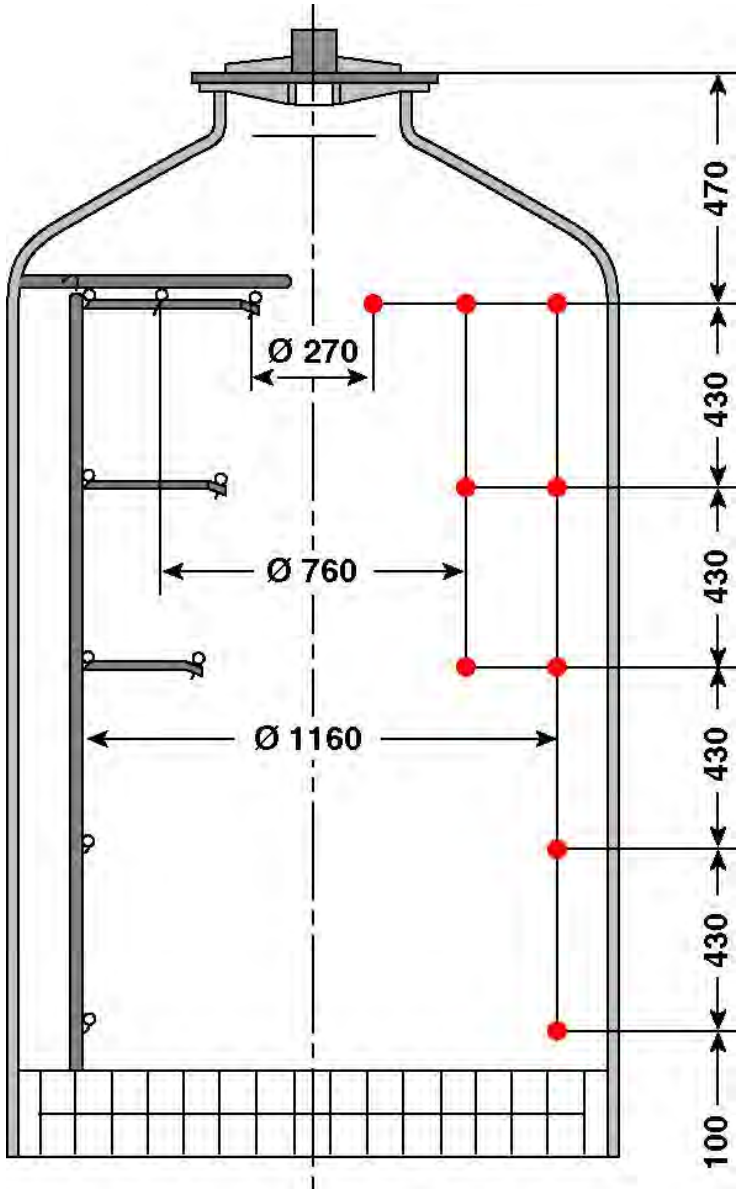
PDF Complete
Your complimentary use period has ended. Thank you for using PDF Complete.
Click Here to upgrade to Unlimited Pages and Expanded Features

Gauges

EADS DEFENCE & SECURITY

6 fictures
x 9 locations =
= 54 diagnostic points

54 dodecahedra
x 11 diaframa =
594 measurements,
distributed over the
radius and height
of the diagnostic vessel



PDF Complete
Your complimentary use period has ended. Thank you for using PDF Complete.
Click Here to upgrade to Unlimited Pages and Expanded Features

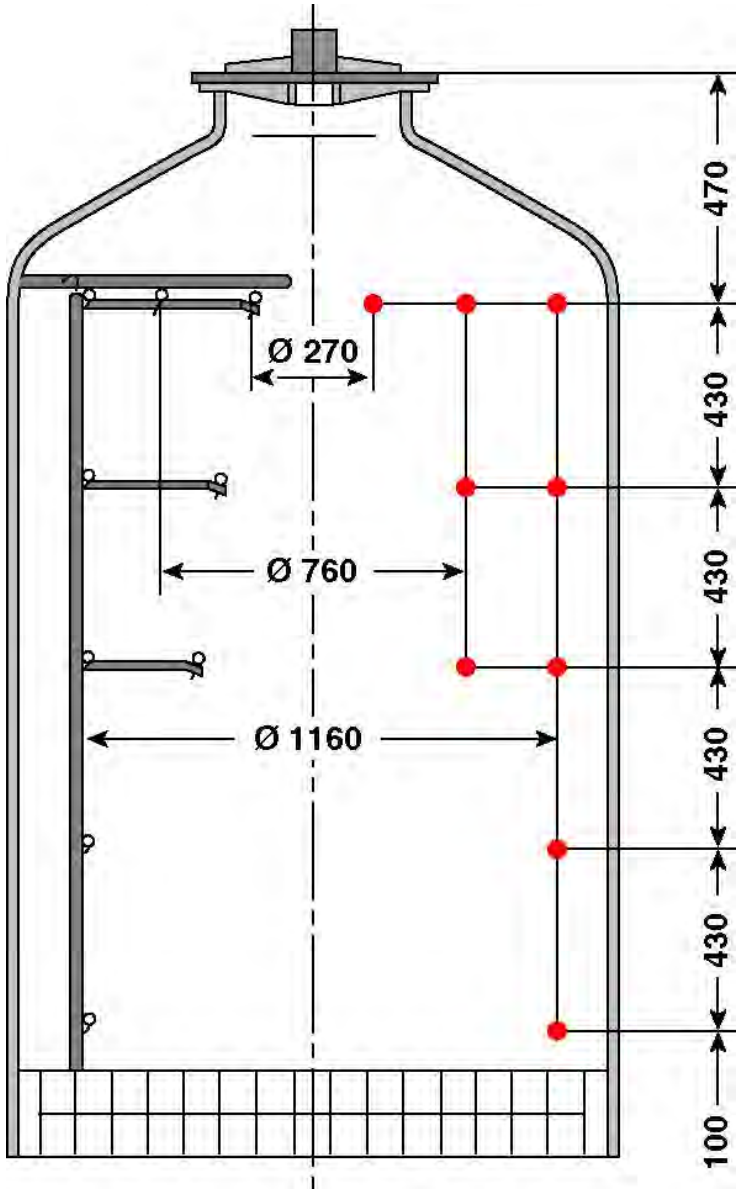
Gauges

EADS DEFENCE & SECURITY

6 fictures
x 9 locations =
= 54 diagnostic points

54 dodecahedra
x 11 diafragma =
594 measurements,
distributed over the
radius and height
of the diagnostic vessel





PDF Complete
Your complimentary use period has ended. Thank you for using PDF Complete.
Click Here to upgrade to Unlimited Pages and Expanded Features

p of diagnostic vessel



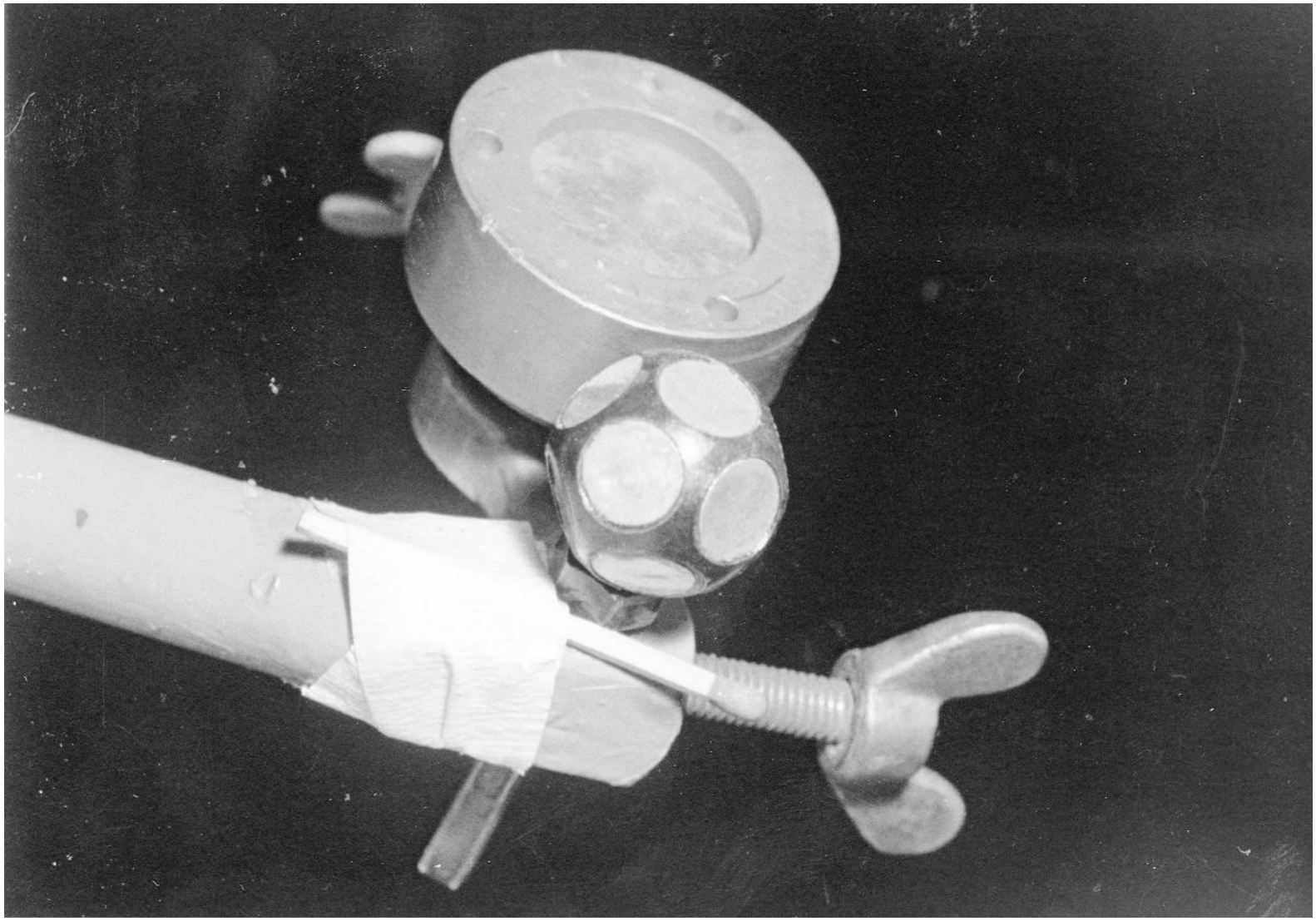
EADS DEFENCE & SECURITY

Fictutures

Expanded metal mesh

PDF Complete
Your complimentary use period has ended. Thank you for using PDF Complete.
Click Here to upgrade to Unlimited Pages and Expanded Features

ecaeder, Matches



EADS DEFENCE & SECURITY

PDF Complete
Your complimentary use period has ended. Thank you for using PDF Complete.
Click Here to upgrade to Unlimited Pages and Expanded Features

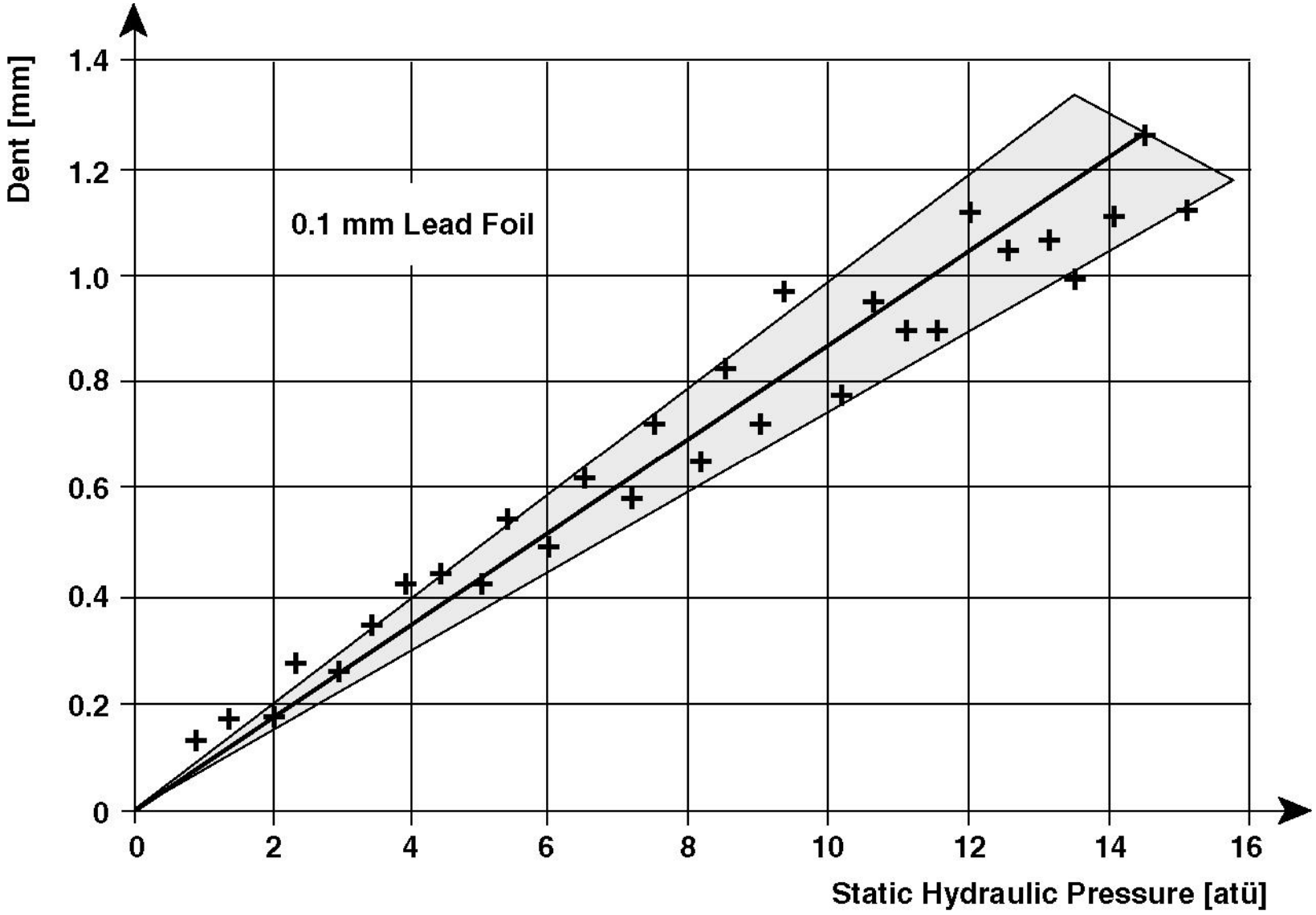
körper“



EADS DEFENCE & SECURITY

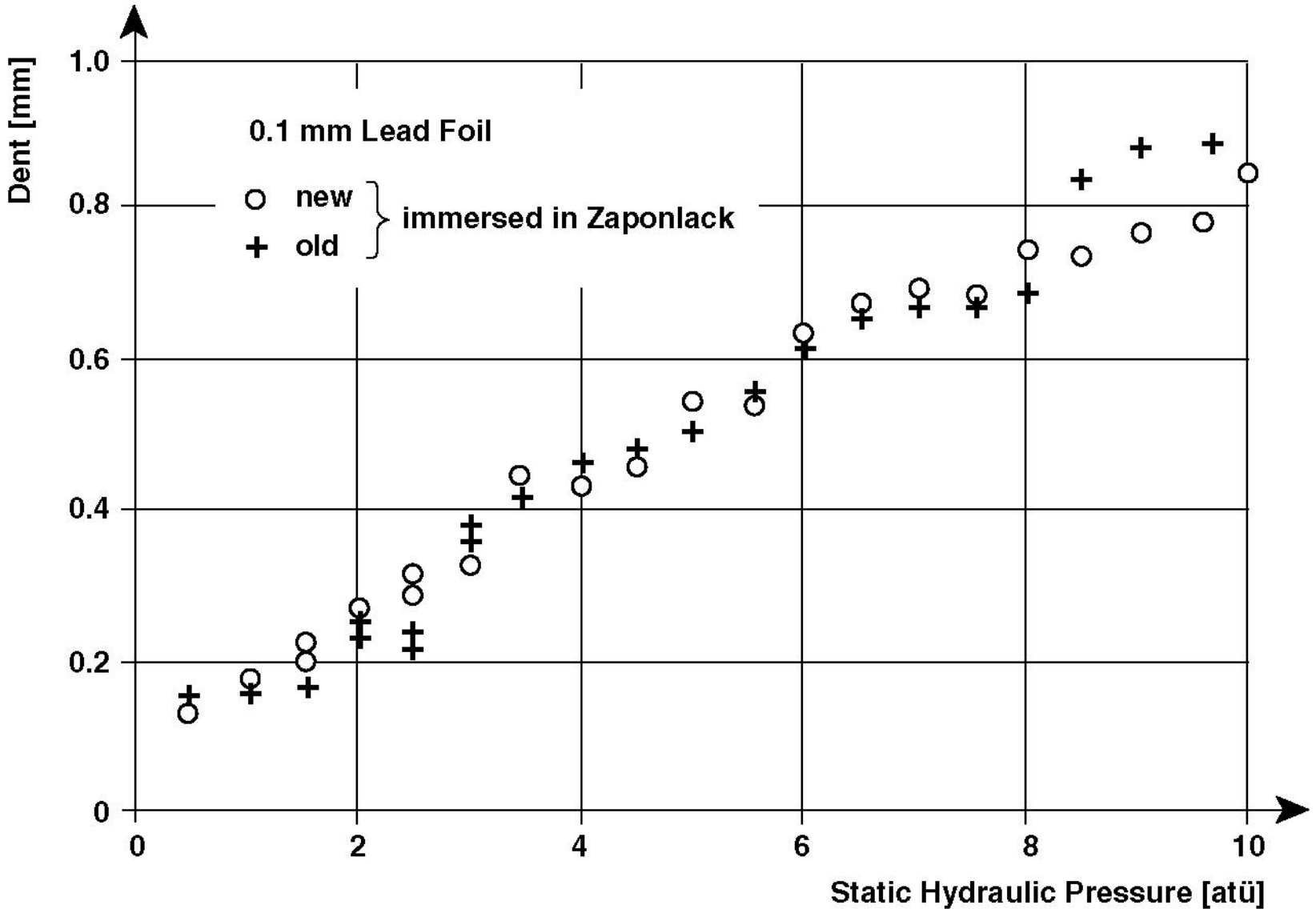
PDF Complete
Your complimentary use period has ended. Thank you for using PDF Complete.
Click Here to upgrade to Unlimited Pages and Expanded Features

suring Device

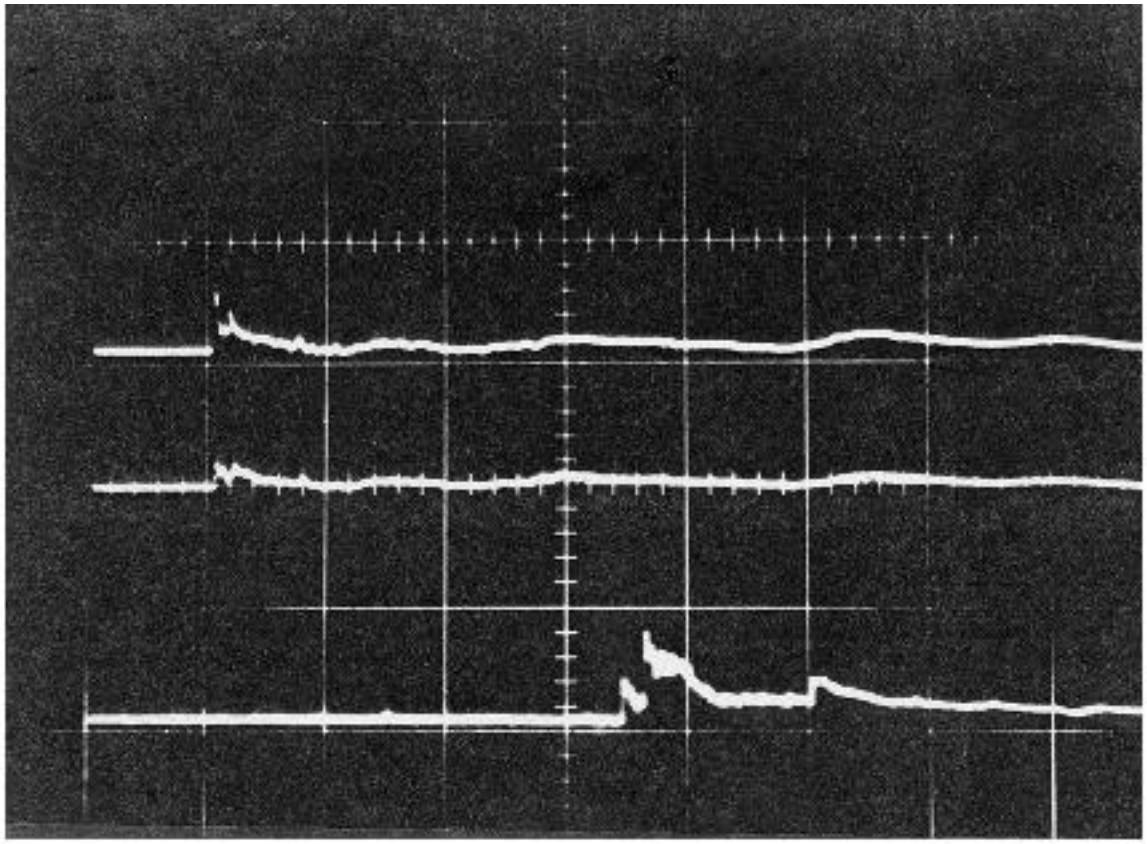


PDF Complete
Your complimentary use period has ended. Thank you for using PDF Complete.
Click Here to upgrade to Unlimited Pages and Expanded Features

suring Device



PDF Complete
Your complimentary use period has ended. Thank you for using PDF Complete.
Click Here to upgrade to Unlimited Pages and Expanded Features



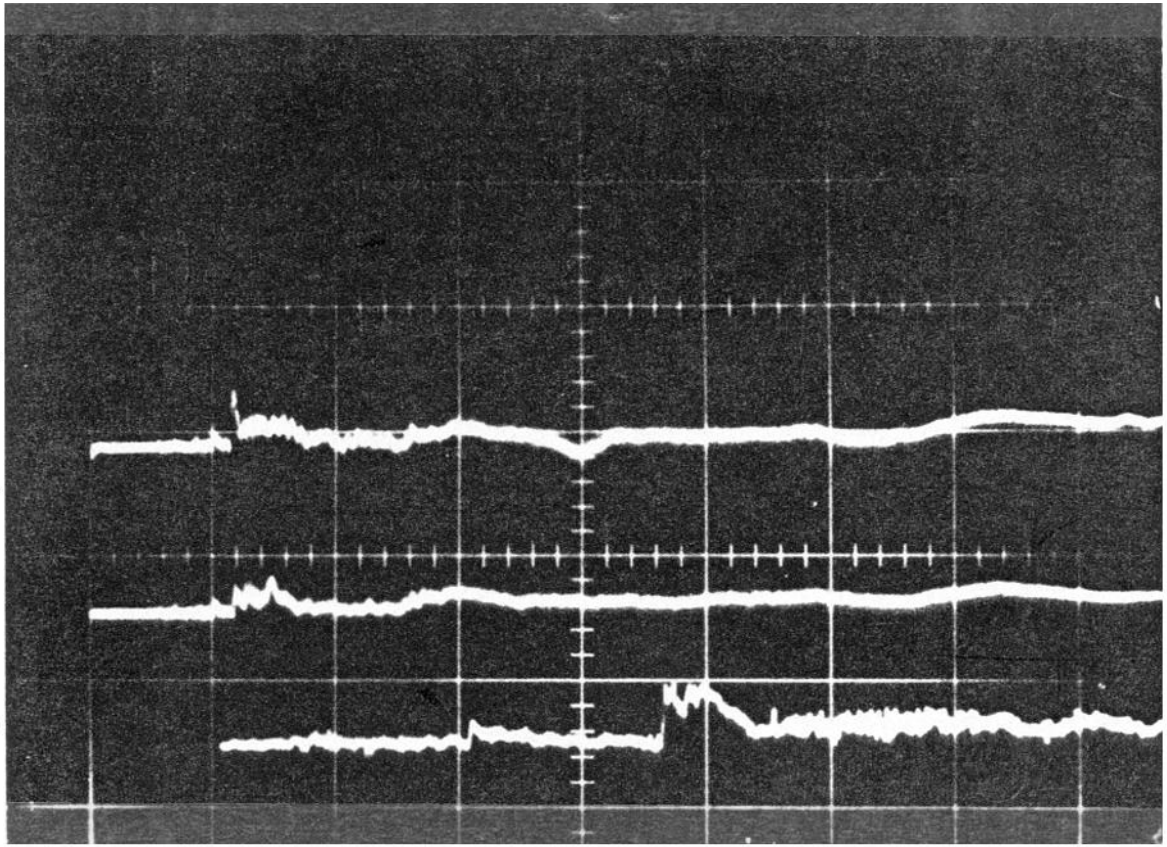
P_R = 2.2 atü

P_S = 0.6 atü

PDF Complete
Your complimentary use period has ended. Thank you for using PDF Complete.
Click Here to upgrade to Unlimited Pages and Expanded Features

00 mm Barrier

EADS DEFENCE & SECURITY



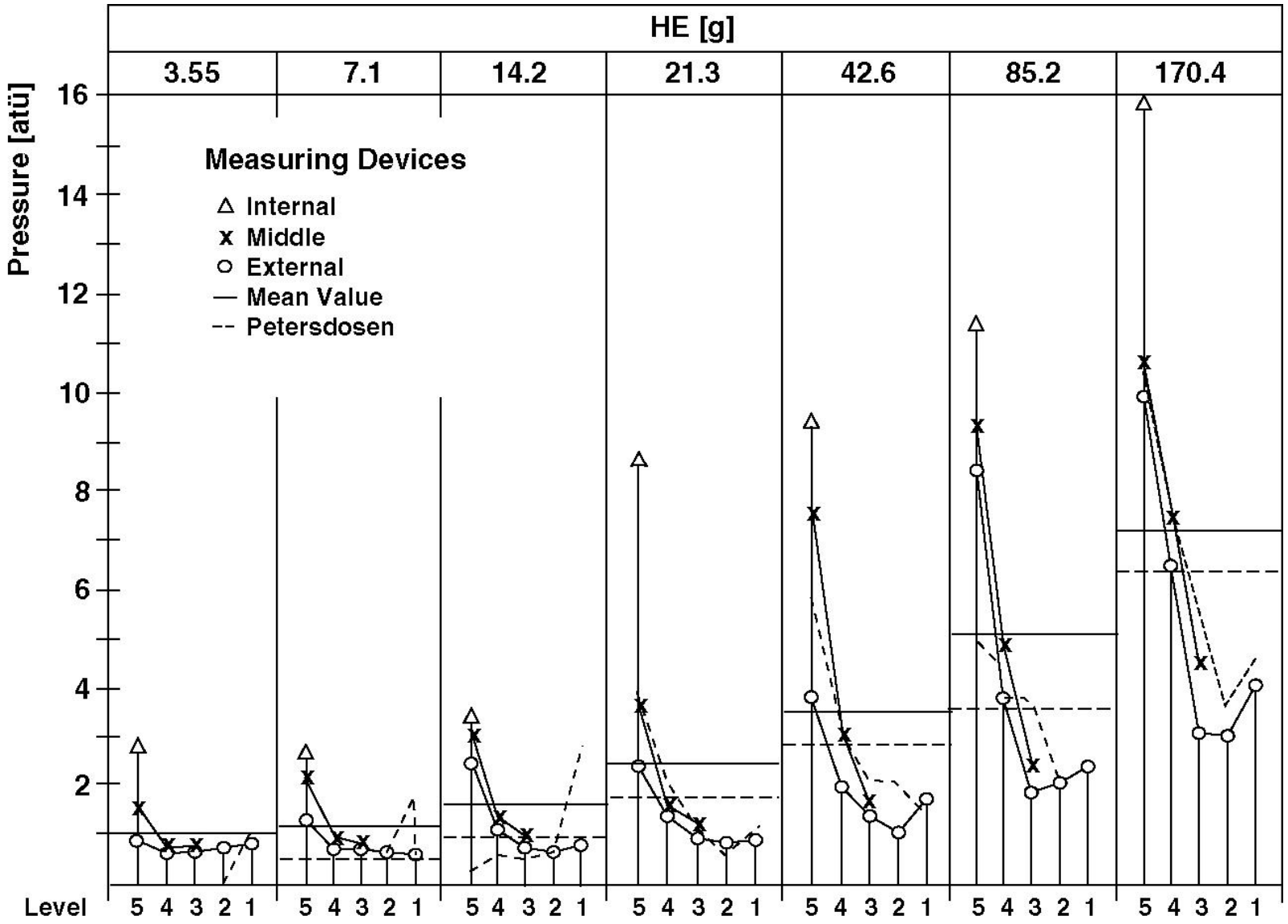
P_R = 1.6 atü

P_S = 0.9 atü

PDF Complete
Your complimentary use period has ended. Thank you for using PDF Complete.
Click Here to upgrade to Unlimited Pages and Expanded Features

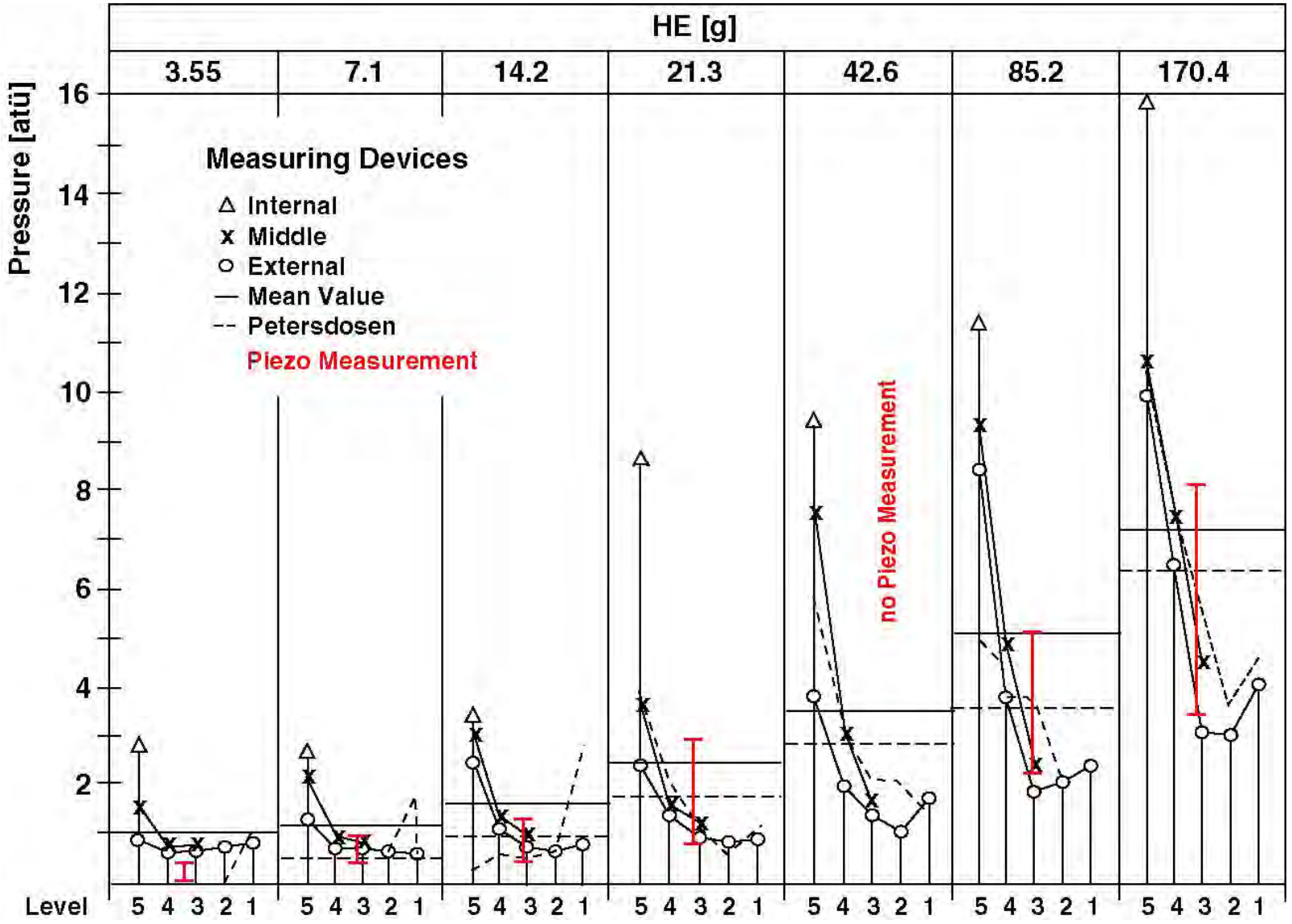
on

EADS DEFENCE & SECURITY



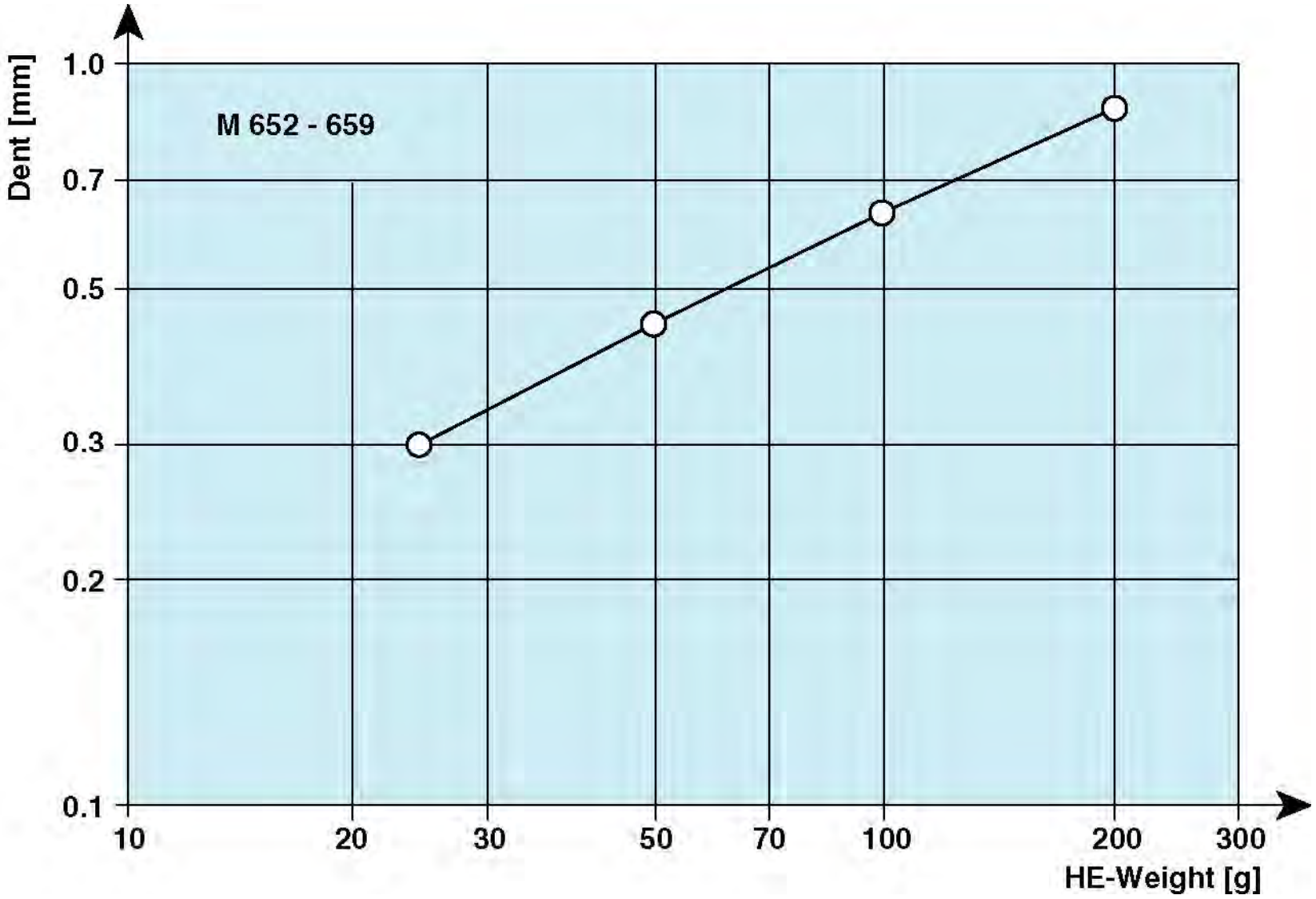
PDF Complete
Your complimentary use period has ended. Thank you for using PDF Complete.
Click Here to upgrade to Unlimited Pages and Expanded Features

EADS DEFENCE & SECURITY



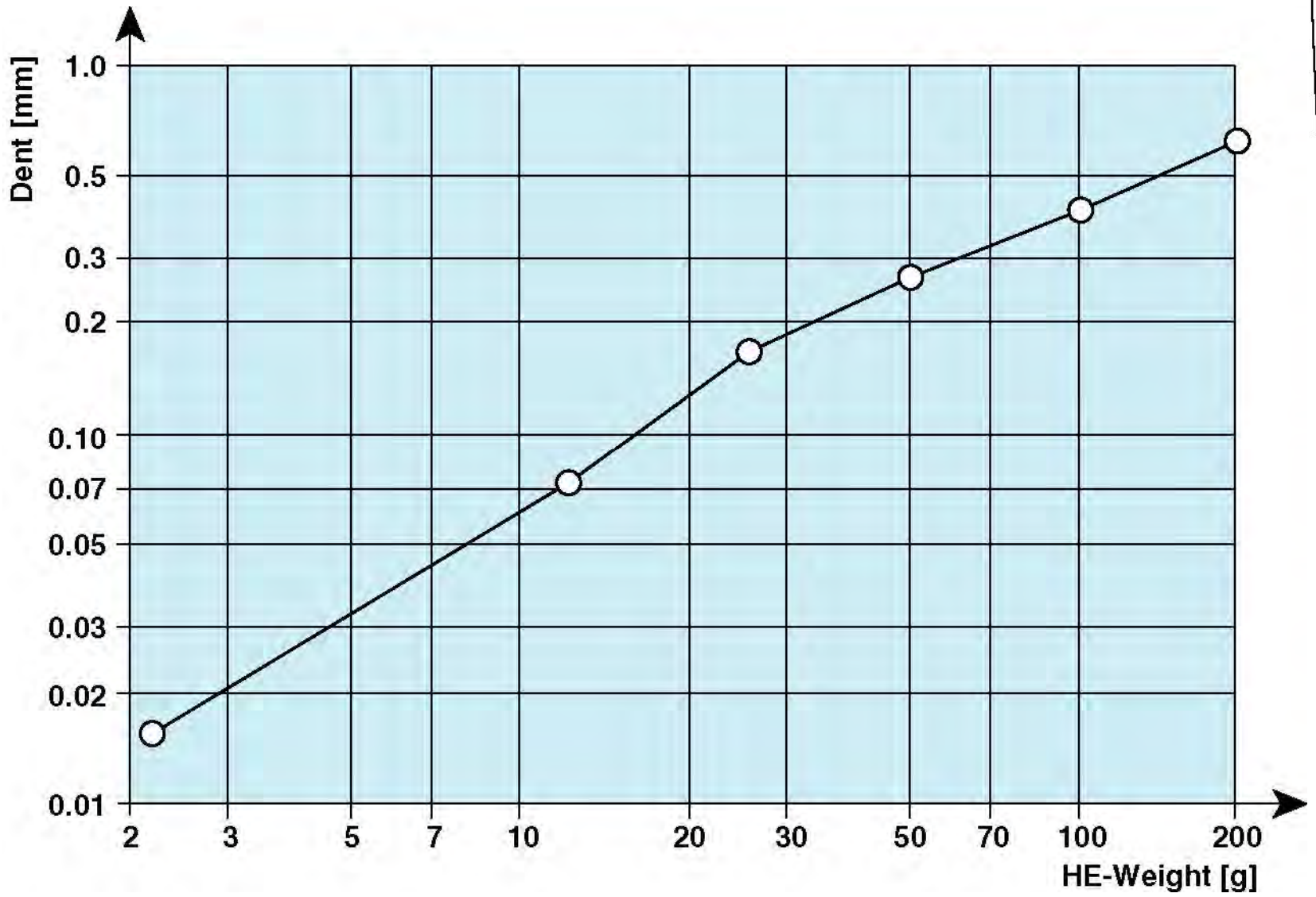
PDF Complete
Your complimentary use period has ended. Thank you for using PDF Complete.
Click Here to upgrade to Unlimited Pages and Expanded Features

EADS DEFENCE & SECURITY



PDF Complete
Your complimentary use period has ended. Thank you for using PDF Complete.
Click Here to upgrade to Unlimited Pages and Expanded Features

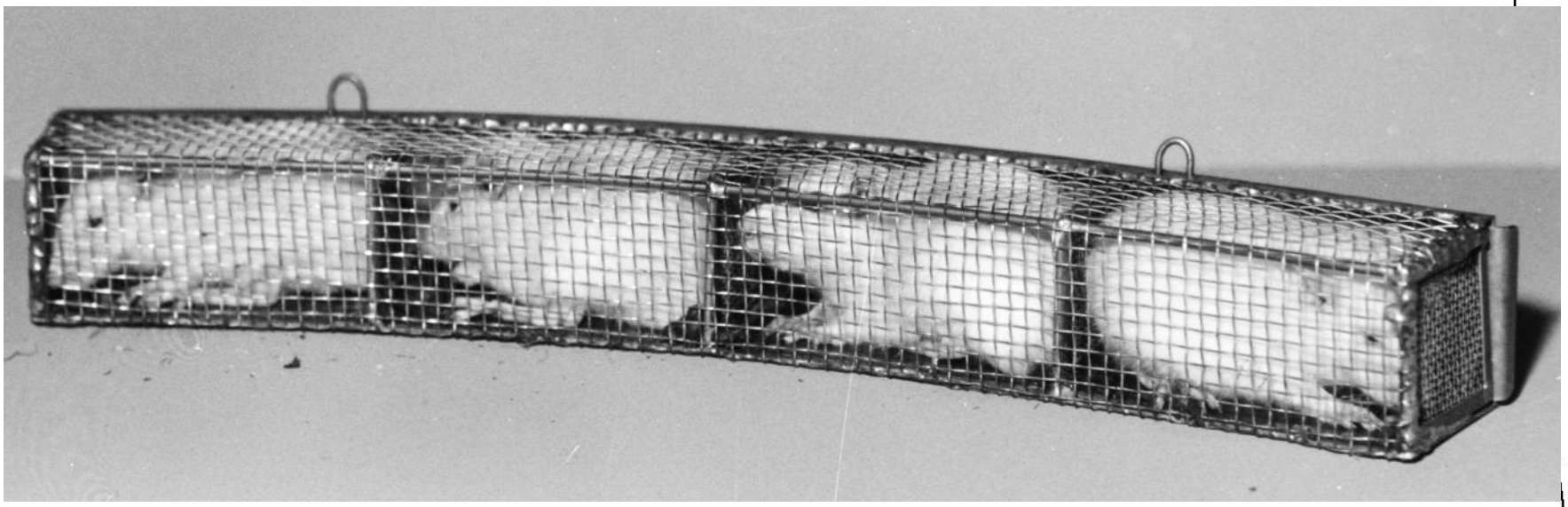
EADS DEFENCE & SECURITY



PDF Complete
Your complimentary use period has ended. Thank you for using PDF Complete.
Click Here to upgrade to Unlimited Pages and Expanded Features

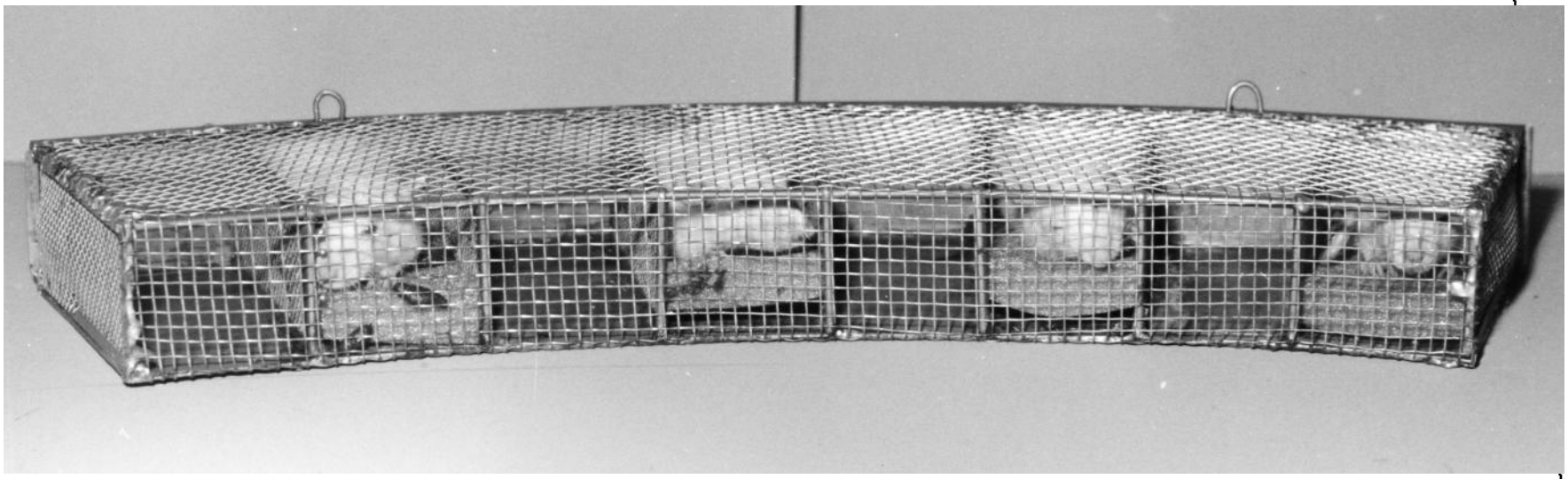
bino Rats

EADS DEFENCE & SECURITY



PDF Complete
Your complimentary use period has ended. Thank you for using PDF Complete.
Click Here to upgrade to Unlimited Pages and Expanded Features

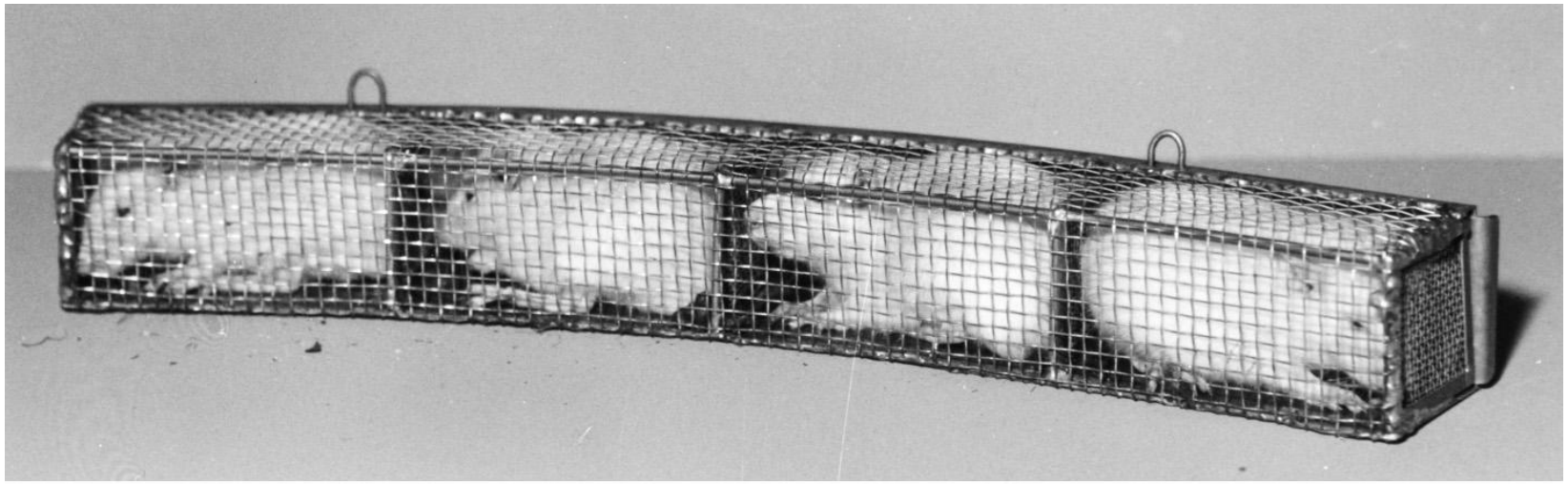
bino Rats

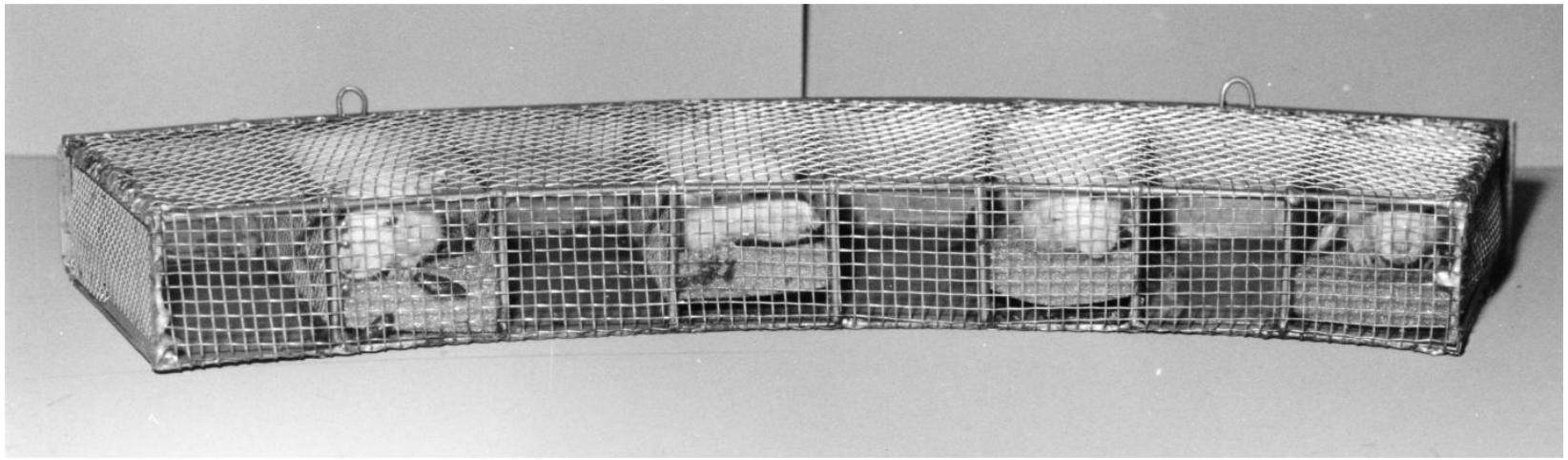


EADS DEFENCE & SECURITY

PDF Complete
Your complimentary use period has ended. Thank you for using PDF Complete.
Click Here to upgrade to Unlimited Pages and Expanded Features

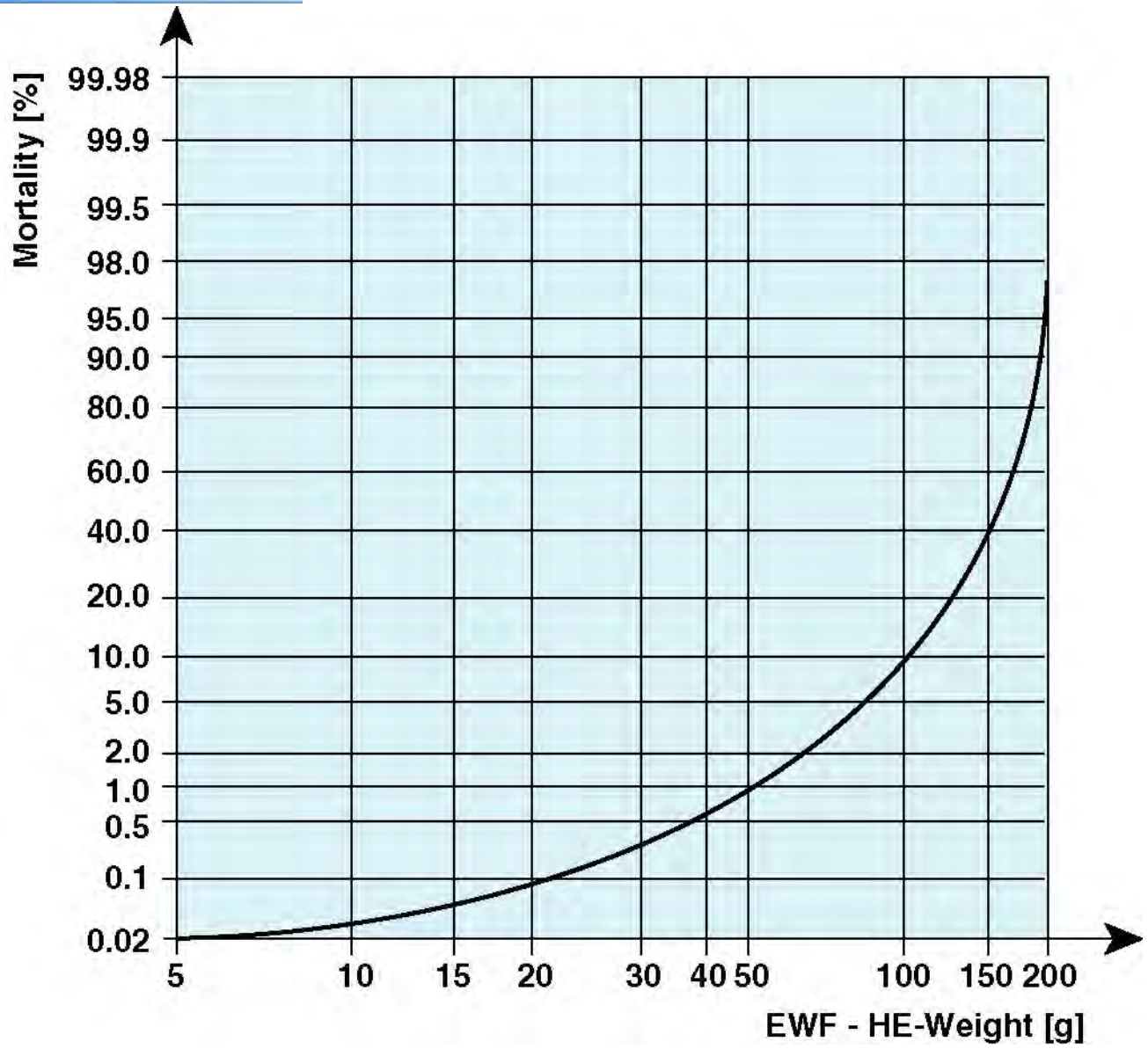
bino Rats





PDF Complete
Your complimentary use period has ended. Thank you for using PDF Complete.
Click Here to upgrade to Unlimited Pages and Expanded Features

Rats 200g



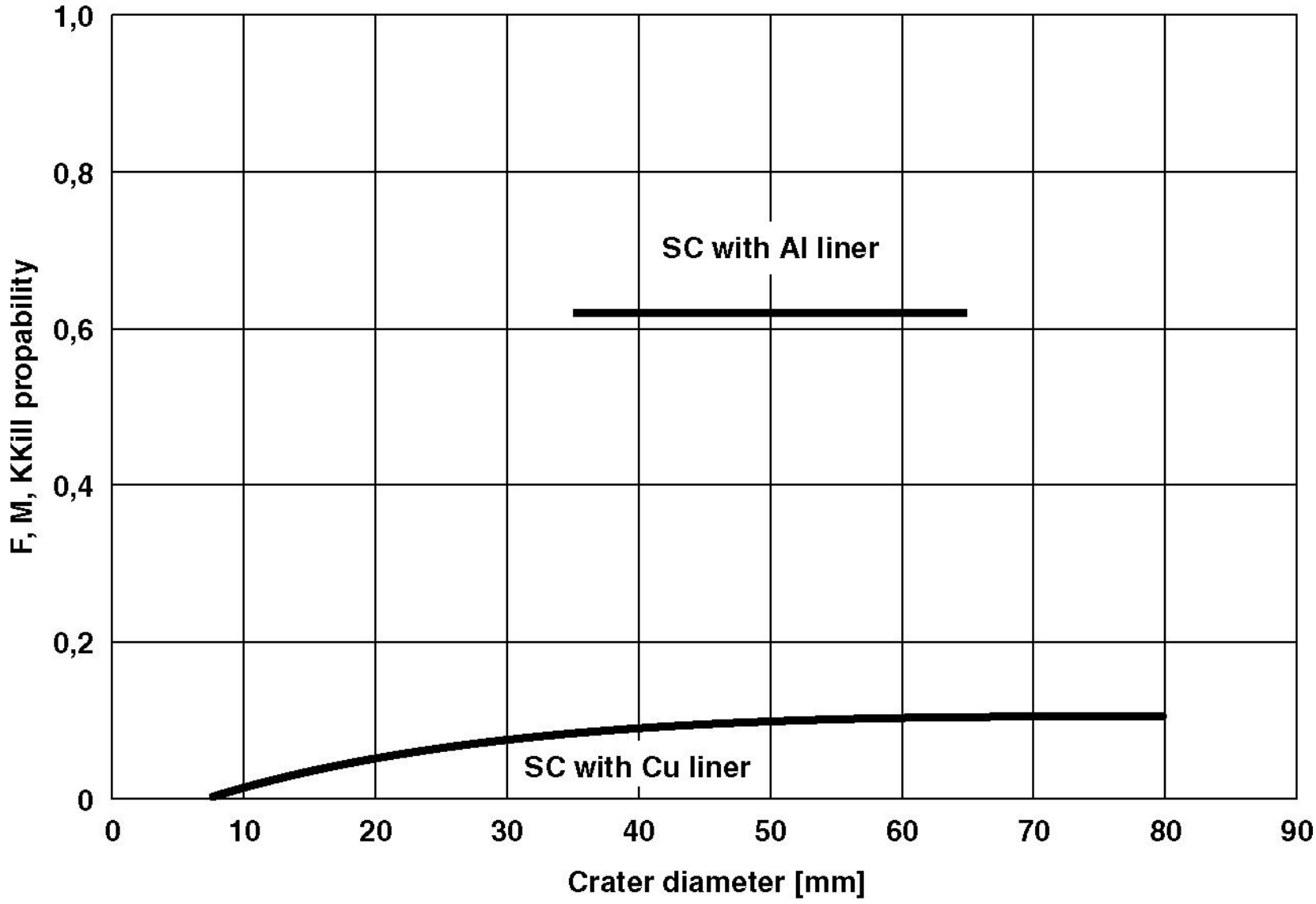
PDF Complete
Your complimentary use period has ended. Thank you for using PDF Complete.
Click Here to upgrade to Unlimited Pages and Expanded Features

EADS DEFENCE & SECURITY

Incendiary Effects

PDF Complete
Your complimentary use period has ended. Thank you for using PDF Complete.
Click Here to upgrade to Unlimited Pages and Expanded Features

EADS DEFENCE & SECURITY



PDF Complete
Your complimentary use period has ended. Thank you for using PDF Complete.
Click Here to upgrade to Unlimited Pages and Expanded Features

EADS DEFENCE & SECURITY



PDF Complete
Your complimentary use period has ended. Thank you for using PDF Complete.
Click Here to upgrade to Unlimited Pages and Expanded Features

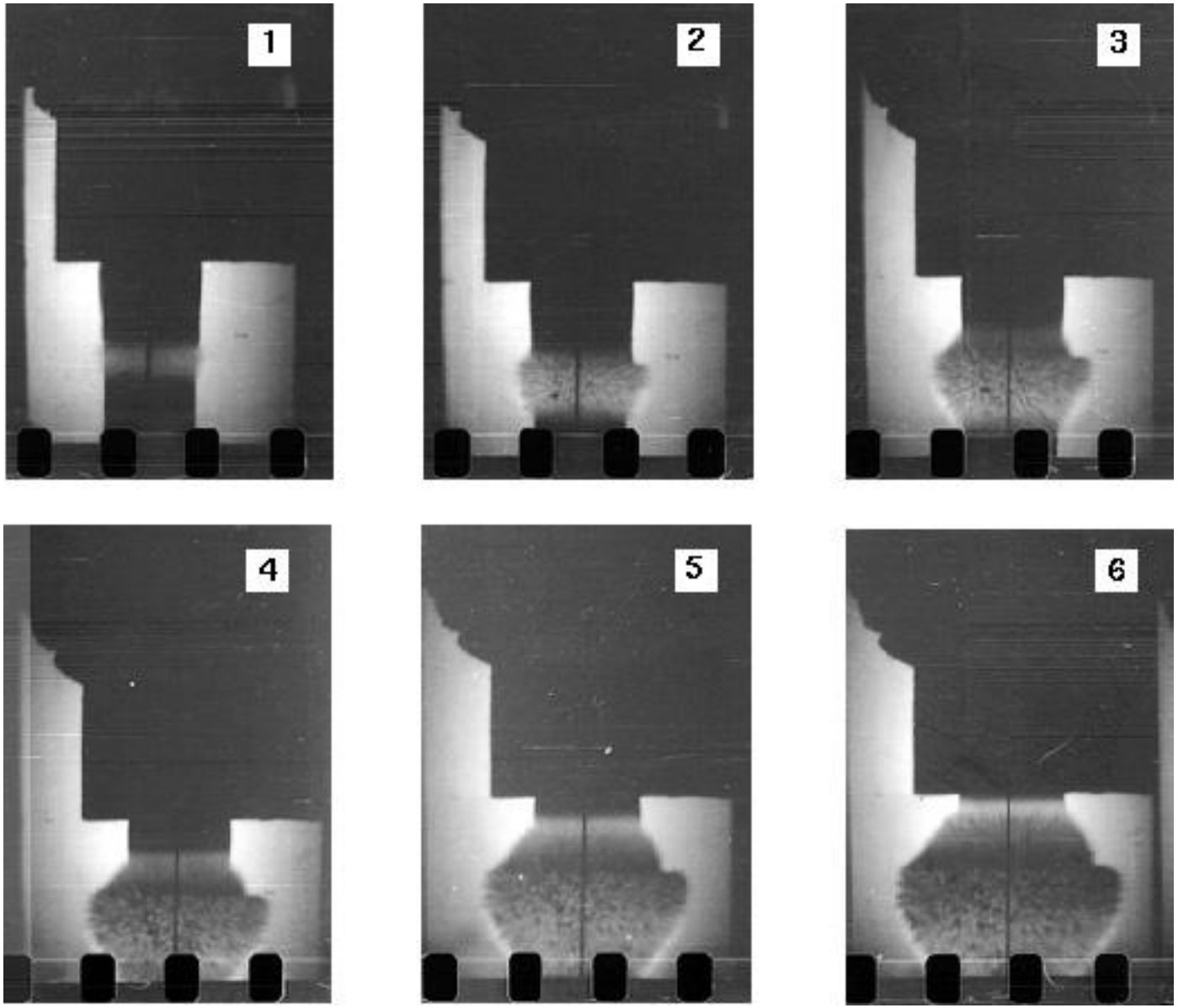
EADS DEFENCE & SECURITY

Ignition &

Initiation Effects

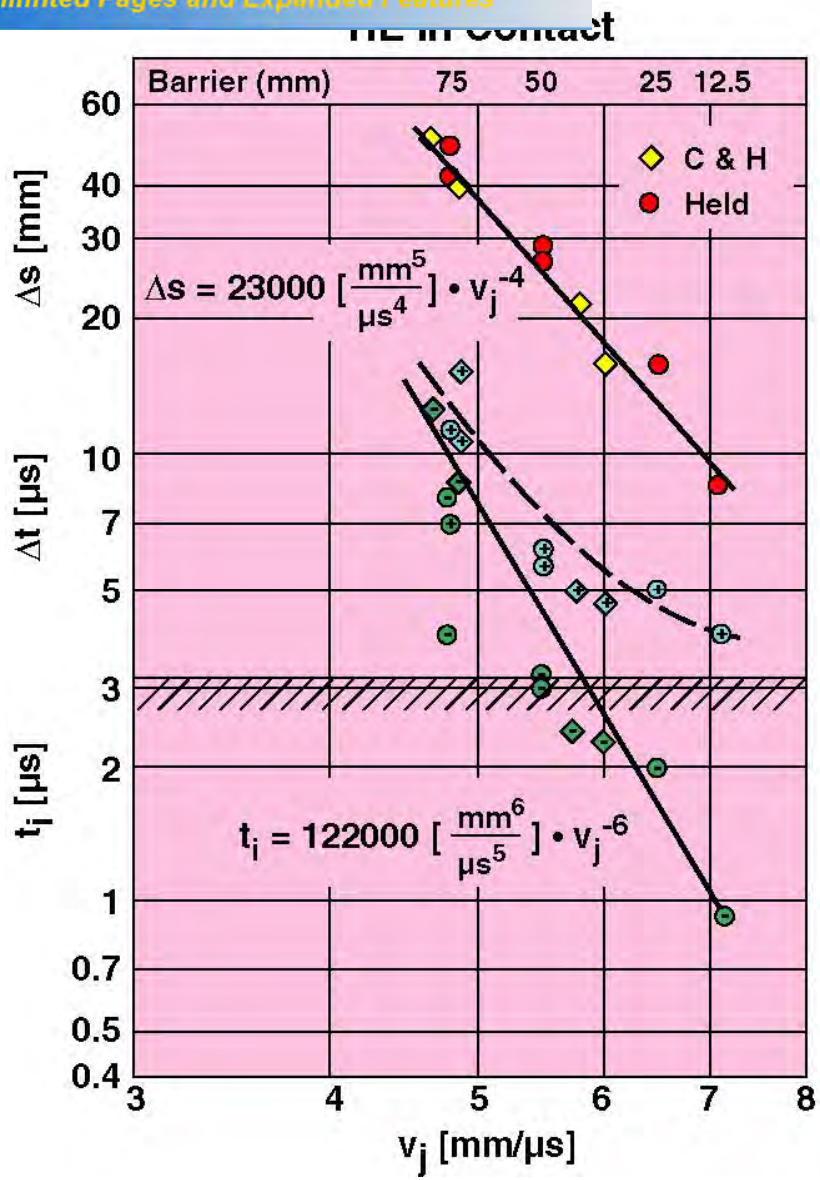
PDF Complete
Your complimentary use period has ended. Thank you for using PDF Complete.
Click Here to upgrade to Unlimited Pages and Expanded Features

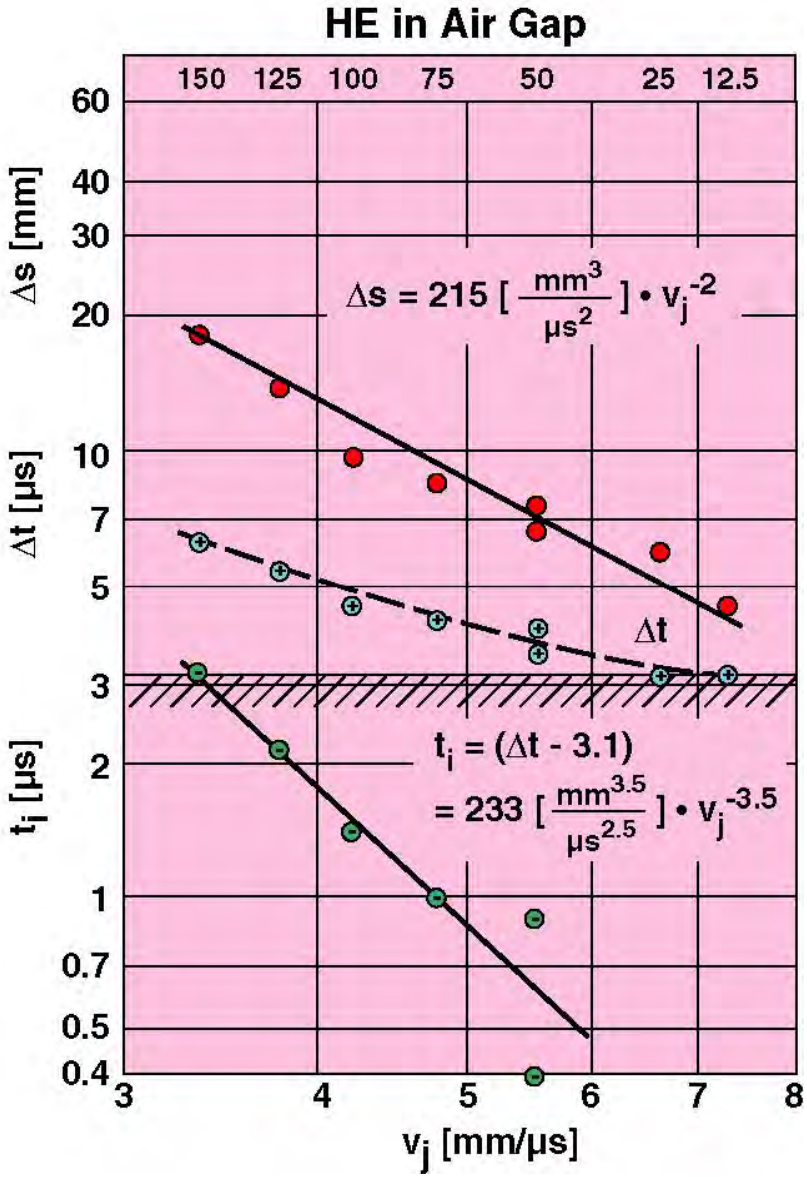
EADS DEFENCE & SECURITY



PDF Complete
Your complimentary use period has ended. Thank you for using PDF Complete.
Click Here to upgrade to Unlimited Pages and Expanded Features

EADS DEFENCE & SECURITY



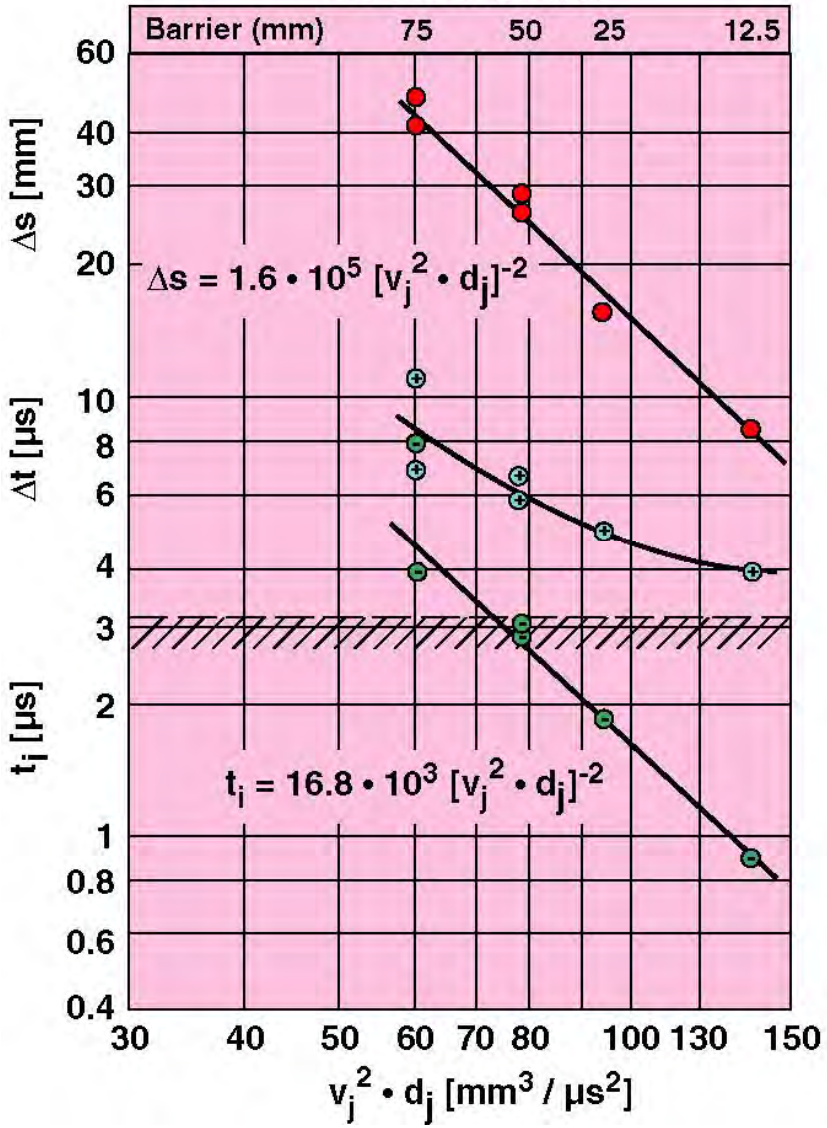


M. Held, 9th Symposium (International) on Detonation 1416 - 1426, **1989**

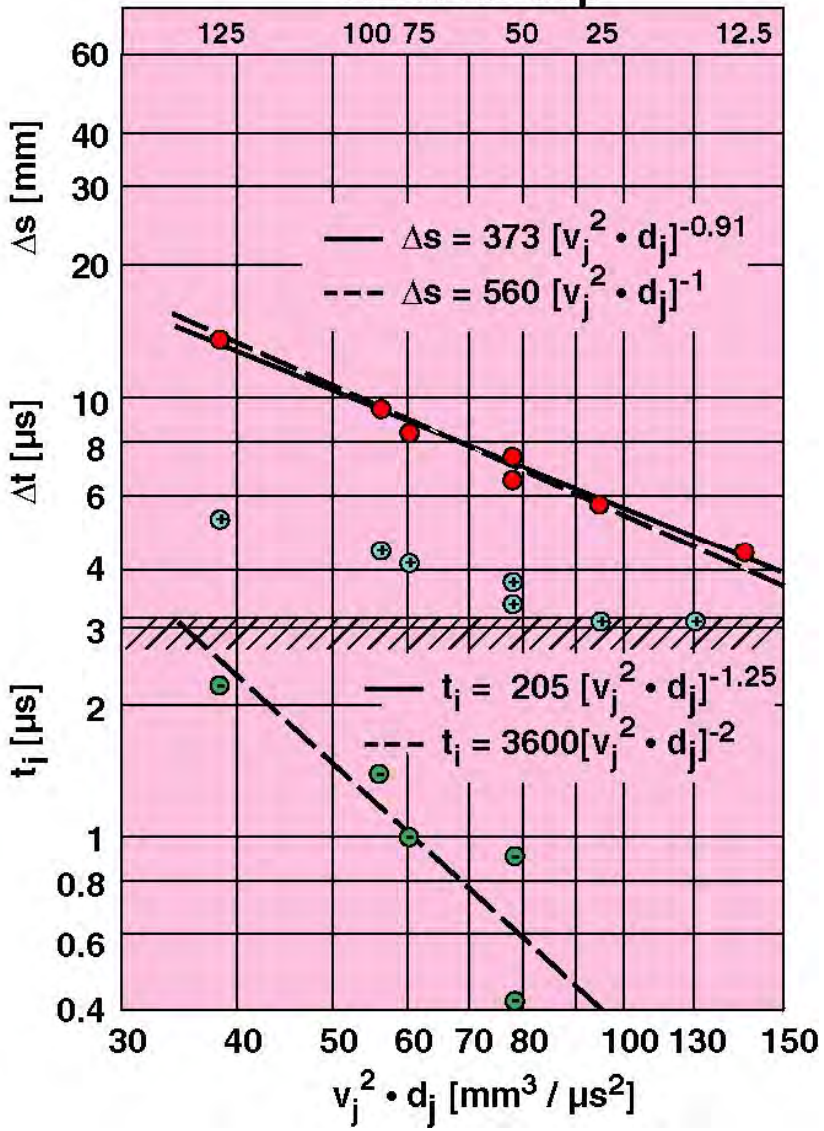
PDF Complete
Your complimentary use period has ended. Thank you for using PDF Complete.
Click Here to upgrade to Unlimited Pages and Expanded Features

EADS DEFENCE & SECURITY

HE in Contact

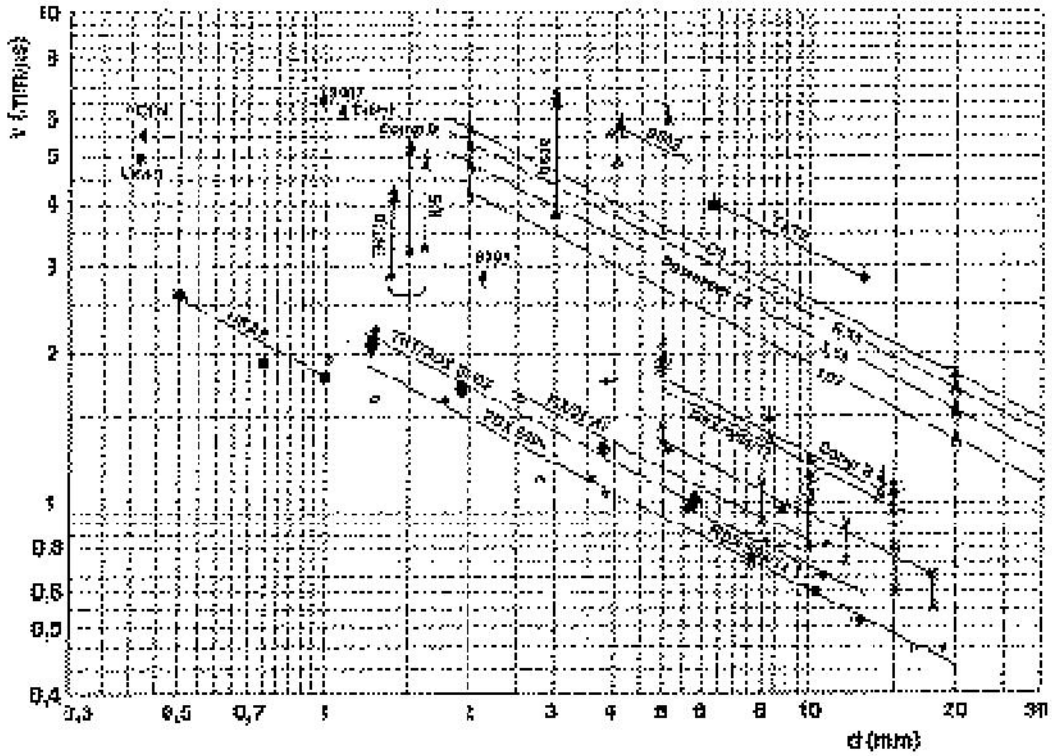


HE in Air Gap



PDF Complete
Your complimentary use period has ended. Thank you for using PDF Complete.
Click Here to upgrade to Unlimited Pages and Expanded Features

EADS DEFENCE & SECURITY



Type of HE	v^2d ($mm^3/\mu s^2$)	Sign in Figure
HNAB	3	■
PBX 9404	4	●
RDX/Wax 88/12	5	●
TNT/RDX 15/65	6	◆
PETN (1.77)	13	▲
Comp. B	16	▲
H6	16.5	▲
Detasheet C3	36 - 53	▲
PBX 9407	40	▲
Tetryl	44	▲
C4	64	▲
TATB	108	■
PBX 9502	128	▲

△ □ ○ - no Initiation ▲ ■ ● - Initiation

The above diagram of the threshold impact velocities as functions of the diameters of the shaped charge jet (▲), projectile (●), flyer foil (■) and from FEM-calculations (x) for different high explosive charges gives a clear indication of the validity of the v^2d-criterion.

M. Held 9th Symposium (int.) on Detonation 1416 - 1426 + 1432 - 1440, 1989

PDF Complete
Your complimentary use period has ended. Thank you for using PDF Complete.
Click Here to upgrade to Unlimited Pages and Expanded Features

EADS DEFENCE & SECURITY

Reactions of Propellants and High Explosives

v^2d or u^2d criterion gives the ignition and initiation threshold values at shaped charge jet impacts

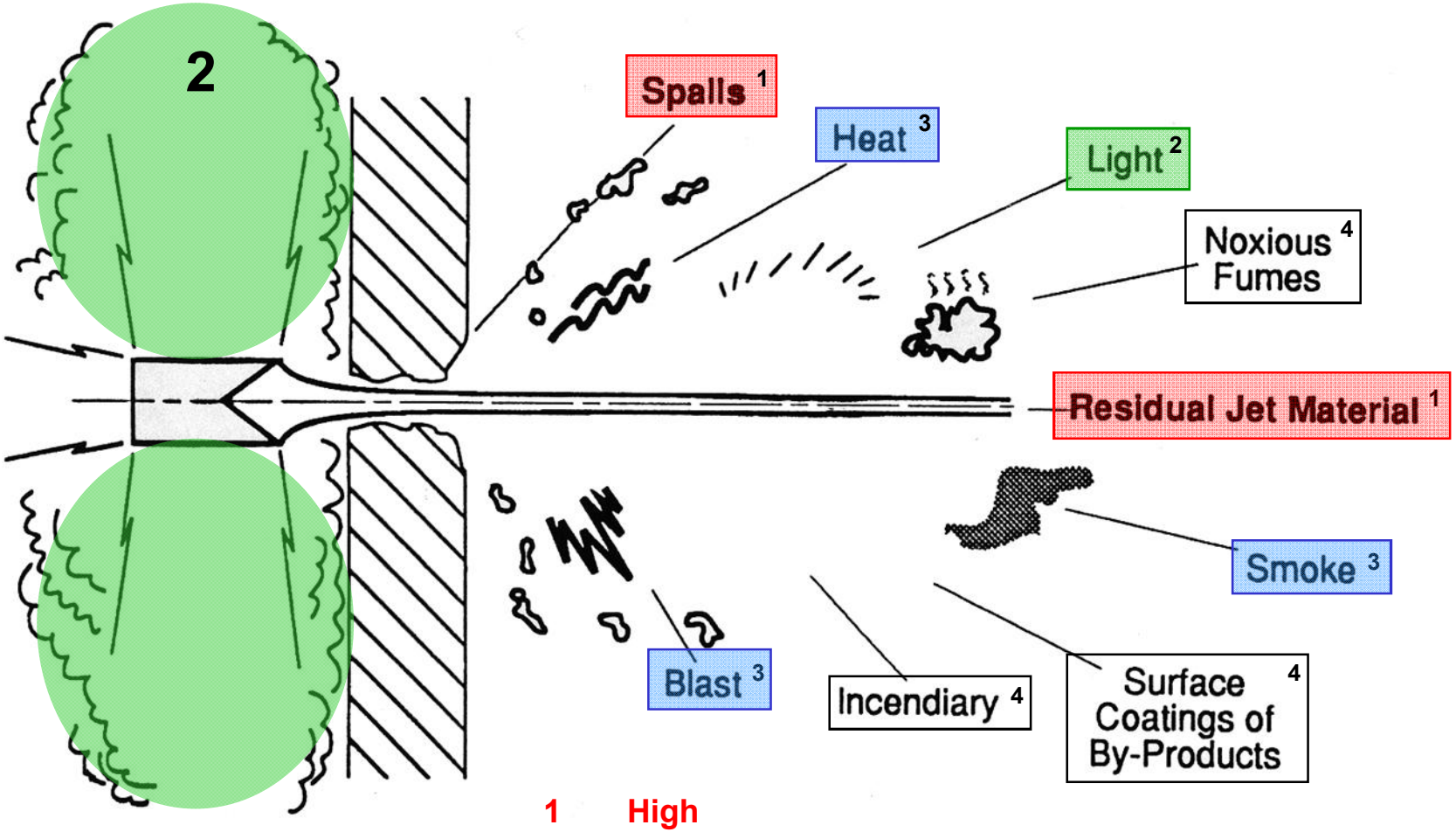
Less sensitive explosives are now not available against shaped charge jet loads

Take no explosives in the crew compartment, if you want to increase the survivability of the crew

PDF Complete
Your complimentary use period has ended. Thank you for using PDF Complete.
Click Here to upgrade to Unlimited Pages and Expanded Features

EADS DEFENCE & SECURITY

nd Armour Effects after Shaped Charge Jets Perforations



1 High
2 Media
3 Minor
4 nothing

PDF Complete
Your complimentary use period has ended. Thank you for using PDF Complete.
Click Here to upgrade to Unlimited Pages and Expanded Features

DEFENCE ACADEMY OF THE UNITED KINGDOM
Cranfield UNIVERSITY
Defence College of Management and Technology

THE VALIDATION OF A THORACIC AND ABDOMINAL TEST RIG FOR BABT SOFT BODY ARMOUR TESTING.

K.Hewins
I.Horsfall
C.Watson
Cranfield University, Shrivenham, UK.
khewins.cu@defenceacademy.mod.uk
+00 (44) 1793 785 330
+00 (44) 7533038677

PDF Complete
Your complimentary use period has ended. Thank you for using PDF Complete.
Click Here to upgrade to Unlimited Pages and Expanded Features

AIMS

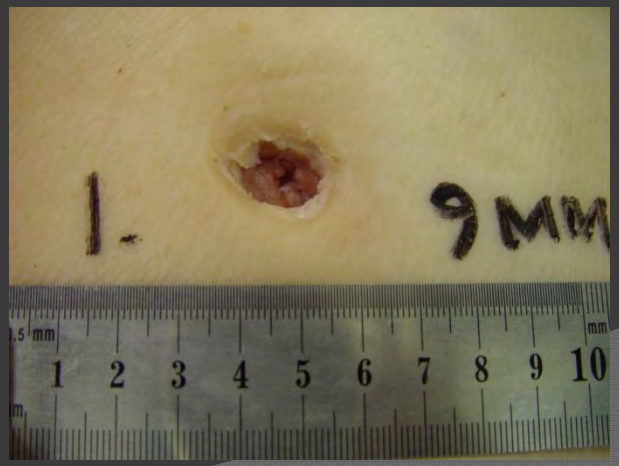
- Define BABT.
- Mechanism of BABT.
- Standards currently in place.
- Problems with current methods.
- The use of a ôTest rigô
- Further Research.

PDF Complete
Your complimentary use period has ended. Thank you for using PDF Complete.
Click Here to upgrade to Unlimited Pages and Expanded Features

RMOUR BLUNT TRAUMA BABT.

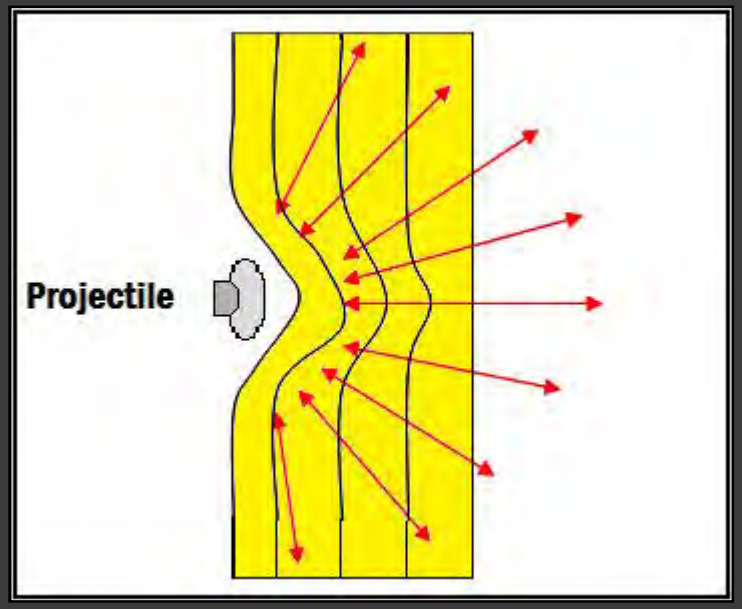
- Law enforcement personal armour.
- High velocity projectile impact.
- Deformation of soft body armour
- Stress waves by initial displacement.
- Shear deformation to viscera.
- Minor and major injuries.



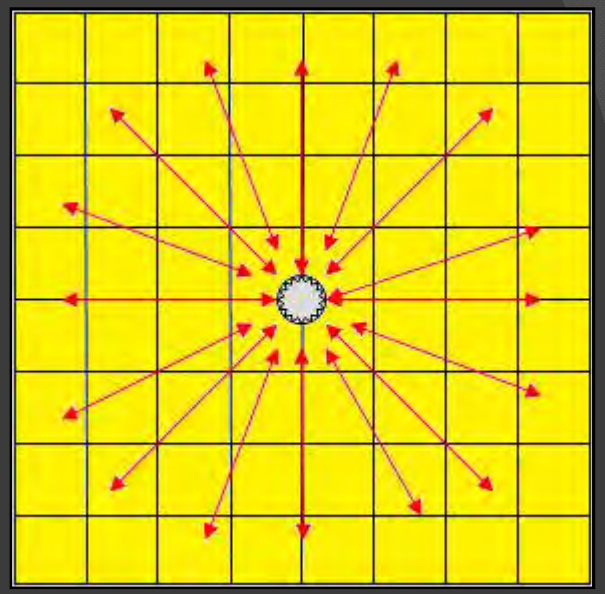


PDF Complete
Your complimentary use period has ended. Thank you for using PDF Complete.
Click Here to upgrade to Unlimited Pages and Expanded Features

MECHANISM OF BABT.



LATERAL ABSORPTION



RADIAL ABSORPTION



PDF Complete
Your complimentary use period has ended. Thank you for using PDF Complete.
Click Here to upgrade to Unlimited Pages and Expanded Features

CURRENT STANDARDS

- Uniform level of resistance to BABT
- UK Home Office ï HOSDB
- US Government ï NIJ
- Plastilina ®
- HG1/A level
- 9mm rounds
- 365 +/- 10m/s
- 44mm





PDF Complete
Your complimentary use period has ended. Thank you for using PDF Complete.
Click Here to upgrade to Unlimited Pages and Expanded Features

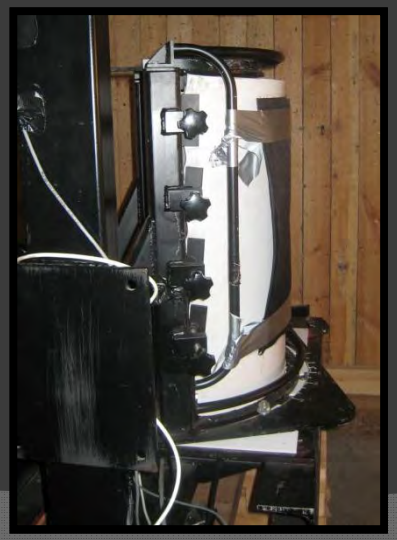
PROBLEMS WITH BABT TESTING

- Biofidelity of Plastilina ®
- Cadaver ï Ethical Issues
- Animal - Ethical Issues
- Hybrid III ï Costly

PDF Complete
Your complimentary use period has ended. Thank you for using PDF Complete.
Click Here to upgrade to Unlimited Pages and Expanded Features

BABT TEST RIG

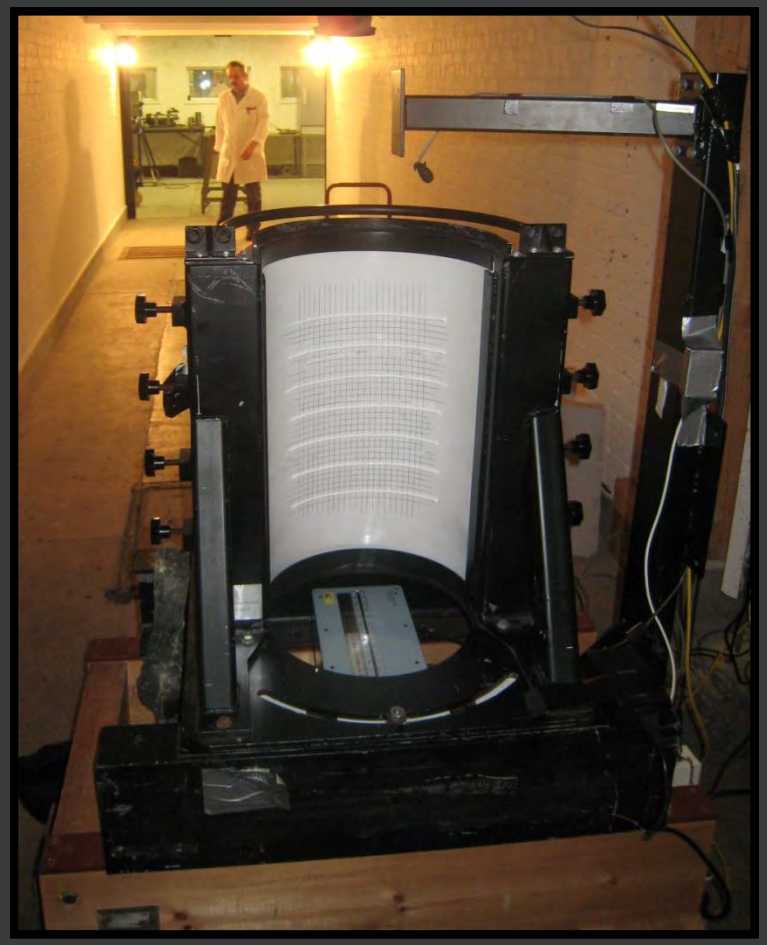


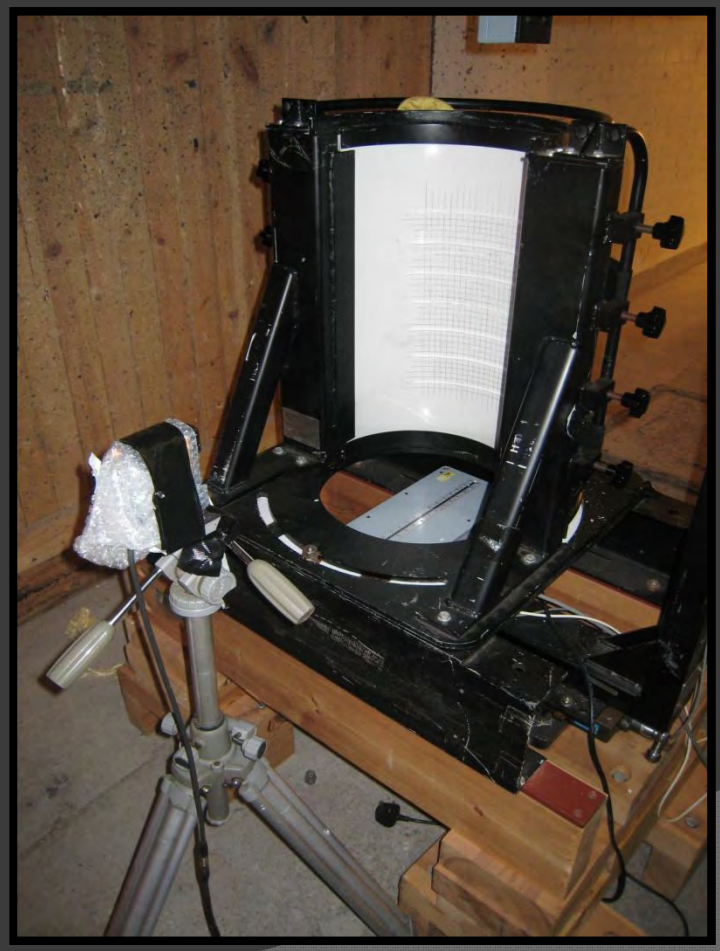


- Three Main Components.
- Response Element
- Lasers
- Framework

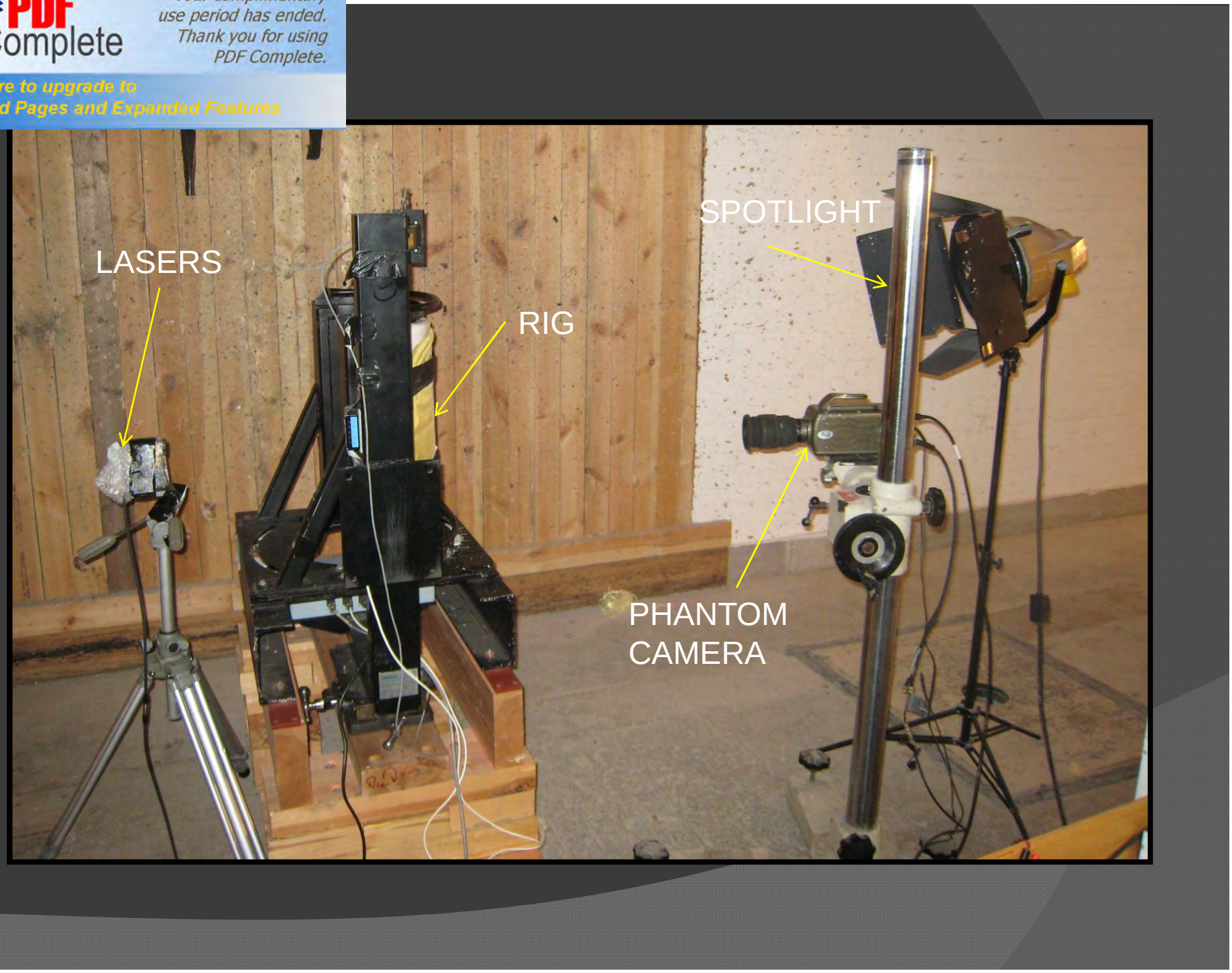
PDF Complete
Your complimentary use period has ended. Thank you for using PDF Complete.
Click Here to upgrade to Unlimited Pages and Expanded Features

DISPLACEMENT LASERS





PDF Complete
Your complimentary use period has ended. Thank you for using PDF Complete.
Click Here to upgrade to Unlimited Pages and Expanded Features



PDF Complete
Your complimentary use period has ended. Thank you for using PDF Complete.
Click Here to upgrade to Unlimited Pages and Expanded Features

JURY CRITERIA

- The Viscous Injury Criterion VC (Lau and Viano 86).
- Severity of Injury.
- Viscous tolerance = risk of soft tissue injury associated with a specific-induced viscous response, VC.
- VC_{max} ï maximum risk.

PDF Complete
Your complimentary use period has ended. Thank you for using PDF Complete.
Click Here to upgrade to Unlimited Pages and Expanded Features

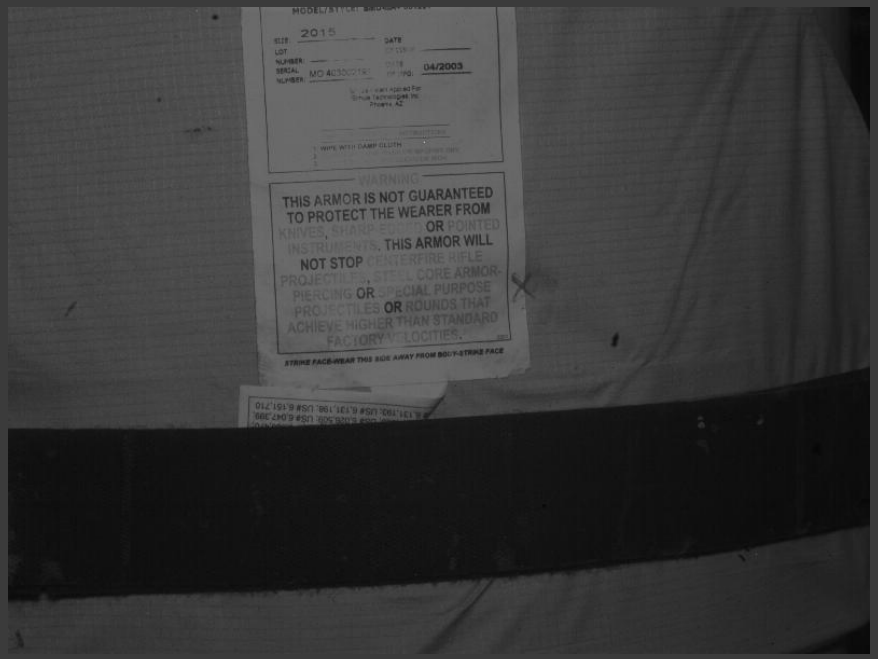
BALLISTIC TEST PROCEDURE

- HOSDB HG1/A Level
- 9x19mm Nobel Dynamit FMJ DM11A1B2
- 5m Range
- Abdominal and Thoracic

- 30 ply Kevlar ® 49
- 30 ply Teijin Twaron ®
- 30ply Zylon ®

PDF Complete
Your complimentary use period has ended. Thank you for using PDF Complete.
Click Here to upgrade to Unlimited Pages and Expanded Features

FRONT IMPACT



THORACIC SIMULANT



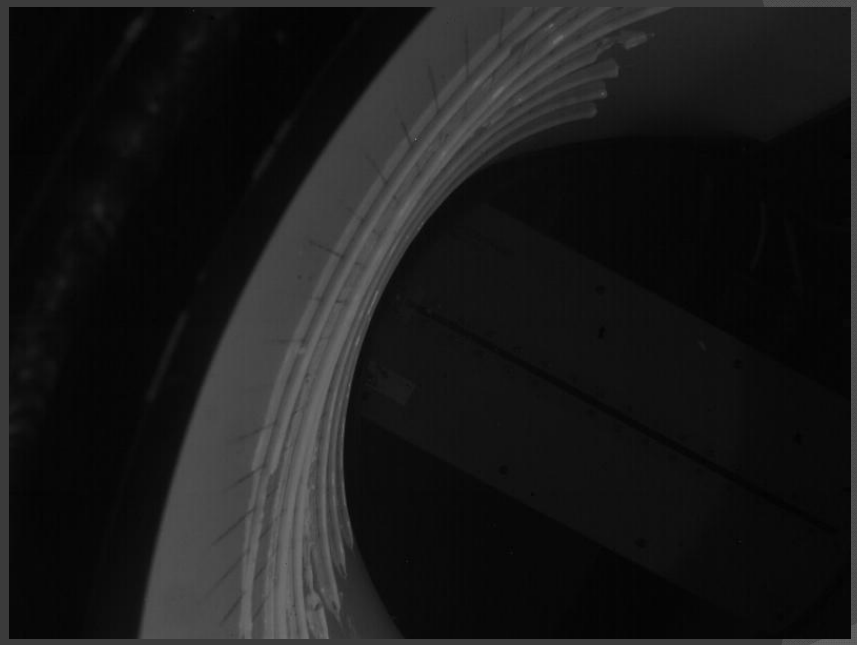
ABDOMINAL SIMULANT

PDF Complete
Your complimentary use period has ended. Thank you for using PDF Complete.
Click Here to upgrade to Unlimited Pages and Expanded Features

TOP IMPACT



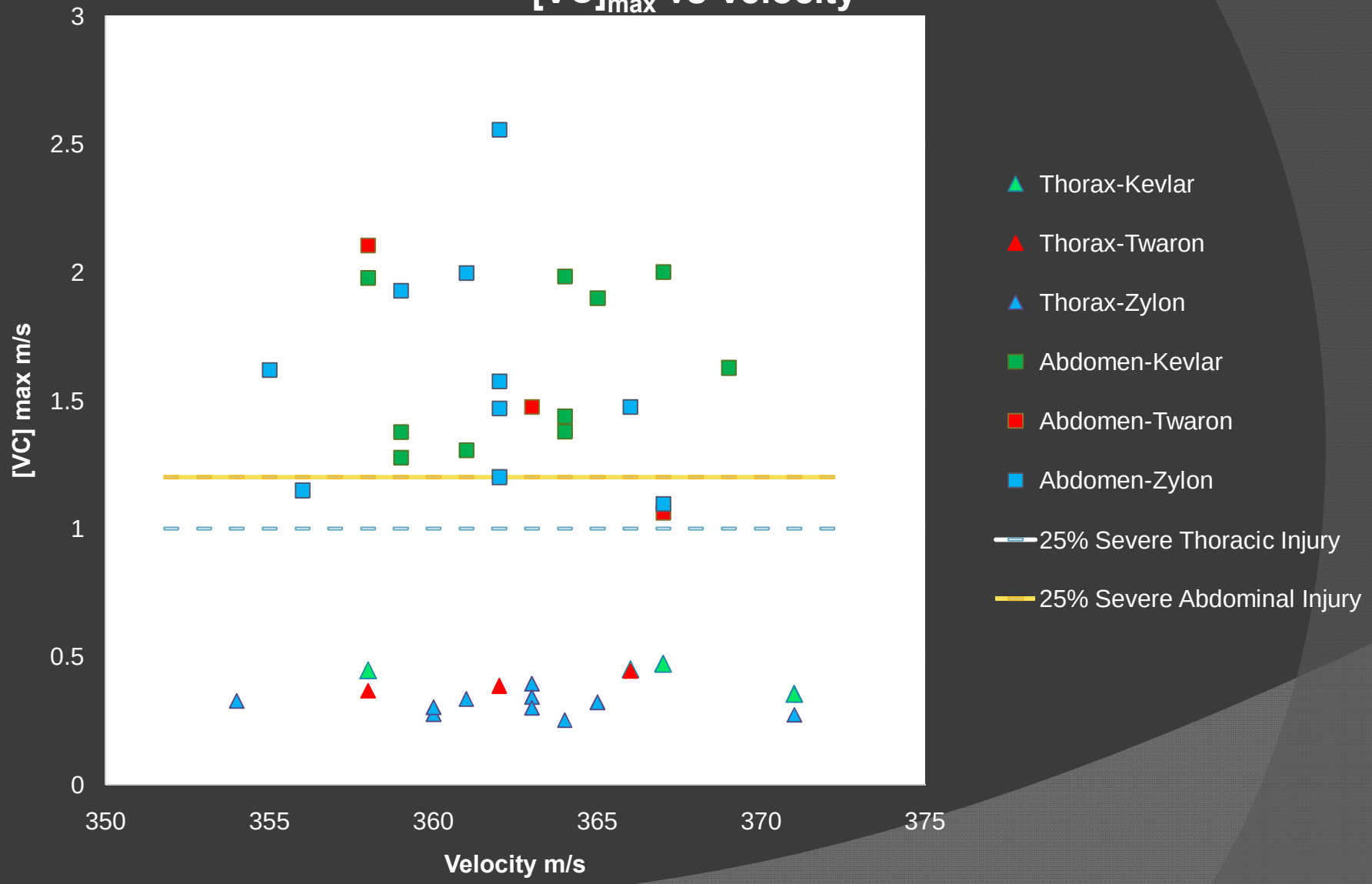
THORACIC SIMULANT



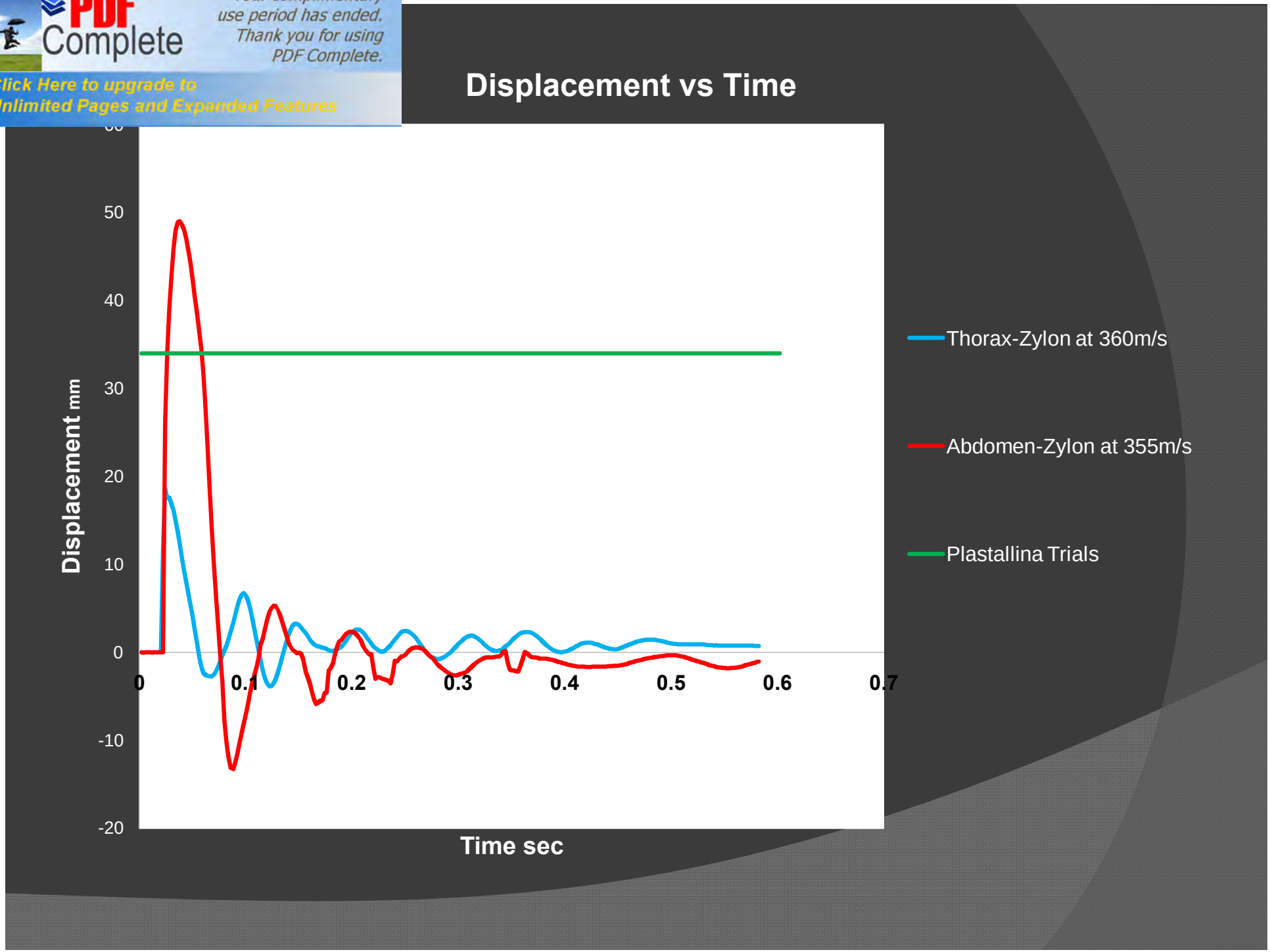
ABDOMINAL SIMULANT

PDF Complete
Your complimentary use period has ended. Thank you for using PDF Complete.
Click Here to upgrade to Unlimited Pages and Expanded Features

Ballistic Testing. $[VC]_{max}$ vs Velocity



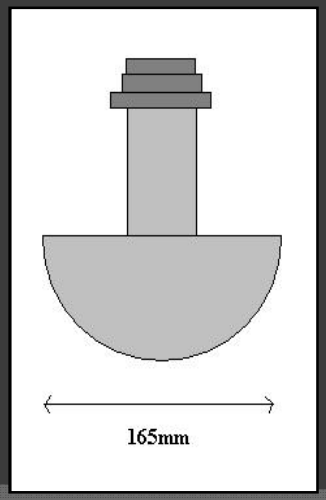
PDF Complete
Your complimentary use period has ended. Thank you for using PDF Complete.
Click Here to upgrade to Unlimited Pages and Expanded Features



PDF Complete
Your complimentary use period has ended. Thank you for using PDF Complete.
Click Here to upgrade to Unlimited Pages and Expanded Features

M 10 INSTRUMENTED DROP TOWER



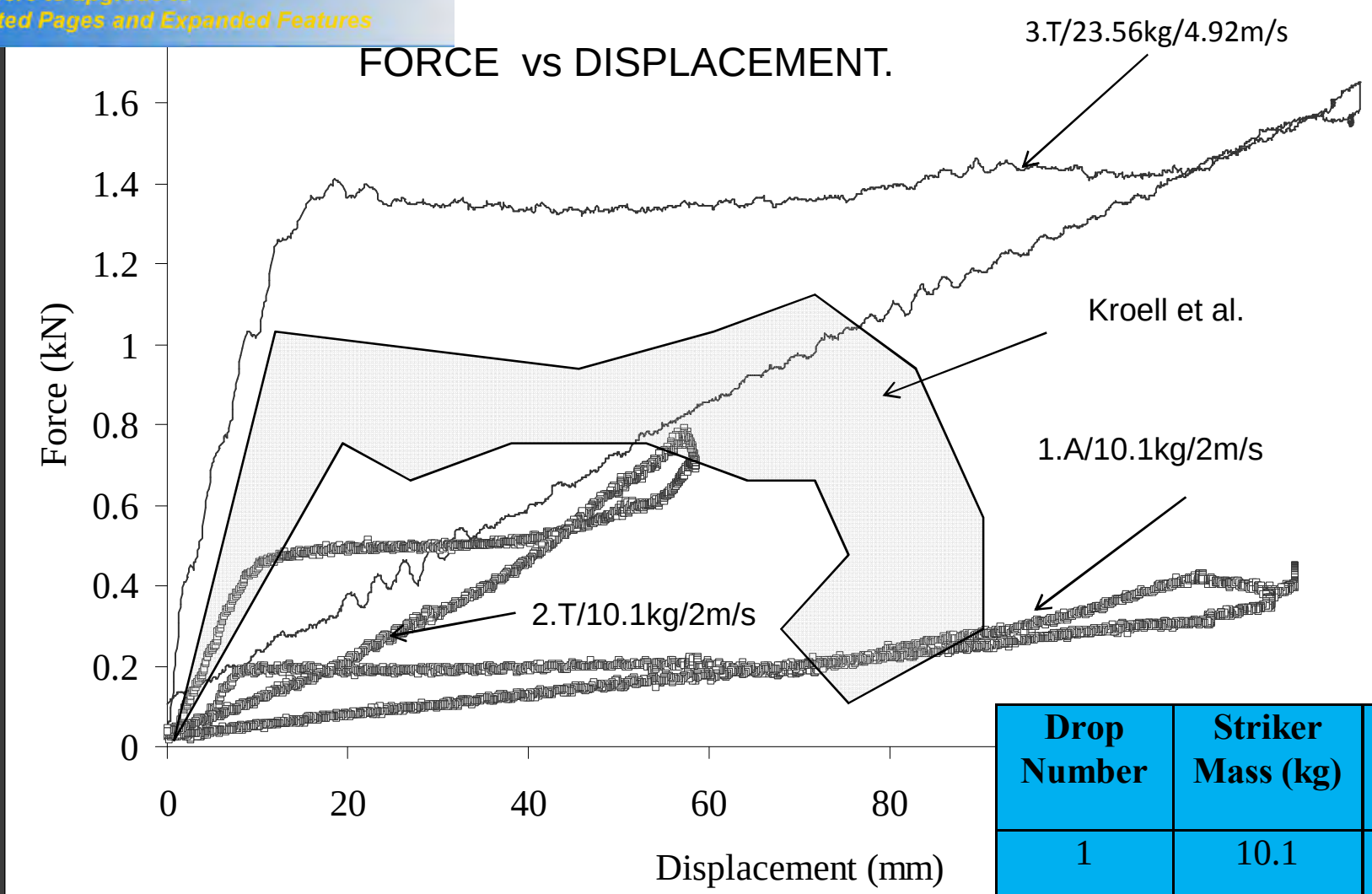


- Displacement/Force/Striker Mass
- Abdomen ï 1.8m/s and 2m/s.

  Striker Mass 10.1kg
- Thorax ï 1.8m/s and 5m/s

  Striker Mass 10.1kg and 23.656kg
- Kroell et al 1974

PDF Complete
Your complimentary use period has ended. Thank you for using PDF Complete.
Click Here to upgrade to Unlimited Pages and Expanded Features



Drop Number	Striker Mass (kg)	Velocity (m/s)
1	10.1	2
2	10.1	2
3	23.56	4.92
Kroell et al	~23	~4.92

PDF Complete
Your complimentary use period has ended. Thank you for using PDF Complete.
Click Here to upgrade to Unlimited Pages and Expanded Features

CONCLUSION

- Positive drop tower results.
- Ability to determine Injury severity.
- New abdominal simulant work.

- Further work to determine ideal thickness.
- Advantages over previous techniques.

PDF Complete
Your complimentary use period has ended. Thank you for using PDF Complete.
Click Here to upgrade to Unlimited Pages and Expanded Features

QUESTIONS?

Thankyou.....

Kate Hewins, Ian Horsfall, Celia Watson.

Cranfield University, Shrivenham, UK.
khewins.cu@defenceacademy.mod.uk
+00 (44) 1793 785 330
+00 (44) 7533038677

IBC Presentation 2008

Bo Janzon
IBC Chairman
(SECRAB, Sweden)
23 September 2008



Tarragona '07 - results of questionnaire

Question	YES [%]	NO [%]	Nil [%]
IBC organisation to remain as is	28	59	13
IBC to become a Society	75	19	6
Will become member of IBS	81	12	7
Be more actively involved?	67	25	8
Publishing in refereed Journal	94	1	5
Full proceedings only on a CD	56	44	1



108 answers out of 333 delegates

at 23rd ISB, Tarragona

Publication

- Will occur in the Journal of Applied Mechanics (JAM”)
- Abstracts for Journal articles due on 1 March 2009
- Manuscripts due 1 August 2009
- Authors notified by 15 November
- Final Manuscripts due 15 February 2010
- Symposium 17-21May 2010
- Publication of JAM special ISB issue September 2010



Publication, 2

- Abstracts to be submitted to ISB '10 Organiser's website
- Manuscripts (for Journal) to be submitted to JAM's website
- Acceptance rate of order of 35 % expected
- Space for 22-25 papers in special issue
- Good papers for which there will be no space can be published later by the JAM



Publication, 3

- Papers for Journal will have extended abstract in Symposium Proceedings
- Other papers will be printed, as usual, in Symposium Proceedings
- See 25th ISB Organiser's website:

www.ISB2010.com

or link from www.ballistics.org



Future Symposia



2010	Beijing, China
2011	Miami, Fl, USA
2013	Freiburg i. B., Germany

IBC 2005 – 2008 – What have we achieved?

- Organisation of future Symposia is stable, planned 4 1/2 years ahead!
- We have achieved scientific review and publication in a Journal, to be implemented in 2010
- We have started preparations for a ”Ballistic Society”, to be carried on by the new board.



The new IBC Executive

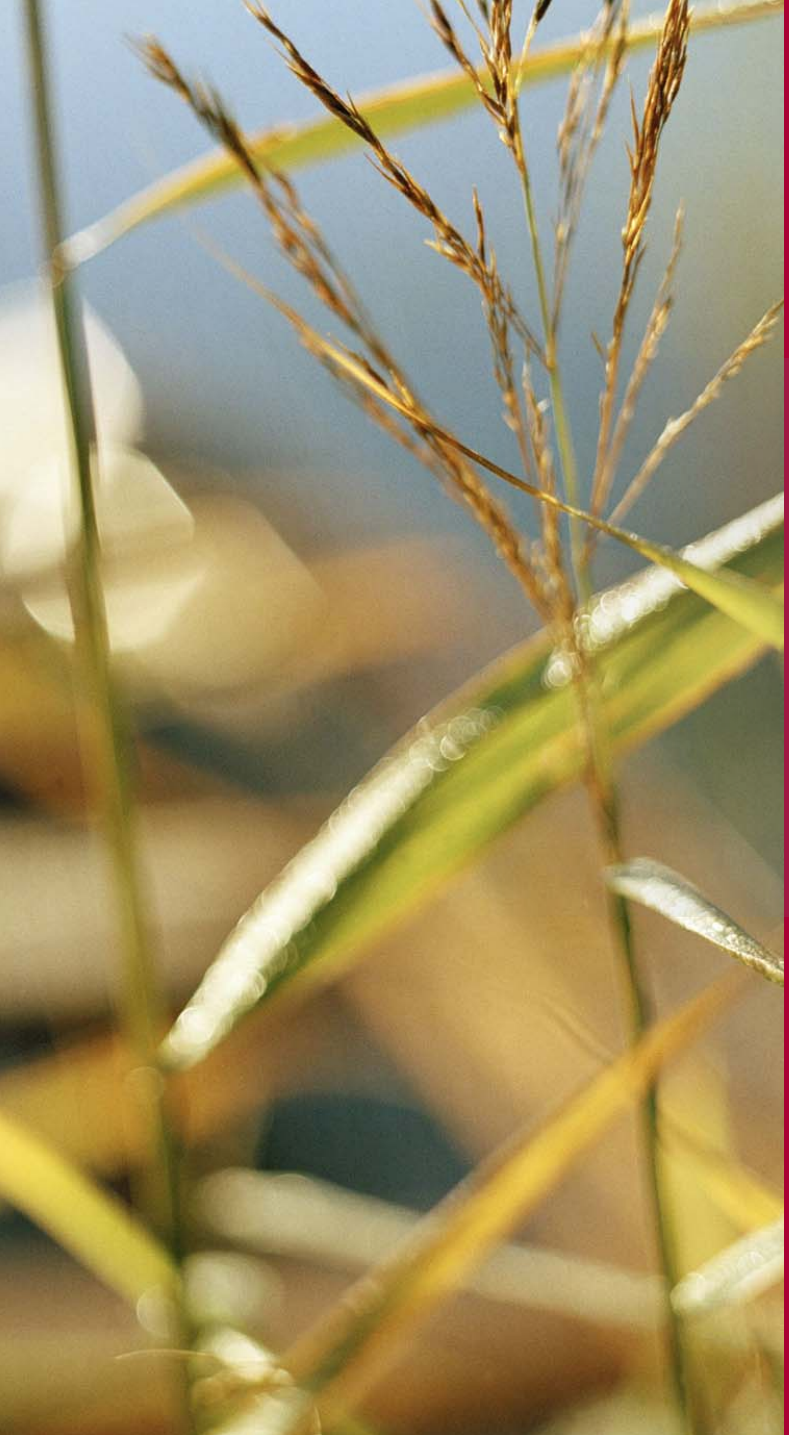


Chairman:	Jack Riegel, US
Vice Chairman:	Ian Cullis, UK
Secretary:	Sidney Chocron, US
Bursar #1:	Richard Fong, US
Bursar #2:	Bill Flis, US
POC Americas:	Michael Murphy, US
POC Europe:	Roxan Cayzac, France
POC OC:	Meir Mayseless, Israel
Past Chairman:	Bo Janzon, Sweden

Contact



www.ballistics.org



See you all at Beijing! in 2010

PDF Complete
Your complimentary use period has ended. Thank you for using PDF Complete.
Click Here to upgrade to Unlimited Pages and Expanded Features

A BRIEF HISTORY OF SHAPED CHARGES

24TH International Symposium on Ballistics
New Orleans, LA
September 2008

PDF Complete
Your complimentary use period has ended. Thank you for using PDF Complete.
Click Here to upgrade to Unlimited Pages and Expanded Features

BILL WALTERS

US ARMY RESEARCH LABORATORY

AMSRD-ARL-WM-TC

Aberdeen Proving Ground, MD

410-278-6062

walters@arl.army.mil

PDF Complete
Your complimentary use period has ended. Thank you for using PDF Complete.
Click Here to upgrade to Unlimited Pages and Expanded Features

MISNOMERS

PDF Complete
Your complimentary use period has ended. Thank you for using PDF Complete.
Click Here to upgrade to Unlimited Pages and Expanded Features



WAR IN IRAQ SATURDAY, FEB. 2, 1991 ••• THE NEWS JOURNAL

llied onslaught viewed om an Iraqi tank

qi tank commander on the battlefield can expect to be threatened by a storm of deadly echnology weapons developed especially to destroy Soviet-built tanks like his. They from modern armor-piercing shells fired by allied tanks to anti-tank guided missiles hed from helicopters, jets, and infantry vehicles. Here is how it all might look on the ing end:

A-10 Thunderbolt II
Close-support "Warthog" jet streaks in at less than 100 feet above the battlefield, then pops up for a good shot.

AH-64 Apache
Heavily armed attack helicopter can maneuver nimbly on the battlefield, firing on tanks from many angles.

Hellfire missile
Precision guided "fire and forget" missile can lock on to its target after firing, while the helicopter evades enemy fire.

HEAT shell
High-explosive, anti-tank rounds are one of four different shells carried by M1A1s (see inset). Only the newest Iraqi tanks have any chance of withstanding a hit.

ger 30mm cannon
nks with up to 70 ring shells per second ven rotating barrels.

Maverick missile
Precision guided tactical missile homes in on tanks at supersonic speed using infrared, TV or laser guidance.

missile
in Vietnam and the 1973 Mideast war. issiles are guided to their by a wire tether ame out t of the as

Tank-piercing HEAT shell
Shell
A shaped charge detonates on impact, liquefying metal, which melts the tank's armor and forces its way through.
Liquefied metal

M2 Bradley
An IFV or infantry fighting vehicle, a cross between a light tank and an armored personnel carrier, armed with TOW missiles and a 25mm cannon.

M1A1 Abrams main battle tank
Most modern version of America's best tank has improved armor protection, better suspension, and a 120mm gun.

heavy tank
t tank is big, fairly fast, Soviet-built, d with a powerful 125mm main gun, some areas protected by HEAT- ing Chobham-type nic-and-metal r plating.

Dug-in tanks
In defensive fortifications, Iraq digs in tanks, half-burying them in the sand. Dug-in tanks cannot maneuver, but they are much harder to hit.

n range of anti-tank ordnance
16 km
4 km
TOW
Hellfire
HEAT
Target
16

PDF Complete
Your complimentary use period has ended. Thank you for using PDF Complete.
Click Here to upgrade to Unlimited Pages and Expanded Features

nating impulse upon striking the tough armour surface of the target. The detonator(s) fire the main body of explosive which, because of its shape, produces a narrow, high temperature plasma jet. The temperature is so high (about 20,000° Celsius) and the pressures developed are so great that even the toughest of alloy armour steels are penetrated. The material forming the jet reaches a density several times that of steel, and the armour becomes plastic and yields whilst the jet torch assists by melting and burning the armour metal.

It will be seen that most of the above is entirely under the control of the anti-tank weapon designer. He can control the speed of the missile, the composition, mass, density and also speed of detonation of the warhead, and finally he can control the time of pre-detonation by changing the length of the stand-off probe.

The designer can modify any of these parameters to produce plasma jets which will defeat the thickest armour, and it is not unknown for the heaviest warhead jets to be capable of piercing one side of a fighting vehicle, and then continuing straight through to pierce the opposite

Since a top attack is often del
a near vertically falling missile, a
ing armour effects will be mini
warhead will attack on the line
resistance. Thus, a smaller an
warhead may be used to pierce
top armour vertically. The mis
becomes small enough to be
in clusters or groups. These
showered down from suitable
canisters which can be delivere
craft or missile.

Thus an advancing armoure
may be attacked by hundreds
shaped-charge bomblets drop
rectly onto the tops of the ar

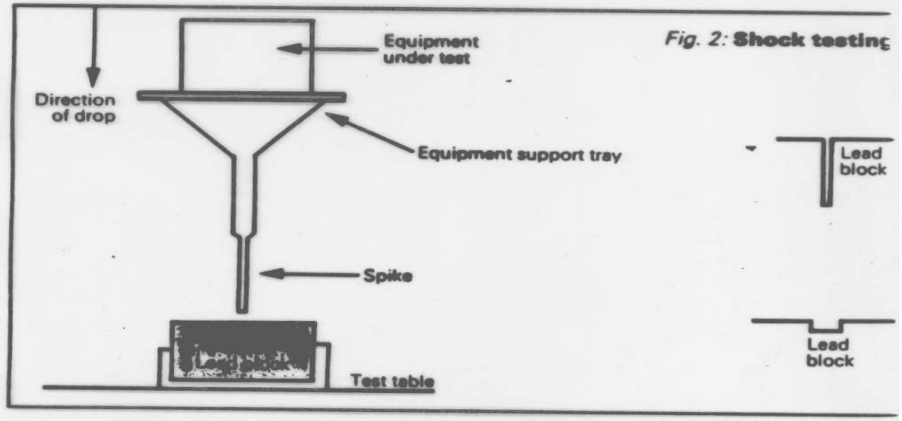


Fig. 2: **Shock testing**

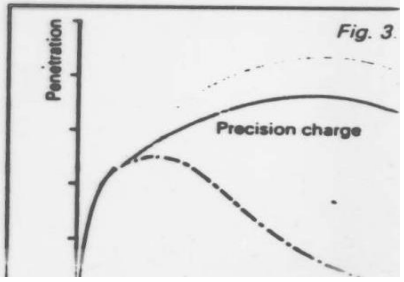
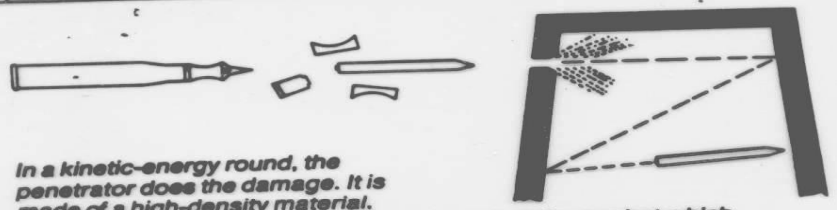


Fig. 3

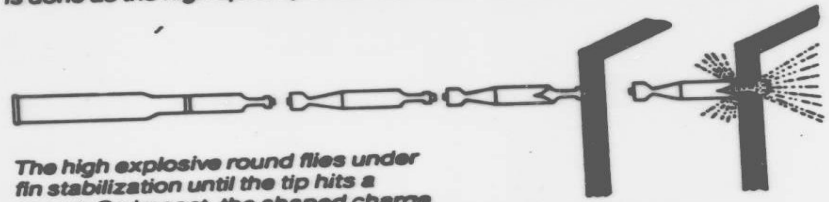
PDF Complete
Your complimentary use period has ended. Thank you for using PDF Complete.
Click Here to upgrade to Unlimited Pages and Expanded Features

TANK KILLERS

The U.S Army now favors the 120 mm smoothbore gun for its main battle tank, replacing the rifled 105 mm. (The Soviets use a smoothbore 125 mm.) The shift from rifled to smoothbore came about chiefly because spinning the round is no longer advantageous. In the days of stubby, full-bore rounds, the projectile behaved much like a rifle bullet and spin stabilization was essential. Today's modern rounds behave poorly when spun. The shaped-charge round does a better job if the warhead has minimum spin when it hits the target. The penetrator of the kinetic energy round now has a such a long length to diameter ratio, (about 18 to 1), that spinning causes it to wobble and lose stability. Instead, rounds are fin stabilized; small vanes are exposed after the round is fired to keep the projectile on course.



In a kinetic-energy round, the penetrator does the damage. It is made of a high-density material. Before the round is fired, the penetrator is held by a sabot which falls away while the projectile is in flight. The sabot allows the full power of a large diameter round to boost the small-diameter projectile. When the penetrator hits the target, its energy drives it through the armor. Once through, it contributes to the destruction by spalling metal from the armor it has penetrated. Most of the damage is done as the high speed penetrator ricochets around inside the tank.



The high explosive round flies under fin stabilization until the tip hits a target. On impact, the shaped charge within the round ignites and begins to play a stream of plasma on the target. Each shaped charge configuration has an optimum distance from the target where the cutting power of the plasma cone is greatest. This detonation distance is established by the length of the warhead tip. The plasma cone burns through the armor and spray molten particles into the tank at speeds of 30,000 fps.

composite armor
dard. It consists of
soft and hard ma
spaces. The dens
entation of the ar
critical to its su
armor is made is
cret. Even knowle
material being u
enemy a good i
much protectior
vides against spe
Composite arm
ject of many rese
ticularly metal r
This family of
exceptional st
weight and
breakthroughs i
How armor is
the tank is ano
and the amount
tect is a trick
tionally, the ta
protected along
forward arc, us
armor sectior
threats, this
positioned. Slo
deflect small ar
new high veloci
recent trend, t
as many sectic
ble. The "boxy
tank designers
Most heavy
armored skirt
The skirt perf
tion and caus
or break up
forces reac
Ideally, the sl
nate and sp
harmlessly i
the penetrat
up or start
reaches the
One of the

PDF Complete
Your complimentary use period has ended. Thank you for using PDF Complete.
Click Here to upgrade to Unlimited Pages and Expanded Features



JSED.

PDF Complete
Your complimentary use period has ended. Thank you for using PDF Complete.
Click Here to upgrade to Unlimited Pages and Expanded Features

COVER STORY

If nuclear weapons really are negotiated out of Europe, what will NATO do to offset the Soviets' 2-to-1 edge in conventional firepower? The answer may lie in the one technological trump card America still holds: Sophisticated microelectronics in "smart" weapons that find their own targets—with deadly accuracy

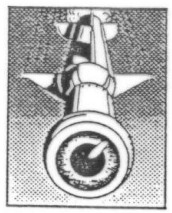
One shot, one kill: A new era of 'smart' weapons

■ *Viewed from the ground, it looks more curious than threatening: A paint can dangling from a tiny parachute, slowly flittering to earth. But suddenly, with a crack and a brilliant white flash, the "paint can" spits out a molten metal slug that crashes at 5,000 miles per hour directly through the engine of the Soviet tank below.*

In the distance, a flock of tiny parachutes drops onto the countryside. Their lethal cargo: A portable mine field that will stay in place until acoustic sensors detect passing Soviet armor. Then they, too, come alive with a barrage of hypervelocity slugs.

Behind the Soviet lines, model-airplane-like drones buzz overhead, relaying high-resolution TV pictures of massing Soviet divisions to the NATO command center hundreds of miles away.

And along the seven railroad lines that the Soviet high command has or-



viding armies with unprecedented mobility. Medieval knights feared the killing potential of the crossbow so much that at the Lateran Council of 1139 it was outlawed as "un-Christian." The invention of gunpowder, the cannon, the breech-loading rifle—each in turn revolutionized warfare. In 1862, Richard Gatling's machine gun introduced a grim new reality to the battlefield. During World War I, the mobility, firepower and armor of the tank began changing the strategy of static and horribly bloody trench warfare.

Yet none of history's revolutionary new weapons and technologies changed one basic fact about war: It has always taken hundreds or thousands of rocks, arrows, bullets, artillery shells or bombs to wipe out a single target. In the end, it has usually been numbers, skill and courage, not technology, that have prevailed on the battlefield.



U.S. AIR FORCE SYSTEMS COMMAND

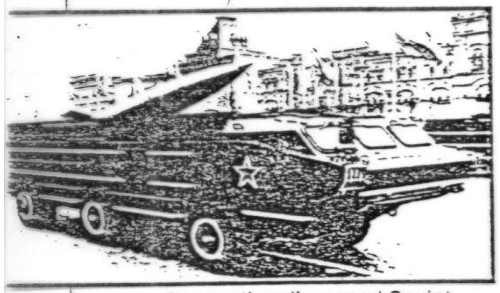
RFIGHTER FOCUSED.

PDF Complete
Your complimentary use period has ended. Thank you for using PDF Complete.
Click Here to upgrade to Unlimited Pages and Expanded Features

THE KREMLIN'S CATCH-UP PLAN

Invest now, build later

Lagging behind in critical computer and sensor technologies, the Soviets aren't trying to match U.S. smart weaponry gadget for gadget. At least not right away. Instead, they are gambling that the Gorbachev economic reforms eventually will so strengthen Moscow's technological base that it can compete both commercially and militarily with the United States. Moreover, some Soviet military theoreticians have been quicker than many of their Western counterparts to grasp the potential of smart weapons.



Conventionally armed Soviet SS-21s threaten NATO airfields

Writing in a Soviet military journal, Marshal Nikolai Ogarkov has observed that "automated search-and-destroy complexes, long-range high-accuracy terminally guided combat systems, unmanned flying machines and qualitatively new electronic-control systems make it possible to sharply increase the destructive potential of conventional weapons, bringing them closer to

Historically, Soviet weapons are made "soldierproof," suitable to the skills of soldiers who receive little technical training. The aim is summed up by reported orders of helicopter designer Mikhail Mil to his engineers: "Make it simple, make it rugged, make it reliable, make it *work*." Argues Christopher Donnelly, a British Soviet expert: "In some respects, by use of good engineering techniques and clever design, the Russians produce better weapons systems than we do with high technology."

The Soviets are also good at coming up with simple fixes to offset the enemy's high-tech weapons. For example, Soviet "reactive" armor seeks to undo the direct-hit capability of smart antitank munitions. When hit by a warhead, an explosive layer sandwiched inside the armor goes off, deflecting the blast to save the tank.

Already the Soviets lead the U.S. in some kinds of laser research, and a Pentagon analysis says they have caught up in six technology areas, including aerodynamics, explosives and optics. They are at work on radar-evading Stealth aircraft, and one smart helicopter antitank missile, the AT-6 Spiral, is said to have antijamming devices and heat sensors that give it a 90 percent kill probability.

"They already have quantity, and now are looking for better quality" that includes computer-chip technology on MiG-29 and MiG-31 fighters and computerized artillery fire-control centers, says

PDF Complete
Your complimentary use period has ended. Thank you for using PDF Complete.
Click Here to upgrade to Unlimited Pages and Expanded Features

Misnomers

- "On impact, the shaped charge within the round ignites and begins to play a stream of plasma on the target. Each shaped charge configuration has an optimum distance from the target where the cutting power of the plasma cone is greatest. This detonation distance is established by the length of the warhead tip. The plasma cone burns through the armor and sprays molten particles into the tank at speeds of 30,000 fps."

PDF Complete
Your complimentary use period has ended. Thank you for using PDF Complete.
Click Here to upgrade to Unlimited Pages and Expanded Features

More Misnomers

- "A shaped charge detonates on impact, liquefying metal, which melts the tanks armor."
- "The jet is a high temperature plasma (about 20,000 C)"
- "The jet reaches a density several times that of steel, and the armor becomes plastic and yields whilst the jet torch assists by melting and burning the armor metal"

PDF Complete
Your complimentary use period has ended. Thank you for using PDF Complete.
Click Here to upgrade to Unlimited Pages and Expanded Features

aped Charge Jet in Air



PDF Complete
Your complimentary use period has ended. Thank you for using PDF Complete.
Click Here to upgrade to Unlimited Pages and Expanded Features

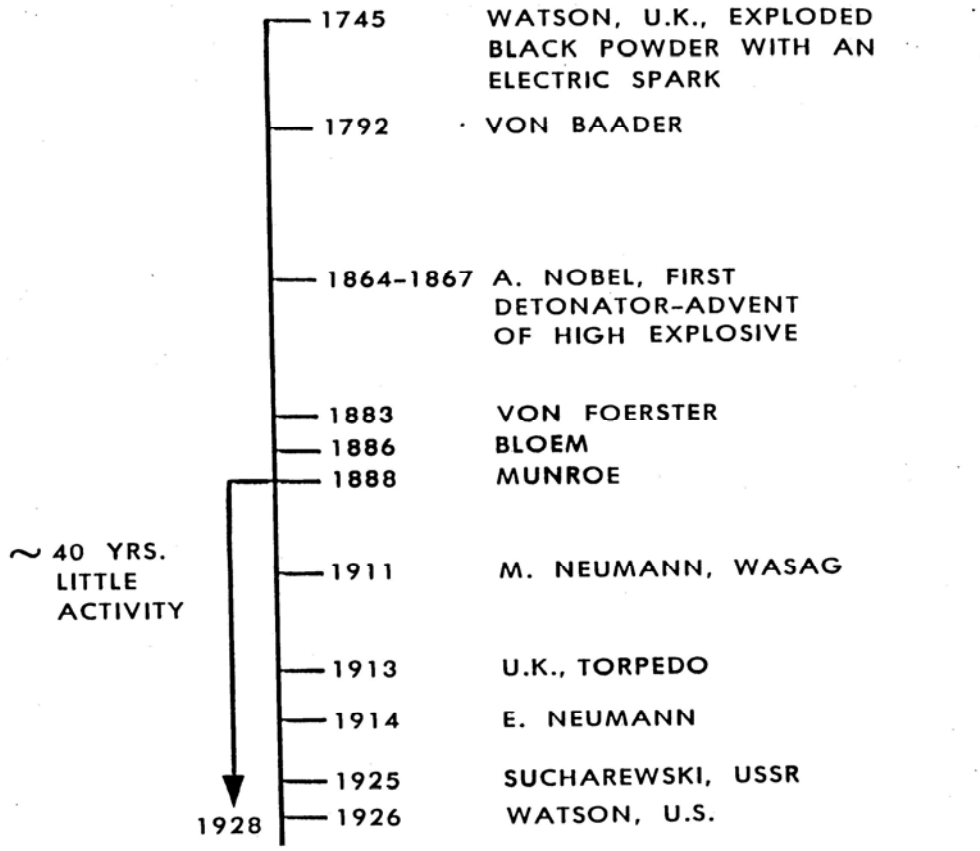
HISTORY OF SHAPED CHARGES

PDF Complete
Your complimentary use period has ended. Thank you for using PDF Complete.
Click Here to upgrade to Unlimited Pages and Expanded Features

HE EARLY HISTORY

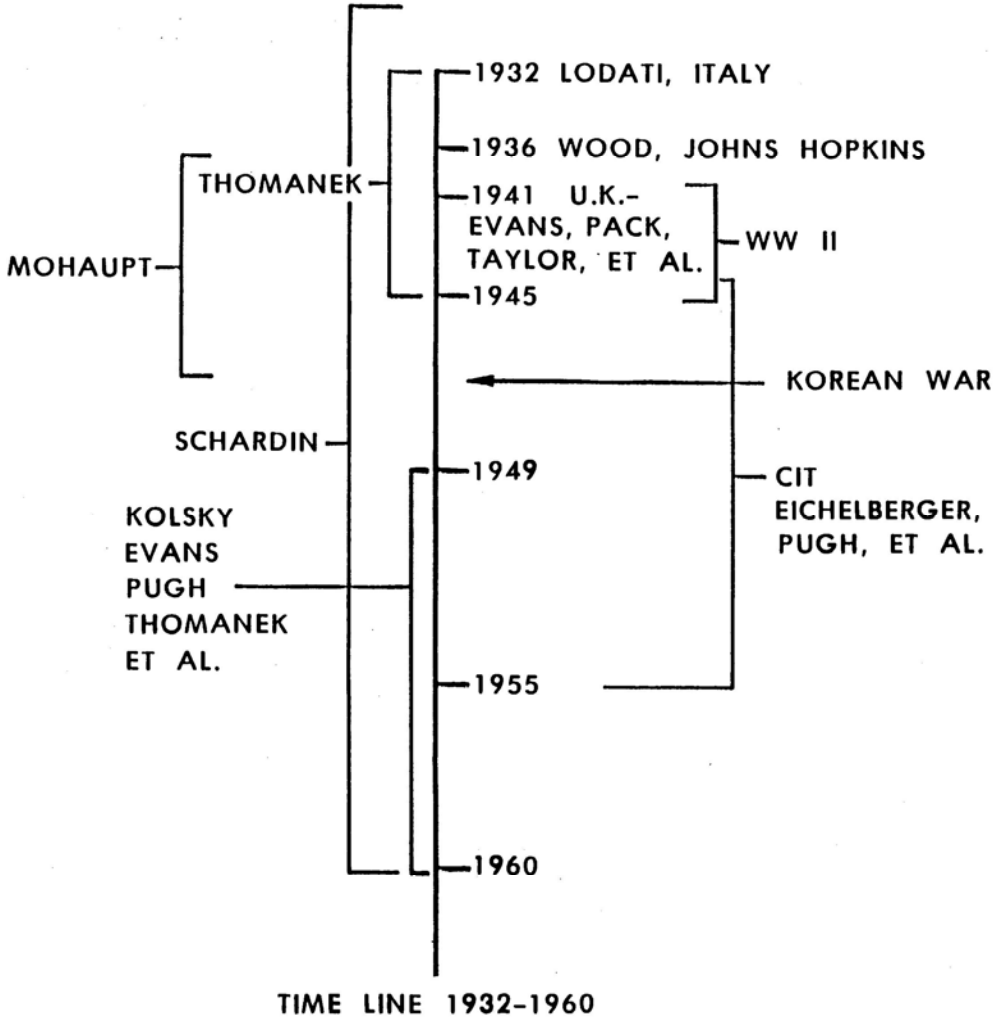
Å von Baader	1792	M. Neumann	1911
Å Nobel	1867	Sukharevskii	1925
Å von Foerster	1883	Lodati	1932
Å Bloem	1886	Wood	1936
Å C. Monroe	1888	Thomanek	1935
Å Lepidi	1891	Mohaupt	1939

PDF Complete
Your complimentary use period has ended. Thank you for using PDF Complete.
Click Here to upgrade to Unlimited Pages and Expanded Features



TIME LINE 1745–1928

PDF Complete
Your complimentary use period has ended. Thank you for using PDF Complete.
Click Here to upgrade to Unlimited Pages and Expanded Features



PDF Complete
Your complimentary use period has ended. Thank you for using PDF Complete.
Click Here to upgrade to Unlimited Pages and Expanded Features

1960

U.S., GERMANY, U.K., FRANCE, U.S.S.R. (GOVERNMENT AND INDUSTRY) CONTINUAL RESEARCH

Former Soviet Union and other countries

1988

TIME LINE 1960-TO DATE

PDF Complete
Your complimentary use period has ended. Thank you for using PDF Complete.
Click Here to upgrade to Unlimited Pages and Expanded Features

IN ABOUT 100 YEARS, THE US PARTICIPATION IN SHAPED CHARGE TECHNOLOGY WENT FROM THE DISCOVERY BY MONROE; 40 YEARS OF LITTLE ACTIVITY UNTIL THE INTRODUCTION TO WEAPONS TECHNOLOGY BY MOHAUPT ABOUT 1940; AND CONTINUOUS RESEARCH TO DATE.

PDF Complete
Your complimentary use period has ended. Thank you for using PDF Complete.
Click Here to upgrade to Unlimited Pages and Expanded Features

PETARDS

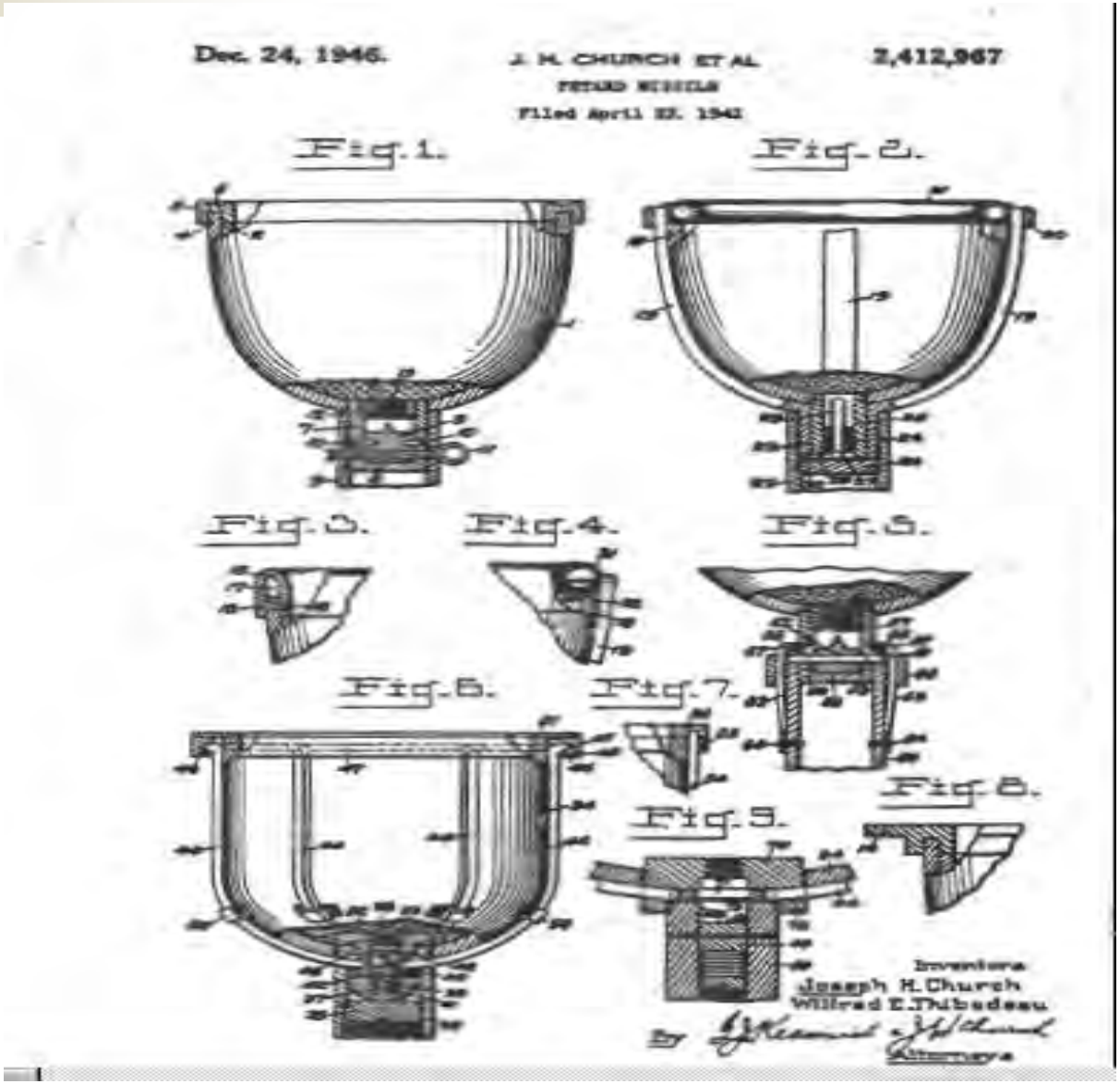
The petard or shaped charge of those times, relates M. F. Massey of the Office, Chief of Ordnance, Washington, D.C., in his ñhistoryò of hollow charges, consisted of a cast or wrought iron case of various shapes. This case was filled with powder moistened with good wine, and pressed or pounded into the case as firmly as possible, care being taken not to crack a grain of the powder, ñas flowers were expensive even then and funerals consume time far better spent in other pursuits.ò The case was then closed with a wooden plug and paper ñwell beaten inò and painted with hot tar. A quick match or a fuse ignited the charge through a hole in the top.

PDF Complete
Your complimentary use period has ended. Thank you for using PDF Complete.
Click Here to upgrade to Unlimited Pages and Expanded Features

PETARD

Years came and went and in 1825, one James Cutbush, Professor of pyrotechnology at West Point, recommended a further improvement in the petard by substituting brandy for wine. That recipe is still in use by makers of consolidated charges and cased telescoped ammunition, except that they use aquaeous solutions of industrial grade alcohol, not brandy. The petard is by no means dead, as US patent 2,412,967, filed in 1943 attests.

PDF Complete
Your complimentary use period has ended. Thank you for using PDF Complete.
Click Here to upgrade to Unlimited Pages and Expanded Features


Dec. 24, 1946. J. H. CHURCH ET AL 2,412,967
Filed April 22, 1942
Fig. 1.
Fig. 2.
Fig. 3.
Fig. 4.
Fig. 5.
Fig. 6.
Fig. 7.
Fig. 8.
Fig. 9.
Inventors
Joseph H. Church
Wilfred E. Thibodeau
By
Attorneys

PDF Complete
Your complimentary use period has ended. Thank you for using PDF Complete.
Click Here to upgrade to Unlimited Pages and Expanded Features

Explosives with Lined Cavities*

Gerald Birkhoff, Donald P. MacDougall, Emmett M. Pugh, and Sir Geoffrey Taylor

(Received January 16, 1948)

Explosives detonated in contact with thick steel plates produce much deeper holes in the steel when there is a cavity in the explosive in contact with the plate. While this phenomenon has been known for more than 150 years, the enormous increase in penetrating power that can be produced by lining the explosive cavity with thin metal has been discovered only recently. During the war a number of light, low velocity, antitank weapons (e.g., the rocket-propelled Bazooka) were developed which made use of this phenomenon to perforate thick armor plate.

A fairly complete mathematical theory of this essentially new phenomenon is presented together with some of the experimental data that aided testing of the theory. The principal phases are: first, the formation of a long thin jet traveling lengthwise (30,000 ft./sec.) and, second, the target material by the extremely high pressures produced by the jet.

The theories of both of these phases of classical hydrodynamics of perfect fluids because the strength of the material at the high pressures

JAP, JUNE 1948

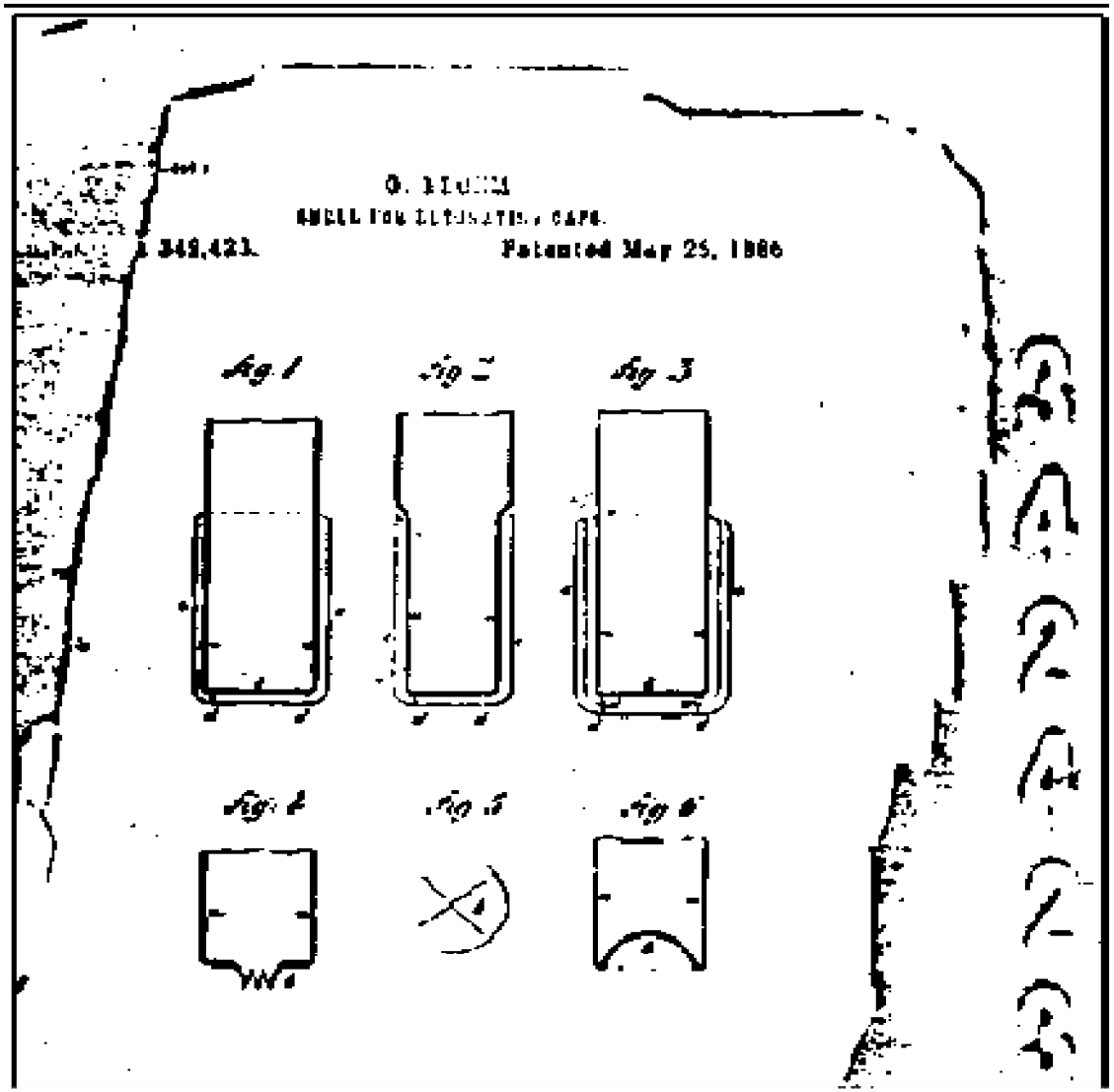
FOR over a century mining engineers have known that some of the force of an explosive charge could be concentrated on a small area by hollowing out the charge opposite to the area ("hollow charge principle"). The earliest known reference to this is 1792; a popular account appeared in von Nostrand's Magazine in 1884. The effect became known as the Munroe effect in England and the United States, and as the Neumann effect in Germany, in honor of later workers (1885, 1915).

Early in the recent war a large number of new weapons, based on an important modification of this principle, appeared almost simultaneously in the armed forces of the major combatants. It had been discovered that by lining the hollow with a thin metal liner it became possible to perforate armor plate, concrete walls, or other structures with a surprisingly small weight of explosive charge. Very often took the form of a projectile charge in the nose. Its advantage over the ordinary in that their ability to per independent of their stick hand placed and statical charges are at least as ef armor as those used in p mate on impact.

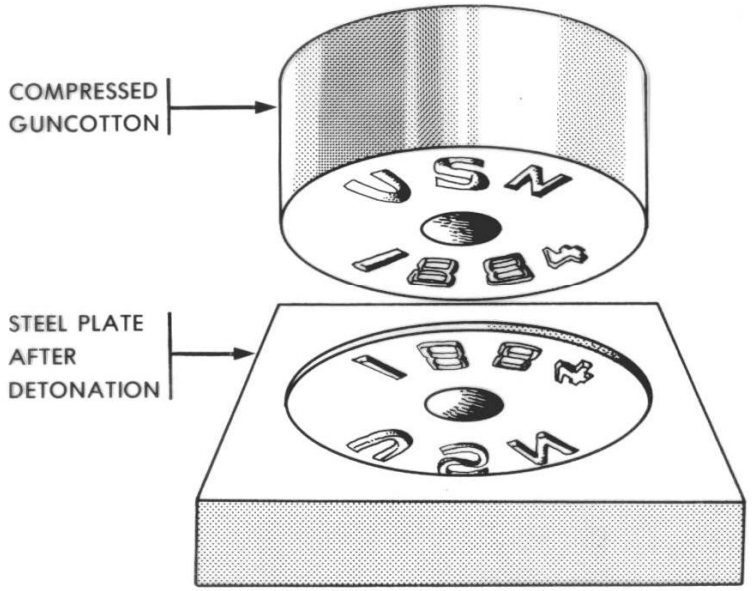
This fact led to a variety the hollow charges to th known method was the us employed in the American which were very effective they had striking velociti the ordinary antitank ar American bazooka could b by individual infantrymen

TECHNOLOGY DRIVEN. WARFIGHTER FOCUSED.

PDF Complete
Your complimentary use period has ended. Thank you for using PDF Complete.
Click Here to upgrade to Unlimited Pages and Expanded Features



PDF Complete
Your complimentary use period has ended. Thank you for using PDF Complete.
Click Here to upgrade to Unlimited Pages and Expanded Features



PDF Complete
Your complimentary use period has ended. Thank you for using PDF Complete.
Click Here to upgrade to Unlimited Pages and Expanded Features

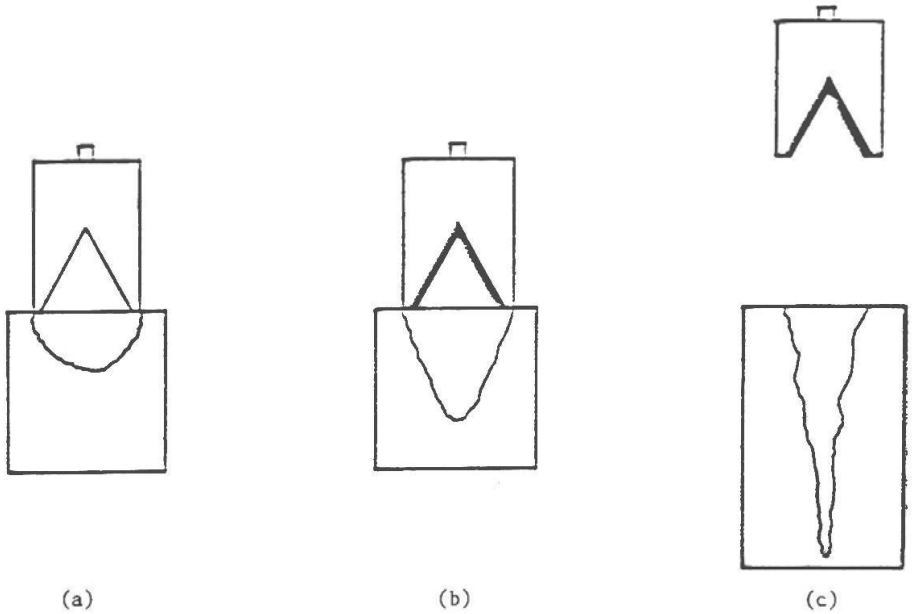
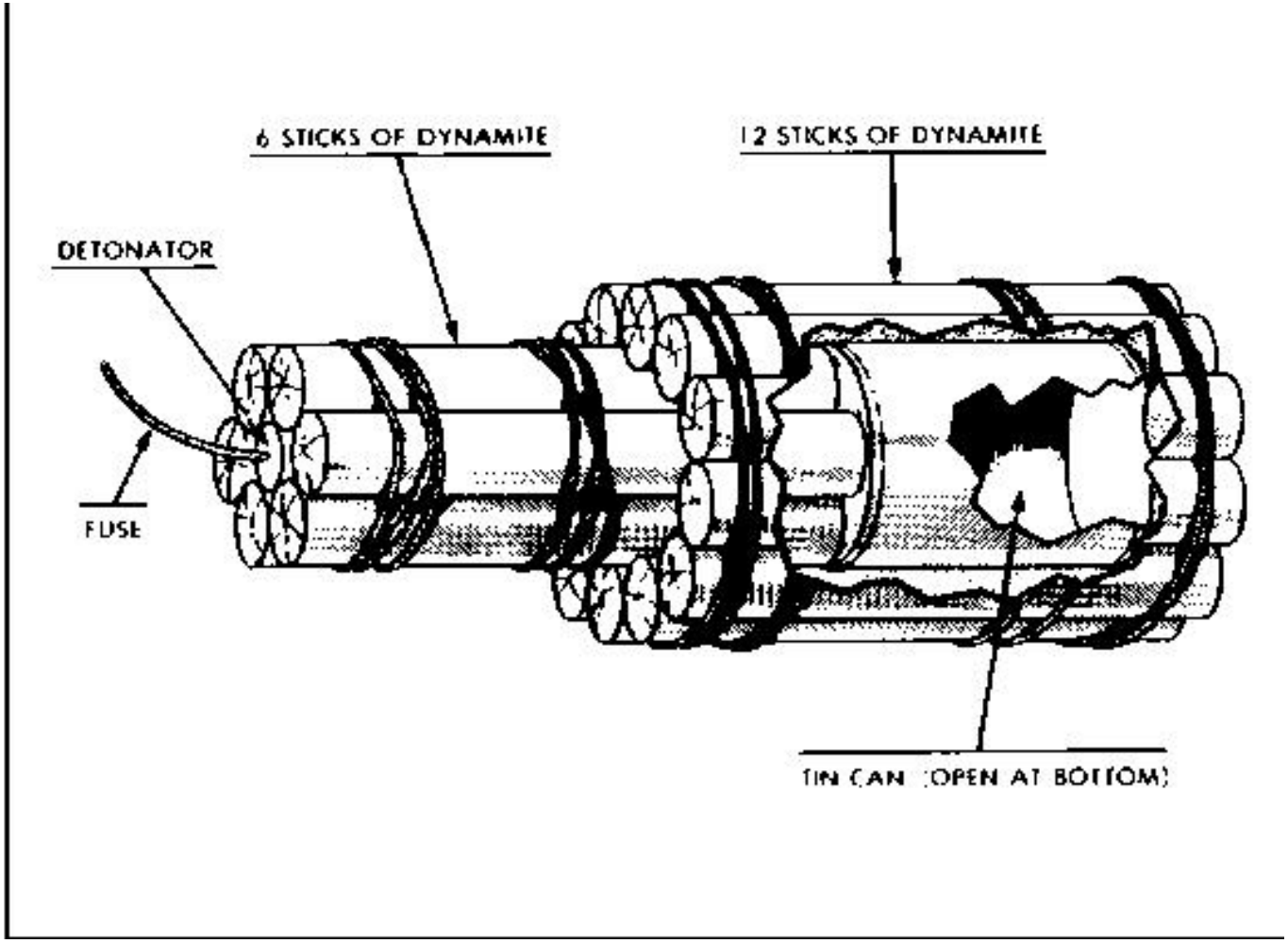


Figure 4. The Lined Cavity Effect

PDF Complete
Your complimentary use period has ended. Thank you for using PDF Complete.
Click Here to upgrade to Unlimited Pages and Expanded Features



PDF Complete
Your complimentary use period has ended. Thank you for using PDF Complete.
Click Here to upgrade to Unlimited Pages and Expanded Features



PDF Complete
Your complimentary use period has ended. Thank you for using PDF Complete.
Click Here to upgrade to Unlimited Pages and Expanded Features

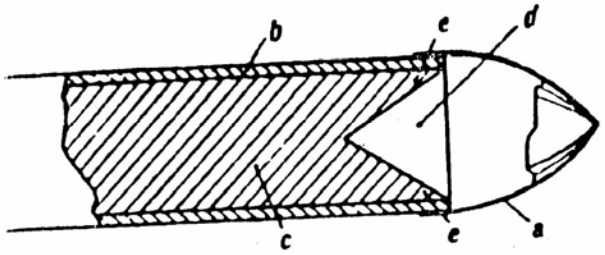


Fig. 2

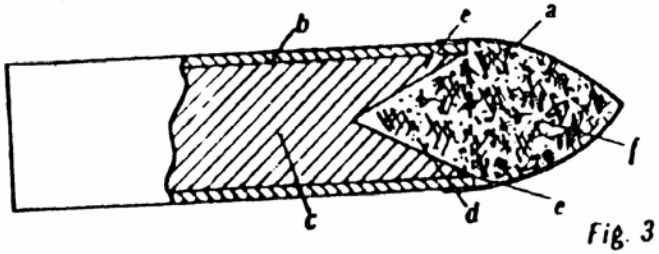
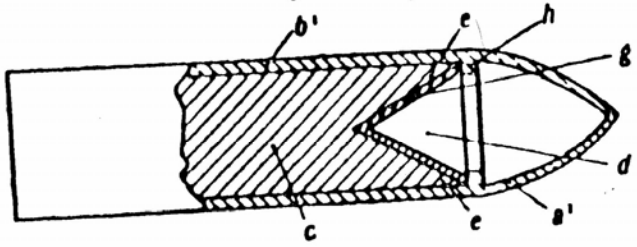
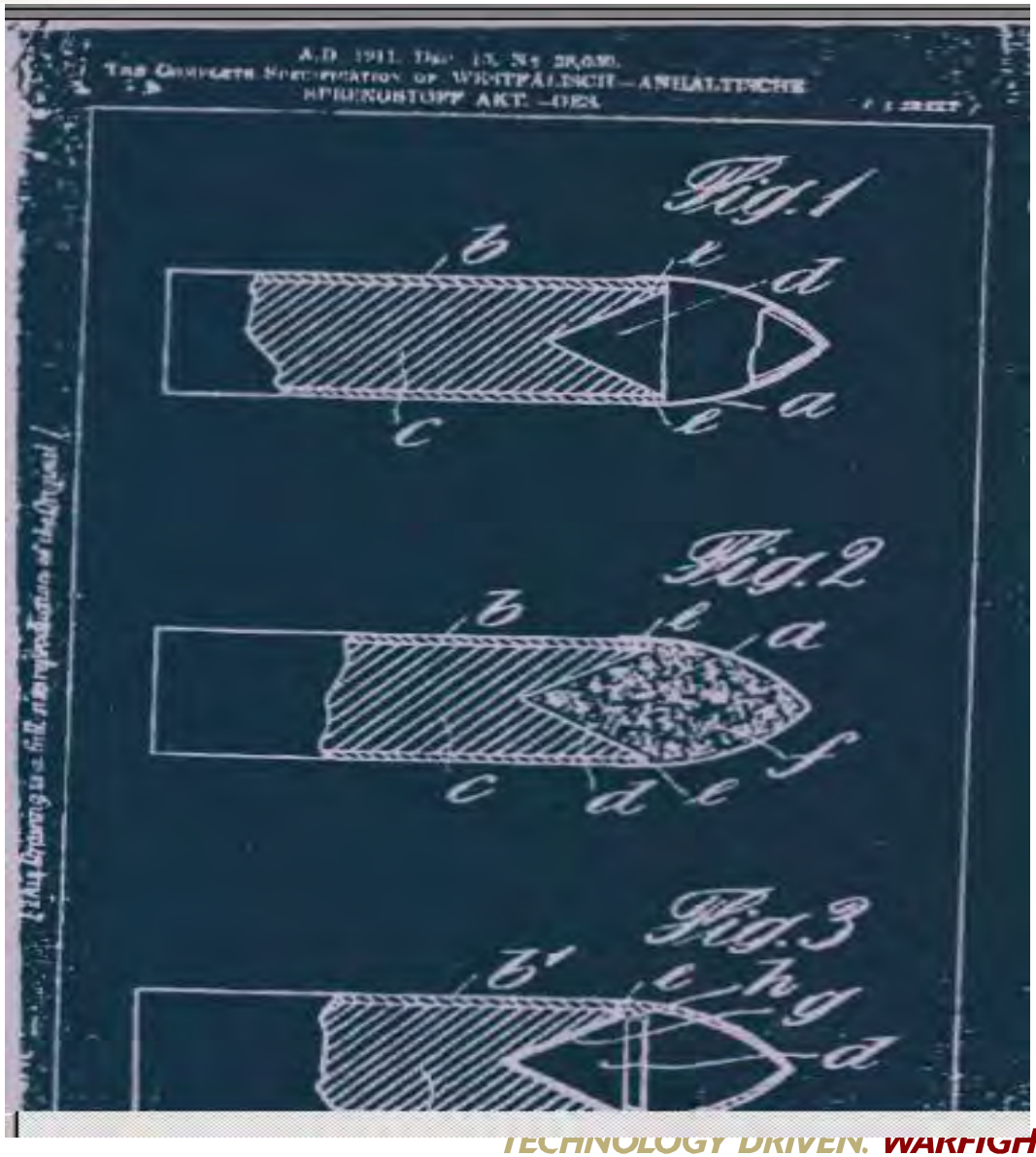


Fig. 3



Projectiles with Hollow Charges
(Note liner (g) in Fig. 3)
(WASAG patent, 1911)

PDF Complete
Your complimentary use period has ended. Thank you for using PDF Complete.
Click Here to upgrade to Unlimited Pages and Expanded Features



PDF Complete
Your complimentary use period has ended. Thank you for using PDF Complete.
Click Here to upgrade to Unlimited Pages and Expanded Features

84 SARRAU et VIEILLE mettent au point la poudre B

von DUTTENHOFER fabrique poudre gelatinisée en grain à Rottweil (D)

85

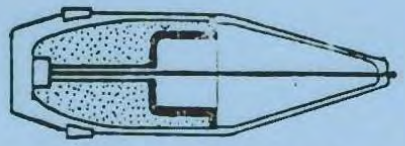
86

87 NOBEL invente la «balistite», poudre à base de ngl et de nc

91 Eclat avec les autorités françaises, NOBEL quitte Paris.

TURPIN détecte à Paris la détonabilité de l'acide picrique. Fabrication de la mélinite en France. Adoption générale pour les charges d'obus. Les études des «canons dynamite» s'arrêtent.

LEPIDI étudie un obus à charge creuse («Obus chambré») au Bouchet. Il détecte l'effet du revêtement et de la distance d'action, mais a à abandonner l'étude quand un tube de canon éclate

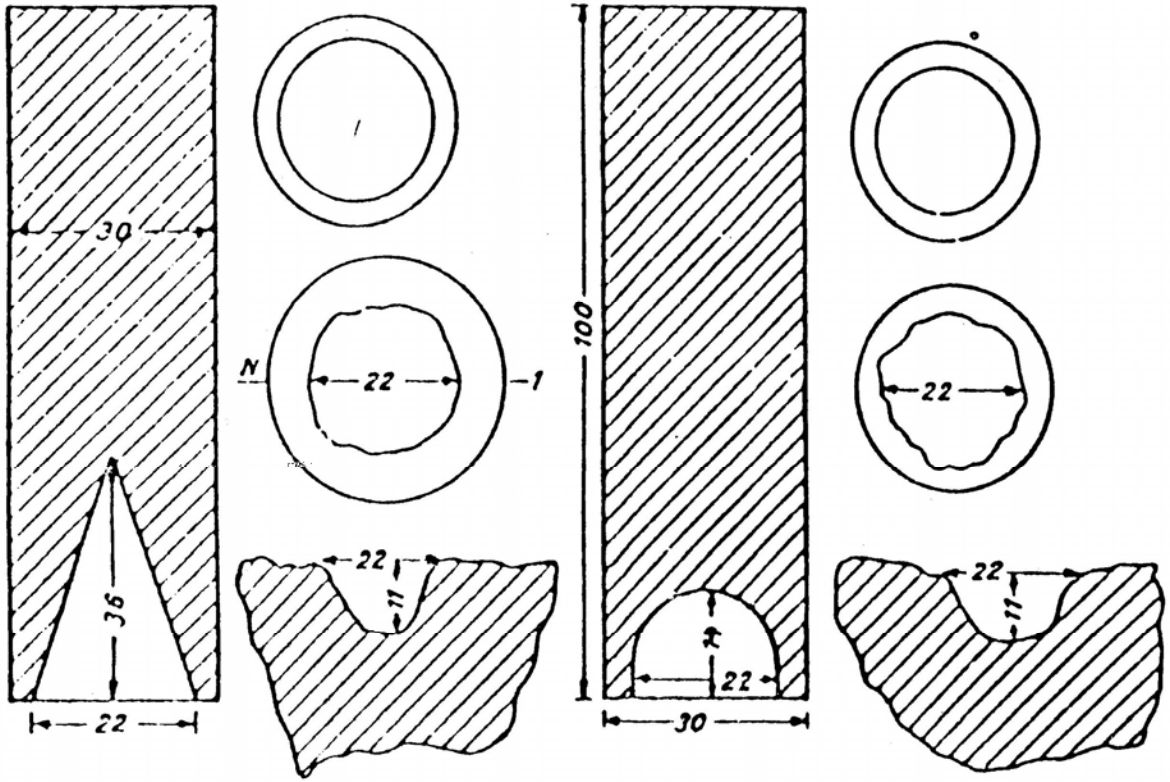


Obus chambré de Lepidi

PDF Complete
Your complimentary use period has ended. Thank you for using PDF Complete.
Click Here to upgrade to Unlimited Pages and Expanded Features

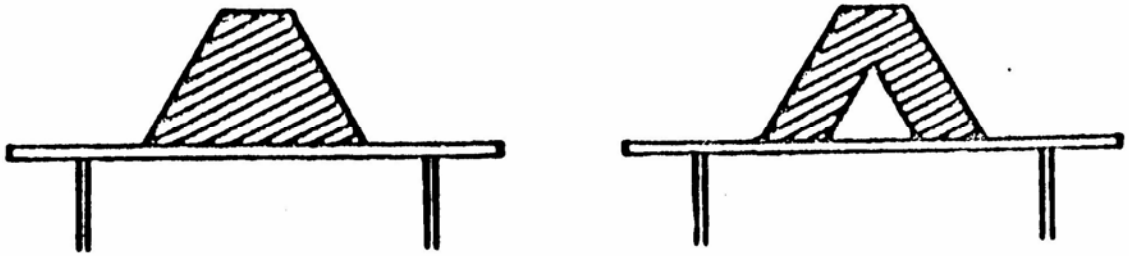
"The most advanced state in the history of shaped-charge was undoubtedly achieved in France. In the gun-powder factory situated in Le Bouchet during the period 1891-1893, a certain captain named LEPIDI worked on a project named "obus chambré", which was nothing other than a HEAT(shaped-charge) shell with a cylindrical liner. During this period, LEPIDI performed a static study of the influence of the liner thickness, of the standoff distance and of the liner material and he was able to statically perforate 140 mm of armor with a 155 mm shell. The final construction of a nearly modern antitank shell failed at that time, only due to troubles with the initiation system. Because of the use of an inadequate time-fuse device, a gun exploded and therefore the experiments were stopped and the results sunk in forgetfulness"

PDF Complete
Your complimentary use period has ended. Thank you for using PDF Complete.
Click Here to upgrade to Unlimited Pages and Expanded Features



Hollow Charges with Increased Explosive Head
(M. Sukharevskii, 1926)

PDF Complete
Your complimentary use period has ended. Thank you for using PDF Complete.
Click Here to upgrade to Unlimited Pages and Expanded Features



Setup to Compare Solid and Hollow Conical Charges
set on steel plate

PDF Complete
Your complimentary use period has ended. Thank you for using PDF Complete.
Click Here to upgrade to Unlimited Pages and Expanded Features

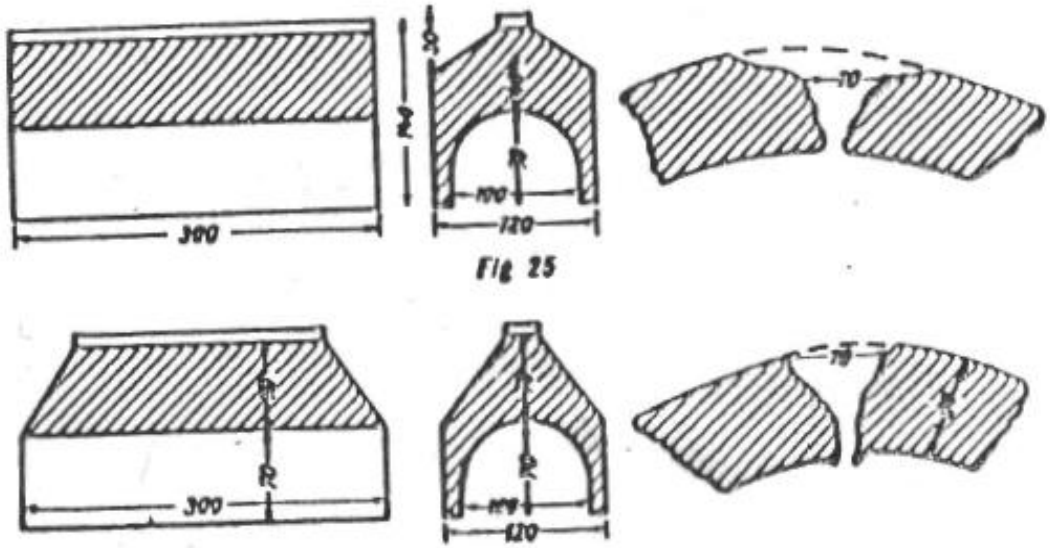
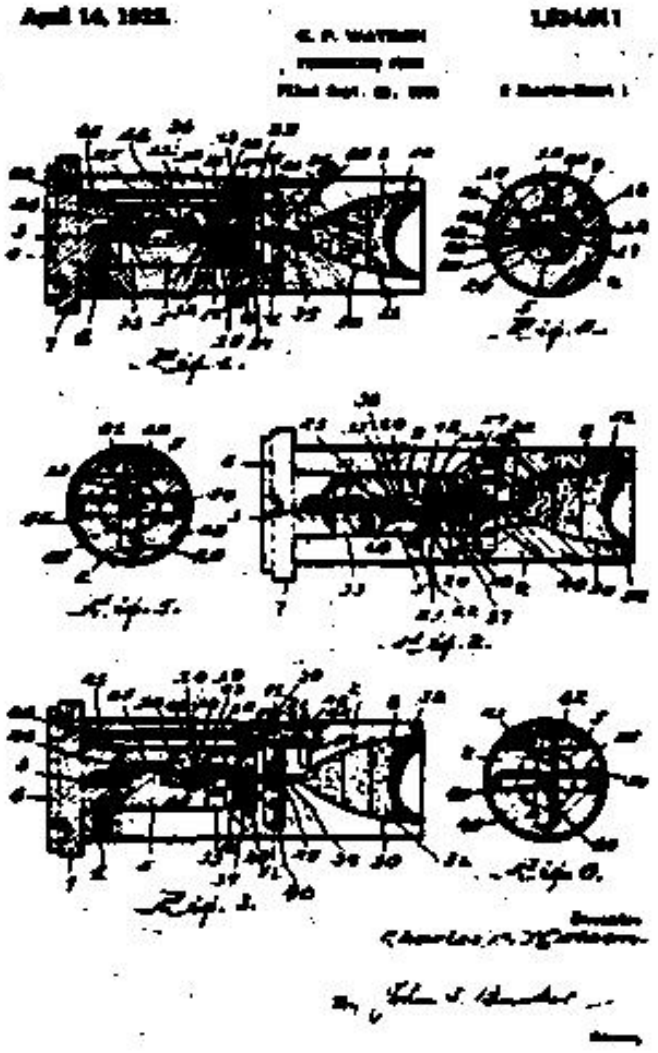


Fig 25

Linear (Unlined) Shaped Charges
(M. Sukharevskii, 1926)

PDF Complete
Your complimentary use period has ended. Thank you for using PDF Complete.
Click Here to upgrade to Unlimited Pages and Expanded Features

The Watson Fuze



PDF Complete
Your complimentary use period has ended. Thank you for using PDF Complete.
Click Here to upgrade to Unlimited Pages and Expanded Features

Poulter's Device

June 3, 1964 T. C. POULTER 3,136,249

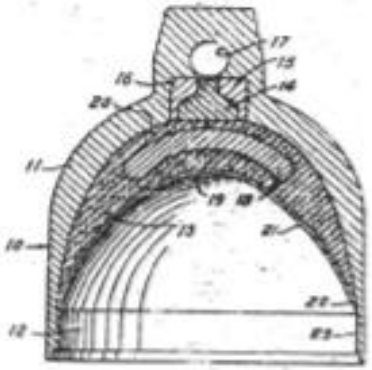


Fig. 1



Fig. 2

Thomas C. Poulter
INVENTOR

ATTORNEY

114

PDF Complete
Your complimentary use period has ended. Thank you for using PDF Complete.
Click Here to upgrade to Unlimited Pages and Expanded Features

Optical and Physical Effects of High Explosives

By R. W. Wood, For. Mem. R.S., Professor of Experimental Physics, Johns Hopkins University

(*Received 25 June*, 1936)

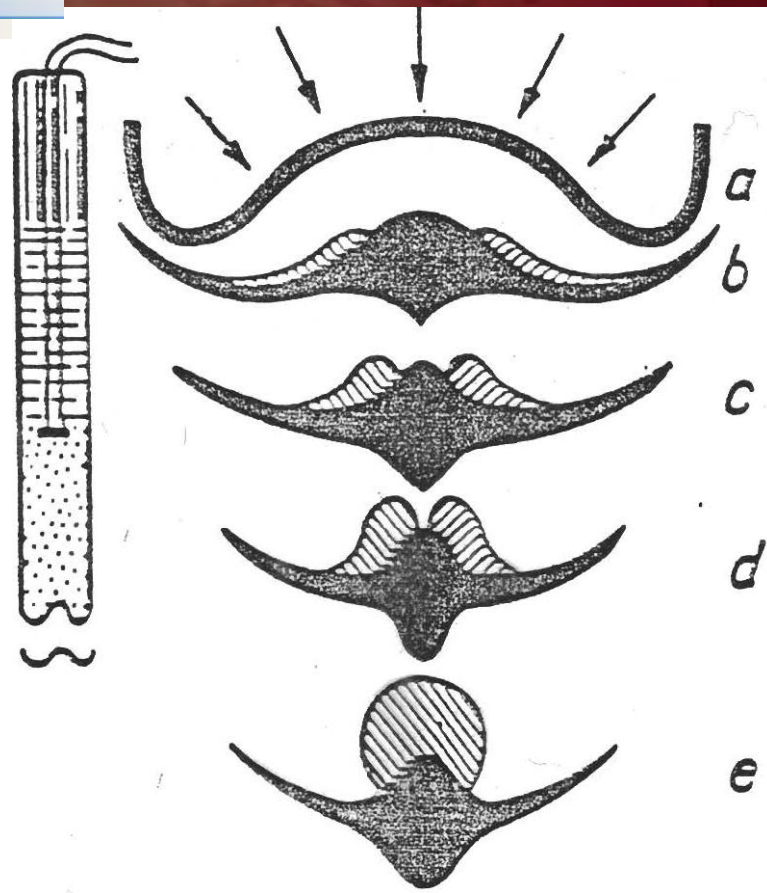
[PLATES 7 AND 8]

I—PLASTIC FLOW OF METALS

My interest in the study of the effects produced by high explosives originated in the investigation of "evidence" in a number of murders by bomb, and more especially in connexion with a most unfortunate and unusual accident which resulted in the almost instant death of a young woman who, on opening the door of the house furnace to see if the fire was burning properly, was struck by a small particle of metal which flew out of the fire and penetrated the breast bone, slitting a large artery and causing death in 2 or 3 minutes from internal haemorrhage. The particle, which was not much larger than a pin-head, was submitted to me for identification, and though its form resembled nothing with which I was familiar, I surmised that it was probably a part of a dynamite-cap or "detonator" used for exploding the dynamite charges in the mines, which, by some carelessness on the part of a miner, had been delivered intact with the coal.

These detonators are soun from very thin sheet copper and consist of

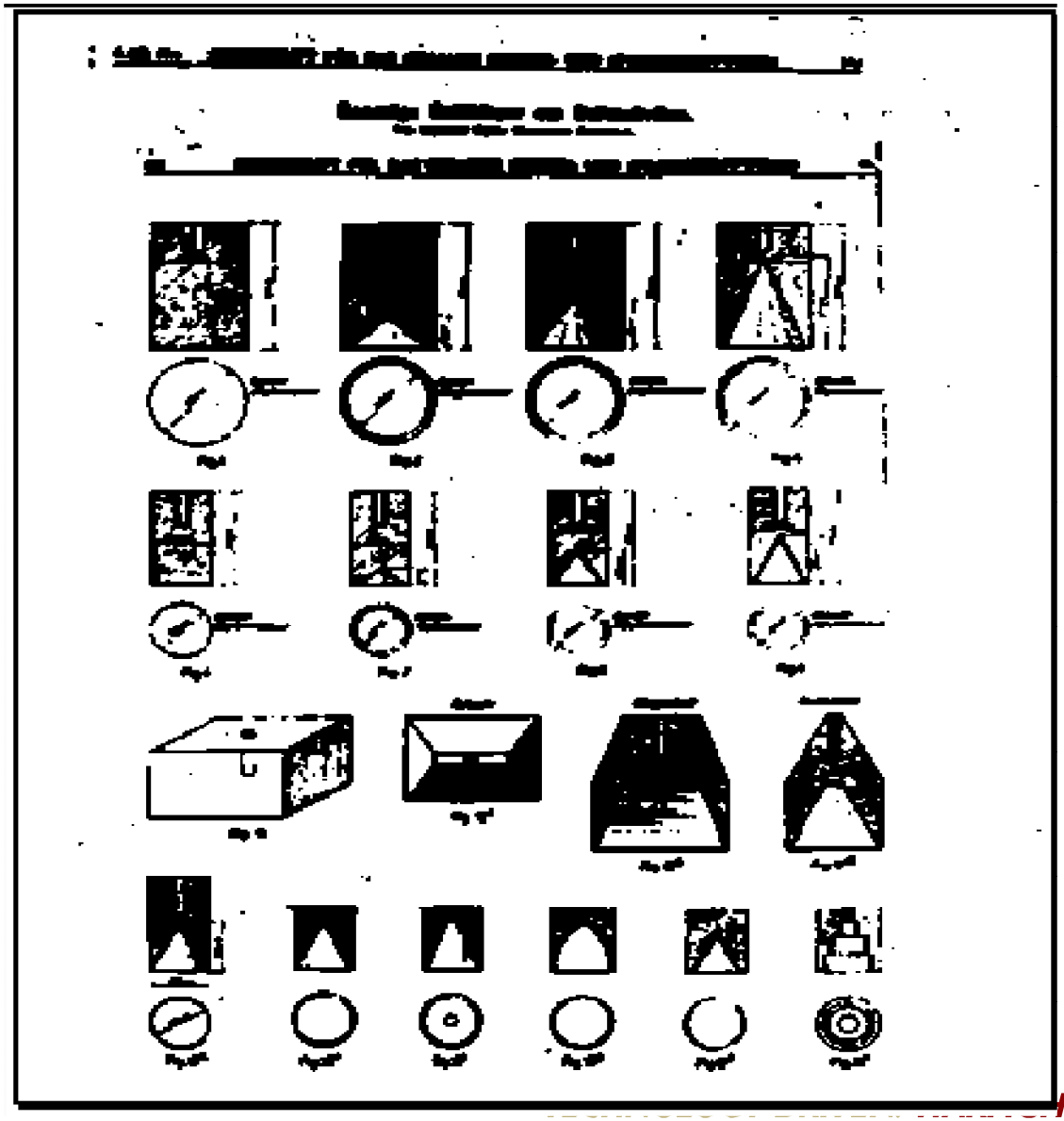
PDF Complete
Your complimentary use period has ended. Thank you for using PDF Complete.
Click Here to upgrade to Unlimited Pages and Expanded Features



Blasting Cap and Postulated Transformation of Lined Bottom following Detonation
(R. W. Wood, 1937)

PDF Complete
Your complimentary use period has ended. Thank you for using PDF Complete.
Click Here to upgrade to Unlimited Pages and Expanded Features

Liner Shapes



PDF Complete
Your complimentary use period has ended. Thank you for using PDF Complete.
Click Here to upgrade to Unlimited Pages and Expanded Features

DEVELOPMENT OF HOLLOW CHARGES (1942) [From (54)]

Historical Survey:

1883	Work by Foerster (hollow charge effect; use in projectiles)
1910	WASAG hollow charge for blasting charges of all types patented. Sheet metal liner used without knowledge of effect
1914	Neumann, "Investigation Into Hollow Charges Without Liner" (also acute angle cone hollow charge)
1926	Hollow charge investigations at inspection of arms and equipment

PDF Complete
Your complimentary use period has ended. Thank you for using PDF Complete.
Click Here to upgrade to Unlimited Pages and Expanded Features

1935/36	Development of armor-piercing projectile by WA A with hollow charge (patent Capt. Wimmer)
Late 1935	Demonstration of anti-tank rifle by Thomanek in presence of Hilter and WA A . No results.
June 1937	Determination of favorable effect of standoff detonation with hemispherical liner (WA F)
Nov/Dec 1938	Proposed introduction of shells with hollow charge and aluminum liner (no increase in effect) by WA Pruf 1

PDF Complete
Your complimentary use period has ended. Thank you for using PDF Complete.
Click Here to upgrade to Unlimited Pages and Expanded Features

Jun 1938-May 1939	Work by Thomanek (employed by Luftwaffe - Gatow); evacuated hollow charge (no improvement); recognition of liner effect by Prof. Schardin; disagreement between Thomanek and Schardin.
15 Feb 1939	Final report by WA Pruf 5 on hollow charge tests; realization of increased effect (independent of Gatow) through solid liner
June 1939	Introduction of 7.5cm projectile with hollow charge and aluminum liner.

PDF Complete
Your complimentary use period has ended. Thank you for using PDF Complete.
Click Here to upgrade to Unlimited Pages and Expanded Features

Dec 1939- Jan 1940	Test results presented by Thomanek to Research Institute Gatow (WA Pruf 1)
May 1940	Use of hollow charge detonations without reinforced liner on Liege fortifications, after development by WA Pruf 5
May 1940	Explosive Experiment Company given green light by WA Pruf 5 for development

PDF Complete
Your complimentary use period has ended. Thank you for using PDF Complete.
Click Here to upgrade to Unlimited Pages and Expanded Features

Most Significant Results:

Casing device for hollow charges (patent applied for 10 August 1940).
Acute angle cone and liner with wall thickness for armor-piercing projectiles (patent applied for 9 September 1940).
Diaphraghm-like liner for hollow charge, 6 November 1940.
Hollow charge for rifle anti-tank land mine, 29 May 1941.

7 Sep 1940 Detonation tests by WA F (without Thomanek) with satisfactory results with acute angle cone hollow charge (solid sheet metal liner) and standoff detonation (cast charge).

PDF Complete
Your complimentary use period has ended. Thank you for using PDF Complete.
Click Here to upgrade to Unlimited Pages and Expanded Features

20-30 Sep 1940	First demonstration of anti-tank rifle grenade (WASAG). Hollow charge with thin liner.
Late 1940	Completion of construction of hollow charge 15 (hollow charge with heavy liner) in Gatow.
March 1941	Testing of hollow charge 15 on Maginot Line forts.
9 May 1941	Delivery of 450 rifle grenades by WASAG for use on Crete.

PDF Complete
Your complimentary use period has ended. Thank you for using PDF Complete.
Click Here to upgrade to Unlimited Pages and Expanded Features

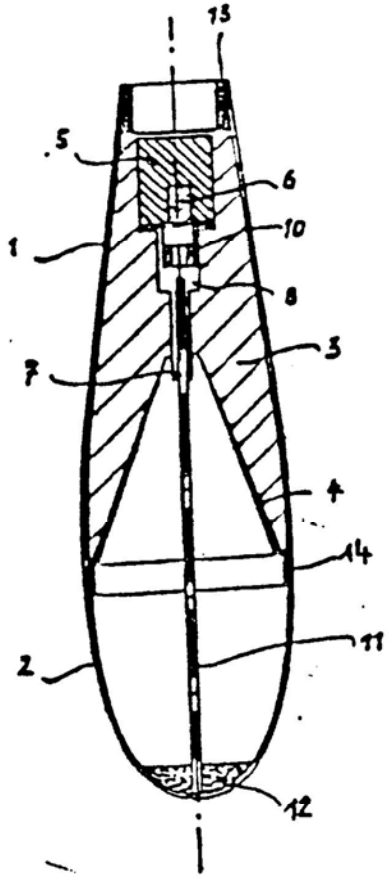
Steel liners (0.5 to 1 mm thick) were found to be superior to gray-iron casting (June 1940). Hollow charges with conical liners (up to 1.5 mm and with angles between 20 - 45 degrees) and proper standoff (25 - 30 mm) would effect perforation of 15 mm armor plate. The charges used were cast. An increase of the diameter of the blast hole was made possible by the use of a bell-shaped hollow charge which would also permit fewer irregularities than with the acute cone. The diameter was 1 cm (of the charge).

PDF Complete
Your complimentary use period has ended. Thank you for using PDF Complete.
Click Here to upgrade to Unlimited Pages and Expanded Features

The idea of firing a hollow charge shell from the shoulder was first conceived in 1937 (i.e., a rifle grenade).

NOTES: WA A is an abbreviation for *Waffenamt* (Army Weapons Office) which had a department designated WA Pruf for the proof testing of weapons. WA Pruf is an abbreviation for *Waffenamt Prufwesen* (Offices of Weapons Proof and Development). WA F means *Waffen Forschung* (weapons research) and worked with shaped charges under the direction of Dr. Schumann. The *Technische Akademie der Luftwaffe* or TAL (Technical Academy of the Air Force) was headquartered at Berlin - Gatow and headed by Dr. Schardin. It was roughly a World War II counterpart of BRL. For additional organizational details see Simon (57).

PDF Complete
Your complimentary use period has ended. Thank you for using PDF Complete.
Click Here to upgrade to Unlimited Pages and Expanded Features



Rifle Grenade (German Patent 975,806)
(F. R. Thomanek, 1941, assigned to WASAG)

PDF Complete
Your complimentary use period has ended. Thank you for using PDF Complete.
Click Here to upgrade to Unlimited Pages and Expanded Features

Source
Ordnance Department, U.S.Army
"The Shaped Charge" lecture by
L.E.Simons 4 April 1947
Technical Division, Picatinny Arsenal

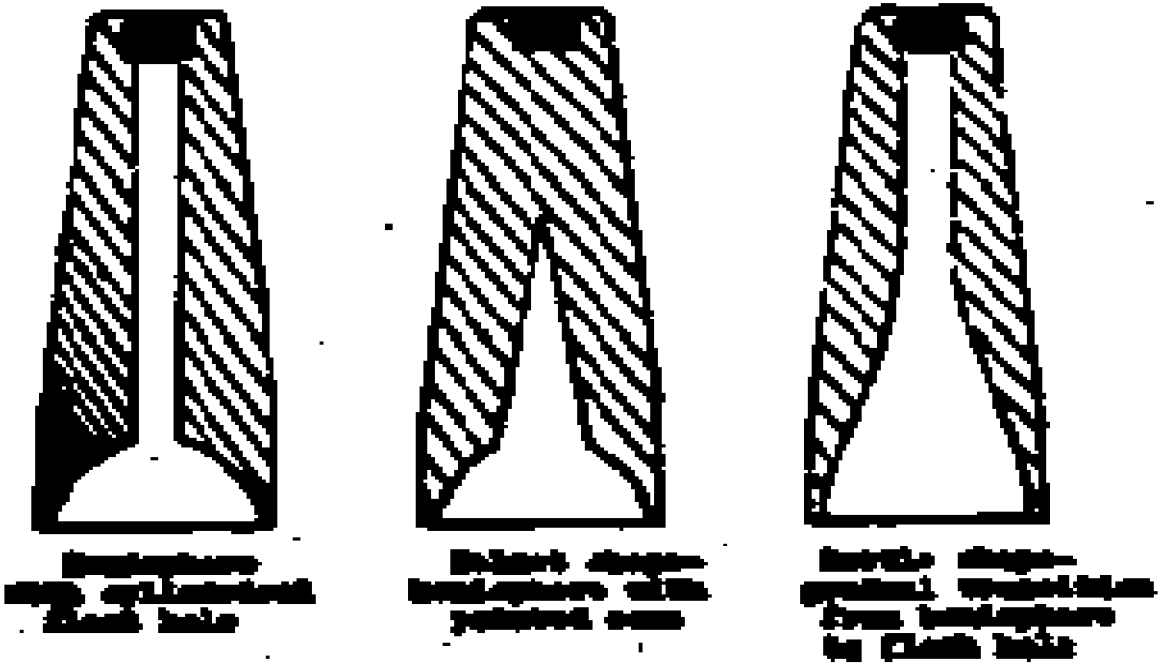
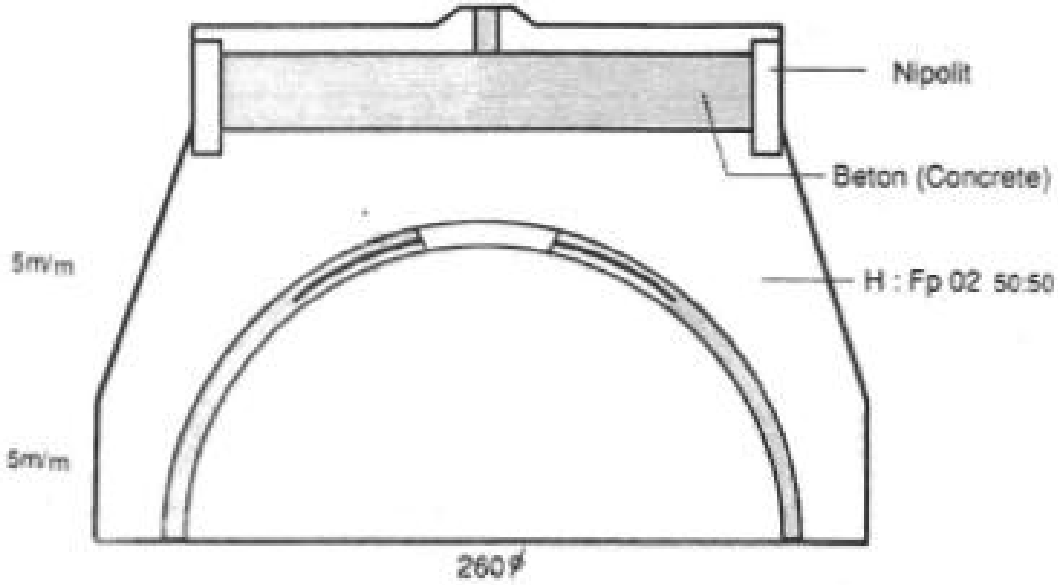


Figure 4

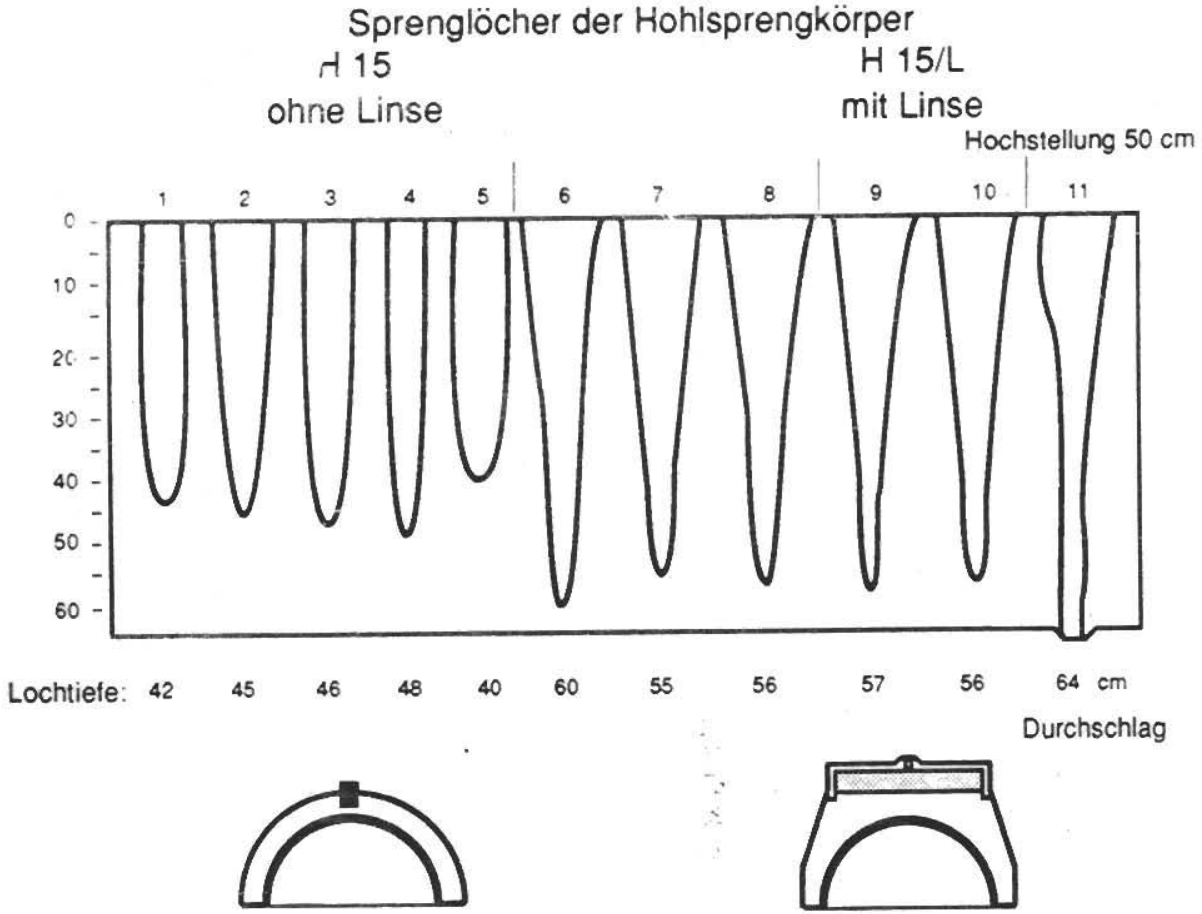
PDF Complete
Your complimentary use period has ended. Thank you for using PDF Complete.
Click Here to upgrade to Unlimited Pages and Expanded Features

1943 German paper "Preliminary Information report about the enhanced performance of hollowcharge bodies by directed initiation (lenses)" von Prof. Dr. Erich Schumann u. Dr. Gerd Hinrichs

H 15/L



PDF Complete
Your complimentary use period has ended. Thank you for using PDF Complete.
Click Here to upgrade to Unlimited Pages and Expanded Features

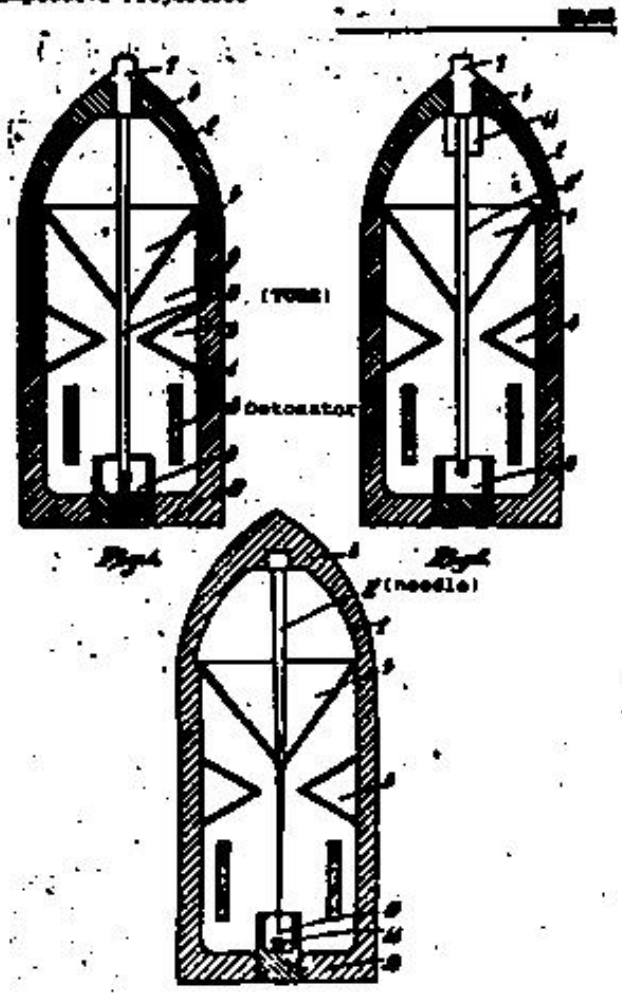


PDF Complete
Your complimentary use period has ended. Thank you for using PDF Complete.
Click Here to upgrade to Unlimited Pages and Expanded Features

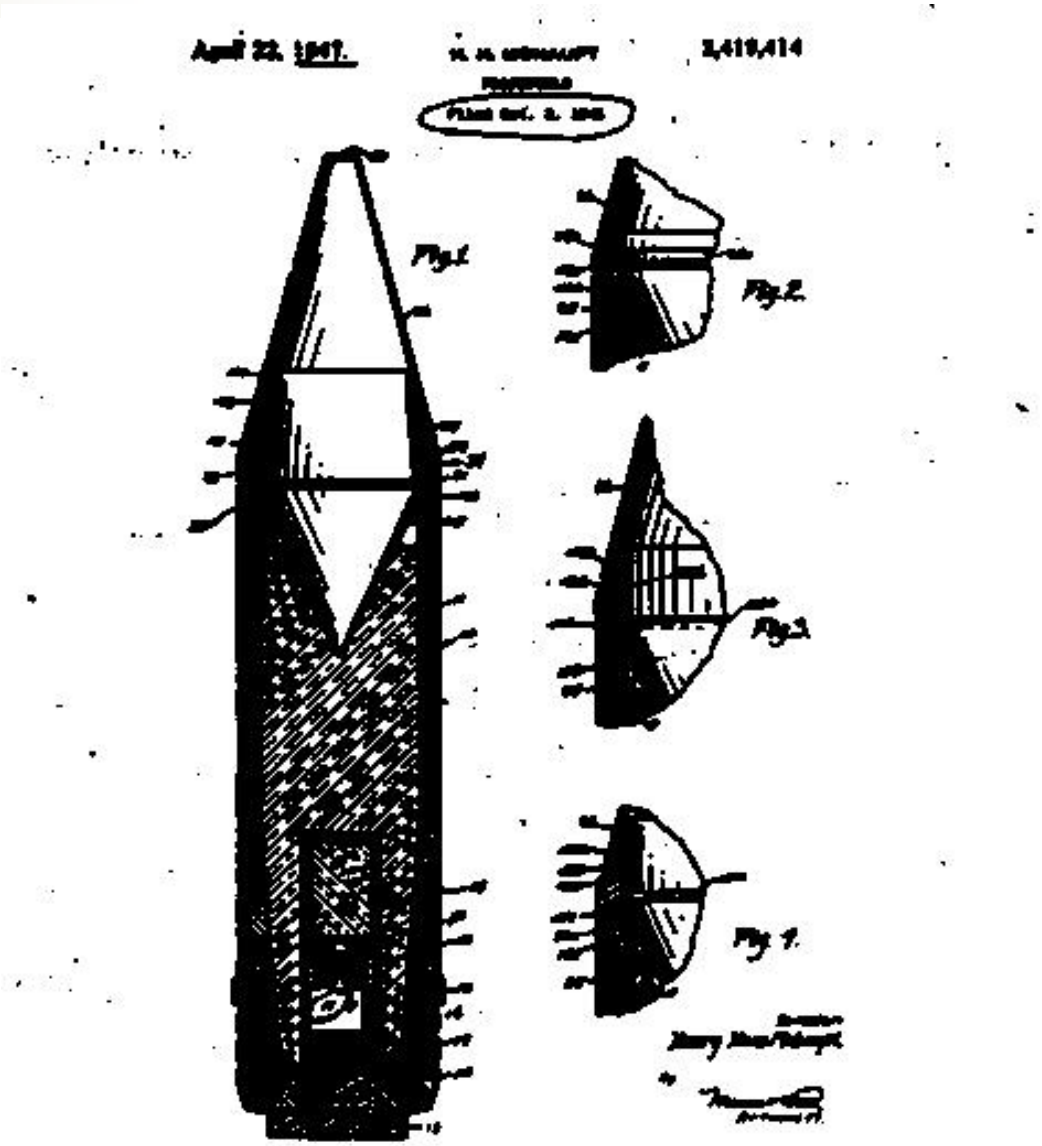
Invention data claimed:
France 9 Nov 1939

Australia 16 Aug 1941
"An Improved Explosive Projectile"

Applicant: Eagar, Societe Anonyme de Gestion et d'Exploitation de Brevets
Assignees: Barthold Nahnsen, Henry Nahnsen, Erich Leuders, of France.



PDF Complete
Your complimentary use period has ended. Thank you for using PDF Complete.
Click Here to upgrade to Unlimited Pages and Expanded Features



PDF Complete
Your complimentary use period has ended. Thank you for using PDF Complete.
Click Here to upgrade to Unlimited Pages and Expanded Features

1942 FIGURE 12

March 14, 1961



Fig. 1.



Fig. 3.



Fig. 2.

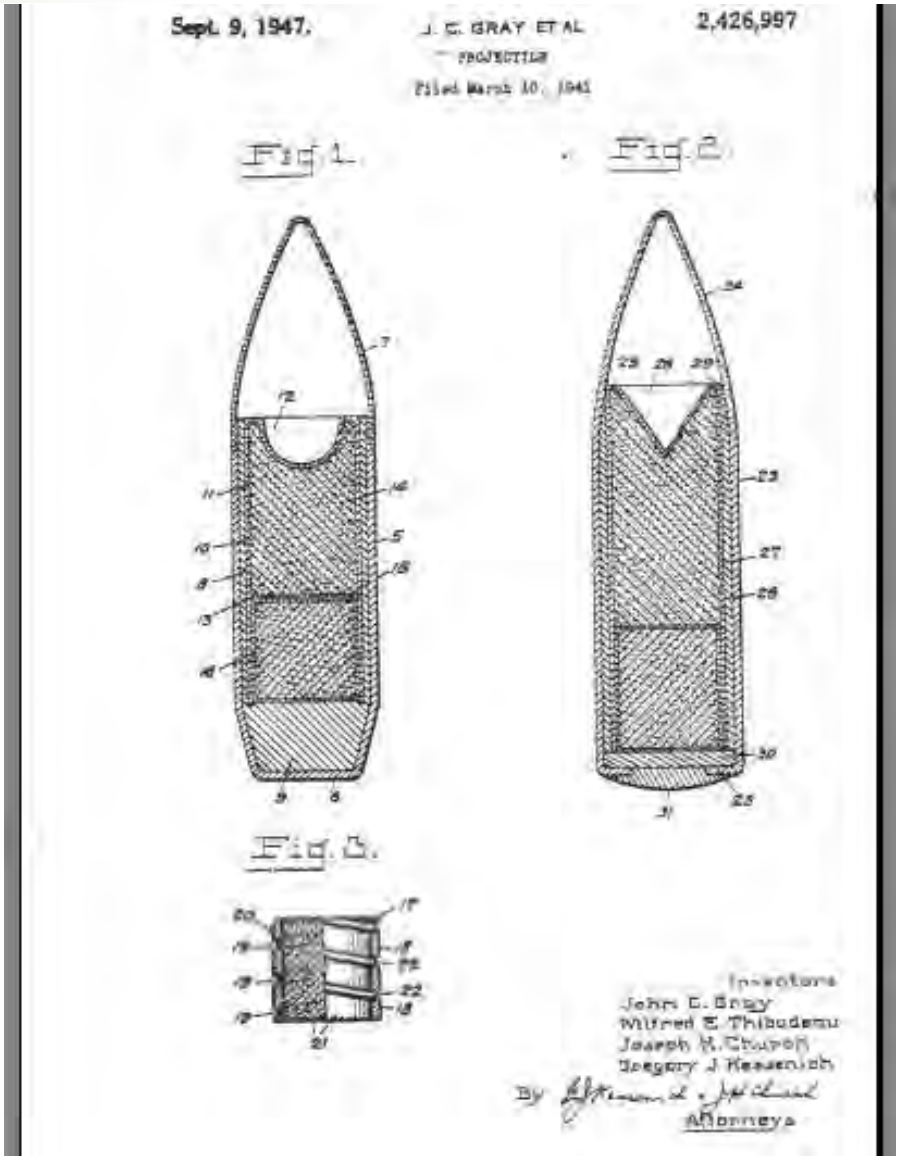


Fig. 5.



Fig. 4.

PDF Complete
Your complimentary use period has ended. Thank you for using PDF Complete.
Click Here to upgrade to Unlimited Pages and Expanded Features



Sept. 9, 1947. J. C. GRAY ET AL 2,426,997

PROJECTILE

Filed March 10, 1941

Fig. 1.

Fig. 2.

Fig. 3.

Inventors
John C. Gray
Wilfred E. Thibodeau
Joseph H. Church
Gregory J. Hasenich
By
Attorneys

PDF Complete
Your complimentary use period has ended. Thank you for using PDF Complete.
Click Here to upgrade to Unlimited Pages and Expanded Features

ANTISUBMARINE SHAPED-CHARGE BOMB*

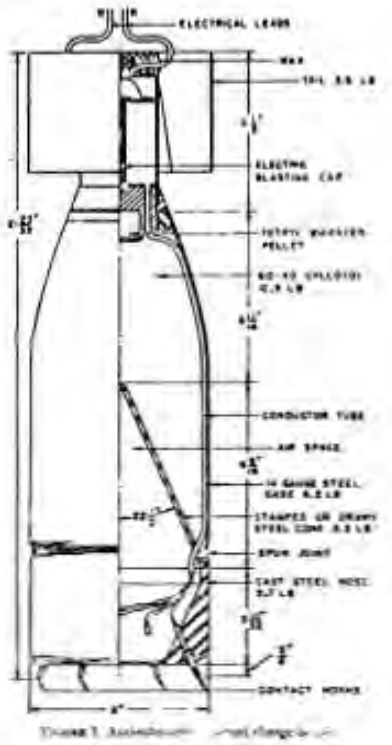
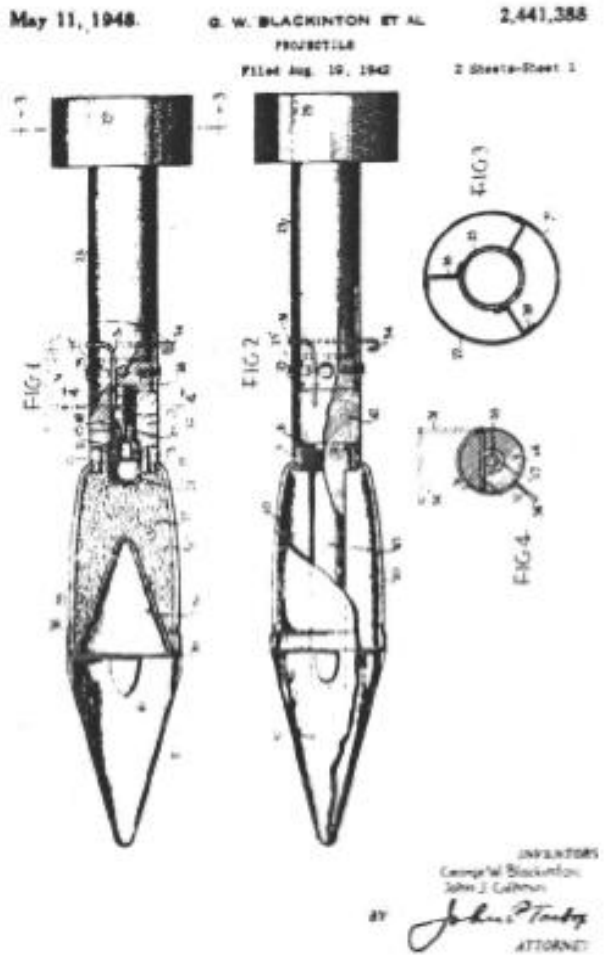


Fig. 36 Antisubmarine HEAT Scatterbomb, U.S. Navy, WWII, ca. 1945

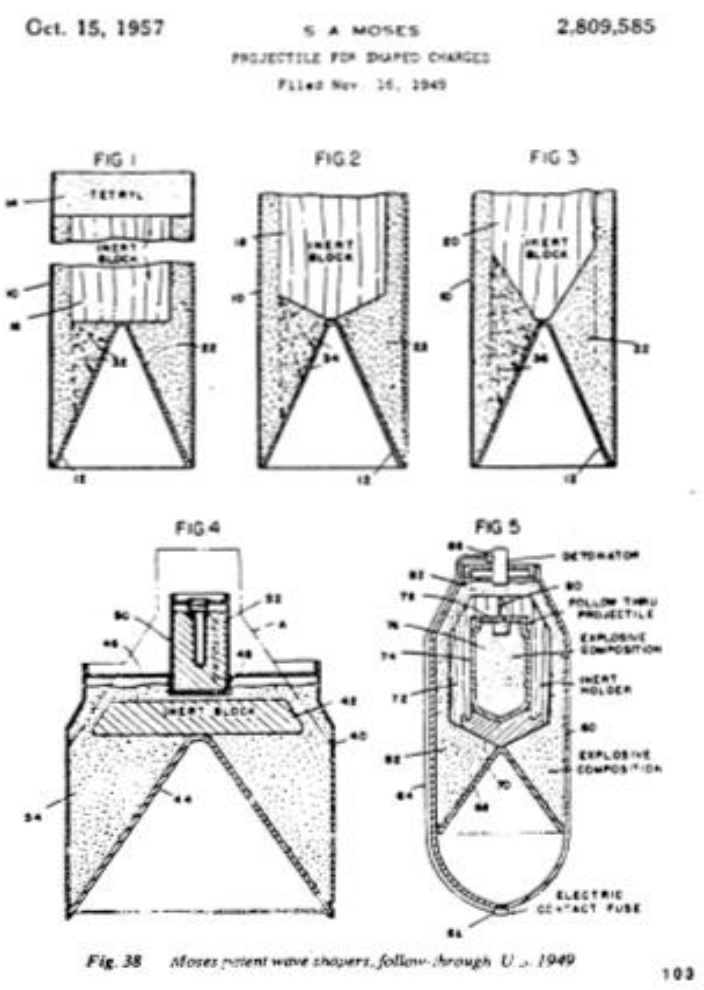
TECHNOLOGY DRIVEN. WARFIGHTER FOCUSED.

PDF Complete
Your complimentary use period has ended. Thank you for using PDF Complete.
Click Here to upgrade to Unlimited Pages and Expanded Features



98 *Fig. 32 Blackington patent filed August 1942. HEAT rifle grenade*

PDF Complete
Your complimentary use period has ended. Thank you for using PDF Complete.
Click Here to upgrade to Unlimited Pages and Expanded Features


Oct. 15, 1957 S. A. MOSES 2,809,585

PROJECTILE FOR SHAPED CHARGES

Filed Nov. 16, 1949

FIG. 1 FIG. 2 FIG. 3

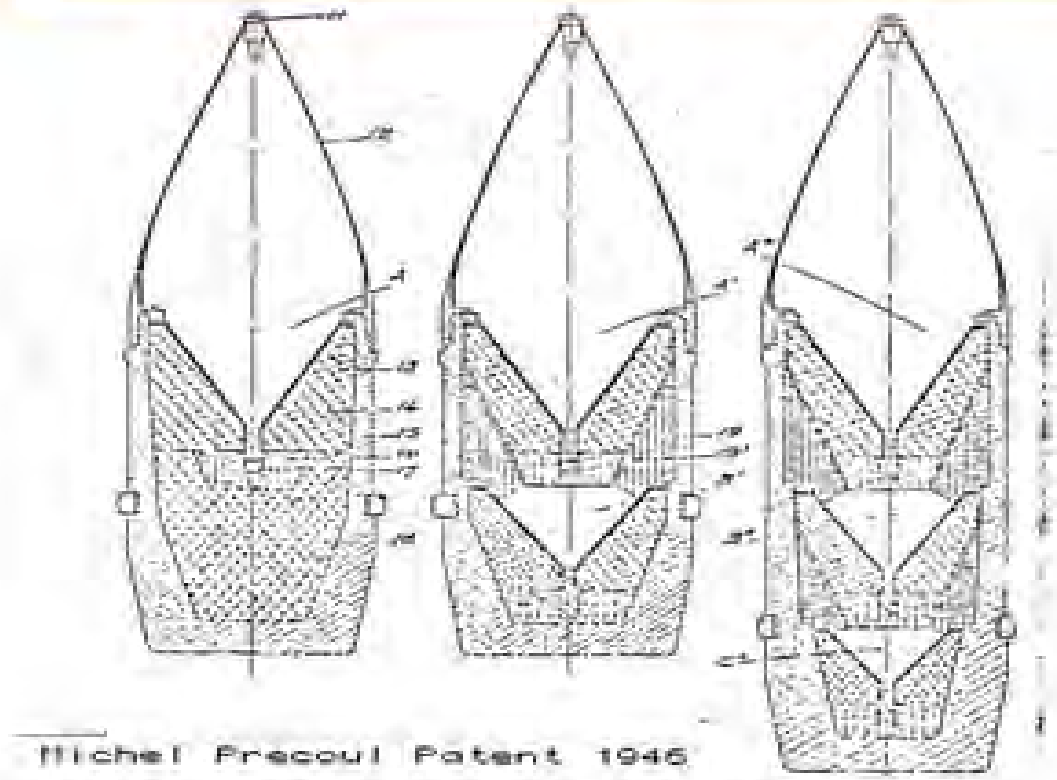
FIG. 4 FIG. 5

Fig. 38 Moses patent wave shapers, follow-through U. S., 1949

103

PDF Complete
Your complimentary use period has ended. Thank you for using PDF Complete.
Click Here to upgrade to Unlimited Pages and Expanded Features

dem Shaped Charge

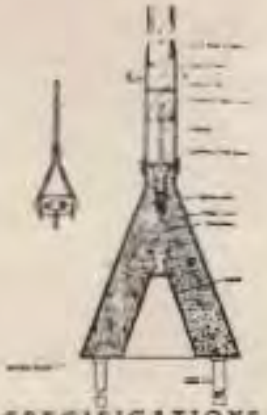


Michel Precoul Patent 1946

Societe' Technique de Recherches Industrielles et Mecaniques

PDF Complete
Your complimentary use period has ended. Thank you for using PDF Complete.
Click Here to upgrade to Unlimited Pages and Expanded Features

ANTITANK "LUNGE" MINE



SPECIFICATIONS



94

Fig. 28 Japanese anti-tank lunge mine (suicide mine) ca. 1944

PDF Complete
Your complimentary use period has ended. Thank you for using PDF Complete.
Click Here to upgrade to Unlimited Pages and Expanded Features

A two meter diameter shaped charge



NUMERICAL ANALYSIS OF BI-METALLIC EXPLOSIVE SHOCK-LOADING AND RELEASE EXPERIMENTS

(Wave Interaction)

Geremy Kleiser, Brian Plunkett, and Lalit Chhabildas
Air Force Research Laboratory – Munitions Directorate – Eglin AFB

September 2008

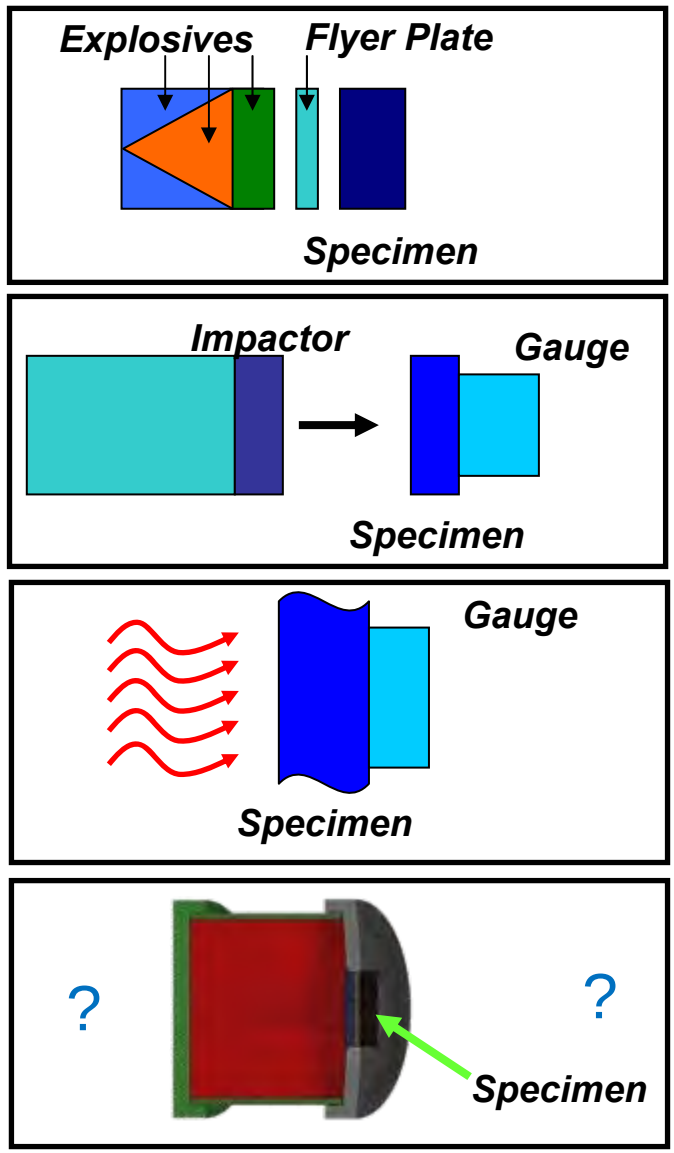


DISTRIBUTION A: Approved for public release; distribution unlimited.
Approval Confirmation 96 ABW/PA No. 07-03-08-312

Shock Loading Techniques

Established Techniques

- **Explosive Loading**
  1. Plane wave lens
  2. Explosively-driven flyers
- **Smooth-bore guns**
  1. Single-stage compressed gas
  2. Propellant
  3. Two-stage light gas
  4. Rail guns
  5. Three-stage light gas
- **Radiation**
  1. Electron beams
  2. Nuclear explosions
  3. Laser beams
  4. Z machine (X- rays, magnetic flux)



Evaluate Explosive End-Projector

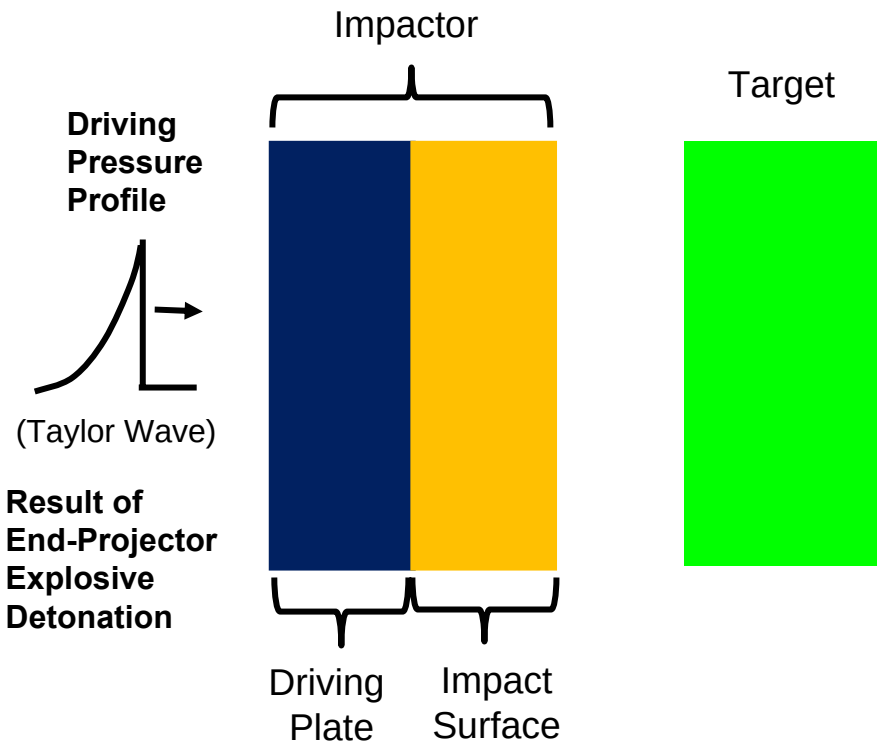
In-house capability but not an established technique

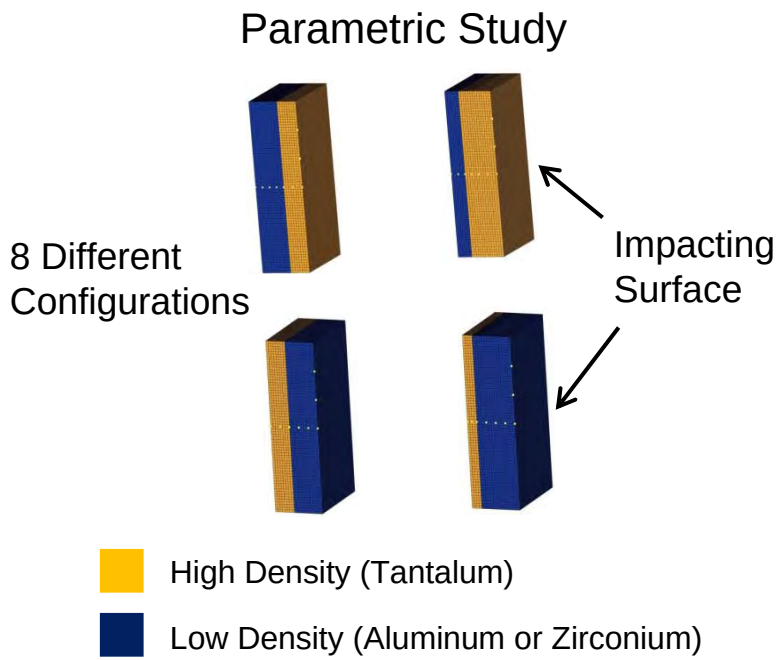
Approved for public release; Distribution Unlimited. Approval Confirmation 96 ABW/PA No. 07-03-08-312

Objective

Effects of the End-Projector on Terminal Velocity

Evaluate loading conditions and its effects (pressure, velocity, strain) through the bonded plates using the End-Projector, and its effects on terminal velocity





Approved for public release; Distribution Unlimited. Approval Confirmation 96 ABW/PA No. 07-03-08-312

Equation of State & Constitutive Parameters

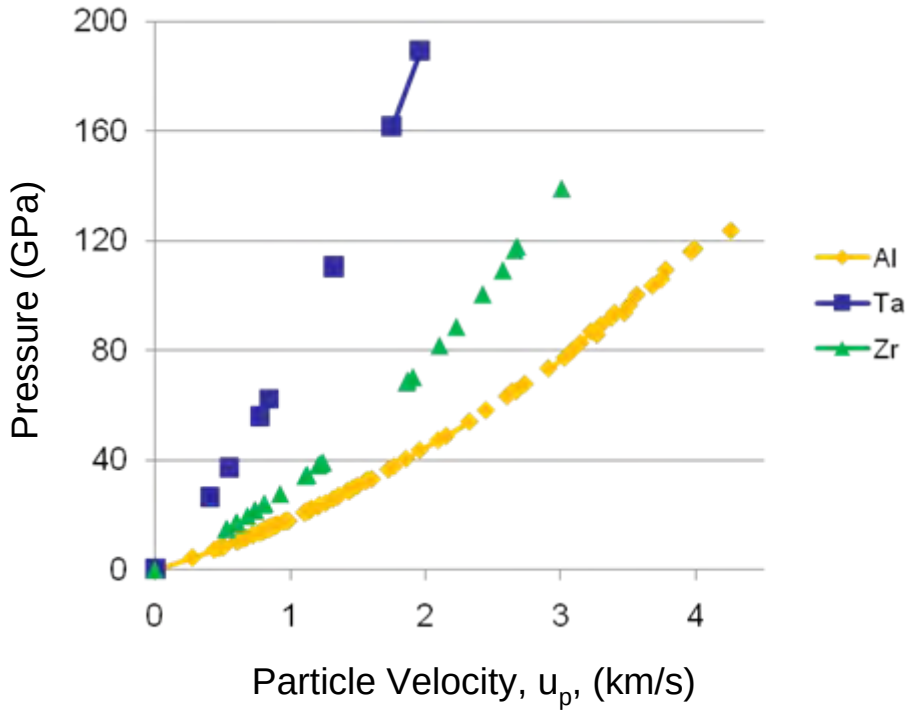
Used to Simulate Material Response - EPIC Hydrocode

Materials:

- Aluminum – Al
- Tantalum – Ta
- Zirconium - Zr

Strength Properties: Johnson-Cook Model
EOS: Mie-Gruneisen Model 2

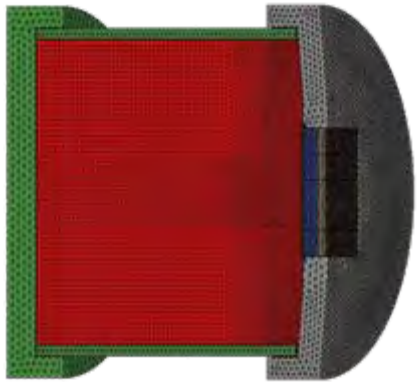
Property	Al	Ta	Zr
Density, ρ_0 (g/cm^3)	2.78	16.6	6.65
Yield Stress (GPa)	0.310	0.170	0.230
Poisson Ratio	0.33	0.34	0.34
Bulk Sound Velocity, C_S (km/s)	5.328	3.414	3.757
U_S / u_P Slope (S)	1.338	1.201	1.271
Spall Strength (GPa)	1.7	6.5	2.16
Impedance , $Z = \rho_0 U_S$	14.8	56.7	25.0



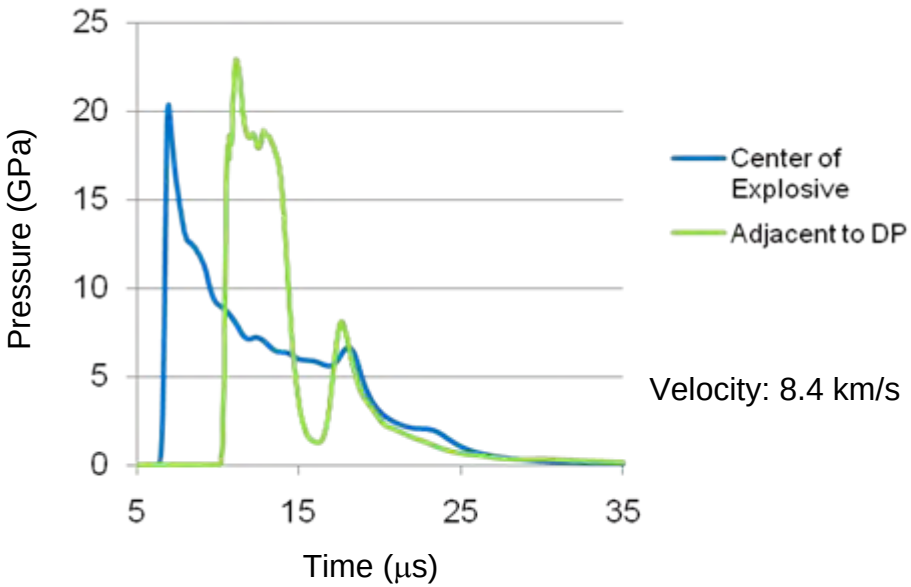
Approved for public release; Distribution Unlimited. Approval Confirmation 96 ABW/PA No. 07-03-08-312

Numerical Configuration

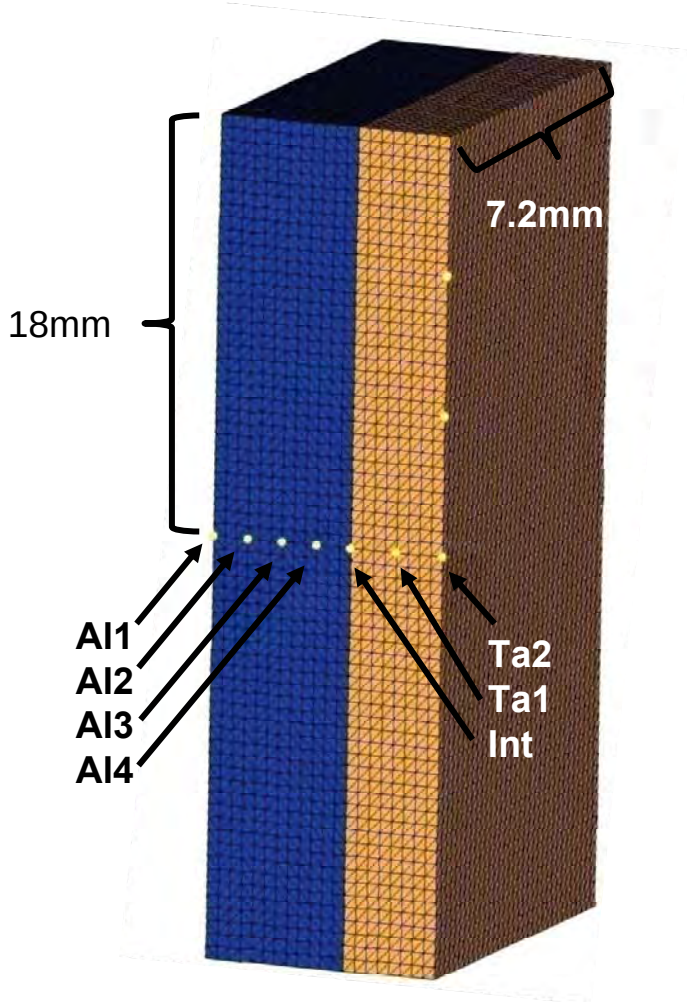
Monitor Through-thickness and Lateral Dimensions



Driving Pressure Profile



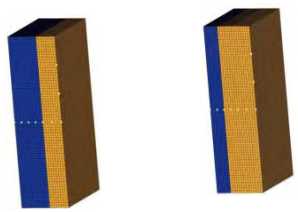
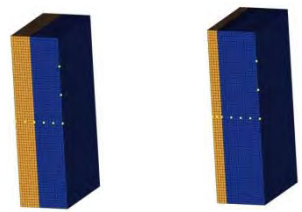
Velocity: 8.4 km/s



Code: EPIC; 1.1 Million Constant-strain Tetrahedral Elements

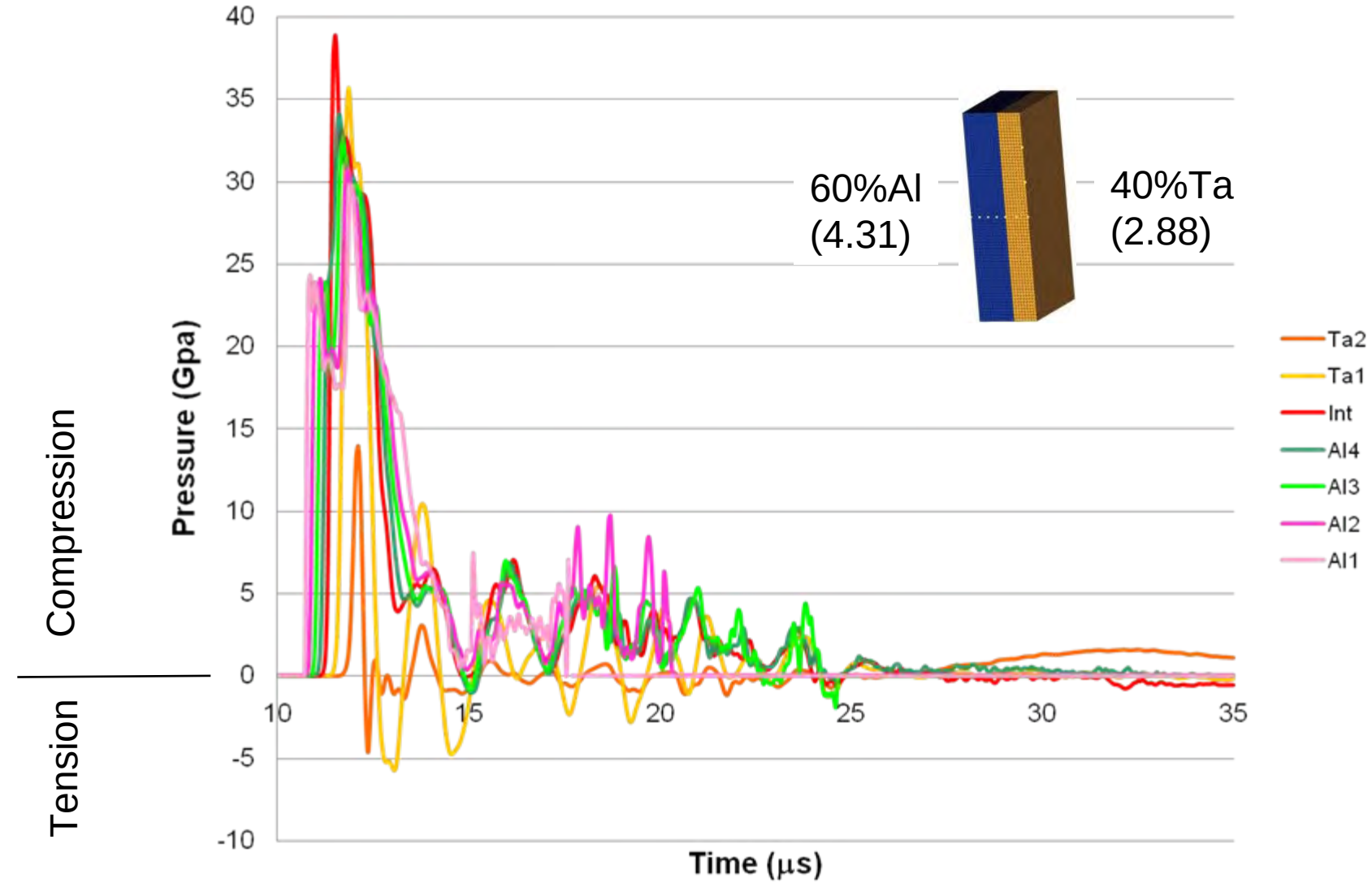
Approved for public release; Distribution Unlimited. Approval Confirmation 96 ABW/PA No. 07-03-08-312

Bimetallic Plate Configuration

Configuration	1	2	3	4	5	6	7	8
Driver Plate Material (Explosive Surface)	Al	Al	Zr	Zr	Ta	Ta	Ta	Ta
Driver Plate Material Thickness (mm)	4.31	2.16	4.31	2.16	2.88	1.44	2.88	1.44
Impactor Surface Material	Ta	Ta	Ta	Ta	Al	Al	Zr	Zr
Impactor Surface Material Thickness (mm)	2.88	5.03	2.88	5.03	4.31	5.75	4.31	5.75
Type	Shock / Release				Shock / Reshock			
High Density (Tantalum) Low Density (Aluminum or Zirconium)								

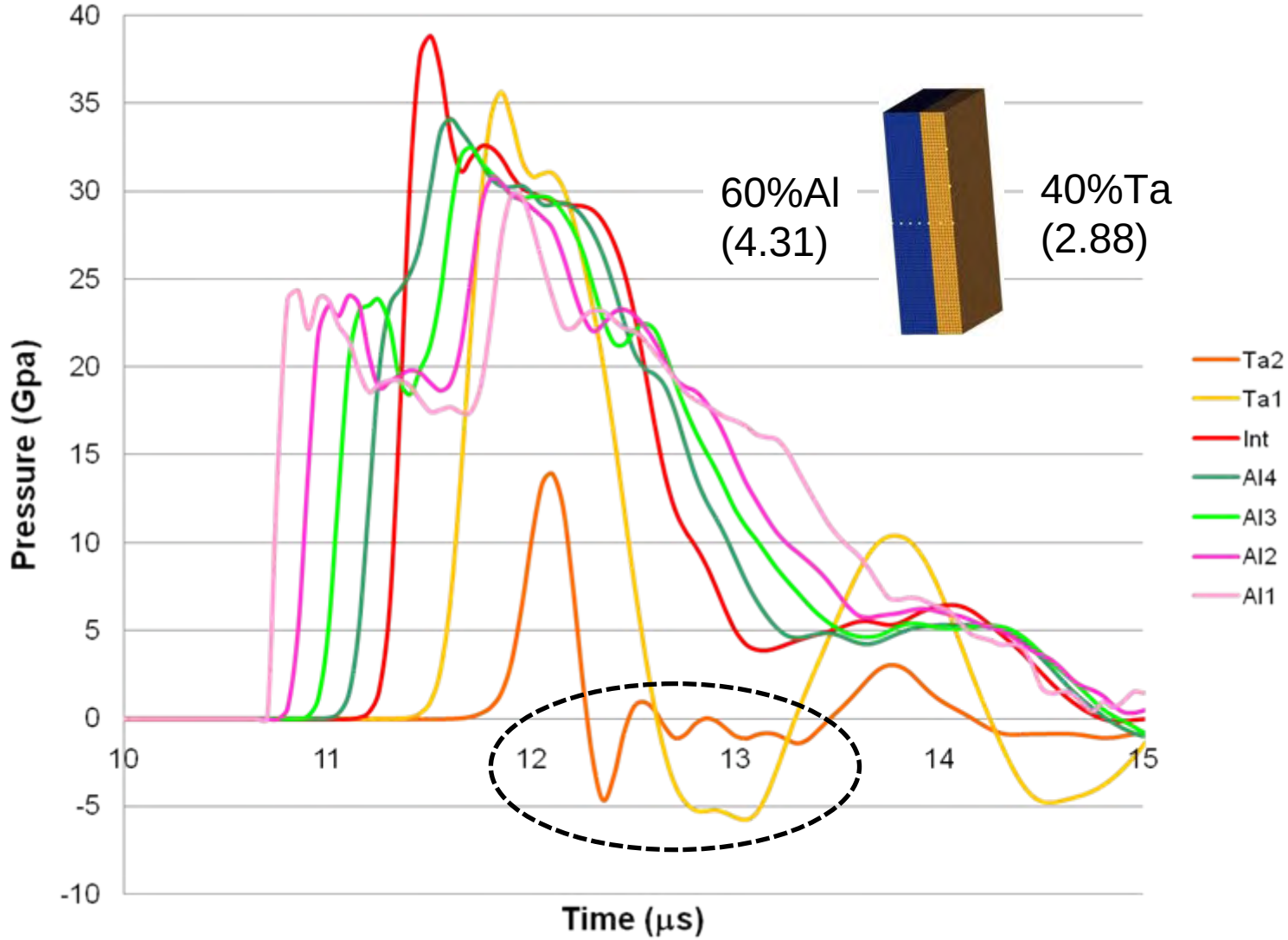
Approved for public release; Distribution Unlimited. Approval Confirmation 96 ABW/PA No. 07-03-08-312

Through Thickness Pressure (Configuration 1)



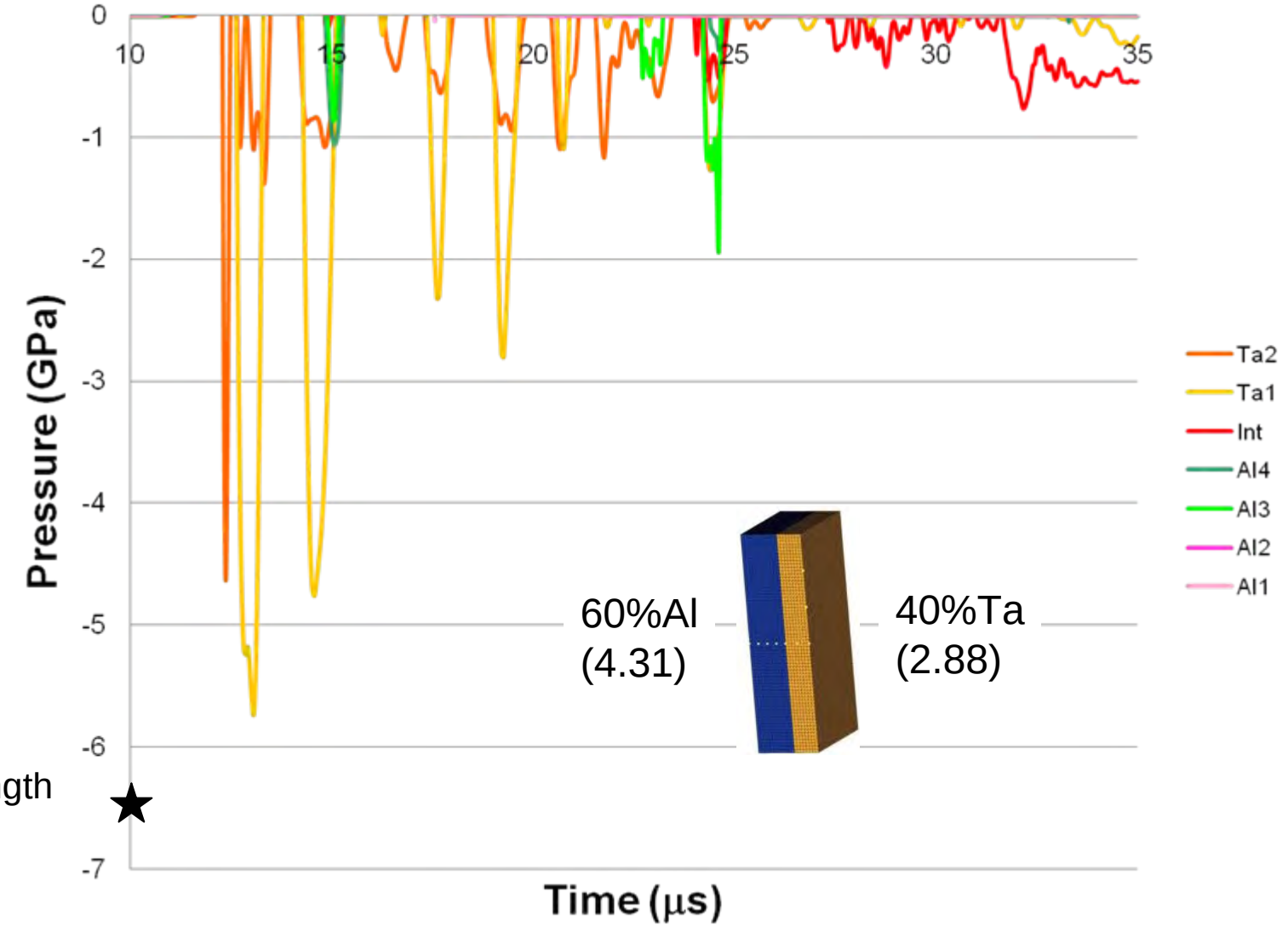
Approved for public release; Distribution Unlimited. Approval Confirmation 96 ABW/PA No. 07-03-08-312

Through Thickness Pressure (Configuration 1)



Approved for public release; Distribution Unlimited. Approval Confirmation 96 ABW/PA No. 07-03-08-312

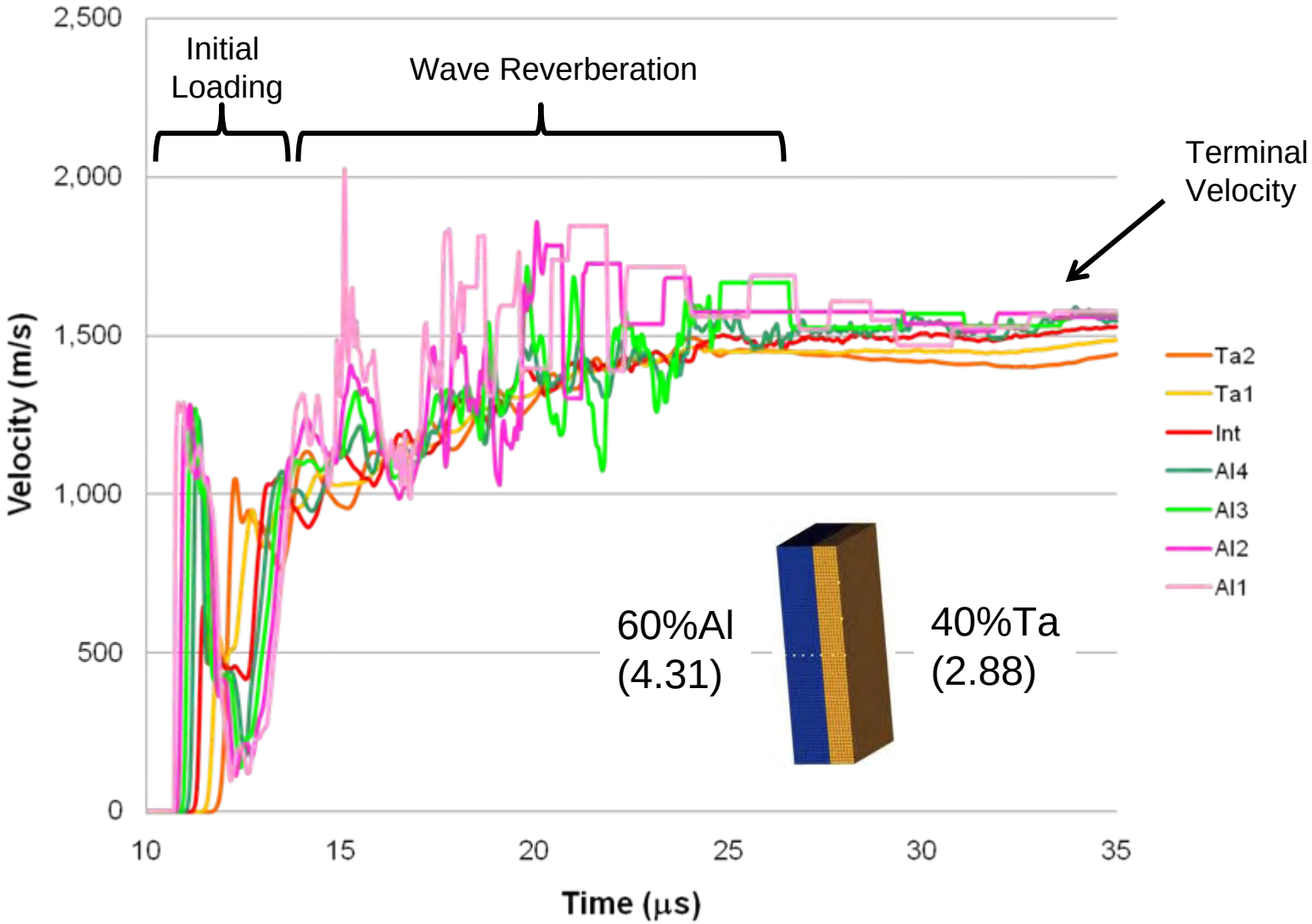
Through Thickness Tension (Configuration 1)



~Spall Strength of Tantalum

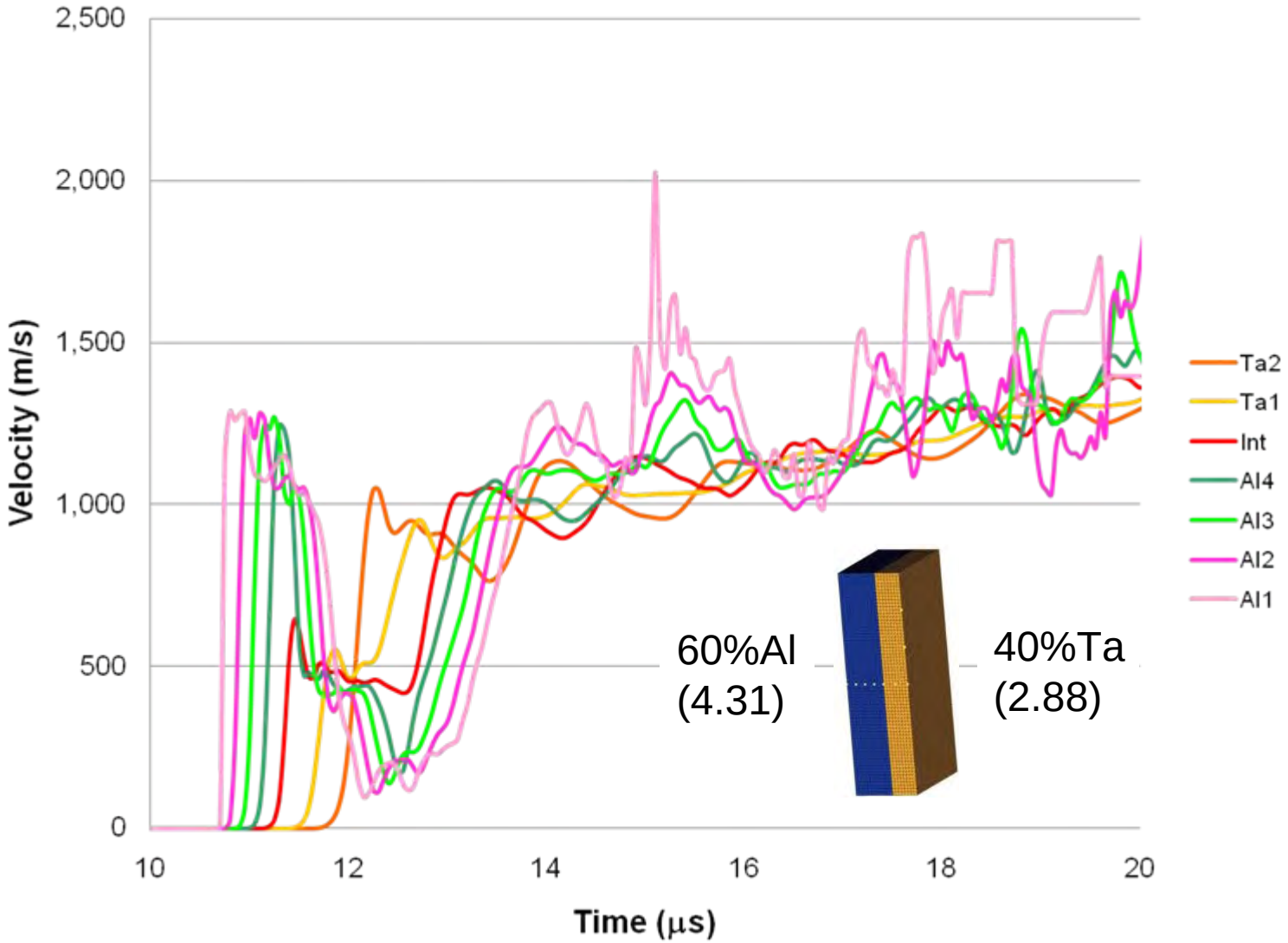
Approved for public release; Distribution Unlimited. Approval Confirmation 96 ABW/PA No. 07-03-08-312

Through Thickness Velocity (Configuration 1)



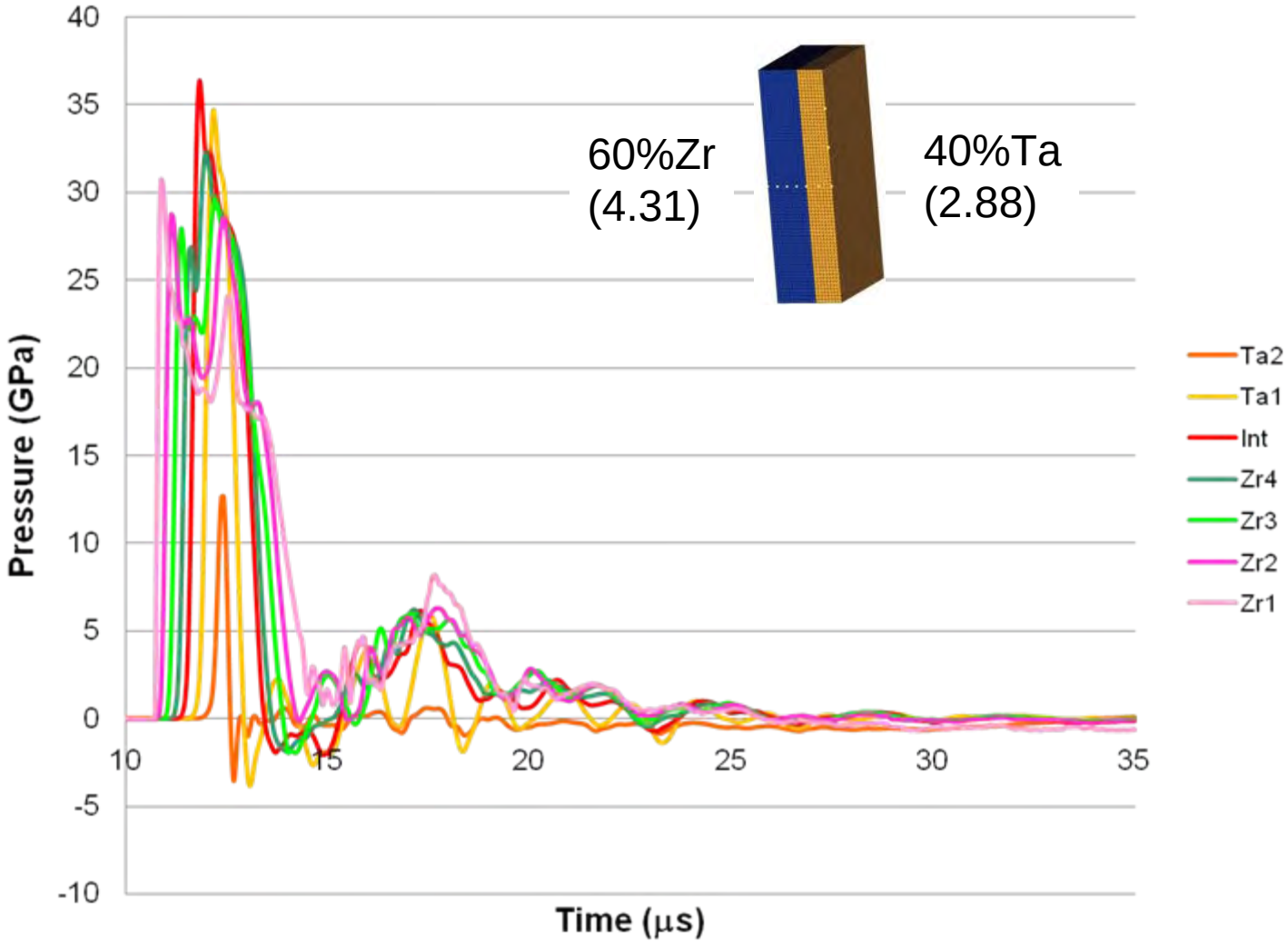
Approved for public release; Distribution Unlimited. Approval Confirmation 96 ABW/PA No. 07-03-08-312

Through Thickness Velocity (Configuration 1)



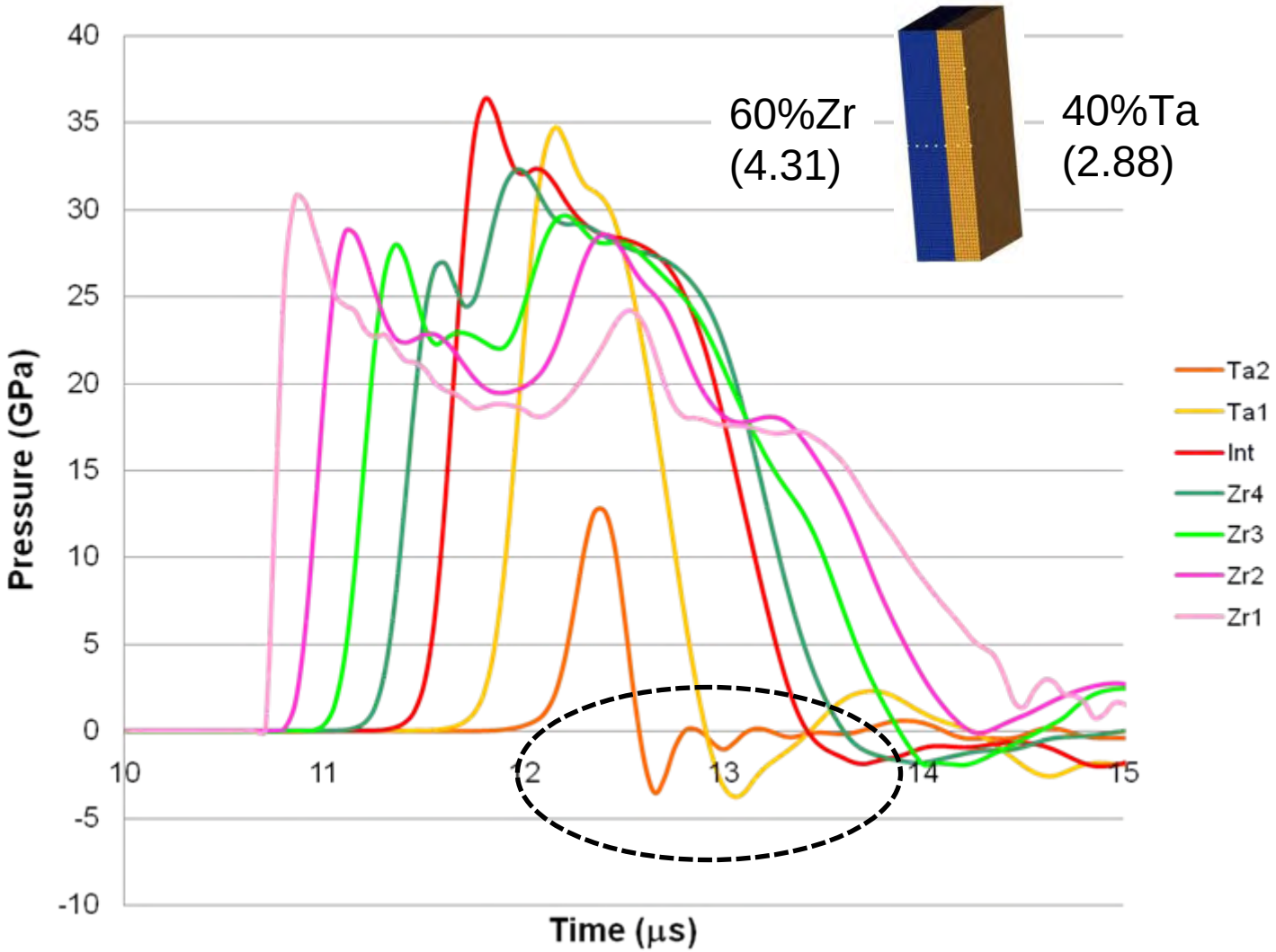
Approved for public release; Distribution Unlimited. Approval Confirmation 96 ABW/PA No. 07-03-08-312

Through Thickness Pressure (Configuration 3)



Approved for public release; Distribution Unlimited. Approval Confirmation 96 ABW/PA No. 07-03-08-312

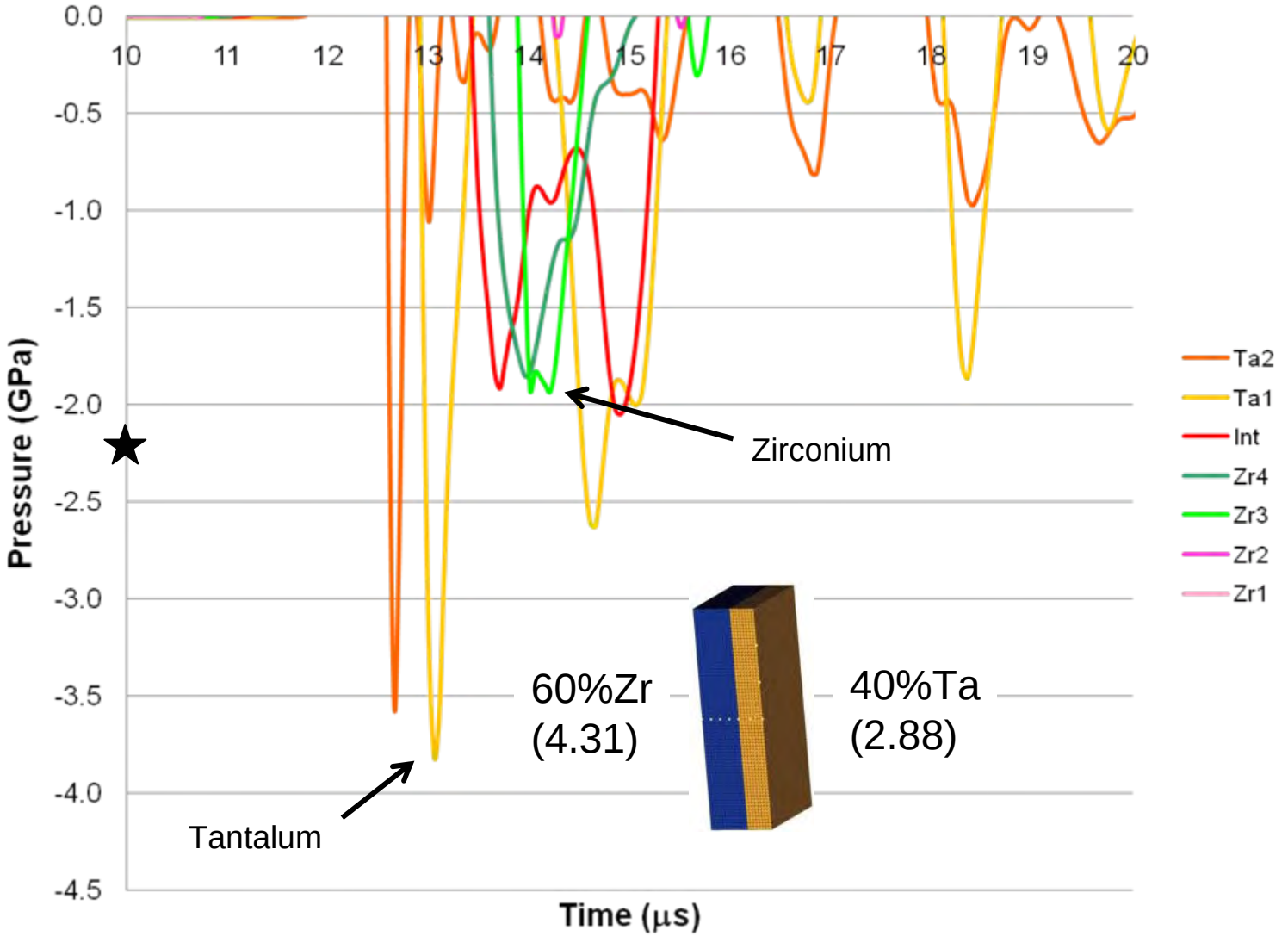
Through Thickness Pressure (Configuration 3)



Approved for public release; Distribution Unlimited. Approval Confirmation 96 ABW/PA No. 07-03-08-312

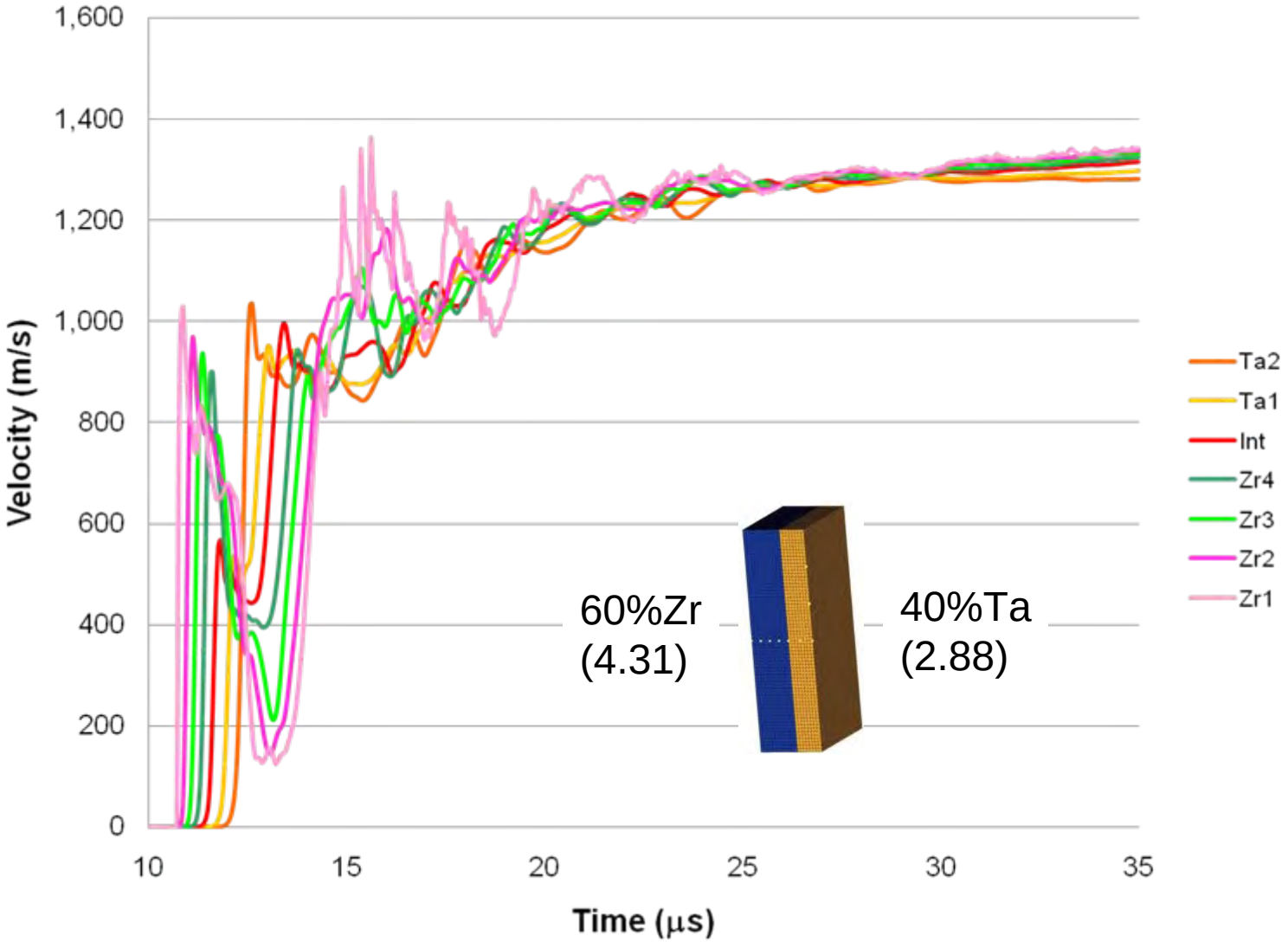
Through Thickness Pressure (Configuration 3)

~Spall Strength of Zirconium



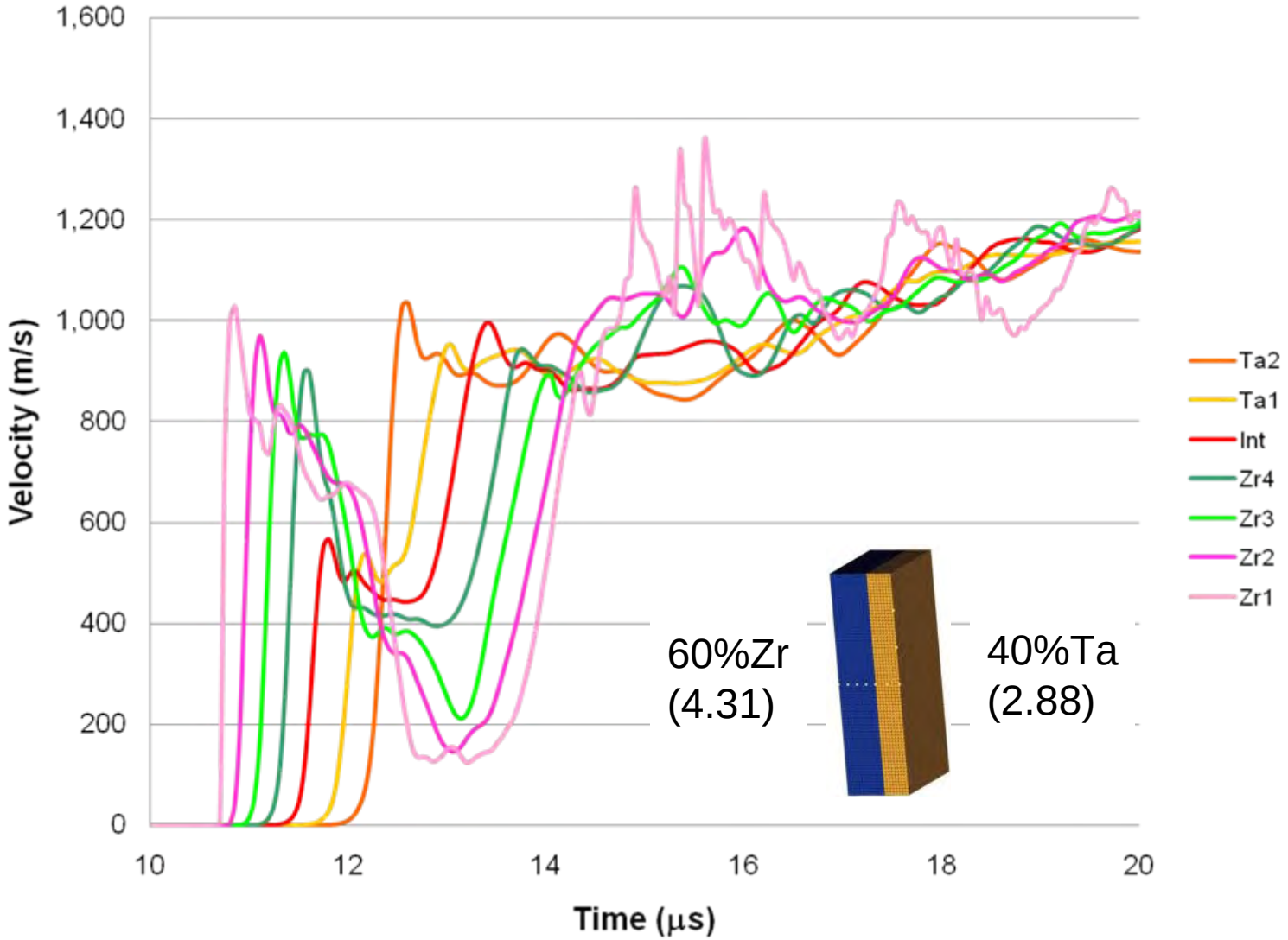
Approved for public release; Distribution Unlimited. Approval Confirmation 96 ABW/PA No. 07-03-08-312

Through Thickness Velocity (Configuration 3)



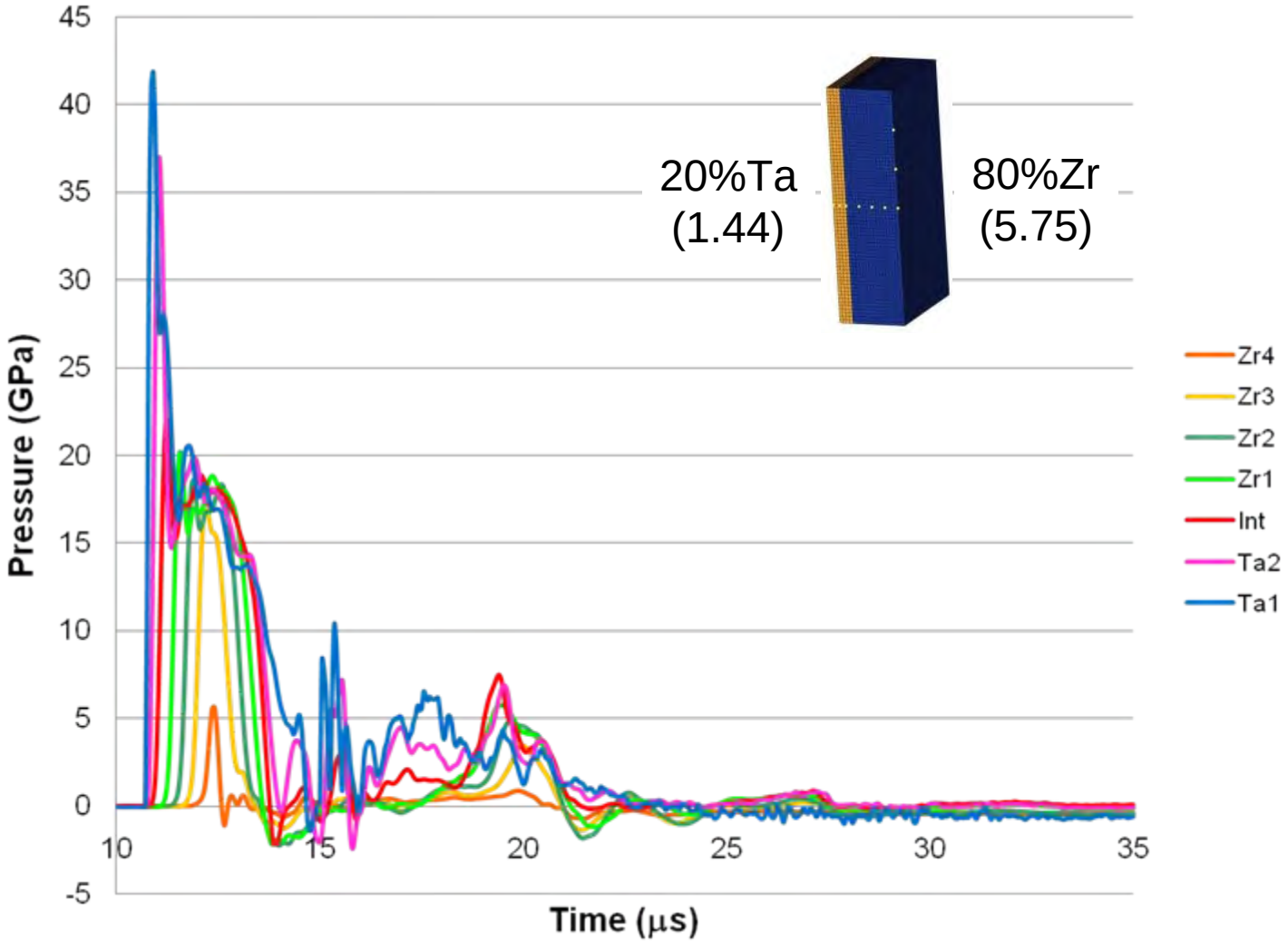
Approved for public release; Distribution Unlimited. Approval Confirmation 96 ABW/PA No. 07-03-08-312

Through Thickness Velocity (Configuration 3)



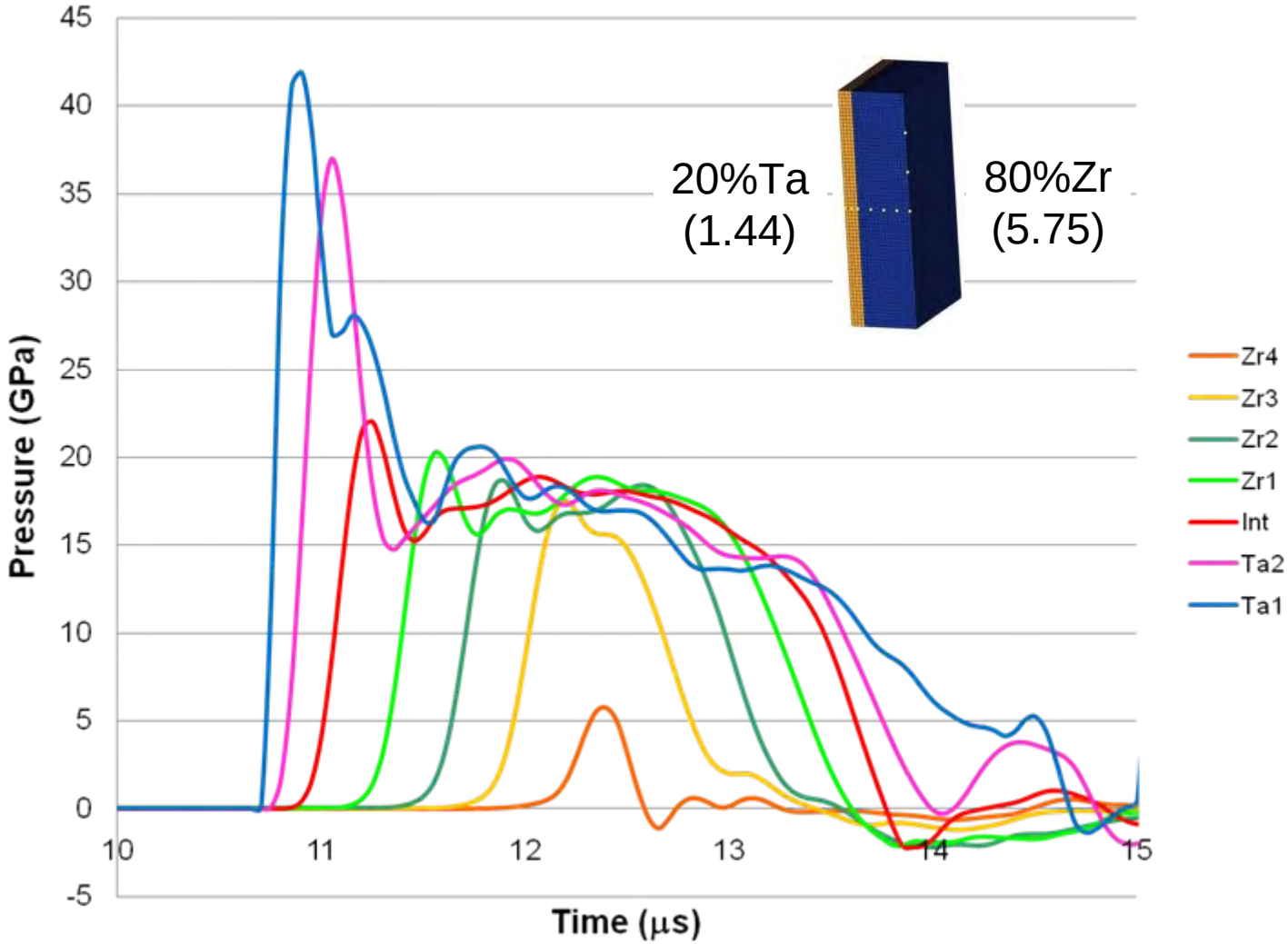
Approved for public release; Distribution Unlimited. Approval Confirmation 96 ABW/PA No. 07-03-08-312

Through Thickness Pressure (Configuration 8)



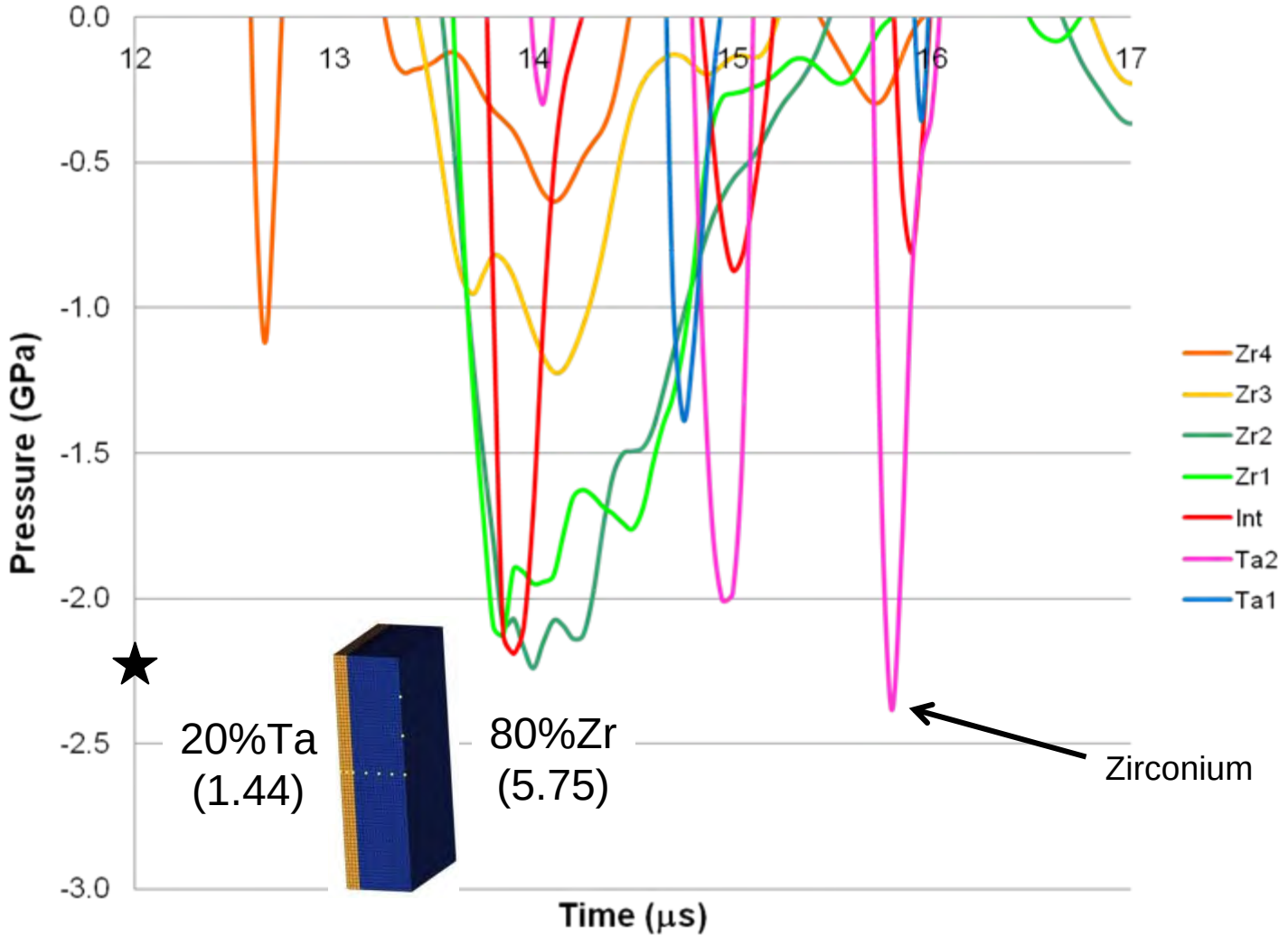
Approved for public release; Distribution Unlimited. Approval Confirmation 96 ABW/PA No. 07-03-08-312

Through Thickness Pressure (Configuration 8)



Approved for public release; Distribution Unlimited. Approval Confirmation 96 ABW/PA No. 07-03-08-312

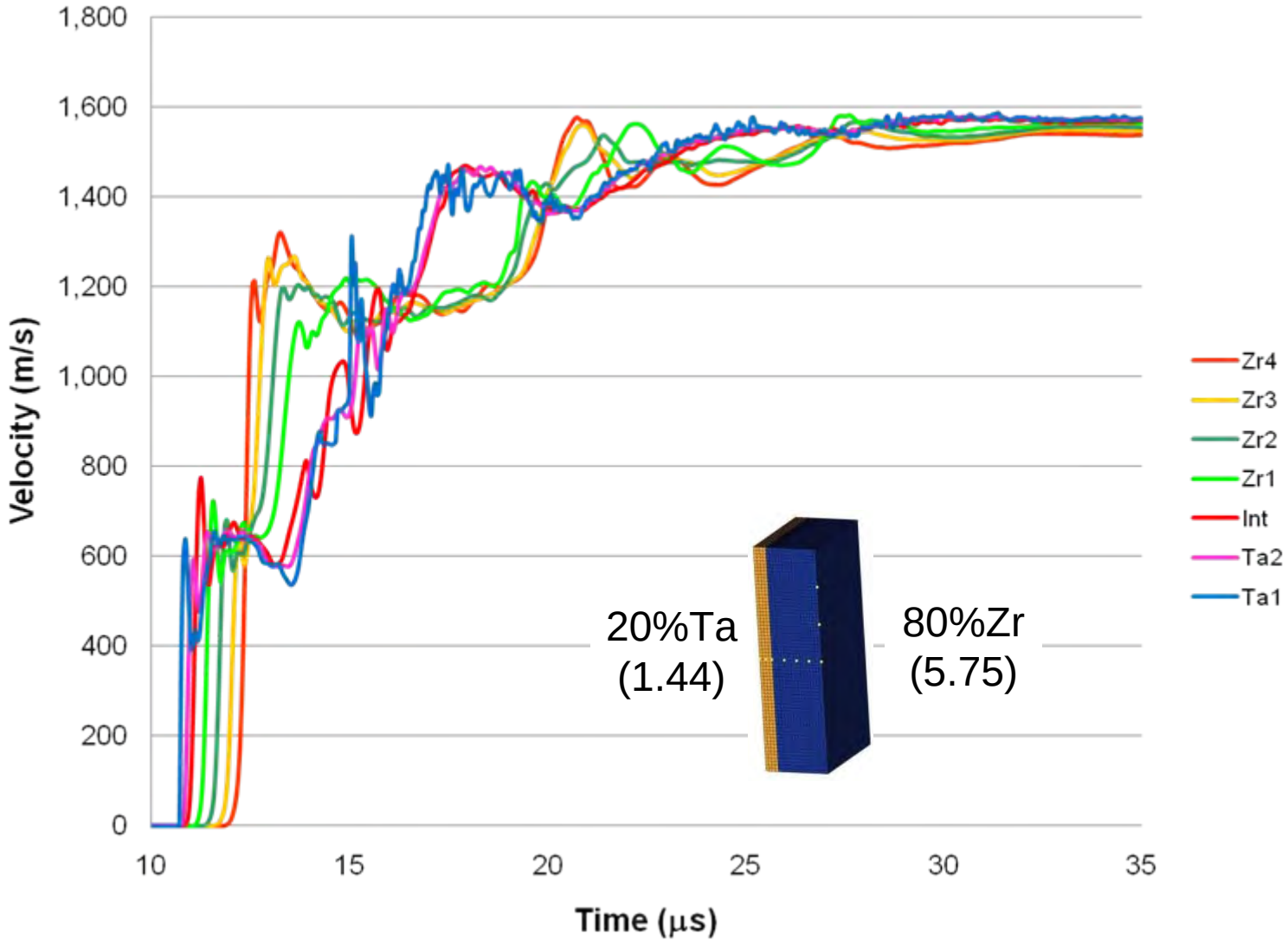
Through Thickness Pressure (Configuration 8)



~Spall Strength of Zirconium

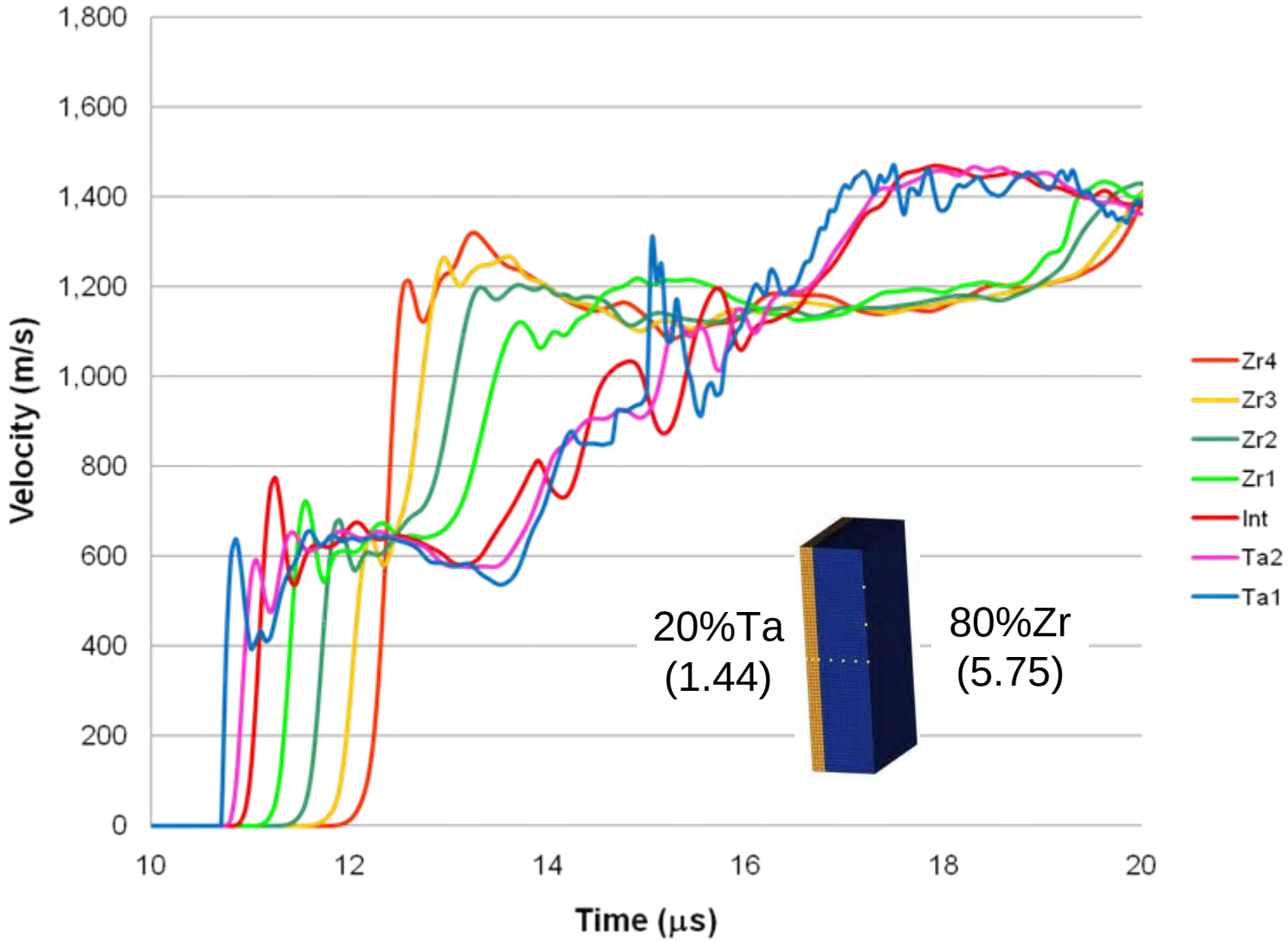
Approved for public release; Distribution Unlimited. Approval Confirmation 96 ABW/PA No. 07-03-08-312

Through Thickness Velocity (Configuration 8)



Approved for public release; Distribution Unlimited. Approval Confirmation 96 ABW/PA No. 07-03-08-312

Through Thickness Velocity (Configuration 8)



Approved for public release; Distribution Unlimited. Approval Confirmation 96 ABW/PA No. 07-03-08-312

Summary

Configuration	1	2	3	4	5	6	7	8
Driver Plate Material (Explosive Surface)	Al	Al	Zr	Zr	Ta	Ta	Ta	Ta
Max Compression (GPa)	32.5	35.5	32.2	34.1	41.9	41.9	41.9	41.9
Max Tension (GPa)	1.88	0.76	1.93	0.83	5.90	4.56	4.26	2.38
Impactor Surface Material	Ta	Ta	Ta	Ta	Al	Al	Zr	Zr
Max Compression (GPa)	35.7	38.8	34.7	37.9	13.3	14.8	18.5	20.2
Max Tension (GPa)	5.7	7.15	3.82	6.86	3.74	4.22	1.51	2.23
Interface								
Max Compression (GPa)	38.9	41.2	36.4	39.8	14.5	15.7	20.4	22.0
Max Tension (GPa)	0.76	1.21	2.05	0.21	5.13	4.08	2.19	2.19
Velocity								
Terminal Velocity (m/s)	1500	1150	1300	1050	1575	2150	1300	1575

Anticipated Spall

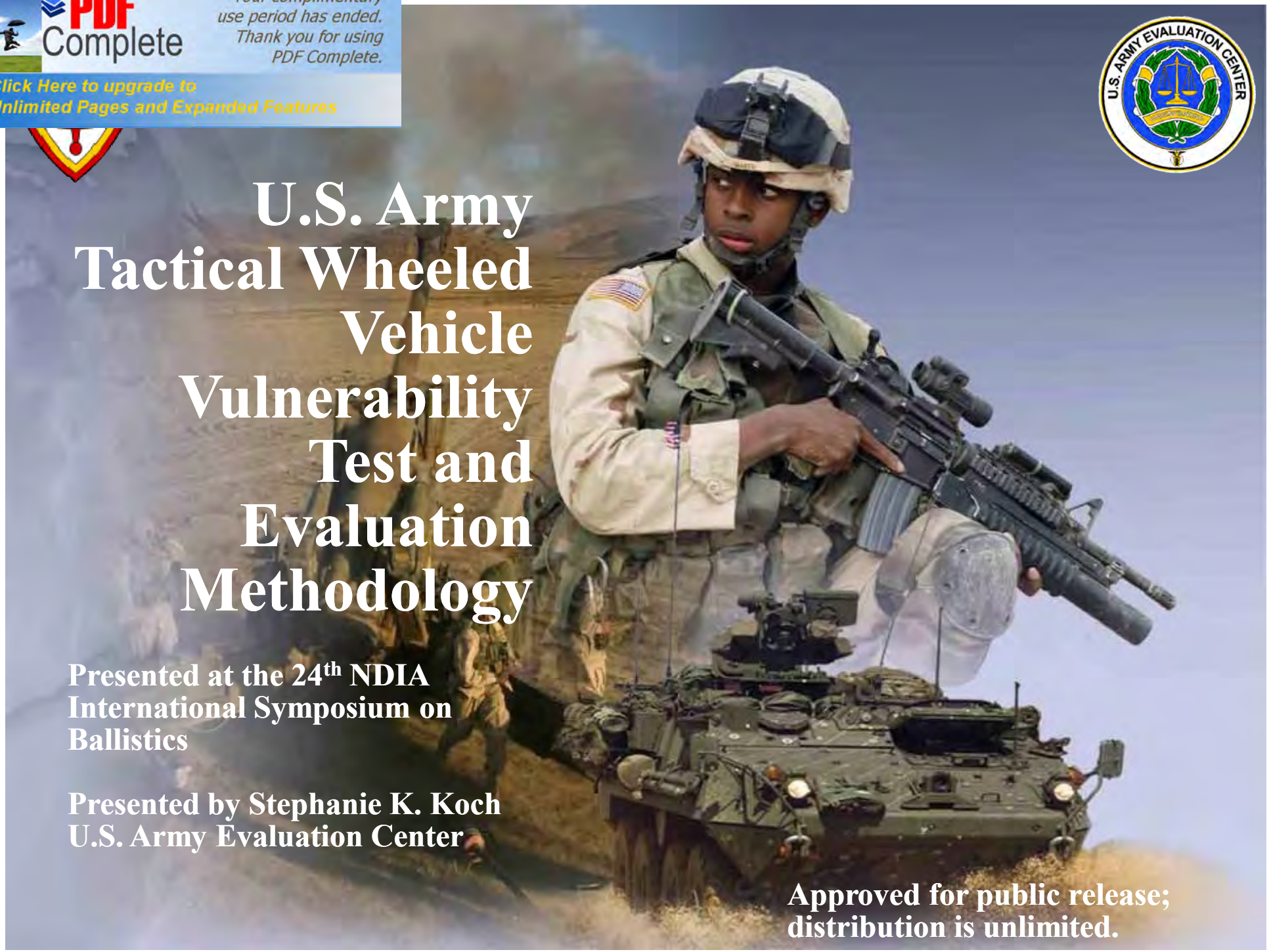
Approved for public release; Distribution Unlimited. Approval Confirmation 96 ABW/PA No. 07-03-08-312

Conclusions

- Good potential for explosively launched bimetallic plates regarding shock loading experiments
- As expected, material choice and dimensions play a key role in the survivability of launching the bonded plates. Lower impedance mismatches reduce spall susceptibility but at expense of reshock
- Shock / Re-shock experiments are more susceptible to spall and thus more challenging to design
- Additional system features may be introduced such as an air gap between the explosive and driver plate which would result in a lower driving pressure and therefore reduced susceptibility to spall.
- It is encouraging that these initial studies are quite promising. Further studies should include using an optimization routine which would include controlling the dimensions of the air gap, and the relative thicknesses of the driver plate and impactor plate.

Approved for public release; Distribution Unlimited. Approval Confirmation 96 ABW/PA No. 07-03-08-312

PDF Complete
Your complimentary use period has ended. Thank you for using PDF Complete.
Click Here to upgrade to Unlimited Pages and Expanded Features



U.S. Army Tactical Wheeled Vehicle Vulnerability Test and Evaluation Methodology

Presented at the 24th NDIA International Symposium on Ballistics

Presented by Stephanie K. Koch
U.S. Army Evaluation Center

Approved for public release; distribution is unlimited.

PDF Complete
Your complimentary use period has ended. Thank you for using PDF Complete.
Click Here to upgrade to Unlimited Pages and Expanded Features

ny TWV T&E Methodology

Introduction

Traditional
Ballistic Vulnerability Candidates





Heavily Armored Combat Vehicles

OEF/OIF
Ballistic Vulnerability Candidates





Unarmored TWVs

PDF Complete
Your complimentary use period has ended. Thank you for using PDF Complete.
Click Here to upgrade to Unlimited Pages and Expanded Features

ny TWV T&E Methodology

Agenda

- Phase 1: Coupon Testing
- Phase 2: Component/Subsystem Testing
- Phase 3: Exploitation Testing
- Phase 4: System Level Testing







PDF Complete
Your complimentary use period has ended. Thank you for using PDF Complete.
Click Here to upgrade to Unlimited Pages and Expanded Features

ny TWV T&E Methodology

Phase 1: Coupon Testing

Coupon testing provides a quick and cost effective means to determine the capabilities of an armor solution.

- A coupon is a 2 x 2 foot piece of the complete armor recipe.
- A coupon test involves testing against various ballistic threats.
- Three phases of coupon testing.
  - V_{50}
  - Requirement
  - Armor Characterization



PDF Complete
Your complimentary use period has ended. Thank you for using PDF Complete.
Click Here to upgrade to Unlimited Pages and Expanded Features

ny TWV T&E Methodology

Phase 1: Coupon Testing

V_{50} coupon testing determines whether or not an armor recipe is worthy of further investigation.

- A V_{50} is the velocity where a complete penetration and partial penetration are equally likely for the threat under consideration.
- The V_{50} is calculated by taking the mean of an equal number of highest partial and lowest complete penetrations.
- The V_{50} for a certain armor recipe is compared to other recipes to determine the performance capabilities.

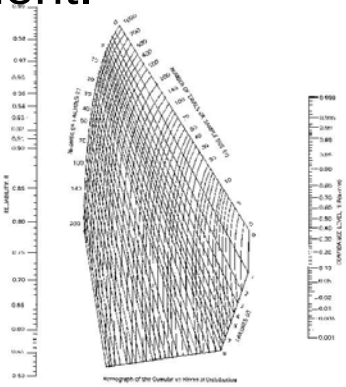
PDF Complete
Your complimentary use period has ended. Thank you for using PDF Complete.
Click Here to upgrade to Unlimited Pages and Expanded Features

ny TWV T&E Methodology

Phase 1: Coupon Testing

Requirements coupon testing determines whether or not an armor recipe meets specific requirements.

- Example requirement: The armor must provide an X% probability of protection against a threat fired at a velocity with a Y% confidence level.
- The cumulative binomial distribution is used to determine the number of partial impacts required to meet the requirement.
- Coupon testing is then conducted.



PDF Complete
Your complimentary use period has ended. Thank you for using PDF Complete.
Click Here to upgrade to Unlimited Pages and Expanded Features

ny TWV T&E Methodology

Phase 1: Coupon Testing

Armor characterization coupon testing primarily supports modeling and simulation efforts.

- Penetration Algorithm Development
- Behind Armor Debris (BAD) Characterization

PDF Complete
Your complimentary use period has ended. Thank you for using PDF Complete.
Click Here to upgrade to Unlimited Pages and Expanded Features

ny TWV T&E Methodology

Phase 2: Component/Subsystem Testing

Component/Subsystem testing determines the affect of certain system components/subsystems on the survivability of the crew.

- Typical combat vehicle evaluations focused heavily on component/subsystem testing to determine the survivability of the system as a whole.
- TWVôs are only required to provide crew protection so those components/subsystem that could affect the survivability of the crew are tested.
  - Fuel Cells
  - Automatic Fire Extinguishing Systems (AFES)

PDF Complete
Your complimentary use period has ended. Thank you for using PDF Complete.
Click Here to upgrade to Unlimited Pages and Expanded Features

ny TWV T&E Methodology

Phase 3: Exploitation Testing

Exploitation testing determines the ballistic vulnerabilities of the integrated armor.

- Exploitation testing addresses the ability of certain projectiles to penetrate vulnerable areas of the armor package as installed on the cab.

PDF Complete
Your complimentary use period has ended. Thank you for using PDF Complete.
Click Here to upgrade to Unlimited Pages and Expanded Features

ny TWV T&E Methodology

Phase 4: System Level Testing

System level testing determines the overall protection provided to the crew of the vehicle under consideration.

- System level testing focuses on addressing crew vulnerabilities against threats that can not be addressed in the other three phases.
  - Typically focuses on blast-type threats.
- System level testing also provides insight into battle damage and repair capabilities.

Event	Location	Test Condition
1. Mine	Under Wheel	Running vehicle, Stowage, Heated Fuel
2. Mine	Underbody	Running vehicle, Stowage, Heated Fuel
3. Fragmenting Round	Side of Vehicle	Not Running, Stowage, Simulated Fuel Tank Weight

PDF Complete
Your complimentary use period has ended. Thank you for using PDF Complete.
Click Here to upgrade to Unlimited Pages and Expanded Features

ny TWV T&E Methodology

Conclusion

The TWV ballistic vulnerability methodology is a detailed, flexible, and judicious building block approach to test and evaluation.

- Phase 1: Coupon Testing
- Phase 2: Component/Subsystem Testing
- Phase 3: Exploitation Testing
- Phase 4: System Level Testing

PDF Complete
Your complimentary use period has ended. Thank you for using PDF Complete.
Click Here to upgrade to Unlimited Pages and Expanded Features

ny TWV T&E Methodology





Questions









PDF Complete
Your complimentary use period has ended. Thank you for using PDF Complete.
Click Here to upgrade to Unlimited Pages and Expanded Features

Engineering

BAE SYSTEMS

Warhead Filling and Casing Interactions affect the Blast Field performance

Authors: Paul Locking – BAE Systems (Land)
Dennis Flynn – BAE Systems (Land)
Jim Dunnett – Fluid Gravity Engineering

PDF Complete
Your complimentary use period has ended. Thank you for using PDF Complete.
Click Here to upgrade to Unlimited Pages and Expanded Features

g effects on Blast

BAE SYSTEMS

ACKNOWLEDGEMENTS

This work was funded by the Weapon & Platform Effectors (WPE) Domain of the UK MoD Research Acquisition Office (RAO) and contracted through QinetiQ, the Prime Contractor.

The authors are grateful for their kind permission to publish this work. RAO has since become the Defence Technology Innovation Centre (DTIC).

PDF Complete
Your complimentary use period has ended. Thank you for using PDF Complete.
Click Here to upgrade to Unlimited Pages and Expanded Features

BAE SYSTEMS

sentation Outline

- Objectives
- Historical Background
- Recent Trials
- Analysis
- Conclusions

PDF Complete
Your complimentary use period has ended. Thank you for using PDF Complete.
Click Here to upgrade to Unlimited Pages and Expanded Features

g effects on Blast

BAE SYSTEMS

Errata

I would like to apologise for one typographical error that got through the proof reading:

óAluminium Alloy 6086T6ô

should read

óAluminium Alloy 6082 to Condition T6ô

PDF Complete
Your complimentary use period has ended. Thank you for using PDF Complete.
Click Here to upgrade to Unlimited Pages and Expanded Features

ojectives

BAE SYSTEMS

- Currently Engineering models predict Blast output from cased warheads use experimentally derived algorithms, e.g. Fano and Fisher curves
- Such curves are typically based upon TNT explosive with the cast iron or steel cases
- Review Historical Data
- Investigate
  - Ideal and Non-Ideal explosives
  - Brittle and Ductile case materials
- Integrated Trials and EDEN hydrocode Modelling to assess these Engineering models
- Establish a preferred model and its fitô parameters with applicability for each case

PDF Complete
Your complimentary use period has ended. Thank you for using PDF Complete.
Click Here to upgrade to Unlimited Pages and Expanded Features

BAE SYSTEMS

Engineering Models

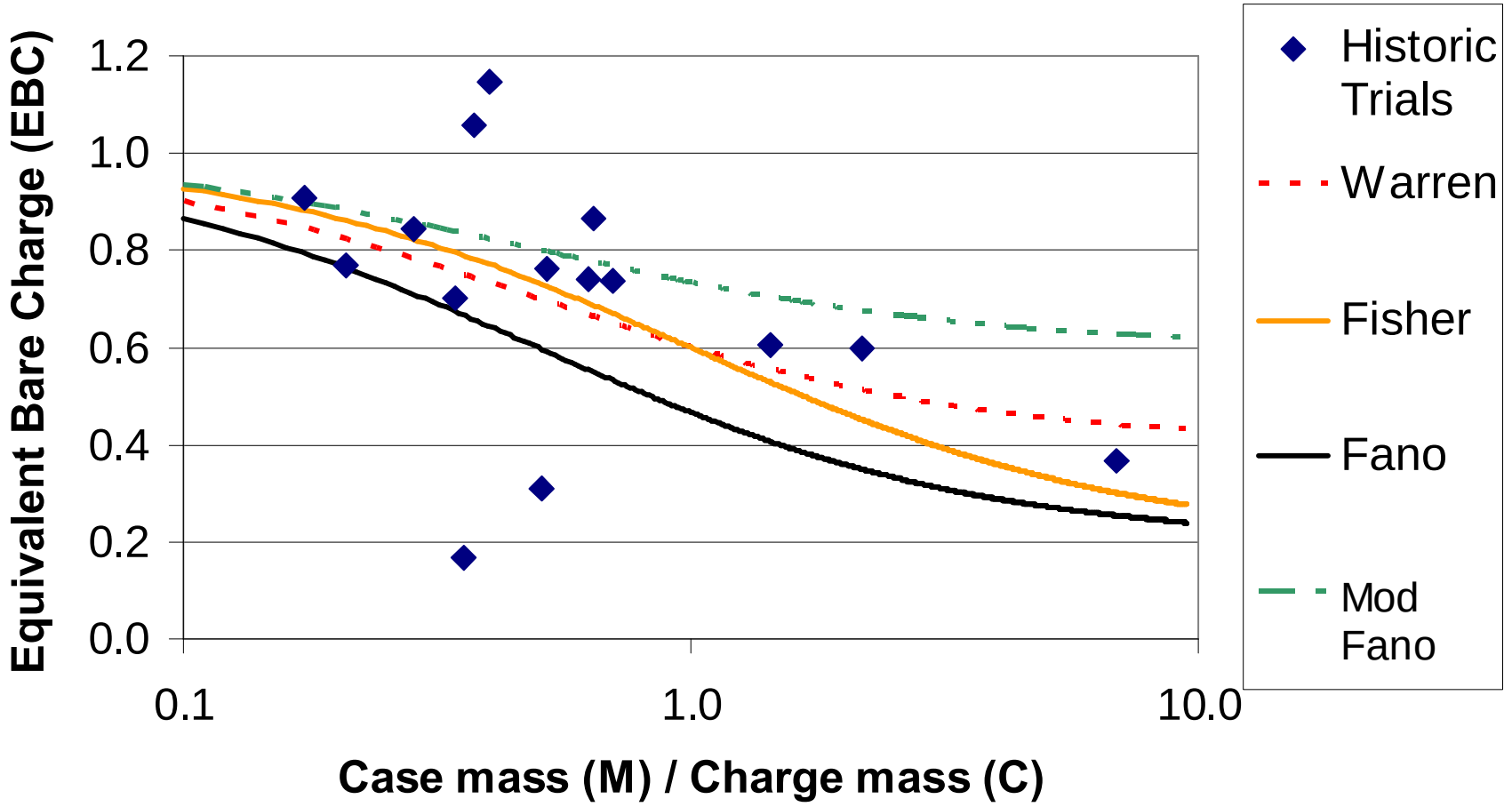
Fisher	$EBC = C \times [0.2 + 0.8/(1 + M/C)]$
Modified Fisher	$EBC = \{C + C \times [0.2 + 0.8/(1 + M/C)]\}/2$
Fano	$EBC = C \times [0.2 + 0.8/(1 + 2 \times M/C)]$
Modified Fano	$EBC = C \times [0.6 + 0.4/(1 + 2 \times M/C)]$
Warren	$EBC = C \times [0.4 + 0.6/(1 + 2 \times M/C)]$
US for Pressure	$EBC = 1.19 \times C \times [1 + M/C \times (1 - M_c)/(1 + M/C)]$
US for Impulse	$EBC = C \times [1 + M/C \times (1 - M_c)/(1 + M/C)]$

EBC = Equivalent Bare Charge
C = Charge mass
M = Mass of metal (in parallel section)
M_c = M/C if M/C <=1.0 or 1.0 otherwise

PDF Complete
Your complimentary use period has ended. Thank you for using PDF Complete.
Click Here to upgrade to Unlimited Pages and Expanded Features

BAE SYSTEMS

or Steel Casings



PDF Complete
Your complimentary use period has ended. Thank you for using PDF Complete.
Click Here to upgrade to Unlimited Pages and Expanded Features

BAE SYSTEMS

ng Case Effects on Blast

- Limited understanding of case effects
- Large scatter of trials data
- Wide choice of ‘Engineering Models’
- Limited data
- Need for updated trials with purpose made hardware and extensive instrumentation
- With experimental controls
- Integrated EDEN hydrocode modelling
- Trials designed specifically for the hydrocode modelling

PDF Complete
Your complimentary use period has ended. Thank you for using PDF Complete.
Click Here to upgrade to Unlimited Pages and Expanded Features

BAE SYSTEMS

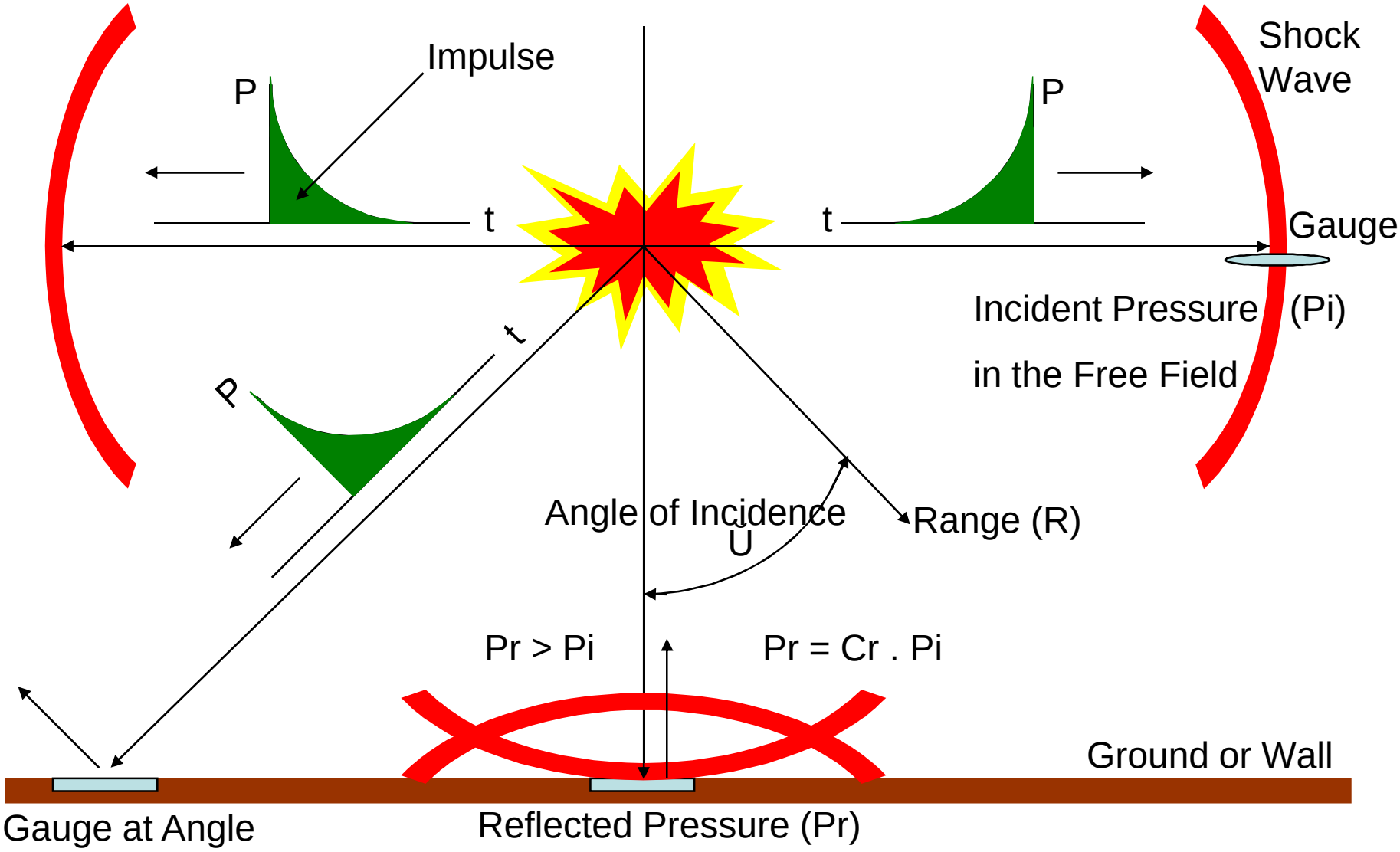
Limitations / Unknowns

- Explosive Type
- Casing Material
- Fragmentation Mechanism (Natural / Pre-fragmented)
- Pressure or Impulse
- Pressure Considered (Incident / Reflected)
- Ground / Air
- Shape (Spherical / Cylindrical)
- Scaling
- Confinement (Uniformly / Heavy Nose)
- Initiation (Central / End)
- Position / Aspect - Best historic trials gauge positions undefined

PDF Complete
Your complimentary use period has ended. Thank you for using PDF Complete.
Click Here to upgrade to Unlimited Pages and Expanded Features

Typical Issues that Arise

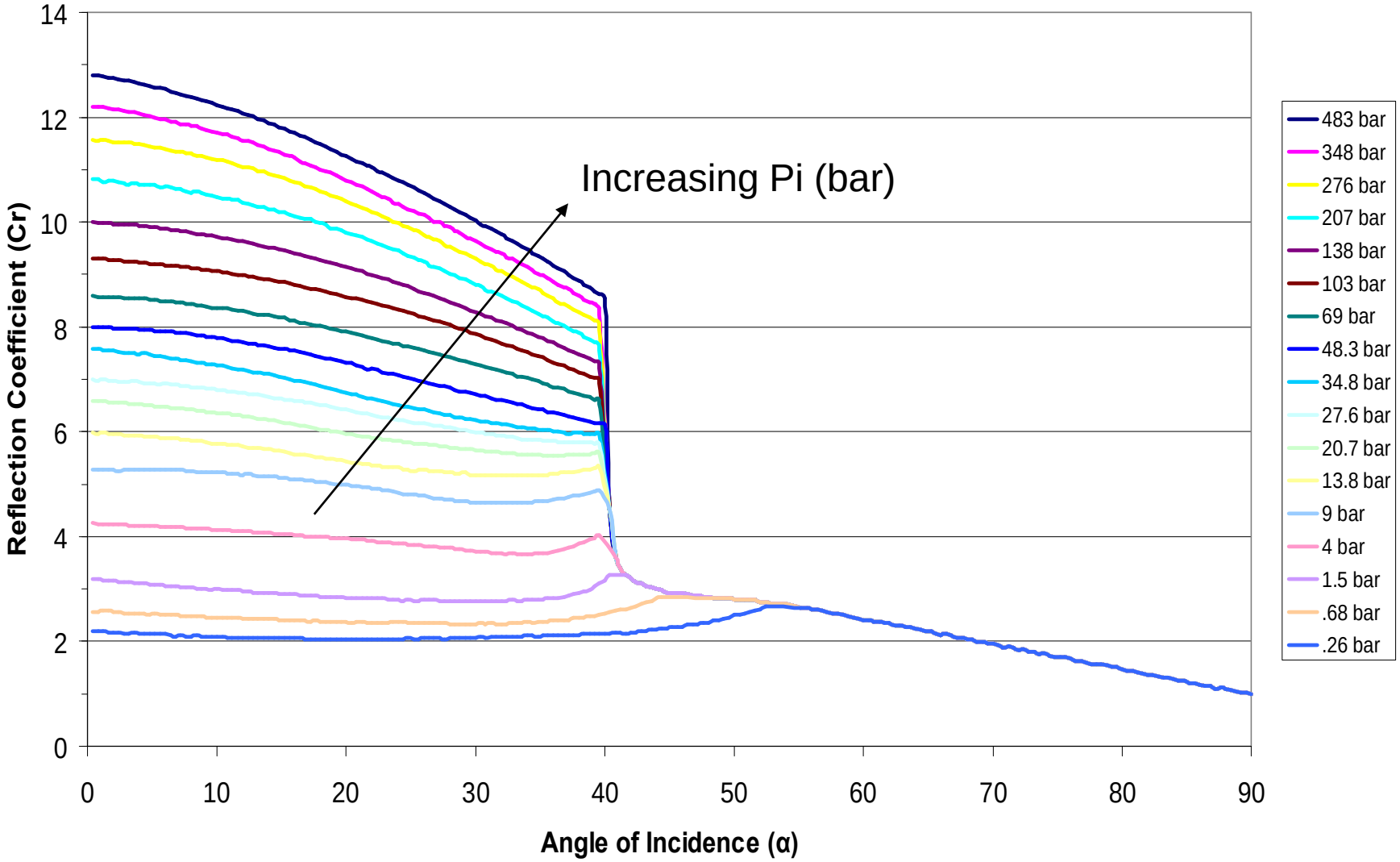
Record Reflected (Pr) pressure, but need to correct to get Incident (Pi) pressure, but it is both Angle (U) and Pressure dependent



PDF Complete
Your complimentary use period has ended. Thank you for using PDF Complete.
Click Here to upgrade to Unlimited Pages and Expanded Features

BAE SYSTEMS

nst Angle of Incidence with Pressure



PDF Complete
Your complimentary use period has ended. Thank you for using PDF Complete.
Click Here to upgrade to Unlimited Pages and Expanded Features

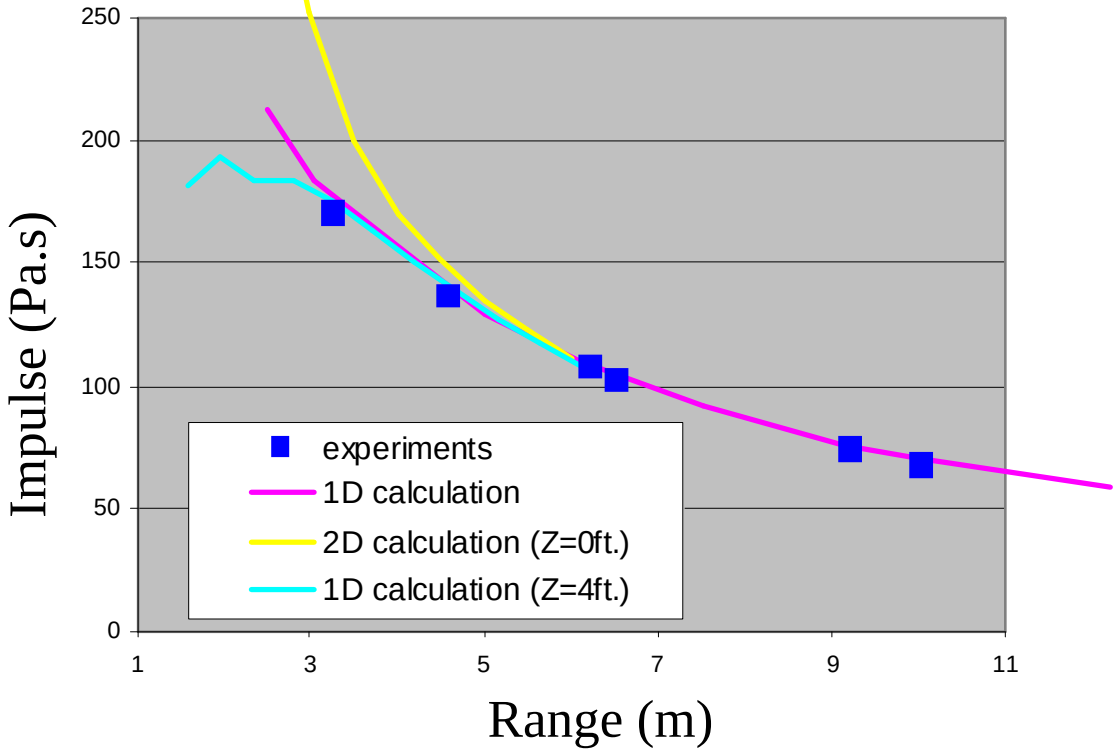
Sheard Analysis

(Royal Society, V187, 1944)

BAE SYSTEMS

Grime and Sheard experiments were found to provide sufficient data about the trial arrangement to attempt to reproduce using the FGE - EDEN hydrocode

- Explosive = Comp-B
- L / D = 2 / 1
- Material = Brass or Steel
- Charge / Weight =
  - 84.4%
  - 62%
  - 25%
  - 5.4%
- End initiated
- End plates similar thickness to case



Gauge positions are not clearly defined. The assumed positions match the reported data.

PDF Complete
Your complimentary use period has ended. Thank you for using PDF Complete.
Click Here to upgrade to Unlimited Pages and Expanded Features

w Trials

BAE SYSTEMS

43 Experimental Firings over 3 years

ÅThree explosive types:

- ï Rx1100 (Ideal) (RDX/Binder 88/12)
- ï Rx1400 (Non-Ideal) (RDX/Al/Binder 66/22/12)
- ï PBX N109 (RDX/Al/Binder 64/20/16)

ÅTwo case materials:

- ï Steel EN24
- ï Aluminium 6082T6

ÅVarying Case mass / Charge mass Ratios (0, 0.5, 2, 5, 10)

PDF Complete
Your complimentary use period has ended. Thank you for using PDF Complete.
Click Here to upgrade to Unlimited Pages and Expanded Features

BAE SYSTEMS

for All Series 1, 2 & 3

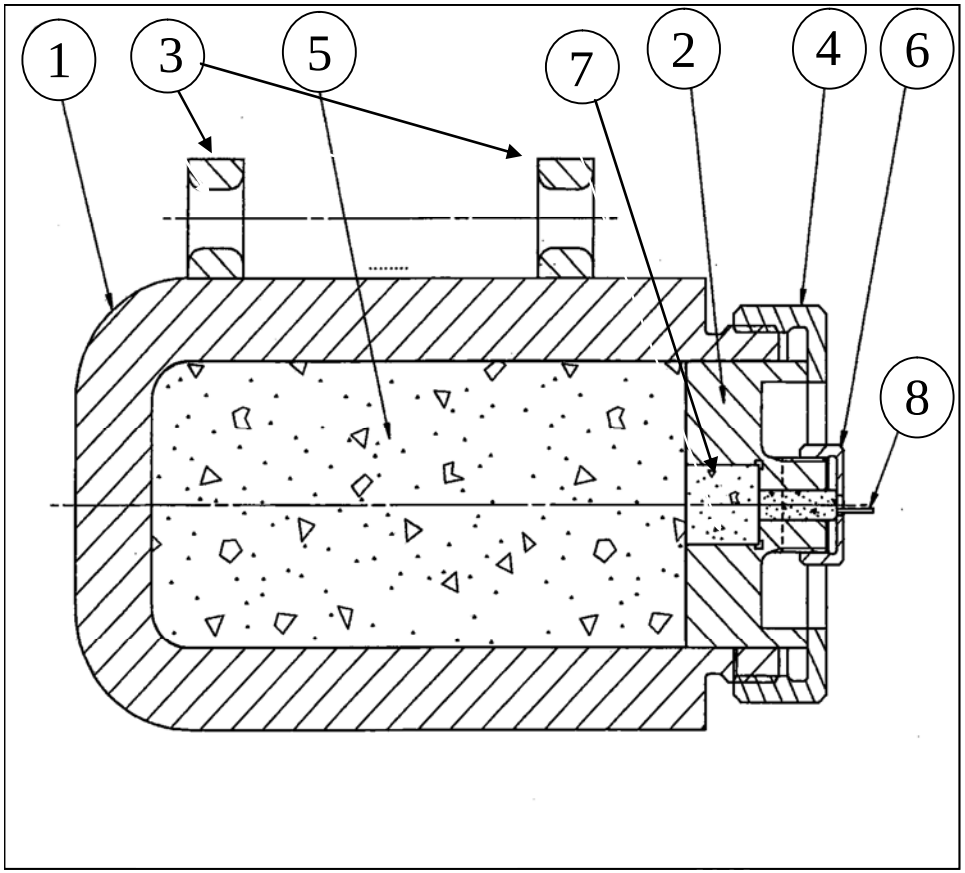
Matrix of Trials – All Series 1, 2 & 3									
Configuration		Case mass (M) to charge mass (C) ratio						Total	
Explosive	Case	0	0.5	2	5	8.46	10		
Rx1100	Bare	3						3	17
	Steel		2	2	2		2	8	
	Al		2	2		2		6	
Rx1400	Bare	3						3	17
	Steel		2	2	2		2	8	
	Al		2	2		2		6	
PBX N109	Bare	3						3	9
	Steel		2		2		2	6	
Total		9	10	8	6	4	6	43	

- Idealô Rx1100 - RDX /Binder 88/12
- Non-Idealô Rx1400 - RDX/Al/Binder 66/22/12
  PBX N109 - RDX/Al/Binder 64/20/16

PDF Complete
Your complimentary use period has ended. Thank you for using PDF Complete.
Click Here to upgrade to Unlimited Pages and Expanded Features

harge Configuration

BAE SYSTEMS



Key

1 ï Fragmenting case (Cylindrical)
2 ï Charge closure
3 ï Lifting eyelets
4 ï Clamp ring
5 ï Charge (1kg nominal, L/D =2)
6 ï Detonator clamp ring
7 ï Booster pellet (Debrix 18AS)
8 ï Detonator (RP 80)

Note: Case thickness chosen to achieve correct case mass (M) to charge mass (C) ratio

PDF Complete
Your complimentary use period has ended. Thank you for using PDF Complete.
Click Here to upgrade to Unlimited Pages and Expanded Features

BAE SYSTEMS

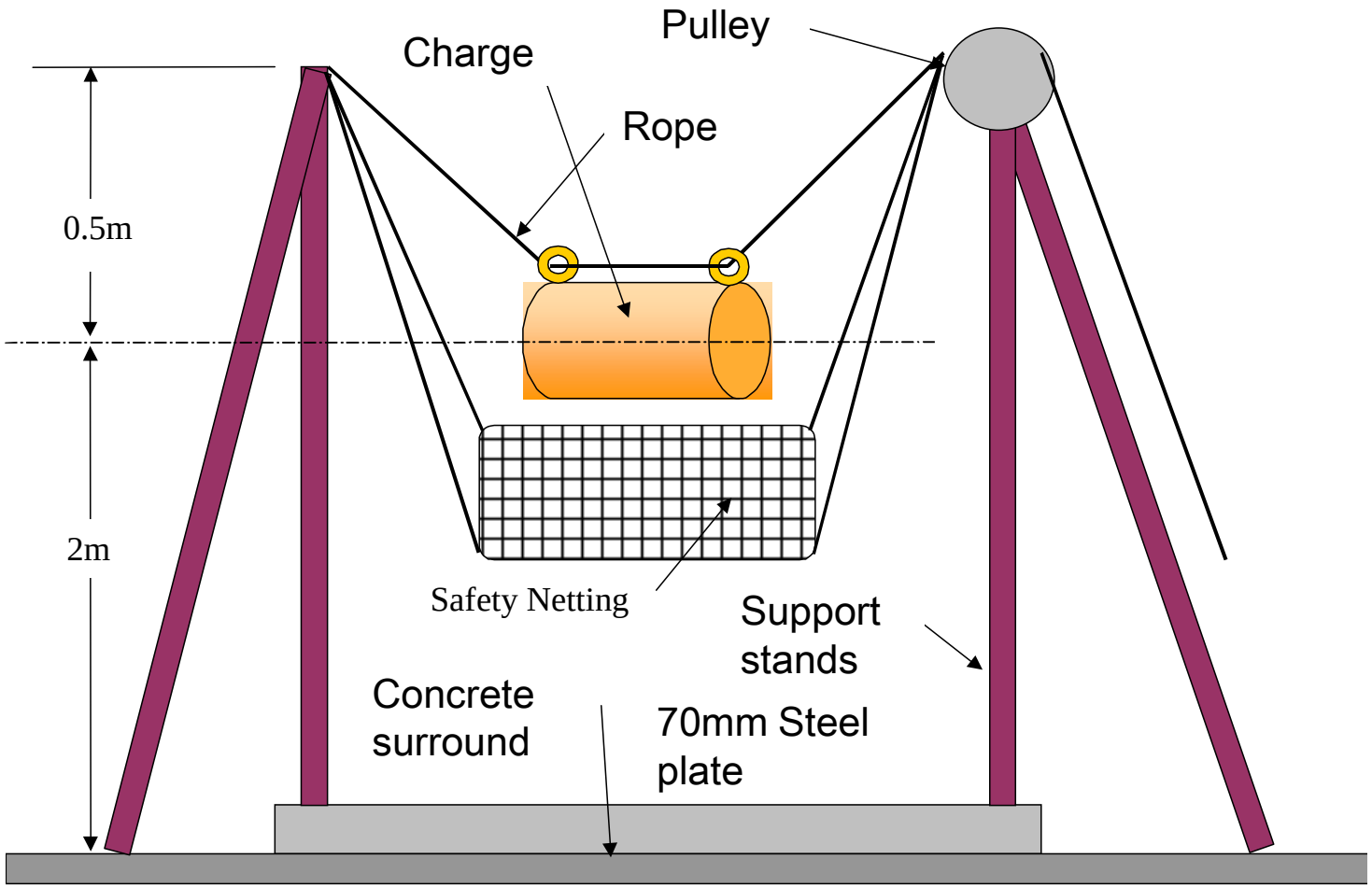
ness - Series 1, 2 & 3

Trial Series 1, 2 & 3					
Case Thickness (mm)	Case Mass to Charge Mass Ratio				
Casing	0.5	2	5	8.458	10
AL 6082T6	4.1	13.6		41.5	
Steel EN24	1.5	5.5	12.1		20.6

PDF Complete
Your complimentary use period has ended. Thank you for using PDF Complete.
Click Here to upgrade to Unlimited Pages and Expanded Features

ls Schematic

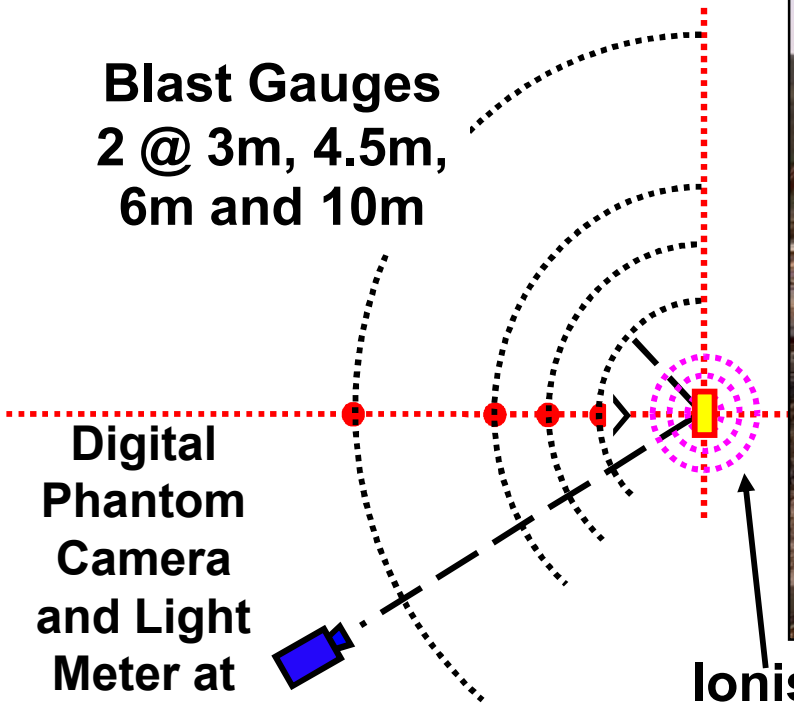
BAE SYSTEMS



PDF Complete
Your complimentary use period has ended. Thank you for using PDF Complete.
Click Here to upgrade to Unlimited Pages and Expanded Features

BAE SYSTEMS

rials Arena





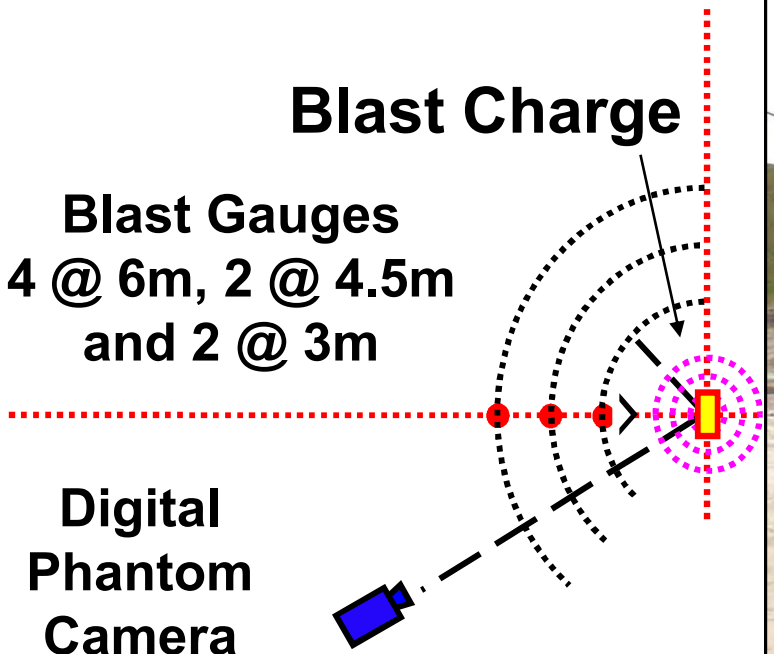
B12 and ICP137
@ 3m, 4.5m
6m and 10m



PDF Complete
Your complimentary use period has ended. Thank you for using PDF Complete.
Click Here to upgrade to Unlimited Pages and Expanded Features

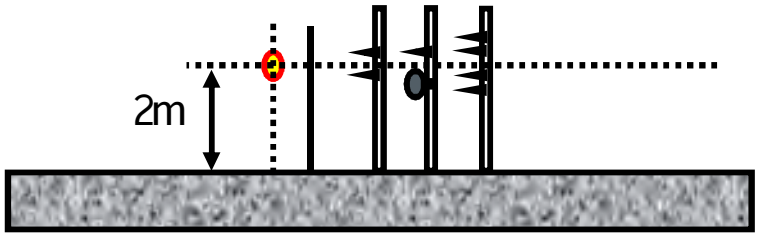
BAE SYSTEMS

rials Arena





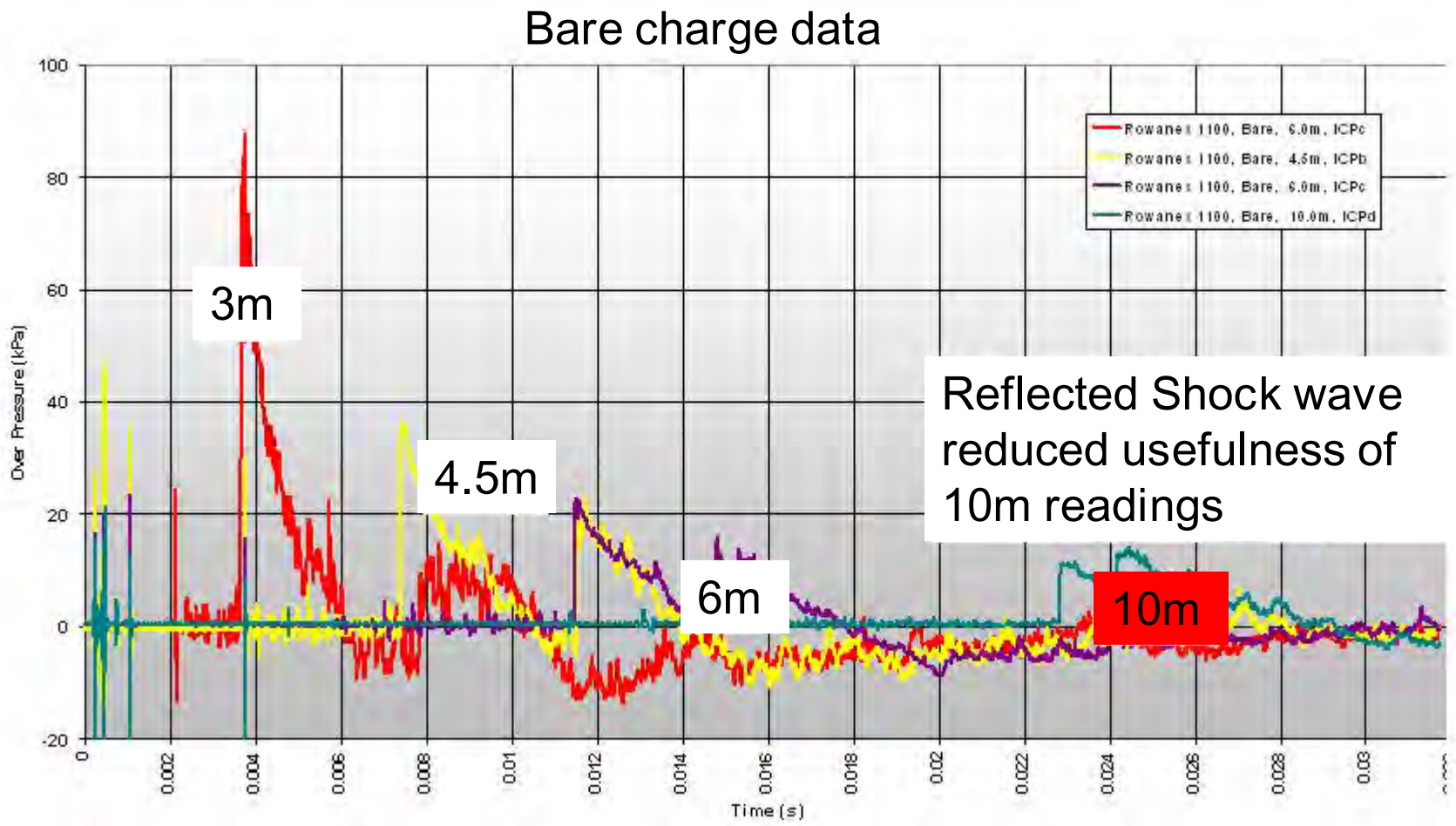
Blast Gauges mainly ICP137 Pairs with one B12 / ICP137 combination



PDF Complete
Your complimentary use period has ended. Thank you for using PDF Complete.
Click Here to upgrade to Unlimited Pages and Expanded Features

BAE SYSTEMS

ast Gauge Output



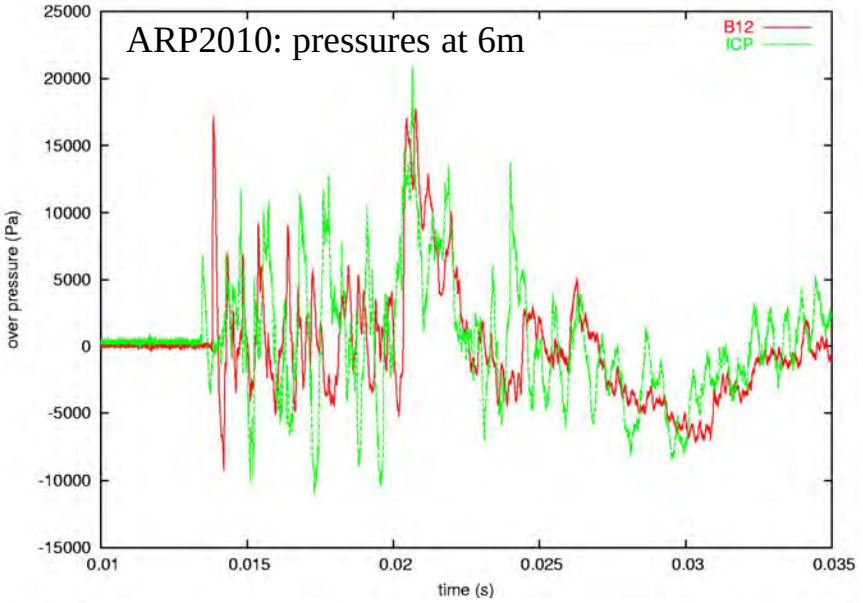
Impulse data is less sensitive to noise than Incident Pressure

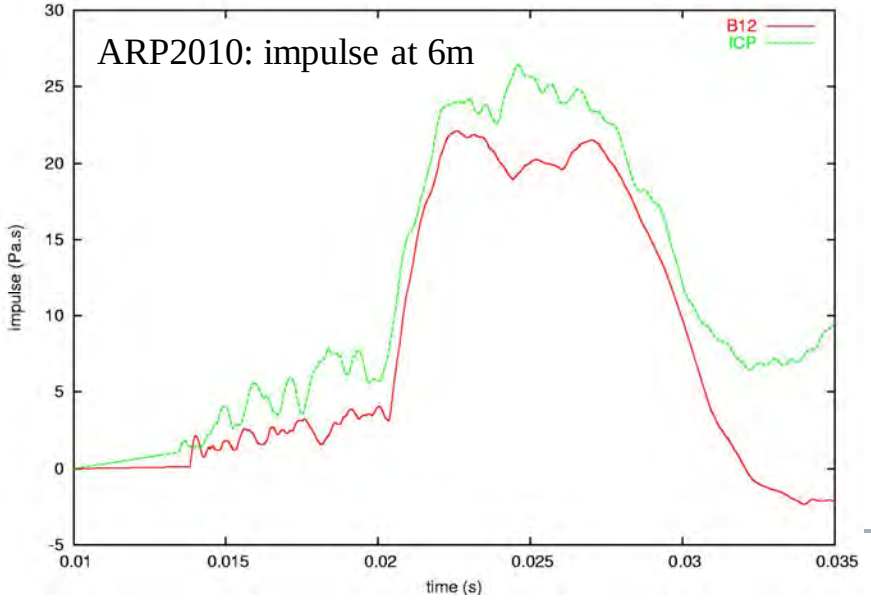
PDF Complete
Your complimentary use period has ended. Thank you for using PDF Complete.
Click Here to upgrade to Unlimited Pages and Expanded Features

BAE SYSTEMS

Cased Results

- Very noisy
- Signal/noise ratio worse as:
  - Case mass increases
  - Increase range
- ICP results marginally worse than B12 gauges
- Little confidence in peak pressures
- Noise integrates to give impulse prior to arrival of signal
  - Adjust for this in peak impulse calculation

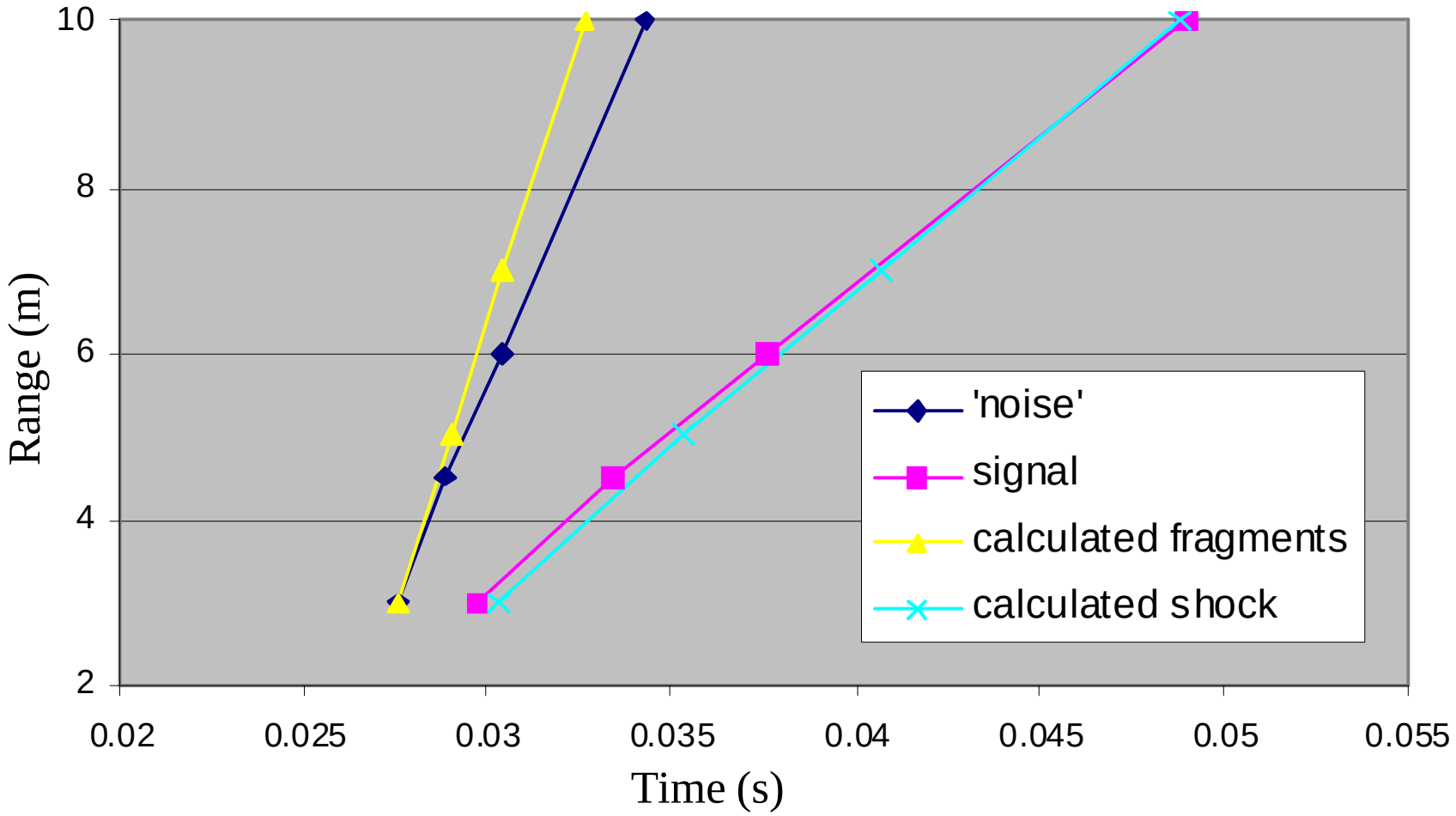




PDF Complete
Your complimentary use period has ended. Thank you for using PDF Complete.
Click Here to upgrade to Unlimited Pages and Expanded Features

BAE SYSTEMS

rom Cased Results



ÅNoise and Blast wave signal with predicted Shock and Fragment position

PDF Complete
Your complimentary use period has ended. Thank you for using PDF Complete.
Click Here to upgrade to Unlimited Pages and Expanded Features

ating Case Effect

BAE SYSTEMS

ÅUse Pressure and Impulse data to compute case effects - i.e. effect case has in reducing Equivalent Bare Charge mass (EBC)

- ï Convert Pressure and Impulse results to EBC masses
- ï Case effect = (EBC from cased result) / (EBC for equivalent bare charge result)

ÅReference curves used to convert Impulse and Pressure results to EBC masses

- ï Use results of 1kg Spherical TNT charge calculation as reference

PDF Complete
Your complimentary use period has ended. Thank you for using PDF Complete.
Click Here to upgrade to Unlimited Pages and Expanded Features

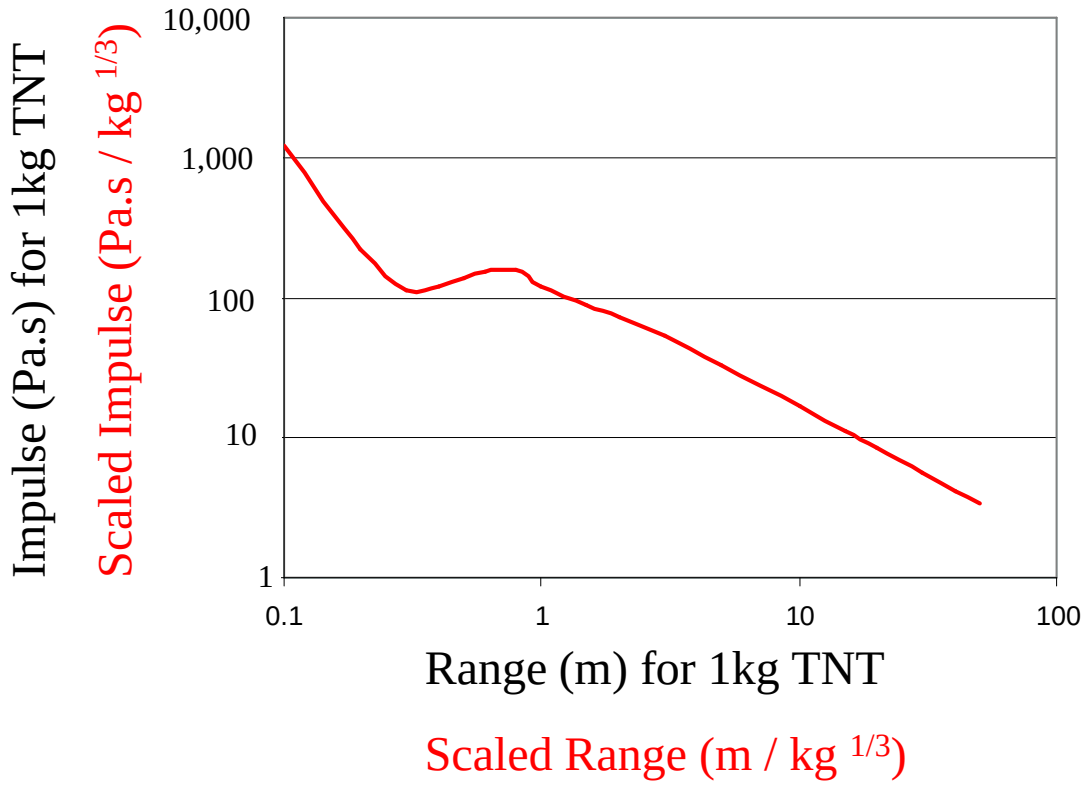
BAE SYSTEMS

ge, for Standard 1kg Spherical TNT charge

Scaled Range (R_{scl}) and Scaled Impulse (I_{scl}) are used to find the Equivalent bare mass of TNT:

$$R_{scl} = R / C^{1/3}$$

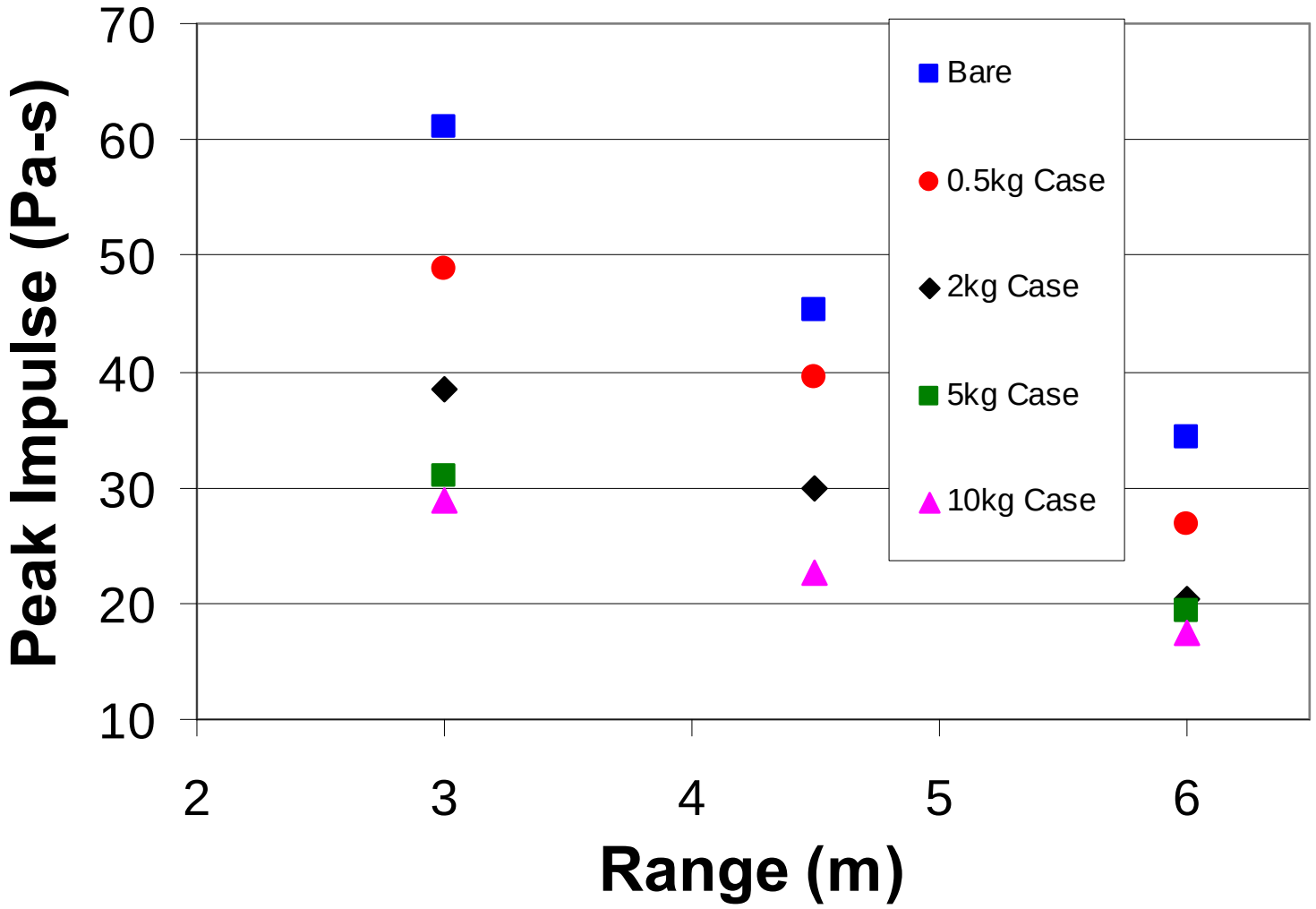
$$I_{scl} = I / C^{1/3}$$



PDF Complete
Your complimentary use period has ended. Thank you for using PDF Complete.
Click Here to upgrade to Unlimited Pages and Expanded Features

BAE SYSTEMS

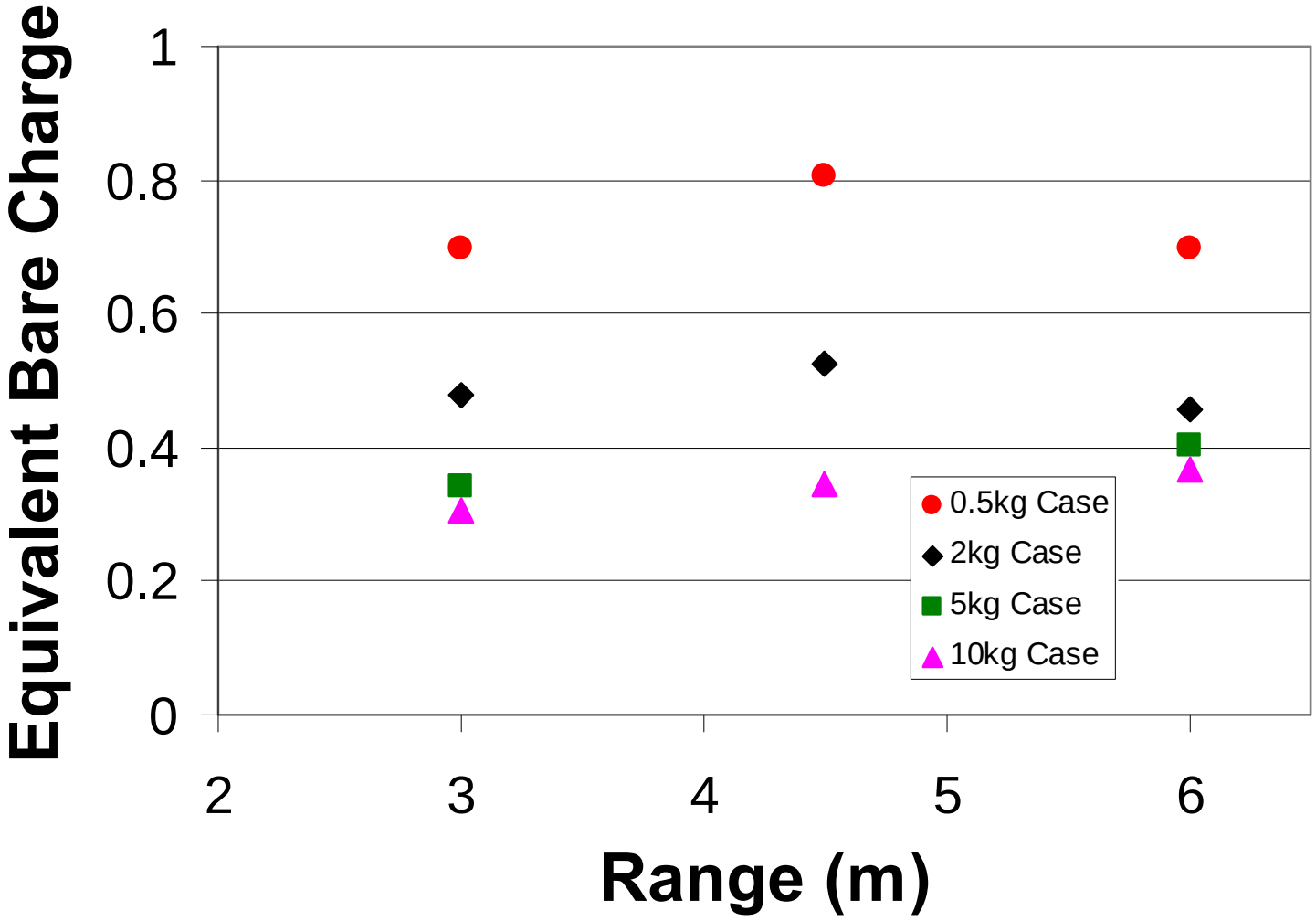
Range (Rx1100/Steel case)



PDF Complete
Your complimentary use period has ended. Thank you for using PDF Complete.
Click Here to upgrade to Unlimited Pages and Expanded Features

BAE SYSTEMS

ith Range (Rx1100/Steel case)



PDF Complete
Your complimentary use period has ended. Thank you for using PDF Complete.
Click Here to upgrade to Unlimited Pages and Expanded Features

/ Fano Equations

BAE SYSTEMS

ÅHistorically, mainly used Fisher or Fano curves
ÅFit Fisher and Fano equations to the experimental data

ÅFisher

ï Fisher curve $$\frac{EBC}{C} = 0.2 + \frac{0.8}{\left(1 + \frac{M}{C}\right)^{\dot{U}}}$$

ï Modified Fisher $$\frac{EBC}{C} = 0.6 + \frac{0.4}{\left(1 + \frac{M}{C}\right)^{\dot{U}}}$$

ï Generalised form $$\frac{EBC}{C} = \alpha + \frac{1 - \alpha}{\left(1 + \frac{M}{C}\right)^{\dot{U}}}$$

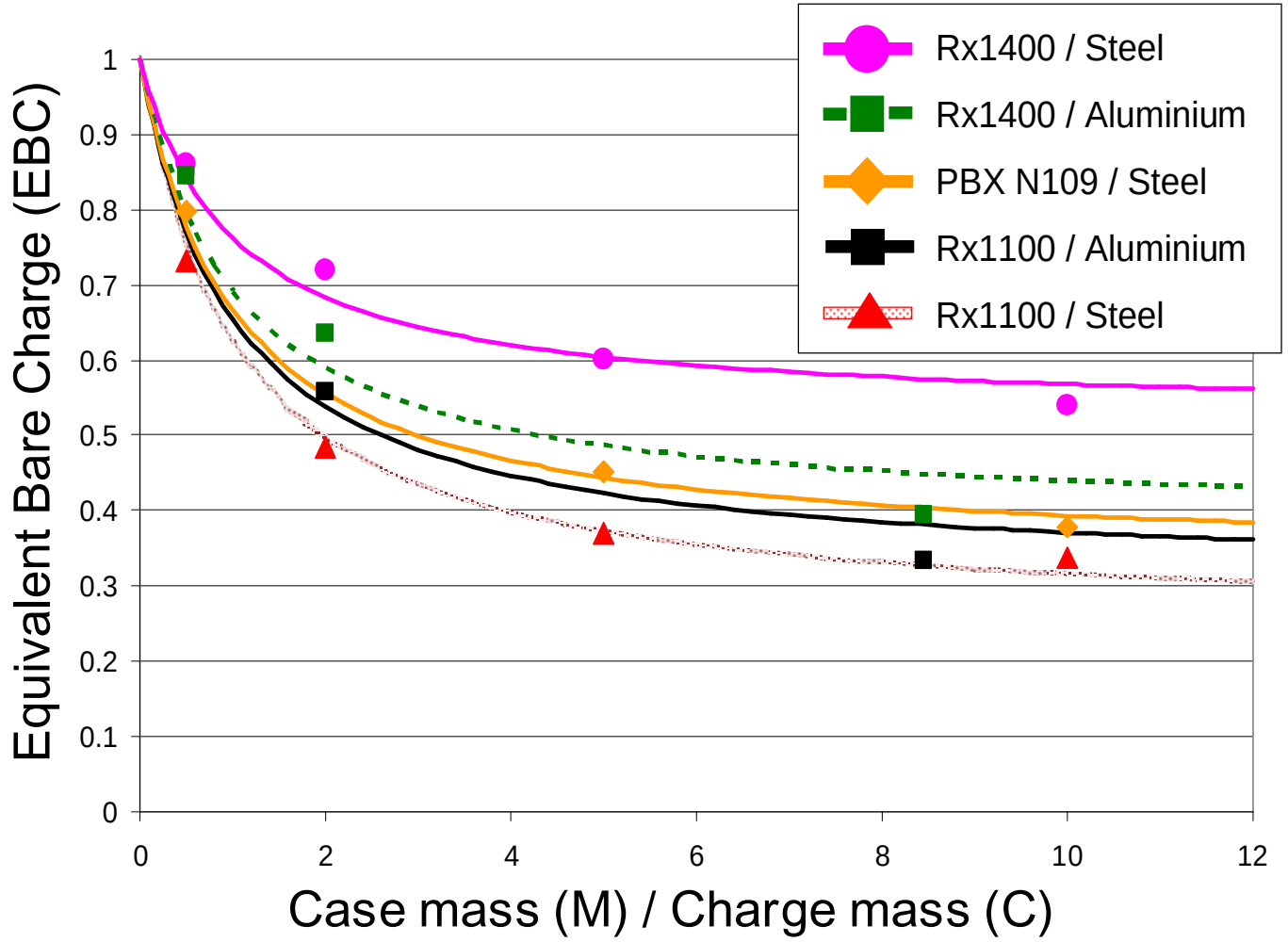
EBC = Equivalent Bare Charge, M = Case mass, C = Charge mass
Ů = Experimentally derived ôbest fitô parameter

ÅBest fit is always the Generalised Fisher Equation rather than Fano

PDF Complete
Your complimentary use period has ended. Thank you for using PDF Complete.
Click Here to upgrade to Unlimited Pages and Expanded Features

BAE SYSTEMS

lent Bare Charge Impulse vs. Case to Charge mass ratio



PDF Complete
Your complimentary use period has ended. Thank you for using PDF Complete.
Click Here to upgrade to Unlimited Pages and Expanded Features

BAE SYSTEMS

sher – Alpha fit for Series 1, 2 & 3

$$\frac{M_{EBC}}{C} = \alpha + \frac{(1-\alpha)}{(1+M/C)}$$

Trial Series 1, 2 & 3 Fitted Results		
Generalised Fisher Alpha	Casing Type	
	Steel	Aluminium
Rx 1100	0.249	0.308
Rx 1400	0.525	0.383
PBX N109	0.333	N/A

Valid for: Case Mass (M) / Charge Mass (C) up to 10:1

N.B. Historically: Standard Fisher, Alpha = 0.2

(Fisher was approximately correct for Steel cased Ideal explosives)

PDF Complete
Your complimentary use period has ended. Thank you for using PDF Complete.
Click Here to upgrade to Unlimited Pages and Expanded Features

Results - 1

BAE SYSTEMS

- Generalised Fano and Fisher models were fitted to the data. Fisher gave the best fit
  - Fisher used an Alpha of 0.2, whilst we predict 0.249
  - Consistent with his use of steel cased Ideal explosives

- Our results show:
- a. Ideal explosive systems, Steel cases have more effect than Aluminium cases
- b. Non Ideal explosive systems, Aluminium cases have the greater effect than steel cases (a great surprise)
- c. Aluminium cased systems, Ideal Explosive show greater casing effects than Non Ideal explosive systems
- d. Cases have a greater effect on Ideal explosive charges than on Non Ideal explosive charges
- e. Case material effect is directly explosive type dependent
- f. Case effects are more diverse than ever expected

PDF Complete
Your complimentary use period has ended. Thank you for using PDF Complete.
Click Here to upgrade to Unlimited Pages and Expanded Features

Results - 2

BAE SYSTEMS

- The Combined casing and explosive as a System is crucial to blast performance and which model

- Casings interact directly with the warhead filling during the early stages of detonation
  - Effects are often counter-intuitive

- PBX-N109 results are interesting. Although it is regarded as similar to Rx1400, we see significant differences
  - Case effects are significantly greater for PBX-N109, Rx1400 outperforms PBX-N109

- Case effects are dramatic enough to indicate that warhead fillings are often incorrect for blast performance
  - An optimised warhead could produce a 20% performance improvement. Perhaps a mid life upgrade

PDF Complete
Your complimentary use period has ended. Thank you for using PDF Complete.
Click Here to upgrade to Unlimited Pages and Expanded Features

...on

BAE SYSTEMS

- Gauge results are noisy from cased trials
  - Little confidence in Peak Pressure
  - Impulse results are reliable
  - Only Impulses have been used in this paper
- Trials have been performed to measure case effects for five different systems
  - Results show case effects depend on both charge type and case material
- Generalised Fisher equation is the best fit to data
  - Good fit for Steel systems, but less satisfactory for Aluminium systems
- The reasons for this observed charge and case material dependence is not understood
  - Crowley has since proposed a model in which the case effect is a function of the ratio of the case yield stress to the pressure in the unexpanded case

PDF Complete
Your complimentary use period has ended. Thank you for using PDF Complete.
Click Here to upgrade to Unlimited Pages and Expanded Features

BAE SYSTEMS

inally

ÅThank you for listening

Any questions?

ÅContact:

Paul Locking

Technical Specialist (Blast & Ballistics)

BAE Systems (Land), UK

Tel: +44-1793-78-6427

Email: paul.locking@baesystems.com

High Speed Penetration into Low Strength Concrete Target

24th International Symposium on Ballistics
September 22-26, 2008
New Orleans, LA

**V. K. Luk, J. A. Dykes, J. E. Bishop,
P. A. Taylor, J. S. Ludwigsen, and D. A. Dederman**

Sandia National Laboratories

Albuquerque, NM 87185-1160, USA

Contact: Vincent K. Luk
E-mail: vkluk@sandia.gov
Phone: 505-844-5498

Sandia is a multiprogram laboratory operated by Sandia Corporation for the United States Department of Energy's National Nuclear Security Administration under contract DE-AC04-94AL85000.

NNSA National Nuclear Security Administration

Sandia National Laboratories

Outline

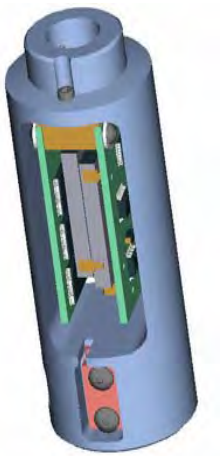
- **Phenomenon study on high speed penetration**
  - **(760 - 1220 m/s, 2500 - 4000 fps)**
- **High speed penetration experiments into low strength concrete targets**
  - **(20.7 MPa, 3.0 Ksi)**
- **Penetration simulations with Alegra/Shism, Emu, and Epic**
- **Summary – future plan**

Acknowledgment: Sponsorship from Defense Threat Reduction Agency, DTRA

Sandia National Laboratories

High Speed Penetration Experiments

- **Goal: to demonstrate the survivability of both the 7.62-cm jointed penetrator and the onboard instrumentation in high speed penetration events**
  - **Locate the appropriate gun launcher**
  - **Develop the launch package of petalled pusher/sabot that houses the subscale penetrator instrumented with triaxial data package, 3AMP**
  - **Conduct experiments at normal incidence into low strength concrete targets**



3AMP



Sandia National Laboratories

High Speed Penetration Experiments

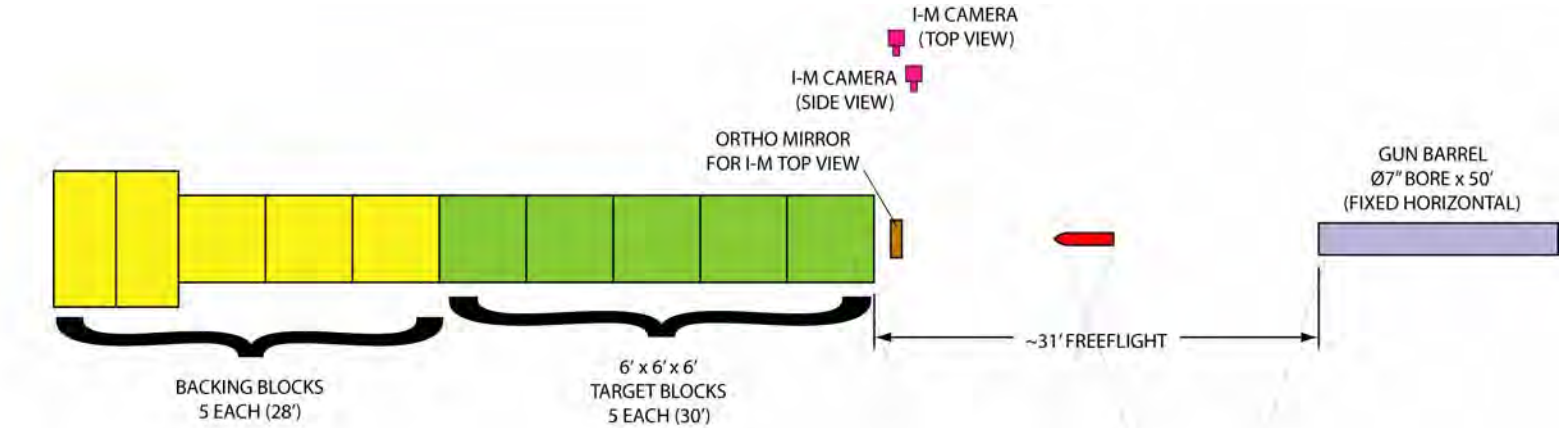
- **Launch facility**
  - **A stationary 17.78-cm (7-inch) powder gun at the Energetic Materials Research and Testing Center (EMRTC) in Socorro, New Mexico**
- **Penetrator design**
  - **A jointed nose of 3 CRH (Caliber Radius Head), 7.62 cm diameter, 53.1 cm long, and a weight of 13.5 Kg**
- **Groutcrete target**

3 KSI Groutcrete UCS DATA			
Block	UCS (psi)		
	7 day	28 day	90 day
1	1715	2520	
2	1410	2335	
3	1335	2195	2785
4	1330	2115	2890
5	---	---	---
6	1380	2325	3040
7	1420	2365	3010
8	1370	2270	3030
9	1480	2335	3010
10	1335	2310	3130
AVERAGE	1419	2308	2985

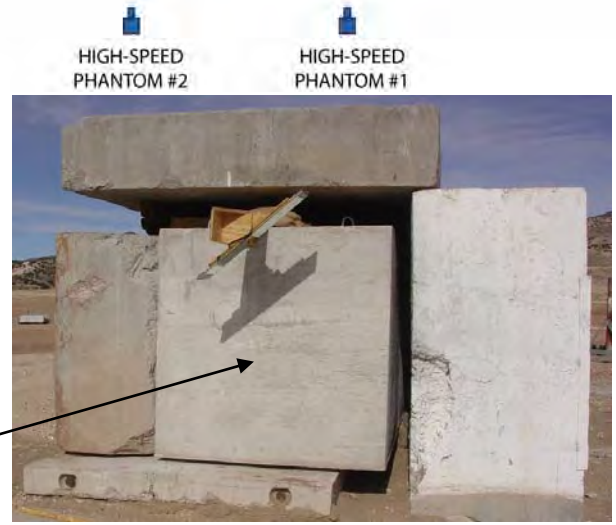
Sandia National Laboratories

High Speed Penetration Experiments

Experimental Layout





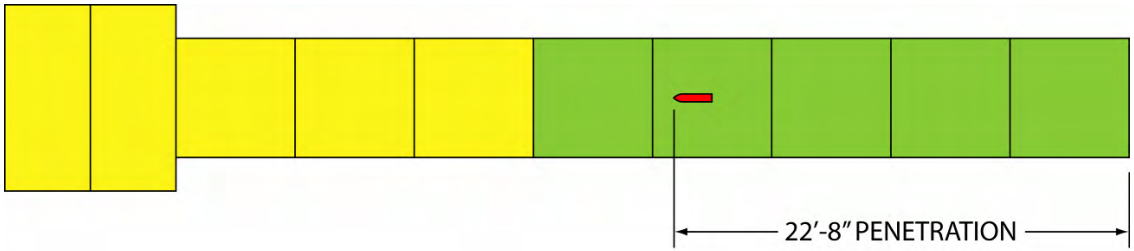


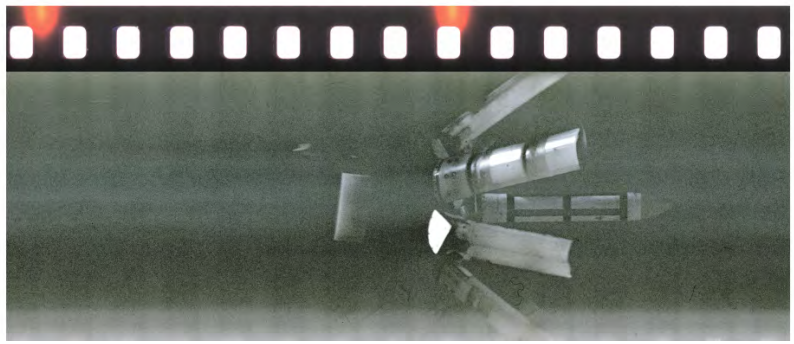
Impact surface

Sandia National Laboratories

High Speed Penetration Experiments

Results from 1st Experiment





3,637 ft/s IMPACT SPEED - MEASURED FROM THE I-M SIDE VIEW FOOTAGE

- **Impact condition: 1107 m/s (3636 fps) at near normal incidence**
- **Pusher/sabot separation occurred as designed**
- **Depth of penetration: 6.9 m (22.7 ft)**
- **3AMP failed to record meaningful data due to high frequency accelerometer ringing during penetration event**

Sandia National Laboratories

High Speed Penetration Experiments

Results from 1st Experiment

Post-test Observations







Target block 4

Penetrator final position

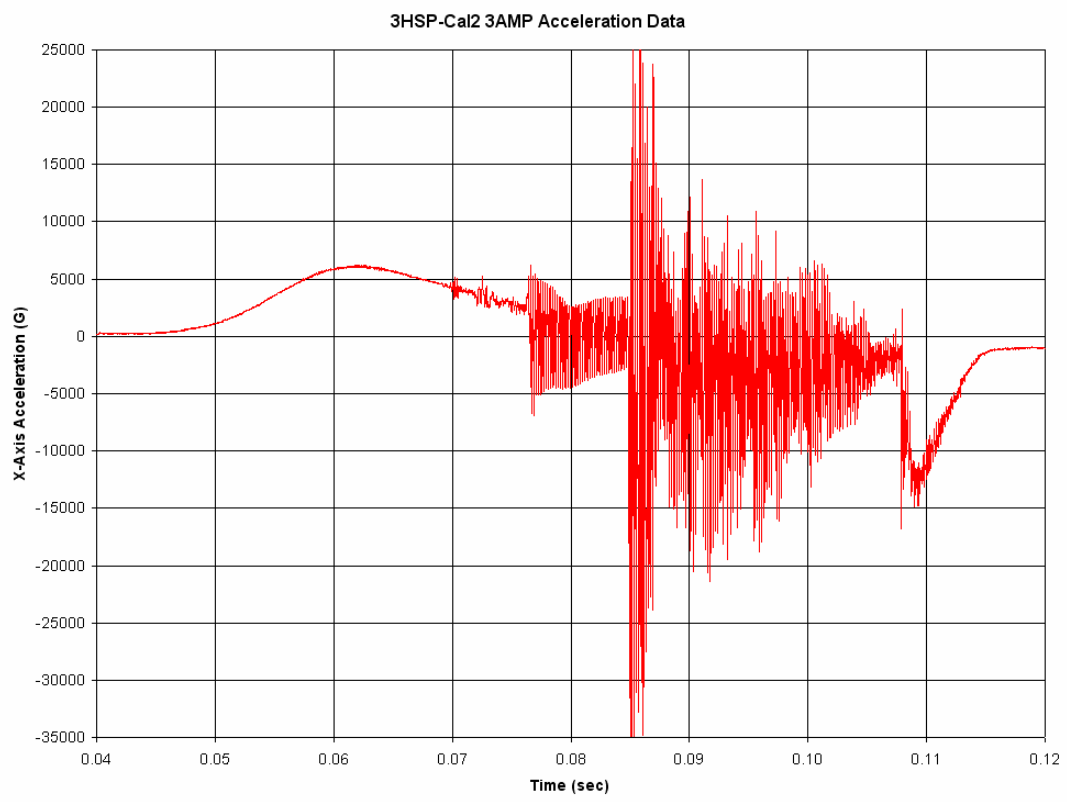
- The penetrator and the nose joint survived
  - Nose threads free of damage and turn easily
  - Threads were hand tight after the test
- Penetrator lost 0.65 inches and 2.1 pounds (originally 20.9 inches long and 29.8 pounds)

Sandia National Laboratories

High Speed Penetration Experiments

Results from 2nd Experiment

- **Impact condition: 1061 m/s (3480 fps) at near normal incidence**
- **Depth of penetration: 6.19 m (20.3 ft)**
- **3AMP recorded meaningful deceleration data**



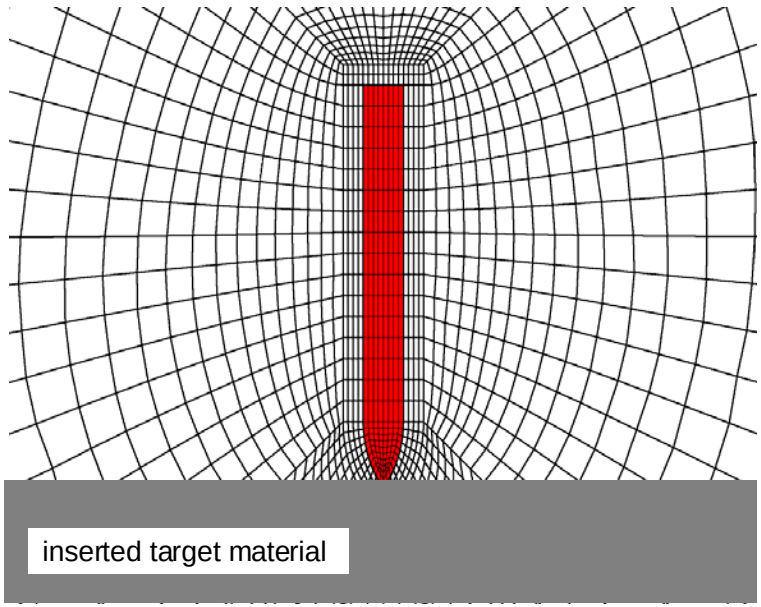
•The axial deceleration limits were recorded at +25000 g and -35000 g.
• A considerable amount of accelerometer ringing still occurred prior to impact, but it might have not affected the performance of the accelerometer.

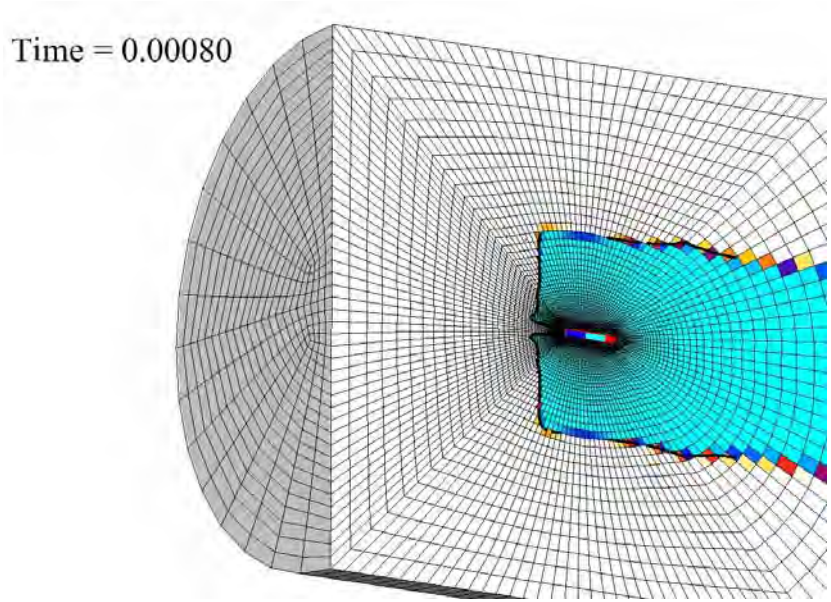
Sandia National Laboratories

High Speed Penetration Analyses

Alegra/Shism

- **Alegra/shism is a specific algorithm for soft/hard impact conditions. For penetration simulations, the Shism takes the penetrator mesh and interface to be Lagrangian and models the target region as ALE.**





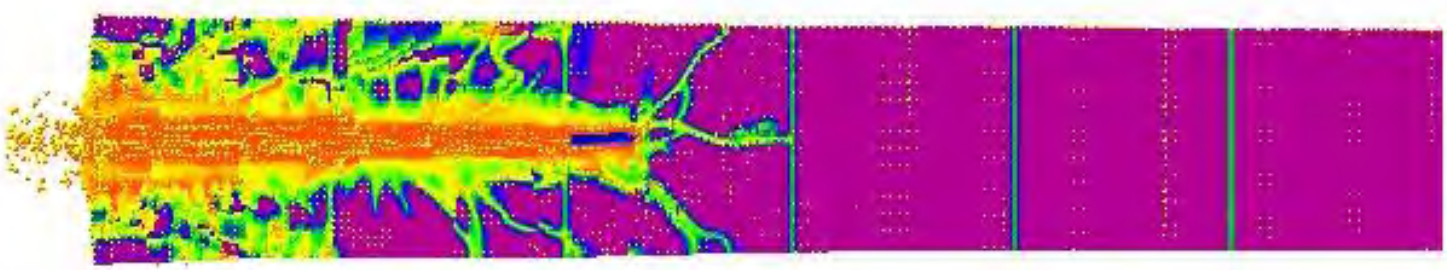
- **Calculated depth of penetration = 4.6 m (Test data: 6.9 m)**

Sandia National Laboratories

High Speed Penetration Analyses

Emu

- **Emu: A Lagrangian code, based of peridynamic theory, uses a mesh-free, particle approach to describe conservation laws in integral equations.**
- **In the penetration model, the concrete was modeled as a brittle elastic-plastic material, and the penetrator as a rigid projectile.**
- **Analysis results:**
  - **Depth of penetration = 4.25 m (Test data: 6.9 m)**
  - **Peak axial deceleration = 48500 g (Test data: 35000 g)**



Final configuration of penetration event with concrete damage

Sandia National Laboratories

High Speed Penetration Analyses

Epic

- **Epic: a general purpose finite element code, capable of solving structural dynamic and penetration problems.**
- **Epic has a large library of material models for isotropic and anisotropic behavior and a selected set of failure criteria. It has a special feature to transform distorted 3D elements into meshless particles.**
- **In the high speed penetration model, the concrete target was modeled with 3D elements using the HJC concrete model with a 24 MPa (3.5 ksi) unconfined concrete compressive strength and a 0.34 MPa (50 psi) tensile strength.**
- **Calculated depth of penetration = 3.05 m (Test data: 6.9 m)**

Sandia National Laboratories

Summary

- **Penetration experiments**
  - **Jointed penetrator design and launch package with petalled pusher/sabot have been developed.**
  - **Onboard 3AMP package survived and recorded deceleration data for high speed penetration experiment with normal incidence into 20.7 MPa concrete target.**
  - **Future tasks include high speed experiments into 39 MPa concrete target.**
- **Penetration analyses**
  - **Sandia has extensive experiences in analyzing penetration events at conventional speeds using Alegra/Shism, Emu, and Epic, and the penetration models perform well.**
  - **However, the high speed penetration models with these codes calculate lower depth of penetration and higher decelerations → target provides much higher penetration resistance.**
  - **New penetration models will be researched and developed to account for radial cracking resulting in material softening of concrete target.**

Sandia National Laboratories

PDF Complete
Your complimentary use period has ended. Thank you for using PDF Complete.
Click Here to upgrade to Unlimited Pages and Expanded Features

ry Industries Ltd. (IMI)
Heavy Ammunition Division



THE APPENDIX

MEIR MAYSELESS, EITAN HIRSCH

SEPTEMBER 2008

PDF Complete
Your complimentary use period has ended. Thank you for using PDF Complete.
Click Here to upgrade to Unlimited Pages and Expanded Features

OUTLINE

- INTRODUCTION
- EXPERIMENTAL RESULTS
- NUMERICAL MODELLING
- DISCUSSION

PDF Complete
Your complimentary use period has ended. Thank you for using PDF Complete.
Click Here to upgrade to Unlimited Pages and Expanded Features

INTRODUCTION

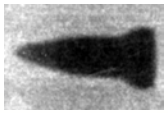
CLASSICAL PARTITION OF THE JET :

MAIN (coherent) JET

SLUG

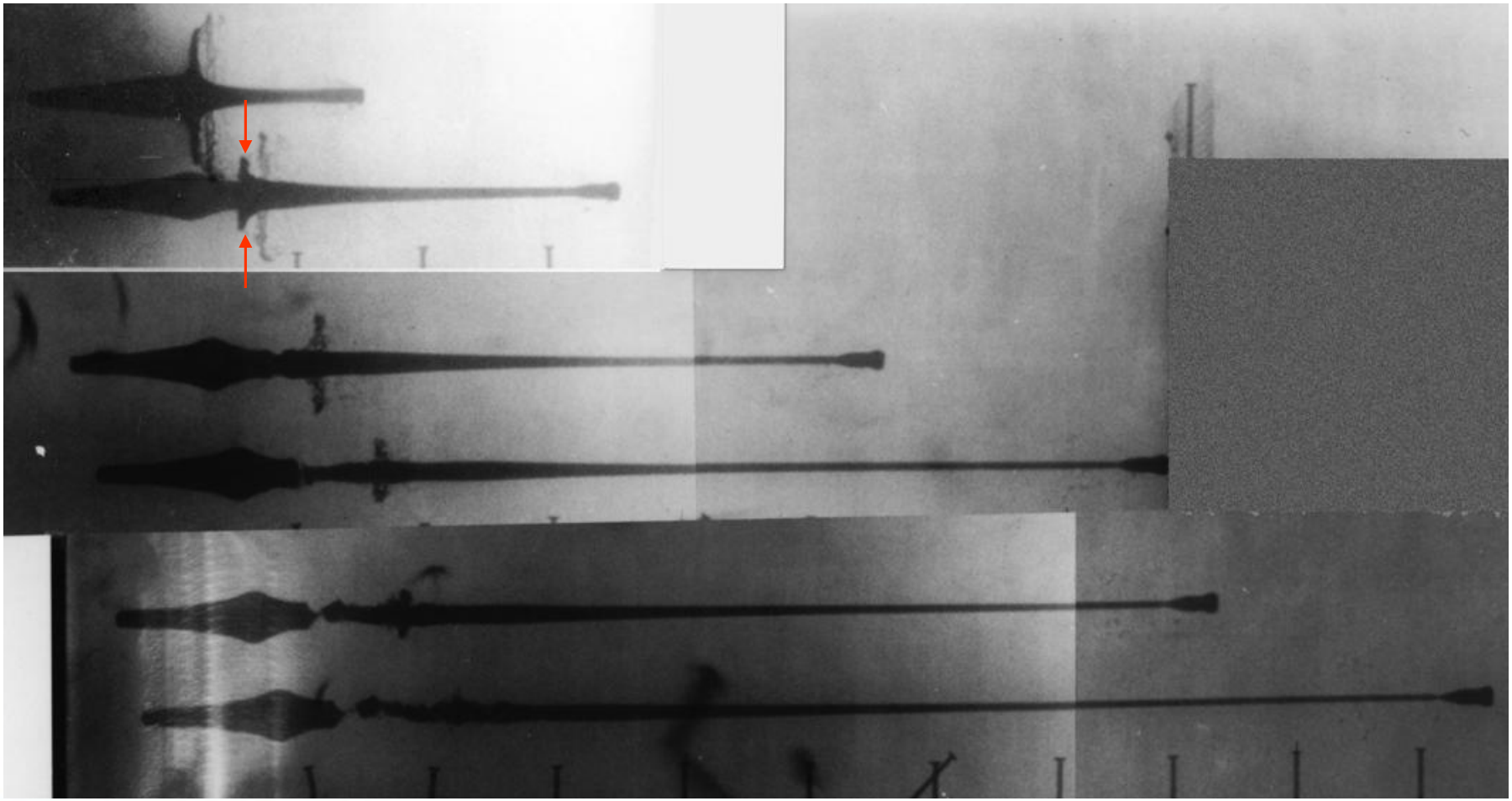






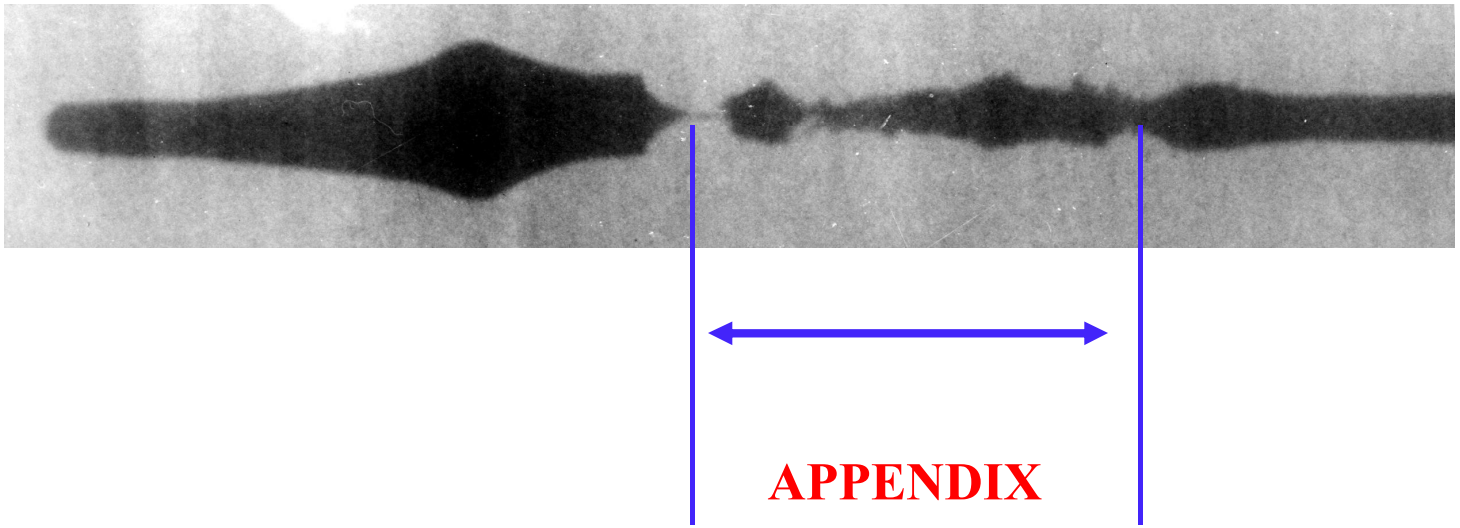
PDF Complete
Your complimentary use period has ended. Thank you for using PDF Complete.
Click Here to upgrade to Unlimited Pages and Expanded Features

BUT IF WE LOOK CLOSER:



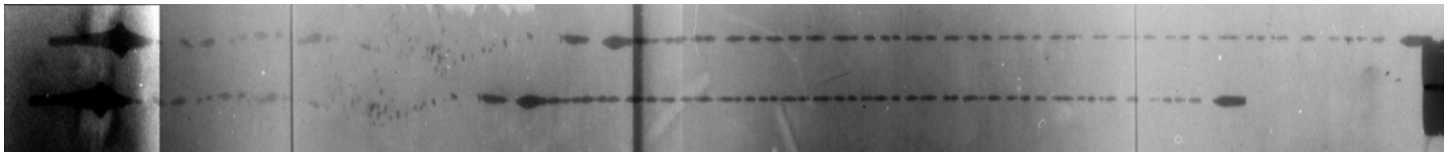
PDF Complete
Your complimentary use period has ended. Thank you for using PDF Complete.
Click Here to upgrade to Unlimited Pages and Expanded Features

AND YET CLOSER:

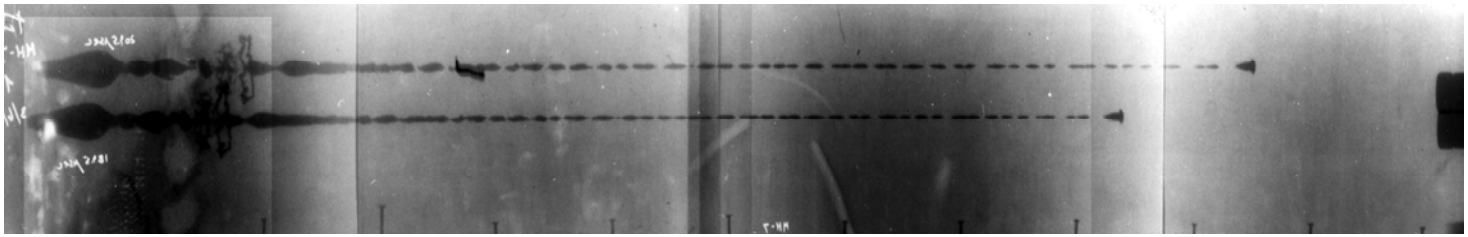


PDF Complete
Your complimentary use period has ended. Thank you for using PDF Complete.
Click Here to upgrade to Unlimited Pages and Expanded Features

EXPERIMENTAL RESULTS

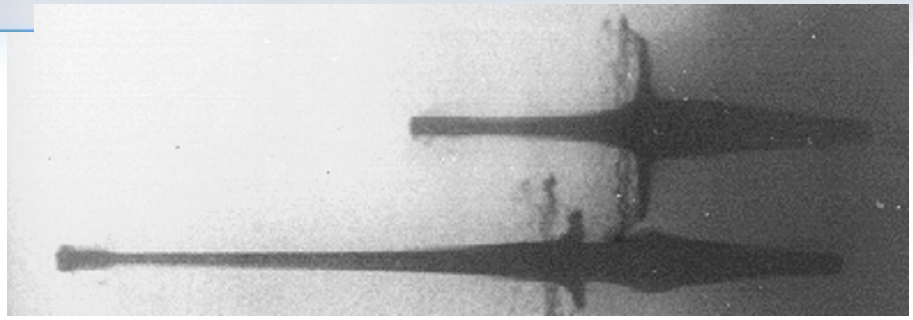


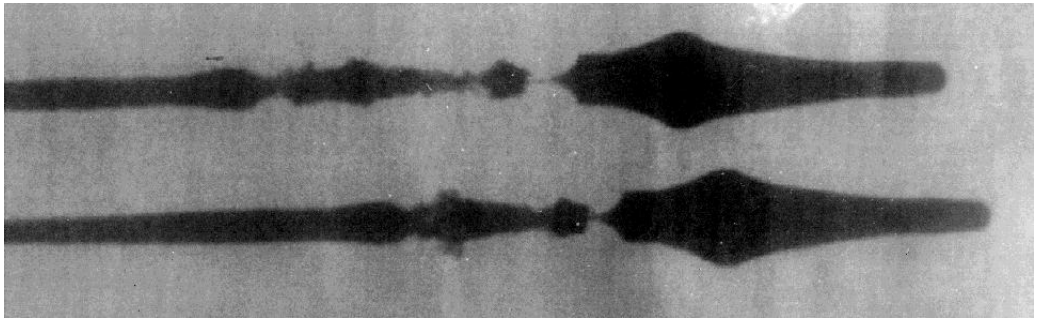
1% CD LINER

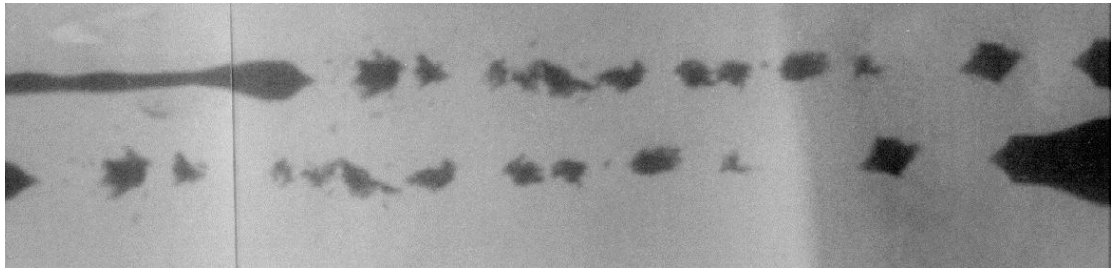


4% CD LINER

PDF Complete
Your complimentary use period has ended. Thank you for using PDF Complete.
Click Here to upgrade to Unlimited Pages and Expanded Features



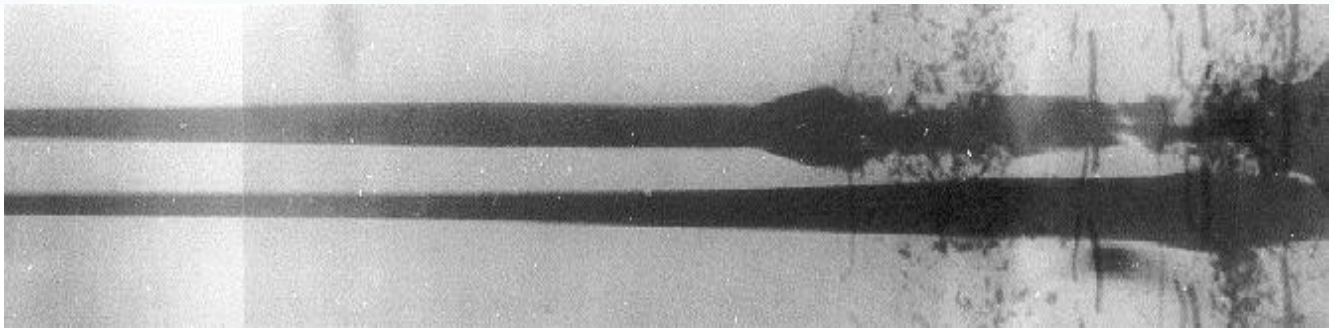


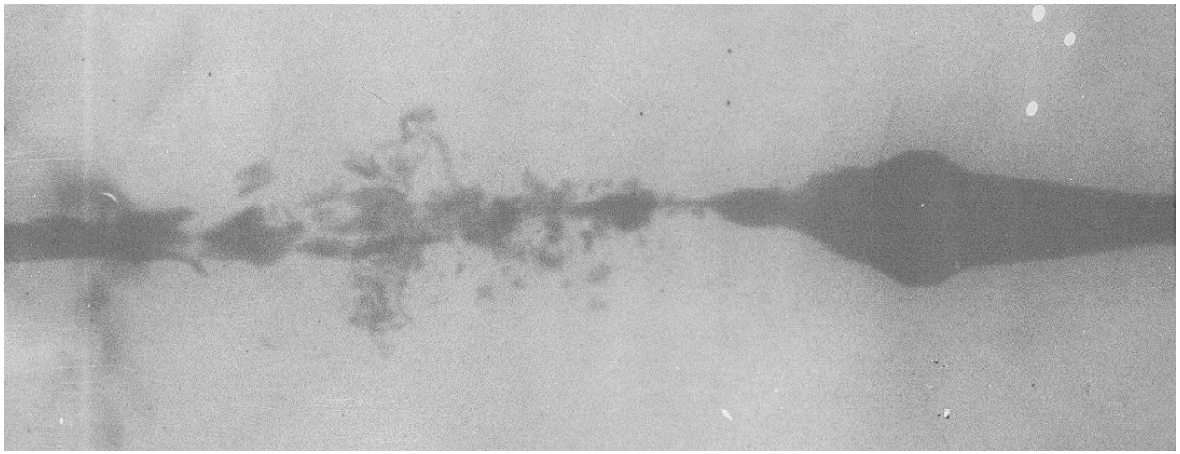


POINT INITIATED UNCONFINED

CHARGE AT 30μS, 45μS, 90μS, 100μS, 180μS & 200μS

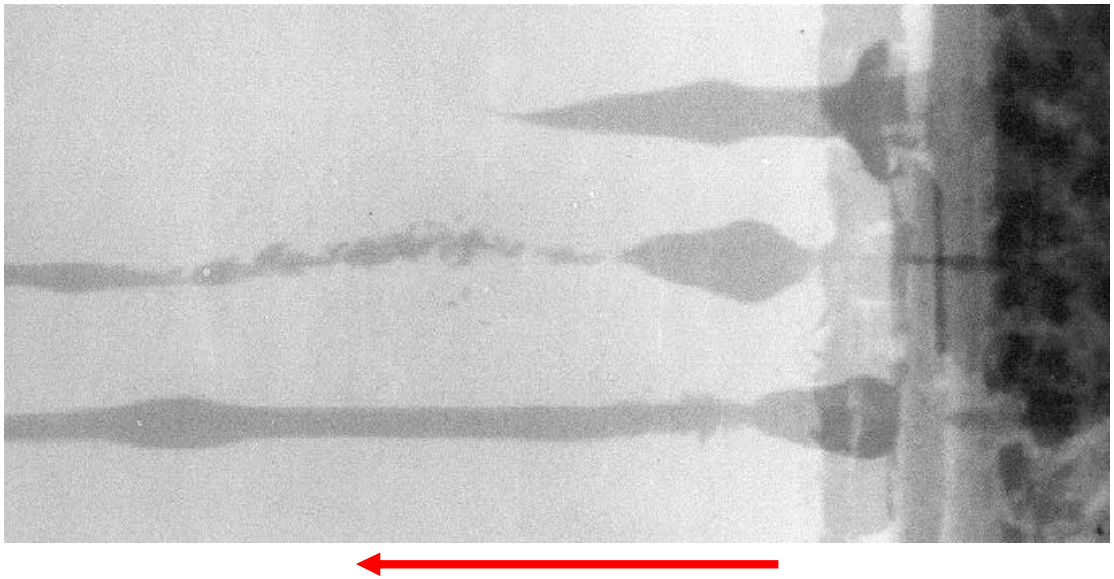
PDF Complete
Your complimentary use period has ended. Thank you for using PDF Complete.
Click Here to upgrade to Unlimited Pages and Expanded Features





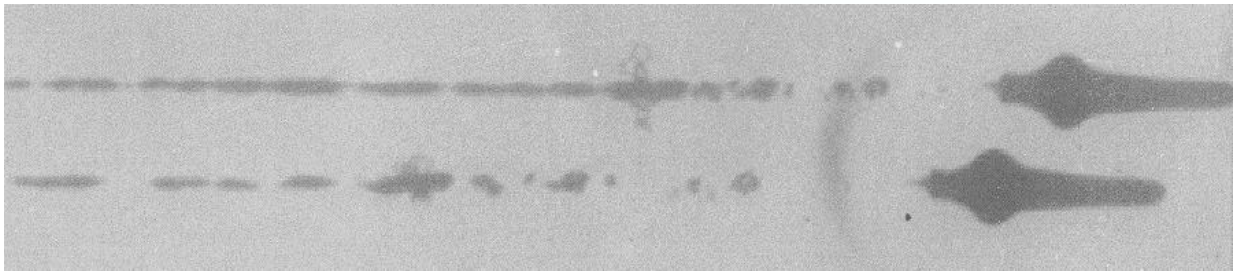
PERIPHERALLY INITIATED CHARGES

PDF Complete
Your complimentary use period has ended. Thank you for using PDF Complete.
Click Here to upgrade to Unlimited Pages and Expanded Features



HEAVILY CONFINED HEMISPHERICAL CHARGE AT 30μS, 50μS AND 80 μS

PDF Complete
Your complimentary use period has ended. Thank you for using PDF Complete.
Click Here to upgrade to Unlimited Pages and Expanded Features

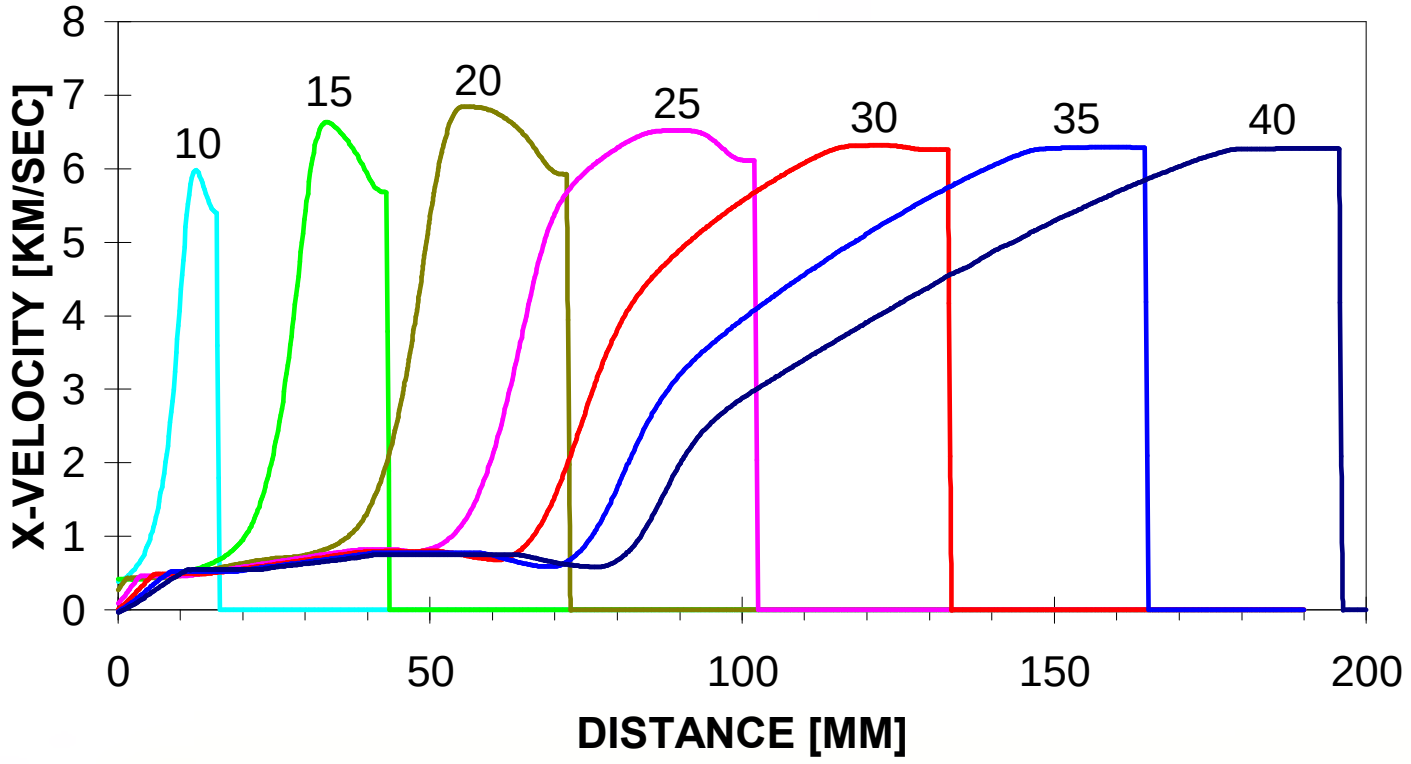


SMALL CHARGE AT 30μS AND 50μS

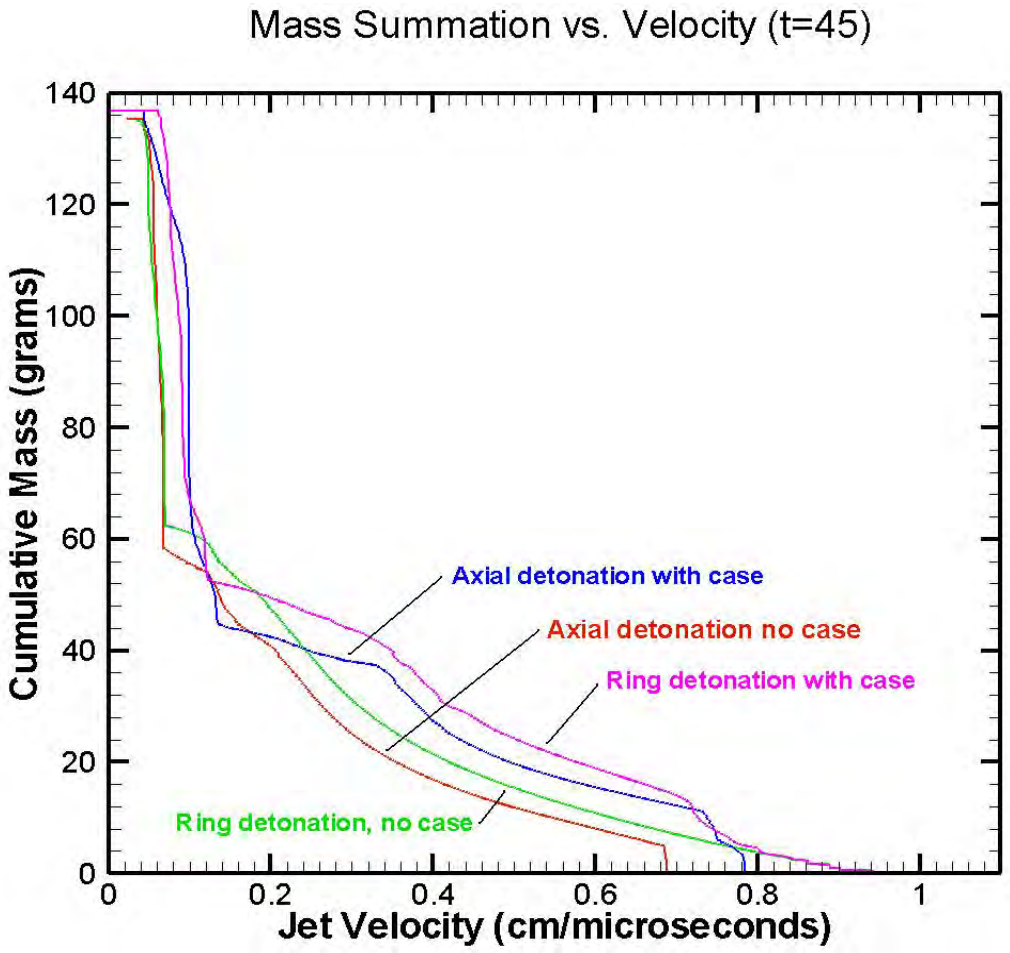
PDF Complete
Your complimentary use period has ended. Thank you for using PDF Complete.
Click Here to upgrade to Unlimited Pages and Expanded Features

SIMULATED VELOCITY PROFILES

FOR P.I. 2% CD LINER THICKNESS



PDF Complete
Your complimentary use period has ended. Thank you for using PDF Complete.
Click Here to upgrade to Unlimited Pages and Expanded Features



PDF Complete
Your complimentary use period has ended. Thank you for using PDF Complete.
Click Here to upgrade to Unlimited Pages and Expanded Features

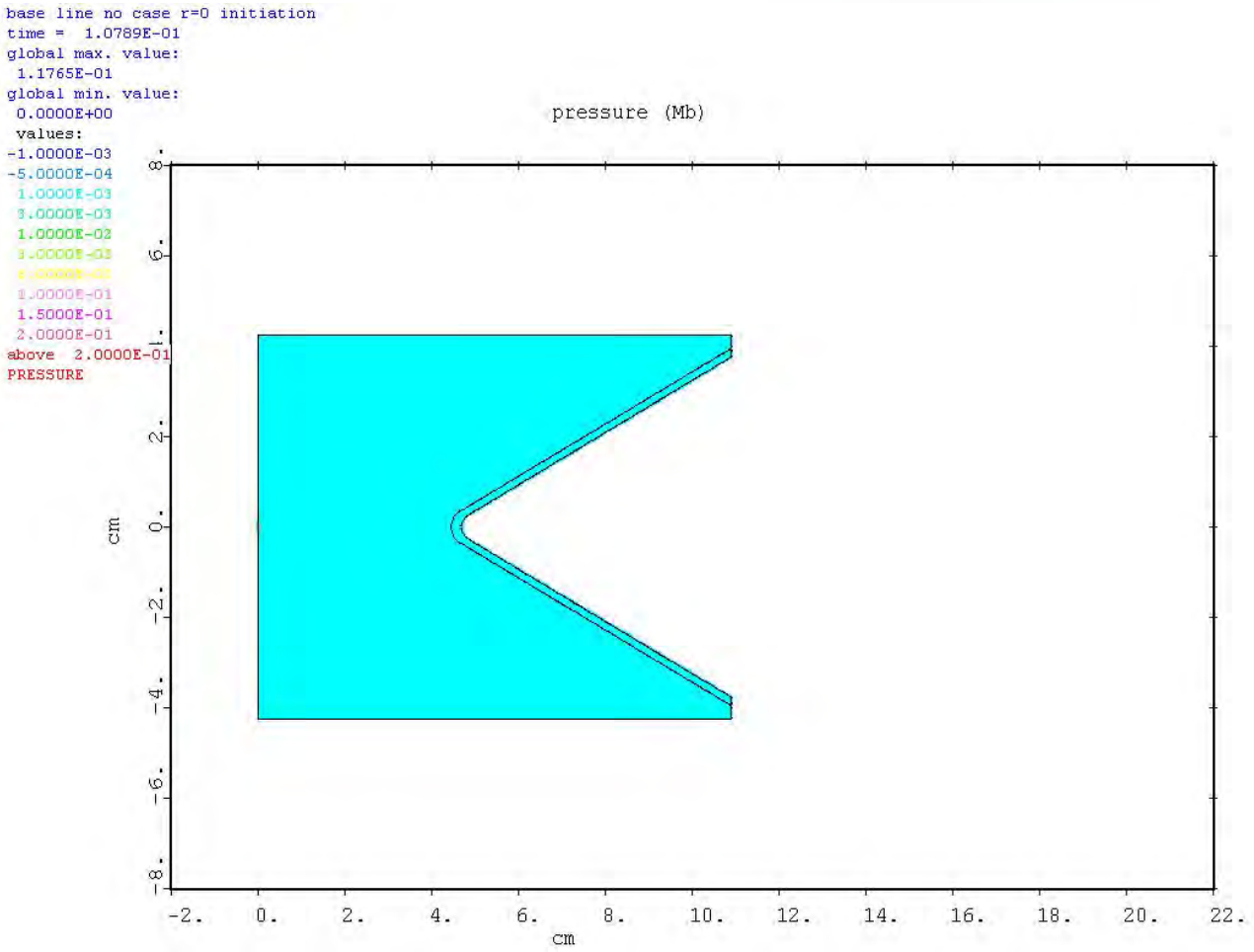
GOALS

IDENTIFY THE APPENDIX

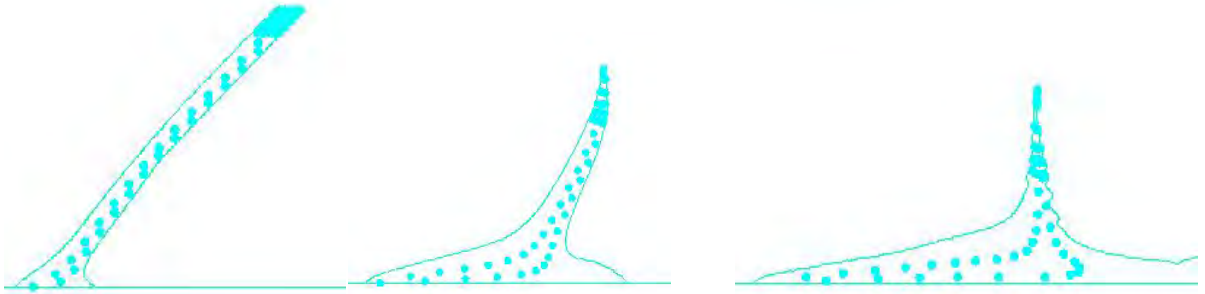
CHARACTERIZING THE APPENDIX

PDF Complete
Your complimentary use period has ended. Thank you for using PDF Complete.
Click Here to upgrade to Unlimited Pages and Expanded Features

Point initiated charge

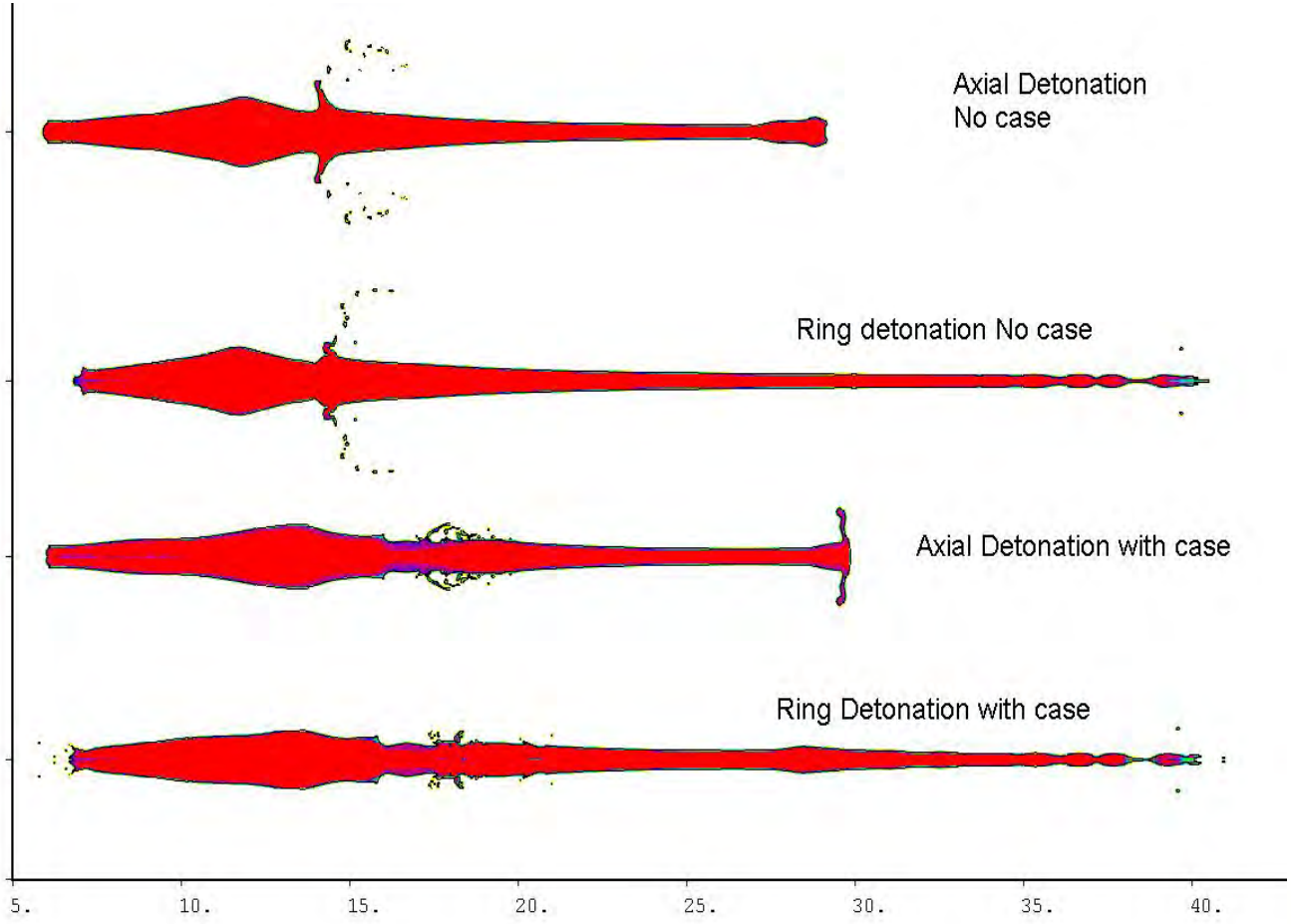


PDF Complete
Your complimentary use period has ended. Thank you for using PDF Complete.
Click Here to upgrade to Unlimited Pages and Expanded Features



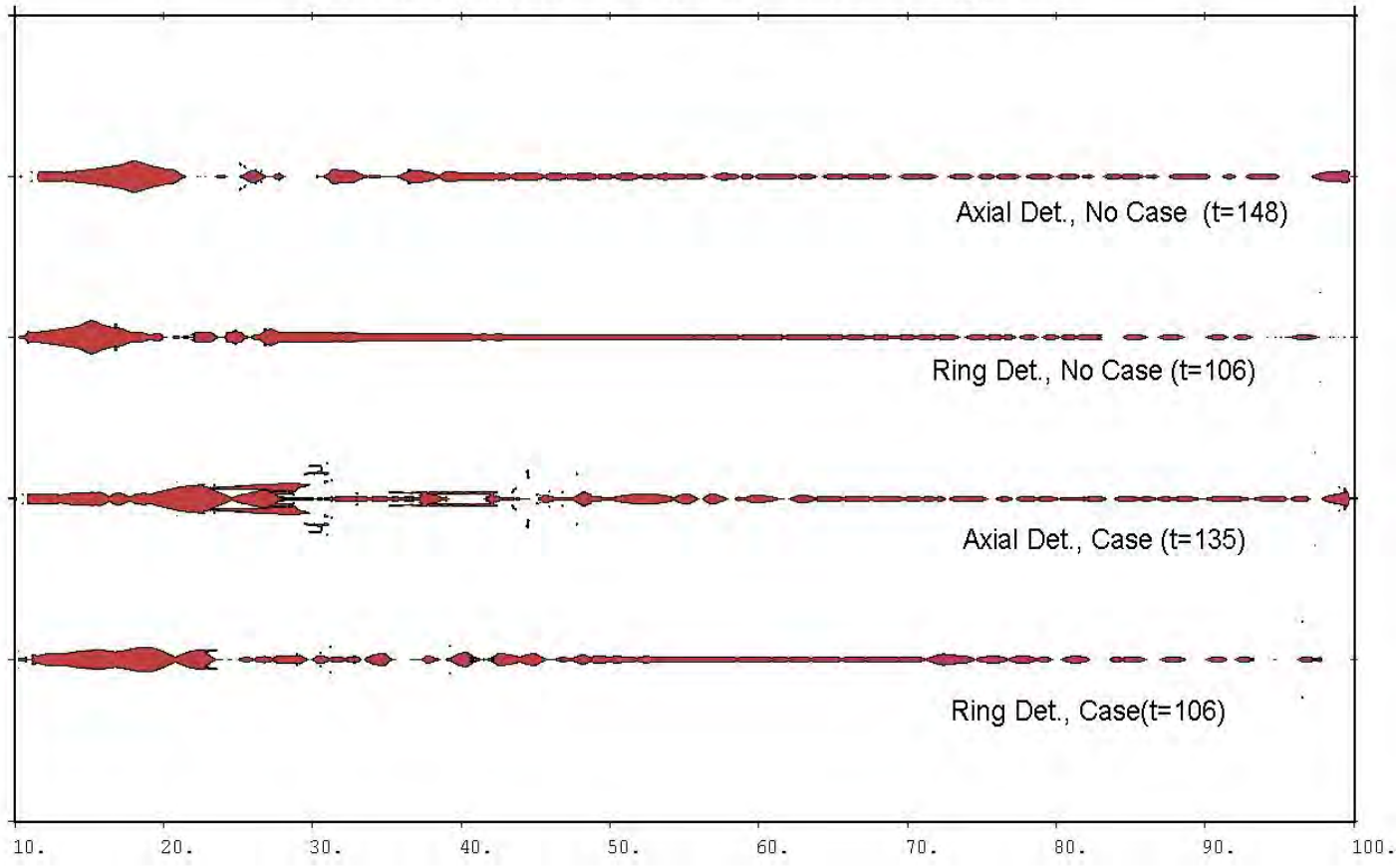
Numerical simulation results of a flow of the liner material points in a point initiated confined charge
at 10 μs (left), 20 μs (center) and 30 μs (right), after initiation.

PDF Complete
Your complimentary use period has ended. Thank you for using PDF Complete.
Click Here to upgrade to Unlimited Pages and Expanded Features



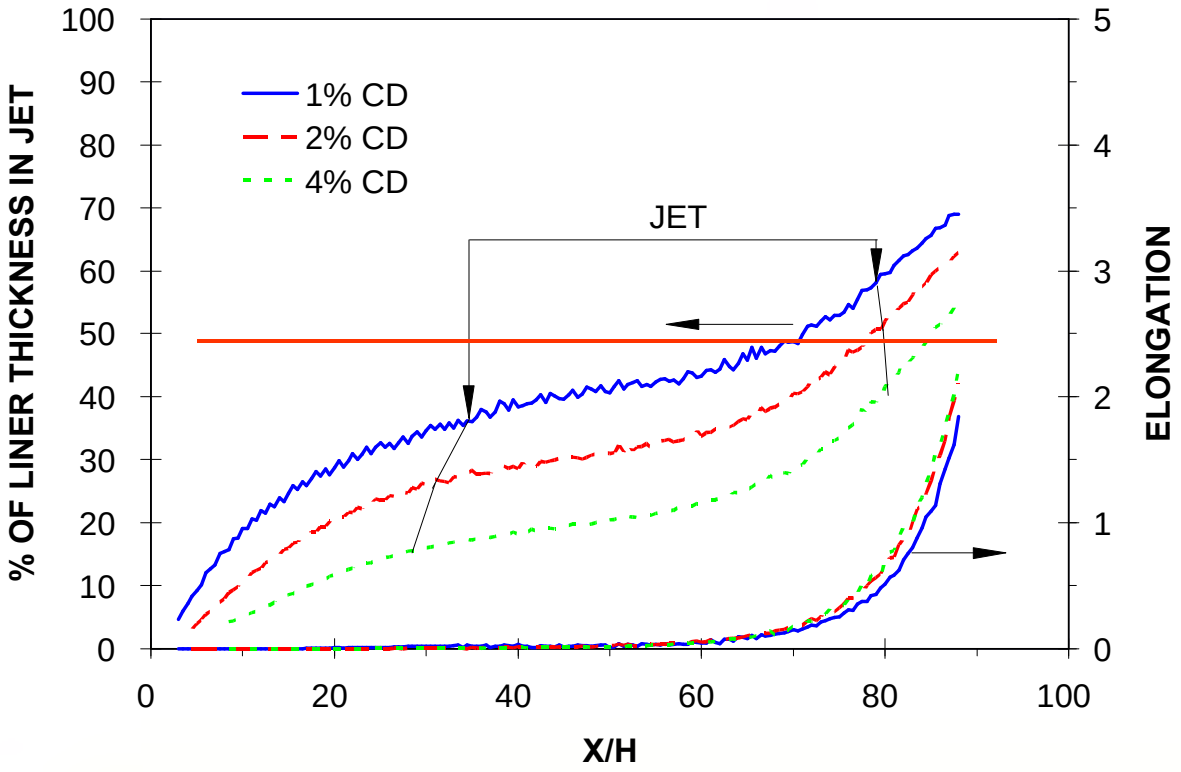
PDF Complete
Your complimentary use period has ended. Thank you for using PDF Complete.
Click Here to upgrade to Unlimited Pages and Expanded Features

Tips are at approximately 90 cm from charge end.



PDF Complete
Your complimentary use period has ended. Thank you for using PDF Complete.
Click Here to upgrade to Unlimited Pages and Expanded Features

SCAN CALCULATION FOR 1%, 2%, 4% CD LINER THICKNESS



PDF Complete
Your complimentary use period has ended. Thank you for using PDF Complete.
Click Here to upgrade to Unlimited Pages and Expanded Features



Figure 5: jet from a 72mm charge, 60°, 0.4mm (0.5%CD) thick copper

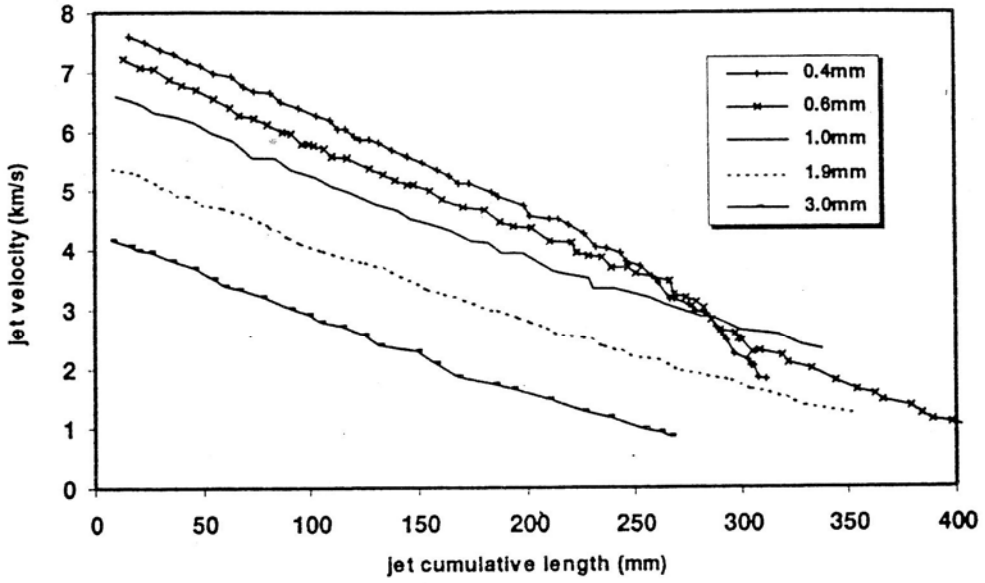


Figure 3: particulation behavior of jets from 60° copper cones with different wall thickness: experimental jet velocity vs. cumulative length from radiographs

P. Y. Chanteret and A. Lichtenberger, "About Varying Shaped Charge Liner Thickness", in Proceedings 17th Int. Symp. On Ballistics, Midrand, South-Africa, 1998.

PDF Complete
Your complimentary use period has ended. Thank you for using PDF Complete.
Click Here to upgrade to Unlimited Pages and Expanded Features

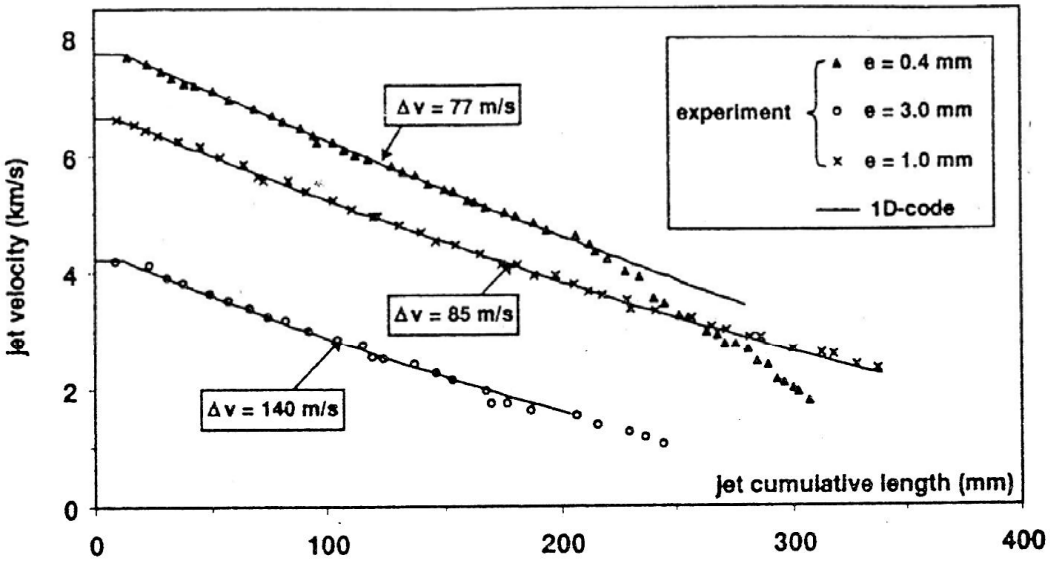


Figure 11: experimental and 1D-code calculated jet velocity vs. cumulative length; 60° copper liners with 0.9%, 2.2% and 6.7% CD liner wall thickness.

PDF Complete
Your complimentary use period has ended. Thank you for using PDF Complete.
Click Here to upgrade to Unlimited Pages and Expanded Features

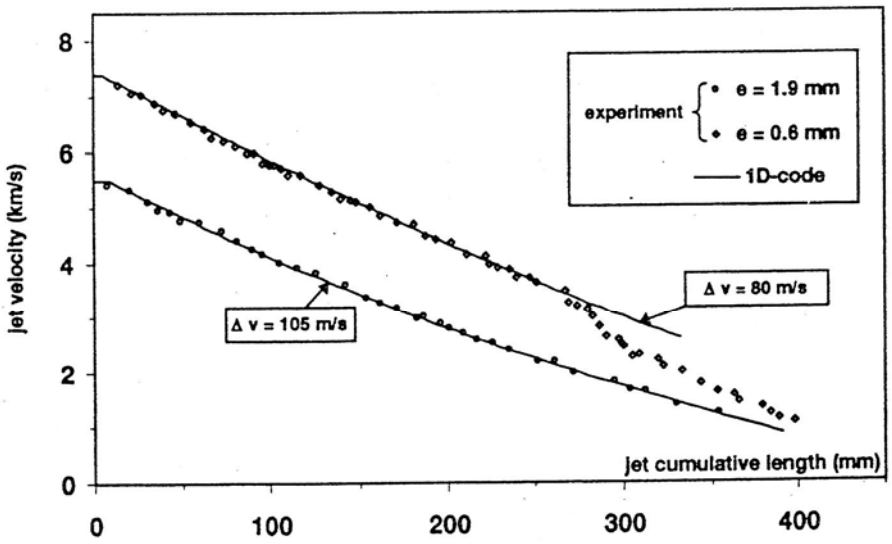
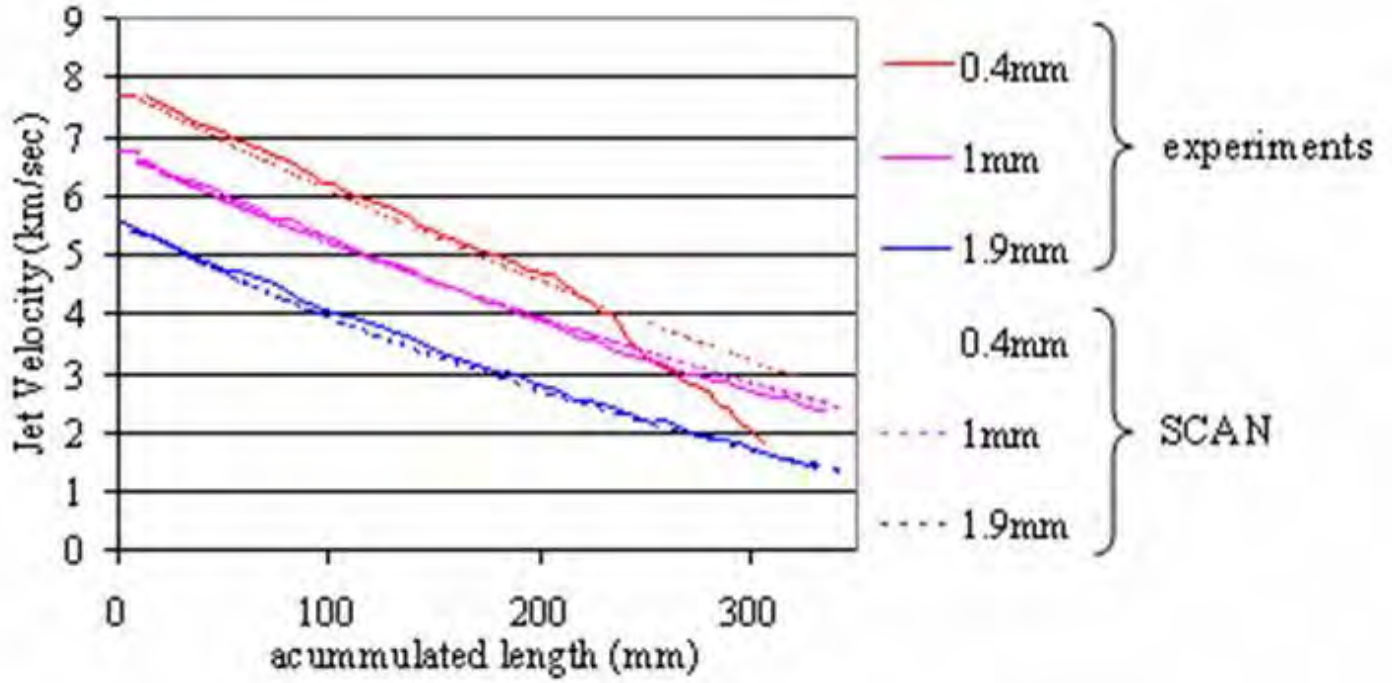


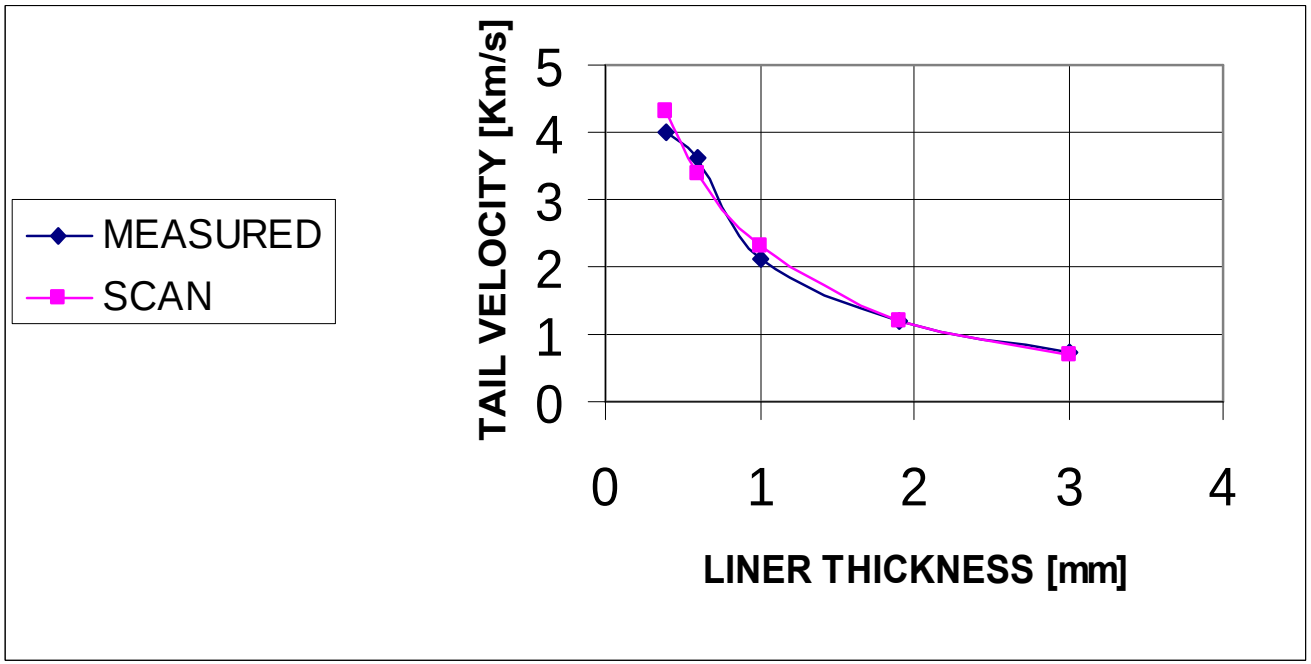
Figure 12: experimental and 1D-code calculated jet velocity vs. cumulative length; 60° copper liners with 1.3% and 4.2% CD liner wall thickness.

PDF Complete
Your complimentary use period has ended. Thank you for using PDF Complete.
Click Here to upgrade to Unlimited Pages and Expanded Features



SCAN calculations compared to Chanteret and Lichtenberger experimental results. The sudden change in the slope seen in the 0.4mm liner characteristic is where the appendix begins to form in this case (it is in the process adjustment) .

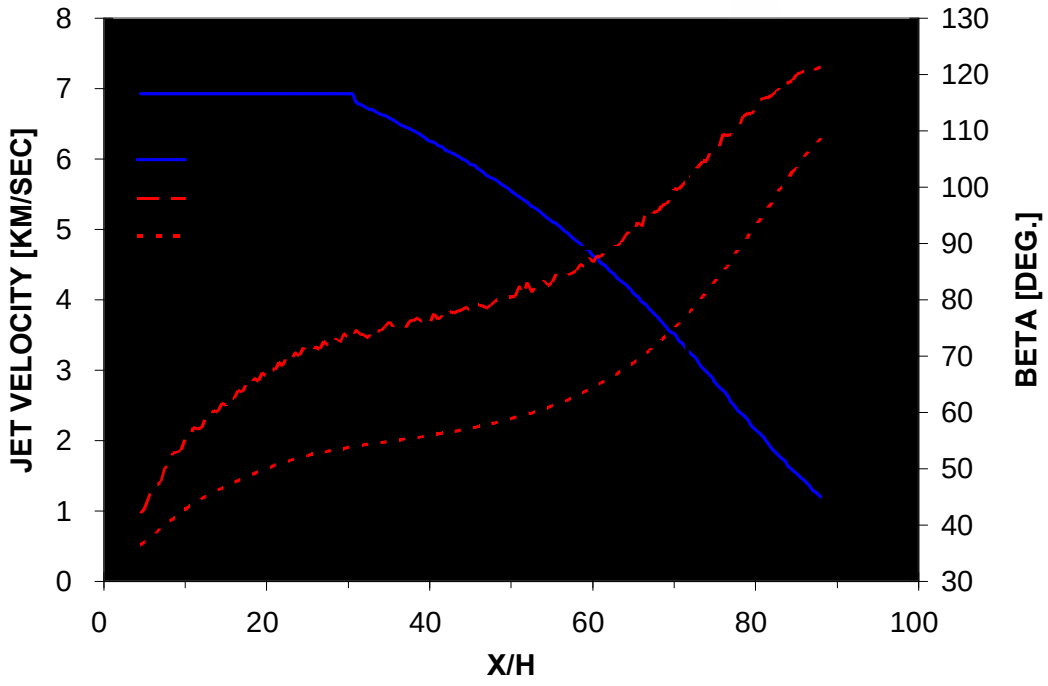
PDF Complete
Your complimentary use period has ended. Thank you for using PDF Complete.
Click Here to upgrade to Unlimited Pages and Expanded Features



Experimental results (Chanteret and Lichtenberger) of the jet velocity where the Appendix starts, as a function of the liner thickness, compared to the SCAN theoretical results.

PDF Complete
Your complimentary use period has ended. Thank you for using PDF Complete.
Click Here to upgrade to Unlimited Pages and Expanded Features

SCAN CALCULATION FOR 2 % CD LINER THICKNESS



PDF Complete
Your complimentary use period has ended. Thank you for using PDF Complete.
Click Here to upgrade to Unlimited Pages and Expanded Features

CONCLUSIONS:

THE APPENDIX REGION WAS IDENTIFIED.

$$\beta \geq 90^\circ$$

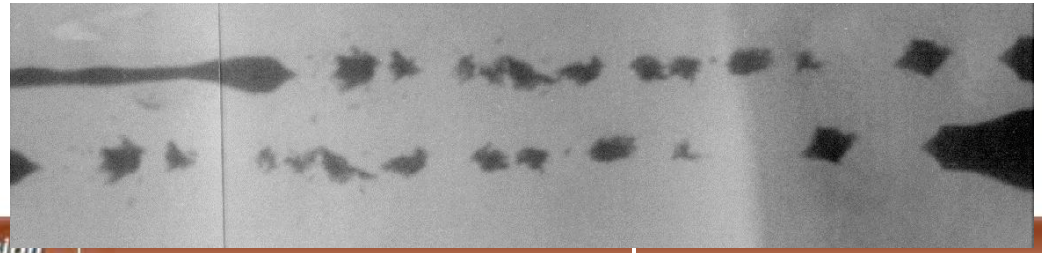
$$V_S = V_1 - V_f < 0$$

HIGH STRAIN RATE.

HIGH VELOCITY DIFFERENCE BETWEEN PARTICLES.

NON STABLE ZONE.

EFFECTIVE FOR PENETRATING SOFT TARGETS.



PDF Complete
Your complimentary use period has ended. Thank you for using PDF Complete.
Click Here to upgrade to Unlimited Pages and Expanded Features

Numerical Simulation of Projectile Acceleration Process Using Solid/Gas Two-Phase Reacting Flow Model

Hiroaki MIURA[1], Akiko MATSUO[1] and Yuichi NAKAMURA[2]

[1]Department of Mechanical Engineering, Keio University, JAPAN

[2]NOF Corporation, JAPAN

PDF Complete
Your complimentary use period has ended. Thank you for using PDF Complete.
Click Here to upgrade to Unlimited Pages and Expanded Features

ystems Utilizing Solid Propellant

Chemical energy of solid propellant
≒ 4MJ/kg

→

Kinetic energy of projectile

Gun System

Military Technology

Cannon



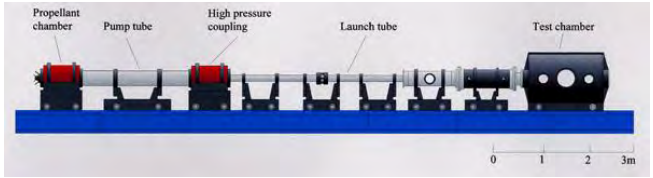
http://www.army-technology.com
/projects/crusader/crusader5.html

Scientific Research

Ballistic Range



http://www.knlab.msl.titech.ac.jp/



http://ceres.ifs.tohoku.ac.jp/~coe/jfacility.html

Solid Rocket

Space Propulsion

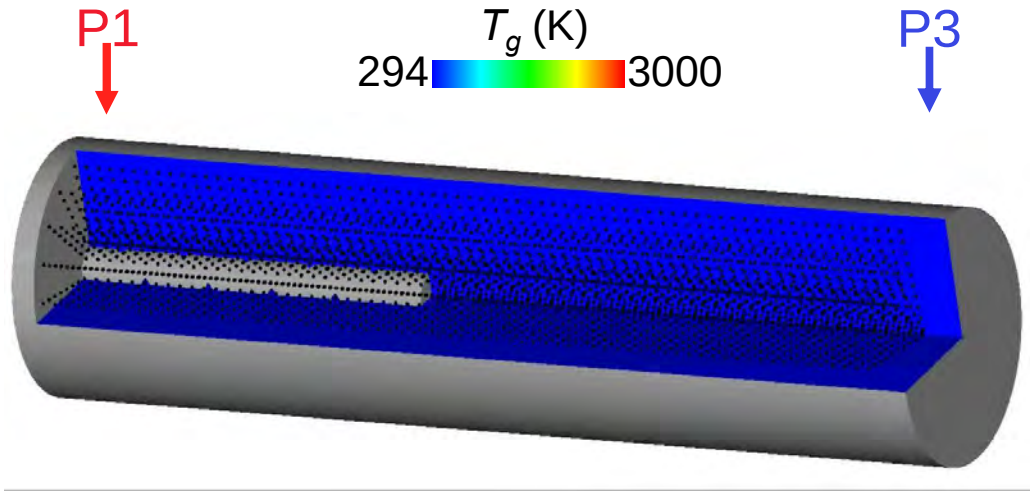
Solid Rocket Booster



http://spaceinfo.jaxa.jp/db/kaihatu/shuttle
/shuttle_g/sts-87-2.jpg

PDF Complete
Your complimentary use period has ended. Thank you for using PDF Complete.
Click Here to upgrade to Unlimited Pages and Expanded Features

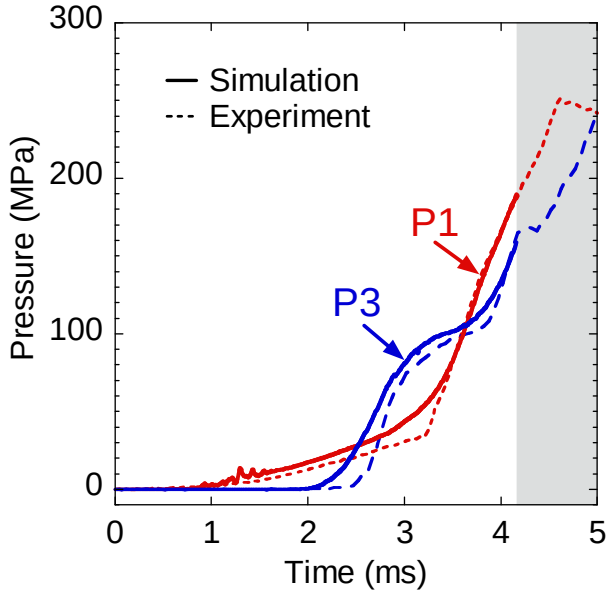
ssure of Granular Solid Propellant



Typical Propellant Chamber



FAS Military Analysis Network



H. Miura *et al*., ISEM2008

The movement of granular solid propellant causes the chamber pressure fluctuations.

↓

Simulation of propellant grains movement is significant to predict the destructive pressure waves generation.

PDF Complete
Your complimentary use period has ended. Thank you for using PDF Complete.
Click Here to upgrade to Unlimited Pages and Expanded Features

bular Solid Propellant

Granular propellant



Characteristics of granular propellant

- ÅLarger surface area
  - Ÿ Rapid fire
- ÅEasy adjustment for propellant mass
- ÅProblem of strong pressure waves

Tubular propellant



Characteristics of tubular propellant

- ÅSmaller surface area
  - Ÿ Slow burning
- ÅUniform ignition and uniform charge concentration

FAS Military Analysis Network

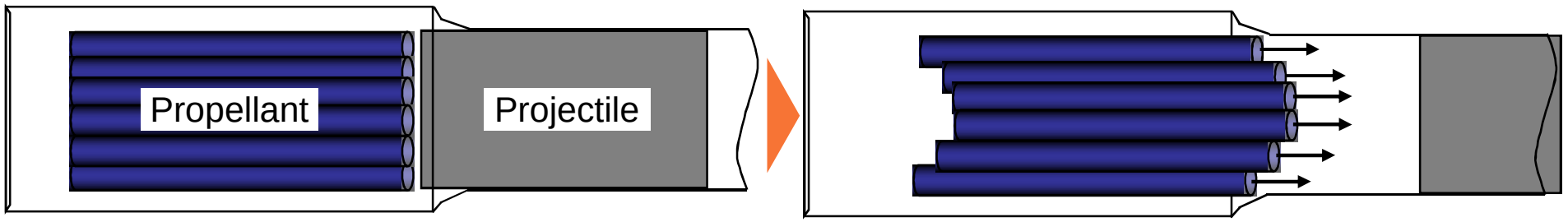
Simulation technique for tubular propellant combustion should be developed.

Modeling for tubular propellant movement with burning

PDF Complete
Your complimentary use period has ended. Thank you for using PDF Complete.
Click Here to upgrade to Unlimited Pages and Expanded Features

n of Tubular Solid Propellant

To simulate tubular propellant behavior in the chamber

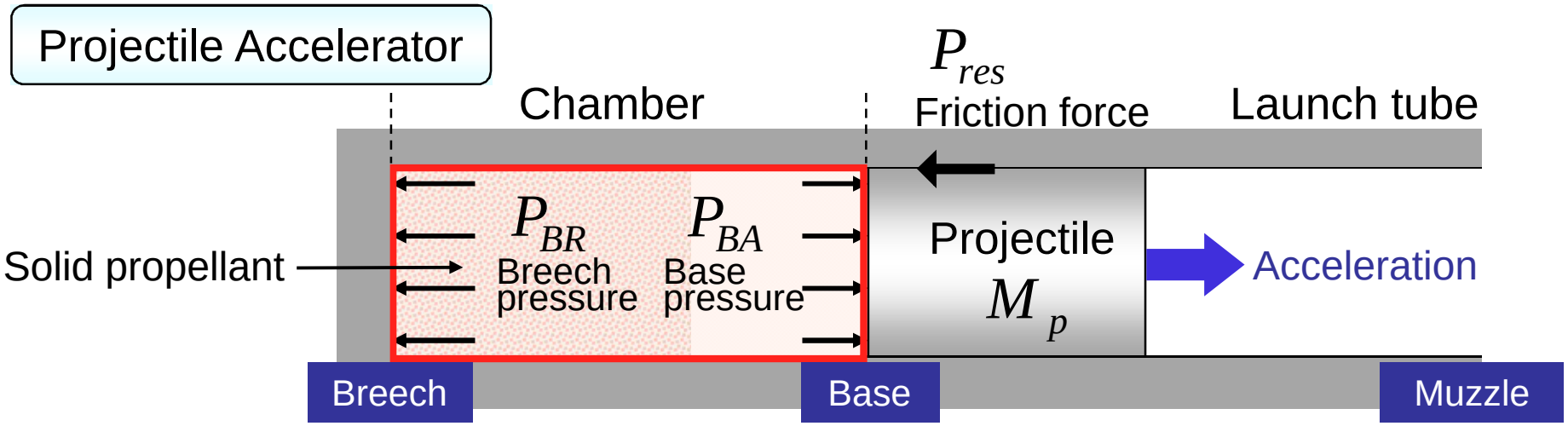


Modeling for tubular propellant movement with burning

- A long tubular propellant lies in the wide range of computational domain.
  - Consideration of property distributions on propellant surface
- Each tubular propellant moves in the chamber.
  - Movement model for propellants by Lagrangian approach

PDF Complete
Your complimentary use period has ended. Thank you for using PDF Complete.
Click Here to upgrade to Unlimited Pages and Expanded Features

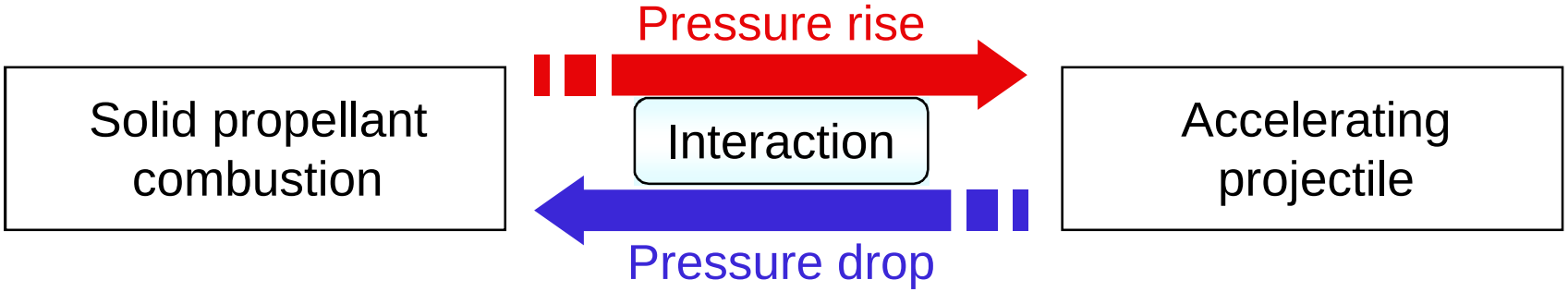
for Projectile Accelerator



- Combustion gas and solid propellant coexist in the chamber.

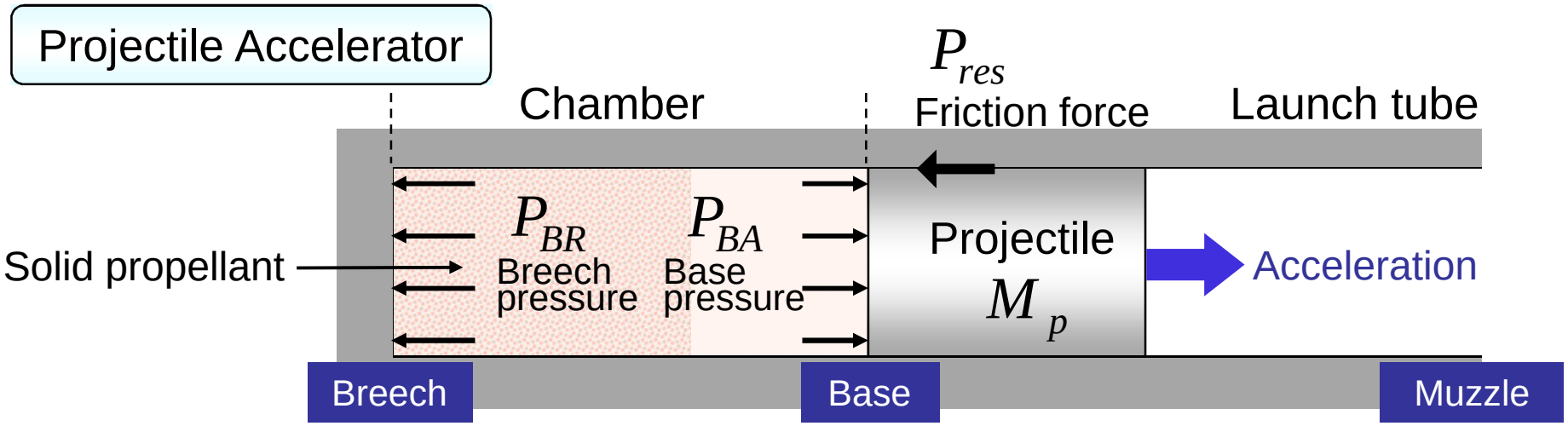


- Chamber volume increases with the projectile movement.



PDF Complete
Your complimentary use period has ended. Thank you for using PDF Complete.
Click Here to upgrade to Unlimited Pages and Expanded Features

nalysis Based on Interior Ballistics



Prediction of events in the accelerator is required.

Elements of accelerating process simulation by numerical analysis

- Solid/Gas two-phase flow
- Solid propellant combustion

  Propellant (Solid phase) → Combustion gas (Gas phase)
- Moving boundary problem

PDF Complete
Your complimentary use period has ended. Thank you for using PDF Complete.
Click Here to upgrade to Unlimited Pages and Expanded Features

Objective

To simulate the process of accelerating a projectile by tubular solid propellant combustion in the 50mm projectile accelerator using the developed 2D axisymmetric two-phase flow code and the moving overlapped grid method.

- Simulation method is validated using experimental data.
  - Breech pressure history
  - Projectile velocity history
- Conditions of projectile mass Mp and propellant mass C are varied for the examination of those effects on the performance of gun system.
  - Maximum breech pressure
  - Projectile muzzle velocity and kinetic energy

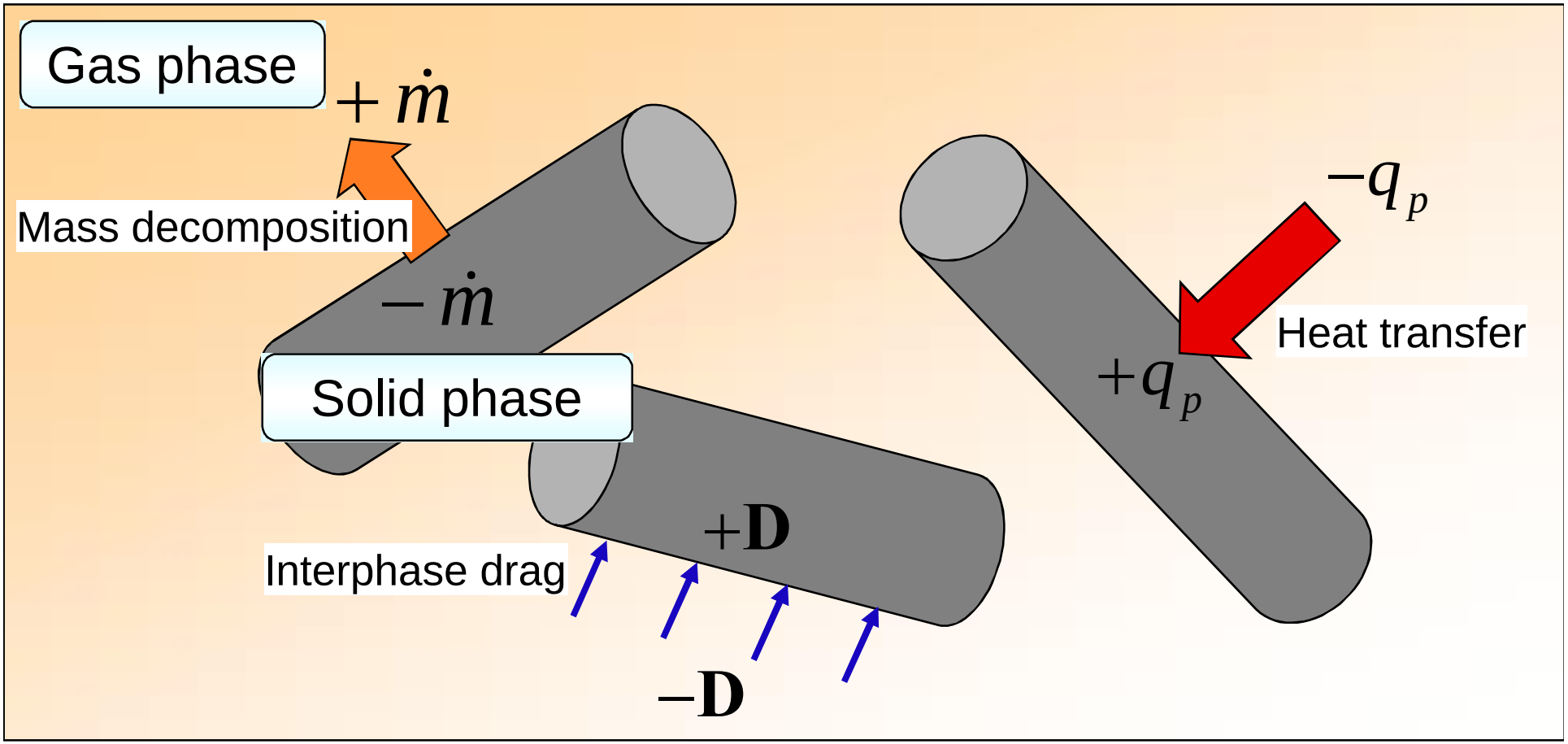
PDF Complete
Your complimentary use period has ended. Thank you for using PDF Complete.
Click Here to upgrade to Unlimited Pages and Expanded Features

Calculation Method for Interior Ballistics Simulation

- Two-phase Fluid Dynamics Code
- Modeling Tubular Propellant
- Modeling Projectile Movement

PDF Complete
Your complimentary use period has ended. Thank you for using PDF Complete.
Click Here to upgrade to Unlimited Pages and Expanded Features

tion Between Two Phases



$$\dot{m} = \dot{m}(r) \qquad r = ap^n \qquad q_p = q_p(T_g - T_p)$$

$$\mathbf{D} = \mathbf{D}(\mathbf{u}_g - \mathbf{u}_p) \qquad T_p \geq T_{ignition} \rightarrow ignition$$

PDF Complete
Your complimentary use period has ended. Thank you for using PDF Complete.
Click Here to upgrade to Unlimited Pages and Expanded Features

Governing Equations

Gas-phase

$$\frac{\partial}{\partial t}(\alpha\rho)+\nabla\cdot(\alpha\rho\mathbf{u})=\dot{m}+\dot{m}_{ig}$$

$$\frac{\partial}{\partial t}(\alpha\rho\mathbf{u})+\nabla\cdot(\alpha\rho\mathbf{u}\mathbf{u})=-\alpha\nabla p-\mathbf{D}+\dot{m}\mathbf{u}_p$$

$$\frac{\partial}{\partial t}(\alpha e)+\nabla\cdot\{\alpha(e+p)\mathbf{u}\}=-\mathbf{D}\cdot\mathbf{u}_p+\dot{m}\left(q+\frac{\mathbf{u}_p\cdot\mathbf{u}_p}{2}\right)+\dot{m}_{ig}q_{ig}-q_p$$

$$\begin{cases}\dfrac{\partial}{\partial t}(\alpha\rho Y_{pr})+\nabla\cdot(\alpha\rho Y_{pr}\mathbf{u})=\dot{m}\\ \dfrac{\partial}{\partial t}(\alpha\rho Y_{ig})+\nabla\cdot(\alpha\rho Y_{ig}\mathbf{u})=\dot{m}_{ig}\\ \dfrac{\partial}{\partial t}(\alpha\rho Y_{a})+\nabla\cdot(\alpha\rho Y_{a}\mathbf{u})=0\end{cases}$$

pr : propellant gas
ig : igniter gas
a : air

Solid-phase $m_{p,i}\dfrac{du_{p,i}}{dt}=(p_L-p_R)A_i+D_i-\dot{m}_i u_{p,i}$ 1D motion of *i*-th propellant

- Gas-phase : Compressible fluid
- Solid-phase : Constant density

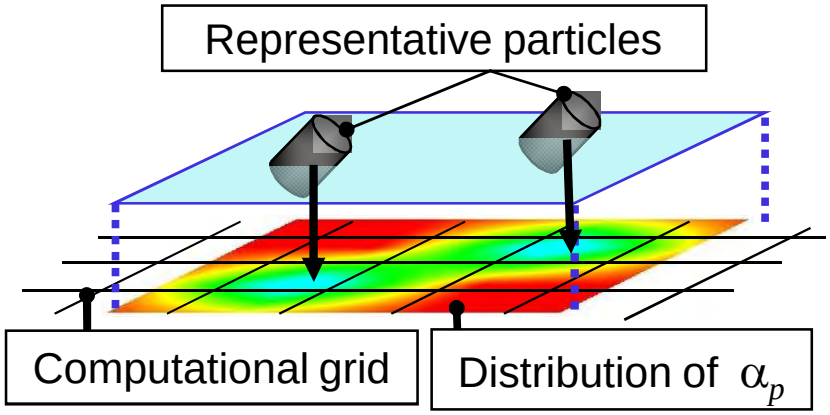
Computational volume is divided into the volume of gas and solid.

α : Volume fraction of gas-phase (porosity)

α_p : Volume fraction of solid-phase

$$\alpha=1-\alpha_p$$

The distribution of α_p is determined from the distribution of representative particles.



PDF Complete
Your complimentary use period has ended. Thank you for using PDF Complete.
Click Here to upgrade to Unlimited Pages and Expanded Features

Governing Equations

Gas-phase

$$\frac{\partial}{\partial t}(\alpha\rho)+\nabla\cdot(\alpha\rho\mathbf{u})=\dot{m}+\dot{m}_{ig}$$

$$\frac{\partial}{\partial t}(\alpha\rho\mathbf{u})+\nabla\cdot(\alpha\rho\mathbf{u}\mathbf{u})=-\alpha\nabla p-\mathbf{D}+\dot{m}\mathbf{u}_p$$

$$\frac{\partial}{\partial t}(\alpha e)+\nabla\cdot\{\alpha(e+p)\mathbf{u}\}=-\mathbf{D}\cdot\mathbf{u}_p+\dot{m}\left(q+\frac{\mathbf{u}_p\cdot\mathbf{u}_p}{2}\right)+\dot{m}_{ig}q_{ig}-q_p$$

$$\begin{cases}\frac{\partial}{\partial t}(\alpha\rho Y_{pr})+\nabla\cdot(\alpha\rho Y_{pr}\mathbf{u})=\dot{m}\\ \frac{\partial}{\partial t}(\alpha\rho Y_{ig})+\nabla\cdot(\alpha\rho Y_{ig}\mathbf{u})=\dot{m}_{ig}\\ \frac{\partial}{\partial t}(\alpha\rho Y_{a})+\nabla\cdot(\alpha\rho Y_{a}\mathbf{u})=0\end{cases}$$

pr : propellant gas
ig : igniter gas
a : air

Solid-phase

$$m_{p,i}\frac{du_{p,i}}{dt}=(p_L-p_R)A_i+D_i-\dot{m}_i u_{p,i}$$

1D motion of *i*-th propellant

- Gas-phase components
  - Propellant combustion gas (*pr*)
  - Igniter combustion gas (*ig*)
  - Air (*a*)
- State equation for gas-phase

$$p=\frac{RT}{(1/\rho-b)}$$

b : Covolume

$\dot{m}$: Propellant mass decomposition rate

$\dot{m}_{ig}$: Igniter mass decomposition rate

$\mathbf{D}$: The interphase drag between two-phase

q : The combustion heat of propellant

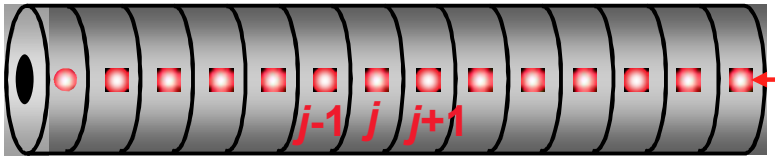
q_{ig} : The combustion heat of igniter

q_p : Heat loss to solid phase

PDF Complete
Your complimentary use period has ended. Thank you for using PDF Complete.
Click Here to upgrade to Unlimited Pages and Expanded Features

entative Particle Properties

Information of propellant geometry for ***j*-th representative particle**



At the end of each tubular propellant

Volume $V_{p,j} = \left(\Delta L_{p,j} - \Delta u_j\right)\left\{\frac{\pi}{4}\left(D_p - 2\Delta u_j\right)^2 - \frac{\pi}{4}\left(d_p + 2\Delta u_j\right)^2\right\}$

Surface area $S_{p,j} = \pi\left(D_p - 2\Delta u_j\right)\left(\Delta L_p - \Delta u_j\right) + \pi\left(d_p + 2\Delta u_j\right)\left(\Delta L_{p,j} - \Delta u_j\right)$

$$+\left\{\frac{\pi}{4}\left(D_p - 2\Delta u_j\right)^2 - \frac{\pi}{4}\left(d_p + 2\Delta u_j\right)^2\right\}$$

$\Delta L_{p,j}$: Divided length of tube

D_p : Outer diameter of tube

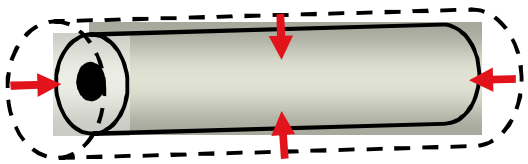
d_p : Inner diameter of tube

$\Delta u_j = \int_0^t r dt \qquad r = ap^n$

At the other position

Volume $V_{p,j} = \Delta L_{p,j}\left\{\frac{\pi}{4}\left(D_p - 2\Delta u_j\right)^2 - \frac{\pi}{4}\left(d_p + 2\Delta u_j\right)^2\right\}$

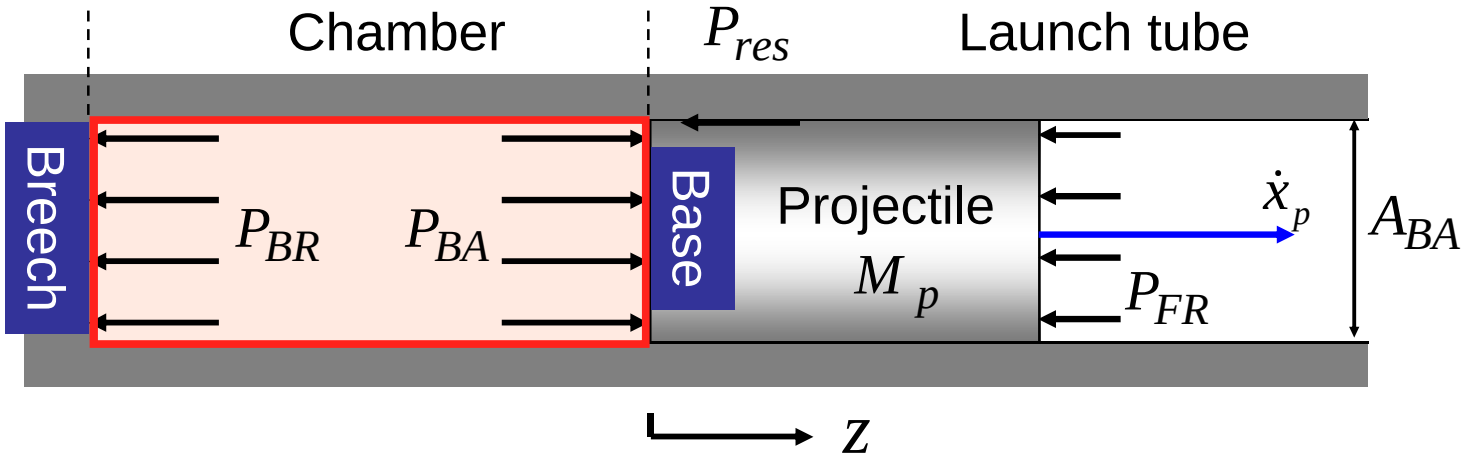
Surface area $S_{p,j} = \pi\left(D_p - 2\Delta u_j\right)\Delta L_p + \pi\left(d_p + 2\Delta u_j\right)\Delta L_{p,j}$



PDF Complete
Your complimentary use period has ended. Thank you for using PDF Complete.
Click Here to upgrade to Unlimited Pages and Expanded Features

ectile Movement in Launch Tube

Kinetic model of projectile movement



P_{BR} : Breech pressure

P_{BA} : Base pressure

P_{res} : Resistive pressure

Projectile velocity $\dot{x}_p = \int_0^t \ddot{x}_p dt = \int_0^t \left(\frac{(P_{BA} - P_{FR} - P_{res}) A_{BA}}{M_p} \right) dt$

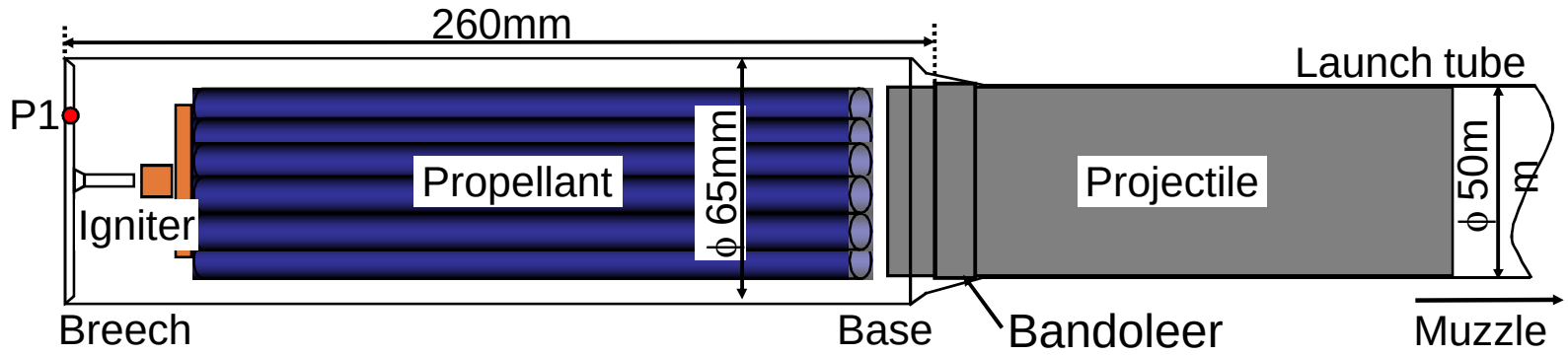
PDF Complete
Your complimentary use period has ended. Thank you for using PDF Complete.
Click Here to upgrade to Unlimited Pages and Expanded Features

Interior Ballistics Simulation of 50mm Gun

PDF Complete
Your complimentary use period has ended. Thank you for using PDF Complete.
Click Here to upgrade to Unlimited Pages and Expanded Features

Computational Model

Reproduction of the experiment of 50mm gun by NOF Corporation



The projectile velocity was recorded using an in-bore Doppler radar system.

Computational data

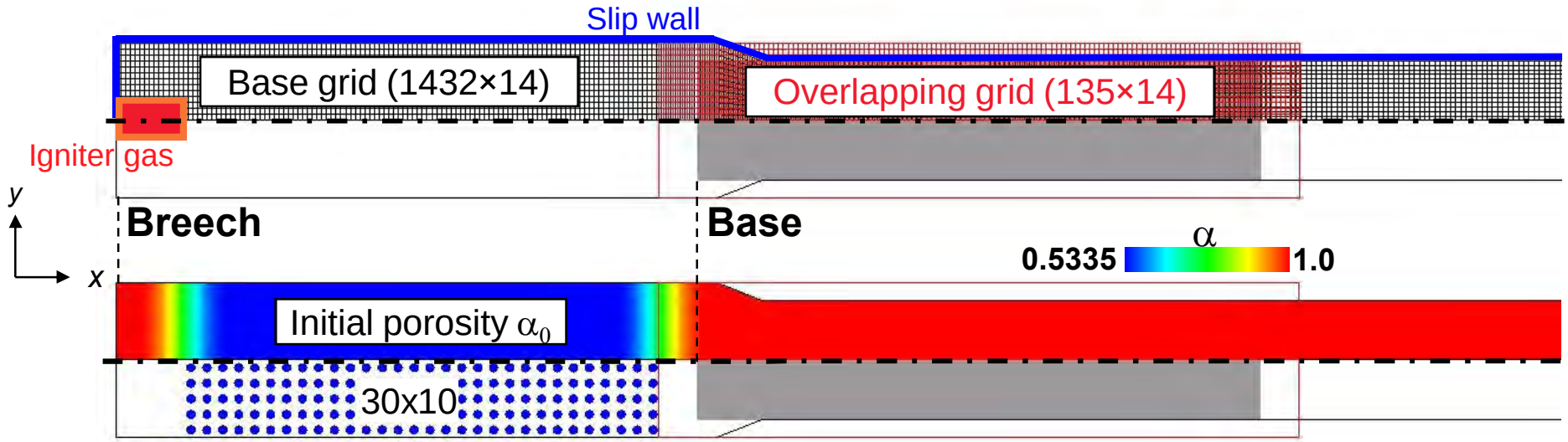
Diameter of tube (mm)	50
Length of tube (mm)	3195
Projectile mass M_p (kg)	2.5, 3.5, 4.5
Propellant mass C (kg)	0.4, 0.5
Propellant type	Double-base
Shape of grain	Tubular (one hole)
Size of grain (mm)	ϕ6.35 x 200

Propellant properties

Adiabatic flame temperature T_0 (K)	3133
Impetus F (J/g)	1036
Specific heat ratio γ	1.232
Density ρ_p (kg/m^3)	1615
Covolume b (cm^3/kg)	993

PDF Complete
Your complimentary use period has ended. Thank you for using PDF Complete.
Click Here to upgrade to Unlimited Pages and Expanded Features

Computational Setup



Calculation condition

Overlapping grid is movable

Wall condition : Adiabatic slip wall

Initial condition : 101kPa, 294K, γ=1.4

Calculation method

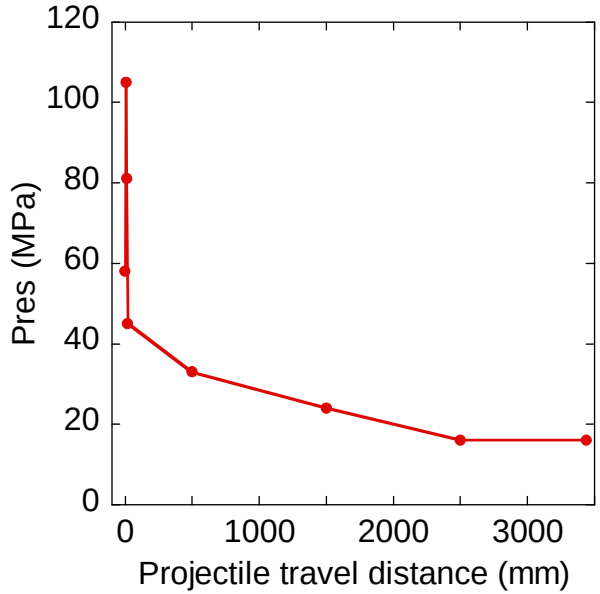
Discretization method of convection term

: SHUS (Shima and Jounouchi, 1995)

Time integration method

: 2-step Runge-Kutta method

Resistive pressure P_{res}



PDF Complete
Your complimentary use period has ended. Thank you for using PDF Complete.
Click Here to upgrade to Unlimited Pages and Expanded Features

Accelerating Process

M_p=4.5kg and C=0.5kg

Pressure / gas temperature distribution



0.1 p (MPa) 390

294 T_g (K) 3000

Propellant / gas velocity distribution

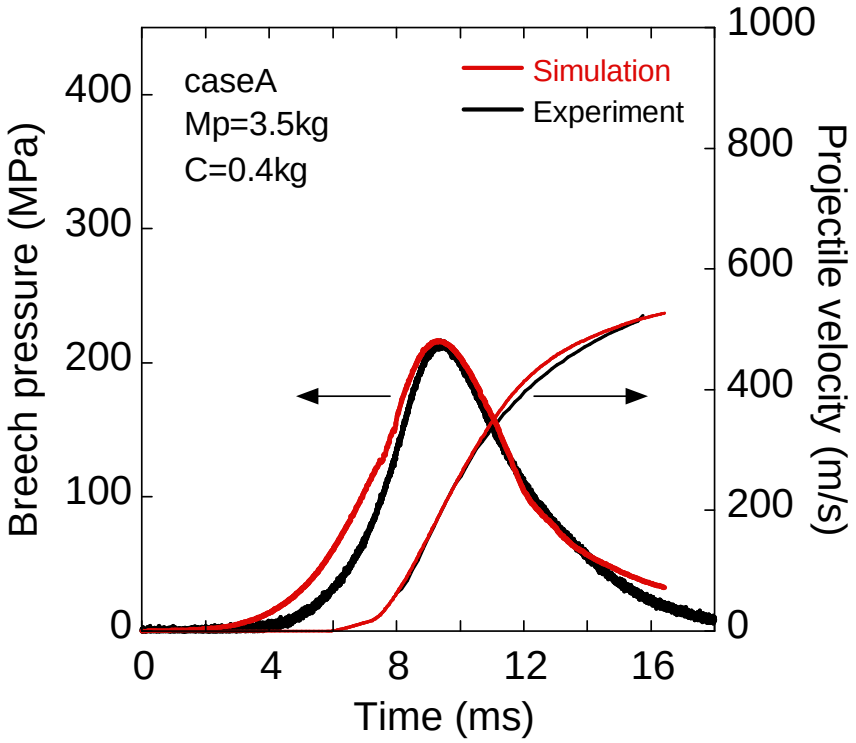


-34 u_g (m/s) 588

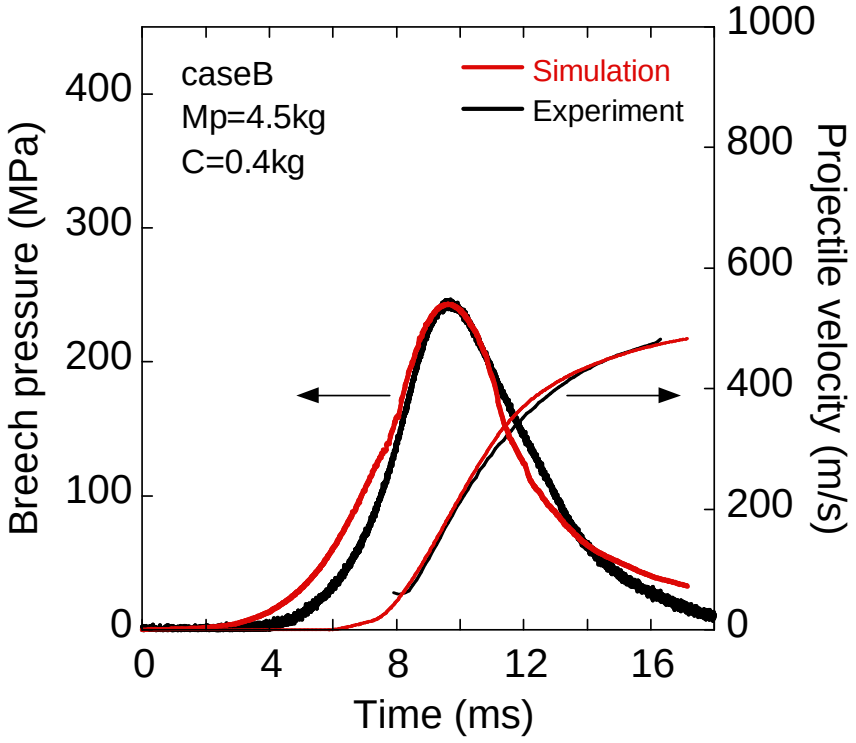
PDF Complete
Your complimentary use period has ended. Thank you for using PDF Complete.
Click Here to upgrade to Unlimited Pages and Expanded Features

f Predicted Data with Experiment

Case A (M_p=3.5kg and C=0.4kg)



Case B (M_p=4.5kg and C=0.4kg)

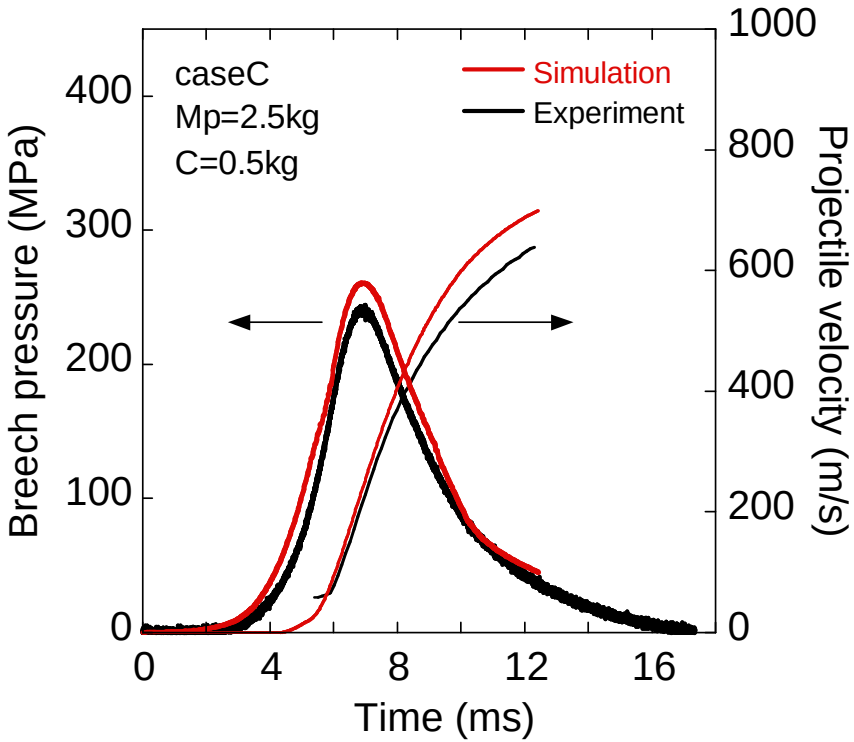


- Predicted histories of the breech pressure and the projectile velocity are in good agreement with the experimental data in the each case.

PDF Complete
Your complimentary use period has ended. Thank you for using PDF Complete.
Click Here to upgrade to Unlimited Pages and Expanded Features

f Predicted Data with Experiment

Case C (M_p=2.5kg and C=0.5kg)

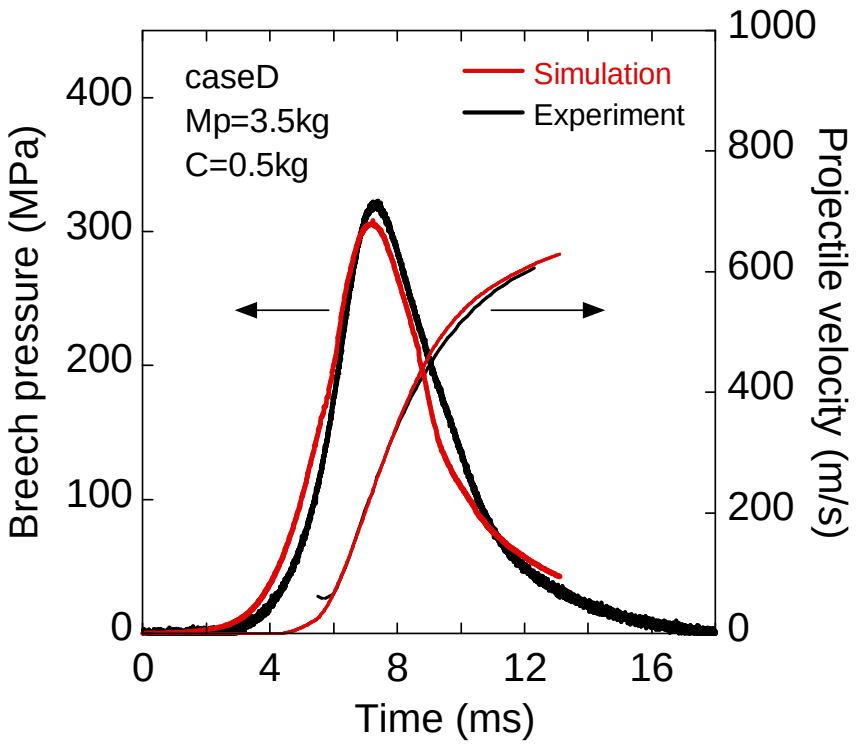


- Predicted breech pressure and projectile velocity are higher than the experimental data in this case.

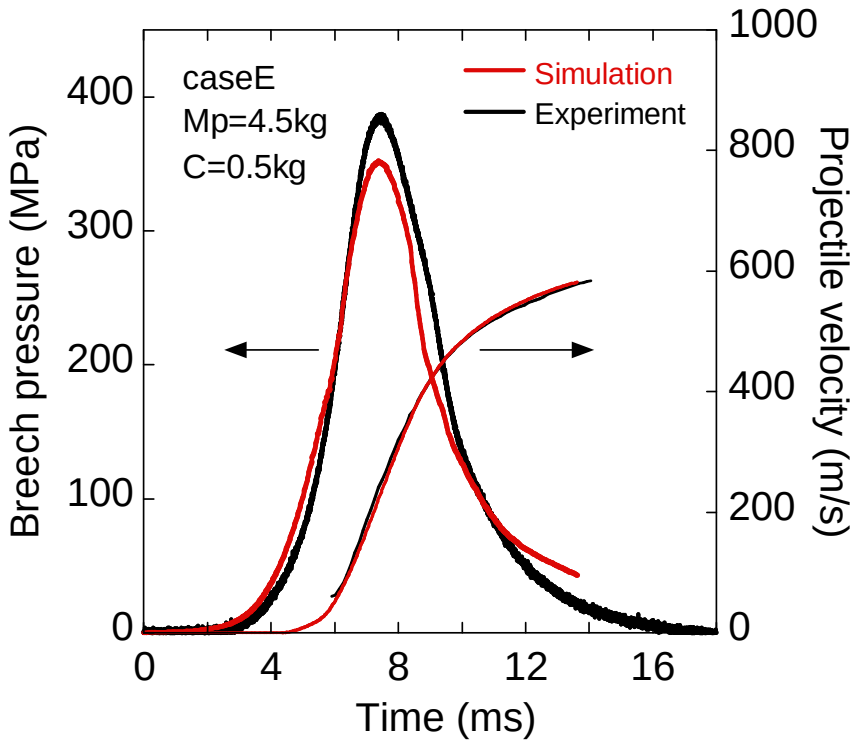
PDF Complete
Your complimentary use period has ended. Thank you for using PDF Complete.
Click Here to upgrade to Unlimited Pages and Expanded Features

f Predicted Data with Experiment

Case D (M_p=3.5kg and C=0.5kg)



Case E (M_p=4.5kg and C=0.5kg)

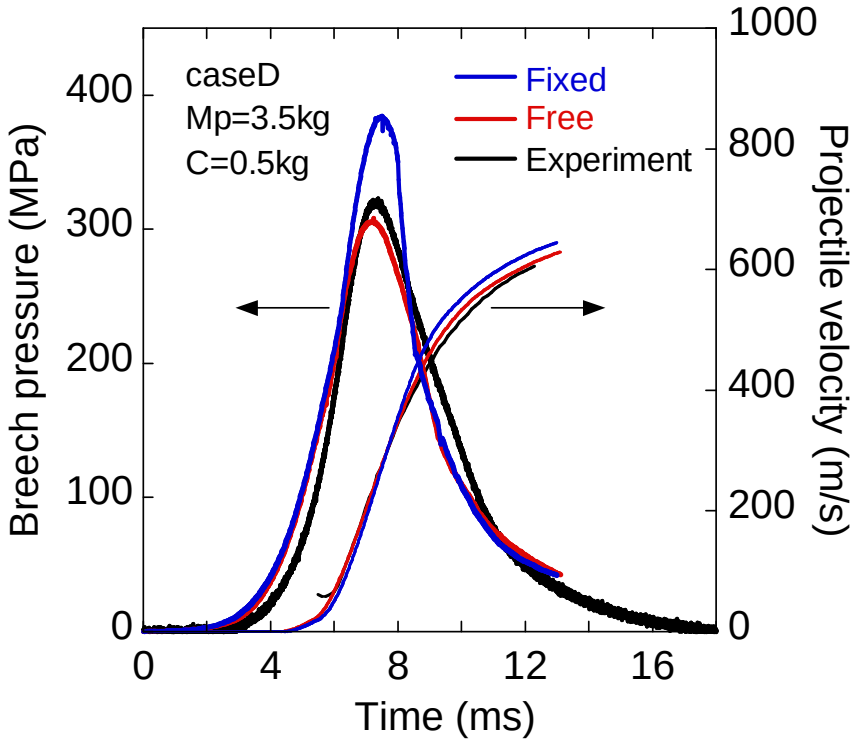


- Predicted histories of the breech pressure and the projectile velocity are in good agreement with the experimental data in the each case.

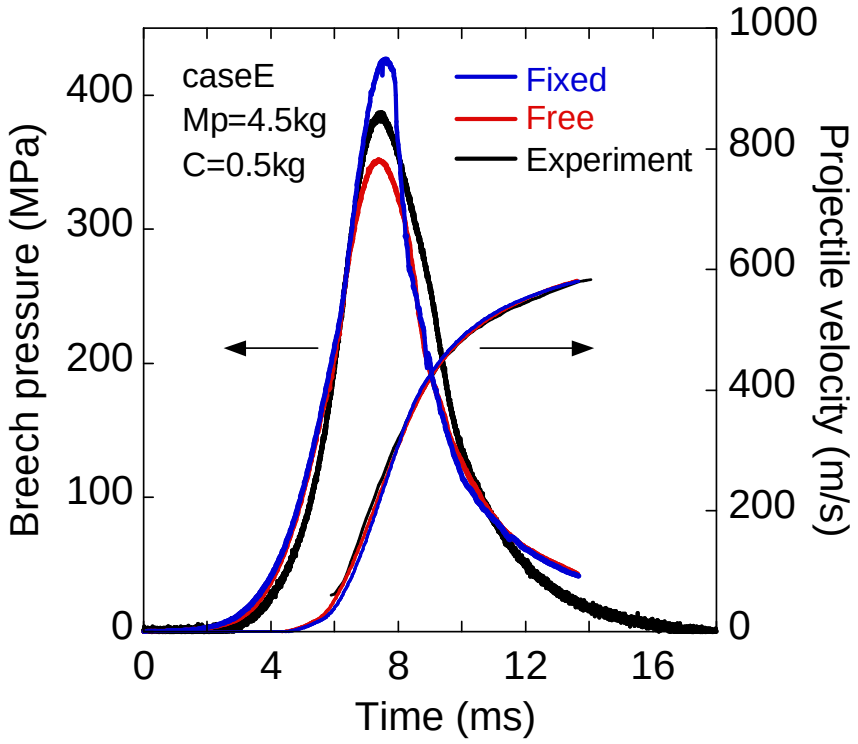
PDF Complete
Your complimentary use period has ended. Thank you for using PDF Complete.
Click Here to upgrade to Unlimited Pages and Expanded Features

nd Fixed Propellant Models

Case D (M_p=3.5kg and C=0.5kg)



Case E (M_p=4.5kg and C=0.5kg)

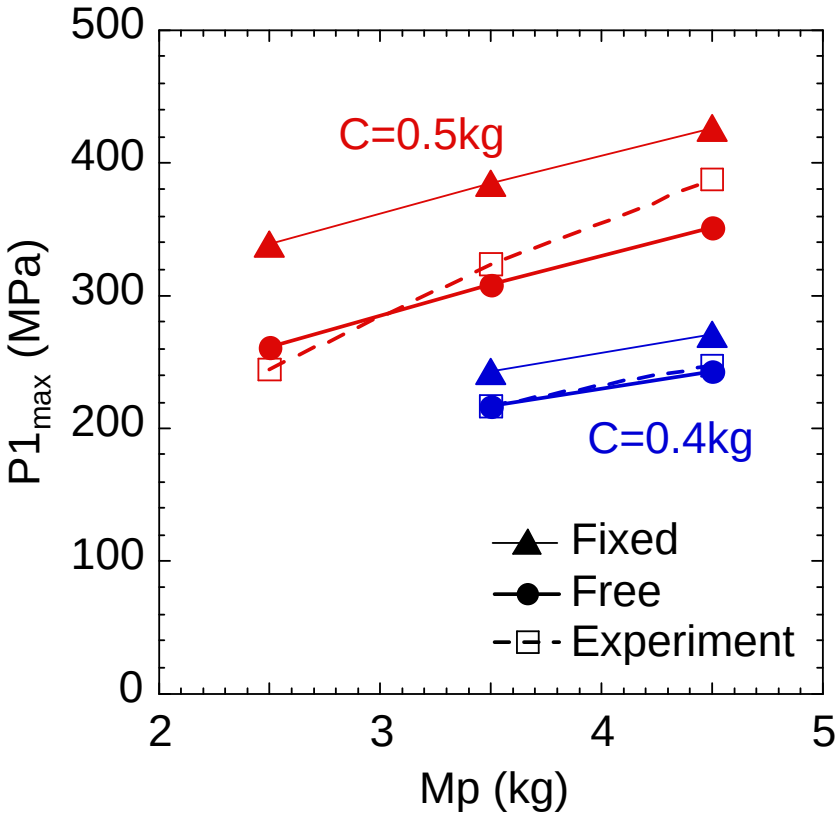


- If we use the fixed propellant model (without propellant movement), the predicted pressure becomes much higher than the free propellant model (with propellant movement).

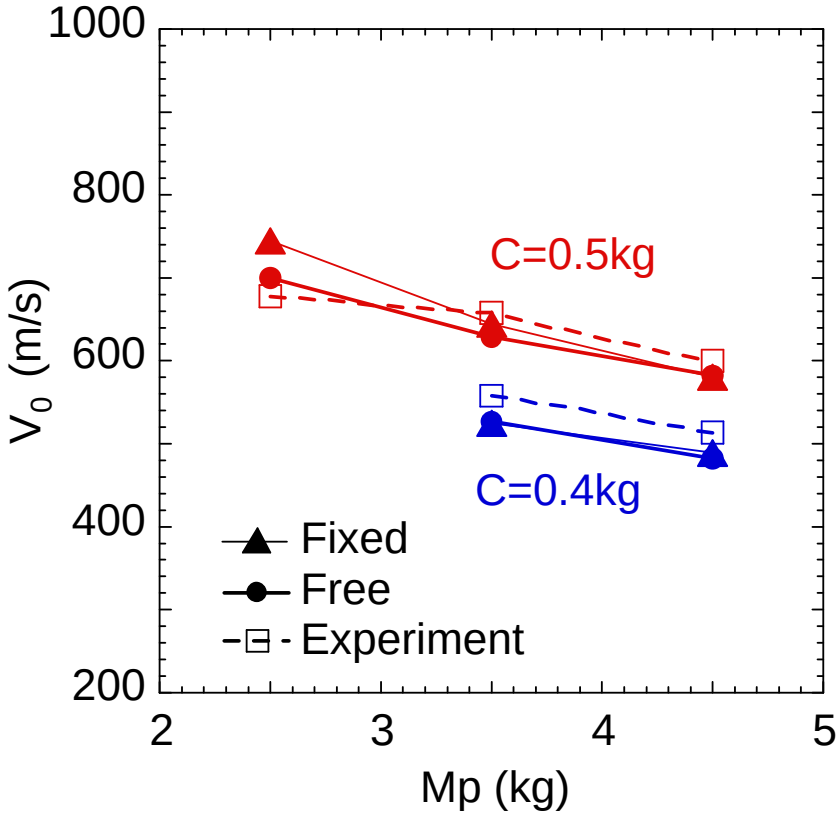
PDF Complete
Your complimentary use period has ended. Thank you for using PDF Complete.
Click Here to upgrade to Unlimited Pages and Expanded Features

nd Fixed Propellant Models

Maximum Breech Pressure



Muzzle Velocity

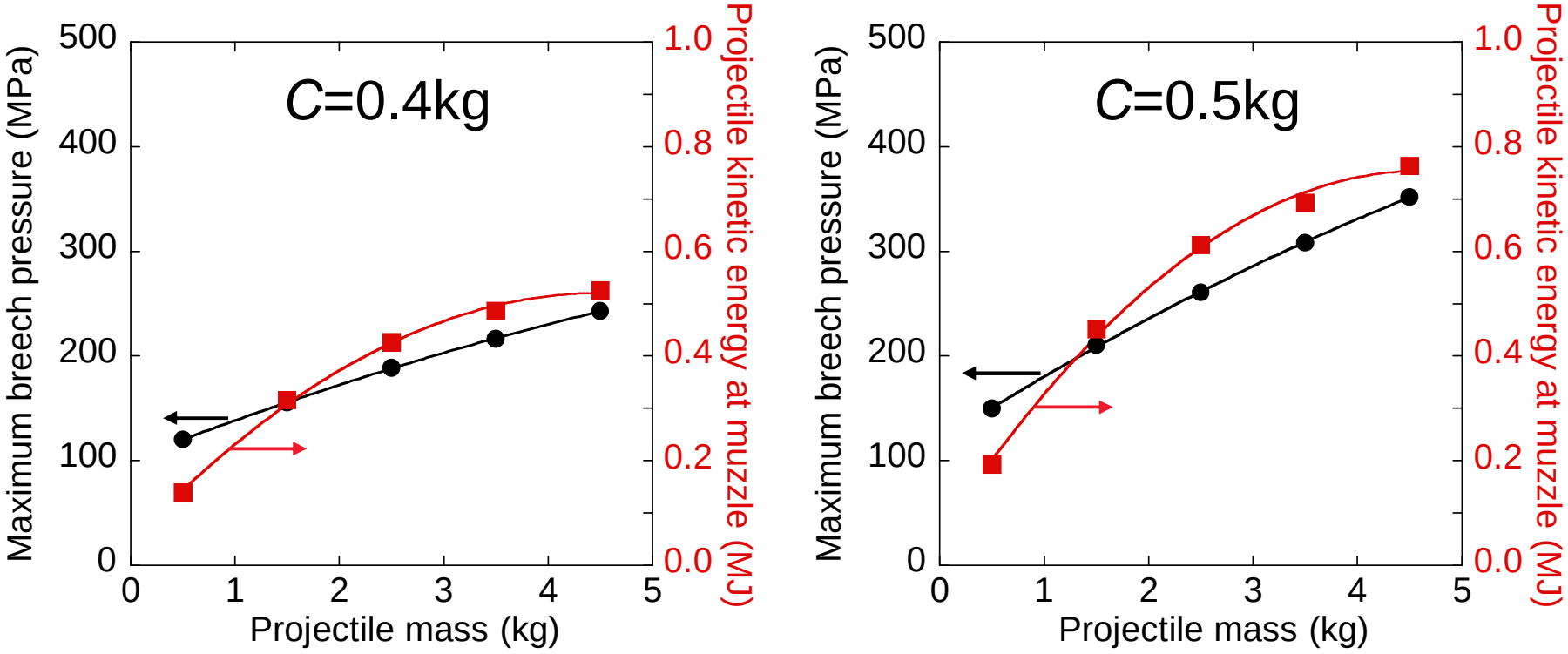


- The muzzle velocities of the two models were almost equivalent. However, the maximum breech pressure was overestimated by the **Fixed Model**, and the **Free Model** well reproduced the experimental maximum pressure.

PDF Complete
Your complimentary use period has ended. Thank you for using PDF Complete.
Click Here to upgrade to Unlimited Pages and Expanded Features

ation of Projectile Mass

Simulated maximum breech pressure and projectile kinetic energy



- The maximum chamber pressure increases linearly whereas the projectile kinetic energy converges with the projectile mass Mp.

PDF Complete
Your complimentary use period has ended. Thank you for using PDF Complete.
Click Here to upgrade to Unlimited Pages and Expanded Features

Conclusion

The processes of accelerating a projectile by tubular solid propellant combustion in the 50mm projectile launch system were simulated for various cases using the developed 2D two-phase flow code and the moving overlapped grid method.

- In the comparison between the predicted results and the experimental data of various Mp and C condition, the results of the simulation with propellant movement showed being in good agreement with the experimental results.

- There was trade-off relation between the chamber pressure suppression and the projectile kinetic energy improvement. However, the projectile kinetic energy at the muzzle converged with increasing the projectile mass Mp.

PDF Complete
Your complimentary use period has ended. Thank you for using PDF Complete.
Click Here to upgrade to Unlimited Pages and Expanded Features

Hiroaki MIURA

Belongs to Department of Mechanical Engineering at Keio University in Japan

miura@mech.keio.ac.jp

dr074673@hc.cc.keio.ac.jp

Development of the NLOS-LS PAM Warhead

24th International Symposium on Ballistics

September 22 – 26, 2008
New Orleans, LA

GENERAL DYNAMICS
Ordnance and Tactical Systems

Raytheon
PO Box 11337
Tucson, AZ 85724-1337

Distribution Statement A – Approved for public release 242-2008

NLOS-PAM Team



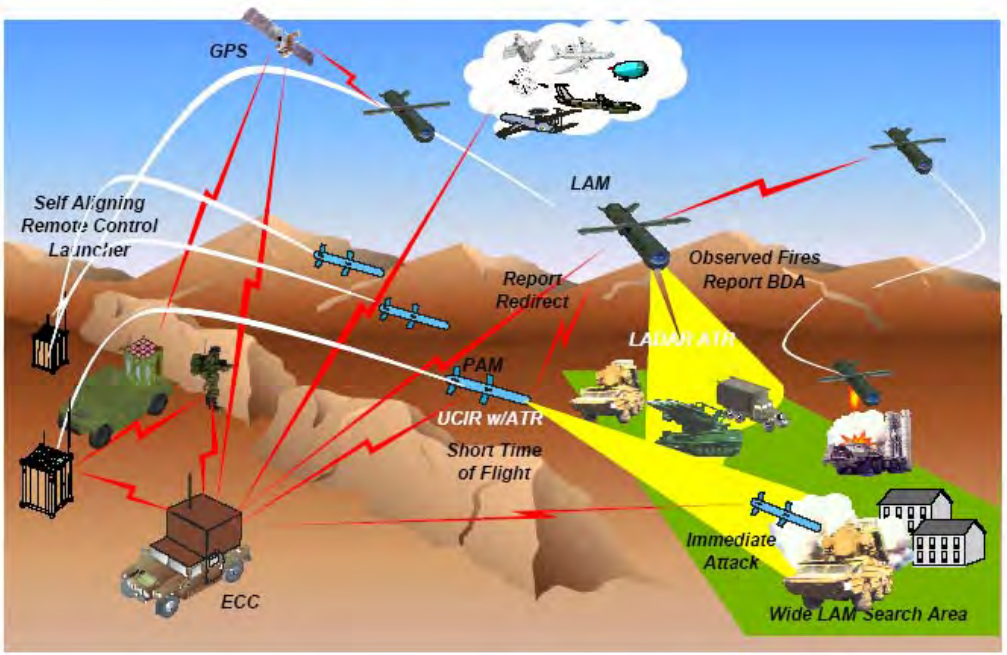
- Prime Contractor: NetFires LLC
  - Raytheon Missile Systems
  - Lockheed Martin Missiles & Fire Control

Distribution Statement A – Approved for public release 242-2008

Raytheon
PO Box 11337
Tucson, AZ 85724-1337

NLOS-PAM Overview

- Low cost, direct attack missile
- Provides precision fire support for the Brigade Combat Team and for USN Littoral Combat Ship





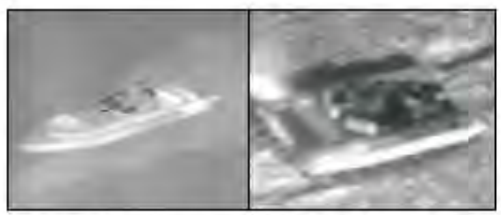
Distribution Statement A – Approved for public release 242-2008

PAM System Description

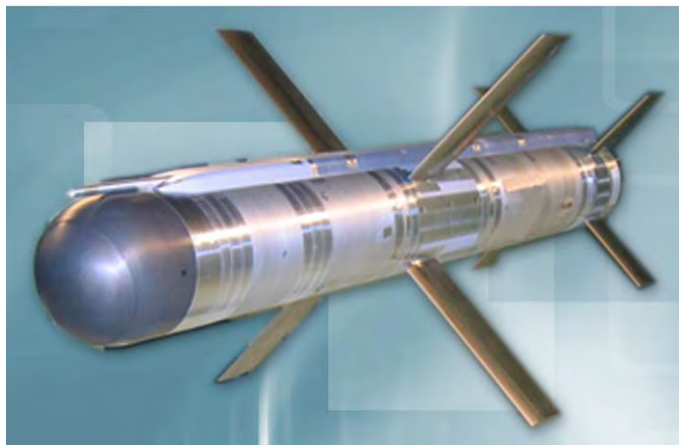
- Large multi-mode warhead
- 7-inch diameter 120 lb class
- Range 0-40 kilometers
- Effective against moving and stationary targets
- In-flight updates, retargeting and image capabilities
- Target sets
  - Light armor
  - Heavy armor
  - Bunkers
  - Fortifications



PAM Warhead Effectiveness



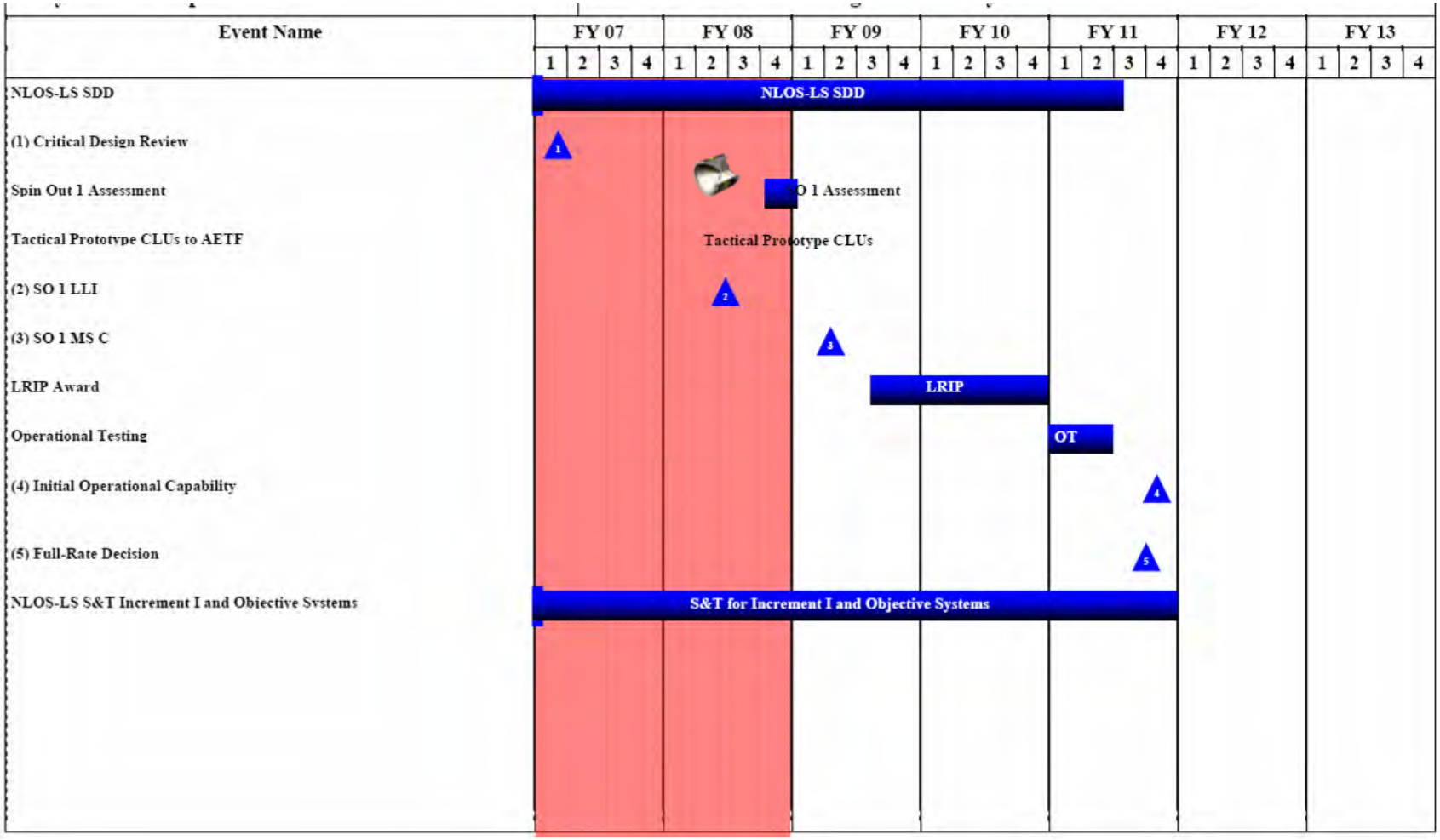
PAM Seeker Image of Land and Sea Targets



Distribution Statement A – Approved for public release 242-2008

Raytheon
PO Box 11337
Tucson, AZ 85724-1337

Program Schedule



GENERAL DYNAMICS
Ordnance and Tactical Systems

Raytheon

PO Box 11337
Tucson, AZ 85724-1337

Distribution Statement A – Approved for public release 242-2008

Multimode Warhead Challenges

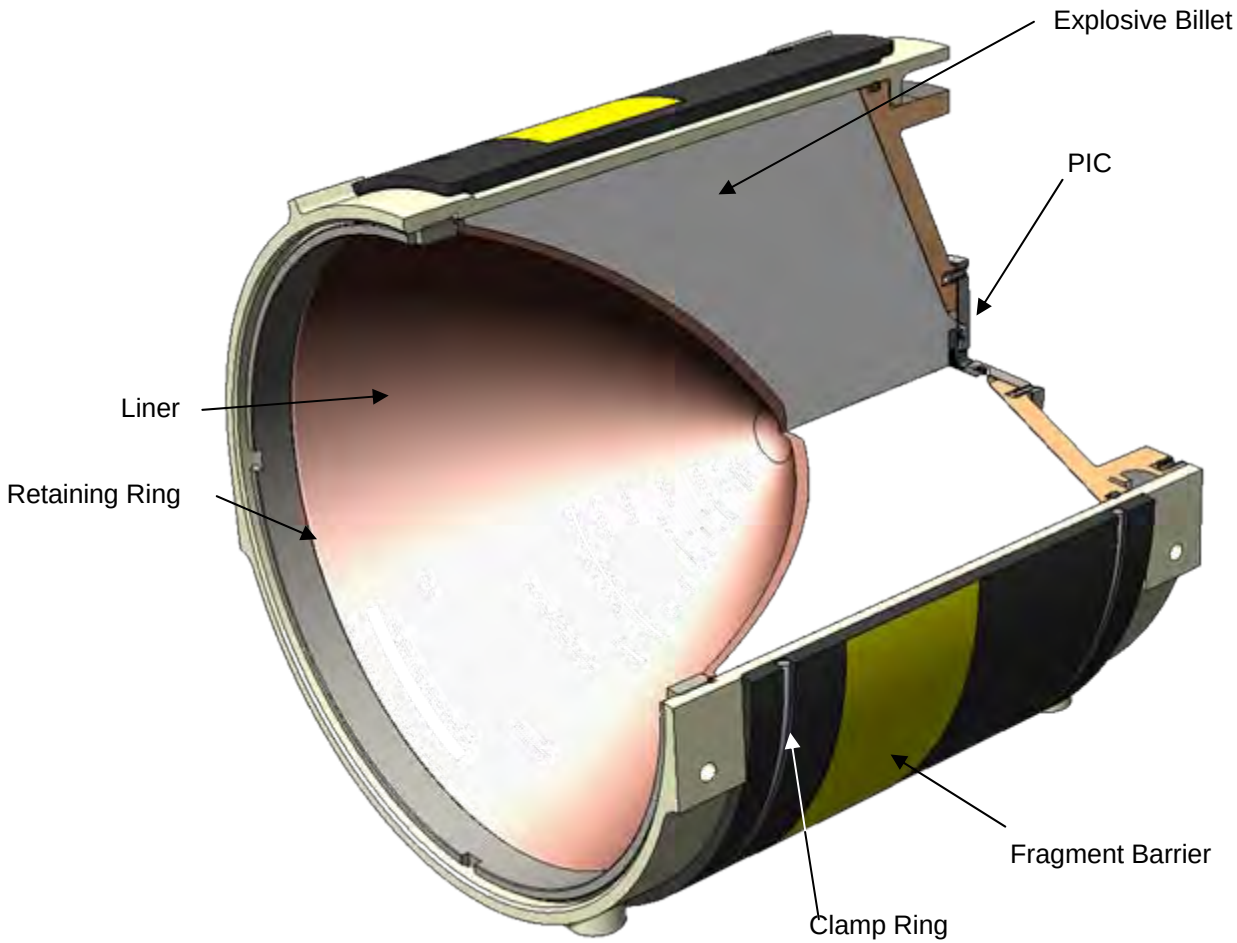


- Short Stand-Off
- High Penetration Performance
- Strict IM requirements
- Cost as a Key Performance Characteristic
- Small Envelope
- Evolving Requirements

Distribution Statement A – Approved for public release 242-2008

Raytheon
PO Box 11337
Tucson, AZ 85724-1337

Warhead Overview



Distribution Statement A – Approved for public release 242-2008

Raytheon
PO Box 11337
Tucson, AZ 85724-1337

Warhead Development



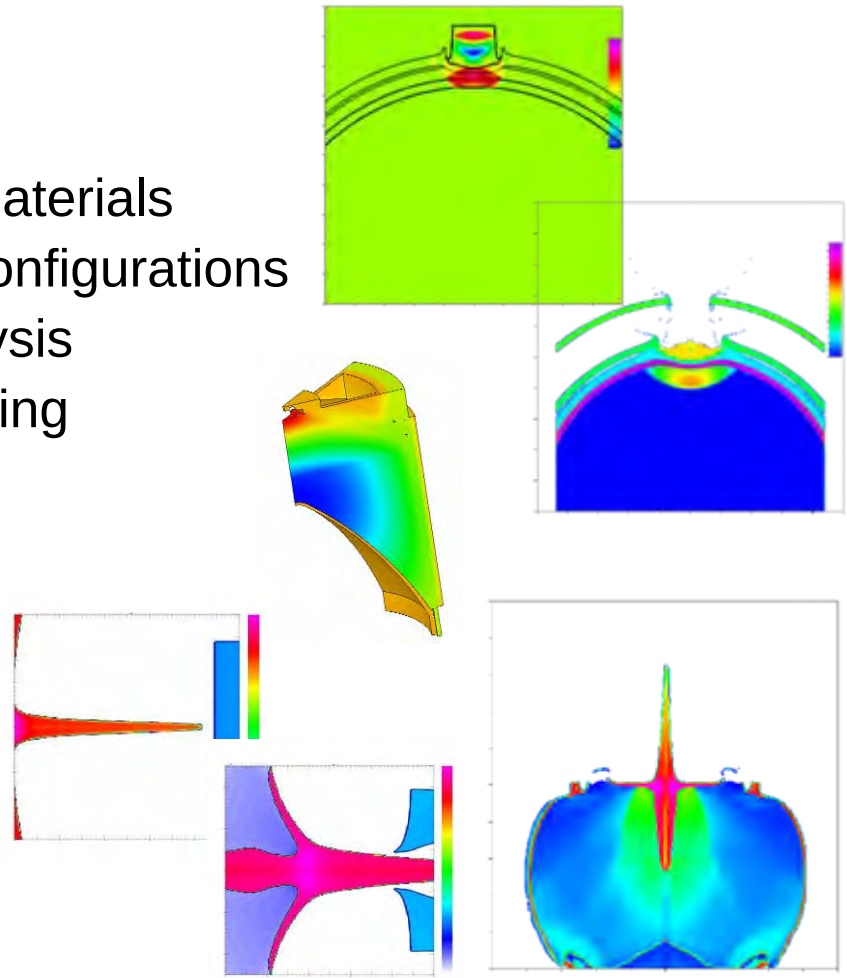
- Competitive Risk Reduction Effort
  - Trade Studies
    - Explosive Material (Penetration Performance vs. IM Performance)
    - Casing Design (Materials to reduce sensitivity to Fragment Impact)
    - Liner Material Study (Penetration Performance vs. Cost)
  - Analysis
    - Penetration Performance (Hydrocode)
    - Seeker Keep Out Zone
  - Testing
    - Jet Characterization
    - RHA and Armor Targets (Penetration Performance)
    - Soft Targets (Arena and Bunker Testing)
    - Insensitive Munitions Testing (Slow Cook-Off and Fragment Impact)
- Followed by the Detail Design Phase

Distribution Statement A – Approved for public release 242-2008

Raytheon
PO Box 11337
Tucson, AZ 85724-1337

Modeling & Simulation

- Fragment Barrier Analysis
  - Understanding the Physics
  - Study the effects of different Materials
  - Study the effects of different configurations
- Slow Cook-Off Performance Analysis
  - Design Features to Allow Venting
  - Thermal Analysis
- Penetration Performance
  - 2D Hydrocode
  - Optimize Design
- Jet Characteristics
  - 3D Hydrocode
  - Ensure Straightness of Jet



Distribution Statement A – Approved for public release 242-2008

Raytheon
PO Box 11337
Tucson, AZ 85724-1337

PAM Warhead Performance

Key Characteristic	Performance
Range target penetration depth	
Range target penetration diameter	
RHA penetration	
Mass	
Design to cost	

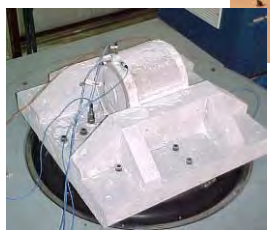
Distribution Statement A – Approved for public release 242-2008

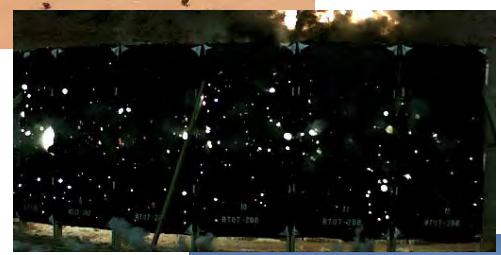
Raytheon
PO Box 11337
Tucson, AZ 85724-1337

Performance Testing

- Tested 5 Different Design Variations
- Conducted over 100 Explosive Tests
  - Arena Testing
  - Jet Characterization
  - RHA Penetration
  - ERA Target Penetration
  - Environmental Testing
  - Behind Armor Debris Testing
  - Reliability (Vari-Comp)

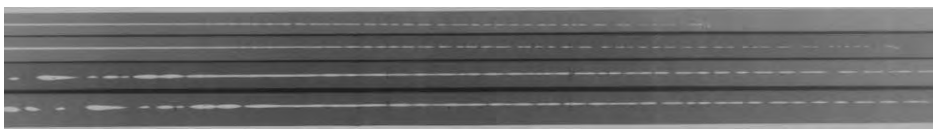














IM Testing













Threat	Test Results
Fast Cook-off	Type V
Slow Cook-off	Type V
Bullet Impact	Type V
Fragment Impact	Type V
Sympathetic Detonation	Type V*
Shaped Charge Jet	Type I*

*=Expected

Production Readiness



- Lean Design Effort
  - Use Low Cost Materials
  - Reduction of the number of Parts
  - Incorporation of Molded Components
  - Detail tolerance stack up analysis to optimize tolerances
  - Work with each component Vendors on reducing Cost Drivers
  - Streamline Assembly Process
- Early Development of Acceptance Testing
  - Perform Lot Acceptance Tests (LAT) to Characterize Variation
- Control of Critical Characteristics
  - Characteristics that mostly control performance variation
- Pilot Production Line incorporated on Qualification Build

Distribution Statement A – Approved for public release 242-2008

Raytheon
PO Box 11337
Tucson, AZ 85724-1337

Design Challenges



- Striking a Balance between Low Cost and High Performance
- Integrating Production Processes early on
- Mitigating Fragment Impact and Slow Cook-Off Hazards
- Maintain Performance with Environmental Factors
- Incorporating Environmentally Compliant Processes and Products

Distribution Statement A – Approved for public release 242-2008

Raytheon
PO Box 11337
Tucson, AZ 85724-1337

Acknowledgements



- Raytheon Missile Systems
  - ➢ Bill Zarr
- ARDEC
  - ➢ Darin Kielsmeier

Distribution Statement A – Approved for public release 242-2008

Raytheon
PO Box 11337
Tucson, AZ 85724-1337



DEFENCE R&D DÉFENSE

Ballistic Performance Assessment of Lightweight Body Armour Material Systems Against IED Threats

by

G. Pageau, Scientific Advisor ISSP
K. Williams, PM AMMPHS TDP, DRDC-Valcartier
D. Bourget, GL PPE Group, DRDC-Valcartier
C. Hedge & M. Cheng, Allen-Vanguard
B. Anctil, Biokinetics Ltd

24th International Symposium on Ballistics
22-26 Sept. 2008, New Orleans, LA, USA



Canada

Overview

- Background
- Goal/approach
- Threat comparison
- Protection levels options
- Test results
- Summary
- Future work
- Questions

Background

- Military soft armors mainly designed to defeat lower mass/velocity fragments from warheads detonating at large distances
- Bullet resistant rigid armors mainly designed to defeat standard rifle bullets fired at close distances, with no fragment resistance specified
- Ballistic threat spectrum wider and more complex
- PPE (soft & hard) not designed and neither specified to protect against blast effects and fragments impacts from IEDs

Goal

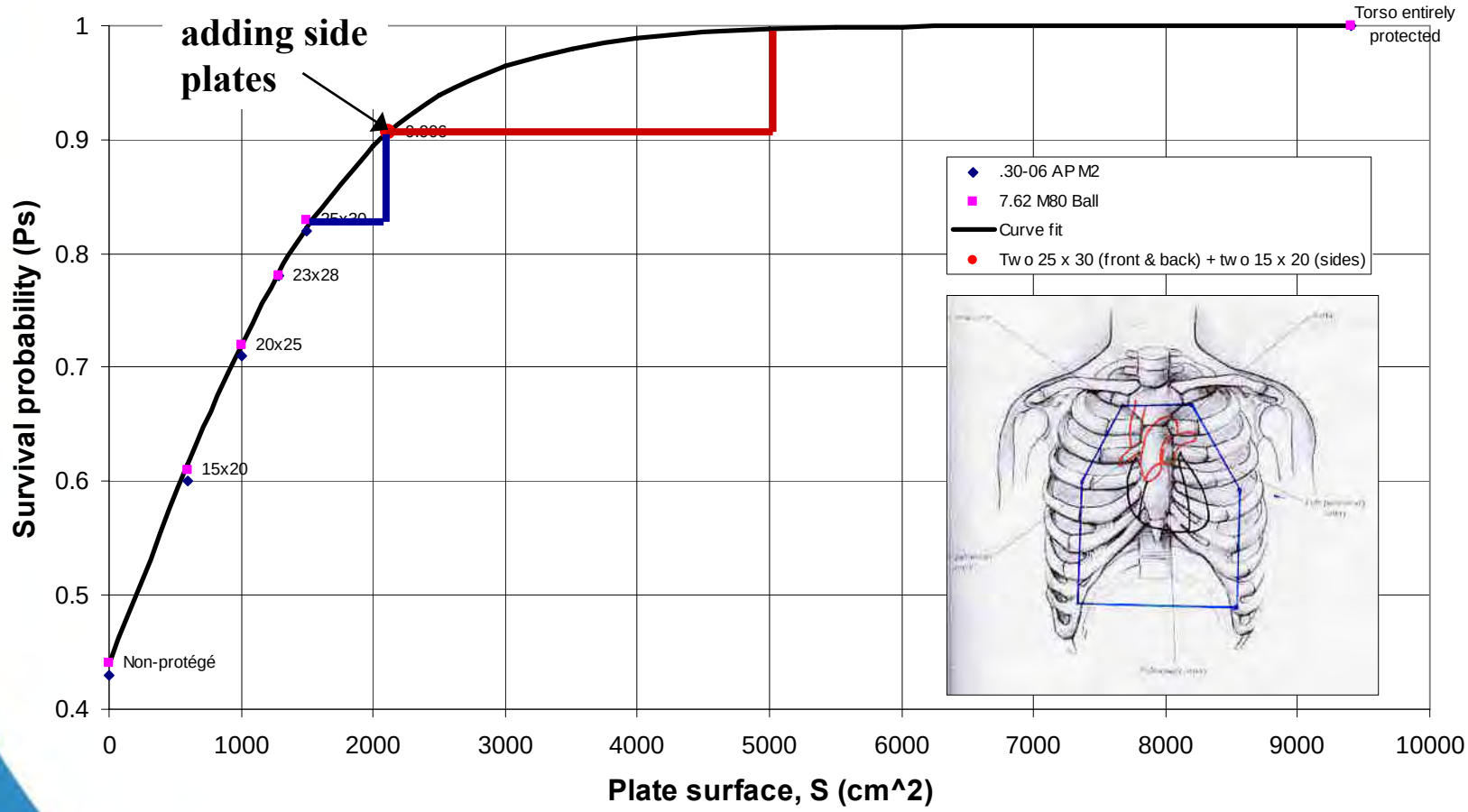
- Increase soldier survivability against IED threats at no extra PPE weight

Approach

- Reduce current PPE weight:
  - Soft Armour:
    - 20% weight saving with same requirements
    - 30% weight saving with lower requirements
  - Hard Armour:
    - 20% weight saving with same requirements
    - 30% weight saving with lower requirements
- Apply weight savings to better match the threat
  - Provide novel IED specific armour components

Torso Coverage Study

- Desirable: uniform coverage of vital organs



Threat Review: Fragments

- Natural fragmenting munitions
  - Large number of fragments (7000-14000) of all sizes (0.5 to 500 gr)
  - Made of steel typically, 30 Rc hardness
  - Initial velocity from 1000 to 1800 m/s
  - L/D or shape factor variable typically 0.5 to 1.1
- Pre-formed fragmenting munitions
  - Spheres:
    - Mines: 7/32 in sphere (0.7 grams)
    - Grenades: 2.5-3.0 mm sphere (0.12 grams)
  - Cubes, steel or tungsten
- Controlled fragmentation

IED Threat Implications

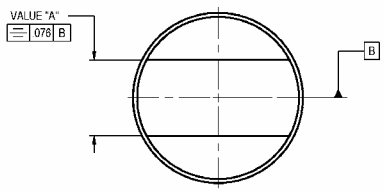
- **Closer proximity from detonation**
  - Higher fragment density & velocity
  - At short range: blast arrive before fragments thus the need for live field tests
  - Fragment impact about simultaneous
  - More frequent negative impact angle
  - Larger fragment variability
    - Size, shape, material

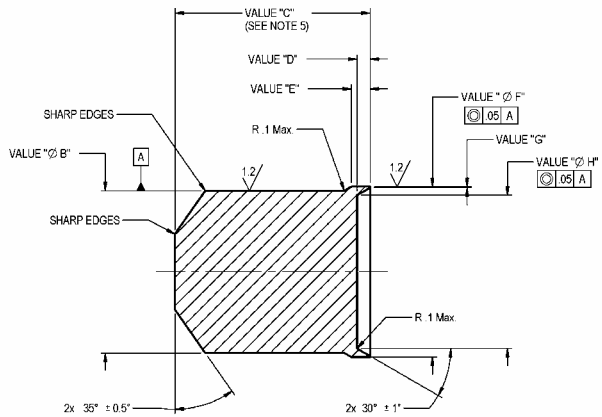
Fragment Surrogates

- Primary fragments:
  - FSP 1.1-g chisel nose, L/D = 1
    (MIL-P-46593 & Stanag 2920 & 4569)
    - Skirted vs unskirted versions
  - RCC flat nose (L/D = 1 or L/D < 1)
    - Required for CRA (Vs-Vr data)
    - Std sizes: 2, 4, 16 and 64-gr, (128-gr)
    - Based on DeLuca work at AAMRC (Vs/Vr match)
- Secondary fragments:
  - Behind armor debris FSP, shorter, L/D = 0.4 (rarely used)
- Possible to design special size for custom threats using homogeneous scaling

Fragment Simulating Projectiles (FSP)
(STANAG 4569)

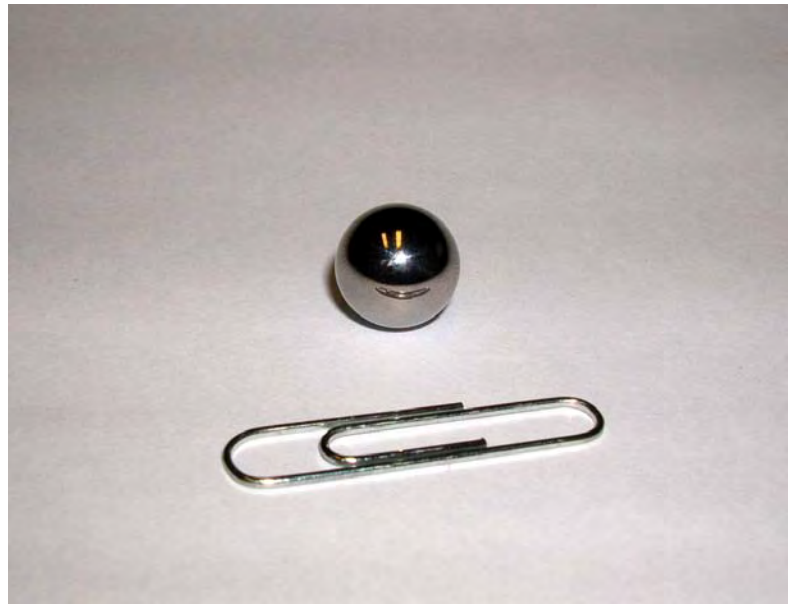
Fragment Simulator	Weight (grains)	A (mm)	Ø B (mm)	C (mm)	D (mm)	E (mm)	Ø F (mm)	G (mm)	Ø H (mm)
FSP 1: 5.56 mm	17±0.5	2.54-0.3	5.46±0.02	6.52	0.4±0.05	0.6±0.05	5.72+0.05	0.08±0.04	5.0±0.1
FSP 2: 7.62 mm	44±0.5	3.45-0.3	7.52±0.02	9.30	0.73±0.05	0.86±0.05	7.87+0.05	0.12 max	6.93±0.25
FSP 3: 9 mm	64±0.5	4.03-0.3	8.69±0.05	9.17	0.4±0.05	0.6±0.05	9.04+0.05	0.12 max	8.42±0.05
FSP 4: 12.7 mm	207±2	5.69-0.4	12.83±0.05	15.24	1.15±0.05	1.47±0.05	12.75+0.08	0.13 max	11.43±0.05
FSP 5: 14.5 mm*	322±2	655-0.4	14.40±0.05	18.00	1.36±0.05	1.68±0.05	15.01+0.08	0.15 max	13.25±0.12
FSP 6: 20 mm	830±4	9.27-0.4	19.89±0.05	24.00	1.62±0.05	2.31±0.05	20.83+0.08	0.2 max	18.80±0.12



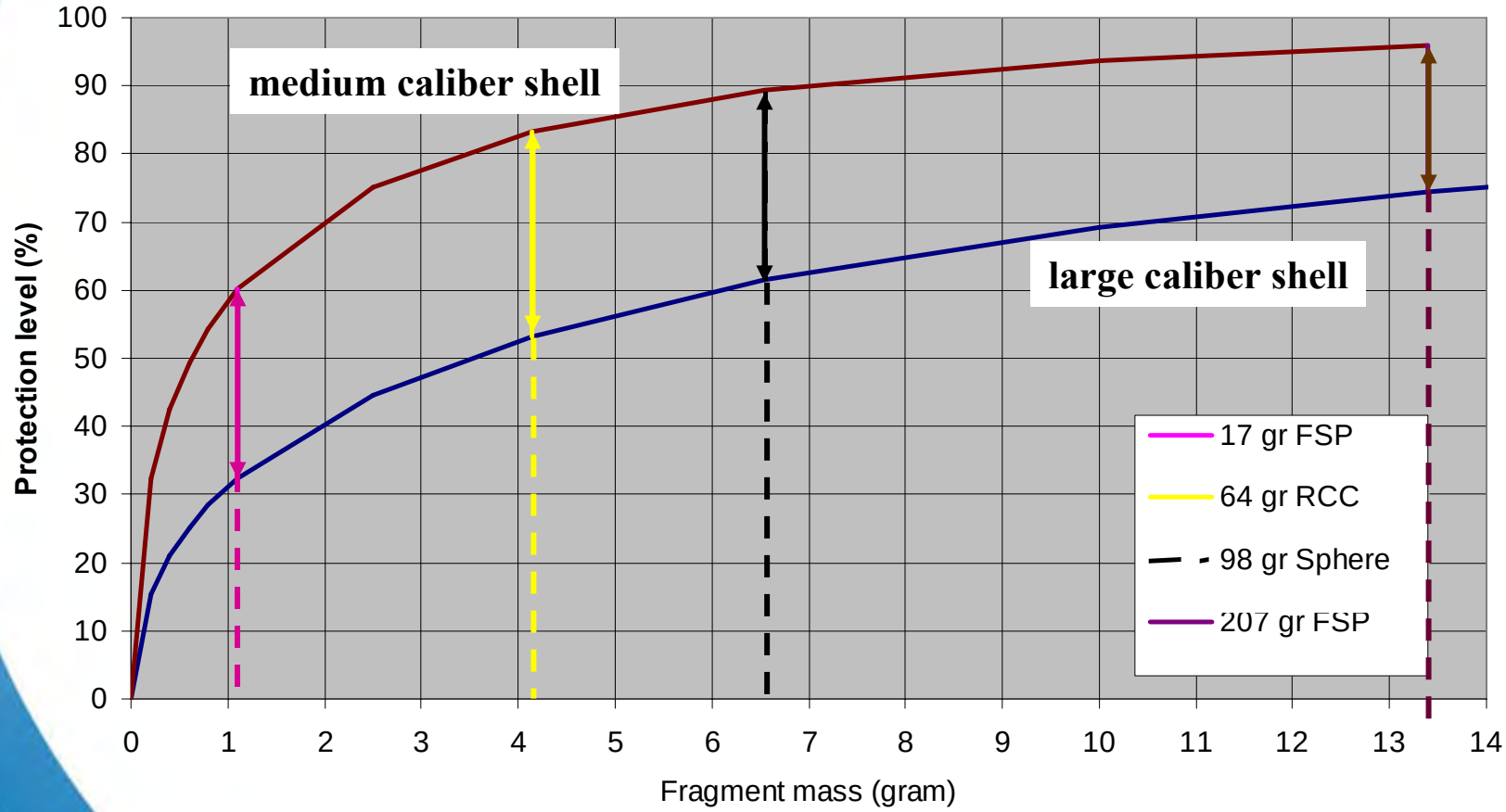


96-gr Sphere Fragment

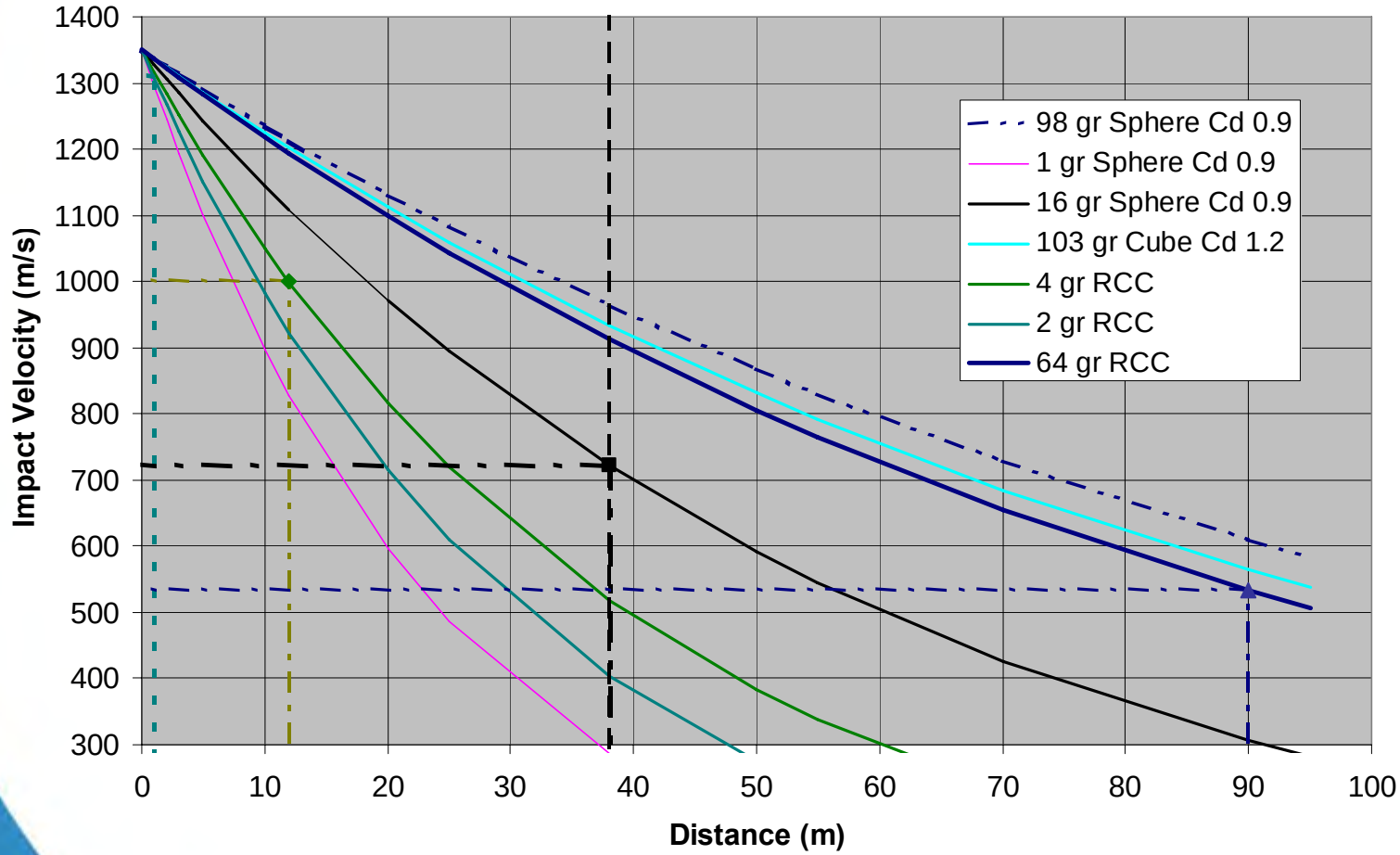
- 11.5 mm diameter, steel HRC 60
- Dimensions, shape & weight very consistent
- Easily available at low cost
- Easily launchable, i.e.: no issues with:
  - sharp edges & hardness
  - flight stability (no yaw)
- More relevant to IEDs & controlled fragment munitions:
- Fill weight gap between 64 gr RCC & 207 gr FSP



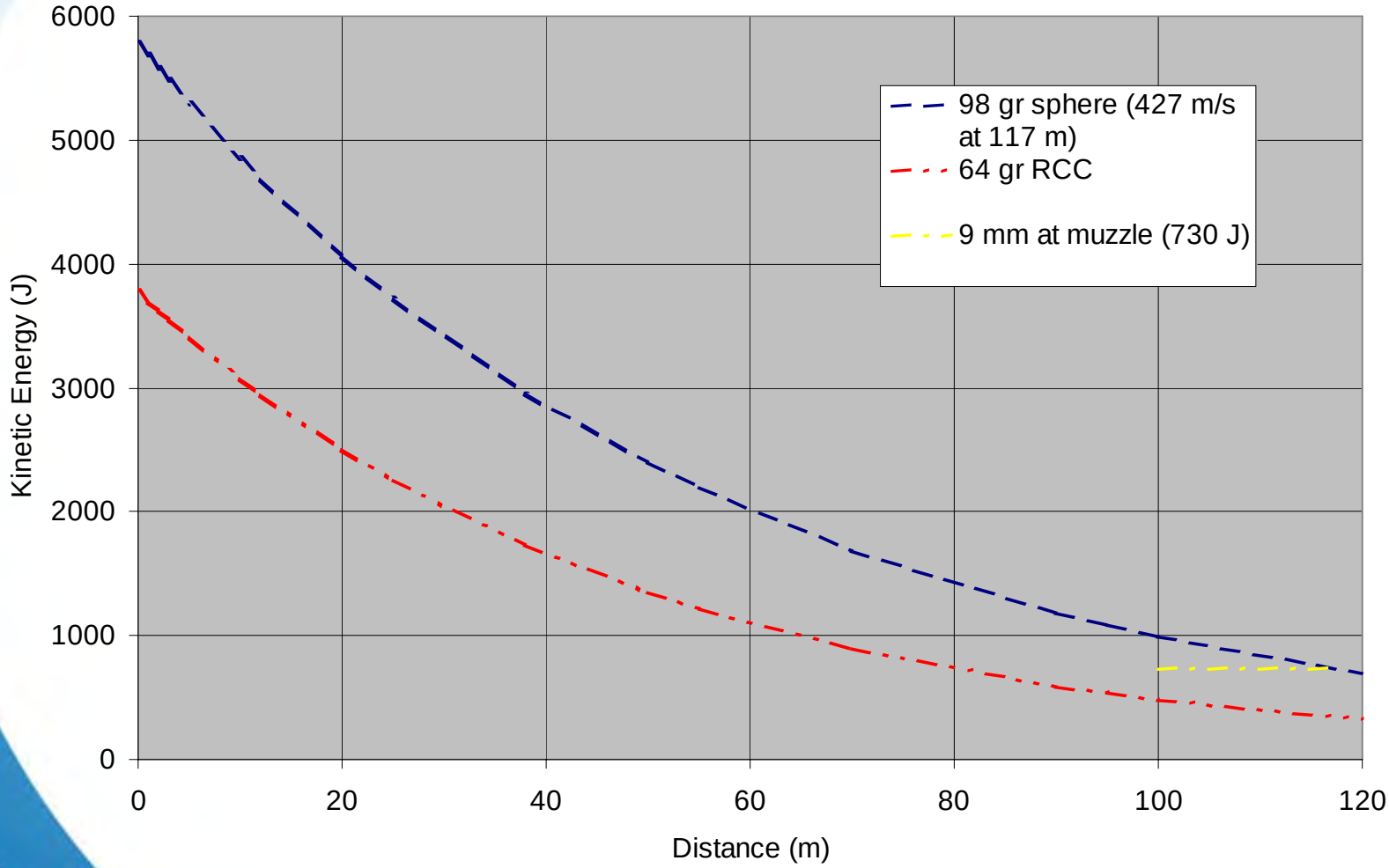
Protection Level vs Fragment Size



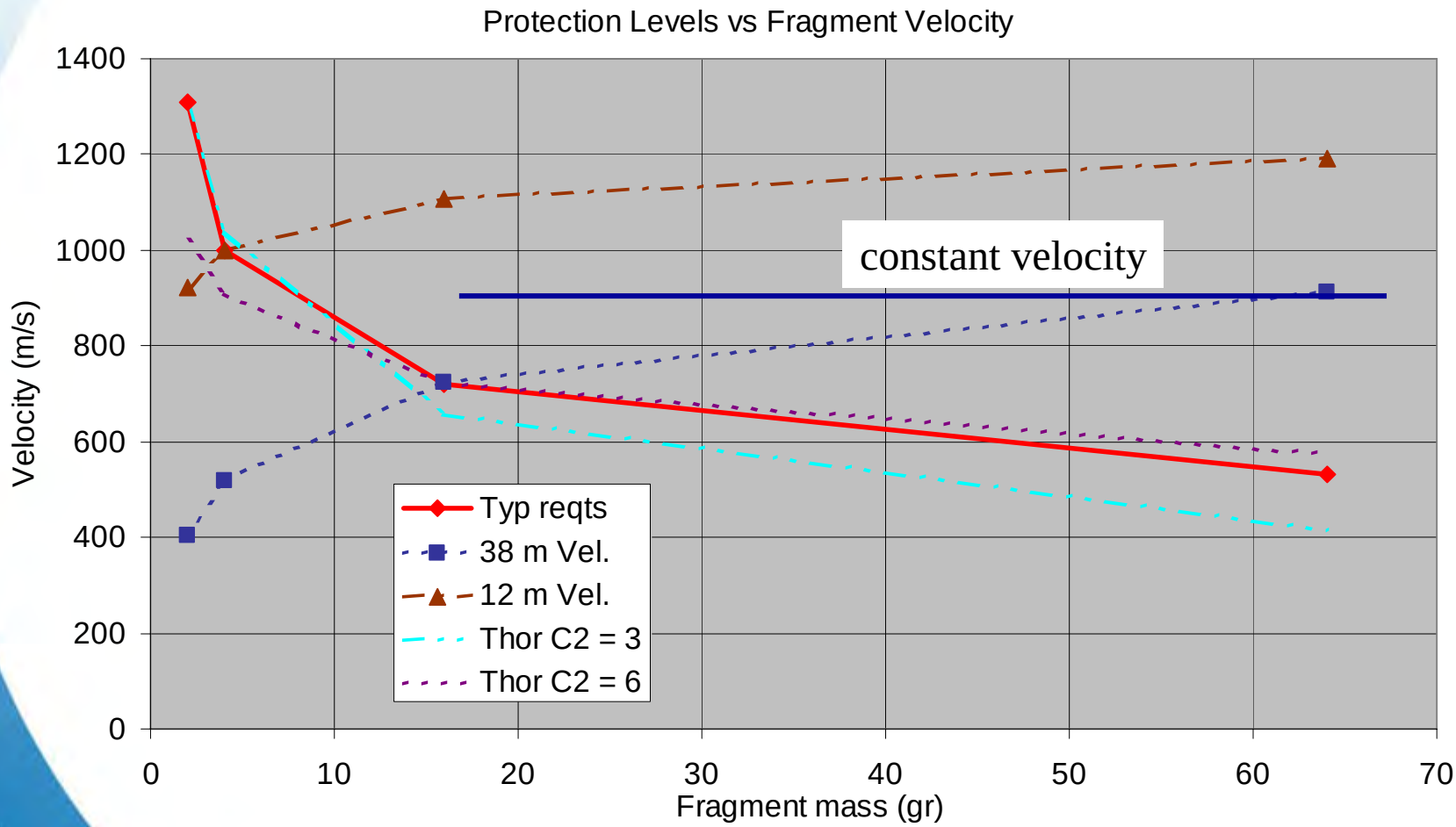
Velocity Decay vs Fragment Mass & Shape



Kinetic Energy Comparison



Threat Velocity Specifications



Test Projectiles

- **Fragments:**
  - 16 gr sphere
  - **96 gr sphere 1000 m/s**
  - 17 gr FSP
  - (207 gr FSP)
- **Bullets:**
  - 9 mm FMJ NIJ level 2
  - 5.56x45 SS109 STANAG level 1
  - 7.62x51 M80 NIJ level 3



Soft Armor Targets
(AD 2.5 kg/m^2)

- Polyethylene (PE) felt
- Aramid fabrics
  - K129
  - KM2
  - Special
- Hybrids






Typical samples photos

Hard Armor Targets
(AD 20 kg/m^2)

- Metallic
  - Aluminum (6061 & 7075-T6)
  - Magnesium (AZ31B-H24)
  - Titanium (Ti-6Al-4V)
- Polyethylene unidirectional composites (PEA, PEB, PEC)
- Metallic/composite
- Ceramic/composite (Plates)
- Hybrid (S-Glass, PE, Aramid + Ti & Al)



Metallic plate



Aluminum (front)



Magnesium (back)

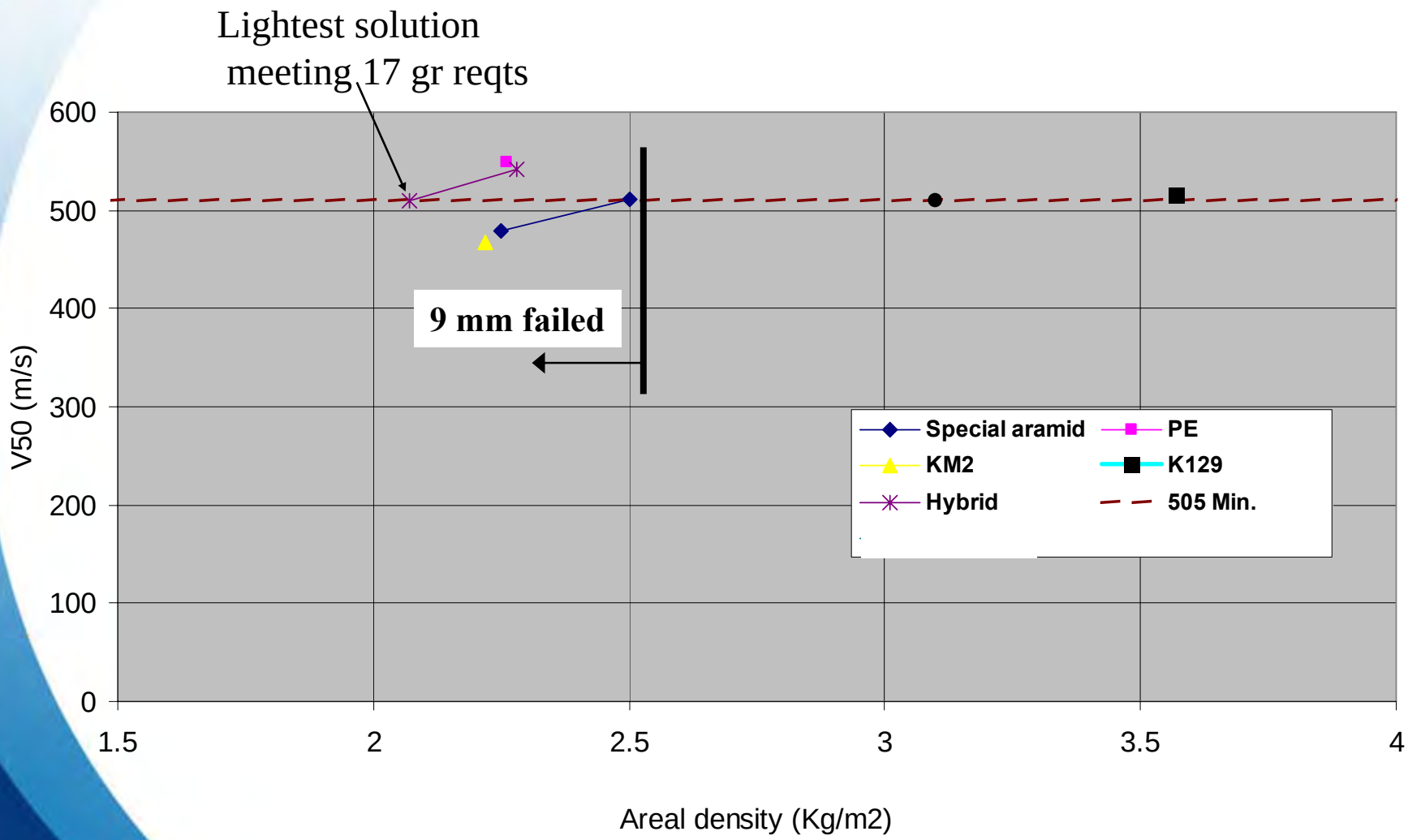
Test Conditions

- 38 x 38 cm samples
- Rigid armour targets tested stand-alone
- Some combinations tested in conjunction with soft armour
- Limited tests done at obliquity

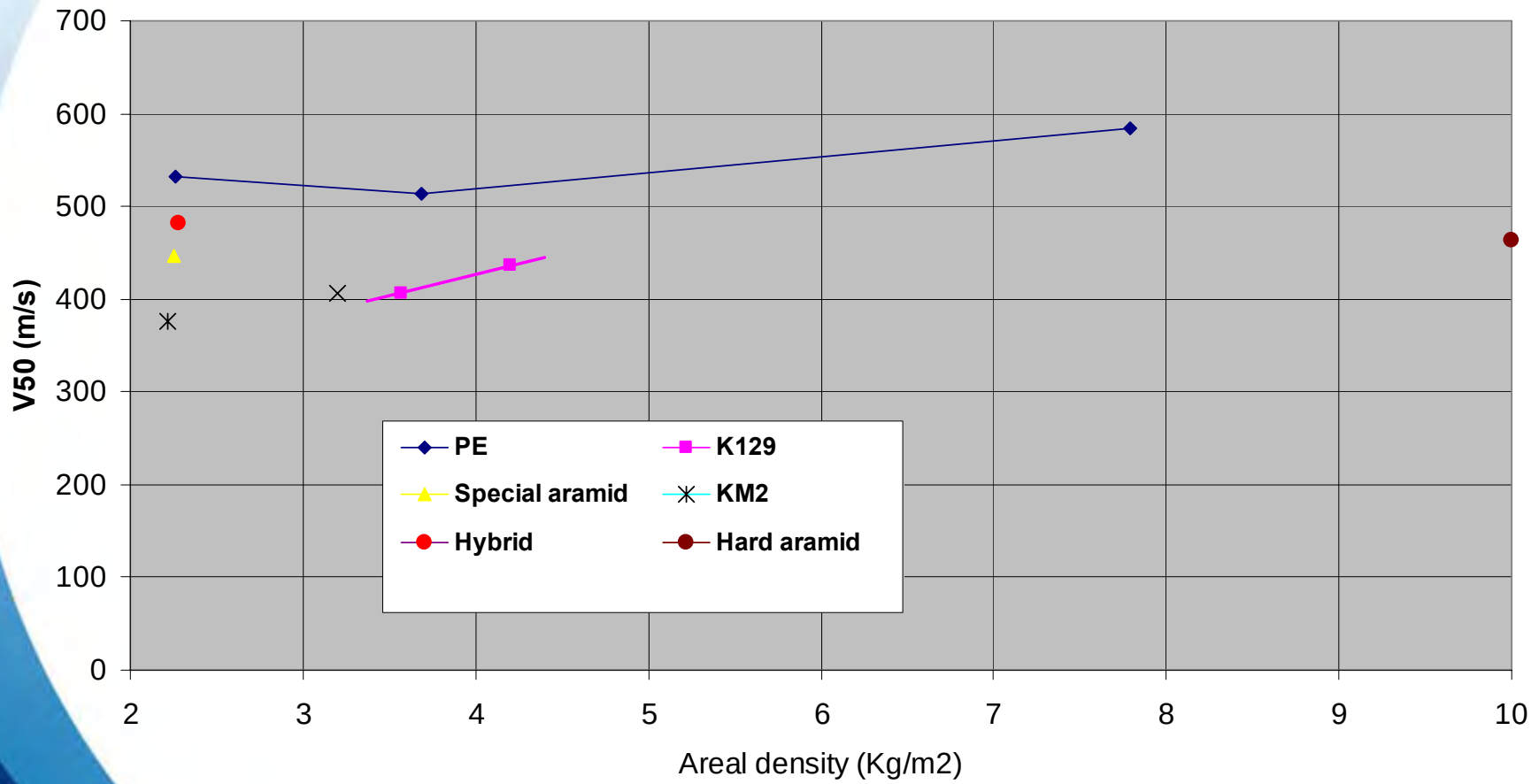
Test Types

- V50 (6 shots)
- Teta 50
- Vproof and backface
- Targets supported on Minicell foam support except for Vbfs using plastilina block

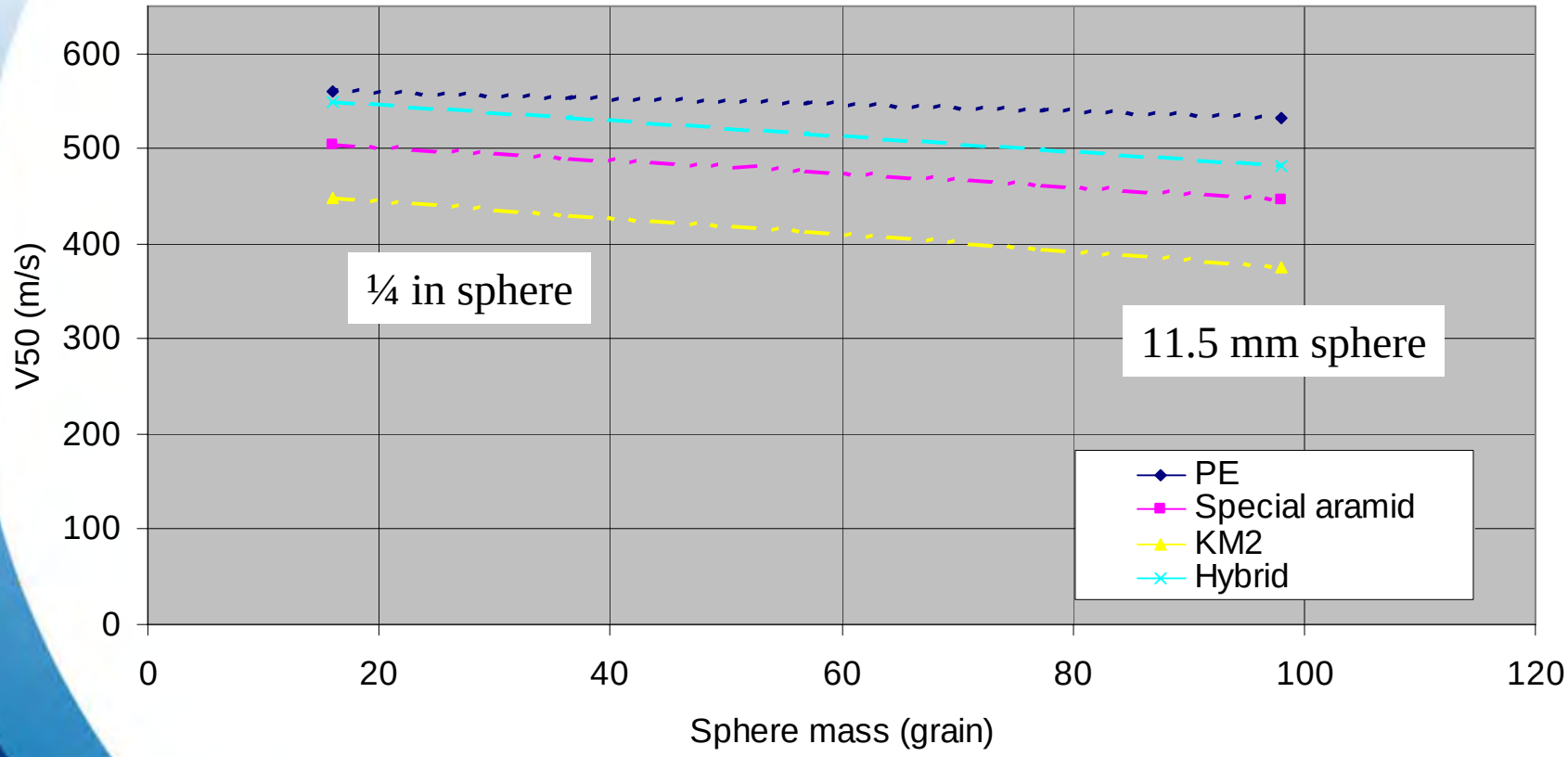
Soft Armor Performance (17-gr FSP)



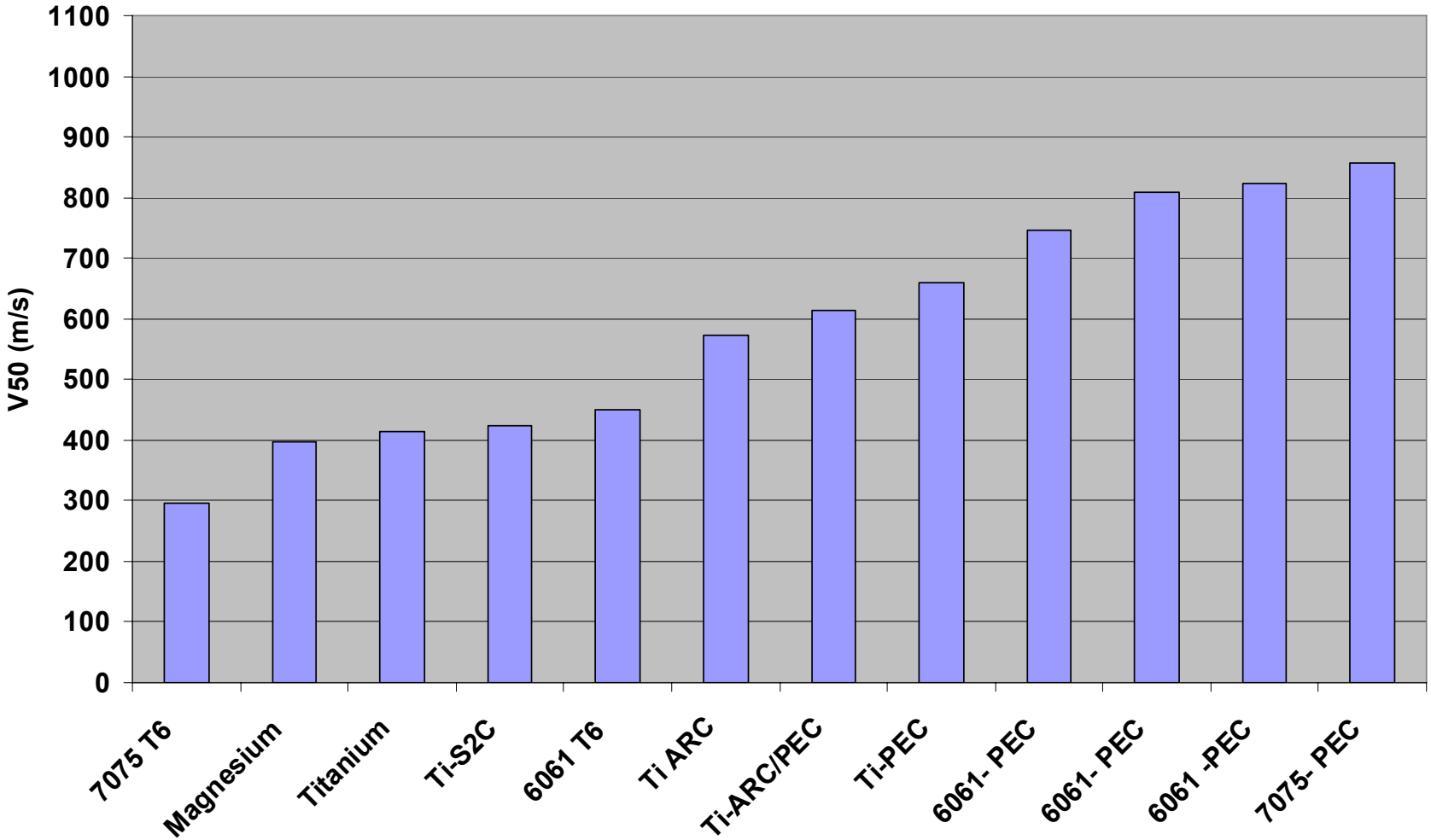
Soft Armor Performance
(96-gr Sphere)



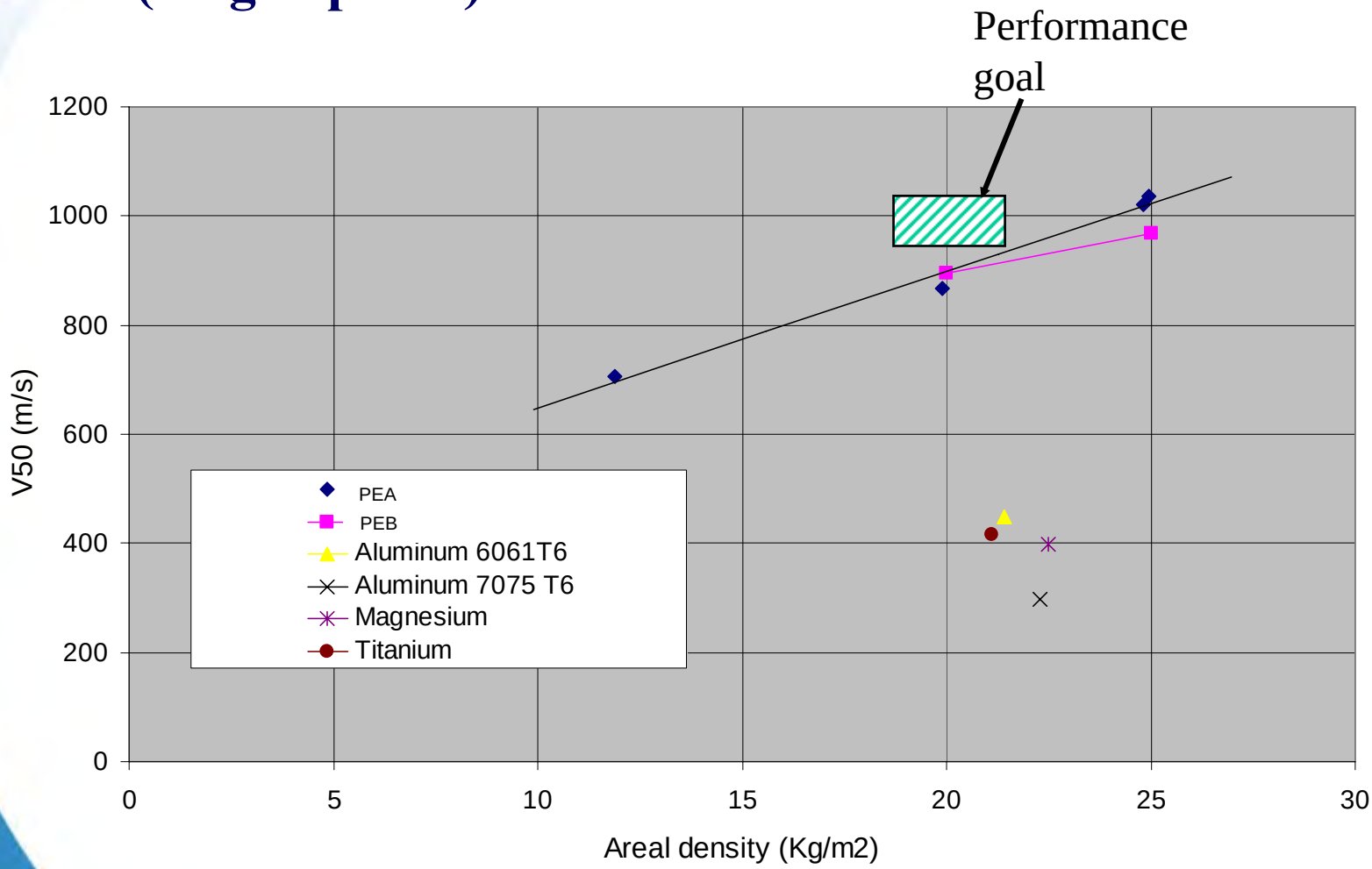
Soft Armors Results vs Sphere Mass



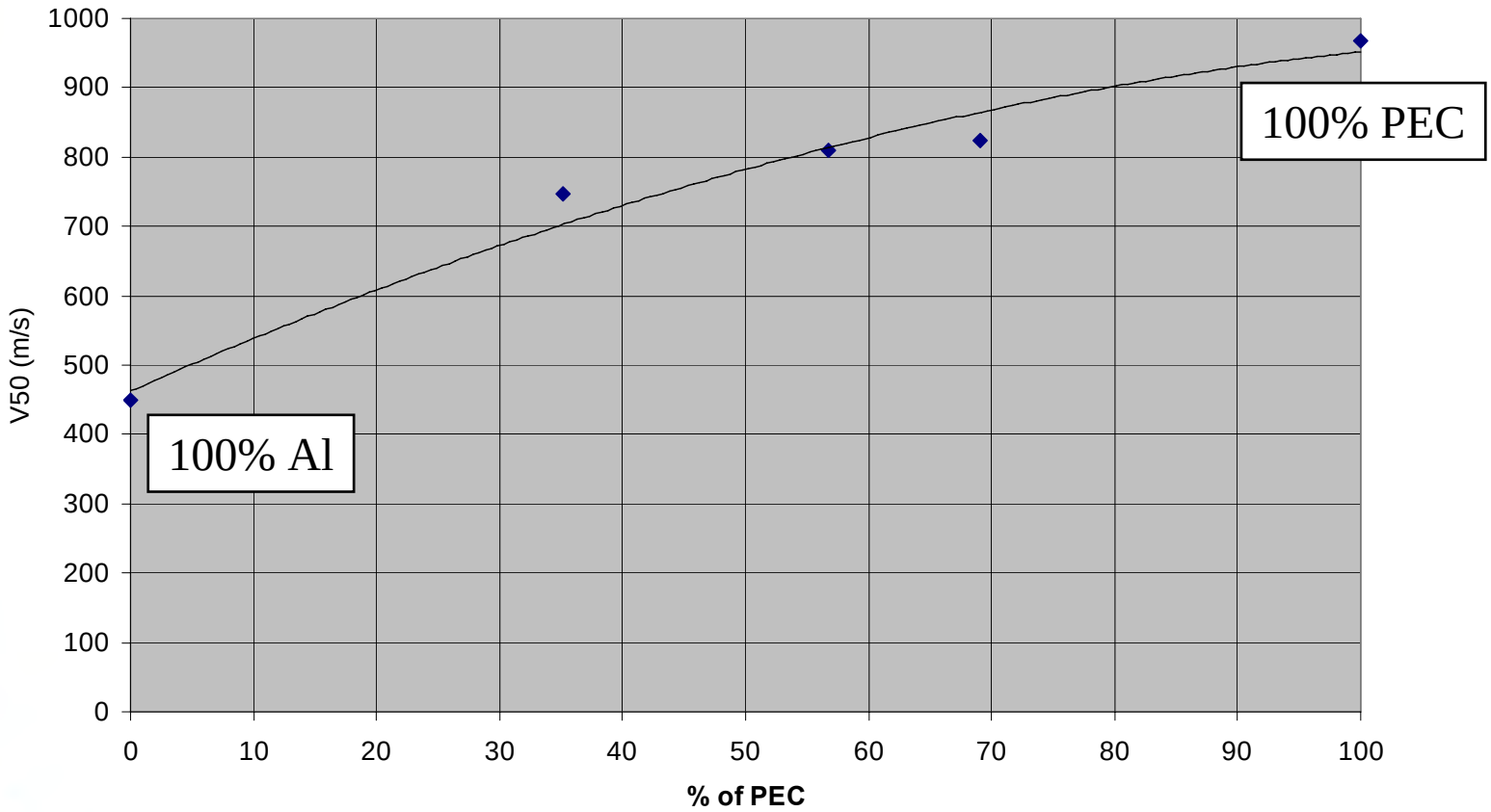
Hard Armor Performance Comparison
(AD 20 Kg/m2)



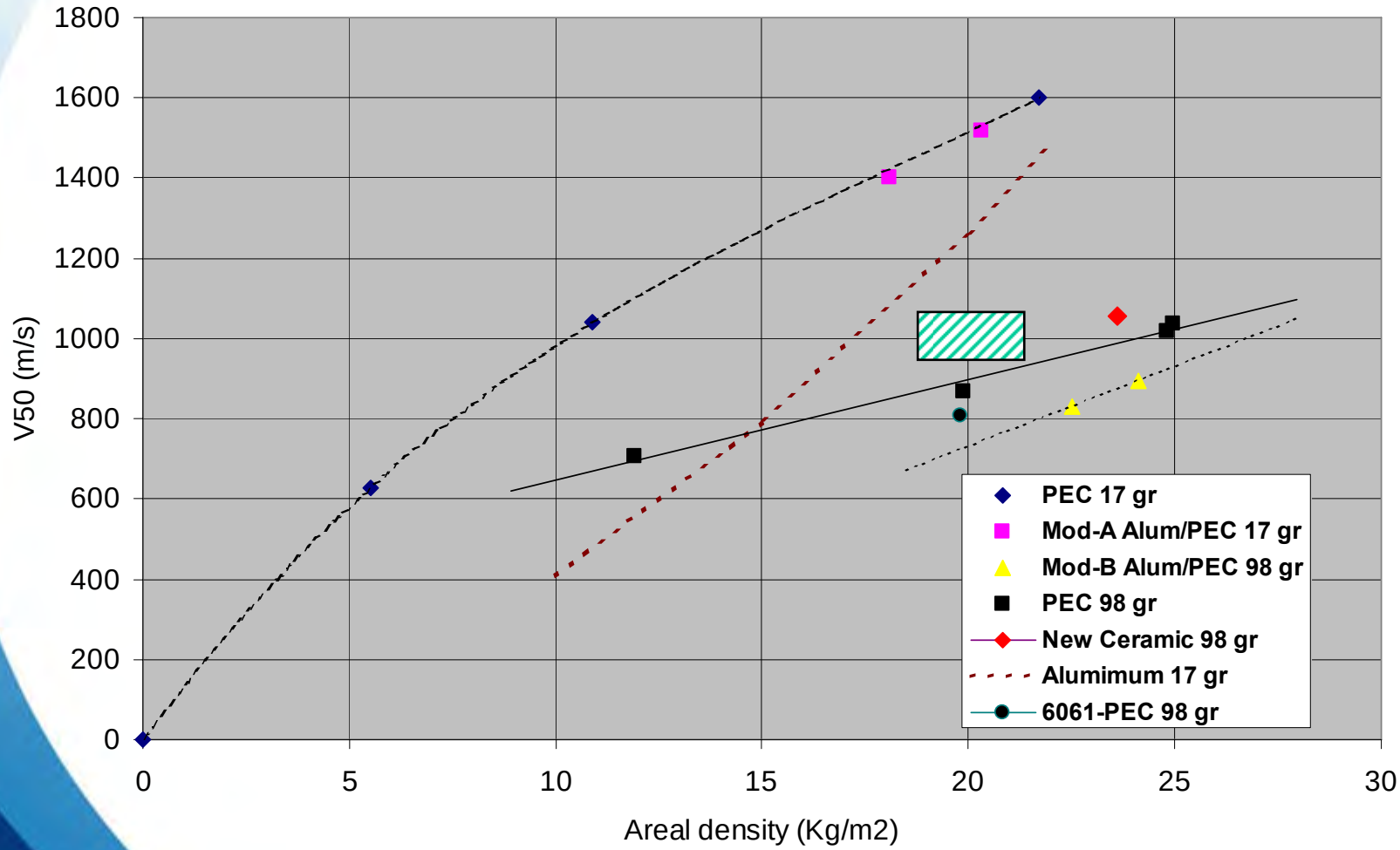
Hard Armour Performance
(96-gr Sphere)



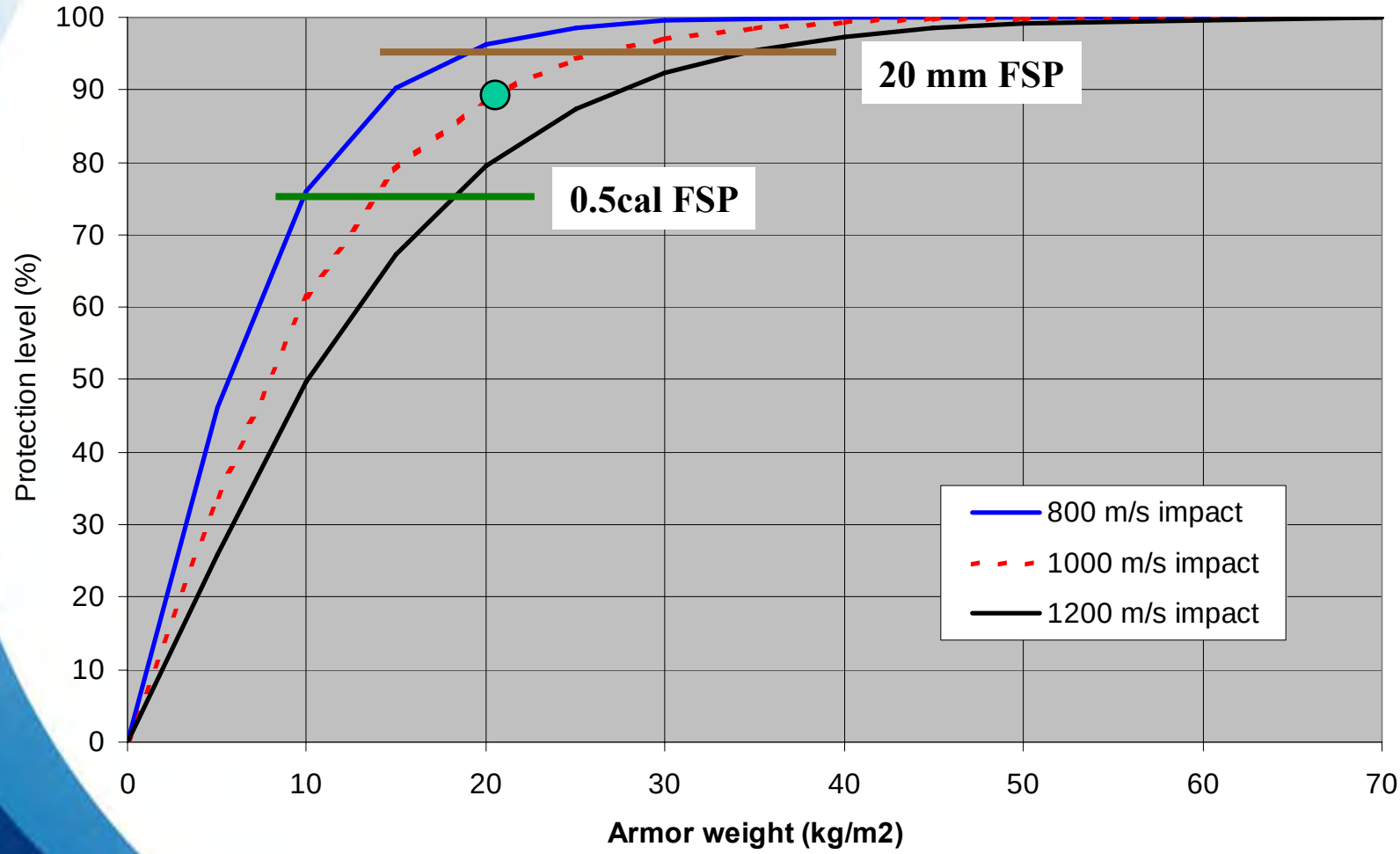
Aluminum/PEC Ratio Study
(96-gr sphere)



Special Hard Armor Configurations
(17-gr and 96-gr fragments)



Protection Level vs Weight & Velocity



Summary

- The 96-gr sphere demonstrated as a viable IED laboratory fragment
- Promising results obtained with some novel armor systems
- Large effects of protection level selected on resulting armour weight
- Level 3+ plate performed quite well vs. fragments & bullets
- Lighter material solutions needed for allowing greater armor coverage & higher protection with no weight penalties
- Trade-off analysis not trivial as many parameters involved

Future work

- Validate performance goals & metrics
  - threat parameters
  - protection/survivability level(s)
  - body coverage
- Conduct detailed trade-off analysis (integrated vs modular vs scaleable)
- Study resulting blast mitigation capabilities
- Further explore new materials and concepts
- …

Key Performance Parameter:
Soldier Acceptance



Biography

Mr. Pageau joined Defence R&D Canada in 1981. He graduated from University of British Columbia with a master degree in Materials Science. He currently works as the scientific advisor for the Integrated Soldier Systems Project within the Directorate of Soldier Systems Program Management in Ottawa. He was exchange scientist at the Natick Soldier Center for two years.

PDF Complete
Your complimentary use period has ended. Thank you for using PDF Complete.
Click Here to upgrade to Unlimited Pages and Expanded Features

The Effect of Velocity on Jacketed Rod Efficiency

Brad Pedersen, Stephan Bless, Robert Fromm

24th International Symposium on Ballistics

New Orleans, Louisiana

September 2008

PDF Complete
Your complimentary use period has ended. Thank you for using PDF Complete.
Click Here to upgrade to Unlimited Pages and Expanded Features

Objective

RDECOM
TECHNOLOGY DRIVEN. WARFIGHTER FOCUSED.

The objective of this work was to determine the penetration performance of steel jacketed rods against armor steel (RHA) targets at velocities above 2.2 km/s.

This effort sought to extend the velocity range above the previously considered 2.2 km/s in an attempt to reach the penetration performance of tungsten rods.

PDF Complete
Your complimentary use period has ended. Thank you for using PDF Complete.
Click Here to upgrade to Unlimited Pages and Expanded Features

Introduction

RDECOM
TECHNOLOGY DRIVEN. WARFIGHTER FOCUSED.

This study consisted of hypervelocity experiments and supporting numerical simulations. Steel jacketed rods with core to jacket diameter ratios (mu) of 0.6 and 0.4 were investigated at nominal velocities of 2.6 and 2.8 km/s.

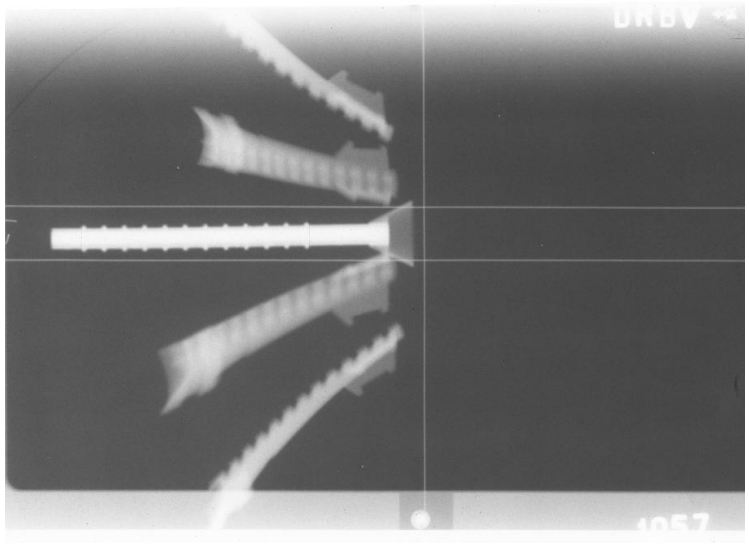
The results of the experiments were compared to the simulations for resultant crater size and normalized penetration (P/L).

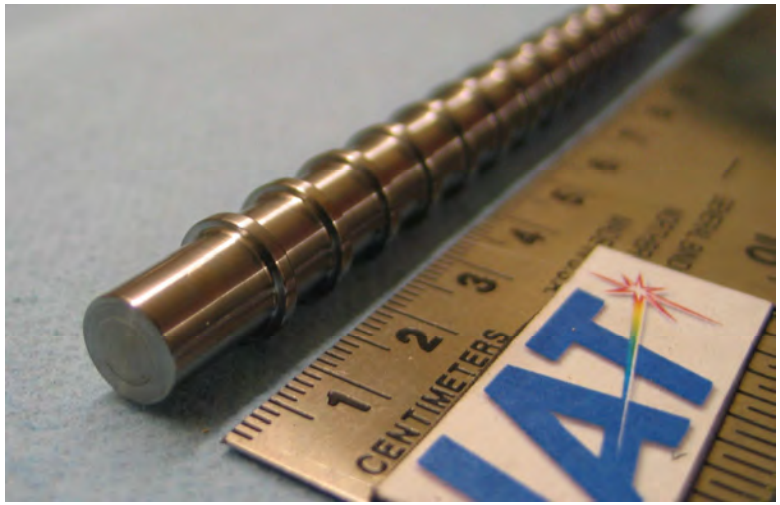
PDF Complete
Your complimentary use period has ended. Thank you for using PDF Complete.
Click Here to upgrade to Unlimited Pages and Expanded Features

Penetrators

RDECOM
TECHNOLOGY DRIVEN. WARFIGHTER FOCUSED.







<u>Materials</u>:
W-Ni-Co Core rod
4340 Steel Jacket
Co-based brazing alloy for bond

ID/OD Ratios (Mu): 0.6, 0.4
L/D = 15
Rod mass and length were constant
Velocities: ~2.6 and 2.8 km/s

PDF Complete
Your complimentary use period has ended. Thank you for using PDF Complete.
Click Here to upgrade to Unlimited Pages and Expanded Features

Penetration Channels

RDECOM
TECHNOLOGY DRIVEN. WARFIGHTER FOCUSED.

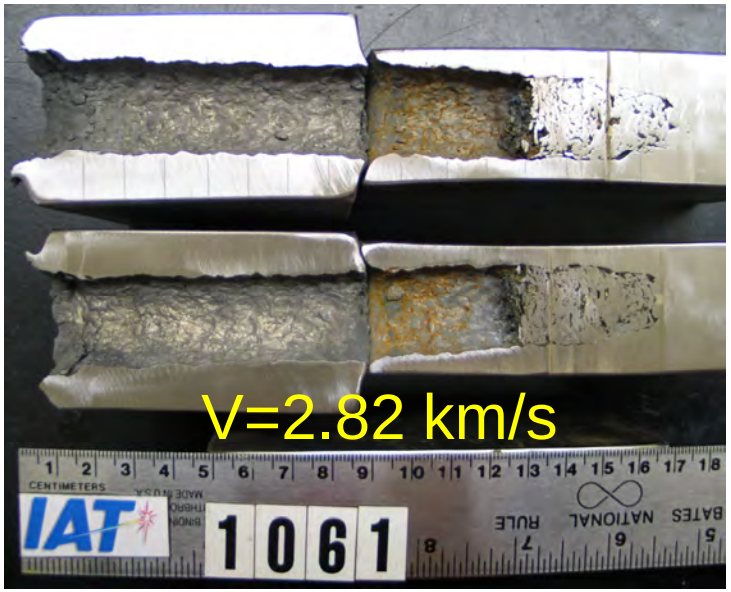
Mu=0.6





Mu=0.4





In general, the mu=0.6 craters were deeper but the mu=0.4 had larger crater diameters and more material in the bottom.

PDF Complete
Your complimentary use period has ended. Thank you for using PDF Complete.
Click Here to upgrade to Unlimited Pages and Expanded Features

malized Crater Diameter

RDECOM
TECHNOLOGY DRIVEN. WARFIGHTER FOCUSED.

A comparison of the normalized crater diameter (H/D) from the jacketed rod tests to the Bjerke* relation for tungsten rods was made. For the jacketed rod data, the crater diameter (H) was normalized by the jacketed rod diameter (D_j) and the diameter of an equal mass and length tungsten rod (D_e).

$$D_e = \left[D_c^2 \left(\left(\frac{1}{\mu^2} - 1 \right) \frac{\rho_j}{\rho_w} + 1 \right) \right]^{1/2}$$

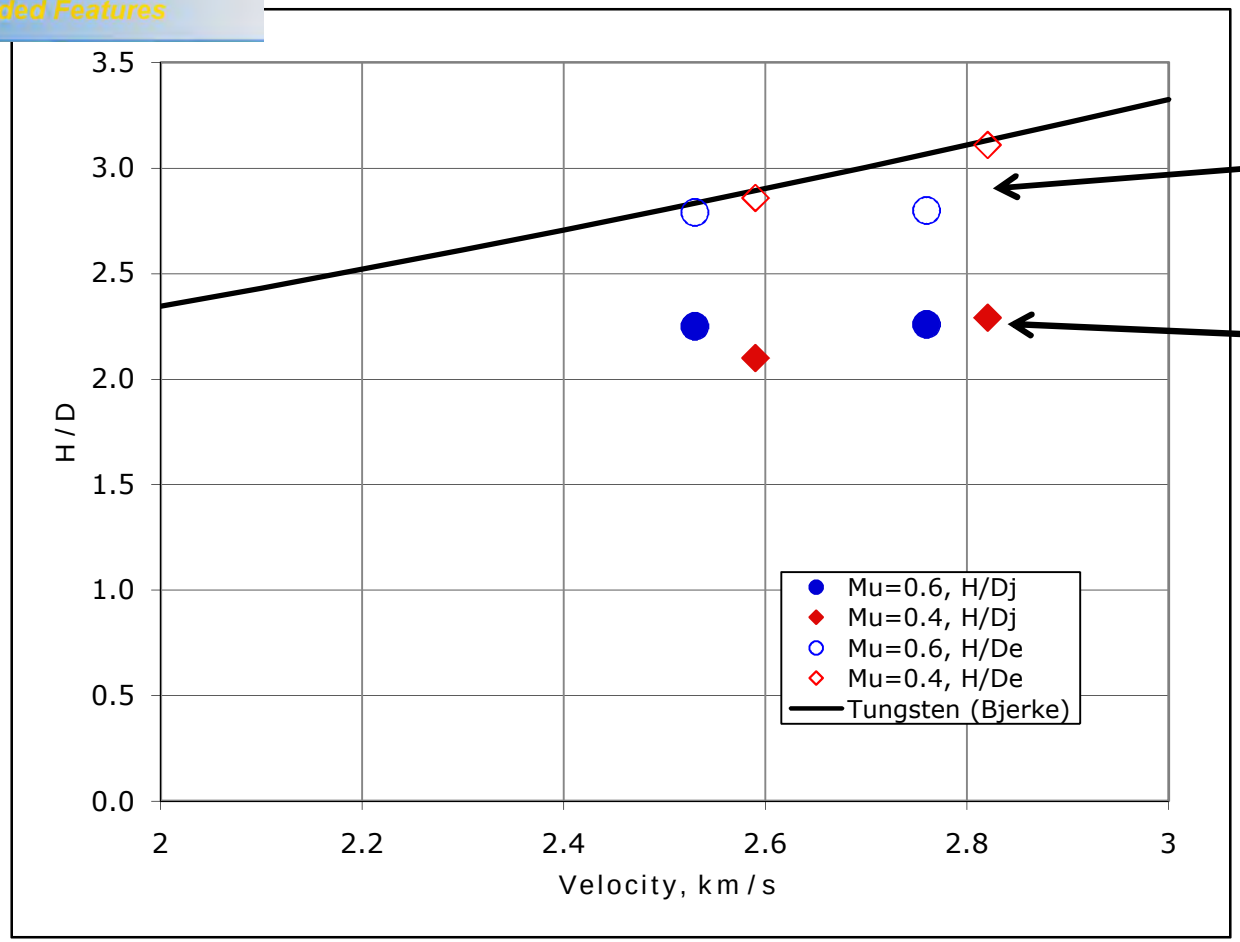
Average density

* Bjerke, Int. J. Impact Engineering **12**, 281-292, 1992

PDF Complete
Your complimentary use period has ended. Thank you for using PDF Complete.
Click Here to upgrade to Unlimited Pages and Expanded Features

malized Crater Diameter

RDECOM
TECHNOLOGY DRIVEN. WARFIGHTER FOCUSED.



H normalized by D_e

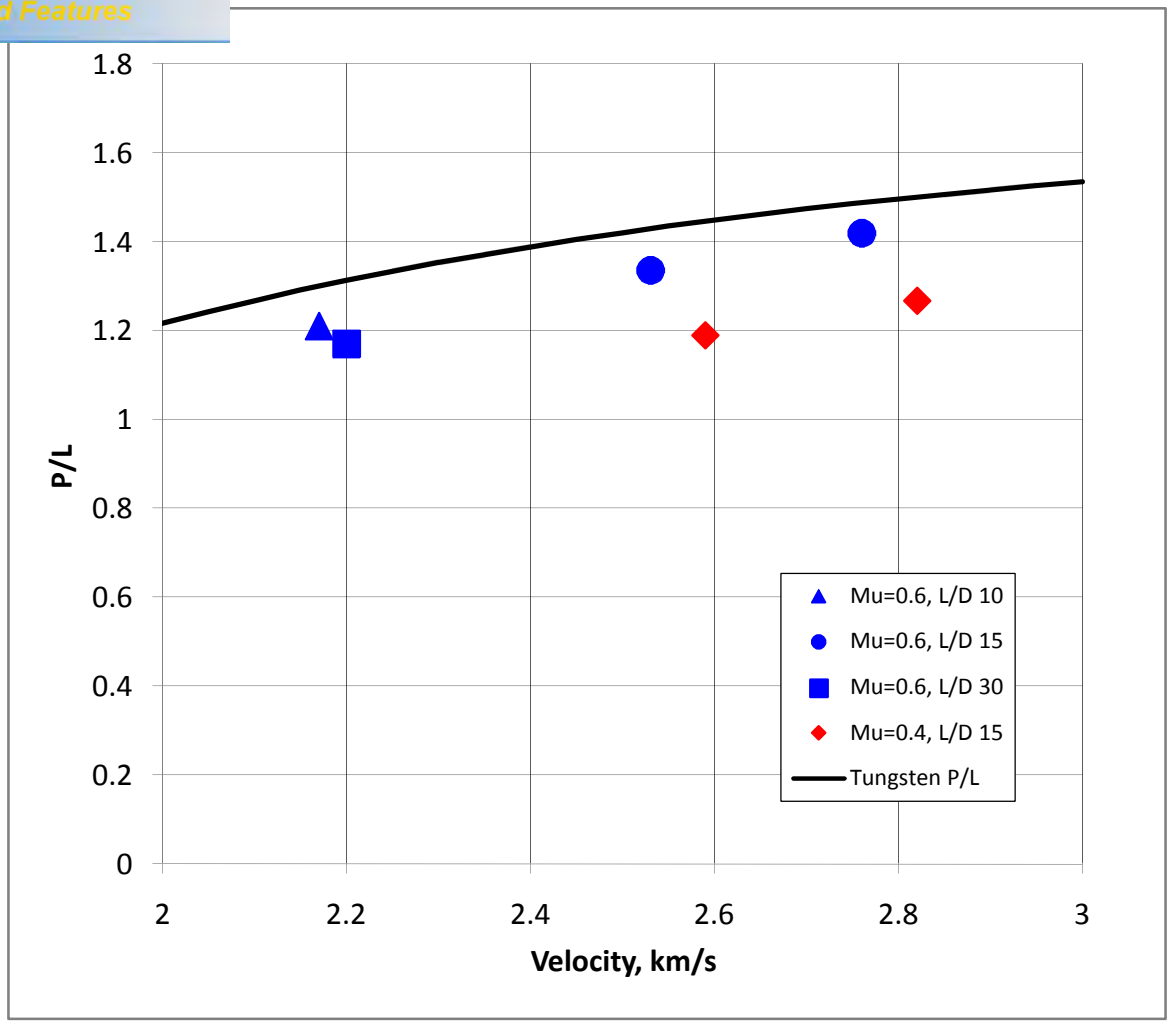
H normalized by D_j

The crater diameter appears to scale as the square root of the average density.

PDF Complete
Your complimentary use period has ended. Thank you for using PDF Complete.
Click Here to upgrade to Unlimited Pages and Expanded Features

Penetration Results

RDECOM
TECHNOLOGY DRIVEN. WARFIGHTER FOCUSED.



P/L does not depend on L/D at 2.2 km/s (10-30).
Jacketed rods never penetrate as well as all-tungsten rods but closely approach the performance as velocity increases.

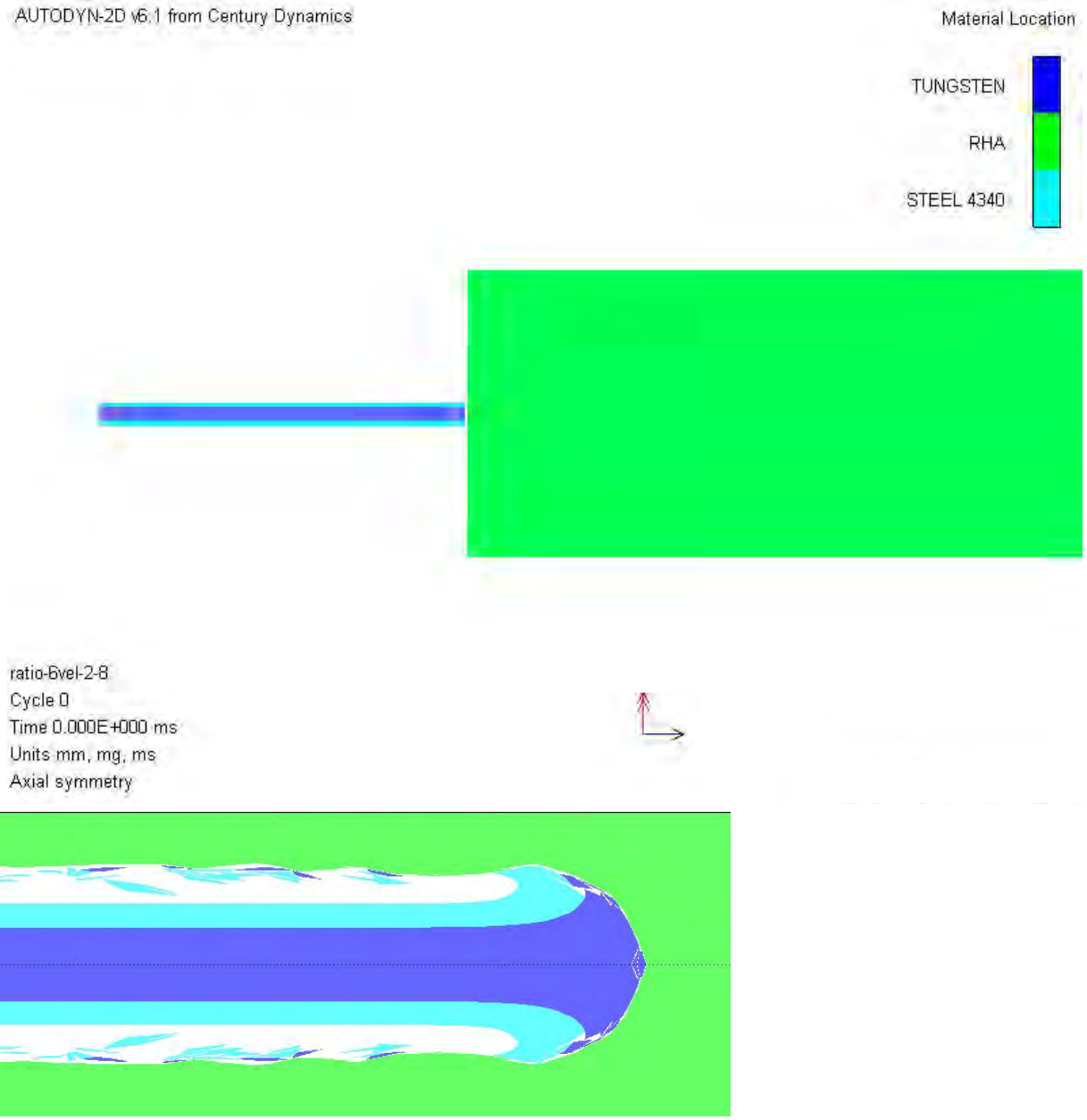
PDF Complete
Your complimentary use period has ended. Thank you for using PDF Complete.
Click Here to upgrade to Unlimited Pages and Expanded Features

Numerical Modeling

RDECOM
TECHNOLOGY DRIVEN. WARFIGHTER FOCUSED.

2D axis-symmetric AUTODYN Lagrangian solver.

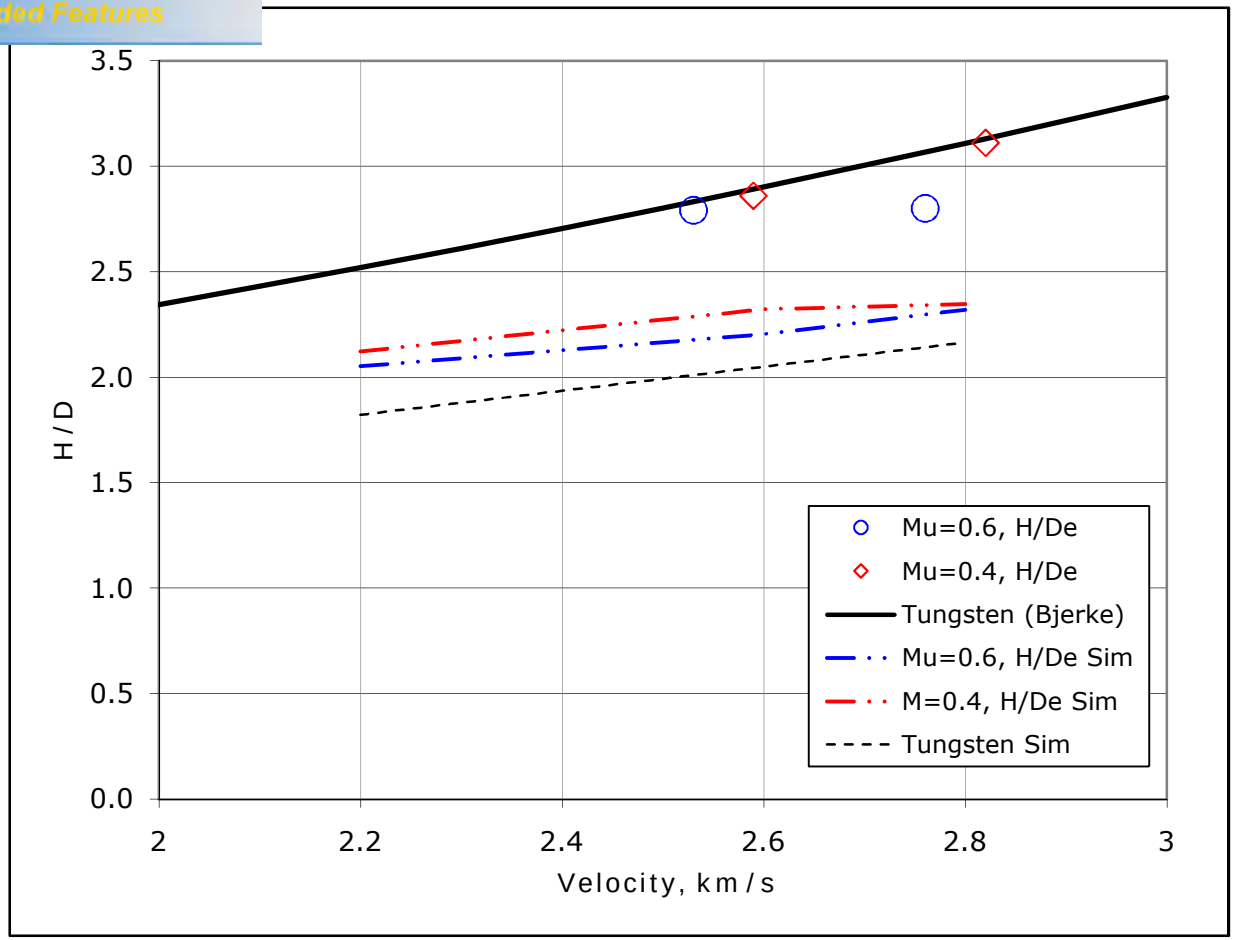
Simulated tungsten rods, and Mu=0.4 and 0.6 jacketed rods at V=2.2, 2.6, 2.8 km/s.



PDF Complete
Your complimentary use period has ended. Thank you for using PDF Complete.
Click Here to upgrade to Unlimited Pages and Expanded Features

rical Modeling – Crater Size

RDECOM
TECHNOLOGY DRIVEN. WARFIGHTER FOCUSED.

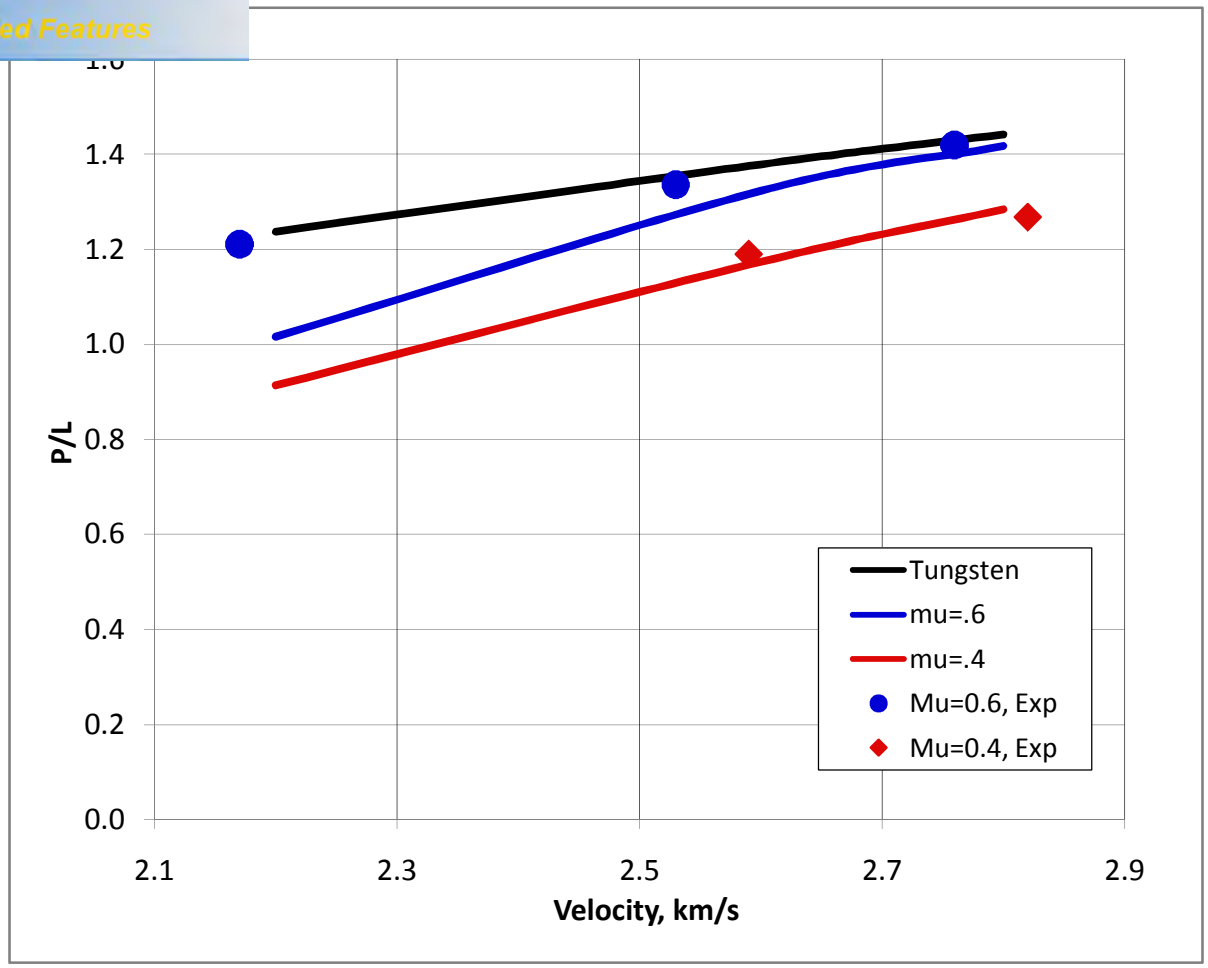


The simulated crater size is significantly less experimental data.
In the simulations, craters from tungsten rods are smaller than craters from jacketed rods, which is not correct.
AUTODYN is not accurately modeling the crater growth.

PDF Complete
Your complimentary use period has ended. Thank you for using PDF Complete.
Click Here to upgrade to Unlimited Pages and Expanded Features

...ical Modeling - Penetration

RDECOM
TECHNOLOGY DRIVEN. WARFIGHTER FOCUSED.



Despite the inaccuracies of the crater size, at high velocity, the simulations agree well with the normalized penetration from the experiments.
At 2.2 km/s, the simulations do not agree with the data. This is likely because in that calculation the crater is not large enough to allow the jacket material to flow freely after it erodes.

PDF Complete
Your complimentary use period has ended. Thank you for using PDF Complete.
Click Here to upgrade to Unlimited Pages and Expanded Features

Conclusions

RDECOM
TECHNOLOGY DRIVEN. WARFIGHTER FOCUSED.

For mu=0.6, jacketed rods approach but never attain the penetration of tungsten rods.

The penetration of mu=0.4 rods is less than mu=0.6 rods.

The simulations matched the penetration for velocities above 2.6 km/s, but under-predicted penetration at 2.2 km/s.

For these jacketed rods, the crater diameter scales as the square root of the average density.

The simulations under-predicted the crater diameters for both jacketed and tungsten rods.

24th International Symposium on Ballistics
New Orleans, LA

Mine Countermeasure Dart Dispense Modeling & Simulation

Gary Prybyla
Naval Surface Warfare Center
Indian Head Division

23 September 08

Contributors/Co-authors

- Digital Fusion, Inc.
  - **William Dietz**
  - **James Baltar**
  - **Kevin Losser**
- NSWC Panama City
  - **Dr. Michael Neaves**

Outline

- Description of Mine Countermeasure Darts
- Background of Dart Dispense Working Group
- Simulation Matrix
- Model Results
- Discussion

Navy Mine Countermeasure Programs

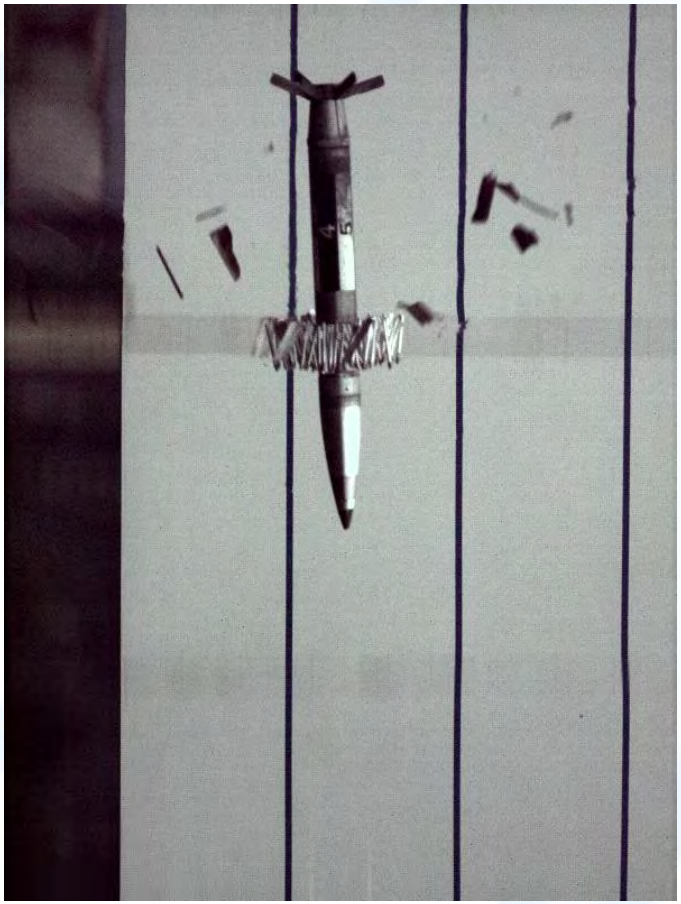


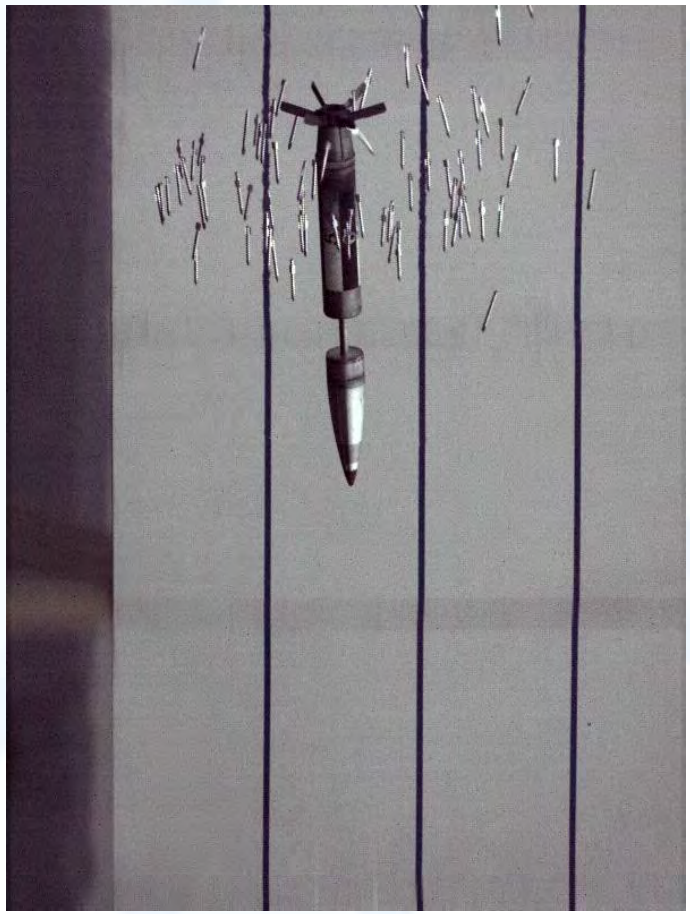
- Indian Head supports 3 Mine Countermeasure Programs w/ Dart Dispense:
  - **MODS**
  - **Hydra 7**
  - **Gun Launched CMCO Round**



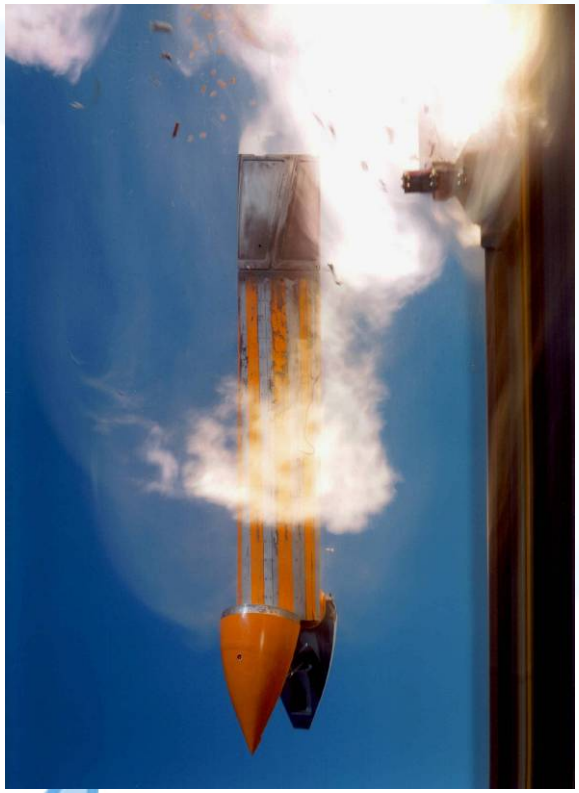
Venom Penetrator Dart

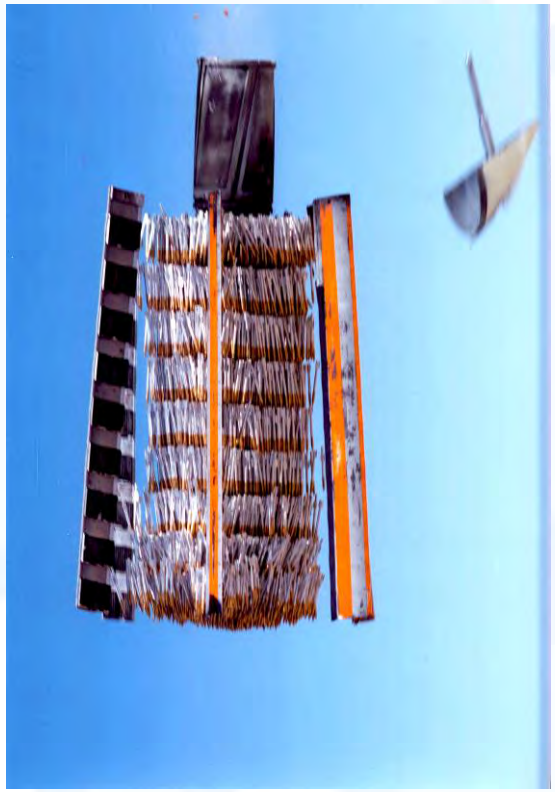
- Naval Gun Fire System CounterMine CounterObstacle Dispense

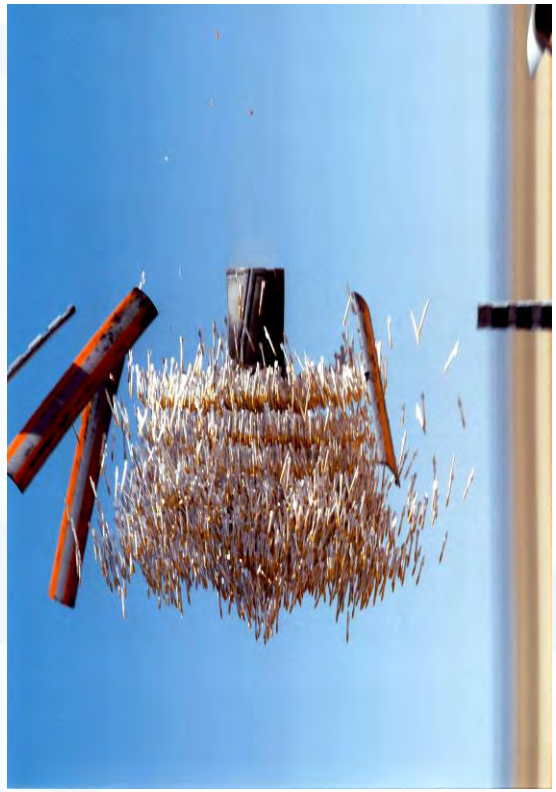




- MODS Dispense of 6000+ darts







Background

- History of Dart Dispense M&S Working Group
  - **Initial Dispensing Technology Workshop, coordinated by Mr. Brian Almquist, Office of Naval Research, held in February 2002**
  - **Working Group formed – kickoff meeting in June 2002**
  - **Team Members:**
    - ONR
    - NSWC/Indian Head
    - NSWC/Panama City
    - Army Aeroflightdynamics Directorate, Ames Research Center
    - NASA/Langley
    - NEAR, Inc.
    - Digital Fusion
  - **DoD High Performance Computer Project "Modeling of Mine Countermeasure Dart Dispense" initiated FY2003**
  - **Challenge Project Status awarded during 2007 & 2008 (1,000,000+ CPU hours per year)**

Objectives of Working Group

- Enhance state-of-the-art techniques for predicting dart aerodynamics during dispense
- Transition techniques to 6-DOF models to predict multiple dart trajectories and impact patterns
- Enhance 6-DOF tools used in Analysis of Alternatives

The Challenge !!

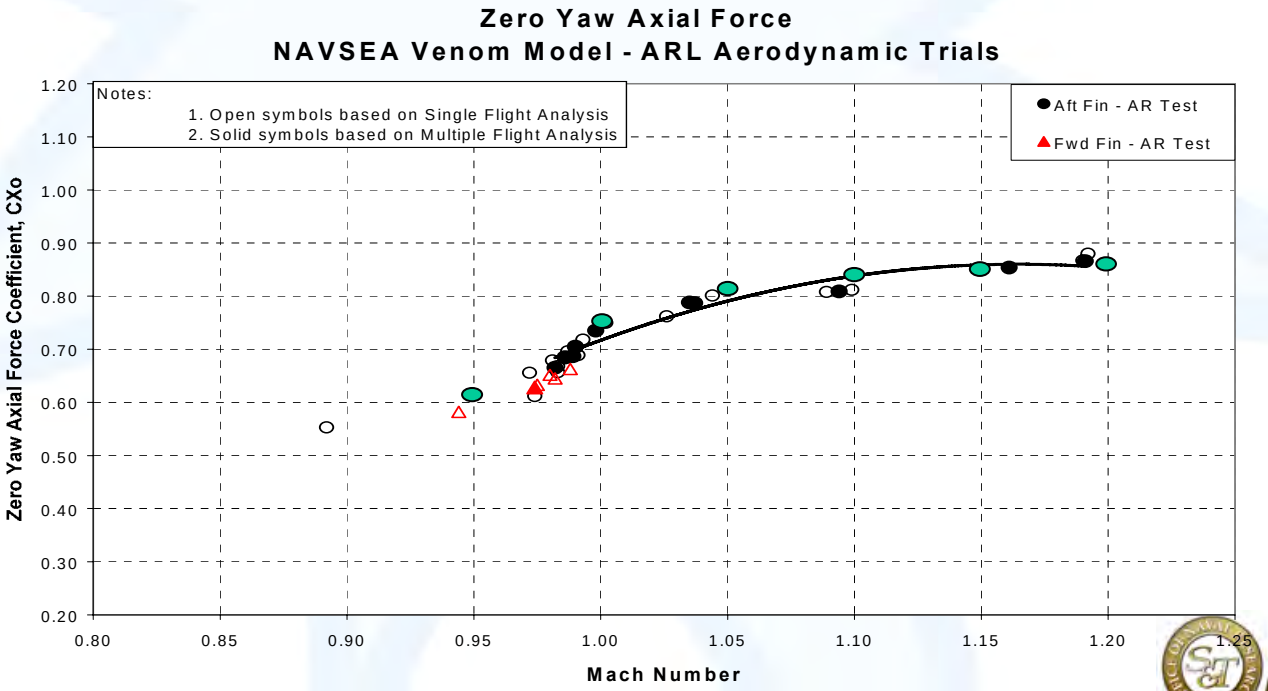
- Accurately model the dispense of multiple darts, approaching a full MODS payload: Multiple-Body Six Degrees-of Freedom (6-DOF) Computational Fluid Dynamics (CFD) with Collisions

- Determine how many darts need to be modeled to capture the overall dispense dynamics

- Given enough memory and computing power, can we model the dispense of all 4000+ darts?

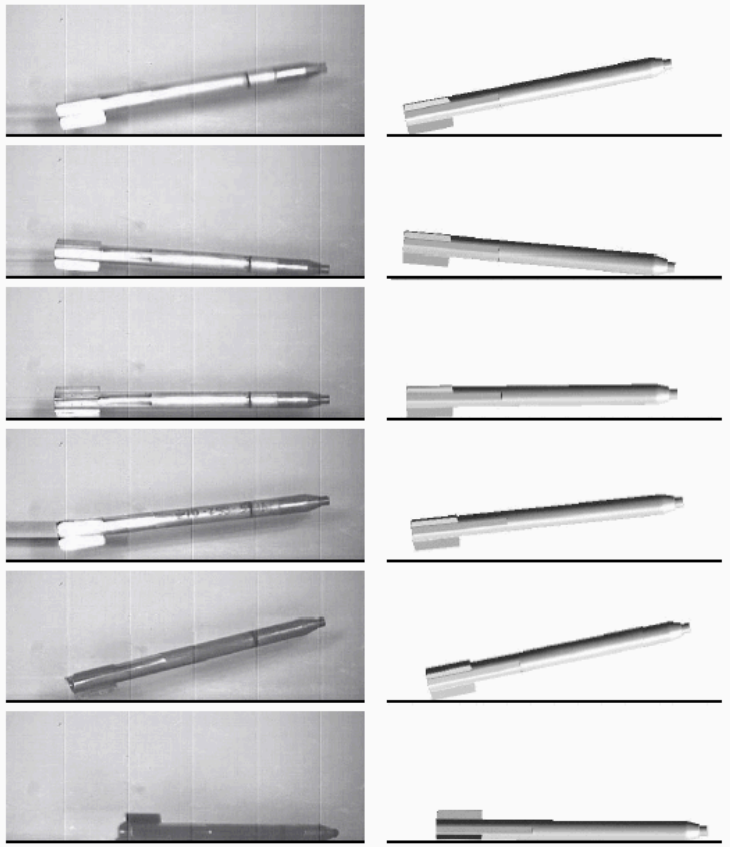
Preliminary CFD Simulations

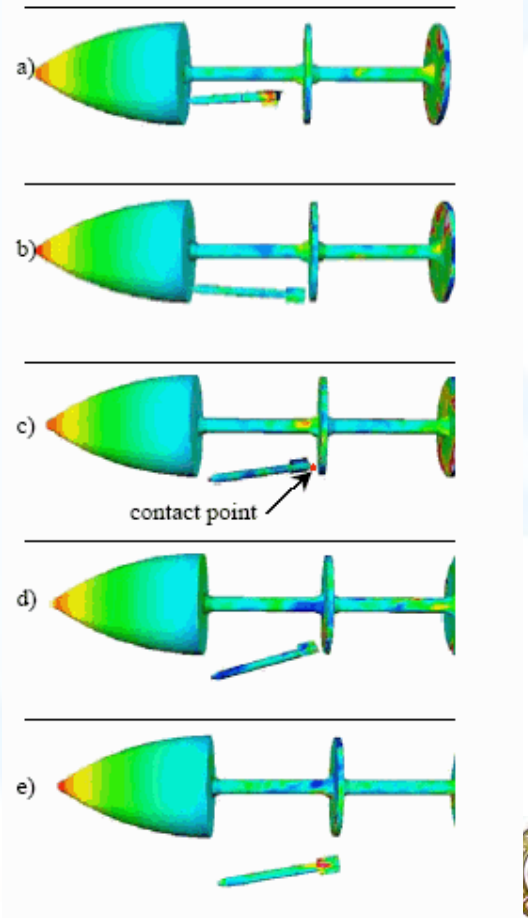
- Evaluated several CFD codes
- Compared results of single dart simulations to Aeroballistic Test Range data (from Aberdeen and Eglin AFB)
- OVERFLOW selected as primary CFD code



Code Modifications

- Collision Module added to OVERFLOW
  - **Provides for dart-to-dart and dart-to-dispenser collisions**
  - **Validated against single dart drop tests**





Simulation Matrix

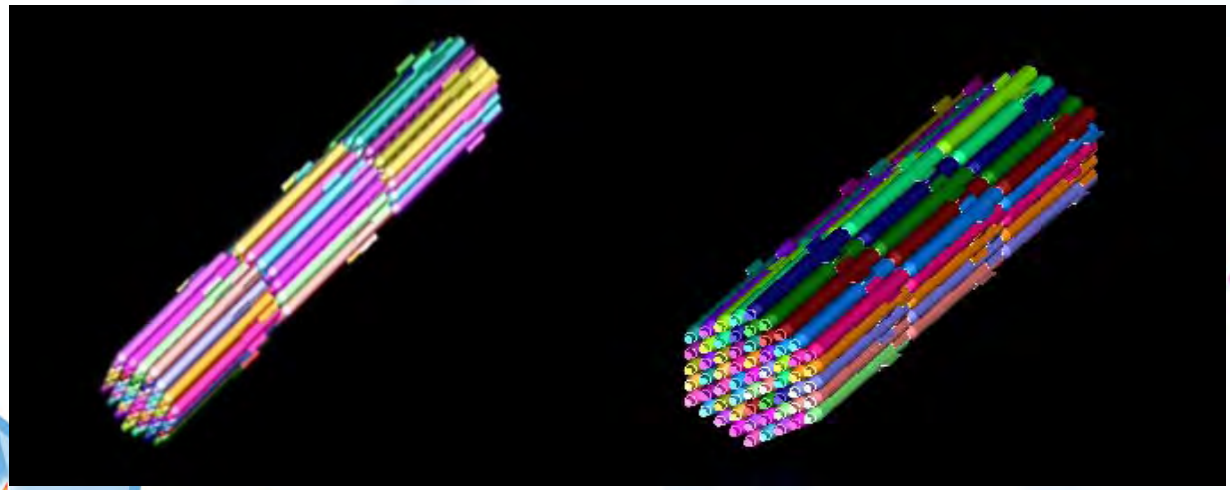
1. 273 darts (3 axial layers x 5 radial rows), 6 Hz spin rate, Mach 1.2
2. 273 darts (3 axial layers x 5 radial rows), 12 Hz spin rate, Mach 1.2
3. 273 darts (3 axial layers x 5 radial rows), 18 Hz spin rate, Mach 1.2

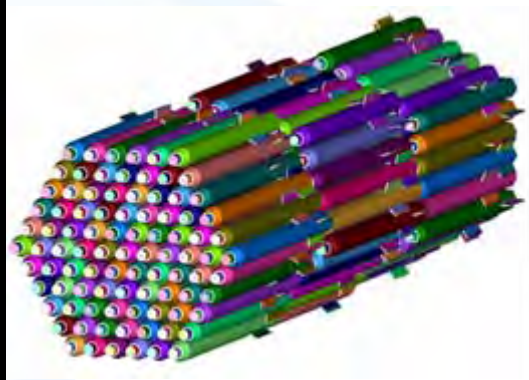
4. 111 darts (3 axial layers x 3 radial rows), 12 Hz spin rate, Mach 1.2
5. 183 darts (3 axial layers x 4 radial rows), 12 Hz spin rate, Mach 1.2
6. 381 darts (3 axial layers x 6 radial rows), 12 Hz spin rate, Mach 1.2

7. 273 darts (3 axial layers x 5 radial rows), 12 Hz spin rate, Mach 1.6
8. 273 darts (3 axial layers x 5 radial rows), 12 Hz spin rate, Mach 2.0

“Number of Darts” Study

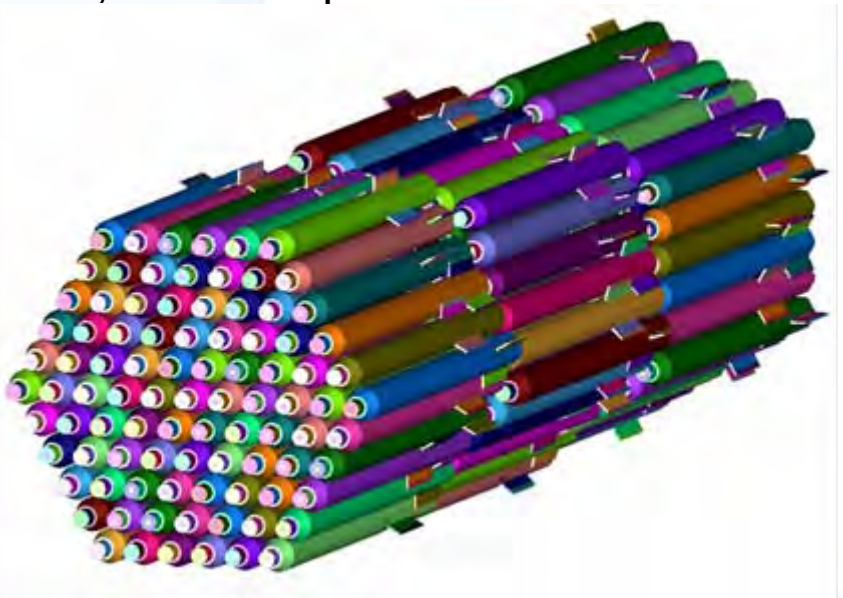
- Compare Matrix runs #2, #4, #5, & #6 to determine differences in dispense behavior resulting from 111, 183, 273, & 381 dart packs
- Matrix run #6 (381 darts) has not been completed
- All runs performed at same Mach number (1.2) and Spin Rate (12 Hz)





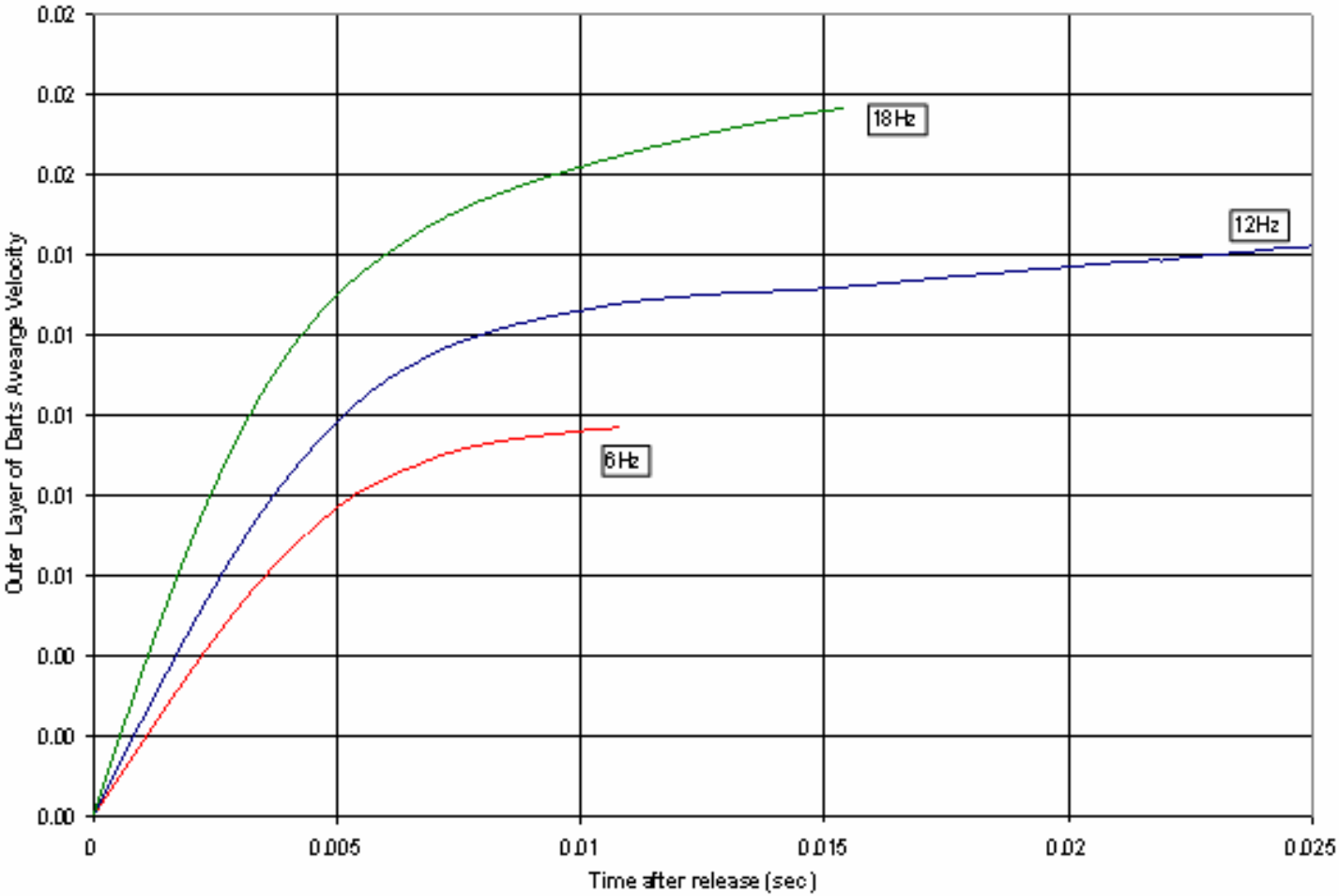
“Spin Rate Effects” Study

- 5 Radial Layers, 91 Darts Per Row, 3 Rows = 273 Darts
- Full 6-DOF Simulation with Collisions, Various spin rates
- ~400 Million Grid Points
- Viscous grid spacing
- Initial Spacing Factor = 1.2
- Physical Run time
    - 6 Hz = ~0.01 seconds
    - 12 Hz = ~0.025 seconds
    - 18 Hz = ~0.015 seconds

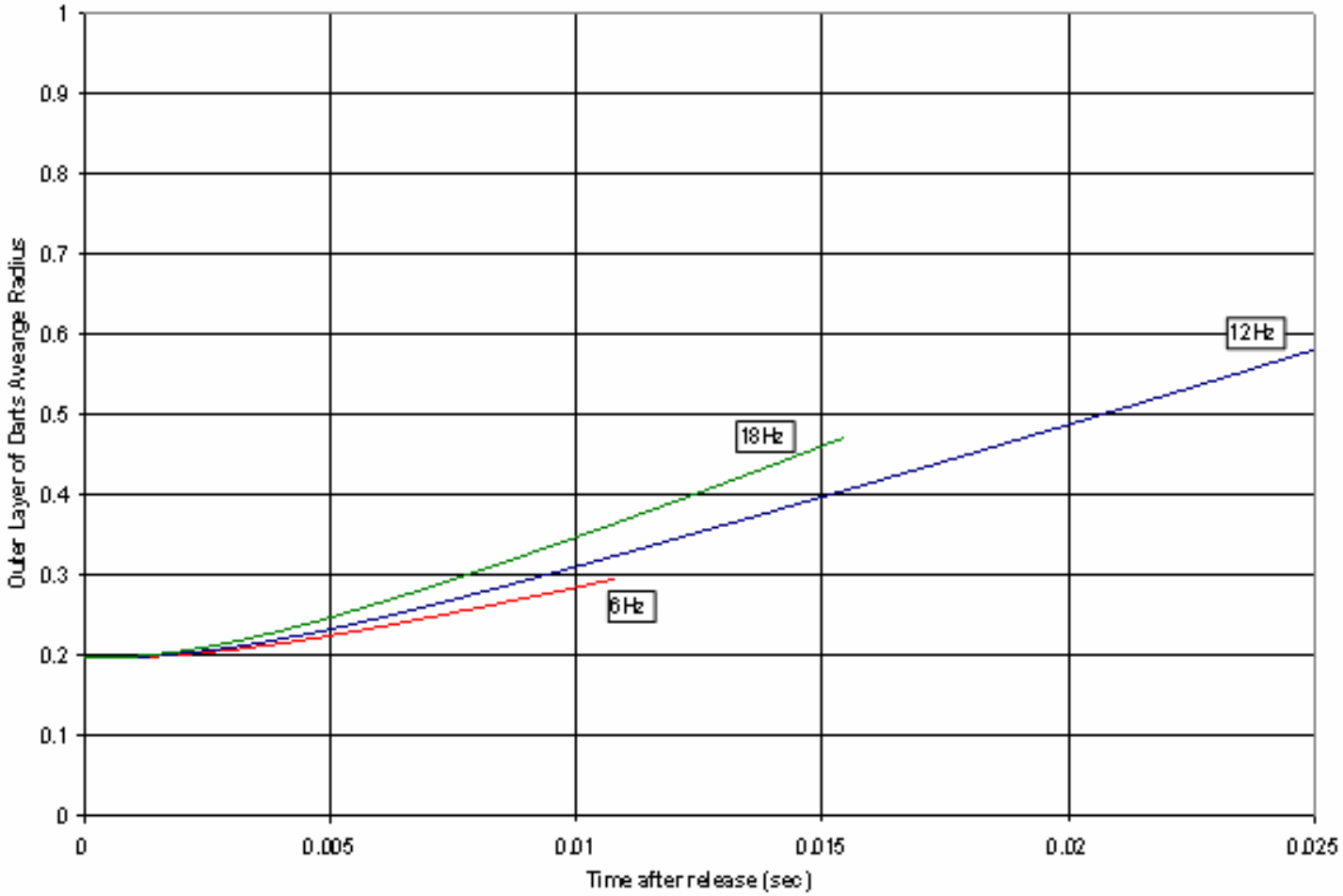


- Errors out due to bugs in OVERFLOW-2 grid adaptation feature (bugs fixed in later versions) and memory limitations

273 Darts – Average Normalized Velocity Comparison



273 Darts – Average Radius Comparison



Revolutionary Research . . . Relevant Results

273 Darts (Longer Run Times)

- 5 Radial Layers, 91 Darts Per Row, 3 Rows = 273 Darts
- Full 6-DOF Simulation with Collisions, 12 Hz spin rate
- ~300 Million Grid Points
- Wall Function Grid, y+ = ~50
- Initial Spacing Factor = 1.1 (previous simulations at 1.2)
- Run time ~0.1 seconds after release
- 600-840 processors
- Errors out due to one dart hitting outer boundary

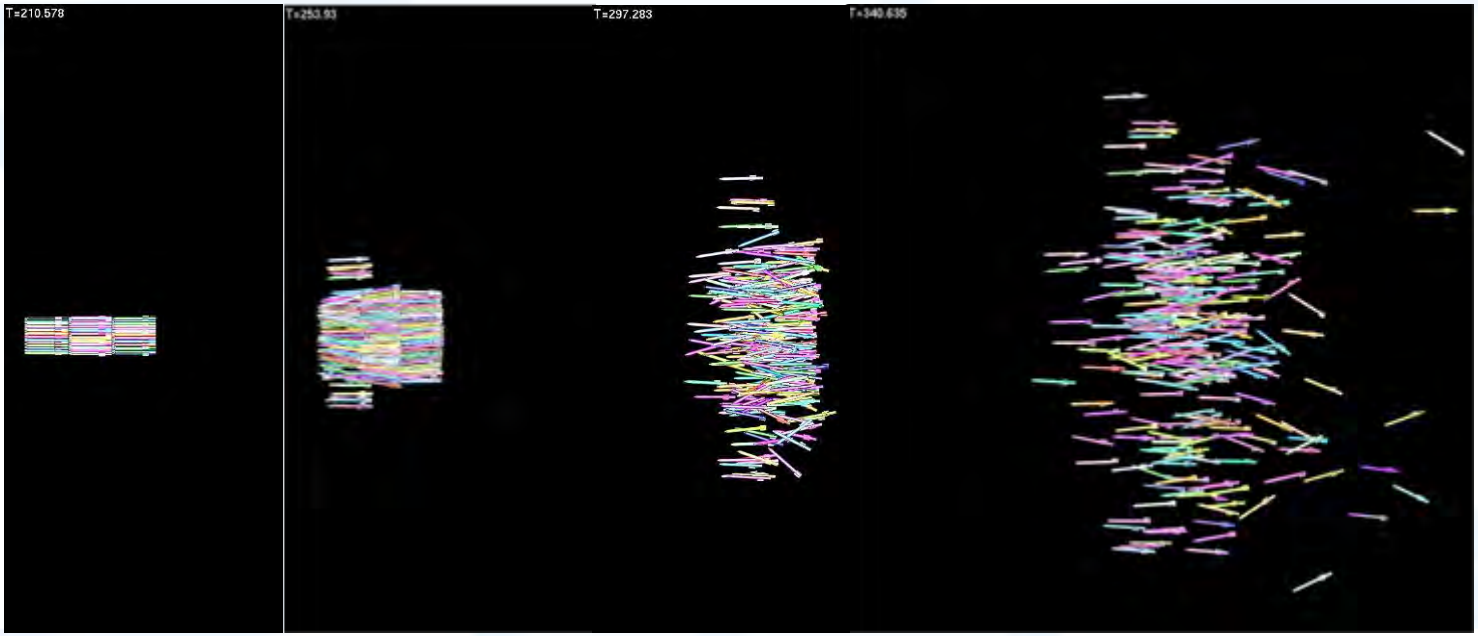
273 Darts (Longer Run Time)

Run to ~0.1 sec after release (MOVIE)
Iso View



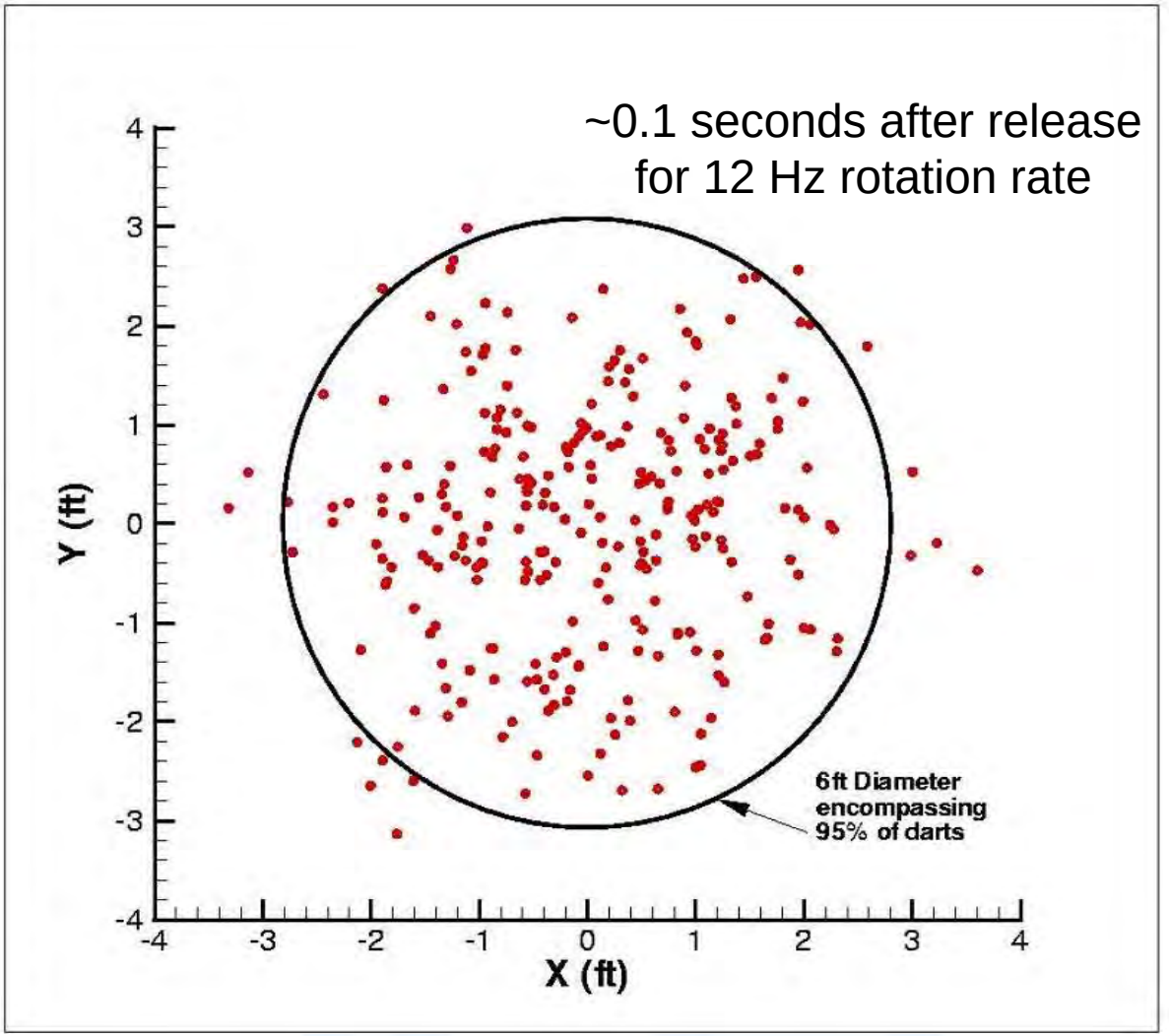
273 Darts (Longer Run Time)

Dispense sequence at Mach 1.2 with 12 Hz rotation rate



T=0s T~0.03s T~0.06s T~0.1s

273 Darts – Spread (12 Hz)



Modeling Lessons Learned

- Wall Functions reduce point count, ease memory requirements
- File size is still a significant problem – storage and transfer
- Memory is limitation, not CPU time
- Increase processor count to get required memory
- Most CPU time spent in initialization and spin
- Graphics/post-processing is a concern

Results/Conclusions

- "Number of Darts" Study
  - **Collisions may play big role in determining pattern size**
  - **Drafting effects are reduced after 3 axial layers**
  - **Additional axial rows of darts may fill in the "gaps" left by the first couple of rows**
  - **Darts are almost independent of each other after 0.1 sec for 273 dart case (small clusters)**
  - **Hexagonal pattern preserved, additional darts on the sides may produce more circular pattern**
- "Spin Rate Effects" Study
  - **Average Radial Dart velocities proportional to spin rates**
  - **Higher spin rates may produce "cleaner" patterns**

Future Plans

- Additional simulations of larger dart packs are progressing (2009 Challenge Project)
- Plan to run Mach 1.6 and Mach 2.0 for 273 darts (Mach number effects study)

NAVSEA
WARFARE CENTERS

HPC Modernization Program
SOLVING THE HARD PROBLEMS

QUESTIONS?

IHDIV
ENERGETIC SYSTEMS

ONR
Revolutionary Research . . . Relevant Results

PDF Complete
Your complimentary use period has ended. Thank you for using PDF Complete.
Click Here to upgrade to Unlimited Pages and Expanded Features

RDECOM

Numerical Computations of Dynamic Pitch-Damping Derivatives using Time-Accurate CFD Techniques

TECHNOLOGY DRIVEN. WARFIGHTER FOCUSED.

Dr. Jubaraj Sahu,
Aerodynamics Branch
U.S. Army Research Laboratory

24th International Symposium on Ballistics
New Orleans, Louisiana
22 ï 26 September, 2008

PDF Complete
Your complimentary use period has ended. Thank you for using PDF Complete.
Click Here to upgrade to Unlimited Pages and Expanded Features

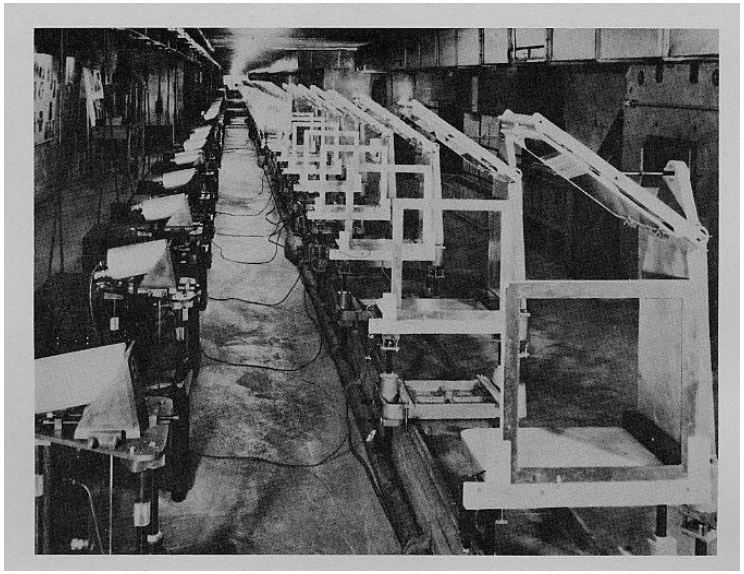
Projectile Aerodynamics

- Wind Tunnel testing
- Actual flight testing
  - Experimental facilities (Aero Range, Transonic Range)
  - Measure the positions and orientations; get Aero from 6-DOF fits
- Empirical codes (AP, DATCOM, PRODAS etc.)
- Computational Fluid Dynamics (CFD)
  - Steady-State Aerodynamics
  - Unsteady Aerodynamics for Magnus, Roll Damping, Pitch Damping using unsteady rolling and imposed pitching motions (Virtual Wind-Tunnel Method)
- CFD and 6-DOF Rigid Body Dynamics Coupling for "Virtual Fly-Outs"
  - Simulate actual free flight (integrated unsteady aero/flight dynamics)
  - Extraction of aerodynamic coefficients (both static and dynamic) from virtual fly-outs
  - Easily extended for computation of dynamic pitch damping moment coefficient using imposed pitching motion– a special case of the virtual fly-out procedure
  - Roll damping and Magnus moment coefficients also are obtained from time-accurate computations of rolling motion, inherently an integral part of the virtual fly-out method

PDF Complete
Your complimentary use period has ended. Thank you for using PDF Complete.
Click Here to upgrade to Unlimited Pages and Expanded Features

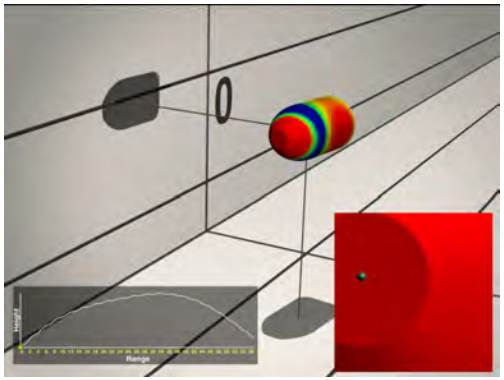
f HPC in the Development of the tal Virtual Aerodynamic Range

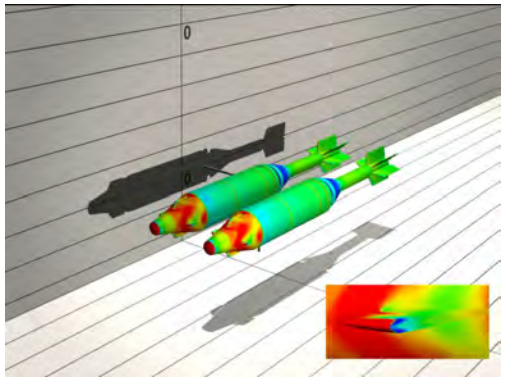
Aerodynamics Experimental Facility



- Measures projectile orientation and position only
  - Pitch, Roll, Yaw
  - X, Y, Z
  - 6DOF fit of range data
  - Limited visualization at a few stations
  - Aerodynamic coefficients determined
  - Characterize observed flight dynamics

Digital Virtual Aerodynamic Range





- Computes entire projectile state
  - Pitch, Roll, Yaw
  - X, Y, Z
  - Linear velocities
  - Pitch, Roll, and Yaw Rates
  - Unlimited flow visualization
  - Integrated Aerodynamics and Flight Dynamics
  - Predictive capability for new geometries
  - Outputs wake and pressure contours

PDF Complete
Your complimentary use period has ended. Thank you for using PDF Complete.
Click Here to upgrade to Unlimited Pages and Expanded Features

tidisciplinary Computational Technique

CFD Computational Technique

- 3-D Unsteady Navier-Stokes equations
- Higher order turbulence modeling including hybrid RANS/LES
- Dual Time-Stepping for transient flow computations
  - Two time-steps
  - First (outer) global or physical step –usually set to 1/100th of the period of oscillation
  - Second (inner) step – 5 to 10 inner iterations
- Grid Motion and BC:
  - Grid moves and rotates as the projectile moves and rotates
  - Free stream is preserved for arbitrary mesh and arbitrary mesh velocity

CFD/RBD COUPLING PROCEDURE

- 6-DOF equations solved at every CFD time-step
- CFD provides aerodynamic forces and moments
- 6-DOF provides the response of the body to the forces and moments
- The response is converted to translational and rotational accelerations
- Integrate the accelerations to obtain translational and rotational velocities
- Integrate once more to obtain linear position and angular orientations
- 6-DOF uses quaternions to define angular orientations
- From the dynamic response, grid point locations and velocities are set

PDF Complete
Your complimentary use period has ended. Thank you for using PDF Complete.
Click Here to upgrade to Unlimited Pages and Expanded Features

e-Accurate CFD Procedures

Complete Virtual Fly-Out Procedure

- STEP 1:
  - "Steady-state" mode
  - Grid velocities account only for translational motion
  - Initial conditions also include the angular orientations
- STEP 2:
  - "Uncoupled" mode (Kinematics)
  - Add rotational component in X (spin, p)
  - Compute for a few spin cycles until solution converges
- STEP 3:
  - "Coupled mode"
  - Add the other rotational components (q and r)
  - Full dynamic calculations

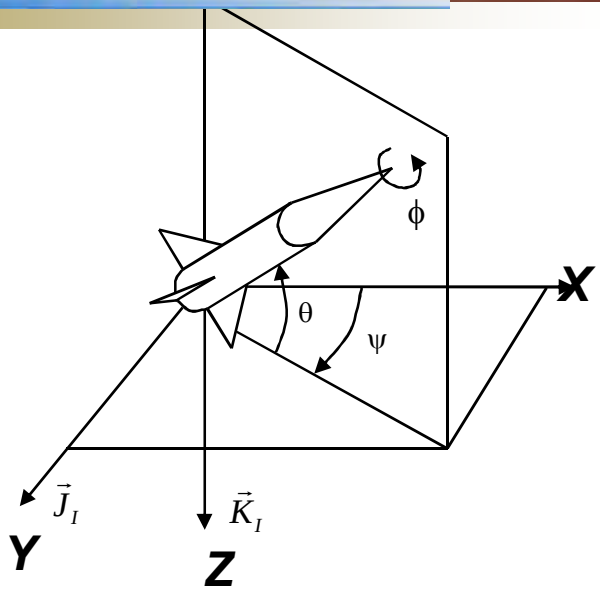
Time-Accurate CFD Procedure for Dynamic Derivatives

- STEP 1:
  - "Steady-state" mode
  - No translation motion
- STEP 2:
  - "Uncoupled" mode (Rolling Motion)
  - Add rotational component (spin, p)
  - Compute for a few spin cycles until solution converges
- STEP 2:
  - "Uncoupled" mode (Pitching Motion)
  - Add the other rotational component (q) i.e. impose pitching motion
  - Pitching motion can be sinusoidal

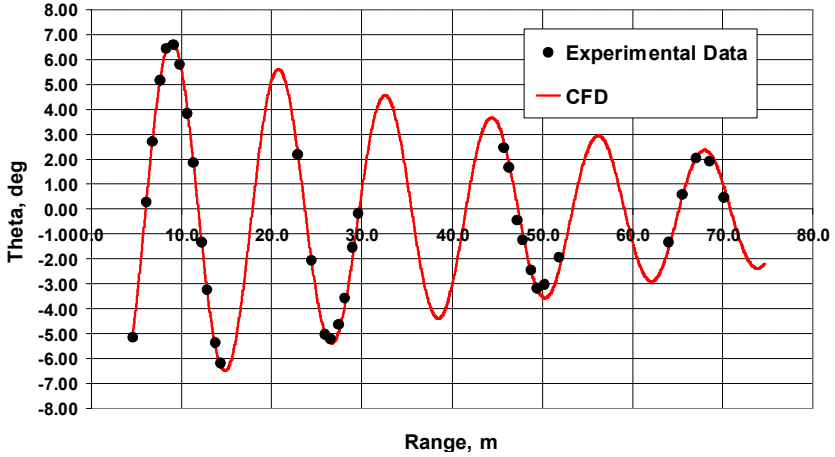
PDF Complete
Your complimentary use period has ended. Thank you for using PDF Complete.
Click Here to upgrade to Unlimited Pages and Expanded Features

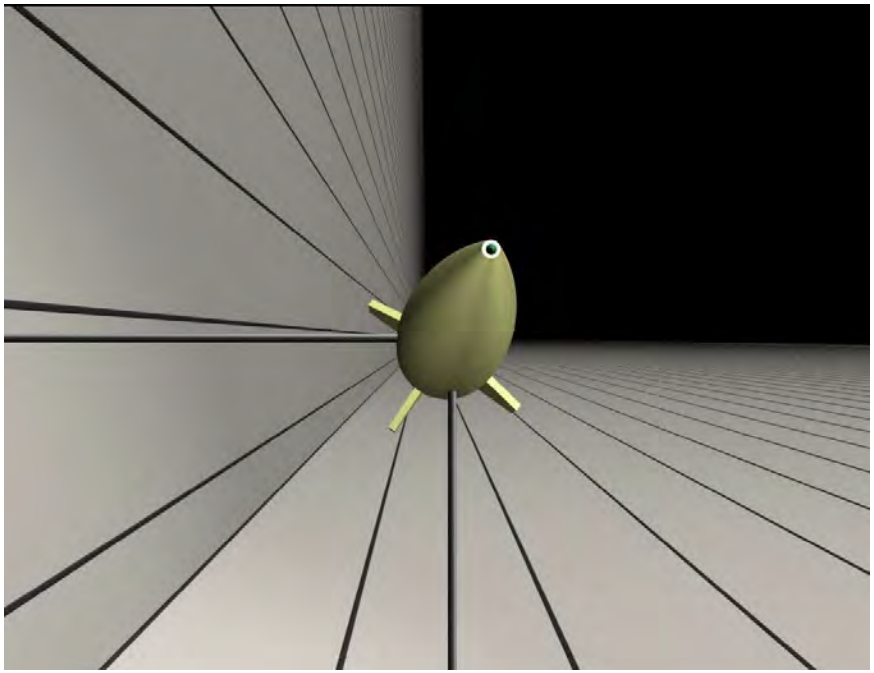
...al Fly-out of a Finned Projectile

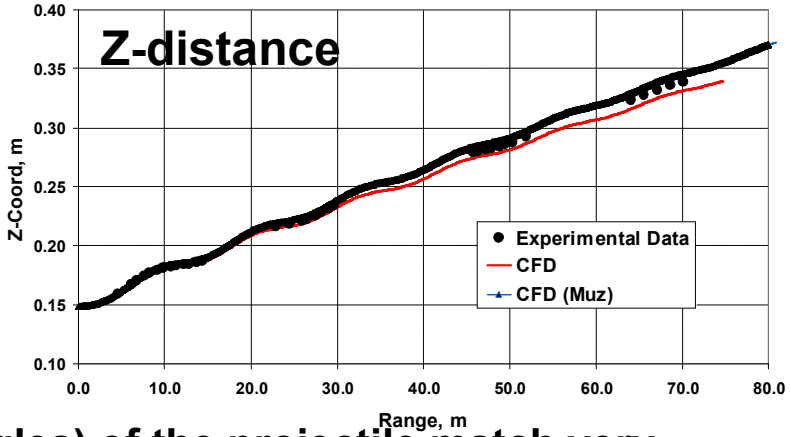
...al Velocity, Mach = 3 (Supersonic)



6-DOF system



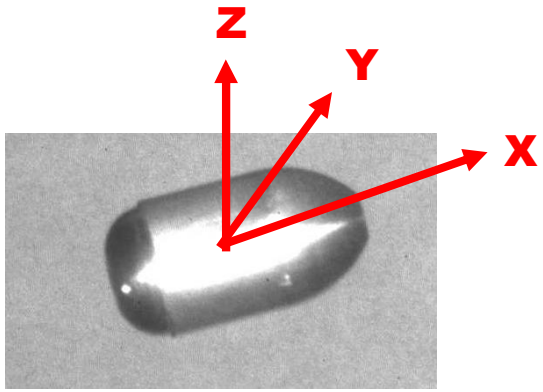


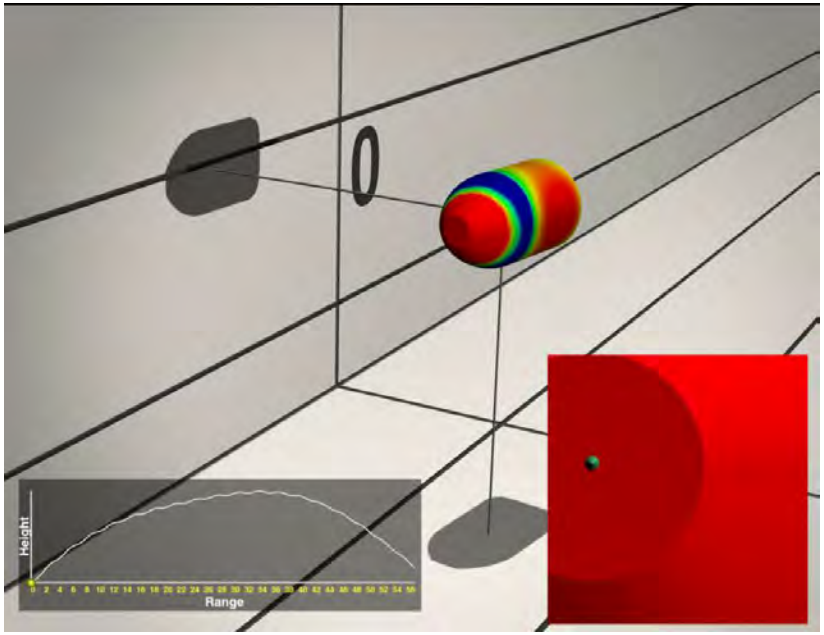


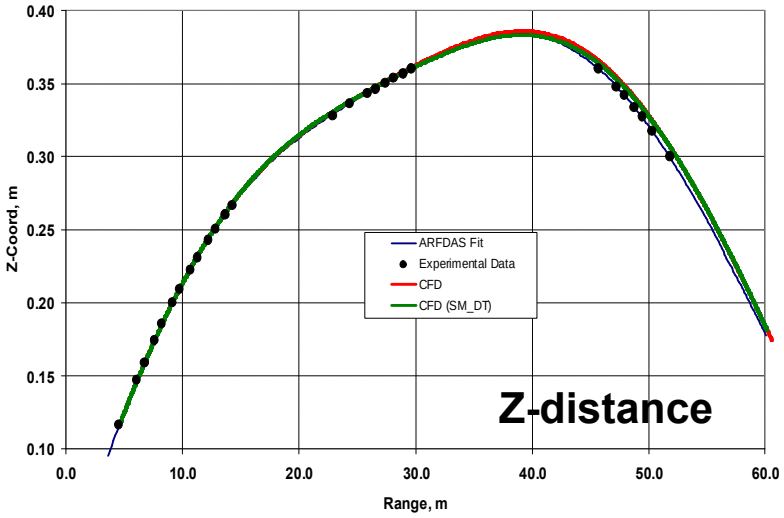
Computed positions and orientations (Euler angles) of the projectile match very well with the data measured in actual free flight tests.

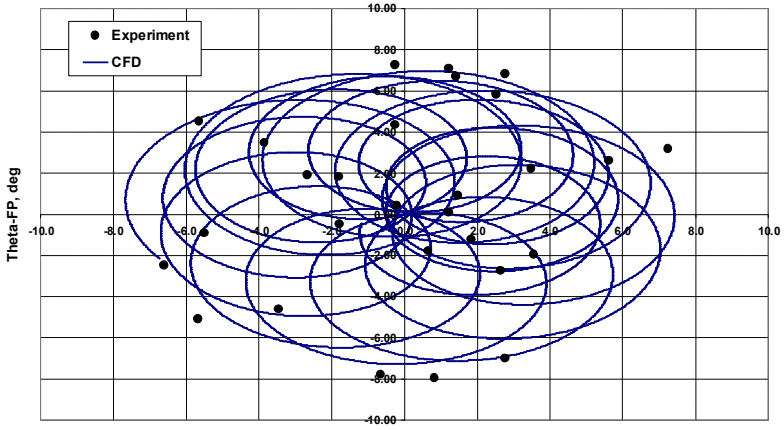
PDF Complete
Your complimentary use period has ended. Thank you for using PDF Complete.
Click Here to upgrade to Unlimited Pages and Expanded Features

Another Example: Spinning Projectile
Initial Mach = 0.4 (Subsonic Flight)





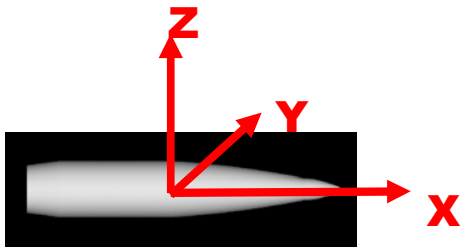


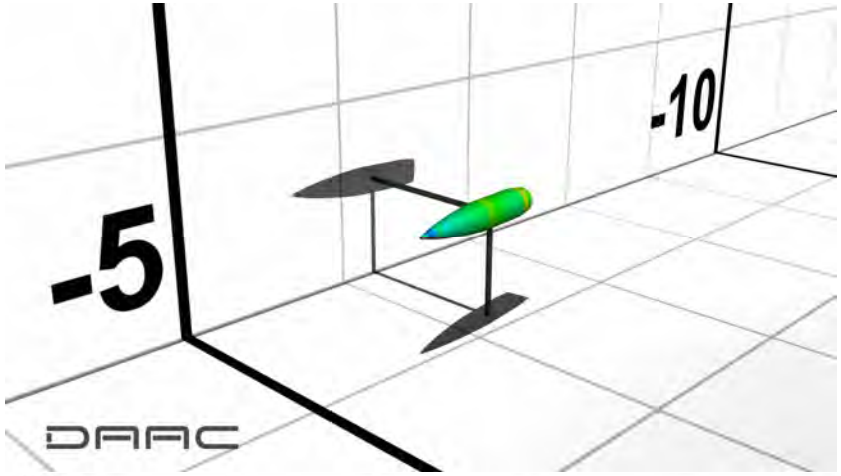


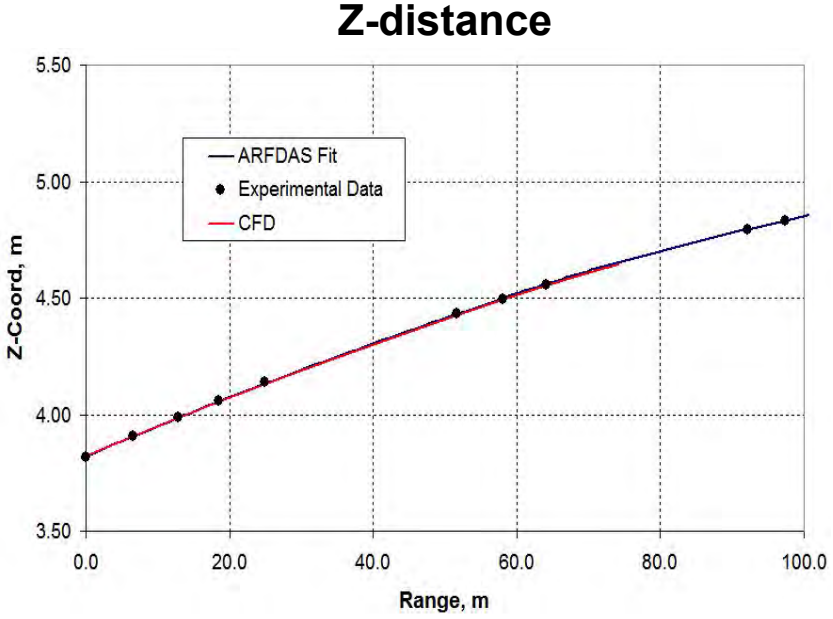
Virtual fly-out technique computes the trajectory of an in-flight spinning projectile; computed results match well with the flight test data

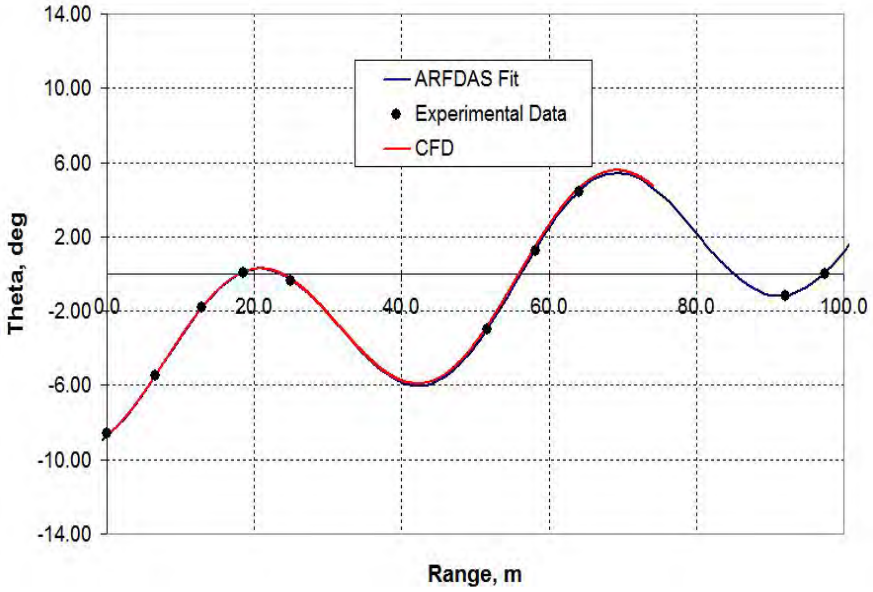
PDF Complete
Your complimentary use period has ended. Thank you for using PDF Complete.
Click Here to upgrade to Unlimited Pages and Expanded Features

ual Fly-Out of a Spinning Projectile
itial Mach = 1.1 (Transonic Flight)





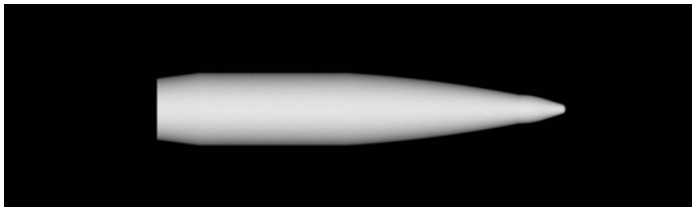




Virtual fly-out technique computes the trajectory of an in-flight spinning projectile; computed results match well with the flight test data.

PDF Complete
Your complimentary use period has ended. Thank you for using PDF Complete.
Click Here to upgrade to Unlimited Pages and Expanded Features

Extraction of Aerodynamic Coefficients from Virtual Fly-Out Simulations



Spinning Projectile

PDF Complete
Your complimentary use period has ended. Thank you for using PDF Complete.
Click Here to upgrade to Unlimited Pages and Expanded Features

Pitch-Damping Moment Coeff.

Virtual fly-outs simulations require only the total aerodynamic forces and moments to fly the projectile.

How do we extract the aerodynamic force and moment coefficients from the virtual fly-out simulations? How good are they?

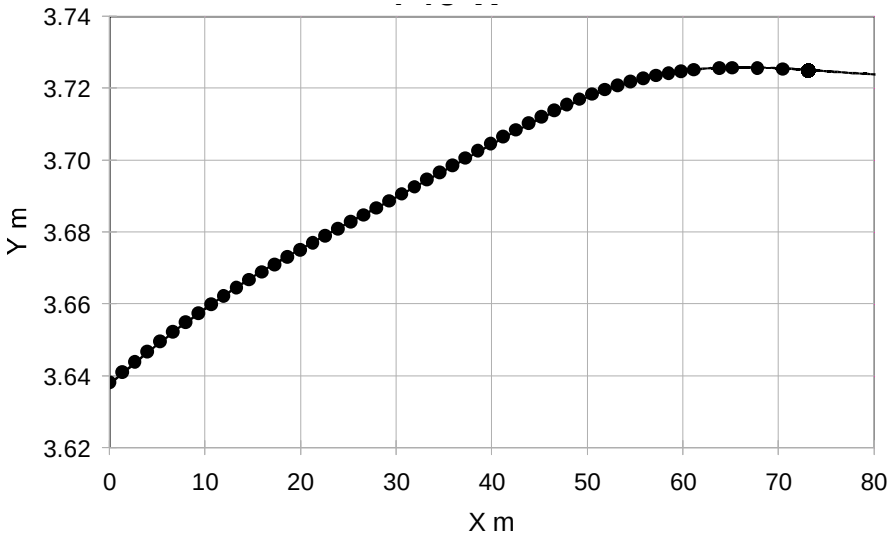
Different Approaches:

1. Aerodynamic coefficients extracted from CFD/RBD virtual fly-out solutions using range reduction software (ARFDAS, for example).
2. PACE - Simple fitting procedure that require a set of short time-histories (virtual fly-outs) at different Mach numbers.

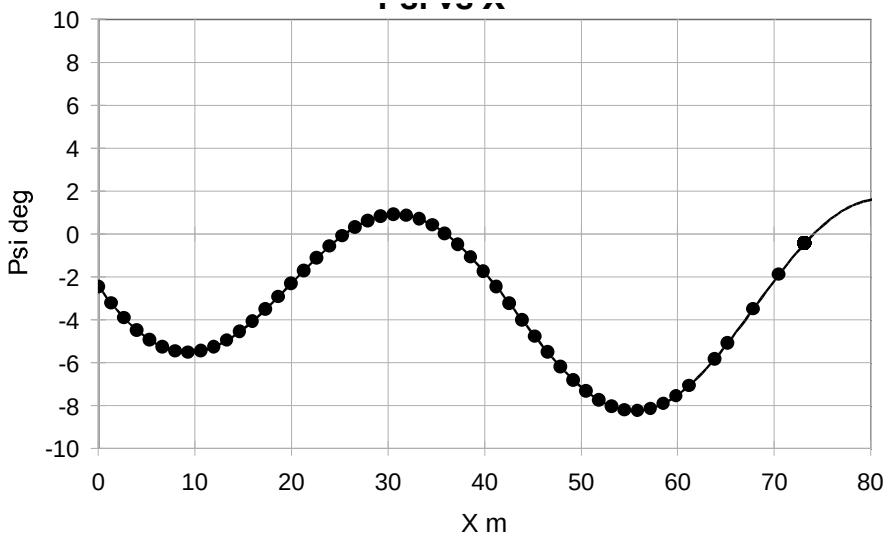
PDF Complete
Your complimentary use period has ended. Thank you for using PDF Complete.
Click Here to upgrade to Unlimited Pages and Expanded Features

RFDAS Fit of CFD Generated data Initial M = 1.1

1. Aerodynamic coefficients extracted from CFD using range reduction software, ARFDAS using the virtual fly-out solutions
2. Position (x,y,z) and the orientation (three Euler angles) of the projectile, obtained from the virtual fly-out simulations were provided as input to ARFDAS. ***Same procedure is used for actual flight measured data.***



Y-distance



Euler roll angle

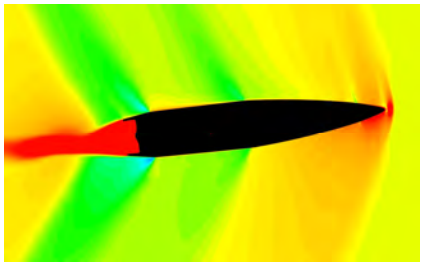
PDF Complete
Your complimentary use period has ended. Thank you for using PDF Complete.
Click Here to upgrade to Unlimited Pages and Expanded Features

Extracted force and moment coefficients (static and dynamic) from virtual fly-out simulation

Data Source	Zero-Yaw Axial Force Coeff., C_{D_0}	Normal Force Coeff. Deriv., C_{N_α}	Pitching Moment Coeff. Deriv, C_{m_α}	Pitch Damping Moment Coeff., Cm_q	Magnus moment Coeff. Deriv., C_{np_α}	Roll Damping Moment Coeff., C_{lp}
Spark Range	0.359	2.081	4.209	-25.3	1.05	-0.019
CFD	0.335	2.362	4.283	-22.9	0.93	-0.019

Aerodynamic coefficients extracted from the virtual fly-out method matches very well with those obtained from free flight tests.

Validate using separate unsteady CFD (Virtual wind tunnel method)



PDF Complete
Your complimentary use period has ended. Thank you for using PDF Complete.
Click Here to upgrade to Unlimited Pages and Expanded Features

Pitch Damping Moment

$$Pitch\ Damping\ Moment = \frac{1}{2}\ \rho\ V^2\ S\ \ d\left(\frac{q\,d}{2V}\right)(C_{m_q} + C_{m_{\dot{\alpha}}})$$

Pitching motion imposed:

$$\alpha = \alpha_m + \alpha_0 \sin(\omega t)$$

Here,

C_{m_q} = pitch damping moment coefficient due to q

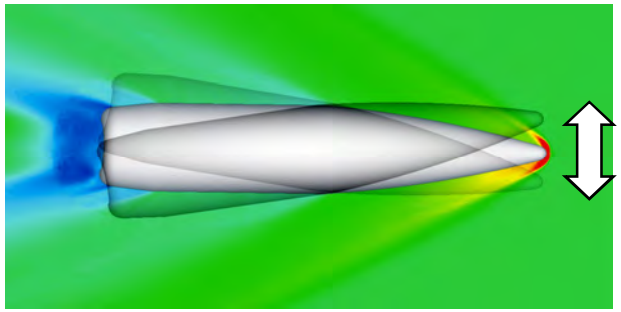
$C_{m_{\dot{\alpha}}}$ = pitch damping moment coefficient due to $\dot{\alpha}$

α = instantaneous angle of attack

α_m = mean angle of attack

α_0 = pitch amplitude

ω = pitch frequency, related to reduced frequency ($k = qd/2V$)

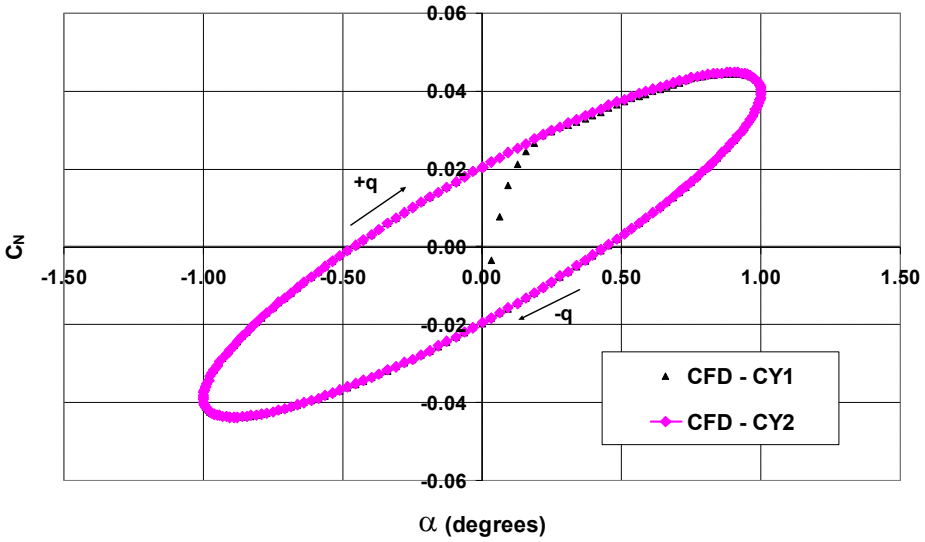


Virtual wind tunnel method (Imposed pitching motion)

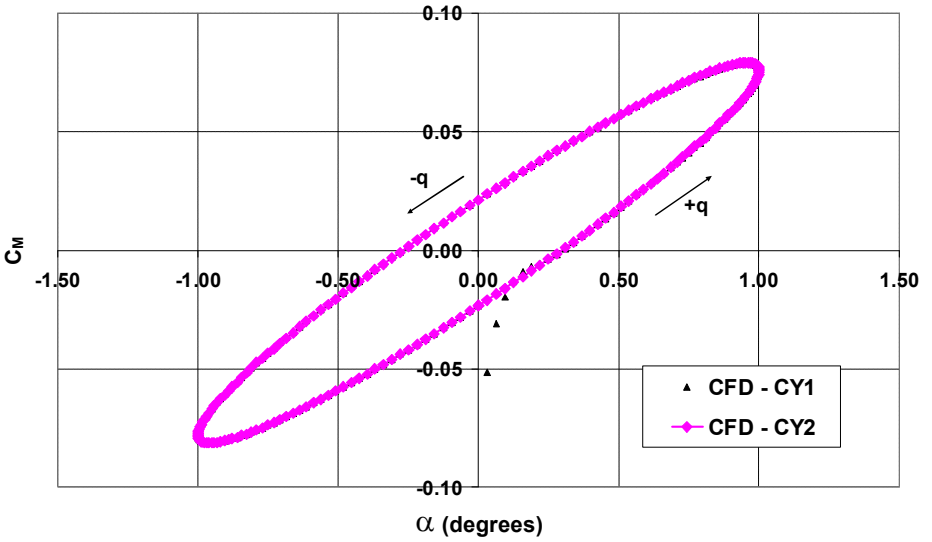
PDF Complete
Your complimentary use period has ended. Thank you for using PDF Complete.
Click Here to upgrade to Unlimited Pages and Expanded Features

-Histories of Normal Force and itching Moment coefficients

Mach = 1.1
α_0 = 1.0, k = 0.1



Normal force



Pitching moment

Pitch damping moment is obtained directly from the time-history plot of the pitching moment coefficient resulting from the imposed pitching motion.

PDF Complete
Your complimentary use period has ended. Thank you for using PDF Complete.
Click Here to upgrade to Unlimited Pages and Expanded Features

tracted force and moment efficients from virtual fly-out

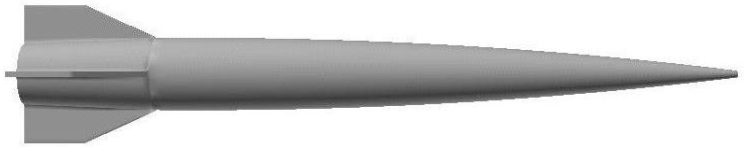
Data Source	Zero-Yaw Axial Force Coeff., C_{D_0}	Normal Force Coeff. Deriv., C_{N_α}	Pitching Moment Coeff. Deriv, C_{m_α}	Pitch Damping Moment Coeff., Cm_q	Magnus moment Coeff. Deriv., C_{np_α}	Roll Damping Moment Coeff., C_{lp}
Spark Range	0.359	2.081	4.209	-25.3	1.05	-0.019
CFD	0.335	2.362	4.283	-22.9	0.93	-0.019

Pitch damping moment extracted from the virtual fly-out method matches very well with that obtained by a separate unsteady CFD approach with prescribed pitching motion.

Computed C_{Mq}= -24.0 using virtual wind-tunnel approach

PDF Complete
Your complimentary use period has ended. Thank you for using PDF Complete.
Click Here to upgrade to Unlimited Pages and Expanded Features

Extraction of Aerodynamic Coefficients from Virtual Fly-Out Simulations

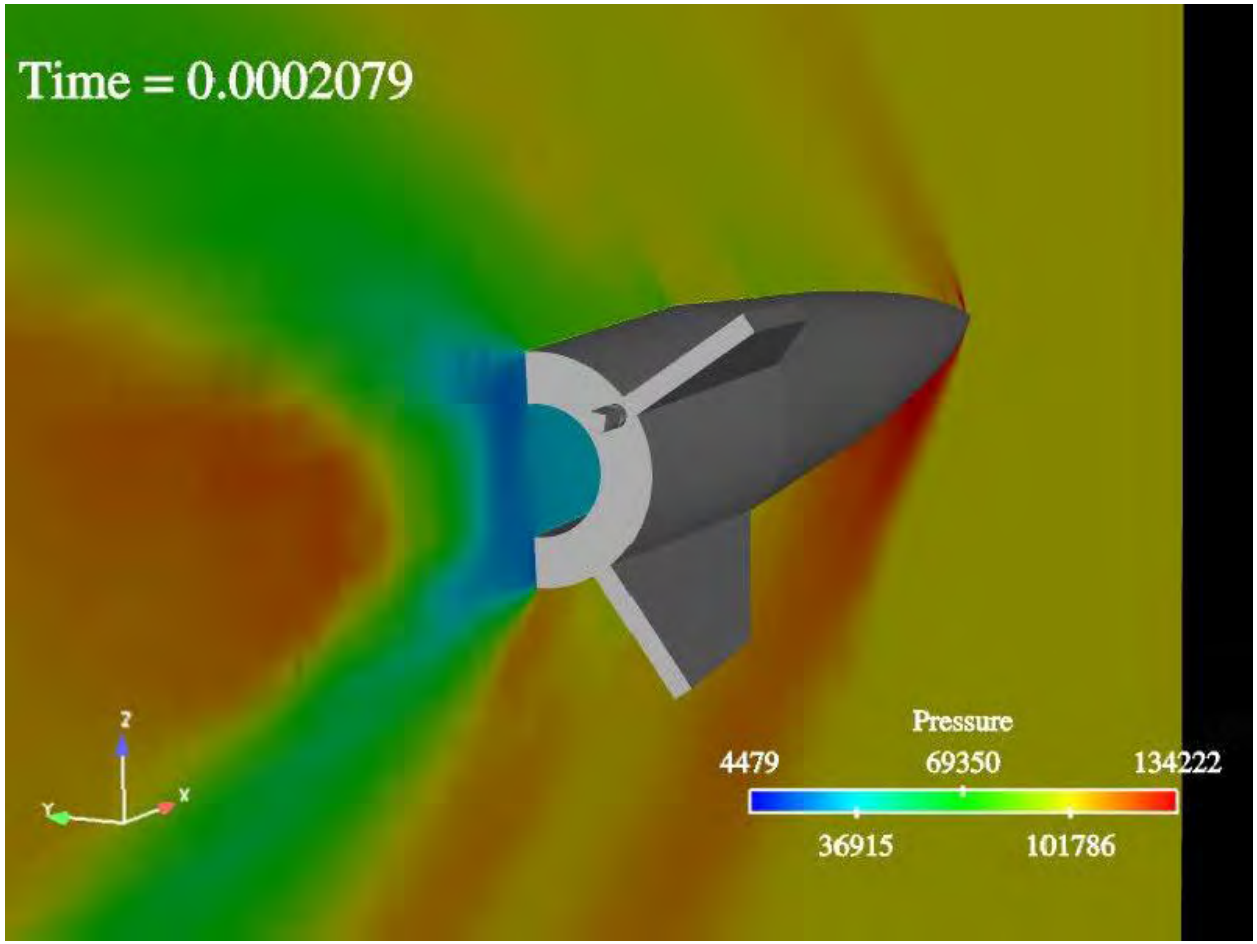


Finned Projectile

PDF Complete
Your complimentary use period has ended. Thank you for using PDF Complete.
Click Here to upgrade to Unlimited Pages and Expanded Features

ıal Fly-out of a Finned Projectile

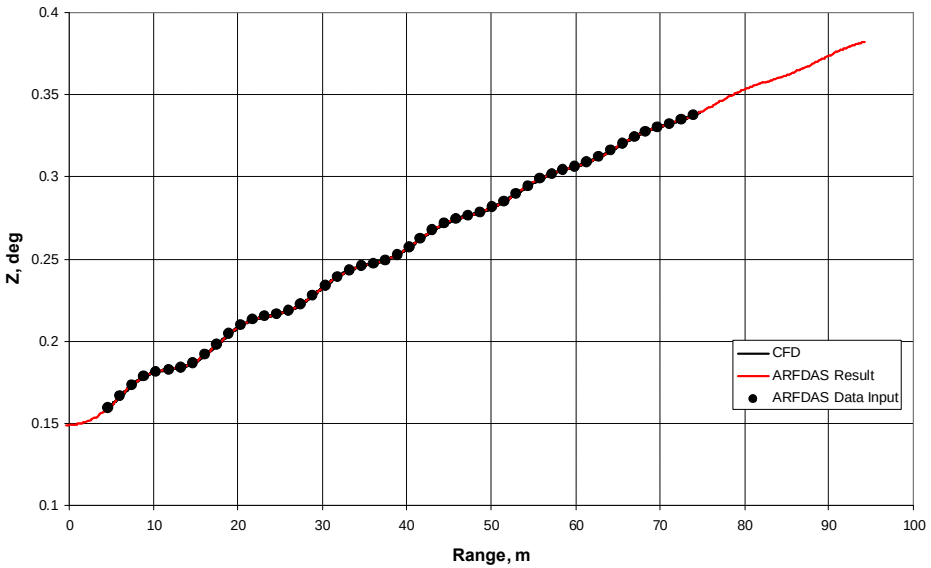
al Velocity, Mach = 3 (Supersonic)



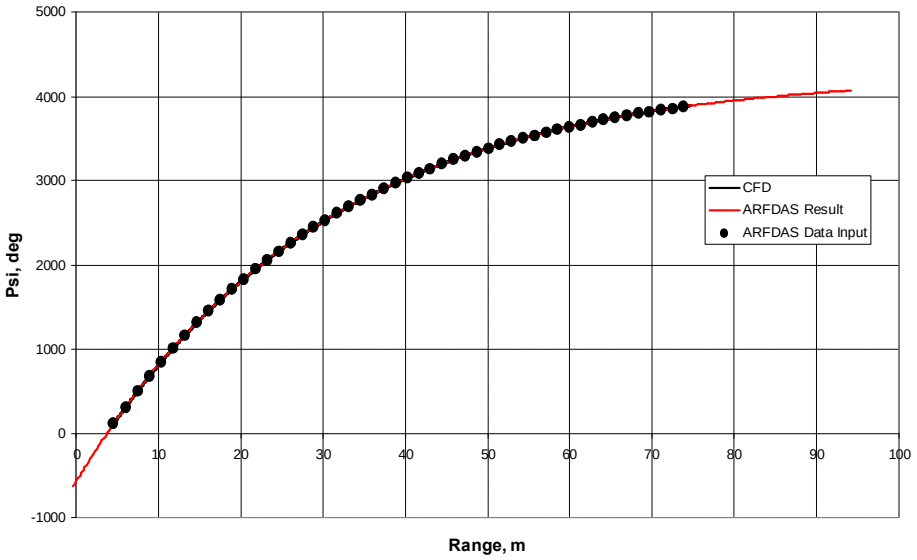
PDF Complete
Your complimentary use period has ended. Thank you for using PDF Complete.
Click Here to upgrade to Unlimited Pages and Expanded Features

RFDAS Fit of CFD Generated data Initial M = 3.0

1. Aerodynamic coefficients extracted from CFD using range reduction software, ARFDAS using the virtual fly-out solutions
2. Position (x,y,z) and the orientation (three Euler angles) of the projectile, obtained from the virtual fly-out simulations, were provided as input to ARFDAS. ***Same procedure is used for actual flight measured data.***



Z-distance



Euler roll angle

PDF Complete
Your complimentary use period has ended. Thank you for using PDF Complete.
Click Here to upgrade to Unlimited Pages and Expanded Features

xtracted Aerodynamic Coefficients from Virtual Fly-Out Simulation

Data Source	Mach No.	CXo	CNa	Cma	Cmq	Clp
Spark Range	3.0	0.221	5.83	-12.60	-196	-2.71
CFD	3.0	0.253	5.88	-12.46	-172	-3.24

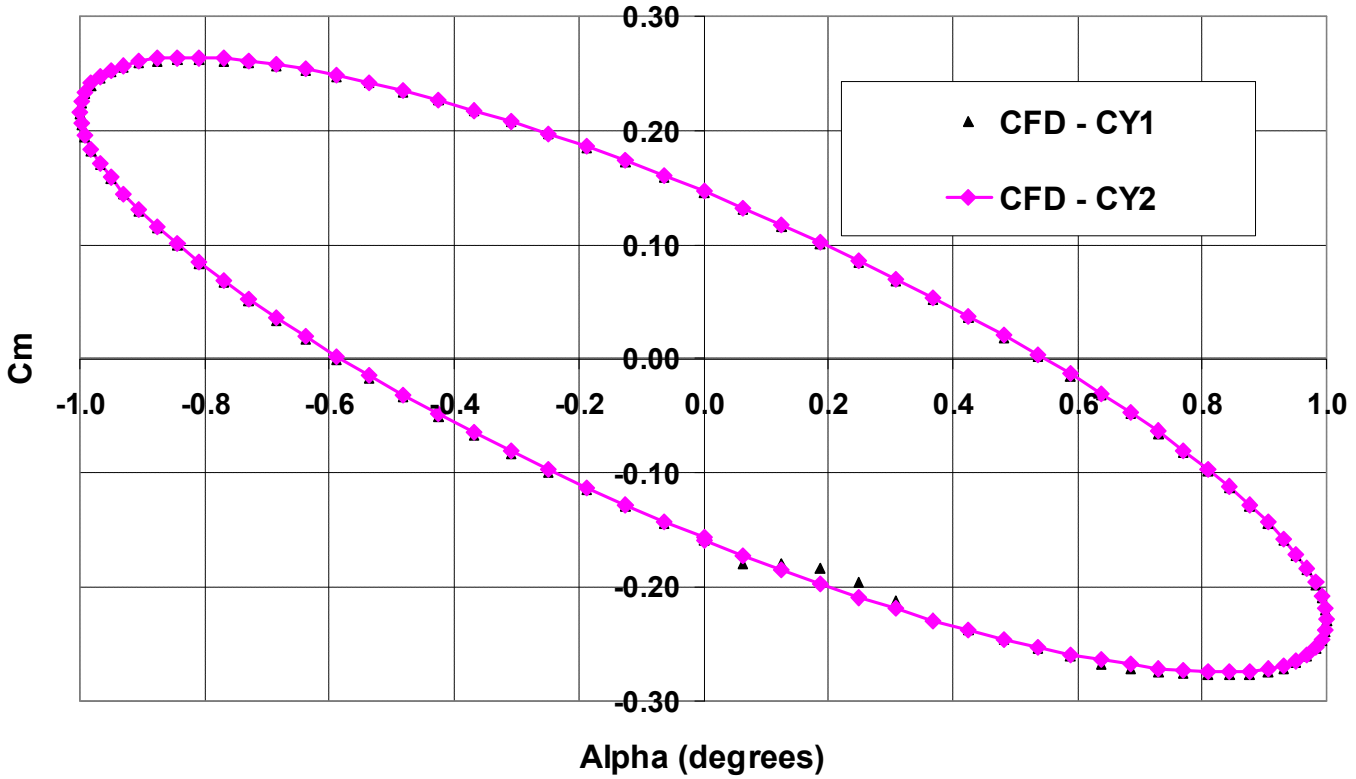
Pitch-Damping Moment Coefficient

PDF Complete
Your complimentary use period has ended. Thank you for using PDF Complete.
Click Here to upgrade to Unlimited Pages and Expanded Features

e-history of the Pitching Moment with Angle of Attack

Mach = 3.0

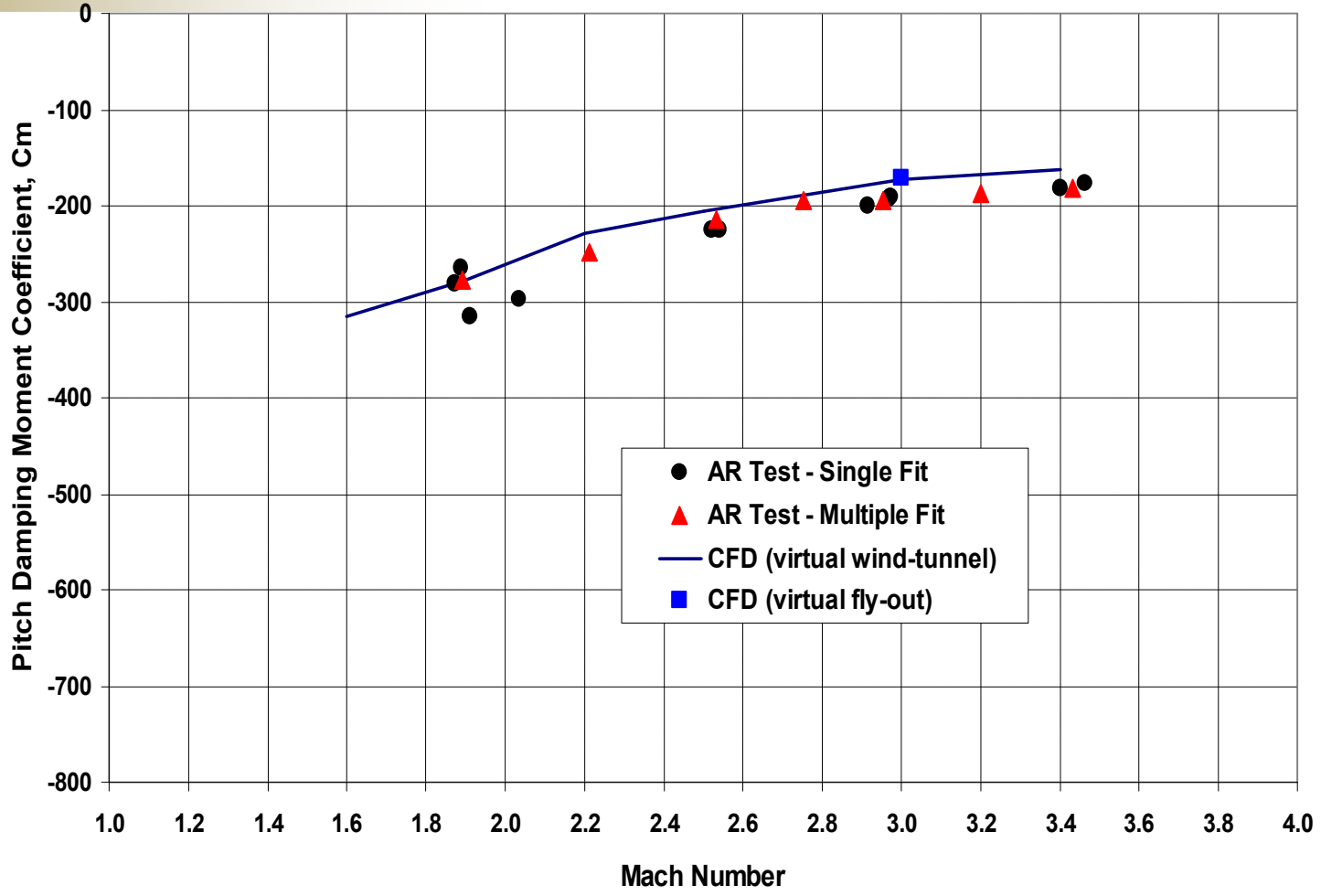
Virtual Wind Tunnel Method



Pitch damping moment is obtained directly from the time-history plot of the pitching moment coefficient resulting from the imposed pitching motion.

PDF Complete
Your complimentary use period has ended. Thank you for using PDF Complete.
Click Here to upgrade to Unlimited Pages and Expanded Features

omputed Pitch-Damping Moment icient as a function of Mach number



- Computed pitch-damping moment coefficients match fairly well with the data obtained from free flight tests.
- Almost identical prediction by both virtual fly-out and virtual wind-tunnel techniques.

PDF Complete
Your complimentary use period has ended. Thank you for using PDF Complete.
Click Here to upgrade to Unlimited Pages and Expanded Features

Concluding Remarks

- Multidisciplinary CFD/Rigid Body Dynamics Coupling for Virtual Fly-Outs
  - Integrated unsteady aerodynamics and flight dynamics
  - All aerodynamic coefficients (static and dynamic) can be easily extracted from the same virtual fly-out solution
  - Technique easily reduces to the virtual wind tunnel approach for computation of dynamic pitch damping derivatives
- Aerodynamic coefficients extracted (both static and dynamic) match fairly well with the data obtained from free flight tests
- Both virtual fly-out and virtual wind-tunnel methods essentially predict the same dynamic pitch damping moment coefficients

A Comparative Study of Penetration Codes for Brittle Materials

Dr. Sikhanda Satapathy, Anthony Dawson, Dr. Gregory Rodin

International Ballistics Symposium
New Orleans, Louisiana
September 23, 2008

Overview

Objective

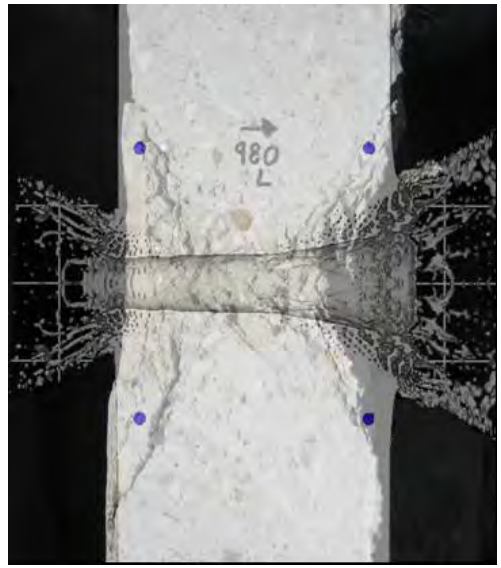
- Identify and exercise computational tools for modeling penetration of concrete targets, and compare with IAT experiments

Back Ground

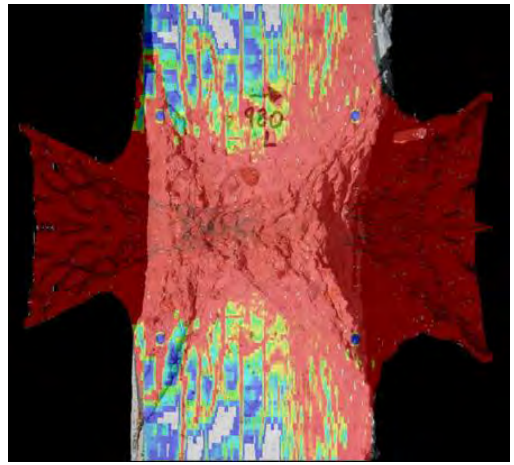
- Earlier comparisons (reported in 2007 HVIS) were not satisfactory
- A non-local peridynamic approach (EMU) was identified for comparison with continuum method (CTH.)

Approach

- Evaluate peridynamics as an alternative approach and compare with CTH's BFK and HJC models.
- Benchmark CTH and EMU with Cavity Expansion Analysis
- Validate with low velocity deceleration data



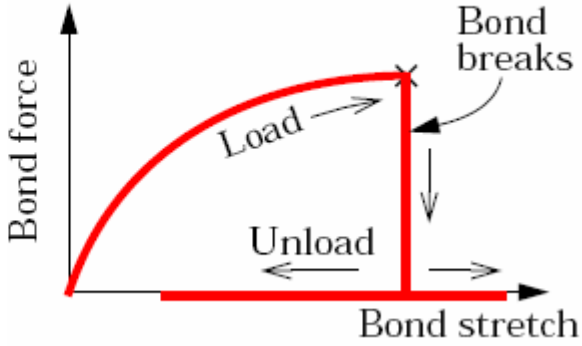
CTH (BFK) model compared with experiment

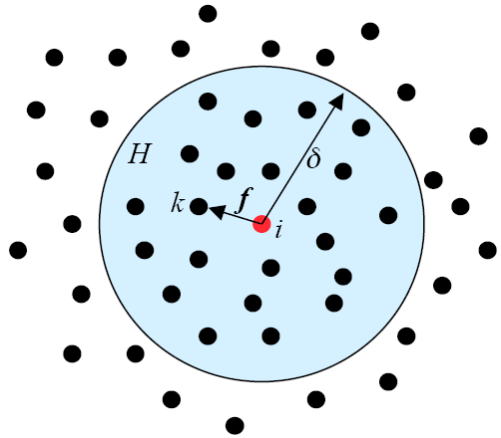


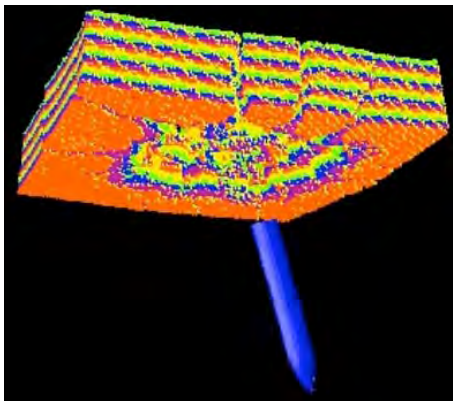
CTH (HJC) model compared with experiment

Peridynamic Method

- Classical Continuum Mechanics uses partial differential equations. However, spatial derivatives may not exist everywhere in the body (i.e. fractures)
- Peridynamic method* uses integral equations which hold everywhere in the body, regardless of any discontinuities
- Cracks form by breaking bonds irreversibly.
- Meshless Lagrangian method





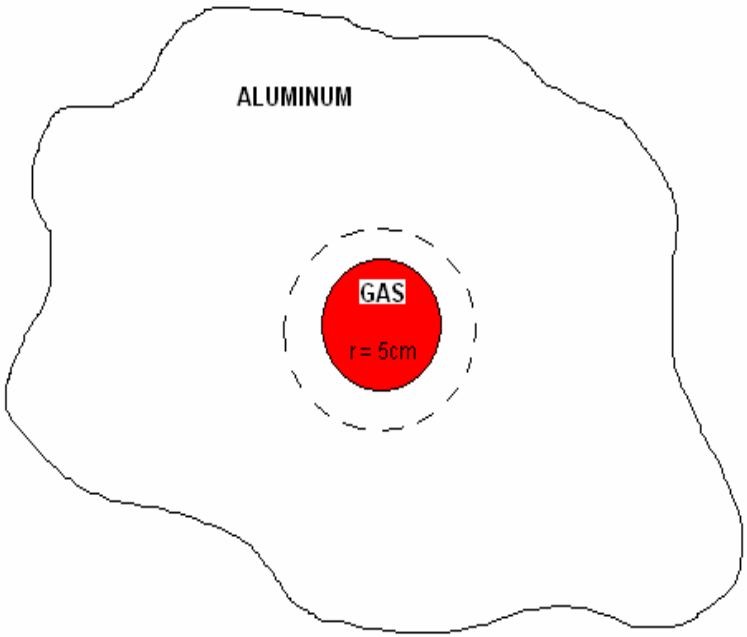


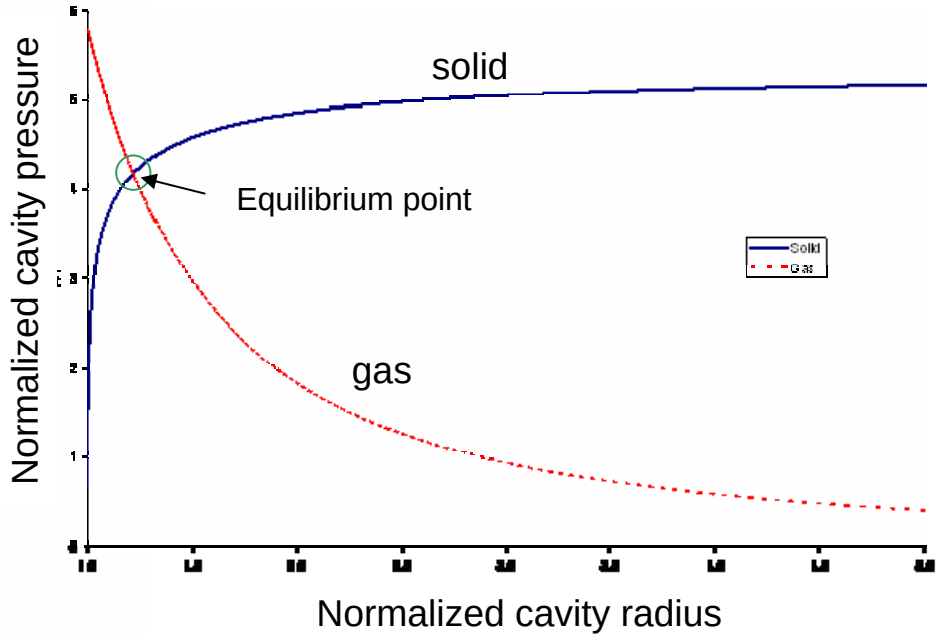
$$\rho\,\ddot{\boldsymbol{u}}_i^n = \sum_{k \in H} \boldsymbol{f}(\boldsymbol{u}_k^n - \boldsymbol{u}_i^n, \boldsymbol{x}_k - \boldsymbol{x}_i)\Delta V_i + \boldsymbol{b}(\boldsymbol{x}_i, t)$$

* Ref. Silling and Askari,Comp. Struct., 2005

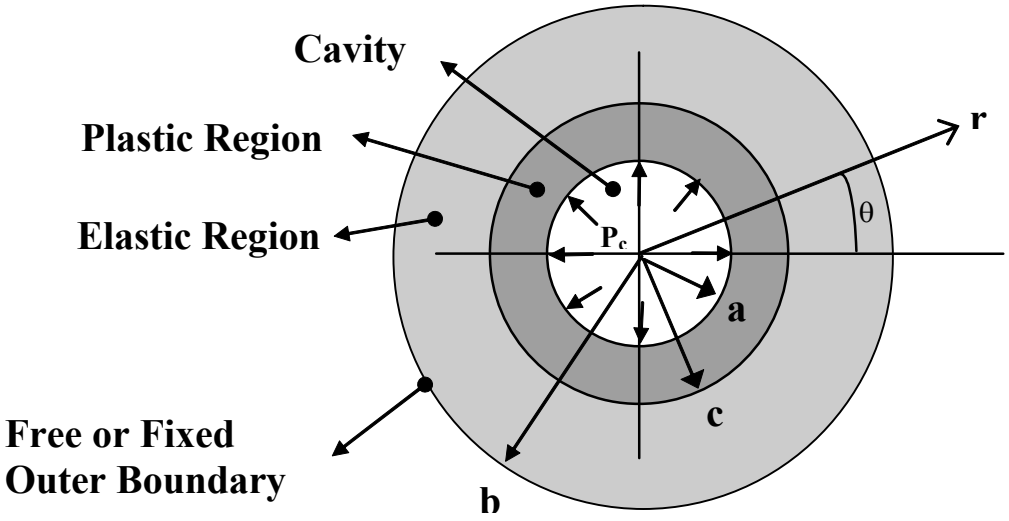
Verification Problem

- Cavity expansion problem was chosen for verification purposes.
- Since traction boundary conditions couldn't be imposed easily neither in CTH nor in EMU, a surrogate problem was chosen
- Cavity was filled with high pressure gas that expanded in an infinite body of aluminum until it reached equilibrium.





Cavity Expansion Theory



Cavity Expansion Pressure

$$\frac{P_c}{Y} = \int_0^{\infty} \frac{f(X)}{\exp(3X/2) - 1} dX$$

P < 2Y/3:

Elastic stress field (r > a)

$$s_r = -P\left(\frac{a_0}{r}\right)^3 \quad \text{and} \quad u_r = \frac{Pa_0^3}{4\mu r^2}$$

P > 2Y/3:

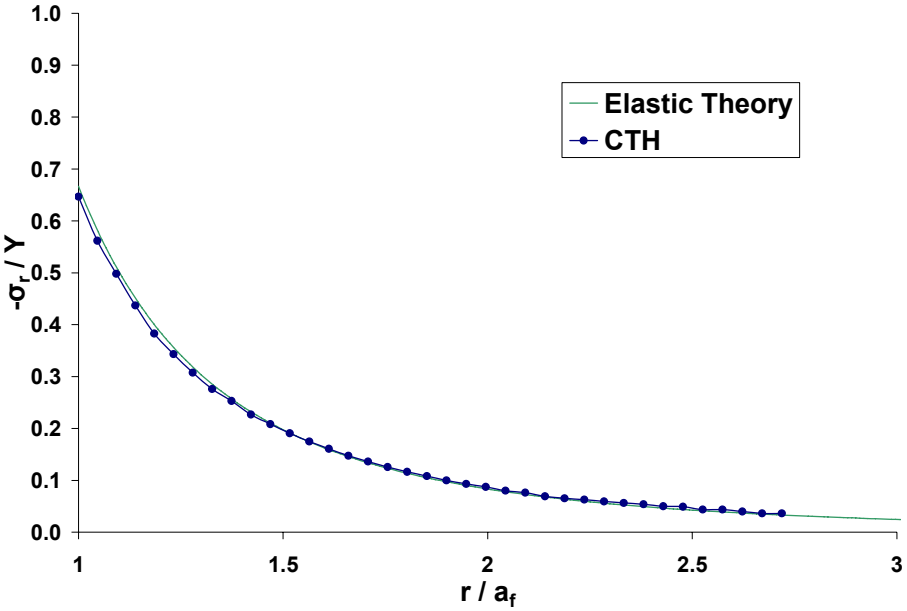
Elastic field (r > c)

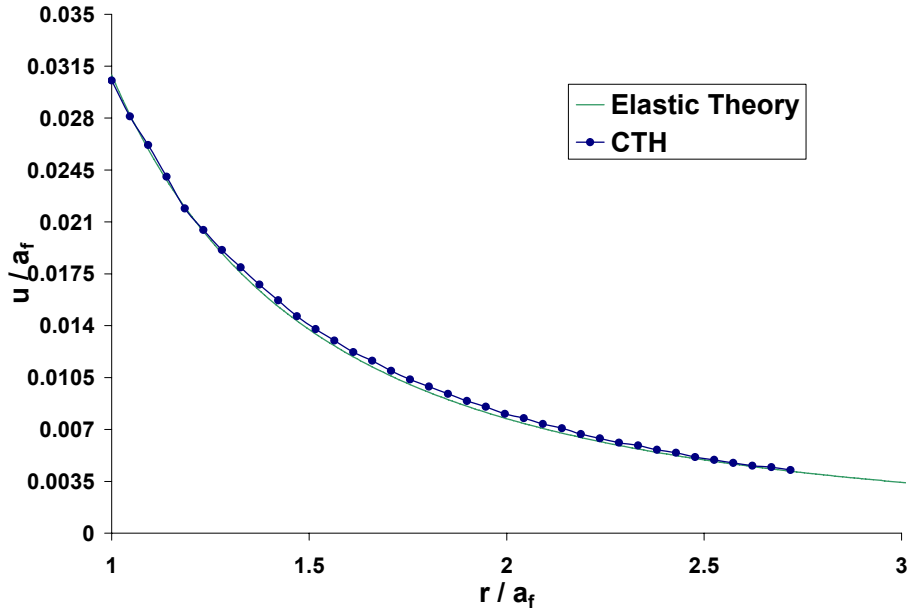
$$\sigma_r = -\left[\frac{2Y}{3}\left(\frac{c}{r}\right)^3\right] \quad \text{and} \quad u_r = \frac{Yc^3}{6\mu r^2}$$

Plastic field (a <r <c)

$$\sigma_r = -\left[\frac{2Y}{3} + 2Y\ln\left(\frac{c}{r}\right)\right] \quad \text{and} \quad u_r = r\left\{1 - \left[1 - \left(\frac{c}{r}\right)^3\left(1 - e^{\frac{-Y}{2\mu}}\right)\right]^{\frac{1}{3}}\right\}$$

CTH: P = 2Y/3 (elastic case)

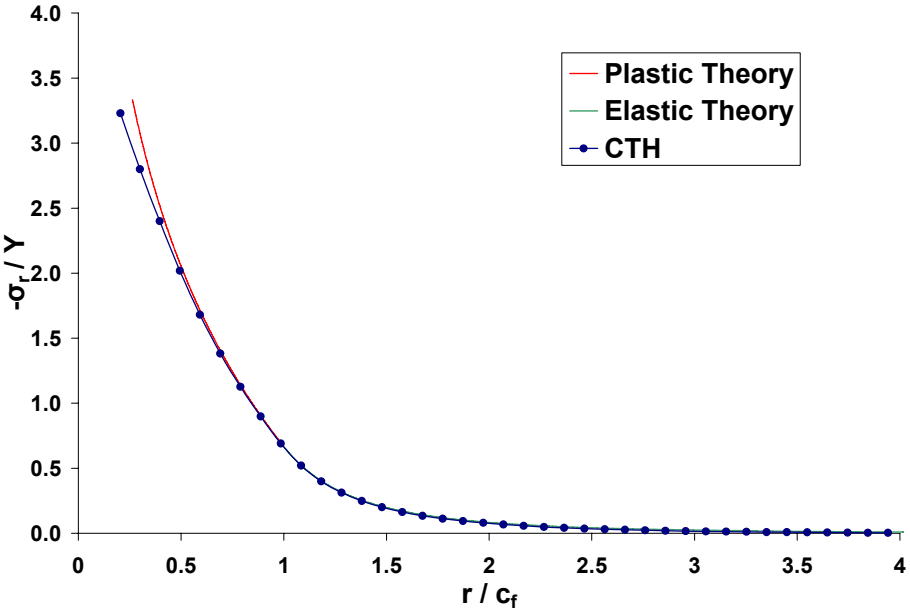


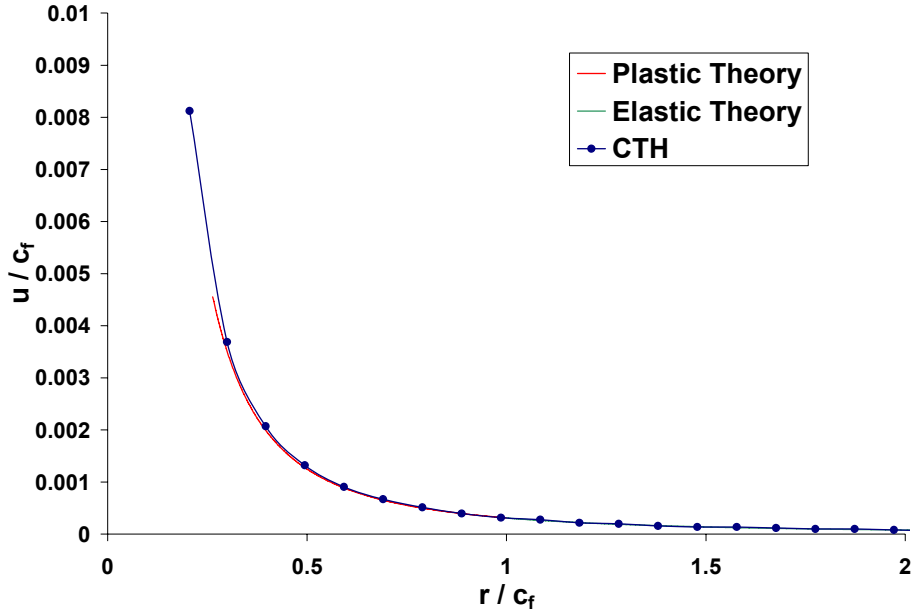


Radial stress and Displacement vs. radius for nominally elastic case

CTH calculation used a linear equation of state and an elastic-plastic strength model

CTH: P > 2Y/3 (elastic-plastic case)

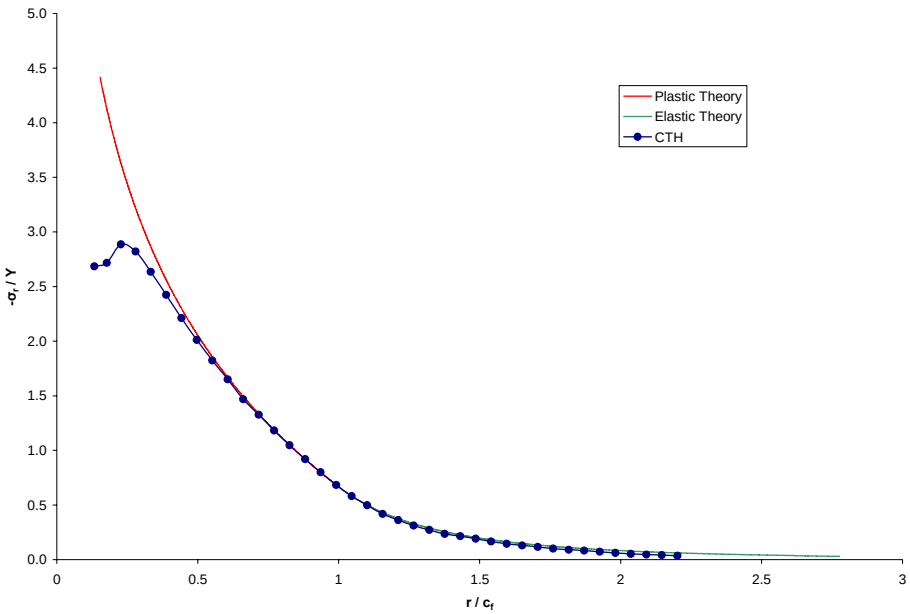


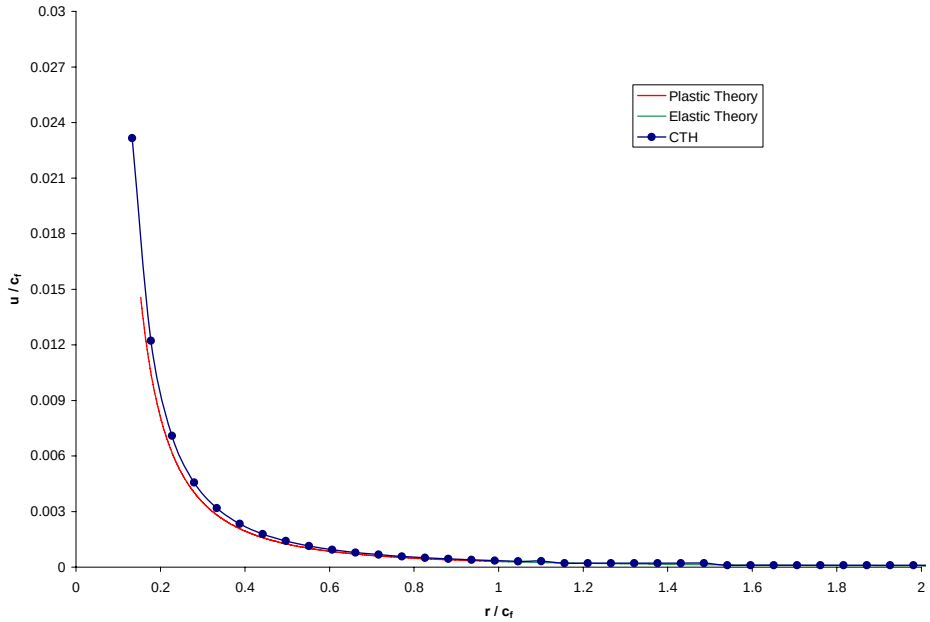


Radial stress and Displacement vs. radius for nominally elastic-plastic case.

Notice the departure of numerical solution from theory near the cavity wall.

CTH: P >> 2Y/3 (elastic-plastic case)





Radial stress and Displacement vs. radius for significant plastic yielding case.

Notice the departure of numerical solution from theory near the cavity wall.

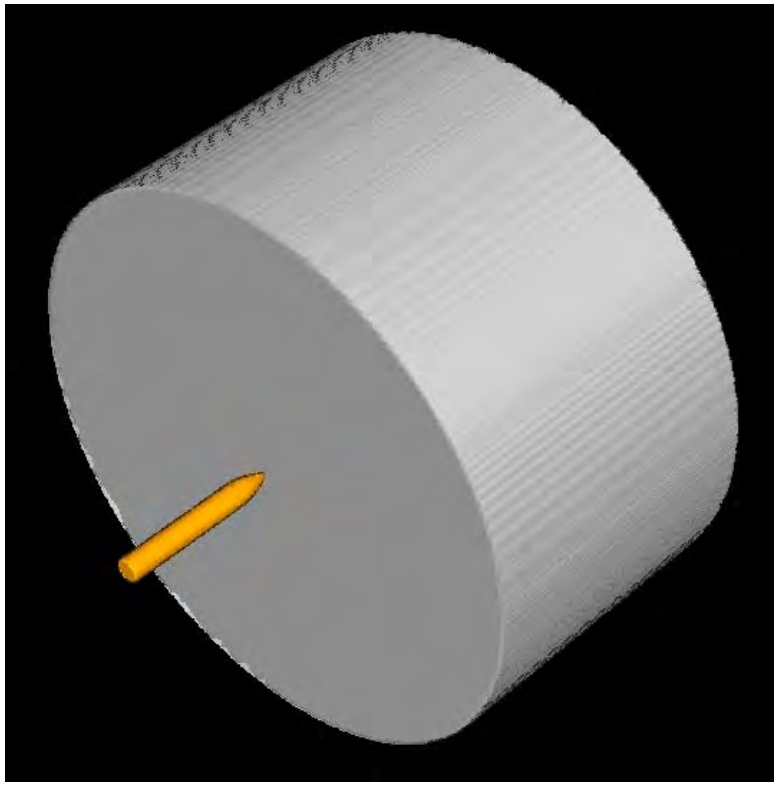
Dynamic Cavity Expansion: $P_0 \left(\frac{a_0}{a}\right)^{3g} - \frac{2Y}{3} + 2Y \ln\left(\frac{c}{a}\right) = b_2 \ddot{a} + b_1 \dot{a}^2$

Verification summary

- CTH produced satisfactory results when dynamic effects were not significant.
- EMU implementation did not produce the desired solution since gas diffusion into solid couldn’t be prevented.
- Code modification needed to complete the verification process for EMU.

Validation Problem

- Rigid penetration into Concrete (1.83 m radius, 23 MPa f'_c)
- Steel Penetrator of 80 mm dia, 13 kg at 380 m/s
- Penetration depth and deceleration measurements taken with accelerometer



Ref: Forrestal et al.,IJIE, 2003

BFK Model

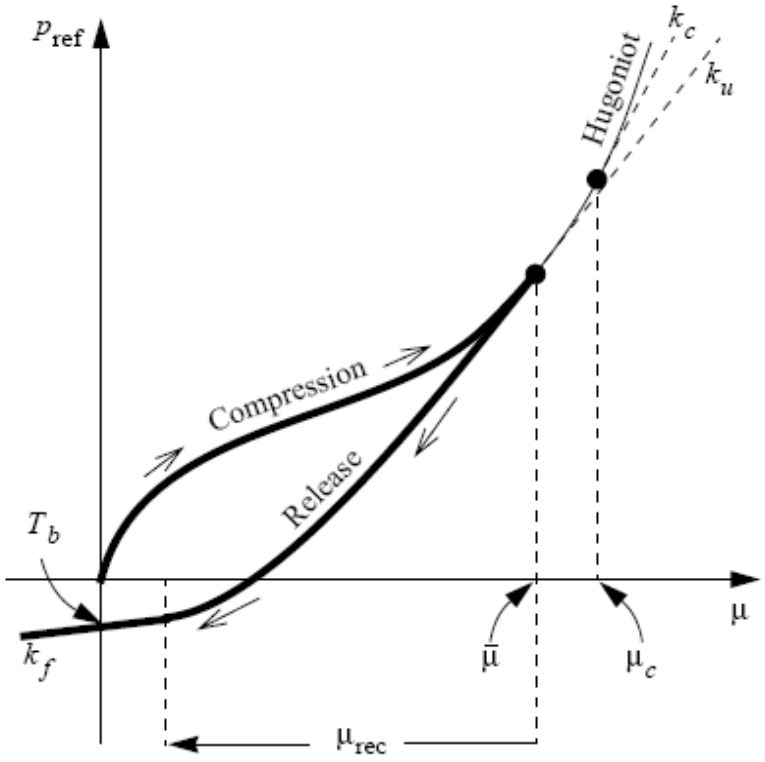


Figure 2.2. Compression (loading) followed by release (unloading) along a reference curve. (Not all the void space is crushed out in this path, $\bar{v} > v_c$.)

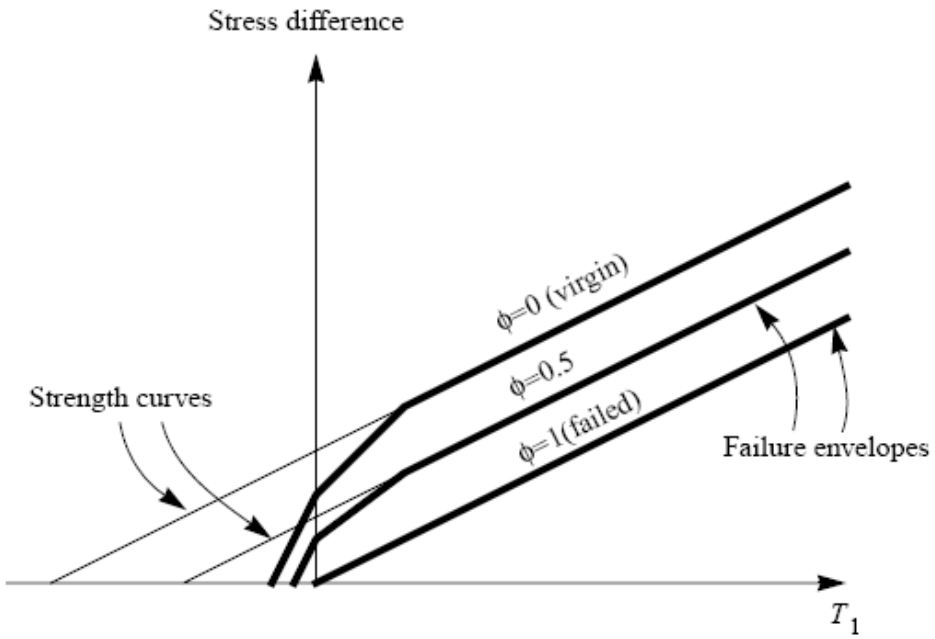
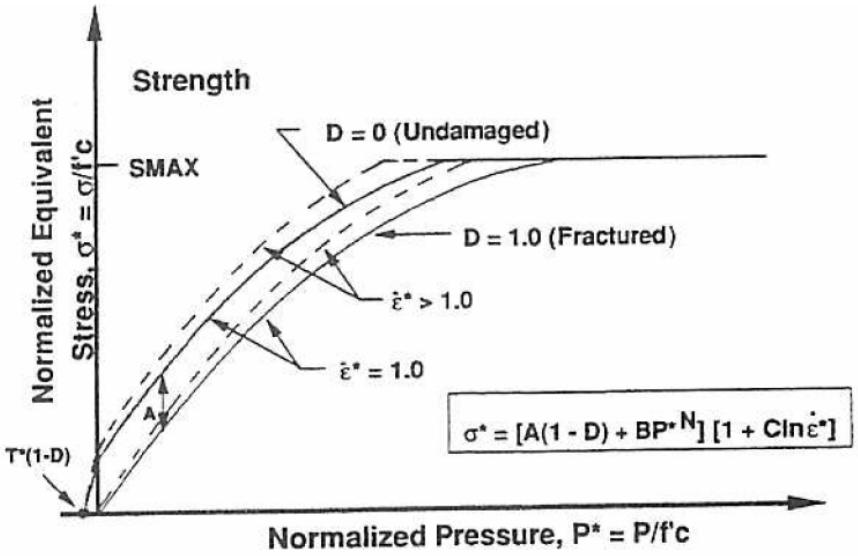
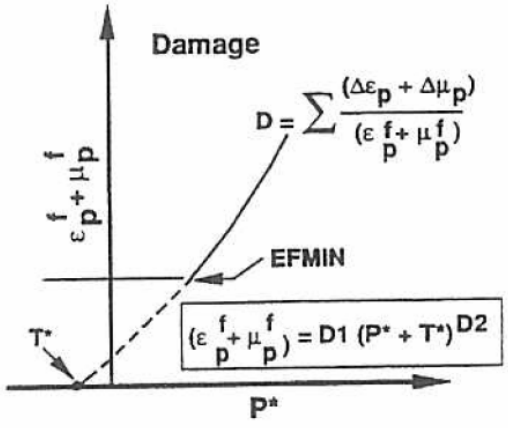


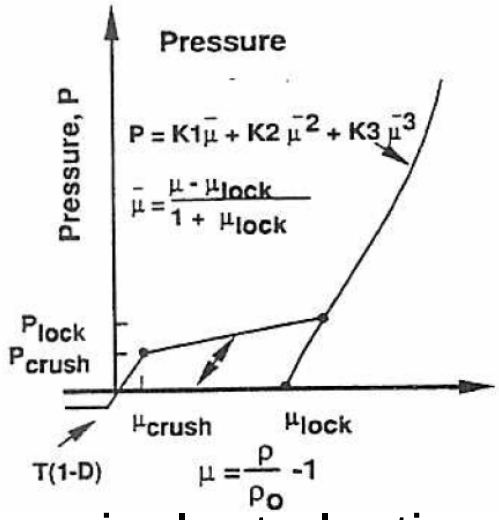
Figure 2.5. Evolution of the failure envelope.

- Scalar damage model explicitly dependent on time
- Damage has three components: brittle, ductile and compressive

HJC Model

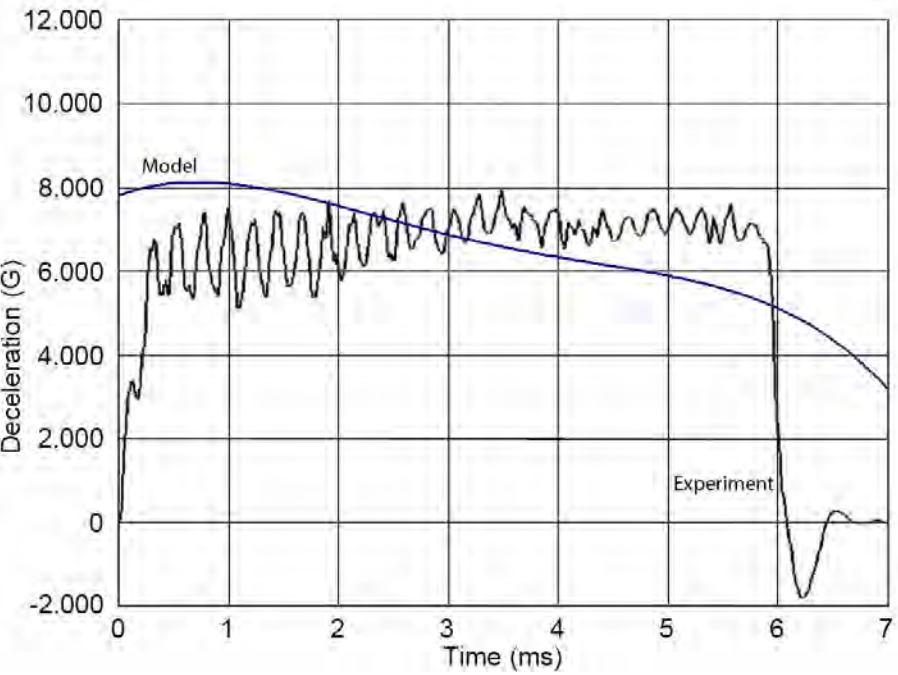






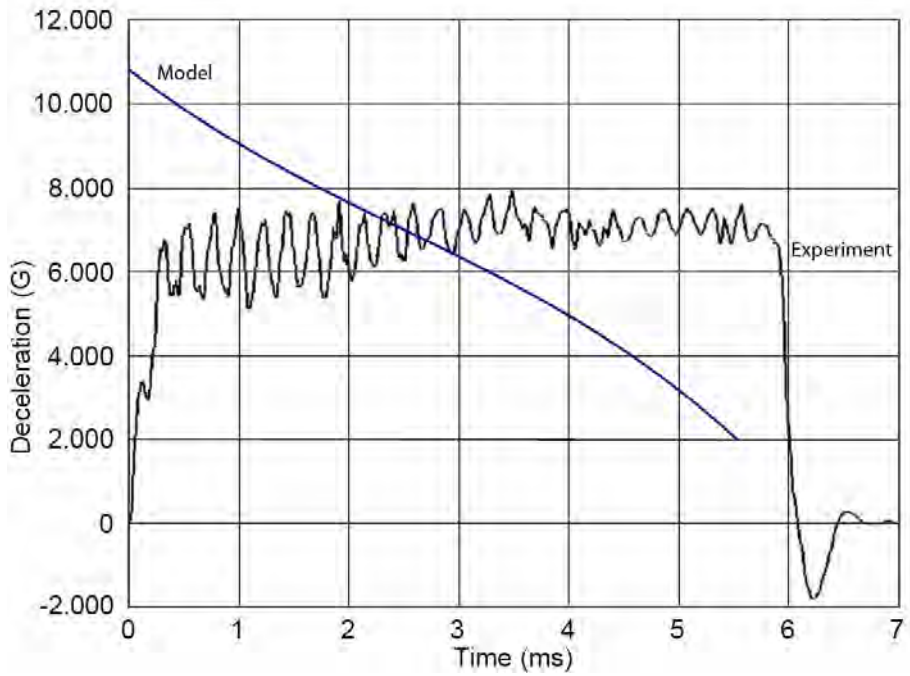
- Damage accumulated from both equivalent plastic strain and plastic volumetric strain (majority from EPS)

CTH Validation Results



BFK

Depth Under-predicted by 5.1%



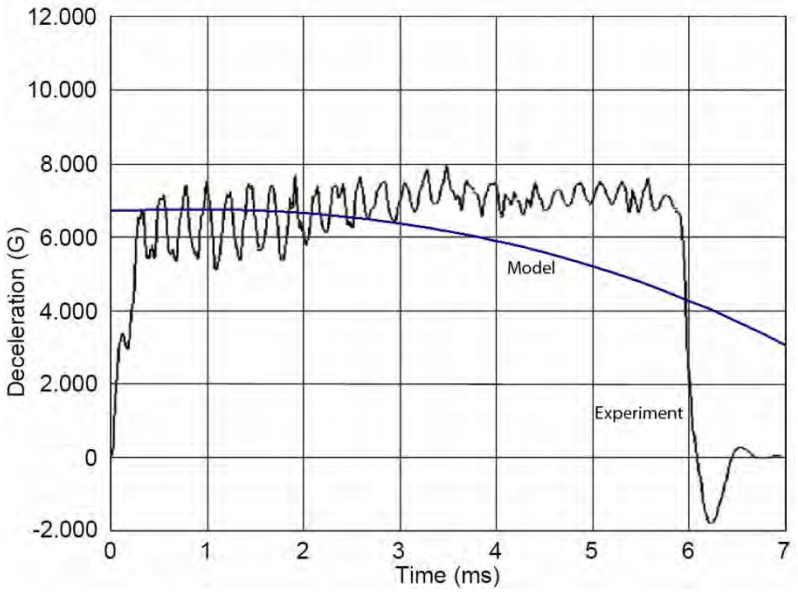
HJC

Depth Under-predicted by 23%

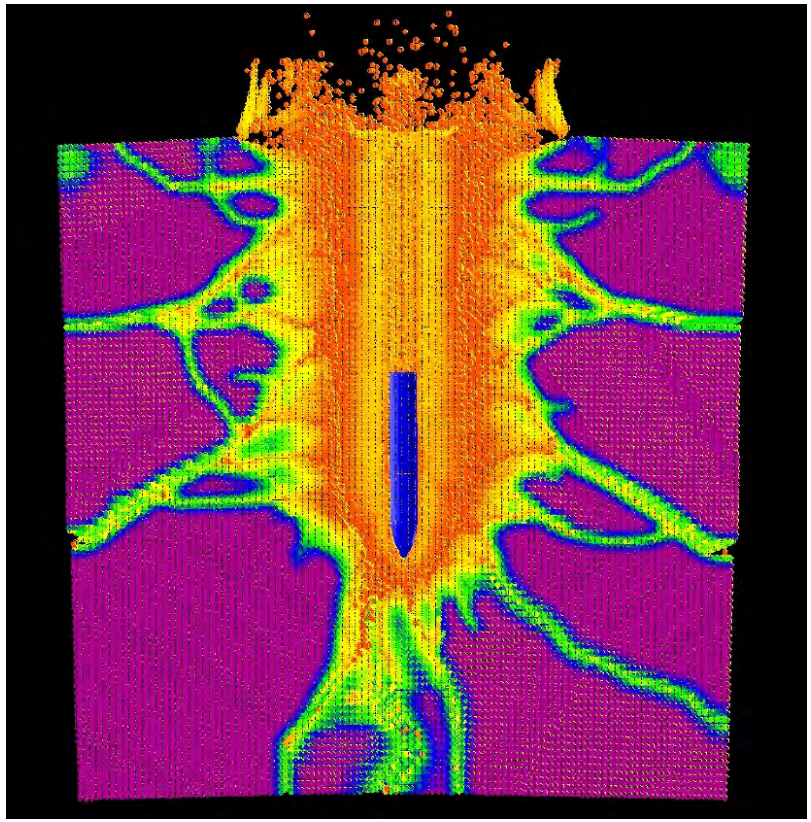
BFK simulation is in much closer agreement with test results than HJC simulation.

Ref: Forrestal et. al. IJIE, 2003

EMU Validation Results



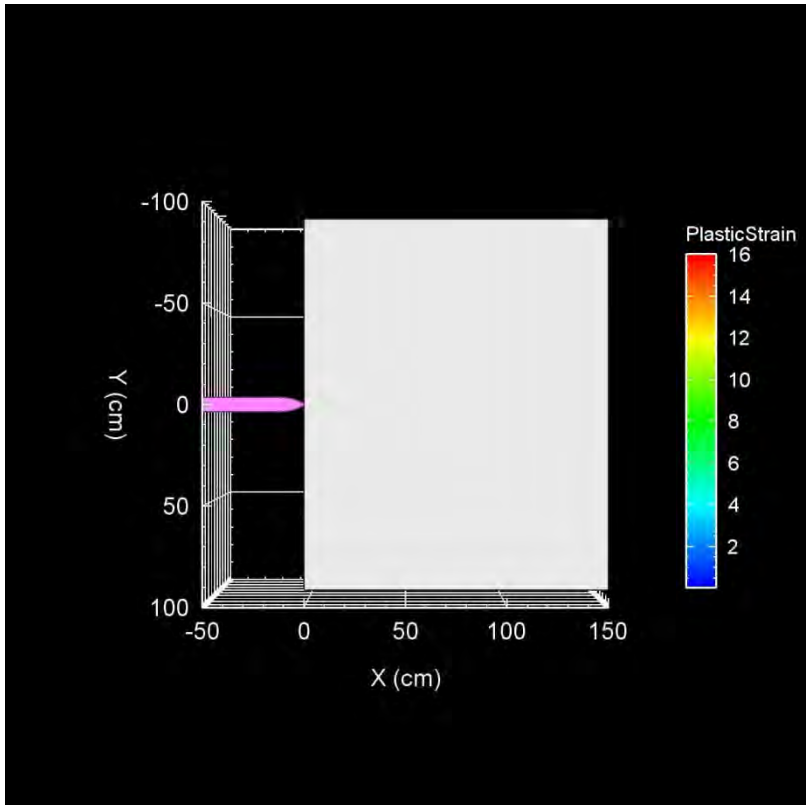
Depth Over-predicted by 0.5%



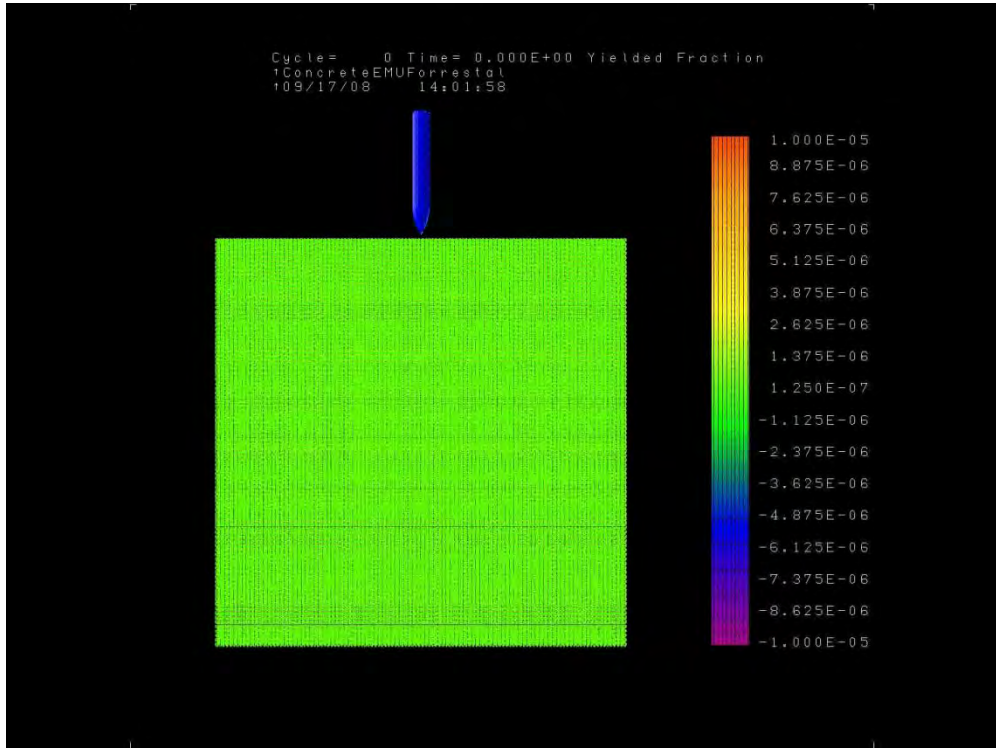
EMU accurately modeled the deceleration

Cracks in target were similar to experimental observations

Simulation Comparison



CTH



EMU

Summary

- CTH verification with cavity expansion solution for elastic-plastic materials was satisfactory when dynamic effects were not significant.
- CTH-BFK model produced reasonable agreement with deceleration data.
- EMU verification couldn’t be completed due to code limitations.
- EMU agreed with deceleration data very well.
- EMU produced fracture patterns similar to that observed in experiments.

Questions?

RDECOM

THE MECHANICS OF PROJECTILE ARREST FOR COMPLIANT CROSS PLIED UNIDIRECTIONAL LAMINATES

Brian Scott
Bryan Cheeseman
ARL, APG MD

TECHNOLOGY DRIVEN. WARFIGHTER FOCUSED.

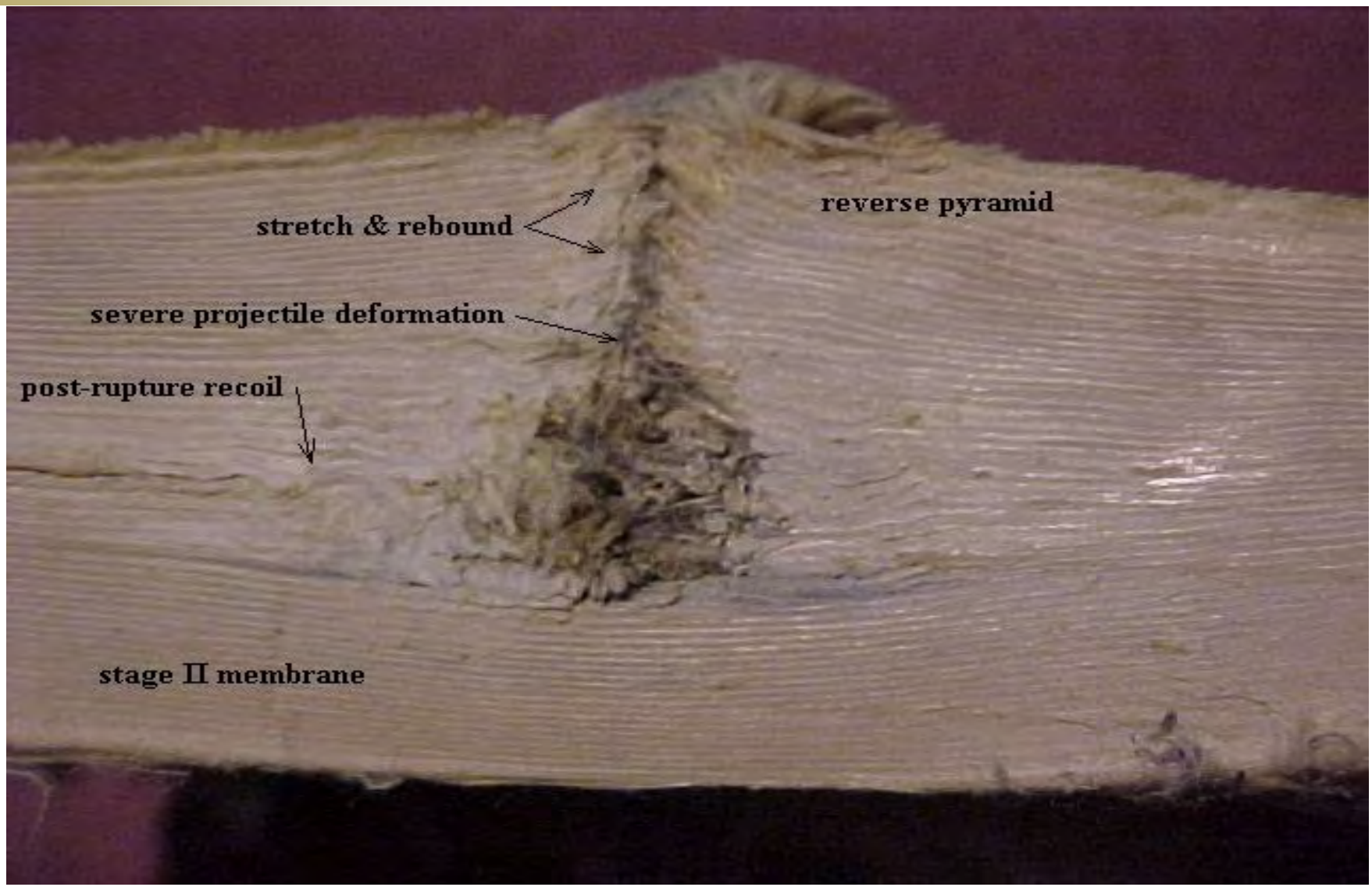
International Symposium on Ballistics
New Orleans, LA
26 September 2008

Outline

- Experimental observations
- Mechanics hypothesis
- Numerical simulations
- Conclusion

- Penetration of Kevlar Laminate by Long Rods and Jets, Scott,B and Walters, W., 12th ISB, San Antonio, 1990
- Good performance with woven architectures of high strength fibers with 20% phenolic matrix
- Better performance is obtained with:
  - Cross ply unidirectional layup
  - Finer ply architecture
  - Higher strength reinforcements
  - Elastomer (thermoplastic or thermoset) matrices
  - Lower resin content laminates

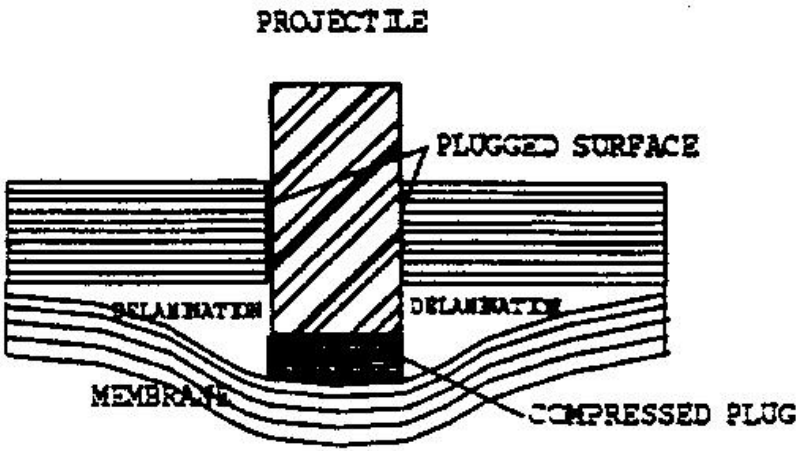
Experimental Observations



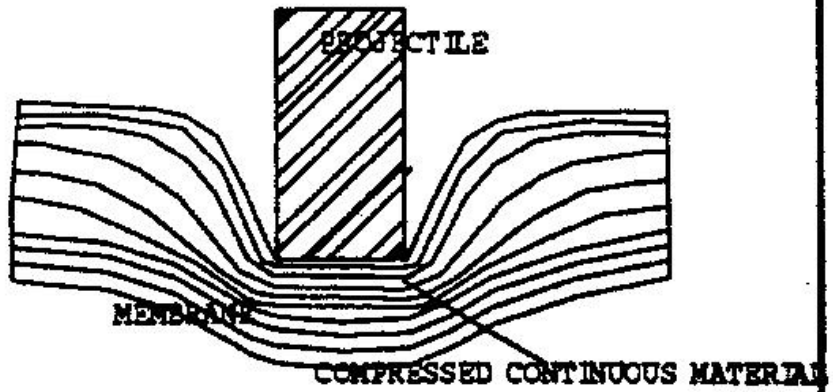
Summary of experimental observations

- **Video observations:**
  - **Uni structures exhibit global extension and displacement (first inward, then outward)**
  - **Woven structures exhibit more localized ruptures with less of the far field deformation**
- **Evidence of fiber stretching prior to tensile rupture**
- **Thru thickness compression of underlying layers**
- **Aramids exhibit little evidence of transverse shear failure**
- **UHMWPE difficult to discern due to localized melting of fiber ends**
  - **Presumably due to passage of or contact with hot projectile**
- **Tensile fiber strength: > 500ksi**
- **Transverse fabric shear strength 3 – 5 ksi (aramid or UHMWPE) ASTM D732**
- **Transverse compression strength ? Not well defined yield point (behaves like elastomer)**
- **UHMWPE 20% thicker than aramid laminate at equal areal density**

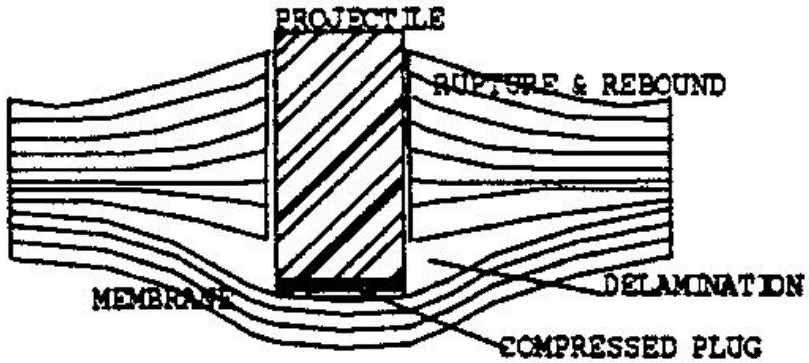
Experimental Observation



Classical Plug & Membrane Behavior



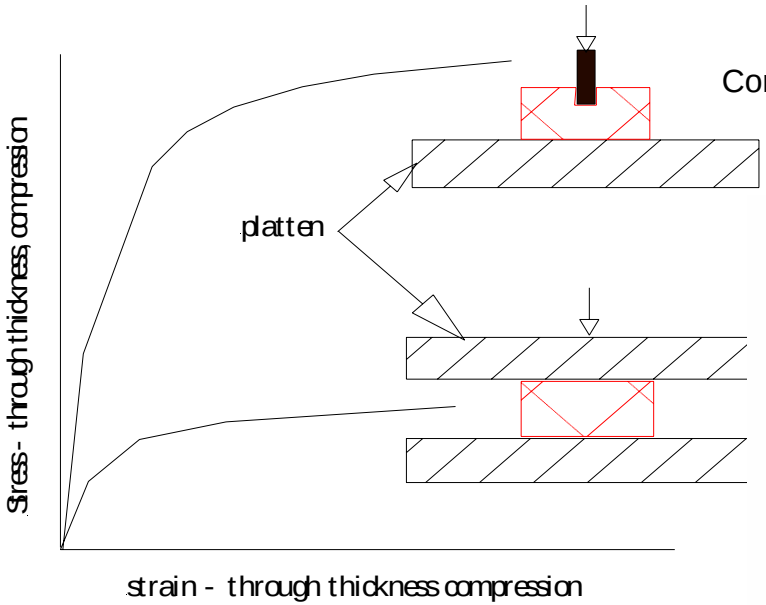
Stage I - Prior to front layer rupture



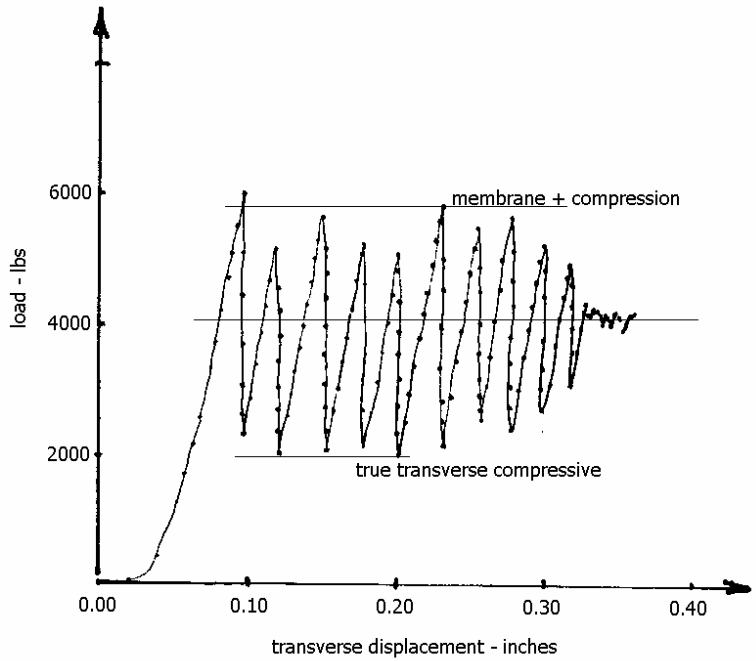
Stage II - Post front layer rupture

Experimental Observation

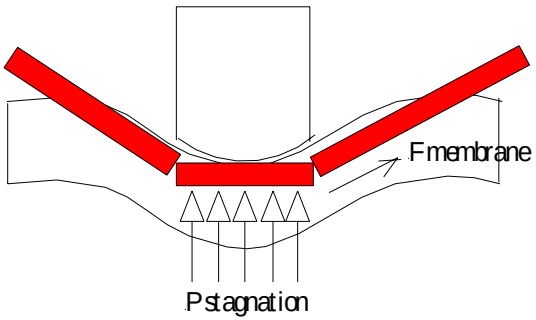
Constrained Compression Test

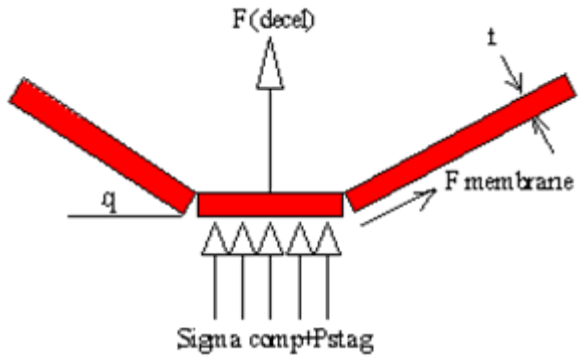


Composites Engineering, Vol 4, No. 3, Woodward, et al, 1994

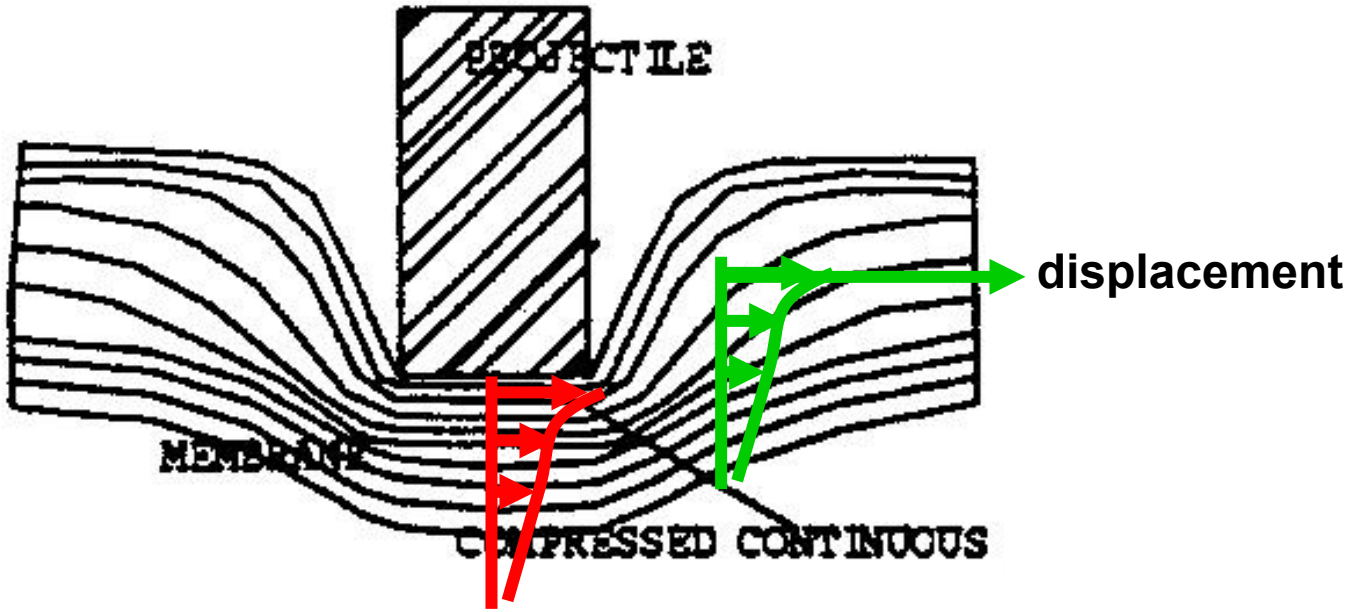


Predominant deceleration forces





Hypothesis



Surface fibers impacted
Material cannot flow until fibers rupture (approx. 4%)
Surface fibers are compressed transversly and forced into underlying layers
“Self-Confined” material develops large comp stress or hydrostatic pressure
Large compressive stresses decelerate projectile

Ansys Autodyn

Dyneema HB2

O'Donoghue, P.E., Anderson, C.E., Jr., Friesenhahn, G. J. and Parr, C. H. 1992. "A Constitutive Formulation for Anisotropic Materials Suitable for Wave Propagation Computer Programs," *J.Comp. Materls*., p.p. 26(13), 1860-1884.

Anderson, C.E., Jr., Cox, P. A., Johnson, G. R. and P.J. Maudlin, P.J. 1994. "A Constitutive Formulation for Anisotropic Materials Suitable for Wave-Propagation Computer Programs 2," *Computational Mechanics*, 15(3), 201-223.

Hiermaier, S., Riedel, W., Clayhurst, C.J., Clegg, R.A. and Wentzel, C.M. 2003. "AMMHIS Advanced Material Models for Hypervelocity Impact Simulations," EMI Report No. 175/03, Freiburg, Germany.

Riedel, W., Harwick, W., White, D.M. and Clegg, R.A. 2003. "ADAMMO Advanced Material Damage Models for Numerical Simulation Codes," EMI Report No. 175/03, Freiburg, Germany.

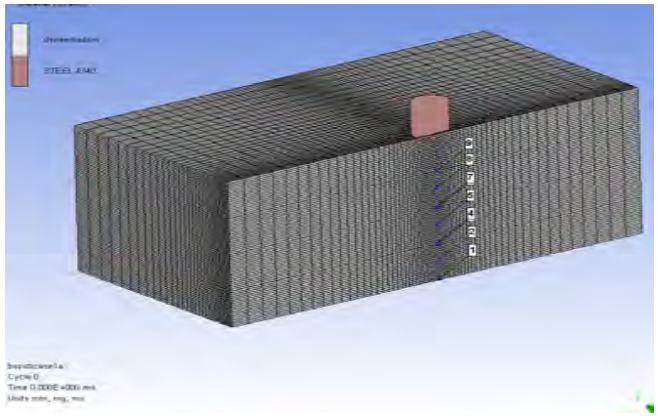
Stijnman, P.W.A., 1995. "Determination of the elastic constants of some composite by using ultrasonic velocity measurements," *Composites*, 26, 597-604.

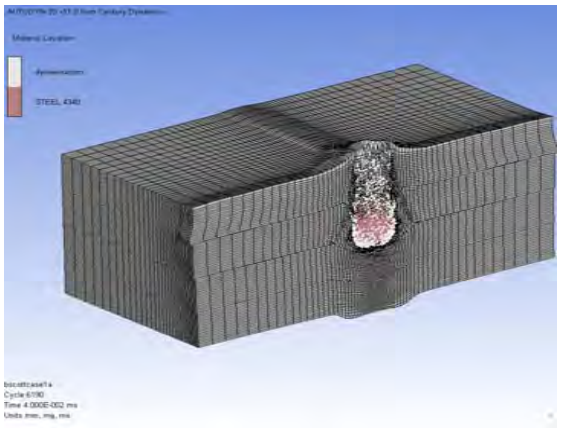
Hayhurst, C., Leahy, J., van der Jagt-Deutekom, M., Jacobs, M. and Kelly, P. 2000. "Development of Material Models for Numerical Simulation of Ballistic Impact onto Polyethylene Fibrous Armour," *Proceeding of the Personal Armour Systems Symposium, Colchester, U.K.*

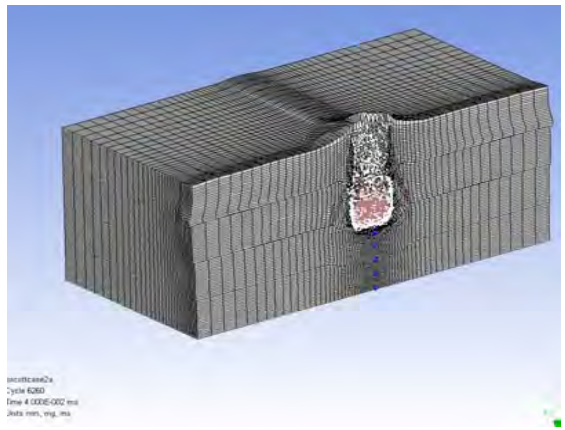
"Data used to model the ballistic behaviour of HB25 in ADAMMO model of Autodyn," Oct. 17 2006. *DSM Dyneema*, Urmond, The Netherlands.

20 mm diameter 50 gram 4340 steel cylinder
2.0 km/s impact velocity
100 mm thick initial 40 microseconds
Two b.c. Rigid backing / simple frame

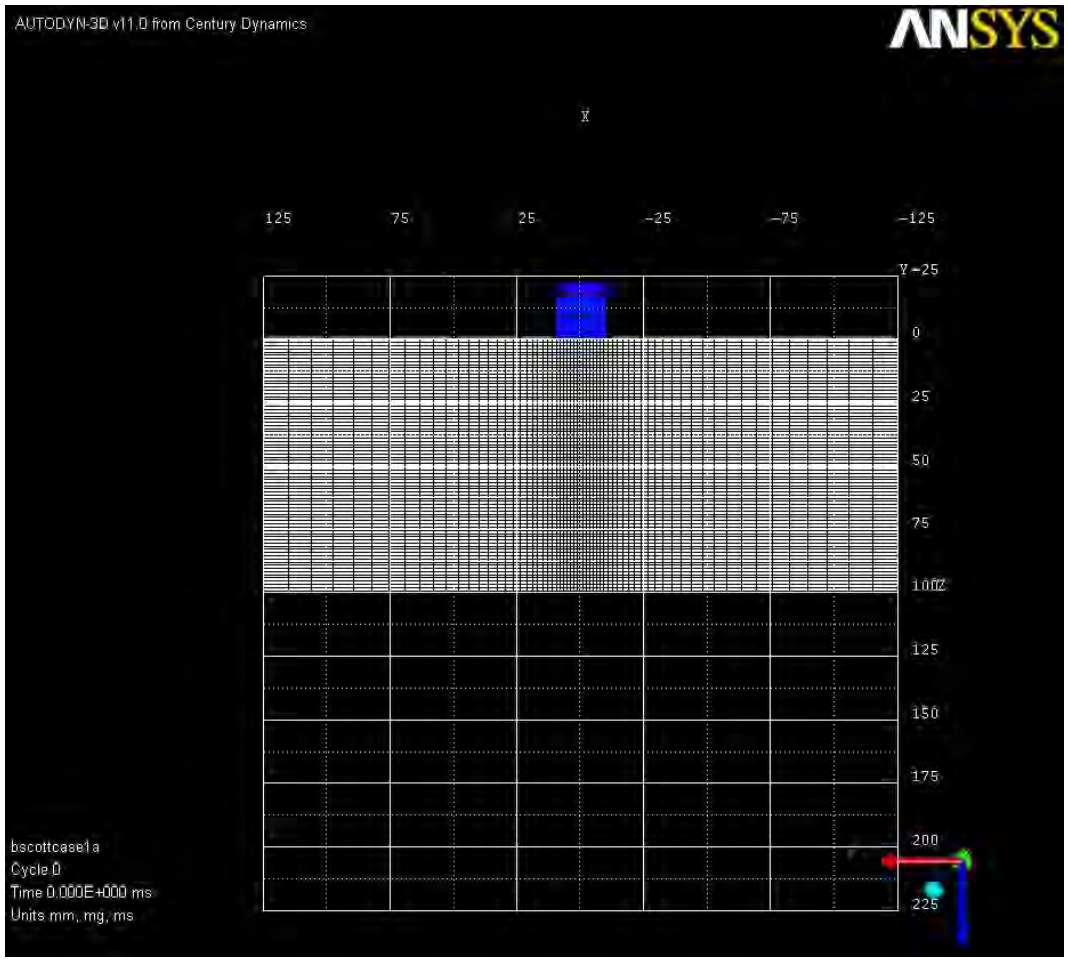
Simulation



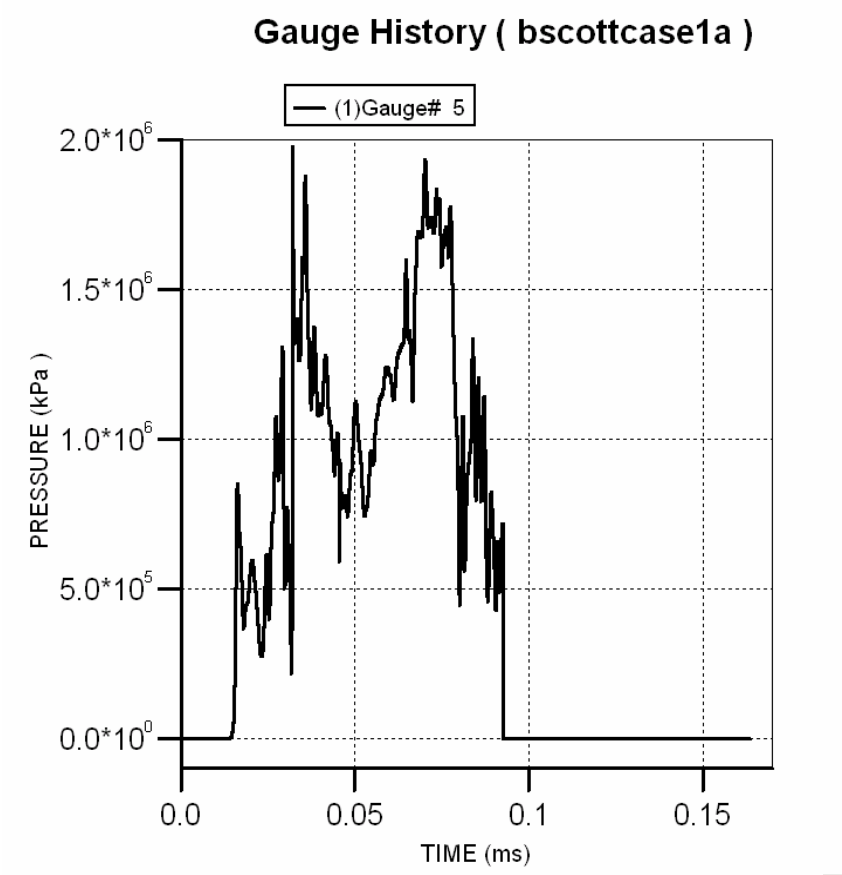




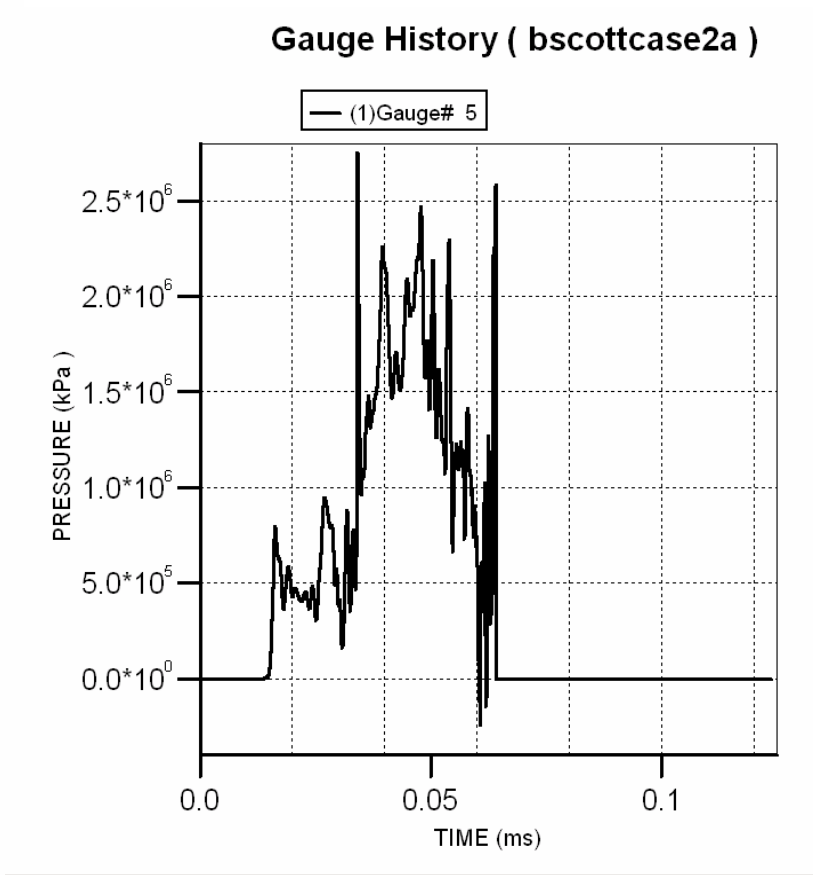
Simple frame b.c. movie



Pressure transient in front of projectile

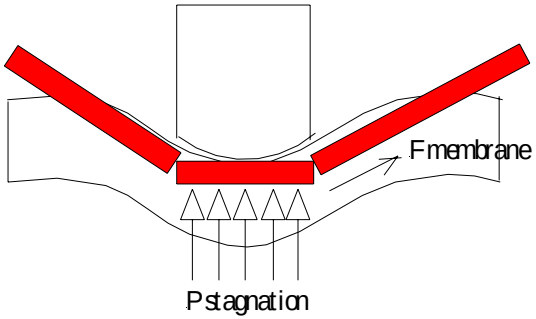


Simple frame b.c.



Rigid backing b.c.

Implication of large pressures



$$\int F \cdot dt = \delta(mv)$$

assume: penetration rate: $u = v/(1+\sqrt{\rho_t / \rho_p})$

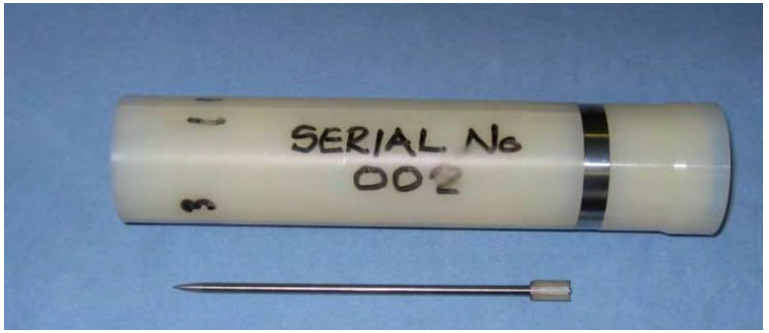
target thickness:	10.0 cm
impact velocity:	2000 m/s
projectile diameter	1.0 cm
projectile mass	5.0 gm
$\sqrt{\rho_t / \rho_p}$	.35
linear f(t)	

Initial axial momentum: 100 kg m/s
Pressure from simulation: 2M kPa (300 ksi)
Assume uniform over cross-section
First 40 microseconds: 25 kg m/s

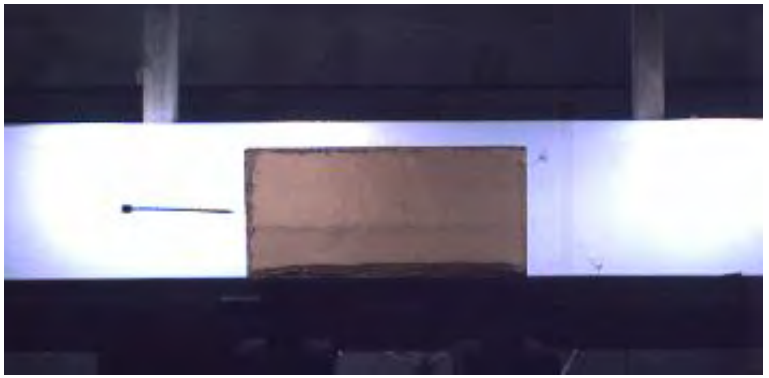
Conclusions

- Hypothesis of self-constrained compression leading to extraordinary axial retardation stresses is confirmed by transient simulations
- Comparing two distinct boundary conditions, we identify the benefit of higher thru thickness pressures with the rigid backing case
- The high pressures account for a large fraction of the impulse delivered to the projectile
- The failure modes involving fiber axial tensile strength and transverse compressive strength appear to be uncoupled
- Uni construction allows for more global extension prior to rupture than woven architecture
- Compliant matrix and elastomeric transverse compressive behavior of fibers may be most important

PDF Complete
Your complimentary use period has ended. Thank you for using PDF Complete.
Click Here to upgrade to Unlimited Pages and Expanded Features







Experiments with Gun Launched Penetrators into Gelatin Target Materials

J.Stubberfield, C. Woodley, N. Lynch and A. Hepper

A presentation to: The 24th International Symposium on Ballistics

25th September 2008

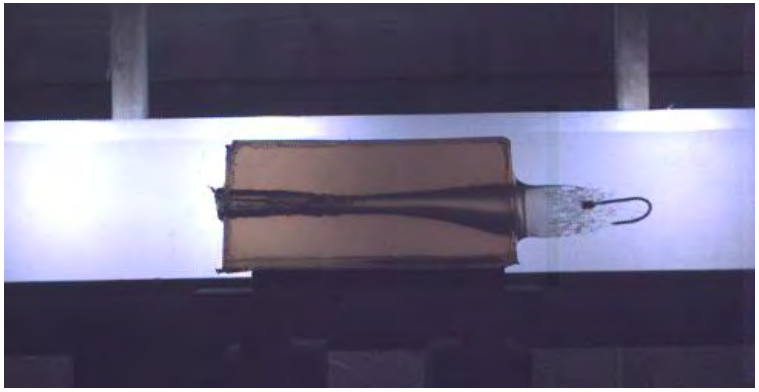
QinetiQ | [dstl]

www.QinetiQ.com

© Copyright QinetiQ Limited 2008

PDF Complete
Your complimentary use period has ended. Thank you for using PDF Complete.
Click Here to upgrade to Unlimited Pages and Expanded Features

01 Penetrator and Launch Package Design
02 Interior Ballistic Modelling
03 Choice of Gun System
04 Instrumentation
05 Experimental Set Up
06 Target Before Penetrator Interaction
07 The Effects of Pitch at Impact
08 Targets After Penetrator Interaction
09 Conclusions
10 Questions



© Copyright QinetiQ Limited 2008

PDF Complete
Your complimentary use period has ended. Thank you for using PDF Complete.
Click Here to upgrade to Unlimited Pages and Expanded Features

01

Penetrator and Launch Package Design

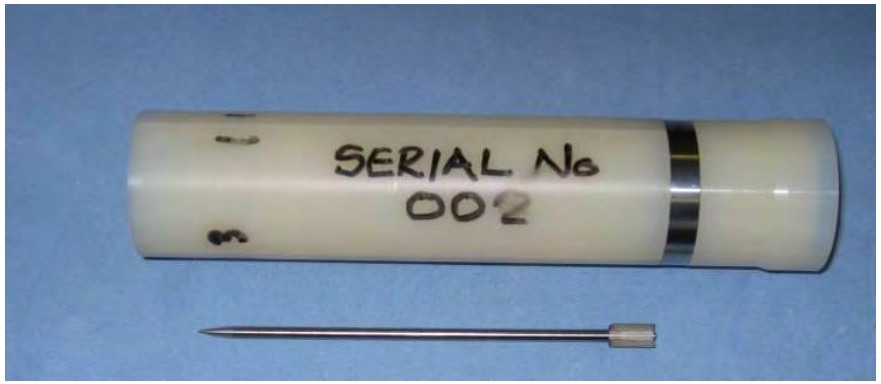


© Copyright QinetiQ Limited 2008

PDF Complete
Your complimentary use period has ended. Thank you for using PDF Complete.
Click Here to upgrade to Unlimited Pages and Expanded Features

Launch Package Design

- Successful launch of unthreaded, high Length to Diameter (L/D) ratio penetrator requires careful design
- Need a light-weight launch package which fully supports the penetrator within the sabot
- Close fitting engineering tolerances to eliminate balloting in-bore
- Light-weight base pushed launch package
- Prevents penetrator buckling in-bore and flexing during its flight to the target





© Copyright QinetiQ Limited 2008

PDF Complete
Your complimentary use period has ended. Thank you for using PDF Complete.
Click Here to upgrade to Unlimited Pages and Expanded Features

02

Interior Ballistic Modelling



© Copyright QinetiQ Limited 2008

PDF Complete
Your complimentary use period has ended. Thank you for using PDF Complete.
Click Here to upgrade to Unlimited Pages and Expanded Features

c Modelling

- Selection of the correct Interior Ballistic (IB) solution critical for sucess
- One dimensional codes can predict muzzle velocities, maximum peak chamber pressures, maximum shot base pressures and other critical characteristics
- Codes identify efficient charge designs to avoid catastrophic effects to the gun system
- The parameters within the code can be used to condition a launch package in-bore, over the longest possible distance and thus creates what is described as a soft launch phenomena
- The QinetiQ Internal Ballistics Simulation (QIBS) version 2.7 was used to predict the IB solution.

© Copyright QinetiQ Limited 2008

PDF Complete
Your complimentary use period has ended. Thank you for using PDF Complete.
Click Here to upgrade to Unlimited Pages and Expanded Features

03
Choice of Gun System



© Copyright QinetiQ Limited 2008

PDF Complete
Your complimentary use period has ended. Thank you for using PDF Complete.
Click Here to upgrade to Unlimited Pages and Expanded Features

System

- 40mm calibre long barrel, smooth bore powder gun system
- Muzzle velocities from ~300m/s to ~2700m/s can be achieved.
- Gun system is a three section, smooth bore barrel system with an overall length of 10 meters
- The barrel is supported over its length with three tripods
- One-piece ammunition system and a modified Bofors 40/70 cartridge case





© Copyright QinetiQ Limited 2008

PDF Complete
Your complimentary use period has ended. Thank you for using PDF Complete.
Click Here to upgrade to Unlimited Pages and Expanded Features

04
Instrumentation

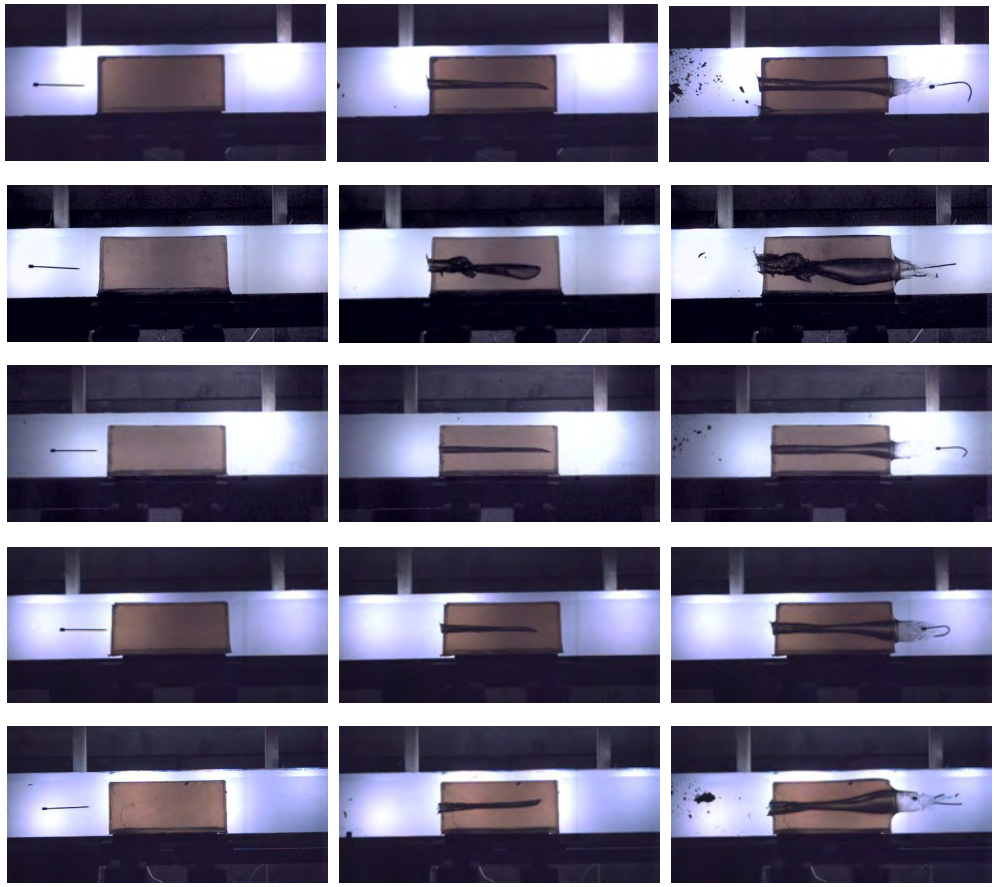


© Copyright QinetiQ Limited 2008

PDF Complete
Your complimentary use period has ended. Thank you for using PDF Complete.
Click Here to upgrade to Unlimited Pages and Expanded Features

n

- High speed video techniques enabled the study of penetrator interactions and penetrator impact and residual velocity data
- Penetrator pitch at impact and at exit and the related cavity formation determined
- Lighting techniques using a diffuser screen and sequential flash bulbs enabled a long capture duration to be used



© Copyright QinetiQ Limited 2008

PDF Complete
Your complimentary use period has ended. Thank you for using PDF Complete.
Click Here to upgrade to Unlimited Pages and Expanded Features

05

Experimental Set Up

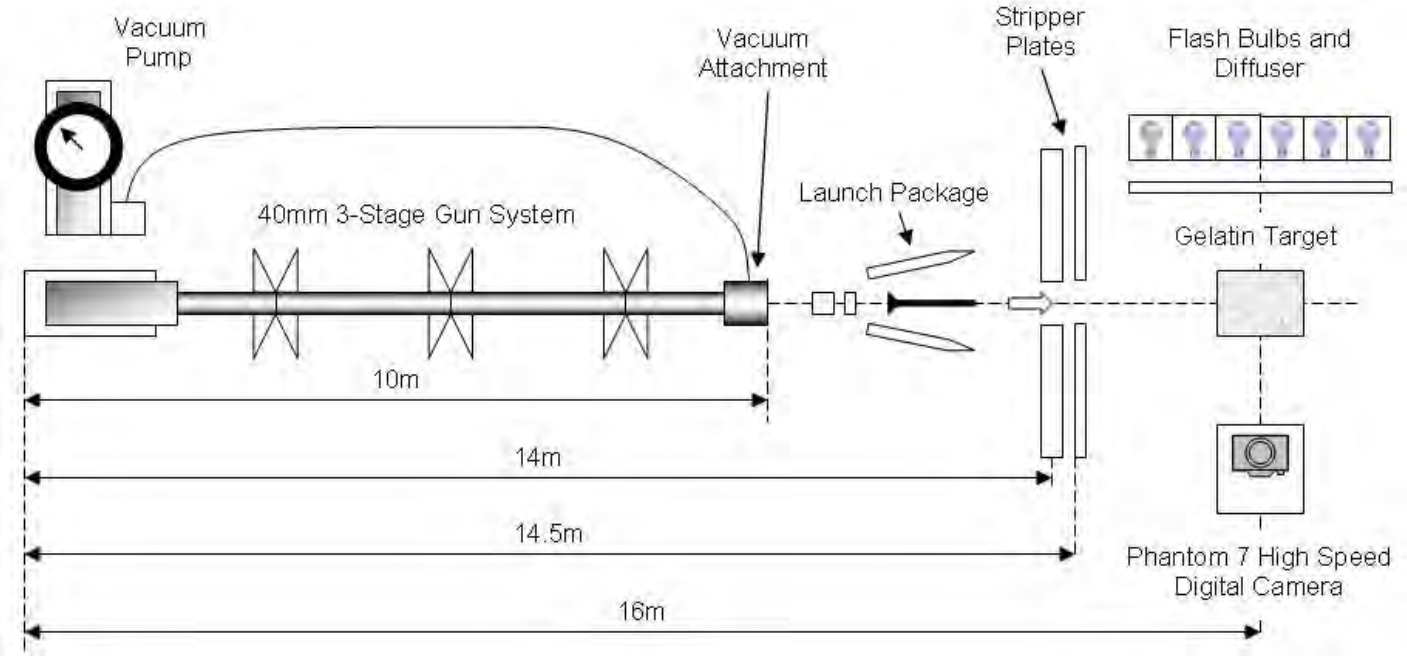


© Copyright QinetiQ Limited 2008

PDF Complete
Your complimentary use period has ended. Thank you for using PDF Complete.
Click Here to upgrade to Unlimited Pages and Expanded Features

Set Up

- Outline diagram showing the overall set up used for the experiments



© Copyright QinetiQ Limited 2008

PDF Complete
Your complimentary use period has ended. Thank you for using PDF Complete.
Click Here to upgrade to Unlimited Pages and Expanded Features

06

Target Before Penetrator Interaction

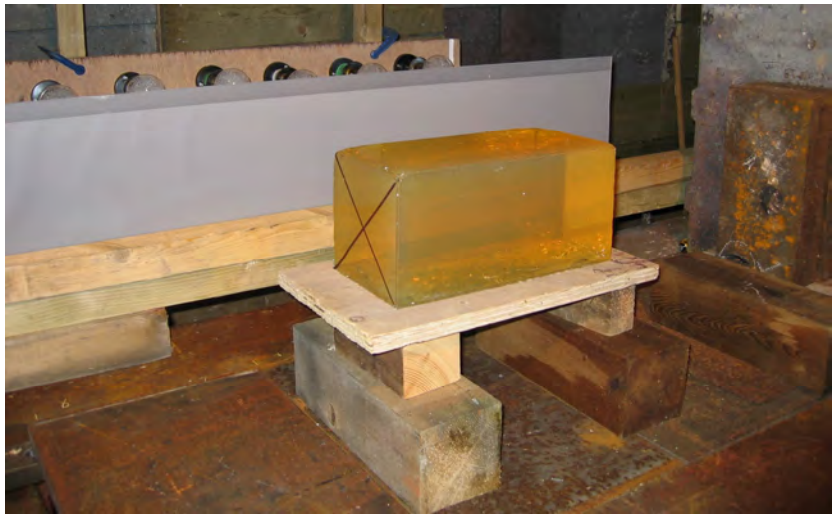


© Copyright QinetiQ Limited 2008

PDF Complete
Your complimentary use period has ended. Thank you for using PDF Complete.
Click Here to upgrade to Unlimited Pages and Expanded Features

Penetrator Interaction

- Targets mounted on a wood platform as the Gelatin target material tends to be mobile in nature
- Target rear illuminated to observe the penetrator interaction and cavity formation through the opaque Gelatin material
- Diffuser screen mounted between the flash bulb array and the target



© Copyright QinetiQ Limited 2008

PDF Complete
Your complimentary use period has ended. Thank you for using PDF Complete.
Click Here to upgrade to Unlimited Pages and Expanded Features

07

The Effects of Pitch at Impact

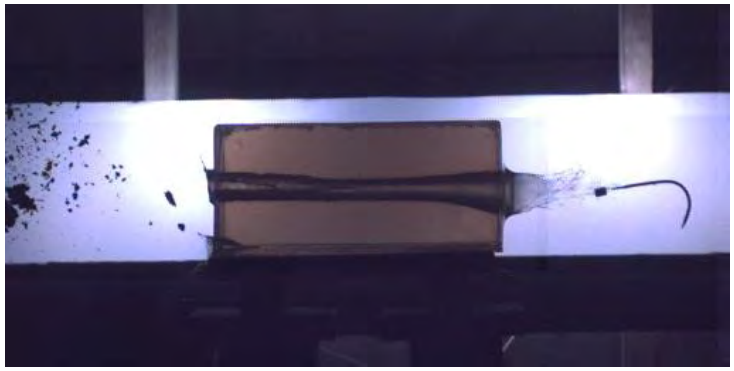


© Copyright QinetiQ Limited 2008

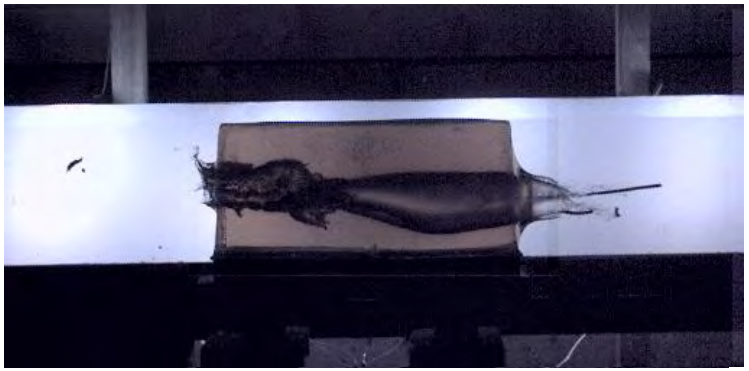
PDF Complete
Your complimentary use period has ended. Thank you for using PDF Complete.
Click Here to upgrade to Unlimited Pages and Expanded Features

Negative Pitch at Impact

- Low negative pitch error: Penetrator exits the target in a severely bent condition
- High negative pitch error: Penetrator exits the target in a broken condition, breaking occurs during interaction with the target



High Speed video of a low negative pitch impact



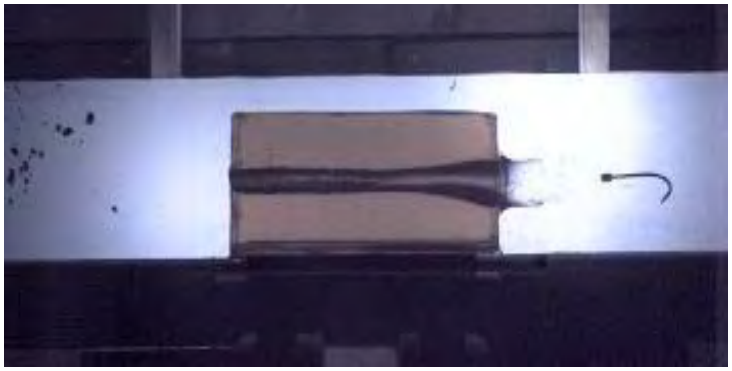
High speed video of a high negative pitch impact

© Copyright QinetiQ Limited 2008

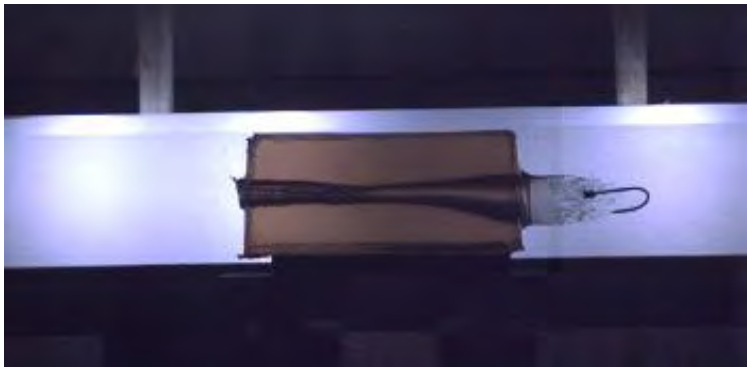
PDF Complete
Your complimentary use period has ended. Thank you for using PDF Complete.
Click Here to upgrade to Unlimited Pages and Expanded Features

Very Low Negative Pitch at Impact

- Low and Very low negative pitch: Penetrator exits the target in a severely bent condition
- In both cases the bending is seen to be progressive during the interaction process and at exit with the target
- The severity of bending is linked to the impact error condition



High Speed video of a very low negative pitch impact



High speed video of a very low negative pitch impact

© Copyright QinetiQ Limited 2008

PDF Complete
Your complimentary use period has ended. Thank you for using PDF Complete.
Click Here to upgrade to Unlimited Pages and Expanded Features

Positive Pitch at Impact

- Positive pitch at impact: Penetrator again exits the target in a broken condition breaking-up during interaction with the target



High Speed video of a positive pitch impact

© Copyright QinetiQ Limited 2008

PDF Complete
Your complimentary use period has ended. Thank you for using PDF Complete.
Click Here to upgrade to Unlimited Pages and Expanded Features

8 Targets After Penetrator Interaction

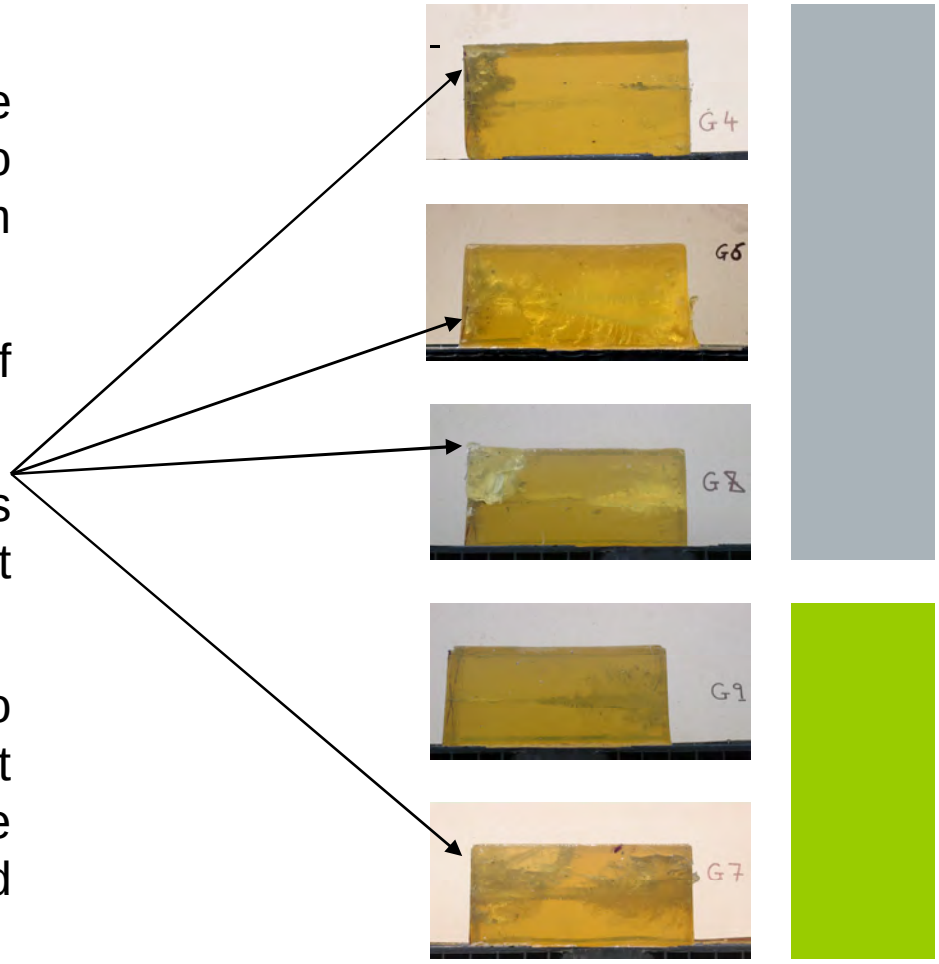


© Copyright QinetiQ Limited 2008

PDF Complete
Your complimentary use period has ended. Thank you for using PDF Complete.
Click Here to upgrade to Unlimited Pages and Expanded Features

enetrator Interaction

- With base pushed launch package designs, it can be difficult to eliminate residual material from interaction with the target
- Stripper plate removes majority of sabot petal component
- This residual material interacts with the Gelatin targets post penetration
- In most cases this was limited to the rear of the target and not considered detrimental to the formations of the observed cavities



© Copyright QinetiQ Limited 2008

PDF Complete
Your complimentary use period has ended. Thank you for using PDF Complete.
Click Here to upgrade to Unlimited Pages and Expanded Features

9 Conclusions



© Copyright QinetiQ Limited 2008

PDF Complete
Your complimentary use period has ended. Thank you for using PDF Complete.
Click Here to upgrade to Unlimited Pages and Expanded Features

- Unthreaded and high L/D ratio penetrators can be launched successfully
- Base pushed launch package designs can be used to launch these penetrators providing close fitting engineering tolerances are applied to the design
- IB modelling is an essential tool which identifies the correct design solutions
- Long barrel gun systems can be used to create soft launch phenomena
- High speed video techniques capture the penetrator performance at relatively low cost
- Low and very low negative pitch at target impact can produce a penetrator which is severely bent at exit from the target
- Higher pitch error at target impact can produce a penetrator which is broken into two or more pieces at exit from the target
- Impact condition is a contributing factor to projectile exit condition and cavity formation

© Copyright QinetiQ Limited 2008

PDF Complete
Your complimentary use period has ended. Thank you for using PDF Complete.
Click Here to upgrade to Unlimited Pages and Expanded Features

10
Questions?





© Copyright QinetiQ Limited 2008

PDF Complete
Your complimentary use period has ended. Thank you for using PDF Complete.
Click Here to upgrade to Unlimited Pages and Expanded Features

QinetiQ

The Global Defence and Security Experts

© Copyright QinetiQ Limited 2008

LOADING MECHANISMS from SHALLOW BURIED EXPLOSIVES

Leslie C. Taylor
William L. Fourney, Ulrich Leiste
Bryan Cheeseman

23 Sept 2008

Acknowledgements

Sponsor
TARDEC

Richard Goetz
David Fox



Team Members

Tim Hennessey	NSWC/IH
Sean Tidwell	NSWC/IH
William Szymczak	NRL
Andrew Wardlaw	ATR Inc.

U of MD Tasks

Using Small-Scale Tests

- Understand interaction between charge and target
- Support development of computational tools
- Explore technology and concepts to mitigate effect of flush & buried charges
- Explore scaling rules
- Measure pressure distribution over face of target as function of time
  - Develop total impulse data
  - Explore effect of target shape on loading
    - Non-deforming targets
      - Vees, pyramids,
      - Others
    - Deforming targets

Loading Mechanisms

Interaction Between Shallow Buried Charge & Target Takes Place in Near Field Of Explosion

- Details Are Important, e.g.:
  - Charge Shape & Detonator Location
  - Charge – Target Geometry
  - Local Soil Properties
    - Including Smoothness of Surface
  - Etc.

Test Charges

PENTOLITE CHARGES (H/D = ~3)

Provided by NSWC/IH

Pressed Pentolite

Explosive Mass: 0.8g 4.4g 8.0g

Detonator – Reynolds RP-87 (0.069g RDX & PETN)

PETN CHARGES (H/D=~3)

DETA Sheet – 63% PETN 37% Binder

Explosive Mass: 0.5g 0.636g 4.4g 8.0g

DETA Mass: 0.68g 0.90g 6.875g 12.59g

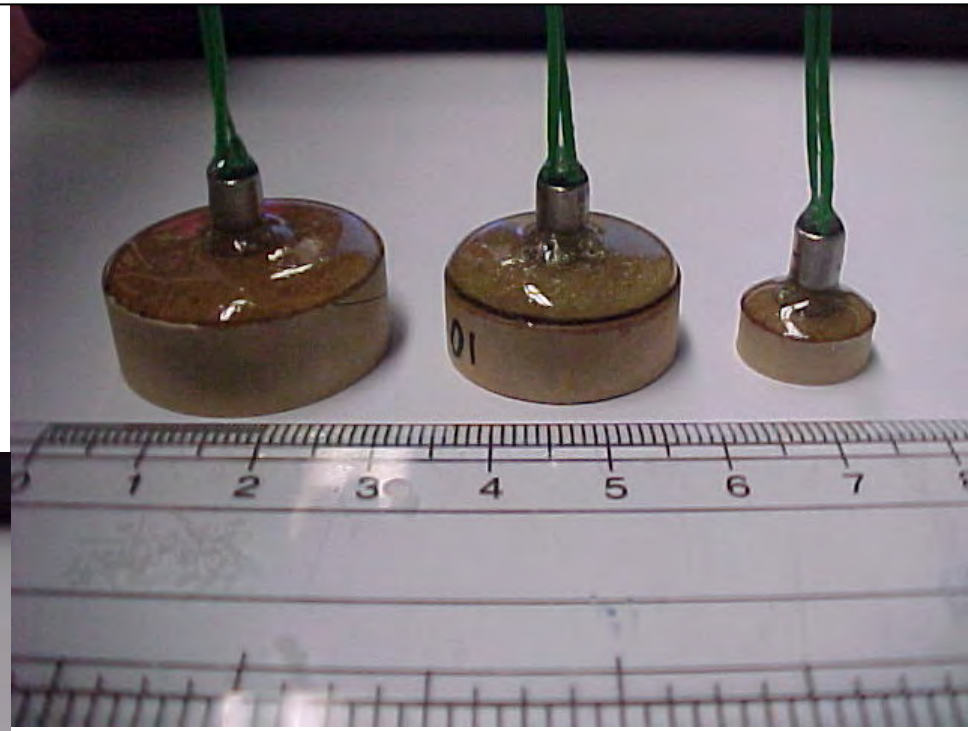
Detonator – Reynolds RP-87 (0.069g RDX & PETN)

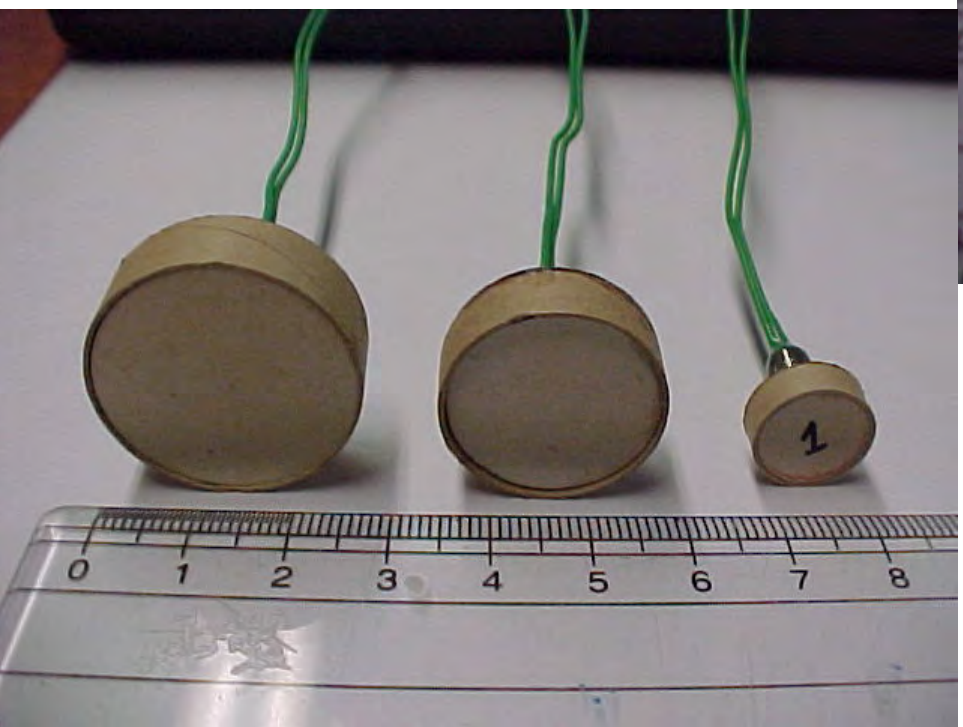
Explosive Mass Always Includes Detonator Explosive

Pentolite Charges

Charge size
(Wt includes RP-87 Det)

Wt.	D(mm)	H(mm)
0.8g	12.0	4.0
4.4g	21.8	7.3
8.0g	26.6	8.9





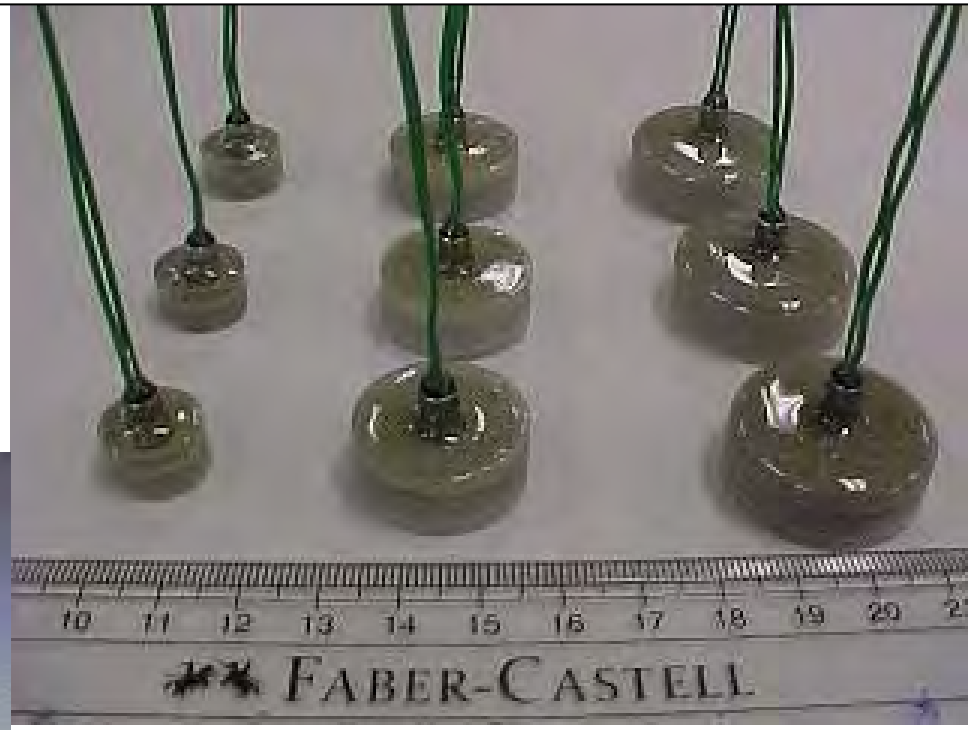
RP-87 contains .069g explosive

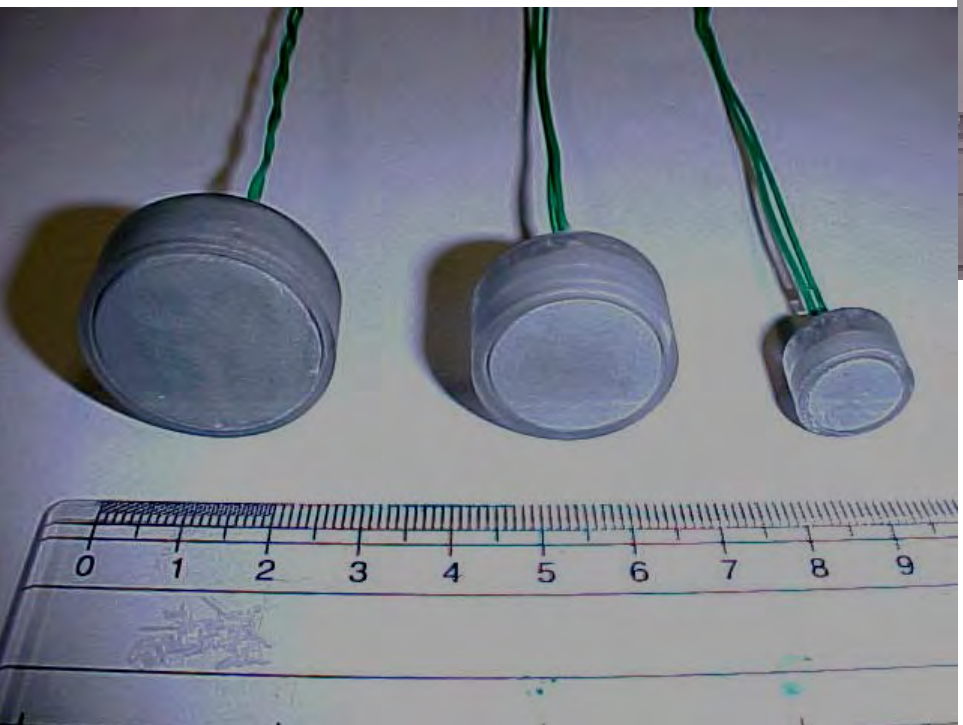
NAVSEA
INDIAN HEAD
Surface Warfare Center Division

DETASHEET Charges

Charge size
(Explosive Weight)
(Wt includes RP-87 Det)

Wt.	D(mm)	H(mm)
0.5g	12.0	2.7
2.5g	21.0	4.6
5.0g	26.0	5.8





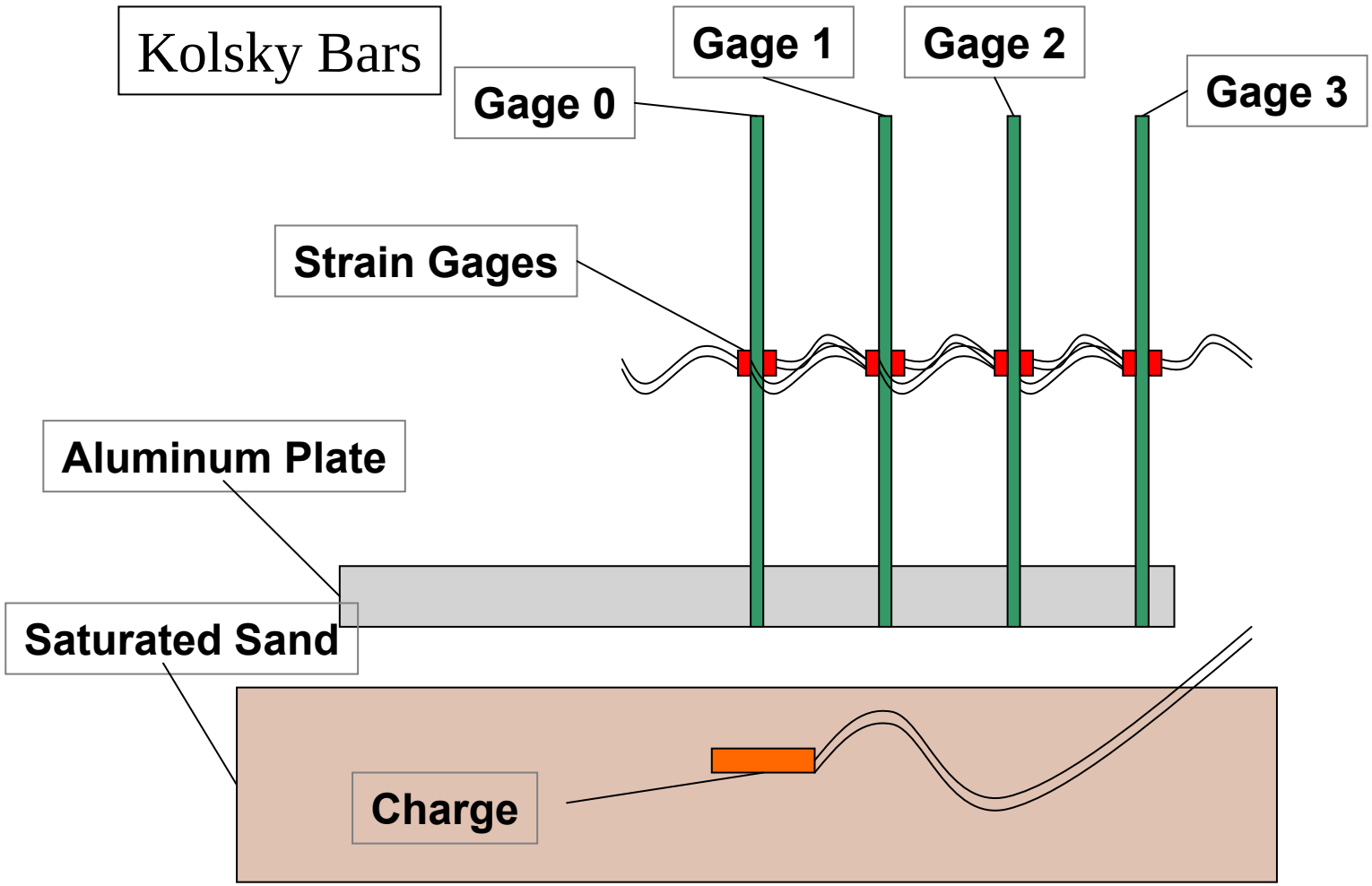
Weight given above is weight of PETN plus RP-87 Det (.069g)
DETASHEET is 63% PETN
Total charge wt – about 1.59 times larger

Pressure

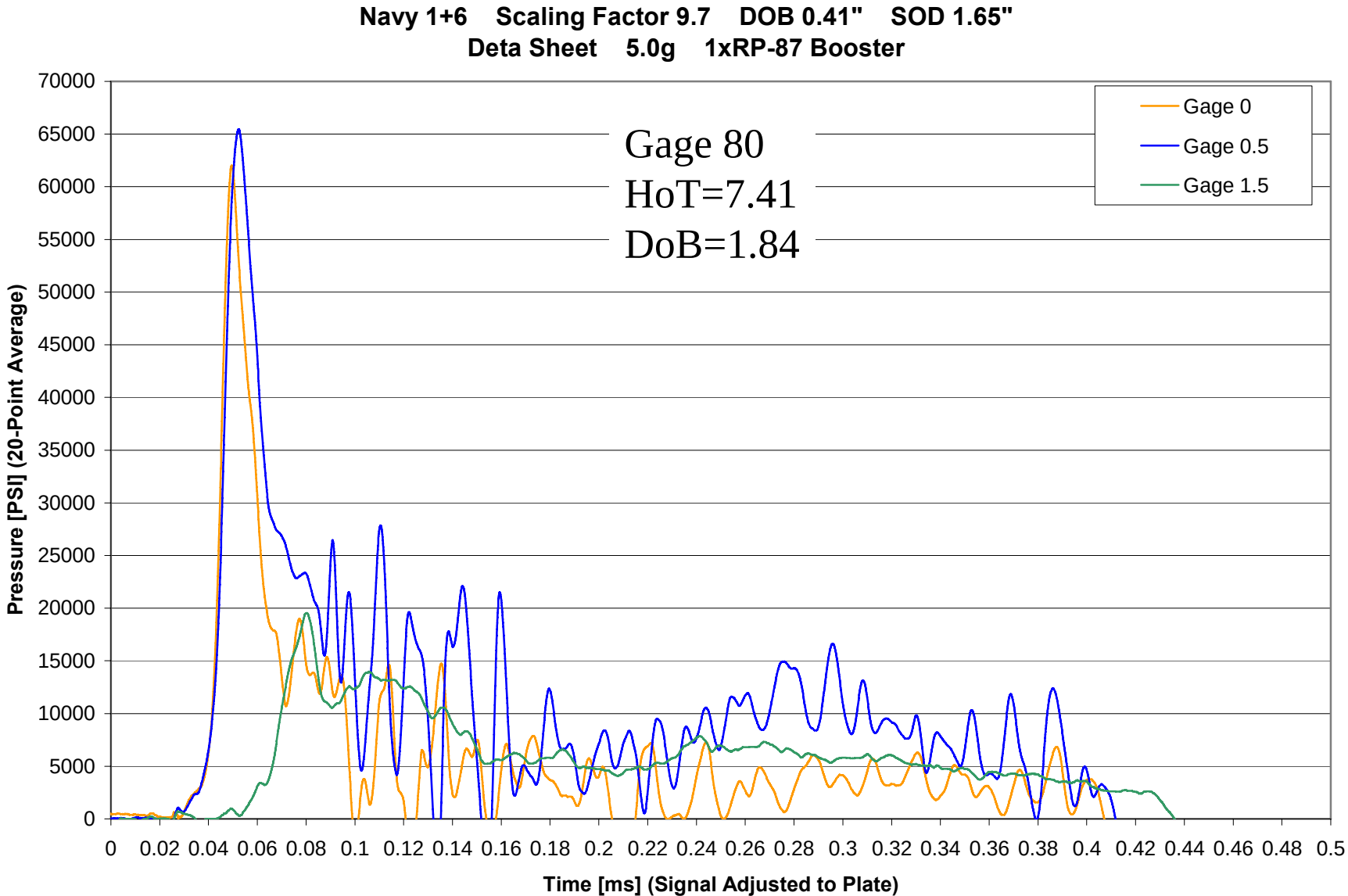
- Pressure at Any Point on Target as Function of Time is Load on Target at That Point
- Pressure Has Proved Very Hard to Measure Accurately
- Substitutes Have Been Used: Integrated Values
  - Impulse Distribution
  - Total Vertical Impulse

Pressure Test

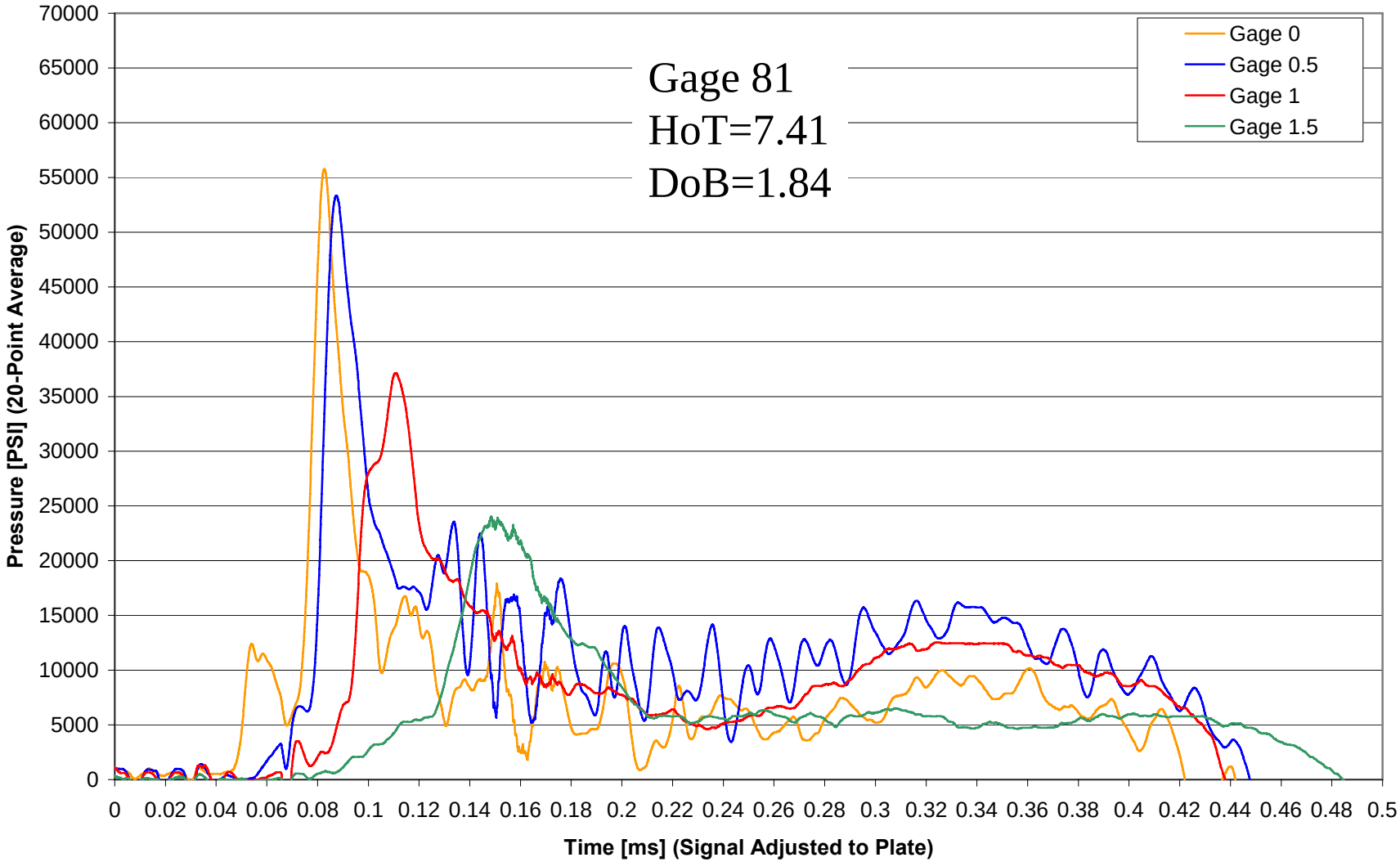
Fixed Plate Pressure Test



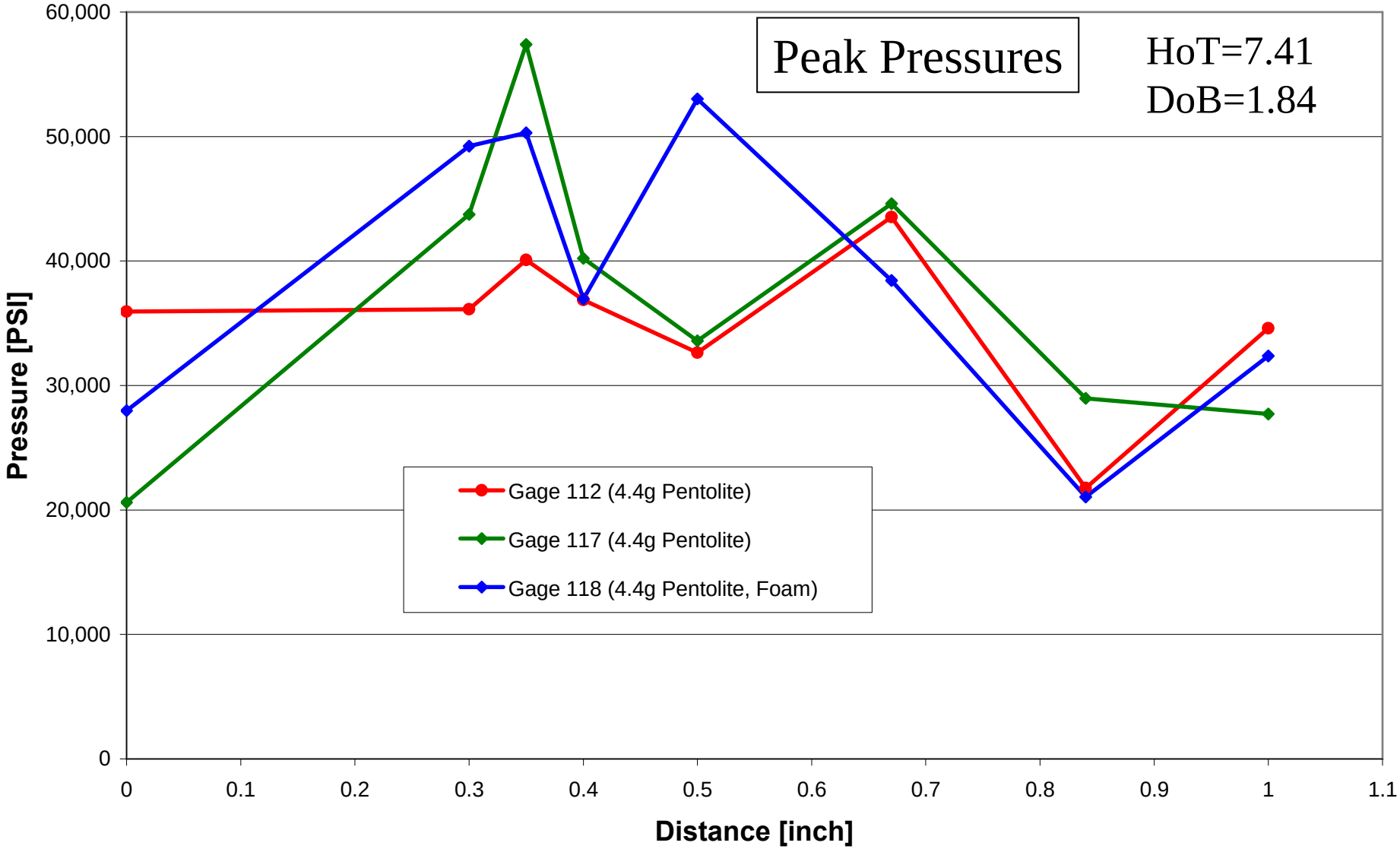
Pressure Test



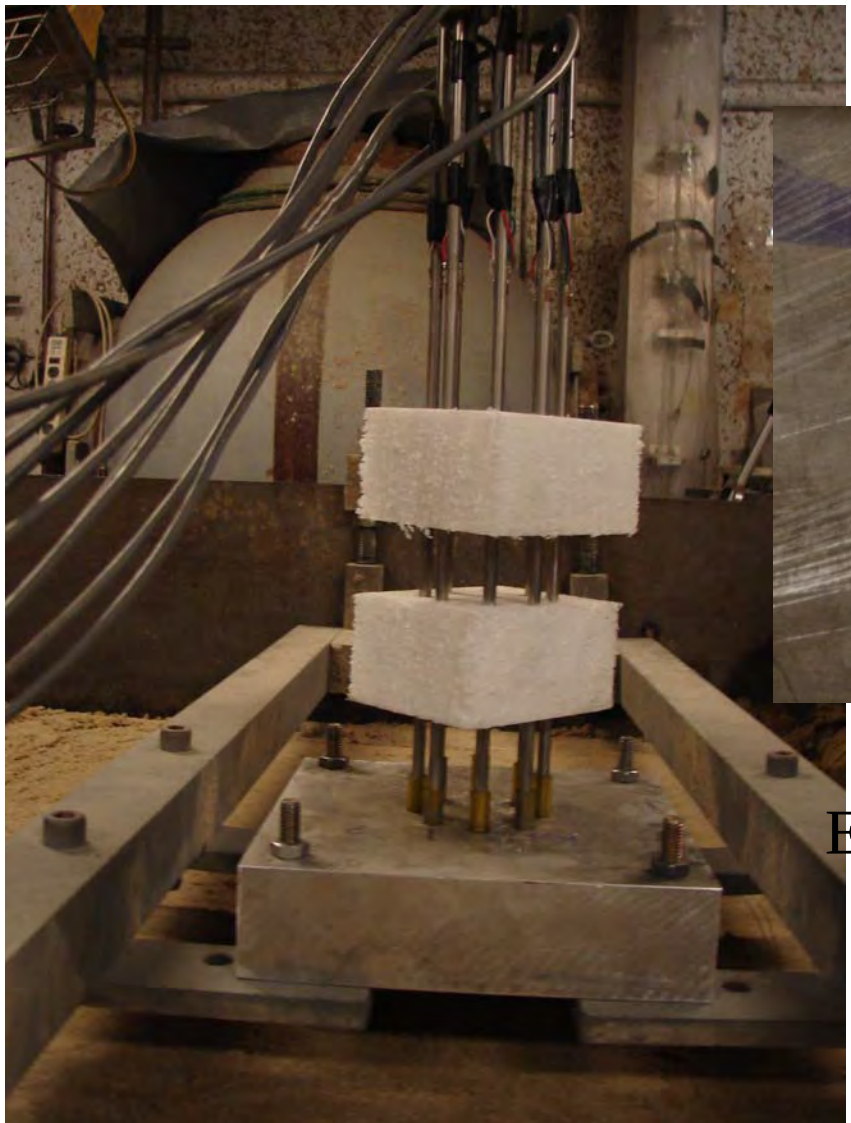
Pressure Test



Pressure Test



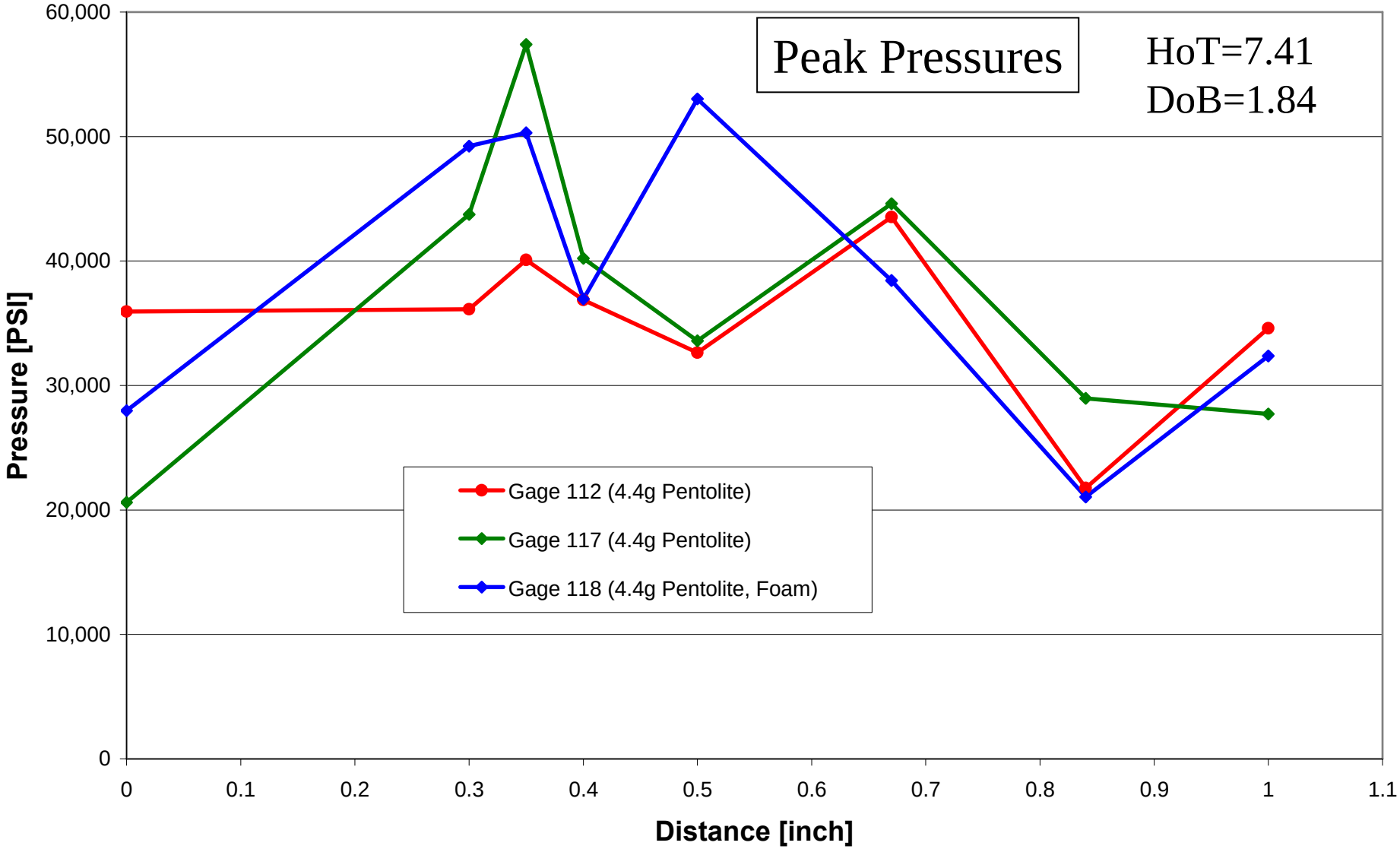
Pressure Test



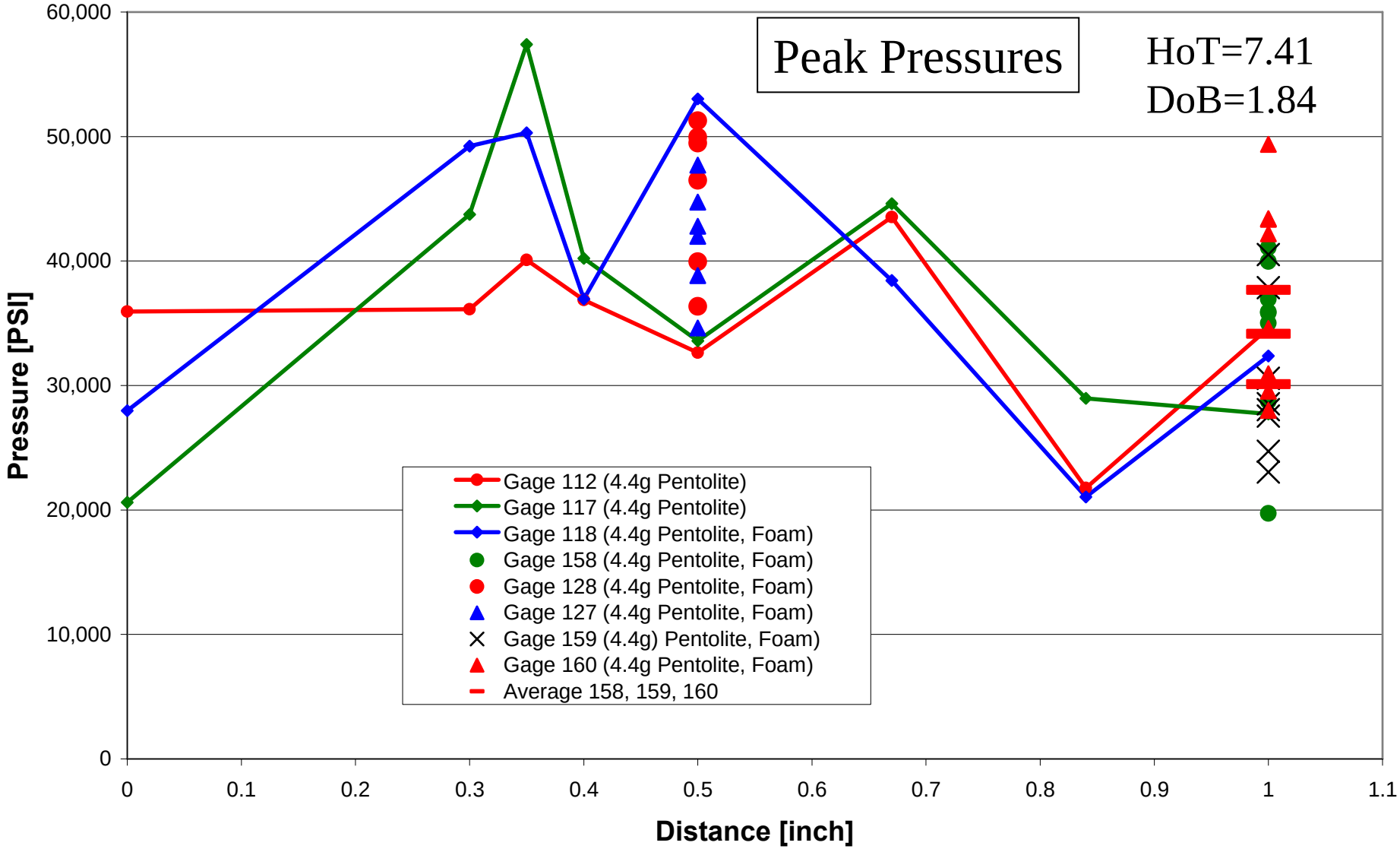


Eight Kolsky Bars in Circle

Pressure Test



Pressure Test



Loading Mechanisms

- Target Loaded by Soil Driven Against Target by Gas Bubble
- Target Loading Not Truly Impulsive
- Occurs Over Finite Time Appropriate to Bubble Processes
  - Generally Millisec Rather Than Microsec
- Target Loading Depends Upon
  - Charge Size & Shape
  - Charge – Target Geometry,
  - Etc.

Loading Mechanisms

Shallow Buried Explosive

- Shockwave does not play *direct* role in target loading
  - Unless target in contact with surface
- Shockwave plays *indirect* role in target loading

Loading Mechanisms

- Target Loaded by Soil Driven Against Target by Gas Bubble

- Soil Cap Directly Over Charge Major Contributor to Load
  - Properties Of This Material When it Hits Target Important
  - They Are Not *In Situ* Properties
  - Properties & Configuration of Soil Modified by Shockwave

- Shockwave Important for What it Does to Soil Not to Target

Early Time Effects

When Charge Detonates

- Emits Shockwave
  - Essentially Parallel to Top of Charge, Because of Charge Shape

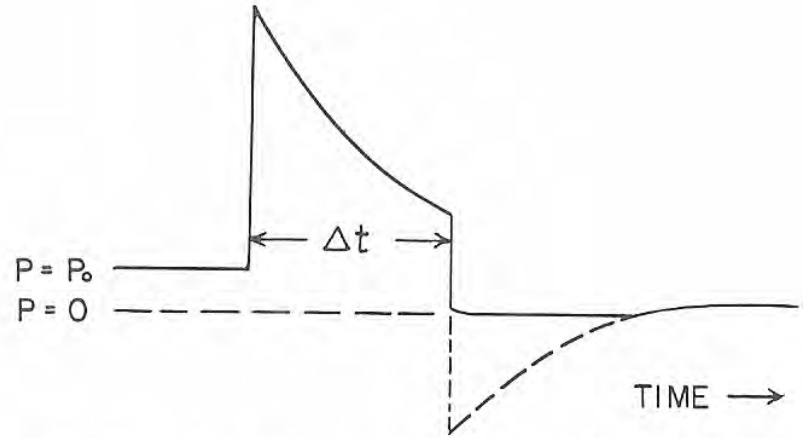


Fig. 7.21 Gauge pressure as a result of surface reflection.

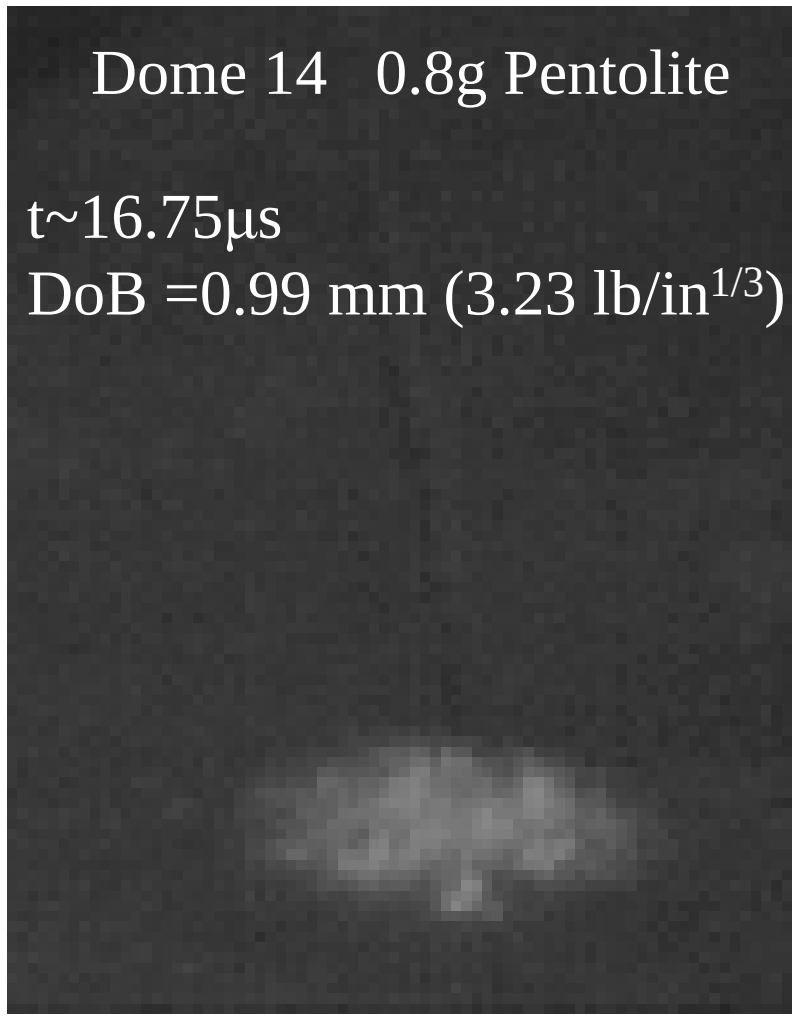
Underwater Explosions, Cole, 1948

- At Surface, Shock Mostly Reflected as Relief Wave in Soil
  - Impedance Mismatch Between Saturated Soil & Air

Early Time Effects

When Charge Detonates

- Not all shock energy reflected
  - Weak shock sent into air
  - Spray thrown up



Early Time Effects

Bulk Cavitation

- Negative Pressure in Relief Wave Interacts With Pressure in Soil Cap
  - Tries To Go Negative
- Water & Saturated Soil Cannot Support Tension – Cavitates
- Bulk Cavitation Creates Three Layers
  - High Density, Low Density, High Density
- If Cavitated Region Present When Soil Cap Hits Target
  - Pressure Rise Interrupted

Early Time Effects

Bulk Cavitation

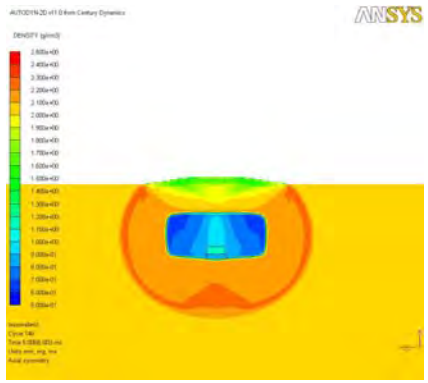
4.4g Pentolite Charge



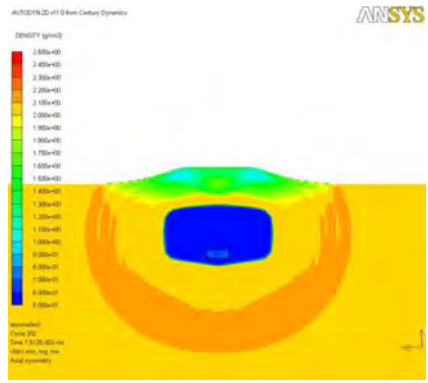
t=0 μs



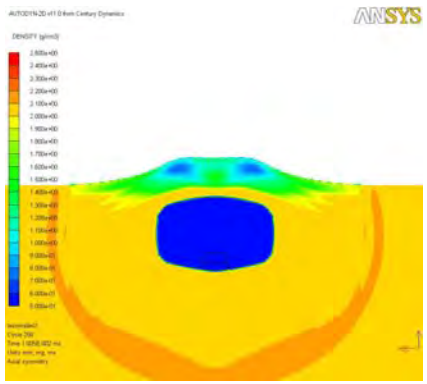
t=2.5 μs



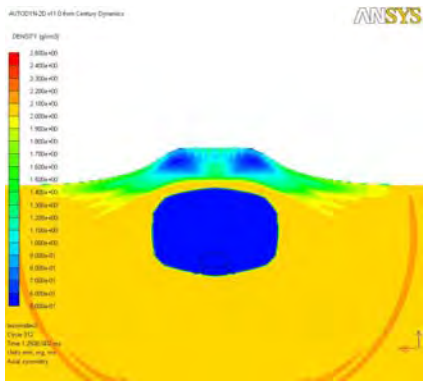
t=5.0 μs



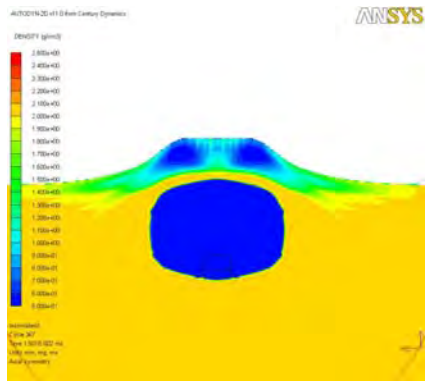
t=7.5 μs



t=10.0 μs



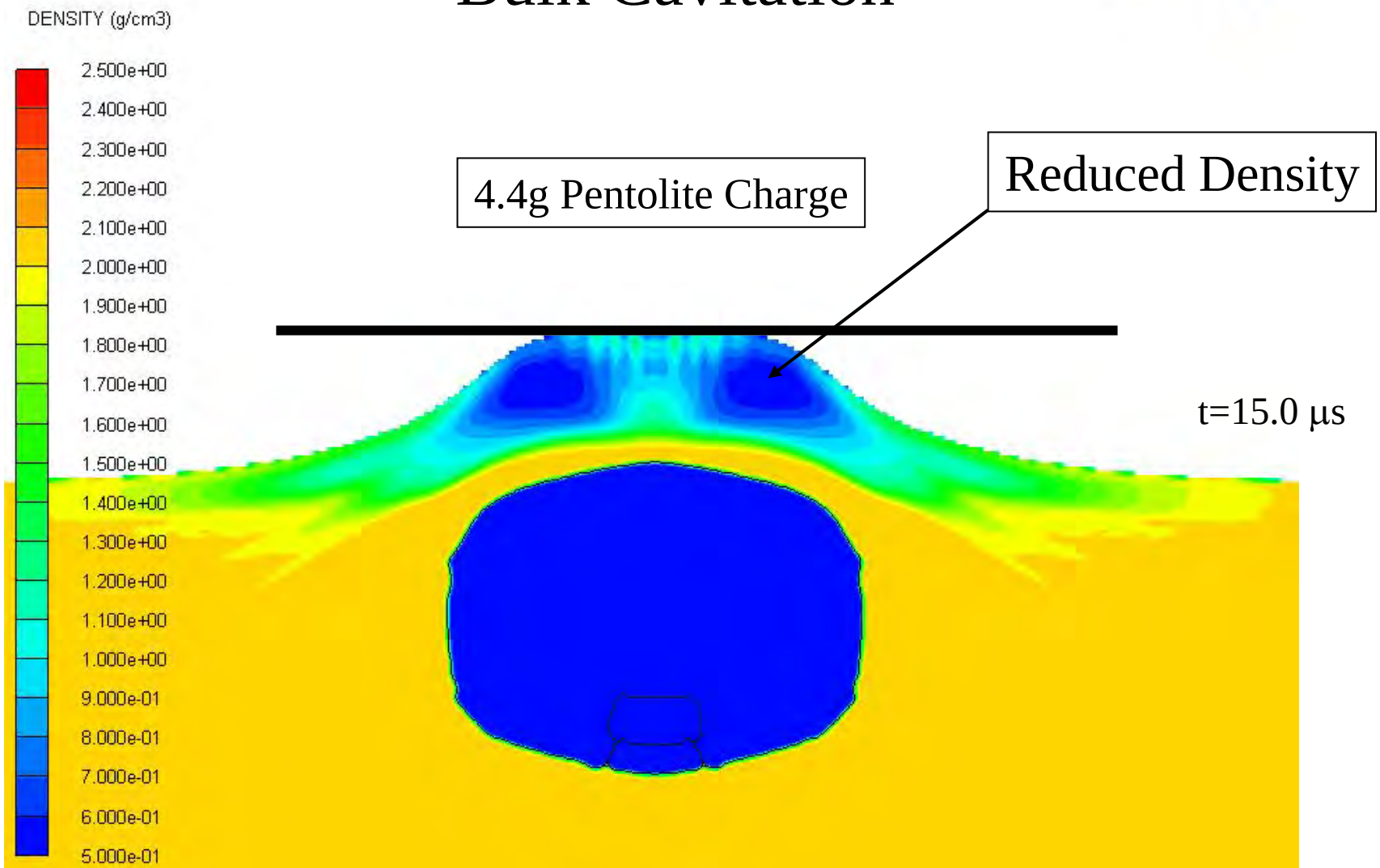
t=12.5 μs



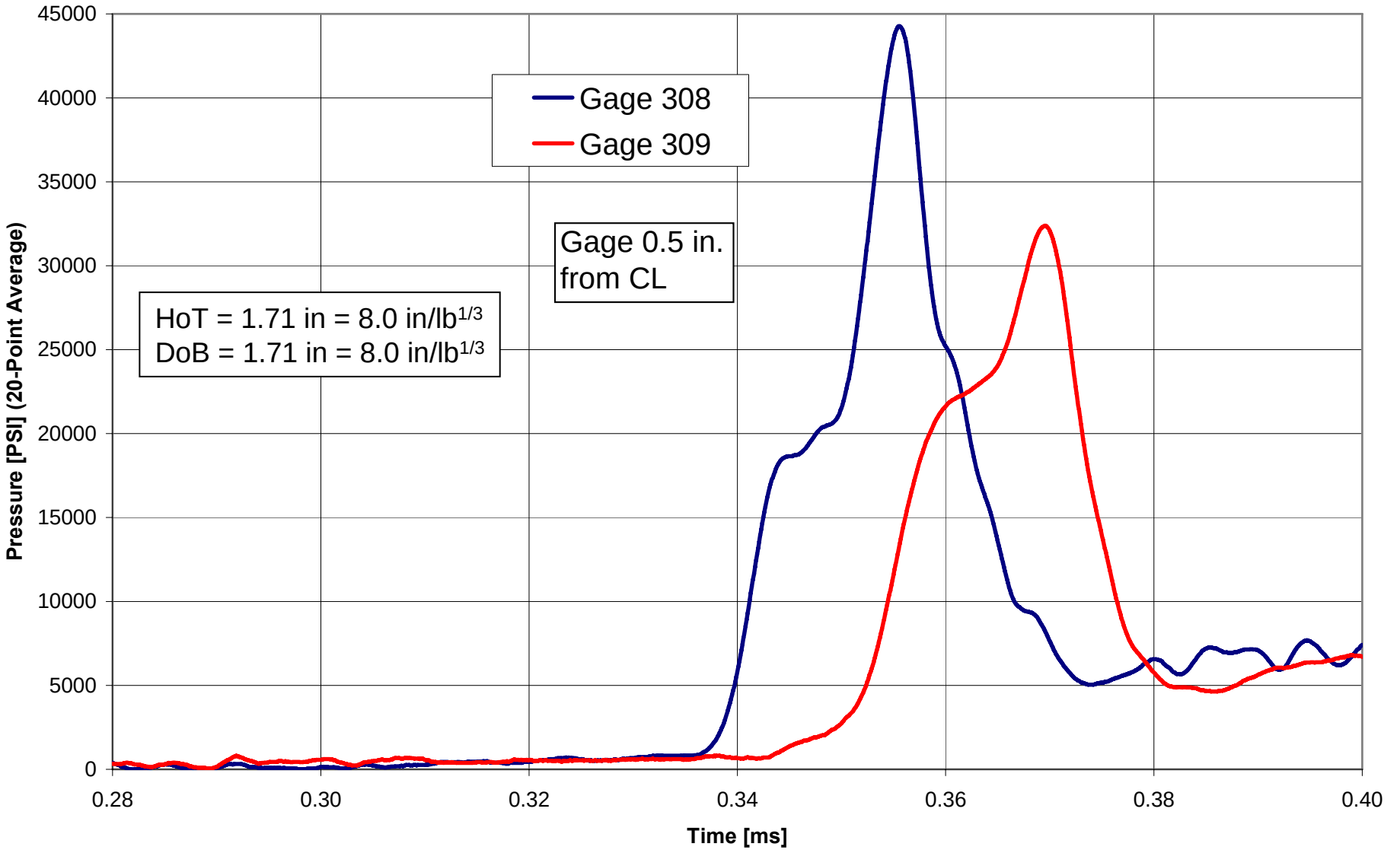
t=15.0 μs

Early Time Effects

Bulk Cavitation



Early Time Effects



Early Time Effects

Richtmyer-Meshkov Instability (RMI)

Occurs when interface between fluids of differing density is impulsively accelerated, e.g. by the passage of shock wave

Development of instability begins with small amplitude perturbations which initially grow linearly with time

Followed by nonlinear regime with spikes appearing in the case of heavy fluid penetrating light fluid

A chaotic regime eventually reached and the two fluids mix

RMI can be considered impulsive-acceleration limit of Rayleigh–Taylor instability.

Early Time Effects

Richtmyer-Meshkov Instability (RMI)

- Our Event Over (Target Hit) Before Chaotic Mixing Phase
- Our Interest – Amplification Of Initial Perturbations
  -Interface Between Soil And Air is Never Smooth
- RMI Origin of Spikes (Fingers) of Material That Move Faster Than Bulk of Soil Cap

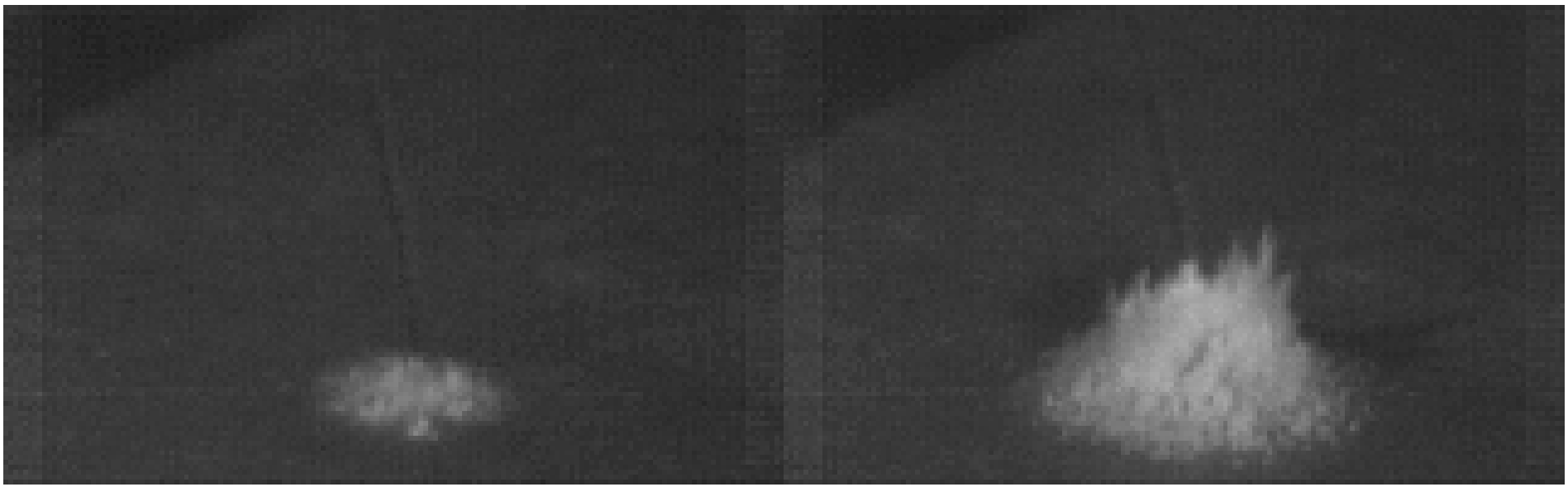
Early Time Effects

Richtmyer-Meshkov Instability (RMI)

Dome 14 0.8g Pentolite
DoB =0.99 mm (3.23 lb/in$^{1/3}$)

t~16.75μs

t=33.5μs later

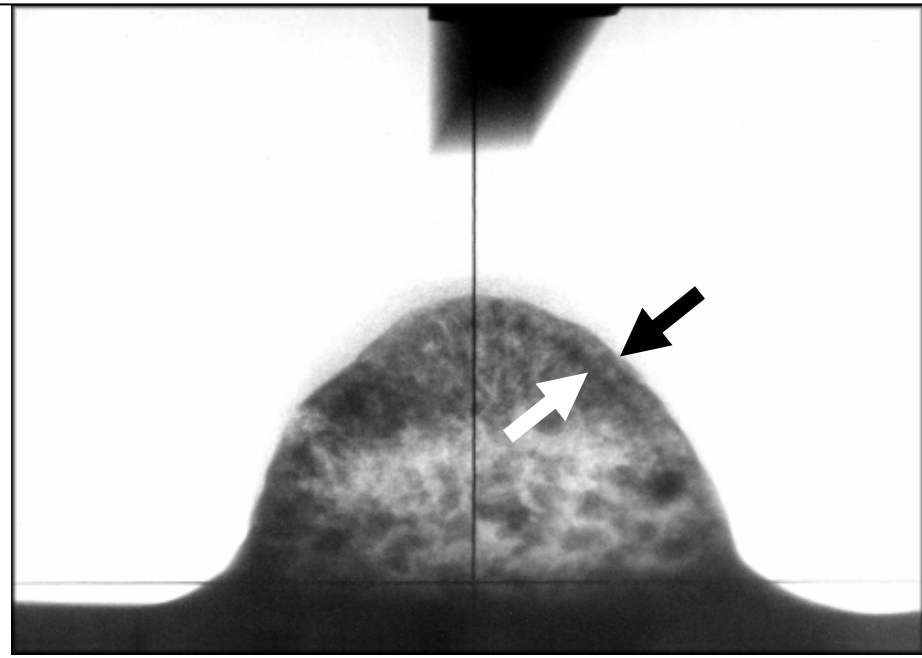


- Since Soil Surface Chaotic, Distribution Of Fingers Chaotic
  - Leads Directly To Difficulty In Measuring Pressure

Early Time Effects

Spherical Spreading

- Soil Cap Quickly Assumes Shape of Rough Hollow Dome
- Soil Cap Thins as Material Above Charge Spreads Over Surface of Dome
- Thinning Shortens Peak Loading Duration



Flash X-Ray

Shot 17-1. 125.9 μs Fairly Dry Sand

Bergeron, Walker & Coffey, DRES-SR-668, April 1998

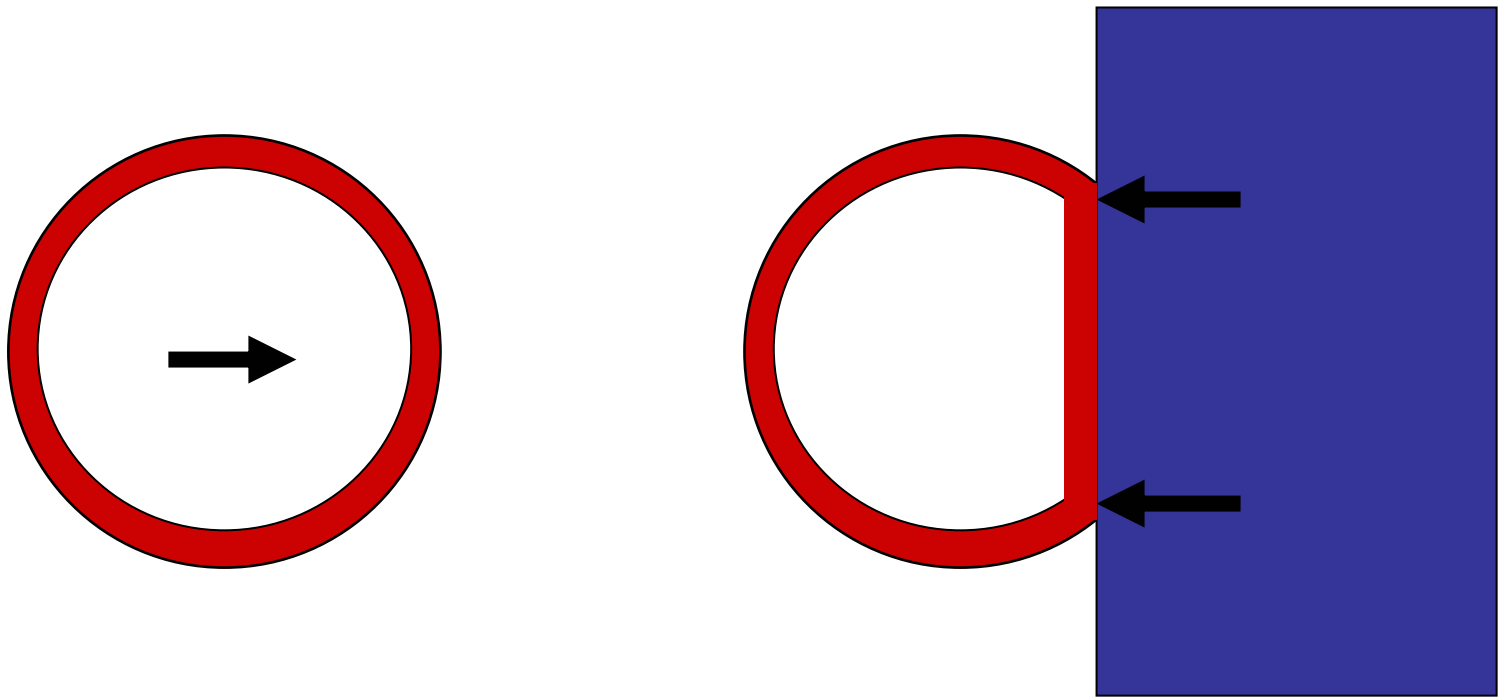
Wt = 106 g
DoB = 30 mm
D = 62mm
T = 22mm
t = 0.1259 ms

If W = 4.4 g
DoB = 10.4 mm
t = 0.0436 ms

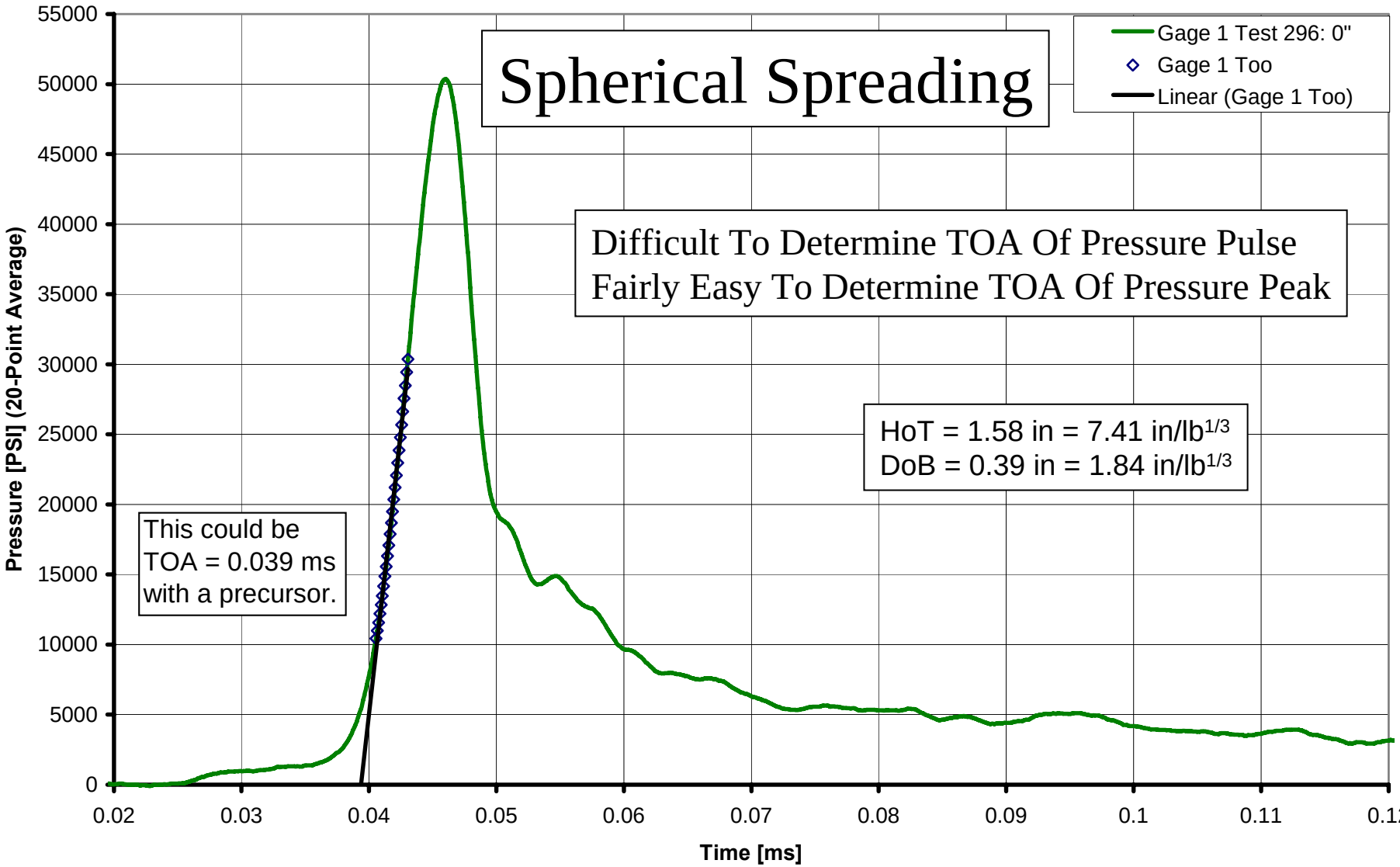
Early Time Effects

Spherical Spreading

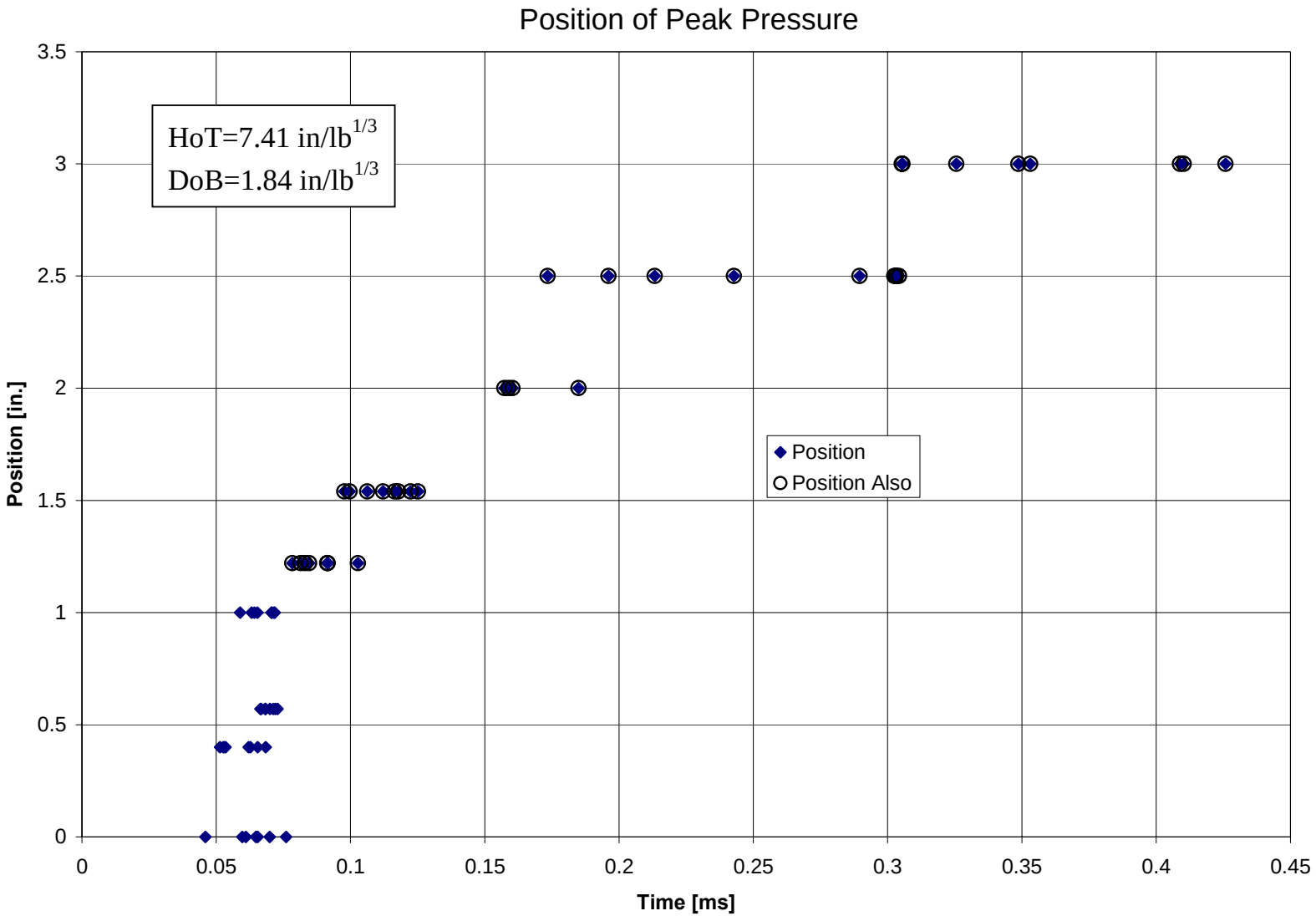
Consider Dome as Hollow Ball Hitting a Plane Target



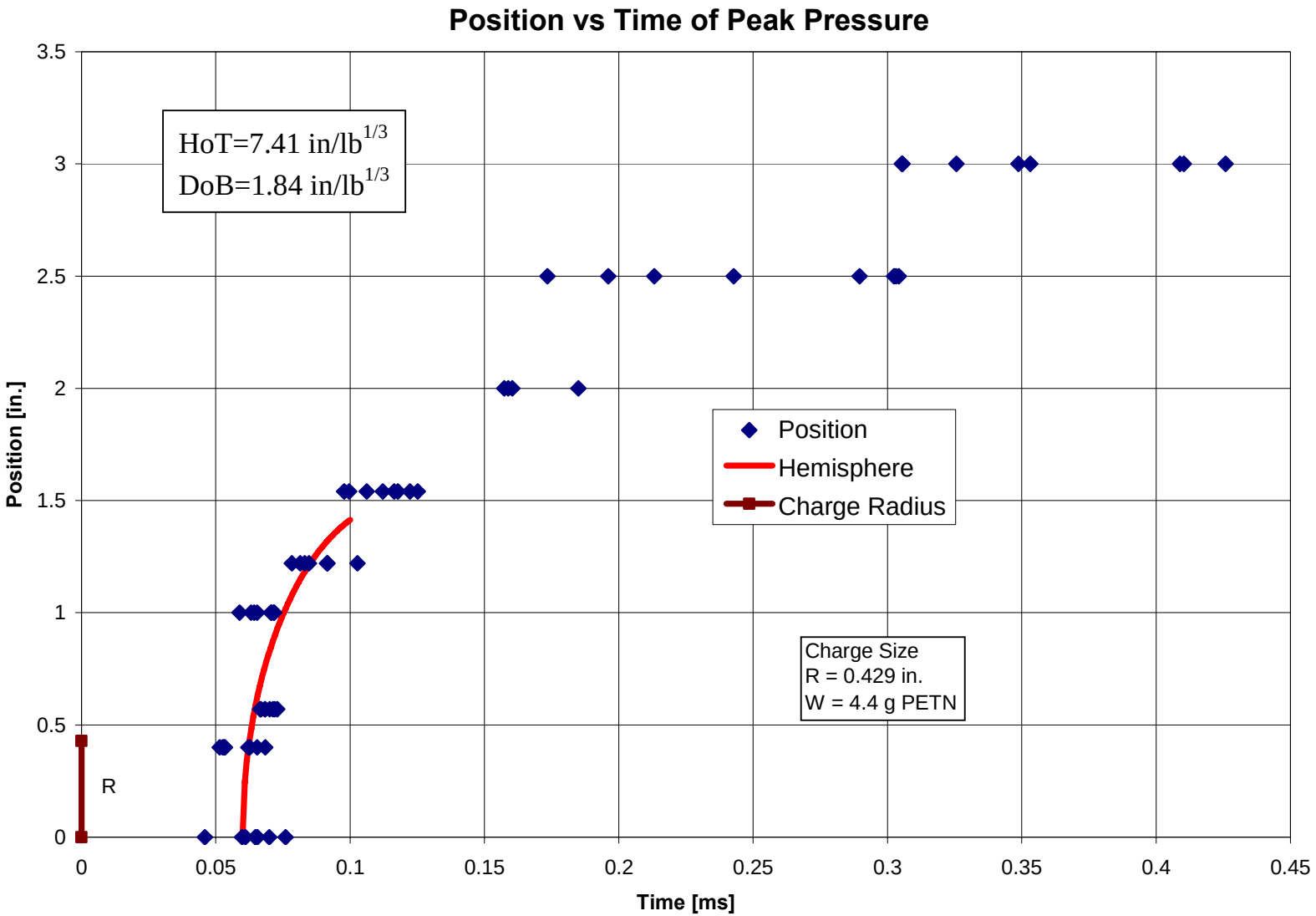
Early Time Effects



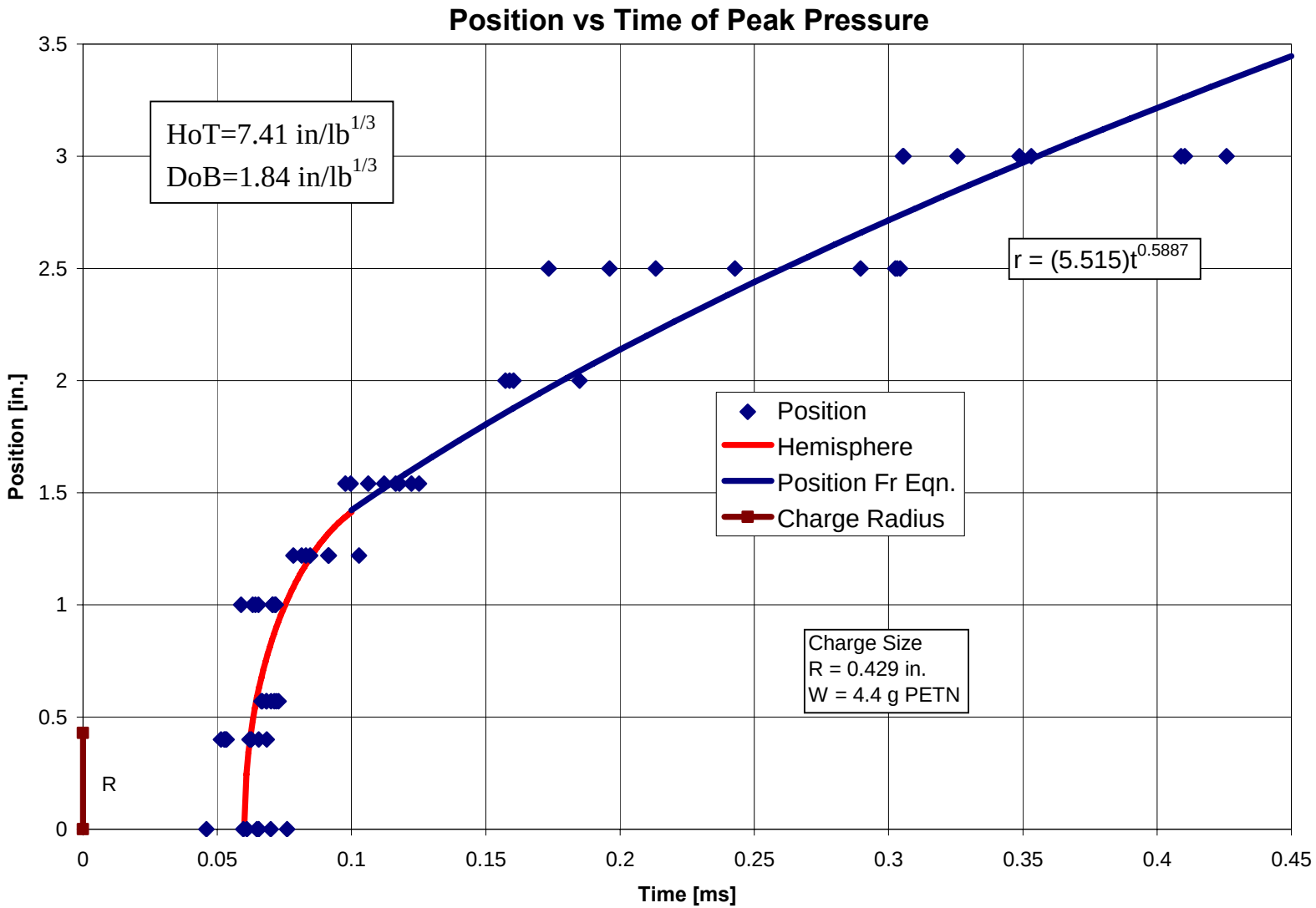
Spherical Spreading



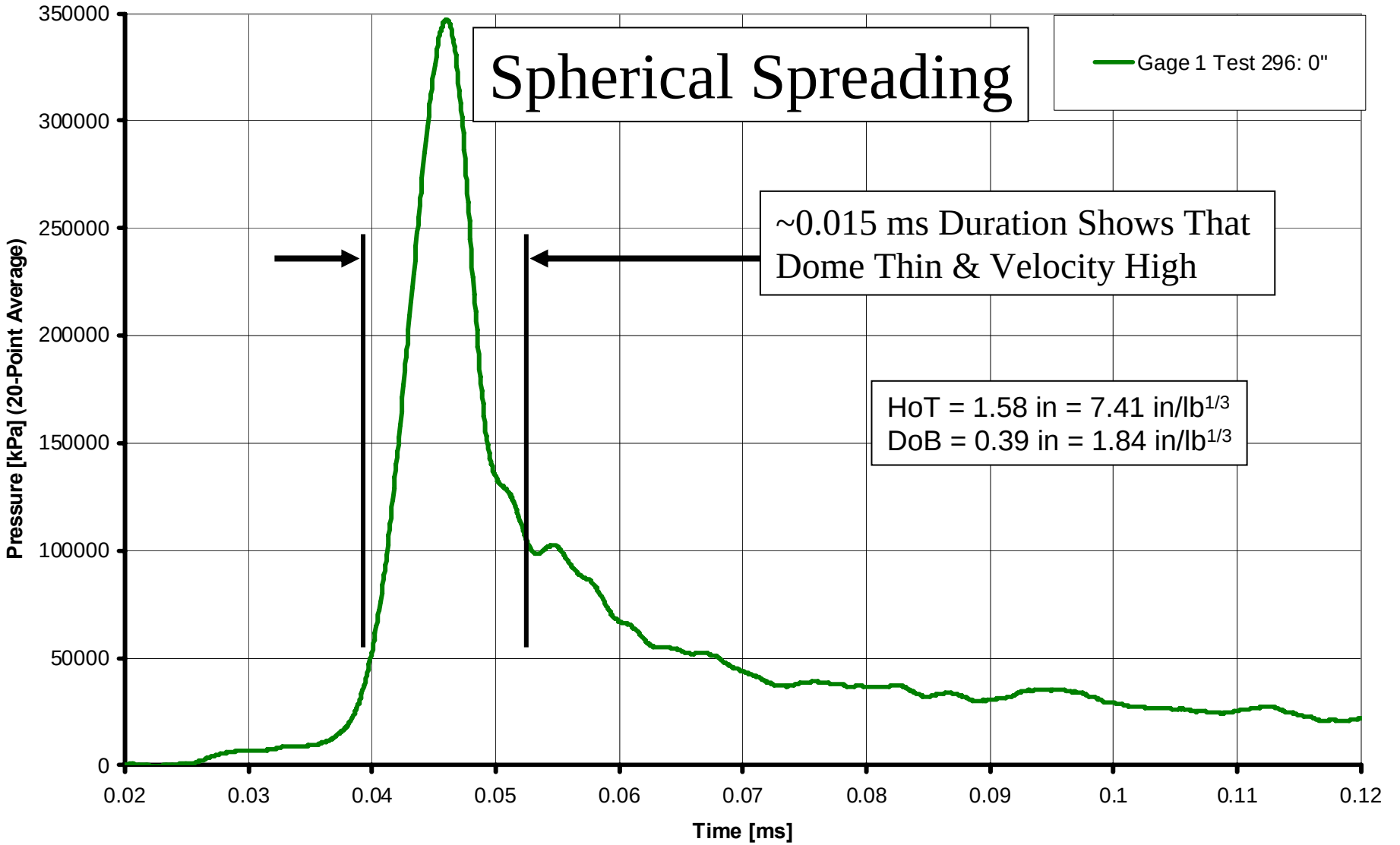
Spherical Spreading



Spherical Spreading



Early Time Effects



Early Time Effects

- Residual Shock in Air & Spray Hitting Target
  - Pressure Precursors
- Cavitation in Soil Cap
  - Variability in Pressure Rise Rate
- Richtmyer-Meshkov Instability
  - Variability in Value & Time of Peak Pressure
- Spherical Spreading & Dome Hitting Target
  - Rapid Initial Pressure Rise & Fall
- All Happens In Very Short Time - e.g. at 4.4 g Scale
  - First 0.1 ms After t = 0
    (Scales to 1ms for 10 lb (4.5 kg) Charge)
- Effect Confined to ~ 3.5 Times Charge Radius

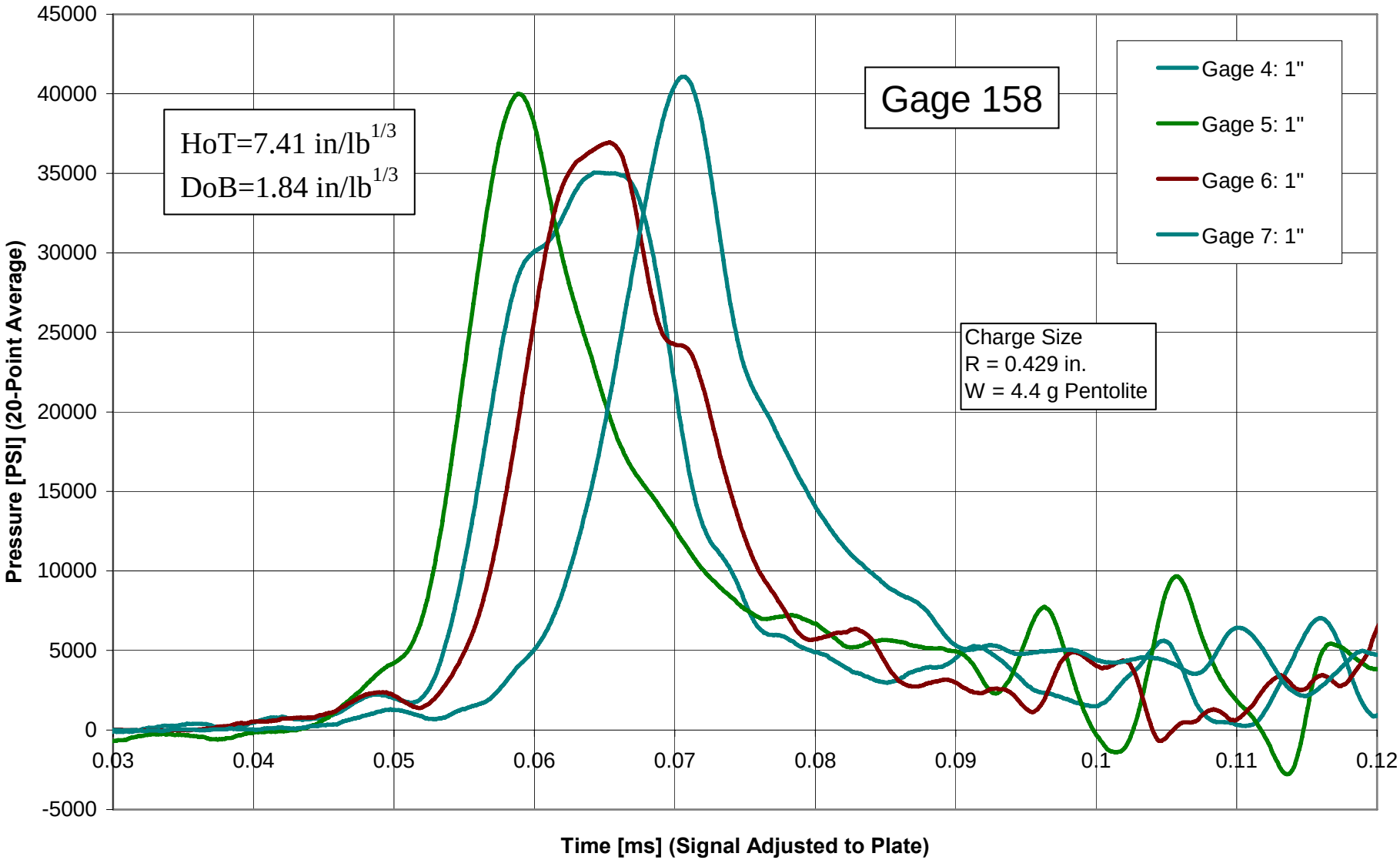
- Not The Whole Story

Late Time Effects

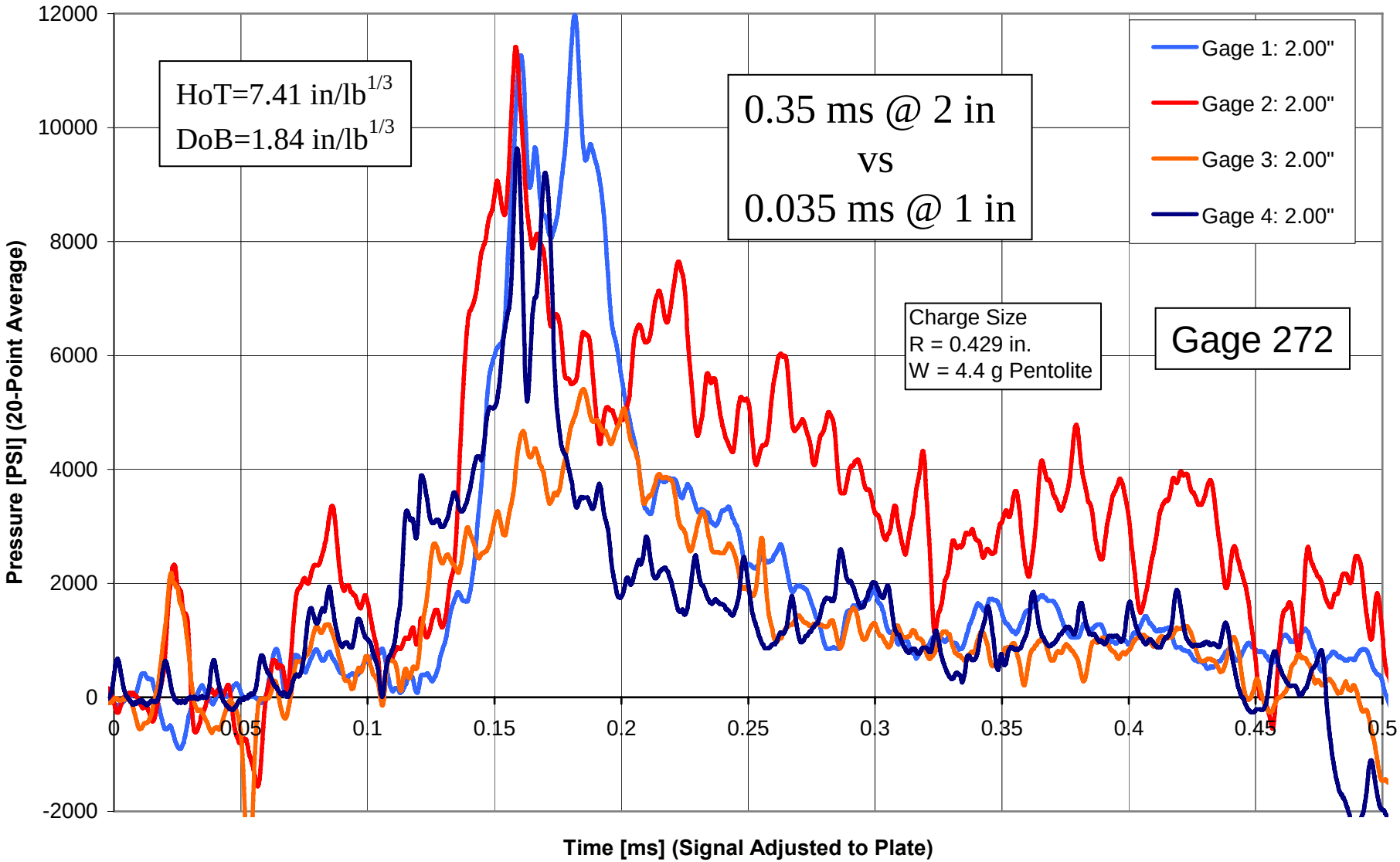
Two Additional Processes

- Material Outside Soil Cap Scooped Out of Crater by Explosive Gas
- Gas Pressure on Bottom of Target Trapped by Material Coming Out of Crater
- Pressures Much Lower
  - Act Over Much Longer Time
  - Act Over Much Greater Area

Late Time Effects



Late Time Effects



Late Time Effects

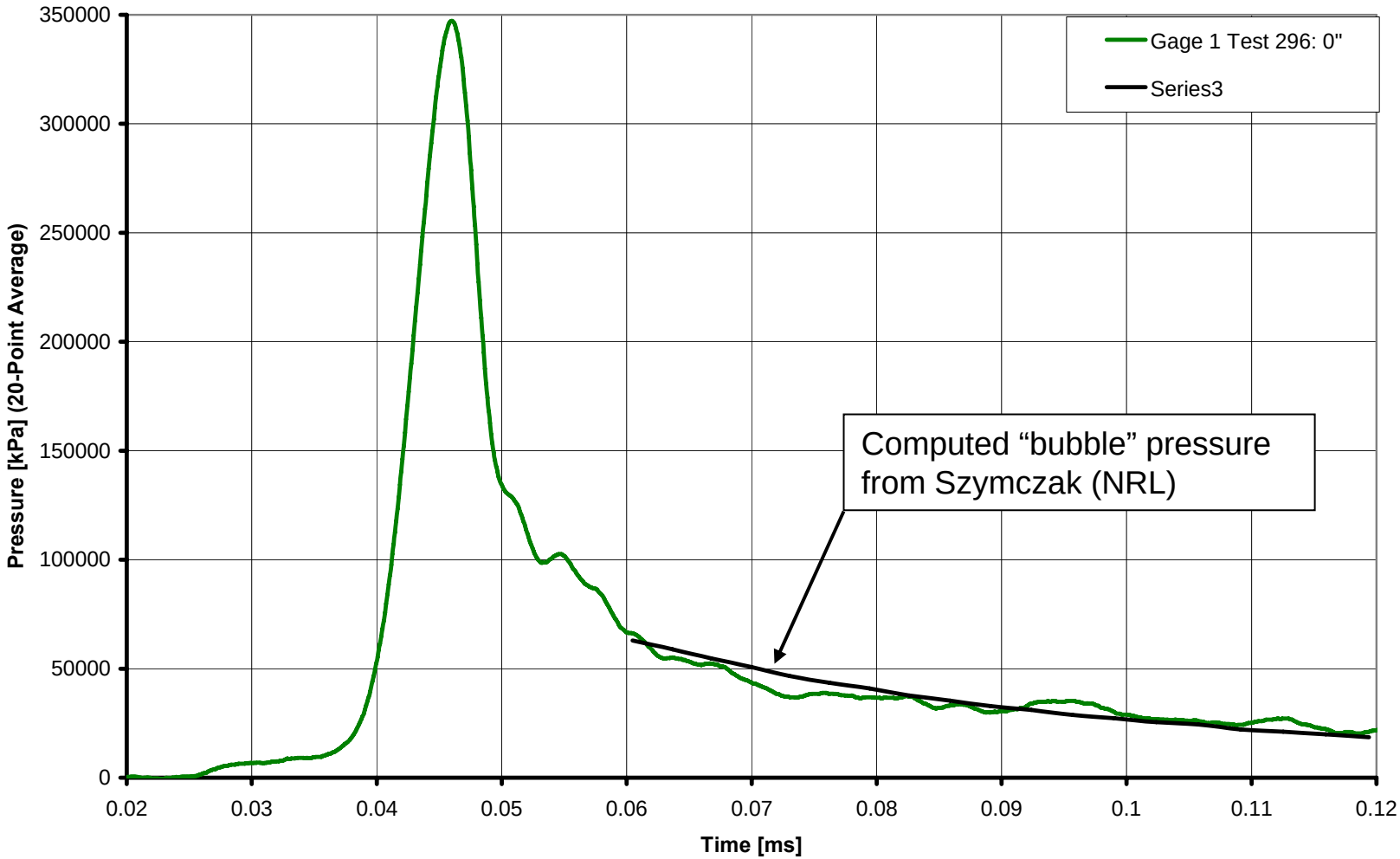
- Material Streaming Out Of Crater & Hitting Target
  - Travels Parallel To Wall Of Crater
  - Ring-shaped Stagnation Region on Target
  - Thickness Of Region Increases Rapidly
  - Vertical & Radial Velocities Comparable

- Lower Pressures & Longer Duration

  t = 0.35 ms @ 50.8 mm vs 0.035 ms @ 25.4mm

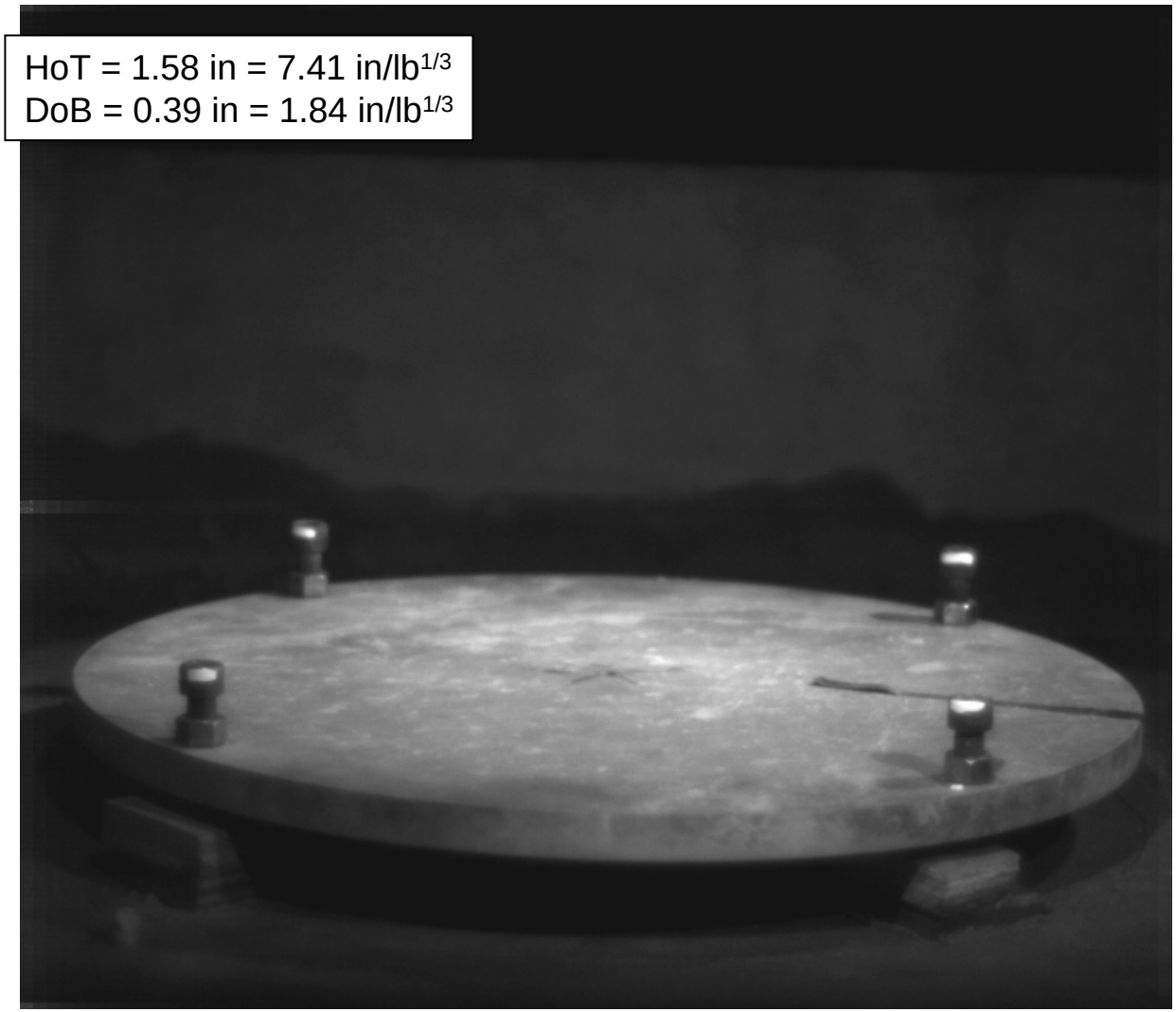
  p_{max}=12,000 psi @ 50.8 mm vs 40,000 psi @ 25.4 mm

Late Time Effects

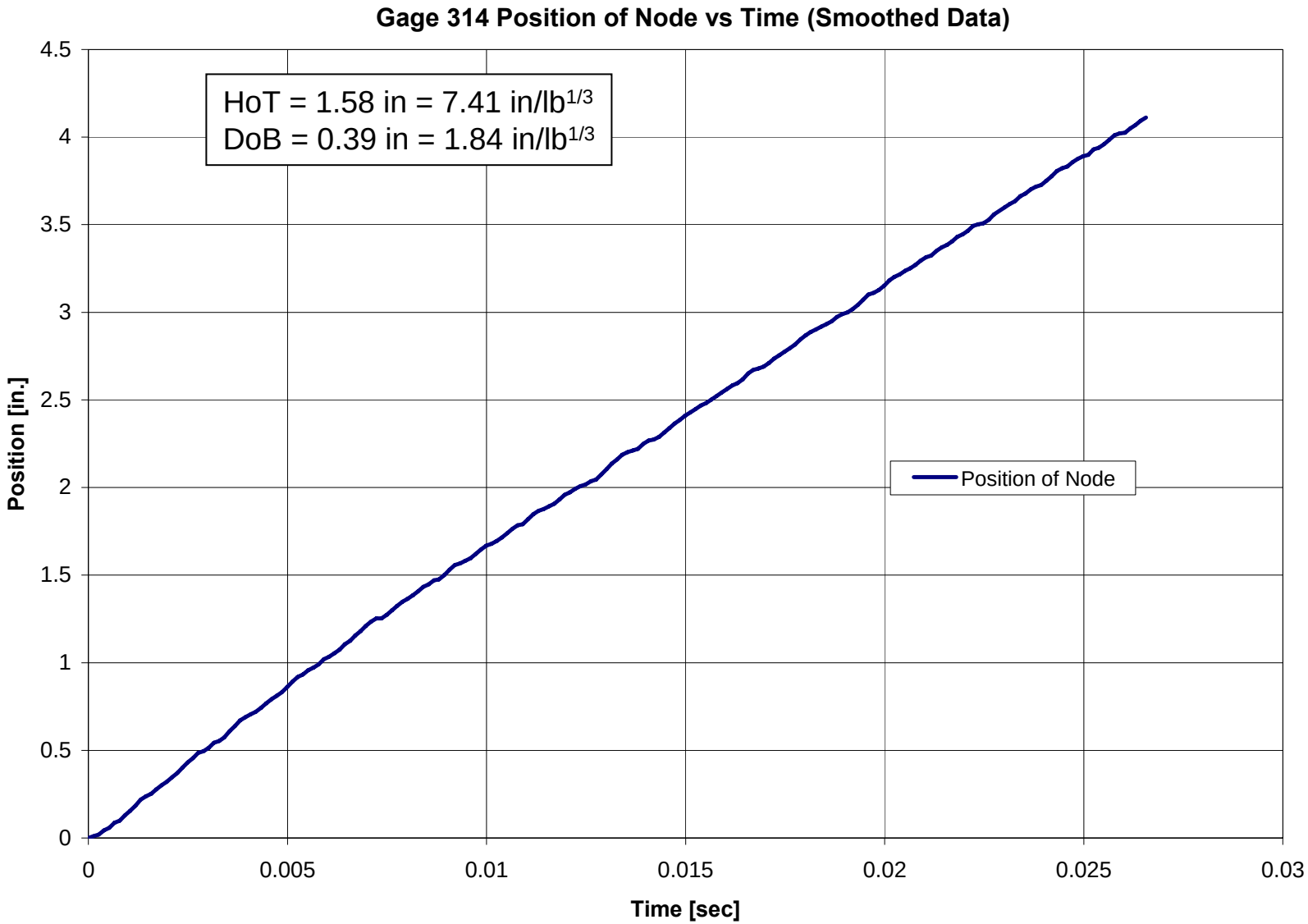


- Annular Jet of Saturated Soil Provides Confinement for Explosive Gas Pressure in “Tail” of Pressure – Time Curve

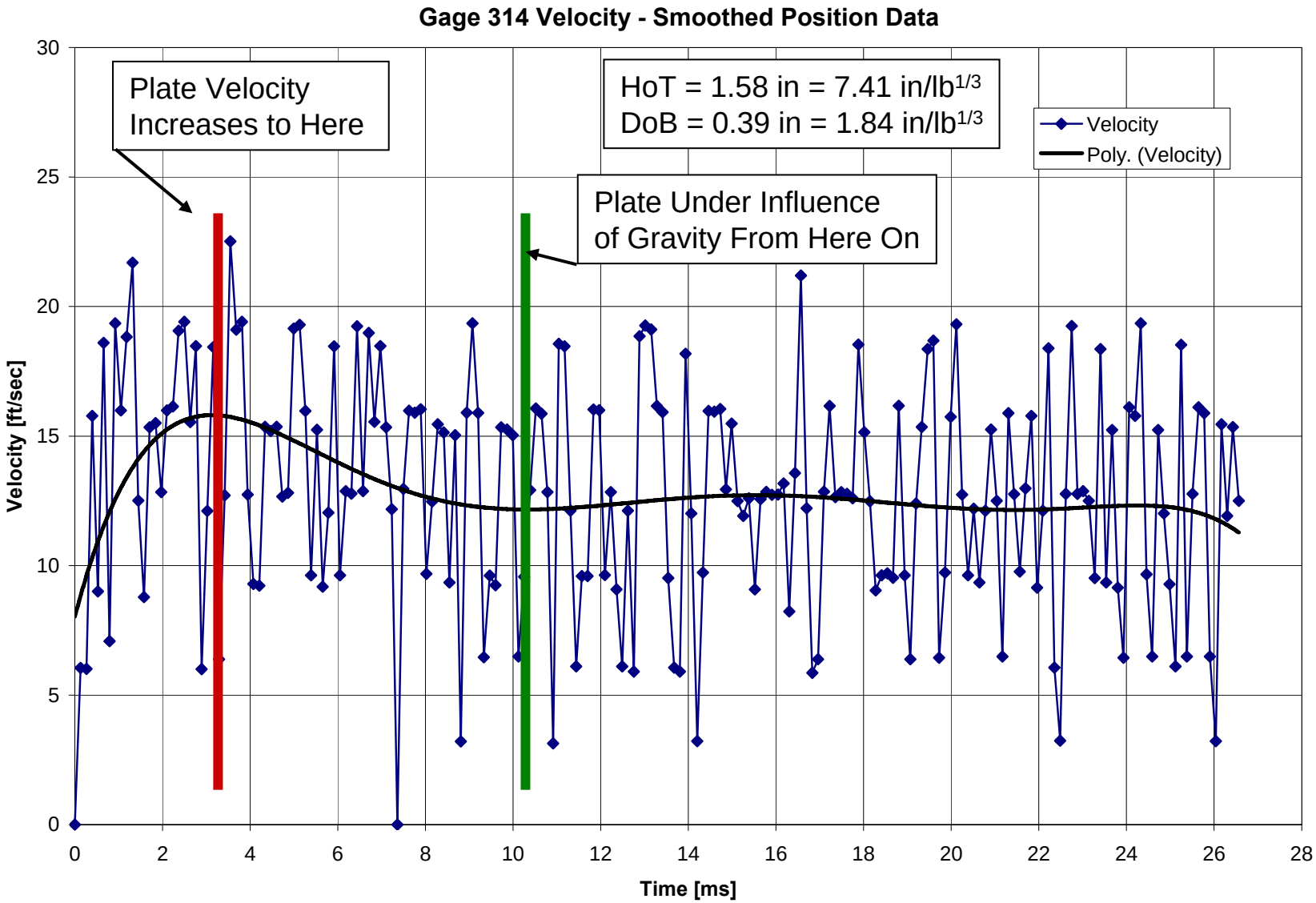
Late Time Effects



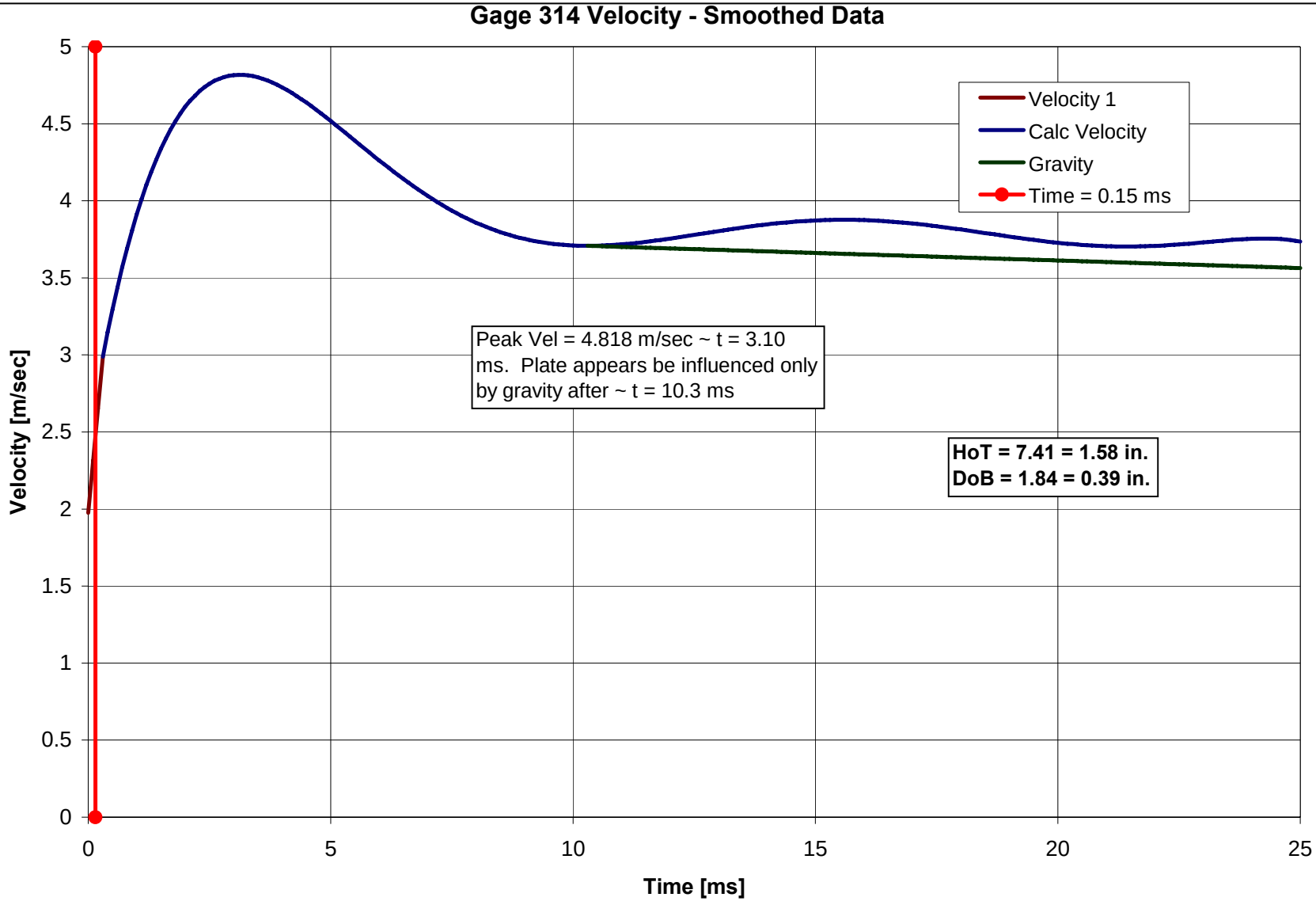
Late Time Effects



Late Time Effects



Late Time Effects



Late Time Effects

- In Spite of Lower Pressures Resulting From
  - Impact of Material From Crater
  - Pressure of Trapped Gas
- Late Time Processes Make Major Contribution to Impulse

- Target Plate Gained Velocity for ~ 3 ms
- Increase After ~ 0.15 ms Due to Late Time Processes

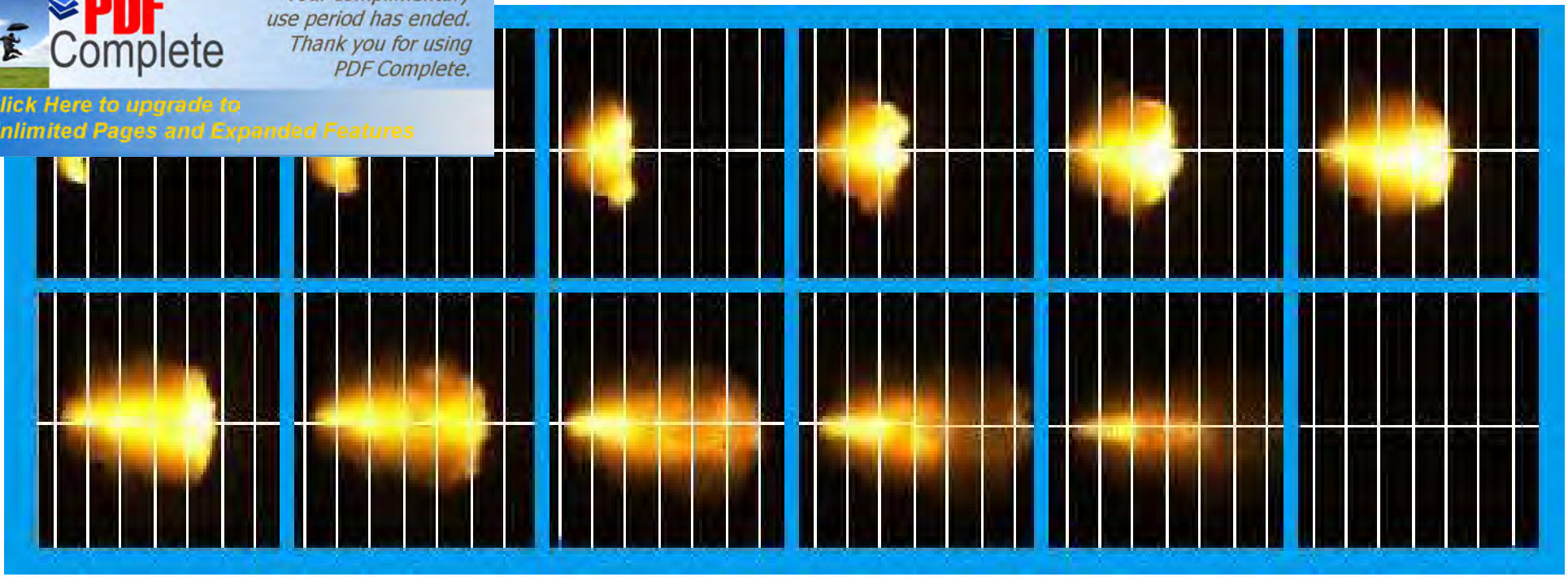
- Also Notice:
  - Plate Slows at Greater Than 1g Until t~10 ms
  - Gas Bubble Can Over-Expand & Slow Plate

Summary

- Primary Loading Mechanism
  - Soil Driven Into Target by Expanding Gas Bubble
- First Phase
  - Complex, Modulated by Shockwave
  - Very Brief
  - Acts on Small Portion of Target
  - Provides About Half Total Vertical Impulse
- Second Phase
  - Dominated By Crater Excavation Processes
  - Pressures Lower
  - Order of Magnitude Greater Duration
  - Much Larger Area of Application
  - Provides About Half Total Vertical Impulse

Leslie C. Taylor
Ph: 301/405-5339
University of Maryland
Paper: ISB 277-2008

PDF Complete
Your complimentary use period has ended. Thank you for using PDF Complete.
Click Here to upgrade to Unlimited Pages and Expanded Features



Consideration of the Ignition Delay of Gun Propellants

M. J. Taylor, C. R. Woodley, S. R. Fuller, S. Gilbert, J. I. Gransden

A presentation to: 24th International Symposium on Ballistics, New Orleans, Louisiana September 22-26, 2008

QinetiQ

© Copyright QinetiQ limited 2008

PDF Complete
Your complimentary use period has ended. Thank you for using PDF Complete.
Click Here to upgrade to Unlimited Pages and Expanded Features

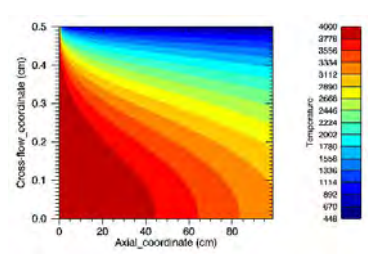
01 Background

02 Empirical Expression for Ignition Delay

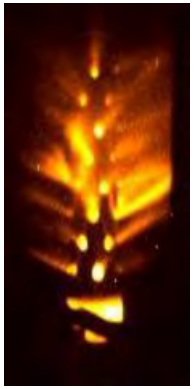
03 The Ablation Coefficient

04 Analytical Treatment of Ignition Delay

05 Conclusions



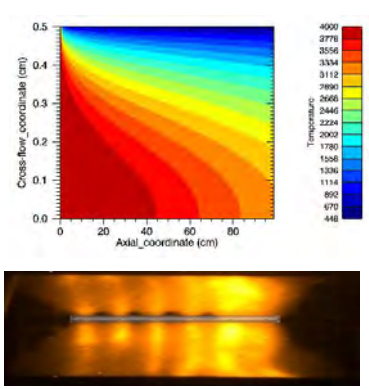




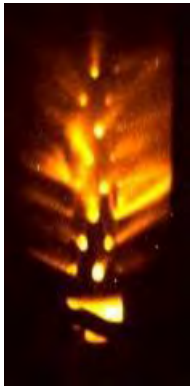
© Copyright QinetiQ limited 2007

PDF Complete
Your complimentary use period has ended. Thank you for using PDF Complete.
Click Here to upgrade to Unlimited Pages and Expanded Features

01
Background

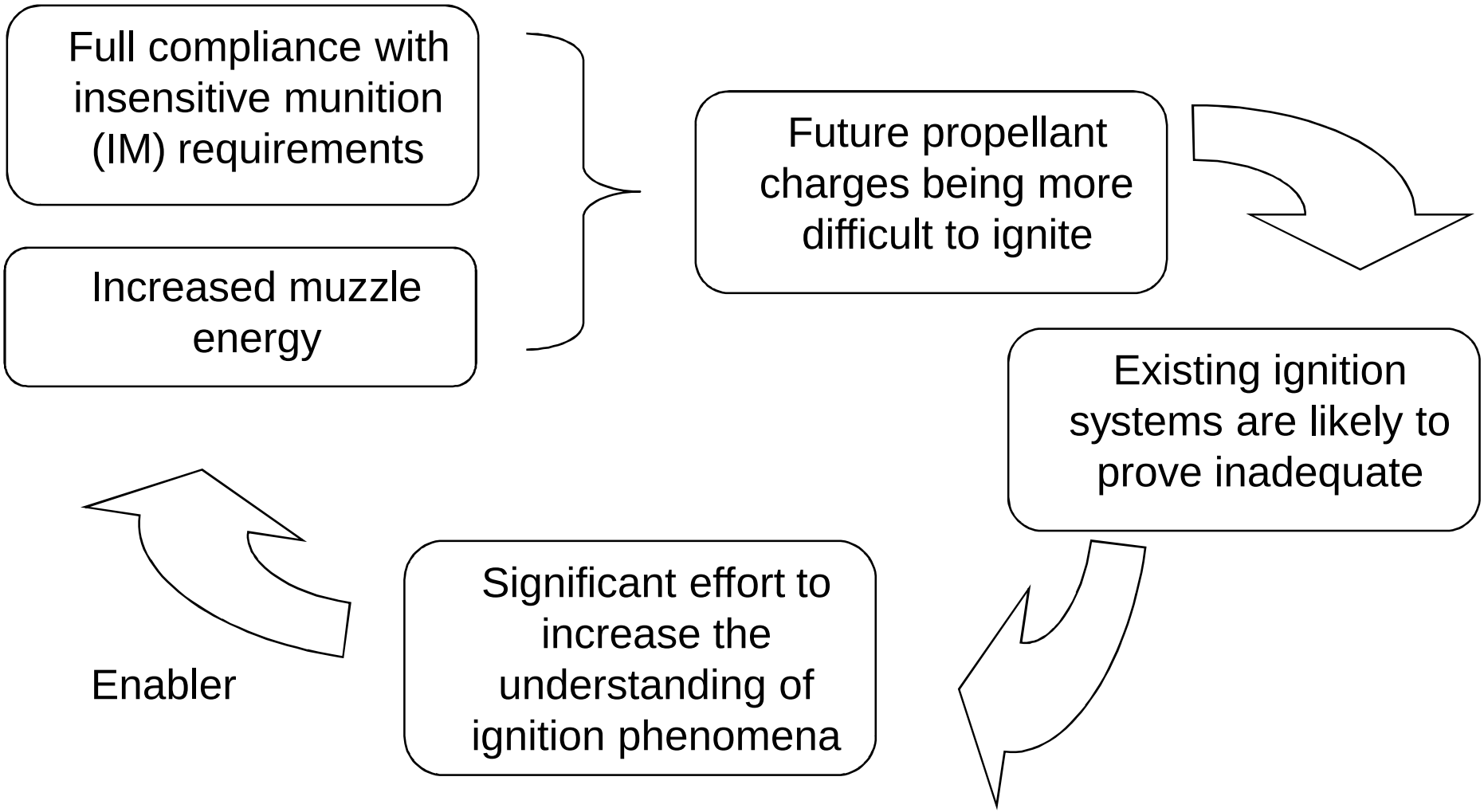






© Copyright QinetiQ limited 2007

PDF Complete
Your complimentary use period has ended. Thank you for using PDF Complete.
Click Here to upgrade to Unlimited Pages and Expanded Features



© Copyright QinetiQ limited 2007

PDF Complete
Your complimentary use period has ended. Thank you for using PDF Complete.
Click Here to upgrade to Unlimited Pages and Expanded Features

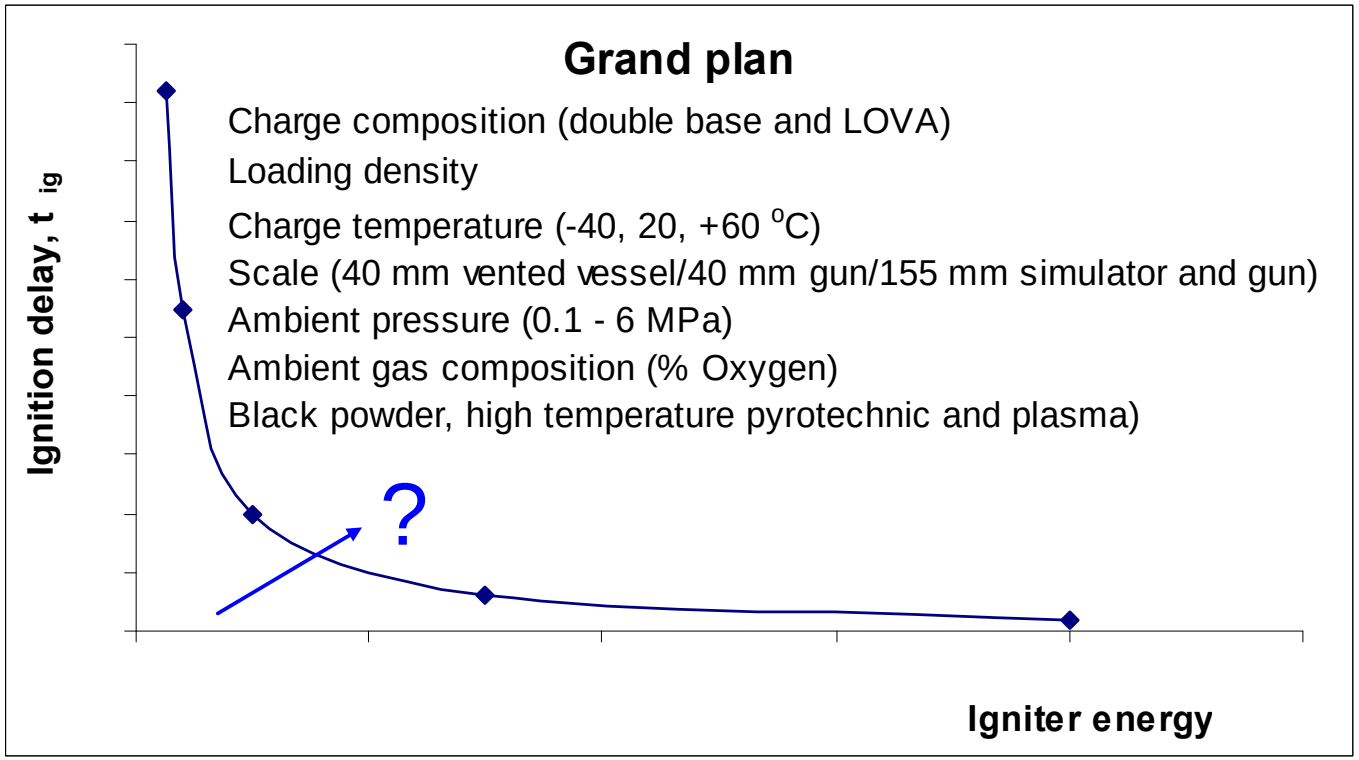
A MOD DTIC programme designed to address this need

Includes the UK component of the EUROPA Ignition Phenomena TA between French, German, Swedish and the UK Govnôs

Aimed at increasing the depth of understanding of ignition by experiment and encapsulate in computer modelling

© Copyright QinetiQ limited 2007

PDF Complete
Your complimentary use period has ended. Thank you for using PDF Complete.
Click Here to upgrade to Unlimited Pages and Expanded Features



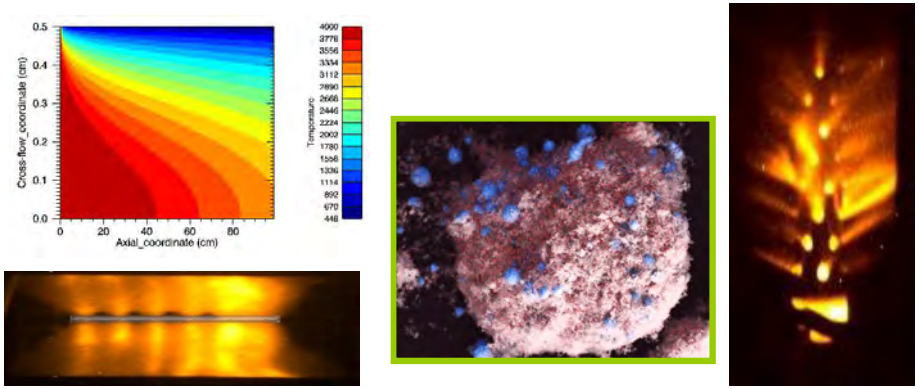
- Ignition delay is an important and sensitive measurand
  - Over-ignition leads to pressure waves: **modelled with reasonable confidence**
  - Under-ignition leads to long ignition delays: **cannot be predictively modelled**

© Copyright QinetiQ limited 2007

PDF Complete
Your complimentary use period has ended. Thank you for using PDF Complete.
Click Here to upgrade to Unlimited Pages and Expanded Features

02

Empirical Expression for Ignition Delay



© Copyright QinetiQ limited 2007

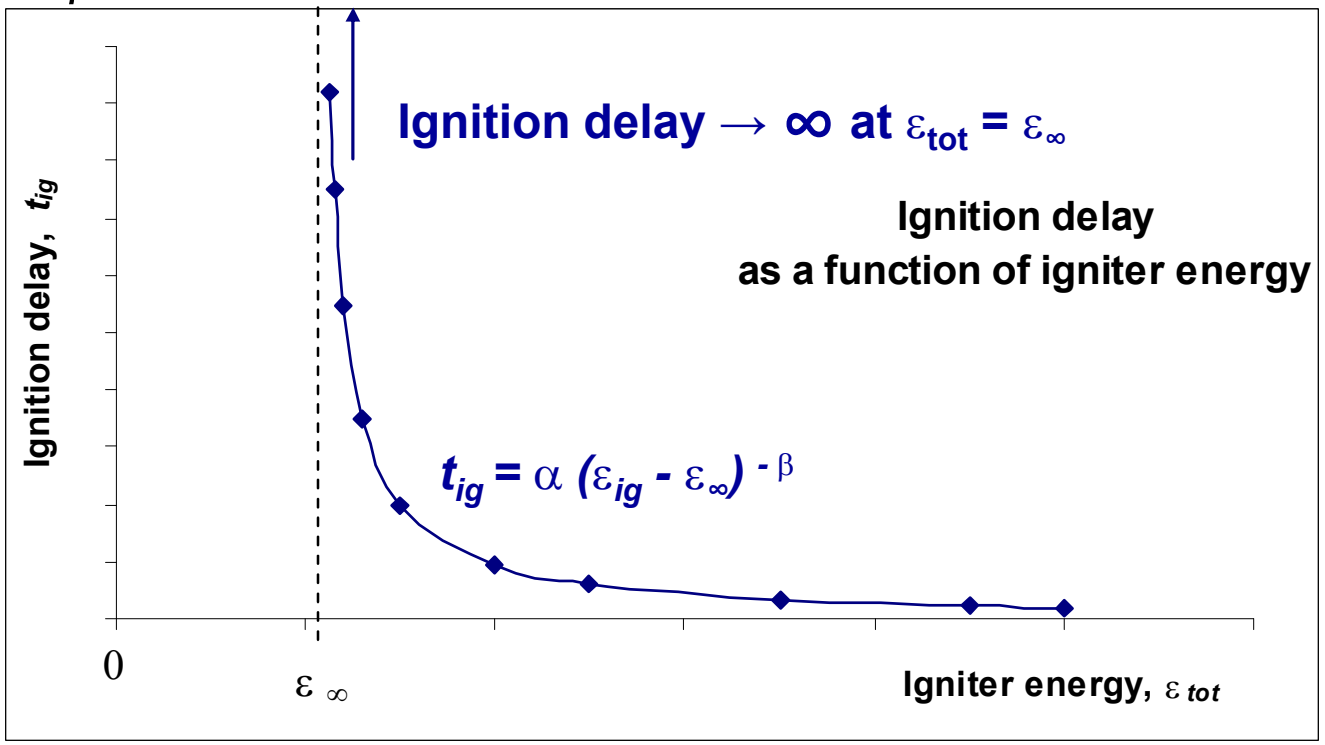
PDF Complete
Your complimentary use period has ended. Thank you for using PDF Complete.
Click Here to upgrade to Unlimited Pages and Expanded Features

ession for Ignition Delay

$$t_{ig} = \alpha\ (\varepsilon_{ig} - \varepsilon_{\infty})^{-\beta} \qquad (1)$$

where ε_{∞} is the energy leading to mis-fire ($t_{ig} = \infty$ when $\varepsilon_{ig} - \varepsilon_{\infty} = 0$);

α, β are constants



Aims:

Determine function coefficients for propellant ignition for a range of parameters

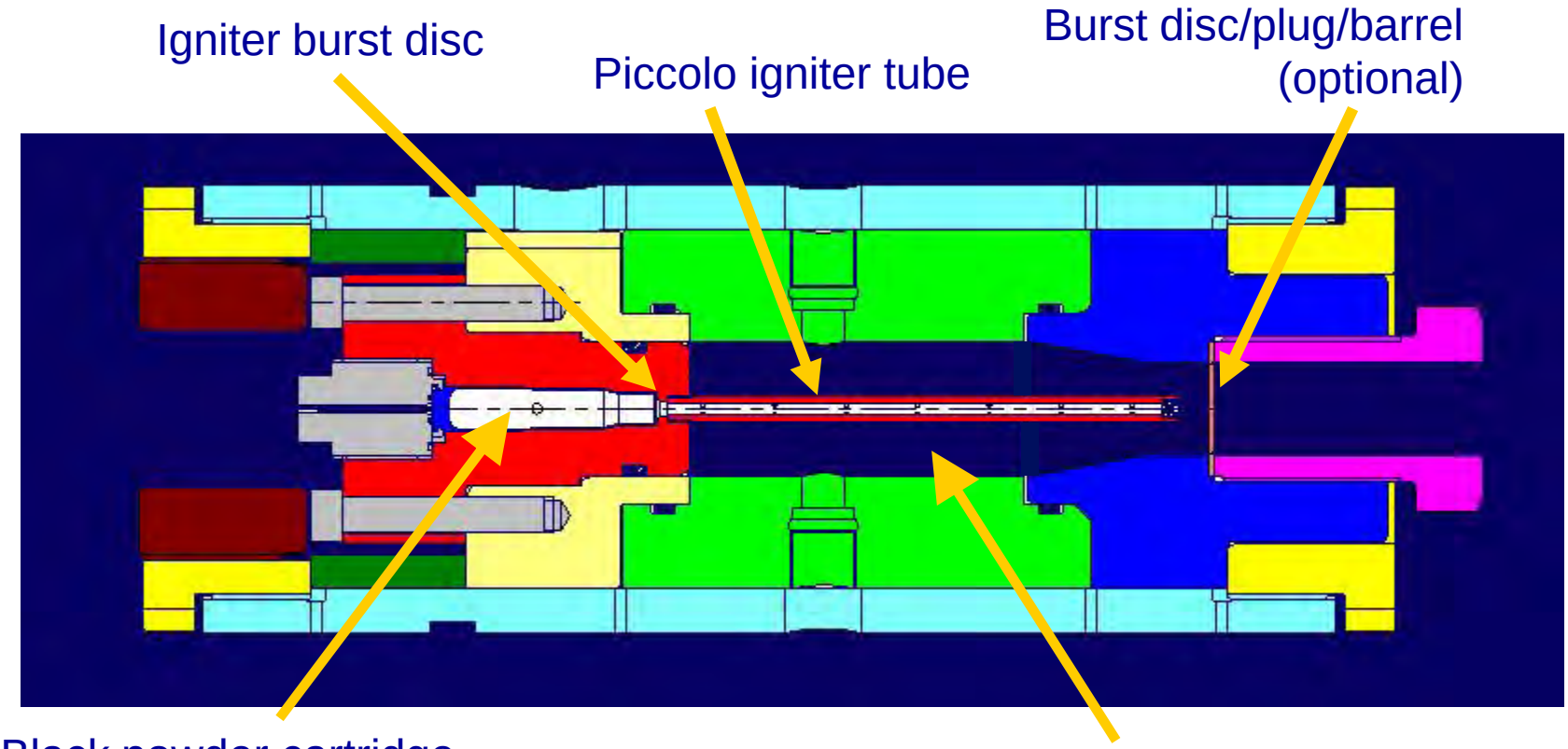
Use data for ignition model validation and model development

© Copyright QinetiQ limited 2007

PDF Complete
Your complimentary use period has ended. Thank you for using PDF Complete.
Click Here to upgrade to Unlimited Pages and Expanded Features

ession for Ignition Delay

Instrumented 40 mm black powder igniter and vessel



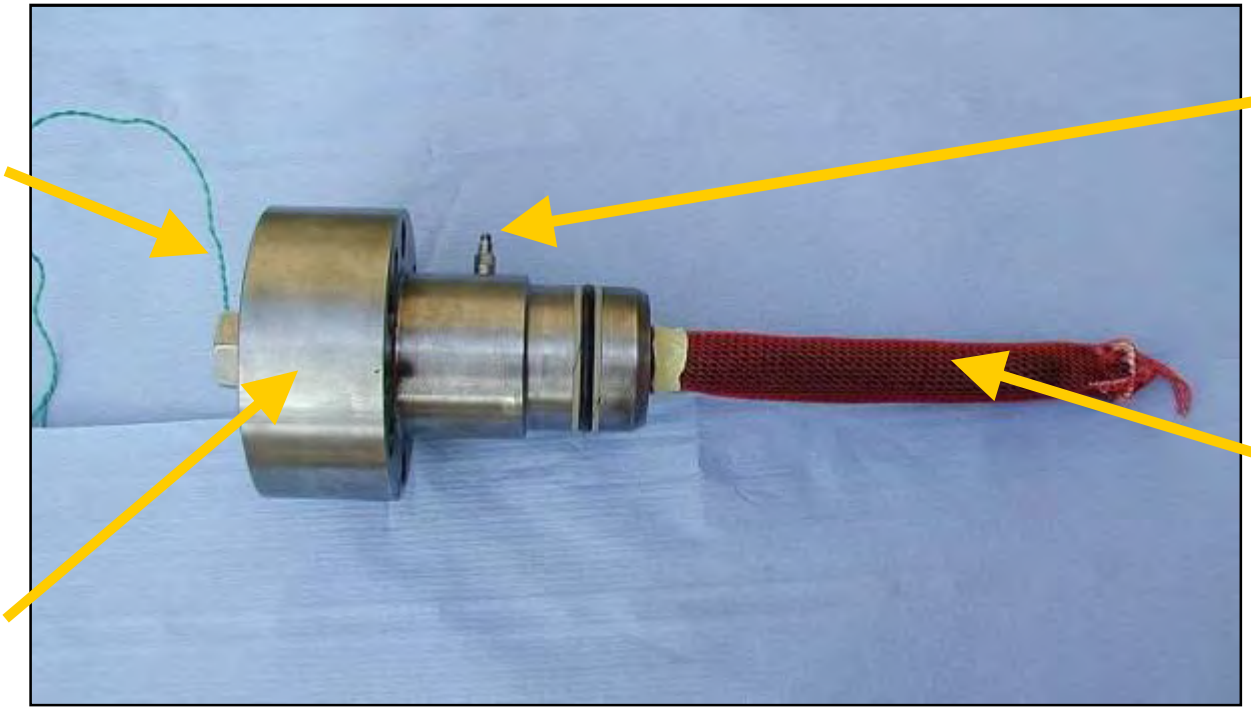
© Copyright QinetiQ limited 2007

PDF Complete
Your complimentary use period has ended. Thank you for using PDF Complete.
Click Here to upgrade to Unlimited Pages and Expanded Features

ession for Ignition Delay

The propellant charge is made around the piccolo tube

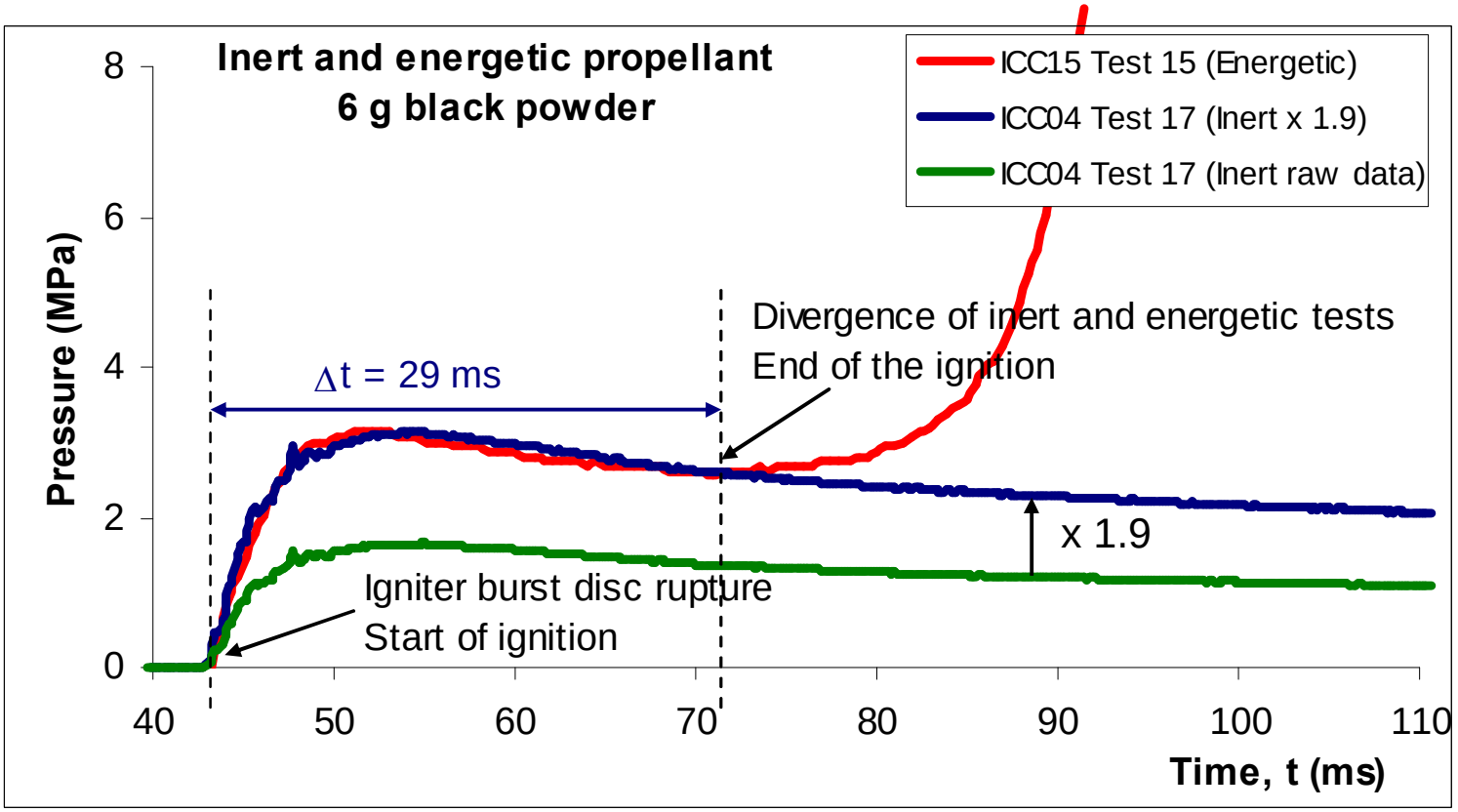
Loading density is adjusted by radial (as opposed to longitudinal) adjustment



© Copyright QinetiQ limited 2007

PDF Complete
Your complimentary use period has ended. Thank you for using PDF Complete.
Click Here to upgrade to Unlimited Pages and Expanded Features

ession for Ignition Delay

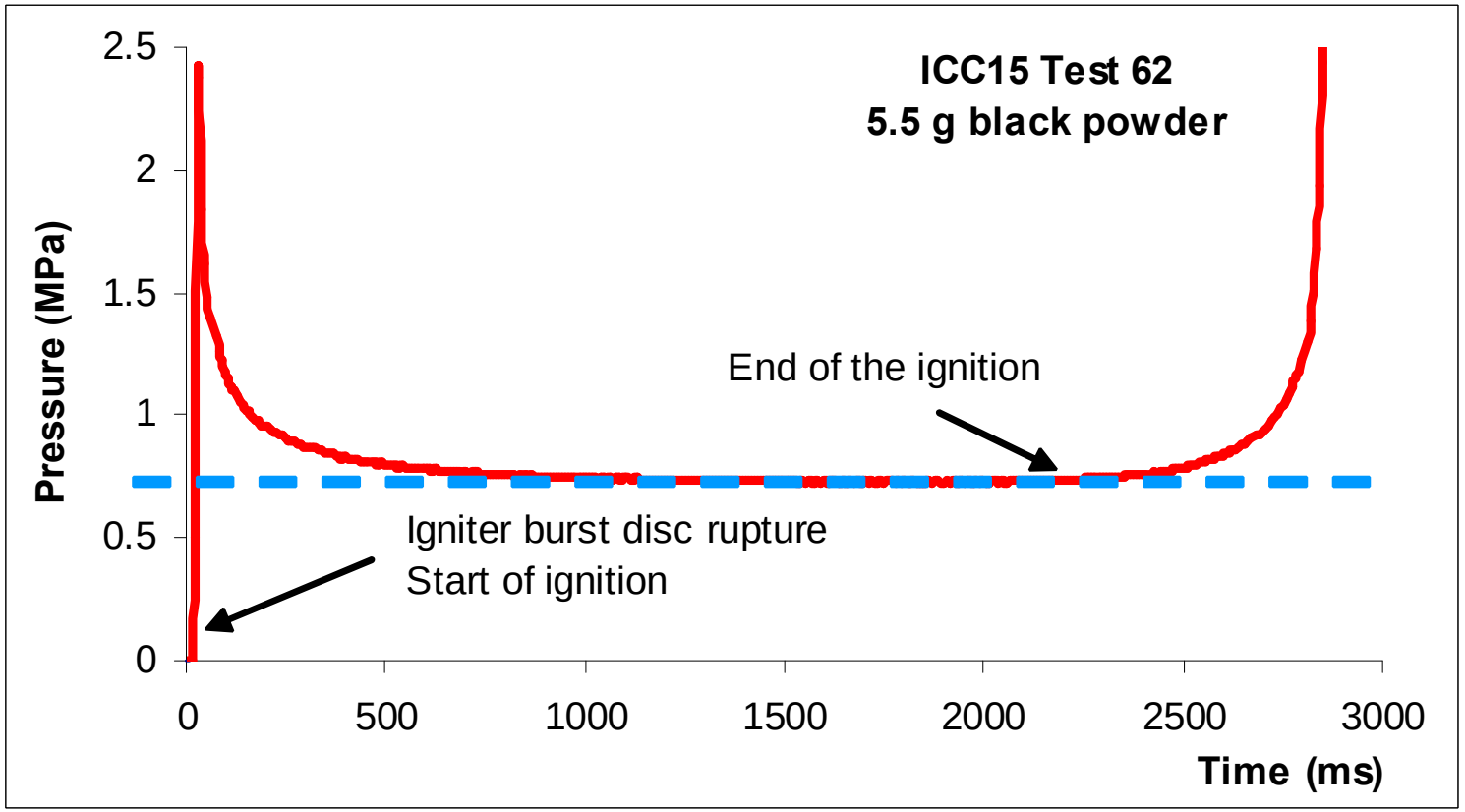


Energetic tests generated up to 4 times more pressure than inert tests

© Copyright QinetiQ limited 2007

PDF Complete
Your complimentary use period has ended. Thank you for using PDF Complete.
Click Here to upgrade to Unlimited Pages and Expanded Features

ession for Ignition Delay

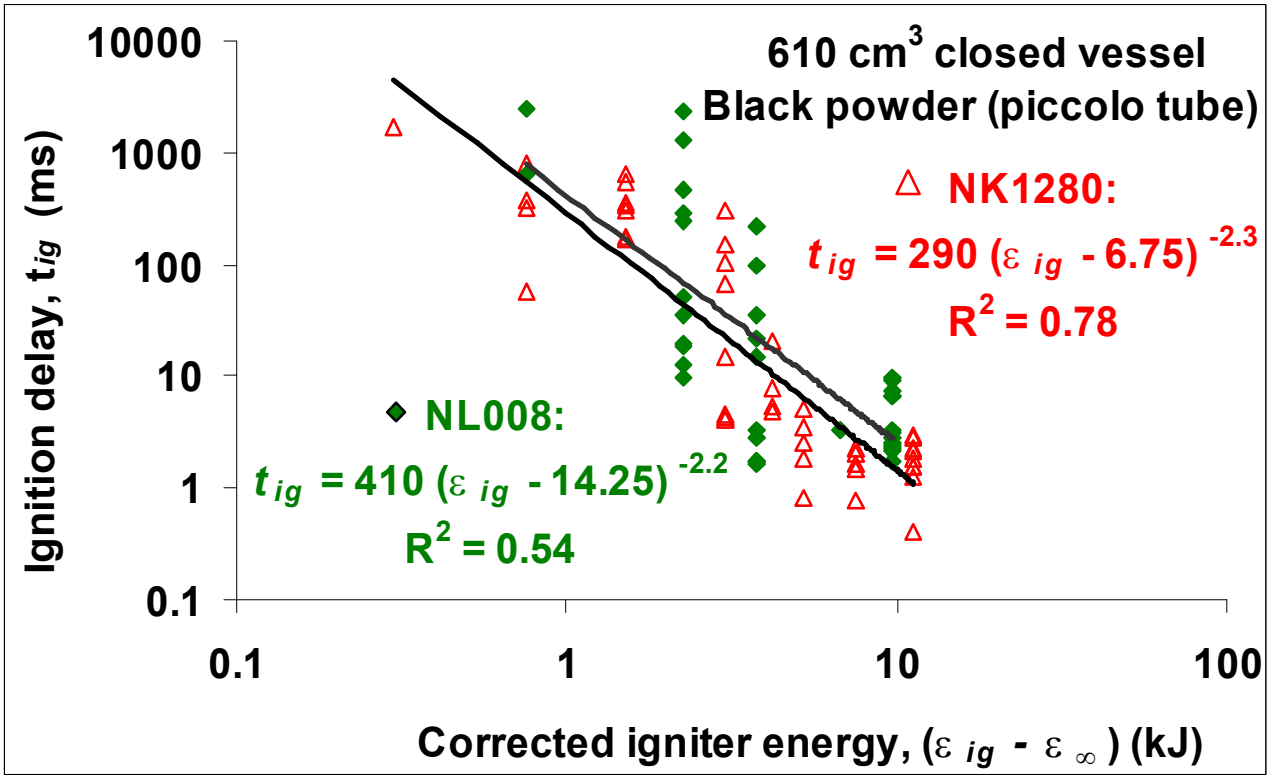


End of ignition can be defined by change in dp/dt

© Copyright QinetiQ limited 2007

PDF Complete
Your complimentary use period has ended. Thank you for using PDF Complete.
Click Here to upgrade to Unlimited Pages and Expanded Features

ession for Ignition Delay

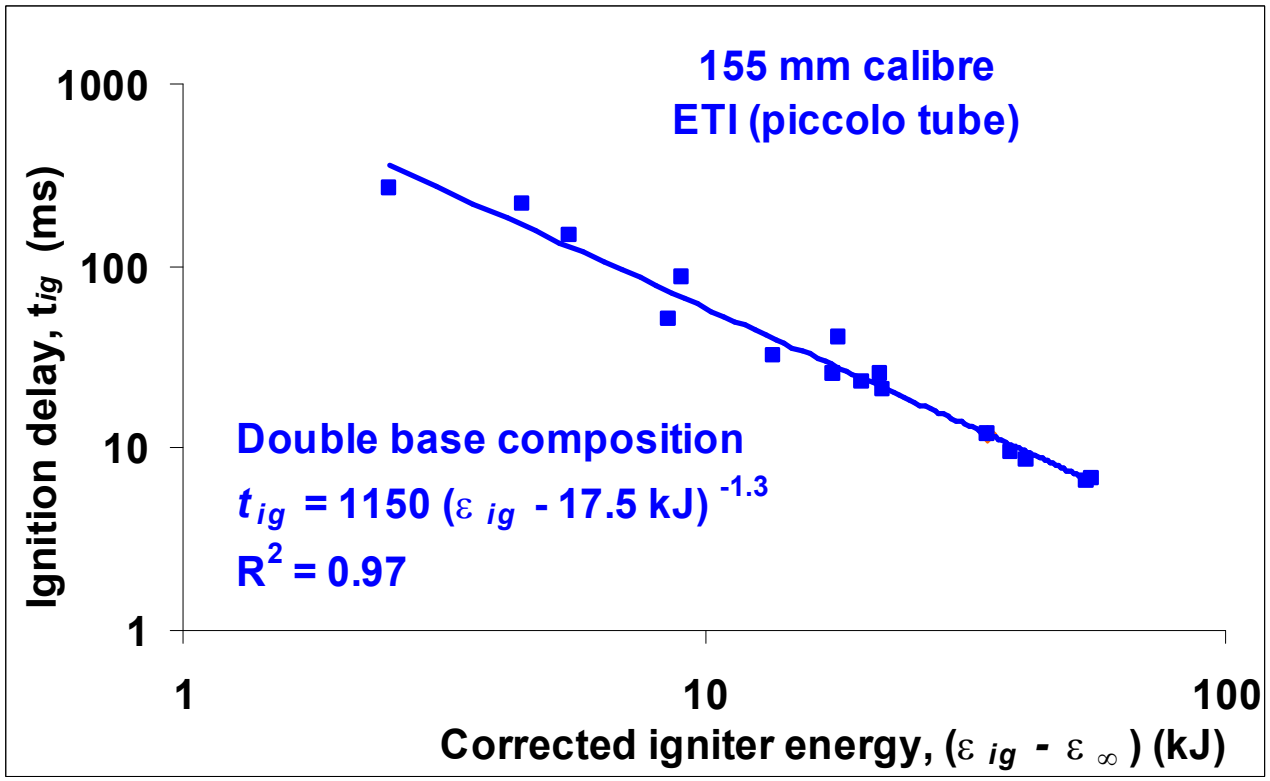


Ignition using a piccolo igniter with black powder ï poor repeatability at cannon calibre

© Copyright QinetiQ limited 2007

PDF Complete
Your complimentary use period has ended. Thank you for using PDF Complete.
Click Here to upgrade to Unlimited Pages and Expanded Features

ession for Ignition Delay

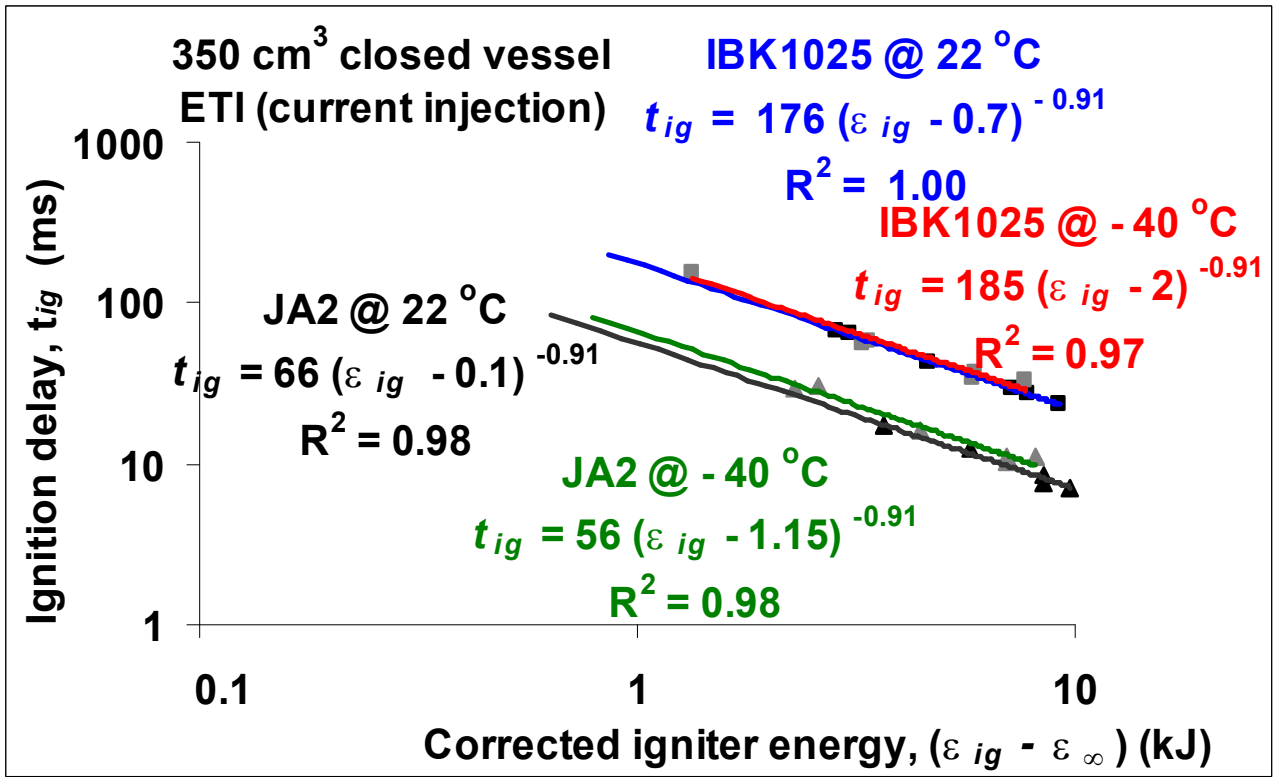


Ignition using a piccolo igniter with black powder ï good repeatability at 155 mm calibre

© Copyright QinetiQ limited 2007

PDF Complete
Your complimentary use period has ended. Thank you for using PDF Complete.
Click Here to upgrade to Unlimited Pages and Expanded Features

ession for Ignition Delay



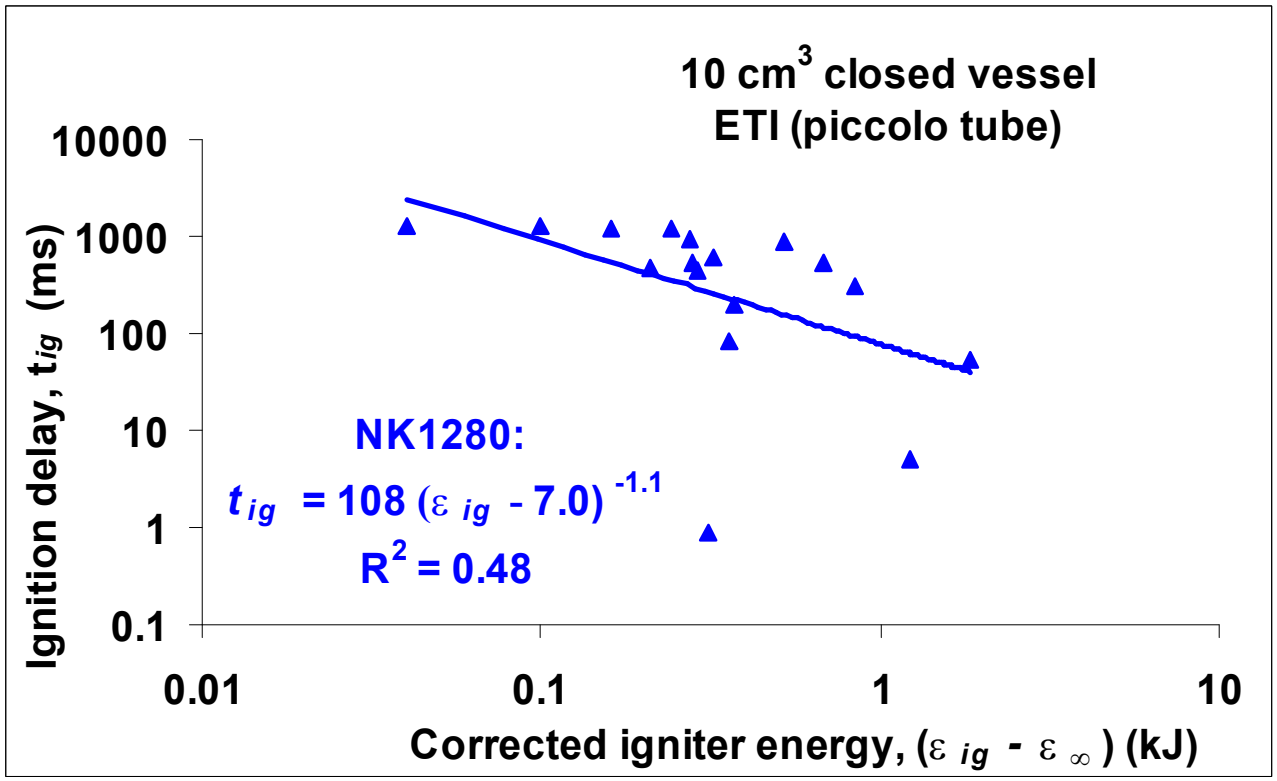
Ignition using a current injection igniter with ETI ï good repeatability at cannon calibre

Results curtsey of TNO - M. Bakker, C. Schoolderman, C. van Driel and E. Folgering, ñETC Ignition of LOVA Gun Propellantsò, 37th Int. Annual Conference of ICT, Karlsruhe, Germany, 27th June - 30th June, 2006

© Copyright QinetiQ limited 2007

PDF Complete
Your complimentary use period has ended. Thank you for using PDF Complete.
Click Here to upgrade to Unlimited Pages and Expanded Features

ession for Ignition Delay



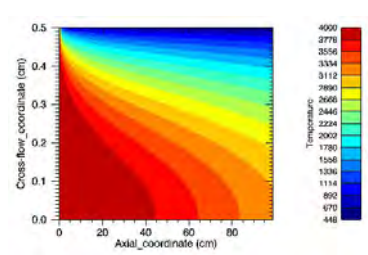
Ignition using a piccolo igniter with ETI ï poor repeatability at cannon calibre

Consistent poor repeatability at cannon calibre with piccolo igniteré .

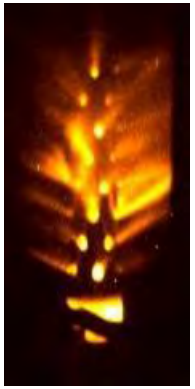
© Copyright QinetiQ limited 2007

PDF Complete
Your complimentary use period has ended. Thank you for using PDF Complete.
Click Here to upgrade to Unlimited Pages and Expanded Features

03
The Ablation Coefficient



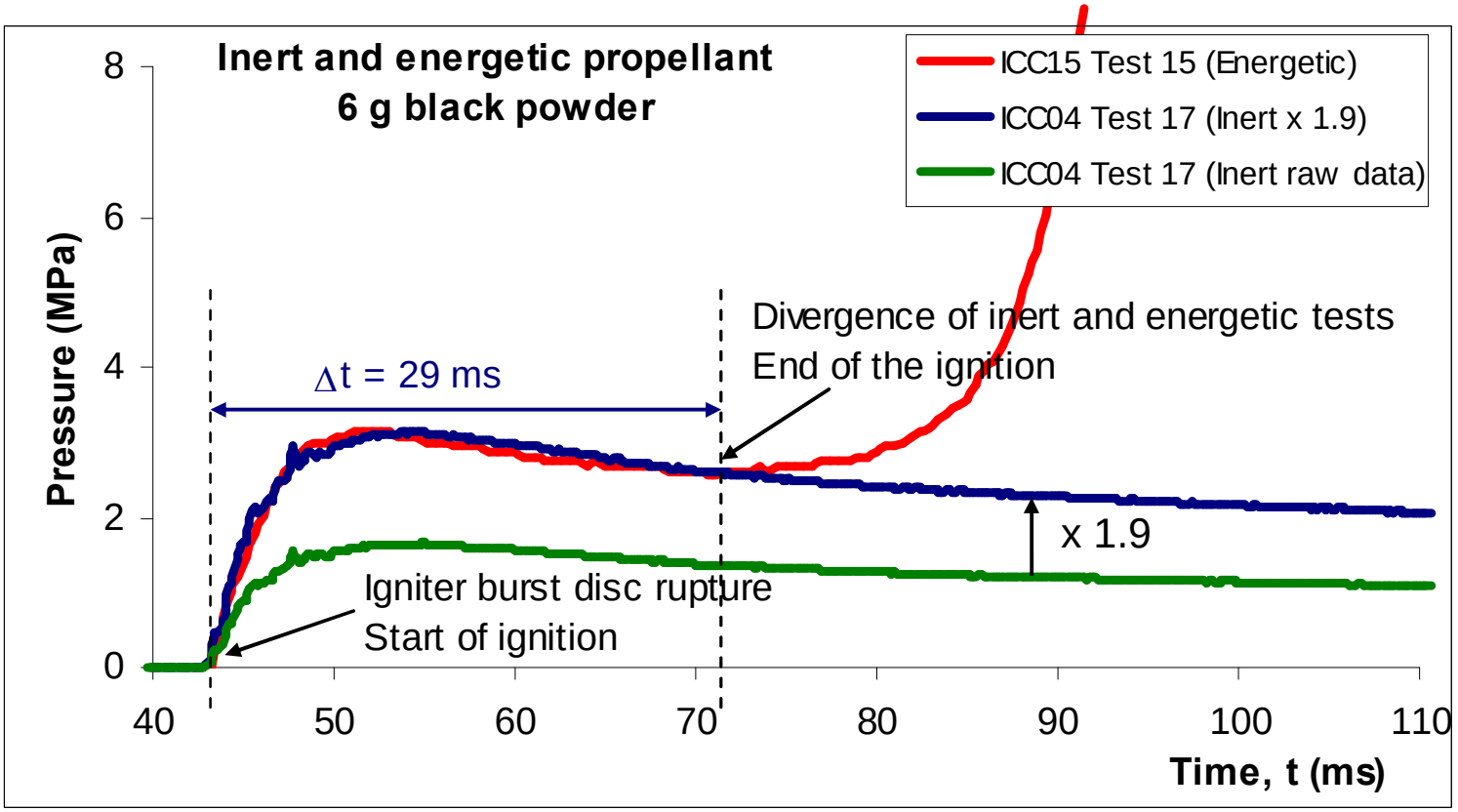




© Copyright QinetiQ limited 2007

PDF Complete
Your complimentary use period has ended. Thank you for using PDF Complete.
Click Here to upgrade to Unlimited Pages and Expanded Features

oefficient



Energetic tests generated up to 4 times more pressure than inert tests

© Copyright QinetiQ limited 2007

PDF Complete
Your complimentary use period has ended. Thank you for using PDF Complete.
Click Here to upgrade to Unlimited Pages and Expanded Features

oefficient

- It is proposed that erosive burning (ablation) of the propellant is caused by the discharging igniter

  This adds energy and pressure to the system during the ignition phase

$$t_{ig} = \alpha\ (\varepsilon_{ig} + ap - \varepsilon_{\infty})^{-\beta} \qquad (2)$$

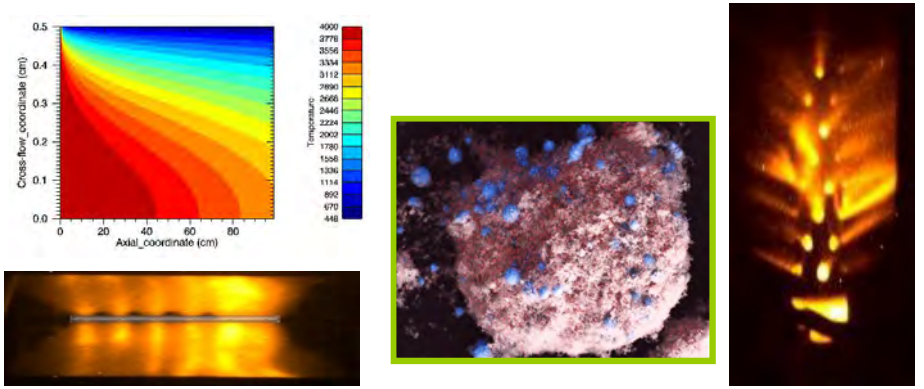
- Variability in ignition delay caused by variability in ablation coefficient, *a*
  - The factor, *a,* slightly varies from test to test
- The factor, *a,* greatly varies with test conditions
  - Cannon calibre ETI using a piccolo igniter gives the largest factor
    - Highly brisant (hard) igniter
  - Cannon calibre ETI using current injection gives the least factor
    - Low brisance (soft) igniter

© Copyright QinetiQ limited 2007

PDF Complete
Your complimentary use period has ended. Thank you for using PDF Complete.
Click Here to upgrade to Unlimited Pages and Expanded Features

04

Analytical Treatment of Ignition Delay



© Copyright QinetiQ limited 2007

PDF Complete
Your complimentary use period has ended. Thank you for using PDF Complete.
Click Here to upgrade to Unlimited Pages and Expanded Features

tment of Ignition Delay

- The time to ignition can also be described by:

$$t_{ig} \sim \tfrac{1}{4} \pi \ \lambda \ \rho \ c_p \ T_p^2 \ I^{-2} + t_{stab} \qquad (2)$$

where

λ is the propellant heat conductivity

ρ is the propellant density

c_p is the propellant specific heat

T_p is the propellant pyrolysis temperature

I is the heat flux

- t_{stab} is the time required for initiation and stabilisation of gas phase reactions and is only significant during over-ignition when the heat flux is large and I^{-2} diminishes (i.e. when ignition delays are small)

© Copyright QinetiQ limited 2007

PDF Complete
Your complimentary use period has ended. Thank you for using PDF Complete.
Click Here to upgrade to Unlimited Pages and Expanded Features

tment of Ignition Delay

- The expressions for ignition delay, equations (2) and (3), are obviously describing the same event but from empirical and theoretical perspectives
  - The theory considers the rate of heat transfer and the experiment considers the time-integrated energy
- However, these expressions can be equated by substituting for heat flux with time-integrated energy in equation (3)

© Copyright QinetiQ limited 2007

PDF Complete
Your complimentary use period has ended. Thank you for using PDF Complete.
Click Here to upgrade to Unlimited Pages and Expanded Features

tment of Ignition Delay

- If the rate of energy transfer is assumed to be constant then, for relatively long ignition delays:

$$t_{ig} = \alpha\,(\varepsilon_{ig} + ap - \varepsilon_{\infty})^{-\beta} = \tfrac{1}{4}\,\pi\ \lambda\ \rho\, c_p\, T_p^{\,2}\, t^2\, A^2\, \varepsilon^{-2} \quad (4)$$

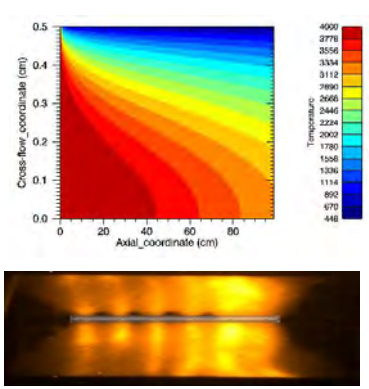
  where ε is the igniter energy transferred to the propellant, t is the time to transfer ε and A is the surface area over which ε is transferred

- This comparison gives a useful platform from which to understand and compare the various values of the igniter coefficients

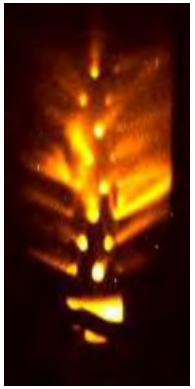
© Copyright QinetiQ limited 2007

PDF Complete
Your complimentary use period has ended. Thank you for using PDF Complete.
Click Here to upgrade to Unlimited Pages and Expanded Features

05
Conclusions







© Copyright QinetiQ limited 2007

PDF Complete
Your complimentary use period has ended. Thank you for using PDF Complete.
Click Here to upgrade to Unlimited Pages and Expanded Features

- Studies have investigated ignition delay of gun propellant
  - An empirical treatment of the relationship between ignition delay and igniter energy agrees in form with an analytical expression
  - The correlation between experiment and theory is excellent under some conditions, but appears to be poor under others
  - An hypothesis to explain this has been put forward, that some igniter designs produce excessive ablation of propellant
- Some of the main assumptions in the theoretical treatment are invalidated, but the comparison between the experiment and theory has been surprisingly successful
- Efforts to understand the physical and chemical processes occurring during the long ignition delays are planned

© Copyright QinetiQ limited 2007

PDF Complete
Your complimentary use period has ended. Thank you for using PDF Complete.
Click Here to upgrade to Unlimited Pages and Expanded Features

QinetiQ

The Global Defence and Security Experts

© Copyright QinetiQ limited 2006

Jacketed penetrators having different thickness

Penetrator performance and production

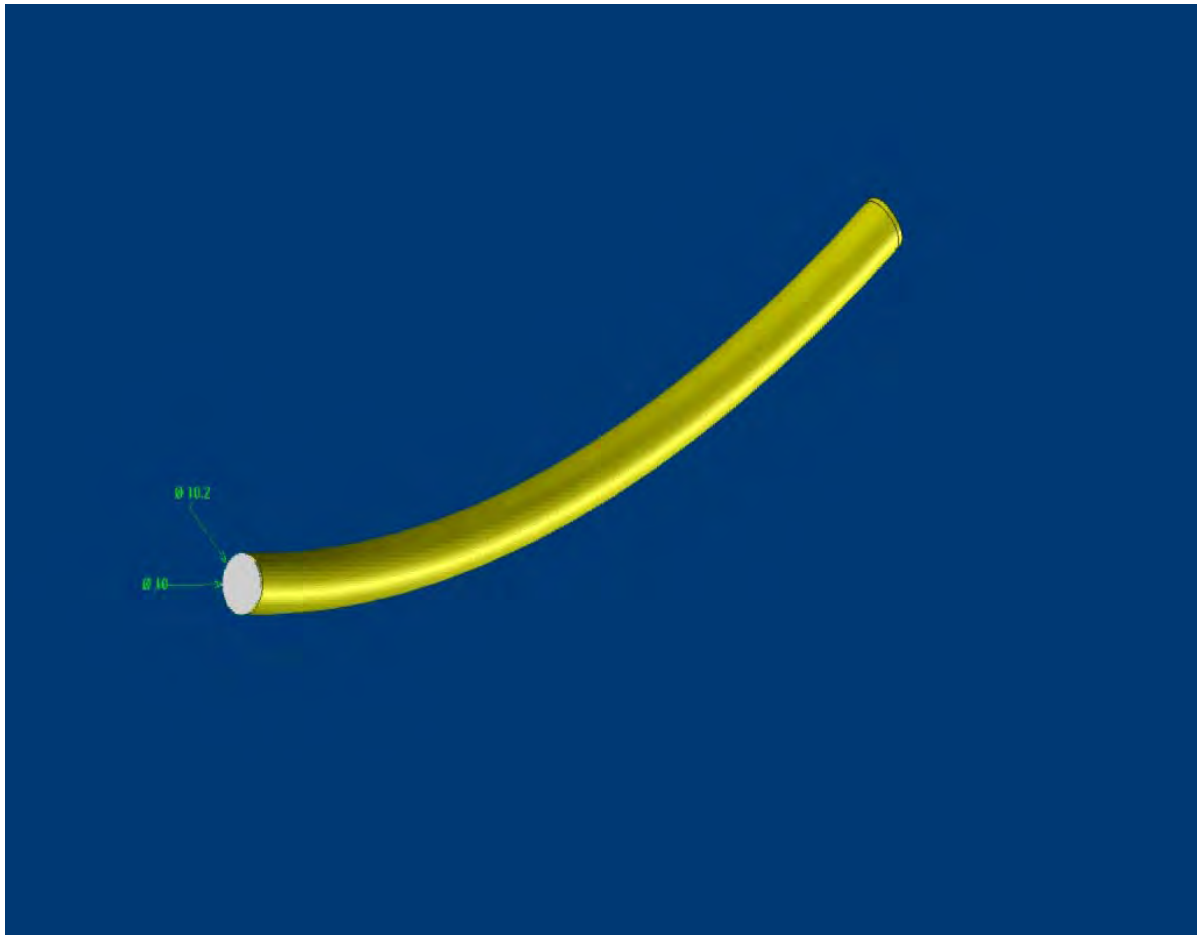
TNO | Knowledge for business



Contributors to this work:

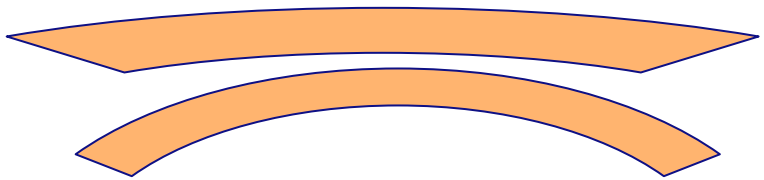
- Dr. Erik Carton
- Dr. Marianne Stuivinga
- Mark Dijkstra, Msc
- Dr. Niels van der Meer
  - TNO Defence, Security and Safety
  - Lange Kleiweg 137, 2280 AA Rijswijk, The Netherlands
  - Phone: +31 15 2843581
  - Fax: +31 15 2843939
  - Email: niels.vandermeer@tno.nl

Increasing the jacket thickness make the penetrator stiffer

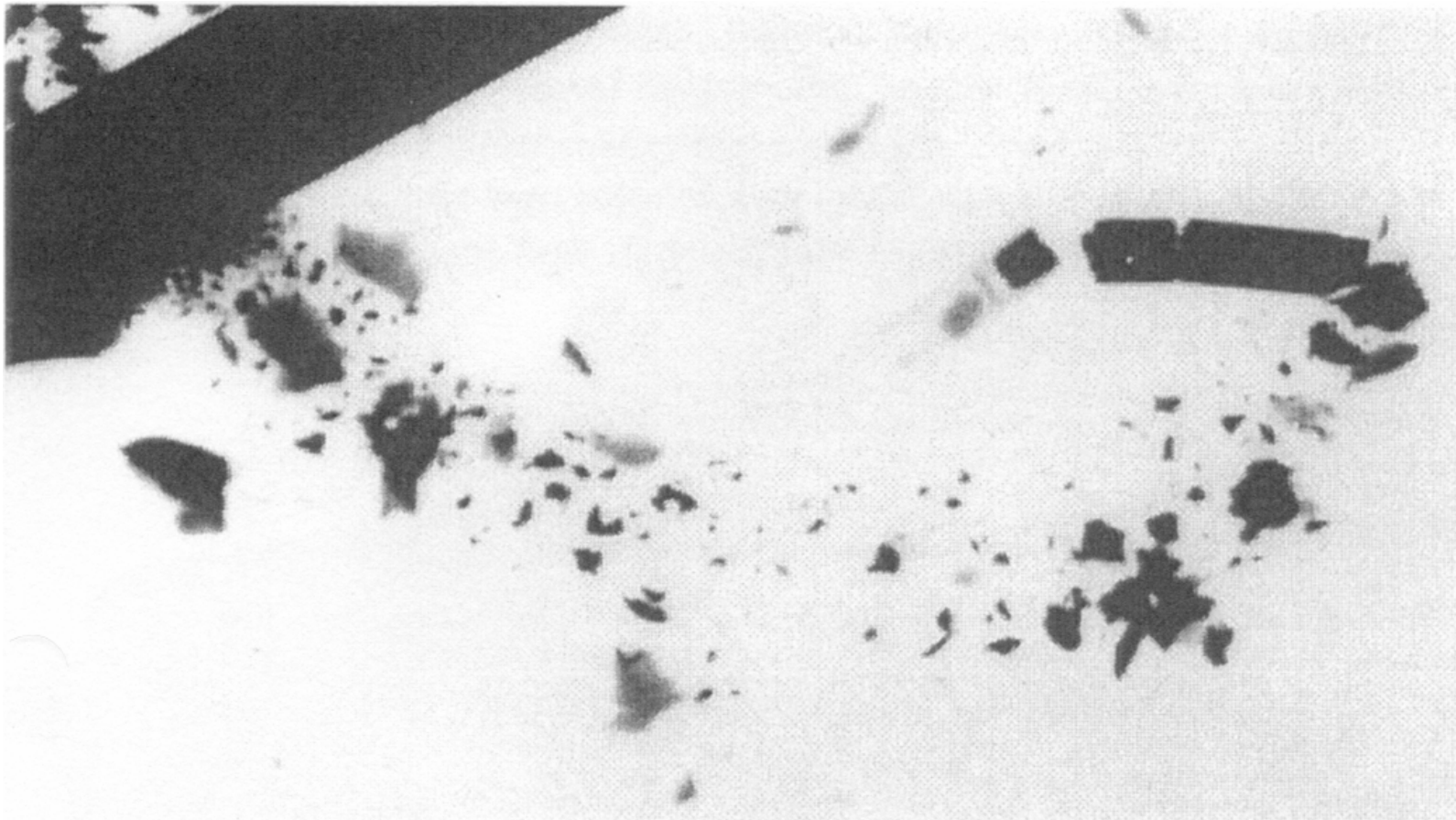


Content of presentation

- Join technique of jacket and core: explosive cladding
- Propellant production and light weight sabot
- Experiments with and results for jacket penetrators
- Conclusions



Limit fragmentation……



Jacketed penetrators obtain higher flexural rigidity with increasing jacket thickness

- Flexural rigidity of a rod $\propto$ E x R^4 (Youngs modulus x radius^4)
- Penetrator mass increase as well $\propto$ $R^{2/3}$ x ρ (radius$^{2/3}$ x mass density)
- Use high Young's modulus, low mass density material for the jacket
- Large radius of low density jacket will reduce penetration capacity of jacketed penetrator
- Commercially available metals (tubes) have been used for jackets

Focus

- Most published work is focussed on the important penetrator depth of penetration (DOP)
- This work is focussed on penetrator condition after perforating spaced/layered thin targets
- Reduced DOP of an intact jacketed penetrator is sometimes preferred over hardly any DOP of a broken penetrator

Under what circumstances can a jacket be useful?

- Thick target plates cause probably too high lateral forces on the penetrator

A jacket could be of advantage in case of:

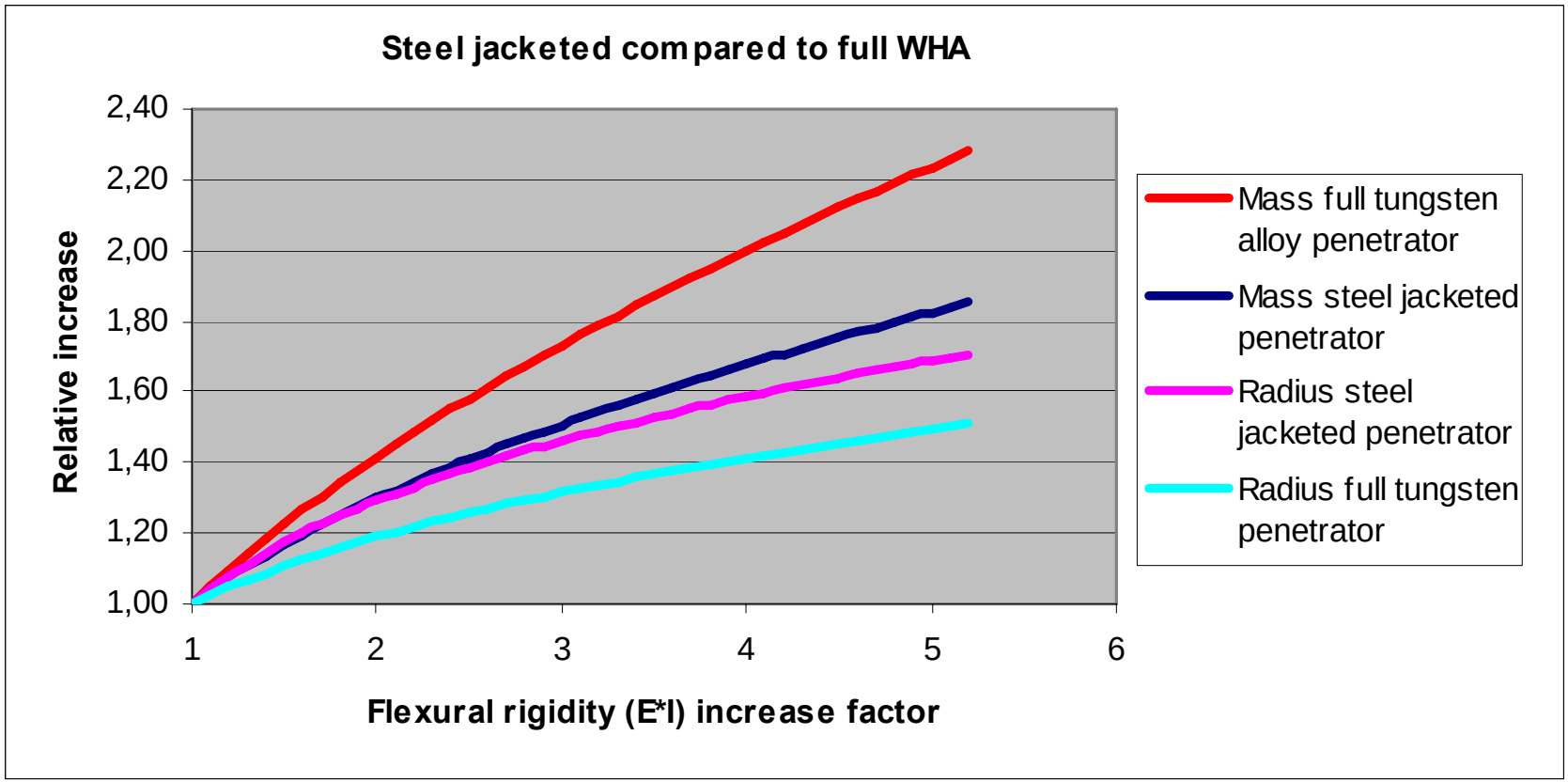
- Spaced target
- Layered target

…..both consisting of relatively thin plates

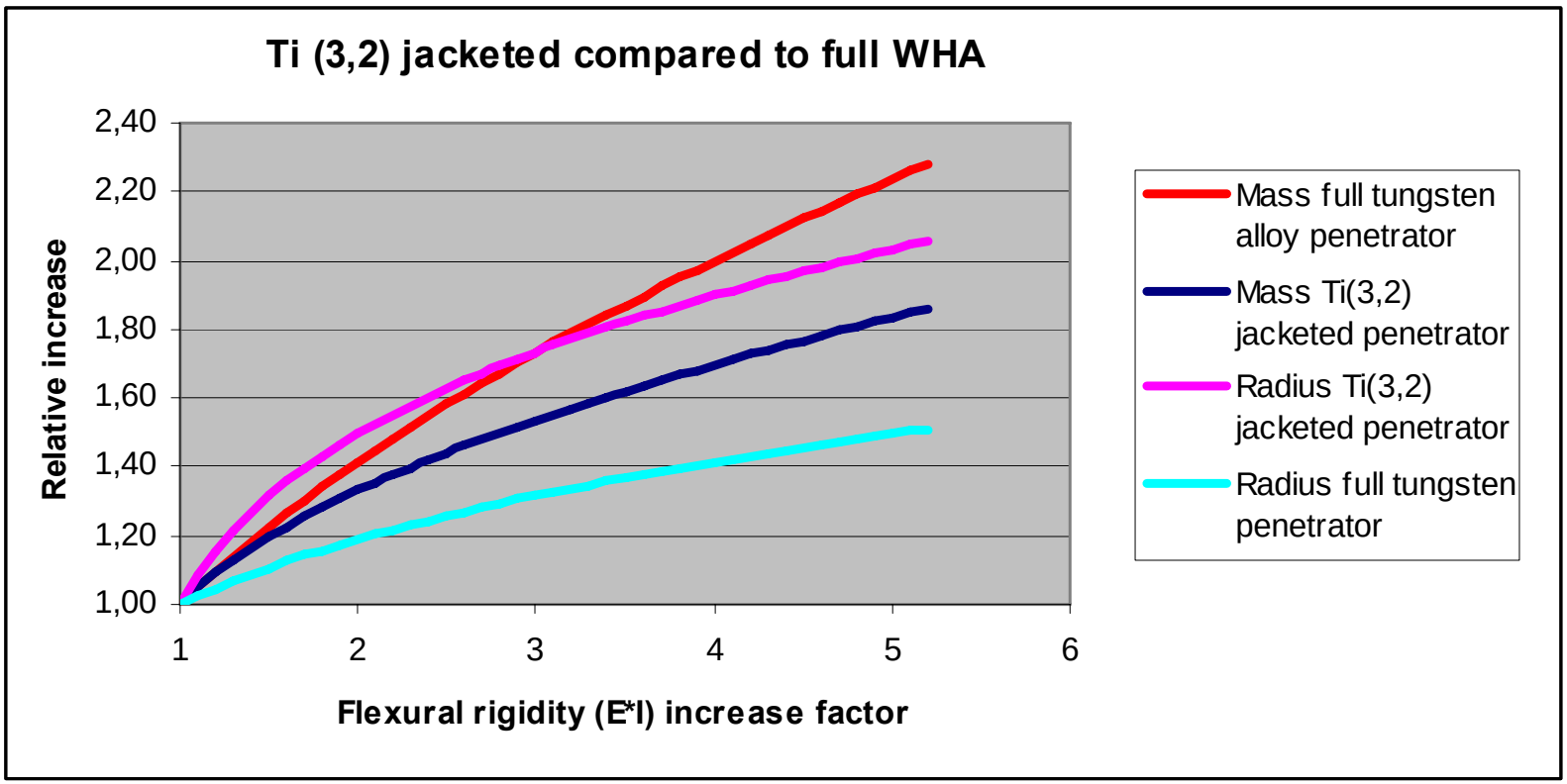
Results of published work

Type of work	D_c/D_j	V_{impact}	***Ref/year***
Computer code	> 0.9	1700 m/s	[2]/1994
Experiment	> 0.8	1800 m/s	[4]/1996
Experiment	> 0.6	2200 m/s	[3]/2001
Experiment	> 0.7	1500 m/s	[5]/2005
Experiment	0.5 – 0.8	1100 – 1300 m/s	this work

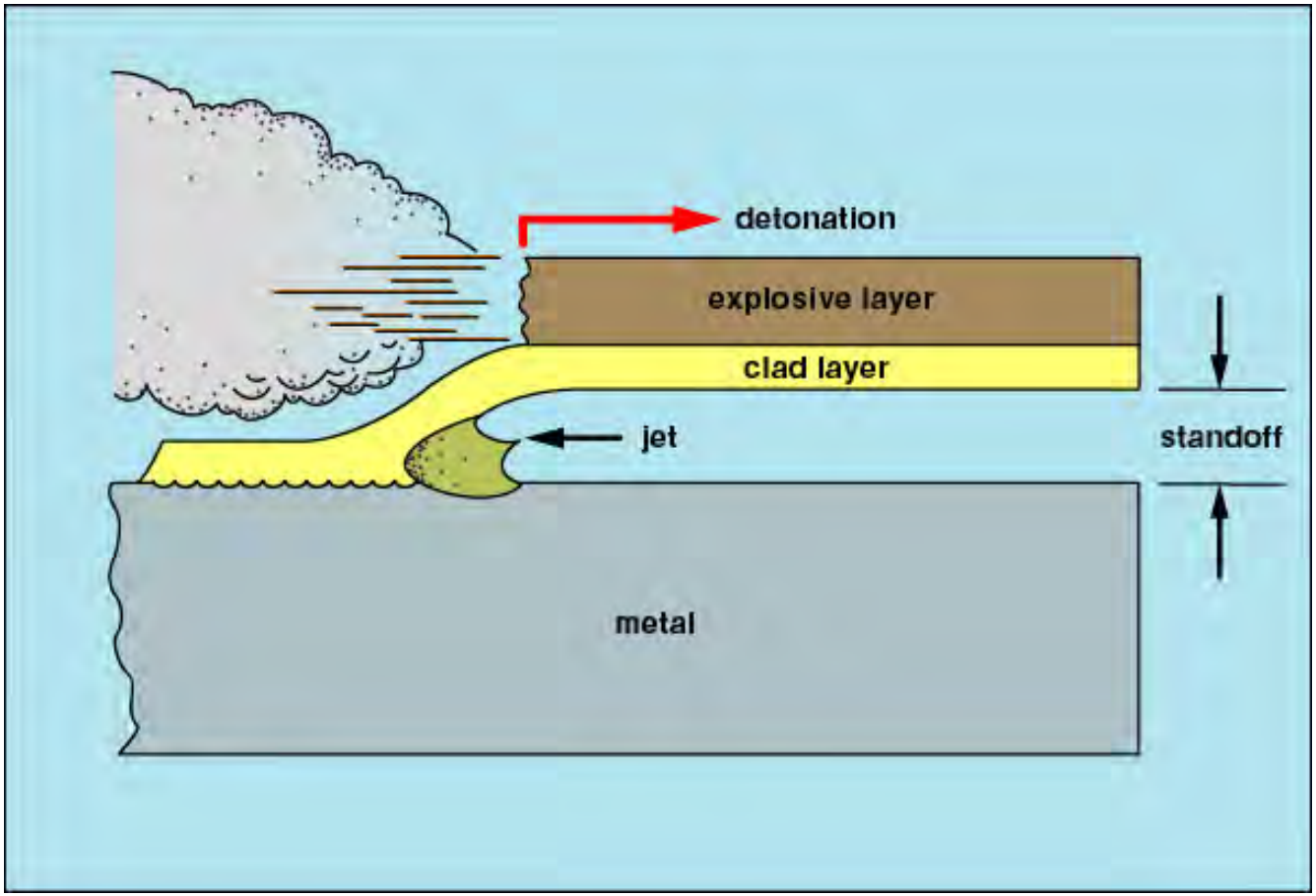
Relative mass and radius increase (1)



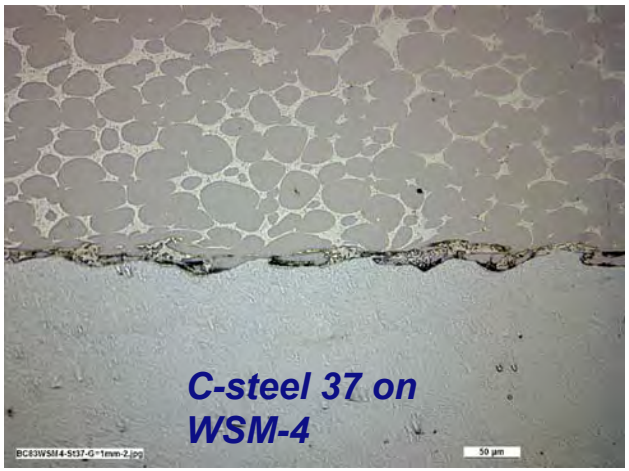
Relative mass and radius increase (2)



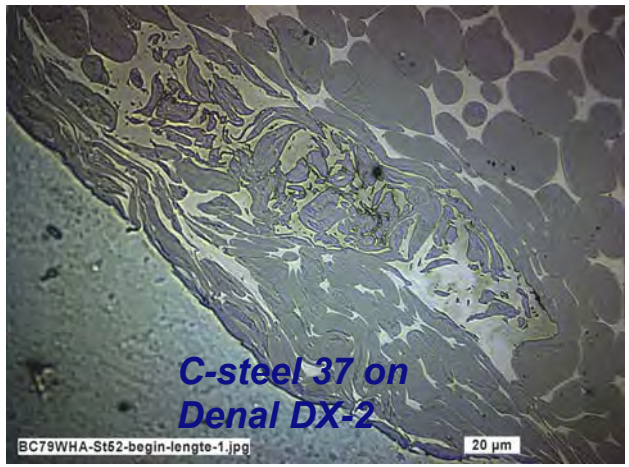
Explosive cladding



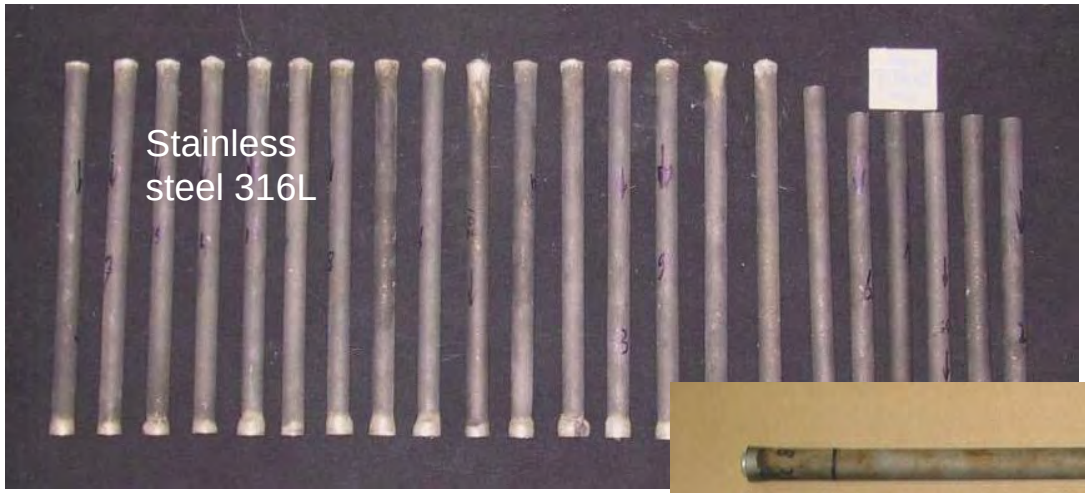
WHA – metal interface

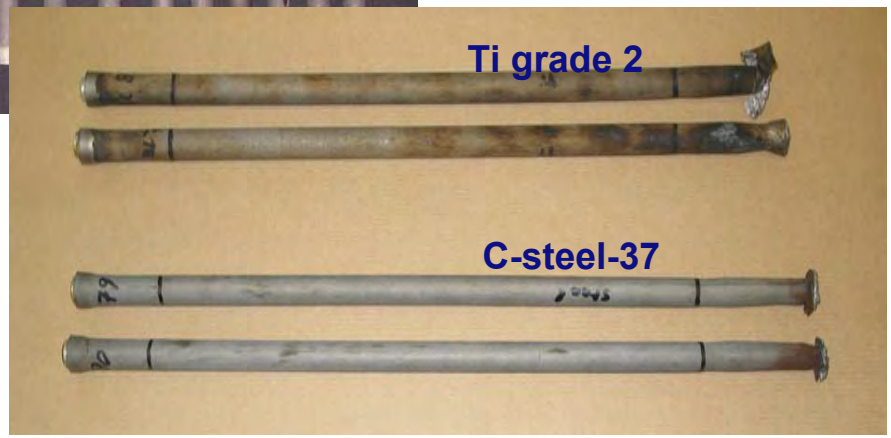






Explosively clad metals on WHA rods

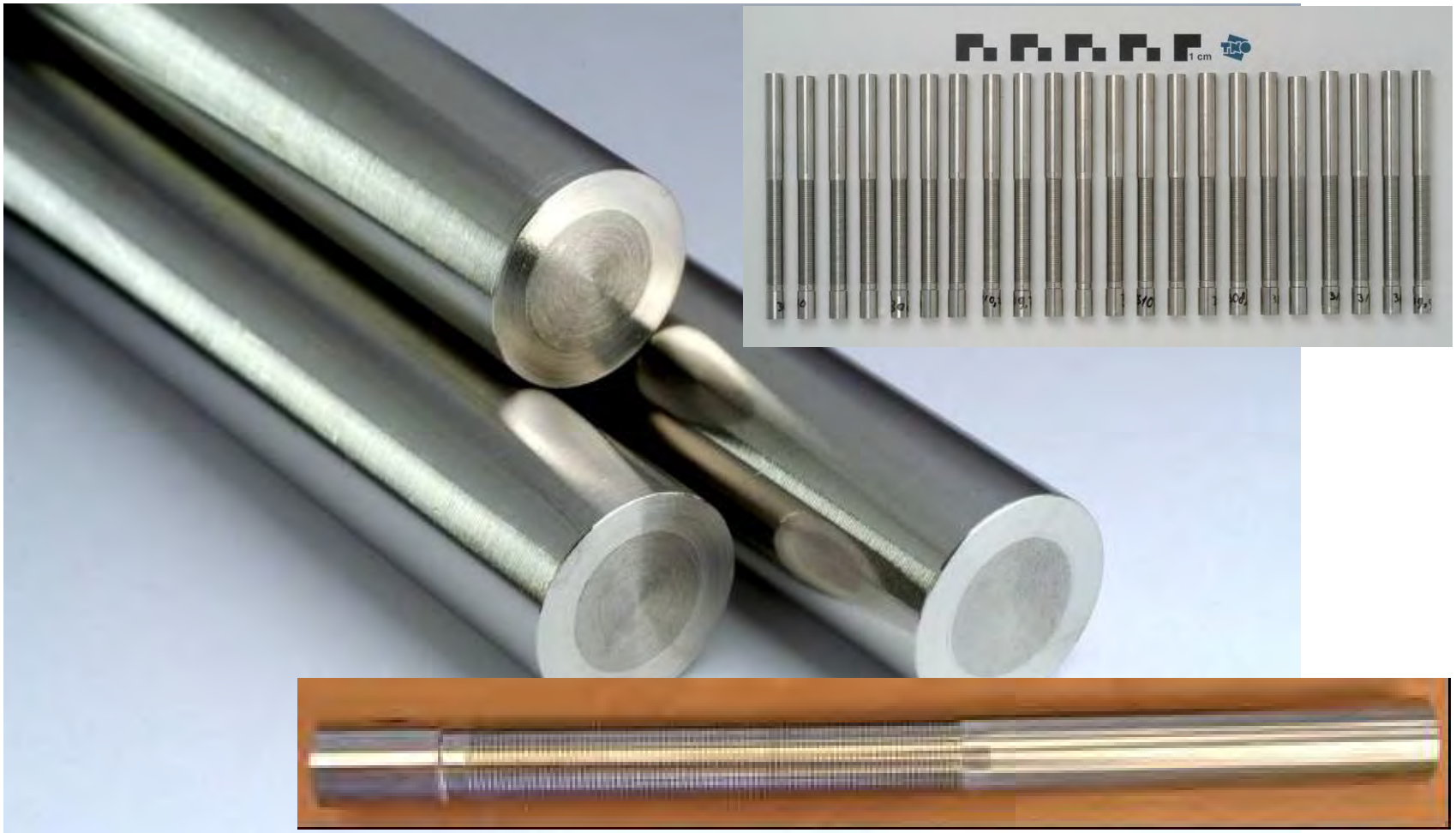




Shear strength data of jacket - core interface

Jacket material	WSM-4 rod diameter (mm)	Jacket thickness (mm)	Shear strength (MPa)
Titanium (3,2)	10	1.2	156
Titanium pure grade 2	15.2	1	159
C-steel-37	14.9	1.3	65

Stainless steel 316L clad on WSM-4 rod

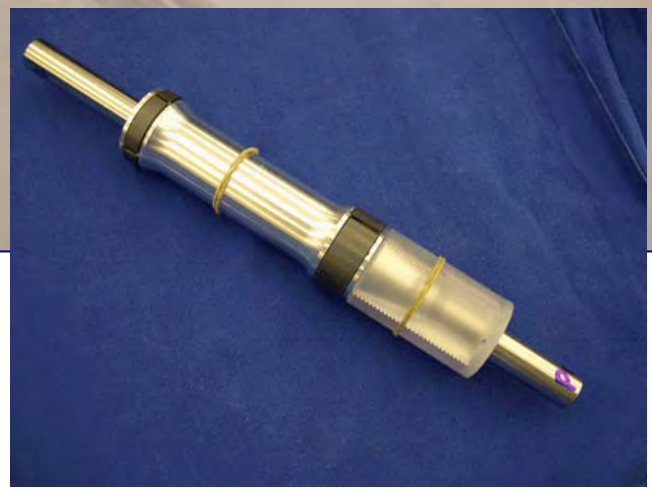


Penetrators having screw thread on the jacket instead in the jacket



Penetrators, sabot and propellant casing







Light weight sabot



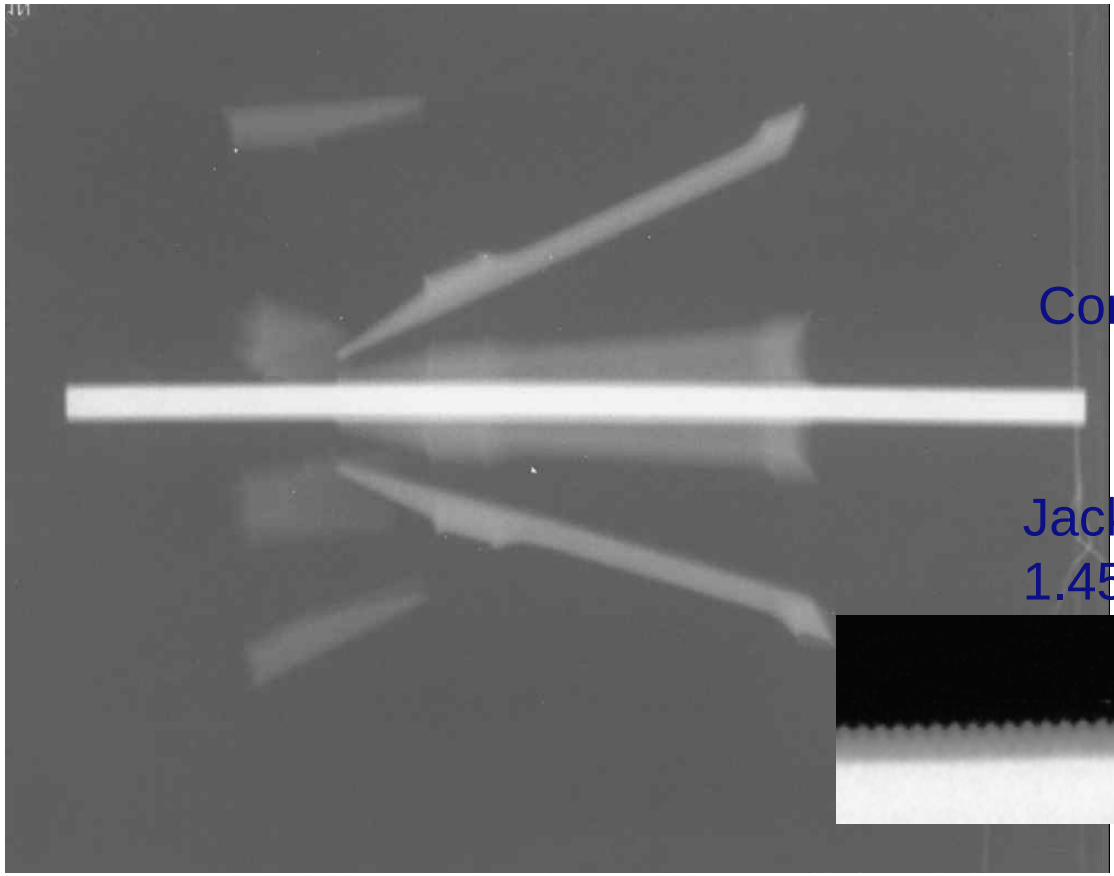
Propellant production facility: extruder



Experimental arrangement

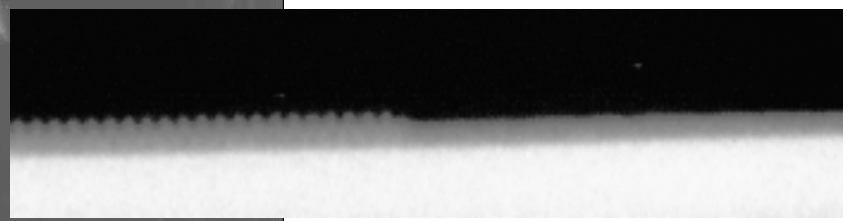


Pure Titanium (grade 2) jacketed penetrator prior to impact (thin jackets)

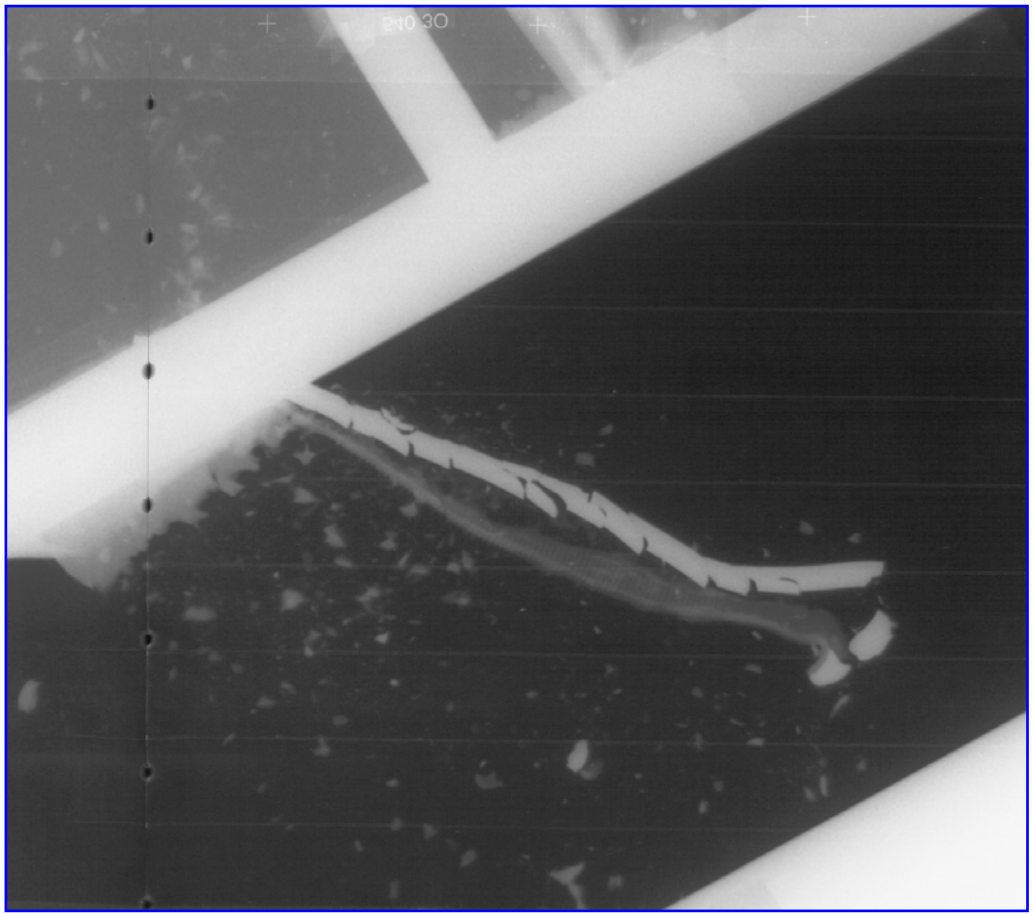


Core diameter: 6.3 mm

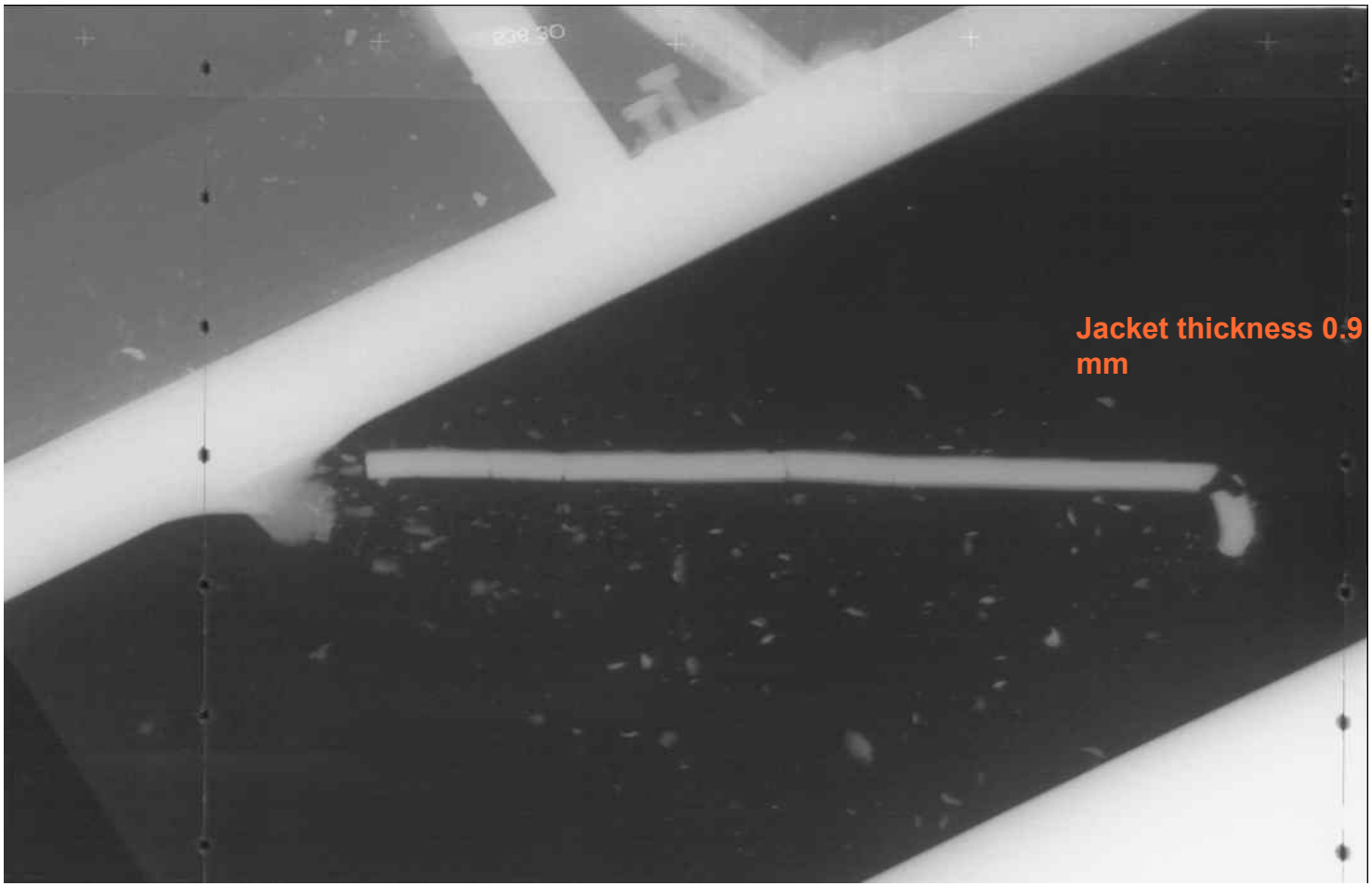
Jacket thickness
1.45 mm



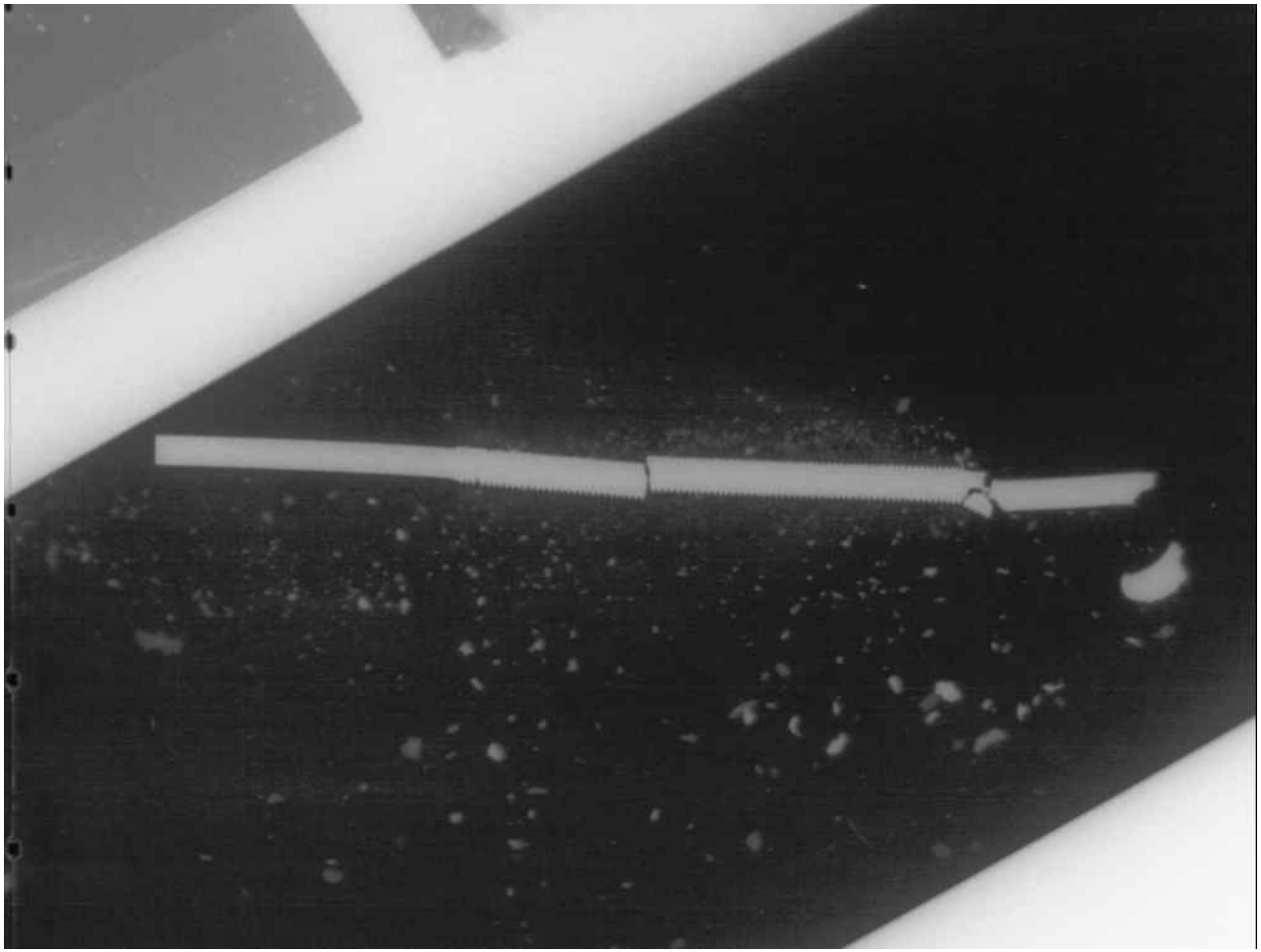
Pure Titanium (grade 2) jacketed penetrator (Denal DX2) after impact of layered steel/rubber/steel target



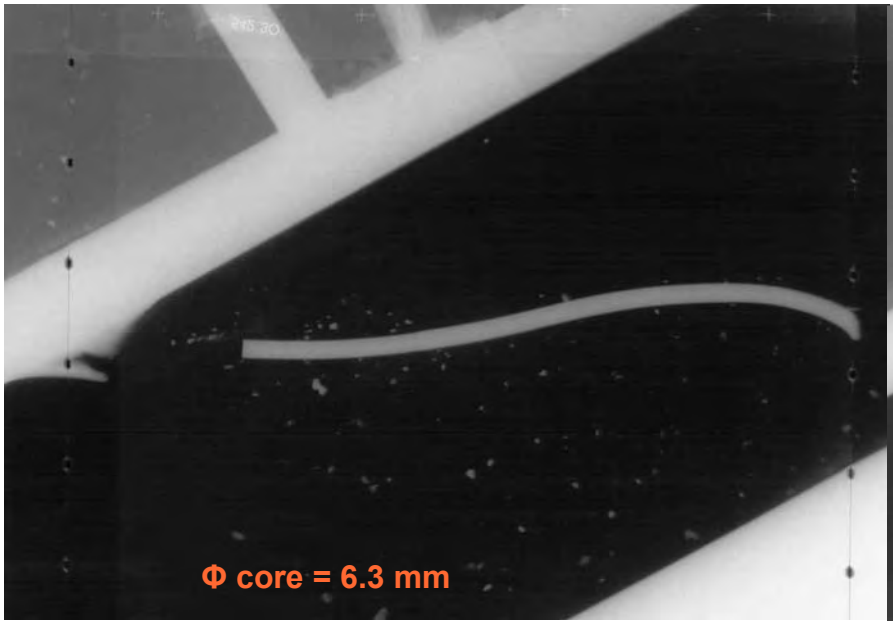
C-steel-37 jacketed penetrator (core: Denal DX 2)

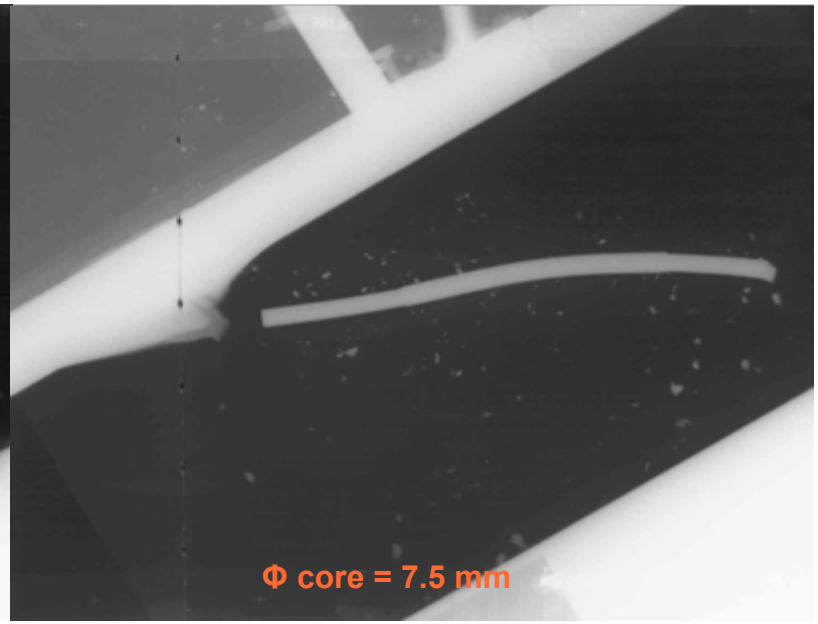


Denal DX 2 penetrator without a jacket

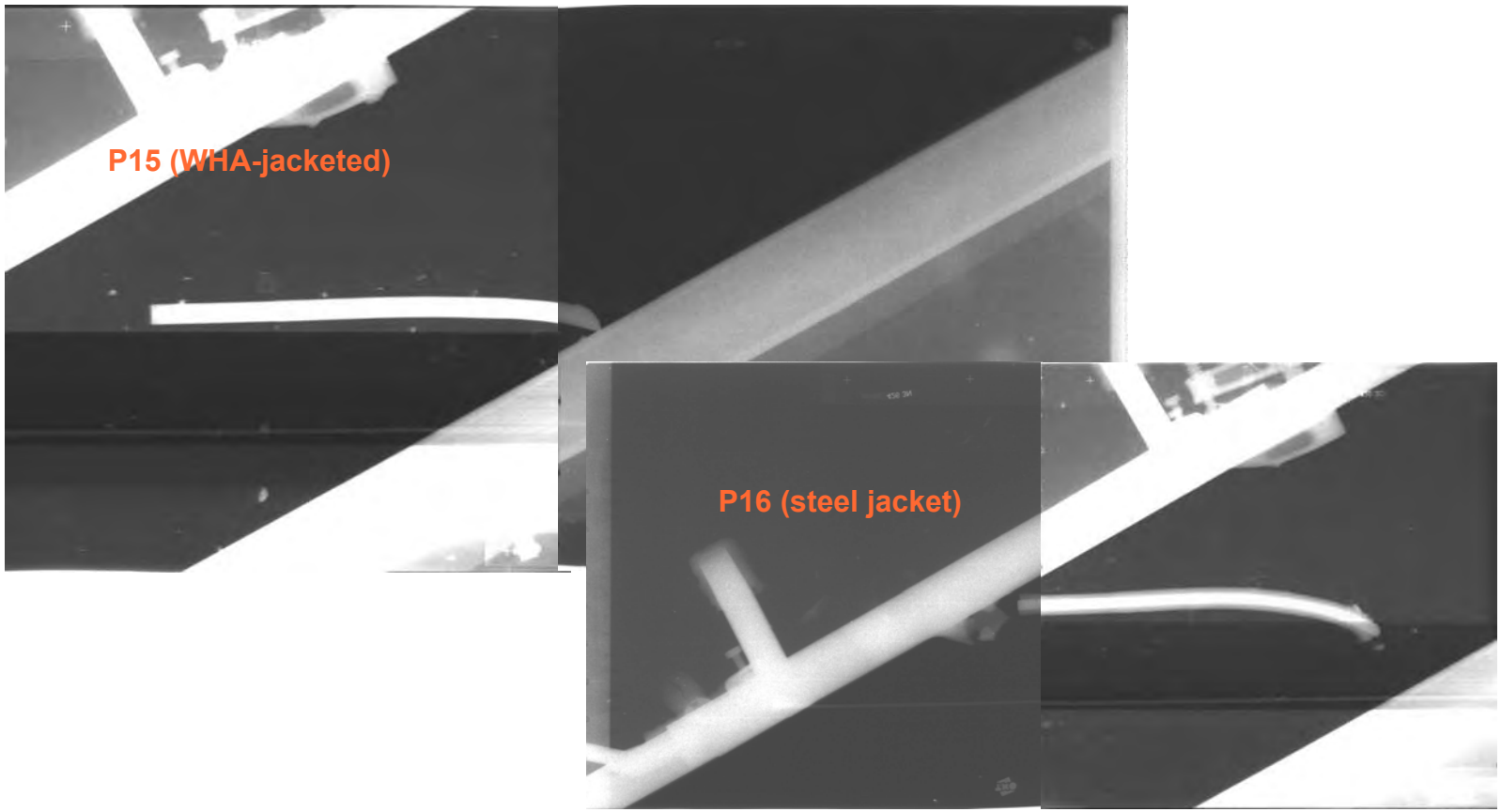


WSM-4 and WSM-4 “jacket”





Thick jackets: WHA “jackets” compared to steel jacketed (core: WSM-4)



DOP reduction

Penetrator	Jacket material	DOP (mm)
423/P15 $\mu = 0.64$	WHA	118
425/P16P $\mu = 0.5$	Steel-37	68

Steel jacketed penetrator



Penetration of stainless steel jacketed penetrator into RHA



Conclusions:

- Jackets can be clad on WHA rods and withstand acceleration forces for muzzle velocities up 1300 m/s (and very likely higher)
- At moderate velocities 1100 -1300 m/s:
  - Jackets can be of advantage:
    - against thin layered targets
    - in case projectile mass is a limiting factor for a firing system;
- Thicker jackets ($\mu \approx 0.5$) jackets reduce “DOP” in semi-infinite RHA-target
- At higher impact velocities, thicker jackets may give advantages as well

PDF Complete
Your complimentary use period has ended. Thank you for using PDF Complete.
Click Here to upgrade to Unlimited Pages and Expanded Features

Symposium on Ballistics
ber 22-26, 2008

Numerical Simulation of Muzzle Exit and Separation Process for Sabot-Guided Projectiles in Supersonic Flight

Dr.-Ing. Jörn van Keuk, Dr.-Ing. Arno Klomfass

Fraunhofer Institut Kurzzeitdynamik Ernst-Mach-Institut

PDF Complete
Your complimentary use period has ended. Thank you for using PDF Complete.
Click Here to upgrade to Unlimited Pages and Expanded Features

- **Introduction / Motivation**
- **Physical Aspects of the Firing Process**
- **Strategies for the Numerical Simulation / Proposed Procedure for the Study**
- **Results for Sabot Separation Simulations**
- **Conclusions / Future Work**

© 2008 Fraunhofer EMI

PDF Complete
Your complimentary use period has ended. Thank you for using PDF Complete.
Click Here to upgrade to Unlimited Pages and Expanded Features

Numerical Investigation of Sabot Separation Processes

Sabot Separation: Coupled Problem of Aerodynamics and Structure Dynamics

Sabot Function:

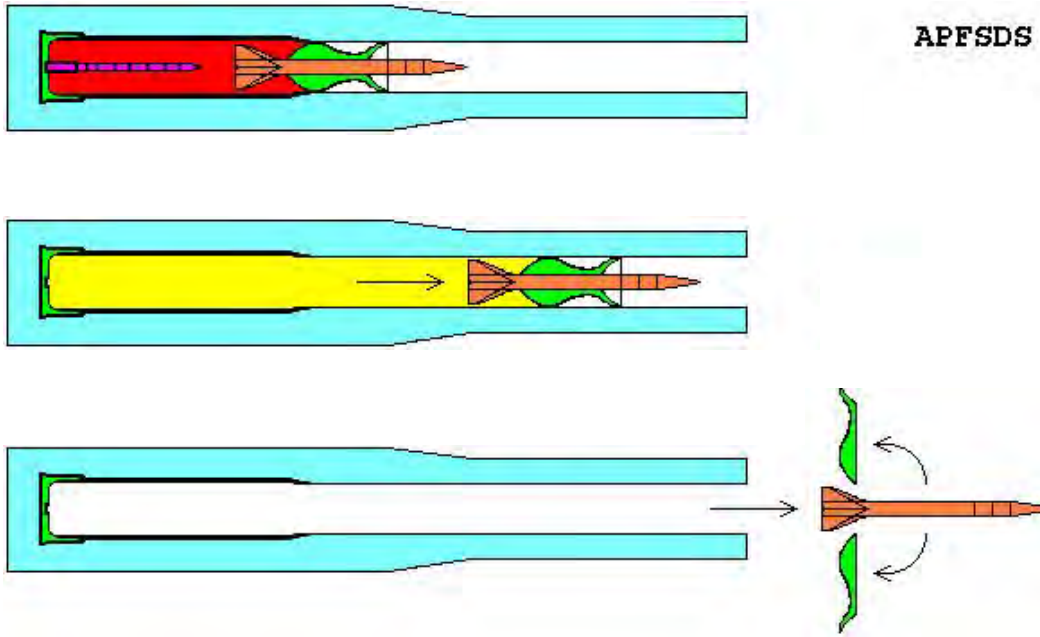
- Guidance of Sub-Caliber Munition

Design Tasks:

- Stability Against Mechanical Loading
- Undisturbed Separation Process
- **Minimum Weight**

Challenges for the Numerical Simulation:

- Highly Unsteady Problem
- Relatively Moving Bodies
- Material Failure Modelling

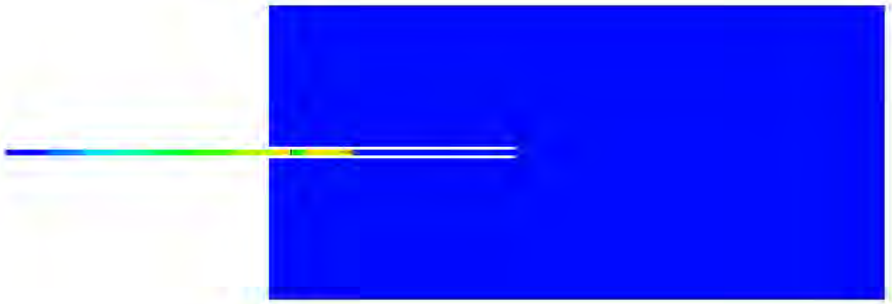


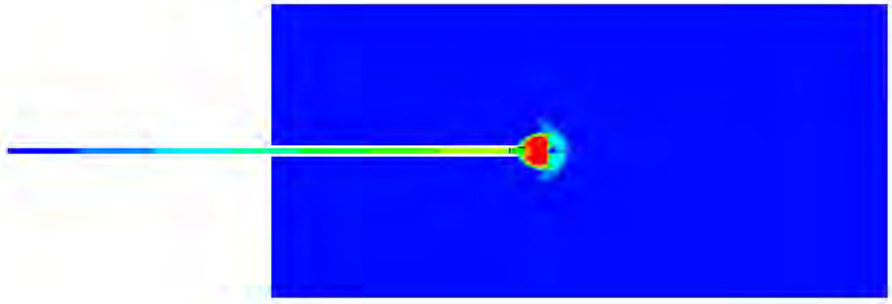
© 2008 Fraunhofer EMI

PDF Complete
Your complimentary use period has ended. Thank you for using PDF Complete.
Click Here to upgrade to Unlimited Pages and Expanded Features

of the Firing Process

ndrical ÆProjectileñ(Autodyn)





Phase 1: Interior Ballistics

- $t_0 < t < t_1$
- Compressed Air Ahead of Projectile
- Interaction: Projectile-Gas-Barrel
- **Not Subject of the Presentation**

Phase 2: Muzzle Exit Ballistics

- $t_1 < t < t_2$
- Front of Projectile Outside the Muzzle
- Risk of Canting / Fracture

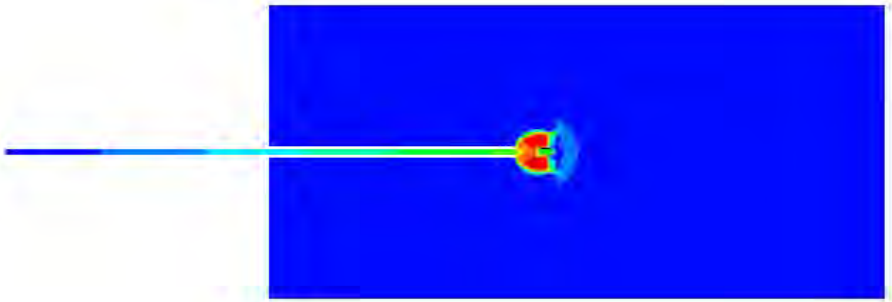
movie1.avi

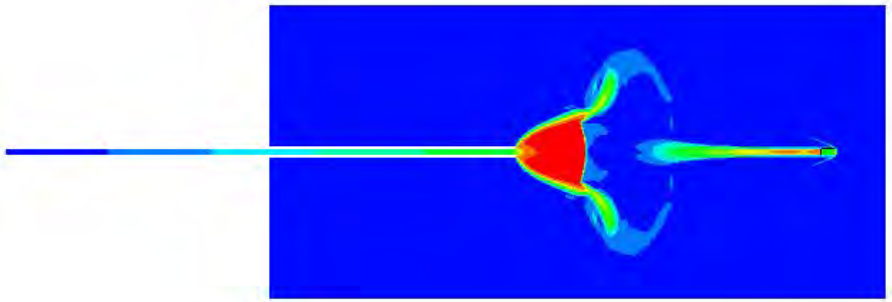
© 2008 Fraunhofer EMI

PDF Complete
Your complimentary use period has ended. Thank you for using PDF Complete.
Click Here to upgrade to Unlimited Pages and Expanded Features

of the Firing Process

ndrical ÆProjectileñ(Autodyn)





Phase 3: Muzzle Exit Ballistics

- $t_2 < t < t_3$
- Projectile Completely Outside the Muzzle
- Significant Incident Flow from Behind

Phase 4: Exterior Ballistics

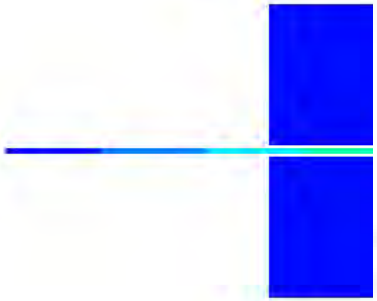
- $t_3 < t < t_4$
- No Interaction with Propellant Gas / Barrel
- Flight Through Undisturbed Atmosphere

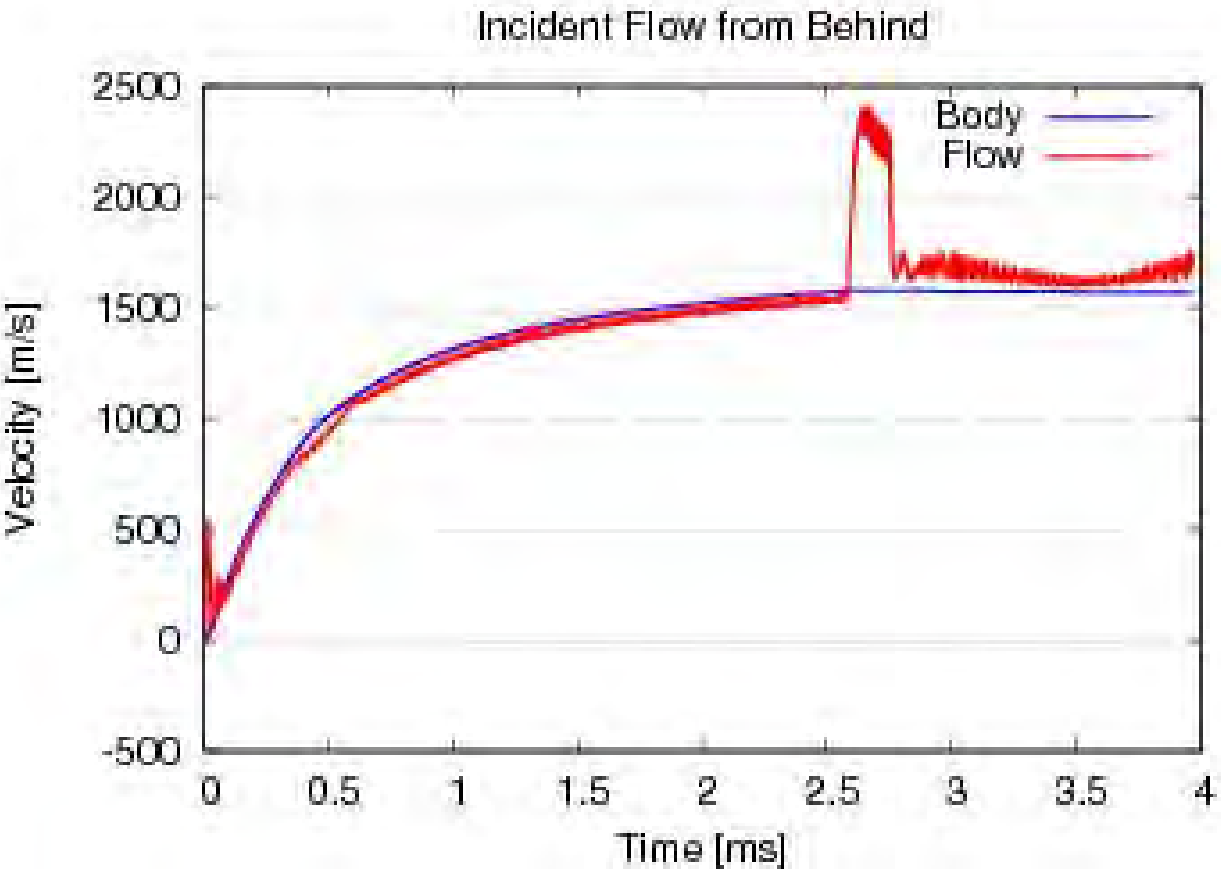
© 2008 Fraunhofer EMI

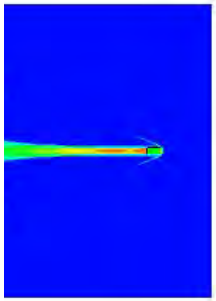
PDF Complete
Your complimentary use period has ended. Thank you for using PDF Complete.
Click Here to upgrade to Unlimited Pages and Expanded Features

of the Firing Process

ndrical ÆProjectileñ(Autodyn)





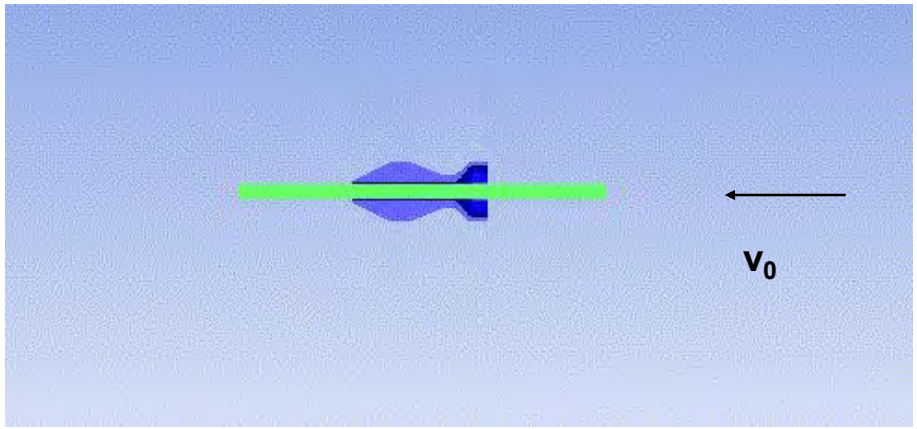


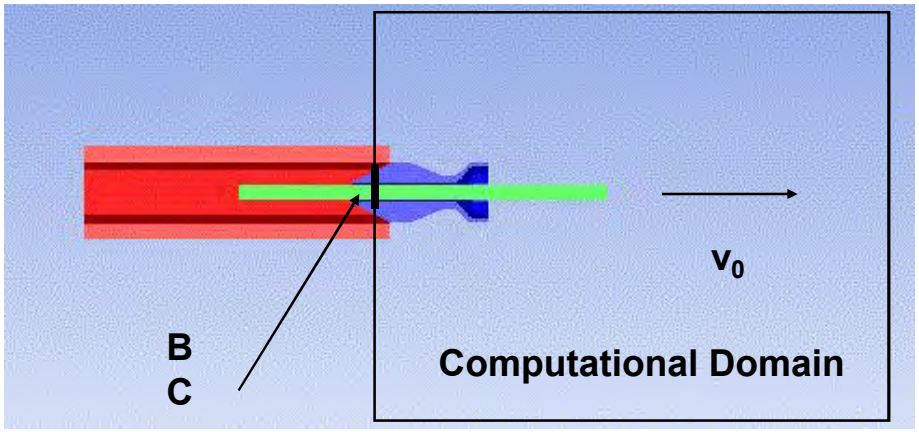
Phase 3: Muzz **ics**

- $t_2 < t < t_3$
- Projectile Comp ellant
- Significant Incic ed Atmosphere

PDF Complete
Your complimentary use period has ended. Thank you for using PDF Complete.
Click Here to upgrade to Unlimited Pages and Expanded Features

Numerical Simulation





Concept A

- Moving Observer
- Instantaneous Inflow

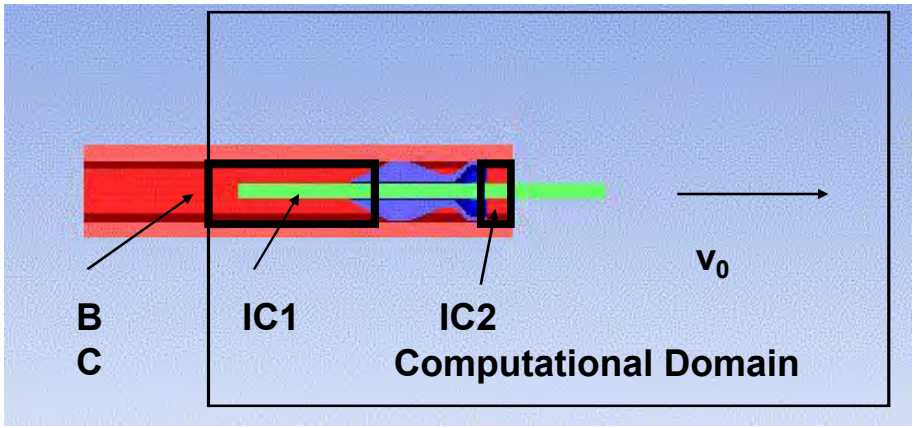
Concept B

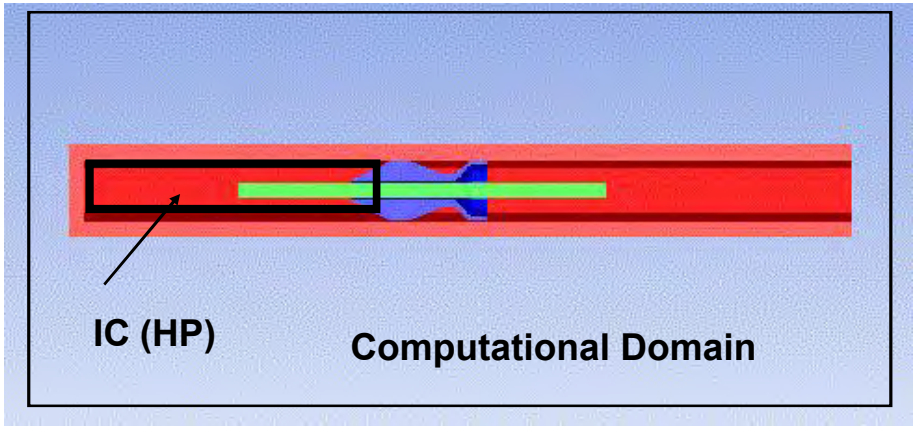
- Earth-Fixed Observer
- Boundary Condition at Muzzle Exit

© 2008 Fraunhofer EMI

PDF Complete
Your complimentary use period has ended. Thank you for using PDF Complete.
Click Here to upgrade to Unlimited Pages and Expanded Features

Numerical Simulation





Concept C

- Earth-Fixed Observer
- Initial and Boundary Conditions Inside the Barrel

Concept D

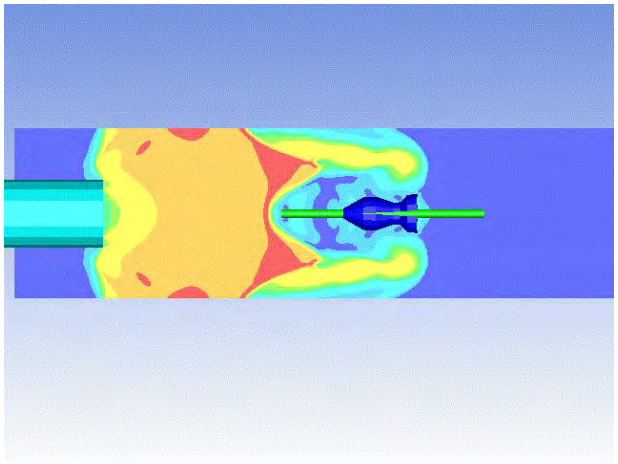
- Earth-Fixed Observer
- Initial Condition Inside the Barrel (**H**igh **P**ressure)
- **Estimation of Required Gridpoints**

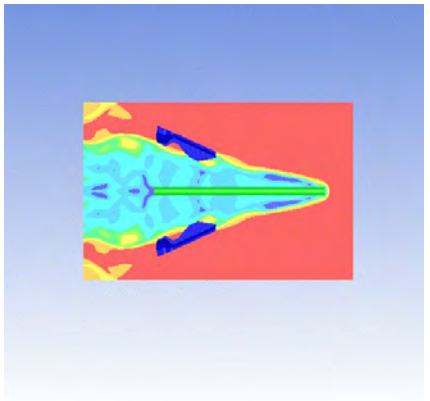
  ~ 90.000.000 → Very Expensive

© 2008 Fraunhofer EMI

PDF Complete
Your complimentary use period has ended. Thank you for using PDF Complete.
Click Here to upgrade to Unlimited Pages and Expanded Features

...ure for the Study
(...pts A und C)





Phase 1:

Earth-Fixed Observer (Concept C)

Phase 2:

Moving Observer (Concept A)

Switch of Coordinate System!

Point of Time: t = t_3

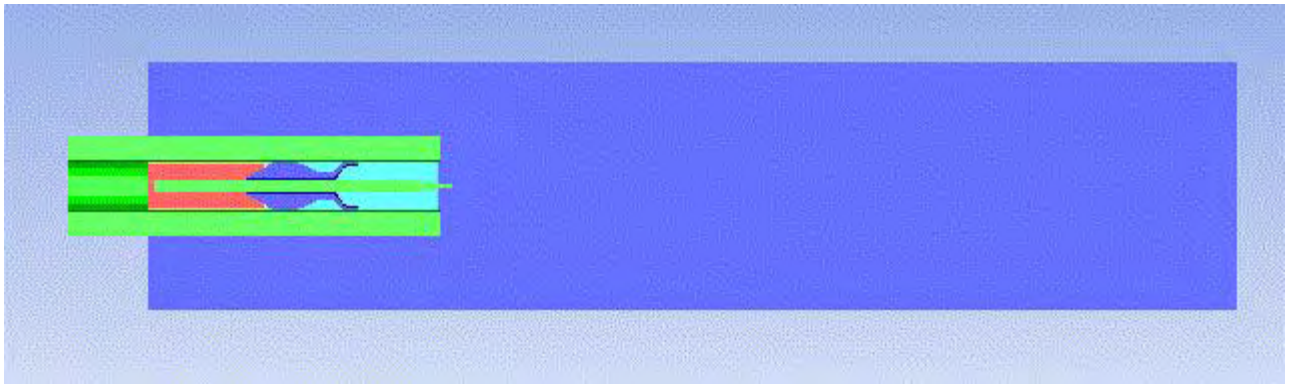
© 2008 Fraunhofer EMI

PDF Complete
Your complimentary use period has ended. Thank you for using PDF Complete.
Click Here to upgrade to Unlimited Pages and Expanded Features

Separation Simulations

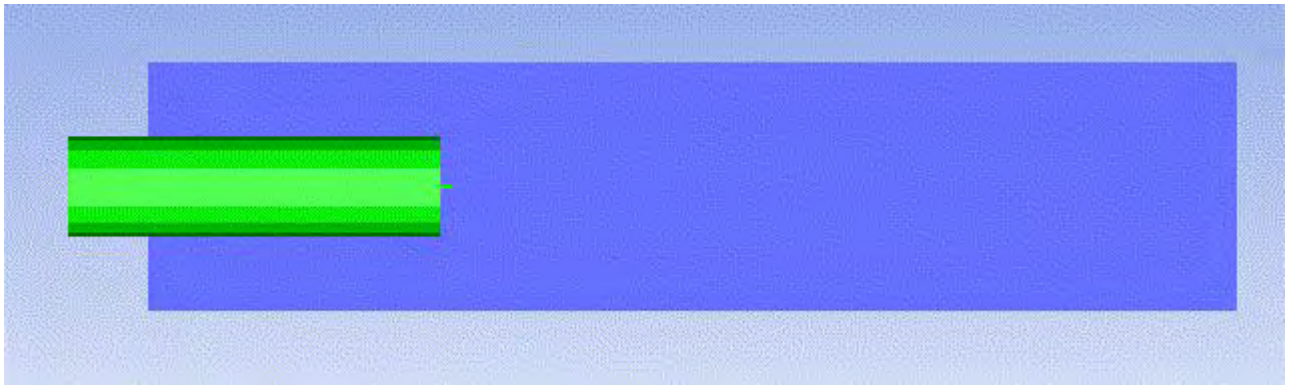
ordinate Switch (Sim. EMI, **Concept C+A**)

Discretization: Air (1.000.000 Points), Sabot (3.900 Points)



Pressure

t = 0.00 ms



Abs. Velocity

© 2008 Fraunhofer EMI

PDF Complete
Your complimentary use period has ended. Thank you for using PDF Complete.
Click Here to upgrade to Unlimited Pages and Expanded Features

Separation Simulations

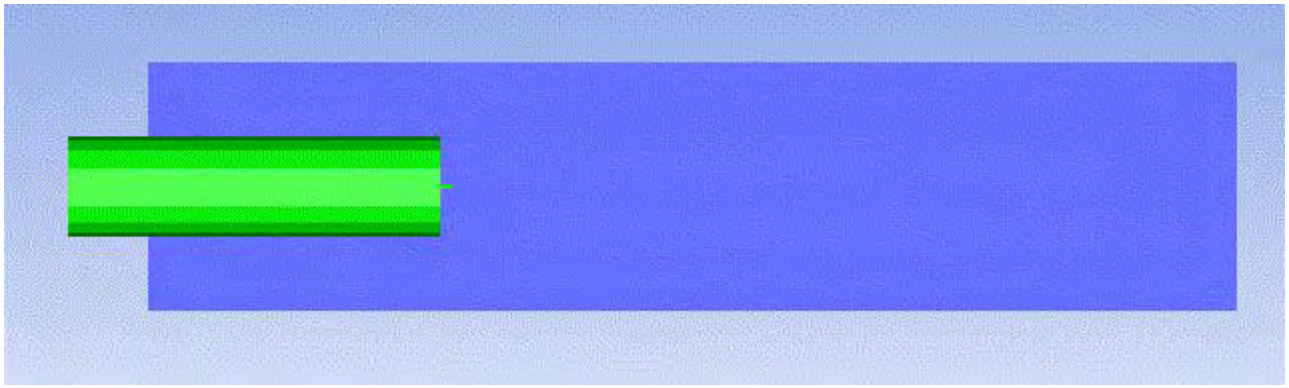
ordinate Switch (Sim. EMI, **Concept C+A**)

Discretization: Air (1.000.000 Points), Sabot (3.900 Points)



Pressure

t = 0.00 ms



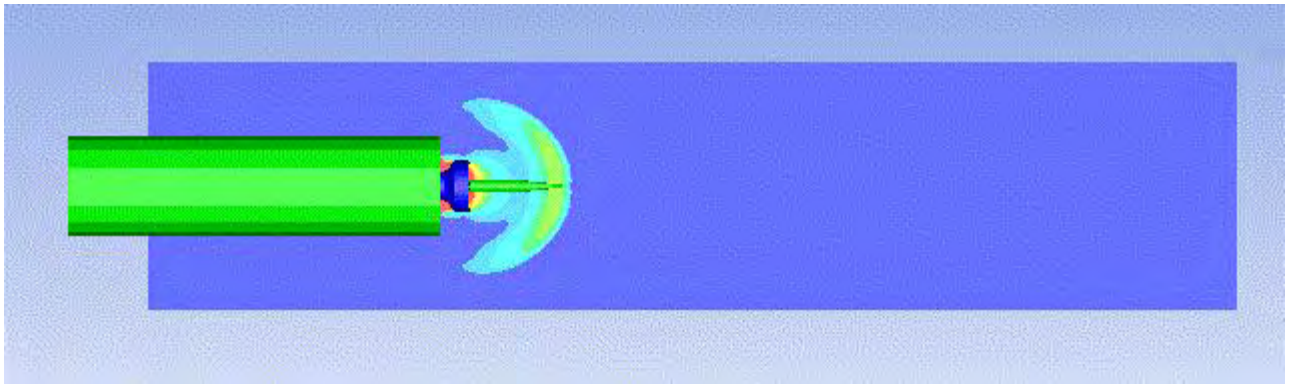
Abs. Velocity

© 2008 Fraunhofer EMI

PDF Complete
Your complimentary use period has ended. Thank you for using PDF Complete.
Click Here to upgrade to Unlimited Pages and Expanded Features

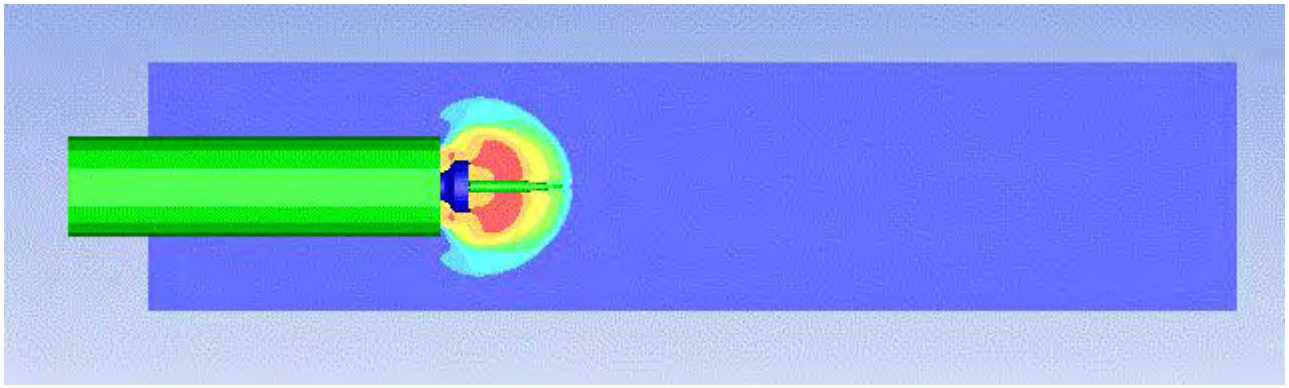
Separation Simulations

ordinate Switch (Sim. EMI, **Concept C+A**)



Pressure

t = 0.06 ms



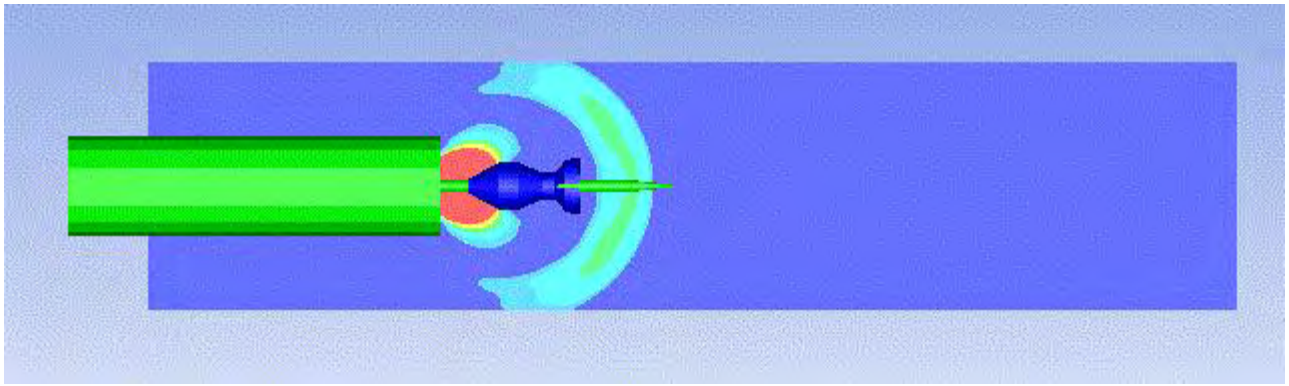
Abs. Velocity

© 2008 Fraunhofer EMI

PDF Complete
Your complimentary use period has ended. Thank you for using PDF Complete.
Click Here to upgrade to Unlimited Pages and Expanded Features

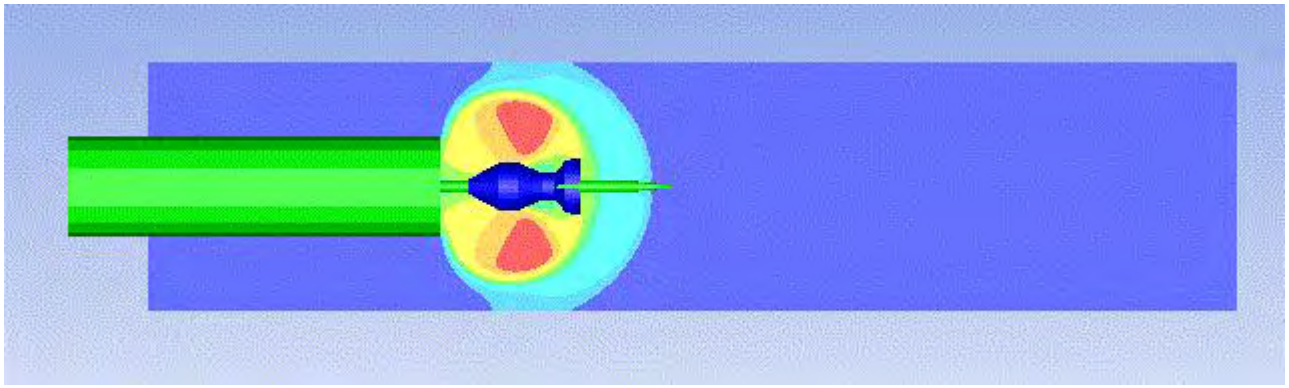
Separation Simulations

ordinate Switch (Sim. EMI, **Concept C+A**)



Pressure

t = 0.12 ms



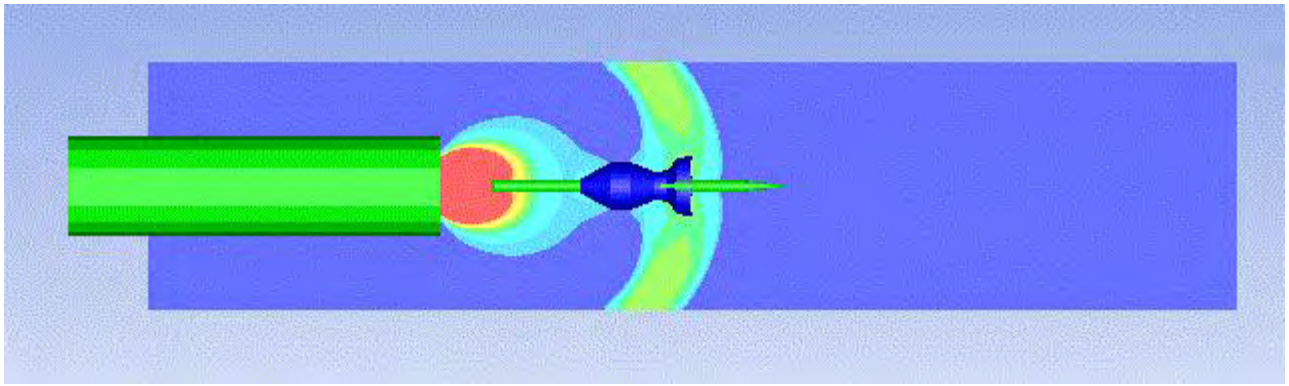
Abs. Velocity

© 2008 Fraunhofer EMI

PDF Complete
Your complimentary use period has ended. Thank you for using PDF Complete.
Click Here to upgrade to Unlimited Pages and Expanded Features

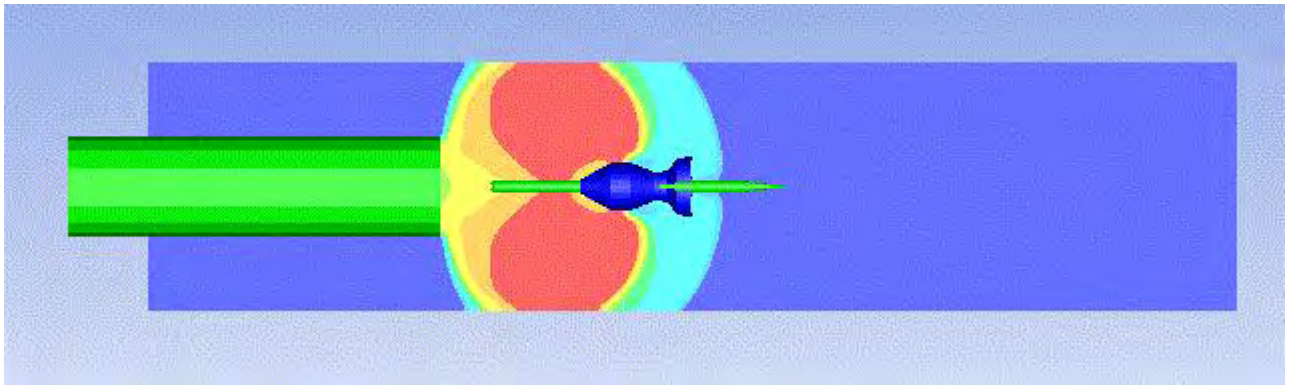
Separation Simulations

ordinate Switch (Sim. EMI, **Concept C+A**)



Pressure

t = 0.18 ms



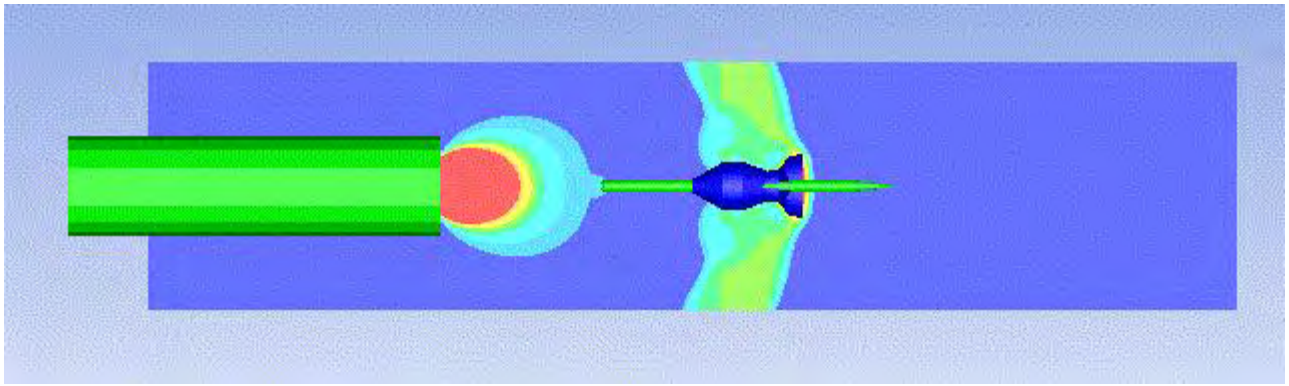
Abs. Velocity

© 2008 Fraunhofer EMI

PDF Complete
Your complimentary use period has ended. Thank you for using PDF Complete.
Click Here to upgrade to Unlimited Pages and Expanded Features

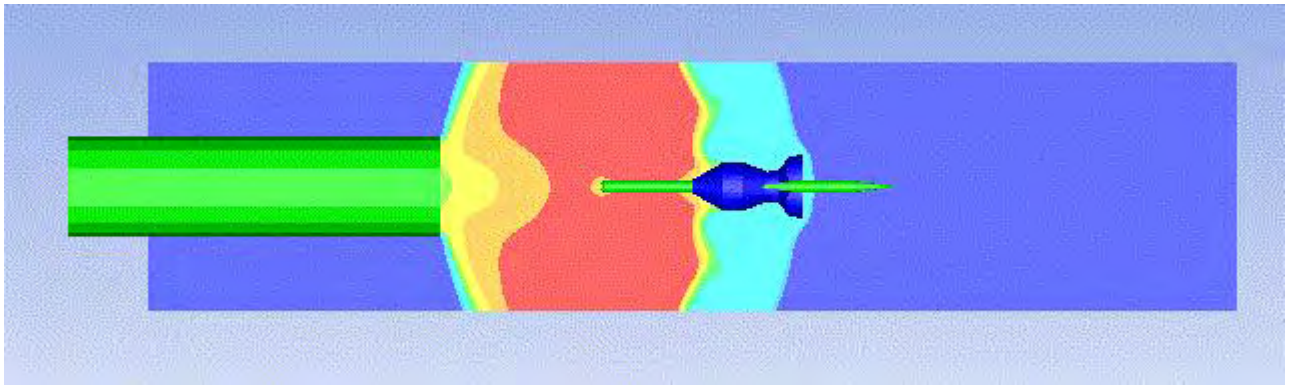
Separation Simulations

ordinate Switch (Sim. EMI, **Concept C+A**)



Pressure

t = 0.23 ms



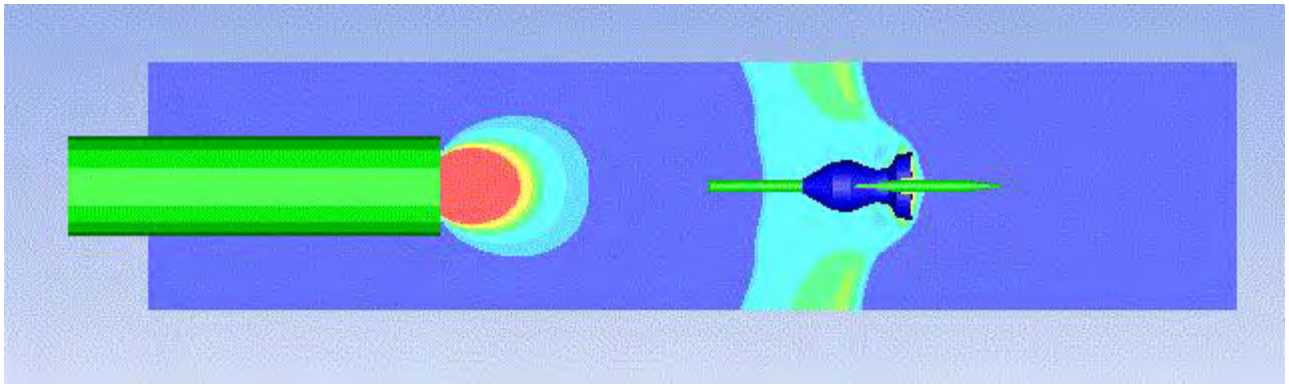
Abs. Velocity

© 2008 Fraunhofer EMI

PDF Complete
Your complimentary use period has ended. Thank you for using PDF Complete.
Click Here to upgrade to Unlimited Pages and Expanded Features

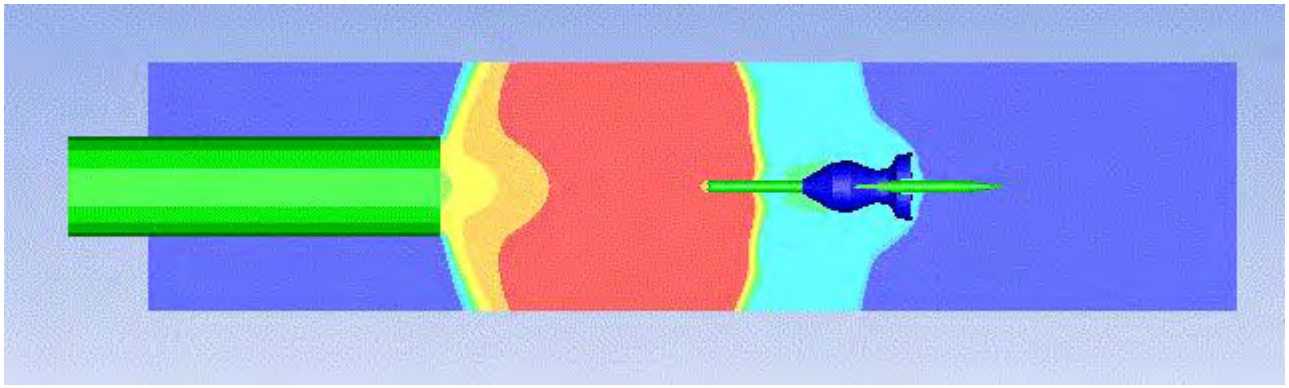
Separation Simulations

ordinate Switch (Sim. EMI, **Concept C+A**)



Pressure

t = 0.29 ms



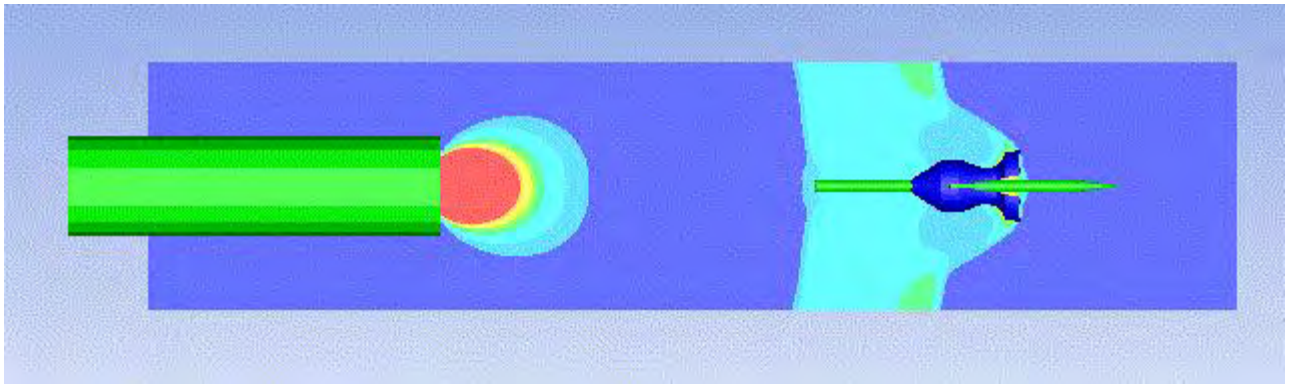
Abs. Velocity

© 2008 Fraunhofer EMI

PDF Complete
Your complimentary use period has ended. Thank you for using PDF Complete.
Click Here to upgrade to Unlimited Pages and Expanded Features

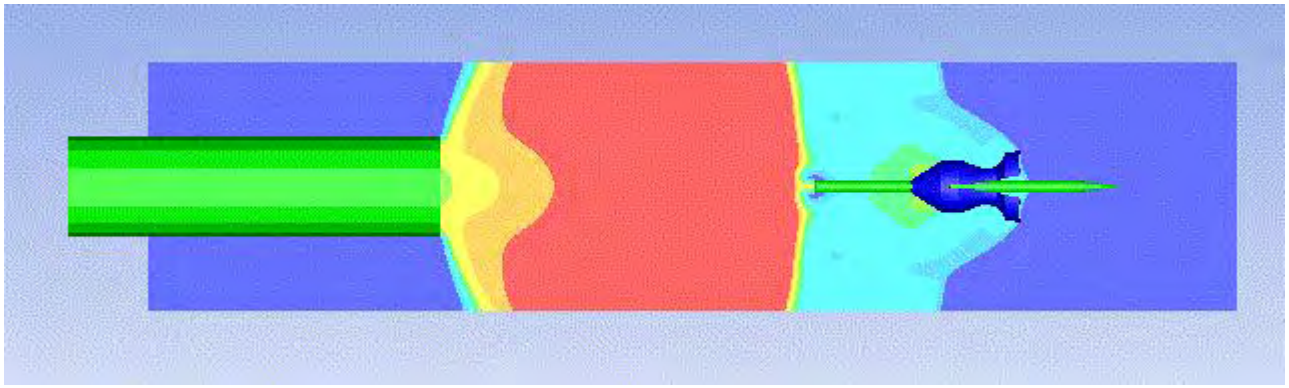
Separation Simulations

ordinate Switch (Sim. EMI, **Concept C+A**)



Pressure

t = 0.35 ms



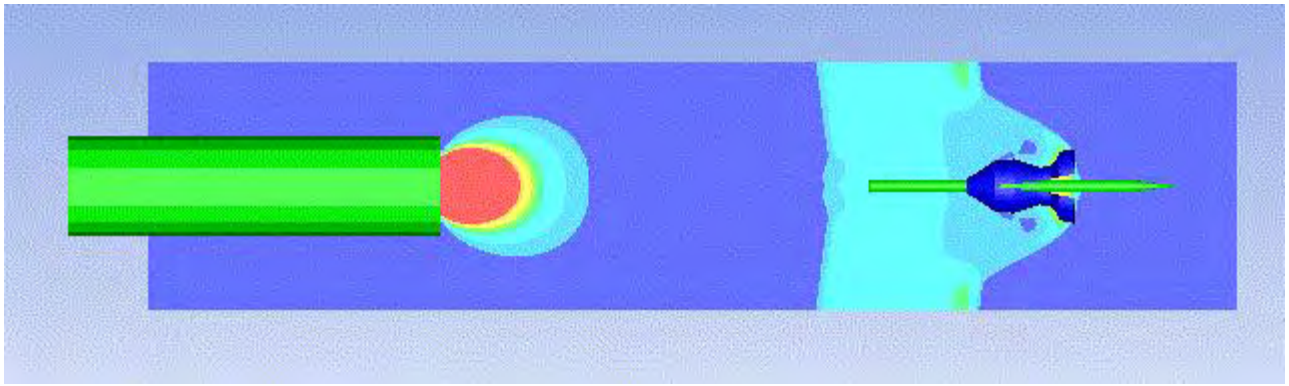
Abs. Velocity

© 2008 Fraunhofer EMI

PDF Complete
Your complimentary use period has ended. Thank you for using PDF Complete.
Click Here to upgrade to Unlimited Pages and Expanded Features

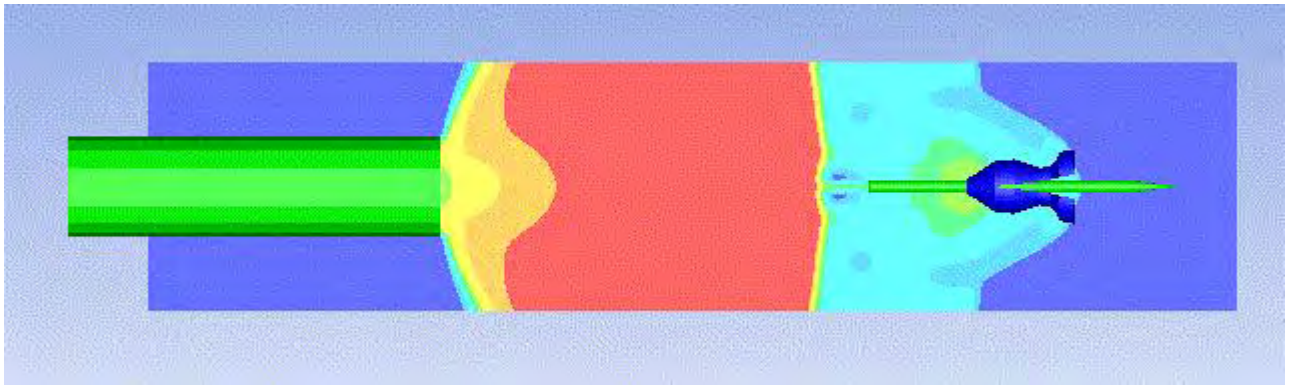
Separation Simulations

ordinate Switch (Sim. EMI, **Concept C+A**)



Pressure

t = 0.38 ms



Abs. Velocity

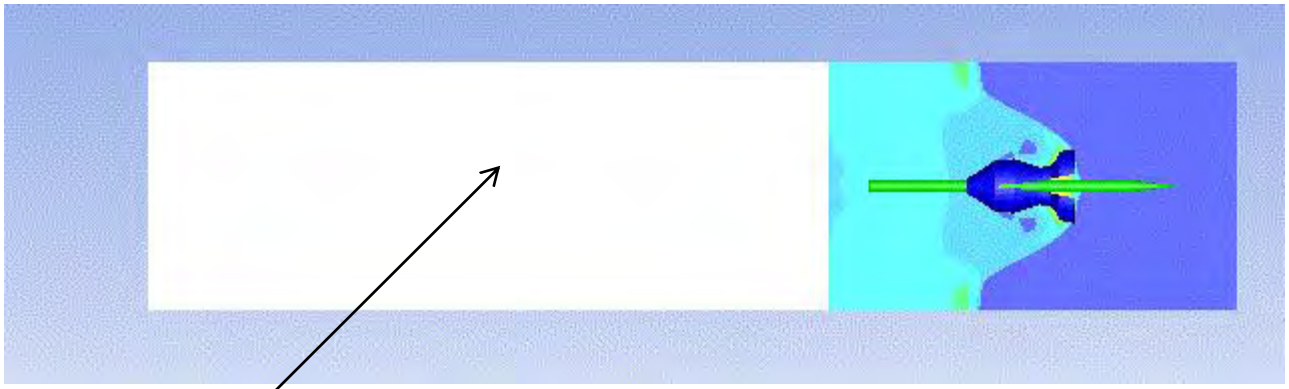
© 2008 Fraunhofer EMI

PDF Complete
Your complimentary use period has ended. Thank you for using PDF Complete.
Click Here to upgrade to Unlimited Pages and Expanded Features

Separation Simulations

ordinate Switch (Sim. EMI, **Concept C+A**)

SWITCH



Pressure

UNUSED

t = 0.38 ms



Abs. Velocity

© 2008 Fraunhofer EMI

PDF Complete
Your complimentary use period has ended. Thank you for using PDF Complete.
Click Here to upgrade to Unlimited Pages and Expanded Features

Separation Simulations

ordinate Switch (Sim. EMI, **Concept C+A**)



Pressure

t = 0.71 ms



Abs. Velocity

© 2008 Fraunhofer EMI

PDF Complete
Your complimentary use period has ended. Thank you for using PDF Complete.
Click Here to upgrade to Unlimited Pages and Expanded Features

Separation Simulations

ordinate Switch (Sim. EMI, **Concept C+A**)



Pressure

t = 1.05 ms



Abs. Velocity

© 2008 Fraunhofer EMI

PDF Complete
Your complimentary use period has ended. Thank you for using PDF Complete.
Click Here to upgrade to Unlimited Pages and Expanded Features

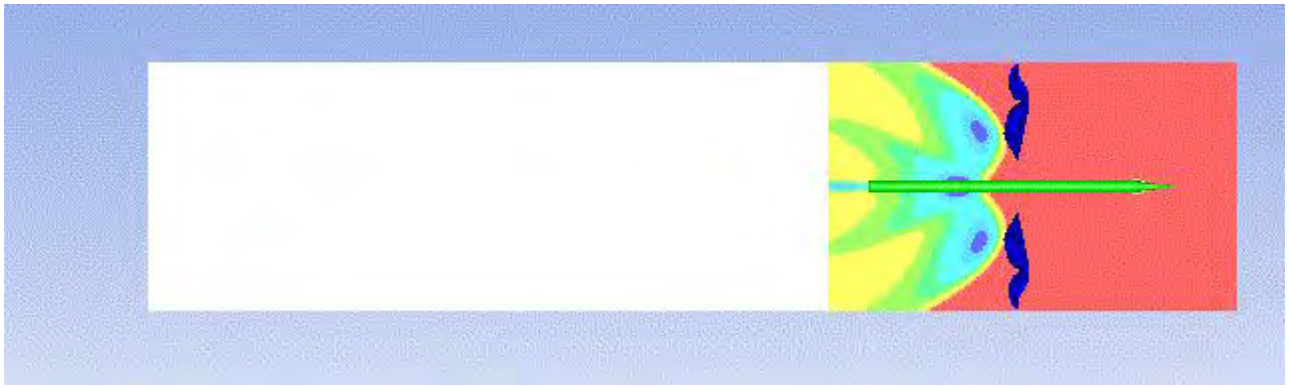
Separation Simulations

ordinate Switch (Sim. EMI, **Concept C+A**)



Pressure

t = 1.39 ms



Abs. Velocity

© 2008 Fraunhofer EMI

PDF Complete
Your complimentary use period has ended. Thank you for using PDF Complete.
Click Here to upgrade to Unlimited Pages and Expanded Features

C xperimental Results (ISL)
E

Penetrator: 10 mm Caliber, 240 mm Length

Sabot: 40 mm Caliber, Magnesium (Magnesium Alloys)

4 Parts → Two-Plane Symmetry

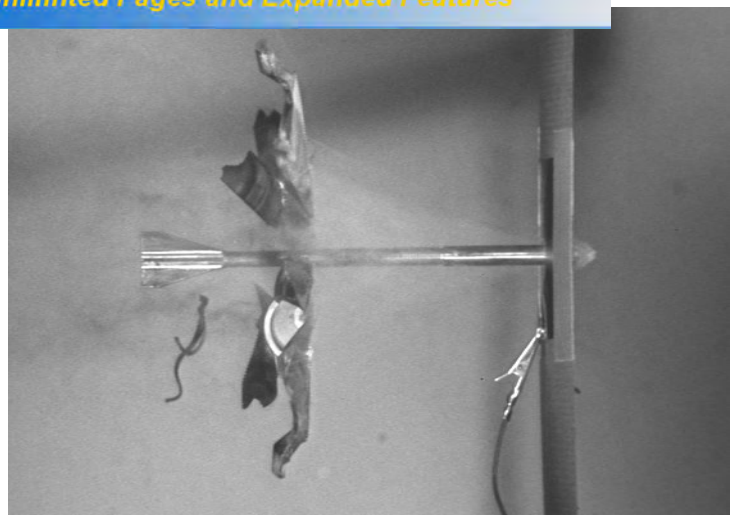
Parameter	Condition A [Schirm, ISL, 2005]	Condition B [Schirm, ISL, 2008]
Material Density Sabot	1.78 g/cm^3 (Mg)	1.52 g/cm^3 (Mg Al3 Li9)
Propellant Mass	0.38 kg	0.40 kg
Maximum Gas Pressure	341.2 MPa	380.3 MPa
Muzzle Velocity	1510 m/s	1633 m/s
Acceleration	794008 m/s^2	897000 m/s^2

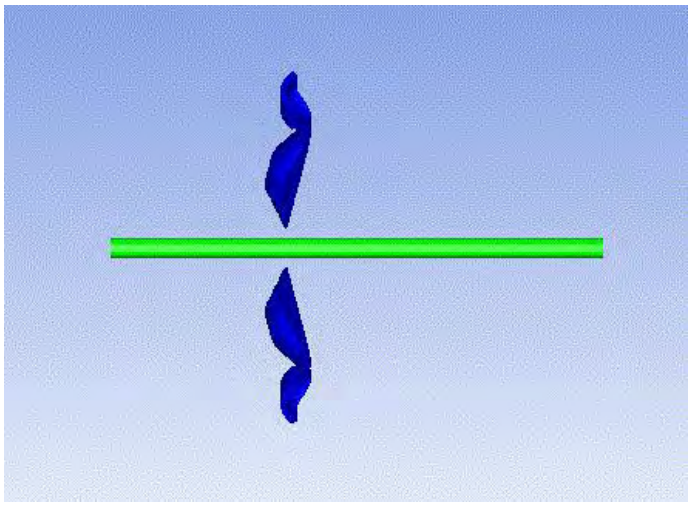
© 2008 Fraunhofer EMI

PDF Complete
Your complimentary use period has ended. Thank you for using PDF Complete.
Click Here to upgrade to Unlimited Pages and Expanded Features

R eparation Simulations

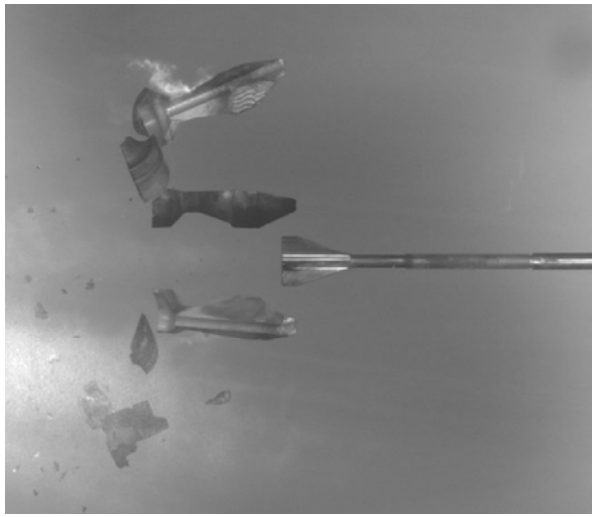
K n: Exp. (ISL) / Sim. (EMI, Condition B)



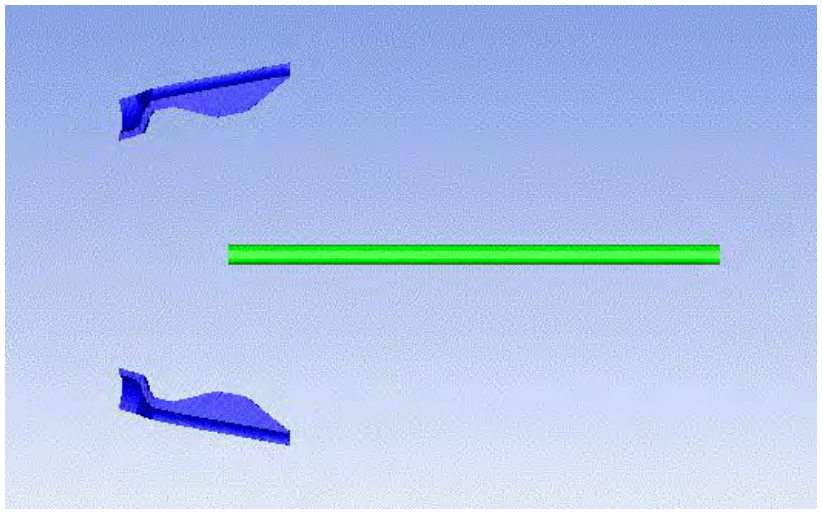


2.0m Behind Muzzle Exit

3.25m Behind Muzzle Exit



Experiment (ISL)

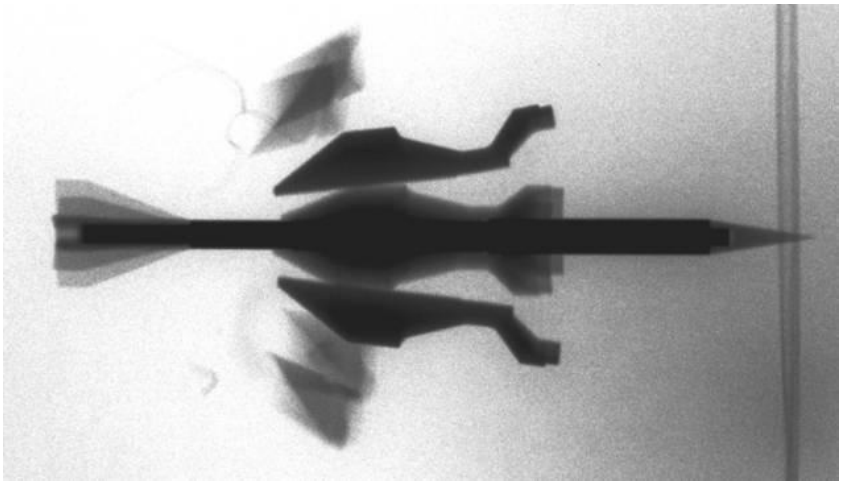


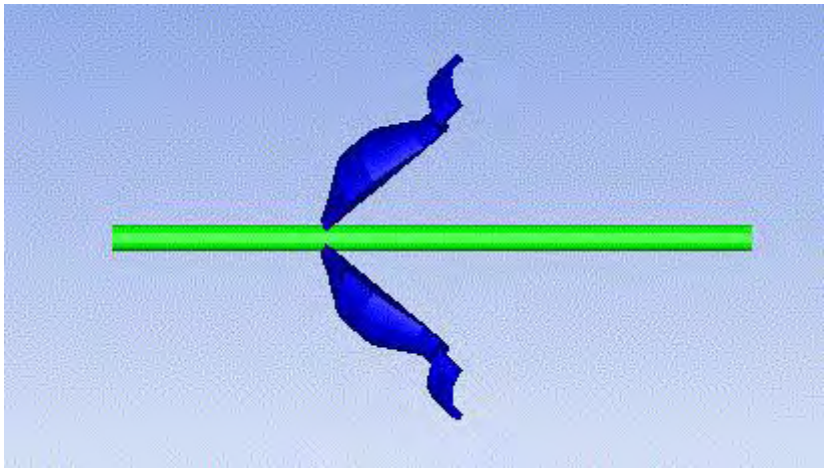
© 2008 Fraunhofer EMI

PDF Complete
Your complimentary use period has ended. Thank you for using PDF Complete.
Click Here to upgrade to Unlimited Pages and Expanded Features

R eparation Simulations

Ki n: Exp. (ISL) / Sim. (EMI, Condition A)

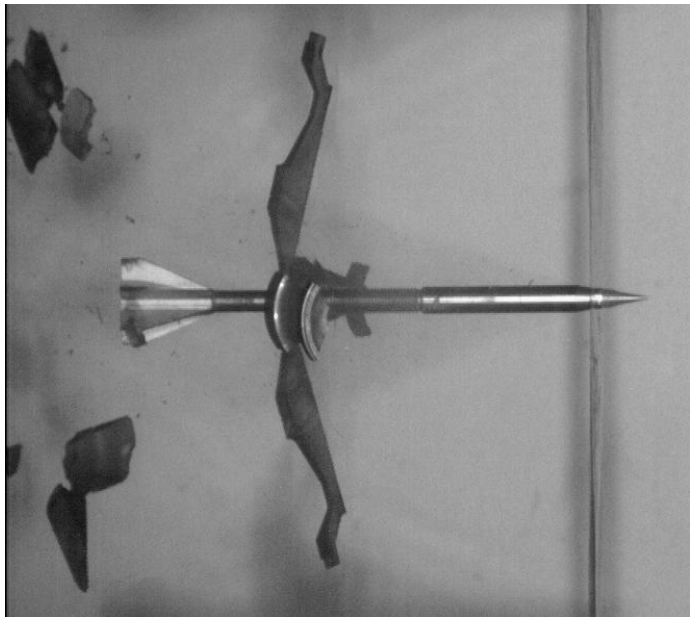


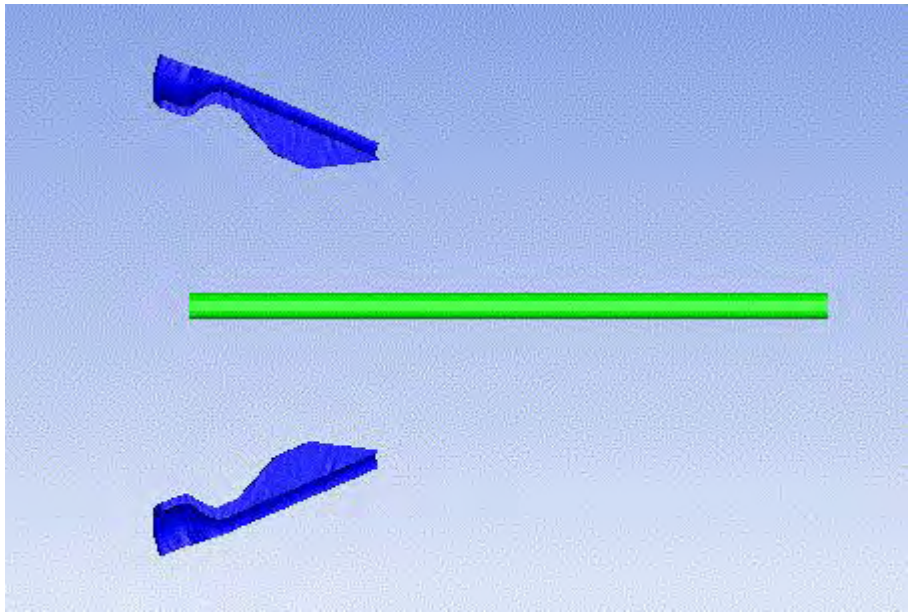


1.8m Behind Muzzle Exit

3.0m Behind Muzzle Exit

Experiment (ISL)



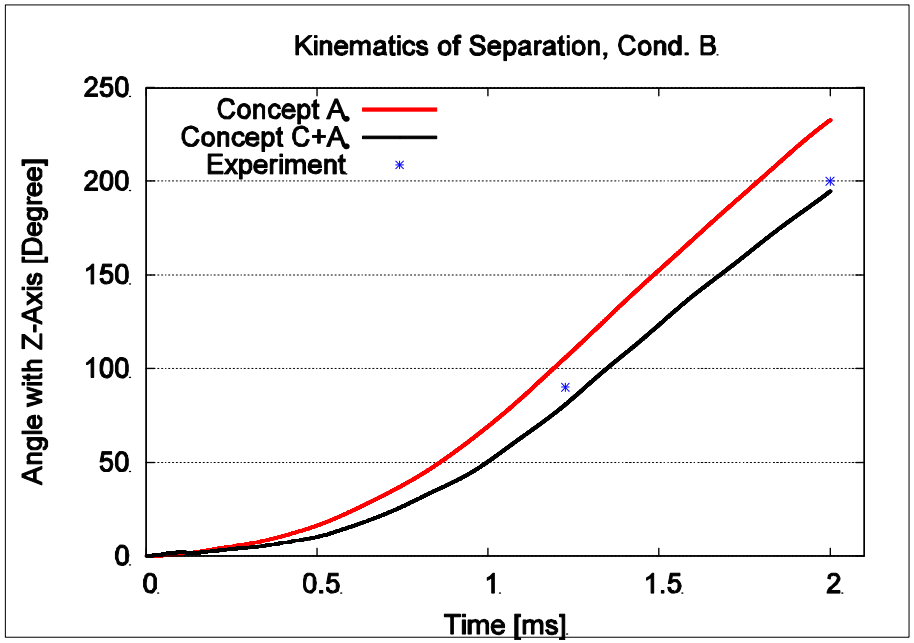


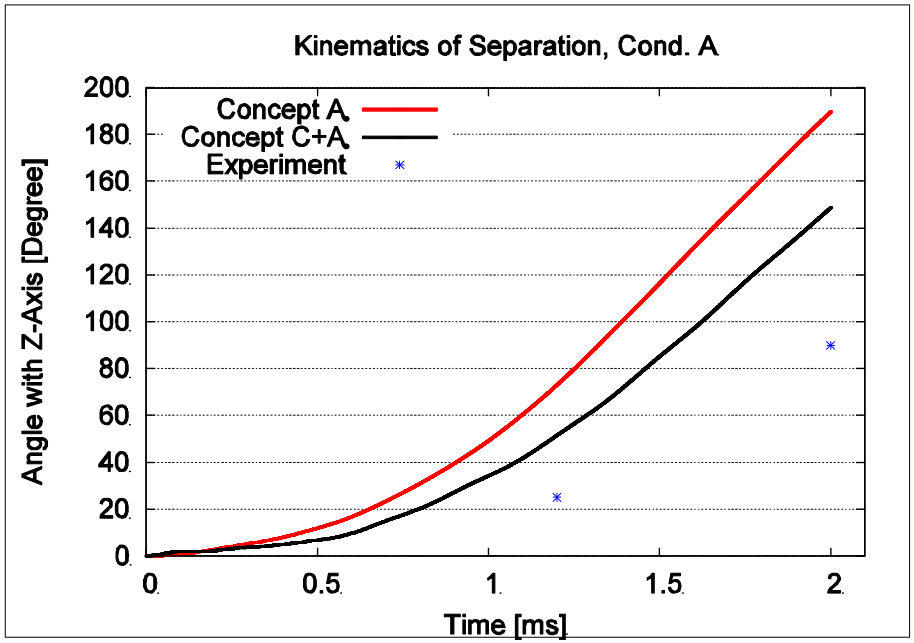
© 2008 Fraunhofer EMI

PDF Complete
Your complimentary use period has ended. Thank you for using PDF Complete.
Click Here to upgrade to Unlimited Pages and Expanded Features

Separation Simulations

tics of Separation (Different Strategies)





Effects of Muzzle Exit have to be Considered (Both Conditions)

Problem of Numerical Capturing (Tracking) of the Penetrator Nose (Geom. Singularity)

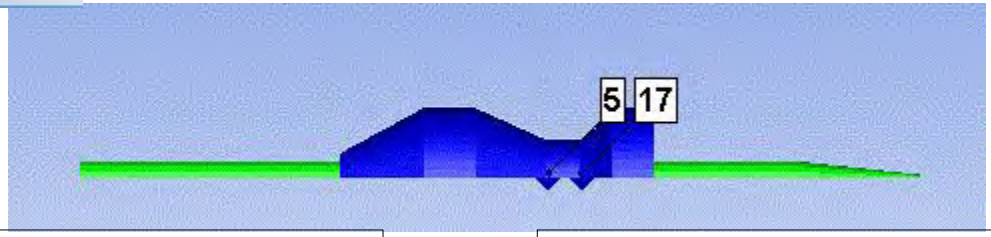
Additional Uncertainties in the Experiments

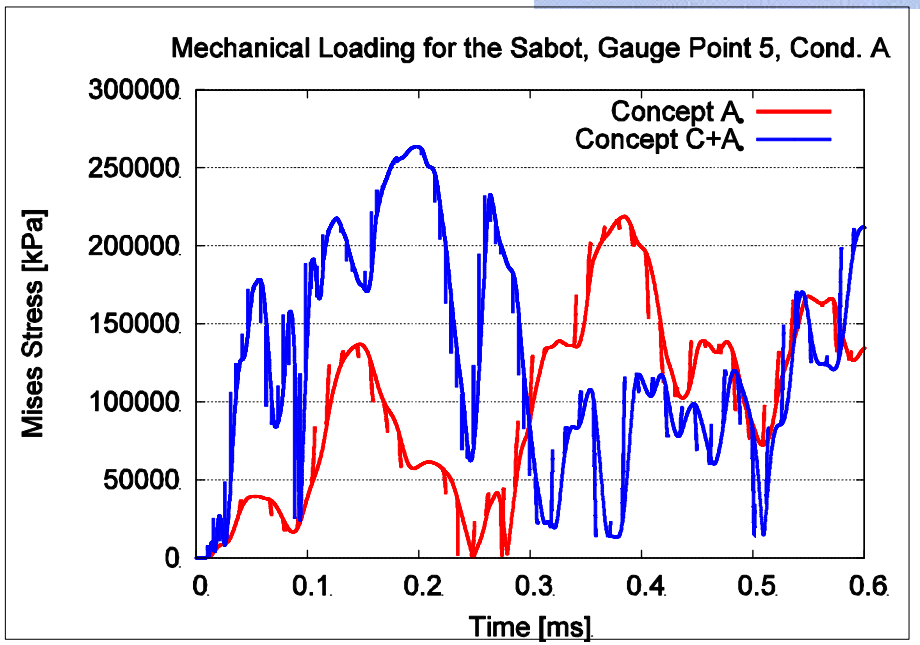
© 2008 Fraunhofer EMI

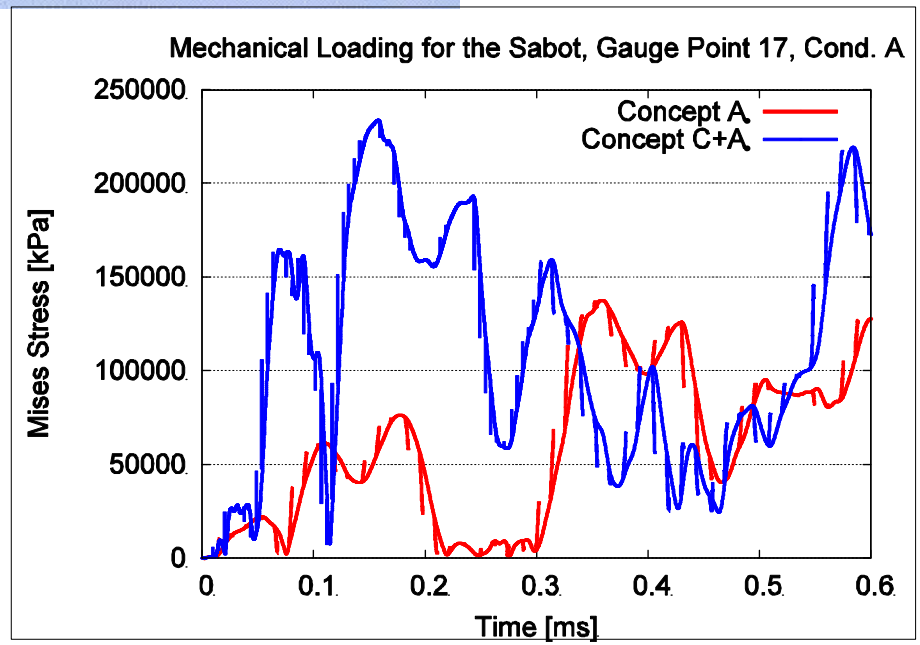
PDF Complete
Your complimentary use period has ended. Thank you for using PDF Complete.
Click Here to upgrade to Unlimited Pages and Expanded Features

Separation Simulations

the Structure (Different Strategies)







Effects of Muzzle Exit Result in Significantly Higher Structure Loads

movie2.avi

© 2008 Fraunhofer EMI

PDF Complete
Your complimentary use period has ended. Thank you for using PDF Complete.
Click Here to upgrade to Unlimited Pages and Expanded Features

(ure Work

- Numerical Simulations for Sabot Separation Processes with Different Approaches
- Ability for Simulation of Muzzle Exit- and Exterior Ballistics by Coordinate Switching
- Future Work:

  - Numerical Investigation of Effects of Experimental Uncertainties (Mass, Geometry,

    Muzzle Exit Velocity / Angle of Attack)

  - Influence of the Penetrator Nose / Fins

  - Sabot Design Optimization

  - „Loading History“ for Separated Structural Calculations

Funded by: Bundeswehr Research Institute for Materials, Explosives, Fuels and Lubricants

DEFENCE ACADEMY
OF THE UNITED KINGDOM
Cranfield UNIVERSITY
Defence College of Management and Technology

Assessment of potential blunt trauma under ballistic helmets

Celia Watson, φAnnette Webb, Ian Horsfall
Impact and Armour Group, Cranfield University Shrivenham,UK.
φ Land Engineering Agency, Australian Department of Defence, Melbourne, Australia

c.h.watson@cranfield.ac.uk



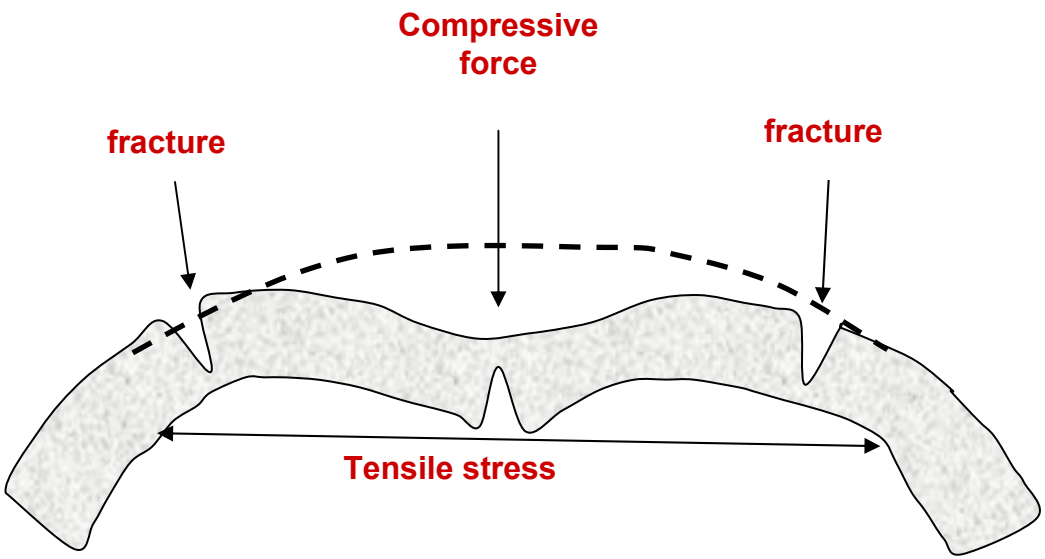
Aims:

To investigate force measurement techniques

Measure head contact loads from non-penetrating ballistic impact on helmets.

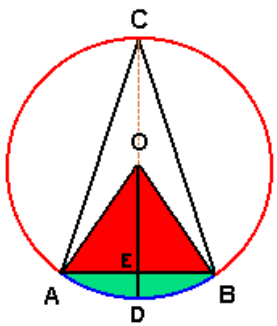
Use the force information to develop a simple method of force measurement for helmet testing.

Forensic analysis



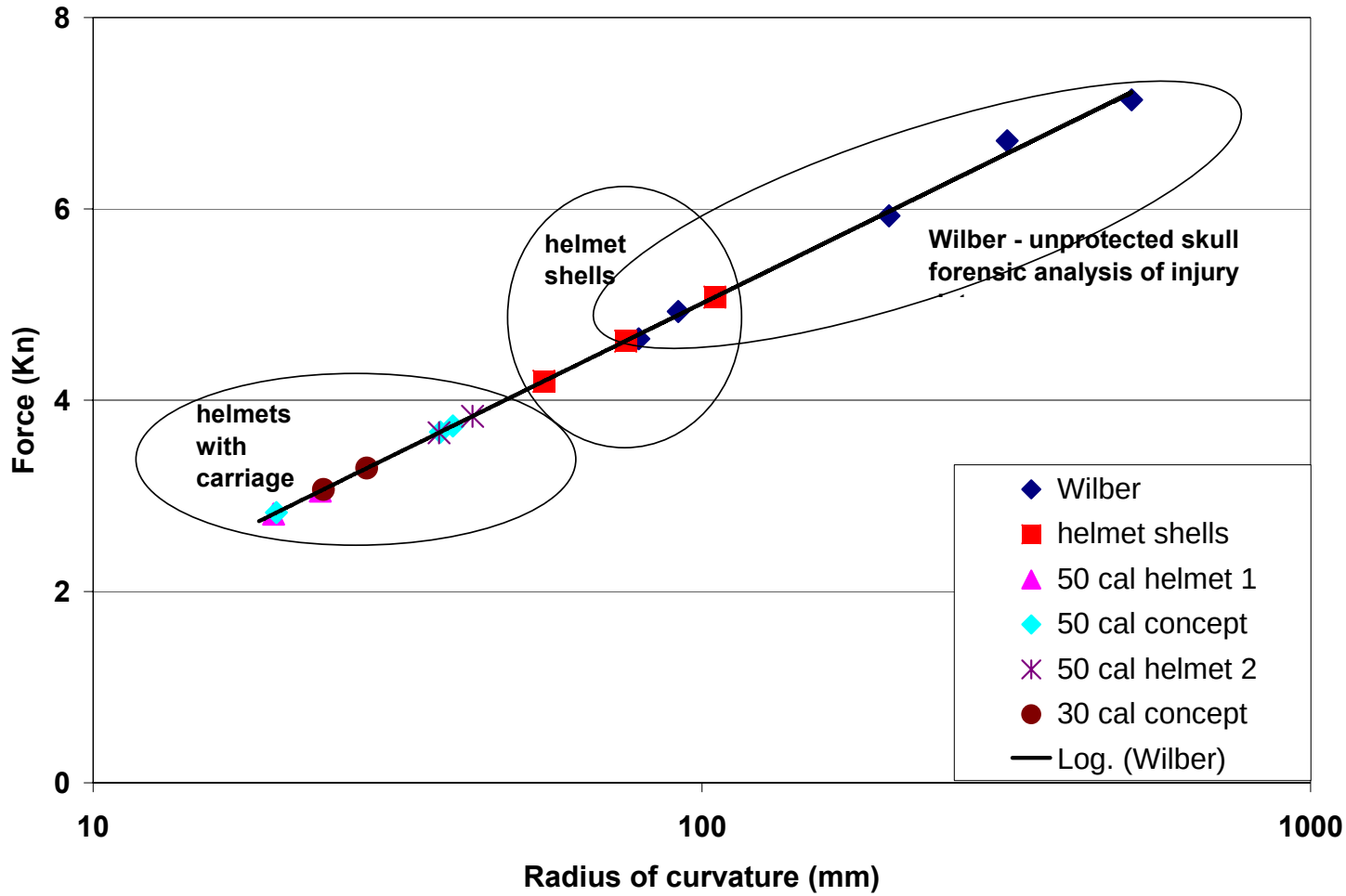
Wilber related the size and shape of fracture damage

To the radius of curvature of the impacting weapon.

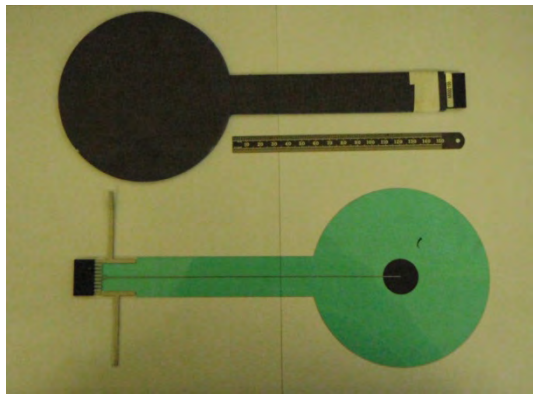


intersecting chord theorem

Force vs Radius of Curvature for Skull Fractures

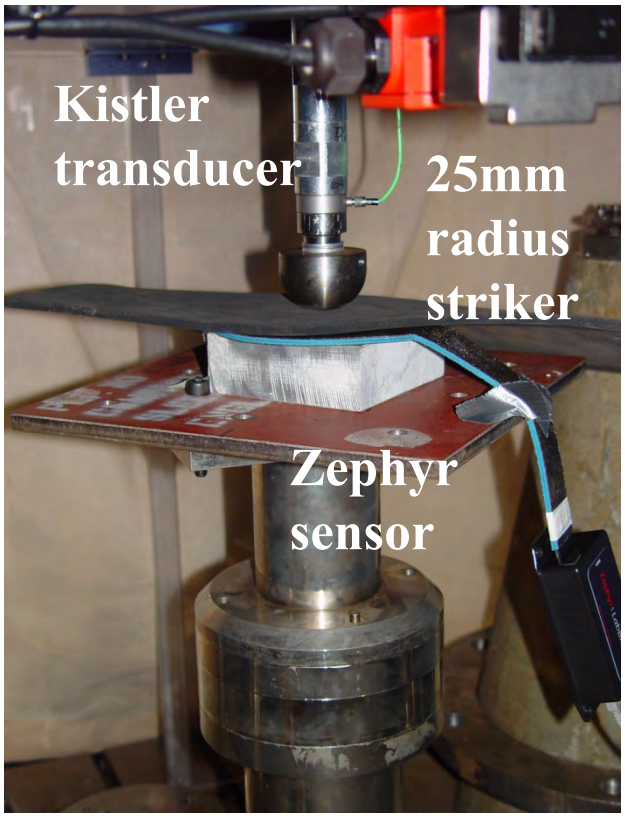


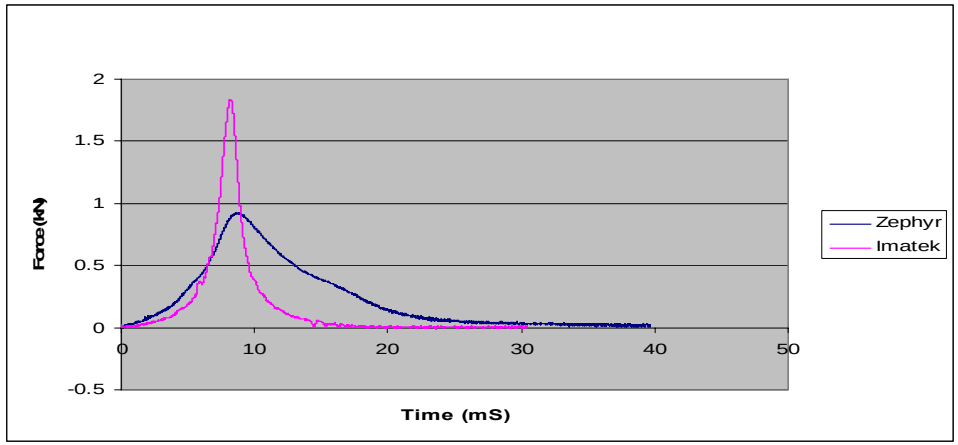




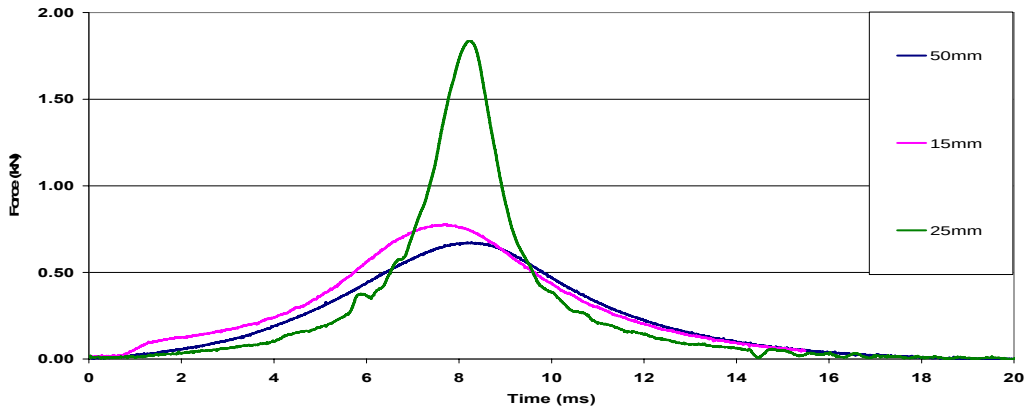
Zephyr® film sensor pads



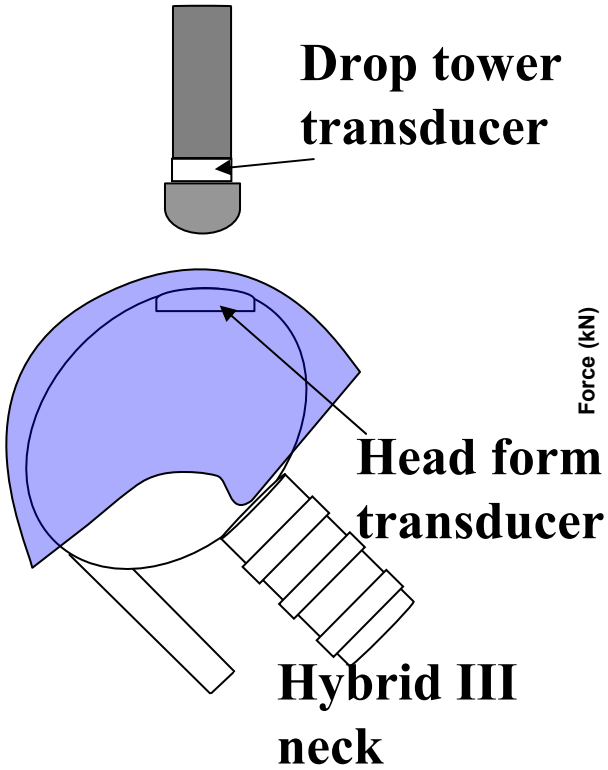


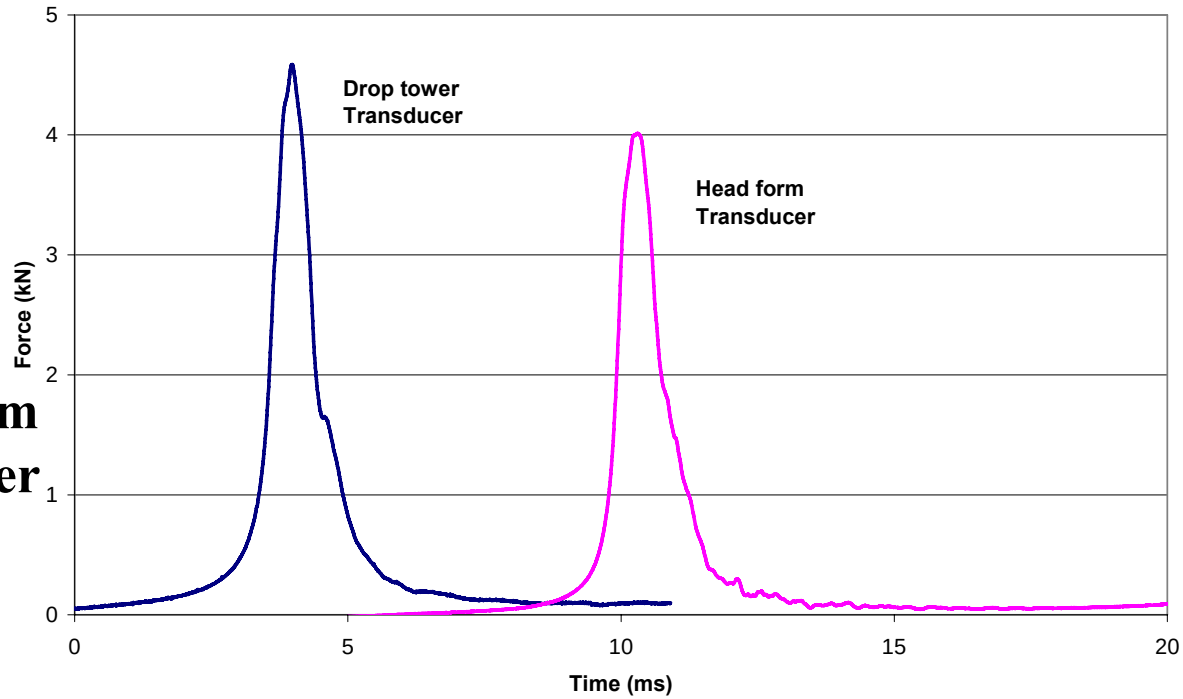


Force output from 9031A Kistler® load cell compared with Zephyr® sensors

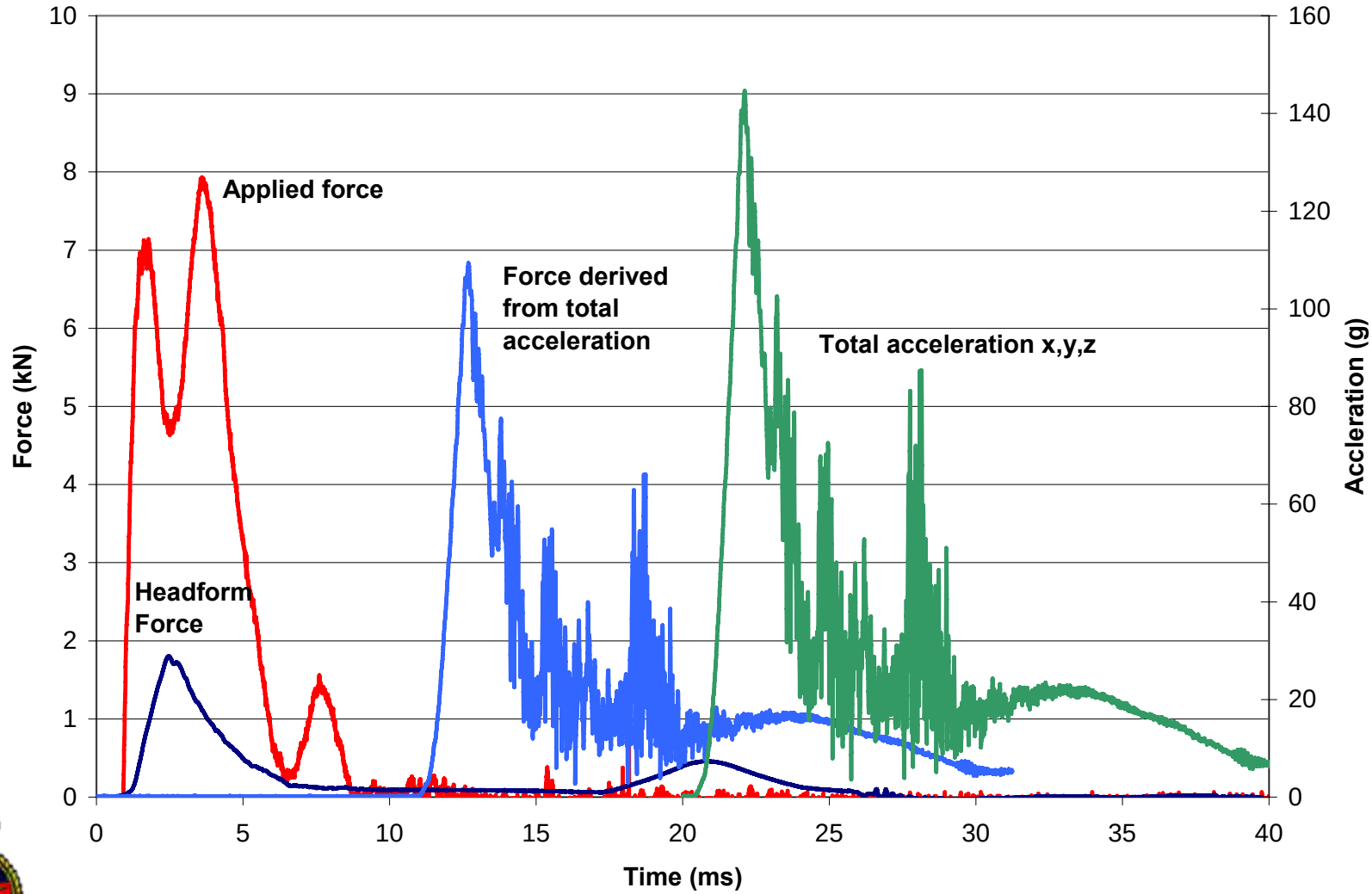


Effect of radius of different strikers





Force vs time - comparison of transducer outputs

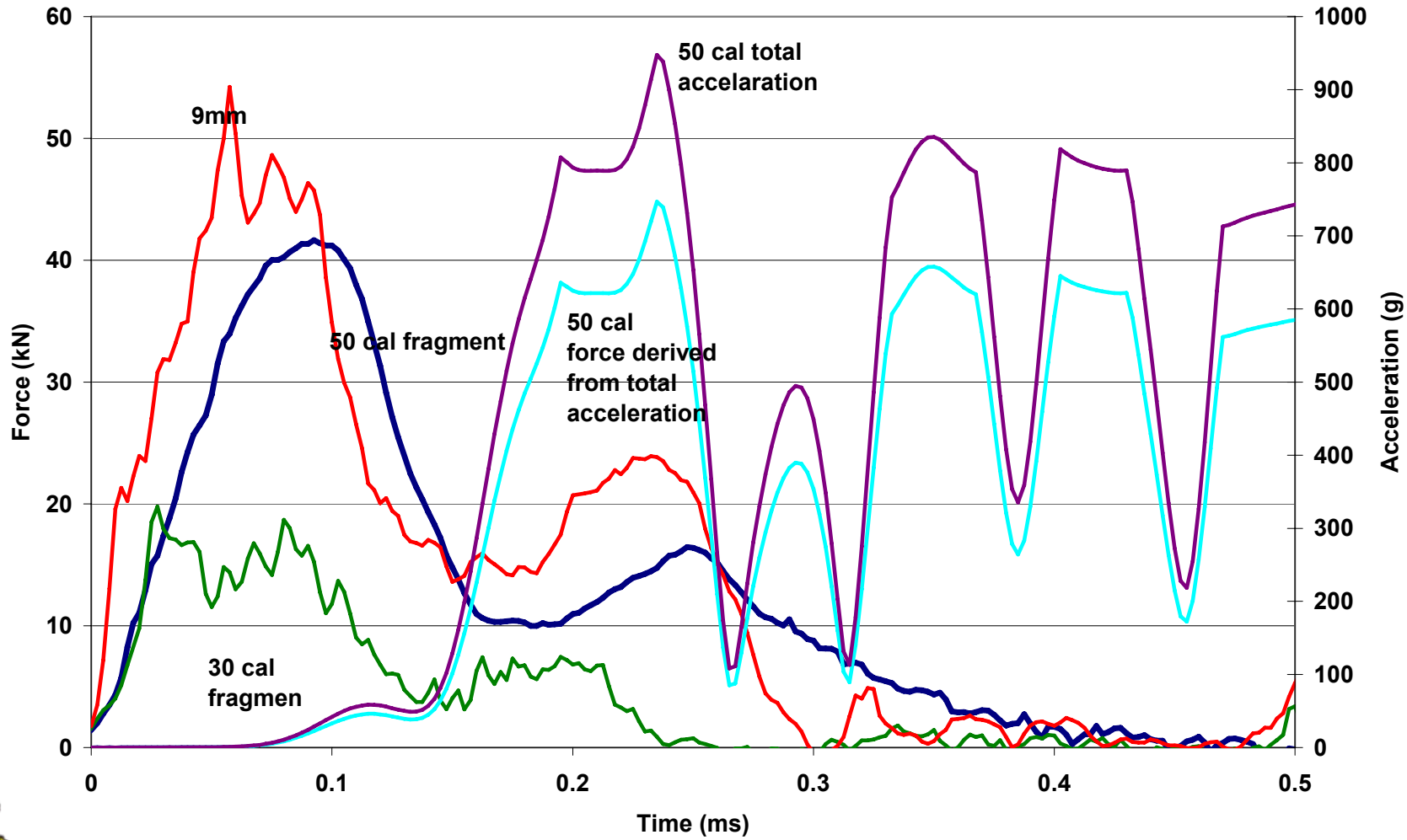

Applied force
Force derived from total acceleration
Total acceleration x,y,z
Headform Force
Force (kN)
Accleration (g)
Time (ms)
0
1
2
3
4
5
6
7
8
9
10
0
20
40
60
80
100
120
140
160
0
5
10
15
20
25
30
35
40



Shots loaded the centre of Film sensors

No standoff other than the mitigation allowed by the carriage system

Kevlar helmet shell with carriage system showing position of Zephyr sensor on Aluminium head form and Hybrid III neck.


60
50
40
30
20
10
0
Force (kN)
1000
900
800
700
600
500
400
300
200
100
0
Acceleration (g)
0
0.1
0.2
0.3
0.4
0.5
Time (ms)
9mm
50 cal fragment
50 cal total accelaration
50 cal force derived from total acceleration
30 cal fragmen

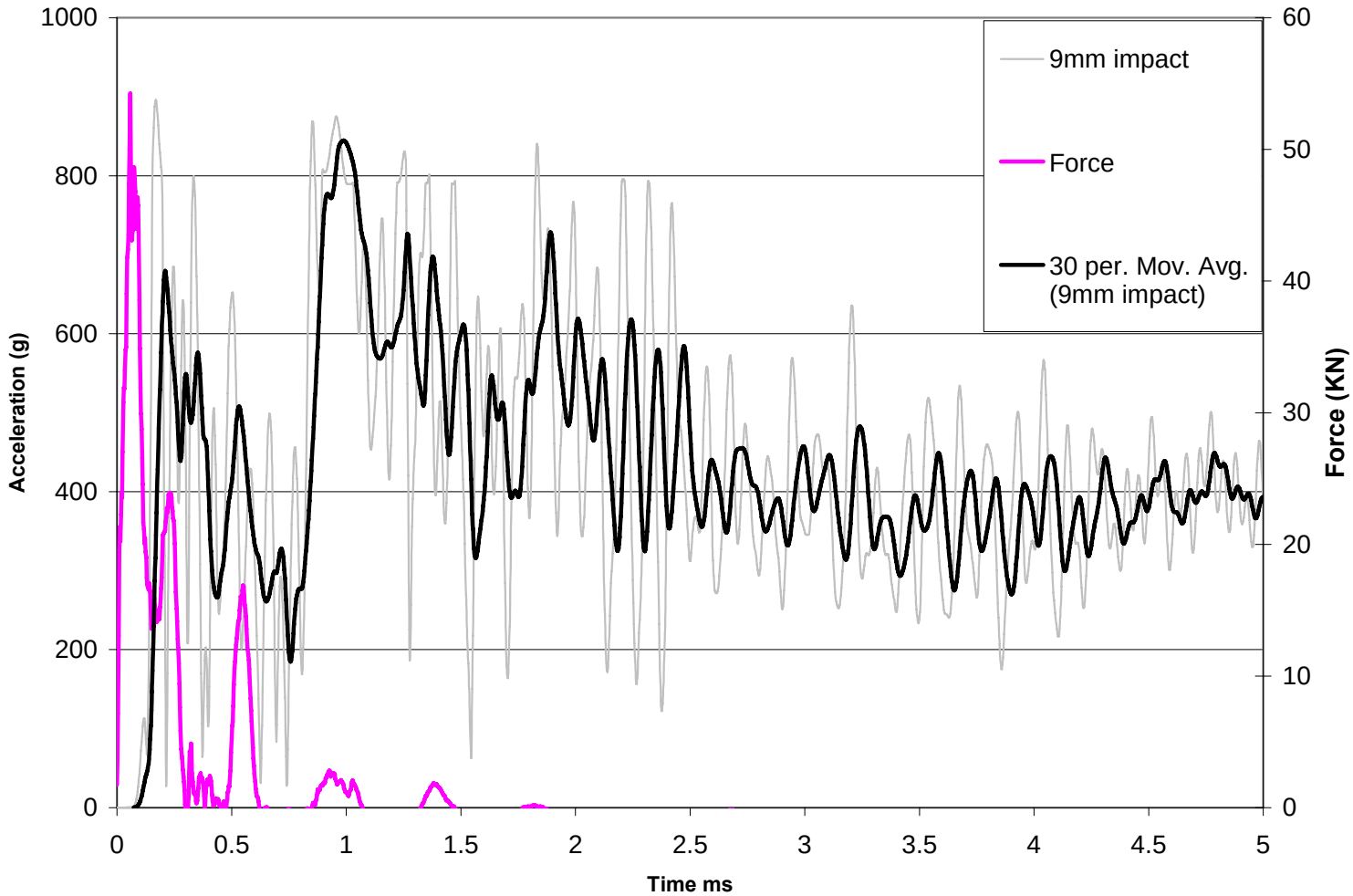
9mm impact on helmet

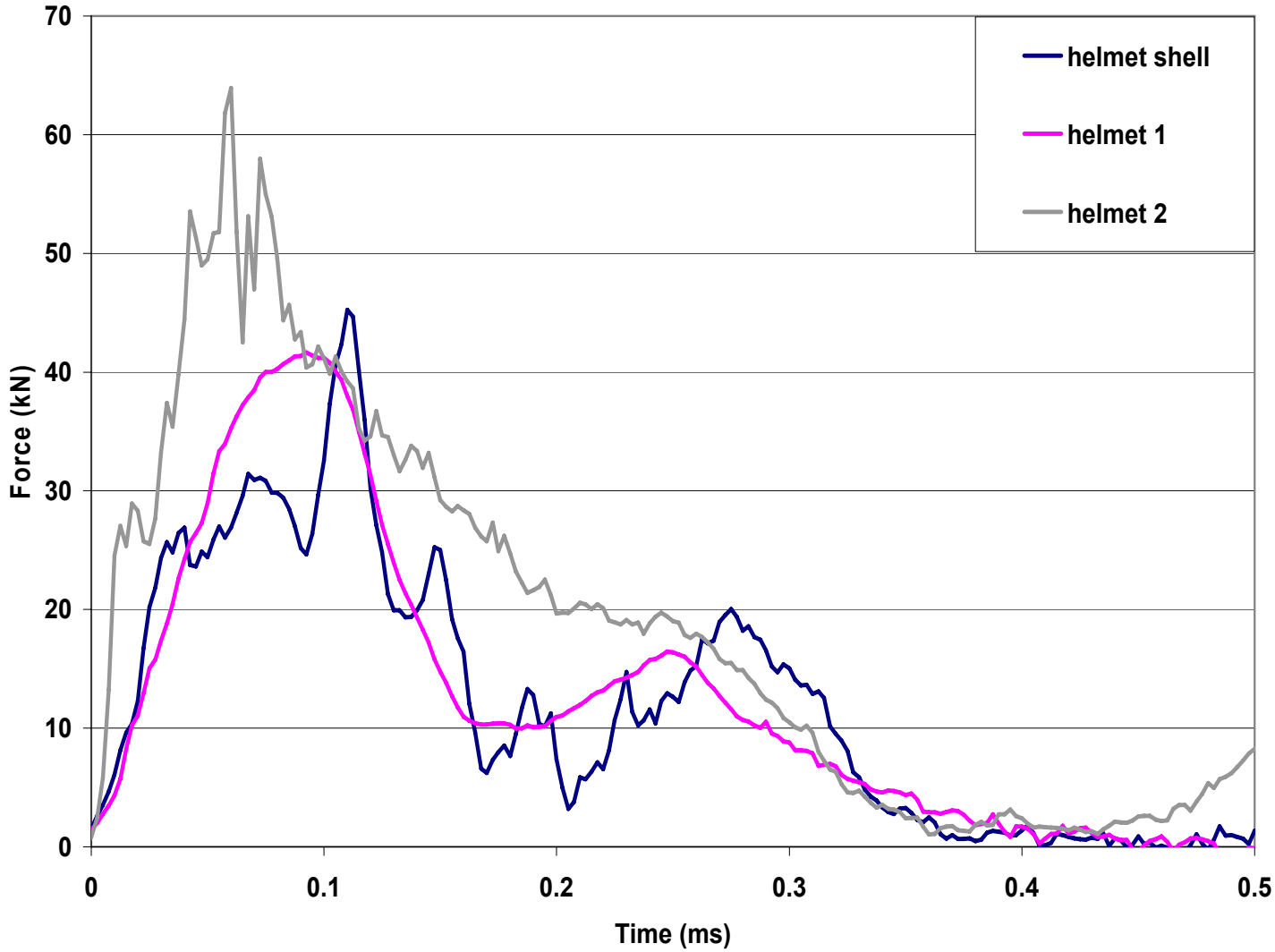


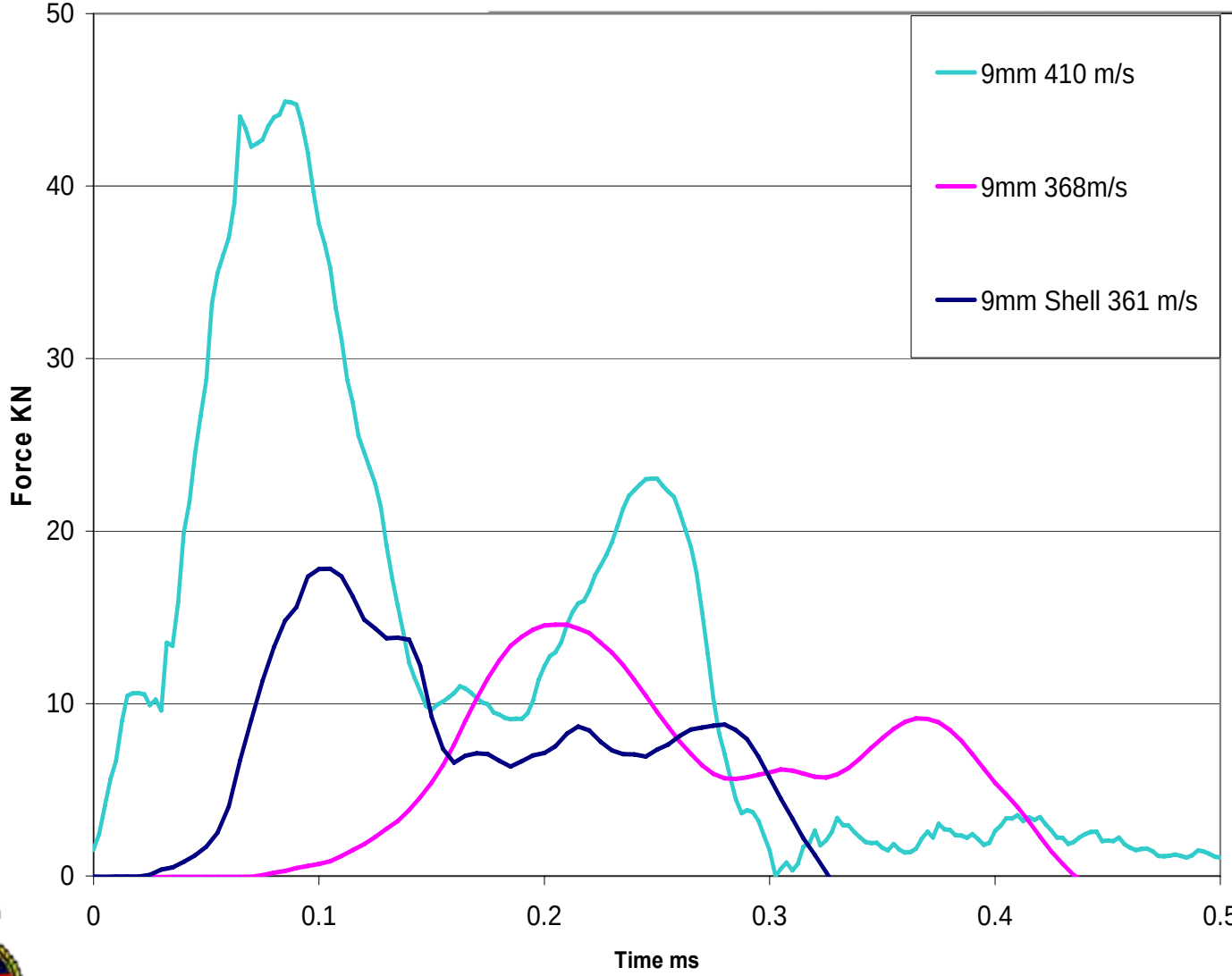
Initial impact



Complete impact motion


1000
800
600
400
200
0
Acceleration (g)
60
50
40
30
20
10
0
Force (KN)
0
0.5
1
1.5
2
2.5
3
3.5
4
4.5
5
Time ms
9mm impact
Force
30 per. Mov. Avg. (9mm impact)


70
60
50
40
30
20
10
0
Force (kN)
0
0.1
0.2
0.3
0.4
0.5
Time (ms)
helmet shell
helmet 1
helmet 2


50
40
30
20
10
0
Force KN
0
0.1
0.2
0.3
0.4
0.5
Time ms
9mm 410 m/s
9mm 368m/s
9mm Shell 361 m/s

Summary

The head form was robust

Peak force results were repeatable.

Time histories of Force and acceleration correlated with high speed video and similar work by other researchers

0.05ms duration of the peak force from ballistic impact is a higher rate than the 15.0ms duration rate accepted as suitable for the HIC

Head form not bio-fidelic and compliance issues will be investigated in further work.

Film sensors show promise but need further development

Trajectory Deflection of Fin- and Spin-Stabilized Projectiles Using Paired Lateral Impulses

Pierre Wey Pierre.Wey@isl.eu

Daniel Corriveau Daniel.Corriveau@drdc-rddc.gc.ca



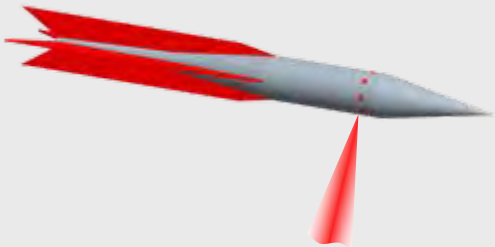


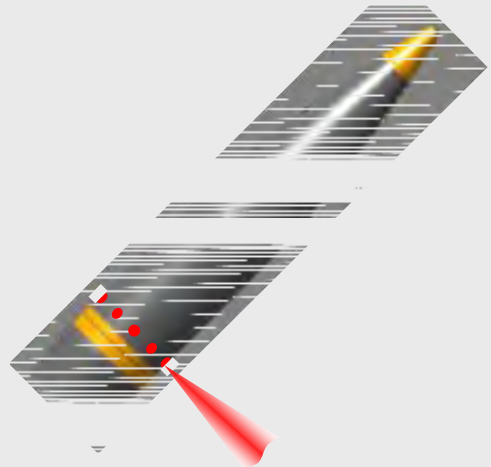
Presentation Overview

- Objective
- Effect of a Lateral Impulse
- Basic Mathematical Model and Analytical Solution
- Pairing the Impulses
- Examples
- Conclusions

Objective

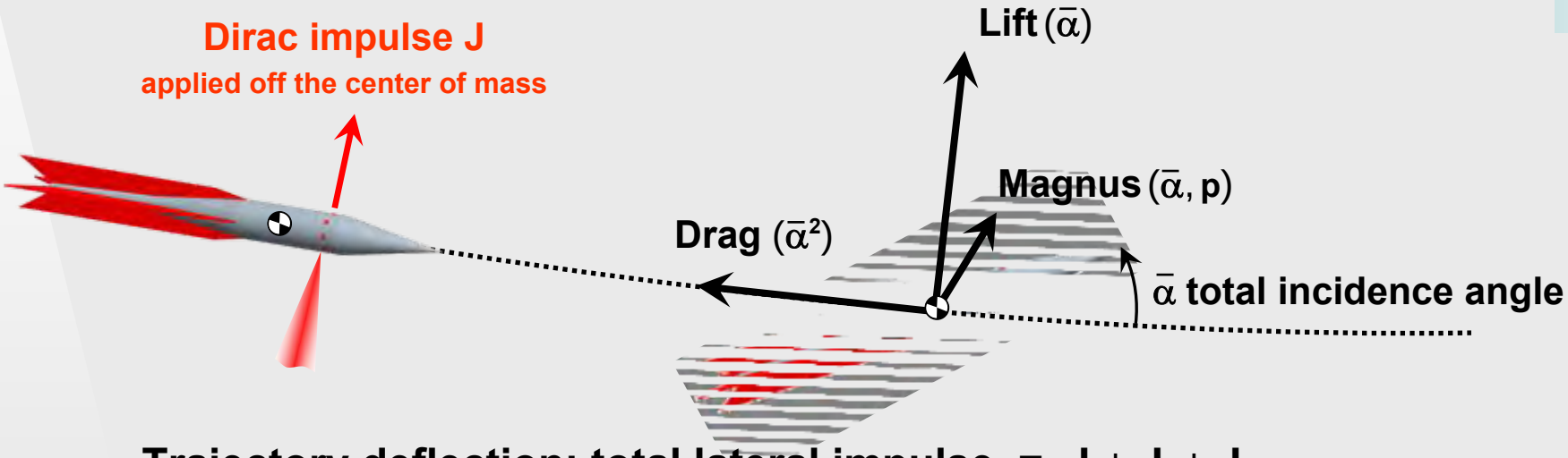
- To developed a well defined procedure for using paired impulses on fin- and spin-stabilized projectiles in order to achieve enhanced drift corrections





ISL DEFENCE R&D DÉFENSE

Effect of a Lateral Impulse (1/2)



Trajectory deflection: total lateral impulse = $J + J_L + J_Y$

- $\int$ Magnus ($\bar{\alpha}$) dt
- $\int$ Lift ($\bar{\alpha}$) dt

Additional velocity decrease: axial impulse = J_{D2}

- $\int$ Drag ($\bar{\alpha}^2$) dt

More challenging to implement properly

Effect of a Lateral Impulse (2/2)

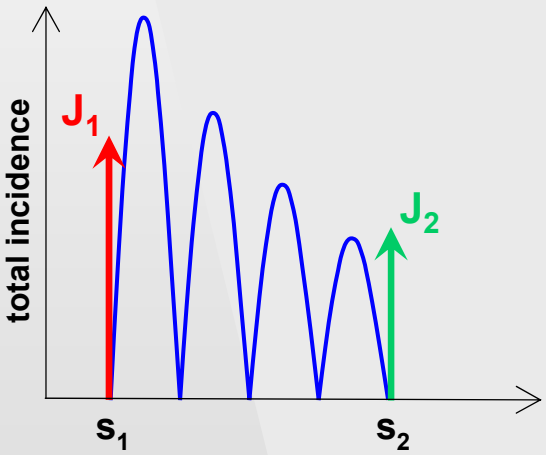
Pairing lateral impulses off the center of mass

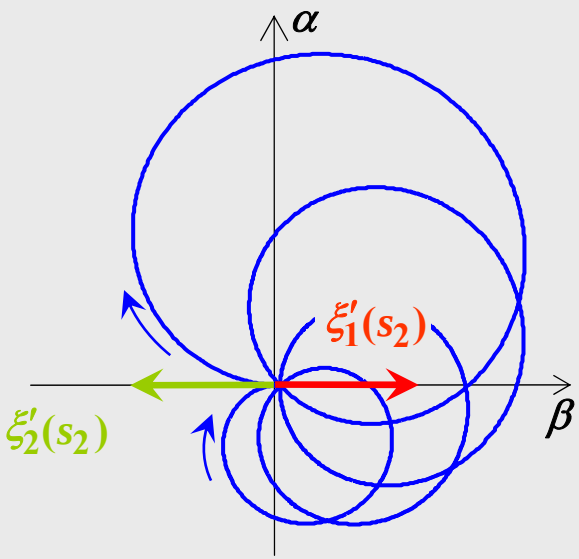
Basic idea: - J_1 triggers the angular motion at s_1

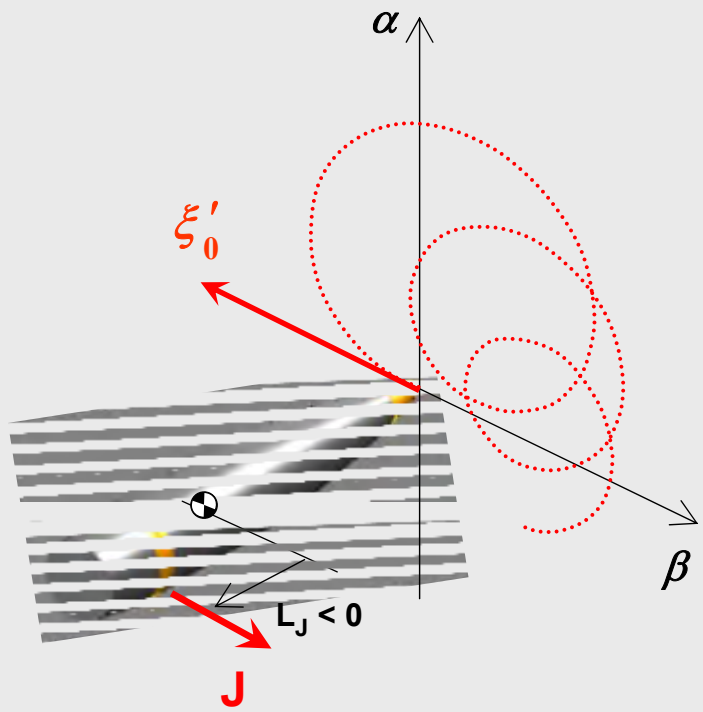
- J_2 stops the angular motion at s_2

Advantages: - the lateral correction is enhanced by the lift impulse resulting from the angular motion

- the range lost is minimized by stopping the angular motion







Basic Mathematical Model (1/4)

Linearized equation of the complex incidence motion:

$$\xi'' + (H - iP)\xi' - (M + iPT)\xi = \xi_0' \delta(s)$$

- $\xi_0' \delta(s)$ — Dirac impulse
- $(M + iPT)\xi$ — Magnus moment + vel. change; $T = \frac{\rho A d}{2m}\left(C_{L\alpha} + \frac{md^2}{I_x} C_{np\alpha}\right)$
- $M\xi$ — Overturning moment (restoring or destabilizing); $M = \frac{\rho A d^3}{2 I_y} C_{m\alpha}$
- $-iP\xi'$ — Gyroscopic effect; $P = \frac{I_x}{I_y}\frac{pd}{V}$
- $H\xi'$ — Damping factor + vel. change; $H = \frac{\rho A d}{2m}\left(C_{L\alpha} - C_D - \frac{md^2}{I_y} C_{mq}\right)$

Basic Mathematical Model (2/4)

Motion = sum of two rotating arms:

$$\xi = K_{F_0} e^{i\phi_{F0}} e^{(\lambda_F + i\phi'_F)s} + K_{S_0} e^{i\phi_{S0}} e^{(\lambda_S + i\phi'_S)s}$$

Angular frequencies

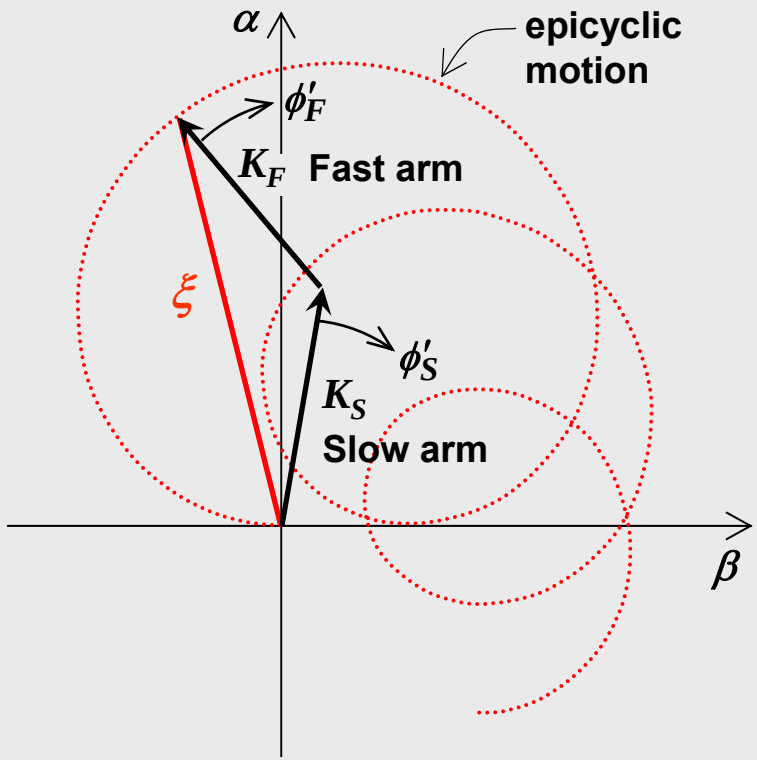
$$\phi'_F = \frac{1}{2}\left(P + \sqrt{P^2 - 4M}\right) \qquad \phi'_S = \frac{1}{2}\left(P - \sqrt{P^2 - 4M}\right)$$

Damping factors

$$\lambda_F = -\frac{1}{2}\left(H - \frac{P(2T - H)}{\sqrt{P^2 - 4M}}\right) \qquad \lambda_S = -\frac{1}{2}\left(H + \frac{P(2T - H)}{\sqrt{P^2 - 4M}}\right)$$

Initial arms

$$K_{F_0} e^{i\phi_{F_0}} = -\frac{i\xi'_0 + \phi'_S \xi_0}{\phi'_F - \phi'_S} \qquad K_{S_0} e^{i\phi_{S_0}} = \frac{i\xi'_0 + \phi'_F \xi_0}{\phi'_F - \phi'_S}$$



Basic Mathematical Model (3/4)

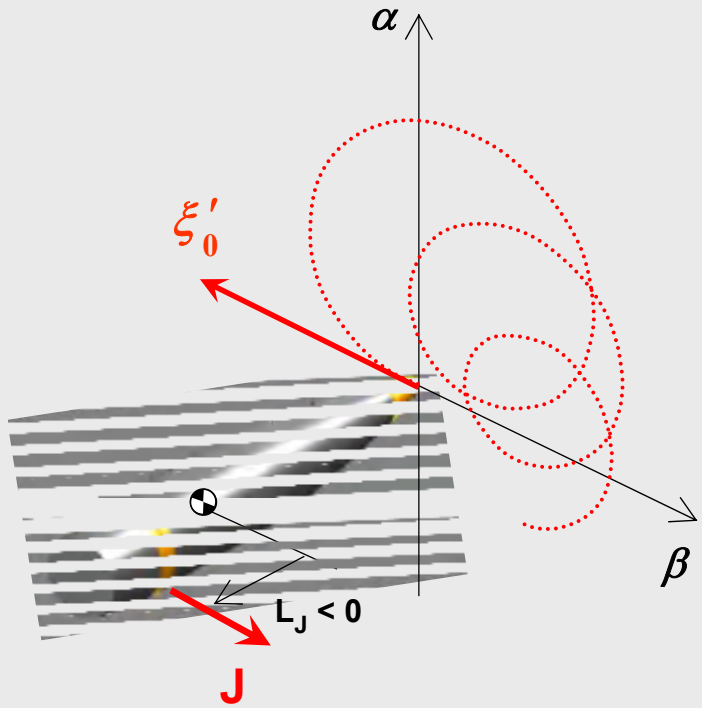
Initial conditions forced by the Dirac impulse:

$$\xi_0 = -\frac{J}{mV}$$

→ negligible in supersonic mode

$$\xi_0' = \frac{J\, L_J\, d^2}{I_y V}$$

→ main cause of angular motion (unless $L_J \to 0$)



Basic Mathematical Model (4/4)

Lateral impulses: Lift + Magnus

$$J_L = \int_0^\infty L(t)\,dt \qquad J_L = \frac{1}{2}\rho A V d C_{L\alpha} \int_0^\infty \xi\,ds \qquad \int_0^\infty \xi\,ds = -\frac{K_{F_0} e^{i\phi_{F_0}}}{\lambda_F + i\phi'_F} - \frac{K_{S_0} e^{i\phi_{S_0}}}{\lambda_S + i\phi'_S}$$

$$J_Y = \int_0^\infty Y(t)\,dt \qquad J_Y = i\frac{C_{Yp\alpha}}{C_{L\alpha}}\frac{pd}{V} J_L$$

Axial impulse: additional Drag

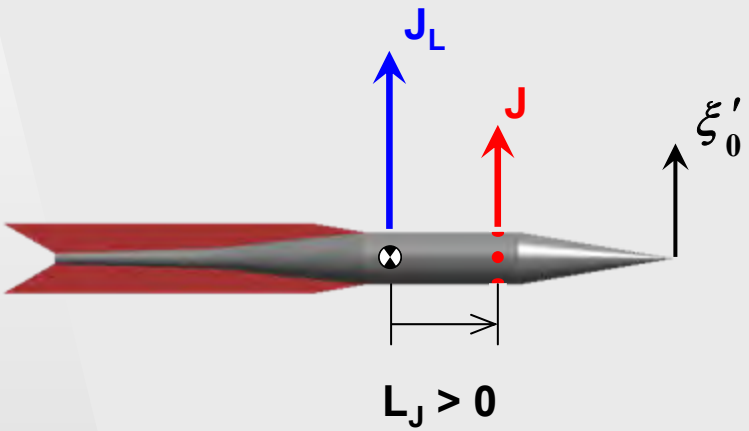
$$J_{D_2} = \int_0^\infty D_2(t)\,dt \qquad C_D = C_{D0} + C_{D_2}\sin^2\bar{\alpha} \qquad J_{D_2} = \frac{1}{2}\rho A V d C_{D_2} \int_0^\infty |\xi|^2\,ds$$

$$\int_0^\infty |\xi|^2\,ds = -\frac{K_{F_0}^2}{2\lambda_F} - \frac{K_{S_0}^2}{2\lambda_S} - \frac{2K_{F_0}K_{S_0}\left[(\lambda_F+\lambda_S)\cos(\phi_{F_0}-\phi_{S_0}) + (\phi'_F-\phi'_S)\sin(\phi_{F_0}-\phi_{S_0})\right]}{(\lambda_F+\lambda_S)^2 + (\phi'_F-\phi'_S)^2}$$

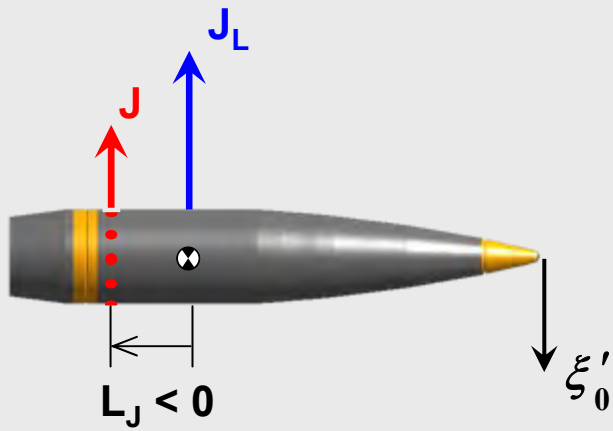
Pairing the Impulses: Location (1/2)

Goal: maximizing $J + J_L$

Fin-stabilized projectile



Spin-stabilized projectile



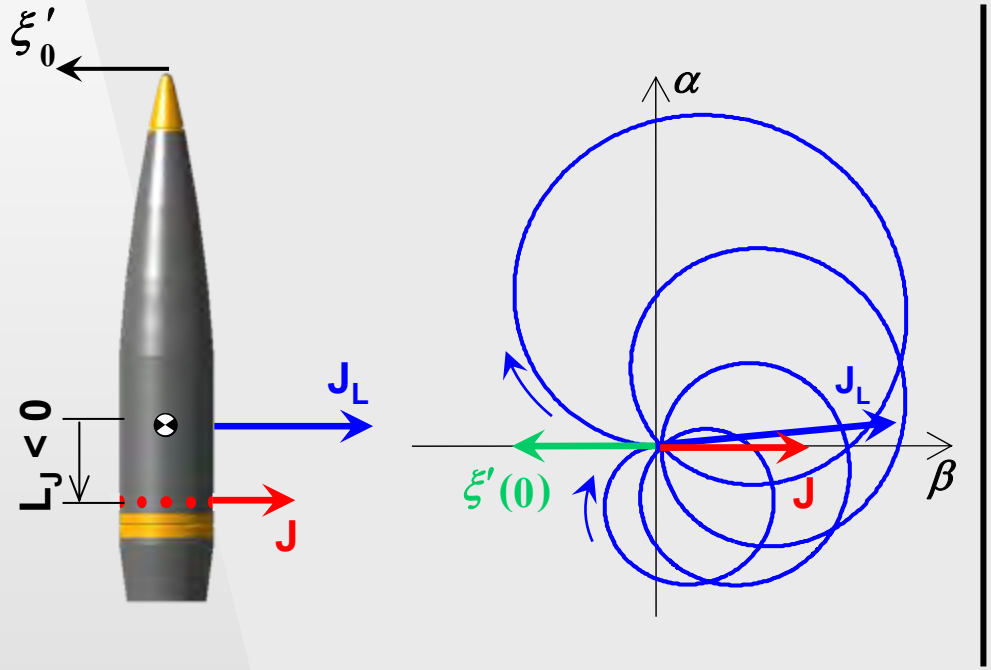
Rule #1: the lateral impulse must be applied
- **ahead of the center of mass for fin-stab. shells**
- **behind the center of mass for spin-stab. shells**

$$J_L = -J L_J \frac{C_{L\alpha}}{C_{m\alpha}} e^{i\Delta\phi}$$

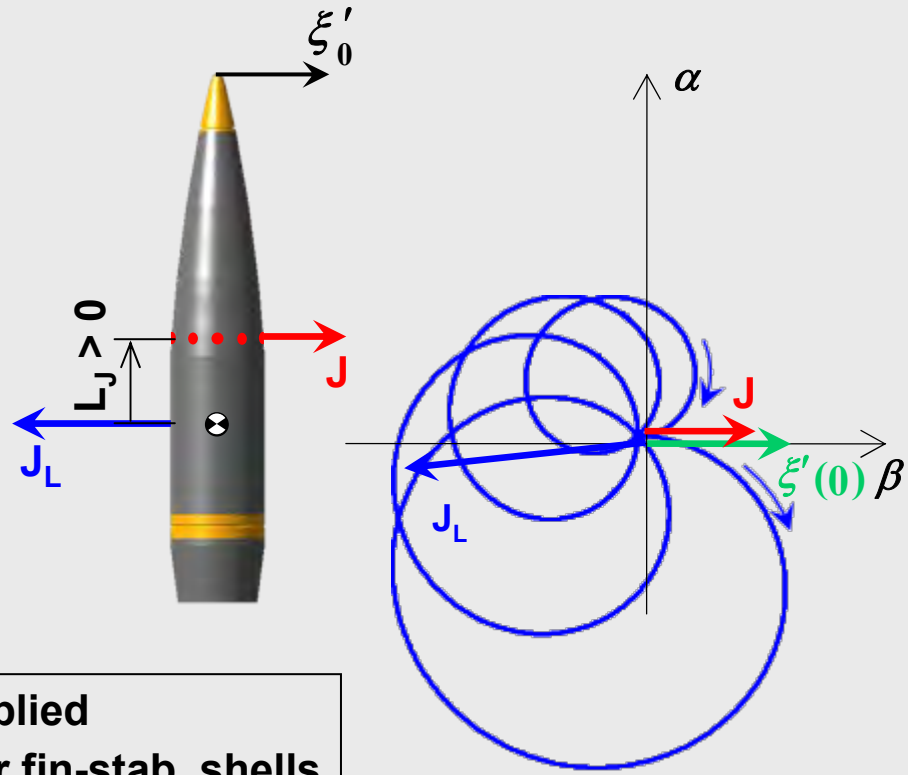
Pairing the Impulses: Location (2/2)

Goal: maximizing J + J_L for spin-stabilized projectile

How to do it:

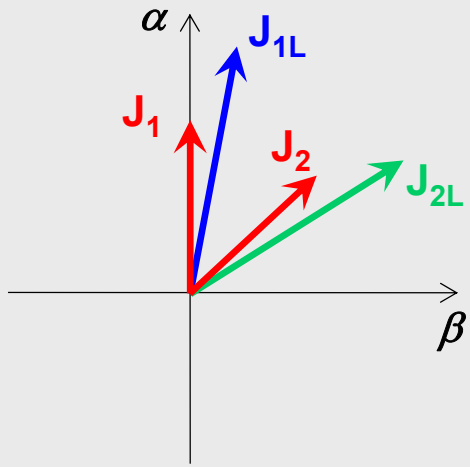


How not to do it:



Rule #1: the lateral impulse must be applied
- **ahead of the center of mass for fin-stab. shells**
- **behind the center of mass for spin-stab. shells**

Pairing the Impulses: Orientation

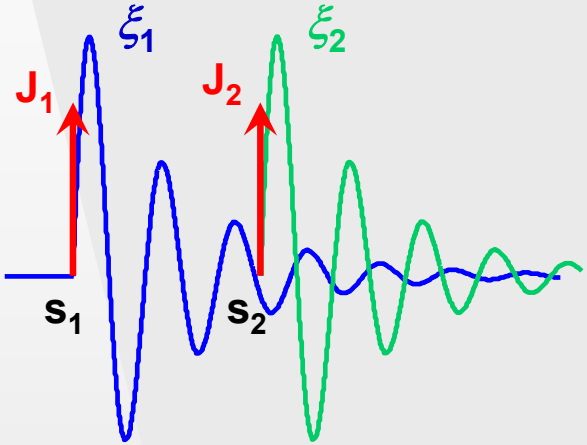


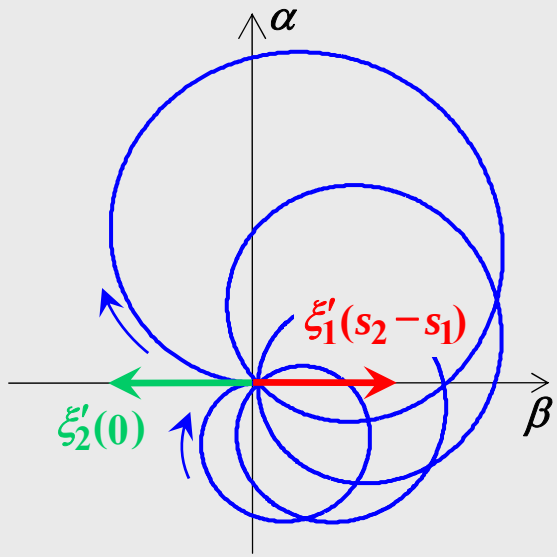
Total lateral impulse = $(J_1 + J_{1L}) + (J_2 + J_{2L})$

- independent of $(s_2 - s_1)$
- maximum if J_1 and J_2 are aligned

Rule #2: J_1 and J_2 must be triggered at the same roll angle

Pairing the Impulses: Timing





Linearized equation of motion:

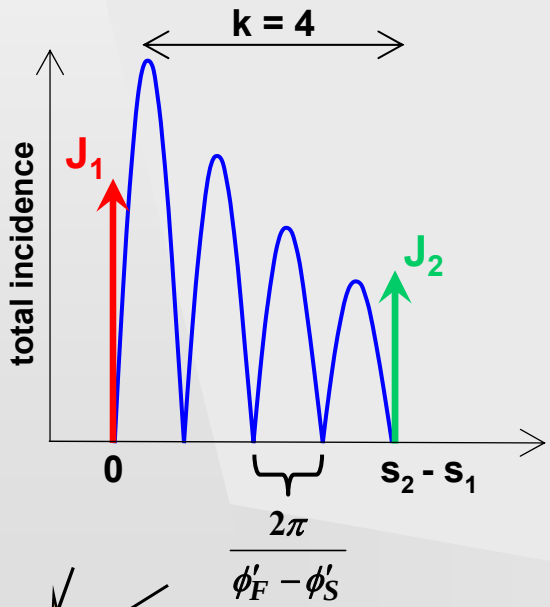
$$\xi = \xi_1 + \xi_2$$

$$\forall s \geq s_2,\ \xi_1(s) + \xi_2(s) = 0$$

Motion strictly opposed if:

$$\xi_1(s_2 - s_1) = \xi_2(0) = 0$$

$$\xi_1'(s_2 - s_1) = -\xi_2'(0)$$



Rule #3:

$$s_2 - s_1 = k \frac{2\pi}{\phi_F' - \phi_S'}$$

$$k = \text{nearest integer to } \frac{\text{sign}(\phi_S')}{2}\left(\frac{\phi_F'}{\phi_S'} - 1\right)$$

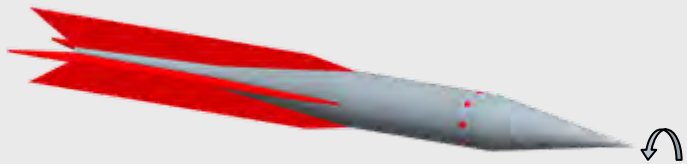
Example: GSP Shell

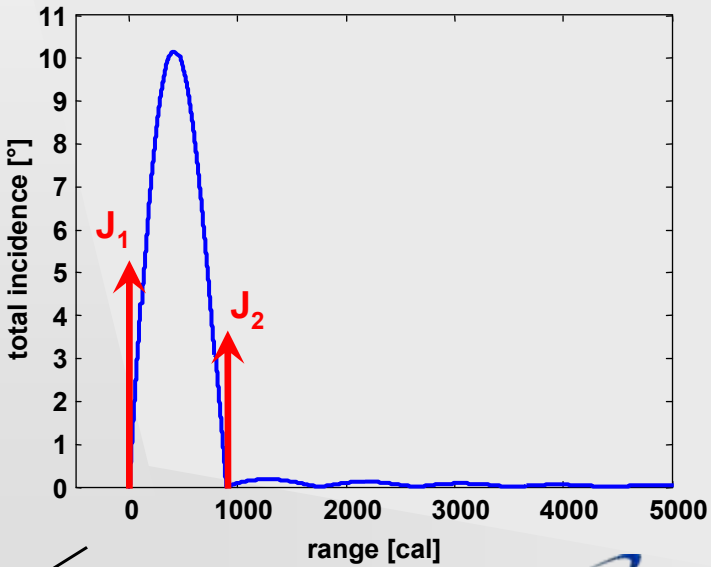
d	m	I_y	Mach	p	CD_0	CLα	CYpα	Cmα	Cmq
30 mm	0.7 kg	5.04e-3 kgm^2	3.5	22 Hz	0.19	7.6	~ 0	-5.3	~ -300

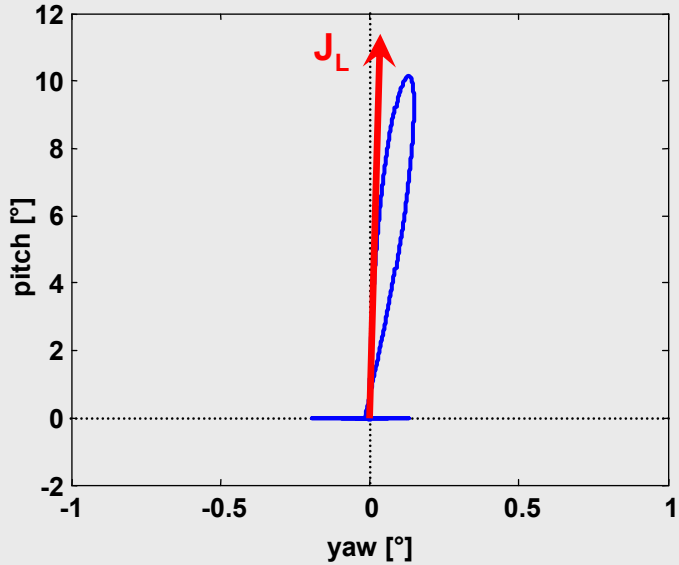
	L_J	2.5 cal
(actual)	J_1	2.0 N·s
	J_2	1.4 N·s
(26.5 m or 22.3 ms)	$s_2 - s_1$	885 cal
	$\bar{\alpha}_{max}$	10.1°

V_J	4.75 m/s
V_L	16.63 m/s
$\Delta\phi$	0.09°
V_Y	0 m/s
V_{D2}	3.98 m/s

GAIN	3.48

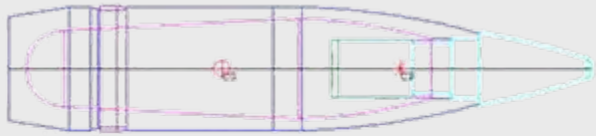






Example: 105 mm Artillery Shell (1/2)

d	m	I_y	Mach	p	CD_0	CLα	CYpα	Cmα	Cmq
105 mm	15.05 kg	2.19e-1 kgm^2	1.5	310 Hz	0.375	2.12	-0.8	3.6	-17

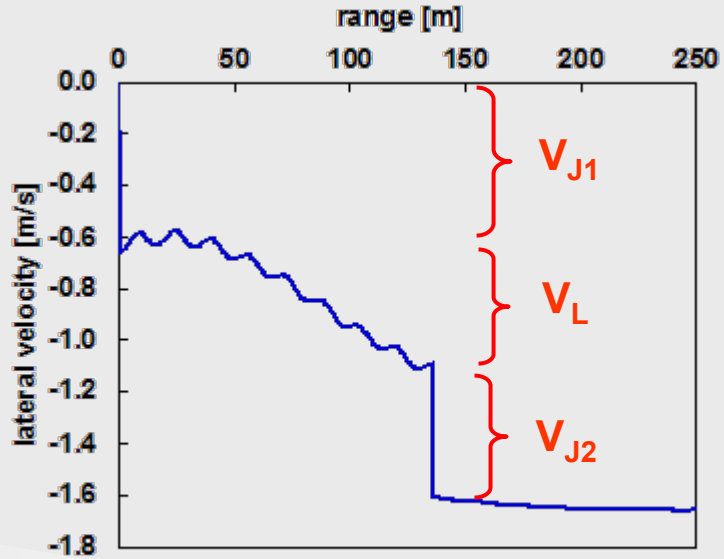




L_J	-0.51 cal
J_1	10 N·s
J_2	7.83 N·s
$s_2 - s_1$	1293 cal
$\bar{\alpha}_{max}$	1.5°

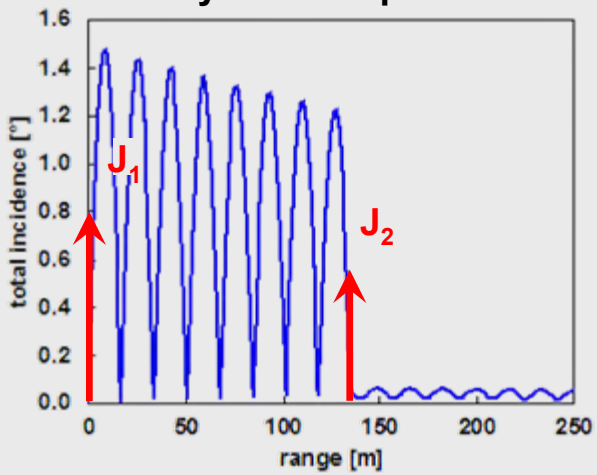
(135.6 m)

V_J	1.18 m/s
V_L	0.36 m/s
$\Delta\phi$	-3.5°
V_Y	0.05 m/s

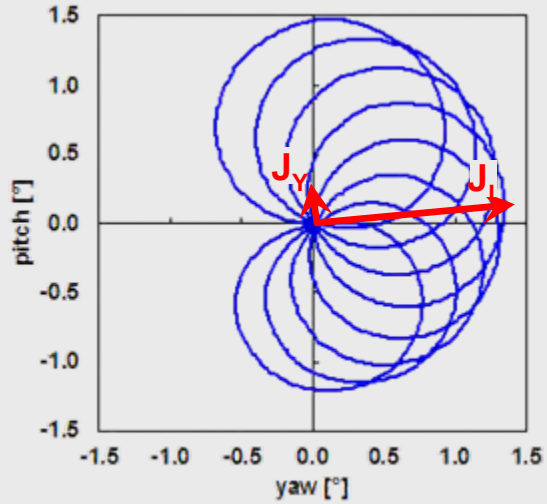


Example: 105 mm Artillery Shell (2/2)

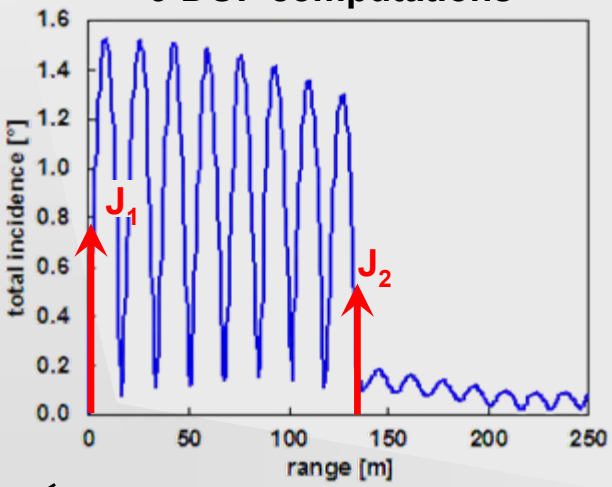
Analytical computations



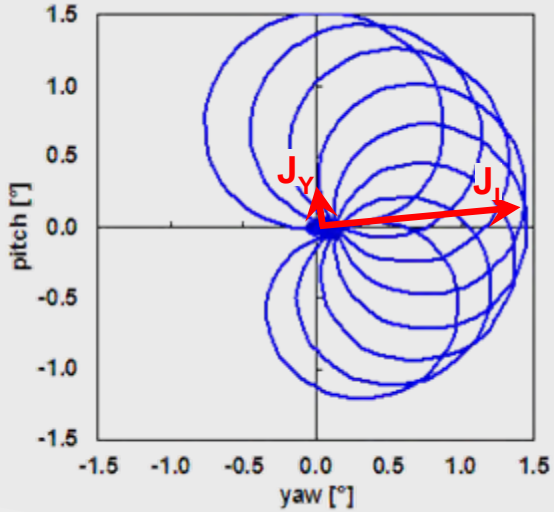
Analytical computations



6-DOF computations



6-DOF computations



ISL DEFENCE R&D DÉFENSE

Conclusions

- An analytical model was developed to predict the angular motion of a projectile subjected to impulse thrusters
- The analytical model predicts the projectile's angular motion very well
- A procedure to properly paired impulses in order to minimize the drag while maximizing the lateral velocity was developed
- The gain in lateral velocity obtained from the induced angular motion is significant

Multiple Effects Warheads for Defeat of Urban Structures and Armour

Anthony J Whelan

24th ISB presentation (New Orleans)



23rd September 2008

www.QinetiQ.com/iX

© Copyright QinetiQ limited 2008

Contents

01 Background

- Defeat of Armour and Structures
- Lethal Mechanisms
- Supporting Technologies
- Combining Technologies

02 Design Study

- Break-in-Charge
- Main warhead
- Tandem Interaction

03 Firing Programme

- Break-in-Charge
- Main warhead

04 Conclusions



Images courtesy of Jane's Information Group

© Copyright QinetiQ limited 2008

01 Background - Defeat of Armour and Structures

Example Targets

- Heavy armour
  - MBT
- Medium armour
  - MRT, SPG, LAFV
- Light armour
  - Logistics, Improvised carrier (Pick-up)
- Urban structures
  - Double skin brick – sand bag fortified
  - Concrete panel – double steel reinforcement



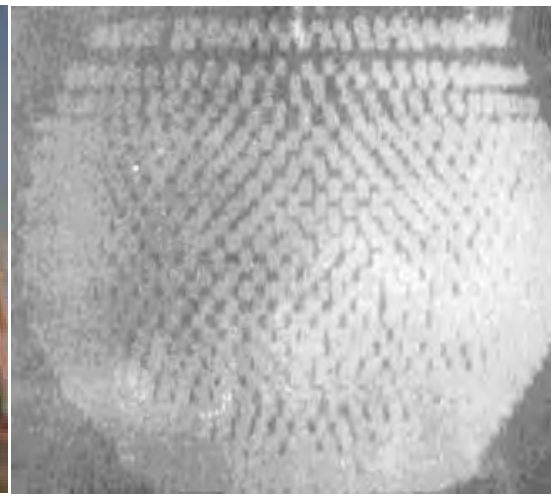
Images courtesy of Jane's Information Group

© Copyright QinetiQ limited 2008

01 Background - Lethal Mechanisms

Several lethal mechanisms required to achieve defeat across the target spectrum

- Blast
- Fragmentation
- Chemical energy – shaped charge, EFP or Slow Stretching Jet (stretching EFP)


© Copyright QinetiQ limited 2008

01 Background – Supporting Technologies

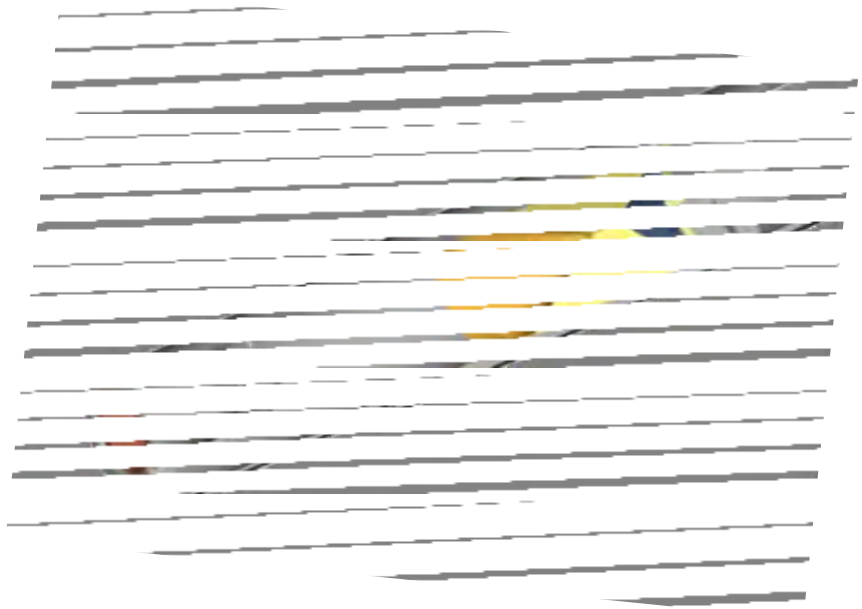
Urban Assault Weapon Programme

- Focussed on structures defeat
  - Utility against light/medium armour
  - Man portable – shoulder launched



High Performance Shaped Charge

- Focussed on heavy armour defeat
  - Tandem shaped charge
  - Crew portable and Air launched

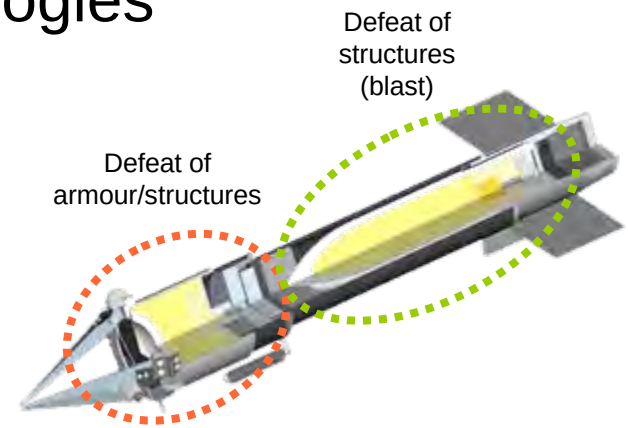


© Copyright QinetiQ limited 2008

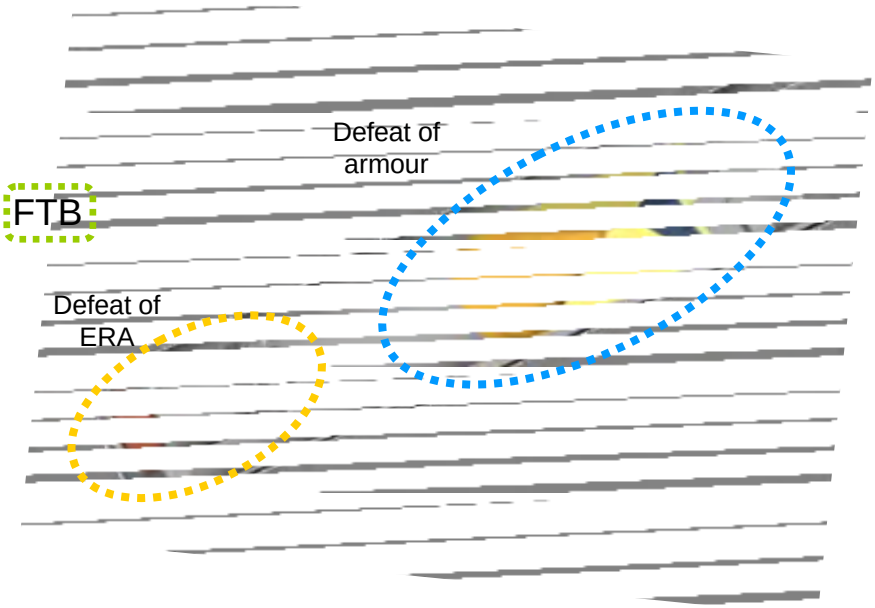
01 Background – Combining Technologies

Enable defeat of armour and structures

- Precursor
  - Combine traditional precursor and BiC warhead functionality



- Main Charge
  - Combine high performance shaped charge with FTB function

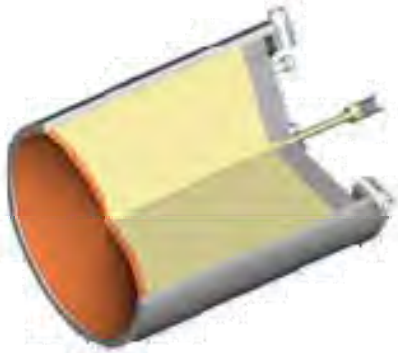


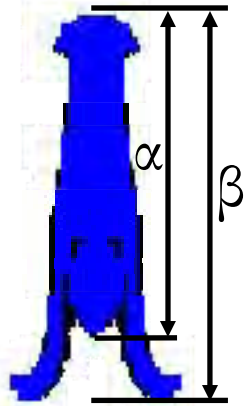
© Copyright QinetiQ limited 2008

02 Design Study – Break-in-Charge

Baseline BiC - SSJ

- EDC1s filled warhead design

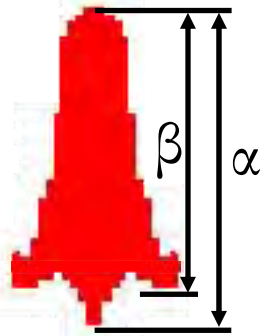




MEW BiC - CSSJ

- PBX filled warhead design
  - PBX replacement – aiding IM compliance
  - Use of PBX reduced CJ pressure by ~7%





Warhead design

- GRIM 2D hydrocode
  - Mass reduced by 30%
  - Volume reduced by 35%
  - 4% reduction in length of central portion of projectile (α)

© Copyright QinetiQ limited 2008

02 Design Study - Break-in-Charge

Target defeat modelling

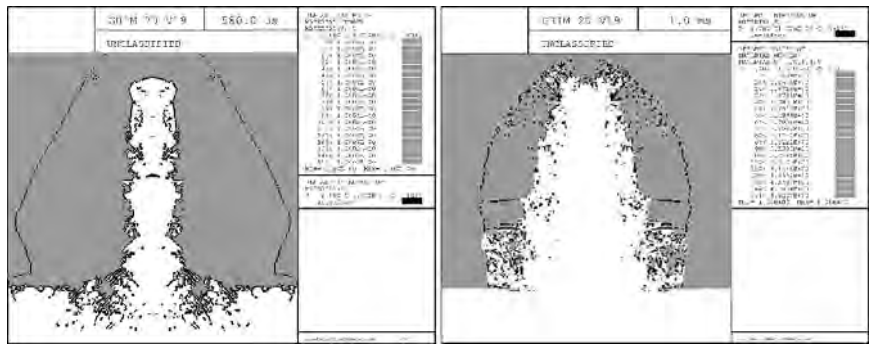
- RHA perforation – hole diameter
  - CSSJ 82% of Baseline hole diameter



SSJ CSSJ

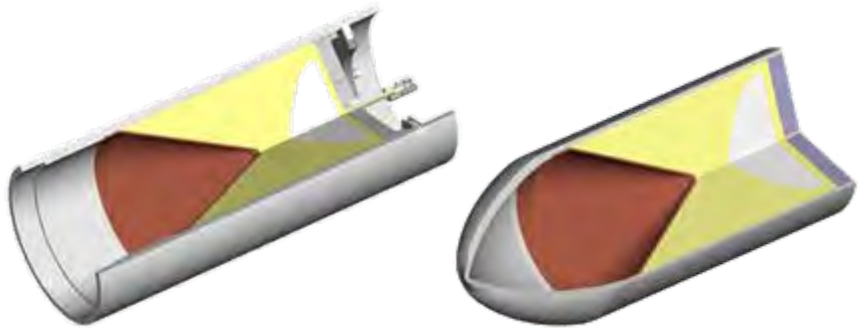
- Concrete penetration

Whd Type	Stand-off (CD)	Bore Depth	Minimum Bore Diameter (CD)	Throat Diameter (CD)
SSJ	1	100%	100%	100%
CSSJ	1	98%	181%	211%



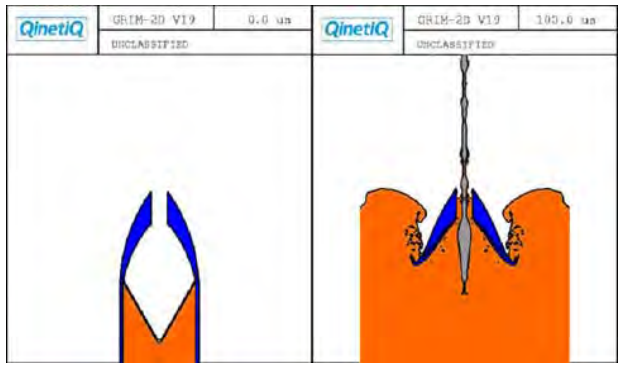
© Copyright QinetiQ limited 2008

02 Design Study – Main Warhead

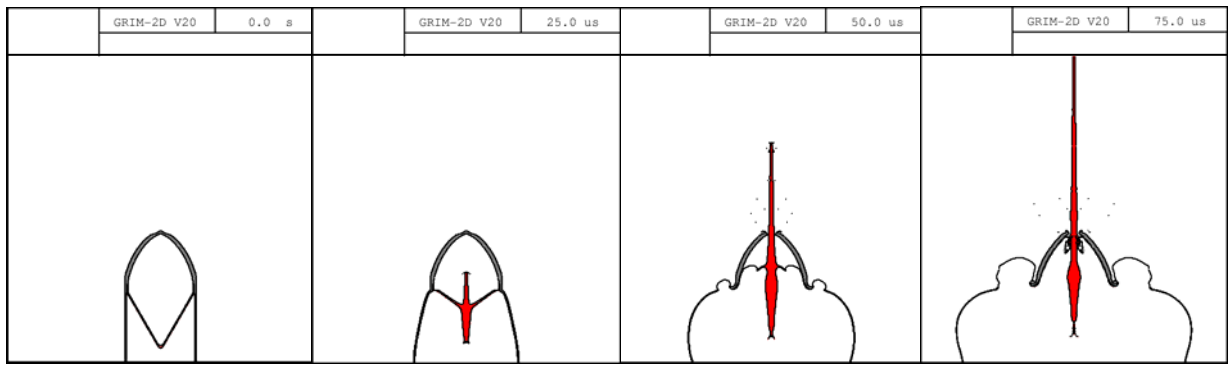


Hydrocode modelling study

- Changes made in several areas
  - Casing material – Aluminium to Steel
  - Casing geometry – inclusion of Ogive
  - Initiation geometry – increase in initiation angle
  - Explosive fill – EDC1s to PBXN-110



Initial design - heavy Ogive



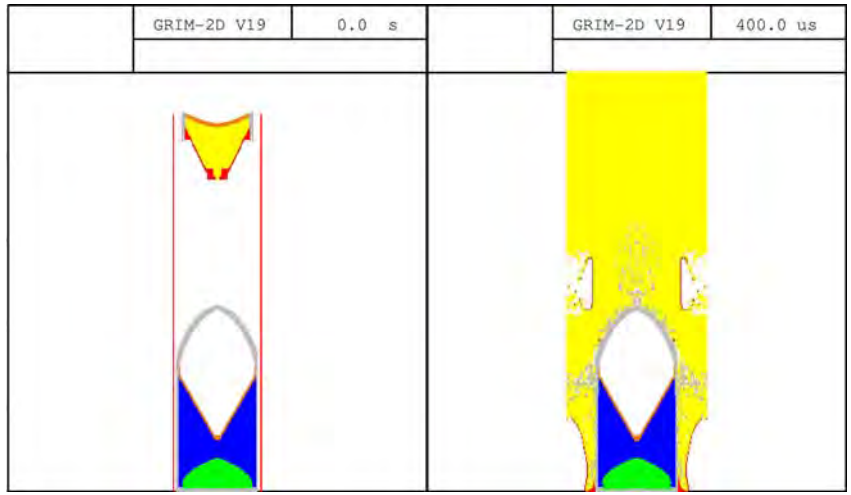
Final design – light Ogive

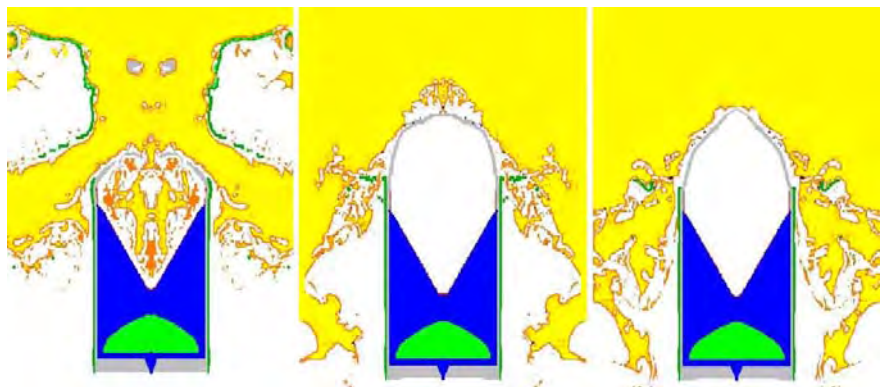
© Copyright QinetiQ limited 2008

02 Design Study – Tandem Interaction

Hydrocode modelling study

- Fixed inter-charge spacing
  - Commensurate with in-service ATGWs
  - No inter-charge barrier
- Several iterations
  - Ogive profile
  - Main warhead casing material – Aluminium to Steel
  - Precursor warhead – Polymer composite rear half of casing
- Survival of main charge





© Copyright QinetiQ limited 2008

03 Firing Programme - Break-in-Charge

BiC warhead Trials

- Anti-structures trial
  - Fortified domestic target
  - Municipal C40 concrete
    - Double steel reinforcement (1/2” bar) to front and rear of target



Double skin brick wall



Sandbag reinforcement to rear of brick wall



Steel reinforced concrete wall

- Trial Results
  - Increase in hole diameter noted
  - Performance level maintained
    - Defeat of targets at normal and 45° obliquities



1.5 CD



2 CD

90° attack



4.5 CD



2.5 CD

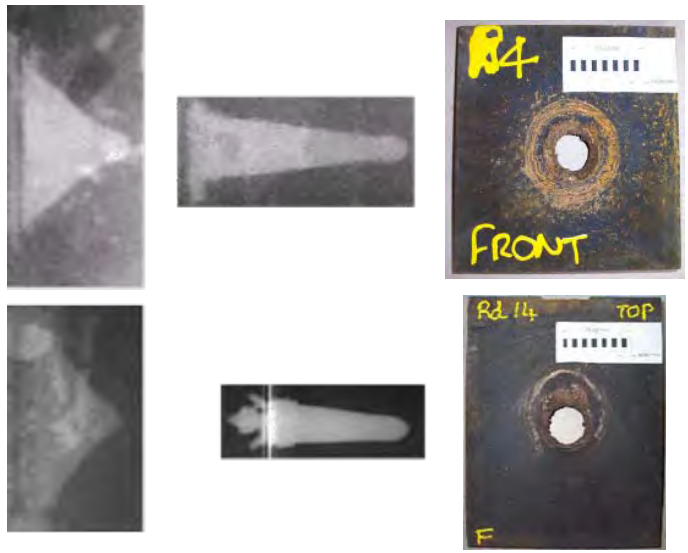
45° attack

© Copyright QinetiQ limited 2008

03 Firing Programme - Break-in-Charge

BiC warhead Trials

- Anti-armour trial
  - RHA plate
  - MBT heavy ERA
- Performance levels
  - Baseline BiC
    - 0.4 CD through hole
  - MEW BiC
    - 0.4 CD through hole
    - Defeat of heavy ERA targets

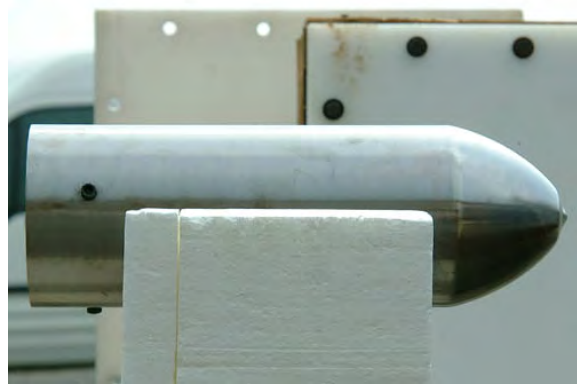


SSJ

CSSJ

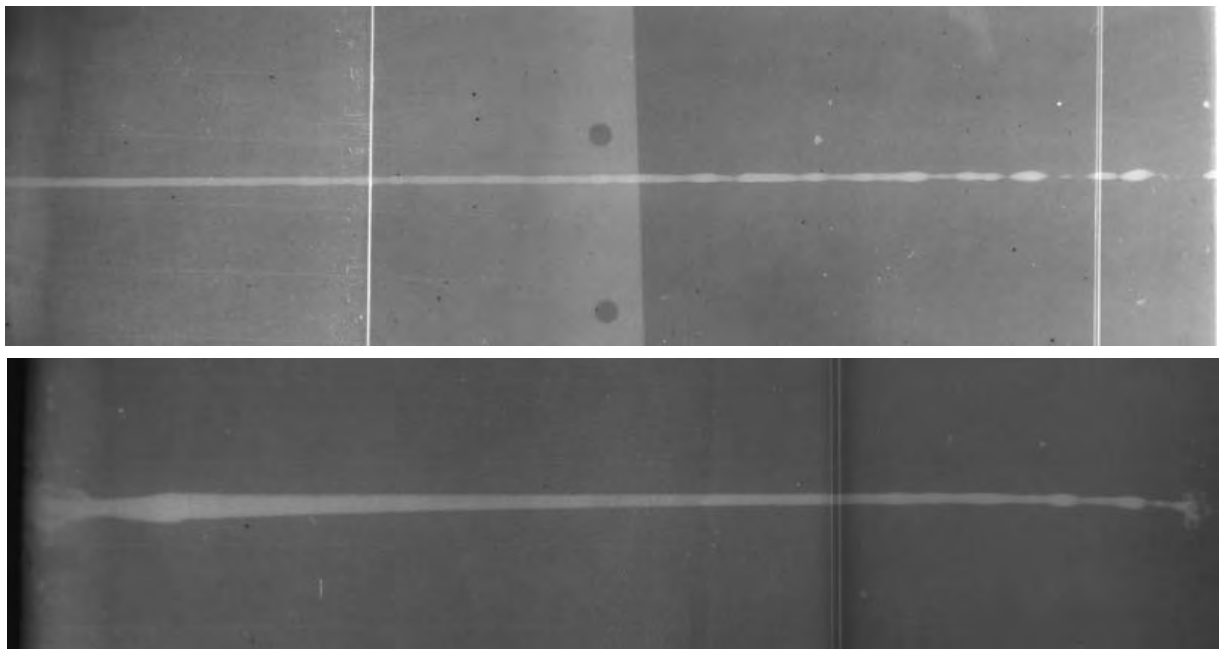
© Copyright QinetiQ limited 2008

03 Firing Programme – Main Warhead



Static main warhead trial

- Variability in warhead performance observed



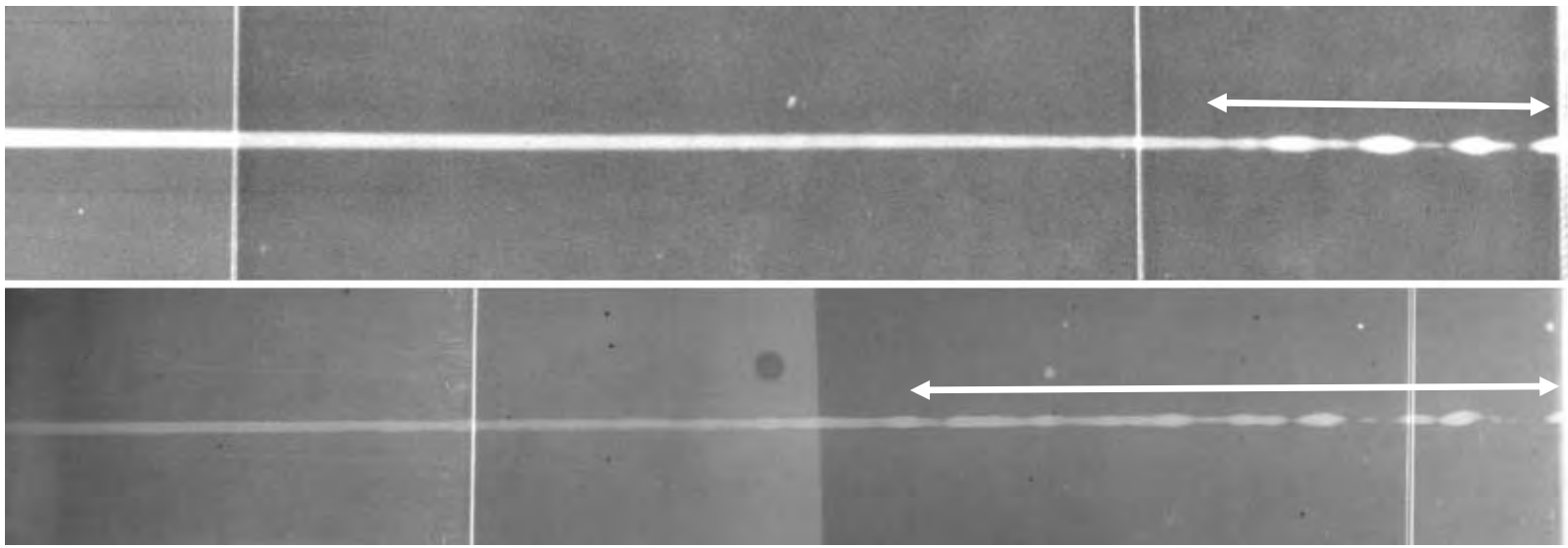
Radiography of two separate FTB/MC firings, (from top) at 100μs, and 170μs

© Copyright QinetiQ limited 2008

03 Firing Programme – Main Warhead

Comparative break-up characteristics

- On-set of break-up occurs earlier
  - Ogive interaction most probable cause



PBXN-110 filled D2 warhead with no ogive (top) PBXN-110 filled FTB/MC (bottom)

© Copyright QinetiQ limited 2008

03 Firing Programme – Main Warhead

Eight main warheads fired

- Firings against RHA
  - Def-Stan 95-13 RHA
  - Various stand-offs
- Large reduction in penetration
  - Jet curvature main cause

Warhead #	Stand-off (CD)	*Average Penetration Reduction (%)	Notes
1	8	19	Jet curvature observed, Jet velocity 8.5mm/μs
2	4	N/A	
3	4	N/A	
4	5	N/A	Jet curvature observed on radiography
5	5	N/A	Curvature at front of jet, jet tip unusual geometry
6	10	17	Target key-holed, jet particulation appears advanced
7	8	19	Jet curvature observed on radiography
8	8	19	Jet velocity 8.65mm/μs

*Average values are those of PBXN-110 filled precision shaped charge

© Copyright QinetiQ limited 2008

04 Conclusions

BiC Warhead

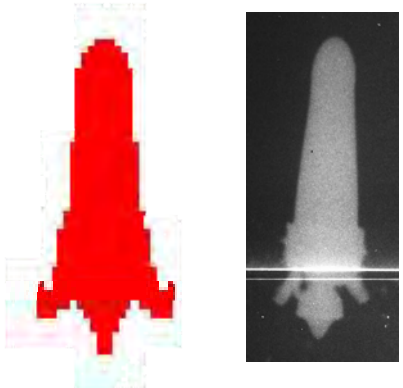
- Performance level maintained
  - More IM compliant explosive
  - Reduced overall mass and volume

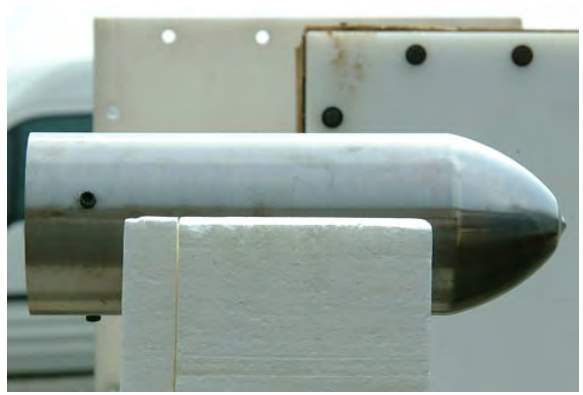
Main Warhead

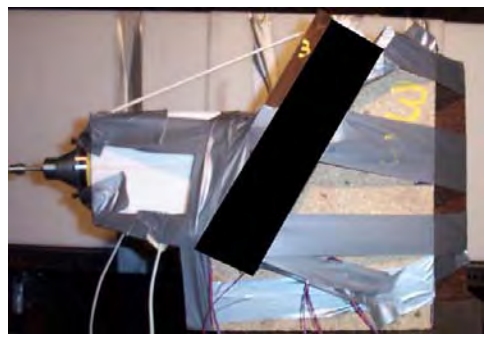
- Reasonable level of RHA penetration
  - Jet curvature through initiation inaccuracies – major loss in performance
  - Ogive – jet interaction

Tandem Interaction

- Hydrocode modelling
  - Main charge appears unaffected by BiC 400µs after detonation







© Copyright QinetiQ limited 2008

04 Conclusions

Overall concept

- Tandem interaction must be observed
  - Current research work is investigating this issue
- Design for production
  - Minor changes required to accommodate through life issues
    - Expansion/contraction of explosive fill under service environment
    - FCO/SCO design features
- Compliancy with system mass/centre of gravity constraints
  - Use in crew portable system
    - Requires re-engineering of warhead solution
  - Use in air launched system
    - No major changes envisaged

© Copyright QinetiQ limited 2008

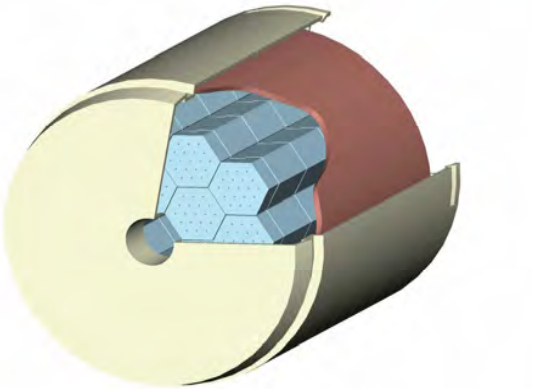


Independent expertise where it matters most.

www.QinetiQ.com/iX

© Copyright QinetiQ limited 2008

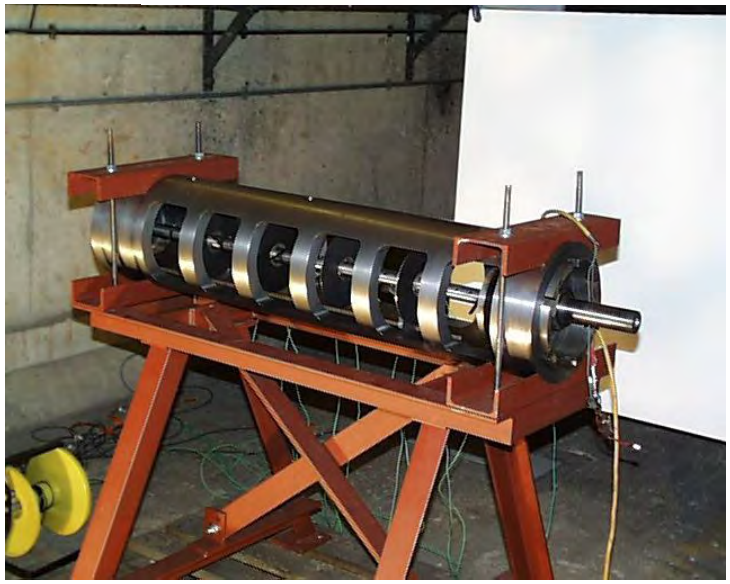
PDF Complete
Your complimentary use period has ended. Thank you for using PDF Complete.
Click Here to upgrade to Unlimited Pages and Expanded Features



Two-dimensional modelling of modular charge gun firings

Clive Woodley, Steve Fuller

A presentation to: 24th International Symposium on Ballistics



September 2008

QinetiQ

www.QinetiQ.com

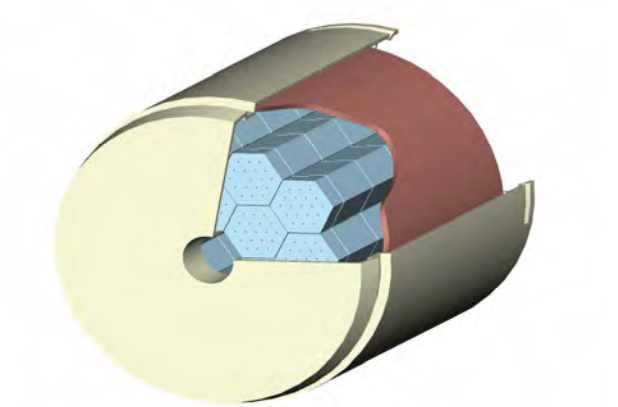
© Copyright QinetiQ limited 2008

PDF Complete
Your complimentary use period has ended. Thank you for using PDF Complete.
Click Here to upgrade to Unlimited Pages and Expanded Features

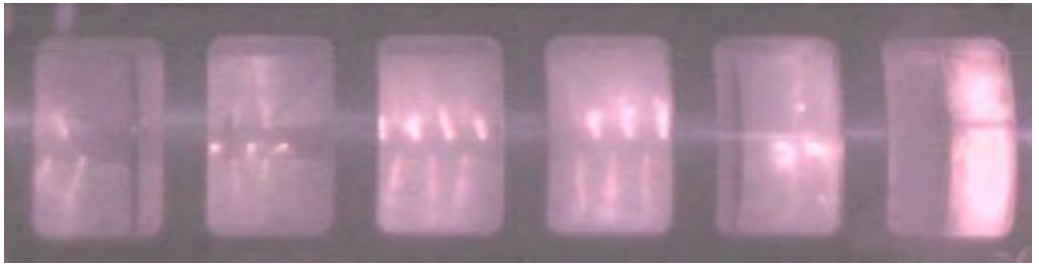
01 Description of UPCS2

02 Description of QIMIBS

03 IB modelling of UPCS2



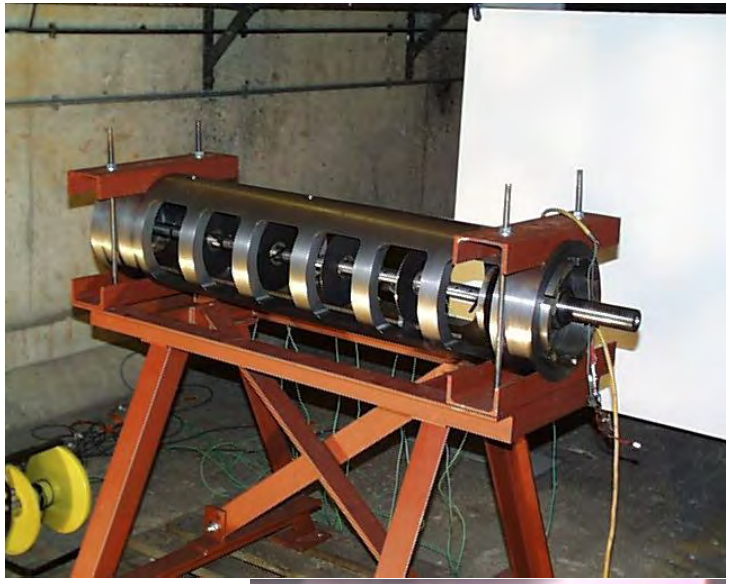


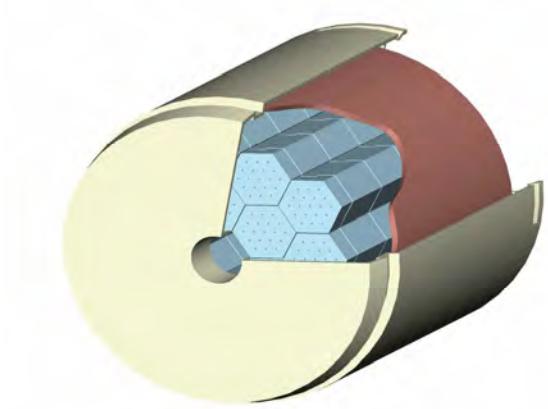


© Copyright QinetiQ limited 2008

PDF Complete
Your complimentary use period has ended. Thank you for using PDF Complete.
Click Here to upgrade to Unlimited Pages and Expanded Features

01
Description of UPCS2







© Copyright QinetiQ limited 2008

PDF Complete
Your complimentary use period has ended. Thank you for using PDF Complete.
Click Here to upgrade to Unlimited Pages and Expanded Features

CS?

Existing 155mm charge inventory replaced with 1 module



© Copyright QinetiQ limited 2008

PDF Complete
Your complimentary use period has ended. Thank you for using PDF Complete.
Click Here to upgrade to Unlimited Pages and Expanded Features

bjectives

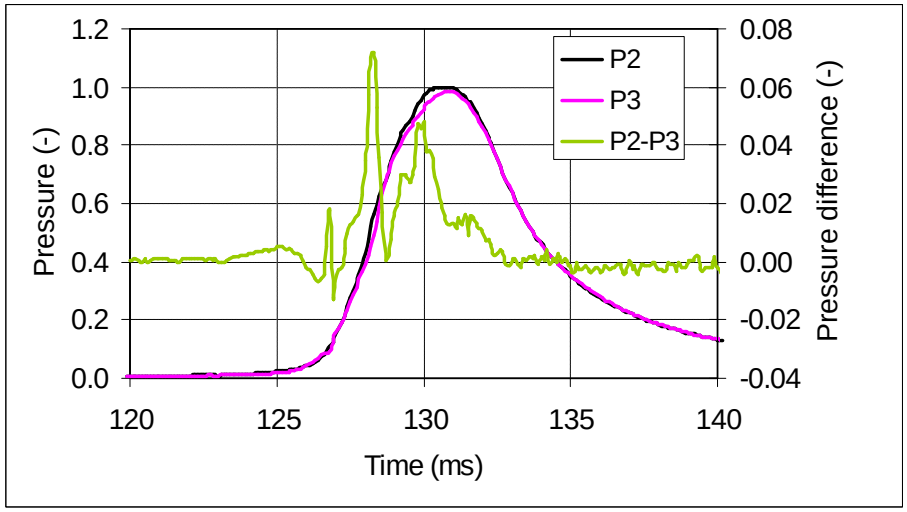
- To determine temperature coefficient data for experimental propellant under gun firing conditions
- To determine top zone performance for experimental propellant
- To determine low zone performance for experimental propellant
- **To investigate the performance of the ignition system**

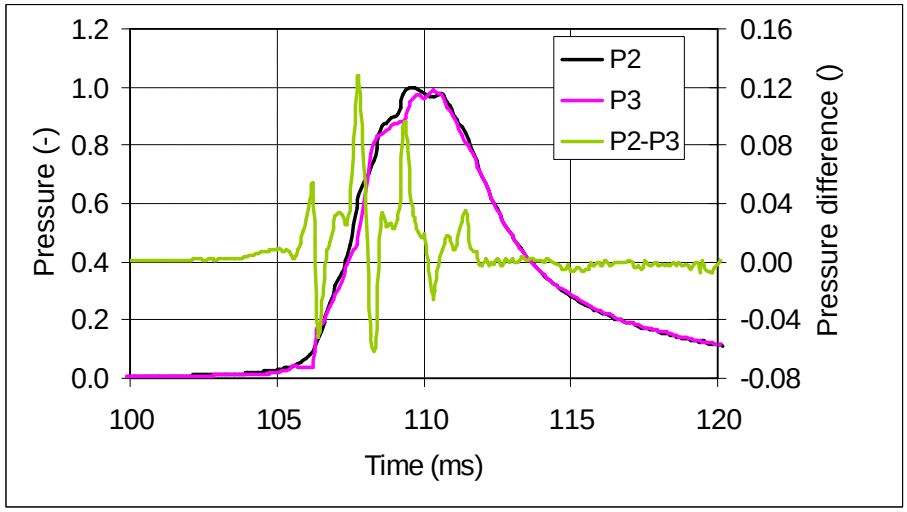
© Copyright QinetiQ limited 2008

PDF Complete
Your complimentary use period has ended. Thank you for using PDF Complete.
Click Here to upgrade to Unlimited Pages and Expanded Features

some results

- Smooth pressure-time profiles were recorded for Z2 and Z3 charges.
- A smooth pressure time profile at zone 4 (+21^{0}C) was also observed
- But so was a ónot so smooth curveô



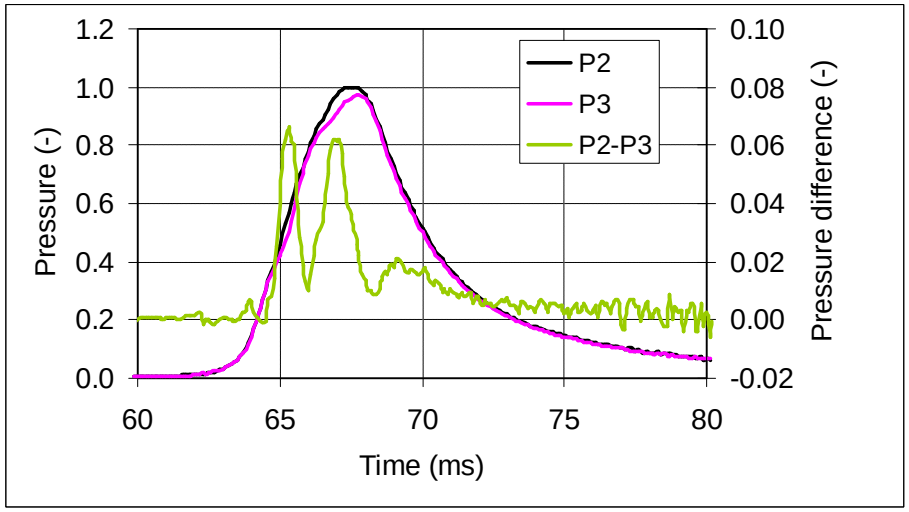


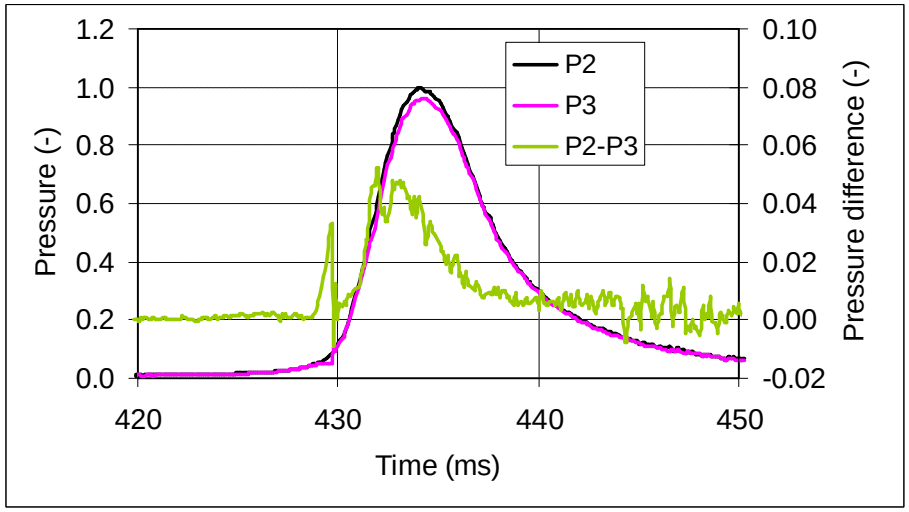
© Copyright QinetiQ limited 2008

PDF Complete
Your complimentary use period has ended. Thank you for using PDF Complete.
Click Here to upgrade to Unlimited Pages and Expanded Features

some results

- Results at zone 4 at 63^{0}C and -33^{0}C were acceptable



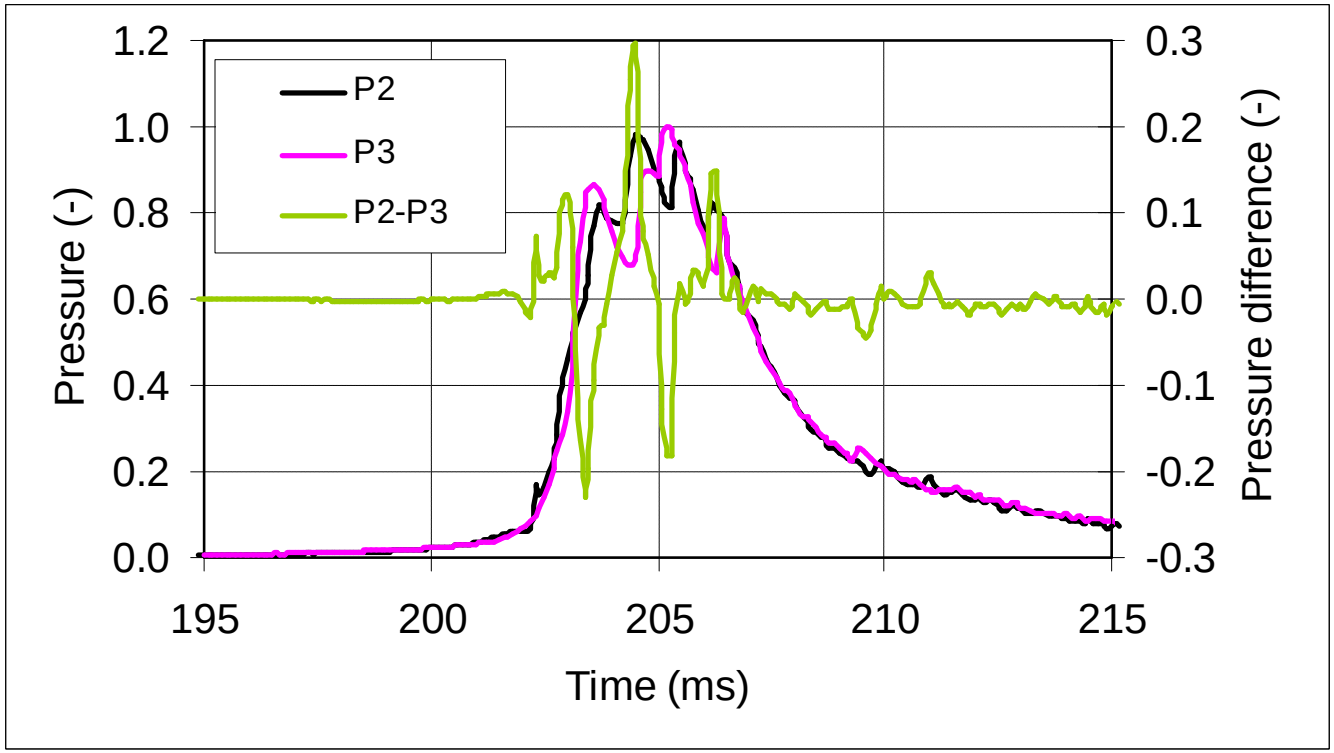


© Copyright QinetiQ limited 2008

PDF Complete
Your complimentary use period has ended. Thank you for using PDF Complete.
Click Here to upgrade to Unlimited Pages and Expanded Features

some results

- 4.5 modules at -33C gave bad results!
- The firing mechanism was forcibly ejected from the gun breech with a substantial velocity



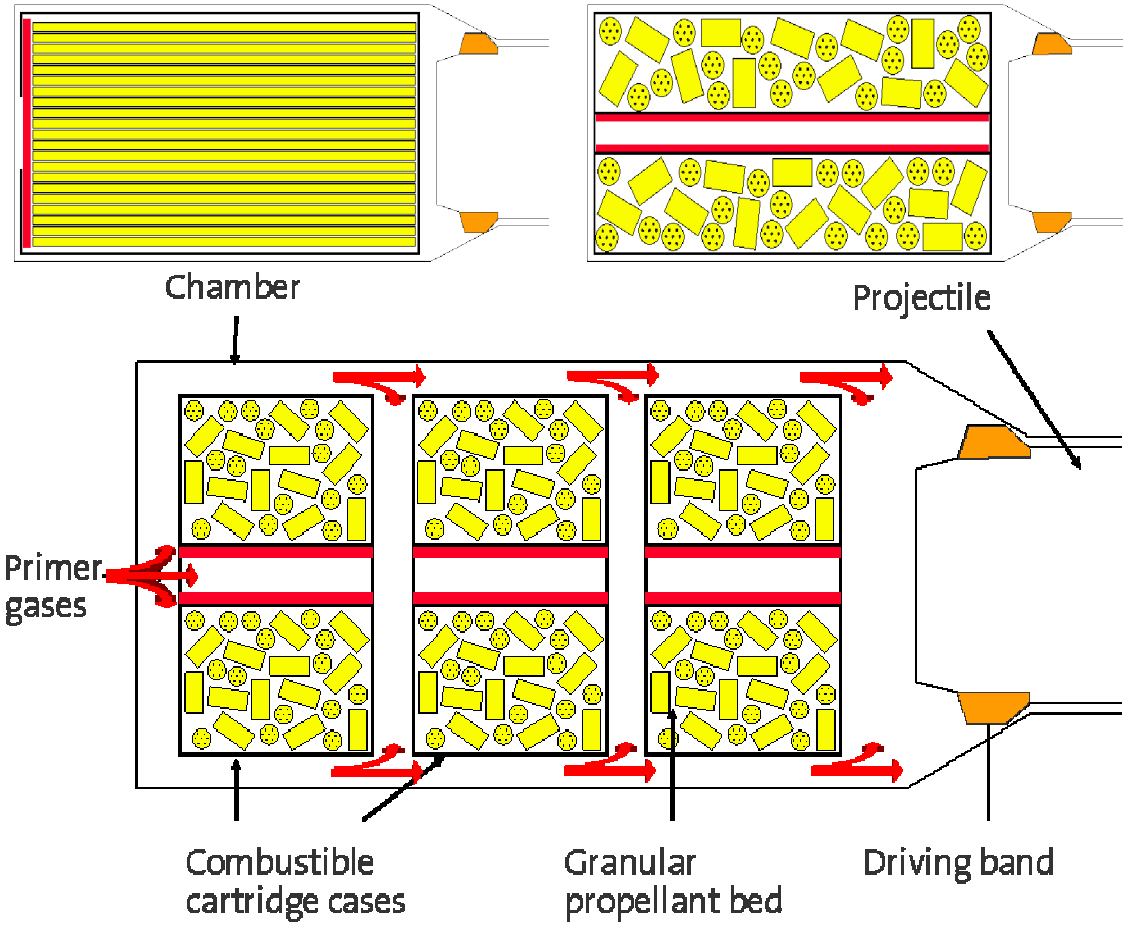
© Copyright QinetiQ limited 2008

PDF Complete
Your complimentary use period has ended. Thank you for using PDF Complete.
Click Here to upgrade to Unlimited Pages and Expanded Features

cs background

Safety & performance are important requirements ï linked to ignition

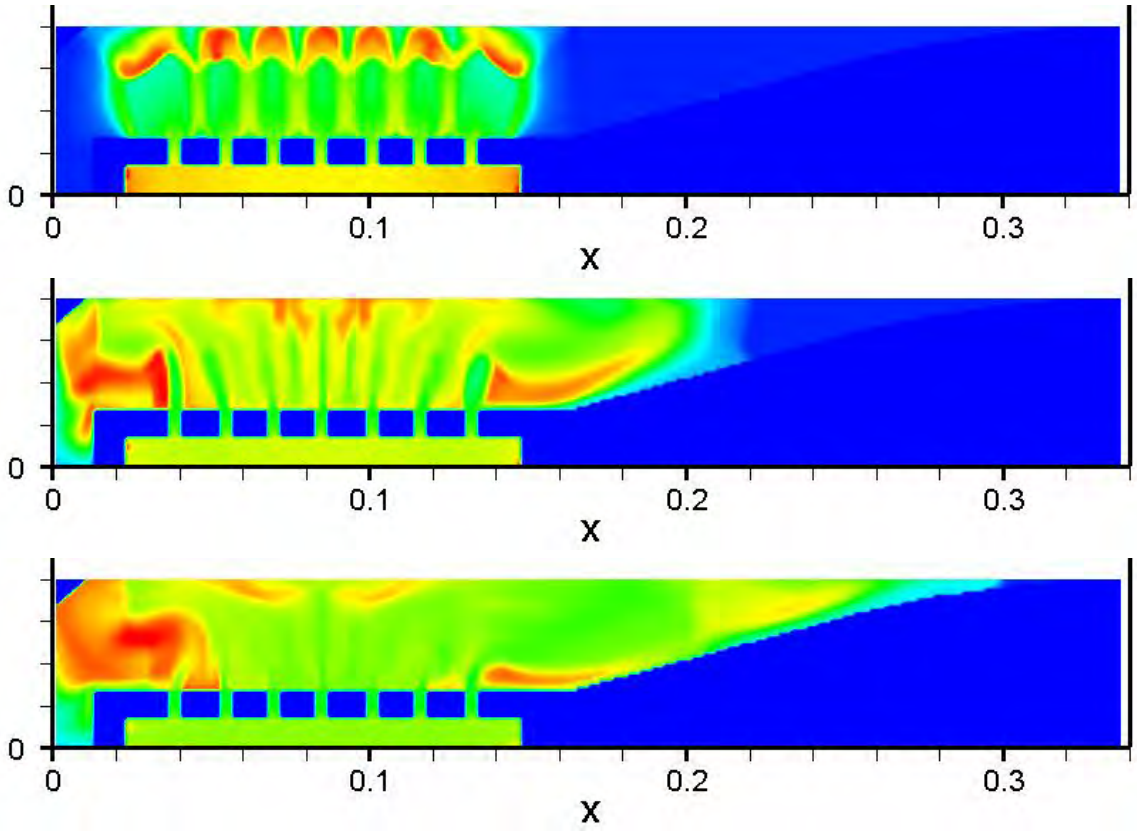
- More conventional charges, comprising stick and granular propellant, can be modelled
- Want any pressure waves to be eliminated or minimised and consistent
- Want simultaneous ignition along length of charge
- Combustible cartridge cases present barrier to flamespread along the propellant bed
- Modules act as projectiles!



© Copyright QinetiQ limited 2008

PDF Complete
Your complimentary use period has ended. Thank you for using PDF Complete.
Click Here to upgrade to Unlimited Pages and Expanded Features

02
Description of QIMIBS



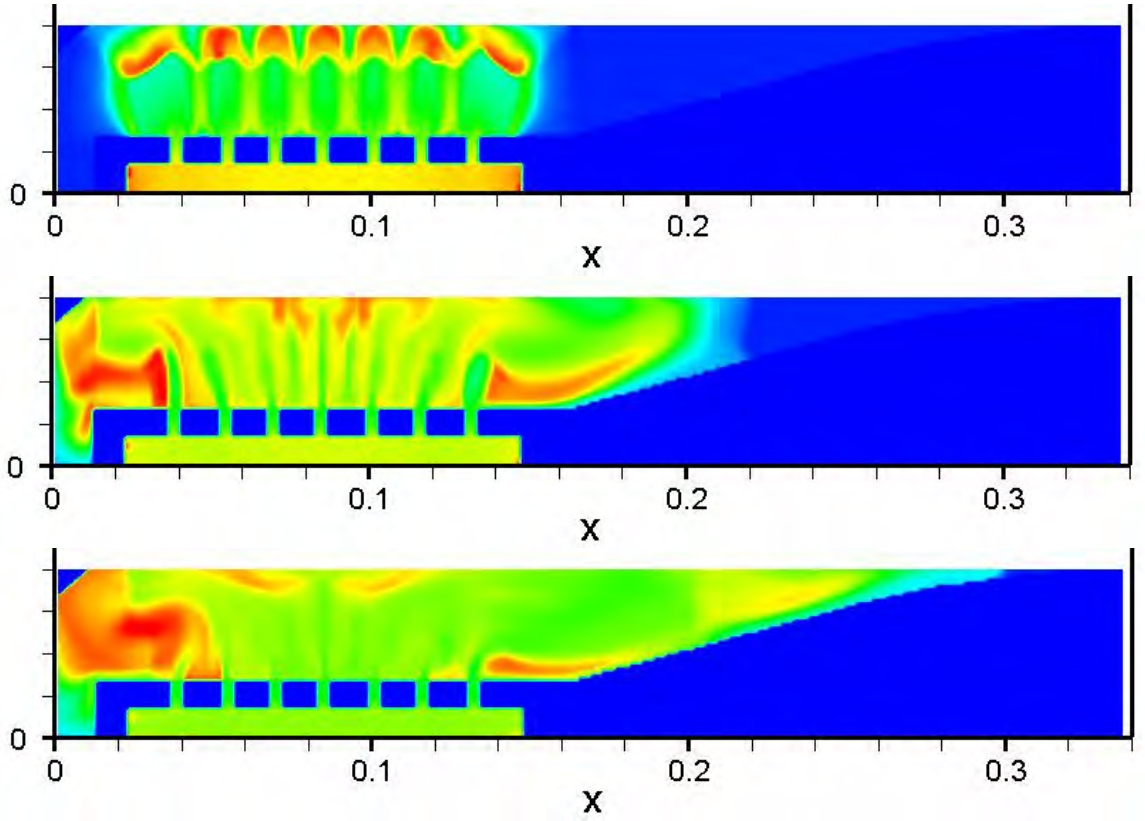
© Copyright QinetiQ limited 2008

PDF Complete
Your complimentary use period has ended. Thank you for using PDF Complete.
Click Here to upgrade to Unlimited Pages and Expanded Features

ground

2D mortar code

- Developed initially with MOD funding
- Developed further using QinetiQ funding
- Details presented at 22nd International Symposium on Ballistics
- Ability to represent internal solid boundaries and burst discs
- Modified for CTA, MCS & other applications



© Copyright QinetiQ limited 2008

PDF Complete
Your complimentary use period has ended. Thank you for using PDF Complete.
Click Here to upgrade to Unlimited Pages and Expanded Features

ase flow equations

$$\frac{\partial}{\partial t}(\rho\varepsilon) + \frac{\partial}{\partial z}(\rho\varepsilon u) + \frac{\partial}{\partial r}(\rho\varepsilon v) = -\frac{\varepsilon\rho v}{r} + \dot{m}_{ig} + \sum_{k=1}^{n} \dot{m}^k$$

$$\frac{\partial}{\partial t}(\rho\varepsilon u) + \frac{\partial}{\partial z}[\varepsilon(\rho u^2 + p)] + \frac{\partial}{\partial r}(\rho\varepsilon uv) = -\frac{\varepsilon\rho uv}{r} + p\frac{\partial\varepsilon}{\partial z} + \sum_{k=1}^{n}(\dot{m}^k u^k - f_z^k)$$

$$\frac{\partial}{\partial t}(\rho\varepsilon v) + \frac{\partial}{\partial z}(\varepsilon\rho uv) + \frac{\partial}{\partial r}[\varepsilon(\rho v^2 + p)] = -\frac{\varepsilon\rho v^2}{r} + p\frac{\partial\varepsilon}{\partial r} + \sum_{k=1}^{n}(\dot{m}^k v^k - f_r^k)$$

$$\frac{\partial}{\partial t}(\rho\varepsilon E) + \frac{\partial}{\partial z}[\varepsilon\rho u(E + p/\rho)] + \frac{\partial}{\partial r}[\rho\varepsilon v(E + p/\rho)] = -\frac{\varepsilon\rho v}{r}(E + p/\rho) + \dot{m}_{ig}Q_{ig}$$

$$-W + E_E + \sum_{k=1}^{n}[\dot{m}^k(Q_p^k + \kappa^k) - p\left(\frac{\partial(\varepsilon^k u^k)}{\partial z} + \frac{\partial(\varepsilon^k v^k)}{\partial r}\right) - u^k f_z^k - v^k f_r^k - q^k N^k S^k]$$

$$\frac{\partial}{\partial t}(\rho^k\varepsilon^k) + \frac{\partial}{\partial z}(\rho^k\varepsilon^k u^k) + \frac{\partial}{\partial r}(\rho^k\varepsilon^k v^k) = -\dot{m}^k - \frac{\varepsilon^k\rho^k u^k}{r}$$

$$\frac{\partial}{\partial t}(\rho^k\varepsilon^k u^k) + \frac{\partial}{\partial z}[\varepsilon^k(\rho^k(u^k)^2 + p + p_{is}^k)] + \frac{\partial}{\partial r}(\rho^k\varepsilon^k u^k v^k) = p\frac{\partial\varepsilon^k}{\partial z} - \frac{\varepsilon^k\rho^k u^k v^k}{r} - \dot{m}^k u^k + f_z^k$$

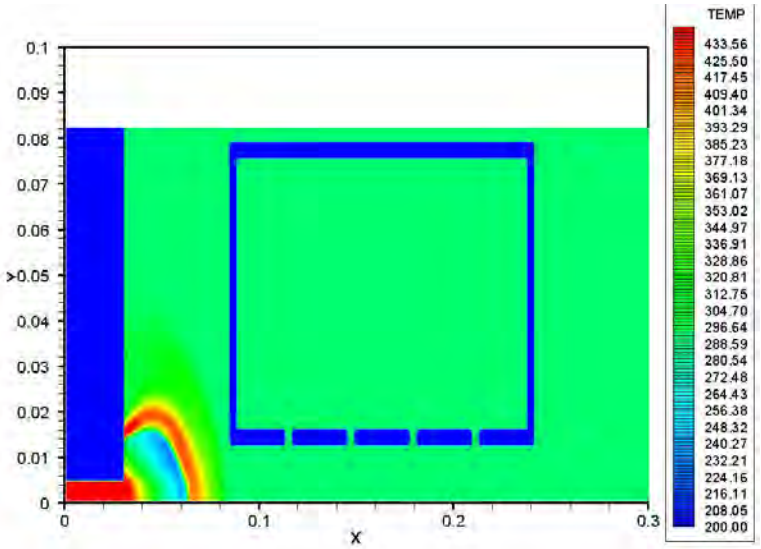
$$\frac{\partial}{\partial t}(\rho^k\varepsilon^k v^k) + \frac{\partial}{\partial z}(\varepsilon^k\rho^k u^k v^k) + \frac{\partial}{\partial r}[\varepsilon^k(\rho^k(v^k)^2 + p + p_{is}^k) = p\frac{\partial\varepsilon^k}{\partial r} - \frac{\varepsilon^k\rho^k(v^k)^2}{r} - \dot{m}^k v^k + f_r^k$$

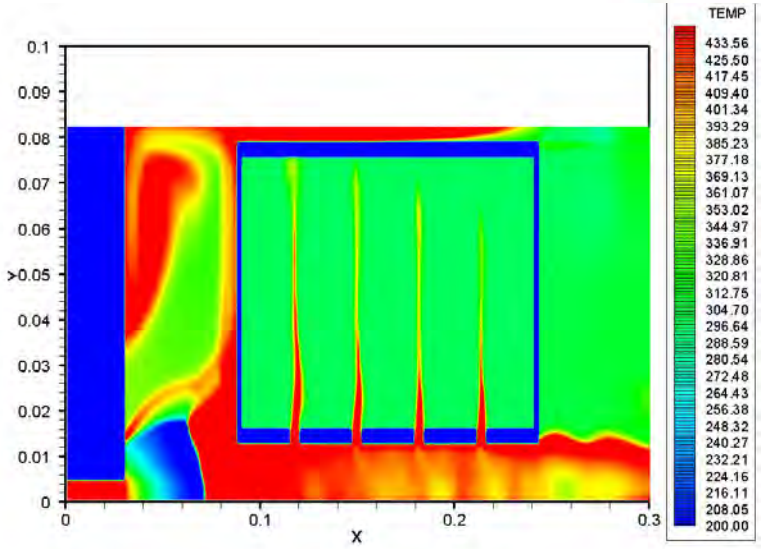
$$\frac{\partial}{\partial t}(N^k) + \frac{\partial}{\partial z}(N^k u^k) + \frac{\partial}{\partial r}(N^k v^k) = -\frac{v^k N^k}{r}$$

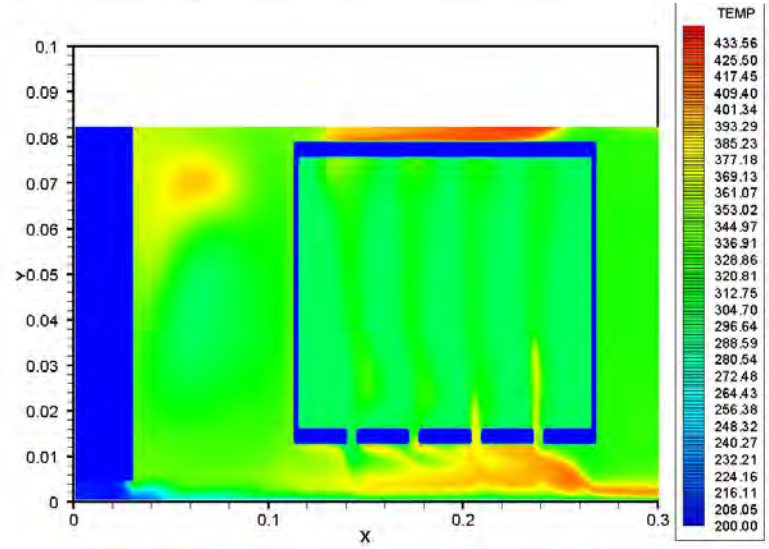
© Copyright QinetiQ limited 2008

PDF Complete
Your complimentary use period has ended. Thank you for using PDF Complete.
Click Here to upgrade to Unlimited Pages and Expanded Features

03
IB Modelling of UPCS2







© Copyright QinetiQ limited 2008

PDF Complete
Your complimentary use period has ended. Thank you for using PDF Complete.
Click Here to upgrade to Unlimited Pages and Expanded Features

modelling strategy

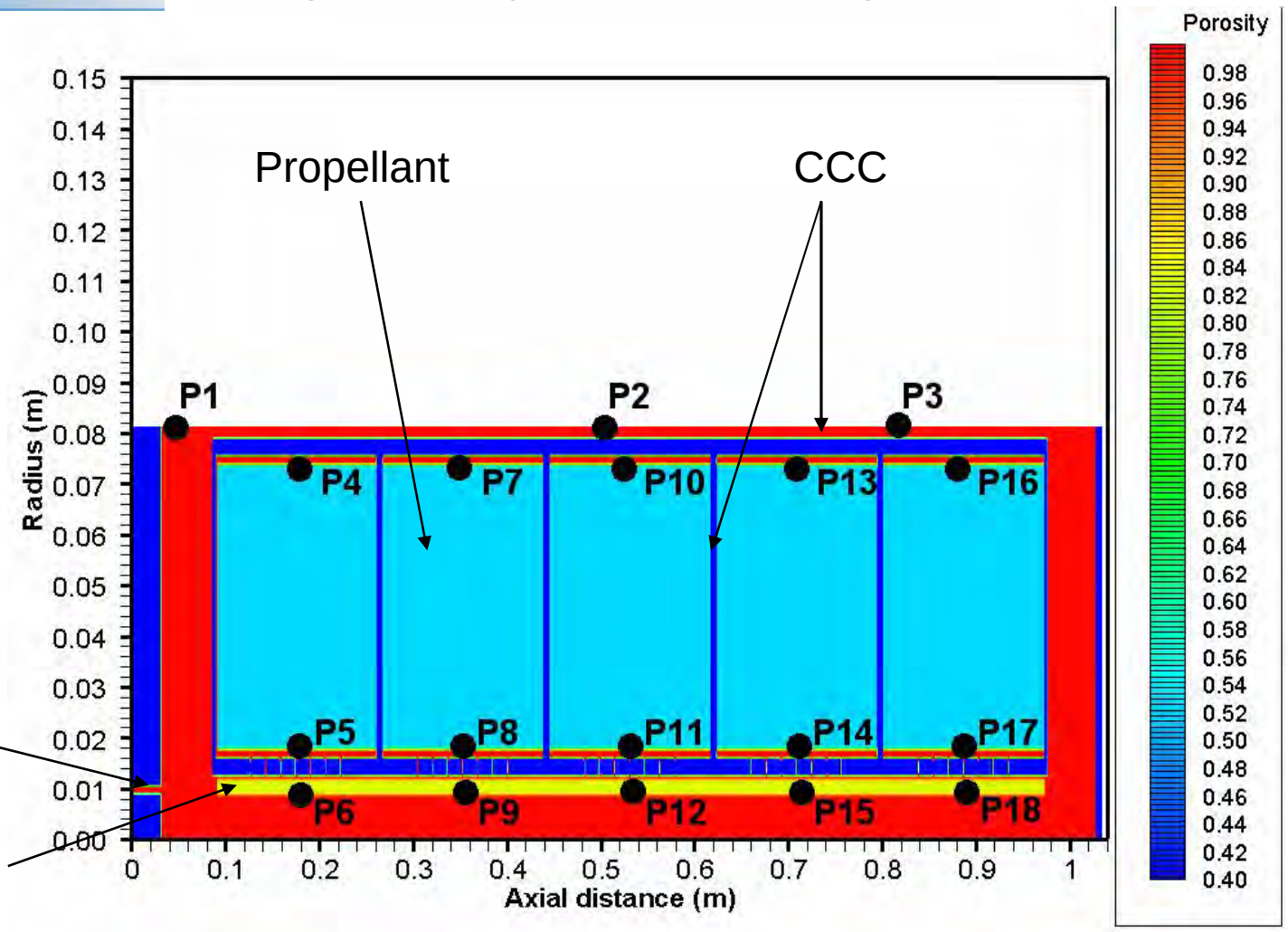
- No single code available that can model all details
- Various ignition scenarios were investigated using QIMIBS
  - Prediction of ignition time for each module
  - Ignition at breech
  - Ignition at projectile
  - Ignition at mid-chamber
- Estimated ignition delays were input to QIBS (1D code)
  - Predicted pressure profiles compared with experiment
- Ignition at breech and mid-chamber did not produce pressure profiles of desired shape
- Most likely ignition scenario was ignition adjacent to projectile

© Copyright QinetiQ limited 2008

PDF Complete
Your complimentary use period has ended. Thank you for using PDF Complete.
Click Here to upgrade to Unlimited Pages and Expanded Features

nitial geometry for modelling

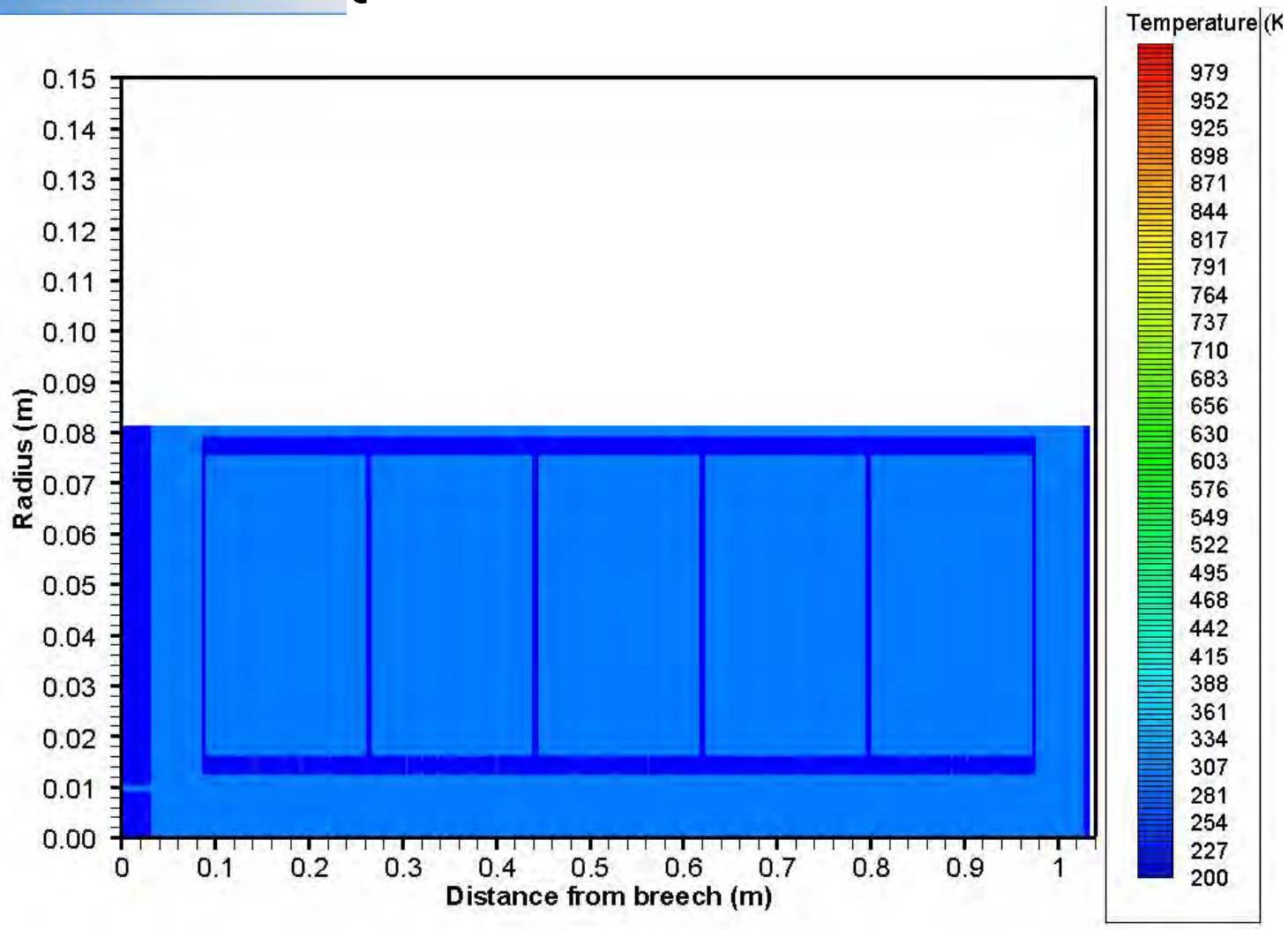
P1-P18 are fictitious pressure gauges



© Copyright QinetiQ limited 2008

PDF Complete
Your complimentary use period has ended. Thank you for using PDF Complete.
Click Here to upgrade to Unlimited Pages and Expanded Features

QIMIBS simulation

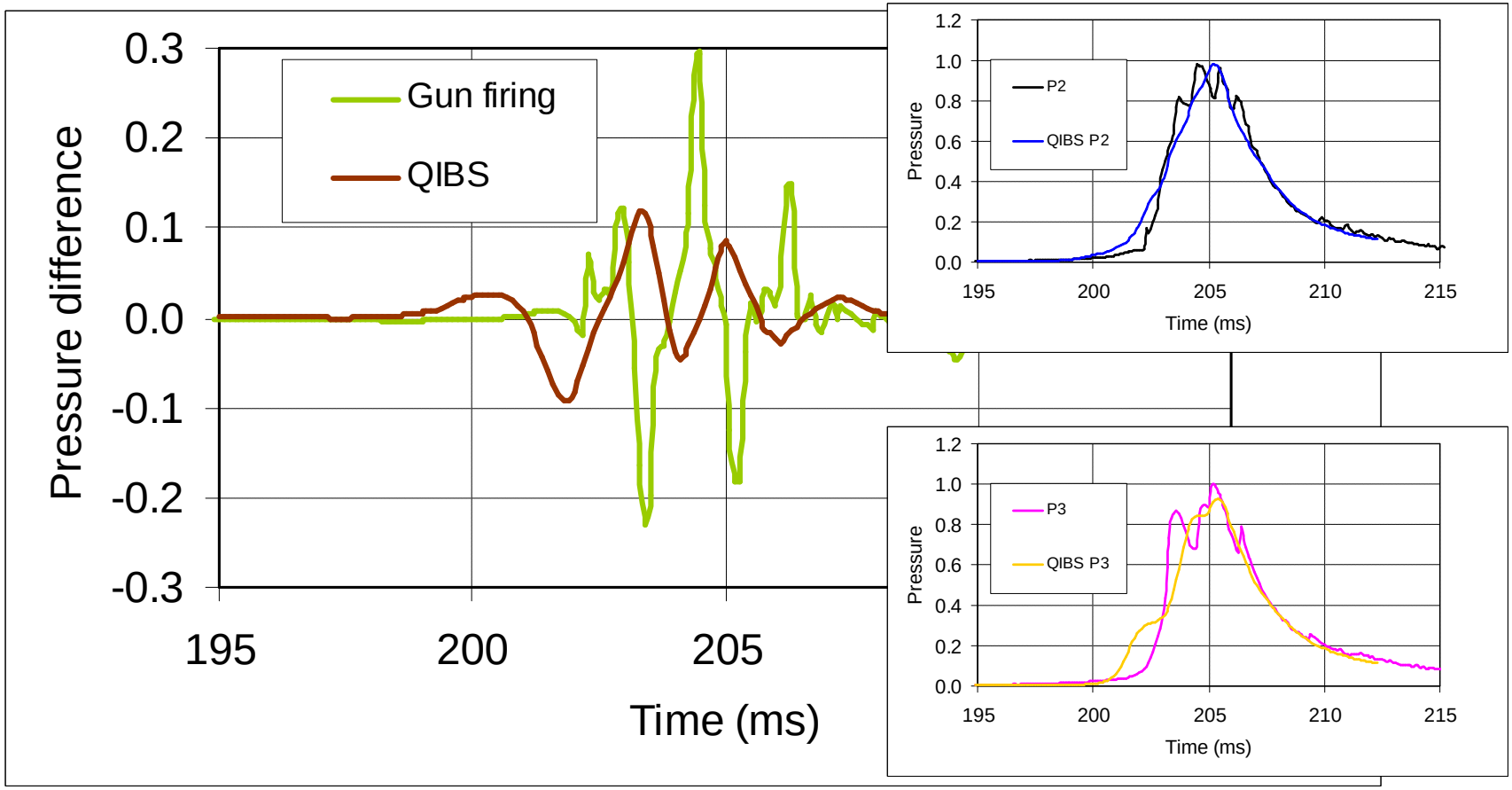


© Copyright QinetiQ limited 2008

PDF Complete
Your complimentary use period has ended. Thank you for using PDF Complete.
Click Here to upgrade to Unlimited Pages and Expanded Features

example ï breech ignition

- Predicted and measured pressure differences are out of phase

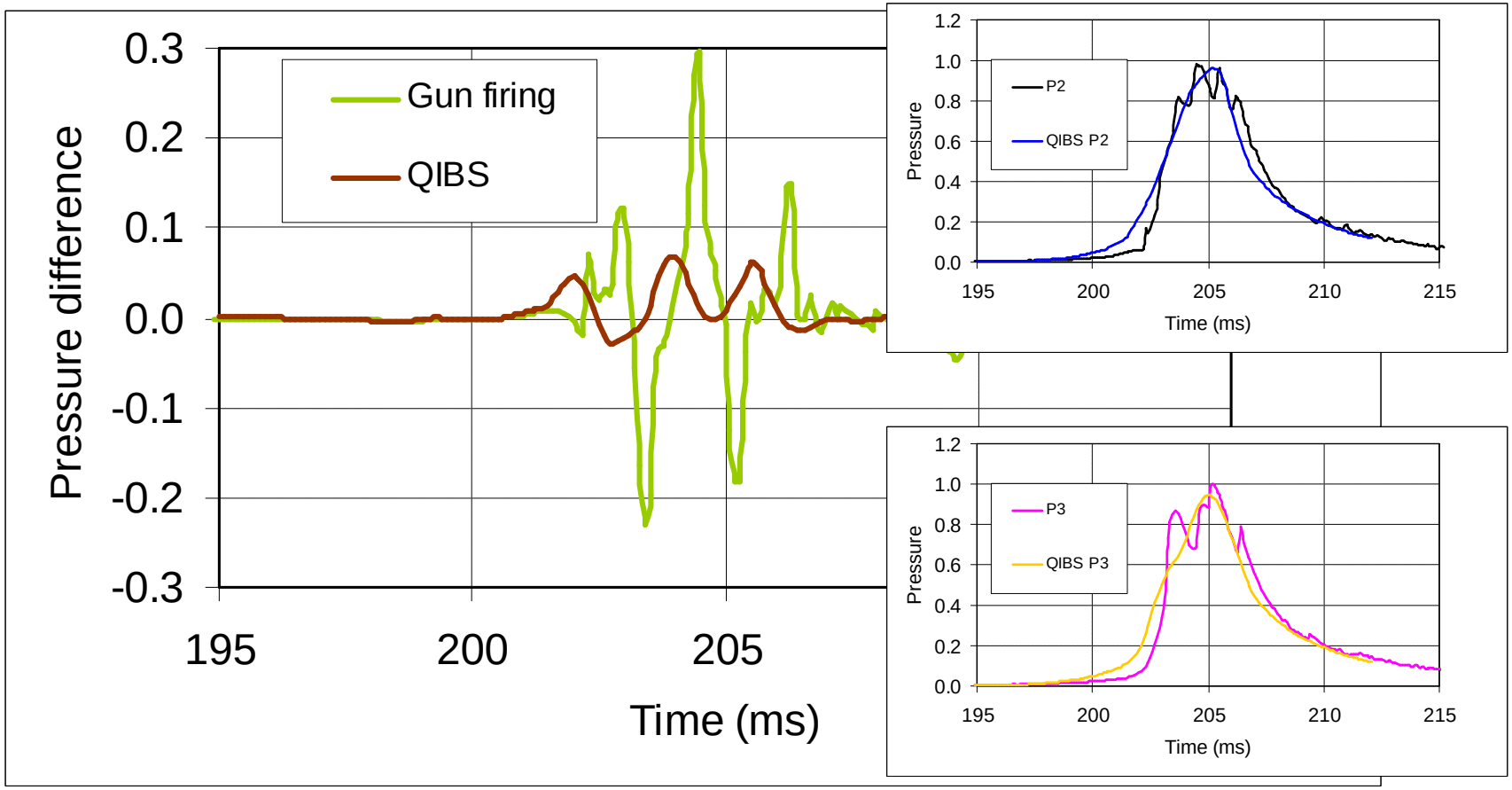


© Copyright QinetiQ limited 2008

PDF Complete
Your complimentary use period has ended. Thank you for using PDF Complete.
Click Here to upgrade to Unlimited Pages and Expanded Features

example ï ignition at projectile

- Predicted and measured pressure differences are slightly out of phase

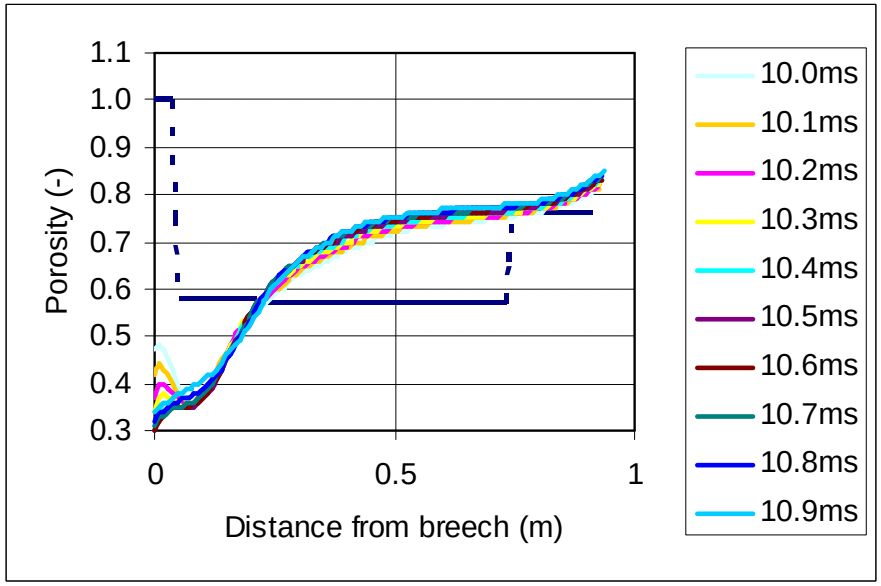


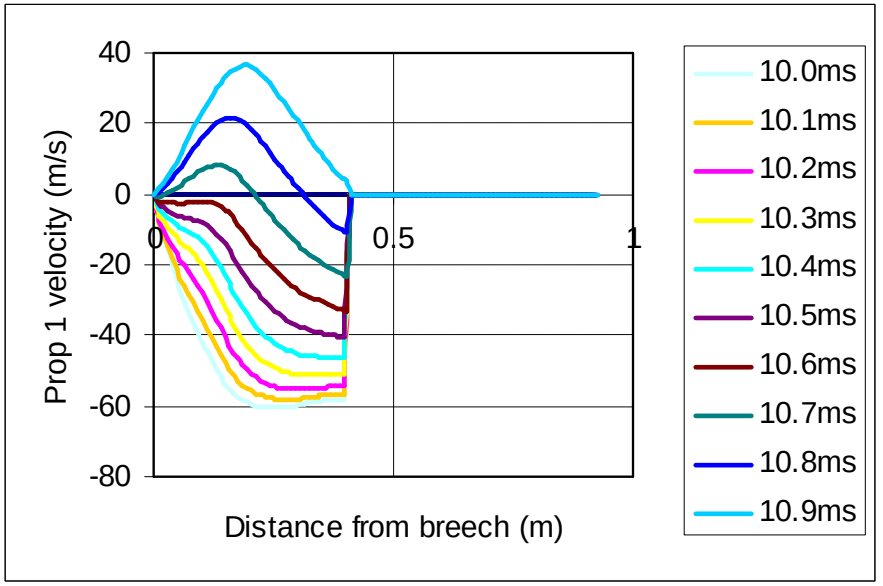
© Copyright QinetiQ limited 2008

PDF Complete
Your complimentary use period has ended. Thank you for using PDF Complete.
Click Here to upgrade to Unlimited Pages and Expanded Features

gnition at projectile

- Analysis of QIBS simulation showed
  - Compression of propellant bed for module 1 propellant at breech
  - Significant rearward propellant velocity
  - Propellant shatter likely



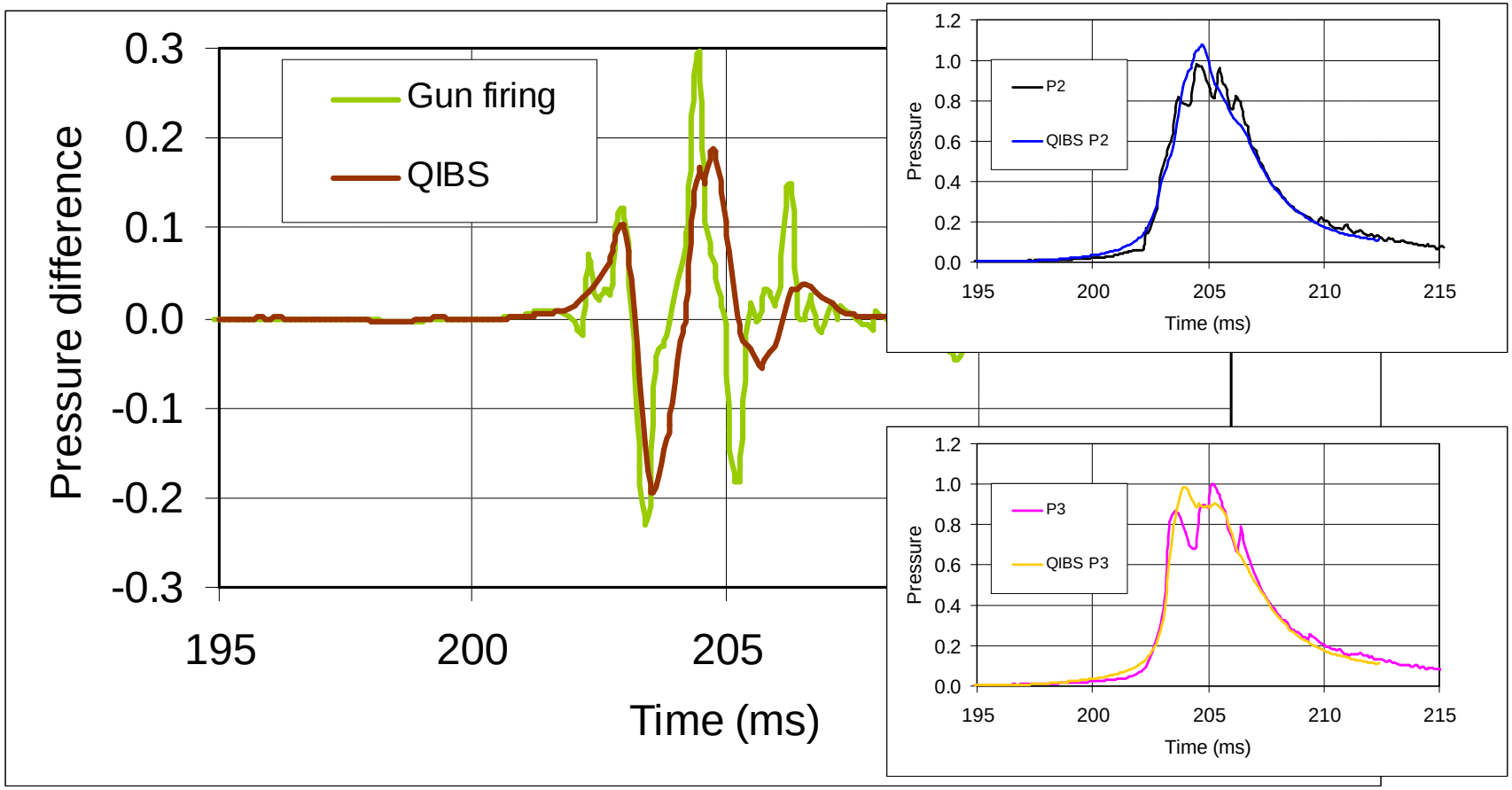


© Copyright QinetiQ limited 2008

PDF Complete
Your complimentary use period has ended. Thank you for using PDF Complete.
Click Here to upgrade to Unlimited Pages and Expanded Features

gnition at projectile ï final simulation

- Excellent agreement up to maximum pressure



© Copyright QinetiQ limited 2008

PDF Complete
Your complimentary use period has ended. Thank you for using PDF Complete.
Click Here to upgrade to Unlimited Pages and Expanded Features

- The quantity of gun powder in the flash tubes was marginal for simultaneous ignition
- The charge appears to have been ignited at the projectile end with the modules closer to the breech then being subsequently ignited in turn
- Ignition at the projectile end then drove the charge towards the breech at over 100 mph and caused shatter of propellant in the module nearest to the breech
- The ensuing pressure wave drove the charge back towards the projectile at over 200 mph and shattered yet more propellant
- Subsequent simulations indicate that gun powder should also be present on the outside of the flash tube (in contact with the propellant) to improve the ignition train
- Future work - better representation of CCC to allow simulation of full IB cycle

© Copyright QinetiQ limited 2008

PDF Complete
Your complimentary use period has ended. Thank you for using PDF Complete.
Click Here to upgrade to Unlimited Pages and Expanded Features

QinetiQ

The Global Defence and Security Experts

© Copyright QinetiQ limited 2008

Launch Dynamics Environment of a Water Piercing Missile Launcher

Jon J. Yagla
DTI Associates, Dahlgren, VA

John Busic, Samuel Koski, Brian Myruski
NSWC Dahlgren Division, Engagement Systems Department, Dahlgren, VA

Chris Weiland and Pavlos Vlachos
Virginia Tech College of Engineering, Blacksburg, VA

INTRODUCTION

The Water Piercing Missile Launcher (WPML) is based on the Concentric Canister Launcher (CCL). The launcher uses the gas jet emitted from the CCL to pierce the ambient water above a submarine or other submerged platform. The missile is then released and flies through the gas column to the surface. The launcher has the potential to eliminate pyrotechnic gas generators and pumps as the means of expelling missiles from submarines, and also has the potential for eliminating complex and noisy pressure balancing systems. Each WPML is a complete launching system, which houses the missile during transport, guides the missile during its initial flight, provides self-contained gas management, and contains all of the necessary electronics to launch a missile [1]. Costs may also be reduced as compared to existing systems that employ pyrotechnic gas generators and complex pressure balancing systems.

The CCL is composed of two concentric tubes joined by longerons running the length of the tubes and spaced at 90-degree intervals, Figure 1. The longerons provide structural support for the CCL. The missile is housed in the inner cylinder. The rocket motor nozzle end of the launcher is capped by a hemisphere, with a radius equal to the outer cylinder radius. Thrust augmentation (gun effect) is controlled by a port near the motor nozzle exit. Exhaust gases from the rocket motor strike the hemispherical end-cap and are re-routed 180-degrees through the annular region between the two cylinders, exiting at the tip of the launcher. Thus, the exhaust gases are safely re-directed along the line of fire, Figure 2.



Figure 1. Concentric Canister Launcher

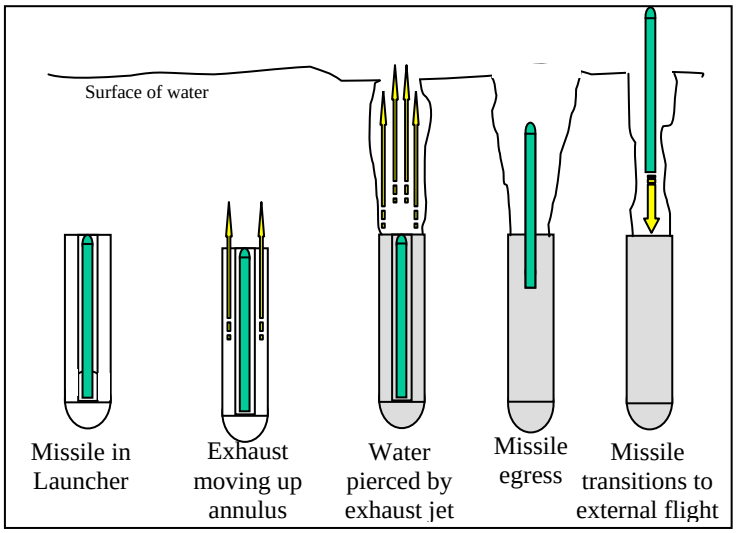


Figure 2. Water Piercing Missile Launcher Concept.

A two-dimensional Navier-Stokes calculation was performed to simulate the effects of 21-inch diameter booster motor inside a submerged CCL. The computer code used was CFDLIB, which was developed by Los Alamos National Laboratory. The water is represented as Lagrangian mass points, related to each other through stress-strain constitutive equations. The stress in the fluid is caused by relative motion of individual particles. An inflow boundary condition of rocket-motor exhaust was located at the exit plane of the CCL. The boundary condition at the exit was calculated using an in-house semi-empirical code called LAX. Figure 3 shows the volume fraction contours for three different time steps using CFDLIB. Superimposed on the contours is an uncoupled rigid-body dynamics solution of a cruise missile exiting the CCL and flying through the missile exhaust. The color fringes are blue for water, red for exhaust gas, and intermediate colors for a mixture of gas and water.

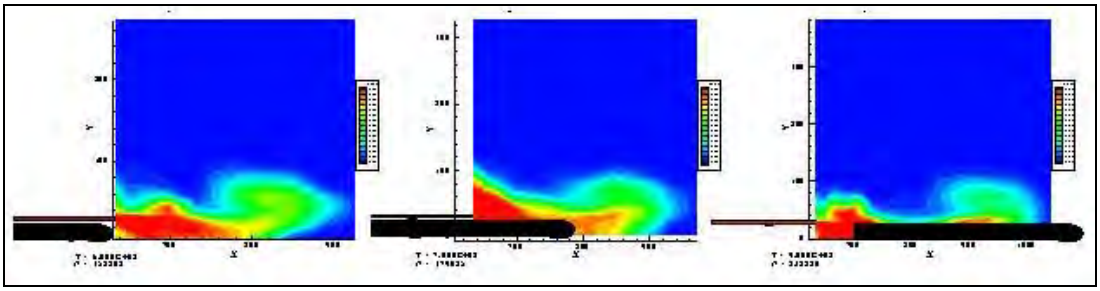


Figure 3. Computer Simulation of Water Piercing Effect and Motion of Missile

Sub scale launchers were built and tested in aquariums. A missile propelled by a 2.75-inch rocket motor was launched and recovered dry from a submerged CCL, Figure 4. Following the favorable result with the 2.75-inch rocket motor, the scale was then doubled and an ~ 8' long x 300 lb. missile propelled by a 5" JATO motor was launched with 20' of water over the launcher, Figures 5 and 6. The figure on the right is a composite view using video camera data for the top half and underwater video for the bottom. The two flashes in the bottom are pyrotechnics fired to release the missile at the right time for it to arrive at the surface at exactly the same time as the jet tip.



Figure 4. Flight Of A Missile Propelled By A 2.75 MK66 Rocket Motor
(The Bright Spot On The Left, Over The Tank, Is The Exhaust).

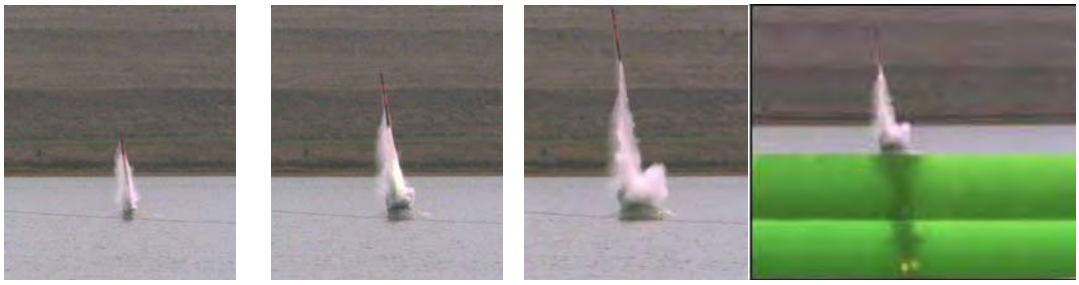


Figure 5. 5-Inch Diameter, 8- Foot Long Missile Propelled By A MK117 JATO Motor.

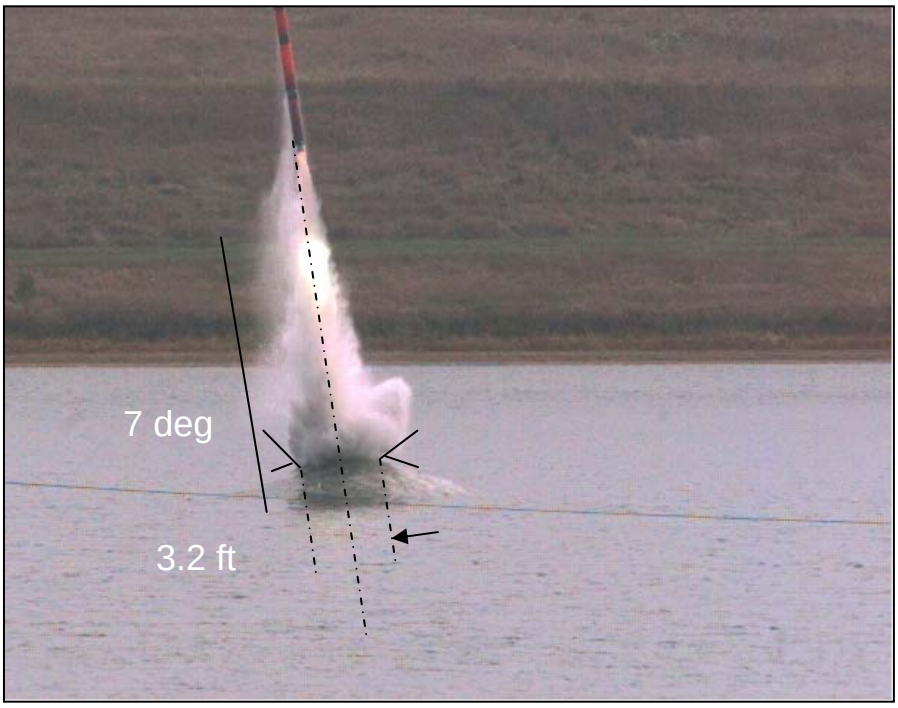


Figure 6. Details The 5-Inch Diameter Missile Transition To Atmospheric Flight.

The remainder of the paper discusses the jet motion and the underwater launch environment. There is very little literature on the formation and initial propagation of transient gas jets in water. Practically all of the literature is about steady jets. Further, there is ample information about water jets in water, and some information about gas jets in air, but very little about gas jets in water.

JET MOTION

The space – time trajectories of the jet tip have been measured for many WPMLs of sizes ranging from 1" to 27" in diameter [2]. The trajectories approximately obey a scaling law, Figure 7. Here the nondimensional jet tip height above the launcher exit plane is plotted against nondimensional time. The jet tip height is nondimensionalized by dividing the observed height by the jet momentum length, L_m, [3]. The nondimensional time is the observed time divided by L_m/V, where V is the jet velocity at the exit plane.

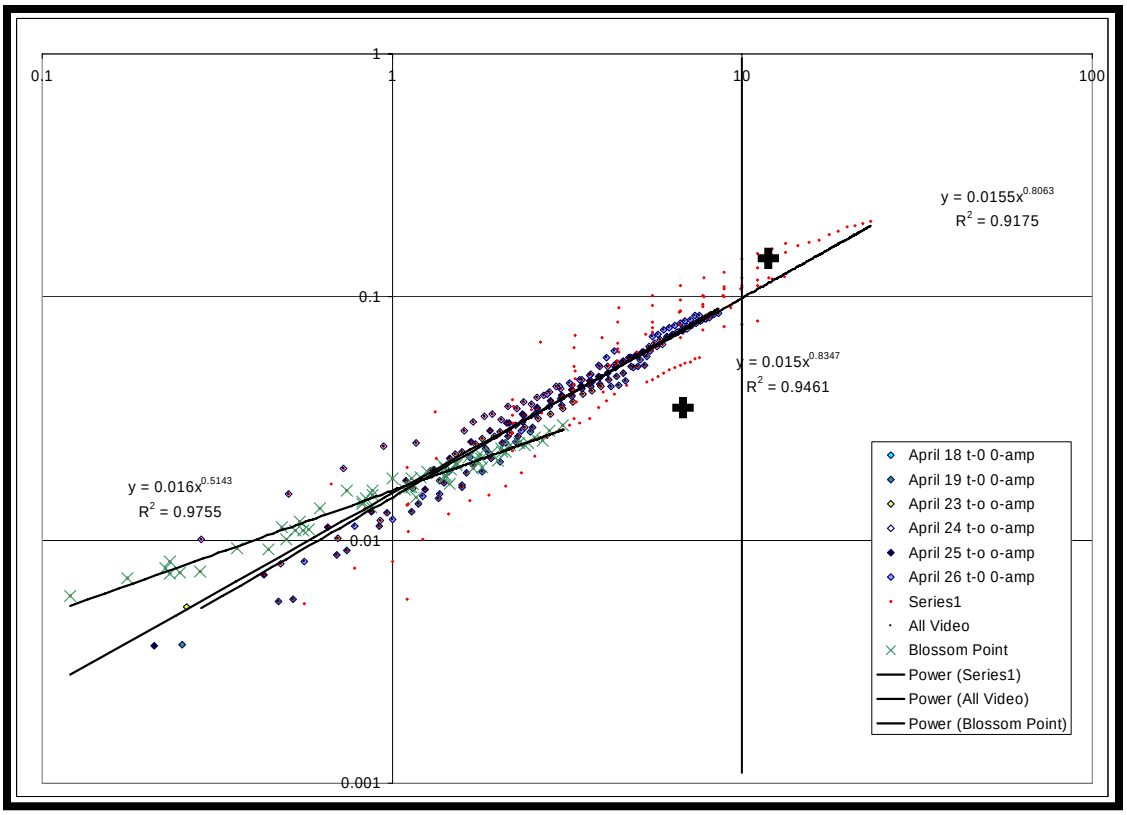


Figure 7. Jet Tip Trajectory Scaled Distance (Ordinate) Versus Scaled Time (Abscissa) Using Data From Mk 66 (2.75-Inch), JATO (5-Inch), And Zuni (5-Inch) Motors At Depths From 6 To 42 Ft. The Mk 66 Motors Were Fired In An 8-Ft Diameter Tank At Blossom Point.

To prepare for the flyout test using the JATO Motor, a preliminary static test with the same launcher was conducted at a depth of 20 ft with only the motor and no missile present. Figure 8 is the space-time trajectory of the JATO at 20 ft depth as determined using an underwater acoustic camera. The formula for the jet tip trajectory is on the upper right corner:

$$y = -6.2508\ t^2 + 24.061\ t + 0.235 \qquad (1)$$

The formula can be differentiated with respect to time to obtain the jet tip velocity:

$$V = -12.5\ t + 24.06 \qquad (2)$$

These formulae are sufficient to determine the time to release missile in order for it to arrive at the surface at the same time as the jet tip reaches the surface. However they do not provide any details on the internal structure of the jet.

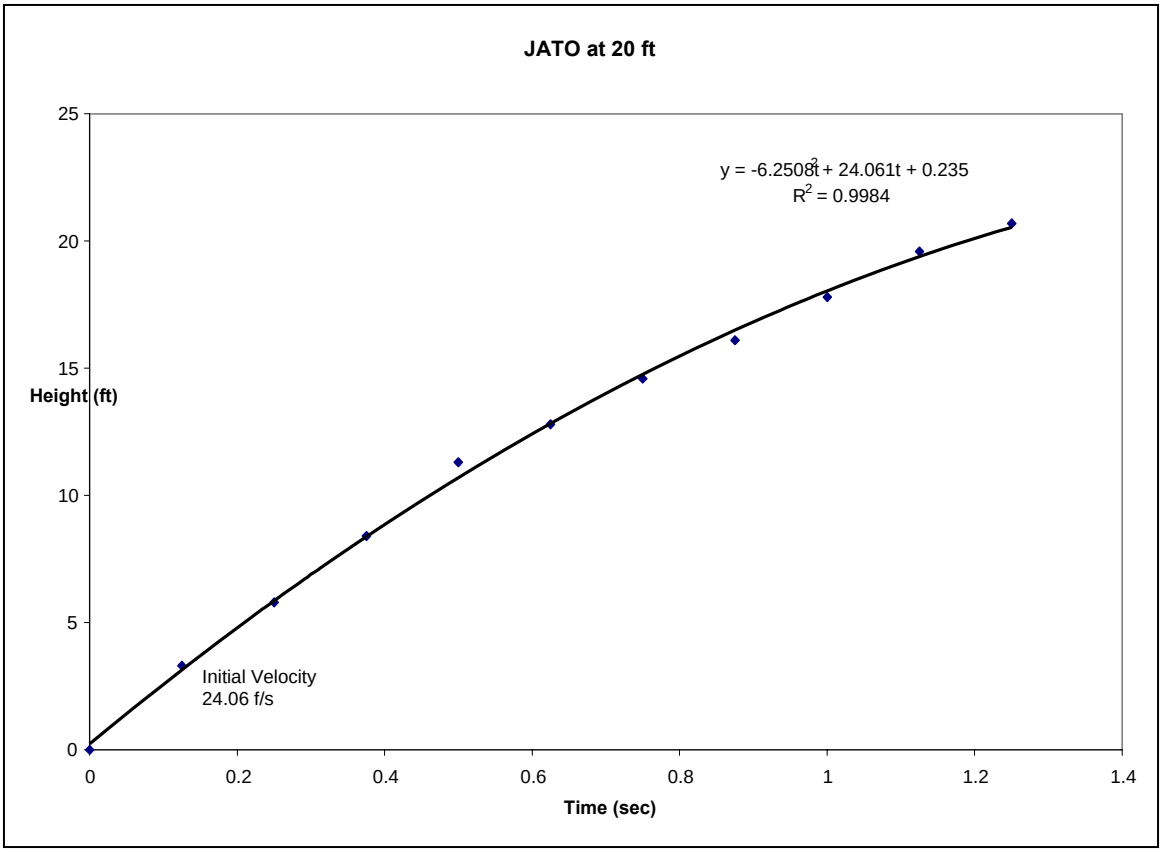


Figure 8. Space-Time Trajectory Of Jet Tip Using JATO Motor And 20 Ft Of Water Over The Launcher.

An assumption that was used to work out the jet flow over the missile is that the jet gas velocity is everywhere the same in the jet and the same as the jet tip: like blowing up a long skinny balloon. There is a high velocity in the filler neck of the balloon, but it fills slowly, so the tip velocity is small by comparison. Equation 2 was used for the jet tip velocity. We consider this a very low order approximation to the launch environment. Better data is now available. However, the launch dynamics were accurately computed with the simple model. There is a considerable effort in the laboratory to refine the launch environment properties using CFD and semi-empirical methods.

JET CHARACTERISTICS

Jet Basics

Figure 9 shows the basic geometry of a steady turbulent round jet [4]. The zone of flow establishment is the region in which the exit geometry is important to the detailed structure of the jet. Beyond this zone the exit geometry doesn't matter, and the profiles of velocity u(x,r) and concentration of entrained materials c(x,r) take

the Gausian shape as shown in the figure. For the WPML, the outlet is an annulus, so the zone of flow establishment can be determined from the equivalent diameter of the annulus. The equivalent diameter is $(4A/\pi)^{1/2}$, where A is the free area of the annulus. For the JATO launcher the free area is 0.599 sq. ft. and the equivalent diameter is 0.87 ft. Therefore the zone of flow establishment should end 5.4 ft above the launcher.

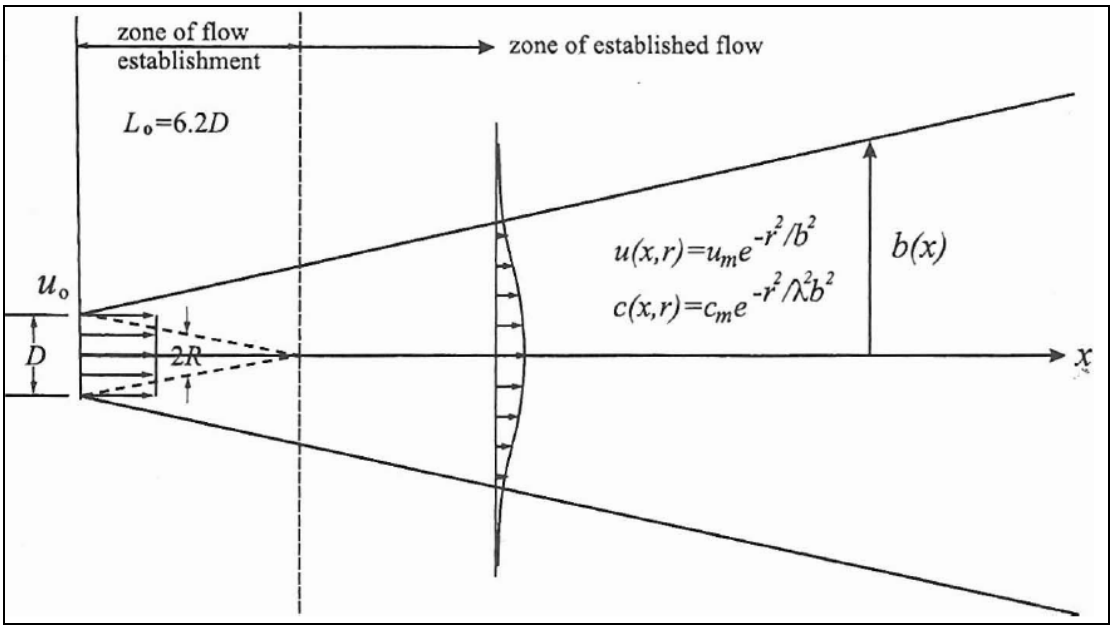


Figure 9. Basic Geometry Of A Turbulent Round Jet.

The data in references 3 and 4 are mainly from water jets discharging into water. For these jets b(x) = 0.12x. Here b(x) is the jet radius. The half angle of the cone is 6.8 degrees. For rocket exhaust jets discharging into air, the jets are broader. Figure 10 shows rocket exhaust jets in air for three cases spanning many orders of magnitude in size. The spreading rate is b(x) = 0.26x and the half angle is 13.7 degrees.

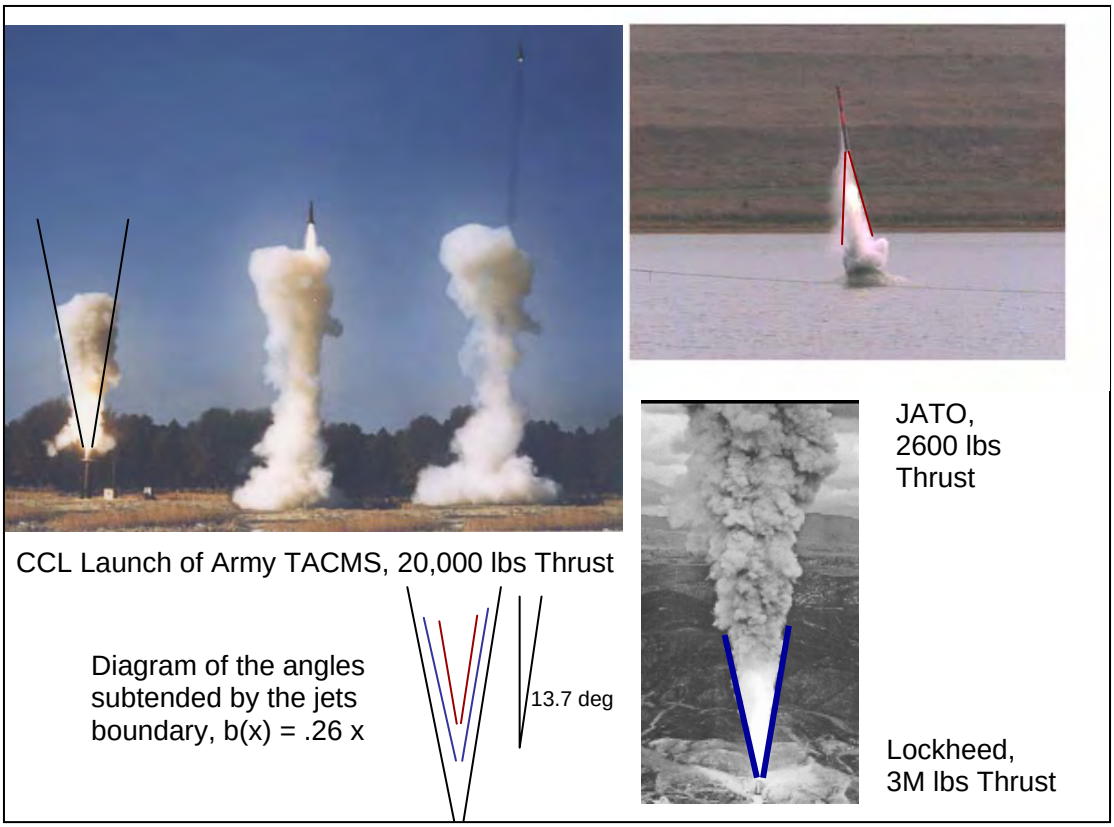


Figure 10. Rocket Exhaust Jets In Air Over A Wide Range Of Motor Sizes.

There is very little data for gas jets discharging into water. Intuition suggests the spreading rate should be insensitive to the exhaust chemical composition and somewhere between the two cases above. A jet from a MK66 motor fired with 10 ft of water over a 7-in diameter CCL is shown in Figure 11. This shows b(x) = 0.13 x and a half angle of 7.4 degrees. The extent to which the cylindrical boundary just four feet from the jet centerline influenced the jet diameter is not known.

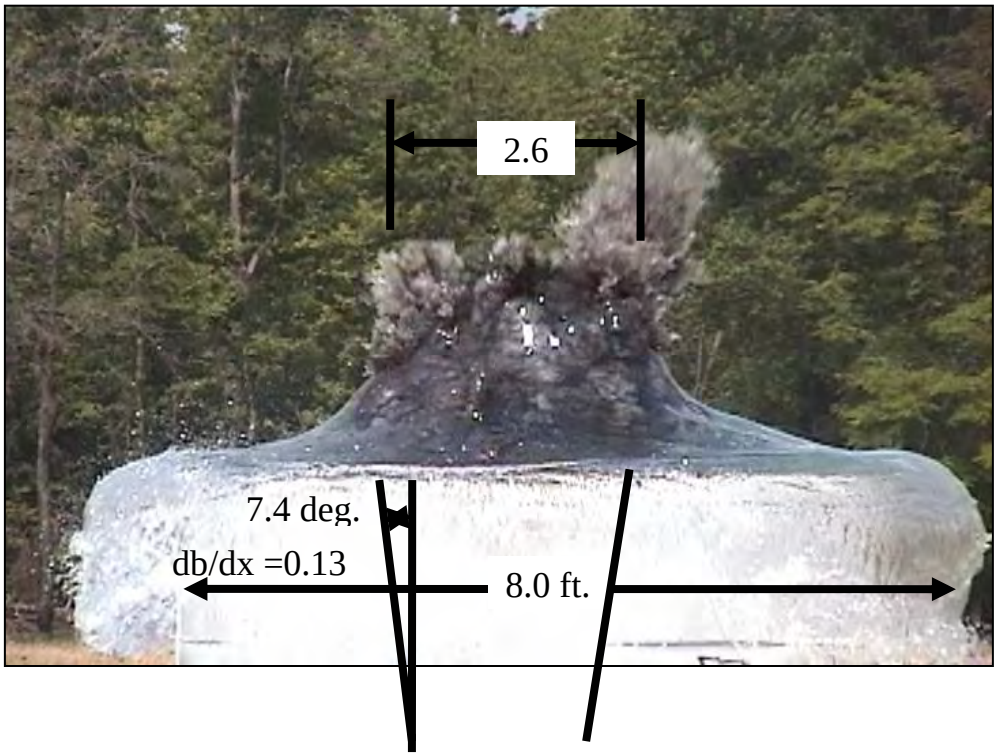


Figure 11. Water Piercing Jet From MK66 Motor At A Depth Of 10 Ft.

The data of Loth and Faeth, [5] for a steady air jet discharging into water show a zone of flow establishment ending at 8 diameters, with a jet width of .5x starting at 8 diameters and diminishing to .4x at 40 diameters, for a broad range of exit conditions from subsonic M~0.6 to supersonic with M>2. Their jet width is defined as twice the radius at which the air/water ratio is 0.5. The slope db/dx would be 0.25 decreasing to 0.2. Their data show at M~0.6, the centerline of the jet out to 20 diameters is pure air. For M =1 the centerline is pure air out to 30 diameters. As the Mach number was increased, penetration of pure air out to 60 diameters along the centerline was observed. Their data also shows that a region of 90% air at least 4 exit diameters in diameter extends out to 80 diameters for M=0.8 and M=1.0 jets, and even broader and farther for higher Mach numbers. The centerline dynamic pressure is constant at the gas outlet value for 6 diameters, then diminishes very rapidly. The dynamic pressure is down to 10% of the outlet value at 30 diameters. Although greatly diminished, the cross section dynamic pressure profiles are broad enough to affect a missile out to 70 diameters where the diameter of the profile is about 20 exit diameters.

We have been able to obtain sonogram type images, Figure 12, of jets from water piercing missile launchers. They show a nearly constant jet diameter of 0.15 the value of x at the surface. The images show a distinct interface, but the gas/air fraction at the image boundary is not known.

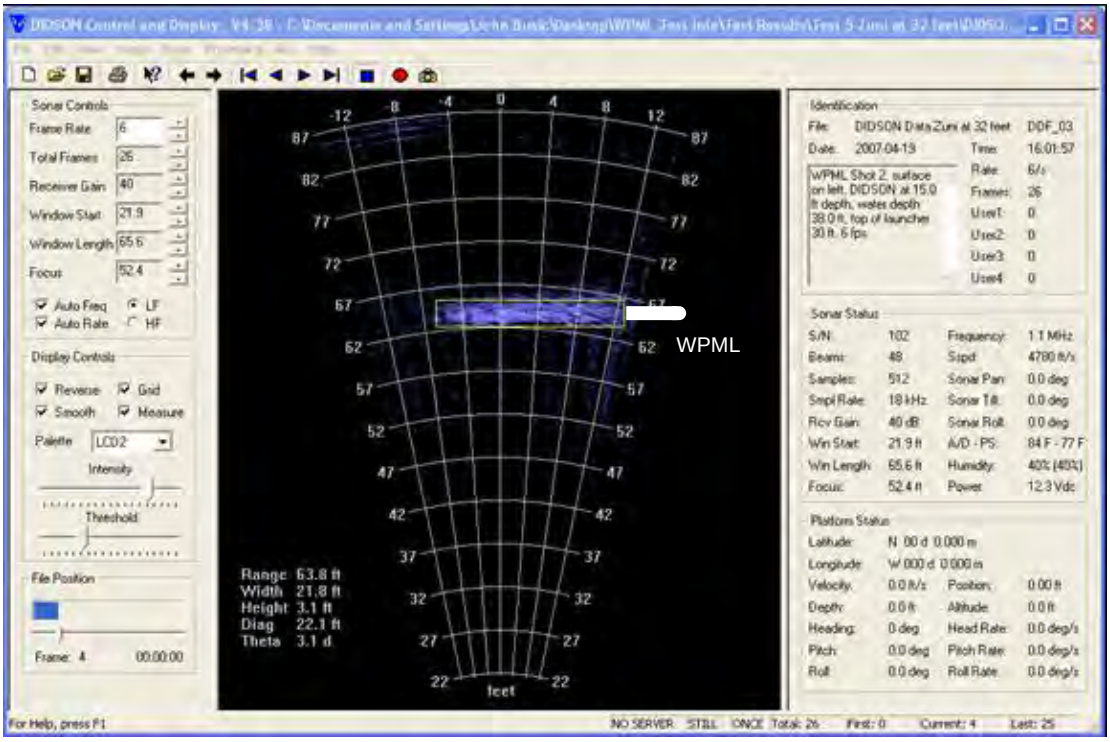


Figure 12. Image Of A Vertical Exhaust Jet From A Water Piercing Missile Launcher From An Acoustic Camera (Rotated 90-Deg, WPML Sketch Added).

LAUNCHER EXIT PLANE PROPERTIES

Computation of the Jet Exit Properties

The jet from a MK117 JATO motor is pure gas as it exits the rocket nozzle and travels up the annular space between the concentric cylinders of the gas management system. The gas properties are computed using the propellant chemical composition and nozzle geometry and an equilibrium thermochemical computer program. The MK 117 JATO motor has properties shown in Table 1. The left side of the table shows the physical properties and the right side shows the thermodynamic state and velocity at the exit. These properties are computed using a one-dimensional CFD program that expands the exhaust into the launcher hemihead and computes wave motion in the annular space. The exit plane ambient pressure depends on the depth over the launcher. The hydrostatic pressure of the water is the exit plane pressure boundary condition for the CFD analysis. This causes the gas to expand to the indicated Mach number. More powerful motors can cause the gas to expand to unity Mach number (choked flow). Notice from the table the sensitivity of the exit condition to the depth.

Table 1. Rocket Exhaust Properties

JATO		
Pressure	**psi**	1800
Temp	**deg K**	2377
Mol. Wt.	**g-mol**	23.23
R	**f^2/(s^2 R)**	2140
Cv	**f^2/(s^2 R)**	9369
Cp	**f^2/(s^2 R)**	11510
Gamma		1.2284

Depth	**ft.**	10.0	20.0
P	**psia**	19.1	23.6
V	**f/s**	1982	1630
Rho	**lb/in^3**	7.50E-06	9.10E-06
Mach		0.680	0.560

The water provides lateral confinement of the jet, so the spreading rate is less than in air. As the jet moves up and away from the launcher, several processes take place. First is turbulent mixing. The jet has a high Reynold's number and is inherently unstable. Eddies form on the interface between the jet and the water. Water eddies are entrained by the jet, and gas eddies are decelerated and enter the water. This is called turbulent mixing and causes the velocity of the gas to decrease and the entire ambient water medium to be set in motion, with streamlines leading in laterally from afar and turning upward and becoming nearly parallel to the jet in the vicinity of the jet boundary. Momentum is conserved. Momentum gained by the entrained water is equal to momentum lost by the jet. This causes the jet to slow down and broaden with height. Figure 5 shows the jet at the time it reaches the surface. The light flashes from the release pyrotechnics are approximately one diameter apart, so the broadening is apparent.

SUFRACE INTERACTION, CROSS FLOW, AND BUOYANCY

Jet Broadening at the Surface and Cross Flow

There are actually two stages of broadening, the first being normal jet broadening due to turbulent mixing, and a second stage of much more rapid broadening immediately near the surface. Figure 13 shows the time averaged shape of the stagnation edge of air jets from a CCL in the water tunnel at Virginia Tech [6]. The cross flow is from right to left. Jet exit Mach numbers in the range of 0.28 to 1.9 are shown. For Mach numbers greater than 0.6 the jet stands up against the cross flow very well. The shape is the same for $.6 < M < 1.67$. Thus a vertical jet from a WPML has the same cross section as a golf tee, i.e. long and slender with a gradual increase of diameter and then a flaring out near the top. Photographs of the jet taken from above the surface are somewhat misleading in that they do not show the diameter of the jet at all, but the flared out diameter which is much larger. Also notice the exaggeration of the horizontal axis.

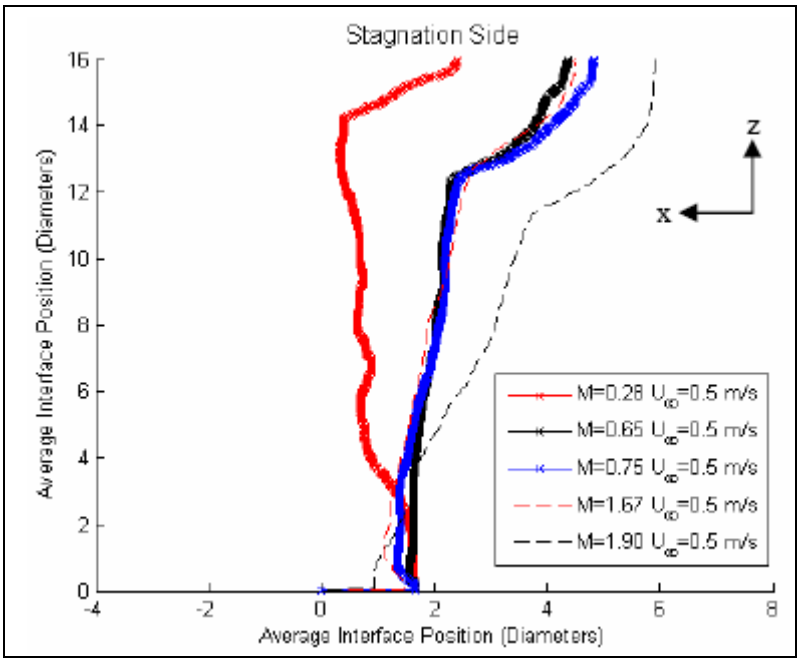


Figure 13. Time average interface position of an air jet in cross flow of .5 m/s (0.96 knot)

For the jets $0.6 < M < 1.67$ the spreading rate db/dx = 0.186 and the half angle is 10.5 degrees. This is a little broader than the tank test result at Blossom Point (7.4 degrees), but much narrower than rocket exhaust in air (13.7 degrees) and broader than water jets in water (6.8 degrees). For the M = 1.67 jet, the values are the same into cross flow as into still water. For jets with Mach numbers less than about .5, they "pinch off" shortly after reaching the surface and do not stand up very well against a cross flow.

Jet Buoyancy

As the jets slow, buoyancy becomes more important and the rate of mixing and spreading change accordingly. Momentum in the jet can be augmented by the buoyant forces and the jet can even be accelerated. For water jets in water the expansion rate is 0.105x in the buoyant region. The "momentum length" of a jet as obtained from dimensional analysis is the distance at which momentum gives way to buoyancy as the dominant mechanism. This has been amply confirmed for water jets in water, where jets inclined relative to vertical bend upward at this distance. The momentum length was used to nondimensionalize the jet trajectory data in Figure 7 above. For the JATO jet at 20 ft depth the momentum length is 240 ft, so buoyancy should not be important. There is no apparent buoyant effect in Figure 5. However, we have some data that show the distance for transition from momentum dominance to buoyancy dominance may be much less than the momentum length for rocket exhaust into water than water jets in water.

The trajectory for the jet tip from a MK-117 JATO motor fired at a depth of 42 ft. is shown in Figure 14. There is a pronounced change in speed at a height of 27 ft. at time 1.8 seconds. The exponent in the trajectory equation obtained from curve fitting shifts from 0.526 to 0.947. The momentum length is 190 ft. for the JATO at 42 ft. depth. From the figure it can be seen flow persists as a jet 0.45 seconds after motor burn out, and then becomes a buoyant plume. The scaled distance at the transition to buoyancy is 0.142 and the scaled time is 11.7. This point is at the upper cross on Figure 7.

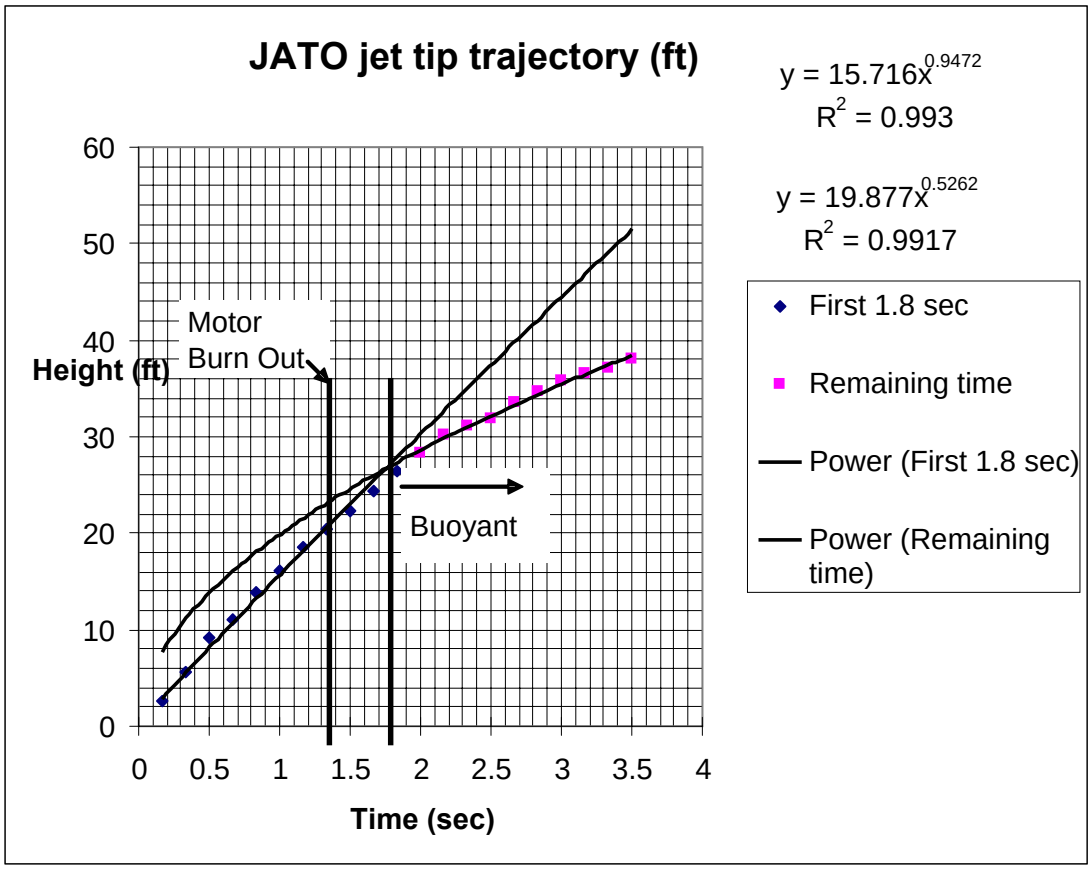


Figure 14. Jet Tip Trajectory For MK117 JATO Fired At A Depth Of 42 Ft.

We fired a SR-121 rocket motor at an inclination of 74.5 degrees to the horizontal (90 degrees is up) at a depth of 30ft. and found the jet turned upward at a distance of 11.5 ft. at time 1.28 seconds. Figure 15 shows the jet transition to a buoyant plume. When the jet got to the surface the time was 2.34 seconds and the knee in the trajectory curve was at 13.8 ft. The theoretical momentum length for this motor fired at 30 ft. is 339 ft. The scaled distance when the jet first turned upward was therefore 0.0339 and the scaled time was 6.79. This point is shown as the lower cross on Figure 7. When the jet arrived at the surface the knee was at a scaled

distance of 0.0407 and the scaled time was 12.45. Even though the momentum length for the SR-121 was greater than the MK-117 JATO, the transition to becoming a plume was closer to the launcher exit. Evidently momentum length is not a good predictor of the transition distance for gas jets in water.

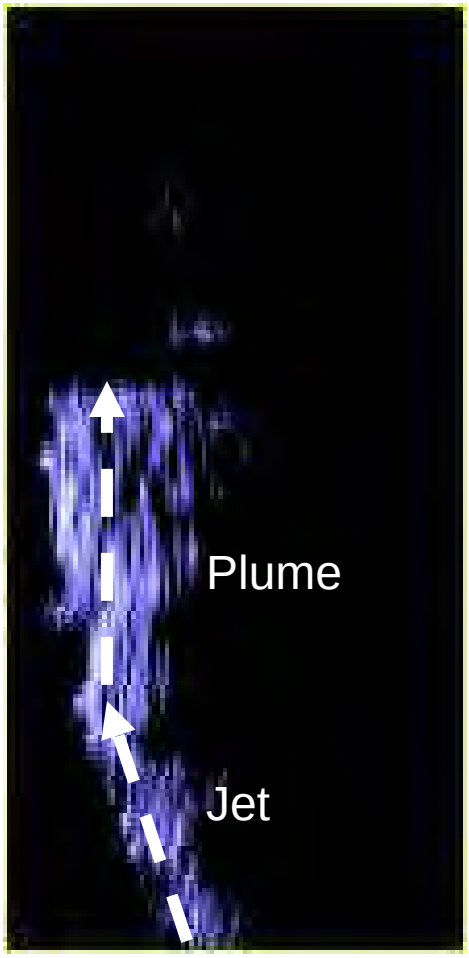


Figure 15. Inclined Jet From SR-121 Rocket Motor Transitioning To Become A Buoyant Plume.

JET INTERNAL STRUCTURE

Jet Cross Sectional Properties and Turbulence

The cross section through the jet at any given height shows nearly Gaussian distributions of the jet density, velocity and other properties. CFD results computed at NSWC are shown at the time the jet tip reaches the surface in Figures 16 and 17. The contours are for pressure and density, with embedded velocity profiles. The contours become Gausian beyond the zone of flow establishment, which ends at 60 inches on the vertical axis. This distance is 6.6 equivalent diameters, which agrees with the zone of flow establishment ending at 6.2 diameters in Figure 9. For positions closer to the exit plane than 30 inches (3.3 equivalent diameters) the

velocity distribution is doughnut shaped. The approximately 7th power velocity distribution of internal flow in the annular space broadens, flattens, and becomes parabolic. At x = 18 (2 equivalent diameters) the parabolic distributions merge. The jet boundary angles from Figure 10, where db(x)/dx is 0.26, are shown in Figure 17.

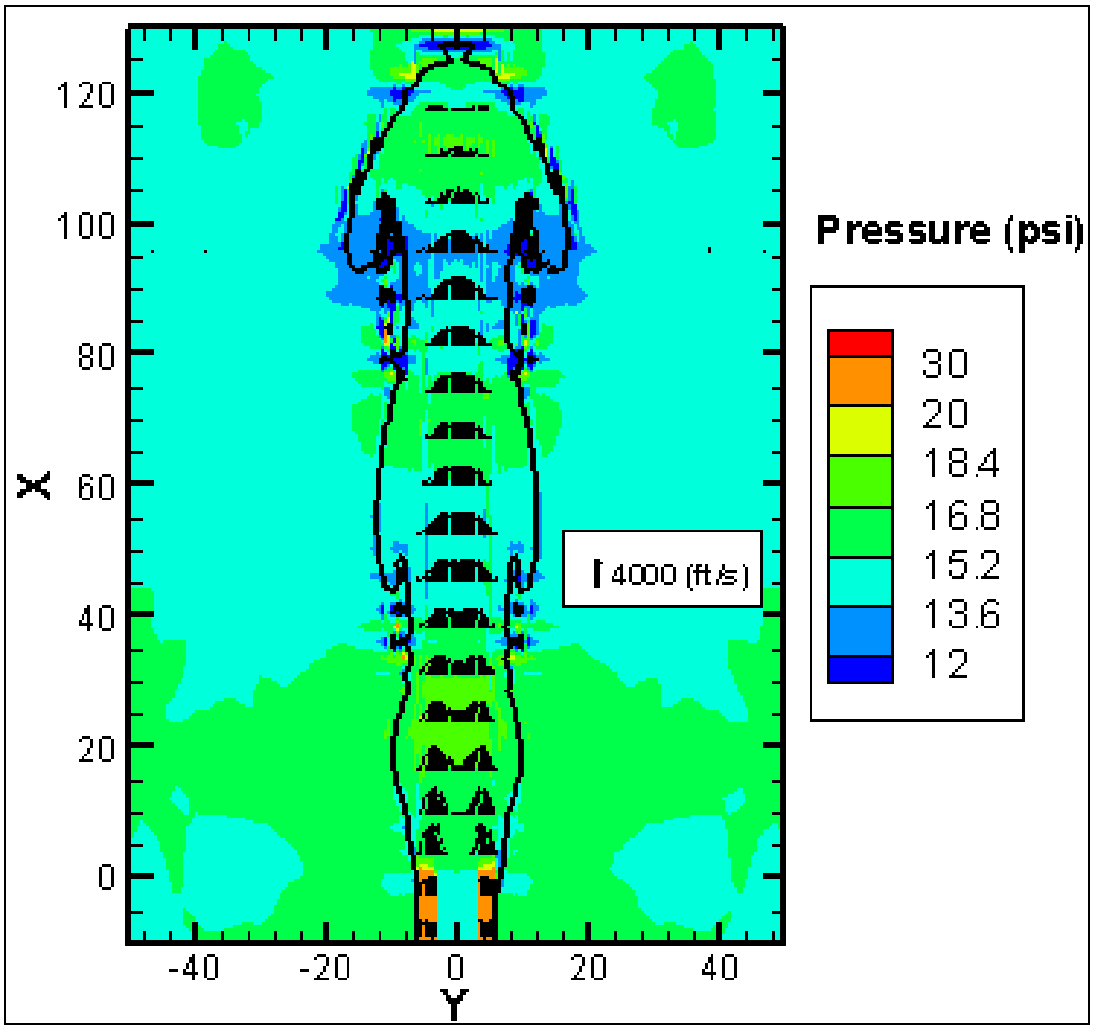


Figure 16. Pressure Contours For Jet. Length Scales Are In Inches.

The contours on Figure 17 show a sudden, near discontinuous change in density. The colors in the range 5 to 35 lb/ft3 are bunched into a solid line. The dark blue region is hot gas with some entrained water. The colors green through red are mainly water with some entrained gas. The computer results are in approximate agreement with the data of Loth and Faeth [5], even though the computer results are for a transient jet that has not reached steady state. The 0.5 air/water region which defines the jet diameter in [5] would be in the middle of the green region, which does not show on the plot because it is in the region of rapid change in the jet boundary.

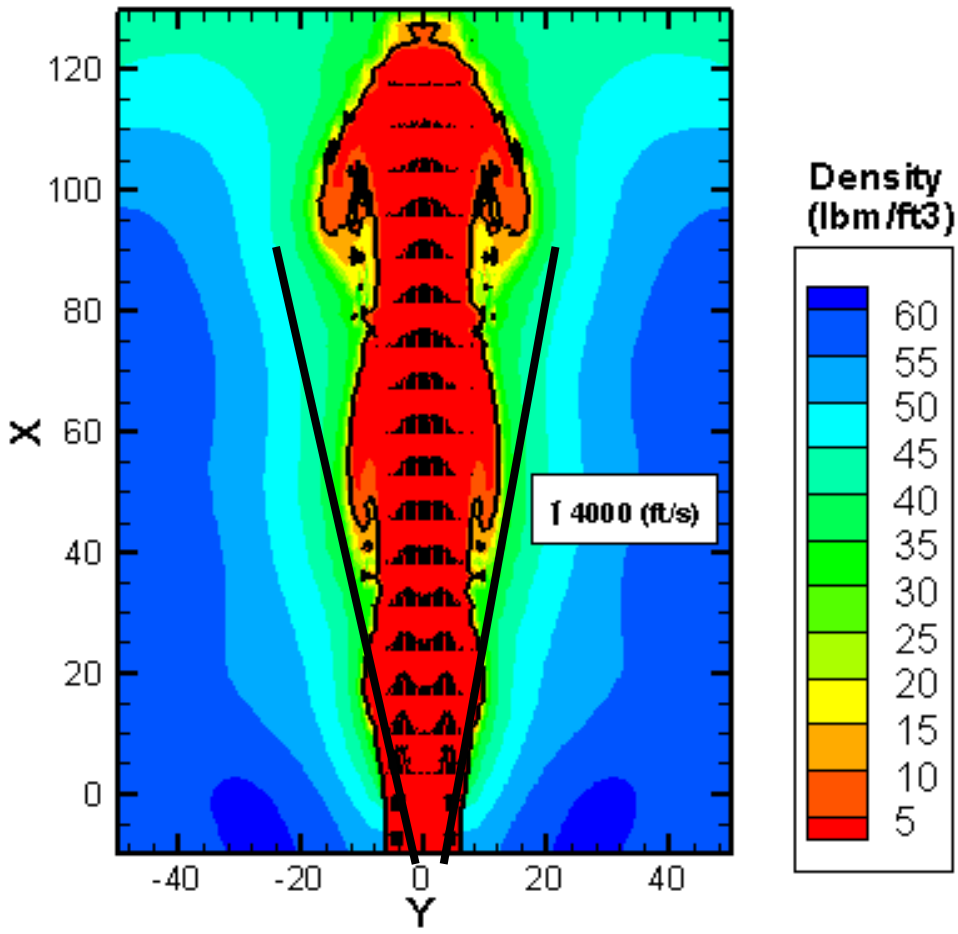


Figure 17. Density Contours For Jet. Length Scales Are In Inches. The Solid Lines Are From Figure 10, Where B(X) = .26 X.

Figure 18 (3.6 in [5]), shows a broad flat contour of turbulent rms intensities of 20-25% of the mean spanning the jet cross section. In the jet the fluctuations are most severe at the interface between the jet and the ambient, and the intensity profile shows two peaks. After the jet slows and becomes a plume, the shear at the interface between the jet and the ambient is less and the profiles show peak intensities along the centerline.

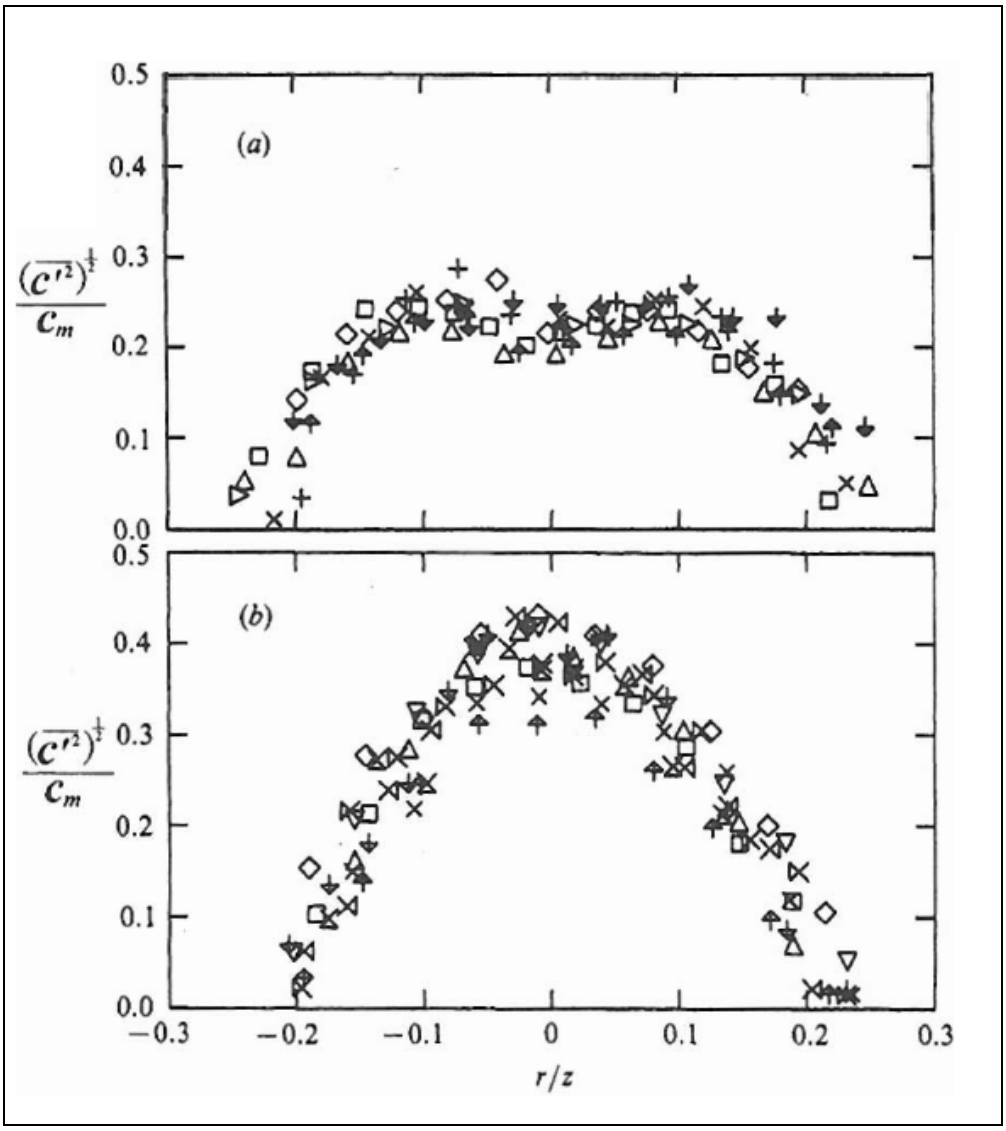


Figure 18. Turbulent Fluctuations Across A Jet (Top) And Plume (Below). The Fluctuations Are Rms Values.

The plots in Figures 16 and 17 show a jet with very high velocities in the core. Even though the core velocity is several thousand feet per second, the jet tip moves much slower. Differentiation of the trajectory equation on Figure 14 with respect to time yields a speed of 14.9 ft. per sec. over most of the burn time. The interface between the jet tip and water is Taylor unstable: a fluid trying to accelerate a second fluid of much higher density. The interface becomes highly irregular and turbulent. The high velocity gas core mixes with water at the jet tip and loses momentum very quickly in the mixing zone. This doesn't seem to cause much of a pressure disturbance in the mixing zone, but the density and velocity fields change very rapidly.

Approximate “low order” models of turbulent jets have been used extensively in civil and environmental engineering. Practically all the models are for steady flow. One example is the “top hat” model, which considers the properties to be uniform across the jet with the value being the average of the more accurate Gaussian distribution. For many problems in civil engineering the top hat model provides nearly the same result for broadening, mixing, and dilution as the Gausian model, with much simplified calculations. The model used in our first try at the launch dynamics problem used a low order balloon filling model discussed above. It is a simple top hat model for nonsteady flow. As more data is obtained and the accuracy of CFD methods is confirmed, CFD will replace the low order semiempirical models.

SUMMARY

Turbulent rocket exhaust jets in water are similar in structure to water jets in water and gas jets in gas. Each case is characterized by a turbulent jet interface region that entrains the surrounding medium. The spreading rate db/dx and the half angle seems invariant with regard to scale and velocity, and unique to the phase of the medium and jet. They seem insensitive to the details of chemical composition. Methods for predicting the exhaust velocity and Mach number were discussed. Water depth is important, as increasing hydrostatic pressure decreases the exit Mach number and velocity. Gas jets can penetrate a considerable distance in water, and maintain a gas column out to at least 80 diameters. As the Mach number of gas jets in water approaches 0.6, the jet has the ability to penetrate a cross flow for a considerable distance. This makes the Water Piercing Missile Launcher plausible for moving platforms. Efforts are under way to develop low order semi-empirical models and computer fluid dynamics approaches to predicting detailed jet structures.

REFERENCES

1. J. Yagla, “Concentric Canister Launcher,” Naval Engineers Journal, May 1997, pages 313-330.
2. Yagla, Jon, Keith deLoach and Chris Weiland “The Water Piercing Missile Launcher,” 21st International Ballistics Symposium, Adelaide Australia
3. Fischer, H., List, J., Koh, R., Imberger, J., and Brooks, N. **Mixing in Inland and Coastal Waters**, Academic Press, New York, 1979.
4. Lee, J.H.W. and V.H. Chu **Turbulent Jets and Plumes**, Kluwer Academic Publishers, Norwell Massachusetts.
5. Loth, E. and G.M. Faeth “Structure of Underexpanded Round Air Jets Submerged in Water” International Journal of Multiphase Flow, Vol. 15, No. 4, pp 589-603, 1989.
6. Weiland, Chris, Jon J. Yagla, and Pavlos Vlachos “Experimental Study of the Stability of a High-Speed Gas Jet Under the Influence of Liquid Cross-Flow Proceedings of FEDSM2007 5th Joint ASME/JSME Fluids Engineering

Conference, July 30-August 2, 2007 San Diego, CA.

Experimental Validation of a Kevlar Fabric Model for Ballistic Impact

Chian-Fong Yen
Tusit Weerasooriya
Paul Moy
Brian Scott
Bryan Cheeseman
ARL, APG MD

TECHNOLOGY DRIVEN. WARFIGHTER FOCUSED.

International Symposium on Ballistics
New Orleans, LA
26 September 2008

Outline

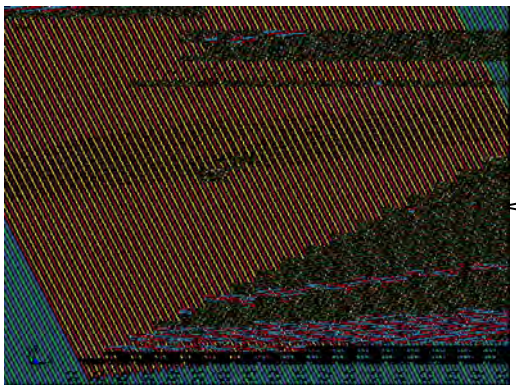
- Experimental Studies
  - Ballistic impact of single layer fabric
- Fabric Modeling
  - Yarn level model
  - Sub-yarn level model*
- Conclusions

* Including results reported in the poster #198 entitled: "**Developing Simulation Capabilities to Link Textile Manufacturing to Ballistic Performance"** by B.A. Cheeseman*, C.F. Yen, B.R. Scott, B. LaMattina, Y. Miao and Y. Wang

Modeling Approach

- Assess current state-of-the-art modeling capabilities and determine the most suitable numerical analysis techniques
- Develop and implement the identified analyses techniques
- Validate analyses techniques with high resolution experiments. Refine modeling capabilities as necessary to ensure the accuracy of the simulation when compared to the experiment

Modeling of Fabrics

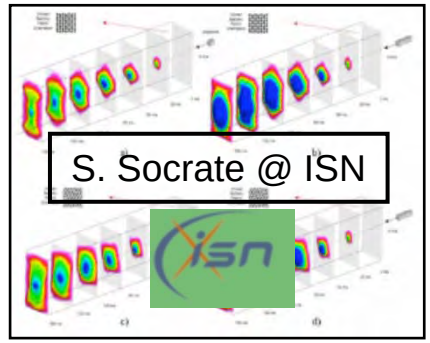


'…the ballistic response of the textile structure depends on the response of the fiber with which it is woven as well as the structural geometry itself." D. Roylance, *Text. Res. J. 1973.*

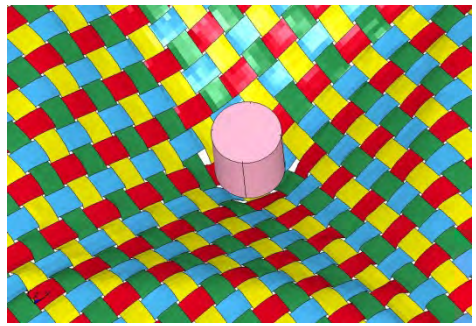
Fabric as a continuum

From Simons, J.W., Erlich, D.C. and Shockey, D.A. 20th Int. Symp.Ballistics, Nov. 2001





Yarn as a continuum



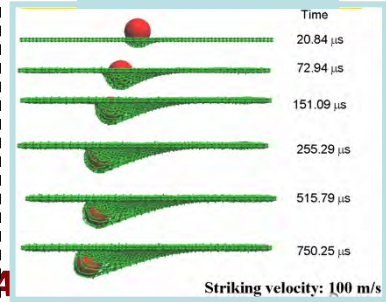
Solid Elements



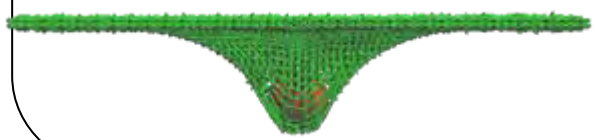
C. Yen

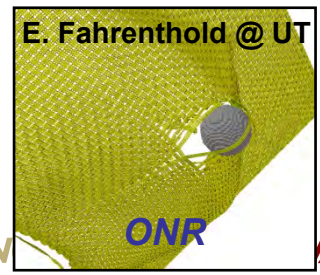


Y. Wang @ KSU



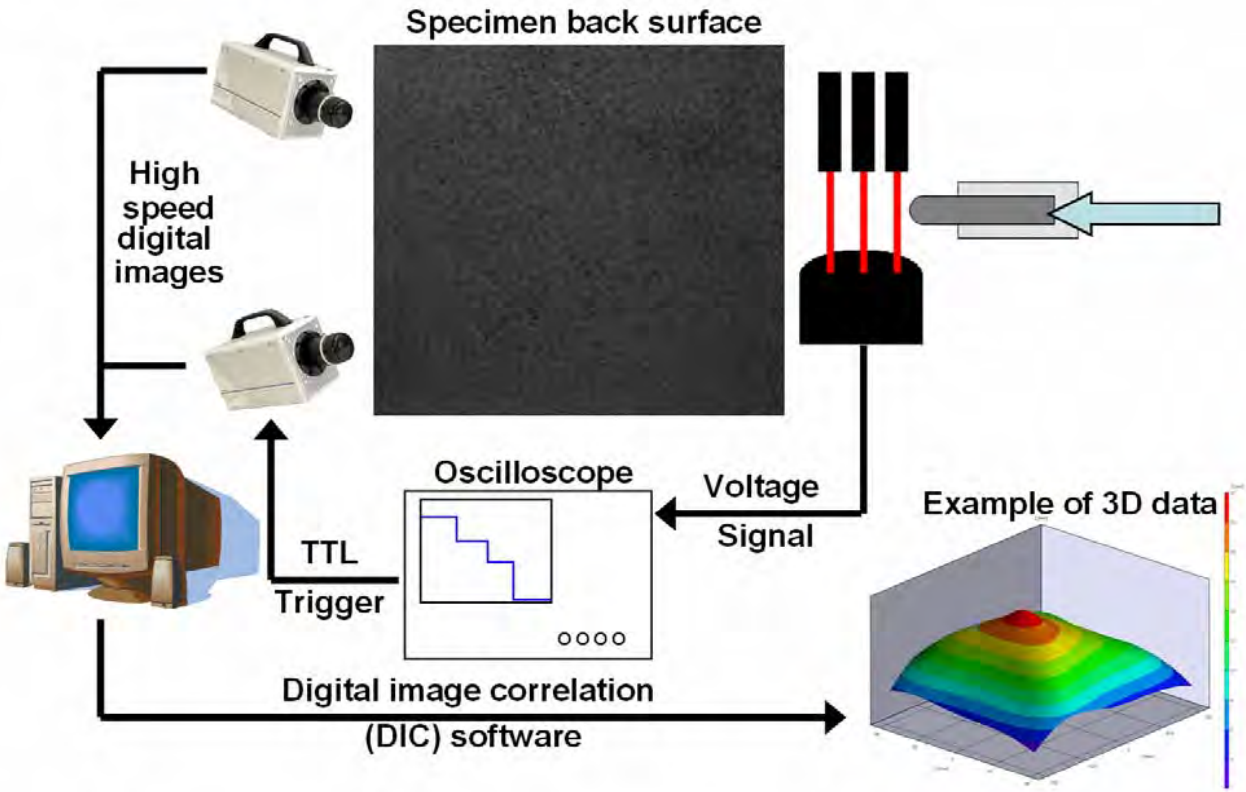
Filament as a continuum

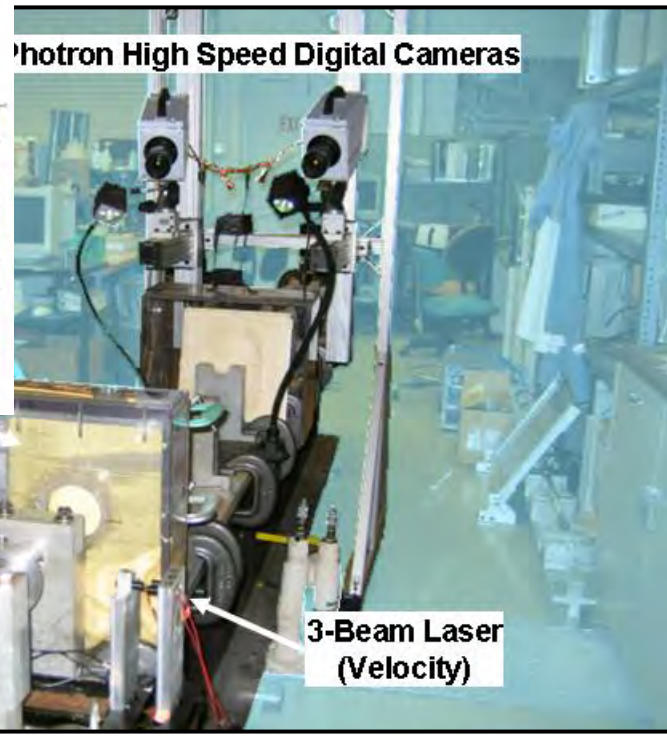




TECHN VA

Fabric Impact Testing: Experimental Setup with High Speed Digital Cameras

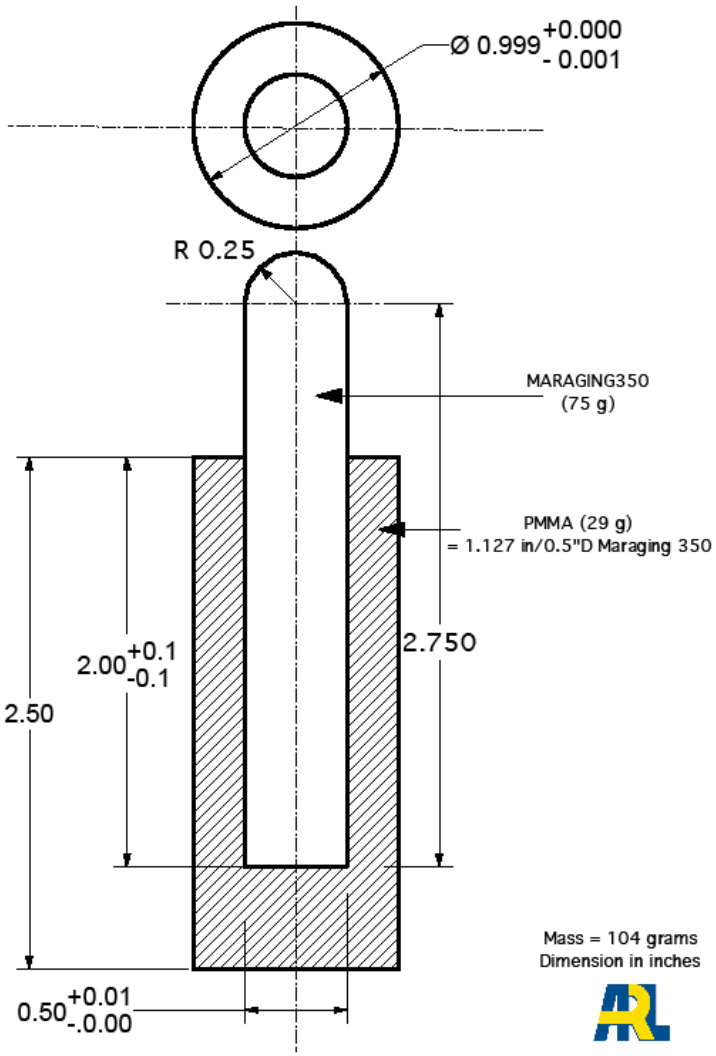




Fabric Impact Testing: Experimental Configurations

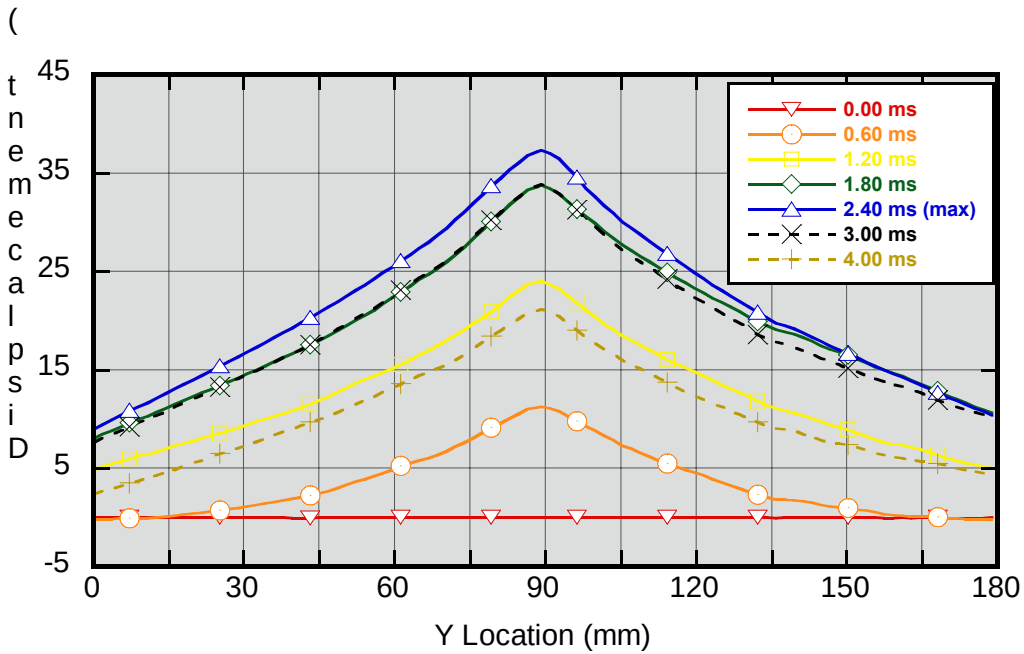
Experimental Results:
May, 2007
Tusit Weerasooriya
ARL

Target:
Hexcel Style 706
Single Layer
Square & Circular Shapes
10”x10” & Diameter = 10”
Fixed boundary
Impact Speed: 22.2m/s



IMPACTOR for DIC on Back Surface

Fabric Impact Testing: Results of Kevlar KM2 Fabric, Displacement Profile, Contours



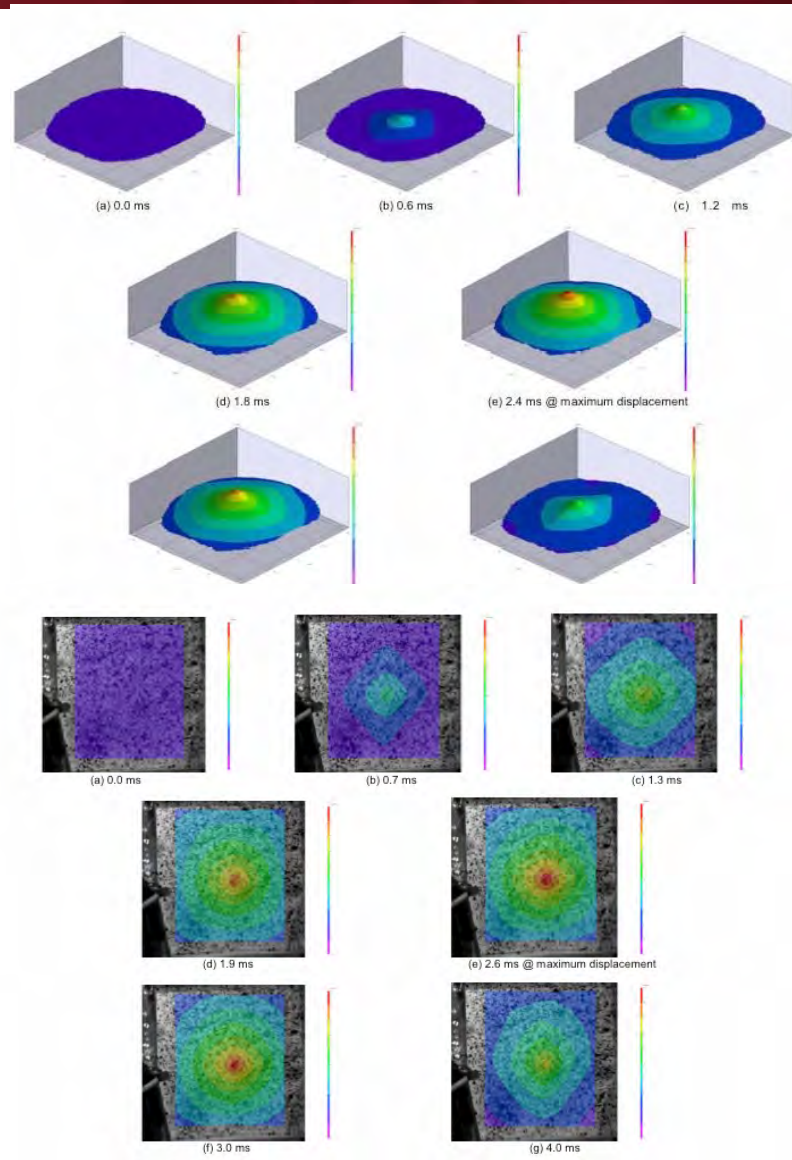
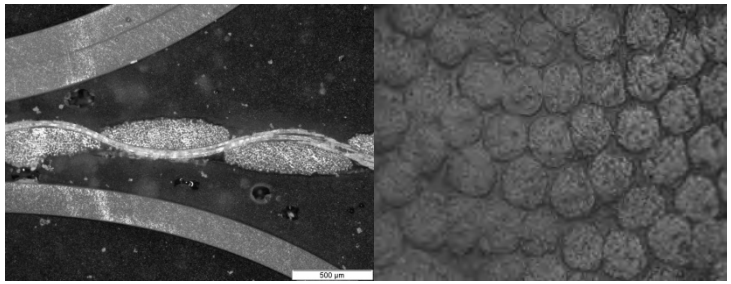


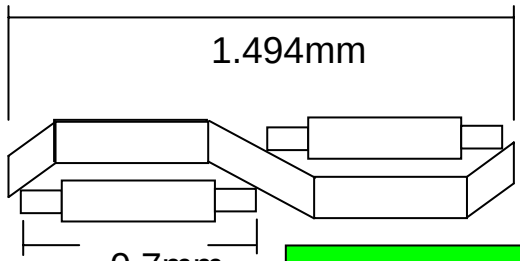
Figure 10. 2D Contour Plot from DIC of Kevlar KM2 on a Square Frame Configuration

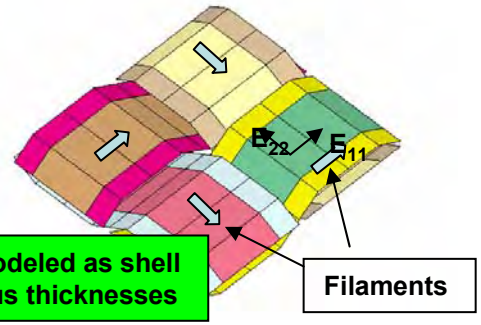
Yarn-Level Modeling Efforts

- **Improved the accuracy of yarn bundle shape and dimensions in a woven structure.**



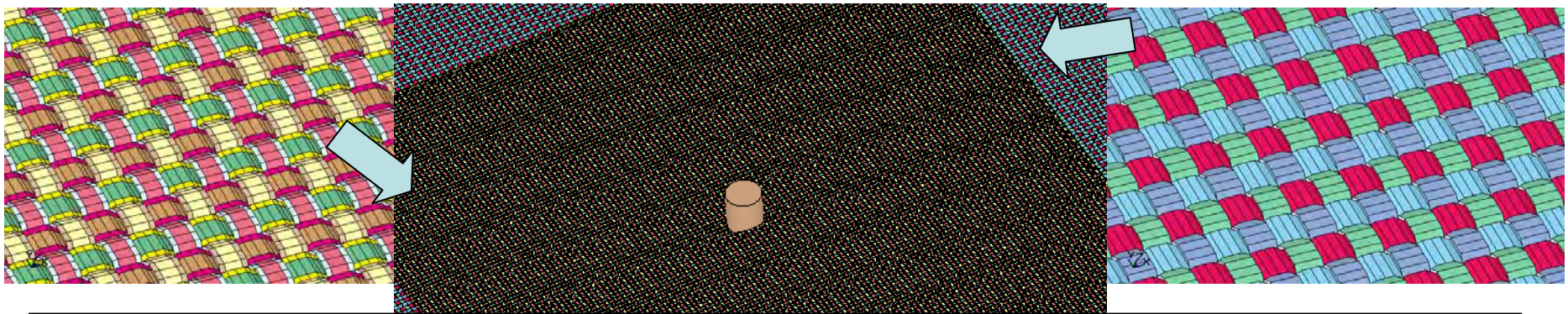
- **Obtained micrographs in order to get more accurate measurements.**





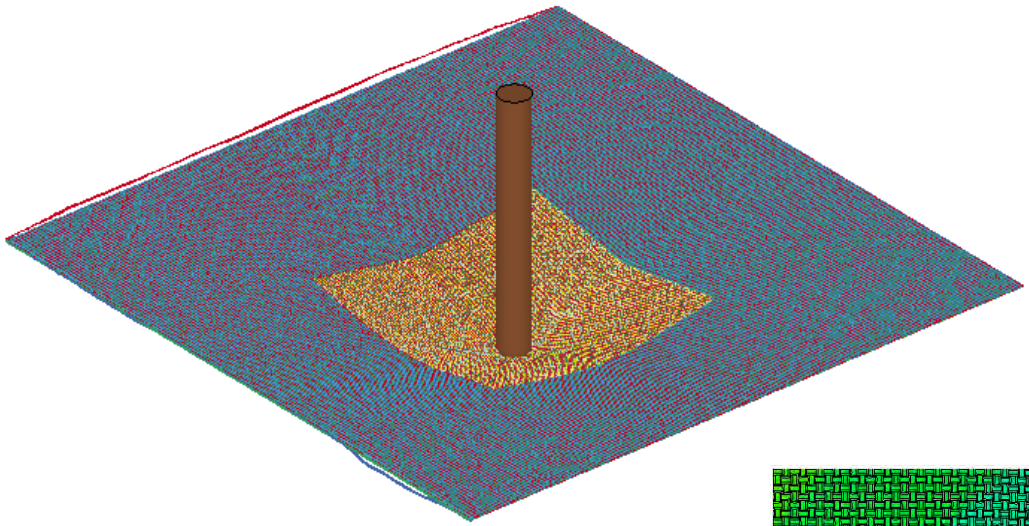
Yarn Bundles are modeled as shell elements with various thicknesses

- **Improved computational efficiency for shorter run times.**
- **Utilized refined mesh in region of impact; less refined elsewhere.**

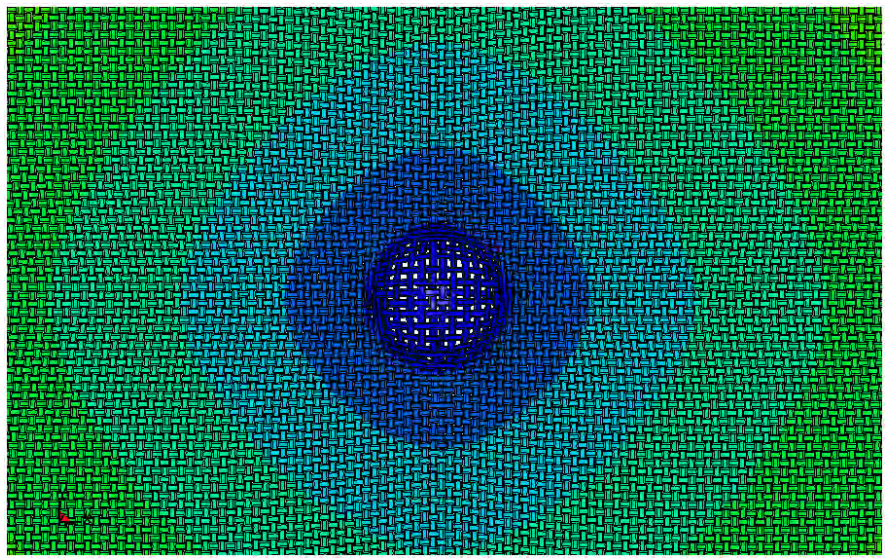


•Using one intg. pt. through bundle thickness to eliminate bundle bending rigidity
•High mesh density in center impact region

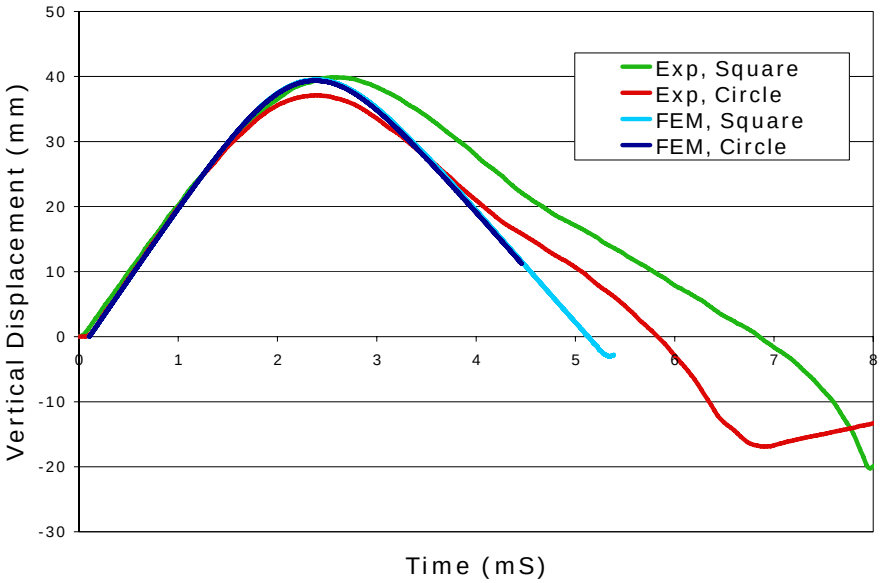
Yarn-Level Modeling: Simulation

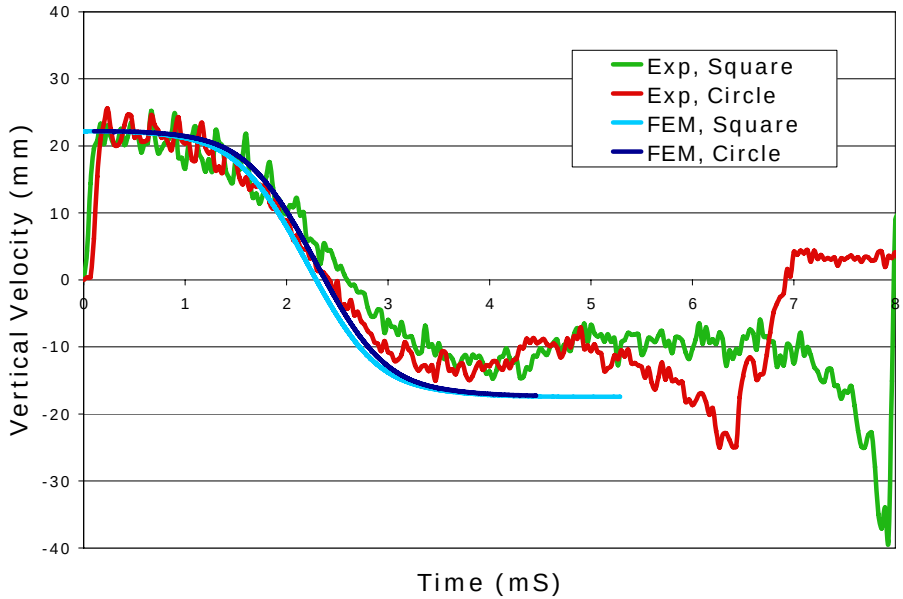


- Deformed mesh of a 34x34 Kevlar fabric layer computed at the peak deflection time of 2.3 msec



Yarn-Level Modeling: Correlation

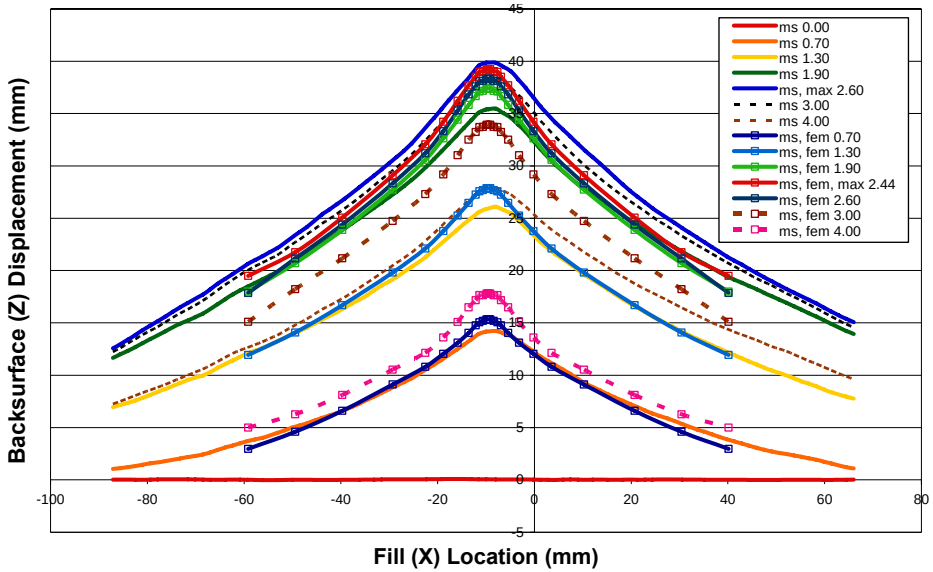




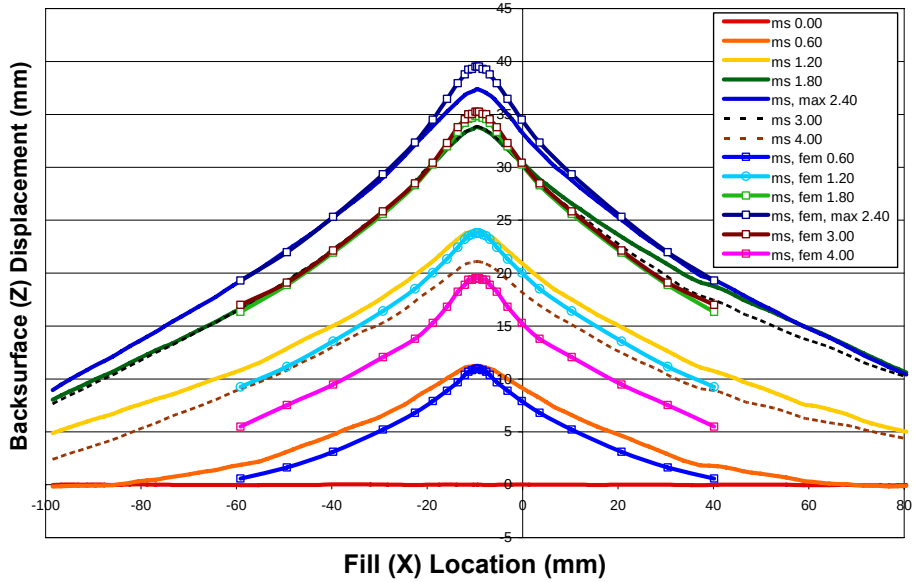
- Displacement -time and velocity – time plots of Kevlar KM2 yarn in weft (x) direction for square support and circular support through the impact point

Yarn-Level Modeling: Correlation

Square Fixture



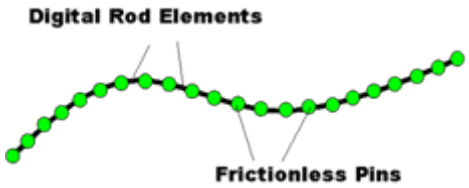
CircularFixture



- Displacement profile of Kevlar KM2 yarn in fill direction for square and circular frame configurations through the impact point

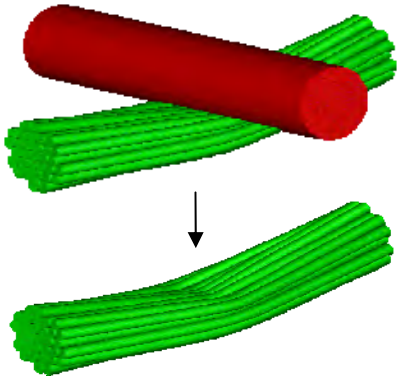
Computational Modeling of Ballistic Textiles: Sub-yarn Level Representation of Fabrics, Kansas State U., Youqi Wang

‘Filament’



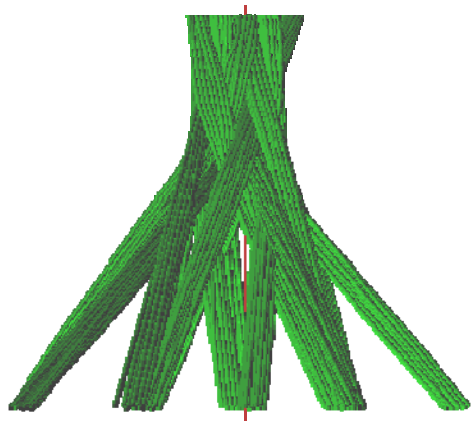
Represented as a series of rod elements connected with frictionless pins = ‘digital chain’

Yarn



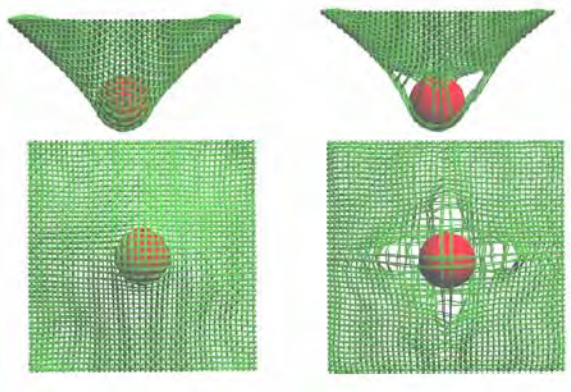
Multi-Digital Chain Yarn Model (Here, each yarn contains 32 digital chains)

Weave or Braid



Yarns utilized to simulate textile manufacturing process

Extended textile manufacturing simulation program to ballistic impact

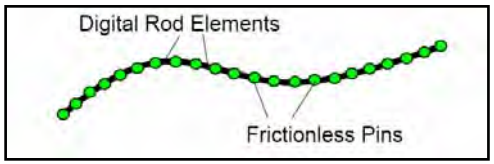


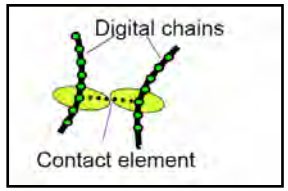
The resulting analysis tool could provide the *critical link* between textile manufacturing and ballistic performance prediction for textile protection systems.

Sub-yarn Fabric Modeling

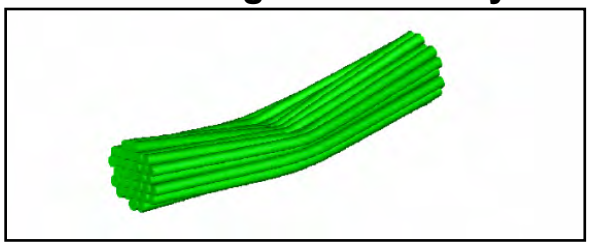
- **Textile manufacturing simulation taking computing time**

'Digital Elements (chains)' = Filaments

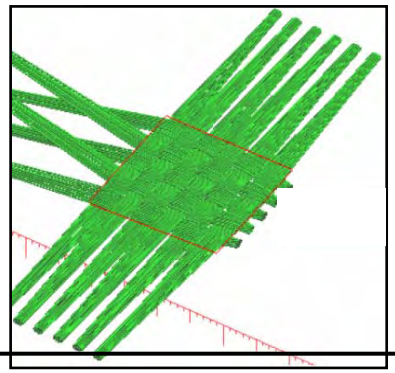


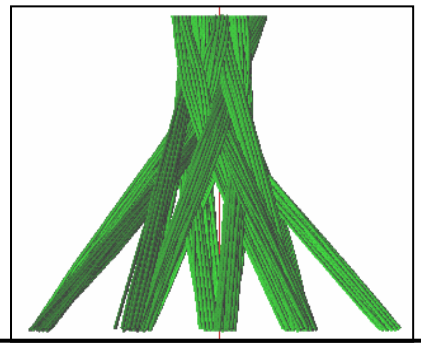


Assemble digital chains = yarn

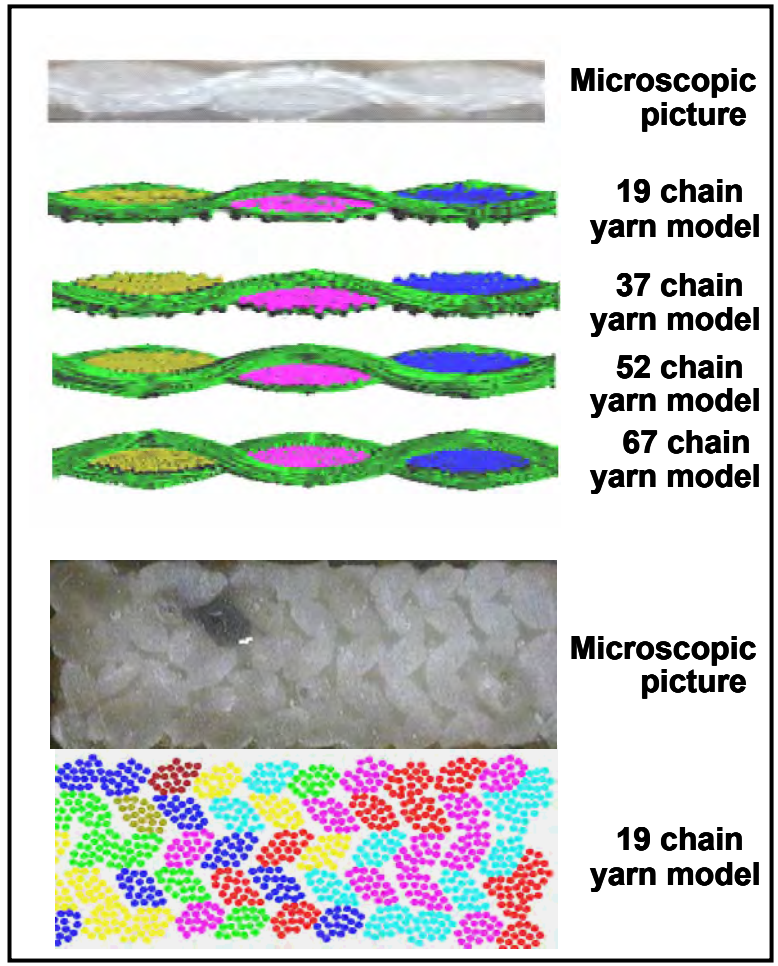


Yarns utilized in textile manufacturing simulation





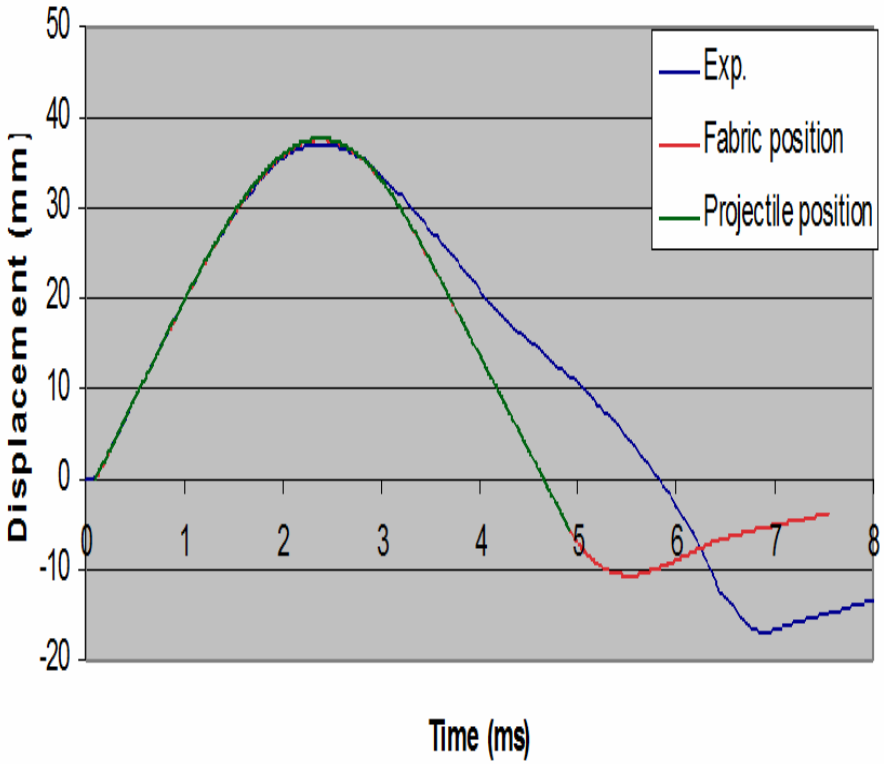
- **Develop explicit formulation for manufacturing process**



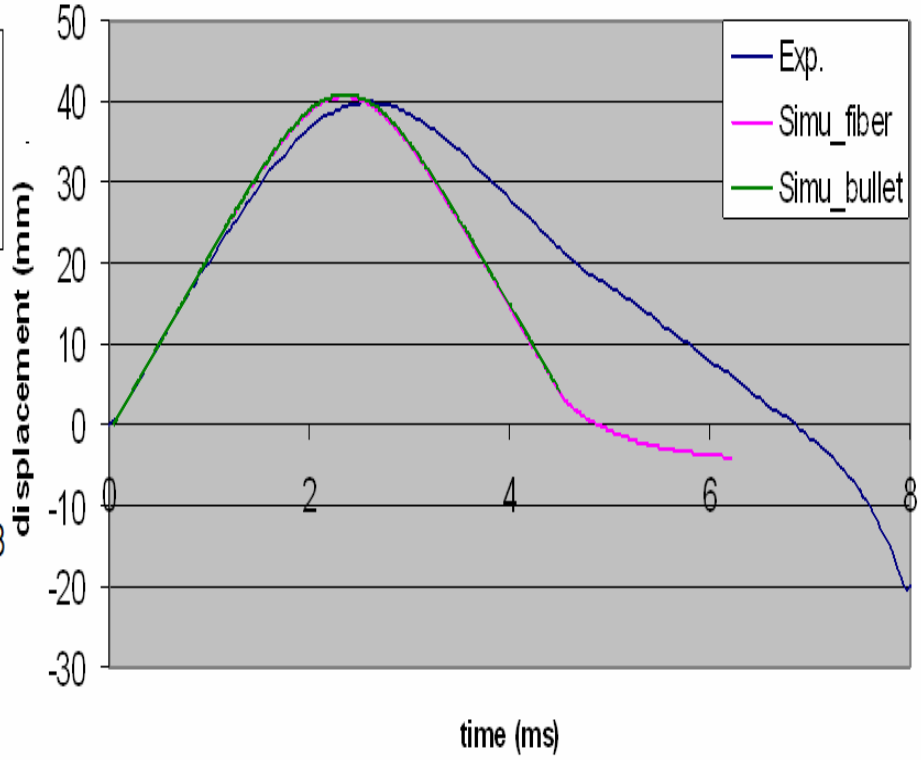
Results reported out at the Army Science Conference, Fiber Society Meeting and two Journal papers

Sub-yarn Level Modeling: Displacement Comparison

Circular Fixture

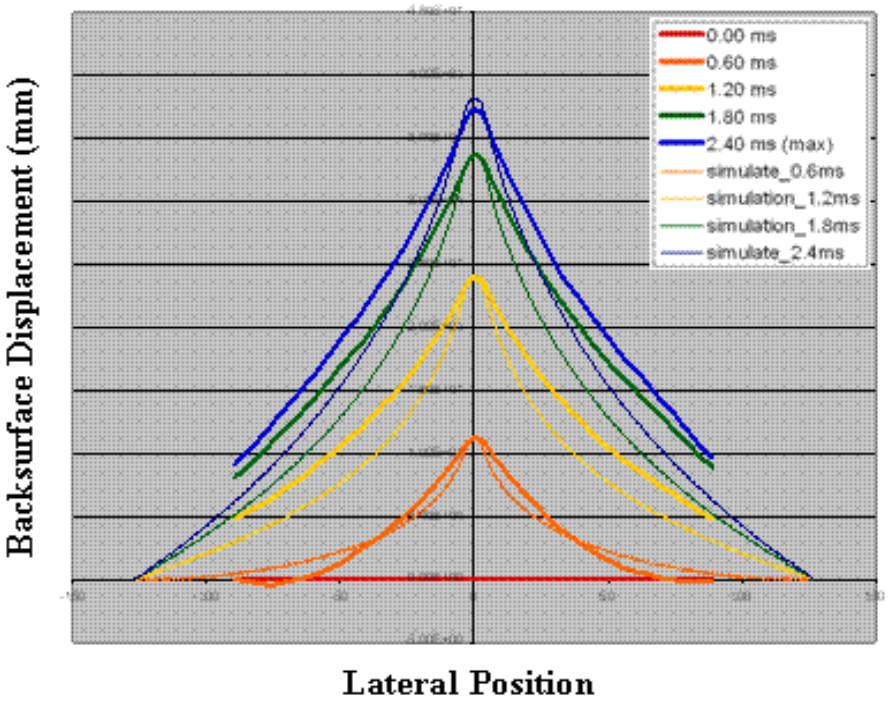


Square Fixture

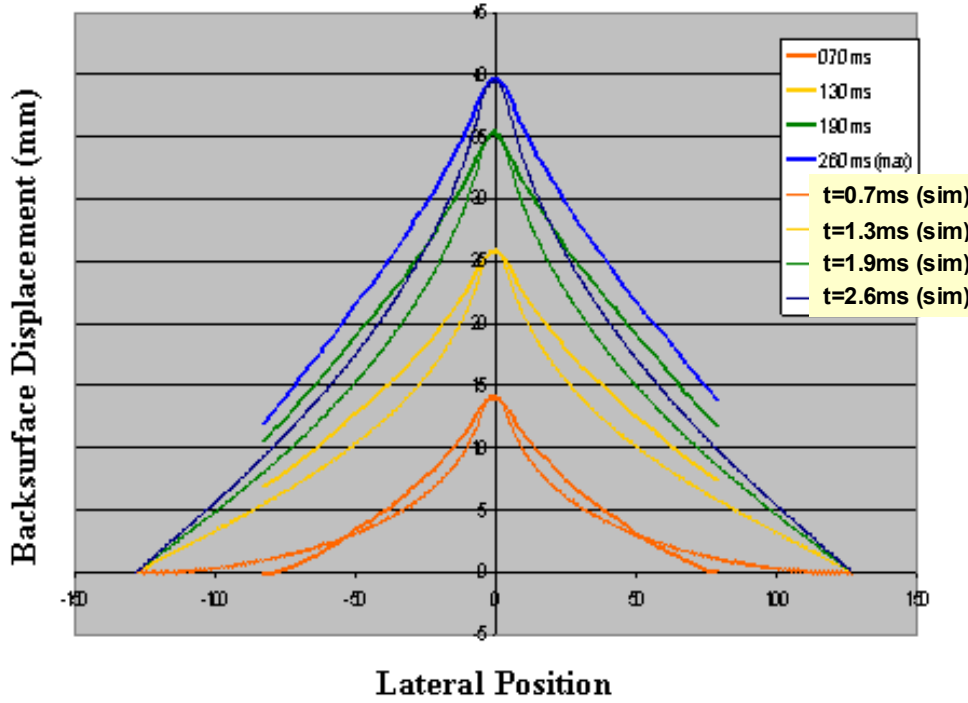


Sub-yarn Level Modeling:
Displacement Profile Correlation

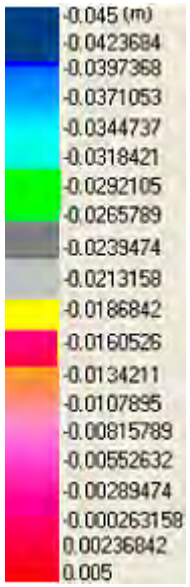
Circular Fixture

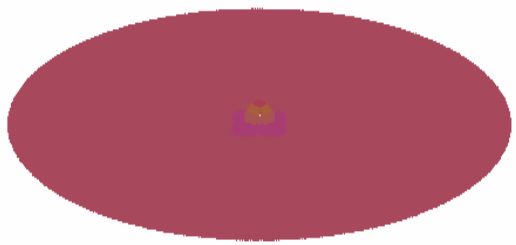


Square Fixture



Fabric deflection (KSU, Num.)

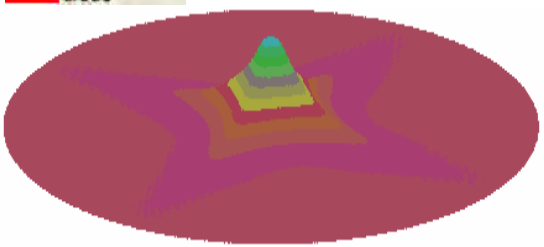




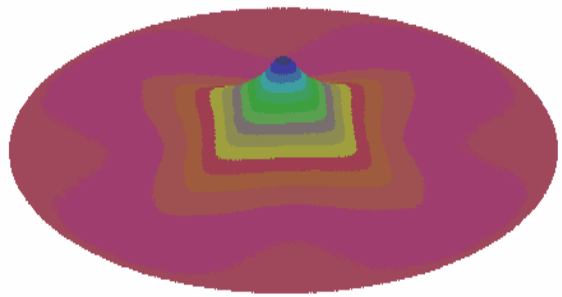
t=0.407 ms



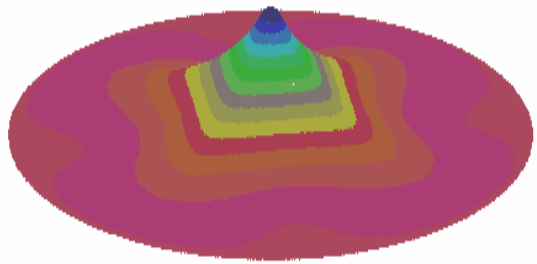
t=0.934 ms



t=0.135 ms



t=0.187ms



0.208 ms

Conclusions

- Two computational approaches have been developed to simulate ballistic impact and penetration of the textile fabric
  - Yarn level model
  - Digital Element model with almost filament level resolution
- Limited validation of the simulation with experiments has been conducted
  - Current results indicate good agreement
  - Further validation is being performed.
- Additional failure mode (filament shearing) and statistical fiber strengths are being incorporated in both models for ballistic modeling
- The developed simulation capabilities would allow a material-by-design approach to textile protection systems
  - Yarn-level model provides computational efficiency on modeling and designing multi-layer fabric protection
  - Sub-yarn-level model by using digital element approach provides
    - Capability of linking the manufacture of a textile to its ballistic performance
    - Quantifying the effect of filament-level parameters such as inter-yarn friction, yarn twisting and pre-yarn tension on the textile fabric ballistic protection efficiency
- When matured and validated, these fabric modeling technologies will allow rapid screening of advanced, novel, hybridized textile systems incorporating differing textile architectures and will enhance our capability for adapting to new threats and integrating new materials as they become available.

Half scale experiments with rig for measuring structural deformation and impulse transfer from land mines

Björn Zakrisson – BAE
Bengt Wikman – BAE
Bo Johansson – FOI

Cooperation during 2007-2008 between:

BAE Systems Hägglunds AB
FOI, Swedish Defence Research Agency

FOI

LULEÅ UNIVERSITY OF TECHNOLOGY

BAE SYSTEMS
HÄGGLUNDS

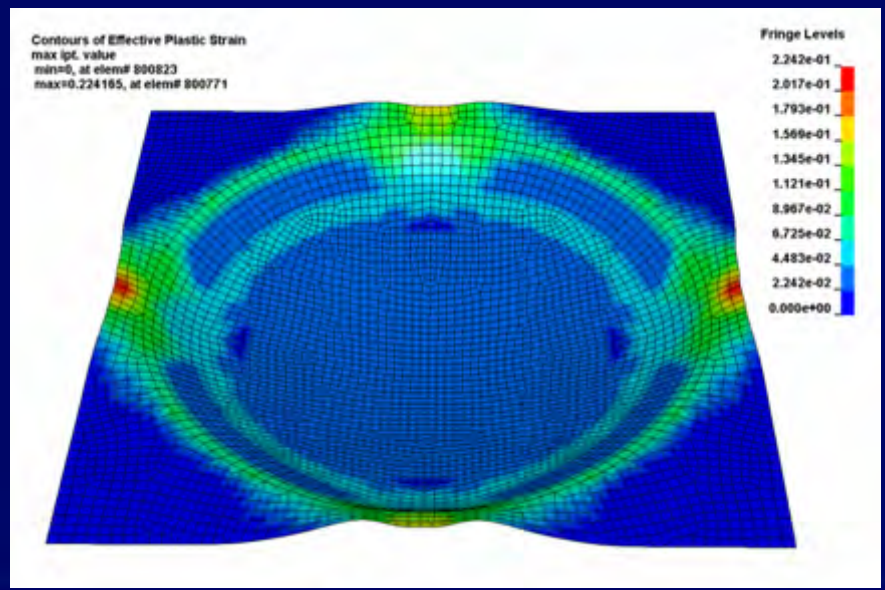
PhD-project PROTECT

In collaboration between :

BAE Systems Hägglunds
Luleå University of Technology

Björn Zakrisson

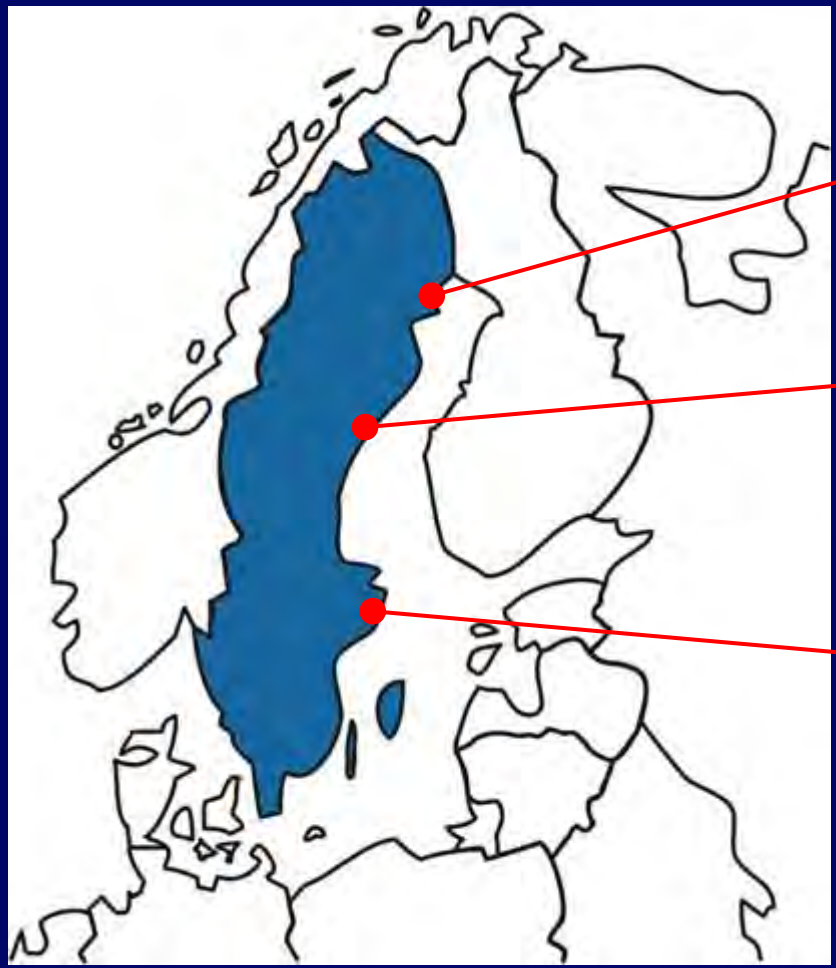




FOI

LULEÅ UNIVERSITY OF TECHNOLOGY

BAE SYSTEMS HÄGGLUNDS



Luleå University of Technology

BAE Systems Hägglunds AB
(Örnsköldsvik, Sweden)

FOI
Swedish Defence Research Agency
(Grindsjön, Tumba, Sweden)

FOI

LULEÅ UNIVERSITY OF TECHNOLOGY

BAE SYSTEMS
HÄGGLUNDS

Scope of work

- Experiments with land mine buried in ground
  - Performed in half scale
- Test parameters:
  - Explosive placed in steel pot or sand
  - Depth of Burial (DOB) in sand 0, 50 och 150 mm
  - Wet or dry sand
- Conditions:
  - Swedish military plastic explosive m/46
    - 86 % PETN 14 % fuel oil
    - Cylindrical with Diameter to Height ratio 3
    - 0.750 kg
  - 0.25 m stand-off distance
- Objective:
  - Detect effects of different test parameters
  - Use test results for validation of numerical model





FOI

LULEÅ UNIVERSITY OF TECHNOLOGY

BAE SYSTEMS HÄGGLUNDS

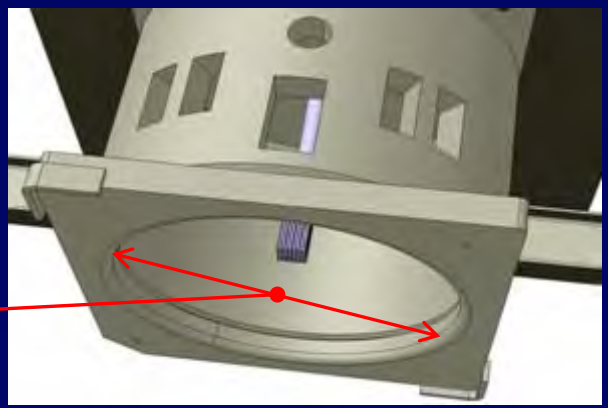
Experimental Setup

Test module viewed from underneath

Plate holder

Weldox 700E
600x600 mm
t=8mm





Diameter
500 mm



Spring-damper system

Test module

Sand box / Steel pot

FOI

LULEÅ UNIVERSITY OF TECHNOLOGY

BAE SYSTEMS HÄGGLUNDS

Measurements

- Maximum vertical jump of the test module
  - Impulse transfer to test module

$$I = m \cdot v_{\max} \approx m \cdot \sqrt{2 \cdot g \cdot z_{\max}}$$

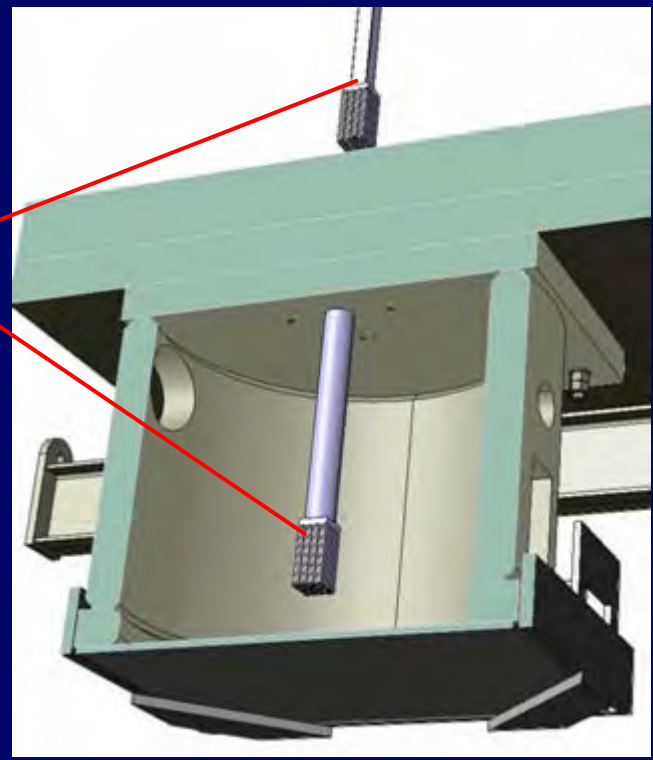
- Maximum dynamic plate deformation
- Residual plate deformation

Measurements (cont.)



Position sensor

Aluminum Honeycomb

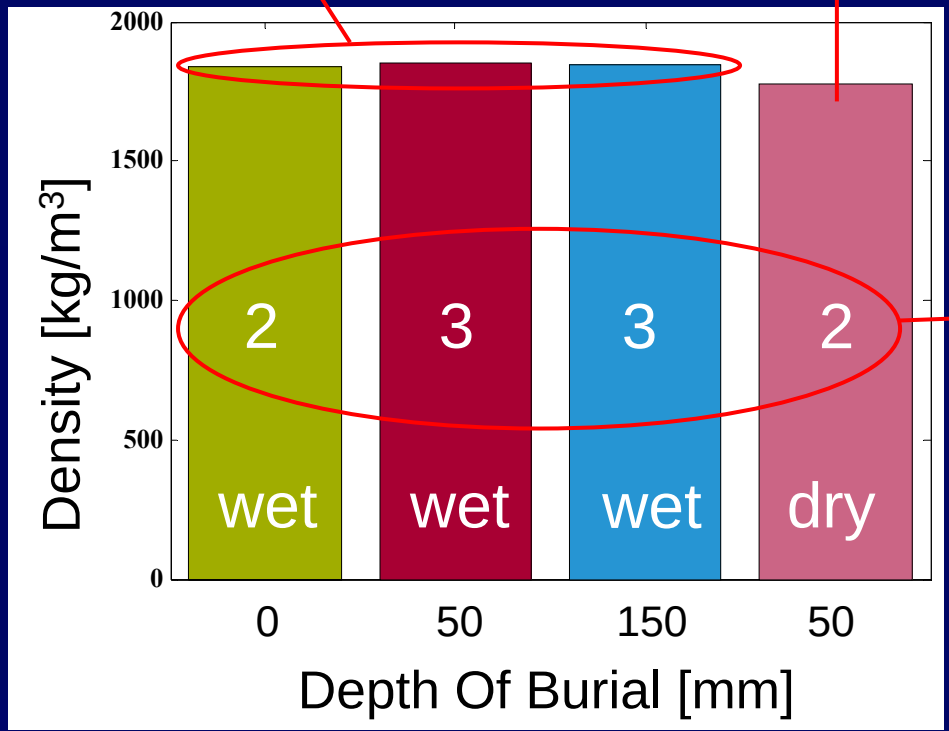


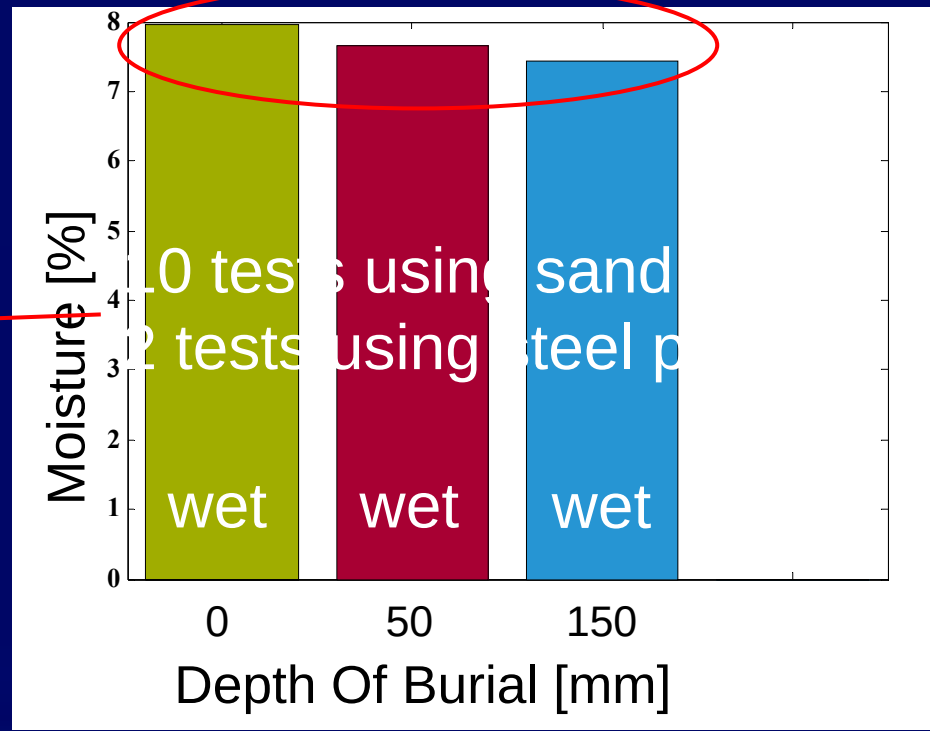
Sand properties

Mean ”wet” density 1845 kg/m^3

Dry density 1771 kg/m^3

Mean moisture 7.7 %





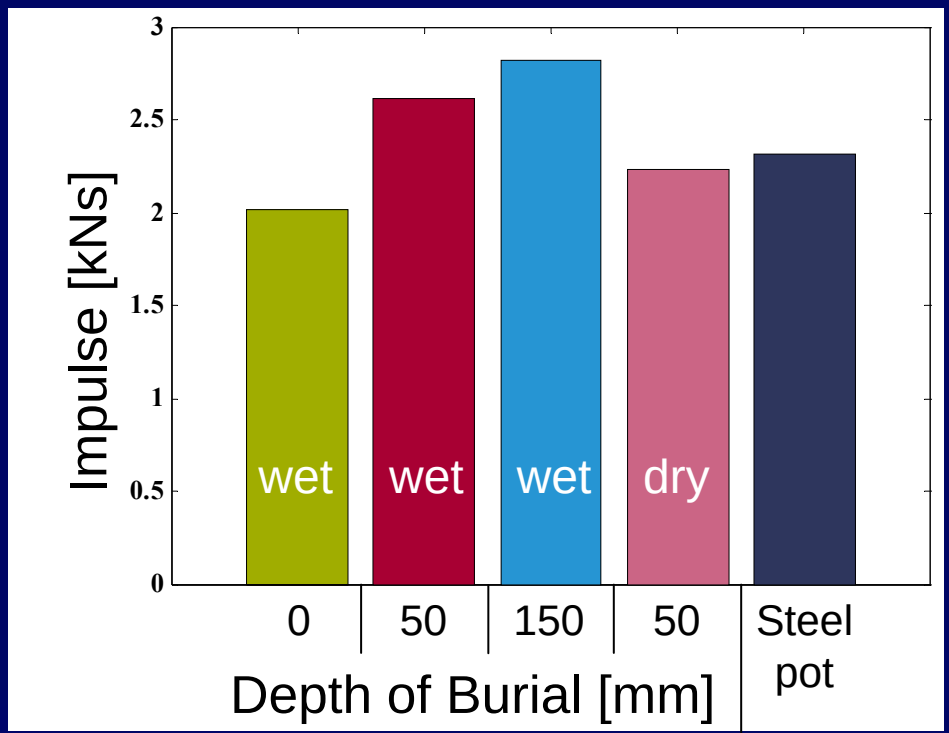
FOI

LULEÅ UNIVERSITY OF TECHNOLOGY

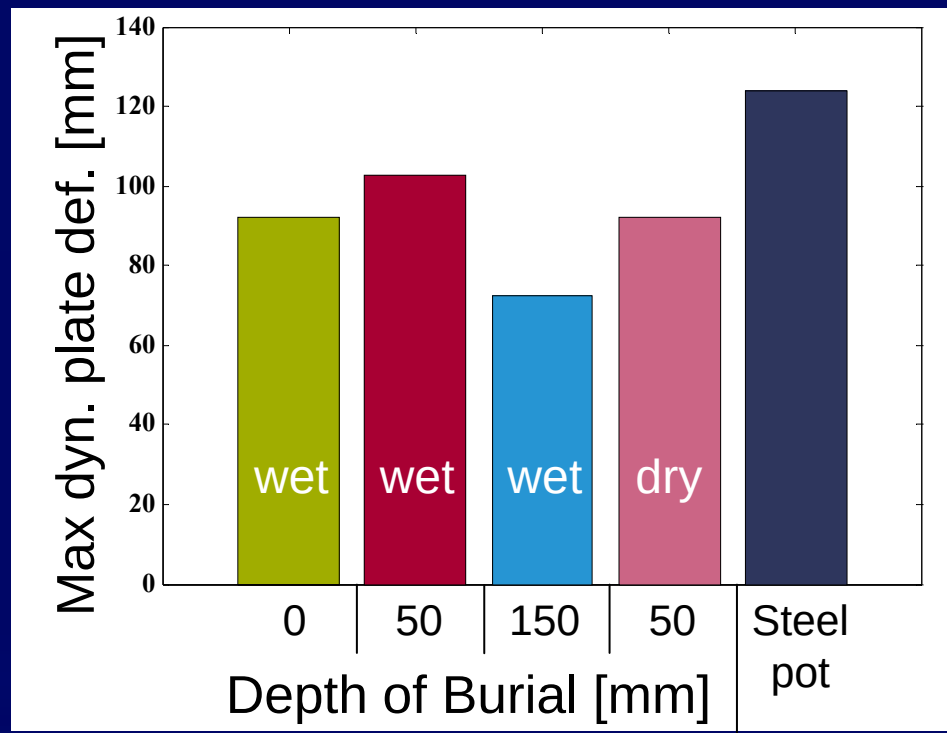
BAE SYSTEMS HÄGGLUNDS

Experimental Results

Impulse transfer to test module



Maximum dynamic plate deformation

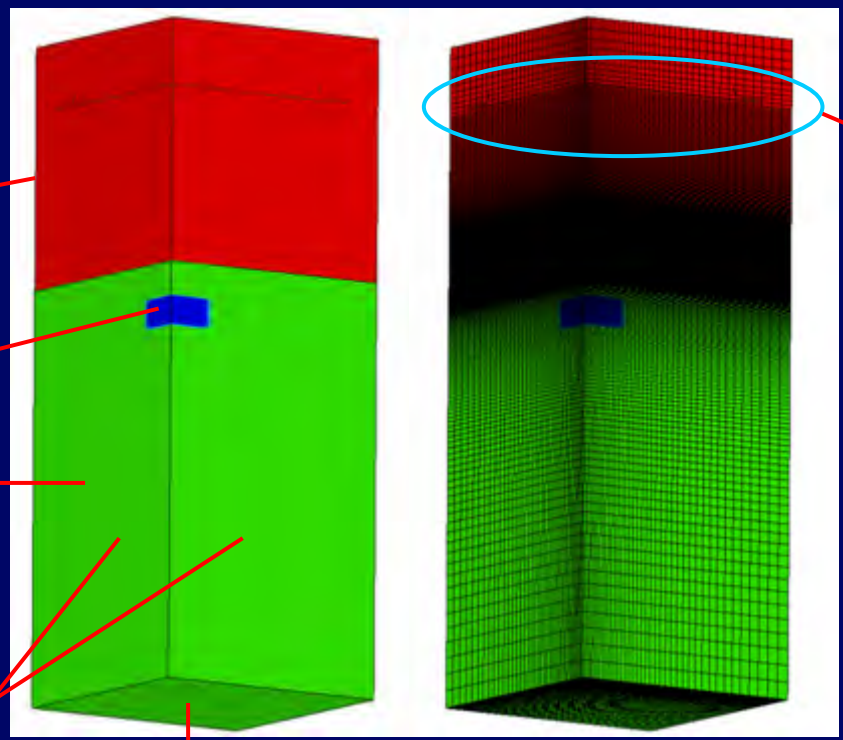


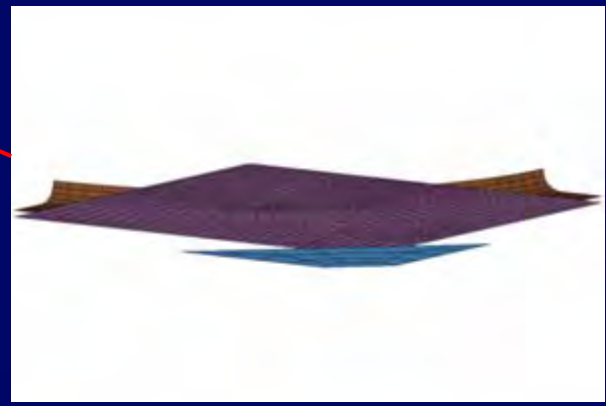
FOI

LULEÅ UNIVERSITY OF TECHNOLOGY

BAE SYSTEMS HÄGGLUNDS

Numerical model
LS-DYNA





- Symmetry model 1/4
- Sand, Air and Explosive modeled with ~536000 Euler elements
- Fluid Structure Interaction couple state variables from gas to structure

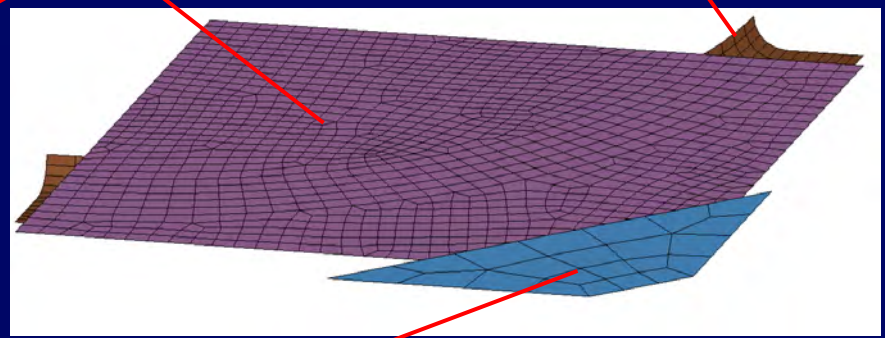
FOI

LULEÅ UNIVERSITY OF TECHNOLOGY

BAE SYSTEMS HÄGGLUNDS

Numerical model (cont.)
LS-DYNA





Numerical model (cont.)
Materials

Sand

- Properties presented by Laine and Sandvik
  - Moisture content 6.57%
  - *Laine L., Sandvik A., "Derivation of mechanical properties for sand", 4th Silos, CI-Premier LTD, p 361-367.*

- Material model
  - Mohr-Coulomb yield surface
  - Tabulated Equation of State
    - ✓ Gives pressure-density relation
  - Initial density set to 1835 kg/m^3

Steel Weldox 700E

- Johnson-Cook model

Explosive m/46

- High Explosive material
  - Equation of state JWL (Jones-Wilkins-Lee)

Air

- Ideal gas

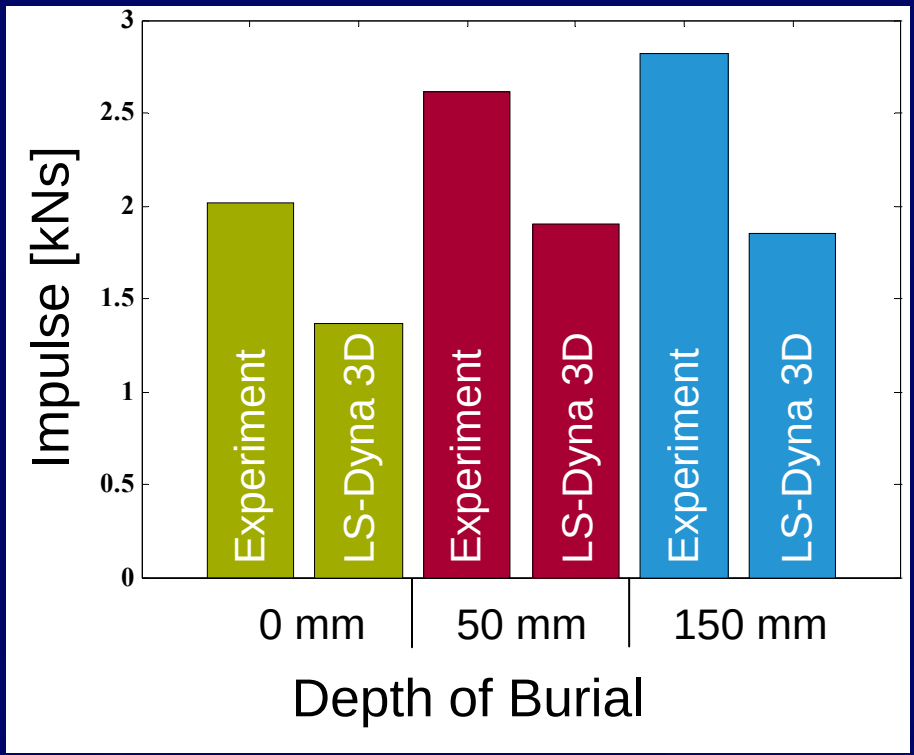
FOI

LULEÅ UNIVERSITY OF TECHNOLOGY

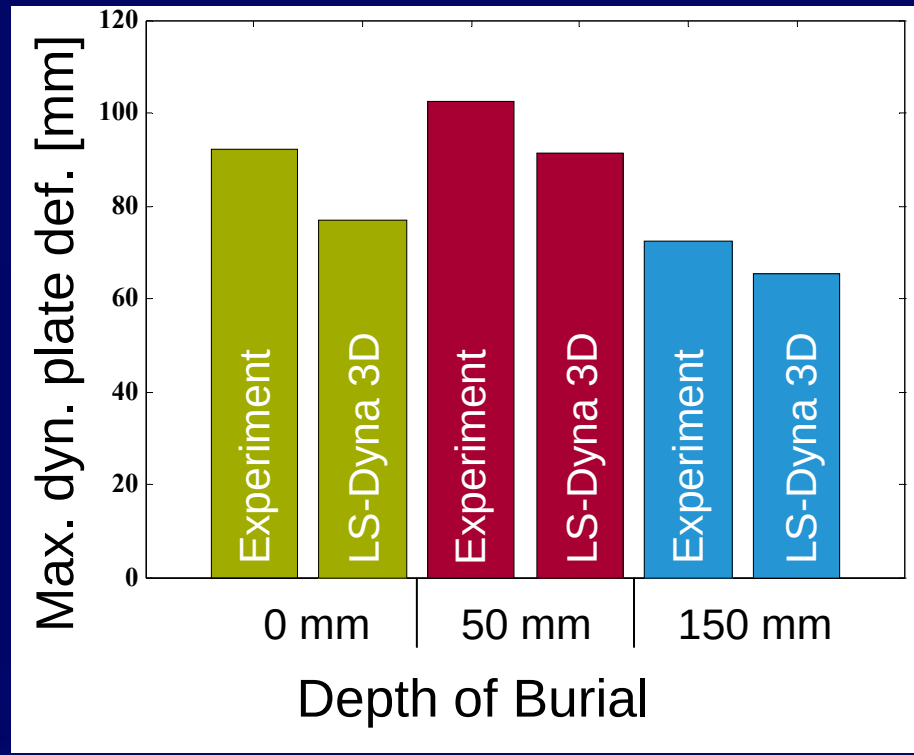
BAE SYSTEMS HÄGGLUNDS

Numerical Results

Impulse transfer to test module



Maximum dynamic plate deformation



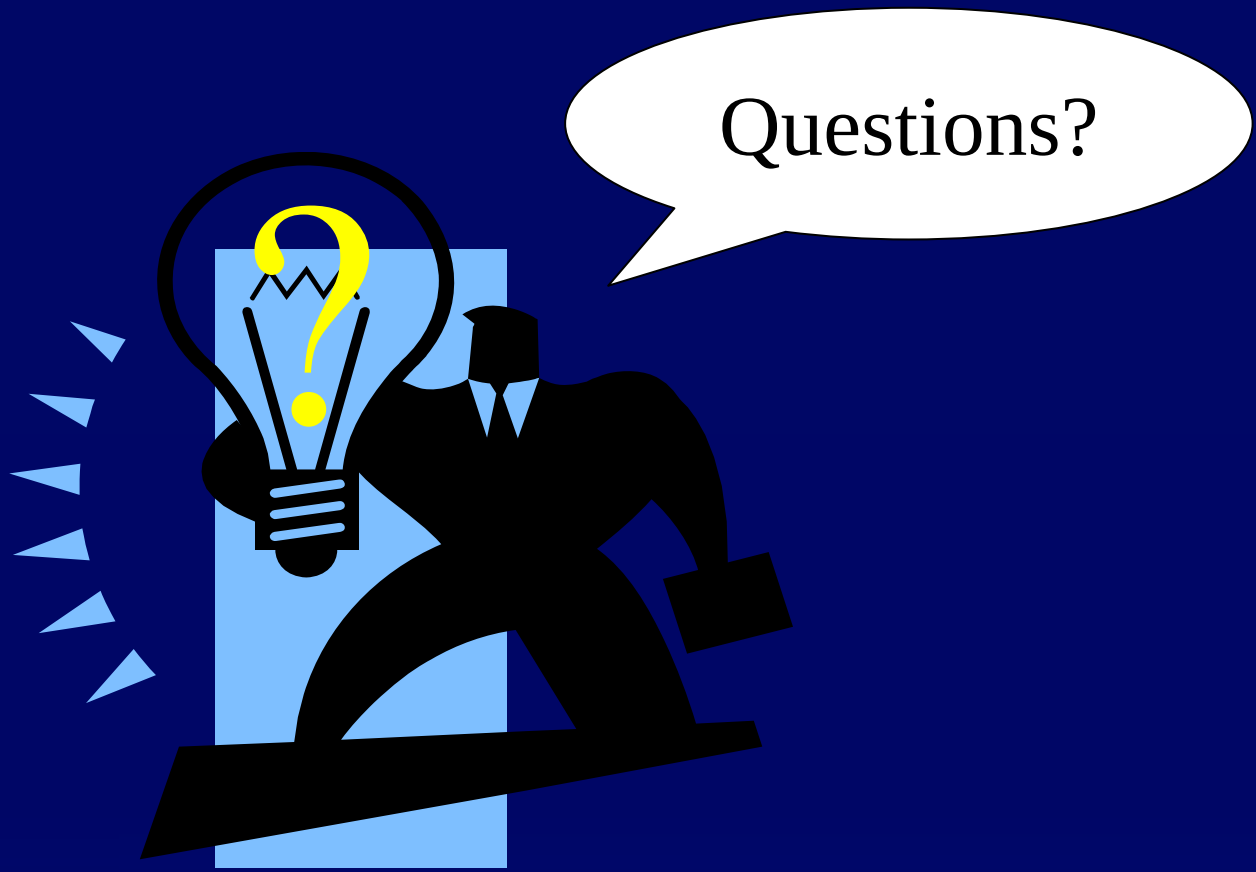
FOI

LULEÅ UNIVERSITY OF TECHNOLOGY

BAE SYSTEMS HÄGGLUNDS

Conclusions

- Transferred impulse increases with the tested DOB in sand
- Measurement methods for test module jump give comparable results
- Wet sand results in larger impulse and plate deformation than dry sand
- Plate deformation increases with DOB up to a limit, decays thereafter
  - Indicates load localization
- Plate deformation largest when using steel pot
- Numerical simulations describe measured trends
  - General underestimation relative measurements
  - Further refinement and investigation needed



FOI

LULEÅ UNIVERSITY OF TECHNOLOGY

BAE SYSTEMS
HÄGGLUNDS

Half scale experiments with rig for measuring structural deformation and impulse transfer from land mines

Name : Björn Zakrisson

Phone : +46 660 80824

Company: BAE Systems Hägglunds AB

E-mail: bjorn.zakrisson@baesystems.se

FOI

LULEÅ UNIVERSITY OF TECHNOLOGY

BAE SYSTEMS HÄGGLUNDS